THE JOURNAL OF
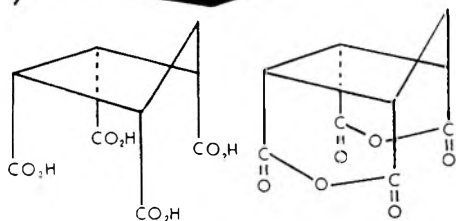# PHYSICAL CHEMISTRY

AUTHOR INDEX

Interaction of Electromagnetic Radiation with Matter. I.

Theory of Optical Rotatory Power: Topic A.

Trigonal Dihedral Compounds[1a]

by Andrew D. Liehr[1b]

Bell Telephone Laboratories, Inc., Murray Hill, New Jersey, and Mellon Institute, Pittsburgh, Pennsylvania
(Received July 24, 1963)

Who shall be a light between truth and intellect.—Dante

A complete theory of the electronic properties of trigonal dihedral compounds is outlined, with special emphasis upon their optical rotatory power. Molecular orbitals are derived, many electron configurations constructed, and various spectral parameters computed. A number of points of general interest have been uncovered and elucidated: (1) a zeroth-order molecular orbital theory is capable of explaining the observed optical rotary strengths of trigonal dihedral compounds; (2) the electron-hole formalism is not directly applicable to optical rotatory or spectral strength calculations; (3) there is a direct correspondence between the rotational and spectral powers of d^n and d^{5+n} ($n = 0, 1, 2, 3, 4, 5$) spin-free systems, between $d^{1,4,6,9}$ spin-free systems, and numerous indirect relationships between these and other systems; (4) strong natural electronic optical rotatory dispersion, dichroism, and dissymmetry are possible in the infrared and microwave regions of the spectrum; (5) spin magnetic dipole transition moments alone, in conjunction with an allowed electric dipole transition moment, may give rise to large rotational strengths; (6) to good approximation, σ- and σ-,π-bonded compounds are formally identical in their dihedral optical rotativity and intensity behavior; (7) electronic transitions to or from bonded and antibonded dihedral molecular states rotate electromagnetic radiation parallelly or oppositely dependent upon conditions; (8) for a fixed molecular conformation, the sign and magnitude of the rotational, dichroic, dissymmetric, and spectral strengths depend upon the degree of local electronic trigonal dihedral asymmetry as measured by such parameters as the covalency and hybridization constants and the angle of metal–ligand orbital mismatch; (9) the absolute and relative geometrical configurations of ground electronic states of chemically distinct and variegated series of trigonal dihedral compounds can be theoretically fixed and correlated, and possible geometric deformations of these configurations in excited electronic states can sometimes be inferred, and their nature guessed, from optical rotatory, circular dichroic, and circular dissymmetric behavior; (10) cubical optical rotatory selection rules do not always hold in zeroth order for trigonal dihedral compounds. Examples have been given, a course for future research outlined, and a plan for closer theoretical–experimental cooperation entered.

TABLE OF CONTENTS

I. Introduction

Of all the natural phenomena observed in nature, none has had so profound an effect on chemical thought as that of natural optical rotatory power. Discovered by Biot in 1812, physically justified by Fresnel in 1822–1824, and structurally interpreted by Pasteur in 1846–1860, this phenomenon has been the foundation upon which all modern structural theory has been built. The modern concept of chemistry in space is a direct outgrowth of its discovery and explanation. Indeed, the tetrahedral geometry of four-coordinate carbon compounds and the octahedral geometry of six-coordinate metal compounds to a large extent owe their final acceptance to the incontrovertible evidence provided for these structures by the resolution of optically active stereoisomers.[2] In this paper we wish to demonstrate the role played by geometry in inducing optical activity in six-coordinate dihedral metal compounds. In later works we shall take up the problem of four-coordinate dihedral compounds and of nondihedral compounds of metals and nonmetals, and in particular of the transition metal and carbon compounds.

II. Theory §1. Molecular Orbitals for Dihedral Compounds: Zero Spin-Orbit Forces

1.1   The σ-Molecular Orbitals. In Fig. 1 we schematically sketch the geometry of a typical σ-bonded (neglecting so-called "ammonia" framework hypercon-

(1) (a) This paper was initially prepared and submitted for possible presentation at the Quantum Chemistry Conference held at Oxford University, Oxford, England, April 10–14, 1961. It was not scheduled in the final select program and, hence, was not officially presented until August, 1961 at the Sixth International Conference on Coordination Chemistry, Wayne State University, Detroit, Michigan, August 27–September 1, 1961. Its main contents also have been disclosed subsequently in the open discussional sessions of the Seventh International Conference on Coordination Chemistry, Stockholm, Sweden, June 25–29, 1962, and of the International Symposium on Molecular Structure and Spectroscopy, Tokyo, September 10–15, 1962. Other more specific portions were detailed at the Symposium on Molecular Structure and Spectroscopy, Ohio State University, Columbus, Ohio, June 10–14, 1963. (b) Mellon Institute, Pittsburgh, Penna.

(2) In this regard, it is interesting to note that it took nearly 20 years for Werner's theory of octahedral metal complexes to gain acceptance, and that this acceptance was finally granted only after he prepared and characterized the optically active dihedral complex potassium trisoxalatochromium(III). For a masterly discussion of the history, theory, and practice of optical rotary phenomena, read T. M. Lowry, "Optical Rotatory Power," Longmans, Green, and Co., London, 1935.

jugative effects) complex cation, the copper(II) tris-ethylenediamine cation. Figure 2 illustrates the idealized disposition of the ligand σ-bond orbitals which we assume in our later numerical work, and Fig. 3 a typical, but not universal, level pattern. Note especially the explicit allowance made in Fig. 2 for an angle of cant, α, between the ligand orbitals and the metal orbitals, which are here imagined to be directed octahedrally along the x, y, and z axes of the figure.
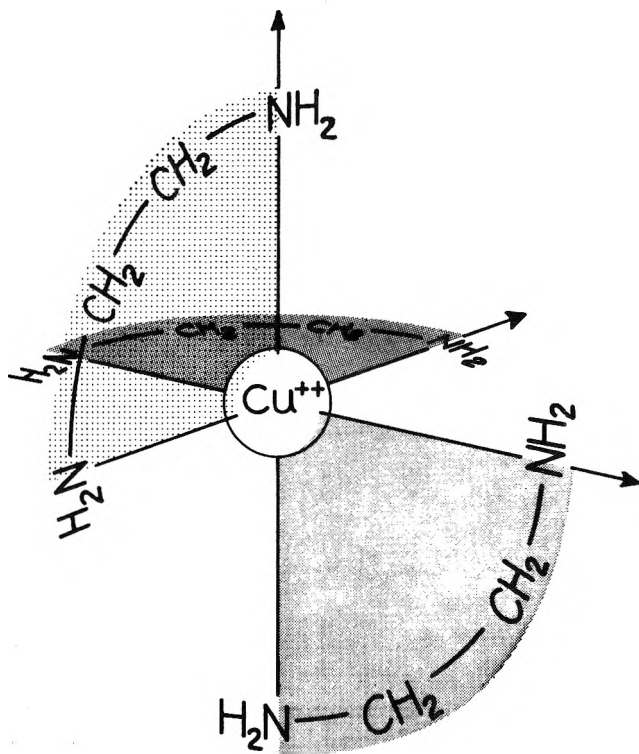
Figure 1. The idealized planar right-angled geometry of the trisethylenediaminecopper(II) cation.

If we designate the localized ligand σ-bond orbitals by the symbol, λ_j, $(j = 0, 1, 2, 3, 4, 5)$, we may approximate the trigonal dihedral one electron σ-molecular orbitals, Λ_s, as a linear combination of these localized orbitals.[3]

$$\Lambda_s = \sum_{j=0}^{5} a_{js}\lambda_j \qquad (1)$$

Now since our molecular system has the symmetry D_3, the threefold axis being the z' axis of Fig. 2, and the three twofold axes being the y' axis and its trigonal equivalents of y'' and y''' [y'' equals $\mathcal{C}_3(z')y'$ and y''' equals $\mathcal{C}_3{}^2(z')y'$ equals $\mathcal{C}_3(z')y''$, where $\mathcal{C}_3(z')$ is a counterclockwise *replacement* rotation (*i.e.*, the so-called rotation operator of the D_3 point group) by 120° about the z' axis defined by Table I], we can always require that
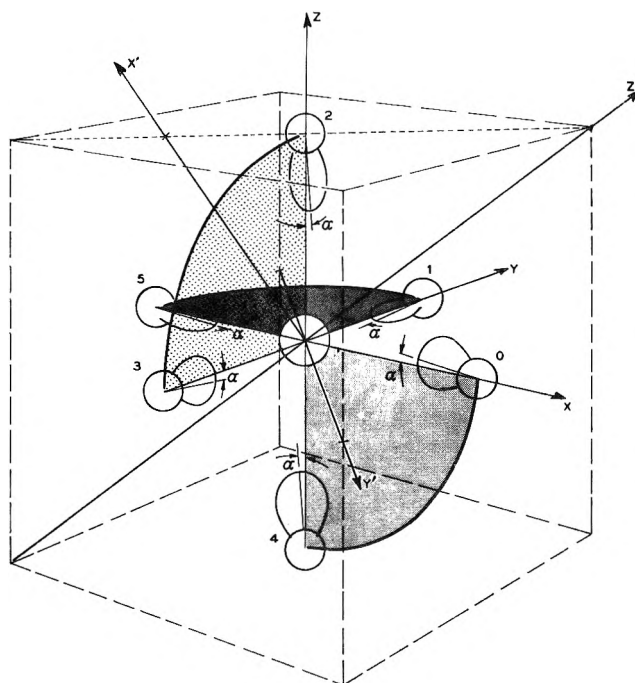
Figure 2. The local ligand orbital spatial disposition for the idealized planar right-angled geometry of the · trisethylenediaminecopper(II) cation.

Table I: Definition of the $\mathcal{C}_3(z')$ and $\mathcal{C}_2(y')$ Symmetry Operations

k	$\mathcal{C}_3(z')k$	$\mathcal{C}_2(y')k$	(kl)	$\mathcal{C}_3(z')(kl)$	$\mathcal{C}_2(y')(kl)$
0	2	3	(04)	(23)	(32)
1	0	5	(23)	(15)	(40)
2	1	4	(15)	(04)	(51)
3	5	0	x	z	$-y$
4	3	2	y	x	$-x$
5	4	1	z	y	$-z$

our molecular orbitals, Λ_s, be trigonally symmetric; that is, that[4]

$$\mathcal{C}_3\Lambda_s = \omega^s\Lambda_s, \quad \omega = e^{2\pi i/3}, \ (s = 0, \pm 1) \qquad (2)$$

(3) It is important to keep in mind that the existence of one-electron molecular orbitals (or atomic orbitals for that matter) is a complete figment of man's imagination. Although pictorially and physically appealing, it is nonetheless only a very rough and ready picture of the actual electronic paths in real molecules. Peruse, *e.g.*, (a) "Papers from the Conference on Molecular Quantum Mechanics, University of Colorado, Boulder, Colorado, June 21–27, 1959," *Rev. Mod. Phys.*, **32**, 169 (1959); and (b) H. Conroy, *J. Chem. Phys.*, **40**, 603 (1964), *et seq.* The use of misguided localized orbitals to form one electron molecular orbitals like those of eq. 1 is not new with the author; they have been employed before by Spitzer, Coulson, and Moffitt, and others. For a review of these uses and of the pertinent literature, read (c) W. H. Flygare, *Science*, **140**, 1179 (1963), and (d) C. A. Coulson and T. H. Goodwin, *J. Chem. Soc.*, 3161 (1963).

(4) For a simple-minded justification of this procedure read A. D. Liehr, "Theory and Structure of Complex Compounds," B. Jezowska-Trzebiatowska, Ed., Pergamon Press, London and New York, 1964, pp. 95–135, and *Progr. Inorg. Chem.*, **5**, 385 (1963).
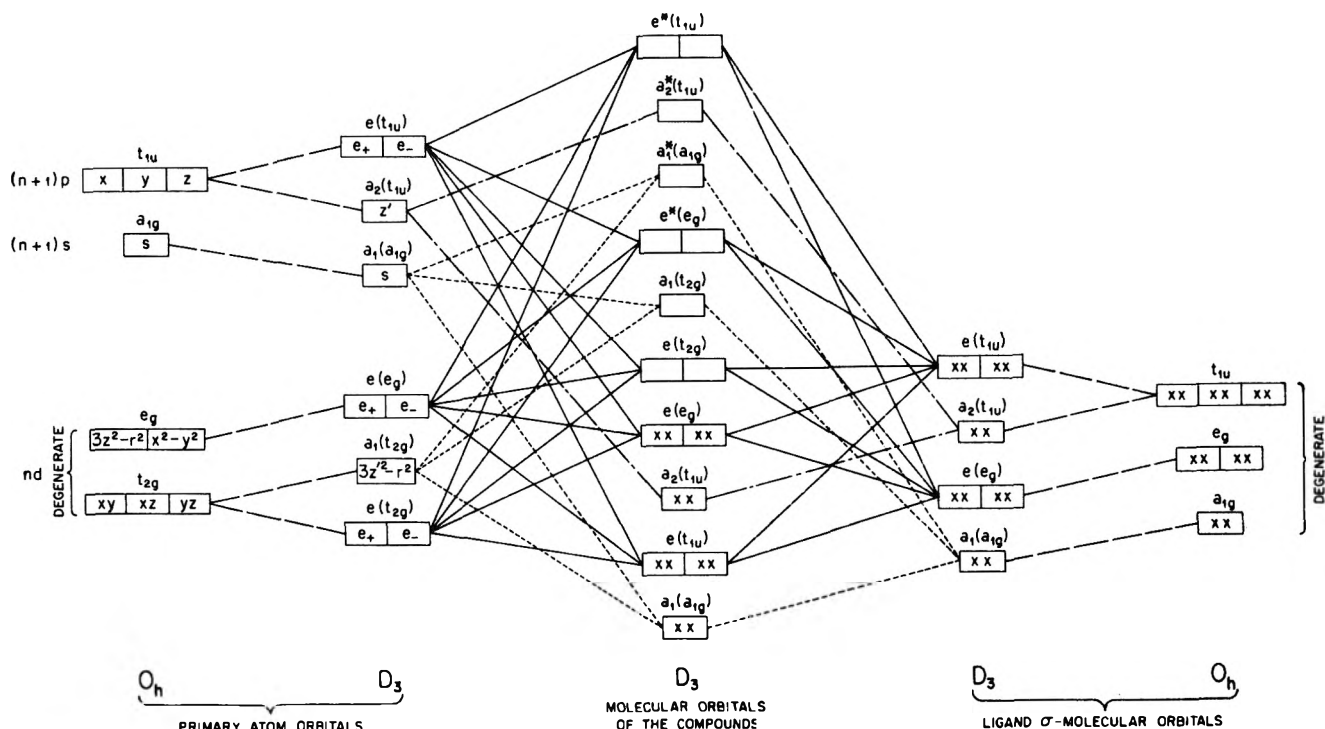
Figure 3. A schematic molecular orbital energy level diagram for a trigonally dihedral transition metal compound in the σ-bond approximation.

In the localized orbital representation, eq. 1, for the one-electron molecular orbitals, Λ_s, we find that the a_{j_s} equal $\omega^{js}a_{0s}$, $(j = 0, 1, 2)$, and $\omega^{js}a_{3s}$, $(j = 3, 4, 5)$, or that [since by eq. 2, ω^{3+j} equals ω^j, $(j = 0, 1, 2)$][4]

$$\Lambda_s = a_{0s} \sum_{j=0}^{2} \omega^{sj}\lambda_j + a_{3s} \sum_{j=3}^{5} \omega^{sj}\lambda_j, \quad (s = 0, \pm1) \quad (3)$$

where the constants a_{0s} and a_{3s} are jointly determined by normalization, further symmetrization, orientation, and/or energy minimization requirements. It will be convenient for later work to define the first member of the two-part summation in eq. 3 as $\Lambda_s^{(1)}$ and the second as $\Lambda_s^{(2)}$.

$$\begin{aligned} \Lambda_s^{(1)} &= a_{0s} \sum_{j=0}^{2} \omega^{sj}\lambda_j \\ \Lambda_s^{(2)} &= a_{3s} \sum_{j=3}^{5} \omega^{sj}\lambda_j, \quad (s = 0, \pm1) \end{aligned} \quad (4)$$

In the case that s equals zero, the symmetrization requirement

$$\mathcal{C}_2\Lambda_0 = \pm\Lambda_0 \quad (5)$$

where $\mathcal{C}_2$ is the $180°$ rotation, $\mathcal{C}_2(y')$, about the y' axis of Fig. 2 which is specified in Table I, fixes a_{3s} as $\pm a_{0s}$, $(s = 0)$, in eq. 3. Hence, with the neglect of localized ligand–ligand overlap, we may write

$$\Lambda_0^{(\pm)} = \frac{1}{\sqrt{6}} \left\{ \sum_{j=0}^{2} \lambda_j \pm \sum_{j=3}^{5} \lambda_j \right\} \quad (6)$$

when $(s = 0)$. For the case $s = \pm1$, however, no such simple symmetrization is possible as the functions $\Lambda_{\pm1}$ are eurythmically doubly degenerate and by definition thus cannot be made simultaneous eigenfunctions of $\mathcal{C}_2(y')$ and $\mathcal{C}_3(z')$. We must therefore be content to work with the functions defined in eq. 4, or suitable linear combinations of these as indicated in eq. 3.[5] In

---

(5) One such linear combination is readily obtained by the orientational requirement $\mathcal{C}_2\Lambda_{\pm1} = + $ or $ - \Lambda_{\mp1}$. This requirement implies that $a_{0s} = \pm a_{3-s}$, a particular solution of which is given by

$$\Lambda_s^{(\pm)} = \frac{1}{\sqrt{6}} \left\{ \sum_{j=0}^{2} \omega^{sj}\lambda_j \pm \sum_{j=3}^{5} \omega^{sj}\lambda_j \right\}$$

where $\mathcal{C}_2\Lambda_s^{(\pm)} = \pm\Lambda_{-s}^{(\pm)}$, $(s = \pm1)$. In terms of these functions, the functions of eq. 4 may be written as $\Lambda_s^{(1)} = a_{0s}^{(1)}\sqrt{3/2}[\Lambda_s^{(+)} + \Lambda_s^{(-)}]$ and $\Lambda_s^{(2)} = a_{3s}^{(2)}\sqrt{3/2}[\Lambda_s^{(+)} - \Lambda_s^{(-)}]$, where $a_{0s}^{(1)}$ and $a_{3s}^{(2)}$ are arbitrary real or complex constants, so that $\mathcal{C}_2\Lambda_s^{(1)} = \Lambda_{-s}^{(2)}$ and $\mathcal{C}_2\Lambda_s^{(2)} = \Lambda_{-s}^{(1)}$ whenever $a_{0s}^{(1)}$ equals $a_{3-s}^{(2)}$. The suitable redefinition of $\Lambda_s^{(-)}$ as $\Lambda_{-1}^{(-)} = -\bar{\Lambda}_{-1}^{(+)}$ and $\Lambda_{+1}^{(-)} = \bar{\Lambda}_{+1}^{(+)}$ allows both $\Lambda_s^{(+)}$ and $\bar{\Lambda}_s^{(+)}$ to satisfy the same $\mathcal{C}_2(y')$ equations, $\mathcal{C}_2\Lambda_{\pm1}^{(+)} = \Lambda_{\mp1}^{(+)}$ and $\mathcal{C}_2\bar{\Lambda}_{\pm1}^{(+)} = \bar{\Lambda}_{\mp1}^{(+)}$, so that both sets of doubly degenerate (E) functions may be properly oriented for combination with compatible central atom orbitals for (D₃) compound formation [see Tables II and III]. It is not impropitious to remember that *only properly, compatibly oriented symmetrized functions may be combined to form molecular orbitals.*

the point group D_3, $\Lambda_0^{(+)}$ is of species A_1, $\Lambda_0^{(-)}$ of species A_2, and $\Lambda_\pm$, $\Lambda_\pm^{(j)}$, or $\overline{\Lambda}_\pm^{(+)}$ (we now drop the subscript 1 in ± 1 for notational convenience)[5] of species E, individually as indicated in Table II.

Table II : The D_3 Point Group and Transformation Standards

D_3	E	$2C_3(z')$	$3C_2(y')$	Transformation standards
A_1	1	1	1	r^2, z'^2, $x'^2 + y'^2$, $\Lambda_0^{(+)}$
A_2	1	1	-1	z', l_z', $\Lambda_0^{(-)}$
E	2	-1	0	(x', y'), (l_x', l_y'), $(x'^2 - y'^2, x'y')$, $(x'z', y'z')$, $\Lambda_{\pm 1}$, $\Lambda_{\pm 1}^{(1,2)}$, $\Lambda_{\pm 1}^{(\pm)}$, $\overline{\Lambda}_\pm^{(+)}$

At this point it is convenient to decompose the localized ligand orbitals λ_j into a "σ-part" and a "π-part" which are separately directed along the axes x, y, and z of Fig. 2 as indicated in Fig. 4.[6] We may then write

$$\lambda_0 = \sigma_{x0} + \pi_{z0}, \ \lambda_2 = \sigma_{z2} + \pi_{y2}, \ \lambda_4 = \sigma_{z4} + \pi_{x4},$$

$$\lambda_1 = \sigma_{y1} + \pi_{x1}, \ \lambda_3 = \sigma_{y3} + \pi_{z3}, \ \lambda_5 = \sigma_{x5} + \pi_{y5} \quad (7)$$

where $[w = x, y, z; \ j = 0, 1, 2, 3, 4, 5]$[6]

$$\sigma_{wj}{}^c = k_s ns_j \mp k_p \cos \alpha \, np_{\sigma_{wj}}, \ \pi_{wj}{}^s = \pm k_p \sin \alpha \, np_{\pi_{wj}} \quad (8)$$

and where a superscript c and s have been added in eq. 8 to indicate the presence of the factors $k_p \cos \alpha$ and $k_p \sin \alpha$ in the σ- and π-like functions, separately. [If these factors are absent, the superscripts c and s are to be discarded.] The $\mp$ and $\pm$ factors in eq. 8 give the phases needed for maximum bonding power [view Fig. 2 and Table V]. In terms of this symbolism we may define

$$\Sigma_0^{(\pm)} = \frac{1}{\sqrt{6}} \left\{ \sum_{j=0}^{2} \sigma_j \pm \sum_{j=3}^{5} \sigma_j \right\},$$

$$\Pi_0^{(\pm)} = \frac{1}{\sqrt{6}} \left\{ \sum_{j=0}^{2} \pi_j \pm \sum_{j=3}^{5} \pi_j \right\}$$

$$\Sigma_s^{(1)} = a_{0s}{}^\sigma \sum_{j=0}^{2} \omega^{sj}\sigma_j, \ \Pi_s^{(1)} = a_{0s}{}^\pi \sum_{j=0}^{2} \omega^{sj}\pi_j$$

$$\Sigma_s^{(2)} = a_{0s}{}^\sigma \sum_{j=3}^{5} \omega^{sj}\sigma_j, \ \Pi_s^{(2)} = a_{3s}{}^\pi \sum_{j=3}^{5} \omega^{sj}\pi_j, \ (s = \pm 1) \quad (9)$$

where the subscript w equals x, y, z, which is rendered redundant by Fig. 2, has been dropped, and where the superscripts c and s must be inserted if the factors

$k_p \cos \alpha$ and $k_p \sin \alpha$ appear in the definitions of the σ- and π-like localized orbitals. The σ-portion of the localized ligand functions, λ_j, may be further arranged to yield a pseudo-octahedral σ-bond system. This arrangement is accomplished by choosing the sums, Σ_s, ($s = 0, \pm 1$), of eq. 9 to transform as do the true octahedral σ-molecular orbitals under the counterclockwise *replacement* rotation, $\mathfrak{C}_4(z)$, about the z axis of Fig. 2 and under the inversion operation i about the coordinate origin of Fig. 2 as indicated in Tables III and IV. Care must be exercised in so doing in order that the resulting functions are properly oriented with respect to the central atom functions with which they are to combine. The result is that the $\Sigma_0^{(+)}$ sum is already the proper pseudo-octahedral molecular orbital of species A_{1g} and that $\Sigma_\pm$ is equal to $\Sigma_s^{(1)} + \Sigma_s^{(2)}$, with a_{0s} and $a_{3-s}{}^*$ equal to $\omega^s/\sqrt{6}$, ($s = \pm 1$), that is

$$\Sigma_\pm = \frac{1}{\sqrt{6}} \omega^{\pm 1} \sum_{j=0}^{2} \omega^{\pm j}\sigma_j + \frac{1}{\sqrt{6}} \omega^{\mp 1} \sum_{j=3}^{5} \omega^{\pm j}\sigma_j \quad (10)$$

(6) For simplicity of illustration, we have assumed the ligating atom to be situated on the x, y, or z axes. In actual practice this will seldom be the case for polydentate ligands due to steric encumbrances [c/. Fig. 16–19, for example]. However, even in the more general case we may still decompose our charge amplitudes into portions directed along lines parallel to metal–ligand nuclear directions [or, if desired, parallel to the x, y, or z axes] and perpendicular to it. This decomposition is most simply and *rigorously* accomplished by the expansion of the ligand charge amplitude function in a Fourier series [if it is taken to be initially axially symmetric] or a spherical harmonic series [if it is not taken to be initially axially symmetric] about the metal–ligand [or coordinate axes] directions, the polar angle being measured from this latter direction and the azimuthal angle [if necessary] being measured about this new direction. If it is assumed, as we shall do presently, that the ligand charge amplitude function is expansible in a cosine Fourier series in which only the first two terms need be kept, we obtain

$$\lambda_j = \lambda(r_j, \bar\theta_j) = \lambda^{(0)}(r_j) + \cos \bar\theta_j \, \lambda^{(1)}(r_j) + \cdots$$

In the two-dimensional case pictured in Fig. 4a, we see that $\bar\theta_j$ equals $|\theta_j - \alpha|$ and so

$$\lambda_j = \lambda(r_j, \bar\theta_j) = \lambda^0(r_j) + \cos(\theta_j - \alpha)\lambda^{(1)}(r_j) + \cdots$$

$$= \lambda^0(r_j) + \cos \theta_j \lambda^{(1)}(r_j) \cos \alpha + \sin \theta_j \lambda^{(1)}(r_j) \sin \alpha + \cdots$$

More generally, in the three-dimensional case drawn in Fig. 4b, we find that $\cos \bar\theta_j = \cos \theta_j \cos \alpha + \sin \theta_j \sin \alpha \cos(\varphi_j - \varphi_\alpha)$, and hence for φ_α equals 0 or 90° as in Fig. 2, we have

$$\lambda_j = \lambda^0(r_j) + \cos \theta_j \lambda^{(1)}(r_j) \cos \alpha +$$

$$\sin \theta_j \begin{Bmatrix} \sin \\ \cos \end{Bmatrix} \varphi_j \lambda^{(1)}(r_j) \sin \alpha + \cdots$$

When the radial functions $\lambda^0(r_j)$ and $\lambda^{(1)}(r_j)$ are identified with atomic-like ligand functions [this does *not* imply that these functions are actually atomic in nature—see A. D. Liehr, to be published, for further discussion, generalizations, and ramifications of this as well as other related matters] of the types ns and np, we have the desired atomic-like basis decomposition

$$\lambda_j = \lambda(r_j, \bar\theta_j) = k_s ns_j + k_p \cos \alpha \, np_{\sigma_j} + k_p \sin \alpha \, np_{\pi_j} = \sigma_j + \pi_j$$

where k_s and k_p are the fractional contents [the so-named "hybridization" ratios (see A. D. Liehr, *ibid.*)] of the ns and np atomic-like basis functions in the Fourier expansion.

is the proper pseudo-octahedral molecular orbital of species E_g.[7] The π-portion of the localized orbitals cannot be so oriented since the six π-like orbitals of eq. 7 do *not* form a symmetrically complete set under $C_4(z)$ and i [for example from Tables IV and V, $i\pi_{z0}$ equals $-\pi_{z5}$ and $C_4\pi_{z1}$ equals $-\pi_{y0}$, neither of which again belongs to the original π-orbital set of eq. 7]. Only when all twelve varieties [Table V] of localized π-orbitals are available [as in the π-bonded complex anions (such as
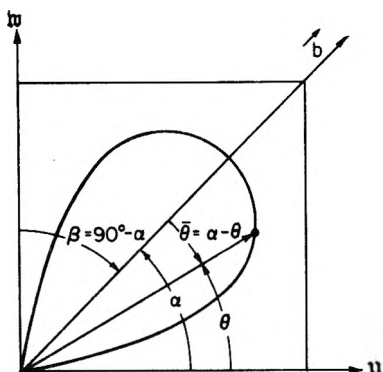
$\therefore$ In the $\mathfrak{u}\mathfrak{w}$ plane $\cos\bar{\theta} = \cos(\alpha - \theta) = \cos\theta\cos\alpha + \sin\theta\sin\alpha$

(a)
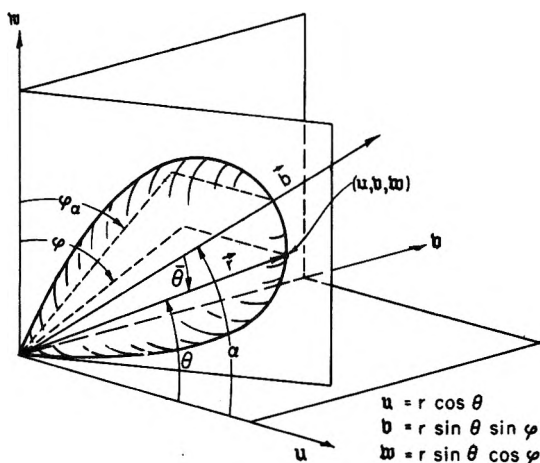
$\vec{r}\cdot\vec{b} = rb\cos\bar{\theta} = \mathfrak{u}\,b_{\mathfrak{u}} + \mathfrak{v}\,b_{\mathfrak{v}} + \mathfrak{w}\,b_{\mathfrak{w}}$

$= rb\,(\cos\theta\cos\alpha + \sin\theta\sin\varphi\sin\alpha\sin\varphi_a + \sin\theta\cos\varphi\sin\alpha\cos\varphi_a)$

$\therefore\ \cos\bar{\theta} = \cos\theta\cos\alpha + \sin\theta\sin\alpha\cos(\varphi - \varphi_a)$

(b)

Figure 4. A diagrammatic picturization of the decomposition of a misaligned ligand orbital into σ- and π-parts. Part a illustrates the divisional procedure for a two-dimensional orbital cross-cut in a coordinate plane and part b illustrates that for the true three-dimensional orbital figure in an arbitrary constellation.

the chromium(III) trisoxalato anion) of the next paragraph, § 1.2] can a pseudo-octahedral combination of π-like orbitals be obtained. By footnote 5, however, we do see that these orbitals are eurythmically complete under $C_2(y')$ [as they must be since this is an operation of the D_3 point group] and obey the relationship $C_2\Pi_{\pm}^{(1)} = \Pi_{\mp}^{(2)}$.

It is now a simple matter to write down the one-electron molecular orbitals of a trigonal dihedral compound: all that need be done is to add, with suitable multiplicative variational constants, the appropriately oriented and symmetrized localized ligand molecular orbitals to the proper central atom orbitals. If we let these multiplicative constants be η, $\xi^{(1)}$, $\xi^{(2)}$, $\rho^{(1)}$, and $\rho^{(2)}$ for the ligand functions $\Pi_0^{s(+)}$, $\Pi_{\pm}^{s(1)}$, $\Pi_{\pm}^{c(1)}$, and $\Sigma_{\pm}^{c(2)}$, respectively, we find that[8]

$$a_1(t_{2g}) = N_{a_1(t)}\{t_{2ga} + \eta\Pi_0^{s(+)}\},\quad a_2 = \Pi_0^{s(-)}$$

$$e_{\pm}(t_{2g}) = N_{e(t)}\{t_{2g(e)}^{b} + \xi^{(\frac{1}{2})}\Pi_{\pm}^{s(1)} + \xi^{(\frac{2}{1})}\Pi_{\pm}^{s(2)}\}$$

$$e_{\pm}(e_g) = N_{e(e)}\{e_{g(b)}^{a} + \rho^{(\frac{1}{2})}\Sigma_{\pm}^{c(1)} + \rho^{(\frac{1}{2})}\Sigma_{\pm}^{c(2)}\}\quad(11)$$

where $N_{a_1(t)}$, $N_{e(t)}$, and $N_{e(e)}$ are the molecular normalization constants which we choose to be real, and where the central atom orbitals are as defined in Table III and ref. 9. The multiplicative constants are not all independent, and hence, eq. 11 may be further simplified. To see this fact all one need note is that the functions $e_{\pm}$ and $e_{\pm}^*$ must have the same energy since the complex conjugate operator, $*$, commutes with the Hamiltonian [*i.e.*, leaves it invariant], and hence, with $N_{e(t)}$ and

(7) These statements follow when it is demanded that the functions $\Sigma_{\pm}$ equal to $\Sigma_r^{(1)} + \Sigma_r^{(2)}$, ($s = \pm 1$), satisfy the selfsame orientation relations with respect to $C_4(z)$, $C_2(y')$, and i as do the central atom orbitals $e_{g(b)}^{a}$ of Table III. Thus the orientational requirements [Tables III and IV] $C_4\Sigma_{\pm} = \Sigma_{\mp}$, $C_2\Sigma_{\pm} = \Sigma_{\mp}$, and $i\Sigma_{\pm} = \Sigma_{\pm}$, uniquely fix a_{0s} and a_{3s}, and hence $\Sigma_{\pm}$, to be as given above in eq. 10.

(8) One might think off-hand that there should be nine constants η, $\xi_{\pm}^{(1)}$, $\xi_{\pm}^{(2)}$, $\rho_{\pm}^{(1)}$, $\rho_{\pm}^{(2)}$ instead of only five as printed in eq. 11. However, this thought is quickly dispelled once it is noted that, as before, orientational and symmetry requirements demand that $C_2(y')e_{\pm}$ equal $e_{\mp}$, since the Hamiltonian is invariant of $C_2(y')$. Hence, we must have [by Table III and footnote 5]

$$C_2e_{\pm}(t_{2u}) = N_{e(t)}\{t_{2g(b)}^{e} + \xi_{\pm}^{(1)}\Pi_{\mp}^{s(2)} + \xi_{\pm}^{(2)}\Pi_{\mp}^{s(1)}\}$$

$$\equiv e_{\mp}(t_{2g}) = N_{e(t)}\{t_{2g(b)}^{e} + \xi_{\mp}^{(1)}\Pi_{\mp}^{s(1)} + \xi_{\mp}^{(2)}\Pi_{\mp}^{s(2)}\}$$

$$C_2e_{\pm}(e_g) = N_{e(e)}\{e_{g(b)}^{a} + \rho_{\pm}^{(1)}\Sigma_{\mp}^{c(2)} + \rho_{\pm}^{(2)}\Sigma_{\mp}^{c(1)}\}$$

$$\equiv e_{\mp}(e) = N_{e(e)}\{e_{g(b)}^{a} + \rho_{\mp}^{(1)}\Sigma_{\mp}^{c(1)} + \rho_{\mp}^{(2)}\Sigma_{\mp}^{c(2)}\}$$

as only one pair of wave functions each can be constructed from the prefactors $N_{e(t)}t_{2g(b)}^{e}$ and $N_{e(e)}e_{g(b)}^{a}$. Therefore, $\xi_{+}^{(1)}$ must equal $\xi_{-}^{(2)}$, $\xi_{-}^{(1)}$ must equal $\xi_{+}^{(2)}$, $\rho_{+}^{(1)}$ must equal $\rho_{-}^{(2)}$, and $\rho_{+}^{(2)}$ must equal $\rho_{-}^{(1)}$, and so we arrive at eq. 11 and its five tentatively independent variational parameters. Actually, of these five parameters only three, η, ξ [equals $\pm|\xi^{(\frac{1}{2})}|$], and ρ [equals $\pm|\rho^{(\frac{1}{2})}|$] are symmetrically independent. The proof of this statement is outlined in the text above and in footnote 10.

(9) A. D. Liehr, *J. Phys. Chem.*, **64**, 43 (1960).

$N_{e(e)}$ real in eq. 11 we must have $e_{\pm}^{*}$ equals $e_{\mp}$. Now by Table III

$$e_{\pm}(t_{2g})^{*} = N_{e(t)}^{*}\{t_{2g(s)} + \xi^{(\frac{1}{2})*}\Pi_{\mp}^{s(1)} + \xi^{(\frac{2}{3})*}\Pi_{\mp}^{s(2)}\}$$

$$e_{\pm}(e_{g})^{*} = N_{e(e)}^{*}\{e_{g(\frac{b}{a})} + \rho^{(\frac{1}{2})*}\Sigma_{\mp}^{c(1)} + \rho^{(\frac{2}{3})*}\Sigma_{\mp}^{c(2)}\}$$

(12a)

and so with $N_{e(t)}$ and $N_{e(e)}$ real, we must have $\xi^{(1)}$ equals $\xi^{(2)*}$, $\xi^{(2)}$ equals $\xi^{(1)*}$, $\rho^{(1)}$ equals $\rho^{(2)*}$, and $\rho^{(2)}$ equals $\rho^{(1)*}$. If we absorb the arbitrary phase factors contained in $\xi^{(\frac{1}{2})}$ and $\rho^{(\frac{1}{2})}$ into the normalization constants $a_{(\frac{0}{3})_{s}}^{\pi}$ and $a_{(\frac{0}{3})_{s}}^{\sigma}$ of the functions $\Pi_{s}^{(\frac{1}{2})}$ and $\Sigma_{s}^{(\frac{1}{2})}$, $(s = \pm 1)$, severally, where[5] $a_{0_{s}}^{\pi}$ equals a_{3-s}^{π} equals $a_{3_{s}}^{\pi*}$ and $a_{0_{s}}^{\sigma}$ equals a_{3-s}^{σ} equals $a_{3_{s}}^{\sigma*}$ [the latter equality of both the π and σ set of equalities is one of arbitrary phase choice associated with the normalization process], and call ξ equal to $+$ or $-|\xi^{(\frac{1}{2})}|$ and ρ equal to $+$ or $-|\rho^{(\frac{1}{2})}|$, we may rewrite eq. 11 in the shape[10]

$$e_{\pm}(t_{2g}) = N_{e(t)}\{t_{2g(\frac{b}{c})} + \xi[\Pi_{\pm}^{s(1)} + \Pi_{\pm}^{s(2)}]\}$$

$$e_{\pm}(e_{g}) = N_{e(e)}\{e_{g(\frac{a}{b})} + \rho[\Sigma_{\pm}^{c(1)} + \Sigma_{\pm}^{c(2)}]\}$$

(12b)

A few final remarks will allow us to deduce the terminal structure of eq. 11 and 12. First, we note that in order for $e_{\pm}(e_{g})$ to reduce to the octahedral e_{c} as the angle of cant, α, goes to zero [this corresponds physically to either increasing the "chain length" of the attached polydentate ligand or to cutting the chain of the attached polydentate ligand to produce a group of monodentate ligands in its stead—study Fig. 1 and 2], the sum $\Sigma_{\pm}^{c(1)} + \Sigma_{\pm}^{c(2)}$ of eq. 12 must reduce to the special form $\Sigma_{\pm}^{c}$ of eq. 10. That is, that the constants $a_{0_{s}}^{\sigma}$ and $a_{3_{s}}^{\sigma}$ of eq. 9 must be chosen to have the values $a_{0_{s}}^{\sigma} = a_{3-s}^{\sigma} = a_{3_{s}}^{\sigma*} = \omega^{s}/\sqrt{6}$, $(s = \pm 1)$. Second, we mark that although the sum $\Pi_{\pm}^{(1)} + \Pi_{\pm}^{(2)}$ cannot reduce to an octahedral t_{2g} π-type ligand molecular orbital as the angle cant, α, becomes zero since the sum vanishes in this limit [Cf. eq. 8. Physically this vanishing is due to the alignment of the ligand orbitals, λ_{j}, along the localized ligand orbital–central atom orbital axis, as shown in Fig. 2. Notice, though, that because of this null value of $\Pi_{\pm}^{(\frac{1}{2})}$ when α vanishes, we have that $e_{\pm}(t_{2g})$ tends to its octahedral $t_{2g(\frac{b}{c})}$ expression as α tends to zero as needed], it can be made to assess correctly the dihedrality of the orbitals. This assertion is readily proved by the consideration of the dihedral molecular orbitals formed by the bidentate localized pairs (15), (23), and (04) of Fig. 2.

$$\Xi_{s} = b_{0_{s}}(15) + b_{1_{s}}(23) + b_{2_{s}}(04)$$

(13)

The eurythmic requirement

$$\mathfrak{C}_{3}\Xi_{s} = \omega^{s}\Xi_{s}, \quad \mathfrak{C}_{2}\Xi_{s} = \Xi_{-s}, \quad (s = 0, \pm 1)$$

(14)

implies[11]

$$\{\Xi_{s} = b_{0_{s}}(15) + \omega^{s}(23) + \omega^{2s}(04)\}$$

(15)

The identification of the bidentate localized pair orbitals (kl) with the pseudo-π-localized orbital pair $\pi_{k} + \pi_{l}$ of eq. 8 and 9 then yields eq. 16.

---

(10) It is readily apparent that any choice of functions

$$\Pi_{\pm}^{(1)'} = e^{\mp i\tau}\Pi_{\pm}^{(1)}, \quad \Pi_{\pm}^{(2)'} = e^{\pm i\tau}\Pi_{\pm}^{(2)}, \quad \Sigma_{\pm}^{(1)'} = e^{\pm i\bar{\tau}}\Sigma_{\pm}^{(1)},$$
$$\Sigma_{\pm}^{(2)'} = e^{\mp i\bar{\tau}}\Sigma_{\pm}^{(2)}$$

will give a satisfactory basis when added to $t_{2g(\frac{b}{c})}$ and $e_{g(\frac{a}{b})}$ as these will likewise behave properly under $\mathfrak{C}_{2}(y')$ and $\mathfrak{C}_{3}(z')$, for arbitrary τ and $\bar{\tau}$, as needed. Furthermore, it is evident that this choice will lead to real values of the covalency parameters $\xi^{(\frac{1}{2})}$ and $\rho^{(\frac{1}{2})}$ as desired, since the selection of a real basis

$$\mathfrak{Re}_{+}(t_{2g}) = N_{e(t)}'\{\mathfrak{Re}t_{2gb} + \xi^{(1)'}\mathfrak{Re}\Pi_{+}^{s(1)'} + \xi^{(2)'}\mathfrak{Re}\Pi_{+}^{s(2)'}\}$$

$$\mathfrak{Im}_{+}(t_{2g}) = N_{e(t)}''\{\mathfrak{Im}t_{2gb} + \xi^{(1)'}\mathfrak{Im}\Pi_{+}^{s(1)'} + \xi^{(2)''}\mathfrak{Im}\Pi_{+}^{s(2)'}\}$$

$$\mathfrak{Re}_{+}(e_{g}) = N_{e(e)}'\{\mathfrak{Re}e_{ga} + \rho^{(1)'}\mathfrak{Re}\Sigma_{+}^{c(1)'} + \rho^{(2)'}\mathfrak{Re}\Sigma_{+}^{c(2)'}\}$$

$$\mathfrak{Im}_{+}(e_{g}) = N_{e(e)}''\{\mathfrak{Im}e_{ga} + \rho^{(1)''}\mathfrak{Im}\Sigma_{+}^{c(1)'} + \rho^{(2)''}\mathfrak{Im}\Sigma_{+}^{c(2)'}\}$$

plus the requirement that these functions transform correctly under $\mathfrak{C}_{2}(y')$ and $\mathfrak{C}_{3}(z')$ [that is, that all these e-type functions obey the relations $\mathfrak{C}_{2}\mathfrak{Re}e = \mathfrak{Re}e$, $\mathfrak{C}_{3}\mathfrak{Im}e = -\mathfrak{Im}e$ (when e is a Π or Σ function $\mathfrak{C}_{2}$ sends superscript (1) into superscript (2) also), and $\mathfrak{C}_{3}\mathfrak{Re}e = -\frac{1}{2}\mathfrak{Re}e - \sqrt{3}/2 \mathfrak{Im}e$, $\mathfrak{C}_{3}\mathfrak{Im}e = \sqrt{3}/2\mathfrak{Re}e - \frac{1}{2}\mathfrak{Im}e$] shows that $N_{e(t)}' = N_{e(t)}''$, $N_{e(e)}' = N_{e(e)}''$, $\xi^{(1)'} = \xi^{(2)'} = \xi^{(1)''} = \xi^{(2)''}$, $\rho^{(1)'} = \rho^{(2)'} = \rho^{(1)''} = \rho^{(2)''}$ with all the constants real [as a real set of basis functions plus a real Hamiltonian must yield real variational parameters. The normalization constants can always be picked real]. The redefinition of the e-type functions as $e_{\pm} = 2^{-1/2}\{\mathfrak{Re}e \pm i\mathfrak{Im}e\}$ then yields the one parameter imaginary e-type trigonal dihedral functions with real variational coefficients as wanted. But note that there are a continuous infinity of such functions which formally differ only in the value of τ or $\bar{\tau}$ assigned (of course, the values of ξ and ρ are also functions of τ and $\bar{\tau}$, individually). This continuous infinity of solutions corresponds in a sense to the formal infinite redundancy of our model, as illustrated in Fig. 5. From this figure we see there are an infinite number of D_{3} geometries corresponding to each bonding scheme, that is, to each localized orbital directive assignment, dependent upon the angle τ or $\bar{\tau}$ of the skewness of the molecular framework with respect to the $x'zz'$ plane. It is important to note though that although a geometry, as far as the orbital phase requirements are concerned, which schematically looks like that of the optical enantiomorph can be obtained by setting both τ and $\bar{\tau}$ equal to $\pi/3$ or $-2\pi/3$, this geometry is definitely not that of the enantiomorph as the associated electronic charge distribution, pictured by the directed ligand orbitals of Fig. 2, is not that correspondent to the enantiomorph but is still that associated with the original conformation under consideration. The true value of τ or $\bar{\tau}$ for a set of real normalization constants $a_{(\frac{0}{3})_{s}}^{\pi}$ and $a_{(\frac{0}{3})_{s}}^{\sigma}$ to be assigned to the molecular framework picked here is determined by cubical (O_{h}) correspondence principles as outlined in the accompanying text. This attendant complication of the trigonal dihedral molecular orbital problem seems to have escaped [because of their neglect of the cant angle α of Fig. 2 or the nonoctahedral placement of the terminal ligand atoms or both] several coetaneous workers in this field [(a) L. E. Orgel, J. Chem. Soc., 3683 (1961); (b) D. W. Barnum, J. Inorg. Nucl. Chem., 21, 221 (1961); 22, 183 (1961); (c) G. Weber, Z. physik. Chem. (Leipzig), 218, 204, 217 (1961)]. Mark that it is not suprising that two parameters ξ and τ or ρ and $\bar{\tau}$ are needed to specify the trigonal dihedral molecular orbitals as three sets of basis functions $t_{2g(\frac{b}{c})}$, $\Pi_{\pm}^{(1)}$, $\Pi_{\pm}^{(2)}$ or $e_{g(\frac{a}{b})}$, $\Sigma_{\pm}^{(1)}$, $\Sigma_{\pm}^{(2)}$ always require two sets [the third is the normalization constant $N_{e(t)}$ or $N_{e(e)}$] to fix the final three sets of molecular orbitals [we here use only two of these three possible sets—the two corresponding to the "metallic" bonding and antibonding molecular orbitals].

(11) Note that $i\Xi_{s}$ is not equal to $\pm\Xi_{s}$ so these functions are not centrosymmetric.

Table III: Central Atom Orbital Transformation Properties

Central atom orbital designation—		d and p representations	Transformation properties		
D_3	O_h		$\mathcal{C}_3(z')$	$\mathcal{C}_2(y')$	$\mathcal{C}_4(z)$
a_1	t_{2ga}	$d\sigma' = d_{3z'^2-r^2}$	t_{2ga}	t_{2ga}	$-\frac{1}{3}t_{2ga} + \frac{2}{3}\omega^{-1/2}t_{2gb} + \frac{2}{3}\omega^{1/2}t_{2gc}$
$e_\pm$	$t_{2g(c)}$	$\sqrt{\dfrac{1}{3}}\,d\pi'_\pm - \sqrt{\dfrac{2}{3}}\,d\delta'_\mp$	$\omega^{\pm 1}t_{2(c)}$	$t_{2g(b)}$	$\frac{2}{3}\omega^{\mp 1/2}t_{2ga} - \frac{1}{3}t_{2g(c)} - \frac{2}{3}\omega^{\pm 1/2}t_{2g(c)}$
$e_\pm$	$e_{g(a)}$	$\sqrt{\dfrac{2}{3}}\,d\pi'_\pm + \sqrt{\dfrac{1}{3}}\,d\delta'_\mp$	$\omega^{\pm 1}e_{g(a)}$	$e_{g(a)}$	$e_{g(a)}$
$e_\pm$	$\cdot\cdot$	$d\pi'_\pm = \sqrt{\dfrac{1}{2}}\,(d_{x'z'} \pm id_{y'z'})$	$\omega^{\pm 1}d\pi'_\pm$	$d\pi'_\mp$	$\mathcal{C}_4(z)\left(\sqrt{\dfrac{1}{3}}\,t_{2g(c)} + \sqrt{\dfrac{2}{3}}\,e_{g(a)}\right)$
$e_\pm$	$\cdot\cdot$	$d\delta'_\pm = \sqrt{\dfrac{1}{2}}\,(d_{x'^2-y'^2} \pm id_{x'y'})$	$\omega^{\mp 1}d\delta'_\pm$	$d\delta'_\mp$	$\mathcal{C}_4(z)\left(-\sqrt{\dfrac{2}{3}}\,t_{2g(c)} + \sqrt{\dfrac{1}{3}}\,e_{g(a)}\right)$
a_2	t_{1ua}	$p\sigma' = p_{z'}$	t_{1ua}	$-t_{1ua}$	$\frac{1}{3}t_{1ua} + \frac{2}{3}\omega^{-1/2}t_{1ub} + \frac{2}{3}\omega^{1/2}t_{1uc}$
$e_\pm$	$t_{1u(c)}$	$p\pi'_\pm = \sqrt{\dfrac{1}{2}}\,(p_{x'} \pm ip_{y'})$	$\omega^{\pm 1}t_{1u(c)}$	$-t_{1u(b)}$	$\frac{2}{3}\omega^{\mp 1/2}t_{1ua} + \frac{1}{3}t_{1u(b)} + \frac{2}{3}\omega^{\pm 1/2}t_{1u(c)}$

$$\Xi_s = b_{0s}\left\{\omega^{-s}\sum_{j=0}^{2}\omega^{sj}\pi_j + \omega^{s}\sum_{j=3}^{5}\omega^{sj}\pi_j\right\}, \quad (s = 0, \pm 1) \tag{16}$$
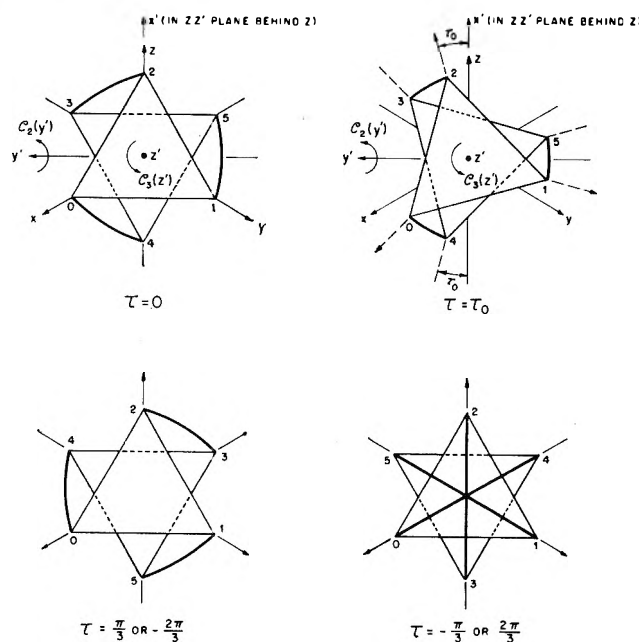
Figure 5. Pictorial representation of the geometrical indeterminateness of the trigonal dihedral architecture. The physical angle τ of relative movement of the equilateral halves of the skewed prismoidal structure can be put in one-to-one correspondence with the mathematical phase angle τ of a molecular orbital treatment of their electronic structure. However, as the geometry remains fixed in a molecular orbital phase variation, τ, but not in a physical variation, τ, this correspondence is not faithful.

Table IV: Definition of the $\mathcal{C}_4(z)$ and i Symmetry Operations

k	$\mathcal{C}_4(z)k$	ik	(kl)	$\mathcal{C}_4(z)(kl)$	$i(kl)$
0	3	5	(04)	(34)	(52)
1	0	3	(23)	(25)	(41)
2	2	4	(15)	(01)	(30)
3	5	1	x	$-y$	$-x$
4	4	2	y	x	$-y$
5	1	0	z	z	$-z$

Comparison with the sum $\Pi_s^{(1)} + \Pi_s^{(2)}$ of eq. 9 and 12 shows that for proper dihedrality, the constants a_{0s}^{π} and a_{3s}^{π} must be taken as $\omega^{-s}b_{0s}$ and $\omega^{s}b_{0s}$, distributively. Normalization of the sum $\Pi_s^{(1)} + \Pi_s^{(2)}$ with the neglect of localized ligand–ligand overlap finally sets a_{0s}^{π} equal to a_{3-s}^{π} equal to $a_{3s}^{\pi*}$ equal to $\omega^{-s}/\sqrt{6}$, $(s = 0, \pm 1)$.[12] Letting $\Pi_\pm$ stand for the sum $\Pi_\pm^{(1)} + \Pi_\pm^{(2)}$ when a_{0s}^{π} and a_{3s}^{π} are as determined above, we may put down the end forms of eq. 11 and 12b as

$$a_1(t_{2g}) = N_{a_1(t)}\left\{t_{2ga} + \eta\Pi_0^{s(+)}\right\}, \quad a_2 = \Pi_0^{s(-)}$$

$$e_\pm(t_{2g}) = N_{e(t)}\left\{t_{2g(c)} + \xi\Pi_\pm^s\right\}$$

$$e_\pm(e_g) = N_{e(e)}\left\{e_{g(a)} + \rho\Sigma_\pm^{c}\right\} \tag{17}$$

where [the symbol $S[\chi_1; \chi_2]$ represents the group overlap of χ_1 and χ_2; their detailed forms are given in the Appendix]

(12) The normalization expressions when ligand–ligand overlap is not neglected are given in the Appendix.

$$N_{a_1(t)} = \left\{ 1 + 2\eta S[t_{2g a}; \; \Pi_0{}^{s(+)}] + \eta^2 \right\}^{-1/2}$$

$$N_{e(t)} = \left\{ 1 + 2\xi S[t_{2g}(^c_b); \; \Pi_\pm{}^s] + \xi^2 \right\}^{-1/2}$$

$$N_{e(e)} = \left\{ 1 + 2\rho S[e_g(^c_b); \; \Sigma_\pm{}^c] + \rho^2 \right\}^{-1/2} \quad (18)$$

and where $\Pi_0{}^{s(+)}$ and $\Sigma_\pm{}^c$ are given by eq. 9 and 10 serially, and [13]

$$\Pi_\pm{}^s = \frac{1}{\sqrt{6}} \, \omega^{\mp 1} \sum_{j=0}^{2} \omega^{\pm j} \pi_j{}^s + \frac{1}{\sqrt{6}} \, \omega^{\pm 1} \sum_{j=3}^{5} \omega^{\pm j} \pi_j{}^s \quad (19)$$

1.2 The π-Molecular Orbitals. When localized ligand functions are available which offer true ligand–central atom π-bond possibilities, the above molecular orbital analysis must be amended accordingly. Figures 6 and 7a picture the geometry and idealized local ligand orbital distribution, individually, for a typical π-bonded trigonal dihedral complex anion, the copper(II) trisoxalato anion, and Fig. 8 illustrates a possible, but not essential, level pattern. Again the σ- and π-ligand frameworks are canted by an angle α to the central atom–ligand atom axes, which have been here taken to be the x, y, z axes for presentational simplicity.

To get the requisite truly π-bonding linear combination of localized ligand orbitals, we proceed as in eq. 1 through 19. We again parse the available localized ligand orbitals when possible. If we denote by $\lambda_j{}^\perp$ the
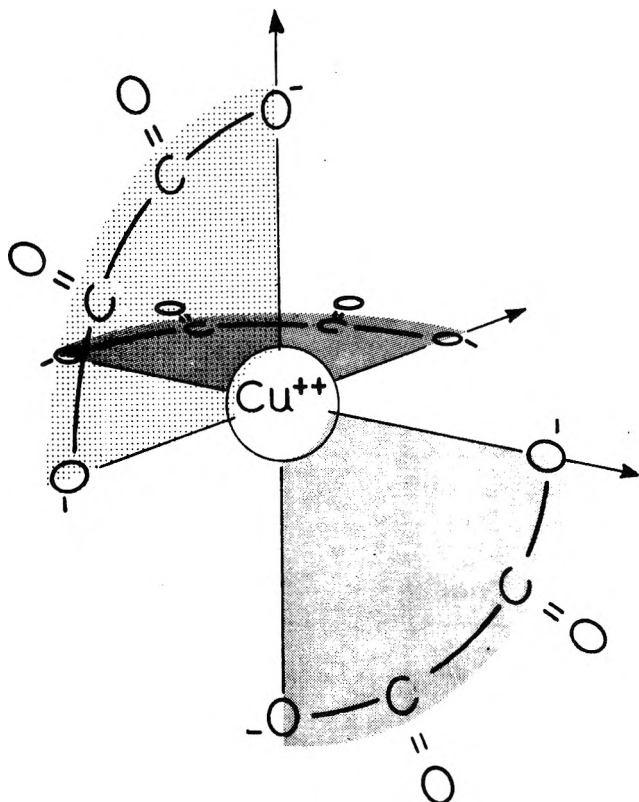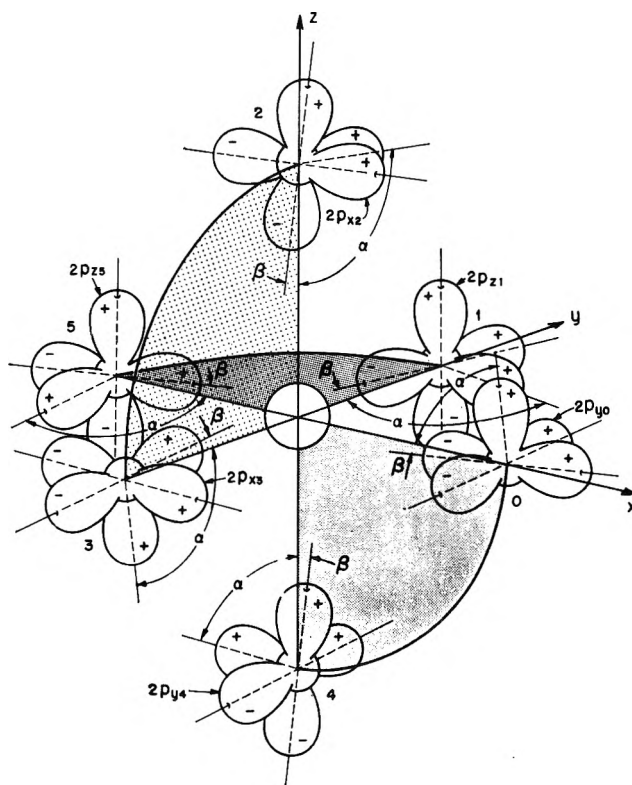
Figure 7a. The diagonal local ligand orbital spatial disposition for the idealized planar right-angled geometry of the trisoxalatocopper(II) anion.

localized π-like ligand orbitals perpendicular to those of eq. 1 through 8, and which lie in the shaded planes of Fig. 7a canted at an angle $\beta = 90° - \alpha$ to the x, y, and z axes of that figure, and by $\bar{\pi}_j$ the π-type orbital of Fig. 7a which is mutually perpendicular to both λ_j and $\lambda_j{}^\perp$, we may scribe[14] eq. 20

(13) Since the $\Sigma_\pm$ functions are centrosymmetric but the $\Pi_0{}^{(\pm)}$, $\Pi_\pm$ ones are not,[11] the only truly dihedrally asymmetric functions of eq. 17 are $a_1(t_{2g})$, a_2, and $e_\pm(t_{2g})$. This circumstance occurs because we have banished the contributions of the t_{1u}-like ligand σ-molecular orbitals in our treatment by our assumption that the σ-bonded dihedral functions $e_\pm(e_g)$ reduce simply to the octahedral σ-bonded functions $e_g(^a_b)(e_g)$ The omission of these t_{1u}-like σ-molecular combinations is the cause of the different phase factors and the different derivations of the $\Sigma_\pm$ and $\Pi_\pm$ ligand molecular orbitals [cf. eq. 10, 15, 16, and 19]

(14) This decomposition is carried out exactly as in footnote 6. To obtain it from footnote 6 one need only rotate the coordinates by 90° about either the x axis or y axis thus replacing cos θ by sin θ sin φ or sin θ cos φ, consecutively. Please mark that here, in sharp contrast to footnote 6, ambiguity may occur in the final choice of a local ligand orbital basis (view Fig. 7b). The use of an alternant such basis, $\{\lambda_j, \lambda_j{}^<, \bar{\pi}_j\}$, as for example that of Fig. 7b, rather than the basis of Fig. 7a, $\{\lambda_j, \lambda_j{}^\perp, \bar{\pi}_j\}$, in the present algebraic formulation, leads to no mathematical structural change: The formal theory abides inviolate whatever the circumstantial local spatial disposition of ligand orbitals chosen. Of course, definitional modifications do enter, as now eq. 20 and 21 must include an altered angle of cant, $\bar{\alpha}$, not equal to either α or 90° − α, hybridization coefficients for the orbitals $np_{\sigma w j}$ and $np_{\pi w j}$ and an additional ns orbital contribution for the orbitals $\sigma^s_{w j}$ of eq. 21.

Figure 6. The idealized planar right-angled geometry of the trisoxalatocopper(II) anion.
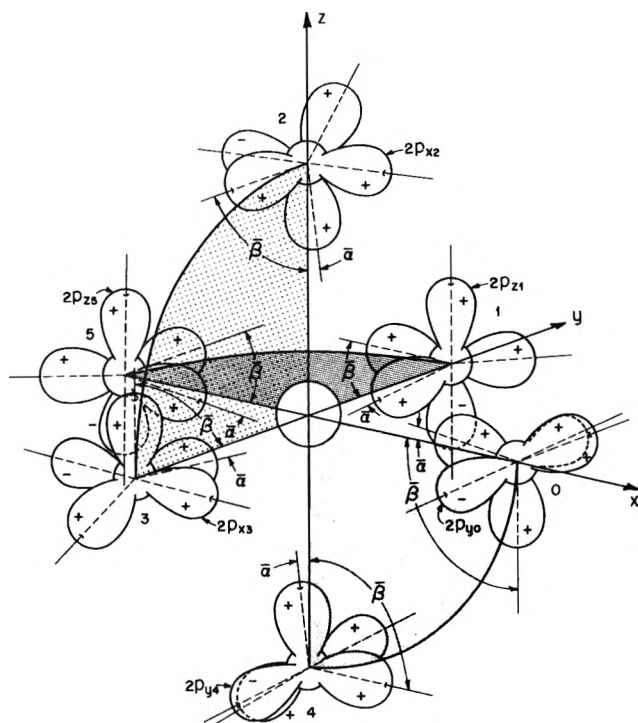
Figure 7b. The isosceles local ligand orbital spatial disposition for the idealized planar right-angled geometry of the trisoxalatocopper(II) anion.

$$\lambda_0^\perp = \sigma_{x0} + \pi_{z0}, \quad \lambda_2^\perp = \sigma_{z2} + \pi_{y2}, \quad \lambda_4^\perp = \sigma_{z4} + \pi_{x4},$$

$$\lambda_1^\perp = \sigma_{y1} + \pi_{\tau1}, \quad \lambda_3^\perp = \sigma_{y3} + \pi_{z3}, \quad \lambda_5^\perp = \sigma_{z5} + \pi_{y5}$$

$$\tag{20}$$

where $[w = x, y, z; \; j = 0, 1, 2, 3, 4, 5]$[14]

$$\sigma_{wj}^{\,s} = \pm\sin \alpha\; np_{\sigma_{wj}}, \quad \pi_{wj}^{\,c} = \pm\cos \alpha\; np_{\pi_{wj}} \tag{21}$$

The use of these functions in conjunction with the dialectics of eq. 1–9 and the data of Tables I–V gives the desired dihedral σ-like one-electron molecular orbitals as

$$\Sigma_s^{\,s(1)} = a_{0_s}^{\,\sigma s} \sum_{j=0}^{2} \omega^{sj}\sigma_j^{\,s}, \quad \Sigma_s^{\,s(2)} = a_{3_s}^{\,\sigma s} \sum_{j=3}^{5} \omega^{sj}\sigma_j^{\,s} \tag{22}$$

The π-like orbitals generated by the $\pi_j^{\,c}$ localized ligand orbitals [we now drop the subscript w equals x, y, z which is made redundant by Fig. 7a and Table V] are likewise given by

$$\Pi_0^{\,c(\pm)} = \frac{1}{\sqrt 6}\left\{\sum_{j=0}^{2} \pi_j^{\,c} \pm \sum_{j=3}^{5} \pi_j^{\,c}\right\}$$

$$\Pi_s^{\,c(1)} = a_{0_s}^{\,\pi} \sum_{j=0}^{2} \omega^{sj}\pi_j^{\,c}, \quad \Pi_s^{\,c(2)} = a_{3_s}^{\,\pi} \sum_{j=3}^{5} \omega^{sj}\pi_j^{\,c},$$

$$(s = \pm 1) \tag{23}$$

Table V: Definition of the Local σ- and π-Orbitals Utilized

j	$\sigma_j^{\,c}$	$\sigma_j^{\,s}$	$\tilde\sigma_j$	π_j	$\pi_j^{\,s}$	$\pi_j^{\,c}$	$\tilde\pi_j$
0	$k_s(2s)_{A_0} - k_p\cos\alpha\,(2p_x)_{A_0}$	$-\sin\alpha\,(2p_z)_{A_0}$	$k_s(2s)_{A_0} - [k_p\cos\alpha + (\rho^s(\tfrac12)/\rho^c(\tfrac12))\sin\alpha](2p_x)_{A_0}$	$(2p_z)_{A_0}$	$k_p\sin\alpha\,(2p_x)_{A_0}$	$\cos\alpha\,(2p_z)_{A_0}$	$(2p_y)_{A_0}$
1	$k_s(2s)_{A_1} - k_p\cos\alpha\,(2p_x)_{A_1}$	$-\sin\alpha\,(2p_z)_{A_1}$	$k_s(2s)_{A_1} - [k_p\cos\alpha + (\rho^s(\tfrac12)/\rho^c(\tfrac12))\sin\alpha](2p_x)_{A_1}$	$(2p_z)_{A_1}$	$k_p\sin\alpha\,(2p_x)_{A_1}$	$\cos\alpha\,(2p_z)_{A_1}$	$(2p_z)_{A_1}$
2	$k_s(2s)_{A_2} - k_p\cos\alpha\,(2p_y)_{A_2}$	$-\sin\alpha\,(2p_z)_{A_2}$	$k_s(2s)_{A_2} - [k_p\cos\alpha + (\rho^s(\tfrac12)/\rho^c(\tfrac12))\sin\alpha](2p_y)_{A_2}$	$(2p_y)_{A_2}$	$k_p\sin\alpha\,(2p_y)_{A_2}$	$\cos\alpha\,(2p_y)_{A_2}$	$(2p_z)_{A_2}$
3	$k_s(2s)_{A_3} + k_p\cos\alpha\,(2p_y)_{A_3}$	$\sin\alpha\,(2p_z)_{A_3}$	$k_s(2s)_{A_3} + [k_p\cos\alpha + (\rho^s(\tfrac12)/\rho^c(\tfrac12))\sin\alpha](2p_y)_{A_3}$	$-(2p_z)_{A_3}$	$-k_p\sin\alpha\,(2p_z)_{A_3}$	$-\cos\alpha\,(2p_z)_{A_3}$	$(2p_z)_{A_3}$
4	$k_s(2s)_{A_4} + k_p\cos\alpha\,(2p_z)_{A_4}$	$\sin\alpha\,(2p_z)_{A_4}$	$k_s(2s)_{A_4} + [k_p\cos\alpha + (\rho^s(\tfrac12)/\rho^c(\tfrac12))\sin\alpha](2p_z)_{A_4}$	$-(2p_z)_{A_4}$	$-k_p\sin\alpha\,(2p_z)_{A_4}$	$-\cos\alpha\,(2p_z)_{A_4}$	$-(2p_z)_{A_4}$
5	$k_s(2s)_{A_5} + k_p\cos\alpha\,(2p_z)_{A_5}$	$\sin\alpha\,(2p_z)_{A_5}$	$k_s(2s)_{A_5} + [k_p\cos\alpha + (\rho^s(\tfrac12)/\rho^c(\tfrac12))\sin\alpha](2p_z)_{A_5}$	$-(2p_y)_{A_5}$	$-k_p\sin\alpha\,(2p_y)_{A_5}$	$-\cos\alpha\,(2p_y)_{A_5}$	$-(2p_x)_{A_5}$

Figure 8. A schematic molecular orbital energy level diagram for a trigonally dihedral transition metal compound in the σ- and π-bond approximation.

Also for the pure π-type molecular orbitals, $\tilde{\Pi}_s$, ($s = 0$, ± 1), created by the $\tilde{\Pi}_j$ network [Fig. 7a and Table V], we can scrive

$$\tilde{\Pi}_0^{(\pm)} = \frac{1}{\sqrt{6}} \left\{ \sum_{j=0}^{2} \tilde{\pi}_j \pm \sum_{j=3}^{5} \tilde{\pi}_j \right\}$$

$$\tilde{\Pi}_s^{(1)} = a_{0_s}{}^{\tilde{\pi}} \sum_{j=0}^{2} \omega^{sj} \tilde{\pi}_j, \quad \tilde{\Pi}_s^{(2)} = a_{3_s}{}^{\tilde{\pi}} \sum_{j=3}^{5} \omega^{sj} \tilde{\pi}_j,$$

$$(s = \pm 1) \quad (24)$$

As in the case of σ-bonded dihedral molecules, it is necessary to orient the σ- and π-like molecular orbitals of the σ- and π-bonded ligands so that they transform in D_3 [i.e., under $C_3(z')$ and $C_3(y')$] as do the central atom orbitals. This orientation [watch Table III] demands that $a_{0_s}{}^{\sigma, \pi, \tilde{\pi}}$ equals $a_{3-s}{}^{\sigma, \pi, \tilde{\pi}}$ equals $a_{3_s}{}^{\sigma, \tilde{\pi}, \pi^*}$, ($s = 0$, ± 1) [the latter equality arises once normalization requirements are prescribed]. The imposition of the further stipulation that these σ-, π-bonded ligands have pseudo-octahedral [i.e., that they also transform under $C_4(z)$ and i in O_h as do the central atom orbitals of Table III] σ-molecular orbitals, $\Sigma_{\pm}{}^s$, equal to $\Sigma_{\pm 1}{}^{s(1)} + \Sigma_{\pm 1}{}^{s(2)}$, determines that $a_{0_s}{}^{\sigma}$ equals $a_{3_s}{}^{\sigma^*}$ equals $\omega^s/\sqrt{6}$; and the stipulation that the π-molecular orbitals $\Pi_{\pm}{}^c$ equal to $\Pi_s{}^{c(1)} + \Pi_s{}^{c(2)}$, ($s = \pm 1$), sets, by eq. 13–16, $a_{0_s}{}^{\pi}$ equals $a_{3_s}{}^{\pi^*}$ to be $\omega^{-s}/\sqrt{6}$, ($s = 0$, ± 1), where

$$\Sigma_{\pm}{}^{s} = \frac{1}{\sqrt{6}}\, \omega^{\pm 1} \sum_{j=0}^{2} \omega^{\pm j}\sigma_j{}^{s} + \frac{1}{\sqrt{6}}\, \omega^{\mp 1}\sum_{j=3}^{5}\omega^{\pm j}\sigma_j{}^{s}$$

$$\Pi_{\pm}{}^{c} = \frac{1}{\sqrt{6}}\,\omega^{\mp 1}\sum_{j=0}^{2}\omega^{\pm j}\pi_j{}^{c} + \frac{1}{\sqrt{6}}\,\omega^{\pm 1}\sum_{j=3}^{5}\omega^{\pm j}\pi_j{}^{c} \quad (25)$$

It will be convenient for our later purposes to construct π-molecular orbitals which possess octahedral symmetry but are of a trigonal orientation. To this goal we define as previously the functions π_j, $\Pi_0{}^{(\pm)}$, $\Pi_{\pm}$ as those functions obtained either from the functions $\pi_j{}^{s}$, $\Pi_0{}^{s(\pm)}$, $\Pi_{\pm}{}^{s}$ of eq. 8, 9, and 17 by dropping the factor $k_p \sin\alpha$ or from the functions $\pi_j{}^{c}$, $\Pi_0{}^{c(\pm)}$, and $\Pi_{\pm}{}^{c}$ of eq. 21, 23, and 25 by dropping the factor $\cos\alpha$. We then find that the sums $\Pi_{0g}{}^{(+)}$, $\Pi_{\pm g}$

$$\Pi_{0g}{}^{(+)} = \frac{1}{\sqrt{2}}\left\{\Pi_0{}^{(+)} + \bar\Pi_0{}^{(+)}\right\},$$

$$\Pi_{\pm g} = -\frac{1}{\sqrt{2}}\left\{\Pi_{\pm} + \bar\Pi_{\pm}\right\} \quad (26)$$

where $\bar\Pi_{\pm}$ is the sum $\bar\Pi_{\pm}{}^{(1)} + \bar\Pi_{\pm}{}^{(2)}$ of eq. 24 with $a_{0_r}{}^{\bar\pi}$ equals $a_{3_r}{}^{\bar\pi}$ equal to $1/\sqrt{6}$

$$\bar\Pi_{\pm} = \frac{1}{\sqrt{6}}\sum_{j=0}^{2}\omega^{\pm j}\bar\pi_j + \frac{1}{\sqrt{6}}\sum_{j=3}^{5}\omega^{\pm j}\bar\pi_j \quad (27)$$

transform under $\mathfrak{C}_3(z')$, $\mathfrak{C}_2(y')$, $\mathfrak{C}_4(z)$, and i as the species T_{2g}, just as do their central atom octahedral counterparts t_{2ga} and $t_{2g(\frac{b}{c})}$, sequentially.[15] From eq. 24, 26, and 27 we see that the imposition of octahedrality on the π-molecular orbital system determines the coefficients $a_{0_r}{}^{\bar\pi}$ and $a_{3_r}{}^{\bar\pi}$ in the sum $\bar\Pi_{\pm}$ equals $\bar\Pi_r{}^{(1)} + \bar\Pi_r{}^{(2)}$, $(s = \pm 1)$, to be $1/\sqrt{6}$. Although functions of the sort given by eq. 26 cannot, of course, be used directly to describe the π-bond molecular orbitals of a dihedral compound, they can be used indirectly as will become apparent.

The molecular orbitals for a σ- and π-bonded dihedral complex may thus be set as

$$a_1(t_{2g}) = N_{a_1(t)}{}^{\sigma,\pi}\left\{t_{2ga} + \eta^s\Pi_0{}^{s(+)} + \eta^c\Pi_0{}^{c(+)} + \bar\eta\bar\Pi_0{}^{(+)}\right\}$$

$$e_{\pm}(t_{2g}) = N_{e(t)}{}^{\sigma,\pi}\left\{t_{2g(\frac{b}{c})} + \xi^{s(\frac{1}{2})}\Pi_{\pm}{}^{s(1)} + \xi^{s(\frac{2}{1})}\Pi_{\pm}{}^{s(2)} + \right.$$
$$\left. \xi^{c(\frac{1}{2})}\Pi_{\pm}{}^{c(1)} + \xi^{c(\frac{2}{1})}\Pi_{\pm}{}^{c(2)} + \bar\xi^{(\frac{1}{2})}\bar\Pi_{\pm}{}^{(1)} + \bar\xi^{(\frac{2}{1})}\bar\Pi_{\pm}{}^{(2)}\right\}$$

$$e_{\pm}(e_g) = N_{e(e)}{}^{\sigma,\pi}\left\{e_{g(\frac{a}{b})} + \rho^{c(\frac{1}{2})}\Sigma_{\pm}{}^{c(1)} + \rho^{c(\frac{2}{1})}\Sigma_{\pm}{}^{(2)} + \right.$$
$$\left. \rho^{s(\frac{1}{2})}\Sigma_{\pm}{}^{s(1)} + \rho^{s(\frac{2}{1})}\Sigma_{\pm}{}^{s(2)}\right\} \quad (28)$$

The reduction of the twelve possible $\xi_{\pm}{}^{\iota}$, $(\iota = 1, 2)$, type coefficients to the six and four, respectively, listed in eq. 28 is accomplished by the orientational symmetry requirement that $\mathfrak{C}_2(y')e_{\pm}$ equals $e_{\mp}$, as before.[8]

We can obtain a considerable simplification of eq. 28 if we add and subtract the quantities $N_{a_1(t)}{}^{\sigma,\pi}\bar\eta\Pi_0{}^{(+)}$ and

$N_{e(t)}{}^{\sigma,\pi}\bar\xi^{(\frac{1}{2})}\Pi_{\pm}$ from the expressions $a_1(t_{2g})$ and $e_{\pm}(t_{2g})$, serially, and subsequently employ the definitions, eq. 26.

$$a_1(t_{2g}) = N_{a_1(t)}{}^{\sigma,\pi}\left\{t_{2ga} + \eta^s\Pi_0{}^{s(+)} + \eta^c\Pi_0{}^{c(+)} - \right.$$
$$\left. \bar\eta\Pi_0{}^{(+)} + \sqrt{2}\,\bar\eta\Pi_{0g}{}^{(+)}\right\}$$

$$e_{\pm}(t_{2g}) = N_{e(t)}{}^{\sigma,\pi}\left\{t_{2g(\frac{b}{c})} + \xi^{s(\frac{1}{2})}\Pi_{\pm}{}^{s(1)} + \xi^{s(\frac{2}{1})}\Pi_{\pm}{}^{s(2)} + \right.$$
$$\xi^{c(\frac{1}{2})}\Pi_{\pm}{}^{c(1)} + \xi^{c(\frac{2}{1})}\Pi_{\pm}{}^{c(2)} - \bar\xi^{(\frac{1}{2})}\Pi_{\pm} - (\bar\xi^{(\frac{1}{2})} -$$
$$\left. \bar\xi^{(\frac{2}{1})})\bar\Pi_{\pm}{}^{(2)} + \bar\xi^{(\frac{1}{2})}[\bar\Pi_{\pm}{}^{(2)} + \bar\Pi_{\pm}{}^{(1)} + \Pi_{\pm}]\right\} \quad (29)$$

Three things now strike us. One is that we can factor out of the expressions $\Pi_0{}^{s(+)}$, $\Pi_{\pm}{}^{s(\frac{1}{2})}$, $\Pi_0{}^{c(+)}$, and $\Pi_{\pm}{}^{c(\frac{1}{2})}$ all multiplicative quantities such as $k_p \sin\alpha$ and $\cos\alpha$, distributively, which appear in them by virtue of the definitions, eq. 8, 9, 21, and 23, to obtain terms of the kind $\eta^{\sigma,\pi}\Pi_0{}^{(+)}$ and $\xi^{\sigma,\pi(\frac{1}{2})}\Pi_{\pm}{}^{(\frac{1}{2})}$ where $\Pi_0{}^{(+)}$ and $\Pi_{\pm}{}^{(\frac{1}{2})}$ are the π-like molecular orbitals of the type indicted in eq. 26; the second is that we can rearrange the expressions $\Sigma_{\pm}{}^{s(\frac{1}{2})}$, $\Sigma_{\pm}{}^{c(\frac{1}{2})}$, by virtue of eq. 8, 9, 21, and 22, to obtain terms of the kind $\rho^{\sigma,\pi(\frac{1}{2})}\bar\Sigma_{\pm}{}^{(\frac{1}{2})}$, where $\bar\Sigma_{\pm}{}^{(\frac{1}{2})}$ are the σ-like molecular orbitals of the types given by eq. 9 and 25; and the third is that the multiplicative factors $\eta^{\sigma,\pi}$, $\xi^{\sigma,\pi(\frac{1}{2})}$, and $\rho^{\sigma,\pi(\frac{1}{2})}$ and the localized σ-basis orbitals, $\bar\sigma_j$, thus introduced take on the structure

$$\eta^{\sigma,\pi} = k_p\eta^s \sin\alpha + \eta^c\cos\alpha - \bar\eta$$

$$\xi^{\sigma,\pi(\frac{1}{2})} = k_p\xi^{s(\frac{1}{2})}\sin\alpha + \xi^{c(\frac{1}{2})}\cos\alpha - \bar\xi^{(\frac{1}{2})}$$

$$\rho^{\sigma,\pi(\frac{1}{2})} = \rho^{c(\frac{1}{2})} \quad (30)$$

$$\bar\sigma_j = k_s n s_j \mp [k_p\cos\alpha + (\rho^{s(\frac{1}{2})}/\rho^{c(\frac{1}{2})})\sin\alpha]n p_{\sigma_{wj}} \quad (31)$$

when the constants $a_{0_r}{}^{\sigma,\pi,\bar\pi,s,c}$ equal $a_{3_r}{}^{\sigma,\pi,\bar\pi,s,c*}$ are picked uniformly [this picking can always be accomplished as all differences can be absorbed into the arbitrary constants $\eta^{s,c}$, $\bar\eta$, $\xi^{s,c(\frac{1}{2})}$, $\bar\xi^{(\frac{1}{2})}$, and $\rho^{s,c(\frac{1}{2})}$]. A particularly simple form for eq. 28 and 29 is gotten when this uniformity is chosen to be that of the pseudo-octahedral basis for which $a_{0_r}{}^{\sigma s,c}$ equals $\omega^r/\sqrt{6}$, $a_{0_r}{}^{\pi s,c}$

(15) A particularly simple way of deriving these formulas, as well as that of eq. 10, is to substitute the σ_j, π_j, and $\bar\pi_j$ orbitals of Table V, i.e., the $p_{\sigma_{wj}}$ and $p_{\pi_{wj}}$-type orbitals into the tetragonally oriented α_{1g}, ϵ_g, τ_{1g}, τ_{2g}, τ_{1u}, τ_{2u} nuclear displacement formulas tabulated in A. D. Liehr and C. J. Ballhausen, *Ann. Phys.* (N. Y.), **3**, 304 (1959), and diagonalize these with respect to $\mathfrak{C}_3(z')$ [this diagonalization is easily accomplished as these displacements behave elementarily under $\mathfrak{C}_3(z')$. As an instance, $\mathfrak{C}_3 S_{ka,b,c} = S_{kb,c,a}$, $(k = 3, 5)$, and $\mathfrak{C}_3(X_a,X_b,X_c) = (-X_b, -X_c, X_a)$, $(X_{a,b,c} = S_{sa,b,c}, R_{1a,b,c})$, so that $S_{kt} = 3^{-1/2}(S_{ka} + \omega^t S_{kc} + \omega^{2t}S_{kb})$, and $X_t = 3^{-1/2}(X_a - \omega^t X_b + \omega^{2t}X_c)$, $(t = 0, \pm 1)$ are diagonal]. This method shows that the related sums $\Pi_{0u}{}^{(-)}$, $\bar\Pi_{0u}{}^{(-)}$, and $\bar\Pi_{0u}{}^{(+)}$, $\Pi_{0g}{}^{(-)} = 1/\sqrt{2}\{\Pi_0{}^{(-)} - \bar\Pi_0{}^{(-)}\}$, $\bar\Pi_{0u}{}^{(\pm)} = 1/\sqrt{2}\{\Pi_0{}^{(\pm)} \mp \bar\Pi^{(\pm)}\}$, are of species T_{1g}, T_{1u}, and T_{2u}, respectively [the other components of the T_{2g}, T_{1u}, and T_{2u} π-like functions are easily generated by the nuclear displacement technique just outlined].

equals $\omega^{-s}/\sqrt{6}$, and $a_{0s}{}^{\pi}$ equals $1/\sqrt{6}$, $(s = 0, \pm 1)$.[10] Then

$$a_1(t_{2g}) = N_{a_1(t)}{}^{\sigma,\pi}\{t_{2g a} + \eta^{\sigma,\pi}\Pi_0{}^{(+)} + \sqrt{2}\bar{\eta}\Pi_{0g}{}^{(+)}\}$$

$$e_\pm(t_{2g}) = N_{e(t)}{}^{\sigma,\pi}\{t_{2g(\frac{b}{c})} + \xi^{\sigma,\pi(\frac{1}{2})}\Pi_\pm{}^{(1)} + \xi^{\sigma,\pi(\frac{2}{2})}\Pi_\pm{}^{(2)} -$$
$$(\xi(\tfrac{1}{2}) - \xi(\tfrac{2}{2}))[\Pi_\pm{}^{(2)} + \tilde{\Pi}_\pm{}^{(2)}] - \sqrt{2}\ \xi(\tfrac{1}{2})\Pi_{\pm g}\}$$

$$e(e_g) = N_{e(e)}{}^{\sigma,\pi}\{e_{g(\frac{a}{b})} + \rho^{\sigma,\pi(\frac{1}{2})}\bar{\Sigma}_{\pm g} -$$
$$(\rho^{\sigma,\pi(\frac{1}{2})} - \rho^{\sigma,\pi(\frac{1}{2})})\bar{\Sigma}_\pm{}^{(2)}\} \quad (32)$$

where the octahedrally oriented functions $\Pi_{0g}{}^{(+)}$, $\Pi_{\pm g}$, and $\bar{\Sigma}_{\pm g}$ are as defined by eq. 26, 27 and 10, 31. When the normalization constants are elected to be real, as earlier, the need that $e_\mp$ and $e_\pm{}^*$ be identical implies that $\xi^{\sigma,\pi}(\tfrac{1}{2})$ equals $\xi^{\sigma,\pi}(\tfrac{2}{1})^*$ and $\xi^{(1)}$ equals $\bar{\xi}^{(2)*}$, and $\rho^{\sigma,\pi}(\tfrac{1}{2})$ equals $\rho^{\sigma,\pi}(\tfrac{2}{1})^*$. Thus the pairs $\xi^{\sigma,\pi(1)}$ and $\xi^{\sigma,\pi(2)}$, $\xi^{(1)}$ and $\bar{\xi}^{(2)}$, and $\rho^{\sigma,\pi(1)}$ and $\rho^{\sigma,\pi(2)}$ differ internally only by a phase factor and not in amplitude. The further requirement that the functions $a_1(t_{2g})$, $e_\pm(t_{2g})$, and $e_\pm(e_g)$ tend to the octahedral one-electron molecular orbitals as the angle of cant, α, tends to zero, demands that $\bar{\eta}$ equals η^c and $\bar{\xi}(\tfrac{1}{2})$ equals $\xi^c(\tfrac{1}{2})$ in this limit (this truth may be conditionally confirmed by a sight of the equality of the pertinent group overlap integrals imprinted in eq. A-12 of the Appendix) so that $\eta^{\sigma,\pi}$ and $\xi^{\sigma,\pi}(\tfrac{1}{2})$ vanish [cf. eq. 30 and Fig. 2], and that $\bar{\xi}^{(1)}$ equals $\bar{\xi}^{(2)}$ equals $\bar{\xi}$ and $\rho^{\sigma,\pi(1)}$ equals $\rho^{\sigma,\pi(2)}$ equals $\rho^{\sigma,\pi}$. For the proper dihedrality of the pair $\Pi_\pm{}^{(1)}$, $\Pi_\pm{}^{(2)}$ at nonzero angles, α, we must have $\xi^{\sigma,\pi(1)}$ equals $\xi^{\sigma,\pi(2)}$ equals $\xi^{\sigma,\pi}$ also when α is not null [cf. eq. 13–16 and footnote 10]. Hence, the ultimate form of eq. 28 is

$$a_1(t_{2g}) = N_{a_1(t)}{}^{\sigma,\pi}\{t_{2g a} + \eta^{\sigma,\pi}\Pi_0{}^{(+)} + \sqrt{2}\ \bar{\eta}\Gamma_{0g}{}^{(+)}\}$$

$$e_\pm(t_{2g}) = N_{e(t)}{}^{\sigma,\pi}\{t_{2g(\frac{b}{c})} + \xi^{\sigma,\pi}\Pi_\pm - \sqrt{2}\ \bar{\xi}\Pi_{\pm g}\}$$

$$e_\pm(e_g) = N_{e(e)}{}^{\sigma,\pi}\{e_{g(\frac{a}{b})} + \rho^{\sigma,\pi}\bar{\Sigma}_{\pm g}\} \quad (33)$$

A comparison of eq. 17 and 33 shows that apart from the added octahedral terms $\Pi_{0g}{}^{(+)}$ and $\Pi_{\pm g}$ the mathematical structures of the σ-bonded and σ-, π-bonded one-electron molecular orbitals are identical. This circumstance will be of great consequence for our later optical intensity and rotativity computations.[16]

§2. Molecular Orbitals for Dihedral Compounds: Nonzero Spin-Orbit Forces

The appropriate trigonal one-electron spin-orbital functions for orbital states of octahedral parentage $e_{g(\frac{a}{b})}$ and $t_{2g(\frac{a}{b})}$ have been worked out previously by the author[9]; hence, we need only summarize the results here.

$$\gamma_{6(\frac{a}{b})}(e_g) = e_\mp(e_g)\zeta'(\pm^1/_2)$$

$$\gamma(\frac{4}{3})(e_g) = \frac{e^{\mp i\beta/4}}{\sqrt{2}}\{e_+(e_g)\zeta'(^1/_2) \mp ie_-(e_g)\zeta'(-^1/_2)\}$$

$$\gamma_{6(\frac{a}{b})}{}^{(7)}(t_{2g}) = \mp\sqrt{^1/_3}t_{2g a}\zeta'(\mp^1/_2) -$$
$$\sqrt{^2/_3}e_\mp(t_{2g})\zeta'(\pm^1/_2)$$

$$\gamma_{6(\frac{a}{b})}{}^{(8)}(t_{2g}) = \pm\sqrt{^2/_3}\ t_{2g a}\zeta'(\mp^1/_2) -$$
$$\sqrt{^1/_3}\ e_\mp(t_{2g})\zeta'(\pm^1/_2)$$

$$\gamma(\frac{4}{3})(t_{2g}) = \frac{e^{\pm i\beta/4}}{\sqrt{2}}\{e_+(t_{2g})\zeta'(^1/_2) \mp ie_-(t_{2g})\zeta'(-^1/_2)\}$$
$$(34)$$

The substitution of either eq. 11, 12, and 17 or eq. 28, 32, and 33 into eq. 34 yields the desired σ-bonded or σ-, π-bonded trigonal dihedral one-electron spin-orbital molecular orbitals. Figure 9 shows the connection of the two schemes, that with and that without spin-orbit forces, in both their one- and nine-electron aspects.

§3. The Optical Rotatory Power

3.1 General Concepts. Before entering upon a detailed exposition of the optical rotatory power of dihedral inorganic compounds, it is necessary to recall a few basic facts. Firstly, one must remember that plane polarized light is a superposition of right and left circularly polarized light [Fresnel, 1822] as pictured in Fig. 10, and that the rotation of the plane of polarization of light incident upon an optically active medium ["optical rotation"] is due to the different indices of refraction,

(16) In both eq. 17 and 33 and their antecedents we have consistently suppressed the contributions of the σ- and π-like octahedral gerade and ungerade orbitals A_{1g} and T_{1g} and T_{1u} and T_{2u}, respectively. The former suppression does no harm as the gerade orbitals cannot contribute to the optical intensity or rotational strengths, except insofar as they alter the normalization constants $N_{a_1(t)}$, $N_{e(t)}$, and $N_{e(e)}$. The latter suppression can do great harm as the ungerade orbitals can contribute quite directly to both the optical intensity and the rotational strengths, as they also allow a nonzero electronic transition moment between the $a_1(t_{2g})$, $e_\pm(t_{2g})$, and $e_\pm(e_g)$ molecular orbitals. The ungerade orbitals were omitted in the present development solely to avoid unnecessary complication and a proliferation of unknown variational constants. Future refinements of the present theory should, of course, include their contributions which are probably far from negligible. For our current purpose of demonstrating the feasibility of the present model, the approximate wave functions of eq. 17 and 33 will more than suffice. Hark that in the limit in which the angle of cant, α, becomes 90° (or in which β equals 90°, α becomes zero) the multiplicative variational constants $\eta^{\sigma,\pi}$ and $\xi^{\sigma,\pi}$ of eq. 33 also vanish as we again obtain an octahedral s- and π-like local ligand electron configuration, which demands that $\bar{\eta}$ equals η^s and $\bar{\xi}(\tfrac{1}{2})$ equals $\xi^s(\tfrac{1}{2})$ in this limit [cf. eq. 30 and Fig. 7a. As before (see text above), this fact may be qualitatively verified by a view of the equality of the relevant group overlap integrals tabulated in eq. A-12 of the Appendix]. Hence in this limit, the one electron trigonal dihedral molecular orbitals, eq. 33, anew become centrosymmetric, and therefore, optically inactive in the electric dipole approximation. [Please note that in this respect a σ-, π-bonded compound differs markedly from its σ-bonded progenitor. Cf. eq. 11 and 17, §1.1.]
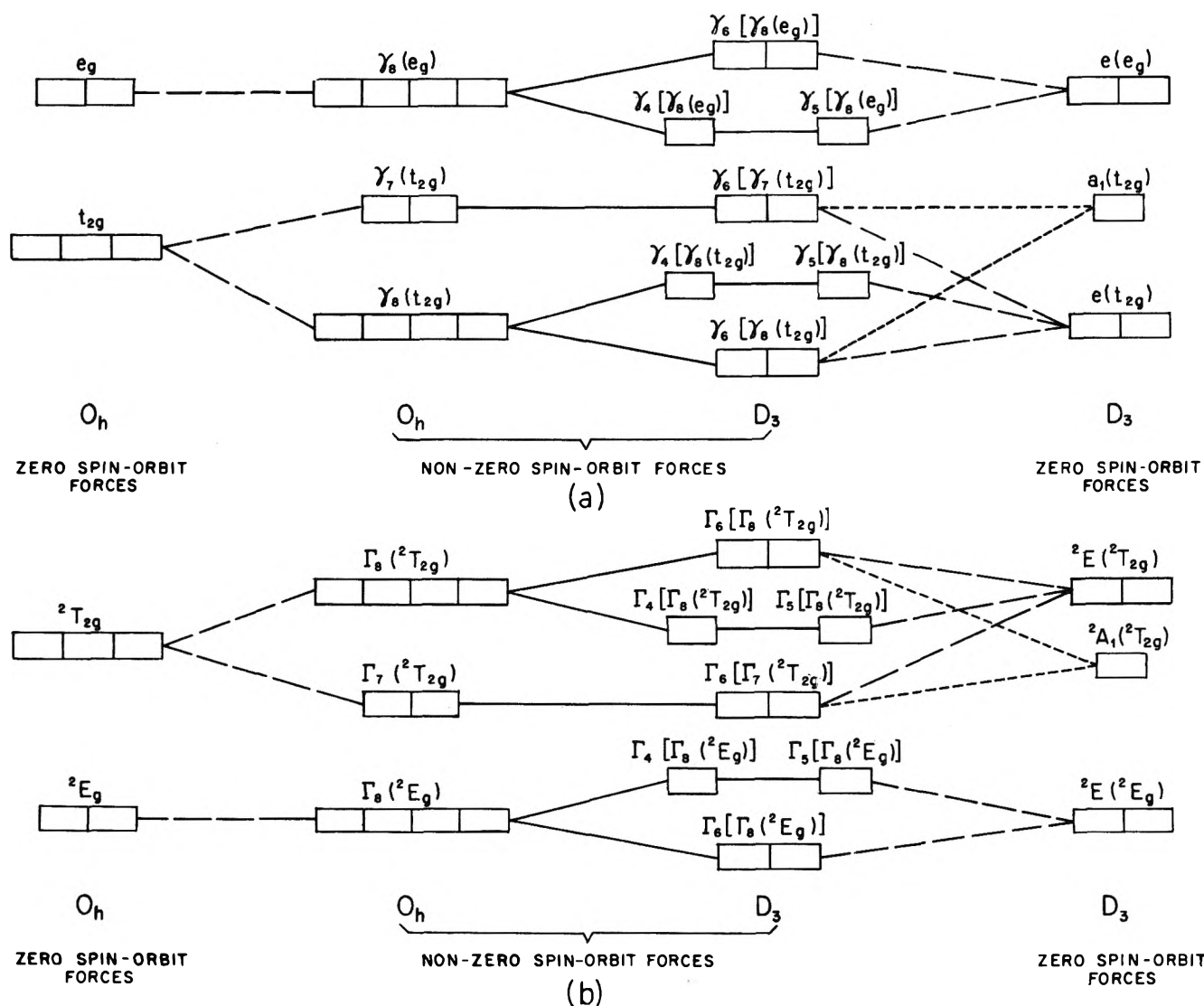
Figure 9. A schematic molecular spin-orbital energy level diagram for a one [part a] and nine [part b] electron transition metal compound.

n_r and n_l, for these two circularly polarized components ["circular birefringence"] as demonstrated in Fig. 11. Secondly, one must remember that the refrangibility of a medium [i.e., its indices of refraction, n_a] is a function of the wave length, λ, or the frequency, ν (or circular frequency ω), of the light employed ["optical dispersion"], and hence that the optical rotation is also a function of the wave length of frequency of the light used ["optical (circular) rotatory dispersion"]. Thirdly, one must remember that optical dispersion is intimately connected with optical absorption, and therefore that optical circular rotatory dispersion, which is due to the existence of two different indices of refraction, n_r and n_l, is also accompanied by optical circular rotatory absorption, due to the correspondent existence of two

different indices of absorption κ_r and κ_l ["circular dichroism"]. Fourthly, one must remember that the presence of two different indices of absorption κ_r and κ_l implies unequal extents of absorption of the right and left circular components of the initially linearly (plane) polarized light, which in turn implies that the resultant rotated emergent light can no longer be linearly (plane) polarized but must now be elliptically polarized with its major axis defining the new (or rotated) direction of the "plane" of polarization of the light as indicated in Fig. 12 and 13. Fifthly, one must remember that the refrangibility and absorptivity of a medium varies strongly and characteristically in regions of optical absorption ["anomalous dispersion and adsorption"], and hence that the optical circular rotatory dispersion

and absorption should likewise vary strongly and characteristically in such regions ["Cotton effects"].

3.2 *Mathematical Considerations.* The basic facts are expressed mathematically as follows. If we let $\vec{D}$ represent the dielectric displacement vector, which
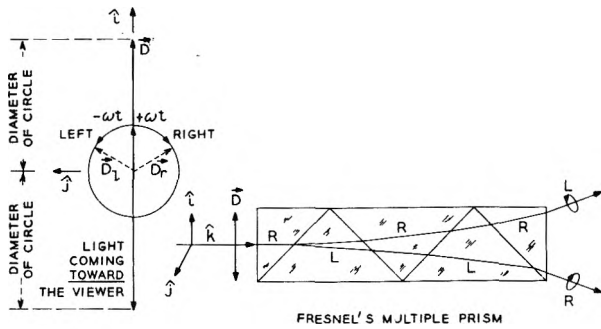
$$\vec{D} = \vec{D}_r + \vec{D}_l = 2D\hat{i} \cos\left(\omega t - \frac{2\pi n z}{\lambda}\right) \quad (36)$$

If now the indices of refraction n_r and n_l in the medium under consideration are different for right and left circularly polarized light but the indices of absorption are

Figure 10. Pictorial and mathematical representation of the Fresnel decomposition of plane polarized light into right and left circularly polarized light.

equals, for an isotropic medium, the dielectric constant, ϵ, times the electric vector, $\vec{E}$, right and left circularly polarized and sinusoidally varying light (traveling along the z axis) may be given the expression

$$\vec{D}_r = D_r\left[\hat{i} \cos\left(\omega t - \frac{2\pi n_r z}{\lambda}\right) - \hat{j} \sin\left(\omega t - \frac{2\pi n_l z}{\lambda}\right)\right]$$

$$\vec{D}_l = D_l\left[\hat{i} \cos\left(\omega t - \frac{2\pi n_r z}{\lambda}\right) + \hat{j} \sin\left(\omega t - \frac{2\pi n_l z}{\lambda}\right)\right]$$

$$(35)$$

where $\vec{D}_r$ and $\vec{D}_l$ are dielectric displacement vectors which rotate in time in a right-hand (clockwise) and left-hand (counterclockwise) direction, respectively, as viewed down the z axis [Fig. 10–13].[17] Thus we see by simple addition that for a medium with equal indices of refraction n_r and n_l [equal n] and equal indices of absorption κ_r and κ_l [equal κ] that $\vec{D}_r + \vec{D}_l$ equals a displacement vector, $\vec{D}$, of amplitude 2D, where D equals D_r equals D_l, directed along the x axis for all time, that is, linearly (plane) polarized along the x axis [Fig. 10]

Figure 11. Pictorial and mathematical demonstration of the rotation of the plane of polarization of a light wave which passes through a medium with different indices of refraction, n_r and n_l, for right and left circularly polarized light, respectively.

still the same, and if we call the sinusoidal arguments $\omega t - 2\pi n_r z/\lambda$ and $\omega t - 2\pi n_l z/\lambda$ appearing in eq. 35, δ_r and δ_l, separately, we further see that the total dis-

(17) This circumstance is most readily seen by examining the time behavior of $\vec{D}_r$ and $\vec{D}_l$ in the plane z equals zero. At time zero, both $\vec{D}_r$ and $\vec{D}_l$ are directed along the positive x axis, and at time $\pi/2\omega$ they are directed along the negative and positive y axis, and hence, they have rotated clockwise and counterclockwise, serially, in time [Fig. 10]. Alternatively, one can see from Fig. 10 that taking components of the vectors $\vec{D}_r$ and $\vec{D}_l$ there pictured, which each make angles ωt with the positive x axis, along the x and y axes leads immediately to eq. 35. The displacement amplitudes D_r and D_l are related to the absorptivities κ_r and κ_l by the relations $D_{(l)} = D_{0}e^{-2\pi\kappa(l)d/\lambda}$. Therefore, for equal absorptivities right and left, D_r equals D_l equals D. [For another expositional survey of the mathematics of the optical rotation problem, read A. D. Liehr, "Advances in the Chemistry of the Coordination Compounds," S. Kirschner, Ed., Macmillan, New York, N. Y., 1961, pp. 422–429.]

$$D_x = \vec{D} \cdot \hat{\imath} = D_r \cos \delta_r + D_L \cos \delta_L$$

$$D_y = \vec{D} \cdot \hat{\jmath} = D_L \sin \delta_L - D_r \sin \delta_r$$

$$D_{x'} = \vec{D} \cdot \hat{\imath}' = D_x(\hat{\imath} \cdot \hat{\imath}') + D_y(\hat{\jmath} \cdot \hat{\imath}') = D_x \cos \delta - D_y \sin \delta$$
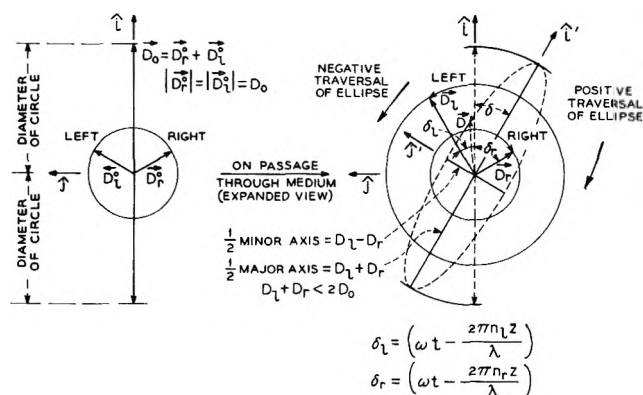
$$D_{y'} = \vec{D} \cdot \hat{\jmath}' = D_x(\hat{\imath} \cdot \hat{\jmath}') + D_y(\hat{\jmath} \cdot \hat{\jmath}') = D_x \sin \delta + D_y \cos \delta$$

Figure 12. Pictorial and mathematical illustration of the
simultaneous rotation and elliptization of a plane polarized
light wave which traverses a medium of different
absorptivities for right and left circular polarized light.
The equations indicate the vectorial decomposition
of the electric displacement vector $\vec{D} = \vec{D}_r + \vec{D}_l$
into components along the two sets of coordinate
axes $\{\hat{\imath}, \hat{\jmath}\}$ and $\{\hat{\imath}', \hat{\jmath}'\}$ defined in the figure.

placement after passage through a thickness z equals d
of the medium is given by[18]

$$\vec{D} = \vec{D}_r + \vec{D}_l = D[\hat{\imath}\,(\cos \delta_r + \cos \delta_l) - \\ \hat{\jmath}(\sin \delta_r - \sin \delta_l)] \quad (37)$$

Hence, the total displacement, $\vec{D}$, which on entering
the medium at z equals zero was directed along the
positive x axis has been turned clockwise and is now
directed at an angle δ to the axis [Fig. 11], where by eq.
37

$$\tan \delta = \frac{\sin \delta_r - \sin \delta_l}{\cos \delta_r + \cos \delta_l} \quad (38)$$

or, by use of the trigonometric identities, $\sin a - \sin b$
$= 2 \cos \frac{1}{2}(a + b) \sin \frac{1}{2}(a - b)$ and $\cos a + \cos b =$
$2 \cos \frac{1}{2}(a + b) \cos \frac{1}{2}(a - b)$ we obtain

$$\tan \delta = \tan \frac{1}{2}(\delta_r - \delta_l) \quad (39)$$

Therefore, we deduce that the total angle of optical
rotation δ is given by

$$\delta = \frac{1}{2}(\delta_r - \delta_l) = \frac{\pi d}{\lambda}(n_l - n_r) \quad (40)$$
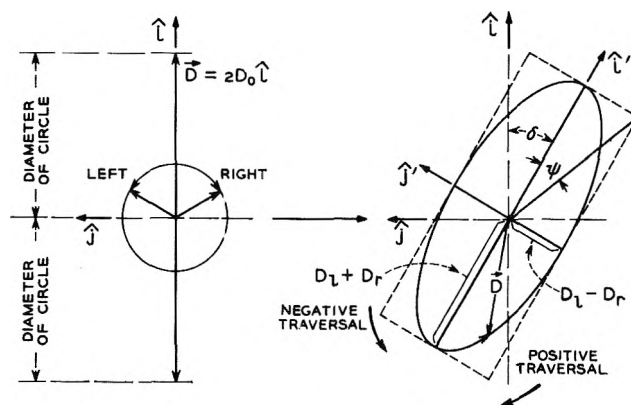
$$\delta = \frac{1}{2}(\delta_r - \delta_l) = \frac{\pi d}{\lambda}(n_l - n_r) \cdot (\text{ANGLE OF ROTATION})$$

$$\text{TAN } \psi = \frac{D_r - D_l}{D_r + D_l}$$

$$\text{IF } D_r = D_0 e^{-\frac{2\pi}{\lambda}\kappa_r d} \quad , \quad D_l = D_0 e^{-\frac{2\pi}{\lambda}\kappa_l d}$$

$$\text{,THEN TAN } \psi = \frac{1 - e^{-\frac{2\pi d}{\lambda}(\kappa_l - \kappa_r)}}{1 + e^{-\frac{2\pi d}{\lambda}(\kappa_l - \kappa_r)}} \approx \frac{\frac{2\pi d}{\lambda}(\kappa_l - \kappa_r)}{2 - \frac{2\pi d}{\lambda}(\kappa_l - \kappa_r)}$$

$$\text{BUT TAN } \psi \approx \psi$$

$$\therefore \psi \approx \frac{\pi d}{\lambda}(\kappa_l - \kappa_r) \cdot (\text{ANGLE OF ELLIPTICITY})$$

Figure 13. Pictorial and mathematical exemplification of the
simultaneous rotation and elliptization of a plane polarized
light wave which goes through a medium of different
indices of absorption, κ_r and κ_l, for right and left
circularly polarized light, respectively. The equations
outline the reduction of the general ellipticity formula,
$\tan \psi = D_r - D_l/D_r + D_l$, to its common
approximate form, $\psi = (\pi d/\lambda)(\kappa_l - \kappa_r)$.

and is independent of time, and that the angle of optical
rotation per unit path length is

$$\phi = \frac{\delta}{d} = \frac{\pi}{\lambda}(n_l - n_r) \quad (41)$$

These results are summarized in Fig. 11.

To see that elliptical polarization of the incident
linearly (plane) polarized light is a necessary accompani-
ment of the rotation of the plane of polarization by a
medium with different indices of refraction and absorp-
tion, n_r, κ_r and n_l, κ_l for right and left circularly polarized
light, separately, let us rewrite eq. 35 and 37 in the form

(18) It is instructive to note that since $2 \cos (\omega t - 2\pi n z/\lambda)$ equals
$e^{+i(\omega t - 2\pi n z/\lambda)} + e^{-i(\omega t - 2\pi n z/\lambda)}$ we can obtain an alternative view
of $\vec{D}$ as equal to $D[e^{+i(\omega t - 2\pi n z/\lambda)} + e^{-i(\omega t - 2\pi n z/\lambda)}]$, which is now
interpreted as a superposition of two vectors rotating in the com-
plex plane with $\vec{D}_r$ identified with $De^{+i(\omega t - 2\pi n z/\lambda)}$ which equals
$\cos (\omega t - 2\pi n z/\lambda) + i \sin (\omega t - 2\pi n z/\lambda)$ and $\vec{D}_l$ identified with
$De^{-i(\omega t - 2\pi z/\lambda)}$ which equals $\cos (\omega t - 2\pi n z/\lambda) - i \sin (\omega t - 2\pi n z/\lambda)$
where the real axis is pointed upward and the imaginary axis
toward the right [cf. Fig. 10 and eq. 35].

$$\vec{D} = \vec{D}_r + \vec{D}_l = D_z\hat{\imath} + D_y\hat{\jmath}$$

$$D_z = \vec{D}\cdot\hat{\imath} = D_r\cos\delta_r + D_l\cos\delta_l, \ D_y = \vec{D}\cdot\hat{\jmath} =$$

$$D_l\sin\delta_l - D_r\sin\delta_r \quad (42)$$

where we have now allowed the indices of absorption κ_r and κ_l and hence[16] the displacement amplitudes D_r and D_l for right and left circularly polarized light to be different. When the amplitudes D_r and D_l are equal, as they are in a medium which absorbs right and left circularly polarized light equally, eq. 42 reduces to our previous equation describing this situation, eq. 37. In this notation it is seen that the components of the displacement vector $\vec{D}$ parallel and perpendicular to the direction $\hat{\imath}'$ [Fig. 12] defined by our previous angle of optical rotation, δ equals $^1/_2(\delta_r - \delta_l)$ of eq. 40, are given by [cf. eq. 42]

$$D_{z'} = \vec{D}\cdot\hat{\imath}' = D_z(\hat{\imath}\cdot\hat{\imath}') + D_y(\hat{\jmath}\cdot\hat{\imath}')$$

$$D_{y'} = \vec{D}\cdot\hat{\jmath}' = D_z(\hat{\imath}\cdot\hat{\jmath}') + D_y(\hat{\jmath}\cdot\hat{\jmath}') \quad (43)$$

As the angle between the $\hat{\imath}'$ and $\hat{\imath}$ axes is δ and that between the $\hat{\imath}'$ and $\hat{\jmath}$ axis is $90° + \delta$ by definition (i.e., geometrical construction) of the direction $\hat{\imath}'$, we have that $(\hat{\imath}\cdot\hat{\imath}')$ equals $\cos\delta$, $(\hat{\jmath}\cdot\hat{\imath}')$ equals $\cos(90° + \delta)$, $(\hat{\imath}\cdot\hat{\jmath}')$ equals $\cos(90° - \delta)$, and $(\hat{\jmath}\cdot\hat{\jmath}')$ equals $\cos\delta$, and so by eq. 42 and the trigonometric sine and cosine addition laws

$$D_{z'} = (D_r\cos\delta_r + D_l\cos\delta_l)\cos\delta -$$

$$(D_l\sin\delta_l - D_r\sin\delta_r)\sin\delta$$

$$D_{z'} = D_r\cos(\delta_r - \delta) + D_l\cos(\delta_l + \delta)$$

$$D_{y'} = (D_r\cos\delta_r + D_l\cos\delta_l)\sin\delta +$$

$$(D_l\sin\delta_l - D_r\sin\delta_r)\cos\delta$$

$$D_{y'} = D_r\sin(\delta - \delta_r) + D_l\sin(\delta_l + \delta) \quad (44)$$

With the substitution of the definition of δ into the sinusoidal arguments of eq. 43, we see that $\delta_r - \delta$ equals $\delta_l + \delta$ equals $^1/_2(\delta_r + \delta_l)$ equals $\omega t - 2\pi n z/\lambda$, where n is the mean index of refraction $^1/_2(n_r + n_l)$. Hence, we may rewrite eq. 44 in the more physically meaningful form

$$D_{z'} = [D_r + D_l]\cos\left(\omega t - \frac{2\pi n z}{\lambda}\right)$$

$$D_{y'} = [D_l - D_r]\sin\left(\omega t - \frac{2\pi n z}{\lambda}\right) \quad (45)$$

which we see is the equation of an ellipse[19]

$$\frac{D_{z'}^2}{[D_r + D_l]^2} + \frac{D_{y'}^2}{[D_l - D_r]^2} =$$

$$\cos^2\left(\omega t - \frac{2\pi n z}{\lambda}\right) + \sin^2\left(\omega t - \frac{2\pi n z}{\lambda}\right) = 1 \quad (46)$$

Thus, the displacement vector $\vec{D}$ equals $D_z\hat{\imath} + D_y\hat{\jmath}$ equals $D_{z'}\hat{\imath}' + D_{y'}\hat{\jmath}'$ traverses in time an ellipse whose major axis lies along the direction $\hat{\imath}'$ and whose minor axis lies along the direction $\hat{\jmath}'$ [inspect eq. 45 and 46]. Therefore, the displacement vector $\vec{D}$, initially polarized along the $\hat{\imath}$ direction, upon traversing the optical medium undergoes an elliptization to become elliptically polarized with the major axis of the ellipse of polarization inclined at an angle δ to the incident direction of linear polarization. The ellipticity of the emergent ellipse is measured by the angle ψ, where $\tan\psi$ is defined as the ratio of the minor to the major axis of the ellipse, $\tan\psi = (D_r - D_l)/(D_r + D_l)$, with the angular sign convention as indicated. The ellipse of polarization is said to be traversed in the positive sense (clockwise) when ψ is greater than zero and in the negative sense (counterclockwise) when ψ is less than zero, that is it is said to be traversed positively (clockwise) if left circularly polarized light is absorbed more strongly than right (κ_l and D_r greater than κ_r and D_l—scan eq. 45 and Fig. 12 and 13), and negatively (counterclockwise) if right circularly polarized light is absorbed more strongly than left (κ_r and D_l greater than κ_l and D_r— look at eq. 45 and Fig. 12 and 13). These results are recapitulated in Fig. 12 and 13.

The magnitude of the optical rotation and elliptization of the plane of (linear) polarization is determined as noted in eq. 41 and Fig. 11 and 13 by the difference in the indices of refraction and absorption, $n_l - n_r$ and $\kappa_l - \kappa_r$, individually, of left and right circularly polarized light. This difference can be shown[20] to depend upon the quantity $\mathfrak{R}_{ab}$, called the rotational strength, where $\mathfrak{R}_{ab}$ equals the imaginary part of the scalar product of the quantum mechanical matrix elements $\langle a|\vec{p}|b\rangle$ and $\langle b|\vec{m}|a\rangle$, and where $\vec{p}$ and $\vec{m}$ are the electronic electric and magnetic dipole operators

(19) A similar but somewhat more complicated derivation of this well known result has been given by F. M. Jaeger, "Spatial Arrangements of Atomic Systems and Optical Activity," The George Fisher Baker Non-Resident Lectures in Chemistry, Cornell University, McGraw-Hill Book Co., Inc., New York, N. Y., 1930. The present derivation was conceived in ignorance of Jaeger's previous pedagogical analysis.

(20) A most excellent demonstration of this fact as well as many others concerning optical rotatory power may be found in the truly wonderful book of J. P. Mathieu, "Les Théories Moléculaires Du Pouvoir Rotatoire Naturel," Centre National De La Recherche Scientifique, Paris, 1946.

$\sum_j e\vec{r}_j$ and $\sum_j \mu_B(\vec{l}_j + 2\vec{s}_j)$, severally,[21,22] and $\langle a|\vec{p}$ or $\vec{m}|b\rangle = \int \chi_a^*(\vec{p}$ or $\vec{m})\chi_b d\tau$. Hence, it is this quantity, the rotational strength, which we wish to assess in order to determine the optical activity of trigonal dihedral compounds.

3.3 *Matrix Elements.* The computation of the requisite matrix elements is straightforward and needs little comment. Since the electric and magnetic dipole moment operators are one-electron operators, the magnitude of their matrix elements between many electron functions is just the sum of their one-electron transition charge density component matrix elements.[23] In the one-electron molecular orbital approximation which we here employ from calculational necessity, this sum of one-electron transition charge density component

matrix elements reduces to a sum of the one-electron molecular orbital matrix elements

$$\left\langle a_1(t_{2g}) \left| \begin{matrix}\vec{p}\\\vec{m}\end{matrix} \right| a_1(t_{2g}) \text{ or } e_\pm(t_{2g} \text{ or } e_g) \right\rangle$$

$$\left\langle e_\pm(t_{2g}) \left| \begin{matrix}\vec{p}\\\vec{m}\end{matrix} \right| e_\pm(t_{2g} \text{ or } e_g) \right\rangle$$

and

$$\left\langle e_\pm(t_{2g}) \left| \begin{matrix}\vec{p}\\\vec{m}\end{matrix} \right| e_\mp(t_{2g} \text{ or } e_g) \right\rangle$$

The use of eq. 11, 17, 33, and 34 and of Tables I–V, together with the neglect of localized ligand–ligand contributions to both the electric dipole and magnetic dipole integrals and of localized ligand–metal contributions to the magnetic dipole interaction, then yields the basic spinless one-electron molecular orbital matrix elements[24]

$$\left\langle a_1(t_{2g}) \left| \begin{matrix}\vec{p}\\\vec{m}\end{matrix} \right| a_1(t_{2g}) \right\rangle \equiv 0$$

$$\left\langle a_1(t_{2g}) \left| \begin{matrix}\vec{p}\\\vec{m}\end{matrix} \right| e_\pm(t_{2g}) \right\rangle = (\hat{\imath} + \omega^{\pm 1}\hat{\jmath} + \omega^{\pm 2}\hat{k})N_{a_1(t)}^*N_{e(t)} \begin{bmatrix} e\xi^{(\frac{1}{2})}\omega^{\mp 1}\sqrt{1/6}k_p \sin\alpha\,(K_{2A_8} + \omega^{\mp 1}K_{3A_8}) - \\ e\xi^{(\frac{2}{3})}\sqrt{1/6}k_p \sin\alpha\,(K_{2A_8} + \omega^{\pm 1}K_{3A_8}) \pm \\ ie\eta^*\omega^{\pm 1}\sqrt{1/2}k_p \sin\alpha\,(K_{3A_8} - K_{2A_8}) \\ \mp \mu_B\sqrt{1/3}\omega^{\pm 1} \end{bmatrix}$$

$$\left\langle a_1(t_{2g}) \left| \begin{matrix}\vec{p}\\\vec{m}\end{matrix} \right| e_\pm(e_g) \right\rangle = (\hat{\imath} + \omega^{\pm 1}\hat{\jmath} + \omega^{\pm 2}\hat{k})N_{a_1(t)}^*N_{e(e)} \begin{bmatrix} \mp i\dfrac{e}{2}\eta^*\omega^{\pm 1}\sqrt{1/2}k_p \sin\alpha\,(\sqrt{3}K_{4A_8} + K_{7A_8}) + \\ e(\rho^{(\frac{1}{2})} - \rho^{(\frac{2}{3})})\omega^{\pm 1}\sqrt{1/6}(k_s K_{0A_8} + k_p \cos\alpha\,K_{2A_8}) \\ \mp \mu_B\sqrt{2/3}\omega^{\pm 1} \end{bmatrix}$$

$$\left\langle e_\pm(t_{2g}) \left| \begin{matrix}\vec{p}\\\vec{m}\end{matrix} \right| e_\pm(t_{2g}) \right\rangle = (\hat{\imath} + \hat{\jmath} + \hat{k})N_{e(t)}^*N_{e(t)} \begin{bmatrix} 0 \\ \mp \mu_B\sqrt{1/3} \end{bmatrix}$$

$$\left\langle e_\pm(t_{2g}) \left| \begin{matrix}\vec{p}\\\vec{m}\end{matrix} \right| e_\pm(e_g) \right\rangle = (\hat{\imath} + \hat{\jmath} + \hat{k})N_{e(t)}^*N_{e(e)} \begin{bmatrix} \dfrac{e}{2}\xi^{(\frac{1}{2})*}\sqrt{1/2}k_p \sin\alpha\,(K_{4A_8} \pm iK_{7A_8}) - \dfrac{e}{2}\xi^{(\frac{2}{3})*}\sqrt{1/2}k_p \sin\alpha\,(K_{4A_8} \mp \\ iK_{7A_8}) - e(\rho^{(\frac{1}{2})} - \rho^{(\frac{2}{3})})\sqrt{1/3}(k_s K_{0A_8} + k_p \cos\alpha\,K_{2A_8}) \\ \pm \mu_B\sqrt{2/3} \end{bmatrix}$$

$$\left\langle e_\pm(t_{2g}) \left| \begin{matrix}\vec{p}\\\vec{m}\end{matrix} \right| e_\mp(t_{2g}) \right\rangle = (\hat{\imath} + \omega^{\pm 1}\hat{\jmath} + \omega^{\pm 2}\hat{k})N_{e(t)}^*N_{e(t)} \begin{bmatrix} e(\xi^{(\frac{1}{2})} + \xi^{(\frac{2}{3})*} - \omega^{\mp 1}(\xi^{(\frac{1}{2})*} + \xi^{(\frac{2}{3})})) \times \\ \sqrt{1/6}k_p \sin\alpha\,(K_{2A_8} + K_{3A_8}) \\ 0 \end{bmatrix}$$

(21) The dipole length representation, $\sum_j e\vec{r}_j$, of the electric dipole operator $\vec{p}$ is by no means the only one possible: the dipole velocity representation $\sum_j i\hbar\vec{\nabla}_j$ can also be used. Indeed, the latter representation is usually the more accurate one for approximate wave functions (as its derivation requires fewer assumptions as to their goodness) and is the one to be preferred in exact calculations. However, in view of the exploratory nature of the present work, we have here followed the historical procedure of preferring the former representation over the the latter in view of its somewhat simpler structure.[22]

(22) For a comparison of the actual performance of these two alternatives in optical intensity and rotativity (part c of this reference)

calculations, read: (a) H. Shull, *Astrophys. J.*, **114**, 546 (1951); *J. Chem. Phys.*, **20**, 18, 1095 (1952); (b) M. Wolfsberg, *ibid.*, **23**, 793 (1955); (c) A. J. Moscowitz, "On Optical Activity—Hexahelicene," Thesis, Harvard University, Cambridge, Mass., 1957, Appendix VII (copies of this thesis are available from Dr. Moscowitz upon request); (d) A. S. Chakravorty and A. D. Liehr, to be published.

(23) For a recent discussion of the theory of one-electron operators, see: (a) M. Karplus, A. Kuppermann, and L. M. Isaacson, *J. Chem. Phys.*, **29**, 1240 (1958); and (b) A. Kuppermann, M. Karplus, and L. M. Isaacson, *Z. Naturforsch.*, **14a**, 311 (1959).

(24) The techniques employed in the evaluation of these matrix elements are well known. However, the use of elementary symmetry concepts to reduce these integrals to more simple forms seems to be less familiar. Thus in the Appendix we have sketched the procedures utilized to obtain the results collected in eq. 47 and 49.

$$\left\langle e_{\pm}(t_{2g}) \left| \frac{\vec{p}}{m} \right| e_{\mp}(e_g) \right\rangle = (\hat{\imath} + \omega^{\pm 1}\hat{\jmath} + \omega^{\pm 2}\hat{k})N_{e(t)}{}^{*}N_{e(e)} \begin{bmatrix} \frac{e}{2}\xi^{(\frac{1}{2})^{*}}\sqrt{1/2}k_p \sin \alpha \,(K_{4A_s} \mp iK_{7A_s}) - \\[2mm] \frac{e}{2}\xi^{(\frac{2}{3})^{*}}\omega^{\mp 1}\sqrt{1/2}k_p \sin \alpha \,(K_{4A_s} \pm iK_{7A_s}) + \\[2mm] 2e(\rho^{(\frac{1}{2})} - \rho^{(\frac{2}{3})})\sqrt{1/3}\omega^{\pm 1}(k_s k_{0A_s} + k_p \cos \alpha \, K_{2A_s}) \\[2mm] \mp \mu_B \sqrt{2/3}\omega^{\pm 1} \end{bmatrix}$$

$$\left\langle e_{\pm}(e_g) \left| \frac{\vec{p}}{m} \right| e_{\pm}(e_g) \right\rangle = 0$$

$$\left\langle e_{\pm}(e_g) \left| \frac{\vec{p}}{m} \right| e_{\mp}(e_g) \right\rangle = (\hat{\imath} + \omega^{\pm 1}\hat{\jmath} + \omega^{\pm 2}\hat{k})N_{e(e)}{}^{*}N_{e(e)} \begin{bmatrix} e(\rho^{(\frac{1}{2})} - \rho^{(\frac{2}{3})} + \rho^{(\frac{1}{2})^{*}} - \rho^{(\frac{2}{3})^{*}}) \times \\[2mm] \omega^{\pm 1}(k_s K_{14A_s} + k_p \cos \alpha \, K_{4A_s}) \\[2mm] 0 \end{bmatrix} \quad (47)$$

In eq. 47 the normalization constants $a_{(\frac{0}{3})_s}^{\sigma, \pi}$, $(s = 0, \pm 1)$, have all been chosen to be of absolute value $\sqrt{1/6}$ and to have complex phases in agreement with our previous conventions.

The addition to these elements of the values

$$\langle '\zeta(\pm 1/2)|2\vec{s}|\zeta'(\pm 1/2)\rangle = \pm \mu_B\sqrt{1/3}(\hat{\imath} + \hat{\jmath} + \hat{k})$$

$$\langle \zeta'(\pm 1/2|2\vec{s}|\zeta'(\mp 1/2)\rangle = \\ \mu_B \omega^{\mp 1}\sqrt{2/3}(\hat{\imath} + \omega^{\mp 1}\hat{\jmath} + \omega^{\mp 2}\hat{k}) \quad (48)$$

allows the determination of the basic one-electron

molecular spin-orbital matrix terms. Since these matrix elements are already quite messy within the mathematical formalism in which $\xi^{(1)}$ equals $\xi^{(2)}$ equals ξ and $\rho^{(1)}$ equals $\rho^{(2)}$ equals ρ, with ξ, ρ, η, $N_{a_1(t)}$, $N_{e(t)}$, and $N_{e(e)}$ real, we shall tabulate them only in this limit. As previously discussed, no actual generality is lost in so doing. If the notationally more general spin-orbital elements are desired, they may be readily generated from eq. 34, 47, and 48 [they are simply appropriate linear combinations of the elements printed in eq. 47 and 48]. The spin-orbital matrix array is then given by

$$\left\langle \gamma_{6a}^{(8)}(t_{2g}) \left| \frac{\vec{p}}{m} \right| \gamma_{6a}^{(7)}(t_{2g}) \right\rangle = (\hat{\imath} + \hat{\jmath} + \hat{k}) \begin{bmatrix} 0 \\ \mu_B\sqrt{2/3}(2/3 + 1/3 N_{e(t)}{}^2) \end{bmatrix}$$

$$\left\langle \gamma_{6a}^{(8)}(t_{2g}) \left| \frac{\vec{p}}{m} \right| \gamma_{6b}^{(7)}(t_{2g}) \right\rangle = (\hat{\imath} + \omega\hat{\jmath} + \omega^2\hat{k}) \begin{bmatrix} -ieN_{a_1(t)}N_{e(t)}\omega\sqrt{1/2}k_p \sin \alpha \,(K_{2A_s}(\xi - \eta) + \eta K_{3A_s}) \\ \mu_B\sqrt{1/3}\omega(2/3 + 1/3 N_{a_1(t)}N_{e(t)}) \end{bmatrix}$$

$$\left\langle \gamma_{6a}^{(8)}(t_{2g}) \left| \frac{\vec{p}}{m} \right| \gamma_{4}(t_{2g}) \right\rangle = (\hat{\imath} + \omega^{-1}\hat{\jmath} + \omega^{-2}\hat{k}) \frac{e^{i\beta/4}}{\sqrt{2}} \begin{bmatrix} -eN_{a_1(t)}N_{e(t)}\omega^{-1}\sqrt{1/3}k_p \sin \alpha \,(K_{2A_s}(\xi - \eta) + \\ \eta K_{3A_s}) - ie\xi N_{e(t)}{}^2\omega^{-1}\sqrt{2/3}k_p \sin \alpha \,(K_{3A_s} + K_{2A_s}) \\ i\mu_B \frac{\sqrt{2}}{3}\omega^{-1}(1 - N_{a_1(t)}N_{e(t)}) \end{bmatrix}$$

$$\left\langle \gamma_{6a}^{(8)}(t_{2g}) \left| \frac{\vec{p}}{m} \right| \gamma_{5}(t_{2g}) \right\rangle = (\hat{\imath} + \omega^{-1}\hat{\jmath} + \omega^{-2}\hat{k}) \frac{e^{-i\beta/4}}{\sqrt{2}} \begin{bmatrix} eN_{a_1(t)}N_{e(t)}\omega^{-1}\sqrt{1/3}k_p \sin \alpha \,(K_{2A_s}(\xi - \eta) + \eta K_{3A_s}) - \\ ie\xi N_{e(t)}{}^2\omega^{-1}\sqrt{2/3}k_p \sin \alpha \,(K_{3A_s} + K_{2A_s}) \\ -i\mu_B \frac{\sqrt{2}}{3}\omega^{-1}(1 - N_{a_1(t)}N_{e(t)}) \end{bmatrix}$$

$$\left\langle \gamma_{6a}^{(7)}(t_{2g}) \left| \frac{\vec{p}}{m} \right| \gamma_{4}(t_{2g}) \right\rangle = (\hat{\imath} + \omega^{-1}\hat{\jmath} + \omega^{-2}\hat{k}) \frac{e^{i\beta/4}}{\sqrt{2}} \begin{bmatrix} eN_{a_1(t)}N_{e(t)}\omega^{-1}\sqrt{1/6}k_p \sin \alpha \,(K_{2A_s}(\xi - \eta) + \eta K_{3A_s}) - \\ ie\xi N_{e(t)}{}^2\omega^{-1}\sqrt{\frac{2}{3}} \, k_p \sin \alpha \,(K_{3A_s} + K_{2A_s}) \\ i\mu_B\omega^{-1}(2/3 + 1/3 N_{a_1(t)}N_{e(t)}) \end{bmatrix}$$

$$\left\langle \gamma_{6a}{}^{(7)}(t_{2g}) \left| \frac{\vec{p}}{m} \right| \gamma_5(t_{2\parallel}) \right\rangle = (\hat{\imath} + \omega^{-1}\hat{\jmath} + \omega^{-2}\hat{k}) \frac{e^{-i\beta/4}}{\sqrt{2}} \begin{bmatrix} -eN_{a_1(t)}N_{e(t)}\omega^{-1}\sqrt{1/6}\,k_p \sin\alpha(K_{2A_2}(\xi - \eta) + \eta K_{3A_2}) - \\ ie\xi N_{e(t)}{}^2\omega^{-1}\frac{2}{\sqrt{3}}k_p \sin\alpha\,(K_{3A_2} + K_{2A_2}) \\ -i\mu_B\omega^{-1}(^2/_3 + {}^1/_3 N_{a_1(t)}N_{e(t)}) \end{bmatrix}$$

$$\left\langle \gamma_4(t_{2g}) \left| \frac{\vec{p}}{m} \right| \gamma_4(e_g) \right\rangle \equiv 0$$

$$\left\langle \gamma_5(t_{2g}) \left| \frac{\vec{p}}{m} \right| \gamma_4(e_g) \right\rangle = (\hat{\imath} + \hat{\jmath} + \hat{k})N_{e(t)}N_{e(e)} \begin{bmatrix} ie\sqrt{1/2}\,k_p \sin\alpha\,\xi K_{7A_2} \\ \sqrt{2/3}\,\mu_B \end{bmatrix}$$

$$\left\langle \gamma_{6a}{}^{(7)}(t_{2g}) \left| \frac{\vec{p}}{m} \right| \gamma_4(e_{\parallel}) \right\rangle = (\hat{\imath} + \omega^{-1}\hat{\jmath} + \omega^{-2}\hat{k}) \frac{e^{-i\beta/4}}{\sqrt{2}} \begin{bmatrix} -\frac{e}{2}\eta N_{a_1(t)}N_{e(e)}\sqrt{1/6}\,k_p \sin\alpha\,\omega^{-1}(\sqrt{3}K_{4A_2} + K_{7A_2}) - \\ i\frac{e}{2}\xi N_{e(t)}N_{e(e)}\sqrt{1/3}\,k_p \sin\alpha\,\omega^{-1}(\sqrt{3}K_{4A_2} - K_{7A_2}) \\ i\mu_B \frac{\sqrt{2}}{3}\omega^{-1}N_{a_1(t)}N_{e(e)} - {}^2/_3\mu_B\omega^{-1}N_{e(t)}N_{e(e)} \end{bmatrix}$$

$$\left\langle \gamma_{6b}{}^{(7)}(t_{2g}) \left| \frac{\vec{p}}{m} \right| \gamma_4(e_g) \right\rangle = (\hat{\imath} + \omega\hat{\jmath} + \omega^2\hat{k}) \frac{e^{-i\beta/4}}{\sqrt{2}} \begin{bmatrix} -i\frac{e}{2}\eta N_{a_1(t)}N_{e(e)}\sqrt{1/6}\,k_p \sin\alpha\,\omega(\sqrt{3}K_{4A_2} + K_{7A_2}) + \\ \frac{e}{2}\xi N_{e(t)}N_{e(e)}\sqrt{1/3}\,k_p \sin\alpha\,\omega(\sqrt{3}K_{4A_2} - K_{7A_2}) \\ -\mu_B \frac{\sqrt{2}}{3}\omega N_{a_1(t)}N_{e(e)} - i^2/_3\mu_B\omega N_{e(t)}N_{e(e)} \end{bmatrix}$$

$$\left\langle \gamma_{6a}{}^{(8)}(t_{2g}) \left| \frac{\vec{p}}{m} \right| \gamma_4(e_g) \right\rangle = (\hat{\imath} + \omega^{-1}\hat{\jmath} + \omega^{-2}\hat{k}) \frac{e^{-i\beta/4}}{\sqrt{2}} \begin{bmatrix} \frac{e}{2}\eta N_{a_1(t)}N_{e(e)}\sqrt{1/3}\,k_p \sin\alpha\,\omega^{-1}(\sqrt{3}K_{4A_2} + K_{7A_2}) - \\ i\frac{e}{2}\xi N_{e(t)}N_{e(e)}\sqrt{1/6}\,k_p \sin\alpha\,\omega^{-1}(\sqrt{3}K_{4A_2} - K_{7A_2}) \\ -i^2/_3\mu_B\omega^{-1}N_{a_1(t)}N_{e(e)} - \mu_B \frac{\sqrt{2}}{3}\omega^{-1}N_{e(t)}N_{e(e)} \end{bmatrix}$$

$$\left\langle \gamma_{6b}{}^{(8)}(t_{2g}) \left| \frac{\vec{p}}{m} \right| \gamma_4(e_g) \right\rangle = (\hat{\imath} + \omega\hat{\jmath} + \omega^2\hat{k}) \frac{e^{-i\beta/4}}{\sqrt{2}} \begin{bmatrix} i\frac{e}{2}\eta N_{a_1(t)}N_{e(e)}\sqrt{1/3}\,k_p \sin\alpha\,\omega(\sqrt{3}K_{4A_2} + K_{7A_2}) + \\ \frac{e}{2}\xi N_{e(t)}N_{e(e)}\sqrt{1/6}\,k_p \sin\alpha\,\omega(\sqrt{3}K_{4A_2} - K_{7A_2}) \\ {}^2/_3\mu_B\omega N_{a_1(t)}N_{e(e)} - i\frac{\sqrt{2}}{3}\mu_B\omega N_{e(t)}N_{e(e)} \end{bmatrix}$$

$$\left\langle \gamma_4(t_{2g}) \left| \frac{\vec{p}}{m} \right| \gamma_{6b}(e_g) \right\rangle = (\hat{\imath} + \omega^{-1}\hat{\jmath} + \omega^{-2}\hat{k}) \frac{e^{-i\beta/4}}{\sqrt{2}} \begin{bmatrix} -\frac{e}{2}\xi N_{e(t)}N_{e(e)}\sqrt{1/2}\,k_p \sin\alpha\,\omega^{-1}(\sqrt{3}K_{4A_2} - K_{7A_2}) \\ i\mu_B\sqrt{2/3}\,\omega^{-1}N_{e(t)}N_{e(e)} \end{bmatrix}$$

$$\left\langle \gamma_5(t_{2g}) \left| \frac{\vec{p}}{m} \right| \gamma_{6b}(e_g) \right\rangle = (\hat{\imath} + \omega^{-1}\hat{\jmath} + \omega^{-2}\hat{k}) \frac{e^{-i\beta/4}}{\sqrt{2}} \begin{bmatrix} \frac{e}{2}\xi N_{e(t)}N_{e(e)}\sqrt{1/2}\,k_p \sin\alpha\,\omega^{-1}(\sqrt{3}K_{4A_2} - K_{7A_2}) \\ -i\mu_B\sqrt{2/3}\,\omega^{-1}N_{e(t)}N_{e(e)} \end{bmatrix}$$

$$\left\langle \gamma_{6a}{}^{(7)}(t_{2g}) \left| \frac{\vec{p}}{m} \right| \gamma_{6b}(e_g) \right\rangle = (\hat{i} + \omega\hat{j} + \omega^2\hat{k}) \begin{bmatrix} i\frac{e}{2}\eta N_{a_1(t)}N_{e(e)}\sqrt{1/6}\,k_p \sin\alpha\,\omega(\sqrt{3}K_{4A_2} + K_{7A_2}) \\ \mu_B \dfrac{\sqrt{2}}{3}\omega N_{a_1(t)}N_{e(e)} \end{bmatrix}$$

$$\left\langle \gamma_{6b}{}^{(7)}(t_{2g}) \left| \frac{\vec{p}}{m} \right| \gamma_{6b}(e_g) \right\rangle = (\hat{i} + \hat{j} + \hat{k}) \begin{bmatrix} -ie\xi N_{e(t)}N_{e(e)}\sqrt{1/3}\,k_p \sin\alpha\, K_{7A_2} \\ -{}^2\!/_3\mu_B N_{e(t)}N_{e(e)} \end{bmatrix}$$

$$\left\langle \gamma_{6a}{}^{(8)}(t_{2g}) \left| \frac{\vec{p}}{m} \right| \gamma_{6b}(e_g) \right\rangle = (\hat{i} + \omega\hat{j} + \omega^2\hat{k}) \begin{bmatrix} -i\frac{e}{2}\eta N_{a_1(t)}N_{e(e)}\sqrt{1/3}\,k_p \sin\alpha\,\omega(\sqrt{3}K_{4A_2} + K_{7A_2}) \\ -{}^2\!/_3\mu_B\omega N_{a_1(t)}N_{e(e)} \end{bmatrix}$$

$$\left\langle \gamma_{6b}{}^{(8)}(t_{2g}) \left| \frac{\vec{p}}{m} \right| \gamma_{6b}(e_g) \right\rangle = (\hat{i} + \hat{j} + \hat{k}) \begin{bmatrix} -ie\xi N_{e(t)}N_{e(e)}\sqrt{1/6}\,k_p \sin\alpha\, K_{7A_2} \\ -\mu_B \dfrac{\sqrt{2}}{3} N_{e(t)}N_{e(e)} \end{bmatrix}$$

$$\left\langle \gamma_4(e_g) \left| \frac{\vec{p}}{m} \right| \gamma_4(e_g) \right\rangle \equiv 0$$

$$\left\langle \gamma_5(e_g) \left| \frac{\vec{p}}{m} \right| \gamma_4(e_g) \right\rangle = (\hat{i} + \hat{j} + \hat{k})e^{-i\beta/2} \begin{bmatrix} 0 \\ \mu_B\sqrt{1/3} \end{bmatrix}$$

$$\left\langle \gamma_{6a}(e_g) \left| \frac{\vec{p}}{m} \right| \gamma_4(e_g) \right\rangle = (\hat{i} + \omega^{-1}\hat{j} + \omega^{-2}\hat{k})\frac{e^{-i\beta/4}}{\sqrt{2}} \begin{bmatrix} 0 \\ -i\mu_B\sqrt{2/3}\,\omega^{-1} \end{bmatrix}$$

$$\left\langle \gamma_{6b}(e_g) \left| \frac{\vec{p}}{m} \right| \gamma_4(e_g) \right\rangle = (\hat{i} + \omega\hat{j} + \omega^2\hat{k})\frac{e^{-i\beta/4}}{\sqrt{2}} \begin{bmatrix} 0 \\ \mu_B\sqrt{2/3}\,\omega \end{bmatrix}$$

$$\left\langle \gamma_{6a}(e_g) \left| \frac{\vec{p}}{m} \right| \gamma_{6a}(e_g) \right\rangle = 0$$

$$\left\langle \gamma_{6a}(e_g) \left| \frac{\vec{p}}{m} \right| \gamma_{6b}(e_g) \right\rangle = 0$$

$$\left\langle \gamma_{6a}{}^{(7)}(t_{2g}) \left| \frac{\vec{p}}{m} \right| \gamma_{6a}{}^{(7)}(t_{2g}) \right\rangle = (\hat{i} + \hat{j} + \hat{k}) \begin{bmatrix} 0 \\ \mu_B\sqrt{1/3}(1/_3 + {}^2\!/_3 N_{e(t)}{}^2) \end{bmatrix}$$

$$\left\langle \gamma_{6a}{}^{(7)}(t_{2g}) \left| \frac{\vec{p}}{m} \right| \gamma_{6b}{}^{(7)}(t_{2g}) \right\rangle = (\hat{i} + \omega\hat{j} + \omega^2\hat{k}) \begin{bmatrix} 0 \\ -\mu_B\sqrt{2/3}\,\omega(1/_3 + {}^2\!/_3 N_{a_1(t)}N_{e(t)}) \end{bmatrix}$$

$$\left\langle \gamma_{6a}{}^{(8)}(t_{2g}) \left| \frac{\vec{p}}{m} \right| \gamma_{6a}{}^{(8)}(t_{2g}) \right\rangle = (\hat{i} + \hat{j} + \hat{k}) \begin{bmatrix} 0 \\ -u_B\sqrt{1/3}(1/_3 - {}^1\!/_3 N_{e(t)}{}^2) \end{bmatrix}$$

$$\left\langle \gamma_{6a}{}^{(8)}(t_{2g}) \left| \frac{\vec{p}}{m} \right| \gamma_{6b}{}^{(8)}(t_{2g}) \right\rangle = (\hat{i} + \omega\hat{j} + \omega^2\hat{k}) \begin{bmatrix} 0 \\ -\mu_B\sqrt{2/3}\,\omega({}^2\!/_3 - {}^2\!/_3 N_{a_1(t)}N_{e(t)}) \end{bmatrix}$$

$$\left\langle \gamma_4(t_{2g}) \left| \frac{\vec{p}}{m} \right| \gamma_4(t_{2g}) \right\rangle = 0$$

$$\left\langle \gamma_5(t_{2g}) \left| \frac{\vec{p}}{m} \right| \gamma_4(t_{2g}) \right\rangle = (\hat{i} + \hat{j} + \hat{k})e^{i\beta/2} \begin{bmatrix} 0 \\ \mu_B\sqrt{1/3}(1 - N_{e(t)}{}^2) \end{bmatrix} \qquad (49)$$

The matrix elements not enrolled in eq. 49 may be effortlessly derived by use of the momentum reversal operator $\mathcal{K}$ and the rotation operators $\mathcal{C}_2(y')$ and $\mathcal{C}_3(z')$ as outlined below.[25]

It is to be especially noted that the magnetic dipole transition moments which are not prefaced by the product of two normalization factors in eq. 49 arise solely from spin alone. The quantities K_{nA_j} which occur in eq. 47 and 49 are certain localized ligand–metal integrals which evaluate the localized electric transition dipole moment in the x direction. These integrals are posted in the Appendix.[26]

3.4 *Rotational and Spectral Strengths.* As mentioned previously, the rotatory power of a substance, as expressed in terms of its rotational dispersion and circular dichroism, is determined by the quantity, $\mathfrak{R}_{ab}$

$$\mathfrak{R}_{ab} = \mathfrak{Im}\{\langle a|\vec{p}|b\rangle\cdot\langle b|\vec{m}|a\rangle\} \qquad (50)$$

the so-called *rotational strength* of the substance. Closely related to this quantity is the so-named (electric dipole) *spectral strength*, S_{ab}

$$S_{ab} = \langle a|\vec{p}|b\rangle\cdot\langle b|\vec{p}|a\rangle = |\langle a|\vec{p}|b\rangle|^2 \qquad (51)$$

which measures the electric dipole absorptive power of a medium. In this paper we shall deal with only what we might designate as the *electronic* rotatory and absorptive power, that is, only that rotatory and absorptive power which owes its origin to the existence of an electronic, as opposed to a vibrational-electronic ["vibronic"], electric transition dipole. Hence, the rotational strength, $\mathfrak{R}_{ab}$, and the spectral strength, S_{ab}, of the electronic transition a to b, as defined here, are only that portion of the total rotational and spectral strength which are nonvibronic in nature. We shall take up the more general case of electronic plus vibronic rotational and spectral strengths in a later publication.[27]

(25) The momentum reversal operator $\mathcal{K}$ applied to the spin-orbital functions of eq. 34 leads to the results $\mathcal{K}\gamma_6(\begin{smallmatrix}a\\b\end{smallmatrix}) = \pm\gamma_6(\begin{smallmatrix}b\\a\end{smallmatrix})$, $\mathcal{K}\gamma(\begin{smallmatrix}4\\5\end{smallmatrix}) = \mp i\gamma(\begin{smallmatrix}5\\4\end{smallmatrix})$ [note the misprint in footnote 37 of ref. 9], regardless of the source, t_{2g} or e_g, of the spin-orbitals, when it is recalled that $\mathcal{K}\zeta'(\pm^1/_2) = \pm\zeta'(\mp^1/_2)$ and $\mathcal{K}c = c^*$ for any constant c [read (a) E. Fick, *Z. Physik*, **147**, 307 (1957), for example]. Hence, when this operator is applied both internally and externally to a typical matrix element such as

$$\left\langle \gamma_{6(\begin{smallmatrix}a\\b\end{smallmatrix})}^{(7)}(t_{2g}) \left|\frac{\vec{p}}{m}\right| \gamma_5(t_{2g}) \right\rangle$$

we find that

$$\mathcal{K}\left\langle \gamma_{6(\begin{smallmatrix}a\\b\end{smallmatrix})}^{(7)}(t_{2g}) \left|\frac{\vec{p}}{m}\right| \gamma_5(t_{2g}) \right\rangle = \left\langle \gamma_{6(\begin{smallmatrix}b\\a\end{smallmatrix})}^{(7)}(t_{2g}) \left|\frac{\vec{p}}{m}\right| \gamma_6(t_{2g}) \right\rangle^* = \left\langle \pm\gamma_{6(\begin{smallmatrix}b\\a\end{smallmatrix})}^{(7)}(t_{2g}) \left|\frac{\vec{p}}{-m}\right| i\gamma_4(t_{2g}) \right\rangle$$

as this matrix element is simultaneously both a constant and a function of the indicated spin-orbitals. Therefore, we derive

$$\left\langle \gamma_{6(\begin{smallmatrix}b\\a\end{smallmatrix})}^{(7)}(t_{2g}) \left|\frac{\vec{p}}{m}\right| \gamma_4(t_{2g}) \right\rangle = i\left[\begin{smallmatrix}\mp\\\pm\end{smallmatrix}\right]\left\langle \gamma_{6(\begin{smallmatrix}a\\b\end{smallmatrix})}^{(7)}(t_{2g}) \left|\frac{\vec{p}}{m}\right| \gamma_5(t_{2g}) \right\rangle^*$$

In general, as a consequence of momentum reversal symmetry, we have for spin-orbitals of either or both t_{2g} and e_g parentage the relations

$$\left\langle \gamma_{6b} \left|\frac{\vec{p}}{m}\right| \gamma_{6b} \right\rangle = \left[\begin{smallmatrix}+\\-\end{smallmatrix}\right]\left\langle \gamma_{6a} \left|\frac{\vec{p}}{m}\right| \gamma_{6a} \right\rangle^*,$$

$$\left\langle \gamma_{6b} \left|\frac{\vec{p}}{m}\right| \gamma_{6a} \right\rangle = \left[\begin{smallmatrix}-\\+\end{smallmatrix}\right]\left\langle \gamma_{6a} \left|\frac{\vec{p}}{m}\right| \gamma_{6b} \right\rangle^*$$

$$\left\langle \gamma_{6b} \left|\frac{\vec{p}}{m}\right| \gamma_4 \right\rangle = i\left[\begin{smallmatrix}-\\+\end{smallmatrix}\right]\left\langle \gamma_{6a} \left|\frac{\vec{p}}{m}\right| \gamma_5 \right\rangle^*,$$

$$\left\langle \gamma_{6b} \left|\frac{\vec{p}}{m}\right| \gamma_5 \right\rangle = i\left[\begin{smallmatrix}+\\-\end{smallmatrix}\right]\left\langle \gamma_{6a} \left|\frac{\vec{p}}{m}\right| \gamma_4 \right\rangle^*$$

$$\left\langle \gamma_5 \left|\frac{\vec{p}}{m}\right| \gamma_5 \right\rangle = \left[\begin{smallmatrix}+\\-\end{smallmatrix}\right]\left\langle \gamma_4 \left|\frac{\vec{p}}{m}\right| \gamma_4 \right\rangle^*,$$

$$\left\langle \gamma_5 \left|\frac{\vec{p}}{m}\right| \gamma_4 \right\rangle = \left[\begin{smallmatrix}-\\+\end{smallmatrix}\right]\left\langle \gamma_4 \left|\frac{\vec{p}}{m}\right| \gamma_5 \right\rangle^*$$

plus those derivable from these by the invocation of the matrix Hermiteness property.

The rotation operators $\mathcal{C}_2(y')$ and $\mathcal{C}_3(z')$ defined in Table I wielded to the spin-orbital functions of eq. 34 brings the disclosures

$$\mathcal{C}_2(y')\gamma_6(\begin{smallmatrix}a\\b\end{smallmatrix}) = \pm\gamma_6(\begin{smallmatrix}b\\a\end{smallmatrix}), \quad \mathcal{C}_2(y')\gamma(\begin{smallmatrix}4\\5\end{smallmatrix}) = \pm i\gamma(\begin{smallmatrix}5\\4\end{smallmatrix})$$

and

$$\mathcal{C}_3(z')\gamma_6(\begin{smallmatrix}a\\b\end{smallmatrix}) = \omega^{\mp1/2}\gamma_6(\begin{smallmatrix}a\\b\end{smallmatrix}), \quad \mathcal{C}_3(z')\gamma(\begin{smallmatrix}4\\5\end{smallmatrix}) = \omega^{\pm3/2}\gamma(\begin{smallmatrix}4\\5\end{smallmatrix})$$

[recall footnote 27 of ref. 9 and that $\omega^{+1/2}$ and $\omega^{-1/2}$ and $\sigma(x' - z')$ and $\mathcal{C}_2(y')$ equals $i\sigma(x' - z')$ are equivalent. The latter equivalence follows as the spin-orbitals there tabulated are even functions, irrespective of the origin, t_{2g} or e_g, of the spin-orbitals, and $\mathcal{C}_2(y')v_{x,y,z} = -v_{y,x,z}$, $\mathcal{C}_3(z')v_{x,y,z} = v_{z,x,y}$ for any true or pseudo-vector $\vec{v}$ [Table I]. Therefore, when these operators are worked both internally and externally on a specimen matrix element like

$$\left\langle \gamma_{6(\begin{smallmatrix}a\\b\end{smallmatrix})}^{(7)}(t_{2g}) \left|\frac{\vec{p}}{m}\right| \gamma_5(t_{2g}) \right\rangle$$

we educe that

$$\mathcal{C}_2\langle\gamma_{6(\begin{smallmatrix}a\\b\end{smallmatrix})}^{(7)}(t_{2g})|v_{x,y,z}|\gamma_5(t_{2g})\rangle = \langle\gamma_{6(\begin{smallmatrix}b\\a\end{smallmatrix})}^{(7)}(t_{2g})|v_{x,y,z}|\gamma_5(t_{2g})\rangle = \pm i\langle\gamma_{6(\begin{smallmatrix}b\\a\end{smallmatrix})}^{(7)}(t_{2g})|v_{y,x,z}|\gamma_6(t_{2g})\rangle$$

and

$$\mathcal{C}_3\langle\gamma_{6(\begin{smallmatrix}a\\b\end{smallmatrix})}^{(7)}(t_{2g})|v_{x,y,z}|\gamma_5(t_{2g})\rangle = \langle\gamma_{6(\begin{smallmatrix}a\\b\end{smallmatrix})}^{(7)}(t_{2g})|v_{z,y,z}|\gamma_5(t_{2g})\rangle = \omega^{\mp1}\langle\gamma_{6(\begin{smallmatrix}a\\b\end{smallmatrix})}^{(7)}(t_{2g})|v_{z,x,y}|\gamma_5(t_{2g})\rangle, (\vec{v} = \vec{p}, \vec{m})$$

as this matrix element is instantaneously both a constant and a function of the denoted spin-orbitals. Thus we elicit

$$\langle\gamma_{6(\begin{smallmatrix}a\\b\end{smallmatrix})}^{(7)}(t_{2g})|v_{x,y,z}|\gamma_5(t_{2g})\rangle = \pm i\langle\gamma_{6(\begin{smallmatrix}b\\a\end{smallmatrix})}^{(7)}(t_{2g})|v_{y,x,z}|\gamma_5(t_{2g})\rangle$$

and

$$\langle\gamma_{6(\begin{smallmatrix}a\\b\end{smallmatrix})}^{(7)}(t_{2g})|v_{x,y,z}|\gamma_5(t_{2g})\rangle = \omega^{\mp1}\langle\gamma_{6(\begin{smallmatrix}a\\b\end{smallmatrix})}^{(7)}(t_{2g})|v_{z,x,y}|\gamma_5(t_{2g})\rangle, (\vec{v} = \vec{p}, \vec{m})$$

These relationships demonstrate, in particular, that

$$\left\langle \gamma_{6(\begin{smallmatrix}a\\b\end{smallmatrix})}^{(7)}(t_{2g}) \left|\frac{p_y}{m_y}\right| \gamma(t_{2g}) \right\rangle = \pm i\left\langle \gamma_{6(\begin{smallmatrix}b\\a\end{smallmatrix})}^{(7)}(t_{2g}) \left|\frac{p_x}{m_x}\right| \gamma_5(t_{2g}) \right\rangle$$

and

$$\left\langle \gamma_{6(\begin{smallmatrix}a\\b\end{smallmatrix})}^{(7)}(t_{2g}) \left|\frac{p_z}{m_z}\right| \gamma_5(t_{2g}) \right\rangle = \omega^{\mp1}\left\langle \gamma_{6(\begin{smallmatrix}a\\b\end{smallmatrix})}^{(7)}(t_{2g}) \left|\frac{p_y}{m_y}\right| \gamma_5(t_{2g}) \right\rangle = \omega^{\pm1}\left\langle \gamma_{6(\begin{smallmatrix}a\\b\end{smallmatrix})}^{(7)}(t_{2g}) \left|\frac{p_x}{m_x}\right| \gamma_5(t_{2g}) \right\rangle$$

and so

$$\left\langle \gamma_6\binom{a}{b}{}^{(7)}(t_{2g}) \left| \frac{\vec{p}}{m} \right| \gamma_5(t_{2g}) \right\rangle =$$

$$(\hat{i} + \omega^{\mp 1}\hat{j} + \omega^{\mp 2}\hat{k}) \left\langle \gamma_6\binom{a}{b}{}^{(7)}(t_{2g}) \left| \frac{p_x}{m_x} \text{ or } \frac{\omega^{\pm 1}p_y}{\omega^{\pm 1}m_y} \text{ or } \frac{\omega^{\pm 2}p_z}{\omega^{\pm 2}m_z} \right| \gamma_5(t_{2g}) \right\rangle$$

[see the Appendix for other examples]. The conjunction of the $\mathfrak{C}_2(y')$ and $\mathfrak{C}_3(z')$ pronouncements then yields

$$\left\langle \gamma_6\binom{a}{b}{}^{(7)}(t_{2g}) \left| \frac{\vec{p}}{m} \right| \gamma_5(t_{2g}) \right\rangle = \omega^{\pm 1}(\hat{i} + \omega^{\mp 1}\hat{j} + \omega^{\mp 2}\hat{k})$$

$$\left\langle \gamma_6\binom{a}{b}{}^{(7)}(t_{2g}) \left| \frac{p_y}{m_y} \right| \gamma_5(t_{2g}) \right\rangle =$$

$$\pm i\omega^{\pm 1}(\hat{i} + \omega^{\mp 1}\hat{j} + \omega^{\mp 2}\hat{k}) \left\langle \gamma_6\binom{b}{a}{}^{(7)}(t_{2g}) \left| \frac{p_x}{m_x} \right| \gamma_5(t_{2g}) \right\rangle$$

or

$$\left\langle \gamma_6\binom{a}{b}{}^{(7)}(t_{2g}) \left| \frac{\vec{p}}{m} \right| \gamma_5(t_{2g}) \right\rangle = \pm i\omega^{\pm 1} \left\langle \gamma_6\binom{b}{a}{}^{(7)}(t_{2g}) \left| \frac{\vec{p}}{m} \right| \gamma_5(t_{2g}) \right\rangle_*$$

where

$$\left\langle \gamma_6\binom{b}{a}{}^{(7)}(t_{2g}) \left| \frac{\vec{p}}{m} \right| \gamma_5(t_{2g}) \right\rangle_*$$

is a matrix element identical with

$$\left\langle \gamma_6\binom{b}{a}{}^{(7)}(t_{2g}) \left| \frac{\vec{p}}{m} \right| \gamma_5(t_{2g}) \right\rangle$$

except that its vectorial direction

$$(\hat{i} + \omega^{\mp 1}\hat{j} + \omega^{\mp 2}\hat{k})$$

is the complex conjugate of that of

$$\left\langle \gamma_6\binom{b}{a}{}^{(7)}(t_{2g}) \left| \frac{\vec{p}}{m} \right| \gamma_5(t_{2g}) \right\rangle$$

In the whole, as an aftermath of the rotational symmetry, we have for the spin-orbitals of either or both t_{2g} and e_g ancestry the connections

$$\left\langle \gamma_{6b} \left| \frac{\vec{p}}{m} \right| \gamma_{6b} \right\rangle = - \left\langle \gamma_{6a} \left| \frac{\vec{p}}{m} \right| \gamma_{6a} \right\rangle,$$

$$\left\langle \gamma_{6b} \left| \frac{\vec{p}}{m} \right| \gamma_{6a} \right\rangle = \omega \left\langle \gamma_{6c} \left| \frac{\vec{p}}{m} \right| \gamma_{6b} \right\rangle_*$$

$$\left\langle \gamma_{6b} \left| \frac{\vec{p}}{m} \right| \gamma_4 \right\rangle = i\omega^{-1} \left\langle \gamma_{6a} \left| \frac{\vec{p}}{m} \right| \gamma_4 \right\rangle_*,$$

$$\left\langle \gamma_{6b} \left| \frac{\vec{p}}{m} \right| \gamma_5 \right\rangle = -i\omega^{-1} \left\langle \gamma_{6a} \left| \frac{\vec{p}}{m} \right| \gamma_5 \right\rangle_*$$

$$\left\langle \gamma\binom{5}{4} \left| \frac{\vec{p}}{m} \right| \gamma\binom{5}{4} \right\rangle = \left\langle \gamma\binom{5}{4} \left| \frac{\vec{p}}{m} \right| \gamma\binom{5}{4} \right\rangle_*,$$

$$\left\langle \gamma\binom{5}{4} \left| \frac{\vec{p}}{m} \right| \gamma\binom{4}{4} \right\rangle = \left\langle \gamma\binom{4}{4} \left| \frac{\vec{p}}{m} \right| \gamma\binom{5}{5} \right\rangle_*$$

These ties together with those of the previous paragraph and of eq. 49 suffice to inpanel all the necessary matrix terms.

It is instructive to rederive the issue of the last paragraph in a somewhat different way. We do this act by transferring to the trigonal basis for the vectors $\vec{p}$ and $\vec{m}$, here given the collective symbol, $\vec{v}$, that is, $\vec{v} \equiv \vec{p}, \vec{m}$. In this basis, $v \equiv v_x'\hat{i}' + v_y'\hat{j}' + v_z'\hat{k}' \equiv v_x\hat{i} + v_y\hat{j} + v_z\hat{k}$, where both $v_{x',y',z'}$ and $\hat{i}', \hat{j}', \hat{k}'$ are related to their tetragonal analogs $v_{x,y,z}$ and $\hat{i}, \hat{j}, \hat{k}$, serially, by the transformation matrix printed in footnote 28 of ref. 9. [Please note that as this matrix is orthonormal its transpose is also its inverse. The coordinate systems in question are pictured in Fig. 2 and 7a]. A rearrangement of the trigonal representation for the vector $\vec{v}$ can always be made such that

$$\vec{v} \equiv 2^{-1/2}(v_{z'} + iv_{y'}) \cdot 2^{-1/2}(\hat{i}' - i\hat{j}') +$$

$$2^{-1/2}(v_{z'} - iv_{y'}) \cdot 2^{-1/2}(\hat{i}' + i\hat{j}') + v_{z'}\hat{k}' \equiv v_{+}'\hat{k}_{-}' +$$

$$v_{-}'\hat{k}_{+}' + v_0'\hat{k}_0,$$

as is quickly verified by multiplicative expansion of the rearrangement. If the components and unit vector bases

$$v_{\pm}' = 2^{-1/2}(v_{z'} \pm iv_{y'}), \quad v_0' = v_{z'} \text{ and}$$

$$\hat{k}_{\pm}' = 2^{-1/2}(\hat{i}' \pm i\hat{j}'), \quad \hat{k}_0' = \hat{k}'$$

are re-expressed in the tetragonal representation by means of the coordinate transformation mentioned above, we find

$$v_j' = 3^{-1/2}\omega^j(v_x + \omega^j v_y + \omega^{2j}v_z), \quad \hat{k}_j' = 3^{-1/2}\omega^j(\hat{i} + \omega^j\hat{j} + \omega^{2j}\hat{k}),$$

$$(j = 0, \pm 1)$$

and

$$\vec{v} \equiv 1/3[(v_x + \omega v_y + \omega^2 v_z)(\hat{i} + \omega^{-1}\hat{j} + \omega^{-2}\hat{k}) + (v_x +$$

$$\omega^{-1}v_y + \omega^{-2}v_z)(\hat{i} + \omega\hat{j} + \omega^2\hat{k}) + (v_x + v_y + v_z)(\hat{i} + \hat{j} + \hat{k})]$$

The symmetry operations $\mathfrak{C}_2(y')$ and $\mathfrak{C}_3(z')$ put to the trigonal vector components v_j', $(j = 0, \pm 1)$, establish $\mathfrak{C}_2 v_j' = -v_{-j}'$ and $\mathfrak{C}_3 v_j' = \omega^j v_j'$, $(j = 0, \pm 1)$, as may be speedily confirmed in either their trigonal or tetragonal representations penciled in the previous sentence. Therefore, if $\langle v \rangle$ designates a matrix constituent of $\vec{v}$, and if the wave function product characteristic of this matrix constituent transforms as ω^j under $\mathfrak{C}_3(z')$, we can say that $\langle v \rangle$ will possess the vectorial dependence $\hat{k}_j'$, $(j = 0, \pm 1)$. In this event we shall obtain $\langle v_z \rangle = \omega^j \langle v_y \rangle = \omega^{2j} \langle v_x \rangle$, so that

$$\langle v_l' \rangle = 3^{-1/2}\omega^l \langle v_x \rangle (1 + \omega^{(l+j)} + \omega^{2(l+j)}) = 3^{1/2}\omega^l \langle v_x \rangle \delta_{l,-j},$$

$$(j, l = 0, \pm 1)$$

and

$$\vec{v} \equiv \left\langle \sum_{l=0,\pm 1} v_l'\hat{k}'_{-l} \right\rangle = 3^{1/2}\omega^{-j} \langle v_x \rangle \hat{k}_j' = (\hat{i} + \omega^j\hat{j} + \omega^{2j}\hat{k})\langle v_x \rangle$$

as previously. The use of $\mathfrak{C}_2(y')$ yields the other desired connections which bring out the harvest reaped before [e.g.

$$\langle \gamma_6\binom{a}{b}(t_{2g})|\vec{v}| \gamma_5(t_{2g}) \rangle = \hat{k}_{\mp}'\langle \gamma_6\binom{a}{b}{}^{(7)}(t_{2g})|v_{\pm}'| \gamma_5(t_{2g}) \rangle =$$

$$\hat{k}_{\mp}'\langle \pm \gamma_6\binom{b}{a}{}^{(7)}(t_{2g}) |-v_{\mp}'| - i\gamma_5(t_{2g}) \rangle =$$

$$\pm i\omega^{\pm 1}\langle \gamma_6\binom{b}{a}{}^{(7)}(t_{2g})|\vec{v}| \gamma_5(t_{2g}) \rangle_*]$$

Similar but different trigonal symmetry arguments for the evaluation of trigonal matrix elements have been given independently by (b) W. E. Moffitt, J. Chem. Phys., 25, 1189 (1956), and (c) S. Sugano and Y. Tanabe, J. Phys. Soc. Japan, 13, 880 (1958).

(26) The null value of the matrix elements

$$\langle \gamma_6\binom{a}{b}|\vec{p}| \gamma_6\binom{a}{b} \rangle, \quad \langle \gamma_6\binom{a}{b}|\vec{p}| \gamma_6\binom{a}{b} \rangle, \quad \langle \gamma\binom{4}{5}|\vec{p}| \gamma\binom{4}{5} \rangle, \text{ and } \langle \gamma\binom{5}{4}|\vec{p}| \gamma\binom{4}{5} \rangle$$

when both spin-orbitals have the same genesis is an offshoot of Kramers' theorem which states that the degeneracy of Kramers' doublets cannot be removed by electric fields [cf. Fick,[25a] Griffith,[34] and Kramers[79]]. In the present case this universal theorem is facilely substantiated by either marking that the momentum reversal and rotation operations, $\mathcal{K}$ and $\mathfrak{C}_2(y')$, and matrix Hermiteness require these elements to be zero, or that the antisymmetric direct product of the integrand wave functions does not contain the D_3 species A_2 and E of $\vec{p}$. [Since the composite angular momentum operator $\vec{m}$ is an imaginary operator, $\vec{m}^*$ equals $-\vec{m}$, it is the symmetric direct product of the integrand wave functions which determines the nullity of its matrix elements (consult Griffith,[34] for example). As the pertinent symmetric direct products all contain either the D_3 species A_1 and A_2 (γ_4, γ_5) or A_2 and E (γ_6), the relevant angular momentum matrix terms do not all group theoretically vanish, a forecast which is obviously required if the last six entries of eq. 49 are to be valid.]

(27) A. D. Liehr, to be published.

(a) No Configuration Interaction: Zero Spin-Orbit Forces. The substitution of eq. 47 into 50 and 51 gives the appropriate basic one-electron rotational and spectral strengths in the absence of spin-orbit forces. To condense the resultant expressions, we now take the normalization constants and variational parameters to be real in accord with our previous discussion of § 1 and footnote 10. We then have

$$\mathfrak{R}[a_1(t_{2g}) \longrightarrow a_1(t_{2g})] = \mathfrak{S}[a_1(t_{2g}) \longrightarrow a_1(t_2g)] \equiv 0$$

$$\mathfrak{R}[(a_1(t_{2g}) \longrightarrow e_\pm(t_{2g})] = -\sqrt{3/2}e\mu_B k_p \sin \alpha\, N_{a_1(t)}{}^2 N_{e(t)}{}^2$$
$$\times (K_{2A_s}(\xi - \eta) + \eta K_{3A_s})$$

$$\mathfrak{S}[a_1(t_{2g}) \longrightarrow e_\pm(t_{2g})] = {}^3/_2 e^2 k_p{}^2 \sin^2 \alpha\, N_{a_1(t)}{}^2 N_{e(t)}{}^2 \times$$
$$(K_{2A_s}(\xi - \eta) + \eta K_{3A_s})^2$$

$$\mathfrak{R}[a_1(t_{2g}) \to e_\pm(e_g)] = \frac{\sqrt{3}}{2} e\mu_B k_p \sin \alpha\, N_{a_1(t)}{}^2 N_{e(e)}{}^2 \times$$
$$(\sqrt{3}K_{4A_s} + K_{7A_s})\eta$$

$$\mathfrak{S}[a_1(t_{2g}) \longrightarrow e_\pm(e_g)] = {}^3/_8 e^2 k_p{}^2 \sin^2 \alpha\, N_{a_1(t)}{}^2 N_{e(e)}{}^2 \times$$
$$(\sqrt{3}K_{4A_s} + K_{7A_s})^2\eta^2$$

$$\mathfrak{R}[e_\pm(t_{2g}) \longrightarrow e_\pm(t_{2g})] = \mathfrak{S}[e_\pm(t_{2g}) \longrightarrow e_\pm(t_{2g})] \equiv 0$$

$$\mathfrak{R}[e_\pm(t_{2g}) \longrightarrow e_\pm(e_g)] =$$
$$\sqrt{3}e\mu_B k_p \sin \alpha\, N_{e(t)}{}^2 N_{e(e)}{}^2 K_{7A_s}\xi$$

$$\mathfrak{S}[e_\pm(t_{2g}) \longrightarrow e_\pm(e_g)] = {}^3/_2 e^2 k_p{}^2 \sin^2 \alpha\, N_{e(t)}{}^2 N_{e(e)}{}^2 K_{7A_s}{}^2\xi^2$$

$$\mathfrak{R}[e_\pm(t_{2g}) \longrightarrow e_\mp(t_{2g})] \equiv 0$$

$$\mathfrak{S}[e_\pm(t_{2g}) \longrightarrow e_\mp(t_{2g})] = 6e^2 k_p{}^2 \sin^2 \alpha\, N_{e(t)}{}^4 \times$$
$$(K_{3A_s} + K_{2A_s})^2\xi^2$$

$$\mathfrak{R}[e_\pm(t_{2g}) \longrightarrow e_\mp(e_g)] = \frac{\sqrt{3}}{2} e\mu_B k_p \sin \alpha\, N_{e(t)}{}^2 N_{e(e)}{}^2 \times$$
$$(\sqrt{3}K_{4A_s} - K_{7A_s})\xi$$

$$\mathfrak{S}[e_\pm(t_{2g}) \longrightarrow e_\mp(e_g)] = {}^3/_8 e^2 k_p{}^2 \sin^2 \alpha\, N_{e(t)}{}^2 N_{e(e)}{}^2 \times$$
$$(\sqrt{3}K_{4A_s} - K_{7A_s})^2\xi^2$$

$$\mathfrak{R}[e_\pm(e_g) \longrightarrow e_\pm(e_g)] = \mathfrak{S}[e_\pm(e_g) \longrightarrow e_\pm(e_g)] \equiv 0$$

$$\mathfrak{R}[e_\pm(e_g) \longrightarrow e_\mp(e_g)] \equiv 0, \quad \mathfrak{S}[e_\pm(e_g) \longrightarrow e_\mp(e_g)] = 0$$
$$(52)$$

These individual rotational and spectral strengths sum to the total rotational and spectral strengths given below.

$$\mathfrak{R}[a_1(t_{2g}) \longrightarrow a_1(t_{2g})] = \mathfrak{S}[a_1(t_{2g}) \longrightarrow a_1(t_{2g})] \equiv 0$$

$$\mathfrak{R}[a_1(t_{2g}) \longrightarrow e(t_{2g})] = 2\mathfrak{R}[a_1(t_{2g}) \longrightarrow e_\pm(t_{2g})]$$

$$\mathfrak{S}[a_1(t_{2g}) \longrightarrow e(t_{2g})] = 2\mathfrak{S}[a_1(t_{2g}) \longrightarrow e_\pm(t_{2g})]$$

$$\mathfrak{R}[a_1(t_{2g}) \longrightarrow e(e_g)] = 2\mathfrak{R}[a_1(t_{2g}) \longrightarrow e_\pm(e_g)]$$

$$\mathfrak{S}[a_1(t_{2g}) \longrightarrow e(e_g)] = 2\mathfrak{S}[a_1(t_{2g}) \longrightarrow e_\pm(e_g)]$$

$$\mathfrak{R}[e(t_{2g}) \longrightarrow e(t_{2g})] \equiv 0$$

$$\mathfrak{S}[e(t_{2g}) \longrightarrow e(t_{2g})] = \mathfrak{S}[e_\pm(t_{2g}) \longrightarrow e_\mp(t_{2g})]$$

$$\mathfrak{R}[e(t_{2g}) \longrightarrow e(e_g)] = \mathfrak{R}[e_\pm(t_{2g}) \longrightarrow e_\pm(e_g)] +$$
$$\mathfrak{R}[e_\mp(t_{2g}) \longrightarrow e_\mp(e_g)] =$$
$$\frac{\sqrt{3}}{2} e\mu_B k_p \sin \alpha\, N_{e(t)}{}^2 N_{e(e)}{}^2(\sqrt{3}K_{4A_s} + K_{7A_s})\xi$$

$$\mathfrak{S}[e(t_{2g}) \longrightarrow e(e_g)] = \mathfrak{S}[e_\pm(t_{2g}) \longrightarrow e_\pm(e_g)] +$$
$$\mathfrak{S}[e_\pm(t_{2g}) \longrightarrow e_\mp(e_g)] =$$
$${}^3/_8 e^2 k_p{}^2 \sin^2 \alpha\, N_{e(t)}{}^2 N_{e(e)}{}^2(4K_{7A_s}{}^2 + (\sqrt{3}K_{4A_s} - K_{7A_s})^2)\xi^2$$

$$\mathfrak{R}[e(e_g) \longrightarrow e(e_g)] \equiv 0, \quad \mathfrak{S}[e(e_g) \longrightarrow e(e_g)] = 0 \quad (53)$$

(b) No Configuration Interaction: Nonzero Spin-Orbit Forces. The insertion of eq. 49 and its momentum reversal related counterparts[25] into eq. 50 and 51 produces the apropos basic one-electron rotational and spectral strengths registered below.[28]

$$\mathfrak{R}[\gamma_6({}^3_5){}^{(8)}(t_{2g}) \longrightarrow \gamma_6({}^3_5){}^{(7)}(t_{2g})] =$$
$$\mathfrak{S}[\gamma_6({}^3_5){}^{(8)}(t_{2g}) \longrightarrow \gamma_6({}^3_5){}^{(7)}(t_{2g})] = 0$$

$$\mathfrak{R}[\gamma_6({}^3_5){}^{(8)}(t_{2g}) \longrightarrow \gamma_6({}^3_5){}^{(7)}(t_{2g})] =$$
$$-\sqrt{1/6}\, e\mu_B k_p \sin \alpha\, N_{a_1(t)}N_{e(t)}(2 + N_{a_1(t)}N_{e(t)}) \times$$
$$(K_{2A_s}(\xi - \eta) + \eta K_{3A_s})$$

$$\mathfrak{S}[\gamma_6({}^3_5){}^{(8)}(t_{2g}) \longrightarrow \gamma_6({}^b_a){}^{(7)}(t_{2g})] =$$
$${}^3/_2 e^2 k_p{}^2 \sin^2 \alpha\, N_{a_1(t)}{}^2 N_{e(t)}{}^2(K_{2A_s}(\xi - \eta) + \eta K_{3A_s})^2$$

$$\mathfrak{R}[\gamma_6({}^3_5){}^{(8)}(t_{2g}) \longrightarrow \gamma_{4\,\text{or}\,5}(t_{2g})] =$$
$$-\frac{(1 - N_{a_1(t)}N_{e(t)})}{(2 + N_{a_1(t)}N_{e(t)})} \mathfrak{R}[\gamma_6({}^3_5){}^{(8)}(t_{2g}) \longrightarrow \gamma_6({}^b_a){}^{(7)}(t_{2g})]$$

---

(28) The coincidence of certain rotational and spectral strengths follows quite naturally from the use of the connections of footnote 25. As a sample, since by footnote 25 we can write

$$\left\langle \gamma_{6a} \left| \frac{\vec{\mathbf{p}}}{m} \right| \gamma({}^4_5) \right\rangle = \pm i \left[{}^+_-\right] \left\langle \gamma_{6b} \left| \frac{\vec{\mathbf{p}}}{m} \right| \gamma({}^5_4) \right\rangle^*$$

and

$$\left\langle \gamma_{6b} \left| \frac{\vec{\mathbf{p}}}{m} \right| \gamma({}^5_4) \right\rangle = \mp i\omega^{-1} \left\langle \gamma_{6a} \left| \frac{\vec{\mathbf{p}}}{m} \right| \gamma({}^5_4) \right\rangle_*$$

we see that

$$\left\langle \gamma_{6a} \left| \frac{\vec{\mathbf{p}}}{m} \right| \gamma({}^4_5) \right\rangle = \omega \left[{}^-_+\right] \left\langle \gamma_{6a} \left| \frac{\vec{\mathbf{p}}}{m} \right| \gamma({}^5_4) \right\rangle^*_*$$

and so

$$\mathfrak{R}[\gamma_{6a} \longrightarrow \gamma_4] = \mathfrak{R}[\gamma_{6b} \longrightarrow \gamma_4] =$$
$$\mathfrak{R}[\gamma_{6a} \longrightarrow \gamma_5] = \mathfrak{R}[\gamma_{6b} \longrightarrow \gamma_5]$$

and similarly for

$$\mathfrak{S}[\gamma_{6a\,\text{or}\,b} \longrightarrow \gamma_{4\,\text{or}\,5}]$$

$$S[\gamma_{6(\frac{a}{b})}{}^{(8)}(t_{2g}) \longrightarrow \gamma_{4 \text{ or } 5}\ (t_{2g})] =$$

$$\tfrac{1}{3}S[\gamma_{6(\frac{a}{b})}{}^{(8)}(t_{2g}) \longrightarrow \gamma_{6(\frac{a}{b})}{}^{(7)}(t_{2g})] +$$

$$e^2 k_p{}^2 \sin^2\alpha\ N_{e(t)}{}^4(K_{3A_1} + K_{2A_1})^2\xi^2$$

$$\mathfrak{R}[\gamma_{6(\frac{a}{b})}{}^{(7)}(t_{2g}) \longrightarrow \gamma_{4 \text{ or } 5}\ (t_{2g})] =$$

$$\tfrac{1}{2}\mathfrak{R}[\gamma_{6(\frac{a}{b})}{}^{(8)}(t_{2g}) \longrightarrow \gamma_{6(\frac{b}{a})}{}^{(7)}(t_{2g})]$$

$$S[\gamma_{6(\frac{a}{b})}{}^{(7)}(t_{2g}) \longrightarrow \gamma_{4 \text{ or } 5}\ (t_{2g})] =$$

$$\tfrac{1}{6}S[\gamma_{6(\frac{a}{b})}{}^{(8)}(t_{2g}) \longrightarrow \gamma_{6(\frac{b}{a})}{}^{(7)}(t_{2g})] +$$

$$2e^2 k_p{}^2 \sin^2\alpha\ N_{e(t)}{}^4(K_{3A_1} + K_{2A_1})^2\xi^2$$

$$\mathfrak{R}[\gamma_{(\frac{4}{5})}(t_{2g}) \longrightarrow \gamma_{(\frac{4}{5})}(e_g)] \equiv S[\gamma_{(\frac{4}{5})}(t_{2g}) \longrightarrow \gamma_{(\frac{4}{5})}(e_g)] \equiv 0$$

$$\mathfrak{R}[\gamma_{(\frac{5}{4})}(t_{2g}) \longrightarrow \gamma_{(\frac{4}{5})}(e_g)] =$$

$$\sqrt{3}\ e\mu_B k_p \sin\alpha\ N_{e(t)}{}^2 N_{e(e)}{}^2 K_{7A_1}\xi$$

$$S[\gamma_{(\frac{5}{4})}(t_{2g}) \longrightarrow \gamma_{(\frac{4}{5})}(e_g)] =$$

$$\tfrac{3}{2}e^2 k_p{}^2 \sin^2\alpha\ N_{e(t)}{}^2 N_{e(e)}{}^2 K_{7A_1}{}^2\xi^2$$

$$\mathfrak{R}[\gamma_{6(\frac{a}{b})}{}^{(7)}(t_{2g}) \longrightarrow \gamma_{4 \text{ or } 5}\ (e_g)] =$$

$$\tfrac{1}{2}\sqrt{\tfrac{1}{3}}\ e\mu_B k_p \sin\alpha\ N_{e(e)}{}^2(N_{e(t)}{}^2(\sqrt{3}K_{4A_1} - K_{7A_1})\xi + \tfrac{1}{2}N_{a_1(t)}{}^2(\sqrt{3}K_{4A_1} + K_{7A_1})\eta)$$

$$S[\gamma_{6(\frac{a}{b})}{}^{(7)}(t_{2g}) \longrightarrow \gamma_{4 \text{ or } 5}\ (e_g)] =$$

$$\tfrac{1}{8}e^2 k_p{}^2 \sin^2\alpha\ N_{e(e)}{}^2(N_{e(t)}{}^2(\sqrt{3}K_{4A_1} - K_{7A_1})^2\xi^2 + \tfrac{1}{2}N_{a_1(t)}{}^2(\sqrt{3}K_{4A_1} + K_{7A_1})^2\eta^2)$$

$$\mathfrak{R}[\gamma_{6(\frac{a}{b})}{}^{(8)}(t_{2g}) \longrightarrow \gamma_{4 \text{ or } 5}\ (e_g)] =$$

$$\tfrac{1}{2}\sqrt{\tfrac{1}{3}}\ e\mu_B k_p \sin\alpha\ N_{e(e)}{}^2(\tfrac{1}{2}N_{e(t)}{}^2(\sqrt{3}K_{4A_1} - K_{7A_1})\xi + N_{a_1(t)}{}^2(\sqrt{3}K_{4A_1} + K_{7A_1})\eta)$$

$$S[\gamma_{6(\frac{a}{b})}{}^{(8)}(t_{2g}) \longrightarrow \gamma_{4 \text{ or } 5}\ (e_g)] =$$

$$\tfrac{1}{8}e^2 k_p{}^2 \sin^2\alpha\ N_{e(e)}{}^2(\tfrac{1}{2}N_{e(t)}{}^2(\sqrt{3}K_{4A_1} - K_{7A_1})^2\xi^2 + \eta^2 N_{a_1(t)}{}^2(\sqrt{3}K_{4A_1} + K_{7A_1})^2)$$

$$\mathfrak{R}[\gamma_{4 \text{ or } 5}\ (t_{2g}) \longrightarrow \gamma_{6(\frac{a}{b})}(e_g)] =$$

$$\frac{\sqrt{3}}{4}\ e\mu_B k_p \sin\alpha\ N_{e(t)}{}^2 N_{e(e)}{}^2(\sqrt{3}K_{4A_1} - K_{7A_1})\xi$$

$$S[\gamma_{4 \text{ or } 5}\ (t_{2g}) \longrightarrow \gamma_{6(\frac{a}{b})}(e_g)] =$$

$$\tfrac{3}{16}e^2 k_p{}^2 \sin^2\alpha\ N_{e(t)}{}^2 N_{e(e)}{}^2(\sqrt{3}K_{4A_1} - K_{7A_1})^2\xi^2$$

$$\mathfrak{R}[\gamma_{6(\frac{a}{b})}{}^{(7)}(t_{2g}) \longrightarrow \gamma_{6(\frac{a}{b})}(e_g)] =$$

$$\frac{2}{\sqrt{3}}\ e\mu_B k_p \sin\alpha\ N_{e(t)}{}^2 N_{e(e)}{}^2 K_{7A_1}\xi$$

$$S[\gamma_{6(\frac{a}{b})}{}^{(7)}(t_{2g}) \longrightarrow \gamma_{6(\frac{a}{b})}(e_g)] =$$

$$e^2 k_p{}^2 \sin^2\alpha\ N_{e(t)}{}^2 N_{e(e)}{}^2 K_{7A_1}{}^2\xi^2$$

$$\mathfrak{R}[\gamma_{6(\frac{a}{b})}{}^{(7)}(t_{2g}) \longrightarrow \gamma_{6(\frac{b}{a})}(e_g)] =$$

$$\tfrac{1}{2}\sqrt{\tfrac{1}{3}}\ e\mu_B k_p \sin\alpha\ N_{a_1(t)}{}^2 N_{e(e)}{}^2(\sqrt{3}K_{4A_1} + K_{7A_1})\eta$$

$$S[\gamma_{6(\frac{a}{b})}{}^{(7)}(t_{2g}) \longrightarrow \gamma_{6(\frac{a}{b})}(e_g)] =$$

$$\tfrac{1}{8}e^2 k_p{}^2 \sin^2\alpha\ N_{a_1(t)}{}^2 N_{e(e)}{}^2(\sqrt{3}K_{4A_1} + K_{7A_1})^2\eta^2$$

$$\mathfrak{R}[\gamma_{6(\frac{a}{b})}{}^{(8)}(t_{2g}) \longrightarrow \gamma_{6(\frac{a}{b})}(e_g)] =$$

$$\tfrac{1}{2}\mathfrak{R}[\gamma_{6(\frac{a}{b})}{}^{(7)}(t_{2g}) \longrightarrow \gamma_{6(\frac{a}{b})}(e_g)]$$

$$S[\gamma_{6(\frac{a}{b})}{}^{(8)}(t_{2g}) \longrightarrow \gamma_{6(\frac{a}{b})}(e_g)] =$$

$$\tfrac{1}{2}S[\gamma_{6(\frac{a}{b})}{}^{(7)}(t_{2g}) \longrightarrow \gamma_{6(\frac{a}{b})}(e_g)]$$

$$\mathfrak{R}[\gamma_{6(\frac{a}{b})}{}^{(8)}(t_{2g}) \longrightarrow \gamma_{6(\frac{b}{a})}(e_g)] =$$

$$2\mathfrak{R}[\gamma_{6(\frac{a}{b})}{}^{(7)}(t_{2g}) \longrightarrow \gamma_{6(\frac{b}{a})}(e_g)]$$

$$S[\gamma_{6(\frac{a}{b})}{}^{(8)}(t_{2g}) \longrightarrow \gamma_{6(\frac{b}{a})}(e_g)] =$$

$$2S[\gamma_{6(\frac{a}{b})}{}^{(7)}(t_{2g}) \longrightarrow \gamma_{6(\frac{b}{a})}(e_g)]$$

$$\mathfrak{R}[\gamma_{(\frac{5}{4})}(e_g) \longrightarrow \gamma_{(\frac{5}{4})}(e_g)] \equiv S[\gamma_{(\frac{5}{4})}(e_g) \longrightarrow \gamma_{(\frac{5}{4})}(e_g)] \equiv 0$$

$$\mathfrak{R}[\gamma_{(\frac{5}{4})}(e_g) \longrightarrow \gamma_{(\frac{4}{5})}(e_g)] \equiv S[\gamma_{(\frac{5}{4})}(e_g) \longrightarrow \gamma_{(\frac{4}{5})}(e_g)] \equiv 0$$

$$\mathfrak{R}[\gamma_{6(\frac{a}{b})}(e_g) \longrightarrow \gamma_{4 \text{ or } 5}\ (e_g)] =$$

$$S[\gamma_{6(\frac{a}{b})}(e_g) \longrightarrow \gamma_{4 \text{ or } 5}\ (e_g)] = 0$$

$$\mathfrak{R}[\gamma_{6(\frac{a}{b})}(e_g) \longrightarrow \gamma_{6(\frac{a}{b})}(e_g)] \equiv$$

$$S[\gamma_{6(\frac{a}{b})}(e_g) \longrightarrow \gamma_{6(\frac{a}{b})}(e_g)] \equiv 0$$

$$\mathfrak{R}[\gamma_{6(\frac{a}{b})}(e_g) \longrightarrow \gamma_{6(\frac{b}{a})}(e_g)] \equiv$$

$$S[\gamma_{6(\frac{a}{b})}(e_g) \longrightarrow \gamma_{6(\frac{b}{a})}(e_g)] \equiv 0$$

$$\mathfrak{R}[\gamma_{6(\frac{a}{b})}{}^{(\frac{7}{8})}(t_{2g}) \longrightarrow \gamma_{6(\frac{a}{b})}{}^{(\frac{7}{8})}(t_{2g})] \equiv$$

$$S[\gamma_{6(\frac{a}{b})}{}^{(\frac{7}{8})}(t_{2g}) \longrightarrow \gamma_{6(\frac{a}{b})}{}^{(\frac{7}{8})}(t_{2g})] \equiv 0$$

$$\mathfrak{R}[\gamma_{6(\frac{a}{b})}{}^{(\frac{7}{8})}(t_{2g}) \longrightarrow \gamma_{6(\frac{b}{a})}{}^{(\frac{7}{8})}(t_{2g})] \equiv$$

$$S[\gamma_{6(\frac{a}{b})}{}^{(\frac{7}{8})}(t_{2g}) \longrightarrow \gamma_{6(\frac{b}{a})}{}^{(\frac{7}{8})}(t_{2g})] \equiv 0$$

$$\mathfrak{R}[\gamma_{(\frac{5}{4})}(t_{2g}) \longrightarrow \gamma_{(\frac{5}{4})}(t_{2g})] \equiv S[\gamma_{(\frac{5}{4})}(t_{2g}) \longrightarrow \gamma_{(\frac{5}{4})}(t_{2g})] \equiv 0$$

$$\mathfrak{R}[\gamma_{(\frac{5}{4})}(t_{2g}) \longrightarrow \gamma_{(\frac{4}{5})}(t_{2g})] \equiv$$

$$S[\gamma_{(\frac{5}{4})}(t_{2g}) \longrightarrow \gamma_{(\frac{4}{5})}(t_{2g})] \equiv 0 \quad (54)$$

These monadal rotational and spectral strengths add to the whole rotational and spectral strengths printed beneath.

$$\mathfrak{R}[\gamma_6{}^{(8)}(t_{2g}) \longrightarrow \gamma_6{}^{(7)}(t_{2g})] =$$

$$\mathfrak{R}[\gamma_{6(\frac{a}{b})}{}^{(8)}(t_{2g}) \longrightarrow \gamma_{6(\frac{a}{b})}{}^{(7)}(t_{2g})]$$

$$S[\gamma_6{}^{(8)}(t_{2g}) \longrightarrow \gamma_6{}^{(7)}(t_{2g})] =$$

$$S[\gamma_{6(\frac{a}{b})}{}^{(8)}(t_{2g}) \longrightarrow \gamma_{6(\frac{a}{b})}{}^{(7)}(t_{2g})]$$

$$\mathfrak{R}[\gamma_6{}^{(8)}(t_{2g}) \longrightarrow \gamma_{4 \text{ or } 5}\ (t_{2g})] =$$

$$\mathfrak{R}[\gamma_{6(\frac{a}{b})}{}^{(8)}(t_{2g}) \longrightarrow \gamma_{4 \text{ or } 5}\ (t_{2g})]$$

$$S[\gamma_6{}^{(8)}(t_{2g}) \longrightarrow \gamma_{4 \text{ or } 5}\ (t_{2g})] =$$

$$S[\gamma_{6(\frac{a}{b})}{}^{(8)}(t_{2g}) \longrightarrow \gamma_{4 \text{ or } 5}\ (t_{2g})]$$

$$\mathcal{R}[\gamma_6{}^{(7)}(t_{2g}) \longrightarrow \gamma_{4\text{ or }5}(t_{2g})] =$$
$$\tfrac{1}{2}\mathcal{R}[\gamma_6{}^{(8)}(t_{2g}) \longrightarrow \gamma_6{}^{(7)}(t_{2g})]$$

$$\mathcal{S}[\gamma_6{}^{(7)}(t_{2g}) \longrightarrow \gamma_{4\text{ or }5}(t_{2g})] =$$
$$\tfrac{1}{6}\mathcal{S}[\gamma_6{}^{(8)}(t_{2g}) \longrightarrow \gamma_6{}^{(7)}(t_{2g})] +$$
$$2e^2 k_p{}^2 \sin^2\alpha\, N_{e(t)}{}^4 (K_{3A_3} + K_{2A_3})^2 \xi^2$$

$$\mathcal{R}[\gamma({}^4_5)(t_{2g}) \longrightarrow \gamma({}^4_5)(e_g)] \equiv \mathcal{S}[\gamma({}^4_5)(t_{2g}) \longrightarrow \gamma({}^4_5)(e_g)] \equiv 0$$

$$\mathcal{R}[\gamma({}^5_4)(t_{2g}) \longrightarrow \gamma({}^4_5)(e_g)] =$$
$$\sqrt{3}\, e\mu_B k_p \sin\alpha\, N_{e(t)}{}^2 N_{e(e)}{}^2 K_{7A_3}\xi$$

$$\mathcal{S}[\gamma({}^5_4)(t_{2g}) \longrightarrow \gamma({}^4_5)(e_g)] =$$
$$\tfrac{3}{2} e^2 k_p{}^2 \sin^2\alpha\, N_{e(t)}{}^2 N_{e(e)}{}^2 K_{7A3}{}^2 \xi^2$$

$$\mathcal{R}[\gamma_6{}^{({7\atop 8})}(t_{2g}) \longrightarrow \gamma_{4\text{ or }5}(e_g)] =$$
$$\mathcal{R}[\gamma_6{}^{({a\atop b})({7\atop 8})}(t_{2g}) \longrightarrow \gamma_{4\text{ or }5}(e_g)]$$

$$\mathcal{S}[\gamma_6{}^{({7\atop 8})}(t_{2g}) \longrightarrow \gamma_{4\text{ or }5}(e_g)] =$$
$$\mathcal{S}[\gamma_6{}^{({a\atop b})({7\atop 8})}(t_{2g}) \longrightarrow \gamma_{4\text{ or }5}(e_g)]$$

$$\mathcal{R}[\gamma_{4\text{ or }5}(t_{2g}) \longrightarrow \gamma_6(e_g)] =$$
$$2\mathcal{R}[\gamma_{4\text{ or }5}(t_{2g}) \longrightarrow \gamma_6({}^a_b)(e_g)]$$

$$\mathcal{S}[\gamma_{4\text{ or }5}(t_{2g}) \longrightarrow \gamma_6(e_g)] = 2\mathcal{S}[\gamma_{4\text{ or }5}(t_{2g}) \longrightarrow \gamma_6({}^a_b)(e_g)]$$

$$\mathcal{R}[\gamma_6{}^{(7)}(t_{2g}) \longrightarrow \gamma_6(e_g)] = \mathcal{R}[\gamma_6({}^a_b)^{(7)}(t_{2g}) \longrightarrow$$
$$\gamma_6({}^a_b)(e_g)] + \mathcal{R}[\gamma_6({}^a_b)^{(7)} \longrightarrow \gamma_6({}^b_a)(e_g)] =$$
$$2\sqrt{1/3}\, e\mu_B k_p \sin\alpha\, N_{e(e)}{}^2 (N_{e(t)}{}^2 K_{7A_3}\xi +$$
$$\tfrac{1}{4} N_{a_1(t)}{}^2 (\sqrt{3}K_{4A_3} + K_{7A_3})\eta)$$

$$\mathcal{S}[\gamma_6{}^{(7)}(t_{2g}) \longrightarrow \gamma_6(e_g)] =$$
$$\mathcal{S}[\gamma_6({}^a_b)^{(7)}(t_{2g}) \longrightarrow \gamma_6({}^a_b)(e_g)] +$$
$$\mathcal{S}[\gamma_6({}^a_b)^{(7)}(t_{2g}) \longrightarrow \gamma_6({}^b_a)(e_g)] =$$
$$e^2 k_p{}^2 \sin^2\alpha\, N_{e(e)}{}^2 (N_{e(t)}{}^2 K_{7A_3}{}^2 \xi^2 +$$
$$\tfrac{1}{8} N_{a_1(t)}{}^2 (\sqrt{3}K_{4A_3} + K_{7A_3})^2 \eta^2)$$

$$\mathcal{R}[\gamma_6{}^{(8)}(t_{2g}) \longrightarrow \gamma_6(e_g)] =$$
$$\mathcal{R}[\gamma_6({}^a_b)^{(8)}(t_{2g}) \longrightarrow \gamma_6({}^a_b)(e_g)] +$$
$$\mathcal{R}[\gamma_6({}^a_b)^{(8)}(t_{2g}) \longrightarrow \gamma_6({}^b_a)(e_g)] =$$
$$\sqrt{1/3}\, e\mu_B k_p \sin\alpha\, N_{e(e)}{}^2 (N_{e(t)}{}^2 K_{7A_3}\xi +$$
$$N_{a_1(t)}{}^2 (\sqrt{3}K_{4A_3} + K_{7A_3})\eta)$$

$$\mathcal{S}[\gamma_6{}^{(8)}(t_{2g}) \longrightarrow \gamma_6(e_g)] =$$
$$\mathcal{S}[\gamma({}^a_b)^{(8)}(t_{2g}) \longrightarrow \gamma_6({}^a_b)(e_g)] +$$
$$\mathcal{S}[\gamma_6({}^a_b)^{(8)}(t_{2g}) \longrightarrow \gamma_6({}^b_a)(e_g)]$$

$$\mathcal{S}[\gamma_6{}^{(8)}(t_{2g}) \longrightarrow \gamma_6(e_g)] = \tfrac{1}{2} e^2 k_p{}^2 \sin^2\alpha\, N_{e(e)}{}^2 \times$$
$$(N_{e(t)}{}^2 K_{7A_3}{}^2 \xi^2 + \tfrac{1}{2} N_{a_1(t)}{}^2 (\sqrt{3}K_{4A_3} + K_{7A_3})^2 \eta^2)$$

$$\mathcal{R}[\gamma_{4\text{ or }5}(e_g) \longrightarrow \gamma_{4\text{ or }5}(e_g)] \equiv$$
$$\mathcal{S}[\gamma_{4\text{ or }5}(e_g) \longrightarrow \gamma_{4\text{ or }5}(e_g)] \equiv 0$$

$$\mathcal{R}[\gamma_6(e_g) \longrightarrow \gamma_{4\text{ or }5}(e_g)] =$$
$$\mathcal{S}[\gamma_6(e_g) \longrightarrow \gamma_{4\text{ or }5}(e_g)] = 0$$

$$\mathcal{R}[\gamma_6(e_g) \longrightarrow \gamma_6(e_g)] \equiv \mathcal{S}[\gamma_6(e_g) \longrightarrow \gamma_6(e_g)] \equiv 0$$

$$\mathcal{R}[\gamma_6({}^7_8)(t_{2g}) \longrightarrow \gamma_6({}^7_8)(t_{2g})] \equiv$$
$$\mathcal{S}[\gamma_6({}^7_8)(t_{2g}) \longrightarrow \gamma_6({}^7_8)(t_{2g})] \equiv 0$$

$$\mathcal{R}[\gamma_{4\text{ or }5}(t_{2g}) \longrightarrow \gamma_{4\text{ or }5}(t_{2g})] \equiv$$
$$\mathcal{S}[\gamma_{4\text{ or }5}(t_{2g}) \longrightarrow \gamma_{4\text{ or }5}(t_{2g})] \equiv 0 \quad (55)$$

(c) Configuration Interaction: Zero and Nonzero Spin-Orbit Forces. In eq. 53 and 55 we see that in the limit of no configuration interaction the $e_\pm(e_g)$ to $e_\pm(e_g)$ set of transitions gives rise to no optical rotatory or refractory power as both the rotational and spectral strengths vanish in this circumstance. When such interaction is considered, however, both rotatory and refractory power do appear, if only slightly and for only certain of the $e_\pm(e_g)$ to $e_\pm(e_g)$ set. To witness this fact, we put the configurationally mixed $e_\pm(e_g)$ wave functions in the form

$$\bar{e}_\pm = \bar{N}_{e\pm}\{e_\pm(e_g) + \kappa_{\pm}e_\pm(t_{2g})\}$$
$$\bar{\gamma}({}^4_5) = \bar{N}({}^4_5)\{\gamma({}^4_5)(e_g) + \bar{\kappa}({}^4_5)\gamma({}^4_5)(t_{2g})\}$$
$$\bar{\gamma}_6({}^a_b) = \bar{N}_6({}^a_b)\{\gamma_6({}^a_b)(e_g) + \kappa_6({}^a_b)^{(7)}\gamma_6({}^a_b)^{(7)}(t_{2g}) +$$
$$\kappa_6({}^a_b)^{(8)}\gamma_6({}^a_b)^{(8)}(t_{2g})\} \quad (56)$$

Symmetry and momentum reversal arguments[10,25] again imply that $\bar{N}_{e\pm}$ equals $\bar{N}_e$, $\kappa_{\pm}$ equals κ_t, $\bar{N}_4$ equals $\bar{N}_5{}^*$, $\bar{\kappa}_4$ equals $\bar{\kappa}_5{}^*$, $\bar{N}_6({}^a_b)$ equals $\bar{N}_6$, $\kappa_6({}^a_b)^{(7)}$ equals $\kappa_6{}^{(7)}$, and $\kappa_6({}^a_b)^{(8)}$ equals $\kappa_6{}^{(8)}$. First-order perturbation theory requires

$$\kappa_t \sim -\frac{\langle e_\pm(t_{2g})|\mathcal{H}_{\text{trigonal}}|e_\pm(e_g)\rangle}{E_t{}^\circ - E_e{}^\circ}$$

$$\bar{\kappa}_4 \sim -\frac{\langle\gamma_4(t_{2g})|\mathcal{H}_{\text{trigonal}}|\gamma_4(e_g)\rangle}{E_t{}^\circ - E_e{}^\circ}$$

$$\kappa_6({}^7_8) \sim -\frac{\langle\gamma_6({}^a_b)^{({7\atop 8})}(t_{2g})|\mathcal{H}_{\text{trigonal}}|\gamma_6({}^a_b)^{({7\atop 8})}(e_g)\rangle}{E_t{}^\circ - E_e{}^\circ} \quad (57)$$

so that $\bar{\kappa}_4$ equals $e^{-i\beta/2}\bar{\kappa}_4$, $\kappa_6{}^{(7)}$ approximately equals both $\sqrt{2}\kappa_6{}^{(8)}$ and $\sqrt{2/3}\kappa_4$ or t, with $\bar{N}_e$, $\bar{N}_4$, $\bar{N}_6$, κ_t, κ_4, $\kappa_6{}^{(7)}$, and $\kappa_6{}^{(8)}$ all real numbers.[29] Therefore, the

(29) These statements are forthwith certified by the insertion of eq. 34 into 58 and the reduction of the ensuing spin-orbital expressions to orbital form. For example, such a reduction leads to a value $-\langle e_\pm(t_{2g})|\mathcal{H}_{\text{trigonal}}|e_\pm(e_g)\rangle/(E_t{}^\circ - E_e{}^\circ)$ for κ_t. As the same Hamiltonian matrix terms enter into a variational calculation of the configuration interaction, the affirmations as to the reality of the constants remain valid in this case also [actually these affirmations are *universally* true as the reality of these constants cannot change as $\mathcal{H}_{\text{trigonal}}$ tends to zero, in which limit perturbation theory is most certainly valid].

desired interacted total rotational and spectral strengths to lowest order in κ_l, κ_4, $\kappa_6^{(7)}$, and $\kappa_6^{(8)}$ are[30]

$$\Re[\bar{e} \longrightarrow \bar{e}] = 0$$

$$S[\bar{e} \longrightarrow \bar{e}] = 4\bar{N}_e^2\kappa_l^2 S[e_\pm(t_{2g}) \longrightarrow e_\mp(t_{2g})]$$

$$\Re[\bar{\gamma}(\substack{4\\5}) \longrightarrow \bar{\gamma}(\substack{4\\5})] \equiv S[\bar{\gamma}(\substack{4\\5}) \longrightarrow \bar{\gamma}(\substack{4\\5})] \equiv 0$$

$$\Re[\bar{\gamma}_4 \longrightarrow \bar{\gamma}_5] = S[\bar{\gamma}_4 \longrightarrow \bar{\gamma}_5] = 0$$

$$\Re[\bar{\gamma}_6 \longrightarrow \bar{\gamma}(\substack{4\\5})] = -\frac{1}{4}e\mu_B k_p \sin\alpha \ \bar{N}_4^2\bar{N}_6^2 N_{a_1(t)}N_{e(e)} \times$$
$$(\sqrt{3}K_{4A_2} + K_{7A_2})(\kappa_6^{(7)} - \sqrt{2}\kappa_6^{(8)})\eta$$

$$S[\bar{\gamma}_6 \longrightarrow \bar{\gamma}(\substack{4\\5})] = \frac{1}{16}e^2k_p^2 \sin^2\alpha \ \bar{N}_4^2\bar{N}_6^2 N_{e(e)}^2 \times$$
$$(N_{a_1(t)}^2(\sqrt{3}K_{4A_2} + K_{7A_2})^2(\kappa_6^{(7)} - \sqrt{2}\kappa_6^{(8)})^2\eta^2 +$$
$$N_{e(t)}^2(\sqrt{3}K_{4A_2} - K_{7A_2})^2(\sqrt{2}\kappa_6^{(7)} + \kappa_6^{(8)} - \sqrt{3}\kappa_4)^2\xi^2))$$

$$(58)$$

Thus, even with configuration interaction the rotational and spectral strengths of the $e_\pm(e_g)$ to $e_\pm(e_g)$ type transitions are small, as $\kappa_6^{(7)} - \sqrt{2}\kappa_6^{(8)}$ and $\sqrt{2}\kappa_6^{(7)} + \kappa_6^{(8)} - \sqrt{3}\kappa_4$ are almost zero in the weak interaction

limit. It is interesting to note, however, that the zeroth-order magnetic dipole which gives the rotational strengths of eq. 58 their nonzero value is entirely of a spin transition moment origin [this situation also holds for the $\bar{\gamma}_4 \rightarrow \bar{\gamma}_5$ transition, but in this latter case the electric dipole transition moment is still zero, and so the over-all rotational strength vanishes anyway].

3.5 *Dissymmetry Factors.* As been shown by Kuhn and others,[2,20,31] the dissymmetry factor, G_{ij}, of an electronic transition of frequency ν_{ij} from the state i to the state j, defined by

$$G_{ij} = 4\frac{\nu}{\nu_{ij}}\frac{\Re_{ij}}{S_{ij}} = \left(\frac{\kappa_l - \kappa_r}{\kappa}\right)_{ij} \approx \left(\frac{n_l - n_r}{n - 1}\right)_{ij} \quad (59)$$

is quite a useful quantity in the analysis of intricate optical rotatory phenomena of the kind observed in actual molecular systems.[32] We therefore tabulate here for ready reference the theoretical values of these factors for the basic one-electron molecular orbitals derived priorly. We shall discuss their significance in a later publication.[33]

(a) *No Configuration Interaction: Zero Spin-Orbit Forces*

$$G[a_1(t_{2g}) \longrightarrow a_1(t_{2g})] = \text{indeterminate}$$

$$G[a_1(t_{2g}) \longrightarrow e(t_{2g})] = -4\sqrt{2/3}\ \frac{\nu}{\nu[a_1(t_{2g}) \longrightarrow e(t_{2g})]}\frac{\mu_B}{e}\frac{1}{k_p \sin\alpha}\frac{1}{(K_{2A_2}(\xi - \eta) + \eta K_{3A_2})}$$

$$G[a_1(t_{2g}) \longrightarrow e(e_g)] = 16\sqrt{1/3}\ \frac{\nu}{\nu[a_1(t_{2g}) \longrightarrow e(e_g)]}\frac{u_B}{e}\frac{1}{k_p \sin\alpha}\frac{1}{(\sqrt{3}K_{4A_2} + K_{7A_2})\eta}$$

$$G[e(t_{2g}) \longrightarrow e(t_{2g})] = 0$$

$$G[e(t_{2g}) \longrightarrow e(e_g)] = 16\sqrt{1/3}\ \frac{\nu}{\nu[e(t_{2g}) \longrightarrow e(e_g)]}\frac{\mu_B}{e}\frac{1}{k_p \sin\alpha}\frac{(\sqrt{3}K_{4A_2} + K_{7A_2})}{(4K_{7A_2}^2 + (\sqrt{3}K_{4A_2} - K_{7A_2})^2)\xi}$$

$$G[e(e_g) \longrightarrow e(e_g)] = \text{indeterminate} \quad (60)$$

(b) *No Configuration Interaction: Nonzero Spin-Orbit Forces*

$$G[\gamma_6^{(8)}(t_{2g}) \longrightarrow \gamma_6^{(7)}(t_{2g})] = -\frac{8}{3}\sqrt{1/6}\ \frac{\nu}{\nu[\gamma_6^{(8)}(t_{2g}) \longrightarrow \gamma_6^{(7)}(t_{2g})]}\frac{\mu_B}{e}\frac{(1 + 2N_{a_1(t)}^{-1}N_{e(t)}^{-1})}{k_p \sin\alpha}\frac{1}{(K_{2A_2}(\xi - \eta) + \eta K_{3A_2})}$$

---

(30) In deriving these results the employment of the rotational symmetry, momentum reversal, and matrix Hermiticity techniques of footnotes 10 and 25 is very helpful. To illustrate, matrix Hermiticity requires that

$$\left\langle e_\pm(e_g) \left|\frac{\vec{p}}{m}\right| e_\mp(t_{2g}) \right\rangle = \left[\substack{+\\-}\right]\left\langle e_\pm(t_{2g}) \left|\frac{\vec{p}}{m}\right| e_\mp(e_g) \right\rangle$$

rotational symmetry under $C_3(z')$ and $C_2(y')$ and matrix Hermiticity requires

$$\left\langle e_\pm(e_g) \left|\frac{\vec{p}}{m}\right| e_\pm(t_{2g}) \right\rangle = \left[\substack{-\\+}\right]\left\langle e_\pm(t_{2g}) \left|\frac{\vec{p}}{m}\right| e_\pm(e_g) \right\rangle$$

and momentum reversal and matrix Hermiticity requires that

$$\left\langle \gamma_4(t_{2g}) \left|\frac{\vec{p}}{m}\right| \gamma_5(e_g) \right\rangle = -\left\langle \gamma_4(e_g) \left|\frac{\vec{p}}{m}\right| \gamma_5(t_{2g}) \right\rangle$$

(31) (a) W. Kuhn, *Trans. Faraday Soc.*, **46**, 293 (1930); (b) W. Kuhn and E. Braun, *Z. physik. Chem.*, **B8**, 281 (1930); (c) W. Kuhn and K. Bein, *ibid.*, **B24**, 335 (1934), *et seq.*

(32) For a survey of these uses read ref. 2, 20, 30 and the recent reviews (a) J. P. Mathieu, "Handbuch der Physik," S. Flügge, Ed., Vol. XXVIII, "Spektroskopie II," Springer-Verlag, Berlin, 1957, pp. 333–432; (b) S. F. Mason, *Quart. Rev.* (London), **27**, 20 (1963).

(33) F. Woldbye and A. D. Liehr, to be published.

$$G[\gamma_6{}^{(8)}(t_{2g}) \longrightarrow \gamma_{1 \text{ or } 5} (t_{2g})] = 4\sqrt{1/6} \frac{\nu}{\nu[\gamma_6{}^{(8)}(t_{2g}) \longrightarrow \gamma_{4 \text{ or } 5} (t_{2g})]} \frac{\mu_B}{e} \frac{N_{a_1(t)}}{N_{e(t)}} \frac{(1 - N_{a_1(t)}N_{e(t)})}{k_p \sin \alpha} \times$$

$$\frac{(K_{2A_s}(\xi - \eta) + \eta K_{3A_s})}{\left(\begin{matrix} N_{e(t)}{}^2 \xi^2 (K_{3A_s} + K_{2A_s})^2 + \\ {}^{1}\!/_{2} N_{a_1(t)}{}^2 (K_{2A_s}(\xi - \eta) + \eta K_{3A_s})^2 \end{matrix} \right)}$$

$$G[\gamma_6{}^{(7)}(t_{2g}) \longrightarrow \gamma_{4 \text{ or } 5} (t_{2g})] = -2\sqrt{1/6} \frac{\nu}{\nu[\gamma_6{}^{(7)}(t_{2g}) \longrightarrow \gamma_{4 \text{ or } 5} (t_{2g})]} \frac{\mu_B}{e} \frac{N_{a_1(t)}(2 + N_{a_1(t)}N_{e(t)})}{N_{e(t)}} \frac{}{k_p \sin \alpha} \times$$

$$\frac{(K_{2A_s}(\xi - \eta) + \eta K_{3A_s})}{\left(\begin{matrix} 2N_{e(t)}{}^2 \xi^2 (K_{3A_s} + K_{2A_s})^2 + \\ {}^{1}\!/_{4} N_{a_1(t)}{}^2 (K_{2A_s}(\xi - \eta) + \eta K_{3A_s})^2 \end{matrix} \right)}$$

$$G[\gamma({}^4_5)(t_{2g}) \longrightarrow \gamma({}^4_5)(e_g)] = \text{indeterminate}$$

$$G[\gamma({}^5_4)(t_{2g}) \longrightarrow \gamma({}^4_5)(e_g)] = 8\sqrt{1/3} \frac{\nu}{\nu[\nu({}^5_4)(t_{2g}) \longrightarrow \gamma({}^4_5)(e_g)]} \frac{\mu_B}{e} \frac{1}{k_p \sin \alpha} \frac{1}{K_{7A_s}\xi}$$

$$G[\gamma_6{}^{(7)}(t_{2g}) \longrightarrow \gamma_{1 \text{ or } 5} (e_g)] = 16\sqrt{1/3} \frac{\nu}{\nu[\gamma_6{}^{(7)}(t_{2g}) \longrightarrow \gamma_{4 \text{ or } 5} (e_g)]} \frac{\mu_B}{e} \frac{1}{k_p \sin \alpha} \times$$

$$\frac{(N_{e(t)}{}^2(\sqrt{3}K_{4A_s} - K_{7A_s})\xi + {}^{1}\!/_{2}N_{a_1(t)}{}^2(\sqrt{3}K_{4A_s} + K_{7A_s})\eta)}{(N_{e(t)}{}^2(\sqrt{3}K_{4A_s} - K_{7A_s})^2\xi^2 \pm {}^{1}\!/_{2}N_{a_1(t)}{}^2(\sqrt{3}K_{4A_s} + K_{7A_s})^2\eta^2)}$$

$$G[\gamma_6{}^{(8)}(t_{2g}) \longrightarrow \gamma_{4 \text{ or } 5} (e_g)] = 16\sqrt{1/3} \frac{\nu}{\nu[\gamma_6{}^{(8)}(t_{2g}) \longrightarrow \gamma_{4 \text{ or } 5} (e_g)]} \frac{\mu_B}{e} \frac{1}{k_p \sin \alpha} \times$$

$$\frac{({}^{1}\!/_{2}N_{e(t)}{}^2(\sqrt{3}K_{4A_s} - K_{7A_s})\xi + N_{a_1(t)}{}^2(\sqrt{3}K_{4A_s} + K_{7A_s})\eta)}{({}^{1}\!/_{2}N_{e(t)}{}^2(\sqrt{3}K_{4A_s} - K_{7A_s})^2\xi^2 + N_{a_1(t)}{}^2(\sqrt{3}K_{4A_s} + K_{7A_s})^2\eta^2)}$$

$$G[\gamma_{4 \text{ or } 5} (t_{2g}) \longrightarrow \gamma_6(e_g)] = 16\sqrt{1/3} \frac{\nu}{\nu[\gamma_{4 \text{ or } 5} (t_{2g}) \longrightarrow \gamma_6(e_g)]} \frac{\mu_B}{e} \frac{1}{k_p \sin \alpha} \frac{1}{(\sqrt{3}K_{4A_s} - K_{7A_s})\xi}$$

$$G[\gamma_6{}^{(7)}(t_{2g}) \longrightarrow \gamma_5(e_g)] = 8\sqrt{1/3} \frac{\nu}{\nu[\gamma_6{}^{(7)}(t_{2g}) \longrightarrow \gamma_6(e_g)]} \frac{\mu_B}{e} \frac{1}{k_p \sin \alpha} \times$$

$$\frac{(N_{e(t)}{}^2 K_{7A_s}\xi + {}^{1}\!/_{4}N_{a_1(t)}{}^2(\sqrt{3}K_{4A_s} + K_{7A_s})\eta)}{(N_{e(t)}{}^2 K_{7A_s}{}^2\xi^2 + {}^{1}\!/_{8}N_{a_1(t)}{}^2(\sqrt{3}K_{4A_s} + K_{7A_s})^2\eta^2)}$$

$$G[\gamma_6{}^{(8)}(t_{2g}) \longrightarrow \gamma_5(e_g)] = 8\sqrt{1/3} \frac{\nu}{\nu[\gamma_6{}^{(8)}(t_{2g}) \longrightarrow \gamma_6(e_g)]} \frac{\mu_B}{e} \frac{1}{k_p \sin \alpha} \times$$

$$\frac{(N_{e(t)}{}^2 K_{7A_s}\xi + N_{a_1(t)}{}^2(\sqrt{3}K_{4A_s} + K_{7A_s})\eta)}{(N_{e(t)}{}^2 K_{7A_s}{}^2\xi^2 + {}^{1}\!/_{2}N_{a_1(t)}{}^2(\sqrt{3}K_{4A_s} + K_{7A_s})^2\eta^2)}$$

$$G[\gamma_{4 \text{ or } 5} (e_g) \longrightarrow \gamma_{4 \text{ or } 5} (e_g)] = \text{indeterminate}, \quad G[\gamma_6(e_g) \longrightarrow \gamma_{4 \text{ or } 5} (e_g)] = \text{indeterminate}$$

$$G[\gamma_6(e_g) \longrightarrow \gamma_6(e_g)] = \text{indeterminate}, \quad G[\gamma_6({}^7_8)(t_{2g}) \longrightarrow \gamma_6{}^{({}^7_8)}(t_{2g})] = \text{indeterminate}$$

$$G[\gamma_{4 \text{ or } 5} (t_{2g}) \longrightarrow {}_{4 \text{ or } 5} (t_{2g})] = \text{indeterminate} \quad (61)$$

(c) Configuration Interaction: Zero and Nonzero Spin-Orbit Forces

$$G[\bar{e} \longrightarrow \bar{e}] = 0, \quad G[\bar{\gamma}_{4 \text{ or } 5} \longrightarrow \bar{\gamma}_{4 \text{ or } 5}] = \text{indeterminate}$$

$$G[\bar{\gamma}_6 \longrightarrow \bar{\gamma}({}^4_5)] = -16 \frac{\nu}{\nu[\bar{\gamma}_6 \longrightarrow \bar{\gamma}({}^4_5)]} \frac{\mu_B}{e} \frac{1}{k_p \sin \alpha} \frac{N_{a_1(t)}}{N_{e(t)}} \times$$

$$\frac{(\sqrt{3}K_{4A_s} + K_{7A_s})(\kappa_6{}^{(7)} - \sqrt{2}\kappa_6{}^{(8)})\eta}{\left(\begin{matrix} N_{a_1(t)}{}^2(\sqrt{3}K_{4A_s} + K_{7A_s})^2(\kappa_6{}^{(7)} - \sqrt{2}\kappa_6{}^{(8)})^2\eta^2 + \\ N_{e(t)}{}^2(\sqrt{3}K_{4A_s} - K_{7A_s})^2(\sqrt{2}\kappa_6{}^{(7)} + \kappa_6{}^{(8)} - \sqrt{3}\kappa_4)^2\xi^2 \end{matrix} \right)} \quad (62)$$

If magnetic dipole or other sources of spectral strength are included in the definition of G_{ij}, eq. 59, the indetermindness of some of the dissymmetry ratios is lifted.

III. Applications. §4. The Many-Electron Systems: Wave Functions and Matrix Elements

4.1 *The One- and Nine-Electron Case.* The relevant rotatory and refractory parameters for one-electron systems have already been given in eq. 47 through 62. Thus we need only consider the nine-electron case at this point. The appropriate orbital wave functions follow.

(a) *No Configuration Interaction: Zero Spin-Orbit Forces.* (*i*) *Wave Functions: One Electron.* These are the same as eq. 17 and 33.

(*ii*) *Wave Functions: Nine Electrons*

$$^2E_\pm[^2E_g(t_{2g}{}^6e_g{}^3)]: \left|a_1(t_{2g})^2e_\pm(t_{2g})^4e_\pm(e_g)^3\right|$$

$$^2A_1[^2T_{2g}(t_{2g}{}^5e_g{}^4)]: \left|a_1(t_{2g})^1e_\pm(t_{2g})^4e_\pm(e_g)^4\right|$$

$$^2E_\pm[^2T_{2g}(t_{2g}{}^5e_g{}^4)]: \left|a_1(t_{2g})^2e_\pm(t_{2g})^3e_\pm(e_g)^4\right| \quad (63)$$

where in eq. 63 the spin function $\zeta'(+^1/_2)$ is associated with a molecular orbital on its first appearance in a determinant and the spin function $\zeta'(-^1/_2)$ on its second. The molecular orbital $e_+(t_{2g}$ or $e_g)$ is ordered before $e_-(t_{2g}$ or $e_g)$ in eq. 63 for a given spin function. A computation of the requisite matrix terms with these functions shows that the nine- and one-electron situations are related as follows

(*iii*) *Matrix Elements: One Electron.* These are the same as eq. 47.

(*iv*) *Matrix Elements: Nine Electrons*

$$\left\langle ^2E_\pm[^2E_g(t_{2g}{}^6e_g{}^3)] \left| \frac{\vec{p}}{m} \right| ^2E_\pm[^2T_{2g}(t_{2g}{}^5e_g{}^4)] \right\rangle =$$
$$- \left\langle e_\mp(t_{2g}) \left| \frac{\vec{p}}{m} \right| e_\mp(e_g) \right\rangle$$

$$\left\langle ^2E_\pm[^2E_g(t_{2g}{}^6e_g{}^3)] \left| \frac{\vec{p}}{m} \right| ^2E_\mp[^2T_{2g}(t_{2g}{}^5e_g{}^4)] \right\rangle =$$
$$- \left\langle e_\pm(t_{2g}) \left| \frac{\vec{p}}{m} \right| e_\mp(e_g) \right\rangle$$

$$\left\langle ^2E_\pm[^2E_g(t_{2g}{}^6e_g{}^3)] \left| \frac{\vec{p}}{m} \right| ^2A_1[^2T_{2g}(t_{2g}{}^5e_g{}^4)] \right\rangle =$$
$$- \left\langle a_1(t_{2g}) \left| \frac{\vec{p}}{m} \right| e_\mp(e_g) \right\rangle$$

$$\left\langle ^2A_1[^2T_{2g}(t_{2g}{}^5e_g{}^4)] \left| \frac{\vec{p}}{m} \right| ^2E_\pm[^2T_{2g}(t_{2g}{}^5e_g{}^4)] \right\rangle =$$
$$- \left\langle e_\mp(t_{2g}) \left| \frac{\vec{p}}{m} \right| a_1(t_{2g}) \right\rangle \quad (64)$$

Because of the great similarity of the predictions which can be made on the basis of eq. 64 to those which can be made on the basis of the nonzero spin-orbit force equation, eq. 66, of the next paragraph, §4.1b, we shall defer discussion of the consequence of this equation until after eq. 66 of that paragraph, and there present a joint analysis of the one- and nine-electron orbital and spin-orbital forecasts.

b) *No Configuration Interaction: Nonzero Spin-Orbit Forces.* The correct spin-orbit wave functions include the following.

(*i*) *Wave Functions: One Electron.* These are the same as eq. 34.

(*ii*) *Wave Functions: Nine Electrons*

$\Gamma_{(\frac{3}{5})}[\Gamma_8(^2E_g)]:$

$$\left| \gamma_6{}^{(3)}(t_{2g})^2\gamma_6{}^{(7)}(t_{2g})^2\gamma_4(t_{2g})^1\gamma_5(t_{2g})^1\gamma(\tfrac{3}{4})(e_g)^1\gamma_6(e_g)^2 \right.$$

$\Gamma_6(\frac{3}{5})[\Gamma_8(^2E_g)]:$

$$\left| \gamma_6{}^{(8)}(t_{2g})^2\gamma_6{}^{(7)}(t_{2g})^2\gamma_4(t_{2g})^1\gamma_5(t_{2g})^1\gamma_4(e_g)^1\gamma_5(e_g)^1\gamma_6(\tfrac{3}{5})(e_g)^1 \right|$$

$\Gamma_6(\frac{3}{5})[\Gamma_7(^2T_{2g}):$

$$\left| \gamma_6{}^{(8)}(t_{2g})^2\gamma_6(\tfrac{3}{5})^{(7)}(t_{2g})^1\gamma_4(t_{2g})^1\gamma_5(t_{2g})^1\gamma_4(e_g)^1\gamma_5(e_g)^1\gamma_6(e_g)^2 \right|$$

$\Gamma_{(\frac{3}{5})}[\Gamma_8(^2T_{2g})]:$

$$\left| \gamma_6{}^{(8)}(t_{2g})^2\gamma_6{}^{(7)}(t_{2g})^2\gamma(\tfrac{3}{4})(t_{2g})^1\gamma_4(e_g)^1\gamma_5(e_g)^1\gamma_6(e_g)^2 \right|$$

$\Gamma_6(\frac{3}{5})[\Gamma_8(^2T_{2g})]:$

$$\left| \gamma_{3(\frac{3}{5})}{}^{(8)}(t_{2g})^1\gamma_6{}^{(7)}(t_{2g})^2\gamma_4(t_{2g})^1\gamma_5(t_{2g})^1\gamma_4(e_g)^1\gamma_5(e_g)^1\gamma_6(e_g)^2 \right|$$
$$(65)$$

In eq. 65 the molecular spin orbital $\gamma_{6a}(t_{2g}$ or $e_g)$ has been placed before $\gamma_{6b}(t_{2g}$ or $e_g)$. A calculation of the needed matrix array with these functions demonstrates that the nine- and one-electron instances are conjoined as indicated.

(*iii*) *Matrix Elements: One Electron.* These are the same as eq. 49.

(*iv*) *Matrix Elements: Nine Electrons*

$$\left\langle \Gamma_4[\Gamma_8(^2E_g)] \left| \frac{\vec{p}}{m} \right| \Gamma_5[\Gamma_8(^2E_g)] \right\rangle = \left\langle \gamma_5(e_g) \left| \frac{\vec{p}}{m} \right| \gamma_4(e_g) \right\rangle$$

$$\left\langle \Gamma_4[\Gamma_8(^2E_g)] \left| \frac{\vec{p}}{m} \right| \Gamma_6(\tfrac{3}{5})[\Gamma_8(^2E_g)] \right\rangle =$$
$$\pm \left\langle \gamma_6(\tfrac{3}{5})(e_g) \left| \frac{\vec{p}}{m} \right| \gamma_4(e_g) \right\rangle$$

$$\left\langle \Gamma_4[\Gamma_8(^2E_g)] \left| \frac{\vec{p}}{m} \right| \Gamma_{(\frac{3}{5})}[\Gamma_8(^2T_{2g})] \right\rangle =$$
$$\mp \left\langle \gamma(\tfrac{3}{5})(t_{2g}) \left| \frac{\vec{p}}{m} \right| \gamma_4(e_g) \right\rangle$$

$$\left\langle \Gamma_4[\Gamma_8(^2E_g)] \left|\frac{\vec{p}}{\vec{m}}\right| \Gamma_{6(^a_b)}[\Gamma_7(^2T_{2g})] \right\rangle =$$

$$\pm \left\langle \gamma_{6(^b_a)}{}^{(7)}(t_{2g}) \left|\frac{\vec{p}}{\vec{m}}\right| \gamma_4(e_g) \right\rangle$$

$$\left\langle \Gamma_4[\Gamma_8(^2E_g)] \left|\frac{\vec{p}}{\vec{m}}\right| \Gamma_{6(^a_b)}[\Gamma_8(^2T_{2g})] \right\rangle =$$

$$\pm \left\langle \gamma_{6(^b_a)}{}^{(8)}(t_{2g}) \left|\frac{\vec{p}}{\vec{m}}\right| \gamma_4(e_g) \right\rangle$$

$$\left\langle \Gamma_{6a}[\Gamma_8(^2E_g)] \left|\frac{\vec{p}}{\vec{m}}\right| \Gamma_{(^4_8)}[\Gamma_8(^2T_{2g})] \right\rangle =$$

$$\pm \left\langle \gamma_{(^4_8)}(t_{2g}) \left|\frac{\vec{p}}{\vec{m}}\right| \gamma_{6b}(e_g) \right\rangle$$

$$\left\langle \Gamma_{6a}[\Gamma_8(^2E_g)] \left|\frac{\vec{p}}{\vec{m}}\right| \Gamma_{6(^a_b)}[\Gamma_7(^2T_{2g})] \right\rangle =$$

$$\mp \left\langle \gamma_{6(^b_a)}{}^{(7)}(t_{2g}) \left|\frac{\vec{p}}{\vec{m}}\right| \gamma_{6b}(e_g) \right\rangle$$

$$\left\langle \Gamma_{6a}[\Gamma_8(^2E_g)] \left|\frac{\vec{p}}{\vec{m}}\right| \Gamma_{6(^a_b)}[\Gamma_8(^2T_{2g})] \right\rangle =$$

$$\mp \left\langle \gamma_{6(^b_a)}{}^{(8)}(t_{2g}) \left|\frac{\vec{p}}{\vec{m}}\right| \gamma_{6b}(e_g) \right\rangle$$

$$\left\langle \Gamma_{6a}[\Gamma_7(^2T_{2g})] \left|\frac{\vec{p}}{\vec{m}}\right| \Gamma_{(^4_8)}[\Gamma_8(^2T_{2g})] \right\rangle =$$

$$\pm \left\langle \gamma_{(^4_8)}(t_{2g}) \left|\frac{\vec{p}}{\vec{m}}\right| \gamma_{6b}{}^{(7)}(t_{2g}) \right\rangle$$

$$\left\langle \Gamma_{6a}[\Gamma_8(^2T_{2g})] \left|\frac{\vec{p}}{\vec{m}}\right| \Gamma_{(^4_8)}[\Gamma_8(^2T_{2g})] \right\rangle =$$

$$\pm \left\langle \gamma_{(^4_8)}(t_{2g}) \left|\frac{\vec{p}}{\vec{m}}\right| \gamma_{6b}{}^{(8)}(t_{2g}) \right\rangle \quad (66)$$

The $\Gamma_5[\Gamma_8(^2E_g)]$ and $\Gamma_{6b}[\Gamma_8(^2E_g)]$ analogs of eq. 66 are immediately obtained upon consultation of footnote 25 and its tabulated momentum reversal connections. As a sample, since by construction $\mathcal{K}\Gamma_{(^4_8)}$ equals $\mp i\Gamma_{(^4_8)}$ and $\mathcal{K}\Gamma_{6(^a_b)}$ equals $\pm\Gamma_{6(^a_b)}$ and since by content $\mathcal{K}\vec{p}$ equals $\vec{p}$ and $\mathcal{K}\vec{m}$ equals $-\vec{m}$ and by definition $\mathcal{K}c$ equals c^*, for any constant c, we have

$$\mathcal{K} \left\langle \Gamma_{6a}[\Gamma_8(^2E_g)] \left|\frac{\vec{p}}{\vec{m}}\right| \Gamma_4[\Gamma_8(^2T_{2g})] \right\rangle$$

equals (by definition)

$$\left\langle \Gamma_{6a}[\Gamma_8(^2E_g)] \left|\frac{\vec{p}}{\vec{m}}\right| \Gamma_4[\Gamma_8(^2T_{2g})] \right\rangle^*$$

equals (by operation of $\mathcal{K}$ on the integrands)

$$\left\langle \Gamma_{6b}[\Gamma_8(^2E_g)] \left|\frac{-i\vec{p}}{+i\vec{m}}\right| \Gamma_5[\Gamma_8(^2T_{2g})] \right\rangle$$

The substitution of eq. 64 and 66 into 50 and 51 demonstrates that the one- and nine-electron rotational and spectral strengths are *directly* related: the nine-electron I to J transition has the same sign and algebraic structure as the one-electron j to i transition $(I,J = A_1(T_{2g})$, $E_\pm(T_{2g})$, $E_\pm(E_g)$, $\Gamma_{(^4_8)}(^2E_g)$, $\Gamma_{6(^a_b)}(^2E_g)$, $\Gamma_{(^4_8)}(^2T_{2g})$, $\Gamma_{6(^a_b)}{}^{(^8_8)}(^2T_{2g})$; $i,j = a_1(t_{2g})$, $e_\pm(t_{2g})$, $e_\pm(e_g)$, $\gamma_{(^4_8)}(e_g)$, $\gamma_{6(^a_b)}(e_g)$, $\gamma_{(^4_8)}(t_{2g})$, $\gamma_{6(^a_b)}{}^{(^7_8)}(t_{2g}))$ [these strengths would also have the same magnitudes if the molecular parameters α, k_p, ξ, η, and K_{nA_j} were by chance the same]. Thus, if *formally* the nine-electron orbital wave functions J $(J = A_1(T_{2g})$, $E_\pm(T_{2g})$, $E_\pm(E_g)$, $\Gamma_{(^4_8)}(E_g)$, etc.) were replaced by the one-electron functions j $(j = a_1(t_{2g})$, $e_\pm(t_{2g})$, $e_\pm(e_g)$, $\gamma_{(^4_8)}(e_g)$, etc.) *in one-to-one correspondence*, as is done in the theory of electron-hole congates,[34] we should find that the one-electron and one-hole configurations rotated oppositely for the same conformation.[35] This discovery, however, is a purely formal one and of academic interest only, as in actuality, energetically correspondent electronic transitions of homomorphous nine- and one-electron configurations rotate electromagnetic radiation isodirectionally [view Fig. 14].[36] It is patent that all that was said of eq. 47 through 62 for the one-electron situation applies equally well for the nine-electron situation. In particular, eq. 56 through 58 of §3.4c apply straightway (with the appropriate sign changes), upon use of the state function correlation suggested by eq. 66.

4.2 *The Two- and Eight-Electron Case.* There are many more electronic dispositions possible for the d^n $(n = 2, 3, 4, 5, 6, 7, 8)$ electron configurations than for the one- and nine-electronic situations. However, of this burgeoned multitude only a few are of great rotational import. This happenstance springs as an effect of the one-electron nature of the electronic electric and magnetic dipole moment operators: matrix elements which connect electronic configurations which differ by more than one orthogonalized electron molecular orbital vanish identically.[23,34] Hence, here and in what succeeds we need only concern ourselves with the

(34) Read J. S. Griffith, "The Theory of Transition Metal Ions," Cambridge University Press, Cambridge, England, 1961.

(35) This assertion follows from the antisymmetry of the rotational strengths [examine eq. 50] with respect to the interchange of their transition indices, that is, $\mathcal{R}_{ij}$ equals $-\mathcal{R}_{ji}$. [Note that this antisymmetry implies that the dissymmetry factors G_{ij} [eq. 59] are likewise antisymmetric in their indices, G_{ij} equals $-G_{ji}$, as the spectral strengths are indicially symmetric, S_{ij} equals S_{ji}, by eq. 51.]

(36) By a homomorphous configuration is meant one of the same conformation in which the two central atoms compared are in the same row of the periodic table, and the two ligand groups compared are of similar bonding tendencies and of similar rows of the periodic table. This reservation is made as there is a slight chance that the integrals K_{nA_j} may change sign on going from one row of the periodic table to another without those of the variational parameters ξ and η changing sign correspondingly, or that the sign of the dihedral trigonality might vary with alternate bonding properties.
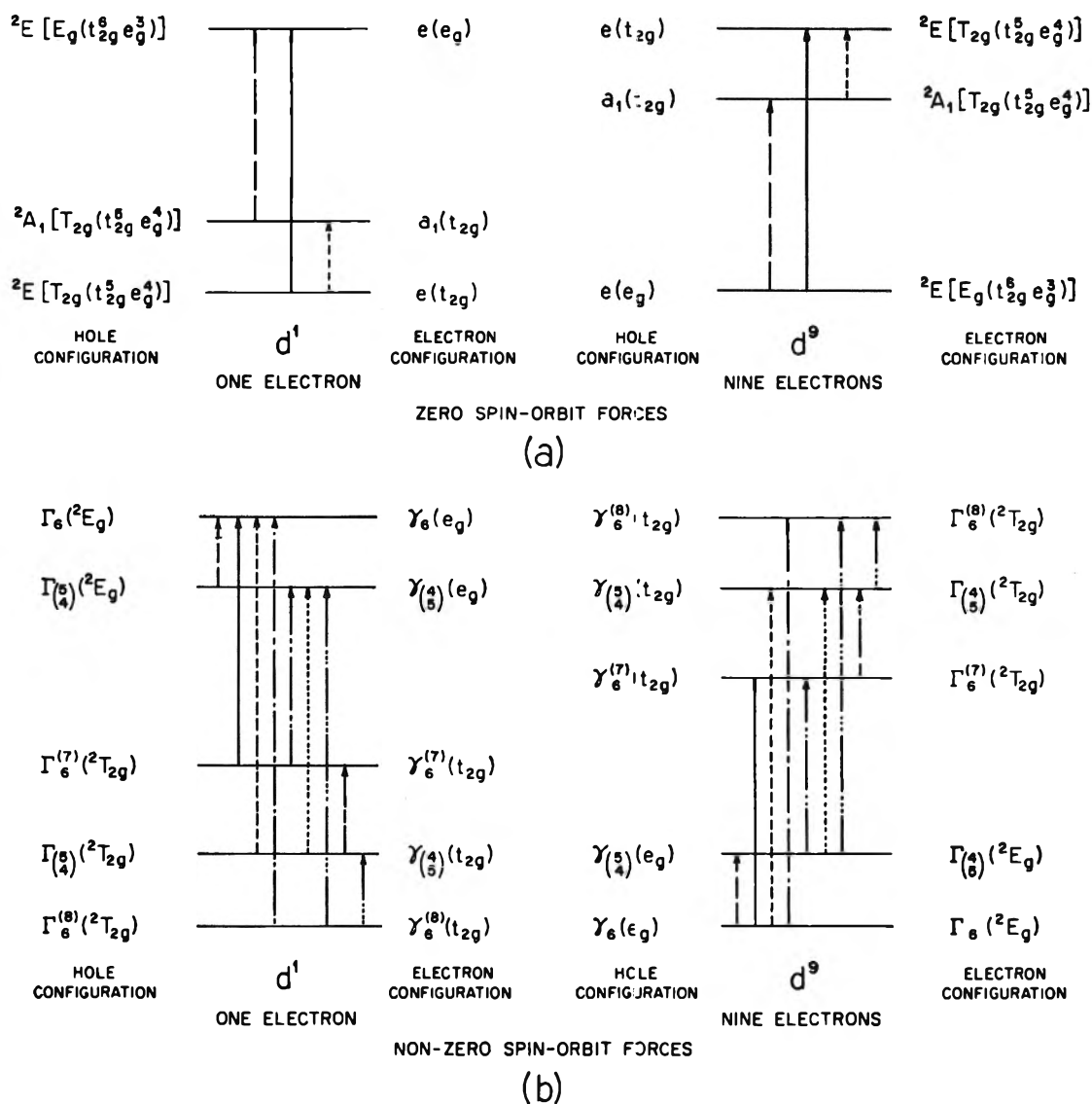
Figure 14. Diagramatic illustration of the conjugate one- and nine-electron electronic transitions in both the orbital [part a] and spin-orbital [part b] representations. Correspondent pairs of transitions are depicted by correspondent lines.

singly excited electronic configurations in order to determine all the transition moments of interest for the discussion of nonmetastable optical rotations. For rotations associated with metastable electronic states (that is, rotations due to electronic transitions between states not inclusive of the (cubical) ground electronic state) further work must be done.[37,38] The rotational and spectral strengths of nonmetastable multi-electron jumps are obtained as functions of those of the related one-electron leaps, as are those of spin-forbidden jumps

Liehr, to be published]. As a preview of the methods employed to set up these sorts of wave functions, a few sentences entered now might not be misplaced [read also ref. 50c]. The $d^{2,8}$ trigonally disposed cubical determinantal wave functions are built by the process of symmetrization and orthnormalization of cubical two-electron determinants composed of the one-electron functions of Table III. [The ancestral one-electron origins as listed in Appendix II of ref. 34 are of great help in formulating these determinants.] All determinantal functions are made to transform in the standard manner of Table III under the symmetry operations $C_4(z)$, $C_3(z')$, and $C_2(y')$ of Tables I and IV. The process is made facile by first fabricating the nondegenerate trigonal components of a given cubical species and then using this component to generate the two doubly degenerate components by means of the $C_4(z)$ symmetry operation [cubically doubly degenerate species, of course, go over into trigonally doubly degenerate species so no significant effort is involved in their reorientation]. The $d^{2,8}$ wave functions may alternatively be manufactured by a direct transformation of their known[34] tetragonal representation to their desired trigonal representation by means of the connections of Table III and eq. 3.4-4 of ref. 59. The apropos configurational wave functions for the d^{10-n} systems are obtained from those for the correspondent d^n ($n = 1, 2, 3, 4$) systems by recourse to electron-hole conjugation.

(37) Actually, the hole-electron formalism allows certain of the metastable rotational and spectral strengths to be determined from eq. 67 through 92 also.

(38) The wave functions and energies for the multiply excited electronic states of transition metal compounds of trigonal and other low symmetries will be the subject of future communication [A. D.

also, by configurational interaction. This process will be discussed later in §4.2c. With these reservations, the apropos two- and eight-electron charge amplitudes follow.

(a) *No Configuration Interaction: Zero Spin-Orbit Forces.* (i) *Wave Functions: Two Electrons*

$${}^3A_2[{}^3T_{1g}(t^2{}_{2g})]: |e_+(t_{2g})e_-(t_{2g})|$$

$${}^3E_\pm{}^3[T_{1g}(t^2{}_{2g})]: \mp |a_1(t_{2g})e_\pm(t_{2g})|$$

$${}^3A_1[{}^3T_{2g}(t_{2g}e_g)]: \frac{1}{\sqrt{2}} \{|e_+(t_{2g})e_-(e_g)| + |e_-(t_{2g})e_+(e_g)|\}$$

$${}^3E_\pm[{}^3T_{2g}(t_{2g}e_g)]: \frac{1}{\sqrt{2}} \{|a_1(t_{2g})e_\pm(e_g)| - |e_\mp(t_{2g})e_\mp(e_g)|\}$$

$${}^3A_2[{}^3T_{1g}(t_{2g}e_g)]: \frac{1}{\sqrt{2}} \{|e_+(t_{2g})e_-(e_g)| - |e_-(t_{2g})e_+(e_g)|\}$$

$${}^3E_\pm[{}^3T_{1g}(t_{2g}e_g)]: \pm \frac{1}{\sqrt{2}} \{|a_1(t_{2g})e_\pm(e_g)| + |e_\mp(t_{2g})e_\mp(e_g)|\}$$

$${}^3A_2[{}^3A_{2g}(e_g{}^2)]: |e_+(e_g)e_-(e_g)|$$

$${}^1A_1[{}^1T_{2g}(t_{2g}{}^2)]: \frac{1}{\sqrt{6}} \{2|a_1(t_{2g})\bar{a}_1(t_{2g})| - |e_+(t_{2g})\bar{e}_-(t_{2g})| + |\bar{e}_+(t_{2g})e_-(t_{2g})|\}$$

$${}^1E_\pm[{}^1T_{2g}(t_{2g}{}^2)]: -\frac{1}{\sqrt{6}} \{|a_1(t_{2g})\bar{e}_\pm(t_{2g})| - |\bar{a}_1(t_{2g})e_\pm(t_{2g})| + 2|e_\mp(t_{2g})\bar{e}_\mp(t_{2g})|\}$$

$${}^1E_\pm[{}^1E_{1g}(t_{2g}{}^2)]: \frac{1}{\sqrt{3}} \{|a_1(t_{2g})\bar{e}_\pm(t_{2g})| - |\bar{a}_1(t_{2g})e_\pm(t_{2g})| - |e_\mp(t_{2g})\bar{e}_\mp(t_{2g})|\}$$

$${}^1A_1[{}^1A_{1g}(t_{2g}{}^2)]: \frac{1}{\sqrt{3}} \{|a_1(t_{2g})\bar{a}_1(t_{2g})| + |e_+(t_{2g})\bar{e}_-(t_{2g})| - |\bar{e}_+(t_{2g})e_-(t_{2g})|\} \quad (67)$$

(ii) *Wave Functions: Eight Electrons.*

$${}^3A_2[{}^3A_{2g}(t_{2g}{}^6e_g{}^2)]: |a_1(t_{2g})^2e_\pm(t_{2g})^4e_+(e_g)e_-(e_g)|$$

$${}^3A_1[{}^3T_{2g}(t_{2g}{}^5e_g{}^3)]:$$

$$\frac{1}{\sqrt{2}} \{|a_1(t_{2g})^2e_+(t_{2g})e_-(t_{2g})^2e_+(e_g)^2e_-(e_g)| + |a_1(t_{2g})^2e_+(t_{2g})^2e_-(t_{2g})e_+(e_g)e_-(e_g)^2|\}$$

$${}^3E_\pm[{}^3T_{2g}(t_{2g}{}^5e_g{}^3)]: \frac{1}{\sqrt{2}} \{|a_1(t_{2g})e_\pm(t_{2g})^4e_\pm(e_g)^2e_\mp(e_g)| - |a_1(t_{2g})^2e_\pm(t_{2g})e_\mp(t_{2g})^2e_\pm(e_g)e_\mp(e_g)^2|\}$$

$${}^3A_2[{}^3T_{1g}(t_{2g}{}^5e_g{}^3)]:$$

$$\frac{1}{\sqrt{2}} \{|a_1(t_{2g})^2e_+(t_{2g})e_-(t_{2g})^2e_+(e_g)^2e_-(e_g)| - |a_1(t_{2g})^2e_+(t_{2g})^2e_-(t_{2g})e_+(e_g)e_-(e_g)^2|\}$$

$${}^3E_\pm[{}^3T_{1g}(t_{2g}{}^5e_g{}^3)]: \pm\frac{1}{\sqrt{2}} \{|a_1(t_{2g})e_\pm(t_{2g})^4e_\pm(e_g)^2e_\mp(e_g)| + |a_1(t_{2g})^2e_\pm(t_{2g})e_\mp(t_{2g})^2e_\pm(e_g)e_\mp(e_g)^2|\}$$

$${}^3A_2[{}^3T_{1g}(t_{2g}{}^4e_g{}^4)]: |a_1(t_{2g})^2e_+(t_{2g})e_-(t_{2g})e_\pm(e_g)^4|$$

$${}^3E_\pm[{}^3T_{1g}(t_{2g}{}^4e_g{}^4)]: \pm |a_1(t_{2g})e_\pm(t_{2g})^2e_\mp(t_{2g})e_\pm(e_g)^4|$$

$${}^1E_\pm[{}^1E_g(t_{2g}{}^6e_g{}^2)]: |a_1(t_{2g})^2e_\pm(t_{2g})^4e_+(e_g)\bar{e}_\mp(e_g)|$$

$${}^1A_1[{}^1A_{1g}(t_{2g}{}^6e_g{}^2)]: \frac{1}{\sqrt{2}} \{|a_1(t_{2g})^2e_\pm(t_{2g})^4e_+(e_g)\bar{e}_-(e_g)| - |a_1(t_{2g})^2e_\pm(t_{2g})^4e_+(e_g)e_-(e_g)|\} \quad (68)$$

The rotatory and spectral matrix elements which follow are facilely obtained from eq. 67 and 68.

(iii) *Matrix Elements: Two Electrons*

$$\left\langle {}^3A_2[{}^3T_{1g}(t_{2g}{}^2)] \left| \frac{\vec{p}}{\vec{m}} \right| {}^3E_\pm[{}^3T_{1g}(t_{2g}{}^2)] \right\rangle = \left\langle e_\mp(t_{2g}) \left| \frac{\vec{p}}{\vec{m}} \right| a_1(t_{2g}) \right\rangle$$

$$\left\langle {}^3A_2[{}^3T_{1g}(t_{2g}{}^2)] \left| \frac{\vec{p}}{\vec{m}} \right| {}^3A_1[{}^3T_{2g}(t_g e_g)] \right\rangle = \sqrt{2} \left\langle e_-(t_{2g}) \left| \frac{\vec{p}}{\vec{m}} \right| e_-(e_g) \right\rangle$$

$$\left\langle {}^3A_2[{}^3T_{1g}(t_{2g}{}^2)] \left| \frac{\vec{p}}{\vec{m}} \right| {}^3E_\pm[{}^3T_{2g}(t_g e_g)] \right\rangle = \pm\frac{1}{\sqrt{2}} \left\langle e_\pm(t_{2g}) \left| \frac{\vec{p}}{\vec{m}} \right| e_\mp(e_g) \right\rangle$$

$$\left\langle {}^3A_2[{}^3T_{1g}(t_{2g}{}^2)] \left| \frac{\vec{p}}{\vec{m}} \right| {}^3A_2[{}^3T_{1g}(t_{2g}e_g)] \right\rangle = 0$$

$$\left\langle {}^3A_2[{}^3T_{1g}(t_{2g}{}^2)] \left| \frac{\vec{p}}{\vec{m}} \right| {}^3E_\pm[{}^3T_{1g}(t_{2g}e_g)] \right\rangle = -\frac{1}{\sqrt{2}} \left\langle e_\pm(t_{2g}) \left| \frac{\vec{p}}{\vec{m}} \right| e_\mp(e_g) \right\rangle$$

$$\left\langle {}^3A_2[{}^3T_{1g}(t_{2g}{}^2)] \left| \frac{\vec{p}}{\vec{m}} \right| {}^3A_2[{}^3A_{2g}(e_g{}^2)] \right\rangle = 0 \quad (69)$$

$$\left\langle {}^3E_\pm[{}^3T_{1g}(t_{2g}{}^2)] \left| \frac{\vec{p}}{\vec{m}} \right| {}^3A_1[{}^3T_{2g}(t_{2g}e_g)] \right\rangle = \pm\frac{1}{\sqrt{2}} \left\langle a_1(t_{2g}) \left| \frac{\vec{p}}{\vec{m}} \right| e_\mp(e_g) \right\rangle$$

$$\left\langle {}^3E_\pm[{}^3T_{1g}(t_{2g}{}^2)] \left| \frac{\vec{p}}{\vec{m}} \right| {}^3E_\pm[{}^3T_{2g}(t_{2g}e_g)] \right\rangle =$$

$$\mp \frac{1}{\sqrt{2}} \left\langle e_\pm(t_{2g}) \left| \frac{\vec{p}}{\vec{m}} \right| e_\pm(e_g) \right\rangle$$

$$\left\langle {}^3E_\pm[{}^3T_{1g}(t_{2g}{}^2)] \left| \frac{\vec{p}}{\vec{m}} \right| {}^3E_\mp[{}^3T_{2g}(t_{2g}e_g)] \right\rangle =$$

$$\mp \frac{1}{\sqrt{2}} \left\{ \left\langle e_\pm(t_{2g}) \left| \frac{\vec{p}}{\vec{m}} \right| e_\mp(e_g) \right\rangle + \left\langle a_1(t_{2g}) \left| \frac{\vec{p}}{\vec{m}} \right| e_\pm(e_g) \right\rangle \right\}$$

$$\left\langle {}^3E_\pm[{}^3T_{1g}(t_{2g}{}^2)] \left| \frac{\vec{p}}{\vec{m}} \right| {}^3A_2[{}^3T_{1g}(t_g e_g)] \right\rangle =$$

$$\frac{1}{\sqrt{2}} \left\langle a_1(t_{2g}) \left| \frac{\vec{p}}{\vec{m}} \right| e_\mp(e_g) \right\rangle$$

$$\left\langle {}^3E_\pm[{}^3T_{1g}(t_{2g}{}^2)] \left| \frac{\vec{p}}{\vec{m}} \right| {}^3E_\pm[{}^3T_{1g}(t_{2g}e_g)] \right\rangle =$$

$$- \frac{1}{\sqrt{2}} \left\langle e_\pm(t_{2g}) \left| \frac{\vec{p}}{\vec{m}} \right| e_\pm(e_g) \right\rangle$$

$$\left\langle {}^3E_\pm[{}^3T_{1g}(t_{2g}{}^2)] \left| \frac{\vec{p}}{\vec{m}} \right| {}^3E_\mp[{}^3T_{1g}(t_{2g}e_g)] \right\rangle =$$

$$- \frac{1}{\sqrt{2}} \left\{ \left\langle e_\pm(t_{2g}) \left| \frac{\vec{p}}{\vec{m}} \right| e_\mp(e_g) \right\rangle - \left\langle a_1(t_{2g}) \left| \frac{\vec{p}}{\vec{m}} \right| e_\pm(e_g) \right\rangle \right\}$$

$$\left\langle {}^3E_\pm[{}^3T_{1g}(t_{2g}{}^2)] \left| \frac{\vec{p}}{\vec{m}} \right| {}^3A_2[{}^3A_{2g}(e_g{}^2)] \right\rangle = 0 \qquad (70)$$

(iv)   Matrix Elements: Eight Electrons

$$\left\langle {}^3A_2[{}^3A_{2g}(t_{2g}{}^6e_g{}^2)] \left| \frac{\vec{p}}{\vec{m}} \right| {}^3A_1[{}^3T_{2g}(t_{2g}{}^5e_g{}^3)] \right\rangle =$$

$$\sqrt{2} \left\langle e_-(t_{2g}) \left| \frac{\vec{p}}{\vec{m}} \right| e_-(e_g) \right\rangle$$

$$\left\langle {}^3A_2[{}^3A_{2g}(t_{2g}{}^6e_g{}^2)] \left| \frac{\vec{p}}{\vec{m}} \right| {}^3E_\pm[{}^3T_{2g}(t_{2g}{}^5e_g{}^3)] \right\rangle =$$

$$\mp \frac{1}{\sqrt{2}} \left\{ \left\langle a_1(t_{2g}) \left| \frac{\vec{p}}{\vec{m}} \right| e_\pm(e_g) \right\rangle + \left\langle e_\pm(t_{2g}) \left| \frac{\vec{p}}{\vec{m}} \right| e_\mp(e_g) \right\rangle \right\}$$

$$\left\langle {}^3A_2[{}^3A_{2g}(t_{2g}{}^6e_g{}^2)] \left| \frac{\vec{p}}{\vec{m}} \right| {}^3A_2[{}^3T_{1g}(t_{2g}{}^5e_g{}^3)] \right\rangle \equiv 0$$

$$\left\langle {}^3A_2[{}^3A_{2g}(t_{2g}{}^6e_g{}^2)] \left| \frac{\vec{p}}{\vec{m}} \right| {}^3E_\pm[{}^3T_{1g}(t_{2g}{}^5e_g{}^3)] \right\rangle =$$

$$\frac{1}{\sqrt{2}} \left\{ \left\langle e_\pm(t_{2g}) \left| \frac{\vec{p}}{\vec{m}} \right| e_\mp(e_g) \right\rangle - \left\langle a_1(t_{2g}) \left| \frac{\vec{p}}{\vec{m}} \right| e_\pm(e_g) \right\rangle \right\}$$

$$\left\langle {}^3A_2[{}^3A_{2g}(t_{2g}{}^6e_g{}^2)] \left| \frac{\vec{p}}{\vec{m}} \right| {}^3A_2[{}^3T_{1g}(t_{2g}{}^4e_g{}^4)] \right\rangle \equiv 0$$

$$\left\langle {}^3A_2[{}^3A_{2g}(t_{2g}{}^6e_g{}^2)] \left| \frac{\vec{p}}{\vec{m}} \right| {}^3E_\pm[{}^3T_{1g}(t_{2g}{}^4e_g{}^4)] \right\rangle = 0 \qquad (71)$$

We again see that the rotational and spectral strengths and dissymetry factors are simply related in a formal algebraic manner to the one-electron mathematical rotational, spectral, and dissymmetry expressions of eq. 52, 53, and 60. Observe that, because of the elementary structure of the one-electron electric and magnetic dipole matrix terms of eq. 47, many electron rotational and spectral strengths due to single electron hops between many electron configurations of the type N and V ($N,V = A_1, A_2, E_\pm$), which depend on sums of the form

$$a \left\langle a_1(t_{2g}) \left| \frac{\vec{p}}{\vec{m}} \right| e_\pm(e_g) \right\rangle \pm b \left\langle e_\pm(t_{2g}) \left| \frac{\vec{p}}{\vec{m}} \right| e_\mp(e_g) \right\rangle$$

can be succinctly expressed as

$$\mathfrak{R}[N \longrightarrow V] =$$

$$a(a \pm b N_{a_1(t)}{}^{-1} N_{e(t)}) \mathfrak{R}[a_1(t_{2g}) \longrightarrow e_\pm(e_g)] +$$

$$b(b \pm a N_{a_1(t)} N_{e(t)}{}^{-1}) \mathfrak{R}[e_\pm(t_{2g}) \longrightarrow e_\mp(e_g)]$$

$$\mathbb{S}[N \longrightarrow V] = a^2 \mathbb{S}[a_1(t_{2g}) \longrightarrow e_\pm(e_g)] +$$

$$b^2 \mathbb{S}[e_\pm(t_{2g}) \longrightarrow e_\mp(e_g)] \pm$$

$$2ab(\mathbb{S}[a_1(t_{2g}) \longrightarrow e_\pm(e_g)] \mathbb{S}[e_\pm(t_{2g}) \longrightarrow e_\mp(e_g)])^{1/2}$$

$$(72)$$

The sign of the square root in eq. 72 is that of the product $\xi\eta$ when the normalization constants of eq. 11, 17, 18, 33, and 47 of §1.1, 1.2, and 3.3 are taken to be positive. The external explicit plus and minus signs are chosen in accord with the rule that when the final state V is of species T_{2g} the sign is positive and when V is of species T_{1g} the sign is negative [cf. eq. 70 and 71]. An equation parallel to (72) may be obtained for the associated dissymmetry factors by substitution into eq. 59 of §3.5. In the case of the electronic transitions N to V, where $\{N,V\}$ equals $\{ {}^3E_\pm(T_{1g}), {}^3E_\mp(T_{1 \text{ or } 2g}) \}$ or $\{ {}^3A_2(A_{2g}), {}^3E_\pm(T_{1 \text{ or } 2g}) \}$, of eq. 70 and 71, in which a and b equal $\pm\sqrt{1/2}$, we can write

$$\mathfrak{R}[N \longrightarrow V] =$$

$$\frac{1}{2} \{ (1 \pm N_{a_1(t)}{}^{-1} N_{e(t)}) \mathfrak{R}[a_1(t_{2g}) \longrightarrow e_\pm(e_g)] +$$

$$(1 \pm N_{a_1(t)} N_{e(t)}{}^{-1}) \mathfrak{R}[e_\pm(t_{2g}) \longrightarrow e_\mp(e_g)] \}$$

$$\mathbb{S}[N \longrightarrow V] = \frac{1}{2} \{ \mathbb{S}[a_1(t_{2g}) \longrightarrow e_\pm(e_g)] +$$

$$\mathbb{S}[e_\pm(t_{2g}) \longrightarrow e_\mp(e_g)] \pm$$

$$2(\mathbb{S}[a_1(t_{2g}) \longrightarrow e_\pm(e_g)] \mathbb{S}[e_\pm(t_{2g}) \longrightarrow e_\mp(e_g)])^{1/2} \} \quad (73)$$

Note that as the rotational and spectral strengths are observables they are invariant of all symmetry operations permitted the conformation and, hence, that they are independent of the subscripts $\pm$ on the many electron state functions or on the one-electron molecular
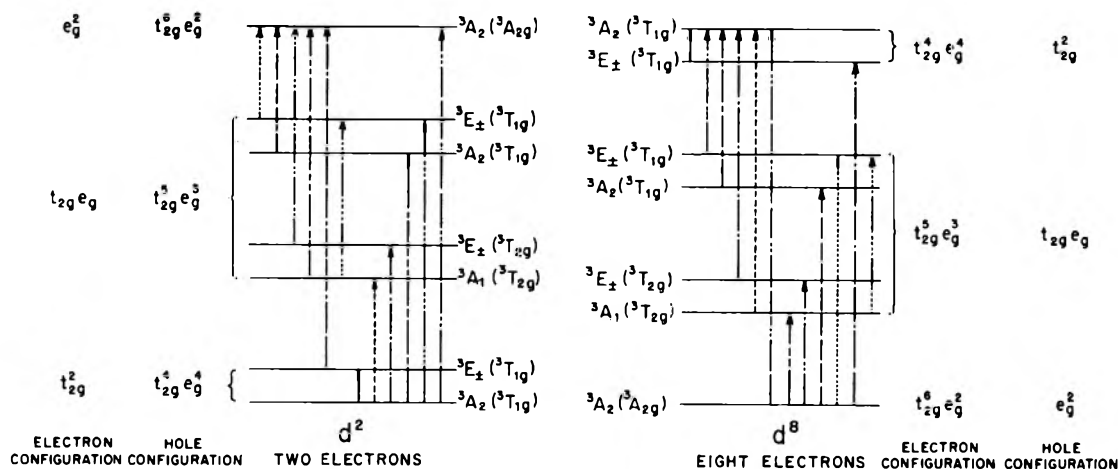
Figure 15. Digramatic illustration of the conjugate two- and eight-electron electronic transitions in the orbital representation. Correspondent pairs of transitions are depicted by correspondent lines.

orbitals, since these subscripts are inverted by the symmetry operation $\mathcal{C}_2(y')$. Therefore, expressions like those of eq. 72 and 73, and their relatives, are independent of the individual signs of the many electron state function subscripts or the one-electron molecular orbital subscripts, but are, of course, dependent upon their relative order, $\{ \pm, \pm \}$ or $\{ \pm, \mp \}$. Witness that, unlike the one- and nine-electron case, there is no formal equivalence of the two- and eight-electron rotational and spectral strengths. This declaration ensues because the electronic leaps of usual practical import are not electron-hole complements [view Fig. 15].

(b) *No Configuration Interaction: Nonzero Spin-Orbit Forces. Two and Eight Electrons.* The many electron spin-orbit wave functions are readily built up by the successive population of the one-electron trigonal molecular spin-orbital functions of eq. 34.[39] It should be noticed, however, that many electron spin-orbit functions of this sort are not simply related to the correspondent orbital functions. For example, from eq. 34, we have

$$\Gamma_1[\gamma_6^{(7)}(t_{2g})^2] = -\frac{1}{3}\left|\bar{a}_1(t_{2g})a_1(t_{2g})\right| +$$

$$\frac{\sqrt{2}}{3}\left|\bar{a}_1(t_{2g})e_+(t_{2g})\right| + \frac{\sqrt{2}}{3}\left|a_1(t_{2g})e_-(t_{2g})\right| -$$

$$\frac{2}{3}\left|\bar{e}_+(t_{2g})e_-(t_{2g})\right|$$

which is a complicated mixture of the usual orbital singlets and triplets formed from the t_{2g}^2 configuration. Hence, for systems of small spin-orbit forces these spin-orbital functions are most inconvenient; for large spin-

orbit forces they are useful, though. In our further work in this paper we shall have no use for functions of this kind, and so we defer to later communication an extensive demonstration of their utility.[40] Needless to say, however, the two- and eight-electron rotational and spectral strengths obtained with such wave functions are simply expressed in terms of those of the one-electron problem as in §4.1a and b.

(c) *Configuration Interaction: Zero and Nonzero Spin-Orbit Forces.* When configuration interaction is included the results summarized in §4.1a and b above are but slightly modified. Two examples should serve to make this point clear. For the two- and eight-electron cases, the trigonal $^3A_2(T_{1g})$ and $^3E(T_{1g})$ state functions can be written as given below.

(i) *Wave Functions: Two Electrons. Zero Spin-Orbit Forces.*

$$\Upsilon(^3A_2) = B{}^3A_2(T_{1g})^{(1)} + C{}^3A_2(T_{1g})^{(2)} + D{}^3A_2(A_{2g}) \quad (74)$$

(ii) *Wave Functions: Eight Electrons. Zero Spin-Orbit Forces*

$$\Upsilon(^3E_\pm) = B{}^3E_\pm(T_{1g})^{(1)} + C{}^3E_\pm(T_{1g})^{(2)} + D{}^3E_\pm(T_{2g})$$
$$(75)$$

where the superscripts (1) and (2) order the cubical $^3T_{1g}$ states and their trigonal components in an energetic sequence. The constants B, C, and D which appear in

(39) Since the author's formulation of this method (1957), reported in ref. 9, the general technique has been applied to a few specific instances by W. E. Moffitt, G. L. Goodman, M. Fred, and B. Weinstock, *Mol. Phys.*, 2, 109 (1959).

(40) A. D. Liehr, to be published.

eq. 74 and 75 are real.[41] With these wave functions, the configurationally interacted rotational strengths become as shown below.

(iii) Rotational Strengths: Two Electrons. Zero Spin-Orbit Forces

$$\Re[^3A_2 \longrightarrow {}^3A_1(T_{2g})] = (B + D)[2(B - D) + C] \times$$
$$\Re[e_-(t_{2g}) \longrightarrow e_-(e_g)] \quad (76)$$

(iv) Rotational Strengths: Eight Electrons. Zero Spin-Orbit Forces

$$\Re[^3A_2(A_{2g}) \longrightarrow {}^3E_\pm] =$$
$$B\Re[^3A_2(A_{2g}) \longrightarrow {}^3E_\pm(T_{1g})^{(1)}] +$$
$$D\Re[^3A_2(A_{2g}) \longrightarrow {}^3E_\pm(T_{2g})] \quad (77)$$

where the rotational strengths $\Re[^3A_2(A_{2g}) \rightarrow {}^3E_\pm(T_{(\frac{1}{2})g})]$ of eq. 77 are as given in eq. 73, with the external plus sign in eq. 73 associated with the upper state $E_\pm(T_{2g})$ and the minus with the upper state $E_\pm(T_{1g})^{(1)}$ [recall eq. 71]. In this connection, note particularly from eq. 71 and 73 that the eight-electron [*e.g.*, nickel(II)] trigonal dihedral electronic leaps to the $^3T_{1g}$-like electronic states from the $^3A_2$ ground electronic state should be much more weakly rotatory than those to the $^3T_{2g}$-like states, as would be predicted on the basis of cubical selection rules [the A_{2g} to T_{1g} transition is magnetically forbidden in the point group O_h], and that the T_{1g}-like electronic states become rotationally active solely by virtue of the difference in bond strengths [as measured by the variational parameters η and ξ] and ligand metal overlaps [as reflected in the different normalization constants $N_{a_1(t)}$ and $N_{e(t)}$] for the $a_1(t_{2g})$ and $e_\pm(t_{2g})$ one-electron molecular orbitals, and by the trigonal mixing of the active $^3T_{2g}$-like states into the $^3T_{1g}$-like states. This weakness is actually observed.[42]

(v) Wave Functions and Rotational Strengths: Two and Eight Electrons. Nonzero Spin-Orbit Forces. Formulas analogous to (74) through (77) can be derived also for the spin-orbital configurational hybrids by straightforward but tedious and lengthy calculations as described in §4.2b. Mark especially in this connection that without spin-orbit forces no rotatory or spectral power is available to the two- and eight-electron singlet electronic states. Only when spin-orbit configurational interaction is included do these states become rotationally active. This topic will be further considered in section IV.

4.3 *The Three- and Seven-Electron Case.* In accord with our earlier comments in §4.2 we confine our considerations of the three- and seven-electron problem to the single electron excitations alone, the others to be

left for ensuant work.[38,43] With this restriction, the suitably oriented trigonal electronic state functions for the three- and seven-electron configurations are as shown below.

(a) No Configuration Interation: Zero Spin-Orbit Forces. (i) Wave Functions: Three Electrons

$$^4A_2[^4A_{2g}(t_{2g}{}^3)]:\left|a_1(t_{2g})e_+(t_{2g})e_-(t_{2g})\right|$$

$$^4A_1[^4T_{2g}(t_{2g}{}^2e_g)]:\frac{1}{\sqrt{2}}\left\{\left|a_1(t_{2g})e_+(t_{2g})e_-(e_g)\right| + \left|a_1(t_{2g})e_-(t_{2g})e_+(e_g)\right|\right\}$$

$$^4E_\pm[^4T_{1g}(t_{2g}{}^2e_g)]:\frac{1}{\sqrt{2}}\left\{\left|a_1(t_{2g})e_\mp(t_{2g})e_\mp(e_g)\right| - \left|e_\pm(t_{2g})e_\mp(t_{2g})e_\pm(e_g)\right|\right\}$$

$$^4A_2[^4T_{1g}(t_{2g}{}^2e_g)]:\frac{1}{\sqrt{2}}\left\{\left|a_1(t_{2g})e_+(t_{2g})e_-(e_g)\right| - \left|a_1(t_{2g})e_-(t_{2g})e_+(e_g)\right|\right\}$$

$$^4E_\pm[^4T_{1g}(t_{2g}{}^2e_g)]:\frac{\mp 1}{\sqrt{2}}\left\{\left|a_1(t_{2g})e_\mp(t_{2g})e_\mp(e_g)\right| + \left|e_\pm(t_{2g})e_\mp(t_{2g})e_\pm(e_g)\right|\right\}$$

$$^4A_2[^4T_{1g}(t_{2g}e_g{}^2)]:\left|a_1(t_{2g})e_+(e_g)e_-(e_g)\right|$$

$$^4E_\pm[^4T_{1g}(t_{2g}e_g{}^2)]:-\left|e_\pm(t_{2g})e_+(e_g)e_-(e_g)\right|$$

$$^2E_\pm[^2E_g(t_{2g}{}^3)]:\frac{1}{\sqrt{3}}\left\{\left|a_1(t_{2g})\bar{a}_1(t_{2g})e_\pm(t_{2g})\right| - \left|a_1(t_{2g})e_\mp(t_{2g})\bar{e}_\mp(t_{2g})\right| + \left|e_\pm(t_{2g})\bar{e}_\pm(t_{2g})e_\mp(t_{2g})\right|\right\}$$

(41) This allegation is hurriedly averred by invocation of symmetry arguments and first-order perturbation theory [recall footnotes 29 and 30]. It is proved by the circumstance that B, C, and D depend on many electron matrix elements of the sort $\langle A_7|\mathcal{H}_{trigonal}|A_2\rangle$ and $\langle E_\pm|\mathcal{H}_{trigonal}|E_\pm\rangle$ which are both proportional to the one-electron matrix element $\langle e_\pm(t_{2g})|\mathcal{H}_{trigonal}|e_\pm(e_g)\rangle$, except that for $E_\pm(T_{2g})$ and $E_\pm^{(1)}(T_{1g})$ which is proportional to $\langle e_\pm(t_{2g})|\mathcal{H}_{trigonal}|e_\pm(t_{2g})\rangle - \langle a_1(t_{2g})|\mathcal{H}_{trigonal}|a_1(t_{2g})\rangle$ [*cf.* eq. 67 and 68]. But as these matrix terms are Hermitean and as $\mathcal{C}_2(y')e_\pm(t_{2g}$ or $e_g)$ equals $e_\mp(t_{2g}$ or $e_g)$, with $e_\pm(t_{2g}$ or $e_g)^*$ equals $e_\mp(t_{2g}$ or $e_g)$, we have that the matrix terms are real, and hence, that the constants B, C, and D are real. Notice in passing that for the two-electron problem, in the limit of first-order perturbation theory, with $A_2(T_{1g})^{(2)}$ and $E_\pm(E_{1g})^{(2)}$ the highest T_{1g}-like states, that the constant C, which mixes the T_{1g}-like state (2) with the T_{1g}-like state (1), is in the ratio of 2:1 for the A_2 and $E_\pm$ state mixtures, respectively.

(42) (a) J. P. Mathieu, *Ann. Phys.*, **19**, 335 (1944); (b) F. Woldbye, "Optical Rotatory Dispersion of Transition Metal Complexes," Final Technical Report to the European Research Office, U. S. Department of the Army, Frankfurt am Main, June 30, 1959, Contract No. DA-91-508-EUC-246.

(43) The trigonally oriented cubical d^n, (n = 3, 4, 5, 6, 7), determinartal wave functions are most painlessly constructed by a two-step procedure. First one constructs the trigonally oriented $d^{1,2,8,9}$ functions by the techniques of ref. 9 and footnote 38, and second one conjoins these by the Tanabe and Sugano parental relations as tabulated, for example, in ref. 34, Appendix 2, making certain that the issuant expressions are both orthonormally and transformationally sound [*cf.* Table III] under integrations and under symmetry operations such as $\mathcal{C}_4(z)$, $\mathcal{C}_3(z')$, and $\mathcal{C}_2(y')$ of Tables I and IV. [The d^{10-n} functions are gotten from the d^n functions, (n = 1, 2, 3, 4), by electron-hole conjugation as before.[38]]

$^2A_1[^2T_{2g}(t_{2g}{}^3)]: \dfrac{1}{\sqrt{2}} \{ |a_1(t_{2g})e_+(t_{2g})\bar{e}_-(t_{2g})| -$

$$|a_1(t_{2g})\bar{e}_+(t_{2g})e_-(t_{2g})| \}$$

$^2E_\pm[^2T_{2g}(t_{2g}{}^3)]: \dfrac{1}{\sqrt{2}} \{ |a_1(t_{2g})\bar{a}_1(t_{2g})e_\pm(t_{2g})| -$

$$|e_\pm(t_{2g})\bar{e}_\pm(t_{2g})e_\mp(t_{2g})| \}$$

$^2A_2[^2T_{1g}(t_{2g}{}^3)]: \dfrac{1}{\sqrt{6}} \{ 2|\bar{a}_1(t_{2g})e_+(t_{2g})e_-(t_{2g}) -$

$$|a_1(t_{2g})e_+(t_{2g})\bar{e}_-(t_{2g})| - |a_1(t_{2g})\bar{e}_+(t_{2g})e_-(t_{2g})| \}$$

$^2E_\pm[^2T_{1g}(t_{2g}{}^3)]: \mp \dfrac{1}{\sqrt{6}} \{ 2|a_1(t_{2g})e_\mp(t_{2g})\bar{e}_\mp(t_{2g})| +$

$$|a_1(t_{2g})\bar{a}_1(t_{2g})e_\pm(t_{2g})| + |e_\pm(t_{2g})\bar{e}_\pm(t_{2g})e_\mp(t_{2g})| \} \quad (78)$$

(ii)   *Wave Functions: Seven Electrons*

$^4A_2[^4T_{1g}(t_{2g}{}^5e_g{}^2)]: |a_1(t_{2g})e_\pm(t_{2g})^4e_+(e_g)e_-(e_g)|$

$^4E_\pm[^4T_{1g}(t_{2g}{}^5e_g{}^2)]: - |a_1(t_{2g})^2e_\pm(t_{2g})^2e_\mp(t_{2g})e_+(e_g)e_-(e_g)|$

$^4A_1[^4T_{2g}(t_{2g}{}^4e_g{}^3)]:$

$$\dfrac{1}{\sqrt{2}} \{ |a_1(t_{2g})e_+(t_{2g})e_-(t_{2g})^2e_+(e_g)^2e_-(e_g)| +$$

$$|a_1(t_{2g})e_+(t_{2g})^2e_-(t_{2g})e_+(e_g)e_-(e_g)^2| \}$$

$E_\pm[^4T_{2g}(t_{2g}{}^4e_g{}^3)]:$

$$\dfrac{1}{\sqrt{2}} \{ |a_1(t_{2g})e_\pm(t_{2g})e_\mp(t_{2g})^2e_\pm(e_g)e_\mp(e_g)^2| -$$

$$|a_1(t_{2g})^2e_\mp(t_{2g})e_\pm(t_{2g})e_\pm(e_g)^2e_\mp(e_g)| \}$$

$^4A_2[^4T_{1g}(t_{2g}{}^4e_g{}^3)]:$

$$\dfrac{1}{\sqrt{2}} \{ |a_1(t_{2g})e_+(t_{2g})e_-(t_{2g})^2e_+(e_g)^2e_-(e_g)| -$$

$$|a_1(t_{2g})e_+(t_{2g})^2e_-(t_{2g})e_+(e_g)e_-(e_g)^2| \}$$

$^4E_\pm[^4T_{1g}(t_{2g}{}^4e_g{}^3)]:$

$$\pm \dfrac{1}{\sqrt{2}} \{ |a_1(t_{2g})e_\pm(t_{2g})e_\mp(t_{2g})^2e_\pm(e_g)e_\mp(e_g)^2| +$$

$$|a_1(t_{2g})^2e_\mp(t_{2g})e_\pm(t_{2g})e_\pm(e_g)^2e_\mp(e_g)| \}$$

$^4A_2[^4A_{2g}(t_{2g}{}^3e_g{}^4]: |a_1(t_{2g})e_+(t_{2g})e_-(t_{2g})e_+(e_g)^2e_-(e_g)^2|$

$^2E_\pm[^2E_g(t_{2g}{}^6e_g)]: |a_1(t_{2g})^2e_\pm(t_{2g})^4e_\pm(e_g)|$

$^2A_2[^2T_{1g}(t_{2g}{}^5e_g{}^2)]: \dfrac{1}{\sqrt{6}} \{ |a_1(t_{2g})e_\pm(t_{2g})^4e_+(e_g)\bar{e}_-(e_g)| +$

$$|a_1(t_{2g})e_\pm(t_{2g})^4\bar{e}_+(e_g)e_-(e_g)| -$$

$$2|\bar{a}_1(t_{2g})e_\pm(t_{2g})^4e_+(e_g)e_-(e_g)| \}$$

$^2E_\pm[^2T_{1g}(t_{2g}{}^5e_g{}^2)]:$

$$\pm \dfrac{1}{\sqrt{6}} \{ |a_1(t_{2g})^2e_\pm(t_{2g})^2e_\mp(t_{2g})\bar{e}_\pm(e_g)e_\mp(e_g)| +$$

$$|a_1(t_{2g})^2\bar{e}_\pm(t_{2g})^2e_\mp(t_{2g})e_\pm(e_g)\bar{e}_\mp(e_g)| -$$

$$2|a_1(t_{2g})^2e_\pm(t_{2g})^2\bar{e}_\mp(t_{2g})e_\pm(e_g)e_\mp(e_g)| \}$$

$^2A_1[^2T_{2g}(t_{2g}{}^5e_g{}^2)]:$

$$\dfrac{1}{\sqrt{2}} \{ |a_1(t_{2g})^2e_+(t_{2g})e_-(t_{2g})^2e_-(e_g)\bar{e}_-(e_g)| +$$

$$|a_1(t_{2g})^2e_+(t_{2g})^2e_-(t_{2g})e_+(e_g)\bar{e}_+(e_g)| \}$$

$^2E_\pm[^2T_{2g}(t_{2g}{}^5e_g{}^2)]: \dfrac{1}{\sqrt{2}} \{ |a_1(t_{2g})e_\pm(t_{2g})^4e_\mp(e_g)\bar{e}_\mp(e_g)| -$

$$|a_1(t_{2g})^2e_\pm(t_{2g})e_\mp(t_{2g})^2e_\pm(e_g)\bar{e}_\pm(e_g)| \}$$

$^2A_2[^2T_{1g}(t_{2g}{}^5e_g{}^2)]:$

$$\dfrac{1}{\sqrt{2}} \{ |a_1(t_{2g})^2e_+(t_{2g})e_-(t_{2g})^2e_-(e_g)\bar{e}_-(e_g)| -$$

$$|a_1(t_{2g})^2e_+(t_{2g})^2e_-(t_{2g})e_+(e_g)\bar{e}_+(e_g)| \}$$

$^2E_\pm[^2T_{1g}(t_{2g}{}^5e_g{}^2)]: \dfrac{\mp 1}{\sqrt{2}} \{ |a_1(t_{2g})e_\pm(t_{2g})^4e_\mp(e_g)\bar{e}_\mp(e_g)| -$

$$|a_1(t_{2g})^2e_\pm(t_{2g})e_\mp(t_{2g})^2e_\pm(e_g)\bar{e}_\pm(e_g)| \}$$

$^2A_1[^2T_{2g}(t_{2g}{}^5e_g{}^2)]: \dfrac{1}{\sqrt{2}} \{ |a_1(t_{2g})e_\pm(t_{2g})^4e_+(e_g)\bar{e}_-(e_g)| -$

$$|a_1(t_{2g})e_\pm(t_{2g})^4\bar{e}_+(e_g)e_-(e_g)| \}$$

$^2E_\pm[^2T_{2g}(t_{2g}{}^5e_g{}^2)]:$

$$-\dfrac{1}{\sqrt{2}} \{ |a_1(t_{2g})^2e_\pm(t_{2g})^2e_\mp(t_{2g})e_\pm(e_g)\bar{e}_\mp(e_g)| -$$

$$|a_1(t_{2g})^2e_\pm(t_{2g})^2e_\mp(t_{2g})\bar{e}_\pm(e_g)e_\mp(e_g)| \} \quad (79)$$

From these functions the gyratory and optical matrix arrays, which succeed, are swiftly determined.

(iii)   *Matrix Elements: Three Electrons*

$$\left\langle {}^4A_2[^4A_{2g}(t_{2g}{}^3)] \left| \dfrac{\vec{p}}{\vec{m}} \right| {}^4A_1[^4T_{2g}(t_{2g}{}^2e_g)] \right\rangle =$$

$$\sqrt{2} \left\langle e_-(t_{2g}) \left| \dfrac{\vec{p}}{\vec{m}} \right| e_-(e_g) \right\rangle$$

$$\left\langle {}^4A_2[^4A_{2g}(t_{2g}{}^3)] \left| \dfrac{\vec{p}}{\vec{m}} \right| {}^4E_\pm[^4T_{2g}(t_{2g}{}^2e_g)] \right\rangle =$$

$$\dfrac{\mp 1}{\sqrt{2}} \left\{ \left\langle e_\pm(t_{2g}) \left| \dfrac{\vec{p}}{\vec{m}} \right| e_\mp(e_g) \right\rangle + \left\langle a_1(t_{2g}) \left| \dfrac{\vec{p}}{\vec{m}} \right| e_\pm(e_g) \right\rangle \right\}$$

$$\left\langle {}^4A_2[^4A_{2g}(t_{2g}{}^3)] \left| \dfrac{\vec{p}}{\vec{m}} \right| {}^4A_2[^4T_{1g}(t_{2g}{}^2e_g)] \right\rangle \equiv 0$$

$$\left\langle {}^4A_2[{}^4A_{2g}(t_{2g}{}^3)]\left|\frac{\vec{p}}{\vec{m}}\right|{}^4E_\pm[{}^4T_{1g}(t_{2g}{}^2e_g)]\right\rangle =$$

$$\frac{1}{\sqrt{2}}\left\{\left\langle e_\pm(t_{2g})\left|\frac{\vec{p}}{\vec{m}}\right|e_\mp(e_g)\right\rangle - \left\langle a_1(t_{2g})\left|\frac{\vec{p}}{\vec{m}}\right|e_\pm(e_g)\right\rangle\right\}$$

$$\left\langle {}^4A_2[{}^4A_{2g}(t_{2g}{}^3)]\left|\frac{\vec{p}}{\vec{m}}\right|{}^4A_2[{}^4T_{1g}(t_{2g}e_g{}^2)]\right\rangle \equiv 0$$

$$\left\langle {}^4A_2[{}^4A_{2g}(t_{2g}{}^3)]\left|\frac{\vec{p}}{\vec{m}}\right|{}^4E_\pm[{}^4T_{1g}(t_{2g}e_g{}^2)]\right\rangle = 0 \qquad (80)$$

(iv) Matrix Elements: Seven Electrons

$$\left\langle {}^4A_2[{}^4T_{1g}(t_{2g}{}^5e_g{}^2)]\left|\frac{\vec{p}}{\vec{m}}\right|{}^4E_\pm[{}^4T_{1g}(t_{2g}{}^5e_g{}^2)]\right\rangle =$$

$$- \left\langle e_\mp(t_{2g})\left|\frac{\vec{p}}{\vec{m}}\right|a_1(t_{2g})\right\rangle$$

$$\left\langle {}^4A_2[{}^4T_{1g}(t_{2g}{}^5e_g{}^2)]\left|\frac{\vec{p}}{\vec{m}}\right|{}^4A_1[{}^4T_{2g}(t_{2g}{}^4e_g{}^3)]\right\rangle =$$

$$\sqrt{2}\left\langle e_-(t_{2g})\left|\frac{\vec{p}}{\vec{m}}\right|e_-(e_g)\right\rangle$$

$$\left\langle {}^4A_2[{}^4T_{1g}(t_{2g}{}^5e_g{}^2)]\left|\frac{\vec{p}}{\vec{m}}\right|{}^4E_\pm[{}^4T_{2g}(t_{2g}{}^4e_g{}^3)]\right\rangle =$$

$$\frac{\pm 1}{\sqrt{2}}\left\langle e_\pm(t_{2g})\left|\frac{\vec{p}}{\vec{m}}\right|e_\mp(e_g)\right\rangle$$

$$\left\langle {}^4A_2[{}^4T_{1g}(t_{2g}{}^5e_g{}^2)]\left|\frac{\vec{p}}{\vec{m}}\right|{}^4A_2[{}^4T_{1g}(t_{2g}{}^4e_g{}^3)]\right\rangle \equiv 0$$

$$\left\langle {}^4A_2[{}^4T_{1g}(t_{2g}{}^5e_g{}^2)]\left|\frac{\vec{p}}{\vec{m}}\right|{}^4E_\pm[{}^4T_{1g}(t_{2g}{}^4e_g{}^3)]\right\rangle =$$

$$- \frac{1}{\sqrt{2}}\left\langle e_\pm(t_{2g})\left|\frac{\vec{p}}{\vec{m}}\right|e_\mp(e_g)\right\rangle$$

$$\left\langle {}^4A_2[{}^4T_{1g}(t_{2g}{}^5e_g{}^2)]\left|\frac{\vec{p}}{\vec{m}}\right|{}^4A_2[{}^4A_{2g}(t_{2g}{}^3e_g{}^4)]\right\rangle \equiv 0 \qquad (81)$$

$$\left\langle {}^4E_\pm[{}^4T_{1g}(t_{2g}{}^5e_g{}^2)]\left|\frac{\vec{p}}{\vec{m}}\right|{}^4A_1[{}^4T_{2g}(t_{2g}{}^4e_g{}^3)]\right\rangle =$$

$$\pm \frac{1}{\sqrt{2}}\left\langle a_1(t_{2g})\left|\frac{\vec{p}}{\vec{m}}\right|e_\mp(e_g)\right\rangle$$

$$\left\langle {}^4E_\pm[{}^4T_{1g}(t_{2g}{}^5e_g{}^2)]\left|\frac{\vec{p}}{\vec{m}}\right|{}^4E_\pm[{}^4T_{2g}(t_{2g}{}^4e_g{}^3)]\right\rangle =$$

$$\mp \frac{1}{\sqrt{2}}\left\langle e_\pm(t_{2g})\left|\frac{\vec{p}}{\vec{m}}\right|e_\pm(e_g)\right\rangle$$

$$\left\langle {}^4E_\pm[{}^4T_{1g}(t_{2g}{}^5e_g{}^2)]\left|\frac{\vec{p}}{\vec{m}}\right|{}^4E_\mp[{}^4T_{2g}(t_{2g}{}^4e_g{}^3)]\right\rangle =$$

$$\mp \frac{1}{\sqrt{2}}\left\{\left\langle e_\pm(t_{2g})\left|\frac{\vec{p}}{\vec{m}}\right|e_\mp(e_g)\right\rangle + \left\langle a_1(t_{2g})\left|\frac{\vec{p}}{\vec{m}}\right|e_\pm(e_g)\right\rangle\right\}$$

$$\left\langle {}^4E_\pm[{}^4T_{1g}(t_{2g}{}^5e_g{}^2)]\left|\frac{\vec{p}}{\vec{m}}\right|{}^4A_2[{}^4T_{1g}(t_{2g}{}^4e_g{}^3)]\right\rangle =$$

$$- \frac{1}{\sqrt{2}}\left\langle a_1(t_{2g})\left|\frac{\vec{p}}{\vec{m}}\right|e_\mp(e_g)\right\rangle$$

$$\left\langle {}^4E_\pm[{}^4T_{1g}(t_{2g}{}^5e_g{}^2)]\left|\frac{\vec{p}}{\vec{m}}\right|{}^4E_\pm[{}^4T_{1g}(t_{2g}{}^4e_g{}^3)]\right\rangle =$$

$$- \frac{1}{\sqrt{2}}\left\langle e_\pm(t_{2g})\left|\frac{\vec{p}}{\vec{m}}\right|e_\pm(e_g)\right\rangle$$

$$\left\langle {}^4E_\pm[{}^4T_{1g}(t_{2g}{}^5e_g{}^2)]\left|\frac{\vec{p}}{\vec{m}}\right|{}^4E_\mp[{}^4T_{1g}(t_{2g}{}^4e_g{}^3)]\right\rangle =$$

$$- \frac{1}{\sqrt{2}}\left\{\left\langle e_\pm(t_{2g})\left|\frac{\vec{p}}{\vec{m}}\right|e_\mp(e_g)\right\rangle - \left\langle a_1(t_{2g})\left|\frac{\vec{p}}{\vec{m}}\right|e_\pm(e_g)\right\rangle\right\}$$

$$\left\langle {}^4E_\pm[{}^4T_{1g}(t_{2g}{}^5e_g{}^2)]\left|\frac{\vec{p}}{\vec{m}}\right|{}^4A_2[{}^4A_{2g}(t_{2g}{}^3e_g{}^4)]\right\rangle = 0 \qquad (82a)$$

$$\left\langle {}^2E_\pm[{}^2E_g(t_{2g}{}^6e_g)]\left|\frac{\vec{p}}{\vec{m}}\right|{}^2A_2[{}^2T_{1g}(t_{2g}{}^5e_g{}^2)]\right\rangle =$$

$$\mp \sqrt{3/2}\left\langle a_1(t_{2g})\left|\frac{\vec{p}}{\vec{m}}\right|e_\mp(e_g)\right\rangle$$

$$\left\langle {}^2E_\pm[{}^2E_g(t_{2g}{}^6e_g)]\left|\frac{\vec{p}}{\vec{m}}\right|{}^2E_\pm[{}^2T_{1g}(t_2{}^5e_g{}^2)]\right\rangle =$$

$$\mp \sqrt{3/2}\left\langle e_\mp(t_{2g})\left|\frac{\vec{p}}{\vec{m}}\right|e_\mp(e_g)\right\rangle$$

$$\left\langle {}^2E_\pm[{}^2E_g(t_{2g}{}^6e_g)]\left|\frac{\vec{p}}{\vec{m}}\right|{}^2E_\mp[{}^2T_{1g}(t_{2g}{}^5e_g{}^2)]\right\rangle =$$

$$\pm \sqrt{3/2}\left\langle e_\pm(t_{2g})\left|\frac{\vec{p}}{\vec{m}}\right|e_\mp(e_g)\right\rangle$$

$$\left\langle {}^2E_\pm[{}^2E_g(t_{2g}{}^6e_g)]\left|\frac{\vec{p}}{\vec{m}}\right|{}^2A_1[{}^2T_{2g}(t_{2g}{}^5e_g{}^2)]\right\rangle =$$

$$- \frac{1}{\sqrt{2}}\left\langle e_\mp(t_{2g})\left|\frac{\vec{p}}{\vec{m}}\right|e_\pm(e_g)\right\rangle$$

$$\left\langle {}^2E_\pm[{}^2E_g(t_{2g}{}^6e_g)]\left|\frac{\vec{p}}{\vec{m}}\right|{}^2E_\pm[{}^2T_{2g}(t_{2g}{}^5e_g{}^2)]\right\rangle =$$

$$\frac{1}{\sqrt{2}}\left\langle e_\pm(t_{2g})\left|\frac{\vec{p}}{\vec{m}}\right|e_\pm(e_g)\right\rangle$$

$$\left\langle {}^2E_\pm[{}^2E_g(t_{2g}{}^6e_g)]\left|\frac{\vec{p}}{\vec{m}}\right|{}^2E_\mp[{}^2T_{2g}(t_{2g}{}^5e_g{}^2)]\right\rangle =$$

$$- \frac{1}{\sqrt{2}}\left\langle a_1(t_{2g})\left|\frac{\vec{p}}{\vec{m}}\right|e_\pm(e_g)\right\rangle$$

$$\left\langle {}^2E_\pm[{}^2E_g(t_{2g}{}^6e_g)]\left|\frac{\vec{p}}{\vec{m}}\right|{}^2A_2[{}^2T_{1g}(t_{2g}{}^5e_g{}^2)]\right\rangle =$$

$$\pm \frac{1}{\sqrt{2}}\left\langle e_\mp(t_{2g})\left|\frac{\vec{p}}{\vec{m}}\right|e_\pm(e_g)\right\rangle$$

$$\left\langle \, {}^2E_\pm[{}^2E_g(t_{2g}{}^6e_g)] \left| \frac{\vec{p}}{\vec{m}} \right| {}^2E_\pm[{}^2T_{1g}(t_{2g}{}^5e_g{}^2)] \, \right\rangle =$$

$$\mp \frac{1}{\sqrt{2}} \left\langle e_\pm(t_{2g}) \left| \frac{\vec{p}}{\vec{m}} \right| e_\pm(e_g) \right\rangle$$

$$\left\langle \, {}^2E_\pm[{}^2E_g(t_{2g}{}^6e_g)] \left| \frac{\vec{p}}{\vec{m}} \right| {}^2E_\mp[{}^2T_{1g}(t_{2g}{}^5e_g{}^2)] \, \right\rangle =$$

$$\pm \frac{1}{\sqrt{2}} \left\langle a_1(t_{2g}) \left| \frac{\vec{p}}{\vec{m}} \right| e_\pm(e_g) \right\rangle$$

$$\left\langle \, {}^2E_\pm[{}^2E_g(t_{2g}{}^6e_g)] \left| \frac{\vec{p}}{\vec{m}} \right| {}^2A_1[{}^2T_{2g}(t_{2g}{}^5e_g{}^2)] \, \right\rangle =$$

$$- \frac{1}{\sqrt{2}} \left\langle a_1(t_{2g}) \left| \frac{\vec{p}}{\vec{m}} \right| e_\mp(e_g) \right\rangle$$

$$\left\langle \, {}^2E_\pm[{}^2E_g(t_{2g}{}^6e_g)] \left| \frac{\vec{p}}{\vec{m}} \right| {}^2E_\pm[{}^2T_{2g}(t_{2g}{}^5e_g{}^2)] \, \right\rangle =$$

$$\frac{1}{\sqrt{2}} \left\langle e_\mp(t_{2g}) \left| \frac{\vec{p}}{\vec{m}} \right| e_\mp(e_g) \right\rangle$$

$$\left\langle \, {}^2E_\pm[{}^2E_g(t_{2g}{}^6e_g)] \left| \frac{\vec{p}}{\vec{m}} \right| {}^2E_\mp[{}^2T_{2g}(t_{2g}{}^5e_g{}^2)] \, \right\rangle =$$

$$\frac{1}{\sqrt{2}} \left\langle e_\pm(t_{2g}) \left| \frac{\vec{p}}{\vec{m}} \right| e_\mp(e_g) \right\rangle \quad (82b)$$

We espy from eq. 80, 81, and 82 that the rotational and spectral strengths of the three- and seven-electron puzzle are simply related to those of the two- and eight-electron problems anteriorly discussed. Indeed, we witness an exact one-to-one correspondence of the two- and seven-electron spin free rotational and spectral strengths and of the three- and eight-electron strengths, respectively. The seven-electron spin-paired rotational and spectral strengths are related multiplicatively to the one, four, six, and nine [confer §3.3, 3.4, 4.1, and 4.4] spin free strengths and to certain of the five-electron spin paired strengths [refer §4.5] as we shall see in §4.4 and 4.5. The far-reaching consequences of this correspondence will be expounded in section IV.

(b) *No Configuration Interaction: Nonzero Spin-Orbit Forces. Three and Seven Electrons.* The comments appropriate to this paragraph are identical with those of §4.2b.

(c) *Configuration Interaction: Zero and Nonzero Spin-Orbit Forces. Three and Seven Electrons.* The effects of configuration interaction are exactly as outlined in §4.2c.

4.4 *The Four- and Six-Electron Case.* Consistent with our antecedent remarks of §4.2, we limit our examination of the four- and six-electron teaser to the single-electron excitations alone, the remainder to be left for subsequent study.[38,43] With this curtailment,

the pertinent trigonally disposed determinantal functions for the four- and six-electron coveys follow.

(a) *No Configuration Interaction: Zero Spin-Orbit Forces.* (i) *Wave Functions: Four Electrons*

$${}^5E_\pm[{}^5E_g(t_{2g}{}^3e_g)] : \pm \left| a_1(t_{2g})e_+(t_{2g})e_-(t_{2g})e_\pm(e_g) \right|$$

$${}^5A_1[{}^5T_{2g}(t_{2g}{}^2e_g{}^2)] : \left| e_+(t_{2g})e_-(t_{2g})e_+(e_g)e_-(e_g) \right|$$

$${}^5E_\pm[{}^5T_{2g}(t_{2g}{}^2e_g{}^2)] : \mp \left| a_1(t_{2g})e_\pm(t_{2g})e_+(e_g)e_-(e_g) \right|$$

$${}^3A_2[{}^3T_{1g}(t_{2g}{}^4)] : \left| a_1(t_{2g})\bar{a}_1(t_{2g})e_+(t_{2g})e_-(t_{2g}) \right|$$

$${}^3E_\pm[{}^3T_{1g}(t_{2g}{}^4)] : \mp \left| a_1(t_{2g})e_\pm(t_{2g})\bar{e}_\pm(t_{2g})e_\mp(t_{2g}) \right|$$

$${}^1E_\pm[{}^1E_g(t_{2g}{}^4)] : \frac{1}{\sqrt{3}} \left\{ \left| a_1(t_{2g})e_\pm(t_{2g})\bar{e}_\pm(t_{2g})e_\mp(t_{2g}) \right| - \right.$$
$$\left| \bar{a}_1(t_{2g})e_\pm(t_{2g})\bar{e}_\pm(t_{2g})e_\mp(t_{2g}) \right| -$$
$$\left. \left| a_1(t_{2g})\bar{a}_1(t_{2g})e_\mp(t_{2g})\bar{e}_\mp(t_{2g}) \right| \right\}$$

$${}^1A_1[{}^1T_{2g}(t_{2g}{}^4)] : \frac{1}{\sqrt{6}} \left\{ 2\left| e_+(t_{2g})\bar{e}_+(t_{2g})e_-(t_{2g})\bar{e}_-(t_{2g}) \right| - \right.$$
$$\left| a_1(t_{2g})\bar{a}_1(t_{2g})e_+(t_{2g})\bar{e}_-(t_{2g}) \right| +$$
$$\left. \left| a_1(t_{2g})\bar{a}_1(t_{2g})\bar{e}_+(t_{2g})e_-(t_{2g}) \right| \right\}$$

$${}^1E_\pm[{}^1T_{2g}(t_{2g}{}^4)] : - \frac{1}{\sqrt{6}} \left\{ 2\left| a_-(t_{2g})\bar{a}_1(t_{2g})e_-(t_{2g})\bar{e}_-(t_{2g}) \right| + \right.$$
$$\left| a_1(t_{2g})e_+(t_{2g})\bar{e}_+(t_{2g})\bar{e}_-(t_{2g}) \right| -$$
$$\left. \left| \bar{a}_1(t_{2g})e_+(t_{2g})\bar{e}_+(t_{2g})e_-(t_{2g}) \right| \right\}$$

$${}^1A_1[{}^1A_{1g}(t_{2g}{}^4)] : \frac{1}{\sqrt{3}} \left\{ \left| e_+(t_{2g})\bar{e}_+(t_{2g})e_-(t_{2g})\bar{e}_-(t_{2g}) \right| - \right.$$
$$\left| a_1(t_{2g})\bar{a}_1(t_{2g})\bar{e}_+(t_{2g})e_-(t_{2g}) \right| +$$
$$\left. \left| a_1(t_{2g})\bar{a}_1(t_{2g})e_+(t_{2g})\bar{e}_-(t_{2g}) \right| \right\}$$

$${}^3E_\pm[{}^3E_g(t_{2g}{}^3e_g)] : \pm \frac{1}{2\sqrt{3}} \left\{ 3\left| a_1(t_{2g})e_+(t_{2g})e_-(t_{2g})\bar{e}_\pm(e_g) \right| - \right.$$
$$\left| a_1(t_{2g})e_+(t_{2g})\bar{e}_-(t_{2g})e_\pm(e_g) \right| -$$
$$\left| a_1(t_{2g})\bar{e}_+(t_{2g})e_-(t_{2g})e_\pm(e_g) \right| -$$
$$\left. \left| \bar{a}_1(t_{2g})e_+(t_{2g})e_-(t_{2g})e_\pm(e_g) \right| \right\}$$

$${}^3A_2[{}^3T_{1g}(t_{2g}{}^3e_g)] : \frac{1}{2\sqrt{3}} \left\{ -2\left| a_1(t_{2g})e_-(t_{2g})e_-(t_{2g})e_-(e_g) \right| - \right.$$
$$\left| a_1(t_{2g})\bar{a}_1(t_{2g})e_+(t_{2g})e_-(e_g) \right| -$$
$$\left| e_+(t_{2g})\bar{e}_+(t_{2g})e_-(t_{2g})e_-(e_g) \right| +$$
$$2\left| a_1(t_{2g})e_+(t_{2g})\bar{e}_+(t_{2g})e_+(e_g) \right| +$$
$$\left| a_1(t_{2g})\bar{a}_1(t_{2g})e_-(t_{2g})e_+(e_g) \right| +$$
$$\left. \left| e_+(t_{2g})e_-(t_{2g})\bar{e}_-(t_{2g})e_+(e_g) \right| \right\}$$

$^3E_{\pm}[^3T_{1g}(t_{2g}{}^3e_g)]: \pm\dfrac{1}{2\sqrt{3}}\{2|\bar{a}_1(t_{2g})e_{\pm}(t_{2g})e_{\mp}(t_{2g})e_{\pm}(e_g)| -$

$\quad |a_1(t_{2g})e_{\pm}(t_{2g})\bar{e}_{\mp}(t_{2g})e_{\pm}(e_g)| -$

$\quad |a_1(t_{2g})\bar{e}_{\pm}(t_{2g})e_{\mp}(t_{2g})e_{\pm}(e_g)| +$

$\quad 2|a_1(t_{2g})e_{\pm}(t_{2g})\bar{e}_{\pm}(t_{2g})e_{\mp}(e_g)| +$

$\quad |a_1(t_{2g})\bar{a}_1(t_{2g})e_{\mp}(t_{2g})e_{\mp}(e_g)| +$

$\quad\quad |e_{\mp}(t_{2g})\bar{e}_{\mp}(t_{2g})e_{\mp}(t_{2g})e_{\mp}(e_g)|\}$

$^3A_1[^3T_{2g}(t_{2g}{}^3e_g)]: -\dfrac{1}{2\sqrt{3}}\{2|a_1(t_{2g})e_-(t_{2g})\bar{e}_-(t_{2g})e_-(e_g)| +$

$\quad |a_1(t_{2g})\bar{a}_1(t_{2g})e_+(t_{2g})e_-(e_g)| +$

$\quad |e_+(t_{2g})\bar{e}_+(t_{2g})e_-(t_{2g})e_-(e_g)| +$

$\quad 2|a_1(t_{2g})e_+(t_{2g})\bar{e}_+(t_{2g})e_+(e_g)| +$

$\quad |a_1(t_{2g})\bar{a}_1(t_{2g})e_-(t_{2g})e_+(e_g)| +$

$\quad\quad |e_-(t_{2g})\bar{e}_-(t_{2g})e_+(t_{2g})e_+(e_g)|\}$

$^3E_{\pm}[^3T_{2g}(t_{2g}{}^3e_g)]: \dfrac{1}{2\sqrt{3}}\{2|\bar{a}_1(t_{2g})e_{\pm}(t_{2g})e_{\mp}(t_{2g})e_{\pm}(e_g)| -$

$\quad |a_1(t_{2g})e_{\pm}(t_{2g})\bar{e}_{\mp}(t_{2g})e_{\pm}(e_g)| -$

$\quad |a_1(t_{2g})\bar{e}_{\pm}(t_{2g})e_{\mp}(t_{2g})e_{\pm}(e_g)| -$

$\quad 2|a_1(t_{2g})e_{\pm}(t_{2g})\bar{e}_{\pm}(t_{2g})e_{\mp}(e_g)| -$

$|a_1(t_{2g})\bar{a}_1(t_{2g})e_{\mp}(t_{2g})e_{\mp}(e_g)| - |e_{\mp}(t_{2g})\bar{e}_{\mp}(t_{2g})e_{\pm}(t_{2g})e_{\mp}(e_g)|\}$

$^3A_1[^3A_{1g}(t_{2g}{}^3e_g)]: \dfrac{1}{\sqrt{6}}\{|e_+(t_{2g})\bar{e}_+(t_{2g})e_-(t_{2g})e_-(e_g)| +$

$\quad |a_1(t_{2g})\bar{a}_1(t_{2g})e_+(t_{2g})e_-(e_g)| -$

$\quad |a_1(t_{2g})e_-(t_{2g})\bar{e}_-(t_{2g})e_-(e_g)| +$

$\quad |e_-(t_{2g})\bar{e}_-(t_{2g})e_+(t_{2g})e_+(e_g)| +$

$|a_1(t_{2g})\bar{a}_1(t_{2g})e_-(t_{2g})e_+(e_g)| - |a_1(t_{2g})e_+(t_{2g})\bar{e}_+(t_{2g})e_+(e_g)|\}$

$^3E_{\pm}[^3E_g(t_{2g}{}^3e_g)]: \dfrac{1}{\sqrt{3}}\{|e_{\mp}(t_{2g})\bar{e}_{\mp}(t_{2g})e_{\pm}(t_{2g})e_{\mp}(e_g)| +$

$|a_1(t_{2g})\bar{a}_1(t_{2g})e_{\mp}(t_{2g})e_{\mp}(e_g)| - |a_1(t_{2g})e_{\pm}(t_{2g})\bar{e}_{\pm}(t_{2g})e_{\mp}(e_g)|\}$

$^3A_2[^3A_{2g}(t_{2g}{}^3e_g)]: \dfrac{1}{\sqrt{6}}\{|e_+(t_{2g})\bar{e}_+(t_{2g})e_-(t_{2g})e_-(e_g)| +$

$\quad |a_1(t_{2g})\bar{a}_1(t_{2g})e_+(t_{2g})e_-(e_g)| -$

$\quad |a_1(t_{2g})e_-(t_{2g})\bar{e}_-(t_{2g})e_-(e_g)| -$

$\quad |e_-(t_{2g})\bar{e}_-(t_{2g})e_+(t_{2g})e_+(e_g)| -$

$|a_1(t_{2g})\bar{a}_1(t_{2g})e_-(t_{2g})e_+(e_g)| + |a_1(t_{2g})e_+(t_{2g})\bar{e}_+(t_{2g})e_+(e_g)|\}$

$^3A_1[^3T_{2g}(t_{2g}{}^3e_g)]: {}^1/_2\{|a_1(t_{2g})\bar{a}_1(t_{2g})e_+(t_{2g})e_-(e_g)| -$

$\quad |e_+(t_{2g})\bar{e}_+(t_{2g})e_-(t_{2g})e_-(e_g)| +$

$|a_1(t_{2g})\bar{a}_1(t_{2g})e_-(t_{2g})e_+(e_g)| - |e_-(t_{2g})\bar{e}_-(t_{2g})e_+(t_{2g})e_+(e_g)|\}$

$^3E_{\pm}[^3T_{2g}(t_{2g}{}^3e_g)]: {}^1/_2\{|a_1(t_{2g})e_{\pm}(t_{2g})\bar{e}_{\mp}(t_{2g})e_{\pm}(e_g)| -$

$\quad |a_1(t_{2g})\bar{e}_{\pm}(t_{2g})e_{\mp}(t_{2g})e_{\pm}(e_g)| -$

$\quad |a_1(t_{2g})\bar{a}_1(t_{2g})e_{\mp}(t_{2g})e_{\mp}(e_g)| + |e_{\mp}(t_{2g})\bar{e}_{\mp}(t_{2g})e_{\pm}(t_{2g})\mp(e_g)|\}$

$^3A_2[^3T_{1g}(t_{2g}{}^3e_g)]: {}^1/_2\{|a_1(t_{2g})\bar{a}_1(t_{2g})e_+(t_{2g})e_-(e_g)| -$

$\quad |e_+(t_{2g})\bar{e}_+(t_{2g})e_-(t_{2g})e_-(e_g)| -$

$|a_1(t_{2g})\bar{a}_1(t_{2g})e_-(t_{2g})e_+(e_g)| + |e_-(t_{2g})\bar{e}_-(t_{2g})e_+(t_{2g})e_+(e_g)|\}$

$^3E_{\pm}[^3T_{1g}(t_{2g}{}^3e_g)]: \pm{}^1/_2\{|a_1(t_{2g})e_{\pm}(t_{2g})\bar{e}_{\mp}(t_{2g})e_{\pm}(e_g)| -$

$\quad |a_1(t_{2g})\bar{e}_{\pm}(t_{2g})e_{\mp}(t_{2g})e_{\pm}(e_g)| +$

$\quad |a_1(t_{2g})\bar{a}_1(t_{2g})e_{\mp}(t_{2g})e_{\mp}(e_g)| -$

$\quad |e_{\mp}(t_{2g})\bar{e}_{\mp}(t_{2g})e_{\pm}(t_{2g})e_{\mp}(e_g)|\}$ (83)

(ii) Wave Functions: Six Electrons

$^5A_1[^5T_{2g}(t_{2g}{}^4e_g{}^2)]: |a_1(t_{2g})\bar{a}_1(t_{2g})e_+(t_{2g})e_-(t_{2g})e_+(e_g)e_-(e_g)|$

$^5E_{\pm}[^5T_{2g}(t_{2g}{}^4e_g{}^2)]:$

$\quad \mp|a_1(t_{2g})e_{\pm}(t_{2g})\bar{e}_{\pm}(t_{2g})e_{\mp}(t_{2g})e_+(e_g)e_-(e_g)|$

$^5E_{\pm}[^5E_g(t_{2g}{}^3e_g{}^3)]:$

$\quad \pm|a_1(t_{2g})e_+(t_{2g})e_-(t_{2g})e_{\pm}(e_g)\bar{e}_{\pm}(e_g)e_{\mp}(e_g)|$

$^1A_1[^1A_{1g}(t_{2g}{}^6)]: |a_1(t_{2g})\bar{a}_1(t_{2g})e_+(t_{2g})\bar{e}_+(t_{2g})e_-(t_{2g})\bar{e}_-(t_{2g})|$

$^1A_2[^1T_{1g}(t_{2g}{}^5e_g)]:$

$\quad {}^1/_2\{|a_1(t_{2g})\bar{a}_1(t_{2g})e_+(t_{2g})\bar{e}_+(t_{2g})e_-(t_{2g})\bar{e}_-(e_g)| -$

$\quad |a_1(t_{2g})\bar{a}_1(t_{2g})e_+(t_{2g})\bar{e}_+(t_{2g})\bar{e}_-(t_{2g})e_-(e_g)| -$

$\quad |a_1(t_{2g})\bar{a}_1(t_{2g})e_+(t_{2g})e_-(t_{2g})\bar{e}_-(t_{2g})e_+(e_g)| +$

$\quad\quad |a_1(t_{2g})\bar{a}_1(t_{2g})\bar{e}_+(t_{2g})e_-(t_{2g})\bar{e}_-(t_{2g})e_+(e_g)|\}$

$^1E_{\pm}[^1T_{1g}(t_{2g}{}^5e_g)]:$

$\quad \pm{}^1/_2\{|\bar{a}_1(t_{2g})e_+(t_{2g})\bar{e}_+(t_{2g})e_-(t_{2g})\bar{e}_-(t_{2g})e_{\pm}(e_g)| -$

$\quad |a_1(t_{2g})e_+(t_{2g})\bar{e}_+(t_{2g})e_-(t_{2g})\bar{e}_-(t_{2g})\bar{e}_{\pm}(e_g)| +$

$\quad |a_1(t_{2g})\bar{a}_1(t_{2g})\bar{e}_{\pm}(t_{2g})e_{\mp}(t_{2g})\bar{e}_{\mp}(t_{2g})e_{\mp}(e_g)| -$

$\quad\quad |a_1(t_{2g})\bar{a}_1(t_{2g})e_{\pm}(t_{2g})e_{\mp}(t_{2g})\bar{e}_{\mp}(t_{2g})\bar{e}_{\mp}(e_g)|\}$

$^1A_1[^1T_{2g}(t_{2g}{}^5e_g)]:$

$\quad {}^1/_2\{|a_1(t_{2g})\bar{a}_1(t_{2g})e_+(t_{2g})\bar{e}_+(t_{2g})\bar{e}_-(t_{2g})e_-(e_g)| -$

$\quad |a_1(t_{2g})\bar{a}_1(t_{2g})e_+(t_{2g})\bar{e}_+(t_{2g})e_-(t_{2g})\bar{e}_-(e_g)| +$

$\quad |a_1(t_{2g})\bar{a}_1(t_{2g})\bar{e}_+(t_{2g})e_-(t_{2g})\bar{e}_-(t_{2g})e_+(e_g)| -$

$\quad\quad |a_1(t_{2g})\bar{a}_1(t_{2g})e_+(t_{2g})e_-(t_{2g})\bar{e}_-(t_{2g})\bar{e}_+(e_g)|\}$

$^1E_{\pm}[^1T_{2g}(t_{2g}{}^5e_g)]:$

$\quad {}^1/_2\{|\bar{a}_1(t_{2g})e_+(t_{2g})\bar{e}_+(t_{2g})e_-(t_{2g})\bar{e}_-(t_{2g})e_{\pm}(e_g)| -$

$\quad |a_1(t_{2g})e_+(t_{2g})\bar{e}_+(t_{2g})e_-(t_{2g})\bar{e}_-(t_{2g})\bar{e}_{\pm}(e_g)| +$

$\quad |a_1(t_{2g})\bar{a}_1(t_{2g})e_{\pm}(t_{2g})e_{\mp}(t_{2g})\bar{e}_{\mp}(t_{2g})\bar{e}_{\mp}(e_g)| -$

$\quad |a_1(t_{2g})\bar{a}_1(t_{2g})\bar{e}_{\pm}(t_{2g})e_{\mp}(t_{2g})\bar{e}_{\mp}(t_{2g})e_{\mp}(e_g)|\}$ (84)

The triplet wave functions, $^3T_{1,2g}(t_{2g}{}^5e_g)$, correspondent to those of $^1T_{1,2g}(t_{2g}{}^5e_g)$ tabulated above are readily generated by a simple change of sign between the conjugate spin exchanged determinantal pairs, in accord with the restrictive conditions $\mathcal{C}_2(y')A_2(T_1) = -A_2(T_1)$, $\mathcal{C}_2(y')E_\pm(T_1) = -E_\mp(T_1)$, $\mathcal{C}_2(y')A_1(T_2) = A_1(T_1)$, $\mathcal{C}_2(y')E_\pm(T_2) = E_\mp(T_2)$.

These functions allow the spiratory and spectral matrix entries, which follow, to be inscribed.

(*iii*) *Matrix Elements: Four Electrons*

$$\left\langle {}^5E_\pm[{}^5E_g(t_{2g}{}^3e_g)] \left| \frac{\vec{p}}{\vec{m}} \right| {}^6A_1[{}^5T_{2g}(t_{2g}{}^2e_g{}^2)] \right\rangle =$$
$$- \left\langle a_1(t_{2g}) \left| \frac{\vec{p}}{\vec{m}} \right| e_\mp(e_g) \right\rangle$$

$$\left\langle {}^5E_\pm[{}^5E_g(t_{2g}{}^3e_g)] \left| \frac{\vec{p}}{\vec{m}} \right| {}^5E_\pm[{}^5T_{2g}(t_{2g}{}^2e_g{}^2)] \right\rangle =$$
$$\left\langle e_\mp(t_{2g}) \left| \frac{\vec{p}}{\vec{m}} \right| e_\mp(e_g) \right\rangle$$

$$\left\langle {}^5E_\pm[{}^5E_g(t_{2g}{}^3e_g)] \left| \frac{\vec{p}}{\vec{m}} \right| {}^5E_\mp[{}^5T_{2g}(t_{2g}{}^2e_g{}^2)] \right\rangle =$$
$$\left\langle e_\pm(t_{2g}) \left| \frac{\vec{p}}{\vec{m}} \right| e_\mp(e_g) \right\rangle \quad (85)$$

$$\left\langle {}^3A_2[{}^3T_{1g}(t_{2g}{}^4)] \left| \frac{\vec{p}}{\vec{m}} \right| {}^3E_\pm[{}^3T_{1g}(t_{2g}{}^4)] \right\rangle =$$
$$\left\langle a_1(t_{2g}) \left| \frac{\vec{p}}{\vec{m}} \right| e_\pm(t_{2g}) \right\rangle$$

$$\left\langle {}^3A_2[{}^3T_{1g}(t_{2g}{}^4)] \left| \frac{\vec{p}}{\vec{m}} \right| {}^3E_\pm[{}^3E_g(t_{2g}{}^3e_g)] \right\rangle =$$
$$\pm \frac{2}{\sqrt{3}} \left\langle a_1(t_{2g}) \left| \frac{\vec{p}}{\vec{m}} \right| e_\pm(e_g) \right\rangle$$

$$\left\langle {}^3A_2[{}^3T_{1g}(t_{2g}{}^4)] \left| \frac{\vec{p}}{\vec{m}} \right| {}^3A_2[{}^3T_{1g}(t_{2g}{}^3e_g)] \right\rangle \equiv 0$$

$$\left\langle {}^3A_2[{}^3T_{1g}(t_{2g}{}^4)] \left| \frac{\vec{p}}{\vec{m}} \right| {}^3E_\pm[{}^3T_{1g}(t_{2g}{}^3e_g)] \right\rangle =$$
$$\frac{-1}{2\sqrt{3}} \left\{ 2\left\langle a_1(t_{2g}) \left| \frac{\vec{p}}{\vec{m}} \right| e_\pm(e_g) \right\rangle + \left\langle e_\pm(t_{2g}) \left| \frac{\vec{p}}{\vec{m}} \right| e_\mp(e_g) \right\rangle \right\}$$

$$\left\langle {}^3A_2[{}^3T_{1g}(t_{2g}{}^4)] \left| \frac{\vec{p}}{\vec{m}} \right| {}^3A_1[{}^3T_{2g}(t_{2g}{}^3e_g)] \right\rangle =$$
$$- \frac{1}{\sqrt{3}} \left\langle e_-(t_{2g}) \left| \frac{\vec{p}}{\vec{m}} \right| e_-(e_g) \right\rangle$$

$$\left\langle {}^3A_2[{}^3T_{1g}(t_{2g}{}^4)] \left| \frac{\vec{p}}{\vec{m}} \right| {}^3E_\pm[{}^3T_{2g}(t_{2g}{}^3e_g)] \right\rangle =$$
$$\frac{\mp 1}{2\sqrt{3}} \left\{ 2\left\langle a_1(t_{2g}) \left| \frac{\vec{p}}{\vec{m}} \right| e_\pm(e_g) \right\rangle - \left\langle e_\pm(t_{2g}) \left| \frac{\vec{p}}{\vec{m}} \right| e_\mp(e_g) \right\rangle \right\}$$

$$\left\langle {}^3A_2[{}^3T_{1g}(t_{2g}{}^4)] \left| \frac{\vec{p}}{\vec{m}} \right| {}^3A_1[{}^3A_{1g}(t_{2g}{}^3e_g)] \right\rangle =$$
$$\sqrt{2/3} \left\langle e_-(t_{2g}) \left| \frac{\vec{p}}{\vec{m}} \right| e_-(e_g) \right\rangle$$

$$\left\langle {}^3A_2[{}^3T_{1g}(t_{2g}{}^4)] \left| \frac{\vec{p}}{\vec{m}} \right| {}^3E_\pm[{}^3E_g(t_{2g}{}^3e_g)] \right\rangle =$$
$$\frac{\mp 1}{\sqrt{3}} \left\langle e_\pm(t_{2g}) \left| \frac{\vec{p}}{\vec{m}} \right| e_\mp(e_g) \right\rangle$$

$$\left\langle {}^3A_2[{}^3T_{1g}(t_{2g}{}^4)] \left| \frac{\vec{p}}{\vec{m}} \right| {}^3A_2[{}^3A_{2g}(t_{2g}{}^3e_g)] \right\rangle \equiv 0$$

$$\left\langle {}^3A_2[{}^3T_{1g}(t_{2g}{}^4)] \left| \frac{\vec{p}}{\vec{m}} \right| {}^3A_1[{}^3T_{2g}(t_{2g}{}^3e_g)] \right\rangle =$$
$$\left\langle e_-(t_{2g}) \left| \frac{\vec{p}}{\vec{m}} \right| e_-(e_g) \right\rangle$$

$$\left\langle {}^3A_2[{}^3T_{1g}(t_{2g}{}^4)] \left| \frac{\vec{p}}{\vec{m}} \right| {}^3E_\pm[{}^3T_{2g}(t_{2g}{}^3e_g)] \right\rangle =$$
$$\pm 1/2 \left\langle e_\pm(t_{2g}) \left| \frac{\vec{p}}{\vec{m}} \right| e_\mp(e_g) \right\rangle$$

$$\left\langle {}^3A_2[{}^3T_{1g}(t_{2g}{}^4)] \left| \frac{\vec{p}}{\vec{m}} \right| {}^3A_2[{}^3T_{1g}(t_{2g}{}^3e_g)] \right\rangle \equiv 0$$

$$\left\langle {}^3A_2[{}^3T_{1g}(t_{2g}{}^4)] \left| \frac{\vec{p}}{\vec{m}} \right| {}^3E_\pm[{}^3T_{1g}(t_{2g}{}^3e_g)] \right\rangle =$$
$$-1/2 \left\langle e_\pm(t_{2g}) \left| \frac{\vec{p}}{\vec{m}} \right| e_\mp(e_g) \right\rangle \quad (86)$$

$$\left\langle {}^3E_\pm[{}^3T_{1g}(t_{2g}{}^4)] \left| \frac{\vec{p}}{\vec{m}} \right| {}^3E_\pm[{}^3E_g(t_{2g}{}^3e_g)] \right\rangle =$$
$$\pm \frac{2}{\sqrt{3}} \left\langle e_\pm(t_{2g}) \left| \frac{\vec{p}}{\vec{m}} \right| e_\pm(e_g) \right\rangle$$

$$\left\langle {}^3E_\pm[{}^3T_{1g}(t_{2g}{}^4)] \left| \frac{\vec{p}}{\vec{m}} \right| {}^3E_\mp[{}^3E_g(t_{2g}{}^3e_g)] \right\rangle =$$
$$\mp \frac{2}{\sqrt{3}} \left\langle e_\pm(t_{2g}) \left| \frac{\vec{p}}{\vec{m}} \right| e_\mp(e_g) \right\rangle$$

$$\left\langle {}^3E_\pm[{}^3T_{1g}(t_{2g}{}^4)] \left| \frac{\vec{p}}{\vec{m}} \right| {}^3A_2[{}^3T_{1g}(t_{2g}{}^3e_g)] \right\rangle =$$
$$\frac{-1}{2\sqrt{3}} \left\{ \left\langle a_1(t_{2g}) \left| \frac{\vec{p}}{\vec{m}} \right| e_\mp(e_g) \right\rangle + 2\left\langle e_\mp(t_{2g}) \left| \frac{\vec{p}}{\vec{m}} \right| e_\pm(e_g) \right\rangle \right\}$$

$$\left\langle {}^3E_\pm[{}^3T_{1g}(t_{2g}{}^4)] \left| \frac{\vec{p}}{\vec{m}} \right| {}^3E_\pm[{}^3T_{1g}(t_{2g}{}^3e_g)] \right\rangle =$$
$$- \frac{\sqrt{3}}{2} \left\langle e_\mp(t_{2g}) \left| \frac{\vec{p}}{\vec{m}} \right| e_\mp(e_g) \right\rangle$$

$$\left\langle {}^3E_\pm[{}^3T_{1g}(t_{2g}{}^4)] \left| \frac{\vec{p}}{\vec{m}} \right| {}^3E_\mp[{}^3T_{1g}(t_{2g}{}^3e_g)] \right\rangle =$$
$$\frac{1}{2\sqrt{3}} \left\{ \left\langle e_\pm(t_{2g}) \left| \frac{\vec{p}}{\vec{m}} \right| e_\mp(e_g) \right\rangle - \left\langle a_1(t_{2g}) \left| \frac{\vec{p}}{\vec{m}} \right| e_\pm(e_g) \right\rangle \right\}$$

$$\left\langle {}^3E_\pm[{}^3T_{1g}(t_{2g}{}^4)] \left| \frac{\vec{p}}{\vec{m}} \right| {}^3A_1[{}^3T_{2g}(t_{2g}{}^3e_g)] \right\rangle =$$

$$\frac{\mp 1}{2\sqrt{3}}\left\{ \left\langle a_1(t_{2g}) \left| \frac{\vec{p}}{\vec{m}} \right| e_\mp(e_g) \right\rangle - 2\left\langle e_\mp(t_{2g}) \left| \frac{\vec{p}}{\vec{m}} \right| e_\pm(e_g) \right\rangle \right\}$$

$$\left\langle {}^3E_\pm[{}^3T_{1g}(t_{2g}{}^4)] \left| \frac{\vec{p}}{\vec{m}} \right| {}^3E_\pm[{}^3T_{2g}(t_{2g}{}^3e_g)] \right\rangle =$$

$$\pm \frac{1}{2\sqrt{3}} \left\langle e_\mp(t_{2g}) \left| \frac{\vec{p}}{\vec{m}} \right| e_\mp(e_g) \right\rangle$$

$$\left\langle {}^3E_\pm[{}^3T_{1g}(t_{2g}{}^4)] \left| \frac{\vec{p}}{\vec{m}} \right| {}^3E_\mp[{}^3T_{2g}(t_{2g}{}^3e_g)] \right\rangle =$$

$$\frac{\mp 1}{2\sqrt{3}}\left\{ \left\langle e_\pm(t_{2g}) \left| \frac{\vec{p}}{\vec{m}} \right| e_\mp(e_g) \right\rangle + \left\langle a_1(t_{2g}) \left| \frac{\vec{p}}{\vec{m}} \right| e_\pm(e_g) \right\rangle \right\}$$

$$\left\langle {}^3E_\pm[{}^3T_{1g}(t_{2g}{}^4)] \left| \frac{\vec{p}}{\vec{m}} \right| {}^3E_\pm[{}^3E_g(t_{2g}{}^3e_g)] \right\rangle =$$

$$\pm \frac{1}{\sqrt{3}} \left\langle e_\mp(t_{2g}) \left| \frac{\vec{p}}{\vec{m}} \right| e_\mp(e_g) \right\rangle$$

$$\left\langle {}^3E_\pm[{}^3T_{1g}(t_{2g}{}^4)] \left| \frac{\vec{p}}{\vec{m}} \right| {}^3E_\mp[{}^3E_g(t_{2g}{}^3e_g)] \right\rangle =$$

$$\pm \frac{1}{\sqrt{3}} \left\langle a_1(t_{2g}) \left| \frac{\vec{p}}{\vec{m}} \right| e_\pm(e_g) \right\rangle$$

$$\left\langle {}^3E_\pm[{}^3T_{1g}(t_{2g}{}^4)] \left| \frac{\vec{p}}{\vec{m}} \right| {}^3A_1[{}^3A_{1g}(t_{2g}{}^3e_g)] \right\rangle =$$

$$\pm \frac{1}{\sqrt{6}}\left\{ \left\langle a_1(t_{2g}) \left| \frac{\vec{p}}{\vec{m}} \right| e_\mp(e_g) \right\rangle + \left\langle e_\mp(t_{2g}) \left| \frac{\vec{p}}{\vec{m}} \right| e_\pm(e_g) \right\rangle \right\}$$

$$\left\langle {}^3E_\pm[{}^3T_{1g}(t_{2g}{}^4)] \left| \frac{\vec{p}}{\vec{m}} \right| {}^3A_2[{}^3A_{2g}(t_{2g}{}^3e_g)] \right\rangle =$$

$$\frac{1}{\sqrt{6}}\left\{ \left\langle a_1(t_{2g}) \left| \frac{\vec{p}}{\vec{m}} \right| e_\mp(e_g) \right\rangle - \left\langle e_\mp(t_{2g}) \left| \frac{\vec{p}}{\vec{m}} \right| e_\pm(e_g) \right\rangle \right\}$$

$$\left\langle {}^3E_\pm[{}^3T_{1g}(t_{2g}{}^4)] \left| \frac{\vec{p}}{\vec{m}} \right| {}^3A_1[{}^3T_{2g}(t_{2g}{}^3e_g)] \right\rangle =$$

$$\mp {}^1/_2 \left\langle a_1(t_{2g}) \left| \frac{\vec{p}}{\vec{m}} \right| e_\mp(e_g) \right\rangle$$

$$\left\langle {}^3E_\pm[{}^3T_{1g}(t_{2g}{}^4)] \left| \frac{\vec{p}}{\vec{m}} \right| {}^3E_\pm[{}^3T_{2g}(t_{2g}{}^3e_g)] \right\rangle =$$

$$\pm {}^1/_2 \left\langle e_\pm(t_{2g}) \left| \frac{\vec{p}}{\vec{m}} \right| e_\pm(e_g) \right\rangle$$

$$\left\langle {}^3E_\pm[{}^3T_{1g}(t_{2g}{}^4)] \left| \frac{\vec{p}}{\vec{m}} \right| {}^3E_\mp[{}^3T_{2g}(t_{2g}{}^3e_g)] \right\rangle =$$

$$\pm {}^1/_2\left\{ \left\langle a_1(t_{2g}) \left| \frac{\vec{p}}{\vec{m}} \right| e_\pm(e_g) \right\rangle + \left\langle e_\pm(t_{2g}) \left| \frac{\vec{p}}{\vec{m}} \right| e_\mp(e_g) \right\rangle \right\}$$

$$\left\langle {}^3E_\pm[{}^3T_{1g}(t_{2g}{}^4)] \left| \frac{\vec{p}}{\vec{m}} \right| {}^3A_2[{}^3T_{1g}(t_{2g}{}^3e_g)] \right\rangle =$$

$$-{}^1/_2 \left\langle a_1(t_{2g}) \left| \frac{\vec{p}}{\vec{m}} \right| e_\mp(e_g) \right\rangle$$

$$\left\langle {}^3E_\pm[{}^3T_{1g}(t_{2g}{}^4)] \left| \frac{\vec{p}}{\vec{m}} \right| {}^3E_\pm[{}^3T_{1g}(t_{2g}{}^3e_g)] \right\rangle =$$

$${}^1/_2 \left\langle e_\pm(t_{2g}) \left| \frac{\vec{p}}{\vec{m}} \right| e_\pm(e_g) \right\rangle$$

$$\left\langle {}^3E_\pm[{}^3T_{1g}(t_{2g}{}^4)] \left| \frac{\vec{p}}{\vec{m}} \right| {}^3E_\mp[{}^3T_{1g}(t_{2g}{}^3e_g)] \right\rangle =$$

$${}^1/_2\left\{ \left\langle a_1(t_{2g}) \left| \frac{\vec{p}}{\vec{m}} \right| e_\pm(e_g) \right\rangle - \left\langle e_\pm(t_{2g}) \left| \frac{\vec{p}}{\vec{m}} \right| e_\mp(e_g) \right\rangle \right\}$$

$$(87)$$

(iv) Matrix Elements: Six Electrons

$$\left\langle {}^5A_1[{}^5T_{2g}(t_{2g}{}^4e_g{}^2)] \left| \frac{\vec{p}}{\vec{m}} \right| {}^5E_\pm[{}^5T_{2g}(t_{2g}{}^4e_g{}^2)] \right\rangle =$$

$$\left\langle a_1(t_{2g}) \left| \frac{\vec{p}}{\vec{m}} \right| e_\pm(t_{2g}) \right\rangle$$

$$\left\langle {}^5A_1[{}^5T_{2g}(t_{2g}{}^4e_g{}^2)] \left| \frac{\vec{p}}{\vec{m}} \right| {}^5E_\pm[{}^5E_g(t_{2g}{}^3e_g{}^3)] \right\rangle =$$

$$-\left\langle a_1(t_{2g}) \left| \frac{\vec{p}}{\vec{m}} \right| e_\pm(e_g) \right\rangle$$

$$\left\langle {}^5E_\pm[{}^5T_{2g}(t_{2g}{}^4e_g{}^2)] \left| \frac{\vec{p}}{\vec{m}} \right| {}^5E_\pm[{}^5E_g(t_{2g}{}^3e_g{}^3)] \right\rangle =$$

$$-\left\langle e_\pm(t_{2g}) \left| \frac{\vec{p}}{\vec{m}} \right| e_\pm(e_g) \right\rangle$$

$$\left\langle {}^5E_\pm[{}^5T_{2g}(t_{2g}{}^4e_g{}^2)] \left| \frac{\vec{p}}{\vec{m}} \right| {}^5E_\mp[{}^5E_g(t_{2g}{}^3e_g{}^3)] \right\rangle =$$

$$-\left\langle e_\pm(t_{2g}) \left| \frac{\vec{p}}{\vec{m}} \right| e_\mp(e_g) \right\rangle \quad (88)$$

$$\left\langle {}^1A_1[{}^1A_{1g}(t_{2g}{}^6)] \left| \frac{\vec{p}}{\vec{m}} \right| {}^1A_2[{}^1T_{1g}(t_{2g}{}^5e_g)] \right\rangle =$$

$$2\left\langle e_-(t_{2g}) \left| \frac{\vec{p}}{\vec{m}} \right| e_-(e_g) \right\rangle$$

$$\left\langle {}^1A_1[{}^1A_{1g}(t_{2g}{}^6)] \left| \frac{\vec{p}}{\vec{m}} \right| {}^1E_\pm[{}^1T_{1g}(t_{2g}{}^5e_g)] \right\rangle =$$

$$\mp\left\{ \left\langle a_1(t_{2g}) \left| \frac{\vec{p}}{\vec{m}} \right| e_\pm(e_g) \right\rangle + \left\langle e_\pm(t_{2g}) \left| \frac{\vec{p}}{\vec{m}} \right| e_\mp(e_g) \right\rangle \right\}$$

$$\left\langle {}^1A_1[{}^1A_{1g}(t_{2g}{}^6)] \left| \frac{\vec{p}}{\vec{m}} \right| {}^1A_1[{}^1T_{2g}(t_{2g}{}^5e_g)] \right\rangle \equiv 0$$

$$\left\langle {}^1A_1[{}^1A_{1g}(t_{2g}{}^6)] \left| \frac{\vec{p}}{\vec{m}} \right| {}^1E_\pm[{}^1T_{2g}(t_{2g}{}^5e_g)] \right\rangle =$$

$$\left\{ -\left\langle a_1(t_{2g}) \left| \frac{\vec{p}}{\vec{m}} \right| e_\pm(e_g) \right\rangle + \left\langle e_\pm(t_{2g}) \left| \frac{\vec{p}}{\vec{m}} \right| e_\mp(e_g) \right\rangle \right\}$$

$$(89)$$

Because of the spin ambiguity and prolificity of the four- and six-electron arrangement, we perceive that no simple relationship exists either within itself or between the one-, two-, three-, seven-, eight-, or nine-electron situations. However, in a restrictive domain such relationships can be uncovered. To elucidate, (1) the quintet four and six electronic state verticilatory and spectral strengths are identical with one another and with the one- and nine-electron strengths, and are multiplicatively related to the spin-paired seven-electron strengths; (2) some of the triplet state four-electron helical and spectral strengths are formally one-half those of the correspondent two- and seven- spin-free electron strengths; and (3) the singlet six-electron rotational and spectral strengths are formally twice those of the kindred three- and eight-electron strengths. These relationships will be again emphasized in section IV.

(b) *No Configuration Interaction: Nonzero Spin-Orbit Forces. Four and Six Electrons.* The remarks apropos to this paragraph are the same as those of §4.2b.

(c) *Configuration Interaction: Zero and Nonzero Spin-Orbit Forces. Four and Six Electrons.* The fruits of configuration interaction are coequal to those of §4.2c.

4.5 *The Five-Electron Case.* Concordant with our prior words of §4.2, we fix our scrutiny of the five-electron enigma and study the single-electron excitations alone, the leftovers to be relegated to future looksees.[38,43] With this circumscription, the apt trigonally directed cubical many electron functions for the five-electron bunch are as given below.

(a) *No Configuration Interaction: Zero Spin-Orbit Forces.* (i) *Wave Functions: Five Electrons*

$^6A_1[^6A_{1g}(t_{2g}{}^3e_g{}^2)]: |a_1(t_{2g})e_+(t_{2g})e_-(t_{2g})e_+(e_g)e_-(e_g)|$

$^4A_2[^4T_{1g}(t_{2g}{}^4e_g)]:$

$$\frac{1}{\sqrt{2}} \{ |a_1(t_{2g})e_+(t_{2g})\bar{e}_+(t_{2g})e_-(t_{2g})e_+(e_g)| -$$
$$|a_1(t_{2g})e_-(t_{2g})\bar{e}_-(t_{2g})e_+(t_{2g})e_-(e_g)| \}$$

$^4E_\pm[^4T_{1g}(t_{2g}{}^4e_g)]:$

$$\mp\frac{1}{\sqrt{2}} \{ |a_1(t_{2g})\bar{a}_1(t_{2g})e_\pm(t_{2g})e_\mp(t_{2g})e_\pm(e_g)| +$$
$$|a_1(t_{2g})e_\pm(t_{2g})e_\mp(t_{2g})\bar{e}_\mp(t_{2g})e_\mp(e_g)| \}$$

$^4A_1[^4T_{2g}(t_{2g}{}^4e_g)]:$

$$\frac{1}{\sqrt{2}} \{ |a_1(t_{2g})e_+(t_{2g})\bar{e}_+(t_{2g})e_-(t_{2g})e_+(e_g)| +$$
$$|a_1(t_{2g})e_-(t_{2g})\bar{e}_-(t_{2g})e_+(t_{2g})e_-(e_g)| \}$$

$^4E_\pm[^4T_{2g}(t_{2g}{}^4e_g)]:$

$$\frac{1}{\sqrt{2}} \{ |a_1(t_{2g})e_\pm(t_{2g})e_\mp(t_{2g})\bar{e}_\mp(t_{2g})e_\mp(e_g)| -$$
$$|a_1(t_{2g})\bar{a}_1(t_{2g})e_\pm(t_{2g})e_\mp(t_{2g})e_\pm(e_g)| \}$$

$^2A_1[^2T_{2g}(t_{2g}{}^5)]: |a_1(t_{2g})e_+(t_{2g})\bar{e}_+(t_{2g})e_-(t_{2g})\bar{e}_-(t_{2g})|$

$^2E_\pm[^2T_{2g}(t_{2g}{}^5)]: |a(t_{2g})\bar{a}_1(t_{2g})e_\pm(t_{2g})\bar{e}_\pm(t_{2g})e_\mp(t_{2g})|$

$^2A_2[^2A_{2g}(t_{2g}{}^4e_g)]:$

$$\frac{1}{\sqrt{6}} \{ |a_1(t_{2g})\bar{a}_1(t_{2g})e_-(t_{2g})\bar{e}_+(t_{2g})e_+(e_g)| -$$
$$|a_1(t_{2g})\bar{a}_1(t_{2g})e_-(t_{2g})\bar{e}_-(t_{2g})e_-(e_g)| +$$
$$|\bar{a}_1(t_{2g})e_+(t_{2g})\bar{e}_+(t_{2g})e_-(t_{2g})e_-(e_g)| -$$
$$|\bar{a}_1(t_{2g})e_+(t_{2g})e_-(t_{2g})\bar{e}_-(t_{2g})e_+(e_g)| +$$
$$|a_1(t_{2g})\bar{c}_+(t_{2g})e_-(t_{2g})\bar{e}_-(t_{2g})e_+(e_g)| -$$
$$|a_1(t_{2g})e_+(t_{2g})\bar{e}_+(t_{2g})\bar{e}_-(t_{2g})e_-(e_g)| \}$$

$^2A_2[^2T_{1g}(t_{2g}{}^4e_g)]:$

$$\frac{1}{2\sqrt{3}} \{ |\bar{a}_1(t_{2g})e_+(t_{2g})\bar{e}_+(t_{2g})e_-(t_{2g})e_-(e_g)| -$$
$$2|a_1(t_{2g})e_+(t_{2g})\bar{e}_+(t_{2g})e_-(t_{2g})\bar{e}_-(e_g)| +$$
$$|a_1(t_{2g})e_+(t_{2g})\bar{e}_+(t_{2g})\bar{e}_-(t_{2g})e_-(e_g)| -$$
$$|\bar{a}_1(t_{2g})e_+(t_{2g})e_-(t_{2g})\bar{e}_-(t_{2g})e_+(e_g)| +$$
$$2|a_1(t_{2g})e_+(t_{2g})e_-(t_{2g})\bar{e}_-(t_{2g})\bar{e}_+(e_g)| -$$
$$|a_1(t_{2g})\bar{e}_+(t_{2g})e_-(t_{2g})\bar{e}_-(t_{2g})e_+(e_g)| \}$$

$^2E_\pm[^2T_{1g}(t_{2g}{}^4e_g)]:$

$$\mp\frac{1}{2\sqrt{3}} \{ |\bar{a}_-(t_{2g})e_\pm(t_{2g})e_\mp(t_{2g})\bar{e}_\mp(t_{2g})e_\mp(e_g)| -$$
$$2|a_1(t_{2g})e_\pm(t_{2g})e_\mp(t_{2g})\bar{e}_\mp(t_{2g})\bar{e}_\mp(e_g)| +$$
$$|a_1(t_{2g})\bar{e}_\pm(t_{2g})e_\mp(t_{2g})\bar{e}_\mp(t_{2g})e_\mp(e_g)| -$$
$$|a_1(t_{2g})\bar{a}_1(t_{2g})e_\pm(t_{2g})\bar{e}_\mp(t_{2g})e_\pm(e_g)| +$$
$$2|a_1(t_{2g})\bar{a}_1(t_{2g})e_\pm(t_{2g})e_\mp(t_{2g})e_\pm(e_g)| -$$
$$|a_1(t_{2g})\bar{a}_1(t_{2g})\bar{e}_\pm(t_{2g})e_\mp(t_{2g})e_\pm(e_g)| \}$$

$^2A_1[^2T_{2g}(t_{2g}{}^4e_g)]:$

$$-\frac{1}{2\sqrt{3}} \{ 2|a_1(t_{2g})\bar{a}_1(t_{2g})e_+(t_{2g})\bar{e}_+(t_{2g})e_+(e_g)| +$$
$$|\bar{a}_1(t_{2g})e_+(t_{2g})e_-(t_{2g})\bar{e}_-(t_{2g})e_+(e_g)| -$$
$$|a_1(t_{2g})\bar{e}_+(t_{2g})e_-(t_{2g})e_-(t_{2g})e_+(e_g)| +$$
$$2|a_1(t_{2g})\bar{a}_1(t_{2g})e_-(t_{2g})\bar{e}_-(t_{2g})e_-(e_g)| +$$
$$|\bar{a}_1(t_{2g})e_+(t_{2g})\bar{e}_+(t_{2g})e_-(t_{2g})e_-(e_g)| -$$
$$|a_1(t_{2g})e_+(t_{2g})\bar{e}_+(t_{2g})\bar{e}_-(t_{2g})e_-(e_g)| \}$$

$^2E_{\pm}[^2T_{2g}(t_{2g}{}^4e_g)]$:

$$\frac{1}{2\sqrt{3}}\left\{2\left|e_{\pm}(t_{2g})\bar{e}_{\pm}(t_{2g})e_{\mp}(t_{2g})\bar{e}_{\mp}(t_{2g})e_{\pm}(e_g)\right|\right.+$$
$$\left|a_1(t_{2g})\bar{a}_1(t_{2g})e_{\pm}(t_{2g})\bar{e}_{\mp}(t_{2g})e_{\pm}(e_g)\right|-$$
$$\left|a_1(t_{2g})\bar{a}_1(t_{2g})\bar{e}_{\pm}(t_{2g})e_{\mp}(t_{2g})e_{\pm}(e_g)\right|+$$
$$2\left|a_1(t_{2g})\bar{a}_1(t_{2g})e_{\pm}(t_{2g})\bar{e}_{\pm}(t_{2g})e_{\mp}(e_g)\right|+$$
$$\left|\bar{a}_1(t_{2g})e_{\pm}(t_{2g})e_{\mp}(t_{2g})\bar{e}_{\mp}(t_{2g})e_{\mp}(e_g)\right|-$$
$$\left.\left|a_1(t_{2g})\bar{e}_{\pm}(t_{2g})e_{\mp}(t_{2g})\bar{e}_{\mp}(t_{2g})e_{\mp}(e_g)\right|\right\}$$

$^2E_{\pm}[^2E_g(t_{2g}{}^4e_g)]$:

$$\frac{1}{\sqrt{3}}\left\{\left|\bar{a}_1(t_{2g})e_{\pm}(t_{2g})e_{\mp}(t_{2g})\bar{e}_{\mp}(t_{2g})e_{\mp}(e_g)\right|-\right.$$
$$\left|a_1(t_{2g})\bar{a}_1(t_{2g})e_{\pm}(t_{2g})\bar{e}_{\pm}(t_{2g})e_{\mp}(e_g)\right|-$$
$$\left.\left|a_1(t_{2g})\bar{e}_{\pm}(t_{2g})e_{\mp}(t_{2g})\bar{e}_{\mp}(t_{2g})e_{\mp}(e_g)\right|\right\}$$

$^2A_1[^2T_{2g}(t_{2g}{}^4e_g)]$:

$$\frac{1}{2\sqrt{3}}\left\{\left|\bar{a}_1(t_{2g})e_+(t_{2g})\bar{e}_+(t_{2g})e_-(t_{2g})e_-(e_g)\right|-\right.$$
$$2\left|a_1(t_{2g})e_+(t_{2g})\bar{e}_+(t_{2g})e_-(t_{2g})\bar{e}_-(e_g)\right|+$$
$$\left|a_1(t_{2g})e_+(t_{2g})\bar{e}_+(t_{2g})e_-(t_{2g})e_-(e_g)\right|+$$
$$\left|\bar{a}_1(t_{2g})e_+(t_{2g})e_-(t_{2g})\bar{e}_-(t_{2g})e_+(e_g)\right|-$$
$$2\left|a_1(t_{2g})e_+(t_{2g})e_-(t_{2g})\bar{e}_-(t_{2g})\bar{e}_+(e_g)\right|+$$
$$\left.\left|a_1(t_{2g})\bar{e}_+(t_{2g})e_-(t_{2g})\bar{e}_-(t_{2g})e_+(e_g)\right|\right\}$$

$^2E_{\pm}[^2T_{2g}(t_{2g}{}^4e_g)]$:

$$\mp\frac{1}{2\sqrt{3}}\left\{\left|\bar{a}_1(t_{2g})e_{\pm}(t_{2g})e_{\mp}(t_{2g})\bar{e}_{\mp}(t_{2g})e_{\mp}(e_g)\right|-\right.$$
$$2\left|a_1(t_{2g})e_{\pm}(t_{2g})e_{\mp}(t_{2g})\bar{e}_{\mp}(t_{2g})\bar{e}_{\mp}(e_g)\right|+$$
$$\left|a_1(t_{2g})\bar{e}_{\pm}(t_{2g})e_{\mp}(t_{2g})\bar{e}_{\mp}(t_{2g})e_{\mp}(e_g)\right|+$$
$$\left|a_1(t_{2g})\bar{a}_1(t_{2g})e_{\pm}(t_{2g})\bar{e}_{\mp}(t_{2g})e_{\pm}(e_g)\right|-$$
$$2\left|a_1(t_{2g})\bar{a}_1(t_{2g})e_{\pm}(t_{2g})e_{\mp}(t_{2g})\bar{e}_{\pm}(e_g)\right|+$$
$$\left.\left|a_1(t_{2g})\bar{a}_1(t_{2g})\bar{e}_{\pm}(t_{2g})e_{\mp}(t_{2g})e_{\pm}(e_g)\right|\right\}$$

$^2A_2[^2T_{1g}(t_{2g}{}^4e_g)]$:

$$-\frac{1}{2\sqrt{3}}\left\{2\left|a_1(t_{2g})\bar{a}_1(t_{2g})e_+(t_{2g})\bar{e}_+(t_{2g})e_+(e_g)\right|+\right.$$
$$\left|\bar{a}_1(t_{2g})e_+(t_{2g})e_-(t_{2g})\bar{e}_-(t_{2g})e_+(e_g)\right|-$$
$$\left|a_1(t_{2g})\bar{e}_+(t_{2g})e_-(t_{2g})\bar{e}_-(t_{2g})e_+(e_g)\right|-$$
$$2\left|a_1(t_{2g})\bar{a}_1(t_{2g})e_-(t_{2g})\bar{e}_-(t_{2g})e_-(e_g)\right|-$$
$$\left|a_1(t_{2g})e_+(t_{2g})\bar{e}_+(t_{2g})e_-(t_{2g})e_-(e_g)\right|+$$
$$\left.\left|a_1(t_{2g})e_+(t_{2g})\bar{e}_+(t_{2g})\bar{e}_-(t_{2g})e_-(e_g)\right|\right\}$$

$^2E_{\pm}[^2T_{1g}(t_{2g}{}^4e_g)]$:

$$\mp\frac{1}{2\sqrt{3}}\left\{2\left|(e_{\pm}(t_{2g})\bar{e}_{\pm}(t_{2g})e_{\mp}(t_{2g})\bar{e}_{\mp}(t_{2g})e_{\pm}(e_g)\right|\right.+$$
$$\left|a_1(t_{2g})\bar{a}_1(t_{2g})e_+(t_{2g})\bar{e}_{\mp}(t_{2g})e_{\pm}(e_g)\right|-$$
$$\left|a_1(t_{2g})\bar{a}_1(t_{2g})\bar{e}_{\pm}(t_{2g})e_{\mp}(t_{2g})e_{\pm}(e_g)\right|-$$
$$2\left|a_1(t_{2g})\bar{a}_1(t_{2g})e_{\pm}(t_{2g})\bar{e}_{\pm}(t_{2g})e_{\mp}(e_g)\right|-$$
$$\left|\bar{a}_1(t_{2g})e_{\pm}(t_{2g})e_{\mp}(t_{2g})\bar{e}_{\mp}(t_{2g})e_{\mp}(e_g)\right|+$$
$$\left.\left|a_1(t_{2g})\bar{e}_{\pm}(t_{2g})e_{\mp}(t_{2g})\bar{e}_{\mp}(t_{2g})e_{\mp}(e_g)\right|\right\}$$

$^2A_1[^2A_{1g}(t_{2g}{}^4e_g)]$:

$$\frac{1}{\sqrt{6}}\left\{\left|\bar{a}_1(t_{2g})e_+(t_{2g})\bar{e}_+(t_{2g})e_-(t_{2g})e_-(e_g)\right|\right.+$$
$$\left|\bar{a}_1(t_{2g})e_+(t_{2g})e_-(t_{2g})\bar{e}_-(t_{2g})e_+(e_g)\right|-$$
$$\left|a_1(t_{2g})e_+(t_{2g})\bar{e}_+(t_{2g})\bar{e}_-(t_{2g})e_-(e_g)\right|-$$
$$\left|a_1(t_{2g})\bar{e}_+(t_{2g})e_-(t_{2g})\bar{e}_-(t_{2g})e_+(e_g)\right|-$$
$$\left|a_1(t_{2g})\bar{a}_1(t_{2g})e_+(t_{2g})\bar{e}_+(t_{2g})e_+(e_g)\right|-$$
$$\left.\left|a_1(t_{2g})\bar{a}_1(t_{2g})e_-(t_{2g})\bar{e}_-(t_{2g})e_-(e_g)\right|\right\}$$

$^2E_{\pm}[^2E_g(t_{2g}{}^4e_g)]$:

$$\frac{1}{\sqrt{3}}\left\{\left|e_{\pm}(t_{2g})\bar{e}_{\pm}(t_{2g})e_{\mp}(t_{2g})\bar{e}_{\mp}(t_{2g})e_{\pm}(e_g)\right|-\right.$$
$$\left|a_1(t_{2g})\bar{a}_1(t_{2g})e_{\pm}(t_{2g})\bar{e}_{\mp}(t_{2g})e_{\pm}(e_g)\right|+$$
$$\left.\left|a_1(t_{2g})\bar{a}_1(t_{2g})\bar{e}_{\pm}(t_{2g})e_{\mp}(t_{2g})e_{\pm}(e_g)\right|\right\}\quad(90)$$

These configurational functions enable the vortical and photical matrix displays, which supervene, to be engraved.

(ii)   Matrix Elements: Five Electrons

$$\left\langle ^2A_1[^2T_{2g}(t_{2g}{}^5)]\left|\frac{\vec{p}}{\vec{m}}\right|^2E_{\pm}[^2T_{2g}(t_{2g}{}^5)]\right\rangle =$$
$$-\left\langle e_{\mp}(t_{2g})\left|\frac{\vec{p}}{\vec{m}}\right|a_1(t_{2g})\right\rangle$$

$$\left\langle ^2A_1[^2T_{2g}(t_{2g}{}^5)]\left|\frac{\vec{p}}{\vec{m}}\right|^2A_2[^2A_{2g}(t_{2g}{}^4e_g)]\right\rangle =$$
$$\sqrt{2/3}\left\langle e_-(t_{2g})\left|\frac{\vec{p}}{\vec{m}}\right|e_-(e_g)\right\rangle$$

$$\left\langle ^2A_1[^2T_{2g}(t_{2g}{}^5)]\left|\frac{\vec{p}}{\vec{m}}\right|^2A_2[^2T_{1g}(t_{2g}{}^4e_g)]\right\rangle =$$
$$-\sqrt{3}\left\langle e_-(t_{2g})\left|\frac{\vec{p}}{\vec{m}}\right|e_-(e_g)\right\rangle$$

$$\left\langle ^2A_1[^2T_{2g}(t_{2g}{}^5)]\left|\frac{\vec{p}}{\vec{m}}\right|^2E_{\pm}[^2T_{1g}(t_{2g}{}^4e_g)]\right\rangle =$$
$$\pm\frac{\sqrt{3}}{2}\left\langle e_{\pm}(t_{2g})\left|\frac{\vec{p}}{\vec{m}}\right|e_{\mp}(e_g)\right\rangle$$

$$\left\langle {}^2A_1[{}^2T_{2g}(t_{2g}{}^5)] \left| \frac{\vec{p}}{\vec{m}} \right| {}^2A_1[{}^2T_{2g}(t_{2g}{}^4e_g)] \right\rangle \equiv 0$$

$$\left\langle {}^2A_1[{}^2T_{2g}(t_{2g}{}^5)] \left| \frac{\vec{p}}{\vec{m}} \right| {}^2E_\pm[{}^2T_{2g}(t_{2g}{}^4e_g)] \right\rangle =$$
$$\frac{1}{2\sqrt{3}}\left\{ 2\left\langle a_1(t_{2g}) \left| \frac{\vec{p}}{\vec{m}} \right| e_\pm(e_g) \right\rangle + \left\langle e_\pm(t_{2g}) \left| \frac{\vec{p}}{\vec{m}} \right| e_\mp(e_g) \right\rangle \right\}$$

$$\left\langle {}^2A_1[{}^2T_{2g}(t_{2g}{}^5)] \left| \frac{\vec{p}}{\vec{m}} \right| {}^2E_\pm[{}^2E_g(t_{2g}{}^4e_g)] \right\rangle =$$
$$\frac{1}{\sqrt{3}}\left\langle e_\pm(t_{2g}) \left| \frac{\vec{p}}{\vec{m}} \right| e_\mp(e_g) \right\rangle$$

$$\left\langle {}^2A_1[{}^2T_{2g}(t_{2g}{}^5)] \left| \frac{\vec{p}}{\vec{m}} \right| {}^2A_1[{}^2T_{2g}(t_c{}^4e_g)] \right\rangle \equiv 0$$

$$\left\langle {}^2A_1[{}^2T_{2g}(t_{2g}{}^5)] \left| \frac{\vec{p}}{\vec{m}} \right| {}^2E_\pm[{}^2T_{2g}(t_{2g}{}^4e_g)] \right\rangle =$$
$$\pm \frac{\sqrt{3}}{2}\left\langle e_\pm(t_{2g}) \left| \frac{\vec{p}}{\vec{m}} \right| e_\mp(e_g) \right\rangle$$

$$\left\langle {}^2A_1[{}^2T_{2g}(t_{2g}{}^5)] \left| \frac{\vec{p}}{\vec{m}} \right| {}^2A_2[{}^2T_{1g}(t_{2g}{}^4e_g)] \right\rangle =$$
$$\frac{1}{\sqrt{3}}\left\langle e_-(t_{2g}) \left| \frac{\vec{p}}{\vec{m}} \right| e_-(e_g) \right\rangle$$

$$\left\langle {}^2A_1[{}^2T_{2g}(t_{2g}{}^5)] \left| \frac{\vec{p}}{\vec{m}} \right| {}^2E_\pm[{}^2T_{1g}(t_{2g}{}^4e_g)] \right\rangle =$$
$$\frac{\pm 1}{2\sqrt{3}}\left\{ \left\langle e_\pm(t_{2g}) \left| \frac{\vec{p}}{\vec{m}} \right| e_\mp(e_g) \right\rangle - 2\left\langle a_1(t_{2g}) \left| \frac{\vec{p}}{\vec{m}} \right| e_\pm(t_{2g}) \right\rangle \right\}$$

$$\left\langle {}^2A_1[{}^2T_{2g}(t_{2g}{}^5)] \left| \frac{\vec{p}}{\vec{m}} \right| {}^2A_1[{}^2A_{1g}(t_{2g}{}^4e_g)] \right\rangle \equiv 0$$

$$\left\langle {}^2A_1[{}^2T_{2g}(t_{2g}{}^5)] \left| \frac{\vec{p}}{\vec{m}} \right| {}^2E_\pm[{}^2E_g(t_{2g}{}^4e_g)] \right\rangle =$$
$$\frac{1}{\sqrt{3}}\left\langle a_1(t_{2g}) \left| \frac{\vec{p}}{\vec{m}} \right| e_\pm(e_g) \right\rangle \quad (91)$$

$$\left\langle {}^2E_\pm[{}^2T_{2g}(t_{2g}{}^5)] \left| \frac{\vec{p}}{\vec{m}} \right| {}^2A_2[{}^2A_{2g}(t_{2g}{}^4e_g)] \right\rangle =$$
$$\pm \frac{1}{\sqrt{6}}\left\{ \left\langle e_\mp(t_{2g}) \left| \frac{\vec{p}}{\vec{m}} \right| e_\pm(e_g) \right\rangle + \left\langle a_1(t_{2g}) \left| \frac{\vec{p}}{\vec{m}} \right| e_\mp(e_g) \right\rangle \right\}$$

$$\left\langle {}^2E_\pm[{}^2T_{2g}(t_{2g}{}^5)] \left| \frac{\vec{p}}{\vec{m}} \right| {}^2A_2[{}^2T_{1g}(t_{2g}{}^4e_g)] \right\rangle =$$
$$\pm \frac{\sqrt{3}}{2}\left\langle a_1(t_{2g}) \left| \frac{\vec{p}}{\vec{m}} \right| e_\mp(e_g) \right\rangle$$

$$\left\langle {}^2E_\pm[{}^2T_{2g}(t_{2g}{}^5)] \left| \frac{\vec{p}}{\vec{m}} \right| {}^2E_\pm[{}^2T_{1g}(t_{2g}{}^4e_g)] \right\rangle =$$
$$\pm \frac{\sqrt{3}}{2}\left\langle e_\pm(t_{2g}) \left| \frac{\vec{p}}{\vec{m}} \right| e_\pm(e_g) \right\rangle$$

$$\left\langle {}^2E_\pm[{}^2T_{2g}(t_{2g}{}^5)] \left| \frac{\vec{p}}{\vec{m}} \right| {}^2E_\mp[{}^2T_{1g}(t_{2g}{}^4e_g)] \right\rangle =$$
$$\mp \frac{\sqrt{3}}{2}\left\{ \left\langle a_1(t_{2g}) \left| \frac{\vec{p}}{\vec{m}} \right| e_\pm(e_g) \right\rangle + \left\langle e_\pm(t_{2g}) \left| \frac{\vec{p}}{\vec{m}} \right| e_\mp(e_g) \right\rangle \right\}$$

$$\left\langle {}^2E_\pm[{}^2T_{2g}(t_{2g}{}^5)] \left| \frac{\vec{p}}{\vec{m}} \right| {}^2A_1[{}^2T_{2g}(t_{2g}{}^4e_g)] \right\rangle =$$
$$\frac{-1}{2\sqrt{3}}\left\{ \left\langle a_1(t_{2g}) \left| \frac{\vec{p}}{\vec{m}} \right| e_\mp(e_g) \right\rangle + 2\left\langle e_\mp(t_{2g}) \left| \frac{\vec{p}}{\vec{m}} \right| e_\pm(e_g) \right\rangle \right\}$$

$$\left\langle {}^2E_\pm[{}^2T_{2g}(t_{2g}{}^5)] \left| \frac{\vec{p}}{\vec{m}} \right| {}^2E_\pm[{}^2T_{2g}(t_{2g}{}^4e_g)] \right\rangle =$$
$$\frac{\sqrt{3}}{2}\left\langle e_\mp(t_{2g}) \left| \frac{\vec{p}}{\vec{m}} \right| e_\mp(e_g) \right\rangle$$

$$\left\langle {}^2E_\pm[{}^2T_{2g}(t_{2g}{}^5)] \left| \frac{\vec{p}}{\vec{m}} \right| {}^2E_\mp[{}^2T_{2g}(t_{2g}{}^4e_g)] \right\rangle =$$
$$\frac{1}{2\sqrt{3}}\left\{ \left\langle a_1(t_{2g}) \left| \frac{\vec{p}}{\vec{m}} \right| e_\pm(e_g) \right\rangle - \left\langle e_\pm(t_{2g}) \left| \frac{\vec{p}}{\vec{m}} \right| e_\mp(e_g) \right\rangle \right\}$$

$$\left\langle {}^2E_\pm[{}^2T_{2g}(t_{2g}{}^5)] \left| \frac{\vec{p}}{\vec{m}} \right| {}^2E_\pm[{}^2E_c(t_{2g}{}^4e_g)] \right\rangle =$$
$$\frac{-1}{\sqrt{3}}\left\langle e_\mp(t_{2g}) \left| \frac{\vec{p}}{\vec{m}} \right| e_\mp(e_g) \right\rangle$$

$$\left\langle {}^2E_\pm[{}^2T_{2g}(t_{2g}{}^5)] \left| \frac{\vec{p}}{\vec{m}} \right| {}^2E_\mp[{}^2E_c(t_{2g}{}^4e_g)] \right\rangle =$$
$$\frac{1}{\sqrt{3}}\left\langle a_1(t_{2g}) \left| \frac{\vec{p}}{\vec{m}} \right| e_\pm(e_g) \right\rangle$$

$$\left\langle {}^2E_\pm[{}^2T_{2g}(t_{2g}{}^5)] \left| \frac{\vec{p}}{\vec{m}} \right| {}^2A_1[{}^2T_{2g}(t_{2g}{}^4e_g)] \right\rangle =$$
$$\frac{\sqrt{3}}{2}\left\langle a_1(t_{2g}) \left| \frac{\vec{p}}{\vec{m}} \right| e_\mp(e_g) \right\rangle$$

$$\left\langle {}^2E_\pm[{}^2T_{2g}(t_{2g}{}^5)] \left| \frac{\vec{p}}{\vec{m}} \right| {}^2E_\pm[{}^2T_{2g}(t_{2g}{}^4e_g)] \right\rangle =$$
$$\mp \frac{\sqrt{3}}{2}\left\langle e_\pm(t_{2g}) \left| \frac{\vec{p}}{\vec{m}} \right| e_\pm(e_g) \right\rangle$$

$$\left\langle {}^2E_\pm[{}^2T_{2g}(t_{2g}{}^5)] \left| \frac{\vec{p}}{\vec{m}} \right| {}^2E_\mp[{}^2T_{2g}(t_{2g}{}^4e_g)] \right\rangle =$$
$$\mp \frac{\sqrt{3}}{2}\left\{ \left\langle a_1(t_{2g}) \left| \frac{\vec{p}}{\vec{m}} \right| e_\pm(e_g) \right\rangle - \left\langle e_\pm(t_{2g}) \left| \frac{\vec{p}}{\vec{m}} \right| e_\mp(e_g) \right\rangle \right\}$$

$$\left\langle {}^2E_\pm[{}^2T_{2g}(t_{2g}{}^5)] \left| \frac{\vec{p}}{\vec{m}} \right| {}^2A_2[{}^2T_{1g}(t_{2g}{}^4e_g)] \right\rangle =$$
$$\frac{\pm 1}{2\sqrt{3}}\left\{ \left\langle a_1(t_{2g}) \left| \frac{\vec{p}}{\vec{m}} \right| e_\mp(e_g) \right\rangle - 2\left\langle e_\mp(t_{2g}) \left| \frac{\vec{p}}{\vec{m}} \right| e_\pm(e_g) \right\rangle \right\}$$

$$\left\langle {}^2E_\pm[{}^2T_{2g}(t_{2g}{}^5)] \left| \frac{\vec{p}}{\vec{m}} \right| {}^2E_\pm[{}^2T_{1g}(t_{2g}{}^4e_g)] \right\rangle =$$
$$\pm \frac{1}{2\sqrt{3}}\left\langle e_\mp(t_{2g}) \left| \frac{\vec{p}}{\vec{m}} \right| e_\mp(e_g) \right\rangle$$

$$\left\langle \,^2E_\pm[\,^2T_{2g}(t_{2g}{}^5)] \left|\frac{\vec{p}}{m}\right| \,^2E_\mp[\,^2T_{1g}(t_{2g}{}^4e_g)] \,\right\rangle =$$

$$\frac{\pm 1}{2\sqrt{3}} \left\{ \left\langle a_1(t_{2g}) \left|\frac{\vec{p}}{m}\right| e_\pm(e_g) \right\rangle + \left\langle e_\pm(t_{2g}) \left|\frac{\vec{p}}{m}\right| e_\mp(e_g) \right\rangle \right\}$$

$$\left\langle \,^2E_\pm[\,^2T_{2g}(t_{2g}{}^5)] \left|\frac{\vec{p}}{m}\right| \,^2A_1[\,^2A_{1g}(t_{2g}{}^4e_g)] \,\right\rangle =$$

$$\frac{1}{\sqrt{6}} \left\{ \left\langle a_1(t_{2g}) \left|\frac{\vec{p}}{m}\right| e_\mp(e_g) \right\rangle - \left\langle e_\mp(t_{2g}) \left|\frac{\vec{p}}{m}\right| e_\pm(e_g) \right\rangle \right\}$$

$$\left\langle \,^2E_\pm[\,^2T_{2g}(t_{2g}{}^5)] \left|\frac{\vec{p}}{m}\right| \,^2E_\pm[\,^2E_g(t_{2g}{}^4e_g)] \,\right\rangle =$$

$$\frac{1}{\sqrt{3}} \left\langle e_\pm(t_{2g}) \left|\frac{\vec{p}}{m}\right| e_\pm(e_g) \right\rangle$$

$$\left\langle \,^2E_\pm[\,^2T_{2g}(t_{2g}{}^5)] \left|\frac{\vec{p}}{m}\right| \,^2E_\mp[\,^2E_g(t_{2g}{}^4e_g)] \,\right\rangle =$$

$$\frac{1}{\sqrt{3}} \left\langle e_\pm(t_{2g}) \left|\frac{\vec{p}}{m}\right| e_\mp(e_g) \right\rangle \quad (92)$$

Again, as in the four- and six-electron situation, the multiplicity of the spin electronic states precludes any close uniform accord of the five-electron vortical and photical strengths with those of the one-, two-, three-, four-, six-, seven-, eight-, or nine-electron bevies; but certain relationships nonetheless exist in bounded domains. As a tutorial, the four- and five- spin-paired trigonally ordered cubical electron collections of the optically allowed single-electron hops can be put in a one-to-one correspondence with each other so that their vertigal and photical strengths become (for the most part) equal when the trigonal and cubical specie subscripts 1 and 2 are interchanged, that is, so that the $A_2(T_{1g})$, $E_\pm(T_{1g})$ to $A_2(T_{1g})$, $E_\pm(T_{1g})$ transition of the four-electron case corresponds to the $A_1(T_{2g})$, $E_\pm(T_{2g})$ to $A_1(T_{2g})$, $E_\pm(T_{2g})$ transition of the five-electron case, and so on [three exceptions to this rule exist: one of the four-electron $A_2(T_{1g})$, $E_\pm(T_{1g})$ to $E_\pm(E_g)$ transitions is four times as strong as the correspondent five-electron transition and one each of the four-electron $A_2(T_{1g})$ $E_\pm(T_{1g})$ to $A_{1,2}(T_{2,1g})$, $E_\pm(T_{2,1g})$ transitions is one-third as strong as its correspondent five electron transition]. It thus follows that the five-electron vertigal and photical strengths are also related to those of the two- and seven-electron spin-free (and hence other) situations, just as were the four-electron strengths of §4.4. In addition, there is a direct multiplicative relationship between the two sets of $^2A_1[\,^2T_{2g}(t_{2g}{}^5)]$, $^2E_\pm[\,^2T_{2g}(t_{2g}{}^5)]$ to $^2E_\pm[\,^2E_g(t_{2g}{}^4e_g)]$ five-electron spin-paired rotational and and spectral strengths and the associate sets of $^2E_\pm[\,^2E_g(t_{2g}{}^6e_g)]$ to $^2A_1[\,^2T_{2g}(t_{2g}{}^5e_g{}^2)]$, $^2E_\pm[\,^2T_{2g}(t_{2g}{}^5e_g{}^2)]$ seven-electron spin-paired strengths [compare eq. 82b

with eq. 91 and 92], as well as several other less direct relationships.

(b) *No Configuration Interaction: Nonzero Spin-Orbit Forces. Five Electrons.* The utterances relevant to this paragraph are coincident with those of §4.2b.

(c) *Configuration Interaction: Zero and Nonzero Spin-Orbit Forces. Five Electrons.* The blossoms from configurational interaction are synonymical with those of §4.2c.

4.6 *A Numerical Example: The Trisethylenediamine- and Trisoxalatocopper(II) Cation and Anion.* To affirm that the electrical asymmetries entertained in the antecedent paragraphs are of a suitable magnitude to rationalize the observed optical rotations of transition metal compounds, we shall here present a numerical examplar. Consider the σ- and σ-,π-bonded complex ions, copper(II) trisethylenediamine and copper(II) trisoxalato, respectively, and assume for the sake of simplicity that these are describable by a linear combination of Slater type metallic and ligand atomic orbitals with Slater (effective charge) exponents 7.85 (Cu: 3d),[44] 3.80 and 3.90 (N:2s, 2p),[45] 4.55 or 4.4456 (O: 2s, 2p, or 2p),[46] with the metal and ligand nuclear centers separated by a distance of 2.00 Å.[44] Also assume that the ligand σ-bond 2s- and 2p-like content, k_s and k_p, are $^1/_2$ and $\sqrt{3}/2$, each,[47] that the

(44) (a) J. Bjerrum, C. J. Ballhausen, and C. K. Jørgensen, *Acta Chem. Scand.*, **8**, 1275 (1954); (b) C. J. Ballhausen, *Dan. Mat. Fys. Mea.*, **29**, No. 4 (1954). Of our two examples of trigonal dihedral optically active copper(II) complex ions, only the copper(II) trisethylenediamine cation has actually been prepared and resolved. Unfortunately, its instability in solutions suitable for optical rotatory dispersion and circular dichroism measurements has thus far precluded any close experimental study of these properties [read (c) G. Gordon and R. K. Birdwhistell, *J. Am. Chem. Soc.*, **81**, 3567 (1959)]. Hence, the computations to be described in what follows are at this time but an indicatrix of things yet to come.

(45) (a) J. Higuchi, *J. Chem. Phys.*, **24**, 534 (1956) [NH$_3$, $Z^N{}_\text{effective}$ = 3.80]; (b) A. B. F. Duncan, *ibid.*, **27**, 423 (1957) [*Errata, ibid.*, **39**, 240 (1963)] NH$_3$, $Z^N{}_\text{effective}$ = 3.90]. With the latter of these two values and the metal-ligand bond distance of 2.00 Å. cited above, the relevant copper(II) K_{nAi} integrals become

$[Z_\text{eff} = 3.90]$ $K_{2A_5} = 2.9898 \times 10^{-10}$, $K_{3A_3} = 5.4703 \times 10^{-11}$
$\qquad K_{4A_3} = -1.4449 \times 10^{-10}$, $K_{7A_3} = -1.0120 \times 10^{-10}$
$\qquad K_{24A_4} = 7.0735 \times 10^{-2}$, $K_{26A_4} = -2.6143 \times 10^{-2}$
$\qquad\qquad K_{32A_5} = -4.5274 \times 10^{-2}$

(46) (a) F. O. Ellison and H. Shull, *J. Chem. Phys.*, **21**, 1420 (1953); **23**, 2348 (1955) [H$_2$O, $Z^O{}_\text{effective}$ = 4.55]; (b) J. Sidman, *ibid.*, **27**, 1270 (1957) [CH$_2$O, $Z^O{}_\text{effective}$ = 4.4456]. With the latter of these two values and the metal-ligand bond distance of 2.00 Å. cited above, the relevant copper(II) K_{nAi} integrals become

$[Z_\text{eff} = 4.4456]$ $K_{2A_5} = 2.3847 \times 10^{-10}$, $K_{3A_3} = 3.3716 \times 10^{-11}$
$\qquad K_{4A_3} = -1.1112 \times 10^{-10}$, $K_{7A_3} = -9.7103 \times 10^{-11}$
$\qquad K_{24A_4} = 6.1327 \times 10^{-2}$, $K_{26A_4} = -2.0399 \times 10^{-2}$
$\qquad\qquad K_{32A_5} = -3.9575 \times 10^{-2}$

(47) These values are very close to those obtained by J. Higuchi,[45a] A. B. F. Duncan,[45b] and H. Kaplan (*J. Chem. Phys.*, **26**, 1704 (1957). [Hartree-Fock nitrogen orbitals]) for ammonia for a variety of different orbital assumptions [their values for k_s are 0.551, 0.439, and 0.442, and for k_p, 0.855, 0.904, and 0.896, apiece, as compared with our convenient "average" of 0.500 and 0.866].

ligand–metal σ-, π-mixture parameters, ξ, η, and ρ, are $^1/_{10}$, $-^1/_{10}$, and $-\sqrt{^1/_2}$, serially,[48] and that the angle of ligand–metal orbital cant, α, is $5°$. Under these conservative conditions the rotational, $\mathfrak{R}$, and spectral, $\mathfrak{S}$, strengths for copper(II) trisethylenediamine ($Z^N_{\text{effective}}$ taken to be[45] 3.90) in the conformation of Fig. 2 become, in the limit to zero spin-orbit forces

$$\mathfrak{R}[^2E(E_g) \longrightarrow {}^2A_1(T_{2g})] =$$
$$-\mathfrak{R}[^2E(E_g) \longrightarrow {}^2E(T_{2g})] = +0.087B$$

$$\mathfrak{S}[^2E(E_g) \longrightarrow {}^2A_1(T_{2g})] =$$
$$1.0 \times 10^{-6}D^2, \mathfrak{S}[^2E(E_g) \longrightarrow {}^2E(T_{2g})] = 2.7 \times 10^{-7}D^2$$

$$\mathfrak{R}[^2A_1(T_{2g}) \longrightarrow {}^2E(T_{2g})] =$$
$$-0.22B, \mathfrak{S}[^2A_1[T_{2g}] \longrightarrow {}^2E(T_{2g})] = 5.7 \times 10^{-6}D^2$$
$$(93)$$

where the symbols B and D denote the fundamental units of rotational and spectral strength, the Biot [10^{-40} c.g.s.] and the Debye [10^{-18} c.g.s.].[49] If further the transition frequencies involved, $\nu[^2A_1(T_{2g}) \rightarrow {}^2E(T_{2g})]$ and $\nu[^2E(E_g) \rightarrow {}^2A_1(T_{2g}), {}^2E(T_{2g})]$ are taken to be of the order of 10^3 cm.$^{-1}$ and 1.5×10^4 cm.$^{-1}$, separately,[44,50]

(48) The sign of these constants is determined by the requirement that their associated wave functions have the antibonding radial nodal pattern. As the ligand metal overlap is negative for the $e_\pm(t_{2g})$ molecular orbital and positive for the $a_1(t_{2g})$ and $e_\pm(e_g)$ molecular orbitals, this nodal pattern is attained only with the sign choice given above (cf. section VII, §5.7, eq. A-12).

(49) We have here introduced a new unit, the Biot, in honor of the great French scientist who first discovered optical rotatory dispersion.[3] We hope that it will find favor. [An alternative unit has recently been introduced by W. E. Moffitt and A. J. Moscowitz (per-use, e.g., A. J. Moscowitz, in C. Djerassi, "Optical Rotatory Dispersion," McGraw-Hill Book Co., New York, N. Y., 1960, Chapter 12). While convenient theoretically, it is experimentally a nuisance because of its nonunit conversion factor, just as would the Debye be if it had been defined inclusive of the magnitude of the electronic charge. The name of Biot has been used, to the author's knowledge, but twice before as a unit. Unfortunately, one of these two uses is also in the field of optical rotatory dispersion and again in a mensural sense (look at W. Heller, "Technique of Organic Chemistry," Vol. I, Part III, "Physical Methods of Organic Chemistry," A. Weissberger, Ed., Interscience, New York, London, 1960, p. 2299. The other use is in the field of electromagnetism where 10 amp. is sometimes called 1 Biot). However, as this previous employment does not seem to have gained wide use, its present proposed utilization is, to a great extent, relatively free of possible confusion. Other equally good names would be[3] the Arago, the Cotton, the Fresnel, and the Pasteur. The initials of several of these (Arago, Cotton, and Fresnel), as luck would have it, coincide with those already in wide use as common units (the Ångstrom, the degree Celsius, the degree Fahrenheit, the Faraday, and the Farad (the Farad is usually abbreviated as a lower case letter)). It is thus six of one and half a dozen of the other! However, by calling Heller's specific and molecular rotations specific Biot and molecular Cotton rotations designated by $[\phi]_B$ and $[\mathfrak{M}]_C$, respectively, all confusion can be eliminated, and our proposed new utilization rendered free and clear]. The individual electric and magnetic dipole matrix elements utilized in eq. 93 are

$$\left\langle a_1(t_{2g}) \left| \frac{\vec{p}}{m} \right| e_\pm(t_{2g}) \right\rangle = \pm \left[\frac{i\bar{r}_0}{-m_0} \right] \hat{k}_\pm{}', \left\langle a_1(t_{2g}) \left| \frac{\vec{p}}{m} \right| e_\pm(e_g) \right\rangle =$$

$$\mp \left[\frac{ir_0}{m_0} \right] \hat{k}_\pm{}', \left\langle e_\pm(t_{2g}) \left| \frac{\vec{p}}{m} \right| e_\pm(e_g) \right\rangle = \pm \left[\frac{ir_1}{m_1} \right] \hat{k}_0{}',$$

$$\left\langle e_\pm(t_{2g}) \left| \frac{\vec{p}}{m} \right| e_\mp(e_g) \right\rangle = \mp \left[\frac{ir_2}{m_2} \right] \hat{k}_\pm{}'$$

where [cf. §3.3, eq. 47, with ξ, η, and ρ real]

$$\bar{r}_0 = e \sqrt{^3/_2} k_p \sin \alpha [K_{2A_3}(\xi - \eta) + \eta K_{3A_3}]N_{a_1(t)}N_{e(t)}$$

$$r_0 = \frac{e}{2} \eta \sqrt{^3/_2} k_p \sin \alpha (\sqrt{3} K_{4A_3} + K_{7A_3})N_{a_1(t)}N_{e(e)}$$

$$r_1 = \frac{e}{2} \xi \sqrt{^3/_2} k_p \sin \alpha (2K_{7A_3})N_{e(t)}N_{e(e)}$$

$$r_2 = \frac{e}{2} \xi \sqrt{^3/_2} k_p \sin \alpha (\sqrt{3} K_{4A_3} - K_{7A_3})N_{e(t)}N_{e(e)}$$

$$\bar{m}_0 = \mu_B N_{a_1(t)}N_{e(t)}$$

$$m_0 = \sqrt{2}\mu_B N_{a_1(t)}N_{e(e)}, m_1 = m_2 = \sqrt{2}\mu_B N_{e(t)}N_{e(e)}$$

In terms of these the appropriate single-electron rotational and spectral strengths are [compare §3.4, eq. 52]

$$\mathfrak{R}[a_1(t_{2g}) \longrightarrow e_\pm(t_{2g})] = -\bar{r}_0\bar{m}_0, \mathfrak{R}[a_1(t_{2g}) \longrightarrow e_\pm(e_g)] = r_0 m_0,$$

$$\mathfrak{R}[e_\pm(t_{2g}) \longrightarrow e_\pm(e_g)] = r_1 m_1, \mathfrak{R}[e_\pm(t_{2g}) \longrightarrow e_\mp(t_{2g})] = r_2 m_2$$

and

$$\mathfrak{S}[a_1(t_{2g}) \longrightarrow e_\pm(t_{2g})] = \bar{r}_0{}^2, \mathfrak{S}[a_1(t_{2g}) \longrightarrow e_\pm(e_g)] = r_0{}^2,$$

$$\mathfrak{S}[e_\pm(t_{2g}) \longrightarrow e_\pm(e_g)] = r_1{}^2, \mathfrak{S}[e_\pm(t_{2g}) \longrightarrow e_\mp(e_g)] = r_2{}^2$$

Their many electron state sums are as cataloged in Tables VI and VII [these sums were obtained from eq. 50, 51, 53, 64, 69–71, 80–82a,b, 85–89, 91, and 92]. The specific numerical values of the individual electric and magnetic dipole strengths for the Cu(II) case may be found by use of the recorded integral magnitudes of footnotes 45 and 46. [For $\alpha = 5°$ and $|\xi| = |\eta| = {}^1/_{10}$, $\rho = -1/\sqrt{2}$, the normalization constants become $N_{a_1(t)}{}^2 = N_{e(t)}{}^2 = 0.99105$, $N_{e(e)}{}^2 = 0.86241$ for Cu(II) trisethylenediamine and the ratios of $r_0:r_1:r_2$ become $2.34: -1.34: -1.00$].

(50) For recent quantitative estimates of typical trigonal field separations, look at (a) S. Geschwind and J. P. Remieka, J. Appl. Phys. Suppl., 33, 370 (1962). Other estimates quantitative and qualitative may be found in (b) H. S. Jarrett, J. Chem. Phys., 27, 1298 (1957) [results marred by an error in ligand field formulation]; (c) M. H. L. Pryce and W. A. Runciman, Discussions Faraday Soc., 26, 34 (1958); (d) S. Sugano and Y. Tanabe, ibid., 26, 43 (1958); (e) S. Yamada and R. Tsuchida, Bull. Chem. Soc. Japan, 33, 98 (1960); (f) T. S. Piper and R. L. Carlin, J. Chem. Phys., 33, 1208 (1960); 35, 1809 (1961); T. S. Piper, ibid., 35, 1240 (1961) [Errata, ibid., 36, 1089 (1962)]; T. S. Piper and R. L. Carlin, ibid., 36, 3330 (1962); Inorg. Chem., 2, 260 (1963); and in ref. 25c [in these references the trigonal field cleavage is variously referred to as $3K$ or v, with v equals $-3K$. So take care to avoid puzzlement]. Trigonal field intensities have also been estimated by (g) T. S. Piper and R. L. Carlin, J. Chem. Phys., 33, 608 (1960). The ref. 11b and 50b and many of the references under 50f pertain to studies of the most enigmatic acetylacetonates. Although we have not explicitly considered these compounds in this paper, it might be hoped that the theory here outlined, suitably generalized to explicitly include the molecular orbitals of predominantly ligand character [view Fig. 8], would be serviceable and help to reveal their secret. [Our theory of inclined bonds is not confined to trisbidentate coordinate situations alone, but is universally applicable, and hence, usable in bisbidentate and mono-bidentate circumstances also (as an instance, bisbidentate compounds of digonal dihedral symmetry may have their rotational and spectral strengths estimated by those of the combined trigonal states $a_1(t_{2g})$, $e_+(t_{2g}) \pm e_-(t_{2g})$, and $e_+(e_g) \pm e_-(e_g)$, respectively, in the absence of configuration interaction). A survey of some of the riddles involved in such circumstances may be found in (h) R. L. Belford, M. Calvin, and G. Belford, J. Chem. Phys., 26, 1165 (1957); (i) J. Ferguson, R. L. Belford, and T. S. Piper, ibid., 37, 1569 (1962); (j) C. K. Jørgensen, Acta Chem. Scand., 16, 2406 (1962); and (k) K. DeArmond and L. S. Forster, Spectrochim. Acta, 19, 1393, 1403, 1687 (1963); P. X. Armendarez and L. S. Forster, J. Chem. Phys., 40, 273 (1964).] Further chemicals of trigonal dihedral form which are also treatable by our theory and which experimentally and theoretically are nettle are discussed in ref. 10c and (l) C. K. Jørgensen, Mol. Phys., 5, 485 (1962); and (m) E. König and H. L. Schläfer, Z. physik. Chem. (Frankfurt), 34, 355 (1962); K. Madeja and E. König, J. Inorg. Nucl. Chem., 25, 377 (1963); E. König, to be published.

Table VI: The Spin-Free d^n (n = 1, 2, 3, 4, 5, 6, 7, 8, 9) Trigonal Dihedral Rotational and Spectral Strengths for Zero Spin-Orbit Forces[a]

n	Transitions	Rotational strengths	Spectral strengths	
			Electric	Magnetic
1(s = 2) and 6(s = 5)	$^aA_1(T_{2g}) \rightarrow {}^aE(T_{2c})$	$-2\bar{r}_0\bar{m}_0$	$2\bar{r}_0{}^2$	$2\bar{m}_0{}^2$
	$\rightarrow {}^aE(E_g)$	$2r_0m_0$	$2r_0{}^2$	$2m_0{}^2$
	$^aE(T_{2g}) \rightarrow {}^aE(E_g)$	$r_1m_1 + r_2m_2$	$r_1{}^2 + r_2{}^2$	$m_1{}^2 + m_2{}^2$
2(s = 3) and 7(s = 4)	$^aA_2(T_{1g}) \rightarrow {}^aE(T_{1c})$	$2\bar{r}_0\bar{m}_0$	$2\bar{r}_0{}^2$	$2\bar{m}_0{}^2$
	$\rightarrow {}^aA_1(T_{2g})$	$2r_1m_1$	$2r_1{}^2$	$2m_1{}^2$
	$\rightarrow {}^aE(T_{2g})$	r_2m_2	$r_2{}^2$	$m_2{}^2$
	$\rightarrow {}^aA_2(T_{1g})$	0	0	0
	$\rightarrow {}^aE(T_{1g})$	r_2m_2	$r_2{}^2$	$m_2{}^2$
	$\rightarrow {}^aA_2(A_{2g})$	0	0	0
	$^aE(T_{1g}) \rightarrow {}^aA_1(T_{2g})$	$^1/_2 r_0 m_0$	$^1/_2 r_0{}^2$	$^1/_2 m_0{}^2$
	$\rightarrow {}^aE(T_{2g})$	$^1/_2 r_1 m_1 + {}^1/_2(r_0 + r_2)(m_0 + m_2)$	$^1/_2 r_1{}^2 + {}^1/_2(r_0 + r_2)^2$	$^1/_2 m_1{}^2 + {}^1/_2(m_0 + m_2)^2$
	$\rightarrow {}^aA_2(T_{1g})$	$^1/_2 r_0 m_0$	$^1/_2 r_0{}^2$	$^1/_2 m_0{}^2$
	$\rightarrow {}^aE(T_{1g})$	$^1/_2 r_1 m_1 + {}^1/_2(r_0 - r_2)(m_0 - m_2)$	$^1/_2 r_1{}^2 + {}^1/_2(r_0 - r_2)^2$	$^1/_2 m_1{}^2 + {}^1/_2(m_0 - m_2)^2$
	$\rightarrow {}^aA_2(A_{2g})$	0	0	0
3(s = 4) and 8(s = 3)	$^aA_2(A_{2g}) \rightarrow {}^aA_1(T_{2g})$	$2r_1m_1$	$2r_1{}^2$	$2m_1{}^2$
	$\rightarrow {}^aE(T_{2g})$	$(r_0 + r_2)(m_0 + m_2)$	$(r_0 + r_2)^2$	$(m_0 + m_2)^2$
	$\rightarrow {}^aA_2(T_{1g})$	0	0	0
	$\rightarrow {}^aE(T_{1g})$	$(r_0 - r_2)(m_0 - m_2)$	$(r_0 - r_2)^2$	$(m_0 - m_2)^2$
	$\rightarrow {}^aA_2(T_{1g})$	0	0	0
	$\rightarrow {}^aE(T_{1g})$	0	0	0
4(s = 5) and 9(s = 2)	$^aE(E_g) \rightarrow {}^aA_1(T_{2g})$	r_0m_0	$r_0{}^2$	$m_0{}^2$
	$\rightarrow {}^aE(T_{2g})$	$r_1m_1 + r_2m_2$	$r_1{}^2 + r_2{}^2$	$m_1{}^2 + m_2{}^2$
	$^aA_1(T_{2g}) \rightarrow {}^aE(T_{2g})$	$2\bar{r}_0\bar{m}_0$	$2\bar{r}_0{}^2$	$2\bar{m}_0{}^2$
5	$^aA_1(A_{1g}) \rightarrow {}^{2,4}A_1(T_{1g})$	0	0	0
	$^{2,4}E(T_{1g})$			
	$^{2,4}A_1(T_{2g})$			
	$^{2,4}E(T_{2g})$			
	$^{2,4}A_2(A_{2g})$			
	$^{2,4}E(E_g)$			
	$^{2,4}A_1(A_{1g})$			

[a] The quantities $\bar{r}_0$, $r_{0,1,2}$, $\bar{m}_0$, $m_{0,1,2}$ are as defined generally and specially in footnote 49.

the oscillator strengths, f, and the dissymmetry factors, G, convert to

$$G[^2E(E_g) \longrightarrow {}^2A_1(T_{2g})] = 0.22 \times 10^{-2}\nu,$$
$$f[^2E(E_g) \longrightarrow {}^2A_1(T_{1g})] = 0.74 \times 10^{-8}$$

$$G[^2E(E_g) \longrightarrow {}^2E(T_{2g})] = -0.87 \times 10^{-2}\nu,$$
$$f[^2E(E_g) \longrightarrow {}^2E(T_{2g})] = 1.9 \times 10^{-9}$$

$$G[^2A_1(T_{2g}) \longrightarrow {}^2E(T_{2g})] = -1.5 \times 10^{-2}\nu,$$
$$f[^2A_1(T_{2g}) \longrightarrow {}^2E(T_{2g})] = 2.7 \times 10^{-9} \quad (94)$$

where ν is the frequency of the measuring light probe in cm.$^{-1}$. If all other things are kept constant except the effective ligand charge, $Z_{\text{effective}}$, the rotatory strengths for the copper(II) trisoxalato anion should be lower than those for the copper(II) trisethylenediamine cation by a factor of about 0.8, and the spectral strengths by a factor of about 0.65, for both $Z^0{}_{\text{effective}}$ = 4.55 and 4.4456. Of course, all else cannot be kept equal because of true π-bond possibilities for the trisoxalato anion. However, the above numbers do show

that the ligand field rotations should be of the same order of magnitude and the same sign for the same ionic conformation.

In actual practice the dihedral rotational strengths run from $\sim$0.5 to $\sim$8B. Hence, the above numerical sample was much too conservative. We know from other sources that the σ- and π-molecular orbital mixing parameters $N_{e(e)}\rho$, $N_{a_1(t_1)}\eta$, are about equal to one another[51] and large[52]—of the order $\sqrt{1/_2}$. Therefore, a more faithful numerical estimate would be had by taking $|\xi|$ equal to $|\eta|$ equal to $|\rho|$ equals $\sqrt{1/_2}$ [this

(51) R. G. Shulman and K. Knox, *Phys. Rev. Letters*, **4**, 603 (1960), *et seq.*

(52) This conclusion comes from electron spin resonance and optical estimates of σ-, π-bond covalency. Eve (a) J. Owen, *Proc. Roy. Soc.* (London), **A227**, 183 (1955), (b) C. J. Ballhausen and A. D. Liehr, *J Mol. Spectry.*, **2**, 342 (1958) [*Errata, ibid.*, **4**, 190 (1960)], and R. Rajan and T. R. Reddy, *J. Chem. Phys.*, **39**, 1140 (1963). (The former reference estimates the hexaamminenickel(II) covalency to be $\sim$38%, and the latter estimates the copper(II) triethylenediamine covalency to be $\sim$50%, for example, which is not far from the values assumed above).

Table VII: The Spin-Paired d^n (n = 1, 2, 3, 4, 5, 6, 7, 8, 9) Trigonal Dihedral Rotational and Spectral Strengths for Zero Spin-Orbit Forces[a]

n	Transitions	Rotational strengths	Spectral strengths — Electric	Spectral strengths — Magnetic
4	$^3A_2(T_{1g}) \rightarrow \,^3E(T_{1g})$	$-2\bar{r}_0\bar{m}_0$	$2\bar{r}_0^2$	$2\bar{m}_0^2$
	$\rightarrow \,^3E(E_g)$	$^8/_3 r_0 m_0$	$^8/_3 r_0^2$	$^8/_3 m_0^2$
	$\rightarrow \,^3A_2(T_{1g})$	0	0	0
	$\rightarrow \,^3E(T_{1g})$	$^1/_6(2r_0 + r_2)(2m_0 + m_2)$	$^1/_6(2r_0 + r_2)^2$	$^1/_6(2m_0 + m_2)^2$
	$\rightarrow \,^3A_1(T_{2g})$	$^1/_3 r_1 m_1$	$^1/_3 r_1^2$	$^1/_3 m_1^2$
	$\rightarrow \,^3E(T_{2g})$	$^1/_6(2r_0 - r_0)(2m_0 - m_2)$	$^1/_6(2r_0 - r_2)^2$	$^1/_6(2m_0 - m_2)^2$
	$\rightarrow \,^3A_1(A_{1g})$	$^2/_3 r_1 m_1$	$^2/_3 r_1^2$	$^2/_3 m_1^2$
	$\rightarrow \,^3E(E_g)$	$^2/_3 r_2 m_2$	$^2/_3 r_2^2$	$^2/_3 m_2^2$
	$\rightarrow \,^3A_2(A_{2g})$	0	0	0
	$\rightarrow \,^3A_1(T_{2g})$	$r_1 m_1$	r_1^2	m_1^2
	$\rightarrow \,^3E(T_{2g})$	$^1/_2 r_2 m_2$	$^1/_2 r_2^2$	$^1/_2 m_2^2$
	$\rightarrow \,^3A_2(T_{1g})$	0	0	0
	$\rightarrow \,^3E(T_{1g})$	$^1/_2 r_2 m_2$	$^1/_2 r_2^2$	$^1/_2 m_2^2$
	$^3E(T_{1g}) \rightarrow \,^3E(E_g)$	$^4/_3 r_1 m_1 + \,^4/_3 r_2 m_2$	$^4/_3 r_1^2 + \,^4/_3 r_2^2$	$^4/_3 m_1^2 + \,^4/_3 m_2^2$
	$\rightarrow \,^3A_2(T_{1g})$	$^1/_{12}(r_0 + 2r_2)(m_0 + 2m_2)$	$^1/_{12}(r_0 + 2r_2)^2$	$^1/_{12}(m_0 + 2m_2)^2$
	$\rightarrow \,^3E(T_{1g})$	$^3/_4 r_1 m_1 + \,^1/_{12}(r_0 - r_2)(m_0 - m_2)$	$^3/_4 r_1^2 + \,^1/_{12}(r_0 - r_2)^2$	$^3/_4 m_1^2 + \,^1/_{12}(m_0 - m_2)^2$
	$\rightarrow \,^3A_1(T_{2g})$	$^1/_{12}(r_0 - 2r_2)(m_0 - 2m_2)$	$^1/_{12}(r_0 - 2r_2)^2$	$^1/_{12}(m_0 - 2m_2)^2$
	$\rightarrow \,^3E(T_{2g})$	$^1/_{12} r_1 m_1 + \,^1/_{12}(r_0 + r_2)(m_0 + m_2)$	$^1/_{12} r_1^2 + \,^1/_{12}(r_0 + r_2)^2$	$^1/_{12} m_1^2 + \,^1/_{12}(m_0 + m_2)^2$
	$\rightarrow \,^3E(E_g)$	$^1/_3 r_0 m_0 + \,^1/_3 r_1 m_1$	$^1/_3 r_0^2 + \,^1/_3 r_1^2$	$^1/_3 m_0^2 + \,^1/_3 m_1^2$
	$\rightarrow \,^3A_1(A_{1g})$	$^1/_6(r_0 + r_2)(m_0 + m_2)$	$^1/_6(r_0 + r_2)^2$	$^1/_6(m_0 + m_2)^2$
	$\rightarrow \,^3A_2(A_{2g})$	$^1/_6(r_0 - r_2)(m_0 - m_2)$	$^1/_6(r_0 - r_2)^2$	$^1/_6(m_0 - m_2)^2$
	$\rightarrow \,^3A_1(T_{2g})$	$^1/_4 r_0 m_0$	$^1/_4 r_0^2$	$^1/_4 m_0^2$
	$\rightarrow \,^3E(T_{2g})$	$^1/_4 r_1 m_1 + \,^1/_4(r_0 + r_2)(m_0 + m_2)$	$^1/_4 r_1^2 + \,^1/_4(r_0 + r_2)^2$	$^1/_4 m_1^2 + \,^1/_4(m_0 + m_2)^2$
	$\rightarrow \,^3A_2(T_{1g})$	$^1/_4 r_0 m_0$	$^1/_4 r_0^2$	$^1/_4 m_0^2$
	$\rightarrow \,^3E(T_{1g})$	$^1/_4 r_1 m_1 + \,^1/_4(r_0 - r_2)(m_0 - m_2)$	$^1/_4 r_1^2 + \,^1/_4(r_0 - r_2)^2$	$^1/_4 m_1^2 + \,^1/_4(m_0 - m_2)^2$
5	$^2A_1(T_{2g}) \rightarrow \,^2E(T_{2g})$	$2\bar{r}_0\bar{m}_0$	$2\bar{r}_0^2$	$2\bar{m}_0^2$
	$\rightarrow \,^2A_2(A_{2g})$	$^2/_3 r_1 m_1$	$^2/_3 r_1^2$	$^2/_3 m_1^2$
	$\rightarrow \,^2A_2(T_{1g})$	$3 r_1 m_1$	$3 r_1^2$	$3 m_1^2$
	$\rightarrow \,^2E(T_{1g})$	$^3/_2 r_2 m_2$	$^3/_2 r_2^2$	$^3/_2 m_2^2$
	$\rightarrow \,^2A_1(T_{2g})$	0	0	0
	$\rightarrow \,^2E(T_{2g})$	$^1/_6(2r_0 + r_2)(2m_0 + m_2)$	$^1/_6(2r_0 + r_2)^2$	$^1/_6(2m_0 + m_2)^2$
	$\rightarrow \,^2E(E_g)$	$^2/_3 r_2 m_2$	$^2/_3 r_2^2$	$^2/_3 m_2^2$
	$\rightarrow \,^2A_1(T_{2g})$	0	0	0
	$\rightarrow \,^2E(T_{2g})$	$^3/_2 r_2 m_2$	$^3/_2 r_2^2$	$^3/_2 m_2^2$
	$\rightarrow \,^2A_2(T_{1g})$	$^1/_3 r_1 m_1$	$^1/_2 r_1^2$	$^1/_3 m_1^2$
	$\rightarrow \,^2E(T_{1g})$	$^1/_6(2r_0 - r_2)(2m_0 - m_2)$	$^1/_6(2r_0 - r_2)^2$	$^1/_6(2m_0 - m_2)^2$
	$\rightarrow \,^2A_1(^2A_{1g})$	0	0	0
	$\rightarrow \,^2E(E_g)$	$^1/_3 r_0 m_0$	$^1/_3 r_0^2$	$^1/_3 m_0^2$
	$^2E(T_{2g}) \rightarrow \,^2A_2(A_{2g})$	$^1/_6(r_0 + r_2)(m_0 + m_2)$	$^1/_6(r_0 + r_2)^2$	$^1/_6(m_0 + m_2)^2$
	$\rightarrow \,^2A_2(T_{1g})$	$^3/_4 r_0 m_0$	$^3/_4 r_0^2$	$^3/_4 m_0^2$
	$\rightarrow \,^2E(T_{1g})$	$^3/_4 r_1 m_1 + \,^3/_4(r_0 + r_2)(m_0 + m_2)$	$^3/_4 r_1^2 + \,^3/_4(r_0 + r_2)^2$	$^3/_4 m_1^2 + \,^3/_4(m_0 + m_2)^2$
	$\rightarrow \,^2A_1(T_{2g})$	$^1/_{12}(r_0 + 2r_0)(m_0 + 2m_2)$	$^1/_{12}(r_0 + 2r_2)^2$	$^1/_{12}(m_0 + 2m_2)^2$
	$\rightarrow \,^2E(T_{2g})$	$^3/_4 r_1 m_1 + \,^1/_{12}(r_0 - r_2)(m_0 - m_2)$	$^3/_4 r_1^2 + \,^1/_{12}(r_0 - r_2)^2$	$^3/_4 m_1^2 + \,^1/_{12}(m_0 - m_2)^2$
	$\rightarrow \,^2E(E_g)$	$^1/_3 r_0 m_0 + \,^1/_3 r_1 m_1$	$^1/_3 r_0^2 + \,^1/_3 r_1^2$	$^1/_3 m_0^2 + \,^1/_3 m_1^2$
	$\rightarrow \,^2A_1(T_{2g})$	$^3/_4 r_0 m_0$	$^3/_4 r_0^2$	$^3/_4 m_0^2$
	$\rightarrow \,^2E(T_{2g})$	$^3/_4 r_1 m_1 + \,^3/_4(r_0 - r_2)(m_0 - m_2)$	$^3/_4 r_1^2 + \,^3/_4(r_0 - r_2)^2$	$^3/_4 m_1^2 + \,^3/_4(m_0 - m_2)^2$
	$\rightarrow \,^2A_2(T_{1g})$	$^1/_{12}(r_0 - 2r_2)(m_0 - 2m_2)$	$^1/_{12}(r_0 - 2r_2)^2$	$^1/_{12}(m_0 - 2m_2)^2$
	$\rightarrow \,^2E(T_{1g})$	$^1/_{12} r_1 m_1 + \,^1/_{12}(r_0 + r_2)(m_0 + m_2)$	$^1/_{12} r_1^2 + \,^1/_{12}(r_0 + r_2)^2$	$^1/_{12} m_1^2 + \,^1/_{12}(m_0 + m_2)^2$
	$\rightarrow \,^2A_1(A_{1g})$	$^1/_8(r_0 - r_2)(m_0 - m_2)$	$^1/_6(r_0 - r_2)^2$	$^1/_6(m_0 - m_2)^2$
	$\rightarrow \,^2E(E_g)$	$^1/_3 r_1 m_1 + \,^1/_3 r_2 m_2$	$^1/_3 r_1^2 + \,^1/_3 r_2^2$	$^1/_3 m_1^2 + \,^1/_3 m_2^2$
6	$^1A_1(A_{1g}) \rightarrow \,^1A_2(T_{1g})$	$4 r_1 m_1$	$4 r_1^2$	$4 m_1^2$
	$\rightarrow \,^1E(T_{1g})$	$2(r_0 + r_2)(m_0 + m_2)$	$2(r_0 + r_2)^2$	$2(m_0 + m_2)^2$
	$\rightarrow \,^1A_1(T_{2g})$	0	0	0
	$\rightarrow \,^1E(T_{2g})$	$2(r_0 - r_2)(m_0 - m_2)$	$2(r_0 - r_2)^2$	$2(m_0 - m_2)^2$
7	$^2E(E_g) \rightarrow \,^2A_2(T_{1g})$	$^3/_2 r_0 m_0$	$^3/_2 r_0^2$	$^3/_3 m_0^2$
	$\rightarrow \,^2E(T_{1g})$	$^3/_2 r_1 m_1 + \,^3/_2 r_2 m_2$	$^3/_2 r_1^2 + \,^3/_2 r_2^2$	$^3/_2 m_1^2 + \,^3/_2 m_2^2$
	$\rightarrow \,^2A_1(T_{2g})$	$^1/_8 r_2 m_2$	$^1/_2 r_2^2$	$^1/_2 m_2^2$
	$\rightarrow \,^2E(T_{2g})$	$^1/_2 r_0 m_0 + \,^1/_2 r_1 m_1$	$^1/_2 r_0^2 + \,^1/_2 r_1^2$	$^1/_2 m_0^2 + \,^1/_2 m_1^2$
	$\rightarrow \,^2A_2(T_{1g})$	$^1/_2 r_2 m_2$	$^1/_2 r_2^2$	$^1/_2 m_2^2$
	$\rightarrow \,^2E(T_{1g})$	$^1/_2 r_0 m_0 + \,^1/_2 r_1 m_1$	$^1/_2 r_0^2 + \,^1/_2 r_1^2$	$^1/_2 m_0^2 + \,^1/_3 m_1^2$
	$\rightarrow \,^2A_1(T_{2g})$	$^1/_2 r_0 m_0$	$^1/_2 r_0^2$	$^1/_3 m_0^2$
	$\rightarrow \,^2E(T_{2g})$	$^1/_2 r_1 m_1 + \,^1/_2 r_2 m_2$	$^1/_2 r_1^2 + \,^1/_2 r_2^2$	$^1/_2 m_1^2 + \,^1/_2 m_2^2$

[a] The quantities $\bar{r}_0$, $r_{0,1,2}$, $\bar{m}_0$, $m_{0,1,2}$ are as defined generally and specially in footnote 49.

choice makes the per cent σ-covalency, equals $N_{e(e)}^2\rho^2$, $\sim 43\%$, and the per cent π-covalency, equals $N_{a_1(t)}^2\eta^2$ or $N_{e(t)}^2\xi^2$, $\sim 33\%$], and also by upping the trigonality by setting α to $\sim 15°$. These modifications toward reality would then increase the rotational strengths by a factor of $\sim 10\sqrt{2}$, the spectral and oscillator strengths by ~ 300, and would decrease the dissymmetry factors by $\sim \sqrt{2}/30$. The rotational, spectral, oscillator, and dissymmetry strengths would then become of the order 1B, $10^{-4}D^2$, 10^{-6}, and $2 \times 10^{-4}\nu$, which are of the order of what is actually observed.[53] [Usually the Slater orbital technique of approximating the electronic electric dipole transition moment integrals, K_{nA_j}, underestimates them,[52b, 54] and thus an additional amplification springs from this source too. Also, from eq. 69 through 92 it is apparent that other multiplicative factors enter into the calculation for d^n systems where n is not equal to one or nine. Therefore, specific computations must be done for each situation separately. These computations will be carried through in other publications.[33]]

IV. Discussion

It is apparent from the foregoing theory that the optical rotatory power of dihedrally asymmetric compounds can be adequately explained on the basis of an internal inherent dihedrally asymmetric local electronic charge distribution, both in quality and in quantity. It is, however, also evident that this theory unfortunately contains a number of difficultly specified parameters and integrals. Despite these hitches, much useful information may still be gathered from the theory with a minimum of effort. First, the sign of the rotation for a given conformation can be determined by simple inspection.[55] Second, the order of magnitude of the rotation may be estimated with relative ease. Third, the degree of covalency, hybridity, and dihedrality may be inferred by comparative means.[56] Fourth, the accuracy of spectral assignments may be checked with little effort.[57] Fifth, the cleavage of the threefold degenerate electronic states may be gaged and assessed.[57,58] Sixth, the proportionate symmetry of ex-

(53) For example, consult A. J. MacCaffery and S. F. Mason, *Trans. Faraday Soc.*, **59**, 1 (1963).

(54) Similar difficulties are encountered in the semi-empirical assessment of the electrostatic ligand field parameter Dq,[44] and of the octahedral vibronic oscillator strengths, f [peruse A. D. Liehr and C. J. Ballhausen, *Phys. Rev.*, **106**, 1161 (1957), and ref. 22d].

(55) The usefulness of such a determination has been re-emphasized and well illustrated in the recent papers of (a) R. E. Ballard, A. J. McCaffery, and S. F. Mason, *Proc. Chem. Soc.*, 331 (1962); (b) A. J. McCaffery and S. F. Mason, *ibid.*, 388 (1962); (c) A. J. McCaffery and S. F. Mason, *Mol. Phys.*, **6**, 359 (1963); (d) *Proc. Chem. Soc.*, 211 (1963). [But be sure to read also the classical papers of (e) W. Kuhn and K. Bein, *Z. anorg. allgem. Chem.*, **216**, 321 (1934), and (f) J. P. Mathieu, *Bull. Soc. Chim. France, 5e série*, **3**, 463, 476 (1936), on this

subject]. In this regard, notice that the $d^{3,6}$ correspondence inferred in ref. 55a is well substantiated by eq. 80 and 81 of §4.3 and 4.4 and by the discussion of §4.4.

(56 These, in a sense fictious (read A. D. Liehr, to be published), parameters can be fixed, for instance, by a comparison of nuclear magnetic resonance, electron spin resonance, optical polarization and intensity, and optical rotatory dispersion and dichroism measurements. Such measurements determine $N_{a_1(t)}\eta$, $N_{e(t)}\xi$, $N_{e(t)}\rho$, k_s, k_p, α, and the sign and magnitude of the trigonal field splitting independently, and their mutual cross-check should be most enlightening as to the physical actuality of the concomitant concepts involved. Some such comparisons have already been made in other connections. View T. S. Piper, *J. Am. Chem. Soc.*, **83**, 3908 (1961) as a sample.

(57 This suggestion although arrived at unaided by the author is not original with him. Others have made the same comment. See, for instance, ref. 25b and (a) S. F. Mason, *Proc. Chem. Soc.*, 137 (1962); (b) J. G. Brushmiller, E. L. Amma, and B. E. Douglas, *J. Am. Chem. Soc.*, **84**, 111, 3227 (1962); B. E. Douglas, J. G. Brushmiller, and E. L. Amma, "Proceedings of the Seventh International Conference on Coordination Chemistry," Stockholm, Sweden, June 25–29, 1962, p. 42, paper 1E2; B. E. Douglas, R. A. Haines, and J. G. Brushmiller, *Inorg. Chem.*, **2**, 1194 (1963); J. G. Brushmiller, E. L. Amma, and B. E. Douglas, *ibid.*, in press; (c) R. D. Gillard, *Nature*, **198**, 580 (1963); (d) Th. Bürer, *Helv. Chim. Acta*, **46**, 2388 (1963). The optical rotatory dispersion and circular dichroism method in principle allows the determination of the symmetries (and thus orders) of the electronic excited states, and of the singular or multiple nature of the associated electronic jumps [in this last regard be sure to read the classic papers (e) W. Kuhn and H. K. Gore, *Z. Physik. Chem.*, **12B**, 389 (1931), and ref. 31c and 55f].

(58) This task may be accomplished by noting the change of sign (or in some cases, the drastic relative reduction in magnitude) of the circular dichroism or dissymmetry factor.[55f,57] The need for such a change (or reduction) is hurriedly seen from eq. 52 through 92 which show that within a cubical triply degenerate band the two trigonal components rotate oppositely. To expound, we consider the sums $1/c \sum \mathcal{R}_{ij}$, where $i(e_g)$ equals $e_\pm(e_g)$ or $\gamma_6(\begin{smallmatrix}9\\b\end{smallmatrix})(e_g)$, $\gamma(\begin{smallmatrix}4\\s\end{smallmatrix})(e_g)$ and $i(e_g), j(t_{2g})$
$j(t_{2g})$ equals $a_1(t_{2g})$, $e_\pm(t_{2g})$ or $\gamma(\begin{smallmatrix}4\\s\end{smallmatrix})(t_{2g})$, $\gamma_6(\begin{smallmatrix}9\\b\end{smallmatrix})(\begin{smallmatrix}7\\8\end{smallmatrix})(t_{2g})$], and where g equals the degeneracy of the ground electronic state [equals two for the spinless orbital set $e_\pm(e_g)$, $a_1(t_{2g})$, $e_\pm(t_{2g})$ and four for the spin orbital set $\gamma_6(\begin{smallmatrix}9\\b\end{smallmatrix})(e_g)$, $\gamma(\begin{smallmatrix}4\\s\end{smallmatrix})(e_g)$, $\gamma(\begin{smallmatrix}4\\s\end{smallmatrix})(t_{2g})$, $\gamma_6(\begin{smallmatrix}9\\b\end{smallmatrix})(\begin{smallmatrix}7\\8\end{smallmatrix})(t_{2g})$]. From eq. 52 and 54 we see that these sums both equal

$$-\frac{\sqrt{3}}{2} e\mu_B k_p \sin\alpha\, N_{e(e)}^2(N_{a_1(t)}^2\eta + N_{e(t)}^2\xi)(\sqrt{3}K_{4A_3} + K_{7A_3})$$

[This statement follows since the molecular spin orbitals of eq. 34 are related to the ordinary molecular orbitals of eq. 17 and 33 by a sort of generalized unitary transformation. Thus since by eq. 50 and 51 the sum considered, as well as the analogous one over S_{ij}, which equals

$$^3/_8 e^2 k_p^2 \sin^2\alpha\, N_{e(e)}^2\{N_{a_1(t)}^2\eta^2(\sqrt{3}K_{4A_3} + K_{7A_3})^2 + N_{e(t)}^2\xi^2[4K_{7A_3}^2 + (\sqrt{3}K_{4A_3} - K_{7A_3})^2]\}$$

is an unitarily invariant diagonal trace, the orbital and spin-orbital sums must coincide. In the general notation of footnote 49, the sums over $\mathcal{R}_{ij}$ and S_{ij} are $r_0 m_0 + r_1 m_1 + r_2 m_2$ and $r_0^2 + r_1^2 + r_2^2$ separately, and that over the magnetic transition dipole moments $\mathfrak{M}_j$ is $m_0^2 + m_1^2 + m_2^2$. These sums reduce to

$$r_0 m_0 \left(1 + \frac{\xi N_{e(t)}^2}{\eta N_{a_1(t)}^2}\right), \quad r_0^2 \left(1 + \frac{1}{2}\frac{\xi^2 N_{e(t)}^2}{\eta^2 N_{a_1(t)}^2}\right) + \frac{1}{2}(r_1 - r_2)^2$$

and

$$m_0^2 \left(1 + 2\frac{N_{e(t)}^2}{N_{a_1(t)}^2}\right)$$

individually, for the molecular orbital model used here, as may readily be checked], and that for equal covalency, where $N_{a_1(t)}^2\eta$ equals $-N_{e(t)}^2\xi$ (recall η and ξ have opposite signs when both are either bonding or antibonding orbitals[48]), these sums vanish [for the catholic symbolism of footnote 49, this limit implies that all m_i, $(i = 0, 1, 2)$, are equal, that $r_1 + r_2 + r_3 = 0$, and that $r_0^2 + r_1^2 + r_2^2 = \frac{3}{2}r_0^2 + \frac{1}{2}(r_1 - r_2)^2$]. For unequal covalencies the sum of the $a_1(t_{2g})$ and $e(t_{2g})$ trigonal component rotational strengths is not fully compensated internally and may attain a nonzero value. As the correspondent sums for all the many electron triply degenerate electronic configurations reduce to multiples of this one-electron sum [cf. eq. 52 through 92], the contention is proved.

cited electronic states may be surmised.[59] Seventh, the overlap of optical absorption bands may sometimes be resolved.[60] Eighth, the possibility of observable spin-only magnetic dipole natural optical rotatory power can be demonstrated.[61] Ninth, the sum of the dihedral rotational strengths within a triply degenerate band need not vanish.[58,62] Tenth, for a fixed electronic configuration, d^n, the sign of the rotation for a given conformation may conceivably change as one proceeds from the first to the second to the third transition series and from ligands in the first to the second to the third, etc., rows of the periodic table.[63] Eleventh, the feasibility of perceptibile electronic natural optical rotary power in the infrared and microwave regions of the spectrum is manifested.[64] Twelfth, the variation of the optical verticity with bidentate (or polydentate for that matter) chain length and bond angle can be predicted,[65] and so on.

Besides the above the theory here developed has several other important advantages. One, it shows that σ- and σ-,π-bonded compounds, to good approximation, have mathematically the same formal expressions which relate rotary and spectral power and covalency.

Two, it reveals the mathematical conjugation of the rotary and spectral strengths of the kd^n and kd^{n+5}, ($n = 0, 1, 2, 3, 4, 5$), spin-free systems. Three, it uncovers the simple formal multiplicative and additive relations among the rotational and optical capacities of non-conjugative kd^n configurations, whether spin-free or spin-paired. Four, it unveils a direct correspondence of the rotational and optical potentialities of the $d^{1,4,6,9}$ spin-free arrangements and a simple multiplicative connection between these and the d^7 spin-paired ar-

(59) The admissable geometries of excited electronic states may be enumerated by symmetry techniques of the kind discussed in footnotes 10 and 25 [read A. D. Liehr, *J. Phys. Chem.*, **67**, 389 (1963)] The assignation as to which geometry is actually attained may be made on the basis of large deviations from the sum rule of footnote 58. Whenever the sum of the circular dichroisms and dissymmetry factors of the components of a triply degenerate band do not any where near vanish [that is, whenever the dichroism and dissymmetry do not come near changing signs somewhere in the band], one of the electronic states must be structurally deformed [Jahn–Teller or otherwise] or a most unlikely inversion of bonding and antibonding properties must have occurred, as only in these fashions can large reductions of one rotational strength with respect to another be attained. [The deformational reduction is obtained by a Franck–Condon dimunition—see A. D. Liehr, to be published]. By this means one would infer that one of the excited states of chromium(III) and cobalt(III) is distorted in certain complexes.[33]

(60) As the circular dichroism and dissymmetry factor curves are much sharper than the analogous absorption curves occasional optical resolutions might be expected [careful dispersion measurements and analyses can also yield identical results[49]]. Illustratively, weak spin forbidden or close spin-orbit component bands might be at times separated out.

(61) As examples, in eq. 55 and 58 the electronic transitions $\bar{\gamma}_6$ to $\bar{\gamma}(\frac{4}{5})$ are rotationally only spin allowed, and those from $\gamma_6^{(8)}(t_{2g})$ to $\gamma_6^{(7)}(t_{2g})$ and $\gamma_6^{(7)}(t_{2g})$ to $\gamma(\frac{4}{5})(t_{2g})$ owe a substantial part of their rotational strength [that portion which is only multiplied by two rather than the usual four normalization constants] to spin magnetic transition moments.

(62) This situation will be the normal occurrence [cf. footnote 58].

(63) This possibility arises from conceivable alterations in the sign of the electronic transition moment integrals K_{nAi} without a concomitant change in that of the variational parameter ξ and η [since these are determined by integrals with different spatial weighing factors] as one changes the radial nodal patterns of the central atom or ligand atoms.

(64) The electronic transitions which might be active in these regions of the spectrum are the internal $\{a_1(t_{2g}), e(t_{2g})\}$, $\{\gamma_6^{(8)}(t_{2g}), \gamma_4(t_{2g}), \gamma_5(t_{2g}), \gamma_6^{(7)}(t_{2g})\}$, and $\{\gamma_6(e_g), \gamma_4(e_g), \gamma_5(e_g)\}$ transitions and their many electron orbital and spin-orbital analogs. [In symmetries lower than trigonal and electronic configurations greater than d^1 (or less than d^9) the possibilities become more pronounced.

(65) The dependence of the rotation and circular dichroism on the local orbital mismatch parameter, α, through the functions ξ sin α or η sin α which occur in all the many electron rotational strength expressions, eq. 59 through 92, foretells that as this angle goes to zero and through it, the rotation will likewise go to zero, and after the angle α has passed through zero, the rotation will re-emerge with unchanged sign (as the sign of ξ and η are fixed by the sign of sin α— look at footnote 48 and section VII, §5.7, eq. A-12). Some experimental evidence exists to substantiate the first of these forecasts. [F. Woldbye, "Proceedings of the Seventh International Conference on Coordination Chemistry, Stockholm and Uppsala, Sweden, June 25–29, 1962," p. 41, paper 1E1; private communications. For a most excellent generalized survey of optical rotatory and dichroism measurements read F. Woldbye, "Technique of Inorganic Chemistry," H. B. Jonassen, Ed., Interscience, New York, London, to be published. A more specialized but equally fine survey has also been given by Th. Bürer, *Helv. Chim. Acta*, **46**, 242 (1963).]
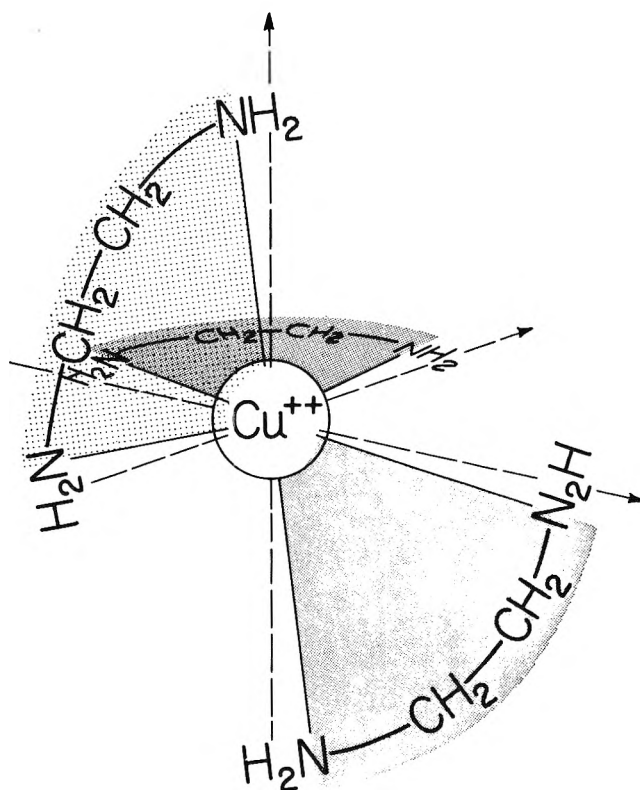
Figure 16. The factualistic acute-angled geometry of the trisethylenediaminecopper(II) cation. (Ligand nonplanarity has been suppressed for illustrative clarity only.)

rangement. Five, it discloses that electronic transitions to or from bonded and antibonded molecular orbitals rotate electromagnetic radiation both parallely and oppositely, dependent upon conditions.[66]

To embellish upon the above mentioned theoretical revelations, a few more comments would not be out of place. (a) In normal circumstances configuration interaction can do little to alter the rotational and spectral trends cataloged aloft.[67] (b) It is only by figuration interaction that spin forbidden electronic states appear in an optical rotatory dispersion or dichroism spectrum.[68] (c) Although formally forbidden to appear in an optical rotatory dispersion or dichroism spectrum on the basis of cubic selection rules, A_1 to T_2 or A_2 to T_1 electronic hops may appear without correlational type electronic configurational interaction within the trigonal field if the molecular orbital covalencies of the $a_1(t_{2g})$ and $e_{\pm}(t_{2g})$ one-electron molecular orbitals differ to a sufficient degree.[69] (d) Due to the one-electron nature of the electric and magnetic dipole operators, no matter how complex the electronic configuration, the many electron theory of optical activity always subsumes the aspect of a one-electron summation.[23] Clearly, further remarks of a similar vein are readily conjured.

At this point it is but logical to inquire as to how the

theory may be improved. Several suggestions immediately advance themselves. (i) The use of improved wave functions, for example, self-consistent field trigonal molecular orbitals should yield a better numerical accord.[70] (ii) The employment of the more exact (for approximate wave functions)[21,22] differential expression $\sum_j \frac{\hbar}{i} \vec{\nabla}_j$, rather than the simpler multiplicative expression, $\sum_j e\vec{r}_j$, for the electric dipole operator should give improved values for the rotatory and spectral powers. (iii) The application of the true ground electronic state molecular geometry to the mathematical development of the theory should produce increased concurrence [cf. Fig. 16-19].[71] (iv) The relaxation of the simplifying restriction that the one-electron molecular orbitals $a_1(t_{2g})$, $e_{\pm}(t_{2g})$, and $e_{\pm}(e_g)$ retain their pseudo cubical character would make an enhanced concert.[72] (v) The inclusion of metal–ligand magnetic transition dipole moment contributions and ligand–ligand electric and magnetic transition dipole moment contributions

(66) This remark follows from the linear dependence of the rotational strength, $\Re_{ij}$, on the sign of the variational parameters ξ and η, and from its indicial antisymmetry[35] [perceive Fig. 3 and 8 for examples. In a later publication, we shall discuss charge-transfer transitions more fully. In this connection it is interesting to notice that the comparison of the sign of the optical rotation of a given bonded to antibonded and antibonded to antibonded transition pair, such as are formed by the $e(e_g)$ and $e(t_{2g})$ pairs of Fig. 3, will afford an experimental proof of the indicial antisymmetry of the rotational strength, $\Re_{ij}$].

(67) By unusual means, configuration interaction can sometimes change the sign of the optical rotation, if for instance, it inverts the positions of two nearby electronic states of opposite verticity.

(68) Elucidatively, the ^2E and ^1E electronic states of chromium(III) and nickel(II), each, attain $\sim$1 to 10% $^4T_{2g}$ and $^3T_{2j}$ character, and hence, should capture $\sim$1 to 10% of the $^4T_{2g}$ and $^3T_{2g}$ rotational strength, seriately, through spin-orbit coupling, in particular instances. [(a) A. D. Liehr and C. J. Ballhausen, Ann. Phys. (N. Y.), 6, 134 (1959); (b) A. D. Liehr, J. Phys. Chem., 67, 314 (1963)]. For a recent application of this concept to the $^1A_{1g} \rightarrow {}^1T_{1g}$ state of cobalt(III) view (c) C. J. Ballhausen, Mol. Phys., 6, 461 (1963).

(69) This fact may be easily manifested by the substitution of the relevant expressions from eq. 69 through 89 into eq. 72.

(70) For an evaluation of the goodness of Slater type wave functions in ligand field calculations read (a) R. L. Belford and M. Karplus, J. Chem. Phys., 31, 394 (1959), and (b) R. E. Watson and A. J. Freeman, Phys. Rev., 120, 1134, 1254 (1960), and related papers.

(71) For actual geometries three principal modifications of the theory would enter. One, the σ-molecular orbitals could no longer be made cubosymmetric,[13,16] and hence, would contribute to the optical activity. Two, the cubical symmetry operations such as $\sigma(x' - z')$, $\mathfrak{C}_4(x)$, $\mathfrak{i}$, etc., could no more be used to equate localized electron transition moment integrals one to another [cf. section VII, §5.3 and 5.4]. Three, an additional angle ι which measured the localized metal-ligand bi- (or poly-) dentate directed orbital nonplanarities would participate [for insight, read (a) E. J. Corey and J. C. Bailar, Jr., J. Am. Chem. Soc., 81, 2620 (1959), and (b) F. Woldbye, Record Chem. Progr., in press. These modifications can be incorproated into the theory without difficulty.[6]

(72) This relaxation would destroy the cubical σ-, π-dichotomy and would invite odd cubical σ-molecular orbitals to enter the calculation, and therefore would enhance the optical rotivity.[16] It would also make possible configurational interaction between the $e_{\pm}(t_{2g})$ and $e_{\pm}(e_g)$ molecular orbitals which would likewise augment the rotivity.
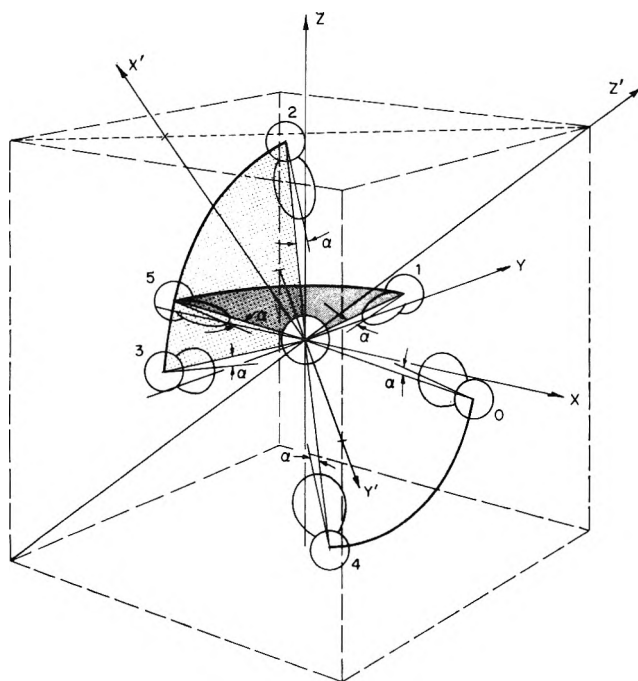
Figure 17. The local ligand orbital spatial disposition for the factualistic acute-angled geometry of the trisethylenediamine-copper(II) cation. (Ligand nonplanarity has been suppressed for illustrative clarity only.)

should create heightened accord.[73] Other emendments should suggest themselves.

A word of comparison: contemporary workers[25b,74] to date have all adopted an electrostatic outlook in the treatment of the optical activity of trigonal dihedral compounds, and have as a consequence fallen into one trap or another.[75] Indeed, the present work was undertaken to rectify the false result of Moffitt[25b] and to demonstrate the inadequacy of his model. Fortunately, a portion of this task which was not too directly connected with the author's purposes was accomplished for him while he has engaged in the present development: Sugano,[74a,76] and later Piper,[74b] Hamer,[74c] Piper and Karipides,[74d] and Poulet[74e] discovered a mislaid minus sign in Moffitt's treatment. This discovery was most gratifying as it had been the author's contention since 1956 that Moffitt's error lay here among other places.[77] Thus the present theory of the trigonally dihedral compounds is the first internally consistent one to be published.[78]

V. Conclusion

To end this disquisition we emphasize the principal finds of this research.
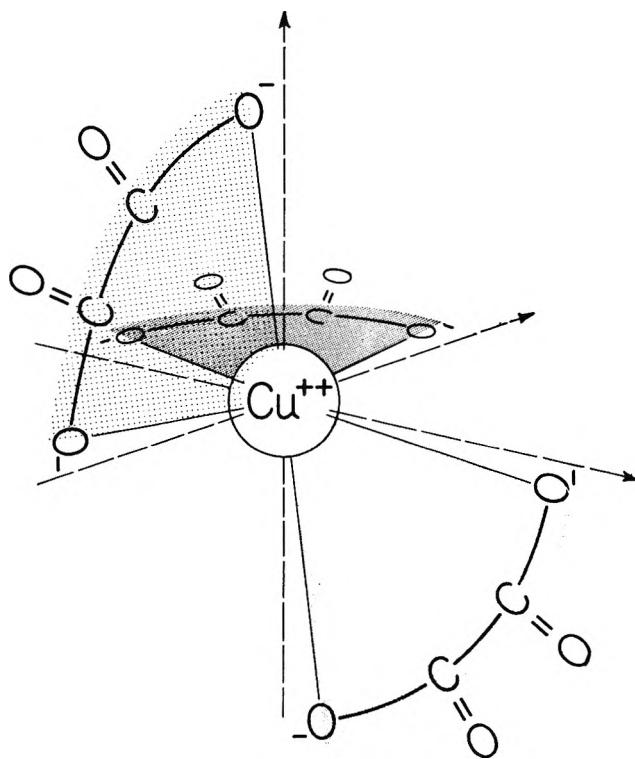

Figure 18.   The factualistic acute-angled geometry of the trisoxalatocopper(II) anion.   (Improbable ligand nonplanarity has been suppressed.)

(1) There is an infinite ambiguity in the mathematical formulation of dihedral molecular orbitals from a directed localized ligand–metal orbital basis.

(2) The optical rotary and spectral powers are directly proportional to the covalent strength of the compound.

(3) The electron-hole formalism is not straightly applicable to optical rotatory or intensiveness computations.

(4) There is a direct correspondence between the ro-

---

(73) The embodiment of ligand–ligand additaments is of paramount importance whenever the angle cant α, and the degree of covalence ξ or η [or ρ if the assumption of pseudo-octahedrality is dropped] are large [see as a sample ref. 10a and (a) A. Carrington and D. S. Schonland, *Mol. Phys*, **3**, 331 (1960)]. In this event quadratic terms in these two sets of parameters, individually, cannot be neglected, as was done in §3.3, eq. 47 and 49 and their descendants. For example, in the approximation of pseudo octahedrality, the σ-bonded electric transition dipole $\langle a_1(t_{2g}) | \vec{p} | e_\pm(t_{2g}) \rangle$ of §3.3, eq. 47, should include the term (neglecting ligand–ligand overlap)

$$\pm i\omega^{\pm 1} \frac{e}{2\sqrt{3}} ak_p^2 \sin^2 x\, N_{a_1(t)}*N_{e(t)}\eta*\xi(\hat{1} + \omega^{\pm 1}\hat{j} + \omega^{\pm 2}\hat{k}),\ \text{where}\ a$$

is the metal–ligand bond length, which arises from the integral $eN_{a_1(t)}*N_{e(t)}\eta*\xi \int \Pi_0{}^{s(+)} \vec{r}\, \Pi_\pm{}^s d\tau$. Note that due to the product $\eta*\xi$ this term is of opposite sign to that given in eq. 47. [Compare also footnotes 45, 46, and 49. This oppositely signed contributent to $\langle a_1(t_{2g}) | \vec{p} | e_\pm(t_{2g}) \rangle$ is only of order $+0.03B$ in the parameterization of eq. 93 and 94, but rapidly attains an order of many-fold times this value as ξ, η, and α increase. Indeed, when $|N_{a_1(t)\eta}|$ and $|N_{e(t)}\xi|$ become $\sim \frac{1}{\sqrt{2}}$ and $\alpha \sim 15°$, this previously neglected ligand–ligand term becomes dominant and exceeds the metal–ligand term of the text by a factor of two! Hence, for large covalencies and cantations the formulas of the text must be supplemented in the manner indicated.] In pseudo-octahedral σ-bonded compounds this is the only such electric transition dipole addition needed [a ligand–ligand magnetic transition dipole additament to $\langle e_\pm(t_{2g}) | \vec{m} | e_{\pm\ or\ \mp}(e_g) \rangle$ also occurs]. However, for pseudo-octahedral σ-,π-bonded compounds and nonpseudo-octahedral σ- or σ-,π-bonded compounds several others also occur [cf. §1.2, eq. 33 and footnotes 71 and 72. In the latter instance (the general case) the matrix expressions become rather cumbersome; cf. (b) part I, topic B, A. D. Liehr, in preparation].

(74) (a) S. Sugano, *J. Chem. Phys.*, **33**, 1883 (1960); (b) T. S. Piper, *ibid.*, **36**, 2224 (1962); (c) N. K. Hamer, *Mol. Phys.*, **5**, 339 (1962); (d) T. S. Piper and A. G. Karipides, *ibid.*, **5**, 475 (1962); (e) H. Poulet, *J. Chim. Phys.*, **59**, 584 (1962); (f) M. Shinada and S. Sugano, International Symposium on Molecular Structure and Spectroscopy, Tokyo, Japan, September 10–15, 1962, private communication, and to be published.

(75) All of these treatments have had difficulty in convincingly reproducing the observed rotations.

(76) Sugano's[74a] investigations on this point were synchronously timed with those of the author while both were neighbors at the Bell Telephone Laboratories, Inc., Murray Hill, N. J His most elegant result rendered the author's planned proof (planned along the lines of Piper's[74b] direct check-see method) both totally redundant and unnecessary [this planned proof was to have been inserted as an appendix to the present paper].

(77) The other errors here implied are in the use of the electrostatic approach in the first place. Shinada and Sugano[74f] are presently attempting to rigorize this approach, however, and have made most impressive progress.

(78) Shinada, Sugano,[74f] and Th. Bürer [(a) *Mol. Phys.*, **6**, 541 (1963), and (b) to be published], and A. G. Karipides and T. S. Piper [(c) *J. Chem. Phys.*, **40**, 674 (1964)] are also at this time developing a harmonious molecular orbital theory of such compounds. It is expected these will be equally good, if not better than the present one.

tational and spectral powers of d^n and d^{5+n}, ($n = 0, 1, 2, 3, 4, 5$), spin-free systems, between $d^{1,4,6,9}$ spin-free systems, and various indirect relationships between these and other d^n, ($n = 0, 1, 2, 3, 4, 5, 6, 7, 8, 9$) configurations.

(9) To good approximation σ- and σ-,π-bonded compounds are formally identical in their mathematical optical rotatativeness and intensiveness behavior.

(10) The optical rotatory and spectral powers of many electron dihedral systems are expressed as multi-
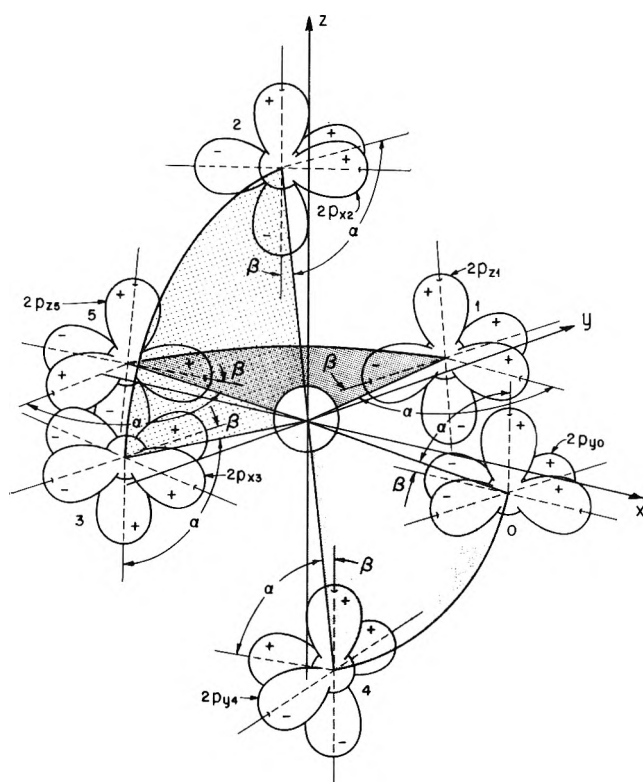
Figure 19a. The digonal local ligand orbital spatial disposition for the factualistic acute-angled geometry of the trisoxalatocopper(II) anion. (Improbable ligand nonplanarity has been suppressed.)
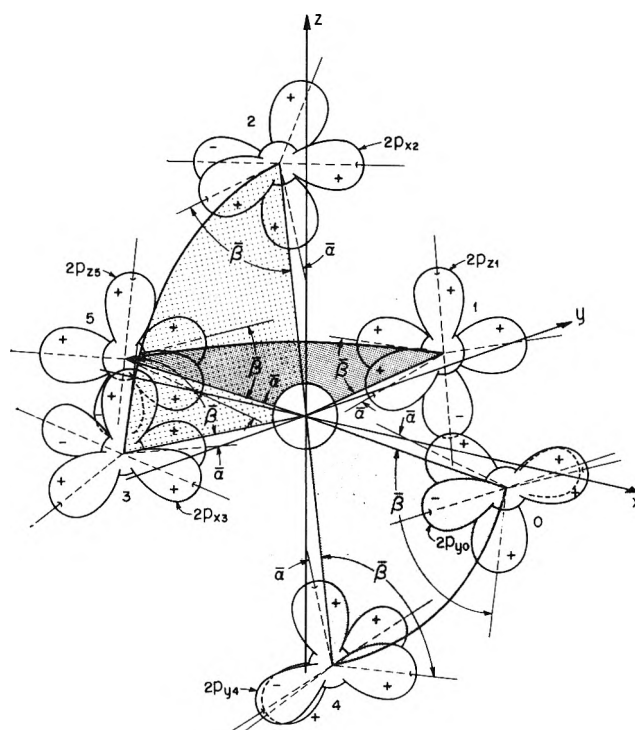
Figure 19b. The isosceles local ligand orbital spatial disposition for the factualistic acute-angled geometry of the trisoxalatocopper(II) anion. (Improbable ligand nonplanarity has been suppressed.)

(5) The sign and magnitude of the optical rotation, the ellipticity, and the dissymmetry, for a given conformation, are directly dependent upon the sign and magnitude of the covalency and hybridization parameters, the localized metal–ligand transition moment, and the angle of bidental cant.

(6) Cubic magnetic and electric selection rules are nontrivially relaxed in zero order in dihedral compounds.

(7) Strong natural electronic optical rotatory dispersion and dichroism are possible in the infrared and microwave regions of the spectrum for spin-orbitally coupled and uncoupled d^n electronic systems.

(8) Spin magnetic dipole transition moments alone, in conjunction with an allowed electric dipole transition moment, can induce large rotational strengths.

plus and simple sums of those of the primogenital one-electron system, and an addition invariance relationship for these expressions.

It is apparent that a large number of further relationships could be derived and recorded by extensions and enlargements of the theory developed above. However, without corroborative detailed experimental information such derivations seem a little premature, at least at this time. It is hoped that at a future date developments will be such as to allow a further evolution of the theory. Plans are now in progress for its accomplishment.[33]

VI. Acknowledgments. The author wishes to take this opportunity to thank his many friends who have aided him in a multitude of diverse and sometimes unknown and forgotten ways in connection with this

paper. In particular, especial thanks are due to Drs.
G. Atkinson, C. H. Brubaker, Jr., Th. Bürer, A. B. F.
Duncan, G. Gordon, E. König, S. F. Mason, J. P.
Mathieu, T. S. Piper, S. Sugano, and F. Woldbye for
their helpful and encouraging communications at times
of need, to R. L. Kornegay for his aid in checking the
algebraic forms of certain integrals and in numerically
evaluating them, and to Messrs. H. M. Yates and C. J.
Jernstedt of the Bell Telephone Laboratories Research
Drafting Department and G. B. Arnold and J. F. Benes
of the Mellon Institute Research Drafting Department
for their wondrous assistance in illustrating this article
under rather arduous conditions.

VII. Appendix §5. Evaluation of the Integrals

5.1 *Algebraic Reduction.* The algebraic reduction
of the requisite molecular and localized integrals to
elementary forms is straightforward. A few samples
will be given here to illustrate the procedure. First,
due to the trigonal dihedral symmetry all vectorial
integrals can be immediately reduced to one component
form. To illustrate, as $\mathcal{C}_3(z')[x,y,z] = [z,x,y]$ and
$\mathcal{C}_3(z')[a_1,e_\pm] = [a_1,\omega^{\pm 1}e_\pm]$ (Fig. 2 and 7 and Tables I
and III), we have[25,30]

$$\int a_1{}^*(t_{2g}) \left|\frac{\vec{p}}{m}\right| e_\pm(t_{2g})\, d\tau =$$

$$(\hat{i} + \omega^{\pm 1}\hat{j} + \omega^{\pm 2}\hat{k}) \int a_1(t_{2g})^* \left[\frac{p_x}{m_x}\right] e_\pm(t_{2g})\, d\tau \quad \text{(A-1)}$$

Thus all integrals may be evaluated with the x-com-
ponent alone. Second, as $\mathcal{C}_2(y')[x,y,z] = (-y,-x,
-z]$ and $\mathcal{C}_2(y')[a_1,e_\pm] = [a_1,e_\mp]$ (Fig. 2 and 7 and Tables
I and III), we also have[25,30]

$$\int e_\pm(t_{2g})^* \left|\frac{\vec{p}}{m}\right| e_\mp(e_g)\, d\tau =$$

$$\omega^{-1} \begin{bmatrix} - \\ + \end{bmatrix} \int e_\mp(e_g)^* \left|\frac{\vec{p}}{m}\right| e_\pm(t_{2g})\, d\tau \quad \text{(A-2)}$$

and so on.

5.2 *Angular Momentum Integrals.* The angular mo-
mentum integrals are readily evaluated if it is assumed
that ligand–metal and ligand–ligand contributions can
be neglected [the neglect corresponds to a first-order ro-
tational strength assessment in terms of the variational
parameters ξ, η, and ρ]. This assumption has been
utilized in the present work to simplify the end ex-
pressions; however, it is by no means a necessary one
as the integrals neglected may be easily evaluated by
the same techniques used for the electronic transition
moment integrals to be described later.[73b] In this ap-
proximation the resolution of the angular momentum
integrals proceeds rapidly once the metal orbitals are

expressed in terms of their trigonal momental basal
representations $d\pi_\pm'$, $d\delta_\pm'$ and $d\sigma'^2$ [Table III] and the
angular momentum components are trigonally oriented
[the latter orientation is accomplished by use of the
vectorial transformation matrix given in ref. 9, footnote
28]. The values of the integrals are then read off by use
of the standard angular momentum matrices as cata-
loged, *e.g.*, by Kramers[79] [but remember in using these
tables the definitions of $d\pi_\pm'$, $d\delta_\pm'$, and $d\sigma'^2$ and their
phase relation to the standard Condon and Shortley
angular momentum bases $|lm_l>$ as given in ref. 9].

5.3 *Local Electronic Transition Moment Integrals.*
The localized electronic transition moment integrals are
not so quickly assessed as were those for the angular mo-
mentum, as the integrals have as their only first-order
nonzero parts those of the metal–ligand cross-term
type. They come in a variety of sorts. To demon-
strate the techniques let us consider the integrals

$$K_{0A_j} = \int (2s)_{A_j}x d_{z'^2}\, d\tau,\quad K_{1A_j} = \int (2p_x)_{A_j}x d_{z'^2}\, d\tau$$

$$K_{2A_j} = \int (2p_y)_{A_j}x d_{z'^2}\, d\tau,\quad K_{3A_j} = \int (2p_z)_{A_j}x d_{z'^2}\, d\tau$$

$$\text{(A-3)}$$

The decomposition of the trigonally oriented metallic
orbital $d_{z'^2}$ into its tetragonal basis, $3^{-1/2}(d_{xy} + d_{xz}
+ d_{yz})$, by means of the transformation matrix printed
in ref. 59, eq. 3.4–4, and the use of the cubical sym-
metry elements then shows that

$$K_{0A_{0,5}} = 0,\quad K_{0A_{1,3}} = -K_{0A_{3,4}},\quad K_{0A_{3,4}} =$$

$$\sqrt{1/3} \int (2s)_{A_3}x d_{zy}\, d\tau$$

$$K_{1A_j} = 0,\quad (j = 0, 1, 2, 3, 4, 5)$$

$$K_{2A_{0,5}} = K_{3A_{0,5}} = \sqrt{1/3} \int (2p_y)_{A_5}x d_{zy}\, d\tau$$

$$K_{2A_{1,3}} = K_{3A_{2,4}} = \sqrt{1/3} \int (2p_y)_{A_3}x d_{zy}\, d\tau$$

$$K_{2A_{2,4}} = K_{3A_{1,3}} = \sqrt{1/3} \int (2p_z)_{A_3}x d_{zz}\, d\tau \quad \text{(A-4)}$$

As an examplar, reflection $[\sigma(x - z)]$ in the x–z plane
(y replaced by $-y$, 1 replaced by 3) of Fig. 2 and 7
shows that $\int (2s)_{A_{1,3}}x d_{zy}\, d\tau$ is zero and $\int (2s)_{A_1}x d_{zy}\, d\tau
= -\int (2s)_{A_3}x d_{zy}\, d\tau$, and reflection $[\sigma(y - z)]$ in the
y–z plane (x replaced by $-x$, 0 replaced by 5) of
Fig. 2 and 7 shows that $\int (2s)_{A_{1,5}}x d_{yz}\, d\tau$ is zero
and that $\int (2s)_{A_0}x d_{zy}\, d\tau = \int (2s)_{A_5}x d_{zy}\, d\tau$, and so
forth. Similarly a counterclockwise rotation of $90°$
$[\mathcal{C}_4(x)]$ about the x axis (0, 1, 2, 3, 4, 5, x, y, z replaced
by 0, 4, 1, 2, 3, 5, x, $-z$, y) of Fig. 2 and 7 shows that
$\sqrt{1/3}\int (2s)_{A_4}x d_{zz}\, d\tau [K_{0A_4}] = \sqrt{1/3}\int (2s)_{A_3}x d_{zy}\, d\tau [K_{0A_3}]$.

(79) H. A. Kramers, "Quantum Mechanics," North-Holland Pub-
lishing Co., Amsterdam, 1958.

The other localized electronic moment integrals are

$$K_{4A_j} = \sqrt{2/3} \int (2p_x)_{A_j} x d_{z^2} \, d\tau,$$

$$K_{5A_j} = -\frac{\sqrt{2}}{3} \int (2p_y)_{A_j} x d_{xy} \, d\tau$$

$$K_{6A} = \frac{\sqrt{2}}{6} \int (2p_z)_{A_j} x d_{xz} \, d\tau,$$

$$K_{7A_j} = \sqrt{2/3} \int (2p_x)_{A_j} x d_{x^2 - y^2} \, d\tau$$

$$K_{8A_j} = \sqrt{1/6} \int (2p_x)_{A_j} x d_{xz} \, d\tau,$$

$$K_{9A_j} = -\sqrt{1/3} \int (2p_x)_{A_j} x d_{x^2 - y^2} \, d\tau$$

$$K_{10A_j} = \sqrt{1/3} \int (2p_z)_{A_j} x d_{zz} \, d\tau,$$

$$K_{11A_j} = \sqrt{1/3} \int (2p_x)_{A_j} x d_{z^2} \, d\tau$$

$$K_{12A_j} = 2/3 \int (2p_y)_{A_j} x d_{xy} \, d\tau,$$

$$K_{13A_j} = -1/3 \int (2p_z)_{A_j} x d_{xz} \, d\tau$$

$$K_{14A_{0,6}} = \sqrt{2/3} \int (2s)_{A_{0,6}} x d_{z^2} \, d\tau,$$

$$K_{15A_{2,4}} = \frac{\sqrt{2}}{6} \int (2s)_{A_{2,4}} x d_{zz} \, d\tau$$

$$K_{16A_{1,3}} = -\frac{\sqrt{2}}{3} \int (2s)_{A_{1,3}} x d_{xy} \, d\tau,$$

$$K_{17A_{0,6}} = \sqrt{2/3} \int (2s)_{A_{0,6}} x d_{x^2 - y^2} \, d\tau$$

$$K_{18A_{2,4}} = \sqrt{1/6} \int (2s)_{A_{2,4}} x d_{xz} \, d\tau,$$

$$K_{19A_{0,6}} = -\sqrt{1/3} \int (2s)_{A_{0,6}} x d_{x^2 - y^2} \, d\tau$$

$$K_{20A_{2,4}} = \sqrt{1/3} \int (2s)_{A_{2,4}} x d_{xz} \, d\tau,$$

$$K_{21A_{0,6}} = \sqrt{1/3} \int (2s)_{A_{0,6}} x d_{z^2} \, d\tau$$

$$K_{22A_{2,4}} = -1/3 \int (2s)_{A_{2,4}} x d_{zz} \, d\tau,$$

$$K_{23A_{1,3}} = 2/3 \int (2s)_{A_{1,3}} x d_{xy} \, d\tau \quad \text{(A-5)}$$

which are straightway obtained by likewise expressing the imaginary trigonal metallic orbitals $d\pi_{\pm}'$ and $d\delta_{\pm}'$ in terms of the real Cartesian trigonal orbitals $d_{z'z'}$, $d_{y'z'}$, $d_{z'^2 - y'^2}$, and $d_{z'y'}$ [Table III], and these in turn in terms of the real Cartesian tetragonal orbitals d_{xy}, d_{zz}, d_{yz}, $d_{x^2 - y^2}$, and d_{z^2} by means of the transformation matrix, eq. 3.4-4 of ref. 59. Note that of these 20 integrals only three, K_{4A_j}, K_{7A_j}, and K_{14A_j}, are really distinct: the remainder are simple multiples of these and of those previously considered in eq. A-3 and 4. The application of the counterclockwise 90° replacement rotation $\mathcal{C}_4(x)$ about the x axis of the last paragraph manifests that not even all of the K_{nA_j}, ($n = 4, 7, 14$), are distinct. As a sample

$$K_{4A_4} = \sqrt{2/3} \int (2p_x)_{A_4} x d_{z^2} \, d\tau \equiv$$

$$\mathcal{C}_4(x) \sqrt{2/3} \int (2p_x)_{A_4} x d_{z^2} \, d\tau =$$

$$\sqrt{2/3} \left\{ -1/2 \int (2p_x)_{A_3} x d_{z^2} \, d\tau - \right.$$

$$\left. \frac{\sqrt{3}}{2} \int (2p_x)_{A_3} x d_{z^2 - y^2} \, d\tau \right\} = -1/2 K_{4A_3} - \frac{\sqrt{3}}{2} K_{7A_3}$$

All other possible integrals besides those listed above vanish.

5.4 *Local Overlap Integrals.* The only nonzero localized overlap integrals are those registered below.

$$K_{24A_j} = \sqrt{2/3} \int (2s)_{A_j} d_{z^2} \, d\tau,$$

$$K_{25A_{0,1,3,6}} = \sqrt{2/3} \int (2s)_{A_{0,1,3,6}} d_{z^2 - y^2} \, d\tau,$$

$$K_{26A_{2,4}} = \sqrt{1/3} \int (2p_x)_{A_{2,4}} d_{xz} \, d\tau,$$

$$K_{27A_{1,3}} = \sqrt{1/3} \int (2p_x)_{A_{1,3}} d_{xy} \, d\tau,$$

$$K_{28A_{2,4}} = \sqrt{1/3} \int (2p_y)_{A_{2,4}} d_{yz} \, d\tau,$$

$$K_{29A_{0,5}} = \sqrt{1/3} \int (2p_y)_{A_{0,5}} d_{zy} \, d\tau$$

$$K_{30A_{0,6}} = \sqrt{1/3} \int (2p_z)_{A_{0,6}} d_{zz} \, d\tau,$$

$$K_{31A_{1,3}} = \sqrt{1/3} \int (2p_z)_{A_{1,3}} d_{yz} \, d\tau$$

$$K_{32A_{0,6}} = \sqrt{2/3} \int (2p_x)_{A_{0,6}} d_{z^2} \, d\tau,$$

$$K_{33A_{1,3}} = \sqrt{2/3} \int (2p_y)_{A_{1,3}} d_{z^2} \, d\tau$$

$$K_{34A_{2,4}} = \sqrt{2/3} \int (2p_z)_{A_{2,4}} d_{z^2} \, d\tau,$$

$$K_{35A_{0,6}} = \sqrt{2/3} \int (2p_x)_{A_{0,6}} d_{z^2 - y^2} \, d\tau$$

$$K_{36A_{1,3}} = \sqrt{2/3} \int (2p_y)_{A_{1,3}} d_{z^2 - y^2} \, d\tau \quad \text{(A-6)}$$

By means of simple coordinate transformations, many of these integrals may be expressed in terms of the others. To indicate, the application of the counterclockwise replacement rotation by 90° $[\mathcal{C}_4(x)]$ yields as before

$$K_{24A_3} \equiv \mathcal{C}_4(x) \sqrt{2/3} \int (2s)_{A_3} d_{z^2} \, d\tau =$$

$$\sqrt{2/3} \left\{ -1/2 \int (2s)_{A_2} d_{z^2} \, d\tau - \right.$$

$$\left. \frac{\sqrt{3}}{2} \int (2s)_{A_2} d_{z^2 - y^2} \, d\tau \right\} = -1/2 K_{24A_2}$$

In truth, such applications show that the sole independent local overlap expressions are K_{24A_j}, K_{26A_4}, and K_{32A_6}.

5.5 *Algebraic Evaluation of the Basic Integrals.* The requisite basic integrals are directly evaluated by the successive use of the standard bipolar and elliptic coordinate transformations.[80] To refresh the memory Fig. 20 and eq. A-7 and 8 exemplify the procedure (a_0 is the Bohr radius) for the localized ligand orbital situated on the negative y axis of Fig. 2 and 7 [atom A_3].

$$\bar{r}_A \sin \gamma_A = \bar{r}_M \sin \gamma_M, \left(\bar{r} = \frac{r}{a_0} \right),$$

$$\bar{r}_M \cos \gamma_M = \bar{a} - \bar{r}_A \cos \gamma_A, \left(\bar{a} = \frac{a}{a_0} \right)$$

---

(80) See, for example, A. D. Liehr, *Z. Naturforsch.*, 13a, 429 (1958), and ref. 23b, among other places.

$\sin \theta_A \sin \varphi_A = \cos \gamma_A$, $\sin \theta_M \sin \varphi_M = -\cos \gamma_M$

$\sin \theta_A \cos \varphi_A = \sin \gamma_A \sin \beta$,

$$\sin \theta_M \cos \varphi_M = \sin \gamma_M \sin \beta$$

$\cos \theta_A = \sin \gamma_A \cos \beta$, $\cos \theta_M = \sin \gamma_M \cos \beta$ (A-7)

$$\bar{r}_A = \frac{\bar{a}}{2}(\lambda + \mu), \quad \bar{r}_M = \frac{\bar{a}}{2}(\lambda - \mu)$$

$$\cos \gamma_A = \frac{1 + \lambda\mu}{\lambda + \mu}, \quad \sin \gamma_A = \frac{\sqrt{(\lambda^2 - 1)(1 - \mu^2)}}{\lambda + \mu}$$

$$d\tau_{AM} = \left(\frac{\bar{a}}{2}\right)^3 (\lambda^2 - \mu^2)d\lambda d\mu d\beta,$$

$$(1 \leq \lambda \leq \infty, -1 \leq \mu \leq 1, 0 \leq \beta \leq 2\pi) \quad (A-8)$$
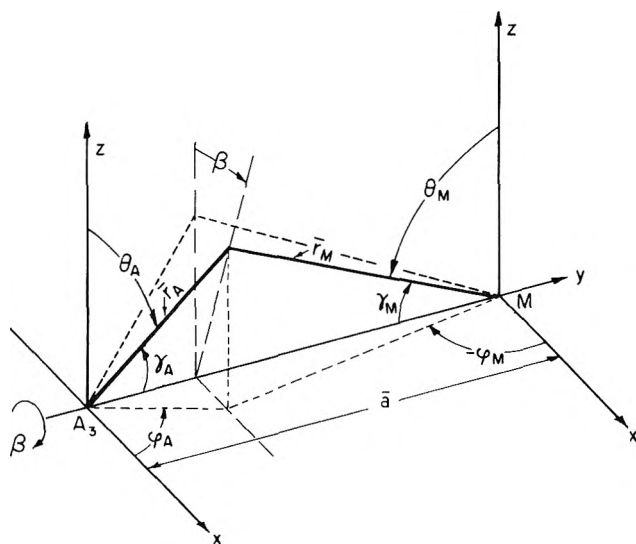
Figure 20. The bipolar coordinate system utilized for the algebraic evaluation of the localized ligand–metal electronic transition dipole moment and overlap integrals.

The employment of these transformations in the integrals leads to their resolution. The emergent expressions are as epitomized beneath.

$$K_{0A_{1,2}} = -K_{0A_{3,4}} = {}^1/_3 \sqrt{{}^2/_3}\, b^{7/2}c^{5/2}a_0 \left(\frac{\bar{a}}{2}\right)^7 \times$$

$$[(A_5 - A_3)(B_0 - 2B_2 + B_4) -$$

$$(A_3 - A_1)(B_2 - 2B_4 + B_6) +$$

$$(A_6 - 2A_4 + A_2)(B_1 - B_3) -$$

$$(A_4 - 2A_2 + A_0)(B_3 - B_5)]$$

$K_{1A_i} \equiv 0$

$$K_{2A_{0,6}} = K_{3A_{0,5}} = \frac{\sqrt{2}}{3} b^{7/2}c^{5/2}a_0 \left(\frac{\bar{a}}{2}\right)^7 \times$$

$$[(A_4 - A_2)(B_0 - B_2) + 2(A_5 - A_3)(B_1 - B_3) +$$

$$(A_6 - A_4)(B_2 - B_4) - (A_2 - A_0)(B_2 - B_4) -$$

$$2(A_3 - A_1)(3_3 - B_5) - (A_4 - A_2)(B_4 - B_6)]$$

$$K_{2A_{1,6}} = K_{3A_{2,4}} = -\frac{\sqrt{2}}{3} b^{7/2}c^{5/2}a_0 \left(\frac{\bar{a}}{2}\right)^7 \times$$

$$[(A_4 - A_2)(B_0 - B_6) + (A_6 - A_0)(B_4 - B_2)]$$

$$K_{2A_{2,4}} = K_{3A_{1,3}} = -\frac{\sqrt{2}}{12} b^{7/2}c^{5/2}a_0 \left(\frac{\bar{a}}{2}\right)^7 \times$$

$$[(A_4 - 2A_2 + A_0)(B_6 - 2B_4 + B_2) -$$

$$(A_6 - 2A_4 + A_2)(B_4 - 2B_2 + B_0)]$$

$$K_{4A_{0,6}} = -\frac{1}{3\sqrt{3}} b^{7/2}c^{5/2}a_0 \left(\frac{\bar{a}}{2}\right)^7 \times$$

$$\{3[(A_4 - A_2)(B_0 - B_2) - (A_6 - A_4)(B_2 - B_4) -$$

$$(A_2 - A_0)(B_2 - B_4) + (A_4 - A_2)(B_4 - B_6)] -$$

$$2[A_4B_0 + 2A_3B_1 - A_6B_2 - 2A_5B_3 - 2A_1B_3 -$$

$$A_0B_4 + 2A_3B_5 + A_2B_6]\}$$

$$K_{4A_{1,6}} = \frac{1}{3\sqrt{3}} b^{7/2}c^{5/2}a_0 \left(\frac{\bar{a}}{2}\right)^7 \times$$

$$[{}^3/_4(A_6 - 2A_4 + A_2)(B_0 - 2B_2 + B_4) -$$

$${}^3/_4(A_4 - 2A_2 + A_0)(B_2 - 2B_4 + B_6) -$$

$$(A_6 - A_4)(B_0 - B_2) - 2(A_5 - A_3)(B_1 - B_3) +$$

$$2(A_3 - A_1)(B_3 - B_5) + (A_2 - A_0)(B_4 - B_6)]$$

$$K_{4A_{2,4}} = -{}^1/_2 K_{A_6} - \frac{\sqrt{3}}{2} K_{7A_6}$$

$$K_{5A_i} = -\sqrt{{}^2/_3}\, K_{2A_i}, \quad K_{6A_i} = \frac{1}{\sqrt{6}} K_{3A_i}$$

$$K_{7A_{0,6}} = -\sqrt{3}\, K_{4A_{0,6}}$$

$$K_{7A_{2,4}} = -\frac{\sqrt{3}}{2} K_{4A_6} + {}^1/_2 K_{7A_2}$$

$$K_{7A_{1,6}} = {}^1/_3 b^{7/2}c^{5/2}a_0 \left(\frac{\bar{a}}{2}\right)^7 \times$$

$$[{}^7/_4(A_6 - 2A_4 + A_2)(B_0 - 2B_2 + B_4) -$$

$${}^7/_4(A_4 - 2A_2 + A_0)(B_2 - 2B_4 + B_6) -$$

$$(A_6 - A_4)(B_0 - B_2) - 2(A_5 - A_3)(B_1 - B_3) +$$

$$2(A_3 - A_1)(B_3 - B_5) + (A_2 - A_0)(B_4 - B_6)]$$

$$K_{8A_j} = \frac{1}{\sqrt{2}} K_{3A_j}, \quad K_{9A_j} = -\frac{1}{\sqrt{2}} K_{7A_j}, \quad K_{10A_j} = K_{3A_j}$$

$$K_{11A_j} = \frac{1}{\sqrt{2}} K_{4A_j}$$

$$K_{12A_j} = \frac{2}{\sqrt{3}} K_{2A_j}, \quad K_{13A_j} = -\frac{1}{\sqrt{3}} K_{3A}$$

$$K_{14A_0} = -K_{14A_6} = \frac{1}{9} b^{7/2} c^{5/2} a_0 \left(\frac{\bar{a}}{2}\right)^7 \times$$

$$\{3[(A_5 - A_3)(B_0 - 2B_2 + B_4) -$$
$$(A_3 - A_1)(B_2 - 2B_4 + B_6) +$$
$$(A_6 - 2A_4 + A_2)(B_1 - B_3) -$$
$$(A_4 - 2A_2 + A_0)(B_3 - B_5) -$$
$$2[A_5(B_0 - B_2) + 2A_4(B_1 - B_3) -$$
$$2A_2(B_3 - B_5) - A_1(B_4 - B_6) +$$
$$(A_6 - A_4)B_1 + 2(A_5 - A_3)B_2 -$$
$$2(A_3 - A_1)B_4 - (A_2 - A_0)B_5]\}$$

$$K_{15A_{2,4}} = \frac{1}{\sqrt{6}} K_{0A_{2,4}}$$

$$K_{16A_{1,3}} = -\sqrt{2/3} K_{0A_{1,3}}, \quad K_{17A_{0,6}} = -\sqrt{3} K_{14A_{0,6}}$$

$$K_{18A_{2,4}} = \frac{1}{\sqrt{2}} K_{0A_{2,4}}$$

$$K_{19A_{0,6}} = \sqrt{3/2} K_{14A_{0,6}}, \quad K_{20A_{2,4}} = K_{0A_{2,4}}$$

$$K_{21A_{0,6}} = \frac{1}{\sqrt{2}} K_{14A_{0,6}}$$

$$K_{22A_{2,4}} = -\frac{1}{\sqrt{3}} K_{0A_{2,4}}, \quad K_{23A_{1,3}} = \frac{2}{\sqrt{3}} K_{0A_{1,3}}$$

$$K_{24A_{0,1,3,5}} = -\frac{1}{2} K_{24A_{2,4}} = -\frac{1}{9} b^{7/2} c^{5/2} \left(\frac{\bar{a}}{2}\right)^6 \times$$

$$[3A_3B_0 + 5A_4B_1 + 3A_5B_2 - A_5B_0 - 3A_1B_2 -$$
$$4A_2B_3 - 3A_3B_4 - 3A_2B_1 - 4A_3B_2 - 3A_4B_3 +$$
$$3B_3A_0 + 5A_1B_4 + 3A_2B_5 - A_0B_5]$$

$$K_{25A_{0,6}} = -K_{25A_{1,3}} = \frac{\sqrt{3}}{2} K_{24A_{2,4}}$$

$$K_{26A_2} = -K_{26A_4} = \frac{\sqrt{2}}{3} b^{7/2} c^{5/2} \left(\frac{\bar{a}}{2}\right)^6 \times$$

$$[(A_4 - A_2)(B_0 - B_2) - (A_2 - A_0)(B_2 - B_4) +$$
$$(A_5 - A_3)(B_1 - B_3) - (A_3 - A_1)(B_3 - B_5)]$$

$$K_{27A_{1,3}} = K_{26A_{2,4}}, \quad K_{28A_{2,4}} = K_{26A_{2,4}}, \quad K_{29A_{0,6}} = K_{26A_{2,4}}$$

$$K_{30A_{0,6}} = K_{26A_{2,4}}, \quad K_{31A_{1,3}} = K_{26A_{2,4}}$$

$$K_{32A_0} = -K_{32A_6} = -\frac{\sqrt{3}}{9} b^{7/2} c^{5/2} \left(\frac{\bar{a}}{2}\right)^6 \times$$

$$\{3[(A_4 - A_2)(B_0 - B_2) - (A_2 - A_0)(B_2 - B_4) -$$
$$(A_5 - A_3)(B_1 - B_3) + (A_3 - A_1)(B_3 - B_5)] -$$
$$2[A_4B_0 - A_5B_1 + 2A_3B_1 - 2A_1B_3 - 2A_4B_2 +$$
$$2A_2B_4 - B_4A_0 + A_1B_5]\}$$

$$K_{33A_{1,3}} = K_{32A_{0,6}}, \quad K_{34A_{2,4}} = -2K_{32A_{0,6}}$$

$$K_{35A_{0,6}} = -\sqrt{3} K_{32A_{0,6}}$$

$$K_{36A_{1,3}} = \sqrt{3} K_{32A_{0,6}} \tag{A-9}$$

where b and c equal $Z_{3d}/3$ and $Z_{2s \text{ or } 2p}/2$, individually, and where the arguments, v, of the auxiliary A_n and B_n integrals

$$A_n(v) = \int_1^\infty \lambda^n e^{-v\lambda} d\lambda, \quad B_n(v) = \int_{-1}^1 \mu^n e^{-v\mu} d\mu \tag{A-10}$$

are $\frac{1}{2}\bar{a}(b + c)$ and $\frac{1}{2}\bar{a}(b - c)$, separately. These latter integrals may be either be evaluated recursively or by recourse to tables.[81]

5.6 *Group Electronic Transition Moment Integrals.* The group electronic transition moment integrals are speedily determined as linear combinations of the localized integrals collected in eq. A-1. Their expressions are

$$T_x[e_{g\binom{a}{b}}; \Sigma_\pm^{c(1)}] = \omega^{\mp 1} T_x[e_{g\binom{a}{b}}; \Sigma_\mp^{c(1)}] =$$
$$k_s K_{14A_6} + k_p \cos \alpha \, K_{4A_6}$$

$$T_x[t_{2ga}; \Sigma_\pm^{c(1)}] = \omega^{\pm 1} \sqrt{1/6} \, (k_s K_{0A_3} + k_p \cos \alpha \, K_{2A_3})$$

$$T_x[t_{2g\binom{b}{c}}; \Sigma_\pm^{c(1)}] = -2\omega^{\mp 1}[t_{2g\binom{b}{c}}; \Sigma_\mp^{c(1)}] =$$
$$-\sqrt{2}\omega^{\mp 1} T_x[t_{2ga}; \Sigma_\pm^{c(1)}]$$

$$T_x[t_{2ga}; \Sigma_\pm^c] \equiv 0, \quad T_x[t_{2g\binom{b}{c}}; \Sigma_\pm^c] \equiv 0$$

$$T_x[\Pi_0^{s(+)}; e_{ga}] = T_x[\Pi_0^{s(+)}; e_{gb}]^* =$$
$$-\frac{i\omega \sin \alpha}{4} k_p(\sqrt{3} \, K_{4A_i} + K_{7A_j})$$

$$T_x[\Pi_\pm^{s(1)}; e_{g\binom{a}{b}}] = -T_x[\Pi_\pm^{s(2)}; e_{g\binom{a}{b}}]^* =$$
$$\frac{1}{2\sqrt{2}} k_p \sin \alpha \, (K_{4A_j} \pm iK_{7A_j})$$

$$T_x[\Pi_\pm^{s(1)}; e_{g\binom{b}{a}}] = -\omega^{\mp 1} T_x[\Pi_\pm^{s(2)}; e_{g\binom{b}{a}}]^* =$$
$$T_x[\Pi_\pm^{s(1)}; e_{g\binom{a}{b}}]^*$$

(81) M. Kotani, A. Amemiya, E. Ishiguro, and T. Kimura, "Table of Molecular Integrals," Maruzen Co., Ltd., Tokyo, 1955.

$$T_x[t_{2ga}; \ \Pi_\pm{}^{s(1)}] = \frac{1}{\sqrt{6}} k_p \omega^{\mp 1} \sin \alpha \ (K_{2A_6} + \omega^{\mp 1} K_{3A_3})$$

$$T_x[t_{2ga}; \ \Pi_\pm{}^{s(2)}] = -\frac{1}{\sqrt{6}} k_p \omega^{\pm 1} \sin \alpha \ (K_{3A_3} + \omega^{\mp 1} K_{2A_6})$$

$$T_x[\Pi_0{}^{s(+)}; \ t_{2g}(^b_c)] = \pm \frac{i}{2} k_p \sin \alpha \ \omega^{\pm 1} (K_{3A_3} - K_{2A_6})$$

$$T_x[t_{2g}(^b_c); \ \Pi_\pm{}^{s(1)}] = -\sqrt{1/6} \ k_p \sin \alpha \ (K_{2A_6} + \omega^{\pm 1} K_{3A_3})$$

$$T_x[t_{2g}(^b_c); \ \Pi_\pm{}^{s(2)}] = \sqrt{1/6} \ k_p \sin \alpha \ (K_{2A_6} + \omega^{\mp 1} K_{3A_3})$$

$$T_x[t_{2g}(^b_c); \ \Pi_\mp{}^{s(1)}] = -\omega^{\mp 1} T_x[t_{2g}(^b_c); \ \Pi_\mp{}^{s(2)}] =$$
$$-\frac{1}{\sqrt{6}} k_p \ \omega^{\mp 1} \sin \alpha \ (K_{2A_3} + K_{3A_3}) \quad \text{(A-11)}$$

where $T_x[\chi_1; \ \chi_2]$ is an ersatz for $\int \chi_1^* x \chi_2 \, d\tau$, and where the functions $\Sigma_\pm{}^{c(1,2)}$, $\Pi_0{}^{(+)}$, $\Pi_\pm{}^{s(1,2)}$ are as defined in the text with $\left| a(^9_3)_s{}^{\sigma,\pi} \right|$ equals $\sqrt{1/6}$, $(s = 0, \pm 1)$. The integrals $T_x[\chi_1; \ \Sigma_{\pm \text{ or } \mp}{}^{c(2)}]$, $(\chi_1 = e_g(^a_s), \ t_{2ga}, \ t_{2g}(^b_c))$, are the negatives of those for $\Sigma_{\pm \text{ or } \mp}{}^{c(1)}$ because of the inversion relation $i\Sigma_\pm{}^{c(1)} = \Sigma_\pm{}^{c(2)}$ [cf. Table IV]. The group electronic transition moments $T_x[t_{2g}(^b_c); \Pi_\pm{}^{s(1,2)}]$ do not appear in the calculations as the matrix elements $\langle e_\pm(t_{2g}) | \vec{p} | e_\pm(t_{2g}) \rangle$ vanish identically [this fact is readily proved by use of the Hermiteness of these matrix elements and their transformation properties under $\mathfrak{C}_2(y')$, where $\mathfrak{C}_2(y')[x', \ y', \ z', \ e_\pm] = [-x', \ y', \ -z', \ e_\mp]$ and $\vec{p} = e(x'\hat{i}' + y'\hat{j}' + z'\hat{k}')$ or $\frac{\hbar}{i}\left(\frac{\partial}{\partial x'}\hat{i}' + \frac{\partial}{\partial y'}\hat{j}' + \frac{\partial}{\partial z'}\hat{k}'\right)$, dependent upon whether the electric dipole length or velocity is employed in the computations].[25] Those involving $\Sigma_\pm{}^{c(1,2)}$ do not appear because of the centrosymmetric nature of $\Sigma_\pm{}^c = \Sigma_\pm{}^{c(1)} + \Sigma_\pm{}^{c(2)}$.

5.7 Group Overlap Integrals. The group overlap integrals are promptly enumerated as linear combinations of the localized overlap integrals gathered before. Their forms are

$$S[e_g(^a_s), \ \Sigma_\pm{}^{c(1,2)}] = \frac{3}{2\sqrt{2}}(k_s K_{24A_4} -$$
$$2k_p \cos \alpha \ K_{32A_6}) = \frac{1}{2} S[e_g(^a_s); \ \Sigma_\pm]$$

$$S[t_{2ga}; \ \Pi_0{}^{s(1,2)}] = -\sqrt{6} \ k_p \sin \alpha \ K_{26A_4} =$$
$$\frac{1}{2} S[t_{2ga}; \ \Pi_0{}^{s(+)}]$$

$$S[t_{2g}(^b_c); \ \Pi_\pm{}^{s(1,2)}] = \sqrt{3/2} \ k_p \sin \alpha \ K_{26A_4} =$$
$$\frac{1}{2} S[t_{2g}(^b_c); \ \Pi_\pm{}^s]$$

$$S[t_{2ga}; \ \bar{\Pi}_0{}^{(1,2)}] = -\sqrt{6} \ K_{26A_4} = \frac{1}{2} S[t_{2ga}; \ \bar{\Pi}_0{}^{(+)}]$$

$$S[t_{2g}(^b_c); \ \bar{\Pi}_\pm{}^{(1,2)}] = \sqrt{3/2} \ K_{26A_4} = \frac{1}{2} S[t_{2g}(^b_c); \ \bar{\Pi}_\pm]$$

$$S[\Sigma_0{}^{(1,2)}; \ \Sigma_0{}^{(2)}] = \frac{1}{2}(k_s^2(1 + 2s_{01}) -$$
$$4k_s k_p \cos \alpha \ \bar{s}_{01} + k_p{}^2 \cos \alpha \ (1 + 2\mathfrak{f}_{01}))$$

$$S[\Sigma_0{}^{(1)}; \ \Sigma_0{}^{(2)}] = \frac{1}{2}(k_s{}^2(2s_{01} + s_{05}) -$$
$$2k_s k_p \cos \alpha \ (2\bar{s}_{01} - \bar{s}_{05}) + k_p{}^2 \cos^2 \alpha \ (2\mathfrak{f}_{01} - \mathfrak{f}_{05}))$$

$$S[\Sigma_0{}^{(+)}; \ \Sigma_0{}^{(+)}] = k_s{}^2(1 + 4s_{01} + s_{05}) -$$
$$2k_s k_p \cos \alpha \ (4\bar{s}_{01} - \bar{s}_{05}) +$$
$$k_p{}^2 \cos^2 \alpha \ (1 + 4\mathfrak{f}_{01} - \mathfrak{f}_{05})$$

$$S[\Sigma_\pm{}^{(1,2)}; \ \Sigma_\pm{}^{(1,2)}] = \frac{1}{2}(k_s{}^2(1 - s_{01}) +$$
$$2k_s k_p \cos \alpha \ \bar{s}_{01} + k_p{}^2 \cos^2 \alpha \ (1 - \mathfrak{f}_{01}))$$

$$S[\Sigma_\pm{}^{(1)}; \ \Sigma_\pm{}^{(2)}] = -\frac{1}{2}(k_s{}^2(s_{01} - s_{05}) -$$
$$2k_s k_p \cos \alpha \ (\bar{s}_{01} + \bar{s}_{05}) +$$
$$k_p{}^2 \cos^2 \alpha \ (\mathfrak{f}_{01} + \mathfrak{f}_{05}))$$

$$S[\Sigma_\pm; \ \Sigma_\pm] = k_s{}^2(1 - 2s_{01} + s_{05}) +$$
$$2k_s k_p \cos \alpha \ (\bar{s}_{01} + \bar{s}_{05}) +$$
$$k_p{}^2 \cos^2 \alpha \ (1 - 2\mathfrak{f}_{01} - \mathfrak{f}_{05})$$

$$S[\Pi_\pm{}^{s(1)}; \ \Pi_\pm{}^{s(2)}] = \frac{1}{2}k_p{}^2 \sin^2 \alpha \ (\mathfrak{f}_{02} - \omega^{\mp 1}\mathfrak{f}_{01})$$

$$S[\Pi_\pm{}^s; \ \Pi_\pm{}^s] = 1 + 2\Re eS[\Pi_\pm{}^{s(1)} \Pi_\pm{}^{s(2)}] =$$
$$1 + k_p{}^2 \sin^2 \alpha \ (\mathfrak{f}_{02} + \frac{1}{2}\mathfrak{f}_{01})$$

$$S[\Pi_\pm{}^{(1)}, \ \bar{\Pi}_\pm{}^{(1)}] = \frac{1}{2}(\mathfrak{f}_{02} - \omega^{\mp 1}\mathfrak{f}_{01}) = S[\Pi_\pm{}^{(2)}; \ \bar{\Pi}_\pm{}^{(2)}]^*$$

$$S[\Pi_\pm{}^{(1)}, \ \bar{\Pi}_\pm{}^{(2)}] = -\frac{1}{2}\mathfrak{f}_{05} = S[\Pi_\pm{}^{(2)}; \ \bar{\Pi}_\pm{}^{(1)}]$$

$$S[\bar{\Pi}_\pm{}^{(1)}, \ \bar{\Pi}_\pm{}^{(2)}] = \frac{1}{2}(\mathfrak{f}_{02} - \omega^{=1}\mathfrak{f}_{01})$$

$$S[\bar{\Pi}_0{}^{(1)}; \ \bar{\Pi}_0{}^{(2)}] = \frac{1}{2}(\mathfrak{f}_{02} - \mathfrak{f}_{01}) = S[\Pi_0{}^{(1)}; \ \Pi_0{}^{(2)}]$$

$$S[\bar{\Pi}_0{}^{(1)}; \ \bar{\Pi}_0{}^{(1)}] = \frac{1}{2}(\mathfrak{f}_{01} + \mathfrak{f}_{02}) = S[\bar{\Pi}_0{}^{(2)}; \ \Pi_0{}^{(2)}]$$

$$S[\bar{\Pi}_0{}^{(1)}; \ \Pi_0{}^{(2)}] = -\frac{1}{2}\mathfrak{f}_{05} = S[\Pi_0{}^{(1)}; \ \Pi_0{}^{(2)}] \quad \text{(A-12)}$$

where $S[\chi_1; \ \chi_2]$, $\mathfrak{f}_{jk}$, $\bar{\mathfrak{f}}_{jk}$, s_{jk}, and $\bar{s}_{jk}$ are replacements for integrals of the sort $\int \chi_1^* \chi_2 d\tau$, $\int (2p_\pi)_{A_j}(2p_\pi)_{A_k} d\tau$, $\int (2p_\sigma)_{A_j}(2p_\sigma)_{A_k} d\tau$, $\int (2s)_{A_j}(2s)_{A_k} d\tau$, $\int (2s)_{A_j}(2p_\sigma)_{A_k} d\tau$, serially. In particular, $\mathfrak{f}_{01}$ equals $\int (2p_z)_{A_0}(2p_z)_{A_1} d\tau$, $\mathfrak{f}_{02}$ equals $\int (2p_z)_{A_0}(2p_z)_{A_2} d\tau$, $\mathfrak{f}_{05}$ equals $\int (2p_z)_{A_0}(2p_z)_{A_5} d\tau$, $\bar{\mathfrak{f}}_{01}$ equals $\int (2p_z)_{A_0}(2p_y)_{A_1} d\tau$, $\bar{\mathfrak{f}}_{05}$ equals $\int (2p_z)_{A_0}(2p_x)_{A_5} d\tau$, s_{01} equals $\int (2s)_{A_0}(2s)_{A_1} d\tau$, s_{05} equals $\int (2s)_{A_0}(2s)_{A_5} d\tau$, $\bar{s}_{01}$ equals $\int (2s)_{A_0}(2p_y)_{A_1} d\tau$, and $\bar{s}_{05}$ equals $\int (2s)_{A_0}(2p_z)_{A_5} d\tau$, each. The local ligand–ligand overlap integrals may be adapted from expressions tabulated by Kotani, Amemiya, Ishiguro, and Kimura[81] or be evaluated directly.[82] The related group overlap integrals for the functions $\bar{\Sigma}_0{}^{(1,2)}$, $\bar{\Sigma}_0{}^{(+)}$, $\bar{\Sigma}_\pm{}^{(1,2)}$ and $\bar{\Sigma}_\pm$ are speedily obtained from those for $\Sigma_0{}^{(1,2)}$, $\Sigma_0{}^{(+)}$, $\Sigma_\pm{}^{(1,2)}$, and $\Sigma_\pm$ enscrolled above by the substitution of $k_p \cos \alpha + (\rho^{s(\frac{1}{2})}/\rho^{c(\frac{1}{2})}) \sin \alpha$ everywhere for $k_p \cos \alpha$. Please note that the functions Π_s and $\bar{\Pi}_s{}^{(1,2)}$ [but not the Σ_s and $\bar{\Sigma}_s$, (see eq. A-12 above)], $(s = 0, \pm 1)$, normalize *exactly* to $1/2$ as a consequence of their textual definition [compare eq. 9 and 24 with Table V].

(82) See ref. 73b, topic B, Appendix.

The Denaturation and Aggregation of Ovalbumin by

Urea in Neutral Solutions

by Walter L. Gagen and John Holme

The Procter and Gamble Company, Miami Valley Laboratories, Cincinnati 39, Ohio   (*Received April 13, 1963*)

Physical properties, such as optical rotation, viscosity, sedimentation, ultraviolet absorption, and partial specific volume of ovalbumin exposed to urea in neutral solutions have been examined. In addition, the reactivity of SH groups in such solutions has been determined by amperometric titration. The changes which occur in these parameters during extended exposure to 6 M urea solutions have been shown to be related to the production of an aggregated form of the ovalbumin macromolecule. Although indirect evidence (*e.g.*, increased levorotation) might suggest that the aggregated form has as its precursor a denatured species, no *direct* evidence for such a species in urea solutions was observed. The conformation of native ovalbumin in urea solutions is not markedly different from its conformation in simple salt solutions. The significant reductions in intrinsic sedimentation coefficients noted in such solutions are adequately described by changes in selective solvation parameters and are not indicative of changes in molecular asymmetry.

Introduction

The examination of changes in various physical and chemical properties that may be related to the denaturation and aggregation of ovalbumin in urea solutions has drawn the attention of numerous workers.

The changes in optical rotation, viscosity, and the gelation of ovalbumin during exposure to various concentrations of urea have been studied by Simpson and Kauzmann,[1] Frensdorff, *et al.*,[2] and Steven and Tristram.[3] The latter workers, in addition, have measured changes in molar extinction coefficients at 295 mμ and, after iodination, at 310 mμ. Imahori[4] and Schellman and Schellman[5] have studied the optical rotatory dispersion of ovalbumin in concentrated urea solutions, while partial specific volume measurements in such systems have been made by McKenzie, *et al.*,[6] and Charlwood.[7] The volume changes accompanying the exposure of this protein to urea have been measured dilatometrically by Christensen[8] and Simpson and Kauzmann.[1]

Generally, these and other similar studies have been interpreted to indicate the existence of a denatured species of ovalbumin in concentrated urea solutions, although Imahori[4] has found that β-form association can and does occur in such solutions.

Recent studies by Holme[9] on the thermal denatura-

tion of ovalbumin have shown, however, that *only* native and aggregated forms of ovalbumin are found in heated solutions. The present study was initiated in an effort to determine whether such was also the case for urea denaturation, and if not, to isolate and characterize the denatured species.

Experimental

Materials. A single lot of crystalline, lyophilized ovalbumin, purchased from Worthington Biochemical Corp., was used throughout. Reagent grade urea and buffer salts were used without further purification.

Preparation of Ovalbumin–Urea Solutions. Ovalbumin was dissolved in distilled water (previously

(1) R. B. Simpson and W. Kauzmann, *J. Am. Chem. Soc.*, **75**, 5139 (1953).
(2) H. K. Frensdorff, W. T. Watson, and W. Kauzmann, *ibid.*, **75**, 5157 (1953).
(3) F. S. Steven and G. R. Tristram, *Biochem. J.*, **73**, 86 (1959).
(4) K. Imahori, *Biochim. Biophys. Acta*, **37**, 336 (1960).
(5) J. A. Schellman and C. Schellman, *Compt. rend. trav. lab. Carlsberg, Ser. chim.*, **30**, 363 (1958).
(6) H. A. McKenzie, M. B. Smith, and R. G. Wake, *Nature*, **176**, 738 (1955).
(7) P. A. Charlwood, *J. Am. Chem. Soc.*, **79**, 776 (1957).
(8) L. K. Christensen, *Compt. rend. trav. lab. Carlsberg, Ser. chim.*, **28**, 37 (1952).
(9) J. Holme, *J. Phys. Chem.*, **67**, 782 (1963).

adjusted to pH 7.0) or phosphate buffer (pH 7.0, ionic strength 0.1). To this was added an equal volume of urea solution, pH 7.0, freshly prepared to avoid the complications of cyanate formation.[10] The solutions were then mixed by very gentle stirring. The final concentrations of ovalbumin and urea are given in the individual experiments. Protein concentrations were determined by semimicro Kjeldahl nitrogen analysis (% N × 6.3) in the absence of urea, and by differential refractometry in the presence of urea.

Density. Solution densities were measured at 30 ± 0.02° using 25-ml. pycnometers. All samples were equilibrated in a constant temperature bath for about 30 min. prior to weighing.

Partial Specific Volume. The conventional pycnometric technique[11] and the ultracentrifugal technique proposed by Martin, *et al.,*[12] were both used for the determination of partial specific volumes.

Using the conventional technique, the apparent partial specific volume, ϕ, at ovalbumin concentrations from 0.23 to 1.80% was calculated from the equation[13]

$$\phi = \frac{1}{\rho_s}\left[1 - \frac{\Delta\rho}{c}\right]$$

where ρ_s is the density of the solvent, $\Delta\rho$ is the increment in density due to the solute, and c is the solute concentration in g./ml. Since ϕ was observed to be independent of ovalbumin concentration, the partial specific volume, $\bar{V}$, was determined as the average of the ϕ-values determined at the various concentrations.

Sedimentation measurements in H_2O and D_2O (at an ovalbumin concentration of 0.25%) permitted calculation of the partial specific volume by the equation of Martin, *et al.*[12]

$$\bar{V} = \left(\frac{\eta_2}{\eta_1} - k\frac{S_1}{S_2}\right)\left(\rho_1\frac{\eta_2}{\eta_1} - \rho_2\frac{S_1}{S_2}\right)^{-1}$$

where η_1, ρ_1, and S_1 are the viscosity, density, and sedimentation coefficients, respectively, in H_2O and η_2, ρ_2, and S_2 are the comparable values in D_2O. A value for k, the ratio of the molecular weights in the two media, 1.015, was calculated from the amino acid composition.

Viscosity. Relative viscosities were determined from the product of the ratio of flow times for solution and solvent and the ratio of their densities, in the usual manner. Flow times were determined at 30 ± 0.2° using an Ostwald–Fenske viscometer having a flow time for phosphate buffer of 59.4 sec. Viscosities are expressed, throughout this paper, in units of (g./

100 ml.)⁻¹. Kinetic correction factors were found to be negligible and were therefore omitted.

Optical Rotation A Rudolph precision polarimeter equipped with a mercury light source (5461 Å.) and a water-jacketed 1-dm. cell maintained at 30 ± 0.2° was used for all optical rotation measurements.

Ultracentrifugation. Sedimentation analyses were made using a Spinco Model E ultracentrifuge equipped with temperature control and a phase-plate schlieren optical system. Sedimentation coefficients were determined in the usual manner[14] from plots of ln x_H vs. time, where x_H has been calculated from the maximal ordinate of the peak position. Peak areas were determined, by planimetry, from tracings of the schlieren patterns that had been enlarged fivefold. Relative concentrations were calculated from the peak areas after correction for radial dilution[14] and Johnston–Ogston[14,15] effects. The correction of sedimentation coefficients to standard conditions is treated in a later section.

Ultraviolet Absorption Spectra. The ultraviolet absorption spectra were obtained using a Beckman DU spectrophotometer with matched 1.00-cm. silica cells. In addition, a limited number of spectra were obtained using a Cary Model 14 recording spectrophotometer with matched 1.00-cm. cells.

Sulfhydryl Determinations. Sulfhydryl groups were measured in TRIS buffer by amperometric titrations[16,17] utilizing silver- or mercury-plated rotating platinum electrodes operating at potentials of -0.1 and -0.2 v./ v., respectively. Titrations were carried out with 10^{-3} M silver nitrate or 10^{-3} M mercuric chloride solutions.

Results and Discussion

Properties of Native Ovalbumin in Urea Solutions. Obviously, the definition of a denatured state of a protein macromolecule in solution requires previous definition of the macromolecule's native state. In this study, the native state was defined as that conforma-

(10) G. R. Stark, W. H. Stein and S. Moore, *J. Biol. Chem.,* **235,** 3177 (1960).

(11) T. Svedberg and K. O. Pedersen, "The Ultracentrifuge," Oxford University Press, London, 1940.

(12) W. G. Martin, W. H. Cook, and C. A. Winkler, *Can. J. Chem.,* **34,** 809 (1956).

(13) E. F. Casassa and H. Eisenberg *J. Phys. Chem.,* **65,** 427 (1961).

(14) H. K. Schachman, "Ultracentrifugation in Biochemistry," Academic Press, New York, N. Y., 1959.

(15) J. P. Johnston and A. G. Ogston, *Trans. Faraday Soc.,* **42,** 789 (1946).

(16) R. E. Benesch, H. A. Lardy, and R. Benesch, *J. Biol. Chem.,* **216,** 663 (1955).

(17) I. M. Kolthoff, W. Stricks, and L. Morren, *Anal. Chem.,* **26,** 366 (1954).
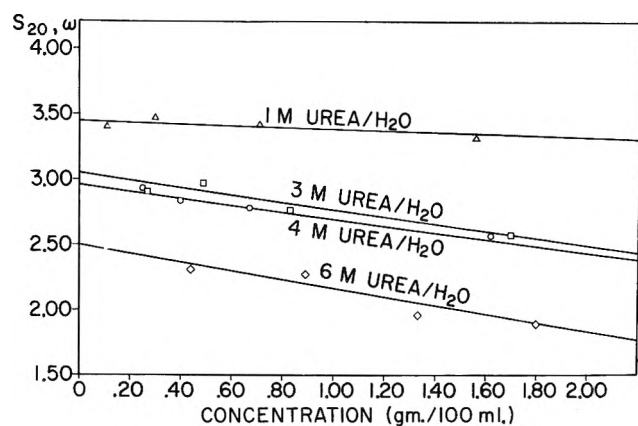
Figure 1. Concentration dependence of sedimentation for ovalbumin in 1, 3, 4, and 6 M urea–water solutions. $s_{20,w}$ values corrected in usual manner ($\bar{V} = 0.750$; see text).

tion naturally assumed by the ovalbumin macromolecule immediately after dissolution in urea solution. In order to define such a state in terms of physical parameters, the properties of ovalbumin immediately after dissolution (or as soon thereafter as experimentally possible) were studied as functions of both urea and protein concentration.

a. *Viscosity.* The reduced viscosities of ovalbumin in 1–6 M urea solutions were measured at various protein concentrations from 0.23 to 1.80%. The intrinsic viscosity (*i.e.*, the reduced viscosity extrapolated to infinite dilution) was found to be 0.040 ± 0.005 regardless of urea concentration.

b. *Optical Rotation.* From measurements of the optical rotation of ovalbumin (at 5461 Å.) as a function of protein concentration in 4 and 6 M urea solutions, it was found that the specific rotation increased only slightly with protein concentration. The specific rotation at infinite dilution was −35 ± 3°.

c. *Sedimentation.* The concentration dependence of sedimentation for ovalbumin in urea solutions was found to be influenced markedly by the urea concentration. If one corrects the sedimentation coefficients to the usual standard conditions,[11,14] the plots shown in Fig. 1 are obtained. Obviously, either the intrinsic sedimentation coefficient is lowered in the presence of urea or the standard conditions correction is not adequate. In attempting to choose between these alternatives, one is immediately confronted with the problem of "correcting" sedimentation coefficients to "standard conditions." Schachman and Lauffer[18] have shown, in studies on tobacco mosaic virus in 40% sucrose solutions, that selective solvation can lead to serious errors in the correction of sedimentation data. As pointed out by these workers, sedimentation data

can be corrected for selective solvation through the substitution of an arbitrarily defined parameter, $\bar{V}_h$ (designated in this paper as the hydrodynamic or effective partial specific volume), for $\bar{V}$ in the standard conditions correction equation. The parameter $\bar{V}_h$ is defined, in hydrodynamic terms, as the reciprocal of the medium density at which the product $\eta s = 0$; *i.e.*

$$\bar{V}_h = 1/\rho^0$$

where ρ^0 is the medium density at $\eta s = 0$ (obtained from the linear plot of ηs *vs.* ρ for the protein in solvents of different viscosity and density). Calculation of $\bar{V}_h$ was accomplished by sedimentation of ovalbumin in H_2O and D_2O containing 3–6 M urea according to the technique of Martin, *et al.*[12] By this technique a value of 0.80 ± 0.01 was found for $\bar{V}_h$. If this value for the *effective* partial specific volume is substituted for $\bar{V}$ (the thermodynamic partial specific volume) in the usual standard conditions correction equation, the sedimentation data shown in Fig. 1 extrapolate to approximately the *same* value (3.5 svedbergs) at *all* urea concentrations. Additional studies concerning the parameter $\bar{V}_h$ and the effect of various additives upon this parameter are now in progress but, for the present study, one need not be disconcerted by the concept of visualizing $\bar{V}_h$ as an *effective* partial specific volume since an alternative procedure for treating the present data is available.

The equation for sedimentation in a mixed-solvent system

$$Nfs = M_p(1 - \bar{V}_p\rho) + \alpha M_1(1 - \bar{V}_1\rho)$$

permits the calculation of sedimentation coefficients in such systems if the selective interaction parameter, α, is known. As shown by Schachman,[14] this parameter can be obtained in a manner similar to that described for $\bar{V}_h$ determinations (*i.e.*, from plots of ηs *vs.* ρ). Thus, as an alternative to the concept of an *effective* partial specific volume, one can determine the selective interaction parameter α (in this instance, 1.39×10^3 moles/mole), use this value in the equation for sedimentation in a mixed-solvent system, and describe the characteristics of *native* ovalbumin in such systems solely in terms of selective interactions. This procedure leads to intercepts ($s_{20,w}^0$) similar to those shown in Fig. 1.

The "β-function" of Scheraga and Mandelkern,[19] which combines data from intrinsic viscosity and sedi-

(18) H. K. Schachman and M. A. Lauffer, *J. Am. Chem. Soc.*, 72, 4266 (1950).

(19) H. A. Scheraga and L. Mandelkern, *ibid.*, 75, 179 (1953).

mentation measurements, allows one to describe more adequately the conformation of a macromolecule in solution (in terms of an effective ellipsoid of revolution) than does either measurement alone. Calculation of β-functions for ovalbumin in 1–6 M urea solutions yields values, at all urea concentrations, not unlike those observed in simple salt solutions (i.e., $\sim 2.4 \times 10^6$). Although the relationship between the effective ellipsoid and the actual conformation of the macromolecule in solution cannot be ascertained from these measurements, it seems obvious that nothing resembling a major conformational change occurs upon the introduction of urea to a neutral solution of ovalbumin. Hence, the decreased intrinsic sedimentation coefficients noted in urea solutions evidently result from factors associated with $\bar{V}_h$ and not from changes in molecular asymmetry.

d. Partial Specific Volume. The partial specific volume of ovalbumin in H_2O was determined pycnometrically to be 0.752. In excellent agreement with this was the value of 0.750 obtained by the ultracentrifugal method.

However, in 3 M urea solution, a partial specific volume of 0.730 ± 0.025 was found by the pycnometric method, while the ultracentrifugal method, as mentioned in the previous section, yielded a value of 0.80 ± 0.01, presumably due to selective solvation effects.

e. Sulfhydryl. The sulfhydryl content of ovalbumin in H_2O and 4 and 8 M urea solutions was found to be 3.9, 4.4, and 4.4 moles of SH/mole of ovalbumin, respectively, when determined by mercurimetric amperometric titration.

On the other hand, argentimetric titrations yielded a value of 3.9 moles of SH/mole of ovalbumin, regardless of urea concentration.

f. Discussion of the Native State. An isotropically expanded or swollen state has been observed in the urea denaturation of bovine mercaptalbumin by Kay and Edsall,[20] for bovine serum albumin by Doty and Katz,[21] for bovine fibrinogen by Scheraga, et al.,[22] and has been suggested by Scheraga and Mandelkern[19] as an explanation for the diffusion and viscosity behavior of horse serum albumin noted by Neurath and Saum.[23] The increased reactivity of the SH groups of ovalbumin to Hg^{+2} ions might suggest that similar swelling behavior also occurs in urea solutions. (The failure of Ag^+ ions to react with such SH groups could be the result of steric hindrances imposed upon the somewhat larger Ag^+ ions.) However, such expansion or swelling would be expected to manifest itself, assuming the shape factor remains constant, as an increase in the intrinsic viscosity. Within the limits of experimental error, no obvious differences between the in-
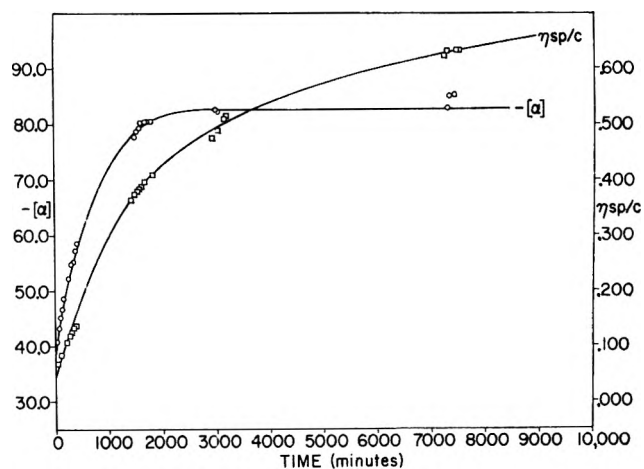
Figure 2. The effect of exposure time on the specific rotation and reduced viscosity of ovalbumin in 6 M urea–water.

trinsic viscosity of ovalbumin in simple salt solutions and that in urea solutions have been noted.

From these various observations, it would appear that native ovalbumin in urea solution at neutral pH assumes a conformation not markedly different from its conformation in simple salt solutions. The significant reductions in the intrinsic sedimentation coefficients noted in such solutions are readily understood in terms of selective solvation effects and are not indicative of changes in molecular asymmetry.

Properties of Ovalbumin during Extended Exposure to 4 M Urea Solution. The specific rotation and reduced viscosity of ovalbumin at a concentration of 1.80% in 4 M urea–water at pH 7.0 were determined at various time intervals during an extended period of exposure at 30 ± 0.2°. The specific rotation was −35 ± 2° and the reduced viscosity was 0.038 ± 0.003 during the entire 0–348 min. observational period.

Studies of a similar nature on ovalbumin in 4 M urea–phosphate buffer at pH 7.0 yielded results not unlike those obtained with 4 M urea–water.

Evidently, the presence of 4 M urea in neutral solutions of ovalbumin produces no marked time-dependent changes in the optical rotation and viscosity of such solutions. The present data, together with data reported by others,[1-3] indicate that the native state of

(20) C. M. Kay and J. T. Edsall, *Arch. Biochem. Biophys.*, **65**, 354 (1956).

(21) P. Doty and S. Katz, Abstracts, 118th National Meeting of the American Chemical Society, Chicago, Ill., September, 1950, p. 14C.

(22) H. A. Scheraga, W. R. Carroll, L. F. Nims, E. Sutton, J. K. Backus, and J. M. Saunders *J. Polymer Sci.*, **14**, 427 (1954).

(23) H. Neurath and A. M. Saum, *J. Biol. Chem.*, **128**, 347 (1939).

Table I : Sedimentation Characteristics of 1.8% Ovalbumin during Extended Exposure to 6 M Urea–Water

Exposure time, min.	$-s_{20,w}$ svedbergs				Relative concentration, %	
	$\bar{V} = 0.75$		$\bar{V}_h = 0.80$			
	Component A	Component B	Component A	Component B	Component A	Component B
25	2.09	...	...	...	100	...
105[a]	2.16	...	2.92	...	~100	...
285[a]	1.91	...	2.58	...	~100	...
717	2.26	~2.8	3.05	~3.8	56	44
1,085	2.43	3.29	3.28	4.43	45	55
1,228	2.00	2.92	2.70	3.95	22	78
1,254	2.07	2.76	2.80	3.73	18	82
1,444	~1.9	2.61	~2.6	3.53	14	86
1,862	~1.9	2.60	~2.6	3.51	10	90
7,214	...[b]	2.21	...[b]	2.99	v. sm.	~100
11,588	...[b]	2.03	...[b]	2.74	v. sm.	~100

[a] Indications of heterogeneity.   [b] Values not determinable.

ovalbumin in urea solutions is stable for prolonged time intervals if the urea concentration is less than 5–6 M.

Properties of Ovalbumin during Extended Exposure to 6 M Urea Solution. a. Optical Rotation, Viscosity, and Sedimentation. Denaturation of proteins by reagents such as urea is generally considered to involve a rather marked unfolding of the naturally-occurring folded macromolecular structure leading to increases in levorotation and reduced viscosity. Aggregation or dissociation into sub-units is frequently observed, but such processes are generally considered to be secondary phenomena.

The specific rotation, reduced viscosity, and sedimentation characteristics of ovalbumin at a concentration of 1.80% in 6 M urea–water and 6 M urea–phosphate buffer at pH 7.0 were examined at various time intervals during an extensive period of exposure at $30 \pm 0.2°$. As shown in Fig. 2, the changes in specific rotation and reduced viscosity in 6 M urea–water solutions take place in two fairly distinct stages: (1) a relatively rapid, initial stage, during which both the specific rotation and reduced viscosity increase at rather rapid rates, lasting for about 1500–2000 min.,

and (2) a relatively slow, secondary stage during which the reduced viscosity continues to increase, although at a somewhat slower rate, after the specific rotation values have reached a plateau. The data for ovalbumin in 6 M urea–phosphate buffer are similar in most respects to those obtained for 6 M urea–water solutions. The primary difference would seem to be that the increases in these parameters occur at a slightly diminished rate and reach lower final values in the presence of phosphate ions.

The sedimentation characteristics of 1.8% ovalbumin in 6 M urea–water solutions show rather marked changes during exposure. Initially, a single, relatively symmetrical, slow-moving boundary, as shown in Fig. 3A, is observed. After progressively longer standing intervals, sedimentation patterns show increasing boundary asymmetry until, after approximately 700 min., a second, slightly faster-moving boundary is resolved (*e.g.*, Fig. 3B). The relative concentration of this faster-moving component progressively increases while that of the slower-moving component decreases (see Fig. 3C), indicating conversion of the slower species to the faster species. Continued exposure yields sedimentation patterns, such as that shown in Fig. 3D, exhibiting an increased sharpening of the faster-moving boundary, and eventually a single, hyper-sharp boundary of gradually decreasing sedimentation rate. This hyper-sharpness and the decreasing sedimentation rate are typical of gels and gel-like materials and are not unexpected in such viscous solutions. The sedimentation data, corrected to standard conditions using $\bar{V} = 0.75$ and $\bar{V}_h = 0.80$, are tabulated in Table I.

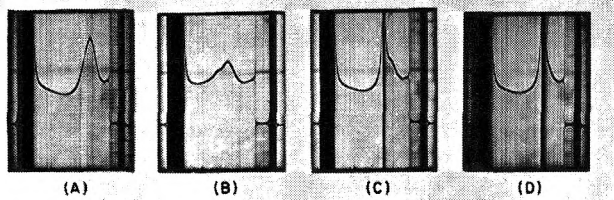The aggregation process begins immediately and closely parallels in extent the changes in optical rotation

Figure 3. Sedimentation patterns for ovalbumin in 6 M urea–water at pH 7.0; speed 59,780 r.p.m.; bar angle = 60°; samples exposed to urea solution, prior to sedimentation analysis, for (A) 24 min.; (B) 1085 min.; (C) 1254 min.; and (D) 11,588 min.

Table II : Sedimentation Characteristics of 1.8% Ovalbumin during Extended Exposure to 6 M Urea-Phosphate

Exposure time, min.	$s_{20,w}$ -svedbergs						Relative concentration, %		
	$\overline{V} = 0.75$			$\overline{V}_h = 0.80$					
	Component A	Component B	Component C	Component A	Component B	Component C	Component A	Component B	Component C
26	2.11	...	...	2.85	...	...	100	..	..
1087	2.20	3.81	...	2.98	5.16	...	40	60	..
1406	2.27	3.81	>3.8	3.07	5.14	>5.1	15	60	25
2843	...	3.96	4.56	...	5.35	6.16	...	55–60	·40–45
7230	...	3.64	4.18	...	4.92	5.65	...	48	52

and viscosity which occur as a function of exposure time, as shown in Fig. 4. Here sedimentation results are superimposed on the optical rotation and viscosity measurements as a function of exposure time.

The results of sedimentation measurements in 6 M urea-phosphate buffer, although less extensive in nature, apparently differ slightly from those observed in urea-water solutions. The resolution of two faster-moving species and slightly increased sedimentation coefficients, the latter presumably due to decreased solution viscosity and diminished charge effects, are the primary differences. These data are shown in Table II.

Several additional sedimentation studies, tabulated in Table III, were conducted on 1.8% ovalbumin exposed to 6 M urea-water, then dialyzed against phosphate buffer prior to sedimentation analyses. As expected, the relative concentration of the monomeric species progressively decreases with time in favor of an aggregated species.

In a second series, a similar concentration of ovalbumin was exposed to 6 M urea-water or 6 M urea-

Table III : Sedimentation Characteristics of 1.8% Ovalbumin in Phosphate Buffer after Extended Exposure to 6 M Urea-Water

Exposure time, min.	$s_{20,w}$, svedbergs		Relative concentration, %	
	$\overline{V} = 0.75$			
	Component A	Component B	Component A	Component B
140	3.2	~10.5	84	16
1,082	3.4	~13.5	40	60
11,000	3.4	~11.9	17	83

phosphate buffer for approximately 1085 min., then subjected to sedimentation analyses under various conditions of solvent environment. The results, shown in Table IV, indicate further the integrity of the two sedimenting species, their relative concentrations not being appreciably altered by mild variations in the solvent medium.

Figure 4. The effect of exposure time on the specific rotation, reduced viscosity, and extent of aggregation of ovalbumin in 6 M urea-water.

Table IV : Sedimentation Characteristics of 1.8% Ovalbumin in Various Media after Extended Exposure to 6 M Urea Solution

Sample A

Exposed @ 30° to 6 M urea-PO₄ for 1087 min.

Sedimentation in 6 M urea-PO₄:
Component 1   2.48 S (40%)
Component 2   4.00 S (60%)

Dialysis vs. H₂O

Sedimentation in H₂O:
Component 1   2.23 S (35%)
Component 2   4.63 S (65%)

Added PO₄ salts

Sedimentation in phosphate buffer:
Component 1   3.45 S (40%)
Component 2   ~13.5 S (60%)

Sample B

Exposed @ 30° to 6 M urea-H₂O for 1082 min.

Added PO₄ salts

Sedimentation in 6 M urea-PO₄:
Component 1   2.89 S (35%)
Component 2   3.48 S (65%)

Dialysis vs. H₂O

Sedimentation in H₂O:
Component 1   2.02 S (30%)
Component 2   4.81 S (70%)

Added PO₄ salts

Sedimentation in phosphate buffer:
Component 1   3.43 S (40%)
Component 2   ~13.5 S (60%)

Figure 5. Ultraviolet absorption spectra for ovalbumin
exposed to 6 M urea-water (concn. = 0.1998 g./100 ml.):
O, 0 min.; △, 30 and 140 min.; and □, 1380 min.
Since the values determined at 30 and 140 min.
were identical, both are identified by the same symbol.
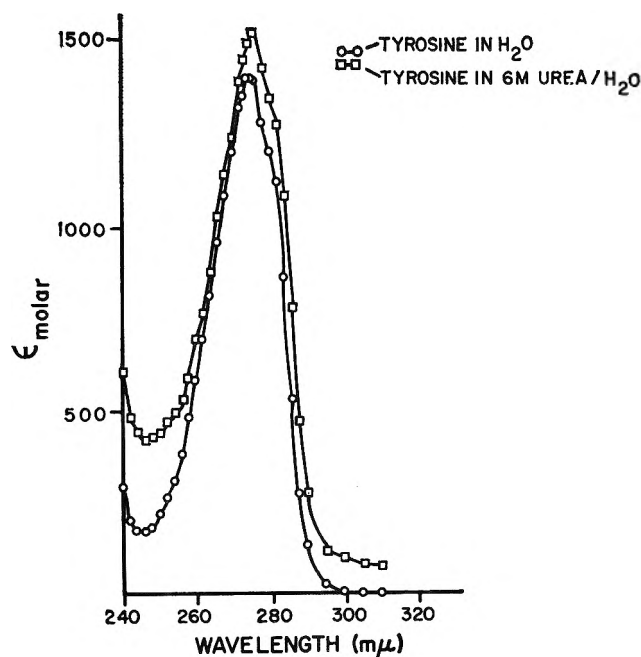
Fig. 6. Ultraviolet absorption spectra for
tyrosine: O, in water; □, in 6 M urea-water.

b. Ultraviolet Absorption Spectra. The ultraviolet absorption spectra for ovalbumin in 6 M urea-water after exposure intervals of 0, 30, 140, and 1380 min. are shown in Fig. 5. The only spectrum which appears to be different from the initial spectrum is that for the 1380-min. sample, which contains more than 80% aggregated form as determined by sedimentation analysis. The spectral broadening and general intensification of absorbancy indicated in Fig. 5 is also evidenced in positive difference spectra obtained on similar solutions using a Cary Model 14 recording spectrophotometer. (It should be pointed out that although the ovalbumin concentrations *during* urea exposure were 1.80%, the ultraviolet spectra were obtained *after* dilution to 0.1–0.2% with urea solution.)
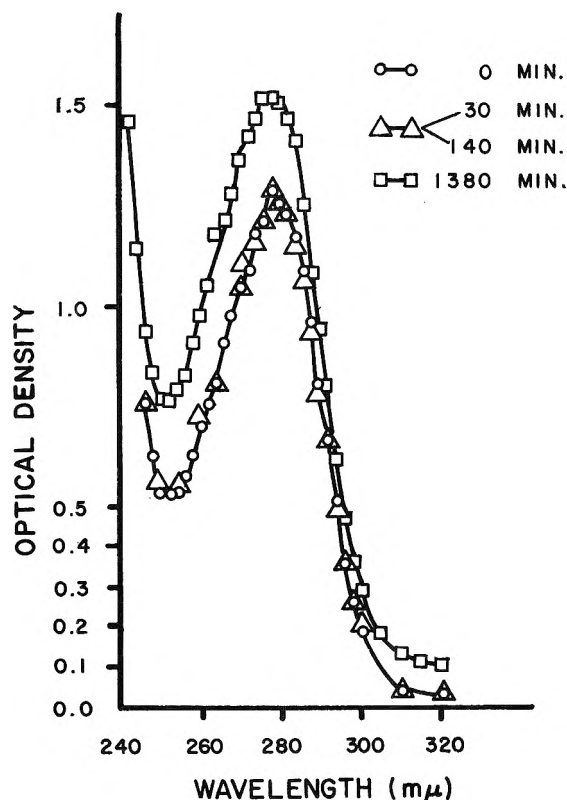
The ultraviolet absorption spectrum of tyrosine, at pH 7.0, is altered significantly by the presence of 6 M urea as shown in Fig. 6. Wetlaufer, *et al.*,[24] have previously reported the difference spectrum of *isoelectric* tyrosine in 6 M urea. Yanari and Bovey[25] have questioned the significance of difference spectra as a measure of solvent-induced spectral shifts. As shown in Fig. 6, the presence of 6 M urea at pH 7.0 does result in both spectral broadening and over-all absorption increases, the primary objectionable aspects indicated by Yanari and Bovey.[25] However, when plotted as difference spectra (*i.e.*, $\Delta\epsilon = \epsilon_{urea} - \epsilon_{water}$ *vs.* λ) a readily discernible "red shift" with maxima at 286 and 278 mμ is indicated in good agreement with the data of Wetlaufer, *et al.*[24] The rather marked increase in absorption in the 295–310-mμ range, which was not noted by Wetlaufer, *et al.*,[24] probably results from the spectral broadening and intensification effects, since Rayleigh scattering corrections have been found to be negligible.

Bigelow and Geschwind[26] have reported similar spectral shifts for tryptophan produced by 3 and 7.5 M urea in 0.1 M KCl. In the present study, individual spectra for tryptophan, at pH 7.0, in water and in 6 M urea-water have been obtained. Although the individual spectra did not appear to be markedly different (probably as a result of the rather low concentration of tryptophan; 1.05×10^{-4} M), the difference spectrum calculated from such measurements was quite similar to that reported by Bigelow and Geschwind.[26]

Hence, the changes in absorption characteristics observed in urea solutions of ovalbumin could result

(24) D. B. Wetlaufer, J. T. Edsall, and B. R. Hollingworth, *J. Biol. Chem.*, 233, 1421 (1958).

(25) S. Yanari and F. A. Bovey, *ibid.*, 235, 2818 (1960).

(26) C. C. Bigelow and I. I. Geschwind, *Compt. rend. trav. lab. Carlsberg*, 31, 283 (1959).

simply from an increased susceptibility of the amino acid residues of the aggregated form to solvent effects in such systems. One cannot, however, overlook the possibility that increased scattering, arising from the aggregation process, could also result in similar behavior. Since Rayleigh scattering corrections were not calculated, the choice between these alternatives cannot be made. Nevertheless, it should be emphasized that *no* spectral change was observed until an appreciable concentration of the aggregated form was produced.

c. Discussion of the Effects of Extended Exposure to 6 M Urea Solution. Simpson and Kauzmann[1] have previously reported observing changes in the specific rotation and reduced viscosity of ovalbumin in concentrated urea solutions which indicated the occurrence of two relatively distinct stages in the denaturation process. It was suggested that the first stage results from an unfolding of the macromolecule, leading to increased levorotation and viscosity, followed by secondary aggregation processes which in the second stage become predominant and produce continued increases in viscosity without further changes in specific rotation.

The optical rotation and viscosity measurements reported here confirm the observation that the changes in these parameters occur in two fairly distinct stages. The sedimentation studies, however, indicate that the observed increases in specific rotation and reduced viscosity are closely paralleled, even during the first stage, by increases in the amount of an aggregated form of ovalbumin in such solutions. Sedimenting species other than the native form or the aggregated forms of ovalbumin have not been observed in such solutions. These observations are similar to the heat denaturation studies of Holme[9] which also yielded evidence for the presence of *only* native and aggregated forms of ovalbumin in heated solutions.

In a sequence, native (N) $\overset{k_1}{\rightleftarrows}$ denatured (D) $\overset{k_2}{\rightarrow}$ aggregate (A), the present results would demand that k_2 be very large in comparison with k_1. However, this in no way implies how D, the necessary intermediate, differs from N, and the present study (and similar studies in the 1–2% protein concentration range) does not provide any assistance here. Studies at lower protein concentrations might be expected to reduce the rate of aggregation and consequently permit one to observe the denatured intermediate. However, because of the relatively small differences in sedimentation coefficients and the large Johnston–Ogston effects, the presence of the aggregate in such solutions would be more difficult to detect by sedimentation in urea.

It has been noted in these studies that the changes in solution properties, including ultraviolet absorption spectra, which occur during exposure to urea, are closely paralleled by the production of aggregated forms. It might be possible that some conformational changes in the monomer take place during or after the aggregation process which make unknown contributions to the properties of such solutions. This would not imply that the aggregation process precedes denaturation (the changes in optical rotation would seemingly preclude this), but simply that the solution properties might be markedly influenced by the aggregation process. It can be concluded that solutions of ovalbumin upon exposure to urea under the conditions described here do not contain a detectable denatured monomer and should not be expected to exhibit properties solely characteristic of the intramolecular change commonly referred to as urea denaturation.

Addendum

Since submission of the present paper, the authors have become aware of the observations on bovine serum albumin and ovalbumin reported by McKenzie, Smith, and Wake[27] and Glazer, McKenzie, and Wake.[28]

The difference spectrum for ovalbumin in 7 *M* urea solution reported by the latter authors[28] (see their Fig. 4) would appear to be in disagreement with the spectra reported in the present paper (see Fig. 5) for 6 *M* urea solutions. However, difference spectra obtained by the present authors, using a Cary Model 14 recording spectrophotometer and employing a modification of the "tandem-cell" technique of Herskovits and Laskowski,[29] have essentially confirmed *both* sets of data under the particular conditions of pH, salt concentration, protein concentration, and urea concentration employed.

(27) H. A. McKenzie, M. B. Smith, and R. G. Wake, *Biochim. Biophys. Acta*, **69**, 222 (1963).

(28) A. N. Glazer, H. A. McKenzie, and R. G. Wake, *ibid.*, **69**, 240 (1963).

(29) T. T. Herskovits and M. Laskowski, Jr., *J. Biol. Chem.*, **237**, 2481 (1962).

The Thermal Decomposition of Irradiated Nickel Oxalate[1]

by Joseph Jach[2]

State University of New York, Stony Brook, New York

and Maurice Griffel[3]

U. S. Naval Postgraduate School, Monterey, California   (*Received May 16, 1963*)

The thermal decomposition of unirradiated and reactor-irradiated dehydrated nickel oxalate has been studied in the temperature range 253–360°. Reaction begins at surface nuclei and there is evidence that the activation energy for nucleus formation is less than for the growth process. In those temperature regions where the amount of decomposition due to the growth of existing nuclei overshadows that due to growth of newly formed nuclei, the acceleratory region is described by a t^2 law. The value of the fraction of total decomposition (α) at the point where the rate is a maximum (the point of inflection) changes drastically with temperature and irradiation. Irradiation appears to increase the number of potential nuclei but does not enhance the growth rate.

Several recent studies[4-6] of the thermal decomposition of nickel oxalate have been published. Attention has also been given to the compound silver oxalate[7,8] which behaves similarly to the nickel salt. In both cases the curve representing α, the fraction of the total decomposition, *vs.* time is sigmoidal. Apparently conflicting rate laws for the acceleratory region have been reported which may be described as the "exponential" and "power" laws, given, respectively, by the equations

$$\alpha = A e^{kt} \tag{1}$$

$$\alpha = B t^m \tag{2}$$

The "exponential" form is generally regarded as indicative of a chain reaction whereby a growing nucleus can branch. The power law is interpreted in terms of a fixed topochemical decomposition scheme in which the power "m" depends upon whether the nuclei grow in one, two, or three dimensions and also depends on the law governing their rate of increase. The contradictions in the silver oxalate work have reportedly been resolved.[8] There seems to be general agreement that aging of a crystal can influence the observed kinetic scheme.

The objectives of thermal decomposition studies are twofold, *i.e.*, answers must be found to the questions where and how do reactions occur? The first question refers to the topochemical behavior while the second refers to the fundamental molecular step leading to the decomposition. Studies of the kind reported here throw light mainly on the first question and it is the object of the current investigation to find such answers with the use of irradiation which has proved to be a powerful tool in such probes.

Experimental

The nickel oxalate was prepared from the nitrate by slow precipitation at 70° in an ammonium acetate–acetic acid buffered solution with the oxalate ion

(1) Work performed primarily at Brookhaven National Laboratory and supported jointly by Picatinny Arsenal and the U. S. Atomic Energy Commission.

(2) Guest Scientist, Brookhaven National Laboratory, Upton. N. Y.

(3) Summer Visitor, Brookhaven National Laboratory. Upton, N. Y.

(4) P. W. M. Jacobs and T. Kureishy, Proceedings of the 4th International Symposium on the Reactivity of Solids, 1960, de Boer, *et al.*, Ed., Elsevier Publishing Co., Amsterdam, 1961, p. 352.

(5) J. A. Allen and D. E. Scaife, *J. Phys. Chem.*, 58, 677 (1954).

(6) V. Danes and V. Ponec. *Collection Czech. Chem. Commun.*, 23, 858 (1958).

(7) A. Finch, P. W. M. Jacobs, and F. C. Tompkins, *J. Chem. Soc.*, 2053 (1954).

(8) R. M. Haynes and D. A. Young, *Discussions Faraday Soc.*, 31, 229 (1961).

being furnished by hydrolysis of diethyl oxalate. This method, adapted from standard procedures, was used in an effort to minimize the precipitation of crystals of colloidal dimensions. The filtered precipitate was washed and dried at room temperature and then dehydrated at 200° in a muffle furnace. The particle size distribution is not known but the crystals are larger than colloidal size.

The decomposition yields only nickel and CO_2 and, within experimental error, eventually goes to completion. The course of the reaction was followed by measurement of the pressure of the CO_2 evolved in a closed system. A Pirani gage was used whose signal was reproduced on a Brown recorder so that data were obtained automatically. The reaction vessel was a long horizontal quartz tube heated by a furnace electronically controlled to ±0.1°. At the part of the tube located at the center of the furnace there was a flat depression 2.5 cm. in length. Reaction occurred in this depression. Located in front of the main furnace and concentric with the tube was an auxiliary heater which could be maintained at 200°.

About 5 mg. of the material were weighed and placed in a small platinum bucket which was attached by a long stiff wire to an iron slug. This unit was placed in the quartz tube the end of which was then closed. After evacuation to about 10^{-5} mm., the platinum bucket was moved by magnetically acting on the slug so that the sample was located in that part of the quartz tube which was maintained at 200°. To remove surface moisture it was left in this position for about 2 hr. During this time the system was still open to the vacuum pump and a liquid nitrogen trap. The pump and trap were then closed off and the sample moved further along the tube into the part heated by the furnace. The crystals were then tipped out of the bucket into the depression and the bucket withdrawn. Pressures were immediately and automatically recorded. One advantage of this system is that final dehydration took place in situ and the samples were thereafter never exposed to the atmosphere. The reaction always occurred on a surface of nickel oxide; the latter was formed by oxidation of deposited nickel by air introduced between runs. The reaction rates thus found were the same within experimental error as those obtained with a bare quartz surface. Before decomposition the dehydrated crystals were a bright yellow.

It was decided that, in the time available for this study, the most profitable experiments would be a set of runs at different temperatures using unirradiated material and a similar set for material subjected to a particular dose of irradiation. A few preliminary neutron and γ-ray irradiations at different doses were

performed in order to determine the order of magnitude of the dose which would be effective in producing large observable effects. The irradiation chosen was a reactor irradiation in the Brookhaven graphite research reactor for 390 hr. at a flux of $10^{13}/cm.^2$ sec. (of which approximately 4×10^{11} were epi-Cd) and at an ambient temperature of 70°. When the irradiated samples were transferred, they were in contact with the atmosphere. They too were subjected to the preliminary in situ heating procedure at 200° to ensure complete dehydration.

The irradiated material was found to be about 15% decomposed by the irradiation (prior to the thermal decomposition). This figure was obtained by examination of the average P_∞/w ratio where P_∞ is the final pressure developed and w is the sample mass. At the end of all runs the temperature was deliberately raised to about 400° to ensure an accurate P_∞ value. The irradiated crystals were black.

Results

The Form of the α–t Curves. The decomposition was studied in the temperature range 253–360° which represents a much wider range than had been used in previous studies. A typical plot of α, the fraction of the total decomposition, *vs.* time is shown in Fig. 1, the open circles being experimental points for unirradiated material. The general form is sigmoidal with a gradual approach to the acceleratory region. There is a small initial gas evolution of one type observed by Jacobs and Kureishy,[4] but the kinetics are obscured by the generally increasing rate before the acceleratory region proper. However, prior to the ac-
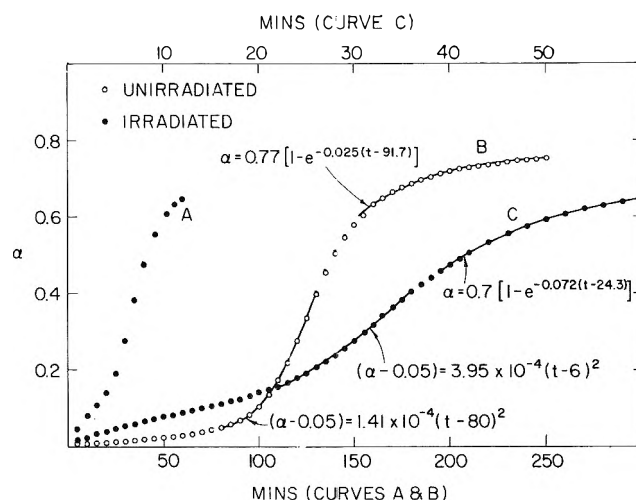
Figure 1. Fractional decomposition (α) *vs.* time:
O, run for unirradiated material at 279.9°;
●, run for irradiated material at 282.7°.
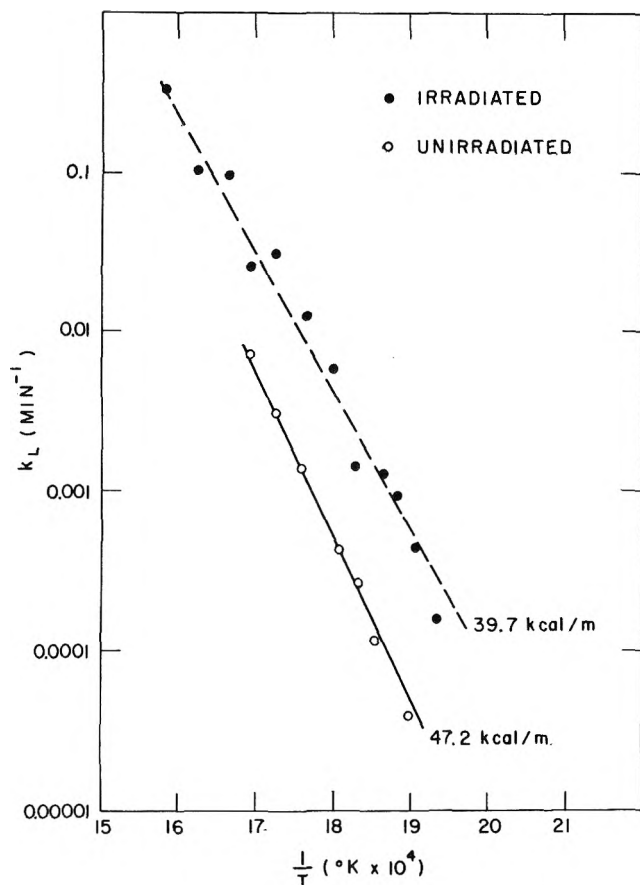
Figure 2. Arrhenius plot of k_L.

Figure 3. Arrhenius plot of k_{max}.

celeratory region proper, it is possible to discern a linear region of low rate from which some kinetic information is obtainable. This rate, k_L, is simply the slope of the line in this region. The acceleratory region is followed by a maximum rate and a subsequent decay stage. The most satisfactory equation describing the acceleratory region is

$$(\alpha - \alpha_0) = a(t - t_0)^m \qquad (3)$$

where a is a rate constant and t_0 and α_0 are constants which separate complicated initial reactions (such as initial surface reactions, etc.) from the acceleratory region.[9] This technique has been extensively used in the field and provided due care is taken in curve analysis and interpretation very much useful information can be obtained from the power "m". In the present case "m" was found to decrease somewhat with increasing values of α_0 but in general was close to a value of 2. If was found that increasing temperature brought "m" to a value of 2 with practically no α_0 correction. The same effect occurred with irradiation at all temperatures.

The decay stage is best described by a simple exponential decay of the form

$$\alpha = D\{1 - \exp[k_d(t - t_0')]\} \qquad (4)$$

Irradiation Effects. The effect of irradiation at a comparable temperature on the form of the α-t curve is shown alongside the "unirradiated" case in Fig. 1. Curve A has the same time scale as the "unirradiated" curve and shows the over-all shape. Curve C is the same run as A but with an expanded time scale to display more details about the acceleratory and decay stages. Three important effects are at once evident: (a) the time required to reach the maximum rate is drastically reduced by irradiation, (b) the value of the maximum rate itself is *not* affected (see also Fig. 3), and (c) the value of α at the point of inflection, *i.e.*, α_{max}, is reduced.

Temperature Effects. Arrhenius plots are shown for the following parameters: (1) the quantity k_L in Fig. 2; (2) the maximum rate, k_{max}, in Fig. 3 (this is

(9) Once α_0 has been chosen t_0 follows since the point α_0, t_0 corresponds to an actual point on the experimental curve.

merely the slope of the curve at the point of inflection);
(3) the quantity k_d in Fig. 4.

A few general features of these plots are worth noting.
First, irradiation has no effect on rate or activation
energy for the region beyond the acceleratory stage,
while it decreases the activation energy and increases
the rate in the early stages of the reaction. Second,
there is a complex temperature dependence of the
maximum rate in the sense that a simple classical
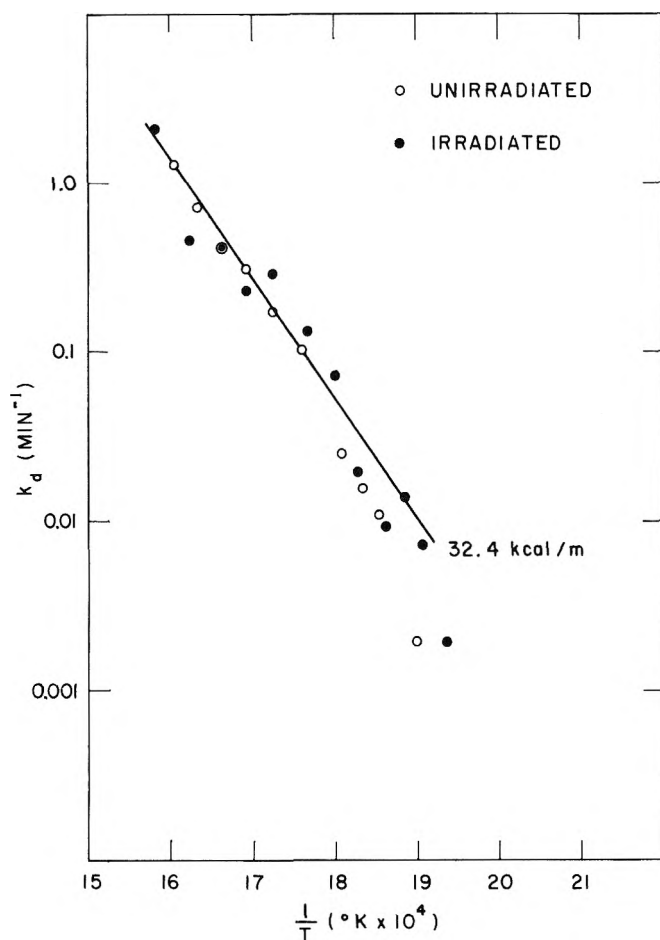
Figure 4. Arrhenius plot of k_d in the equation
$\alpha = D\{1 - \exp\{-k_d(t - t_0)\}\}$.

straight line Arrhenius plot is not observed. This
complexity is much smaller for the k_d plot, i.e., for the
end of the reaction.

Another temperature effect is that of the quantity
α_{max} which is the value of α at the inflection point or
maximum rate. A plot of this vs. temperature is
shown in Fig. 5. With unirradiated material a large
increase of α_{max} with temperature is evident (from
32% to about 48%). Irradiation results in a marked
decrease of α_{max} and although it is possible that here too
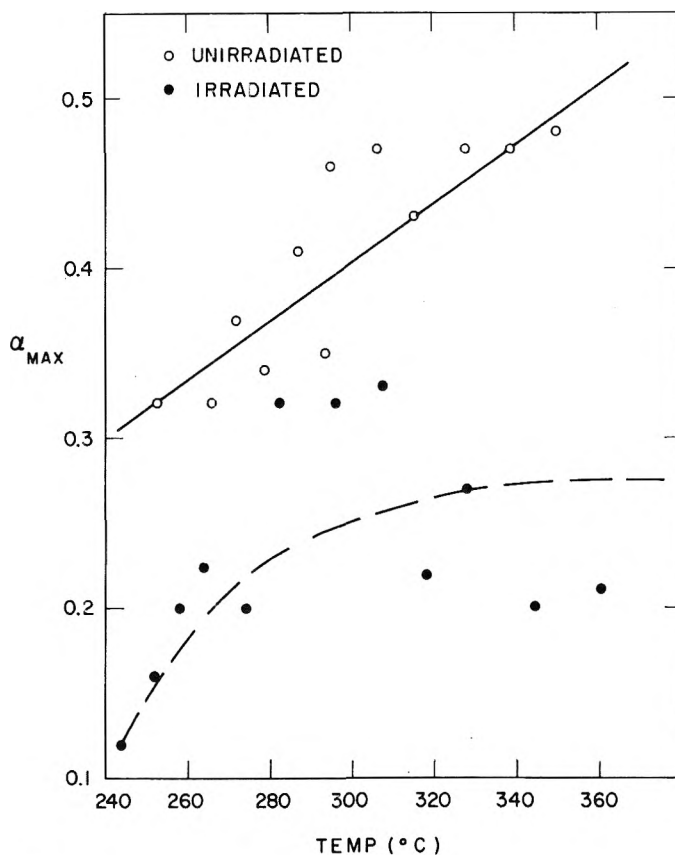
Figure 5. α_{max} vs. temperature.

an increase of temperature causes an increase in α_{max},
the scatter is too large to allow a definite conclusion.

Discussion

We believe that the results can be interpreted in
terms of the following topochemical model. Reaction
begins at the surface of each crystallite from a certain
number of potential nuclei which become activated by
change thermal fluctuations. Growth then proceeds
two-dimensionally into the crystallite, probably along
preferred planes. The square law is evidence for this.
Jacobs and Kureishy[4] draw the same conclusion. The
activation energy for the nucleation process is some-
what lower than that for growth. Irradiation greatly
enhances the number of potential nuclei but does not
affect the rate of growth.

The justification for this model is as follows. The
complexity in the Arrhenius plot indicates that two
or more processes of different activation energies are
occurring simultaneously. There are many reasons for
believing that these two processes are nucleation and
growth. At the beginning of the reaction these two
processes would occur simultaneously and the activa-
tion energy (k_L) would represent some complex com-
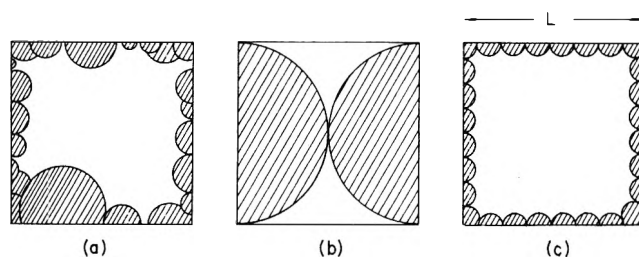
Figure 6. Simplified topochemical model.

posite of that for nucleation and growth and would be higher than for growth alone. At the end of the reaction where nucleation is either complete or its effects completely dominated by growth, the activation energy (k_d) is much lower and represents growth alone.[10] If the activation energy for growth is higher than for nucleation, it is expected that at elevated temperatures growth would dominate the rate $(d\alpha/dt)$. This is responsible for the diminishing value of the slope in the Arrhenius plot at high temperatures. The fact that the value of the power "m" settles down to a value of 2 (even for no α_0 correction) at high temperatures tends to confirm the hypothesis that growth alone is dominant in causing a given amount of decomposition, for the nucleation, which is shown below to add one to the power m, is not effective, whereas at low temperatures the power is higher than 2 (see Appendix). It is of interest to note that Jacobs and Kureishy obtain a value of $m = 2$. The model is further strengthened by the behavior of α_{max}. This quantity represents that stage of the reaction when growing nuclei begin to overlap. A simplified picture of this process is shown in Figure 6a where random nucleation (in terms of position and time) began on the surface and pictures the situation at the maximum rate or α_{max}. Clearly any further reaction results in a contracting area and thus smaller values of $d\alpha/dt$. The fact that α_{max} is higher at higher temperatures means that less nuclei can be formed before the maximum rate stage. An extreme case is shown in Fig. 6b where only two nuclei could be formed before the rapidly growing nuclei overlapped. In this case $\alpha_{max} = 79\%$ as compared to 21% for the situation represented by Fig. 6c.

The effects of irradiation tend to confirm the correctness of the model. The induction period is vastly reduced as would be the case if the number of potential nuclei were increased by the irradiation, for then the time required to reach any given rate must be reduced. There are two concurrent events at the beginning of the reaction, nucleation and growth. Since there are now so many more potential nuclei and hence more growing nuclei after a given time, the power law tends

to reflect growth alone and so the observed drop in "m" to 2 upon irradiation, even without any α_0 correction, is understandable. The drop in activation energy of the beginning stages of reaction upon irradiation is also understandable, since now the activation energy is closer to that for pure growth. The maximum rate is unaffected by irradiation. Referring to Fig. 6c one can make a simplified calculation of the maximum rate as follows: Suppose there are N nuclei and L is the length of the side of the crystallite (assumed to be a square). The radius of each nucleus (assuming they all started growing at the same time and were equally spaced around the crystallite) is $2L/N$. If the reaction front moves with a velocity v, it can be easily shown that

$$\left(\frac{d\alpha}{dt}\right)_{max} = \frac{2\pi v}{L} \tag{5}$$

which is independent of N.[11] This equation also shows why the activation energy for the maximum rate is unaffected by irradiation, since the only temperature dependent quantity in eq. 5 is v which we believe is not affected by irradiation. However, the fact that N is larger with irradiated material implies that the value α_{max} would be lower. Figure 5 shows that indeed this is the case. It is also easy now to understand why the activation energy is changed by irradiation only near the beginning of the reaction for in the later stages the growth of existing nuclei masks growth due to new nuclei since the former are so much bigger.

There remains the decay stage. The fact that it follows a simple exponential decay rather than a contracting area formula does not mean that a contracting area mechanism is not operative. This has been amply demonstrated in the literature.[12]

There are many complicated events that can render the decay stage exponential. An exponential particle size distribution resulting from break-up due to strains is one example. We, therefore, have no reason to believe that the decay stage is anything other than a continuation of the growth after nuclei overlap. One would then, of course, not expect irradiation to have any effect since nucleation has at this point long

(10) The amount of decomposition contributed by a nucleus of radius r growing two-dimensionally is proportional to r^2. A nucleus of any size other than the very smallest and newest will contribute very much more to the total decomposition than will a newly born growth nucleus.

(11) At the maximum rate, the radius of each nucleus is $2L/N$ and the total length of the reaction "front" is $2\pi L(N - 2)/N$. In time dt, the increase in area $d\alpha = 2\pi L(N - 2)vdt/N$ and therefore the increase in α, $d\alpha = d\alpha/L^2 = 2\pi(N - 2)vdt/NL$. Therefore, $(d\alpha/dt)_{max} = 2\pi(N - 2)v/NL$; when N is large, $(d\alpha/dt)_{max} = 2\pi v/L$.

(12) See, for example, J. Jach, ref. 4, p. 8.

ceased to be influencial. This lack of effect is demonstrated in Fig. 4.

Acknowledgment. The authors wish to thank Miss E. Moorehead for her help in the experimentation and curve fitting.

Appendix

The supposed nucleation results from random thermal fluctuations. Their number will then be given as a function of time t by

$$N_0[1 - \exp(-kt)]$$

where N_0 is the number of potential nuclei, k being a rate constant. If the velocity of radial growth of a nucleus is ν and L^2 is the area of a platelet then

$$\alpha = \frac{kN_0\pi\nu^2}{2L^2} \int_0^t (t - y)^2 e^{ky} dy$$

where the integration accounts for nuclei beginning to grow at time $t = y$.[13]

This equation evaluates to

$$\alpha = \frac{N_0\pi\nu_2}{k^2L^2}\left[1 - kt + \frac{k^2t^2}{2} - \exp(-kt)\right]$$

This equation reduces to a t^3 dependence for small t and t^2 for high t, at which point the effect of nucleation is outweighed by the t^2 growth dependence.

(13) For more details, see W. E. Garner, "Chemistry of the Solid State," Butterworths Inc., Washington, D. C., 1955, Chapter 7.

Dielectric Dispersion in the Microwave Region of

Certain Alkyl Amines[1a]

by Surendra K. Garg[1b] and Prasad K. Kadaba

Department of Electrical Engineering, University of Kentucky, Lexington, Kentucky (*Received July 29, 1963*)

The dielectric constant and loss of the following amines have been measured at 10, 3, 2, and 1 cm. from 0° downward over a range of temperatures in the solid phase: ethyl, *n*-propyl, *n*-butyl, *n*-amyl, diethyl, di-*n*-propyl, and di-*n*-butyl. The static dielectric constants of these compounds have also been measured over the same temperature range. The relaxation times and the thermodynamic parameters of the molecules have been determined. The dielectric constants in the solid phase were computed using an IBM 1620 computer. The data in the solid phase do not lend themselves to quantitative interpretation; nevertheless, the results provide evidence of rotation over hindering potential energy barriers in the crystal lattice in a temperature region not far below the respective melting points in the case of primary amines. The secondary amines, on the other hand, do not show a transition to a rotator phase. The difference in the behavior of *n*-amyl-amine and other amines is emphasized.

Introduction

The general behavior of polar liquids has been investigated for many years, but the complicated nature of liquid structure where clear indications as to molecular configurations and motions are not readily obtained has made a detailed molecular interpretation of dielectric relaxation difficult. The study of dielectric dispersion during phase transition provides, in general, considerable information about the molecular mechanism of dielectric relaxation and also gives an insight into molecular kinetic behavior. In particular, the interaction of polar molecules and their neighbors is revealed, the effective viscosity of the medium for molecular motion is determined, and the freedom of motion of the polar groups in the solid state is measured. The problem is of further interest, since very little theoretical or experimental work is reported in the literature on the processes responsible for anomalous behavior during such transitions in simple polar liquids. Hill,[2] on the basis of available experimental data, has divided polar liquids into two categories. In the first category are liquids with rigid molecules where the rotation of the dipoles is prevented upon solidification and an equilibrium equation similar to Debye's can be used to relate their dielectric relaxation times with the corresponding viscosities. In the second category are liquids such as the tetrasubstituted methanes investigated by Powles, Williams, and Smyth.[3] No relationship need exist between their respective relaxation times and viscosities, as the type of association which gives rise to viscosity may have little or no effect on dipole rotation. The dielectric constants of such liquids are not altered much by solidification, indicating that the dipoles have considerable freedom of rotation in the solid state. This freedom of rotation is lost at a transition point considerably below the freezing point. The relaxation times of these liquids can be related theoretically to the transition point at which the freedom of dipolar rotation is lost. Hoffman[4] has developed a theory relating the hindered rotation with the thermal and dielectric properties of long-chain compounds. The theory is based on the assumption

(2) N. E. Hill, *Proc. Roy. Soc.* (London), **A240**, 101 (1957).

(3) J. G. Powles, D. E. Williams, and C. P. Smyth, *J. Chem. Phys.*, **21**, 136 (1953).

(4) J. D. Hoffman, *ibid.*, **20**, 541 (1952).

that the rotation in the solid phase is hindered by potential energy barriers which give one deep minimum and a number of relatively shallow minima.

In a previous investigation by one of the authors,[5] the microwave absorption of several amines was investigated in the liquid phase above 0°. The results on primary amines gave an indication of free rotation of the –NH₂ group around the C–N axis. The purpose of the present investigation is to extend the measurements to temperatures below 0° and to investigate in particular to what extent freedom of dipolar orientation exists in the solid phases of primary and secondary amines.

Experimental

The real and imaginary parts of the dielectric constants of ethyl-, n-propyl-, n-butyl-, n-amyl-, diethyl-, di-n-propyl-, and di-n-butylamine have been measured from 0° downward over a range of temperatures in the solid phase at 10, 3, 2, and 1 cm. The method of measurement was different in the liquid phase as compared with that in the solid phase. The method would also depend on the loss-tangent tan δ of the substance under investigation. For the liquid phase, three methods have been used. For the range of tan δ between 0.1 and 0.5, a reflection method based upon the variation in the reflection coefficient of a uniform layer of the dielectric[6] was used. Very good results have been obtained using a method developed by Poley.[7] The values of the dielectric constant obtained by the above two methods were self-consistent within the limits of experimental errors. For some of the measurements in the solid phase, a technique[8] which involves the determination of the circuit parameters of a four-terminal dissipating network was tried. The method of Roberts and Von Hippel[9] was to be preferred, however. During the course of calculations the charts of ζ vs. $1/c$, developed by Von Hippel, were found to be inadequate. So the results were programmed on an IBM 1620 computer yielding the final values of ϵ' and ϵ''. The accuracy in the determination of ϵ' was 1% and in the determination of ϵ'', 3%.

The static dielectric constant of the various amines were measured at a frequency of 1 Mc. using the General Radio Type 916-A bridge and a superheterodyne receiver for the detector.

A Dry Ice–acetone bath was used up to −75°. The temperatures below −75° were obtained with the help of liquid nitrogen. The flow of liquid nitrogen was controlled by a three-way solenoid valve. The valve was actuated by a United Electric thermoregulator set at a desired temperature. Compressed nitrogen gas was used to force the coolant into the sys-

tem. The liquid nitrogen bath used was similar in construction to the bath described by Vajda and Hart.[10] The accuracy of temperature measurement was ±1° throughout the investigation.

Materials. The various amines used were obtained from Matheson, Coleman and Bell Co. and were of C.P. grade. Their melting points are as follows: ethyl, −80.6°; n-propyl, −83°; n-butyl, −50.5°; n-amyl, −55°; diethyl, −49°; and dipropyl, −39.6°.

Results and Discussion

The values of the dielectric constants ϵ' and the losses ϵ'' of the various alkyl amines measured at wave lengths of 1, 2, 3, and 10 cm. from 0° downward over a range of temperatures in the solid phase are given in Table I. The so-called static dielectric constants ϵ_0 measured at 1 Mc. are also included in the same table.

Cole–Cole arc plots[11] have been constructed from the data in Table I. Table II contains the values of the high frequency dielectric constants ϵ_∞, the distribution parameters α, and the critical wave lengths λ_m, obtained in the usual manner[12] from the arc plots.

The macroscopic relaxation times are calculated by the equation

$$\tau_m = \frac{\lambda_m}{2\pi c} \tag{1}$$

where c is the velocity of light.

Cole–Cole arc plots for some of the representative amines are given in Fig. 1. Since the points are nicely distributed over the arc, the arc is a good representation of the data.

The method of absolute rate theory[13,14] has been used to calculate, from the temperature dependence of the relaxation times, the thermodynamic parameters governing the relaxation process. These are the most probable free energy of activation ΔF_0 and the

(5) S. K. Garg, Ph.D. Thesis (unpublished), University of Allahabad, 1960.
(6) W. H. Surber, Jr., *J. Appl. Phys.*, **19**, 514 (1948).
(7) J. P. Poley, *Australian J. Phys.*, **6**, 352 (1955).
(8) "Handbook of Microwave Measurements," Polytechnic Institute of Brooklyn, Microwave Research Institute, 1954, Chapter IV, pp. 77–82.
(9) "Dielectric Materials and Applications," A. R. Von Hippel, Ed., John Wiley and Sons, Inc., New York, N. Y., 1954, pp. 88–103.
(10) J. Vajda and D. P. Hart, *Rev. Sci. Instr.*, **24**, 354 (1953).
(11) K. S. Cole and R. H. Cole, *J. Chem. Phys.*, **9**, 341 (1941).
(12) C. P. Smyth, "Dielectric Behavior and Structure," McGraw-Hill Book Co., Inc., New York, N. Y., 1955, pp. 69, 70.
(13) S. Glasstone, J. Laidler, and H. Eyring, "The Theory of Rate Processes," McGraw-Hill Book Co., Inc., New York, N. Y., 1941, Chapter IX.
(14) W. Kauzmann, *Rev. Mod. Phys.*, **14**, 12 (1942).

Table I: Values of the Dielectric Constants ϵ', Losses ϵ'', and the Static Dielectric Constants ϵ_0 of the Various Amines

| | \-\-\-\-\-\-\-\-\-\-\-\-\-\-\-\-\-\-\-Temperature, °C\-\-\-\-\-\-\-\-\-\-\-\-\-\-\-\-\-\-\- | | | | | | | | |
	0	−10	−20	−30	−40	−50	−60	−70	−80
				Ethylamine					
ϵ_0	8.7	9.3	10.1	10.8	11.9				
				$\lambda = 10$ cm.					
ϵ'	8.6	9.0	9.5	9.6	9.7				
ϵ''	0.6	0.9	1.9	2.1	2.9				
				$\lambda = 3$ cm.					
ϵ'	8.0	8.1	8.2	8.2	7.8				
ϵ''	1.7	2.15	2.7	3.0	3.7				
				$\lambda = 2$ cm.					
ϵ'	6.8	7.0	7.0	6.8					
ϵ''	2.6	2.8	3.05	3.4					
				n-Propylamine					
ϵ_0	5.90	6.30	6.55	7.25	7.75	8.20	8.60	8.90	
				$\lambda = 10$ cm.					
ϵ'	5.85	6.25	6.55	6.8	7.0	7.0	6.85	6.5	6.05
ϵ''	0.3	0.5	0.75	1.05	1.4	1.75	2.2	2.65	3.25
				$\lambda = 3$ cm.					
ϵ'	5.75	5.8	5.9	5.75	6.0	5.0	4.35	3.75	3.25
ϵ''	0.95	1.2	1.55	2.05	2.3	2.4	2.35	2.1	1.15
				$\lambda = 2$ cm.					
ϵ'	5.45	5.35	5.15	4.9	4.65	4.3	3.95	3.5	3.15
ϵ''	1.25	1.6	1.95	2.2	2.35	2.35	2.2	1.75	1.25
				$\lambda = 1$ cm.					
ϵ'	4.75	4.5	4.3	3.75	3.75	3.4	3.2	3.05	2.95
ϵ''	1.8	1.95	2.05	2.1	2.0	1.8	1.4	1.1	0.9
				n-Butylamine	(−49°)				
ϵ_0	5.4	5.65	5.95	6.15	6.35	6.55	6.74 (−52°)	6.85 (−55°)	3.0 (−56°)
				$\lambda = 10$ cm.					
ϵ'	5.35	5.5	5.6	5.65	5.62	5.57			
ϵ''	0.25	0.55	0.75	0.95	1.1	1.25			
				$\lambda = 3$ cm.					
ϵ'	5.07	5.05	4.95	4.75	4.40	4.00			
ϵ''	0.92	1.20	1.42	1.57	1.62	1.57			
				$\lambda = 2$ cm.					
ϵ'	4.62	4.45	4.20	3.95	3.65	3.40			
ϵ''	1.40	1.55	1.65	1.65	1.57	1.40			
				$\lambda = 1$ cm.					
ϵ'	4.0	3.75	3.55	3.3	3.2	3.0			
ϵ''	1.65	1.85	1.8	1.65	1.45	1.2			
				n-Amylamine					
ϵ_0	4.6	4.75	4.88	5.03	5.2	5.375	5.68 (−65°)	5.75 (−67°)	
				$\lambda = 10$ cm.					
ϵ'	4.4	4.5	4.5	4.45	4.35	4.05			
ϵ''	0.44	0.52	0.65	0.8	0.91	0.98			

Table I *Continued*

	0	−10	−20	−30	−40	−50	−60	−70	−80
					Temperature, °C				

n-Amylamine

λ = 3 cm.

	0	−10	−20	−30	−40	−50
ϵ'	4.2	4.15	4.1	4.0	3.85	3.6
ϵ''	0.7	0.9	1.0	1.12	1.12	1.05

λ = 2 cm.

ϵ'	3.85	3.75	3.65	3.45	3.25	3.05
ϵ''	1.0	1.03	1.15	1.13	1.08	0.98

λ = 1 cm.

ϵ'	3.5	3.4	3.3	3.15	3.0	2.98
ϵ''	1.22	1.24	1.24	1.2	1.13	0.95

Diethylamine (−49°)

	0	−10	−20	−30	−40	−50	−60	−70
ϵ_0	4.5	4.85	5.2	5.55	6.0	6.35	6.6 (−51°)	2.42 (−52°)

λ = 10 cm.

ϵ'	4.45	4.65	4.7	4.6	4.25	3.7
ϵ''	0.3	0.67	0.95	1.3	1.4	1.47

λ = 3 cm.

ϵ'	3.75	3.05	3.3	3.2	3.0	2.9
ϵ''	1.06	1.25	1.3	1.3	1.17	1.0

λ = 2 cm.

ϵ'	3.3	3.15	3.0	2.9	2.75	2.7
ϵ''	1.06	1.22	1.36	1.07	0.91	0.84

λ = 1 cm.

ϵ'	2.9	2.8	2.75	2.7	2.65	2.6
ϵ''	1.14	1.06	1.0	0.92	0.84	0.78

Di-*n*-propylamine

	0	−10	−20	−30	−40	−50	−60	−70	−80
ϵ_0	3.73	4.0	4.2	4.3	4.4	4.475	4.5 (−55°)	3.32 (−56°)	3.20 (−60°)

λ = 10 cm.

ϵ'	3.4	3.5	3.5	3.425	3.25	3.0
ϵ''	0.5	0.6	0.7	0.8	0.9	0.85

λ = 3 cm.

ϵ'	2.95	2.9	2.825	2.75	2.625	2.575
ϵ''	0.67	0.715	0.72	0.69	0.63	0.56

λ = 2 cm.

ϵ'	2.65	2.625	2.575	2.50	2.45	2.40
ϵ''	0.67	0.73	0.68	0.58	0.46	0.37

λ = 1 cm.

ϵ'	2.50	2.475	2.45	2.425	2.40	2.375
ϵ''	0.59	0.56	0.51	0.47	0.40	0.23

Di-*n*-butylamine

	0	−10	−20	−30	−40	−50	−60	−70	−80
ϵ_0	3.20	3.27	3.34	3.41	3.48	3.56	3.62	3.7 (−65°)	3.11 (−70°)

λ = 10 cm.

	0	−10	−20	−30	−40	−50	−60
ϵ'	3.075	3.025	2.95	2.85	2.70	2.575	2.475
ϵ''	0.34	0.46	0.50	0.525	0.51	0.46	0.33

Table I *Continued*

	0	−10	−20	−30	−40	−50	−60	−70	−80
					Temperature, °C				
				Dibutylamine					
				$\lambda = 3$ cm.					
ϵ'	2.525	2.50	2.45	2.45	2.40	2.375	2.35		
ϵ''	0.52	0.525	0.49	0.44	0.39	0.35	0.31		
				$\lambda = 2$ cm.					
ϵ'	2.375	2.375	2.35	2.325	2.325	2.30	2.30		
ϵ''	0.05	0.44	0.395	0.36	0.33	0.28	0.20		
				$\lambda = 1$ cm.					
ϵ'	2.30	2.30	2.30	2.275	2.25	2.25	2.25		
ϵ''	0.41	0.39	0.36	0.32	0.28	0.23	0.17		

Table II: Values of the High Frequency Dielectric Constants ϵ_∞, Distribution Parameters α, Relaxation Times τ, and Critical Wave Lengths λ_m for the Various Amines

	0	−10	−20	−30	−40	−50	−60	−70
				Temperature, °C				
				Ethylamine				
ϵ_∞	2	2	2	2	2			
α	0.07	0.11	0.13	0.16	0.17			
$\tau \times 10^{-12}$, sec.	4.72	5.75	7.39	9.16	17.04			
λ_m, cm.	0.89	1.084	1.39	1.73	3.21			
				n-Propylamine				
ϵ_∞	1.95	1.95	1.95	1.95	1.95	1.95	1.95	2.60
α	0.0	0.05	0.05	0.12	0.13	0.15	0.18	0.09
$\tau \times 10^{-12}$	4.0	4.95	6.94	8.97	12.78	15.31	24.77	35.71
λ_m	0.75	0.93	1.31	1.69	2.41	2.89	4.67	6.73
				n-Butylamine	(−49°)			
ϵ_∞	2.05	2.0	2.0	2.0	2.0	2.0		
α	0.0	0.02	0.08	0.13	0.17	0.21		
$\tau \times 10^{-12}$	5.74	6.12	8.66	10.84	15.23	17.25		
λ_m	1.08	1.15	1.63	2.04	2.87	3.25		
				n-Amylamine				
ϵ_∞	1.95	1.95	1.95	1.925	1.90	1.90		
α	0.08	0.11	0.13	0.18	0.22	0.29		
$\tau \times 10^{-12}$	5.01	6.12	7.12	10.23	13.17	17.55		
λ_m	0.96	1.15	1.35	1.93	2.48	3.31		
				Diethylamine	(−49°)			
ϵ_∞	2.05	2.07	2.07	2.07	2.1	2.1		
α	0.07	0.07	0.12	0.14	0.19	0.21		
$\tau \times 10^{-12}$	8.16	12.32	17.40	23.96	30.68	48.10		
λ_m	1.54	2.32	3.28	4.52	5.79	9.06		
				Di-n-propylamine				
ϵ_∞	2.05	2.05	2.05	2.13	2.25	2.25		
α	0.13	0.17	0.18	0.23	0.13	0.13		
$\tau \times 10^{-12}$	12.44	17.70	21.10	30.95	45.15	56.97		
λ_m	2.35	3.34	3.98	5.84	8.51	10.74		
				Di-n-butylamine				
ϵ_∞	2.11	2.13	2.13	2.17	2.17	2.17	2.17	
α	0.00	0.01	0.06	0.05	0.12	0.16	0.20	
$\tau \times 10^{-12}$	17.09	21.51	25.88	32.53	39.08	54.02	30.71	
λ_m	3.22	4.05	4.88	6.13	7.36	10.18	5.79	

Table III: Values of the Most Probable Free Energy of Activation ΔF_0 (kcal.) for the Various Amines

					Temperature, °C				
	0	−10	−20	−30	−40	−49	−50	−60	−70
Ethylamine	1.873	1.887	1.902	1.940	2.073		1.961		
n-Propyl-	1.783	1.809	1.890	1.920	1.986				
n-Butyl-	1.959	1.920	2.002	2.011	2.067	2.025			
n-Amyl-	1.913	1.920	1.908	1.947	1.999	2.031			
Diethyl-	2.169	2.285	2.353	2.395	2.391	2.481			
Di-n-propyl-	2.398	2.475	2.450	2.470	2.570	2.557			
Di-n-butyl-	2.571	2.577	2.552	2.542	2.503		2.519	2.557	

Table IV: Values of the Most Probable Entropy of Activation ΔS_0 (e.u.) for the Various Amines (All Negative)

					Temperature, °C				
	0	−10	−20	−30	−40	−49	−50	−60	−70
Ethylamine	1.36	1.47	1.59	1.81	2.46				
n-Propyl-	0.94	1.07	1.44	1.62	1.97		1.94	2.49	2.77
n-Butyl	2.73	2.69	3.11	3.32	3.66	3.62			
n-Amyl-	2.40	2.52	2.57	2.83	3.19	3.45			
Diethyl-	1.28	1.77	2.10	2.36	2.45	2.95			
Di-n-propyl-	4.32	4.78	4.87	5.15	5.57	5.98			
Di-n-butyl-	5.20	5.43	5.54	5.72	5.81		6.14	6.61	

most probable entropy of activation ΔS_0 and are given in Tables III and IV, respectively.

The ΔF_0 values for primary amines in Table III are nearly the same irrespective of the size of the molecule. This indicates that the rotating unit is of the same size in all the molecules. For the secondary amines cited, the increase in ΔF_0 with molecular size is from about 2.169 to 2.571 kcal.

The ΔS_0 values given in Table IV are found to be more and more negative as the size of the molecule increases. This would be possible if we assume that the molecules neighboring the rotating molecule pack themselves closely together in order to allow the central molecule to move. The total decrease in entropy of these neighbors might be greater than the increase in entropy of the rotating molecule itself, yielding a net negative entropy change. The larger the central molecule, the greater is the degree of packing required and therefore the more negative is the entropy change.

The dielectric constant and loss values of some of the representative amines at different wave lengths are plotted against temperature in Fig. 2 and 3. The plots extend from the liquid phase through the solid phase.

The dielectric constant of diethylamine drops upon freezing and there is an absence of frequency dependence
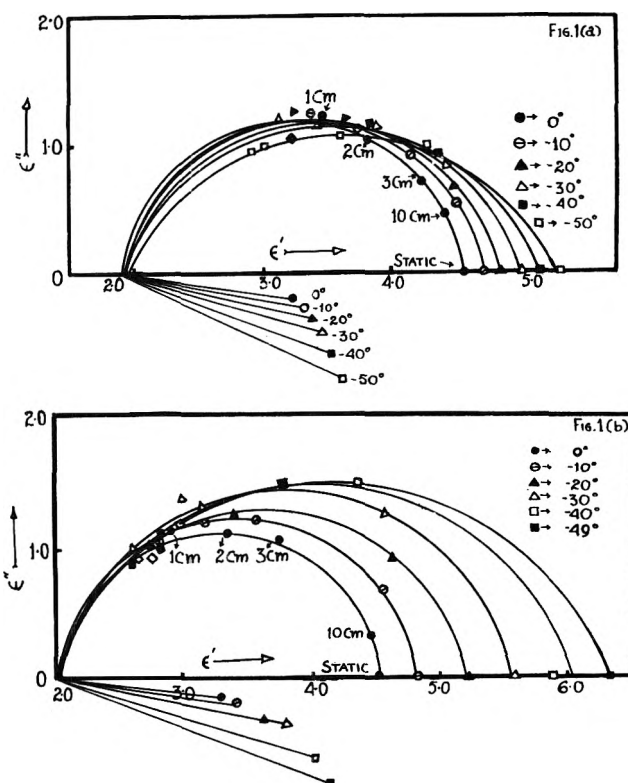

Figure 1. (a) Cole–Cole arc plots of n-amylamine at 0, −10, −20, −30, −40, and −50°. (b) Cole–Cole arc plots of diethylamine at 0, −10, −20, −30, −40, and −49°.

in the solid phase. This result is indicative of the fact that in crystalline diethylamine, the molecules are frozen rigidly in their locations and hence there cannot be any appreciable contribution from the dipoles to the dielectric constant of the material. It has been observed that other secondary amines also do
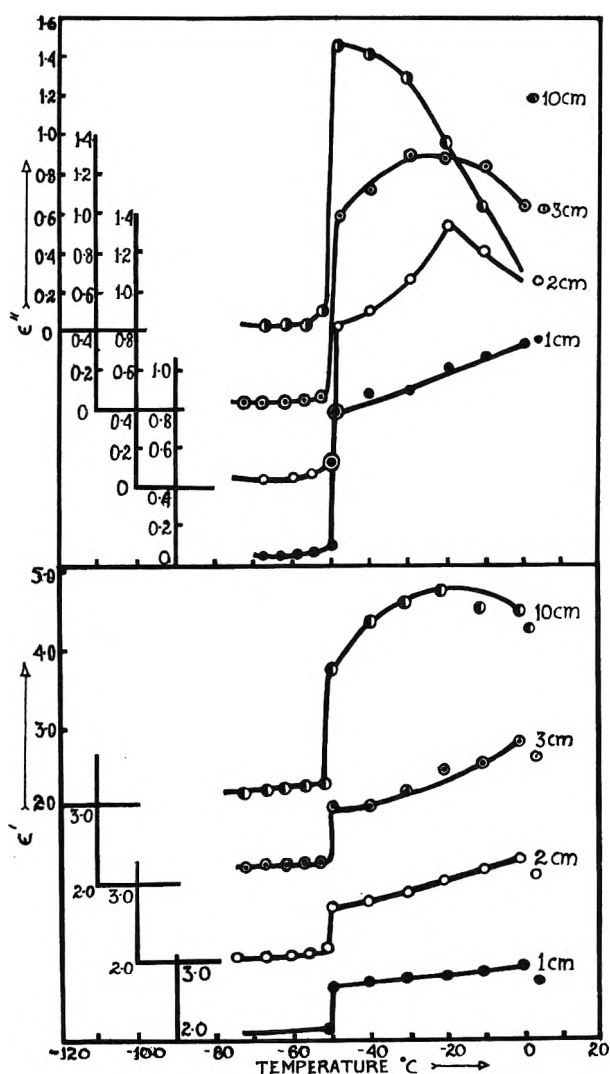

Figure 2. Dielectric constant ϵ' and loss ϵ'' vs. temperature of diethylamine at 1, 2, 3, and 10 cm.

not possess any appreciable amount of molecular orientational freedom in the solid phase.

The behavior of n-amylamine differs markedly from those of the secondary amines. There is no drop in the dielectric constant at the freezing point, indicating some degree of dipolar orientation in the solid phase. A sharp drop, however, at a few degrees below the freezing point indicates a transition involving probably the cessation of rotational jumps around the C–N

axis. The evidence of some degree of molecular rotation has been indicated previously[15] in n-octylamine and n-dodecylamine, although no such freedom was found in the higher members of the series. Dielectric loss decreases markedly at the freezing point, probably as the result of greater hindrance to rotation near the
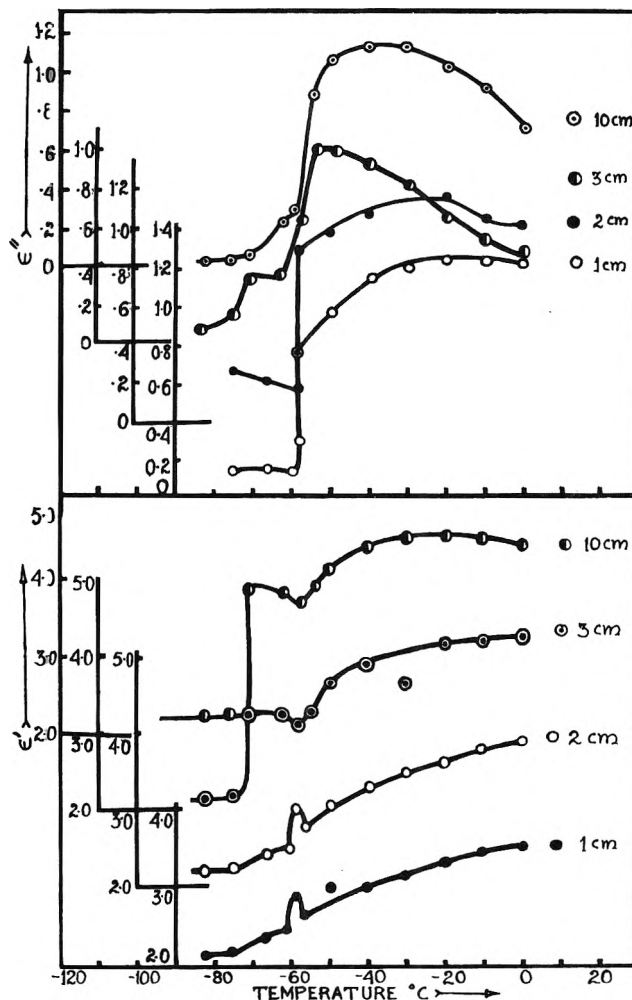

Figure 3. Dielectric constant ϵ' and loss ϵ'' vs. temperature of n-amylamine at 1, 2, 3, and 10 cm.

me_ting point and in the solid phase. This hindrance is probably due to association in amines and is generally considered to be the result of H-bond formation. The nitrogen atom being a good "donor" but a poor "acceptor," the association in primary amines would be much less than that in alcohols, however. In alcohols, the oxygen atom being a good donor as well as a good acceptor, the association would be more pronounced at lower frequencies.

(15) J. D. Hoffman and C. P. Smyth, J. Am. Chem. Soc., 71, 3591 (1949).

In conclusion, the present investigation indicates clearly that primary amines can rotate in their crystal lattices over hindering potential energy barriers in a temperature region not far below their melting points. The extreme sharpness of the drop in the dielectric constant at the transition testifies to the purity of the materials. The secondary amines do not show a transition to a rotator phase as evidenced by the sharp drop in their dielectric constants at the freezing points and by the absence of any appreciable loss in their solid phases.

Isotopic Fractionation of Hydrogen between Water

and the Aqueous Hydrogen Ion[1]

by Karl Heinzinger[2] and Ralph E. Weston, Jr.

Department of Chemistry, Brookhaven National Laboratory, Upton, New York (*Received August 13, 1963*)

The fractionation of hydrogen isotopes between aqueous solutions of perchloric acid and the vapor phase in equilibrium with the solutions has been measured at 13.5°. With the usual assumption that the proton is solvated in the form H_3O^+, the separation factor thus obtained can be used to calculate the equilibrium constant, K_L, for the isotope exchange equilibrium, $H_2O + H_2DO^+ = HDO + H_3O^+$. The value of 0.96 ± 0.02 determined in this work is in good agreement with values obtained by other, generally indirect, methods. It is shown that our results are consistent with those obtained by other types of measurement only if the proton is formulated as H_3O^+.

Some thirty years ago, an explanation for the kinetic behavior of acid-catalyzed reactions in mixtures of light and heavy water was proposed by Gross and co-workers[3-5] and by Butler and co-workers.[6-8] They developed a theory for the effect of deuterium in the aqueous solvent on the ionization constants of weak acids and on the experimental rate constant of acid-catalyzed reactions following the mechanism

$$S + H^+ \rightleftharpoons SH^+ \text{ (rapid)}$$

$$SH^+ \longrightarrow \text{product (rate-determining)}$$
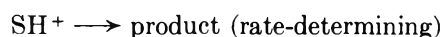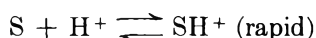
In a solvent composed of light and heavy water, the isotopic composition of the solvated hydrogen ion differs from that of the solvent. These two quantities are related by equilibrium constants such as

$$K_L = (H_3O^+)(HDO)/(H_2DO^+)(H_2O) \qquad (1)$$

(1) Research performed under the auspices of the U. S. Atomic Energy Commission.

(2) On leave from the Max Planck-Institut für Chemie, Mainz, Germany.

(3) P. Gross, H. Steiner, and F. Krauss, *Trans. Faraday Soc.*, **32**, 877 (1936).

(4) P. Gross and H. Wischen, *ibid.*, **32**, 879 (1936).

(5) P. Gross, H. Steiner, and H. Suess, *ibid.*, **32**, 883 (1936).

(6) J. C. Hornel and J. A. V. Butler. *J. Chem. Soc.*, 1361 (1936).

(7) W. J. C. Orr and J. A. V. Butler. *ibid.*, 330 (1937).

(8) W. E. Nelson and J. A. V. Butler, *ibid.*, 958 (1938).

This may be recognized as the equilibrium constant for the isotope exchange reaction

$$H_2O + H_2DO^+ = HDO + H_3O^+ \qquad (2)$$

A further simplification results from the assumption of the rule of the geometric mean[9] as applied to the isotopically homologous series H_3O^+, H_2DO^+, HD_2O^+, and D_3O^+. This makes it possible to relate all the equilibria such as (2) to a single one, which has traditionally been described by the equilibrium constant L.

$$2D_3O^+ + 3H_2O = 2H_3O^+ + 3D_2O \qquad (3)$$

The isotopic fractionation between solvent and hydronium ion is reflected in the behavior of the rate constant as a function of the isotopic content of the solvent. For this reason, the kinetic behavior of acid-catalyzed reactions in mixtures of light and heavy water has been used for many years as a criterion of a mechanism which involves a rapid equilibrium between reactant and hydrogen ion.

A few years ago, this problem was examined again by Purlee,[10] who re-evaluated L from modern data. His paper was rapidly followed by several other communications on the subject. In one of these, Gold[11] points out that in most of the data used by Purlee the value of L is extremely sensitive to small errors in the experimental values of rate constants. He also showed that similar solvent isotope effects may be expected in reactions which have a proton transfer as the rate-determining step. Swain and co-workers[12,13] evaluated L from the vibrational frequencies of H_3O^+ and D_3O^+, and also from a somewhat different treatment of electrochemical data than that of Purlee, obtaining a value of L about 25% lower than Purlee's value. Halevi, Long, and Paul[14] have also discussed this problem, and in particular, have emphasized the importance of the changing medium on ionic activity coefficients. Recently, Kresge[15] has derived, very generally, the equations for protolytic reactions in mixtures of H_2O and D_2O. Equilibrium and rate expressions for both rapid and rate-determining proton transfer reactions are considered.

Until very recently there has been no direct measurement of an equilibrium constant related to L. There now are two sets of experiments[16,17] which give data leading directly to L. These depend upon the fact that the position of the proton n.m.r. peak in an aqueous acid solution is related to the concentration of the hydrogen ion. By measuring this shift in H_2O and in a mixture of D_2O and H_2O, it is possible to obtain relative hydrogen ion concentrations in the two solvents and thus to evaluate L. The agreement

between these two sets of experiments is within experimental error. In this type of measurement, it is tacitly assumed that there is no significant contribution to the n.m.r. shift from the water molecules solvating the anion.[18]

We have now made a direct measurement of the equilibrium constant K_L using a quite different technique. Essentially, this involves the determination of the isotopic composition of the water in an aqueous acid solution by measuring the D/H ratio of the vapor phase (which contains only water) in equilibrium with the acid solution. Knowing the analogous separation factor for pure water and the isotopic composition of the entire liquid phase together with the concentration and extent of dissociation of the acid, one can calculate K_L.

Principle of the Measurement. The equation which relates the separation factor between vapor and liquid of an aqueous acid solution to the desired equilibrium constant K_L can be derived by the same method as that used by Wetzel[19] to describe the fractionation in an azeotropic acid-water mixture.

In our experiments the atom fraction of deuterium is so small ($\sim 3 \times 10^{-4}$) that molecular species containing more than one deuterium atom need not be considered. In addition, $N_{HDO} \ll N_{H_2O}$, $N_{H_2DO^+} \ll N_{H_3O^+}$, and $N_{DA} \ll N_{HA}$. Also, it was shown experimentally that, for our case, no acid is in the vapor phase. This being so, the fractionation factor is given by

$$\alpha_A = \frac{(D/H)_{liquid}}{(D/H)_{vapor}} = \frac{N_{HDO} + N_{DA} + N_{H_2DO^+}}{2N_{H_2O} + N_{HA} + 3N_{H_3O^+}} \frac{2N'_{H_2O}}{N'_{HDO}}$$

$$(4)$$

In this equation, the prime refers to the vapor phase, the N's are mole fractions, and HA represents the undissociated acid. Isotope fractionation due to hydration other than the primary hydration of the proton

(9) J. Bigeleisen, *J. Chem. Phys.*, **23**, 2264 (1955).

(10) E. L. Purlee, *J. Am. Chem. Soc.*, **81**, 263 (1959).

(11) V. Gold, *Trans. Faraday Soc.*, **56**, 255 (1960).

(12) C. G. Swain and R. F. W. Bader, *Tetrahedron*, **10**, 182 (1960).

(13) C. G. Swain, R. F. W. Bader, and E. R. Thornton, *ibid.*, **10**, 200 (1960).

(14) E. A. Halevi, F. A. Long, and M. A. Paul, *J. Am. Chem. Soc.*, **83**, 305 (1961).

(15) A. J. Kresge, paper No. SM-50/32 of the International Atomic Energy Agency Symposium on Isotope Mass Effects in Chemistry and Biology, Vienna, 1963; *Pure Appl. Chem.*, to be published.

(16) A. J. Kresge and A. L. Allred, *J. Am. Chem. Soc.*, **85**, 1541 (1963).

(17) V. Gold, *Proc. Chem. Soc.*, 141 (1963).

(18) J. C. Hindman, *J. Chem. Phys.*, **36**, 1000 (1962).

(19) K. Wetzel, *Isotopentechnik*, **1**, 15 (1960).

is neglected in this equation. The following additional relations are needed:

(a) the separation factor for pure water

$$\alpha_w = \frac{N_{HDO}N'_{H_2O}}{N_{H_2O}N'_{HDO}} \tag{5}$$

(b) the equilibrium constant for the exchange between acid and water

$$K_A = \frac{N_{HA}N_{HDO}}{N_{DA}N_{H_2O}} \tag{6}$$

(c) the mole ratio of acid species in solution

$$r = \frac{N^0{}_{HA}}{N^0{}_{H_2O}} = \frac{N_{HA} + N_{H_3O^+}}{N_{H_2O} + N_{H_3O^+}} \tag{7}$$

where the superscript zero refers to the "formal" concentration.

(d) the fraction of dissociation of the acid HA

$$q = N_{H_3O^+}/(N_{H_3O^+} + N_{HA}) \tag{8}$$

(e) $N_{H_2O} + N_{HA} + N_{H_3O^+} + N_{A^-} =$
$$N_{H_2O} + N_{HA} + 2N_{H_3O^+} = 1 \tag{9}$$

since the concentrations of deuterated species are negligible.

The combination of eq. 4–9 leads to the expression

$$K_L = \frac{rq}{(\alpha_A/\alpha_w)[1 + (r/2)] - 1 + rq + r(1 - q)/K_A} \tag{10}$$

In the case of a completely dissociated acid this simplifies to

$$K_L = \frac{r}{(\alpha_A/\alpha_w)[1 + (r/2)] - 1 + r} \tag{11}$$

In the above derivation we have neglected a possible effect of the anion of the acid on the separation factor of water. The effect of dissolved electrolytes has been measured by Googin and Smith,[20] who ascribe most of the effect to the anion and show that it is a linear function of the anion mole fraction. Therefore, the value of α_w in eq. 10 and 11 should be replaced by

$$\alpha_w' = (1 - bN_{A^-})\alpha_w \tag{12}$$

where b depends on the anion.

Experimental Procedure

The separation factors α_w, α_A, and α_w' were determined simply by measuring the isotopic composition of the vapor phase in equilibrium with the appropriate solution, together with the isotopic composition of the solution. A 500-ml. Pyrex bulb, into which the

solution was introduced, was connected with a 6-mm. bore stopcock to a 1-l. bulb, in which the vapor was isolated by closing the stopcock. Before the experiment, the solution was degassed and the entire vessel was evacuated, in order to speed up the equilibration rate. The lower bulb was immersed in a thermostat at a temperature of 13.5 ± 0.5°, while the upper bulb was at room temperature. This temperature difference was necessary to prevent condensation in the upper bulb. One day sufficed to give complete equilibration between vapor and liquid. In order to minimize the effect of temperature fluctuations or other systematic errors, both α_w and α_A (or α_w and α_w') were determined simultaneously, i.e., a vessel containing pure water was placed in the thermostat together with one containing the appropriate solution, and they were removed at the same time.

Solutions were made up from a large supply of triply distilled water which served as the isotopic standard, and from 70% perchloric acid (Baker's Analyzed) or sodium perchlorate (Amend Drug and Chemical Co.).

Vapor samples were removed from the upper bulb by condensation in a trap at −196° and were subsequently prepared for mass spectrometric analysis by reduction over uranium turnings at 700°.[21] An acidimetric analysis of the vapor in equilibrium with a 4.35 M HClO$_4$ solution indicated that the acid concentration in the vapor was $\leq 3.6 \times 10^{-4}$ M (i.e., $r \leq 10^{-5}$ for the vapor compared with ~0.1 for the solution). This justifies the assumption that the vapor phase contains only water, which was used in deriving eq. 10.

Samples from the liquid phase were reduced in an identical manner in the case of pure water. In the case of acid solutions, they were first neutralized with sodium carbonate, after which the water was removed from the resulting sodium perchlorate solution by heating it to dryness while the vapor was collected in a trap at −196°. With increasing concentration of acid, a decreasing D/H ratio in the liquid sample was found, which indicates that the D/H ratio in the 70% perchloric acid used in this work was lower than that of the triply distilled water used for dilution.

The factor b was determined by measuring the separation factor (α_w') for a 7.15 M solution of NaClO$_4$. For this solution, with $N_{A^-} = 0.1628$, we obtained $\alpha_w'/\alpha_w = 1 - bN_{A^-} = 0.9887 \pm 0.002$. This gives a value of 0.069 ± 0.012 for b, which agrees well with that found by Googin and Smith.[20] The value of

(20) J. M. Googin and H. A. Smith, J. Phys. Chem., 61, 345 (1957).
(21) J. Bigeleisen, M. L. Perlman, and H. C. Prosser, Anal. Chem., 24, 1356 (1952).

Table I : Data Used to Obtain K_L

HClO₄, moles/l.	r	N_{A^-}	α_A/α_w	$1 - bN_{A^-}$	α_A/α_w'	K_L Uncorrected $q = 1$	$q \neq 1$	K_L Corrected $q = 1$	$q \neq 1$	q
0.958	0.0181	0.0178	0.9905	0.9988	0.9917	1.031	1.038	0.964	0.970	0.985
4.353	0.0965	0.0880	0.9552	0.9939	0.961₁	0.987	1.030	0.929	0.962	0.920
7.125	0.1829	0.1546	0.9249	0.9893	0.9349	0.951	1.025	0.899	0.957	0.855

α_w' at other anion concentrations were calculated from eq. 12.

The isotopic analysis was done with a Model M86 mass spectrometer manufactured by Atlas Werke, Bremen, Germany. The measured mass 3/mass 2 ratio must be corrected for the production of H_3^+ in the ion source by extrapolation to zero pressure in the source.[22] (The pressure is indicated by the peak height for mass 2.) For a few samples, the pressure dependence of the 3/2 ratio was measured and compared with that of the standard. Within experimental error, the same slope was obtained. In this case, one obtains

$$\frac{\alpha_A}{\alpha_w} = \frac{1 - [(R_{L,W} - R_{V,W})/R^0_{L,W}]}{1 - [(R_{L,A} - R_{V,A})/R^0_{L,A}]} \quad (13)$$

where R is the 3/2 ratio measured at some arbitrary pressure which is the same for both samples, R^0 the corresponding value obtained by extrapolation to zero pressure, and the indices V, L, W, and A refer to vapor phase, liquid phase, water, and acid.

Results and Discussion of Errors

The results of these measurements for three different acid concentrations are given in Table I. The number of experiments carried out was: 1 M HClO₄, 2; 4 M HClO₄, 4; 7 M HClO₄, 4; and 7 M NaClO₄, 4. The factors which enter into the calculation of K_L require some discussion. The "uncorrected" values are those in which b is assumed to be zero, i.e., the anion effect is neglected. It is seen that this correction has a substantial effect on K_L. There is some doubt about the proper value of q. The values listed in Table I are those obtained from n.m.r. measurements by Hood and Reilly,[23] although Young[24] has made some preliminary Raman measurements which indicate that q is close to unity even in 10 M solutions. Our results show a definite trend with concentration if we assume q is unity, which is absent if we use the values of q obtained by Hood and Reilly. However, the experimental error in K_L is such that it permits deviations of several per cent from Hood and Reilly's values for q.

If q is not unity, a value of K_A is needed. Equation 6 can be rewritten as

$$K_A = \frac{N_{HA}N_{HDO}}{N_{DA}N_{H_2O}} = \frac{N'_{HA}N'_{HDO}}{N'_{DA}N'_{H_2O}} \frac{\alpha_w}{\alpha_{HA}} \quad (14)$$

The first term can be written in terms of reduced partition function ratios[25] as f_{HDO}/f_{DA}. The value used for f_{HDO} in this temperature region was calculated from the data of Libby[26] and may be expressed as

$$f_{HDO} = 1.2752 \exp(886/T) \quad (15)$$

The corresponding value for perchloric acid and perchloric acid-d can be calculated approximately from the vibrational frequencies of Giguère and Savoie[27] to be

$$f_{HClO_4} = 0.439 \exp(1020/T) \quad (16)$$

with an uncertainty of about 10%.

There are no experimental data on the value of α_{HA}. One would guess that it would be greater than unity for a hydrogen-bonded molecule such as perchloric acid. For example, in a series of aliphatic alcohols, α is between 1.04 and 1.08 at 20°.[28] Conversely, however, for nitric acid at 0°, α is found to be 0.935.[29] Therefore the possible range of α_{HA}/α_w is about 0.86 to 1.00. The final value of K_A lies between the rather wide limits of 1.82 to 2.11. This is close to the statistical value of 2.00, which we have used in our calculations.

By taking suitable partial derivatives of K_L in eq. 10, one obtains an approximate expression for the error in K_L

$$\pm \Delta K_L = \frac{1}{qr} \left| \Delta \left(\frac{\alpha_A}{\alpha_w'}\right)\right| + \frac{1}{2qr}\left|\Delta r\right| +$$
$$\frac{1}{2q}\left|\Delta q\right| + \frac{1 - q}{qK_A^2}\left|\Delta K_A\right| \quad (17)$$

(22) I. Friedman, *Geochim. Cosmochim. Acta*, 4, 89 (1953).

(23) G. C. Hood and C. A. Reilly, *J. Chem. Phys.*, 32, 127 (1960).

(24) Quoted in ref. 18, and private communication from Professor Young.

(25) J. Bigeleisen and M. G. Mayer, *J. Chem. Phys.*, 15, 261 (1947).

(26) W. F. Libby, *ibid.*, 11, 101 (1943).

(27) P. A. Giguère and R. Savoie, *Can. J. Chem.*, 40, 495 (1962).

(28) I. B. Rabinovich, N. A. Sokolov, and P. A. Artyukhin, *Dokl. Akad. Nauk SSSR*, 105, 762 (1955).

(29) J. G. Dawber and P. A. H. Wyatt, *J. Chem. Soc.*, 3636 (1958).

Table II: Estimate of the Error in K_L

HClO₄, moles/l.	$\left\|\dfrac{1}{qr}\right\|$	$\|\Delta r\|$	$\left\|\dfrac{1}{2qr}\Delta r\right\|$	$\left\|\Delta\dfrac{\alpha_A}{\alpha_w}\right\|$	$\left\|\dfrac{1}{qr}\Delta\dfrac{\alpha_A}{\alpha_w}\right\|$	$\left\|\dfrac{1-q}{q}\Delta K_A\right\|$	$\|\Delta K_L\|$ uncor.	$\left\|\Delta\dfrac{\alpha_A}{\alpha_w'}\right\|$	$\left\|\dfrac{1}{qr}\Delta\dfrac{\alpha_A}{\alpha_w'}\right\|$	$\|\Delta K_L\|$ cor.
0.958	56	0.0002	0.006	0.0005	0.028	0.001	0.035	0.0008	0.044	0.051
4.353	11	0.0004	0.002	0.0014	0.015	0.003	0.020	0.0024	0.026	0.031
7.125	6	0.0006	0.002	0.0002	0.001	0.006	0.009	0.0022	0.013	0.021

Table III: Comparison of Values of K_L and L

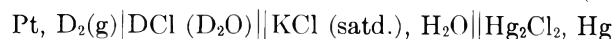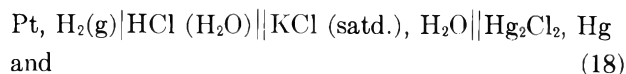| t, °C.	K_L	L	Method	Ref.
25	0.99	11.0	E.m.f. data[a]	10
25	0.98	10.1	Dissociation constants and rate constants	10
25	0.95	8.4	E.m.f. data	12
31	0.97 ± 0.03	9.7 ± 1.5	N.m.r.	17
(25)	0.97	10.0–10.4	Preceding value corrected to 25°	
?	1.00 ± 0.01	11.4	N.m.r.	16
13.5	0.96 ± 0.02	8.9	Fractionation between solution and vapor	This work
(25)	0.95	8.0–8.4	Preceding value corrected to 25°	

[a] These values are probably incorrect. See text.

The estimated magnitudes of the error terms are given in Table II. The effect of an error in q is not tabulated, since Hood and Reilly do not give any estimate of the precision with which they have measured this quantity.

It may be noted that the value of α_w obtained in this work agrees exactly with a value of 1.088 at 13.5° obtained by interpolating the data of Merlivat, et al.[30]

A useful quantity is the reduced partition function ratio for the hydronium ion, $f_{H_2DO^+}$, which can be obtained from K_L, f_{HDO}, and α_w. At 13.5°, $f_{H_2DO^+}$ is 31.9; if the symmetry numbers for H_3O^+ and H_2DO^+ are 3 and 1, respectively, then the nonclassical part of this (sf/s') is 10.6.

Comparison with Other Measurements. The values of K_L and L obtained in this work are compared with previous results in Table III. Some comment on the other types of measurement is necessary.

Purlee evaluated L from the electromotive force measurements of Schwarzenbach and co-workers[31] for the cells

Pt, $H_2(g)|HCl$ $(H_2O)||KCl$ (satd.), $H_2O||Hg_2Cl_2$, Hg

and   (18)

Pt, $D_2(g)|DCl$ $(D_2O)||KCl$ (satd.), $H_2O||Hg_2Cl_2$, Hg

Purlee assumed that the measurements with these cells eliminated the problem of the free energy of transfer

of an anion from light to heavy water. This is seen to be incorrect, however, when the actual cell reactions are considered

$$H_2 = 2H^+ (H_2O) + 2e^- (H_2O)$$

$$Hg_2Cl_2 + 2e^- (H_2O) = 2Hg + 2Cl^- (H_2O) \quad (19)$$

$$D_2 = 2D^+ (D_2O) + 2e^- (D_2O)$$
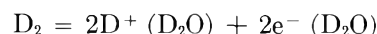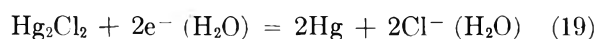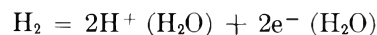
The calomel reference electrode is the same for both cells and the difference in the e.m.f. values corresponds to the reaction

$$H_2 + 2D^+ (D_2O) + 2e^- (D_2O) =$$
$$D_2 + 2H^+ (H_2O) + 2e^- (H_2O) \quad (20)$$
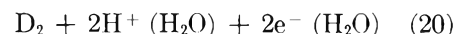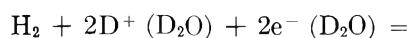
L was obtained from the combination of the free energy of reaction 20 with that for reaction 21, which is known from both thermochemical[32] and spectroscopic[33] data.

$$D_2(g) + H_2O(l) = H_2(g) + D_2O(l) \quad (21)$$
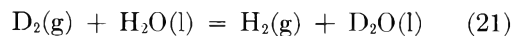
However, there remains a contribution from the transfer

(30) L. Merlivat, R. Botter, and G. Nief, *J. chim. phys.*, **60**, 56 (1963).

(31) G. Schwarzenbach, *Z. Elektrochem.*, **44**, 302 (1938); G. Schwarzenbach, A. Epprecht, and H. Erlenmeyer, *Helv. Chim. Acta*, **19**, 1292 (1936).

(32) F. D. Rossini, J. W. Knowlton, and H. L. Johnston, *J. Res. Natl. Bur. Std.*, **24**, 369 (1940).

(33) H. C. Urey, *J. Chem. Soc.*, 562 (1947).

Table IV: Vibrational Frequencies of the Hydronium Ion

$\nu_1(a_1)$	$\nu_2(a_1)$	$\nu_3(e)$	$\nu_4(e)$	$\nu_L(f)$	Substance	Method and ref.
				H_3O^+		
3235	1060	2590	1700	770	OH_3Cl (solid)	Infrared (34)
3285	1182	~3285?	1577	995?	OH_3ClO_4 (solid)	Raman (35)
	1205	2900	1750	605–625	HCl (soln.)	Infrared (36)
2600	1190	3025	1720	675	HCl (soln.)	Infrared (37)
3025		(3025)			HCl (soln.)	Raman (38)
				643	HCl (soln.)	Infrared (12, 13)
				D_3O^+		
2455	785	2000	1255		OD_3Cl (solid)	Infrared (34)
	960	2170	~1400		DCl (soln.)	Infrared (36)
				465	DCl (soln.)	Infrared (12, 13)

of a solvated electron from one solvent to the other. The value of L thus derived by Purlee should be corrected for the free energy of this transfer process.

Purlee also obtained L from a large number of experimental data for dissociation constants of weak acids and for rate constants of acid-catalyzed reactions. The value of L thus obtained is in good agreement with the value obtained from electrochemical data.

Very recently, Gold[17] and Kresge and Allred[16] have measured an equilibrium constant for the exchange

$$D_3O^+ + HDO = HD_2O^+ + D_2O \qquad (22)$$

which is

$$K_N = (H/D)_{\text{solvated proton}}/(H/D)_{\text{water}} = L^{1/6} \qquad (23)$$

Their measurements depend upon the fact that the proton n.m.r. signal in an acidic aqueous solution is a single peak, owing to the rapid proton exchange between hydronium ion and water molecules. The shift of the peak from that of the pure solvent is related to the concentration of hydronium ion, and the measurement of this shift in light water and almost pure heavy water leads to K_N. In this work it has been tacitly assumed that any shift caused by the anion of the acid used (*i.e.*, effects of the type treated by Hindman[18]) will cancel out in the comparison of light and heavy water solvents. The fact that we have tried to correct for such an anion effect in our vapor pressure measurements may account, to some extent, for the difference in the values obtained by the two methods. Deviations from the rule of the geometric mean could also lead to a discrepancy.

Swain and Bader[12,13] have proposed a model for calculating the partition function ratio for D_3O^+/H_3O^+ in aqueous solution. They find a free energy differ-

ence of 9270 cal. mole^{-1} between H_3O^+ and D_3O^+. While they do not describe their calculations in detail, it is apparent that there is an error in them. The intramolecular vibrational frequencies of H_3O^+ and D_3O^+ have been measured both in acid solutions and in hydronium ion salts,[34-38] but there is considerable disagreement as to the assignments, particularly of the O–H stretching frequencies (*cf.* Table IV). We have calculated the partition function ratio from the vibrational frequency assignment of Ferriso and Hornig together with the estimated librational frequencies of Swain and Bader. In this way (presumably that followed by Swain and Bader) we obtain $F_{D_3O^+} - F_{H_3O^+} = -5500$ cal. mole^{-1} compared with their value of -9270 cal. mole^{-1}.

Both Purlee and Swain and Bader have emphasized the care which must be taken to exclude contributions to L from the process of transferring an ion from light to heavy water. The latter authors have proposed a model for calculating thermodynamic quantities for such a transfer of single ions. In the case of the hydronium ion, it is believed that its effect on the structure of water is relative slight, since it is capable of hydrogen bonding. Similar arguments have been used (for example, by Hindman[18]) in the case of the ammonium ion. The assumption is made, therefore, that the free energy of transfer of the hydronium ion is zero, and that ΔF_L, the free energy change corresponding to L, is given by the isotopic free energy differences of H_3O^+ and H_2O. If this is done with the values obtained from the spectra of

(34) C. C. Ferriso and D. F. Hornig, *J. Chem. Phys.*, **23**, 1464 (1955).

(35) R. C. Taylor and G. L. Vidale, *J. Am. Chem. Soc.*, **78**, 5999 (1956).

(36) M. Falk and P. A. Giguère, *Can. J. Chem.*, **35**, 1195 (1957).

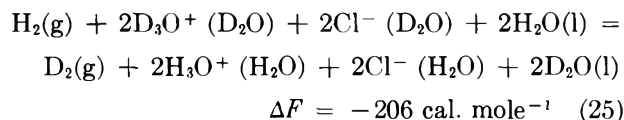(37) G. E. Walrafen, *J. Chem. Phys.*, **36**, 1035 (1962).

(38) W. R. Busing and D. F. Hornig, *J. Phys. Chem.*, **65**, 284 (1961).

H_3O^+, one obtains $L = 24.0$. (The value of ΔF used by Swain and Bader leads to L less than unity.) It is apparent that the spectroscopic data are not a good basis for the calculation of L, since an error of 50 cm.$^{-1}$ in the zero-point energy difference between H_3O^+ and D_3O^+ produces a 25% error in L.
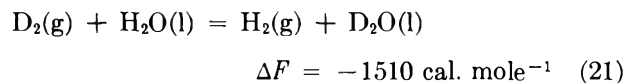
If one accepts the calculations of Swain and Bader for ion transfer processes, another possible route toward L is open, which they have utilized. This involves the e.m.f. measurements by Noonan and La Mer[39] on the cell
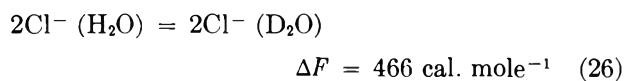
$$H_2, HCl(H_2O)|Ag, AgCl||Ag, AgCl|DCl (D_2O), D_2 \quad (24)$$

the over-all reaction for which may be written

$$H_2(g) + 2D_3O^+ (D_2O) + 2Cl^- (D_2O) + 2H_2O(l) =$$
$$D_2(g) + 2H_3O^+ (H_2O) + 2Cl^- (H_2O) + 2D_2O(l)$$
$$\Delta F = -206 \text{ cal. mole}^{-1} \quad (25)$$

This may be combined with the ΔF values[12,32] for

$$D_2(g) + H_2O(l) = H_2(g) + D_2O(l)$$
$$\Delta F = -1510 \text{ cal. mole}^{-1} \quad (21)$$

and

$$2Cl^- (H_2O) = 2Cl^- (D_2O)$$
$$\Delta F = 466 \text{ cal. mole}^{-1} \quad (26)$$

to give $\Delta F_L = -1250$ cal. mole^{-1} and $L = 8.25$ at $25°$. If the anion transfer effect were neglected, the value of L would be 18.1 at $25°$. This same value (i.e., with the anion transfer effect neglected) has been obtained by Kingerley and La Mer[40] from measurements with the quinhydrone electrode in light and heavy water.

The Effect of Temperature on L. In order to compare the experimental values of L or K_L obtained at various temperatures, some estimate of H_L is needed. In view of the uncertainty of the spectroscopic data for the hydronium ion, it seems useless to attempt to calculate $H_{H_3O^+} - H_{D_3O^+}$ from that direction.

The combination of ΔH values for reactions 25, 21, and 26 gives $\Delta H_L = -1096$ cal. mole^{-1}. The one doubtful quantity here is the heat of transfer of a chloride ion from light to heavy water. If this contribution is set equal to zero, then ΔH_L is almost twice as large, with the value of -1856 cal. mole^{-1}.

Another method of evaluating the temperature coefficient is to calculate the entropy difference between H_3O^+ and D_3O^+ and to combine this with an experimental value of L to obtain ΔH_L. If this is done with the vibrational frequencies used to calculate L (only

the librations and bending vibrations contribute) and our value of $L = 9.1$, we find -1555 cal. mole^{-1} for ΔH_L. The rather unreasonable assumption of free rotation for the ion in solution would lead to a value of -760 cal. mole^{-1}.

Fortunately, this temperature effect is reduced by a factor of six in its effect on K_L, so that the uncertainty does not exceed the experimental error in K_L. We have used an approximate value of -1000 cal. mole^{-1} for ΔH_L to correct K_I to the values given in Table III.

Structure of the Hydrogen Ion in Aqueous Solution. In the preceding section of the paper we have shown that our value of K_L is in good agreement with that from other measurements, if we assume that the solvated proton is formulated as H_3O^+. We shall now show that such agreement is found only for this formulation, and that any other one leads to disagreements outside the limits of experimental error.

Let us rewrite eq. 3 in the more general form

$$2D^+ (D_2O)_n + (2n + 1)H_2O =$$
$$2H^+ (H_2O)_n + (2n + 1)D_2O \quad (27)$$
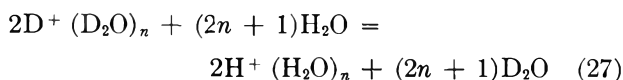
where there are $2n + 1$ equivalent hydrogen atoms in the solvated proton. The equilibrium constant is

$$\lambda = \frac{(D_2O)^{2n+1}[H^+ (H_2O)_n]^2}{(H_2O)^{2n+1}[D^+ (D_2O)_n]^2} \quad (28)$$

and of course, λ is identical with L when n is unity. The constant $\varkappa_L$ for the general form of the equilibrium

$$H_2O + D^+ (H_2O)_n = HDO + H^+ (H_2O)_n \quad (29)$$

now becomes

$$\varkappa_L = 2\lambda^{1/2(2n+1)}/(2n + 1) \quad (30)$$

while the quantity measured in the n.m.r. experiments is

$$(H/D)_{solvated\ proton}/(H/D)_{water} = \varkappa_N = \lambda^{1/2(2n+1)} \quad (31)$$

This leads to

$$\varkappa_L = \frac{2}{2n + 1} \varkappa_N \quad (32)$$

We should also reformulate the expression for $\varkappa_L$ in terms of our experimental quantities. Equations 5 and 6 are unchanged, while eq. 1, 4, and 7–11 now become

$$\varkappa_L = \frac{N_{HDO}N_{H^+(H_2O)_n}}{N_{H_2O}N_{D^+(H_2O)_n}} \quad (33)$$

(39) E. C. Noonan and V. K. La Mer, *J. Phys. Chem.*, **43**, 247 (1939).
(40) R. W. Kingerley and V. K. La Mer, *J. Am. Chem. Soc.*, **63**, 3256 (1941).

$$\alpha_A = \frac{(D/H)_L}{(D/H)_V} = \frac{N_{HDO} + N_{DA} + N_{D^+(H_2O)_n}}{2N_{H_2O} + N_{HA} + (2n + 1)N_{H^+(H_2O)_n}}$$

(34)

$$r = \frac{N^0_{HA}}{N^0_{H_2O}} = \frac{N_{HA} + N_{H^+(H_2O)_n}}{N_{H_2O} + nN_{H^+(H_2O)_n}}$$

(35)

$$q = \frac{N_{H^+(H_2O)_n}}{N_{H^+(H_2O)_n} + N_{HA}}$$

(36)

$$N_{H_2O} + N_{HA} + 2N_{H^+(H_2O)_n} = 1$$

(37)

$$x_L = \frac{rq}{(\alpha_A/\alpha_w)[1 + (r/2)] - 1 + rqn - r(1 - q)/K_A}$$

(38)

If $q = 1$

$$x_L = \frac{r}{(\alpha_A/\alpha_w)[1 + (r/2)] - 1 + rn}$$

(39)

The dependence on n is more apparent when we write

$$x_L^{-1} = n + (rq)^{-1}[(\alpha_A/\alpha_w)(1 + r/2) - 1] - (1 - q)/K_A q$$

(40)

A comparison of our values for x_L for different values of n with those of Gold[17] and of Kresge and Allred[16] is given in Table V. Agreement with both sets of

Table V: Relation between x_L and x_N

n	x_L	$\frac{2}{2n+1} x_N$ Gold[a]	$\frac{2}{2n+1} x_N$ Kresge and Allred[b]
0	23.8	2.92	2.80
1	0.96	0.97	0.98
2	0.49	0.58	0.63
3	0.33	0.42	0.50
4	0.25	0.32	0.49

[a] See ref. 17. [b] See ref. 16.

n.m.r. measurements is found only when n is unity, although the two n.m.r. experiments were treated slightly differently.

We have indicated above that there are difficulties in the evaluation of λ from electrochemical data or from the dependence of rate and equilibrium constants on solvent isotopic composition. Because of this, we consider a comparison of x_N and x_L values a better way of determining n than a comparison of either of these with λ. Furthermore, the comparison of x_L and λ is particularly insensitive to n because of the way in which x_L is determined from experimental parameters. As n increases, x_L from either eq. 30 or 40 approaches n^{-1}. For example, if λ is either 8.1 or 18.1, the agreement between the experimental value of x_L and $2\lambda^{1/2(2n+1)}/(2n + 1)$ is within experimental error for $n \geq 1$.

These conclusions do not exclude the model for the hydrogen ion proposed several years ago by Wicke, et al.,[41] in which a hydronium ion is further solvated by three water molecules hydrogen-bonded to the ion. Support for this model comes from heat capacities and molal volumes, which are markedly similar for solutions of HCl and LiCl, for example. The formulation above is a slight over-simplification, in that the effect on the three hydrogen-bonded solvent molecules is neglected. That is, the n.m.r. shift for these protons is neglected by comparison with those on the central ion. This appears to be a not unreasonable simplification, in view of the relative magnitude for the shifts caused by the hydrogen ion and other cations.[17] Similar considerations should apply to the effect on the separation factor between liquid and vapor.

(41) E. Wicke, M. Eigen, and T. Ackermann, Z. Physik. Chem. (Frankfurt), 1, 340 (1954).

Chain Reactions in the Chemiluminescent Oxidation of Certain

Phthalazinediones by Potassium Peroxydisulfate[1]

by John R. Totter, Wayne Stevenson, and G. E. Philbrook

Chemistry Department, University of Georgia, Athens, Georgia   *(Received August 14, 1963)*

A study of the relationship between maximum intensity of chemiluminescence of mixtures of phthalazinedione and peroxydisulfate ions in 0.1 M NaOH has been made for 5-[N-methylamino]-2,3-dihydro-1,4-phthalazinedione. The results may be explained on a kinetic basis by the assumption that a chain reaction is initiated by a reaction between the phthalazinedione and peroxydisulfate which produces a radical from each reactant. Chains are presumably terminated by reaction of the SO_4^- radical with H_2O and subsequent decomposition of the OH formed, and by a reaction of two phthalazinedione radicals with $S_2O_8^{-2}$ with no radical end products. Similar studies with the 5-hydroxy-2,3-dihydro-1,4-phthalazinedione indicate that this compound reacts only very slowly with peroxydisulfate ion; hence a mixture of the two serves as a chemiluminescent "indicator" for radicals which are capable of initiating a similar chain reaction at rates above the spontaneous rate for SO_4^- radical formation. 5-Amino-2,3-dihydro-1,4-phthalazinedione luminescence (as well as that of other phthalazinediones) is sharply reduced by the addition of a radical scavenger which does not react at an appreciable rate with peroxydisulfate ion.

Introduction

Although there have been numerous theories concerning the course of reaction of phthalazinediones with oxidizing agents leading to the emission of light, few of these have been based upon extensive kinetic data.[2-4] In part, this doubtless results from the fact that the end product of the reaction leading to light emission has not been identified with certainty. In addition, it is hazardous to base conclusions on data derived from a disappearance of the reactants when the light-emitting reaction may be only a minor fraction of the total reaction taking place. Bremer[4] and others have suggested that the chemiluminescence probably arises from the reaction of two radicals: one derived from the phthalazinediones, the other arising from the oxidizing agent, whether this is oxygen or some other substance. It was pointed out by Bremer that it is unlikely that nonradical reactions could provide the energy of 75 kcal./einstein required to emit the short wave lengths characteristic of luminol (5-amino-2,3-dihydro-1,4-phthalazinedione) chemiluminescence.

Recent revival of interest in the possibility of using the phthalazinediones as "indicators" of radical involvement in other reactions[5-7] has encouraged us to restudy some of the kinetics of chemiluminescence in this series. It is hoped that careful studies may lead to a sounder basis upon which to construct hypotheses concerning the reactions leading to light emission.

(1) This work was supported in part by a grant from the Air Force Office of Research and Development (AFOSR-62-73), and by a contract with the U. S. Atomic Energy Commission (AT-(40-1)-2851). The authors are indebted to Dr. W. J. DeAngelis of the Department of Chemistry of The University of Georgia for the preparation of the xanthine oxidase used in the experiment.

(2) P. C. Wilhelmsen, R. Lumry, and H. Eyring, in "The Luminescence of Biological Systems," F. H. Johnson, Ed., American Association for the Advancement of Science, Washington, D. C., 1955, pp. 75-98.

(3) F. H. Johnson, H. Eyring, and M. J. Polissar, "The Kinetic Basis of Molecular Biology," John Wiley and Sons, New York, N. Y., 1954, pp. 139-186.

(4) T. Bremer, *Bull. soc. chim. Belges*, 62, 569 (1953).

(5) J. R. Totter, V. J. Medina, and J. L. Scoseria, *J. Biol. Chem.*, 235, 238 (1960).

(6) J. R. Totter, E. C. de DuGros, and C. Riveiro, *ibid.*, 235, 1839 (1960).

(7) L. Greenlee, L. Fridovich, and P. Handler, *Biochemistry*, 1, 779 (1962).

At the same time, efforts have been made to identify the product whose activated state emits light. The latter studies have been only partially successful, owing to the difficulty that the product is unstable in the presence of oxidizing agents used for its production. It is for this reason that kinetic studies based on the disappearance of the reactants or the appearance of any single end product are unsatisfactory. The present report, therefore, deals chiefly with the relationship of the concentration of the reactants to maximum light intensity, which is taken to be a measure of the rate of formation of the significant activated intermediate.

Light emission from 5-amino-2,3-dihydro-1,4-phthalazinedione (luminol) in the presence of peroxydisulfate ion was noted by Steigmann[8] some years ago. This reaction has been investigated further by Totter and Gordillo,[9] who noted sustained light emission suggestive of a chain reaction when luminol and potassium peroxydisulfate are mixed under proper pH conditions. It was suggested by these authors that the relationship between light intensity and hydroxyl ion concentration might be used as a measure of dissociation constant of OH radicals, since a typical titration curve was observed. Subsequent work, however, indicates that such a titration curve cannot always be seen, especially if highly purified luminol is employed in the determinations.

It may be assumed that if oxidations not requiring a chain mechanism are the only reactions involved in the production of luminescence in mixtures of potassium peroxydisulfate and phthalazinediones under alkaline conditions, the maximum light intensity under appropriate conditions should bear a simple relationship to the concentrations of reactants. However, if a chain mechanism is operative, one would expect that there might be deviations from such a relationship. Accordingly, the maximum light intensities have been determined for mixtures of certain phthalazinediones and potassium peroxydisulfate with wide variations in reactant concentrations. It was in fact observed, in some cases at least, that the maximum intensities do not bear a relationship to the product of the concentrations of the two reactants expressible with a single proportionality constant. In the case of 5-[N-methylamino]-2,3-dihydro-1,4-phthalazinedione with peroxydisulfate concentration held constant, the relationship apparently varies from the $^1/_2$ power of the phthalazinedione to the $^3/_2$ power at extreme ranges of concentrations tested. Other phthalazinediones show less marked deviations, but in some cases tested, the plot of the logarithm of the maximum intensity of light against the logarithm of the concentration of the phthalazinedione at constant peroxydisul-

Table I: Ultraviolet Spectra of Phthalazinediones

Substituent	Concn. of NaOH, mole l.$^{-1}$	Wave length max., mμ	ϵ, l. cm.$^{-1}$ mole^{-1}
5-NH$_2$	0.1	348	7870
		315	7210
5-OH	0.1	332	7133
		315	6620
5-[N-methylamino]	0.01	366	7850
		303	8150
		223	7800

fate concentration gives either a curved line (as in the case with the 5-[N-methylamino] compound) or a line which has a slope differing more or less from 1, indicating the occurrence of fractional powers in the kinetic equations describing the reactions. This behavior is characteristic of chain reactions, and other data available support the conclusion that a chain reaction is important in the chemiluminescent oxidation of certain of the phthalazinediones by peroxydisulfate in alkaline solutions.

Experimental

5-[N-Methylamino]-2,3-dihydro-1,4-phthalazinedione was prepared according to the method of Drew and Hatt[10] and purified by repeated recrystallization from acetic acid with charcoal treatment. 5-Hydroxy-2,3-dihydro-1,4-phthalazinedione was prepared from 3-hydroxyphthalimide by the method of Drew and Pearman.[11] 5-Amino-2,3-dihydro-1,4-phthalazinedione was prepared by the method of Drew and Pearman[12] from the corresponding phthalimide.

Ultraviolet absorption data on these compounds are presented in Table I. The spectral data and paper chromatograms indicate only very minor amounts of impurities.

Measurements of the intensity of the light emitted were made by means of a photomultiplier with amplifier and recorder similar to that described by Cormier.[13] A tritiated light source (Tracerlab Corp.) with an area of 1 cm.^{2} emitting approximately 1×10^{11} quanta/sec. with a wave length maximum at 500 mμ was used to determine instrumental corrections for amplifier

(8) A. Steigmann, *J. Soc. Chem. Ind.*, **61**, 68 (1942).

(9) J. R. Totter and A. E. Gordillo, *Anales Fac. Med., Montevideo*, **46**, 37 (1961).

(10) H. D. K. Drew and H. H. Hatt, *J. Chem. Soc.*, **140**, 16 (1937).

(11) H. D. K. Drew and F. H. Pearman, *ibid.*, **140**, 26 (1937).

(12) H. D. K. Drew and F. H. Pearman, *ibid.*, **140**, 686 (1937).

(13) M. J. Cormier and L. S. Dure, *J. Biol. Chem.*, **238**, 785 (1963).

variation. The equipment indicated a current of 7×10^{-6} amp. with this source in the sample position.

Mixtures of potassium peroxydisulfate and sodium hydroxide, prepared in a 1.2×10.0 cm. test tube so that the final volume would be 5 ml. of solution 0.1 M in sodium hydroxide, were placed in the sample compartment with the shutter closed. Oxygen was bubbled through the samples for 1–2 min. before adding an appropriate amount of the phthalazinedione from a pipet and throughout the course of the subsequent readings. The sample holder was closed and the shutter opened as quickly as possible. The readings were taken immediately or after the light intensity had reached its maximum in those cases where the maximum was delayed presumably because of traces of scavenging impurities. Underestimation of the maximum light intensity, because of the speed of the reaction, occurred only when the phthalazinedione concentration was higher than 0.01 M. In all of the cases there was ample time for the manipulations before the intensity reached its maximum or the decline in intensity was sufficiently slow that extrapolation to mixing time was possible.

Temperature variations were less than $\pm 0.5°$. The actual temperatures of the solutions are given in legends to the figures.

Results

The data from a series of experiments with 5-[N-methylamino]-2,3-dihydro-1,4-phthalazinedione are shown in Fig. 1. Empirically it was determined that a
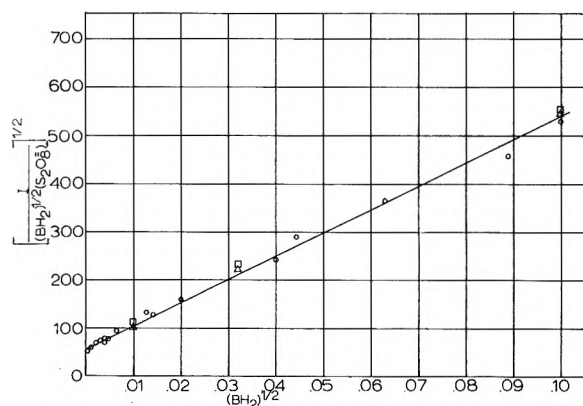

Figure 1. The relationship between maximum chemiluminescence intensity in 0.1 M NaOH and the concentrations of $S_2O_8^{-2}$ ion and 5-[N-methylamino]-2,3-dihydro-1,4-phthalazinedione. Ordinate: $[I/(BH_2)^{1/2}(S_2O_8^{-2})]^{1/2}$; abscissa: $(BH_2)^{1/2}$; the intensity is given in arbitrary units; O, $(S_2O_8^{-2})$ 1 $\times$ 10^{-2} M; □, 5 $\times$ 10^{-3} M; △, 5 $\times$ 10^{-5} M; $T = 25.5°$. The observed values for 5 $\times$ 10^{-5} M $(S_2O_8^{-2})$ have been multiplied by 1.09 to correct for photomultiplier sensitivity.
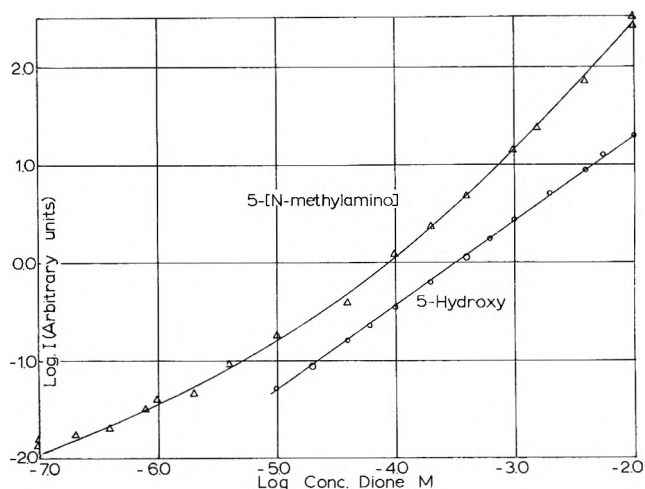

Figure 2. The relationship between maximum chemiluminescence intensity and 5-hydroxy-2,3-phthalazine-1,4-dione concentration in 0.1 M NaOH. Ordinate: logarithm of maximum intensity in arbitrary units; abscissa: logarithm of the phthalazinedione concentration. The upper curve is the theoretical curve calculated from the constants obtained from Fig. 1. The points are typical results with 5-[N-methylamino]-2,3-phthalazine-1,4-dione; temperature, 26°.

straight line was given when $[I/(BH_2)^{1/2}(S_2O_8^{-2})]^{1/2}$ was plotted against the square root of the phthalazinedione concentration.[14] A large number of experiments of this type were conducted and the results invariably conformed to the relationship shown in Fig. 1. (Many of the points have been omitted for the purpose of clarity.) The relationship

$$ I = K_1^2(BH_2)^{1/2}(S_2O_8^{-2}) + $$
$$ 2K_1K_2(BH_2)(S_2O_8^{-2}) + K_2^2(BH_2)^{3/2}(S_2O_8^{-2}) $$

was derived from the data of Fig. 1. This equation has been tested with phthalazinedione concentrations from 10^{-7} to 10^{-2} M and $S_2O_8^{-2}$ concentrations from 5×10^{-5} to 1×10^{-2} M with no indication of systematic deviation from the stated relationship. So far as can be determined without the use of high speed equipment, the equation is applicable to the initial stages of the reaction up to and including the maximum, provided extraneous scavengers are rigidly excluded. The reproducibility of determinations is fair considering that this is probably a free radical system. Twenty-four replicates of one experiment gave an average deviation from the mean of 12% with a maximum deviation of 26%.

In contrast to the 5-[N-methylamino]-2,3-dihydro-1,4-phthalazinedione, similar experiments with 5-

(14) Where I is the maximum chemiluminescence intensity, (BH_2) is the concentration of phthalazinedione, and $(S_2O_8^{-2})$ is the concentration of peroxydisulfate.
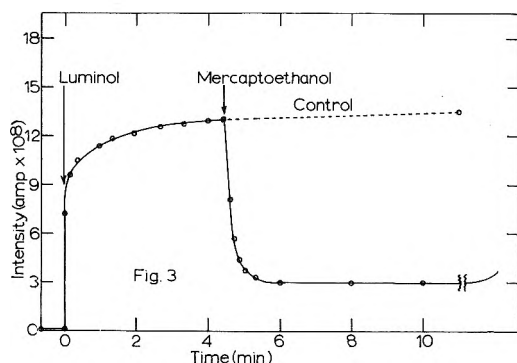
Figure 3. Effect on luminescence intensity of addition of mercaptoethanol to 8×10^{-5} M (at arrow) to a 2.5×10^{-4} M 5-amino-2,3-phthalazine-1,4-dione solution in 0.1 M NaOH and 5×10^{-3} M $K_2S_2O_8$.
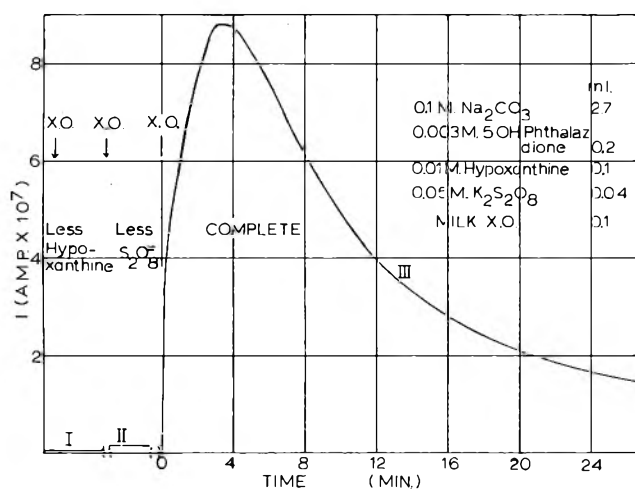

Figure 4. Effect of enzymatic oxidation of hypoxanthine on chemiluminescence of 5-hydroxy-2,3-phthalazine-1,4-dione in the presence of $K_2S_2O_8$. Conditions: 2×10^{-4} M phthalazinedione; 3.3×10^{-4} M hypoxanthine; 6.7×10^{-4} M $K_2S_2O_8$; 0.09 M Na_2CO_3 and 0.1 ml. milk xanthine oxidase solution added at arrows to a total volume of 3 ml. Blanks: hypoxanthine omitted in first test, $K_2S_2O_8$ in second.
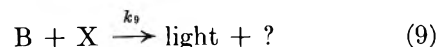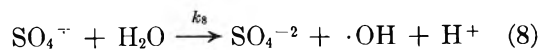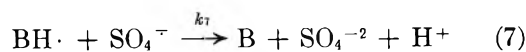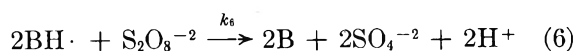
hydroxy-2,3-dihydro-1,4-phthalazinedione resulted in the data shown in Fig. 2, where the logarithm of the maximum intensity is plotted against the logarithm of the phthalazinedione concentration. In this case the deviation from a straight line is very slight. The curve obtained with the 5-[N-methylamino] analog is shown on the same figure for comparison. Conditions were comparable for the two compounds.

The postulate that these reactions follow a radical mechanism is supported by the results shown in Fig. 3 and 4. Figure 3 shows that a known radical scavenger, mercaptoethanol, is capable of dramatically reducing the light emission for the 5-[N-methylamino]

compound even when the scavenger concentration is very low compared with the oxidizing agent concentration. With 5-hydroxy-2,3-dihydro-1,4-phthalazinedione it is possible to increase greatly the light output by adding a source of "radicals" as shown in Fig. 4. This was accomplished by adding the enzyme xanthine oxidase and its substrate, hypoxanthine, to the chemiluminescent system. The oxidation catalyzed by this enzyme is known from the work of others[15-17] to produce radicals. Differences as observed in this case were scarcely detectable with the 5-[N-methylamino] compound and are relatively small with luminol itself.

Discussion

The following reactions may account for the kinetics observed and are among those which might be postulated to occur in alkaline mixtures of phthalazinediones and peroxydisulfate ions.

$$S_2O_8^{-2} \xrightarrow{k_1} 2SO_4^- \quad (1)$$

$$BH_2 + O_2 \xrightarrow{k_2} BH\cdot + O_2H\cdot \quad (2)$$

$$BH_2 + S_2O_8^{-2} \xrightarrow{k_3}$$
$$BH\cdot + SO_4^- + SO_4^{-2} + H^+ \quad (3)$$

$$SO_4^- + BH_2 \xrightarrow{k_4} BH\cdot + SO_4^{-2} + H^+ \quad (4)$$

$$BH\cdot + S_2O_8^{-2} \xrightarrow{k_5}$$
$$B + SO_4^- + SO_4^{-2} + H^+ \quad (5)$$

$$2BH\cdot + S_2O_8^{-2} \xrightarrow{k_6} 2B + 2SO_4^{-2} + 2H^+ \quad (6)$$

$$BH\cdot + SO_4^- \xrightarrow{k_7} B + SO_4^{-2} + H^+ \quad (7)$$

$$SO_4^- + H_2O \xrightarrow{k_8} SO_4^{-2} + \cdot OH + H^+ \quad (8)$$

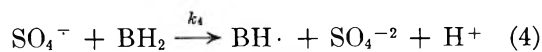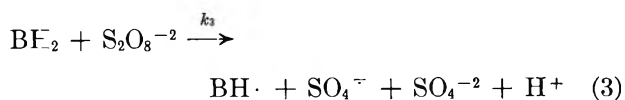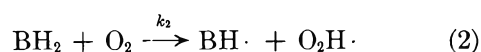$$B + X \xrightarrow{k_9} light + ? \quad (9)$$
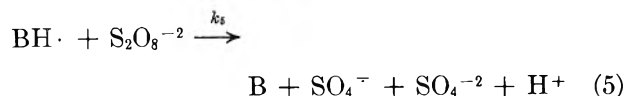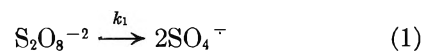
Under conditions where reaction 3 is much faster than reactions 1 and 2, these latter may be ignored. A steady-state solution for light intensity when reaction 5 is the major source of B (hence (4) and (5) are going at about the same rates) is approximated by the equation

(15) G. Parravano, *J. Am. Chem. Soc.*, **73**, 183 (1951).
(16) R. C. Bray, B. G. Malmström, and T. Vänngard, *Biochem. J.*, **71**, 24p (1959).
(17) I. Fridovich and P. Handler, *J. Biol. Chem.*, **233**, 1578 (1958).

$$I \propto k_9(B)(X) = \left[\frac{k_3}{2k_6}\right]^{1/2} k_5(BH_2)^{1/2}(S_2O_8^{-2}) +$$

$$k_3(BH_2)(S_2O_8^{-2}) + \left[\frac{k_3^{3/2}}{(2k_6)^{1/2}k_8}\right]\left[\frac{(BH_2)^{3/2}(S_2O_8^{-2})}{(H_2O)}\right]$$

(10)

If

$$\left[\frac{2k_5}{k_6}\right]^{1/2} = k_8(H_2O)$$　　　(11)

the relationship is a perfect square and may be expressed in the form

$$\left[\frac{k_9(B)(X)}{(BH_2)^{1/2}(S_2O_8^{-2})}\right]^{1/2} = \left[\frac{k_3}{2k_6}\right]^{1/4} k_5^{1/2} +$$

$$\left[\frac{k_3^{3/4}}{2k_6^{1/4}k_8^{1/2}(H_2O)^{1/2}}\right](BH_2)^{1/2}$$

which is analogous to the square root of the empirical equation given above. The constant (k_3) and the ratio of constants obtainable from Fig. 1, however, contain an expression for the quantum yield and geometry of the light measuring system, neither of which is known accurately.

It may be objected that it is improbable that eq. 11 should be valid fortuitously. No simpler expression which reduces the number of constants has been found satisfactory, however, and most of the eq. 1–9 appear to be unobjectionable. Equations 1 and 8 have been postulated by Kolthoff and Miller[18] and by Wilmarth and collaborators,[19] who have made recent studies of the decomposition of peroxydisulfate. The OH radical may be equivalent to the SO_4 radical, but if so must also disappear by a first-order reaction to satisfy the experimental data. Equation 2 helps to account for a small amount of light given by solutions of phthalazinediones in alkali. It is not used in the derivation of eq. 10 but may be of some significance in chemiluminescence of the 5-hydroxy compound.

Equation 3 is similar to initiation reactions of other types as discussed by Frost and Pearson[20]; reactions 4 and 5 are typical chain propagation reactions. Chain breaking must involve a reaction which is second order with respect to BH· in order to account for the fractional powers seen in the kinetic measurements and (6) may be written in other ways. However, the method chosen, even though it involves a third-order reaction, appears the most satisfactory since all other formulations tried created additional complexities. The substance X in reaction 9 may be oxygen (or an oxygen-containing radical) as indicated by Bremer's conclusion

(5). Oxygen is required as shown by a sharp reduction in light intensity (less than 5% of that with O_2) when the oxygen is replaced by N_2. Wilhelmsen, et al.,[2] have studied the effects of oxygen concentration in the hydrogen peroxide oxidation. The end product is unknown, however, and must be left unidentified.

The fact that the theoretical equation appears to be valid over a wider range than is justified by the assumptions used in its derivation may be due to compensating adjustments in the rates as (7) becomes quantitatively important as a termination reaction. Thus the $BH_2^{1/2}$ in the third term of (10) approaches BH_2^2 as reaction 7 increases in importance and is compensated for by an increased rate of disappearance of SO_4^-.

With the clarification of the series of reactions involved (at least in a kinetic, if not in a mechanistic sense) it was evident at once that if a chemiluminescent phthalazinedione could be found that did not react rapidly with peroxydisulfate to initiate chains as in reaction 3, it would be possible to use it in the presence of $S_2O_8^{-2}$ to demonstrate by chemiluminescence the presence of radicals from other sources when these were capable of reacting with either BH_2 or $S_2O_8^{-2}$ to start a chain. 5-Hydroxy-2,3-dihydro-1,4-phthalazinedione is such a compound. The "blank" light intensity with this compound arises presumably chiefly from reaction 5, the chains being initiated by reactions 1 and to a lesser extent by (2). The BH· concentration does not get high enough from (2) to make the third-order reaction quantitatively important, although the line relating light intensity to phthalazinedione concentration does show a slight curvature (Fig. 2). The fulfillment of the prediction based upon the kinetic studies is seen in Fig. 4 as indicated above. It is interesting that in experiments not shown, the addition of P^{32} as a "source" of radicals caused no increase in light intensity above the blank value unless H_2O_2 was substituted for $S_2O_8^{-2}$. This undoubtedly indicates some qualitative difference in the types of radicals derived from this source as compared with the enzymic reaction.

Although the precise reactions involved are not necessarily indicated by a set of equations satisfactory from the kinetic point of view, the equations postulated above are highly suggestive. It has not been possible, for example, to obtain a satisfactory kinetic solution with a one-equivalent oxidation of luminol

(18) I. M. Kolthoff and I. K. Miller, J. Am. Chem. Soc., **73**, 3055 (1951).

(19) M. Tsao and W. K. Wilmarth, J. Phys. Chem., **63**, 346 (1959).

(20) A. A. Frost and R. G. Pearson, "Kinetics and Mechanism," 2nd Ed., John Wiley and Sons, New York, N.Y., 1961, pp. 236–261.

followed solely by reactions with other oxidizing radicals.

The two-equivalent oxidation prior to chemiluminescence strongly suggests that the activated intermediate which emits light might be derived from "B" by the spontaneous elimination of N_2 followed by reaction with oxygen of the substituted phthalyl biradical left. A similar reaction occurs when phenyl-

hydrazine is oxidized with oxyhemoglobin giving rise to N_2, and apparently fleetingly to phenyl radical and H atoms which appear as benzene.[21-23]

(21) G. H. Beaven and J. C. White, Nature, 173, 389 (1954).

(22) H. H. Rostorfer and J. R. Totter, J. Biol. Chem., 221, 047 (1956).

(23) H. H. Rostorfer and M. J. Cormier, Arch. Biochem. Biophys., 71, 235 (1957).

The Exchange of Twenty Metal Ions with the Weakly

Acidic Silanol Group of Silica Gel[1,2]

by Donald L. Dugger, Jimmy H. Stanton, Bobby N. Irby, Bobby L. McConnell, William W. Cummings, and Russell W. Maatman[3]

Department of Chemistry, The University of Mississippi, University, Mississippi   (Received August 26, 1963)

Free energies, heats, and enthalpies are reported for the exchange of 17 metal ions, and free energies for three other ions, with the weakly acidic silanol (-SiOH) groups of the surface of hydrated silica gel. The reaction is that of the formation of a metal–surface complex infinitely dilute on the surface. The acid dissociation constant of -SiOH is estimated to be 10^{-6} to 10^{-8}; with this value the free energy of the $-SiO^-$–metal ion bond is calculated. The bond free energy depends to a first approximation upon the charge density at the surface of the bare ion and not upon the electronegativity of the corresponding atom or the ability of the ion to form inner complexes. The free energy of the bond is proportional to log K for the association of the metal ion with one hydroxyl ion. The surface complex exhibits the chelate effect.

Introduction

The silanol group (-SiOH) of the hydrated silica gel surface is weakly acidic and there is therefore some cation exchange when the gel is mixed with an aqueous electrolyte. The reaction

$$M^{n+} + m(-SiOH) \rightleftharpoons M(OSi-)_m^{n-m} + mH^+ \quad (I)$$
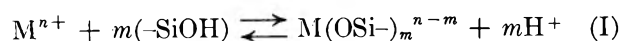
is reversible in acid solution.[4-6]

The purpose of the present work is the determination of the thermodynamic functions of cation exchange at infinite surface dilution and interpretation of the results in terms of a ligand–cation type of reaction.

Other workers have generally been interested in exchange at a finite amount of metal coverage. Earlier,

(4) J. Stanton and R. W. Maatman, J. Colloid Sci., 18, 132 (1963).

(5) A. M. Petrov, Tr. Khim. i Khim. Tekhnol., 1, 229 (1958).

(6) D. N. Strazhesko and G. F. Yankovskaya, Ukr. Khim. Zh., 25, 471 (1959).

we reported results for UO_2^{2+} [4] and Th^{4+} [7]; the results for 20 more cations are given here, and it is now possible to make some general conclusions.

Experimental

Materials. Code 40 Davison silica gel, 6–12 mesh, was acid-washed according to the procedure of Ahrland, Grenthe, and Noren, who showed that the product is completely in the silanol form.[8] The pore volume (water absorption) is 0.40 ml./g. and the surface area (B.E.T.) is 498 m.^{2}/g.[9]

To avoid metal-solution anion reaction, the salts used were nitrates, except for Fe^{3+}, where it was necessary to use the perchlorate. The salts used and their sources were: ferric perchlorate (containing some $HClO_4$), K and K Laboratories; the nitrates of gadolinium, strontium, and samarium from Lindsay, Mallinckrodt, and Fairmount, respectively; the nitrates of barium and nickel, Baker; lanthanum nitrate, A. D. Mackay and Fisher; scandium nitrate, special preparation from Fisher; other salts, Fisher reagent grade.

Buffer of pH 4.00 ± 0.01, 4.0, and 7.0 ± 0.02 were obtained from Fisher, Sargent, and Beckman, respectively. A pH 2.0 buffer was made by diluting to 100 ml. a mixture of 5.3 ml. of 0.200 M HCl and 25 ml. of 0.200 M KCl.

General Procedure. In the standard experiment the ratio of the volume of the salt solution used to the weight of the gel was 1.667 ml./g.; usually, 20 ml. of solution was mixed with 12 g. of gel. The solution and gel remained in contact, with frequent shaking, for 48 hr. except where otherwise noted. The temperature was controlled by using either a room controlled at 20° or a water bath; at the elevated temperatures the solution-gel mixtures were kept in flasks fitted with reflux condensers. Analyses for both hydrogen ion and metal ion were carried out on aliquots of the stock solution and the equilibrium solution.

Analytical. The metal ion and method of analysis, respectively, were: alkali metal and Ba^{2+}, drying of nitrate at 110° for at least 18 hr.; Ag^+, thiocyanate titration; Cr^{3+}, spectrophotometric (Beckman DU); all others, EDTA titration.

The pH values were measured on a Beckman Model GS pH meter. The determination of hydrogen ions produced, as distinguished from hydrogen ions produced by hydrolysis, was made in systems where hydrolysis was significant by the special titration technique described earlier.[4] With Li^+, Na^+, K^+, Mg^{2+}, Ca^{2+}, Sr^{2+}, Ba^{2+}, Ni^{2+}, Zn^{2+}, Cd^{2+}, Ag^+, La^{3+}, Sm^{3+}, and Gd^{3+}, hydrolysis is slight and the hydrogen ion production by the gel reaction was calculated directly

from pH measurements on the stock and equilibrium solutions. No correction due to gel-water interaction was necessary, since the pH values at equilibrium in 5 and 20° blanks, respectively, were 6.25 and 6.29, much higher than all solution equilibrium values.

Silver chloride precipitation prevents the use of an ordinary calomel electrode in the determination of the pH of a silver salt solution. A Beckman sleeve-type electrode, with KCl in the inner compartment and saturated $NaNO_3$ in the outer, was used.

Results

Determination of n and m in Reaction I. Cation hydrolysis was minimized by carrying out experiments at low pH. With Fe^{3+} acid was added to repress hydrolysis. Hydrolysis is not a serious problem with the other ions. Thus for Cr^{3+}, the ion which hydrolyzes more than any other of the group, log $*K_1$ for hydrolysis is -3.9^{10}; in the most dilute Cr^{3+} solution used (9.0×10^{-3} M) at the temperature of the most hydrolysis (65°) 10% of the chromium in the stock solution hydrolyzed, and in the solution which equilibrated with the gel, 2.5% hydrolyzed. Thus, n is essentially the charge of the unhydrolyzed ion.

For the four monovalent ions, m is of course equal to n; the same was shown earlier for UO_2^{2+} and Th^{4+}. By the same technique (determining the number of hydrogen ions produced per metal ion in the pores at equilibrium at low concentrations) it was shown that $m = n$ for Fe^{3+}, one of the ions reported in the present work. Thus for seven of the twenty-two ions considered, $m = n$, and no exception is known. Some assumption about the relationship between m and n for the other fifteen ions is necessary for the calculation of the thermodynamic functions for those ions. It is assumed that $m = n$ in all cases. This assumption is plausible, since it leads to reasonable relationships between the calculated values of the thermodynamic functions for all ions, including the group for which it is known that $m = n$. In addition, it may be inferred from the results of Kozawa in a study of the Zn^{2+} and Cu^{2+} reactions with silica gel that $m = n$ under the

(7) J. Stanton and R. W. Maatman, *J. Colloid Sci.*, 18, 878 (1963).

(8) S. Ahrland, I. Grenthe, and B. Noren, *Acta Chem. Scand.*, 14, 1059 (1960).

(9) For the UO_2^{2+} study[4] a higher surface area was incorrectly used; the UO_2^{2+} values used here therefore differ slightly from those reported.

(10) The equilibrium constants used in this work are taken from (a) the best-value table of D. D. Hedberg, "Sargent Equilibrium Constants of Inorganic Compounds," Copyright 1963 by E. H. Sargent and Co., and (b) estimates of best values from the values compiled by J. Bjerrum, G. Schwarzenbach, and L. G. Sillén, "Stability Constants of Metal-Ion Complexes. Part II. Inorganic Ligands," The Chemical Society, London, 1958.

conditions of our experiment.[11] Where it has not been proved that $m = n$, experiments at very low metal concentrations, such as are possible with radioactive tracer methods, may be carried out later to settle the matter.

The Equilibrium Constant. The apparent equilibrium, K', for reaction I was calculated for several concentrations for all ions and for several temperatures for all but three ions. Assuming that the –SiOH and $M(OSi-)_m$ surface species constitute a surface solution, and that their activities are proportional to their mole fractions, K' is given by

$$K' = \left[\frac{1 - \theta}{m\theta^m}\right]\left[\theta + \frac{1 - \theta}{m}\right]^{m-1} \frac{(C_{H^+})^m}{C_{M^{n+}}}$$

where $m = n$, θ is the fraction of $-SiO^-$ groups in the hydrogen form, and C_{H^+} and $C_{M^{n+}}$ are equilibrium molar concentrations. If there is molecular adsorption of electrolyte on the gel surface, it is slight[12,13]; at any rate, it is irrelevent for the present purpose because K' does not depend upon the amount of adsorbed metal ion. The "constant" K' is designated "apparent"

Table I: Values of pK for Metal Ion–Gel Reaction

Cation	5°	20°	35°	50°	65°
Li$^{+b,c}$	7.2(12)	7.4(11)	7.8(5)	7.5(10)	
Na$^{+b,c}$	6.9(12)	7.0(9)	7.2(5)	7.1(5)	
K$^{+b,c}$	6.9(10)	6.9(12)	7.1(9)	7.1(9)	
Mg$^{2+b,c}$	12.4(6)	12.5(6)	12.5(6)		
Ca$^{2+h,d}$		12.1(7)			
Sr$^{2+b,e}$		12.2(6)			
Ba$^{2+b,c}$	11.9(11)	11.9(10)	11.9(5)		
Al$^{3+c,f}$	9.6(10)	8.5(20)	7.9(10)	7.5(5)	6.4(8)
Sc$^{3+f,g}$	7.6(5)	7.6(10)	7.3(10)	7.1(5)	
Cr$^{3+f,g}$		10.1(8)	9.2(8)	8.6(8)	8.2(8)
Fe$^{3+c,h}$		4.3(16)	4.0(15)	3.7(10)	3.5(10)
Co$^{2+b,g}$		11.2(10)	11.2(10)	11.2(10)	
Ni$^{2+b,g}$	11.7(10)	11.8(10)	11.9(10)	12.0(10)	
Cu$^{2+b,g}$		10.9(4)	10.9(5)	10.8(4)	
Zn$^{2+b,g}$	12.1(5)	11.9(5)	11.7(5)	11.6(5)	
Ag$^{+b,c}$		6.1(4)			
Cd$^{2+b,g}$	12.1(5)	11.9(5)	11.9(5)	11.8(5)	
La$^{3+b,c}$	14.9(10)	14.9(10)	15.0(10)	15.0(13)	
Sm$^{3+b,c}$	13.9(10)	13.7(8)	13.6(10)	13.6(13)	
Gd$^{3+b,c}$	15.9(9)	15.8(10)	15.8(10)	15.6(9)	

^{a} Average error in pK is ± 0.2. Number of pK' values in plots given in parentheses after pK. ^{b} pH values at equilibrium between 3.00 and 4.40. ^{c} Equilibrium concentration lower limit between 0.01 and 0.05 M; upper, between 0.3 and 0.6 M. ^{d} Equilibrium concentrations between 0.11 and 0.91 M. ^{e} Equilibrium concentrations between 0.09 and 0.60 M ^{f} pH values at equilibrium between 1.00 and 2.70. ^{g} Equilibrium concentration lower limit between 0.01 and 0.05 M; upper, between 0.07 and 0.13 M. ^{h} pH values at equilibrium < 1.30.

Table II: Thermodynamic Functions for the Reaction of Metal Ions and the Uranyl Ion with the Surface of Silica Gel^a

Cation	$\Delta F°_{298}$, kcal.	$\Delta H°$, kcal.	$\Delta S°_{298}$, e.u.	$\Delta F_2°/m$, kcal.
Li$^+$	10.1	-3.5	-45.5	0.5
Na$^+$	9.6	-2.6	-40.9	0.0
K$^+$	9.6	-2.5	-40.2	0.0
Mg^{2+}	17.0	-1.4	-61.9	-1.1
Ca^{2+}	16.2^b			-1.5^b
Sr^{2+}	16.4^b			-1.4^b
Ba^{2+}	16.2	0.0	-54.3	-1.5
Al^{3+}	11.5	21.6	34.0	-5.8
Sc^{3+}	10.2	7.3	10.0	-6.2
Cr^{3+}	13.3	24.6	38.0	-5.2
Fe^{3+}	5.8	8.6	9.5	-7.7
Co^{2+}	15.3	0.0	-51.4	-2.0
Ni^{2+}	16.2	-2.0	-61.0	-1.5
Cu^{2+}	14.9	2.0	-56.5	-2.2
Zn^{2+}	16.1	4.2	-39.8	-1.6
Ag$^+$	8.1^b			-1.5^b
Cd^{2+}	16.3	3.1	-44.5	-1.5
La^{3+}	20.2	-1.7	-73.6	-2.9
Sm^{3+}	18.7	3.2	-52.0	-3.4
Gd^{3+}	21.6	2.2	-65.2	-2.4
Th^{4+c}	8.3	11.0	9.1	-7.5
UO$_2^{2+d}$	7.0	3.6	-11.5	-6.1

^{a} Average error in $\Delta F°_{298}$ is ~ 0.3 kcal.; $\Delta H°$, ~ 0.5 kcal. ^{b} For 293°K. ^{c} See ref. 7. ^{d} See ref. 4.

because there are nonideal factors at finite concentrations. For each experiment, θ was calculated from a comparison of the number of hydrogen ions released with the number of silanol groups present $(7.85/m\mu^2$ [14]$)$. Usually θ was well above 0.99. The logarithm of the thermodynamic constant, K, was obtained by extrapolation of log K' to $C_{M^{n+}} = 0$ in a log K' vs. $C_{M^{n+}}$ plot.

The standard states for the species in reaction I are the usual ones for the ions in solution, the pure silanol surface for –SiOH, and for $M(OSi-)_m$ the surface fully covered with metal, with each site possessing the properties it has when infinitely dilute on the surface. In Table I are the pK values at various temperatures for all the cations. In Table II are the free energy, heat (calculated from the temperature coefficient of pK), and entropy of reaction, at 25° except where noted

(11) A. Kozawa. *J. Inorg. Nucl. Chem.*, **21**, 315 (1961).

(12) While there was considerable discussion many years ago whether or not silica gel adsorbed acid, it is now generally agreed that electrolyte adsorption other than exchange is due chiefly to gel impurities.[13]

(13) F. Umland and K. Kirchner. *Z. anorg. allgem. Chem.*, **280**, 211 (1955).

(14) R. K. Iler, "The Colloid Chemistry of Silica and Silicates," Cornell University Press, New York, N. Y., 1955, p. 242.
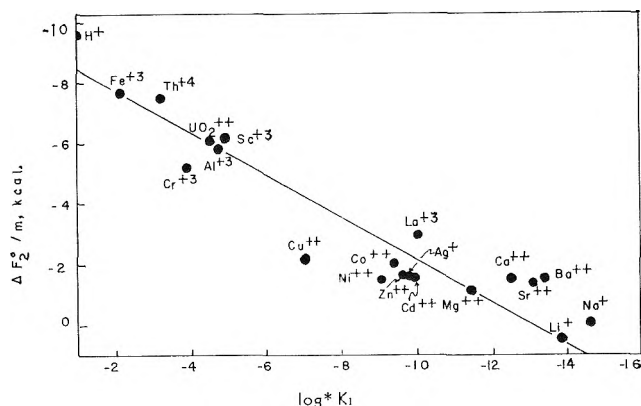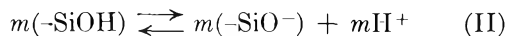
Figure 1. Plot of $\Delta F_2°/m$ vs. log $*K_1$. Three 293°K. values of Table II and $\Delta F_1°$ are included.

Discussion

Nature of the Metal–Oxygen Bond. Reaction I is the sum of two reactions

$$m(\text{-SiOH}) \rightleftarrows m(\text{-SiO}^-) + m\text{H}^+ \quad \text{(II)}$$

$$\text{M}^{n+} + m(\text{-SiO}^-) \rightleftarrows \text{M(OSi-)}_m{}^{n-m} \quad \text{(III)}$$

The free energy of reaction III is of interest in comparing cations. Let $\Delta F_1°$ and $\Delta F_2°$ be the standard free energies of reactions II and III, respectively. In assigning $\Delta F_2°$ values to the various cations, the $\Delta F_2°$ values for K^+ and Na^+ were assumed to be 0.0 ± 1.4 kcal. The assumed values were obtained by considering that the association constants of Na^+ and K^+ with oxygen-containing anions of moderate complexity are within an order of magnitude of 1 M^{-1} (*i.e.*, a free energy of reaction of 0.0 ± 1.4 kcal.). Since

$$\Delta F°_{298} = m\Delta F_1° + \Delta F_2°$$

and since the $\Delta F°_{298}$ values for Na^+ and K^+ are 9.6 kcal.

$$\Delta F_1° = 9.6 \pm 1.4 \text{ kcal}.$$

(Therefore, the dissociation constant of the silanol group, for the first hydrogen to leave the pure silanol surface, is 10^{-6} to 10^{-8}.) For any ion

$$\Delta F_2° = \Delta F°_{298} - 9.6m$$

The free energy of the single metal surface bond, $\Delta F_2°/m$, is of interest and is given in the last column of Table II. (All $\Delta F_2°/m$ values would be in error by the same amount were the assumptions concerning Na^+ and K^+ in error.)

In general, the greater the ionic charge density (as defined by the ratio of the charge to the crystal radius[15]), the greater the negative value of $\Delta F_2°/m$. A secondary effect is the chelate effect: for a given charge density the per-bond stability of the monovalent ions is less than the divalent, etc. The importance of the ionic contribution to the metal–surface bond is further shown by a lack of correlation between $\Delta F_2°/m$ and electronegativity, and by the absence of an unusual stability of bonds with metals which can form inner complexes. Others have concluded this bond to be essentially ionic.[16–19]

The environment of the oxygen atoms of -SiO^- and aqueous OH^- may be similar enough so that the reactions of each with metal ions may be comparable. This is confirmed by the plot of Fig. 1, where even H^+ falls near the curve.

(15) G. H. Cartledge, *J. Am. Chem. Soc.*, **50**, 2855 (1928).

(16) S. S. Bhatnagar, K. N. Mathur, and P. L. Kapur, *Indian J. Phys.*, **3**, 53 (1928).

(17) M. T. Rogers and R. Vancer Vennen, *J. Am. Chem. Soc.*, **75**, 1751 (1953).

(18) C. M. French and J. P. Howard, *Trans. Faraday Soc.*, **52**, 712 (1956).

(19) R. J. Faber and M. T. Rogers, *J. Am. Chem. Soc.*, **81**, 1849 (1959).

Evidence for Thermal Hydrogen Atoms and Other Reactive

Species in Irradiated Liquid Hydrogen Halides[1]

by Robert C. Rumfeldt and David A. Armstrong

Department of Chemistry, University of Alberta, Calgary, Alberta, Canada (*Received September 3, 1963*)

The effects of each of the scavengers, ethylene, chlorine, and bromine, on the hydrogen yield from liquid HCl irradiated at $-79°$ can be interpreted in terms of a competition between HCl and the scavenger, S, for thermal hydrogen atoms. The observed rate constant ratios, k_{H+HCl}/k_{H+S} (1.7×10^{-3} for S = Cl_2, 0.79×10^{-3} for S = Br_2, and 5.9×10^{-3} for S = C_2H_4), are in agreement with ratios calculated on the basis of the available kinetic data for hydrogen atom reactions. In contrast to these compounds, sulfur hexafluoride does not have an appreciable effect on the hydrogen yield. The use of bromine as a scavenger in mixtures of HCl and HBr permitted an evaluation of the ratio k_{H+HBr}/k_{H+Br_2}. The value observed in mixtures containing less than 10 mole % HBr is in excellent agreement with the well-established and virtually temperature independent value (0.12 ± 0.02) obtained from investigations of the gas phase bromination of hydrogen. These results provide convincing evidence that the more easily scavenged of the hydrogen-forming species in liquid hydrogen halides (H') is a thermal hydrogen atom and in liquid HCl $G_{H'} = 2.2 \pm 0.3$. It has also been shown that in HCl–HBr mixtures the yield, $G_{H''}$, of the remaining hydrogen-forming species increases much more rapidly than $G_{H'}$ as the proportion of HBr is increased. Reasons for believing that excited molecules (or hot H atoms formed from them) are responsible for a significant portion of the hydrogen yield from HBr are presented.

Introduction

Earlier studies[2] of the radiolysis of the hydrogen halides were confined largely to the gas phase and did not fully exploit the use of radical scavengers to elucidate the mechanisms involved. Recently, the use of chlorine[3] and bromine[4] in this way has demonstrated that more than one reactive species contributes to hydrogen formation from liquid HCl irradiated at $-79°$. It has been suggested that the first or more easily scavenged of these is a thermal hydrogen atom. The yield ($G_{H'}$) of this species, henceforth referred to as H', was found to be 2.3 ± 0.1, and the total hydrogen yield was $G(H_2)_{HCl, -79°} = 6.53 \pm 0.1_0$. Thus the yield of the remaining hydrogen-forming entities must be $G_{H''} = 4.2 \pm 0.2$. It has also been shown[4] that the radiation sensitivity of liquid HBr is much greater ($G(H_2)_{HBr, -79°} = 12.4$) than that of HCl.

To acquire further and more definite information concerning the identity of H' we have examined and now report the effects of ethylene and sulfur hexafluoride on the hydrogen yield from liquid HCl. In addition, the large difference between the radiation sensitivities of HBr and HCl has prompted us to use bromine as a radical scavenger to determine the yields of H' and H'' in mixtures containing varying proportions of HCl and HBr. It was expected that the results of these experiments would permit more detailed conclusions regarding the origin of the difference between HCl and HBr.

Experimental

Apparatus and Materials. The mercury-free vacuum line for purifying and storing the hydrogen halides and solute gases and the hydrogen analysis system have already been described.[3] The methods of purification of HCl, HBr, and bromine were identical with those previously employed.[4] Ethylene and sulfur hexafluoride were obtained from the Matheson Co., degassed, and subjected to bulb-to-bulb distillation. After this they were stored as gases. Nitric oxide, which was used to inhibit the free radical chain addition of HCl to ethylene, was dried over fused potassium hydroxide and degassed by bulb-to-bulb distillations in which only the middle fractions were retained. It was used immediately after purification.

Dosimetry. Dose rates were calculated in units of e.v./g./min. from measurements of ferrous–ferric conversion in the Fricke dosimetry solution. Corrections for differences in the number of electrons per gram in liquid HCl, liquid HBr, and the dosimetry solution were made on the basis of the Compton scattering process alone. The scattering cross sections per electron were assumed to be identical in all three liquids. $G(Fe^{+3})$ was taken as 15.6 molecules/100 e.v. and the value used for $\epsilon_{Fe^{+3}}$, the extinction coefficient of ferric ions at 304 mμ in the dosimetry solution, was 2220 at 25° (+0.6%/°C.). In mixtures of HBr and HCl the total dose was taken as the sum of the individual doses calculated separately. Dose rates were in the range 5–9 $\times$ 10^{15} e.v./g./min.

Results

As in previous studies, the yields of hydrogen from liquid HCl and HBr were found to be linear with dose both in the presence and absence of scavengers. The
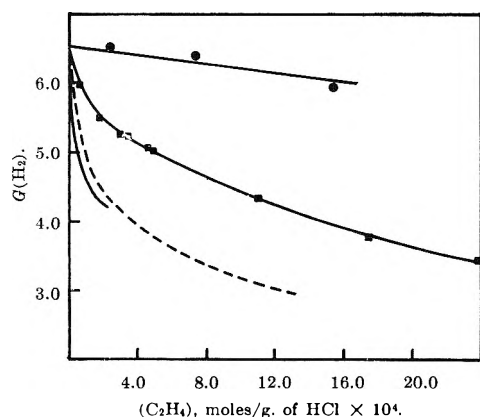
Figure 2. The reciprocal of the reduction in the hydrogen yield $(1/\Delta G(H_2))$ plotted against the reciprocal of the ethylene concentration $(1/(C_2H_4))$ in liquid HCl at $-79°$.

effects of sulfur hexafluoride and ethylene at several different concentrations on the hydrogen yields from HCl are shown in Fig. 1, and for purposes of comparison the earlier data obtained with chlorine and bromine are included. The marked decrease in hydrogen yield at low ethylene concentrations, followed by the continued but more gradual reduction at concentrations in excess of 4 $\times$ 10^{-4} mole/g., is qualitatively similar to the effects originally observed with chlorine in HCl. However, ethylene is clearly a less efficient scavenger than either chlorine or bromine, since much higher concentrations of it were required to suppress the hydrogen formation. Because of this a determination of $G_{H'}$ from the data for ethylene is less likely to reflect the true yield of H' in pure HCl.

In the first study[3] it was shown that 0.1 mole % nitric oxide had no effect on the hydrogen yield from liquid HCl, and such a percentage of nitric oxide has also been shown to inhibit the free-radical chain addition of hydrogen halides to olefins completely.[5] Since this quantity of nitric oxide was added to all samples containing mixtures of ethylene and HCl, the consumption of ethylene in the addition reaction during the course of the radiolyses could not have been significant.

If H' is assumed as before to be a thermal hydrogen atom, then the depletion of the hydrogen yield by ethylene must be attributed to a competition between reactions 1 and 2

$$H + HCl \longrightarrow H_2 + Cl \qquad (1)$$

$$H + C_2H_4 \longrightarrow C_2H_5 \qquad (2)$$

Figure 1. Variation of $G(H_2)$ from γ-irradiated liquid HCl at $-79°$ with scavenger concentration: ●, SF$_6$ as scavenger; ■, C$_2$H$_4$ as scavenger; – – – –, data obtained earlier with Cl$_2$; ———, data obtained earlier with Br$_2$.

(5) R. C. Rumfeldt, Ph.D. Thesis, University of Alberta, Calgary, Alberta, Canada, 1963. Spontaneous Markownikoff addition of HCl to ethylene is negligibly slow.

Table I : Summary of Kinetic Data for HCl and HBr–HCl Mixtures

Medium	H atom scavenger	$G_{H'}$	$G_{H''}$	Competitive reactions	Rate constant ratios Obsd.	Rate constant ratios Calcd.	
HCl	Cl_2	2.3	4.2	$H' + HCl/H' + Cl_2$	1.7×10^{-3}	$2.6 \pm 1.2 \times 10^{-3}$ [a]	A
HCl	C_2H_4	2.0	4.5	$H' + HCl/H' + C_2H_4$	5.9×10^{-3}	8.6×10^{-3} [b]	B
HCl	Br_2	2.4	4.1	$H' + HCl/H' + Br_2$	7.9×10^{-4}	1×10^{-4} to 9×10^{-4} [c]	C
HCl–HBr mixtures							
4.37 mole % HBr	Br_2	2.5	4.9	$H' + HBr/H' + Br_2$	1.20×10^{-1} (D_1)	$1.20 \pm 0.20 \times 10^{-1}$ [d]	D
7.62 mole % HBr	Br_2	2.6	5.4	$H' + HBr/H' + Br_2$	1.05×10^{-1} (D_2)	$1.20 \pm 0.20 \times 10^{-1}$ [d]	D
24.8 mole % HBr	Br_2	3.0	6.4	$H' + HBr/H' + Br_2$	$6.3_8 \times 10^{-2}$ (D_3)	$1.20 \pm 0.20 \times 10^{-1}$ [d]	D
HCl–HBr							
4 to 8 mole % HBr	HBr			$H' + HCl/H' + HBr$	6.6×10^{-3}	8×10^{-4} to 8.7×10^{-3} [e]	E

[a] Calculated with the expression of Klein and Wolfsberg (see text).[14] [b] Calculated using the kinetic parameters given by Yang[15] for the ethylene–hydrogen atom reaction ($\log k_{H+C_2H_4} = 9.10 + 0.5 \log T - (2600/2.303RT)$) and $\log k_{H+HCl} = 9.40 + 0.5 \log T - (4700/2.303RT)$). The latter expression was derived from the data for the reverse reaction and the equilibrium constant for H + HCl ⇌ H_2 + Cl computed by the methods of statistical mechanics.[6] E for Cl + H_2 must lie between 4.6 and 6.1 kcal.[6,16] Since the heat of reaction is 1.0 kcal., E for the reaction H + HCl must be in the range 3.6 to 5.1 kcal. The value used here is slightly different from that given by Benson, but it is still within the acceptable range. [c] Derived from k_{H+HBr} and the ratio D (see below). [d] Determined from the inhibitory effect of HBr in the bromination of hydrogen and found to be independent of temperature over the range 300–1700°K. (see ref. 6 and 7). [e] The extreme values of E_{Br+H_2} in the data summarized by Britton and Cole are 18.0 and 18.8 kcal./mole. Thus $k_{Br+H_2} = 3.35 \times 10^9 \times T^{1/2} \exp -((18,000 \text{ to } 18,800)/RT)$, using their mean value of the pre-exponential factor. From this expression, the heat of reaction and the equilibrium constant derived on the basis of statistical mechanics one finds $k_{H+HBr} = 1.3 \times 10^9 \times T^{1/2} \exp -((1800 \text{ to } 2600)/RT)$. This expression was used in conjunction with the one given above for $\log k_{H+HCl}$ to evaluate ratio E. The calculated value of ratio C must be $0.12 \times$ ratio E. The ratio of the pre-exponential factors A_1/A_4 is $(2.5/1.3) \times 0.12 \cong 0.25$.

The usual steady-state approximation leads to the relation

$$\frac{1}{\Delta G(H_2)} = \frac{1}{G_{H'}} \left\{ 1 + \frac{k_1(HCl)}{k_2(C_2H_4)} \right\} \quad \text{(i)}$$

between the observed reduction in the hydrogen yield ($\Delta G(H_2)$), the yield ($G_{H'}$) of thermal hydrogen atoms in the system, and the ratio $k_1(HCl)/k_2(C_2H_4)$. The plot of $1/\Delta G(H_2)$ against $1/(C_2H_4)$ in Fig. 2, where (C_2H_4) has been expressed in terms of moles of ethylene per gram of HCl, exhibits the sharp break indicative of two hydrogen-forming species. Considering the much larger concentrations of ethylene which were employed, the value of 2.0 ± 0.3 calculated for $G_{H'}$ from the first intercept compares favorably with those observed earlier with chlorine and bromine. The rate constant ratio k_1/k_2 was found from the slope of the upper linear portion to be 5.9×10^{-3} (see Table I, ratio B). The lower and more steeply sloping portion of the curve in Fig. 2 indicates that ethylene also suppresses hydrogen formation by H''.

In contrast to ethylene and the halogens, sulfur hexafluoride has a very low efficiency for suppressing the hydrogen yield from liquid HCl (see Fig. 1).

Experiments with this solute in liquid HBr were unfortunately restricted because of its low solubility. However, the decrease in yield ($\Delta G(H_2) = 0.27$) caused by approximately 1 mole % (0.91×10^{-4} mole of SF_6/g. of HBr) was again relatively small. Although the effects of this solute cannot be attributed with certainty to the scavenging of any particular reactive intermediate, it can be shown that for both liquid hydrogen halides the ratio $k_{H' + HX}/k_{H' + SF_6}$ may be of the order of but not less than 10^{-1}.

The results of the experiments in which bromine was used as a scavenger in mixtures of HCl and HBr were also qualitatively similar to those observed earlier with bromine and chlorine in pure HCl (see Fig. 1). In these solutions reaction 1 and the analogous and more rapid reaction for HBr

$$H + HBr \longrightarrow H_2 + Br \quad (3)$$
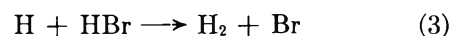
will both contribute to hydrogen formation. When bromine is added there will be a competition for hydrogen atoms between reactions 1 and 3 and reaction 4

$$H + Br_2 \longrightarrow HBr + Br \quad (4)$$
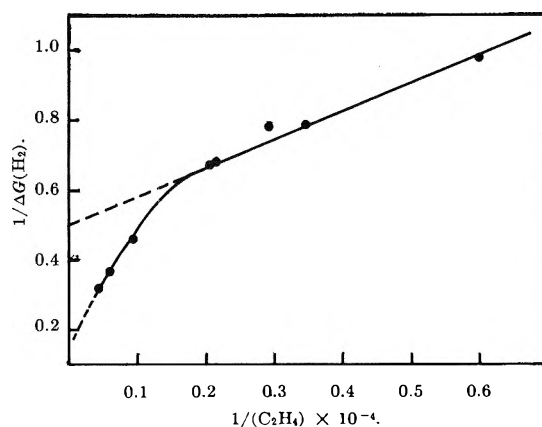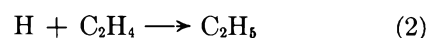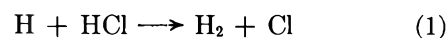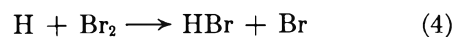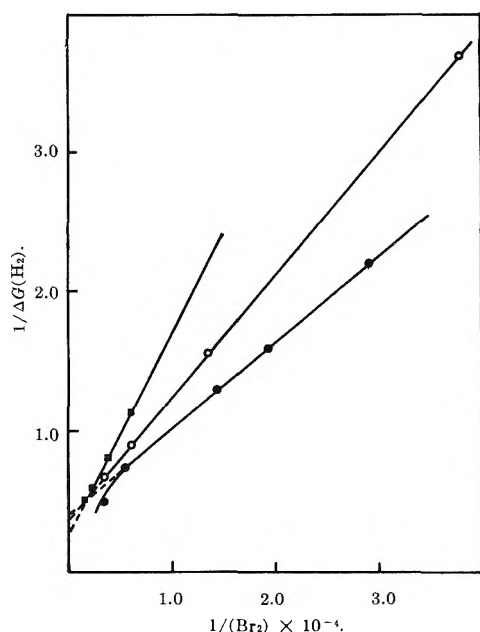
Figure 3. The reciprocal of the reduction in the hydrogen yield $(1/\Delta G(H_2))$ plotted against the reciprocal of the bromine concentration $(1/(Br_2))$ in liquid mixtures of HCl and HBr at $-79°$: ●, 4.37 mole % HBr; ○, 7.62 mole % HBr; ■, 24.80 mole % HBr. (Br_2) is expressed as moles/g. of $(HCl + HBr)$.

Figure 4. The reciprocal of the reduction in the hydrogen yield $(1/\Delta G(H_2))$ plotted against the reciprocal of the bromine concentration in liquid HBr at $-79°$; inset: higher concentrations of bromine.

For a particular concentration of bromine, the observed value of $G(H_2)$ will be given by the expression

$$G(H_2) = G_{H'} \left\{ \frac{k_1(HCl) + k_3(HBr)}{k_1(HCl) + k_3(HBr) + k_4(Br_2)} \right\} + G_{H''}$$

(ii)

In this, $G_{H''}$ may be taken as constant when only low concentrations of bromine are required to deplete the yield of hydrogen formed by H′, and it can be shown that

$$\frac{1}{\Delta G(H_2)} = \frac{1}{G_{H'}} \left\{ 1 + \frac{k_1(HCl) + k_3(HBr)}{k_4(Br_2)} \right\}$$

(iii)

The quantity $1/\Delta G(H_2)$ has been plotted in Fig. 3 against $1/(Br_2)$ over the range of bromine concentrations in which scavenging of H′ is the major effect. The three lines are for HCl–HBr mixtures of different compositions. The values of $G_{H'}$ obtained from their intercepts are presented in Table I. From (iii) it can be seen that the ratio k_3/k_4 may be evaluated from the slopes of these lines on substitution of $1/G_{H'}$, the concentrations of HCl and HBr and the value of k_1/k_4 previously obtained[4] from experiments with bromine in pure HCl (ratio C in Table I). As shown in Table I, the values of k_3/k_4 in the two mixtures which contain the lower proportions of HBr (ratios D_1 and D_2) are in reasonable agreement. Moreover, their

mean value (1.13) is consistent with the value of the same ratio obtained from conventional gas phase kinetic studies[6,7] of the inhibitory effect of HBr on the bromination of hydrogen (0.12 ± 0.02). This reaction has been studied over a wide range of temperatures and k_3/k_4 has been shown to be essentially independent of temperature. The much smaller value of ratio D_3, which was observed in the mixture containing 24.8 mole % HBr, will be discussed later.

The solubility of bromine was greater in the HCl–HBr mixtures than in pure HCl (cf. ref. 4), and the bromine concentrations employed ranged from 0.2 to 7.5×10^{-4} mole/g. (i.e., up to about 3 mole %). In the case of the most dilute solution of HBr in HCl the value of $G(H_2)$ fell from 7.4$_3$ in the absence of bromine to 5.3$_4$ at 3.05×10^{-4} mole/g. A further increase in the bromine concentration to a value of 6.4$_1$ × 10^{-4} mole/g. reduced $G(H_2)$ to 5.0$_2$. It is clear from this that bromine does not compete very effectively for H″ with the hydrogen halide mixture, of which HCl in this case constitutes 95.6 mole %. In fact if H″ is a hot hydrogen atom, which undergoes a set of reactions analogous to (1), (3), and (4) with rate constants k_{1*}, k_{3*} and k_{4*}, it can be shown by a more detailed kinetic analysis (cf. ref. 3) that k_{1*}/k_{4*} must lie in the range 0.2–0.3. This value is very close to the magnitude of the ratio of the pre-exponential factors for the reactions of HCl and bromine with thermal hydrogen atoms (see ref. 6 and footnotes to Table I).

(6) S. W. Benson, "The Foundations of Chemical Kinetics," McGraw-Hill Book Co., Ltd., Toronto, 1960.

(7) D. Britton and R. M. Cole, J. Phys. Chem., 65, 1302 (1961).

The effects of bromine on the hydrogen yield from liquid HBr were investigated over a much wider range of concentrations (0 to 7 mole %) than was employed in the mixtures. The plot of $1/\Delta G(H_2)$ vs. $1/(Br_2)$ in Fig. 4 shows only a gradual curvature (cf. Fig. 1), and the reciprocal of the intercept of the lower portion (12.5 ± 0.8, see inset in Fig. 4) is in agreement with the total hydrogen yield. From the slope of this lower portion the ratio of the rate constants for the reactions of the hydrogen-forming species with HBr and bromine was found to be 0.1_1. This agrees well with the rate constant ratio k_3/k_4 for thermal hydrogen atoms (see above), which was also shown by Eyring, Hirschfelder, and Taylor[8] to be consistent with the effects of bromine at high concentrations in the gas phase radiolysis. Consequently, it would appear that only a single hydrogen-forming species, the thermal hydrogen atom, is produced in irradiated HBr. However, since k_3/k_4 is known to be essentially independent of temperature, the activation energies of reactions 3 and 4 must be virtually identical, and 0.12 is actually the ratio of their pre-exponential factors. This should also be a reasonable ratio for the rate constants of the corresponding reactions of hot hydrogen atoms (i.e., k_{3*}/k_{4*}), provided their energy is not excessively high.[9] It is not therefore possible to exclude hot hydrogen atom reactions on the basis of the observed ratio. Furthermore, the smaller slope and the intercept of the upper portion of the curved plot in Fig. 4 suggest that in pure HBr there is in fact a hydrogen-forming species, which corresponds to H' in HCl and the HCl–HBr mixtures. This would have a ratio of rate constants much less than 0.12 ($D_4 \simeq 2 \times 10^{-2}$) and a yield, $G_{H'}$, of about 3.0. The remainder of the hydrogen would then have to be attributed to a second species, H'', analogous to that occurring in HCl and the mixtures, and with a yield of $G_{H''} \simeq 9$. A feature of the results in Table I which supports such an interpretation of Fig. 4 is the fact that, while $G_{H'}$ increases rather slowly with increasing proportion of HBr in the mixtures, $G_{H''}$ rises rapidly, and at 24.8 mole % HBr is already equivalent to the total hydrogen yield from pure HCl. Thus the proportion of H'' resulting from HBr must be larger than that from HCl. Further supporting evidence comes from a study[10] of the effects of bromine and sulfur hexafluoride on hydrogen yields from the gaseous hydrogen halides. This study has demonstrated that two hydrogen-forming species are produced in both HCl and HBr. In the latter gas the first species, H', contributes some 30% of the total observed hydrogen yield, which is similar in magnitude to that reported here. Because the rate constant ratios for H' and H'' differ much more in gaseous HBr

(see below), the resolution of the two species is considerably easier than in liquid HBr.

Discussion

The ionic and free-radical reactions which are likely to occur in these systems have already been discussed[3,4,8] and only those of particular relevance need be considered here. One important point which should be mentioned at the outset is the fact that both sulfur hexafluoride[11] and bromine[12] have been shown experimentally to have zero energy thresholds for electron capture. They should therefore have high cross sections for reaction with thermal electrons, a property which in the case of sulfur hexafluoride has been confirmed by experiment ($\sigma = 5.7 \times 10^{-16}$ cm.^{2}).[13] Thus, these two scavengers should compete with ion–electron combinations and also with electron capture by hydrogen halide molecules. If these competitions are important at scavenger concentrations similar to (or lower than) those required for the scavenging of hydrogen atoms, then the observed rate constant ratios should differ markedly from those calculated purely for hydrogen atom reactions. Such effects have in fact been found in the gaseous hydrogen halides[10] at 25°, where the rate constant ratios for the reactions of the first species ($k_{H' + HCl}/k_{H' + Br_2} = 2 \times 10^{-4}$, $k_{H' + HBr}/k_{H' + Br_2} = 5 \times 10^{-3}$, $k_{H' + HCl}/k_{H' + SF_6} \simeq 10^{-4}$, and $k_{H' + HBr}/k_{H' + SF_6} = 5 \times 10^{-3}$) are much smaller than those observed in this study.

The first six columns of Table I summarize the values of $G_{H'}$, $G_{H''}$, and the rate constant ratios obtained with different scavengers in HCl and HCl–HBr mixtures. The experimental ratios are in all cases considered to be reliable within $\pm 15\%$. In the case of ratios A and C, the reliability is probably considerably better than this. Column seven contains the corresponding ratios calculated for hydrogen atom reactions on the basis of information from conventional gas kinetic studies. The origin of ratio D has already been given and its reliability is unquestionable. Somewhat similar considerations apply to the corresponding ratio for

(8) Cf. their interpretation of the Lind Livingston data: H. Eyring, J. O. Hirschfelder, and H. S. Taylor, J. Chem. Phys., 4, 570 (1936), and ref. 2.

(9) Some experimental evidence which supports this has been summarized by J. L. Magee and W. H. Hamill, J. Chem. Phys., 31, 1380 (1959).

(10) (a) R. A. Lee and D. A. Armstrong, in press; and (b) further work with R. S. Davidow, which indicates that SF₆ is unreactive toward thermal H atoms and behaves essentially as an electron scavenger.

(11) W. M. Hickman and R. E. Fox, J. Chem. Phys., 25, 622 (1956); D. C. Frost and C. A. McDowell, ibid., 29, 503 (1958).

(12) D. C. Frost and C. A. McDowell, Can. J. Chem., 38, 407 (1960).

(13) N. S. Buchelnickova, Soviet Phys. Tech. Phys., 35, 783 (1959).

chlorine and hydrogen chloride (ratio A). This was evaluated earlier[3] from the data of Klein and Wolfsberg[14] and has been included here for the sake of completeness. The remaining ratios B, C, and E were calculated using kinetic parameters for the individual reactions obtained from the recent literature.[15,16] It can be seen that the calculated and observed values for ratio B are in fair agreement. In the case of ratios C and E, which should be considered together, the observed values are within the estimated ranges. It should be noted that the smaller value of $E_3 = E_4 = 0.9$ kcal./mole, which was previously accepted,[6] would predict much lower values for C and E than were found. Such discrepancies are in the wrong direction to be accounted for on the basis of competitions for electrons as well as hydrogen atoms. Thus the results of the present study support the conclusions of Britton and Cole (that the value of $E_3 = E_4 \simeq 2$ kcal./mole), and are at the same time compatible with Yang's investigations, which indicate a minimum value of about 2.6 kcal./mole for $E_{H + C_2H_4}$.

Taken as a whole the data of Table I are consistent with and strongly support the hypothesis that in liquid HCl H' consists of thermal hydrogen atoms. Furthermore, the agreement between the observed and calculated values of ratios D_1 and D_2 shows that, over the concentration range of bromine necessary to scavenge about 80% of H' (0 to 1.0 mole %) in the two more dilute solutions of HBr in HCl, it does not react significantly with species other than H. Electrons must therefore be captured much more rapidly in these liquids than in the corresponding gaseous systems. The comparatively small effect of sulfur hexafluoride leads to a similar conclusion, and we attribute this capture to reaction 5, which involves molecular agglomerates of two or more hydrogen halide molecules (HX), viz.

$$e + H\text{-}X\text{-} \text{-}H\text{-}X \longrightarrow H + X\text{-}H\text{-}X^- \quad (5)$$
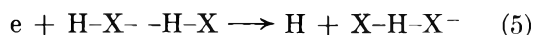
It is perhaps worth restating the reasons for expecting this reaction to replace reaction 6 in the liquid phase

$$e + HX \longrightarrow H + X^- \quad (6)$$

Hydrogen halide molecules are known to undergo mutual association as a result of hydrogen bonding.[17] A similar but rather stronger association occurs between halide ions and hydrogen halide molecules.[18] The energy of both of these interactions will become an integral part of the over-all energy change in reaction 5 and will have the effect of reducing its energy threshold below that of reaction 6 (0.7 e.v. for HCl and 0.2 e.v. for HBr). Reaction 5 should therefore be more efficient for electrons of thermal or very low

energies, and should give rise to thermal hydrogen atoms.

Turning to a consideration of the lower value of ratio D_3, we see that it is in fact part of a general trend (cf. D_1, D_2, and D_4) as the proportion of HBr is increased. There are indications that the effects of sulfur hexafluoride are largely due to electron scavenging.[10b] Thus $k_{e + HX}/k_{e + SF_6}$ in the liquid hydrogen halides should be of the order of 10^{-1}. Since bromine and sulfur hexafluoride have much the same efficiency for reducing the gas phase hydrogen yields, $k_{e + HX}/k_{e + Br_2}$ in liquid hydrogen halides also ought to be approximately 10^{-1}. On this basis, $G_{H'}$ in expression (ii) will depend on the bromine concentration and be equal to $G_e\{1 + [10(Br_2)/(HX)]\}^{-1}$. In accordance with our previous remarks the quantity in brackets is not very different from unity (~ 0.90) at 1 mole % bromine. However, at bromine concentrations equal to and greater than 2 mole % a rather larger proportion of the electrons ($\geqslant 20\%$) would be scavenged by bromine. Because k_3 is much larger than k_1, this is precisely the concentration range of bromine necessary to achieve a significant reduction of the hydrogen yield in pure HBr and the 24.8 mole % solution of HBr in HCl. Hence in these solutions the scavenging of thermal hydrogen atoms and their electron precursors would occur over the same range of bromine concentrations, and the lower rate constant ratios for H' may be attributed to the combination of these two effects. Though the slight difference between D_1 and D_2 is within experimental error, it may be caused by the same effect, since there will obviously be some electron scavenging below 2 mole % bromine. The trend in rate constants may therefore be explained without postulating reactions other than those previously considered in HCl.

The following points are of particular interest in relation to the very large yield of hydrogen from liquid HBr.

(1) The ionization of HBr molecules should be followed by rapid proton transfer to form H_2Br^+. If reaction 5 did not occur, then on energetic grounds the neutralization of this species by electrons could give rise to two hydrogen atoms, thus providing two mole-

(14) F. S. Klein and M. Wolfsberg, J. Chem. Phys., 34, 1494 (1961).

(15) K. Yang, J. Am. Chem. Soc., 84, 3795 (1962).

(16) P. G. Ashmore and J. Chanmugan, Trans. Faraday Soc., 49, 254 (1953).

(17) D. F. Hornig and W. E. Osberg, J. Chem. Phys., 23, 662 (1955); D. F. Hornig and G. L. Hiebert, ibid., 27, 752 (1957).

(18) T. C. Waddington, J. Chem. Soc., 1708 (1958); D. W. A. Sharp, ibid., 2558 (1958); S.-S. Chang and E. F. Westrum, J. Chem. Phys., 36, 2571 (1962); D. G. Tuck and E. J. Woodhouse, Proc. Chem. Soc., 53 (1963).

cules of hydrogen per ionization. However, it would be difficult to explain the large yield of hydrogen which persists in the presence of 7 mole % bromine ($G(H_2)$ = 8.5) entirely on the basis of electron–ion recombinations. In any case, electron capture is a highly probable process in HBr even with isolated molecules (σ = 5.8 × 10^{-17} cm.^{2}),[13] and all of the data to date are consistent with it.

(2) If reaction 5 is accepted, then the neutralization of the resulting Br–H–Br⁻ ions and the H_2Br^+ ions must be considered as a possible source of hydrogen (atomic or molecular). Since recent studies[19] of acid–base reactions in liquid HBr have provided evidence for an autoprotolysis equilibrium similar to that occurring in HCl

$$3HX \rightleftharpoons H_2X^+ + X{-}H{-}X^- \qquad (7)$$
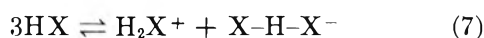
it seems likely that neutralization should occur in the reverse of this process. Alternative neutralization reactions should only take place in cases where ion combination preceded dielectric relaxation. This would presumably require that electrons be captured very close to the parent positive ions and seems improbable.

(3) Although the above reaction sequence cannot be entirely excluded, it is obviously rather difficult to account for H′, H″, and the large total yield from liquid HBr on the basis of simple ionization alone. Other possibilities are dissociative ionization, for which there is evidence from the mass spectrum of HBr,[20] and excitation. A large number of the low lying excited states[21] of the hydrogen halides dissociate or predissociate to ground state halogen and hydrogen atoms, the latter possessing an excess of kinetic energy. This makes excitation a particularly plausible source of H″, since it would not involve the disadvantages of ion–electron combinations as did (1) above. Fur-

thermore, the observed rate constant ratios for H″ were seen to be in accord with reasonable expectations for those of hot hydrogen atoms. For these reasons we are of the opinion that electronic excitation to low lying dissociative states plays an important role in the decomposition of hydrogen halide molecules, particularly in HBr. More detailed conclusions regarding the exact numbers of these species formed in HCl and HBr are not, however, possible at present.

Summary

There is evidence for two hydrogen-forming species in HCl and also in HCl–HBr mixtures. The first of these, H′, has kinetic characteristics which strongly support its identification as a thermal hydrogen atom. The second, H″: (1) becomes more prominent in HCl–HBr mixtures as the proportion of HBr is increased, (2) is scavenged by chlorine in HCl[3] and by bromine in HCl–HBr mixtures, the ratios of the rate constants $k_{H'' - HX}/k_{H'' + X_2}$ in each case being close to the ratios of the pre-exponential factors for the corresponding reactions of thermal hydrogen atoms. There are indications that analogous species are formed in HBr, and that H″ may consist largely of hot hydrogen atoms arising from excited molecules.

(19) .. A. White and T. C. Waddington, *J. Chem. Soc.*, 2697 (1963).

(20) W. H. Johnston and J. R. Arnold, *J. Chem. Phys.*, 21, 1499 (1953).

(21) R. S. Mulliken, *Phys. Rev.*, 51, 310 (1937); R. F. Barrow and J. G. Stamper, *Proc. Roy. Soc.* (London), A263, 259, 277 (1961).

Vaporization Behavior and Phosphorus Decomposition

Pressures of Tungsten Monophosphide

by K. A. Gingerich

Department of Chemistry, The Pennsylvania State University, University Park, Pennsylvania
(Received September 6, 1963)

The vaporization of tungsten monophosphide, WP, has been studied by Knudsen effusion techniques in combination with a mass spectrometer. The major vapor species was P_2 with a small amount of P_4. No tungsten-containing species was observed. At 1000° tungsten monophosphide vaporizes by decomposition into gaseous phosphorus and tungsten metal saturated with phosphorus. No range of homogeneity was observed for WP. An average molal enthalpy of decomposition, $H_{1100°K}$, of 75.63 ± 1.06 kcal. per mole of $P_2(g)$ was obtained from a second law treatment for the composition range $WP_{0.96}$–$WP_{0.65}$, where the uncertainty represents the standard deviation. The temperature dependence of the P_2 decomposition pressure was found to be linear over the temperature range from 950 to 1250°K. and can be expressed by the equation

$$\log p \text{ (atm.) } [P_2] = -\frac{16,534}{T} + 8.501 \pm 0.111$$

Introduction

The system tungsten–phosphorus has been included as part of a program in which the high temperature properties of the most thermodynamically stable transition metal phosphides are investigated.[1-4] These phosphides are expected to form with the inner transition metals and the d block transition metals of groups III–V. Preliminary experiments have shown that compact tungsten metal shows little tendency to react with phosphorus and that it forms phosphides of relatively low stability. For these reasons, and because of its high melting point, tungsten metal has been found to be a suitable oxygen-free container which may be used for more stable transition metal phosphides during preparations and property measurements at high temperatures. In order to predict and to understand possible interactions of tungsten with gaseous phosphorus and with other transition metal phosphides, the vaporization behavior of tungsten phosphides has been studied and vapor pressures have been measured in order to obtain thermodynamic properties of the processes involved.

The system W–P has been studied by tensimetric and X-ray powder methods by Faller, et al.[5] According to these authors only WP and WP_2 occur as intermediate phases. The phosphorus decomposition pressures of WP could not be determined by these authors because they were too low. They succeeded, however, in degradating WP in vacuo to metallic tungsten at 1050°. Schönberg,[6] Bachmeyer, et al.,[7] and Rundqvist[8] have confirmed that WP has the MnP(B31)-type structure and have determined the unit cell dimensions. According to Rundqvist and Lundström[9]

(1) K. A. Gingerich and J. Efimenko, "Thermodynamics of Nuclear Materials," International Atomic Energy Agency, Vienna, 1962, p. 477.

(2) K. S. Irani and K. A. Gingerich, *Phys. Chem. Solids*, 24, 1153 (1963).

(3) K. A. Gingerich, P. K. Lee, and J. Efimenko, *Nature*, 200, 774 (1963).

(4) K. A. Gingerich, *ibid.*, 200, 778 (1963).

(5) F. E. Faller, W. Biltz, K. Meisel, and M. Zumbusch, *Z. anorg. allgem. Chem.*, 248, 209 (1941).

(6) N. Schönberg. *Acta Chem. Scand.*, 8, 226 (1954).

(7) K. Bachmeyer, H. Nowotny, and A. Kohl, *Monatsh. Chem.*, 86, 39 (1955).

(8) S. Rundqvist, *Acta Chem. Scand.*, 16, 287 (1962).

(9) S. Rundqvist and T. Lundström, *ibid.*, 17, 27 (1963).

WP_2 has the orthorhombic MoP_2-type structure with the possible space group $Cmc2_1$. These authors also report that the compositions of the monophosphide WP and of the diphosphide WP_2 correspond closely to stoichiometry and that there are no indications of extended homogeneity ranges. The existence of W_3P is still controversial. Hsu, et al.,[10] prepared W_3P by fused salt electrolysis below 900° and reported its X-ray diffraction powder data. After W_3P was heated to 1050° and quenched, it was found to be disproportionated into W and WP. Other authors[5,9] were unable to prepare W_3P by direct synthesis.

In the present investigation, the vaporization of tungsten monophosphide, WP, has been studied by Knudsen effusion techniques in combination with a mass spectrometer in order to identify the various species produced and to obtain thermodynamic data for the reaction involved. Preliminary results have already been reported.[4]

Experimental

As starting material, a monophosphide produced by fused salt electrolysis[10] was used. For the mass spectrometric studies a 60°-sector, 12-in. radius, first-order, directional focusing instrument manufactured by Nuclide Analysis Associates Inc. was used. The sample was placed directly into a tungsten Knudsen cell which had an orifice area of 1.52×10^{-2} cm.^{2} and a Clausing factor of 0.71. The ratio of the orifice area to the geometrical surface area of the sample was less than 1:88. The temperature was measured by a Pt vs. Pt-10% Rh thermocouple which was inserted into a hole at the bottom of the cell. The heating was by radiation from a single tungsten ribbon that was arranged in a concentric spiral around the Knudsen cell. Due to the thermocouple arrangement and the fact that the sample was placed directly in the tungsten effusion cell, the temperatures reported should have given the sample temperature accurately within a few degrees. The molecular beam was ionized with 55 e.v. electrons. The ions were detected with an electron multiplier and the ion current was recorded automatically. The variation of ion intensity of a particular species was observed as a function of temperature and composition. Species effusing from the Knudsen cell were distinguished from background species by placing a shutter into the beam periodically.

Results and Discussion

The vaporization of tungsten monophosphide, WP, was investigated over a temperature range of 950–1300°K. and an approximate composition range of $WP–WP_{0.1}$. The following ionic species were observed

in the effusing vapor: P^+, P_2^+, and P_4^+. No P_3^+, nor any species containing tungsten and phosphorus could be detected. From the experimental conditions under which the check for tungsten-containing species was carried out, it can be concluded that their concentration is less than 1/1000 of that of the phosphorus vapor concentration in equilibrium with the solid. The appearance potentials of P^+ and P_2^+ were found to be 13.4 e.v. and 9.2 e.v., respectively, on a relative scale, but they show that P_2^+ is a primary species and P^+, a secondary one. If one considers the shift in electron energy scale to lower values by a factor of approximately 0.9 as derived from the ratio 9.2 : 10.2 of the measured value for P_2 to the accepted value, the appearance potential for P^+ becomes 14.9 e.v. Taking this shift into account, the difference between the appearance potentials of P^+ and P_2^+ is 4.7 e.v., which is in fair agreement with the dissociation energy of P_2 of 5.0 e.v.[11] This shows, in addition, that P^+ is primarily produced by fragmentation of P_2, most likely by the reaction

$$P_2 + e^- = P^+ + P + 2e^- \qquad (1)$$
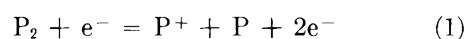
Additional proof that the P^+ ion is produced by fragmentation of P_2 can be derived from the observation that, over the whole temperature range of investigation, the ion intensity of P_2^+/P^+ had a constant value of 10. The contribution to the P^+ intensity from the fragmentation of P_4 is considered to be minor, because the ion intensity of P_4^+ is, under experimental conditions, less than that of P_2^+ by a factor of 20 to 30. Because of the low intensity of P_4, its appearance potential was not measured. It is assumed that the parent of P_4^+ ion is P_4. In Fig. 1, the ionization efficiency curves for P^+ and P_2^+ are represented. Analysis of these ionization efficiency curves shows further that the concentration of primary monatomic phosphorus was too low to be detected.

The observed ion intensity of P_2^+ was independent of composition and a reversible function of temperature over the composition range $WP_{0.96}–WP_{0.65}$. This indicates that equilibrium conditions were prevailing and that the rate of effusion out of the Knudsen cell was smaller than the rate of diffusion of phosphorus through the phase formed on each individual grain by the decomposition of WP. In checking the reversibility of the ion intensity with temperature, it was observed that the largest source of error was the slowness in attainment of temperature equilibrium. The attain-

(10) S. S. Hsu, P. N. Yocom, and T. C. C. Cheng, Interim Report from December, 1953, to July, 1955, Contract N6ori-071(50), Office of Naval Research, Department of the Navy.

(11) G. Herzberg, Ann. Physik, 15, 677 (1932).
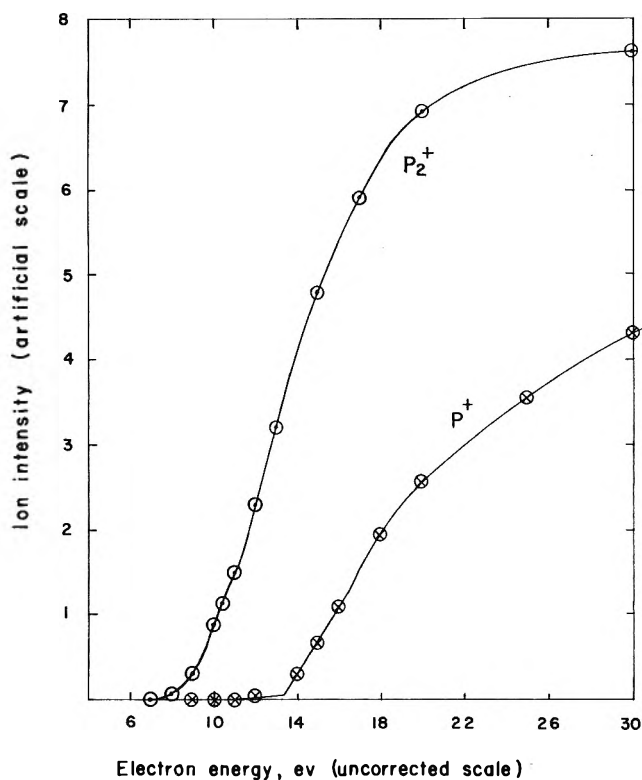
Figure 1. Ionization efficiency curves for
P⁺ and P₂⁺ observed over W–WP.
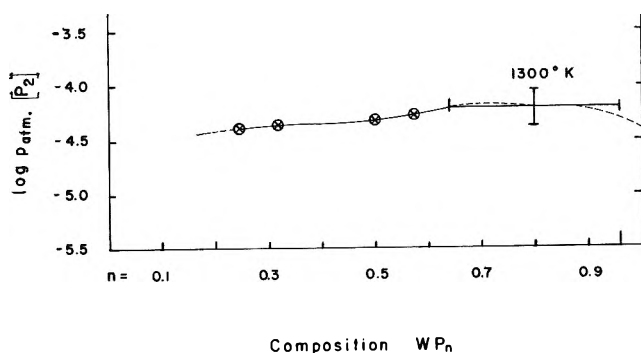
Figure 2. P₂ decomposition pressures as a function
of composition in the system W–WP at 1300°K.

ment of temperature equilibrium after each change in temperature was tested by reaching constant temperature and constant intensity. The constancy in temperature as indicated from the thermocouple reading was reached somewhat earlier than the constancy in ion intensity, which is assumed to be due to the low thermal conductivity within the powdered sample. As a result, vapor pressure values which were obtained while raising the temperature are, on the average, slightly lower, as are those obtained during cooling. The general observation that the ion intensity of P_2^+

is reversible with temperature is modified by observations made in the initial and final stages of the tensimetric analysis of WP in this investigation. Although thermal equilibrium was attained, a set of intensity data obtained in the composition range $WP-WP_{0.96}$ at the beginning of the experiment shows values that are too low. A possible explanation is that in the early stage of vaporization a fraction of the phosphorus vapor reacted with the tungsten effusion cell to form a solid solution of phosphorus in tungsten. This process would have to occur at a more rapid rate than the rate of vaporization of WP. As the rate of phosphorus take-up by the tungsten cell falls markedly below that of the vaporization of WP, the equilibrium pressure observed in the Knudsen cell corresponds closely to the equilibrium pressure of the WP phase. In the later stage of vaporization, while at a constant high temperature and high ion intensities, a decrease in the ion intensity with decreasing phosphorus content of the solid was observed for the composition range $WP_{0.65}-WP_{0.1}$. This is illustrated in Fig. 2, in which the relation between the logarithm of the P_2 partial pressure and composition at 1300°K. is represented. Two possible interpretations are suggested for this observation. (a) It may be because of kinetic effects such as a diffusion barrier caused by the tungsten coat formed on each WP grain that becomes larger as the coat grows in thickness, or to a bulk diffusion barrier that becomes more pronounced as the rate of vaporization increases. (b) It may indicate the presence of a homogeneity range of a condensed phase with lower phosphorus content, the phosphorus-rich boundary of which has a phosphorus activity similar to that of WP. X-Ray analysis of the final product showed that it consisted largely of metallic tungsten. Additional very weak lines observed on an overexposed film were analysed for WO_2, W_4O_9, $W_{18}O_9$, $W_{18}O_{19}$, $W_{20}O_{28}$, β-W_2C, and WC by comparison with the corresponding ASTM data and for W_3O, W_3P, and WP by comparison with the corresponding X-ray diffraction patterns. They could not be identified with any of these substances. It was, however, possible to attribute all but one of these additional lines to the most intense tungsten reflections for Cu Kβ and Fe Kα radiation, respectively. The fact that no WP could be detected would indirectly support explanation b. It is, however, more likely that so little WP was left that it was not visible by X-ray diffraction and that explanation a accounts for the observed decrease in ion intensity. In support of this, the standard deviation is shown in Fig. 2 by the vertical line on the curve, indicating that the effects discussed above are small and of the order of the standard deviation. If ex-

planation b were to hold, a much larger intensity decrease with change in composition, as well as the appearance of a new phase on the X-ray diffraction pattern would be expected.

The fact that the end product was largely tungsten metal and that there was no significant abrupt change in ion intensity at any composition covering the range $WP-WP_{0.1}$ indicates that there is no stable phase existing between WP and W above 1000°. Thus above 1000°, WP vaporizes incongruently[1] by decomposition into gaseous phosphorus and phosphorus-saturated tungsten metal according to the equation

$$\frac{2}{a} WP = \frac{2}{a} WP_{1-a} + \frac{2}{x} P_x \qquad (2)$$
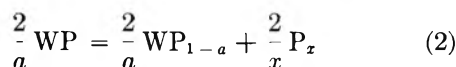
where $a < 1$ and x is either 2 or 4.

For the composition range $WP_{0.96}-WP_{0.65}$ over which the ion intensity of P_2^+ was independent of composition, the variation of ion intensity I of P_2^+ has been determined as a function of temperature over the
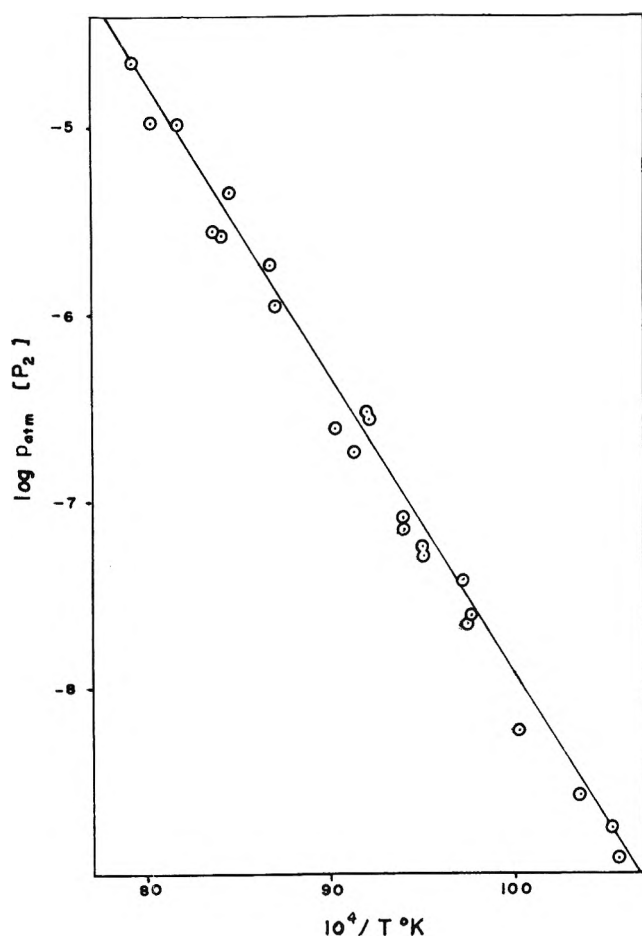
Figure 3. Second-law plot for the reaction:
$(2/a)WP = (2/a)WP_{1-a} + P_2$.

Table I: Mass Spectrometric Vaporization Data for $WP_{0.96-0.65}$[a]

Temp., °K.	$10^4/T$	$I(P_2^+)$, arbitrary units	$p(atm.)[P_2]$	$-\log p(atm.) [P_2]$
992	10.079	13.9	5.85×10^{-9}	8.233
969	10.320	6.50	2.67×10^{-9}	8.573
949	10.535	3.45	1.39×10^{-9}	8.868
948	10.553	3.20	1.29×10^{-9}	8.891
1026	9.751	50.9	2.22×10^{-8}	7.655
1051	9.516	116.1	5.18×10^{-8}	7.286
1065	9.394	167.7	7.58×10^{-8}	7.121
1065	9.390	169.5	7.66×10^{-8}	7.116
1096	9.123	398	1.85×10^{-7}	6.732
1192	8.388	5590	2.83×10^{-6}	5.548
1187	8.423	5290	2.67×10^{-6}	5.574
1220	8.200	20610	1.07×10^{-5}	4.972
1219	8.202	20600	1.07×10^{-5}	4.972
1153	8.672	3890	1.90×10^{-6}	5.720
1152	8.685	3850	1.87×10^{-6}	5.739
1085	9.217	631	2.91×10^{-7}	6.537
1085	9.214	658	3.03×10^{-7}	6.518
1026	9.747	57	2.48×10^{-8}	7.605
1183	8.457	8820[b]	4.43×10^{-6}	5.354
1219	8.206	20100[b]	1.04×10^{-5}	4.993
1182	8.643	6330[b]	3.18×10^{-6}	5.498
1148	8.711	2330[b]	1.14×10^{-6}	5.945
1096	9.124	549[b]	2.55×10^{-7}	6.539
1054	9.491	128[b]	5.73×10^{-8}	7.242
1027	9.740	54.3[b]	2.37×10^{-8}	7.626
1262	7.925	41800	2.24×10^{-5}	4.650
1262	7.923	41700	2.23×10^{-5}	4.651

[a] The sequence of data corresponds to decreasing phosphorus content in the solid. [b] Values were measured as $I(P^+)$ and converted to $I(P_2^+)$ by multiplication by 10.

temperature range from 950 to 1250°K. From the reversible ion intensity–temperature relationship, the average enthalpy of decomposition, ΔH_{1100}, for reaction 2 was obtained from a second-law treatment of the dependence of the decomposition pressure upon temperature.

$$\Delta H_{1100} = 75.66 \pm 1.06 \text{ kcal./mole } P_2(g) \qquad (3)$$

The uncertainty given represents the standard deviation. The accuracy is probably lower because of a possible temperature gradient between the position of the thermocouple and the location of the sample.

(12) W. A. Chupka and M. G. Inghram, J. Phys. Chem., 59, 100 (1955).

(13) M. G. Inghram, W. A. Chupka, and R. F. Porter, J. Chem. Phys., 23, 2159 (1955).

(14) J. W. Otvos and D. P. Stevenson, J. Am. Chem. Soc., 78, 546 (1956).

(15) S. Dushman and J. M. Lafferty, "Scientific Foundation of Vacuum Technique," 2nd Ed., John Wiley and Sons, Inc., New York, N. Y., 1962, p. 94.

The ion intensities of P_2^+ were correlated to vapor pressures through an external silver calibration.[12,13] The difference in electron multiplier efficiencies of Ag^+ and P_2^+ were determined separately. Corrections for fragmentation and double ionization were considered. For the relative ionization cross section of Ag the value given by Otvos and Stevenson[14] was used. For the cross section of P_2, a value of 21.8 was estimated with reference to the cross section of 13.8 for P by considering the geometrical shape of the molecule. The Clausing factor for the geometry of the cell orifice was taken into account.[15] The results are represented in Fig. 3 and in Table I. The temperature dependence of the P_2 partial pressures over the temperature range 950–1250°K. and the composition range $WP_{0.95}$–$WP_{0.65}$ is linear within the limits of experimental error and can be expressed by the equation

$$\log p \text{ (atm.) } [P_2] = \frac{-16{,}534}{T} + 8.501 \pm 0.111 \quad (4)$$

The rather large standard deviation reflects in part the influence of the observations made during the initial and final stages of the investigation into the region selected for the computation of vapor pressures. In the selection of ion intensity values, the main consideration was attainment of temperature equilibrium. Possible slight deviations from temperature equilibrium are, however, included in the standard deviation since the values used correspond to three different temperature cycles. An additional source for the large standard deviation comes from the observation of a possible reaction of phosphorus vapor with the tungsten cell. As indicated earlier, this effect appeared to be most pronounced at the very beginning of the investigation, but is estimated to have continued to the extent indicated by the dotted line in Fig. 2 for the composition region WP–$WP_{0.65}$. Reaction of part of the phosphorus would make the pressures reported too low. A systematic error in addition to that reflected in the standard deviation may be because of the change in sensitivity of the instrument during the 1-week period between the silver calibration and the investigation of WP. Additional experiments have shown, however, that the sensitivity fluctuation of the mass spectrometer–Knudsen cell assembly over a 1-year period is within 30%. An additional systematic error would arise from a vaporization coefficient, α, which is considerably less than unity. The ratio of orifice to sample area applied in this investigation would require a vaporization coefficient less than 10^{-2} before it would influence the vapor pressure values markedly. That a low value of α must be considered as a possibility is apparent from estimates by Lewis and Myers[16] for the vaporization of iron phosphides where α is estimated to be between 4×10^{-5} and 6×10^{-2}.

(16) G. Lewis and C. E. Myers, *J. Phys. Chem.*, **67**, 1289 (1963).

The Adsorption of Water Vapor onto Silver Iodide

by Noubar Tcheurekdjian, A. C. Zettlemoyer, and J. J. Chessick

Surface Chemistry Laboratory, Lehigh University, Bethlehem, Pennsylvania   *(Received September 16, 1963)*

Four adsorption isotherms of water vapor on silver iodide were obtained in the temperature interval of -15.8 to $20°$. Water coverage is only about one-quarter of the argon area at the nominal monolayer value and, therefore, the surface is largely hydrophobic. In accord with similar hydrophobic surfaces possessing isolated hydrophilic sites, adsorption is weak such that the isosteric heats are below the heat of liquefaction, amounts adsorbed at the same relative pressure increase with increasing temperature, and the entropy of the adsorbed molecules is high, indicating considerable lateral movement. No phase change is apparent down to $-15.8°$. As the pressure is increased, the adsorbed molecules form clusters. These clusters are no doubt precursors to ice nucleation when silver iodide is employed as a cloud seeder in supercooled atmospheres.

In an earlier communication[1] we reported on the curious state of affairs concerning the nature of the surface of silver iodide. It had been regarded as being hydrophobic in classical colloid chemistry[2] but as hydrophilic in cloud physics.[3] Our preliminary report indicated that three different preparations gave ratios of B.E.T. specific surface areas for water to nitrogen from 0.07 to 0.37, meaning that the surface was largely hydrophobic. Hence, the historical conclusion of the colloid chemist was correct, yet his argument was specious, since the particles simply flocculate and settle out of sols due to gravity when the electrical double layers are reduced.

Recently, Hall and Tompkins[4] confirmed our findings of Type II isotherms plus sparse coverage by water and, from multitemperature isotherms, calculated isosteric heats of adsorption *vs.* coverage. They then developed an adsorption model based on an idealized uniform surface. Sites in a regular array were supposedly induced by the first water molecules adsorbed, followed by gradual clustering around these sites which made up about one-fifth of the total surface area.

The few earlier investigations of the adsorption of water by silver iodide led to quite different conclusions. Coulter and Candela[5] reported Type III isotherms and isosteric heats of *ca.* 11 kcal./mole. Birstein[6] also reported Type III isotherms, a fantastically large number of adsorbed layers (150) before saturation

pressure, and isosteric heats of 18 kcal./mole. In contrast, Moskvitin, Dubinin, and Sarakhov[7] obtained Type II isotherms and, using benzene to monitor the surface area, concluded that water adsorbs in a close-packed film on silver iodide; they also reported a phase transition around $0°$. One of the purposes of the present study was to discover the cause of these anomalous results.

Water adsorption measurements were made on several different preparations to try to establish differences. Much effort was first expended in attempting to prepare a sample of high specific surface area so that good precision could be obtained and so that extension to measurements of heats of immersion would be possible with ordinary calorimetry.[8] In accord with the recent

(1) A. C. Zettlemoyer, N. Tcheurekdjian, and J. J. Chessick, *Nature*, 192, 653 (1961).

(2) J. T. G. Overbeek, in "Colloid Science," H. R. Kruyt, Ed., Elsevier Publishing Co., Amsterdam, 1952.

(3) B. J. Mason, "The Physics of Clouds," Oxford University Press, London, 1957. A gradual recognition of the hydrophobic character of AgI has been emerging; see, *e.g.*, N. H. Fletcher, *J. Meteorol.*, 16, 173 (1959), on contact angles.

(4) F. G. Hall and F. C. Tompkins, *Trans. Faraday Soc.* 58, 1734 (1962).

(5) L. V. Coulter and G. A. Candela, *Z. Elektrochem.*, 56, 449 (1952).

(6) S. J. Birstein, *J. Meteorol.*, 12, 324 (1955).

(7) N. H. Moskvitin, M. M. Dubinin, and A. I. Sarakhov, *Izv. Akad. Nauk SSR, Otd. Khim. Nauk*, 12, 2080 (1959).

(8) J. J. Chessick and A. C. Zettlemoyer, *Advan. Catalysis*, 11, 233 (1959).

findings of Corrin and Storm,[9] it was found that silver iodide sinters much too rapidly, even at room temperature, to work with high area samples. Most of the results reported here were obtained with a stabilized low area sample.

Experimental

Adsorption Apparatus. A sensitive spoon gage was used to measure pressure.[10] It was nulled by an inert gas monitored by an oil manometer. Thus, water vapor and organic vapors could be used as adsorbates without concern for dissolution by the manometer liquid or stopcock grease. Over-all accuracy of the determination of dosing and equilibrium pressures was ±0.03 mm. Measurements were made at −15.8, 0, 10, and 20°.

Silver Iodide Preparation. Numerous methods were employed to attempt to prepare high area samples. Sublimation in an inert atmosphere in the dark (added iodine vapor was sometimes employed) yielded a surface area of 15 m.^{2}/g. This product sintered rapidly even at 0° in an inert atmosphere.[9]

Main effort was centered on a precipitate from solutions of potassium iodide and silver nitrate following the method of Birstein.[6] The sample was aged to a stable area of 0.11 m.^{2}/g. as determined by argon adsorption at liquid nitrogen temperature. The average area as determined by water adsorption (10.5 Å.^{2} per molecule) at the four temperatures was 0.032 m.^{2}/g. An important finding was that the water–argon surface area ratio was not constant from preparation to preparation in accord with our earlier report.[1]

Samples were also prepared at various excesses of iodide and nitrate, and were washed until apparently free of contaminants. A sample was also prepared in a drybox filled with nitrogen using freshly boiled and still hot solutions to attempt to avoid contamination by oxygen. The precipitate was filtered and dried as quickly as possible. Finally, a sample was precipitated using ammonium iodide in place of the potassium iodide solution to reproduce the results reported by Coulter and Candela[5] and by Birstein.[6]

The solutions were prepared from Baker Analyzed reagents. The silver nitrate was reported to be 100.0%; the potassium iodide 99.8% (0.002% insoluble matter, 0.02% water); and the ammonium iodide 100.0% (insoluble matter 0.003%). Of course, trace amount of impurities could be of critical importance with regard to surface cleanliness of the precipitated silver iodide.

A few adsorption results were also obtained on a commercial product (Baker's C.P.); the water–argon ratio was also low.

Results

Results of the studies of the effect of surface contaminants will be discussed first and then results obtained with the main preparation will be presented.

Surface Contamination of Silver Iodide. No trends in the water–argon surface area ratios were uncovered for the preparations from the different excesses of iodide and nitrate. The sample prepared in the absence of all but trace oxygen gave a ratio of 0.19 instead of 0.29 obtained with the main preparation. This decrease is in the proper direction to account for
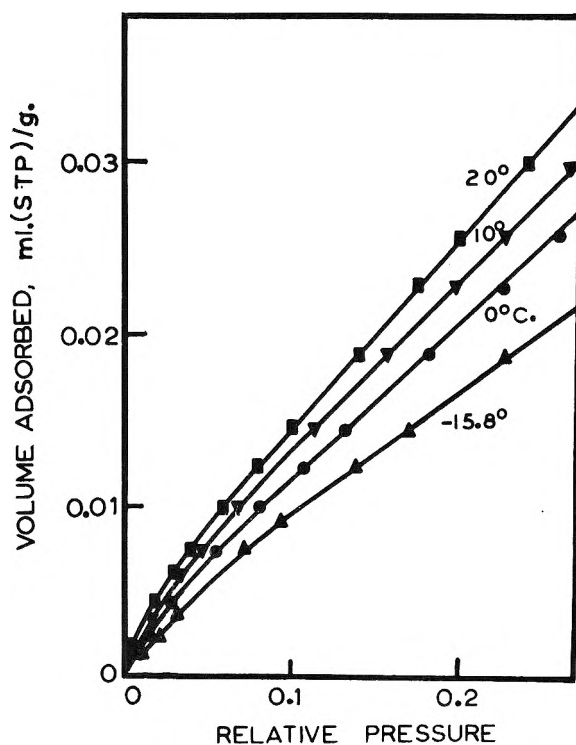
Figure 1. Adsorption isotherms for water vapor on AgI. Note increasing adsorption with increasing temperature; argon area, 0.11 m.^{2}/g.

water adsorption occurring on oxygenated, hydrophilic sites. The decrease is, however, too small to be decisive.

The effect of sintering on the relative amount of water adsorption was also studied on a sample which had an argon surface area of 2.3 m.^{2}/g. at the outset. The water area remained *ca.* 0.02 m.^{2}/g. as the argon area was reduced to 0.04 m.^{2}/g. In other words, the number of polar sites remained essentially constant while the total area was reduced 56-fold.

(9) M. L. Corrin and N. S. Storm, *J. Phys. Chem.*, **67**, 1509 (1963).
(10) Y. F. Yu, J. J. Chessick, and A. C. Zettlemoyer, *ibid.*, **63**, 1626 (1959).
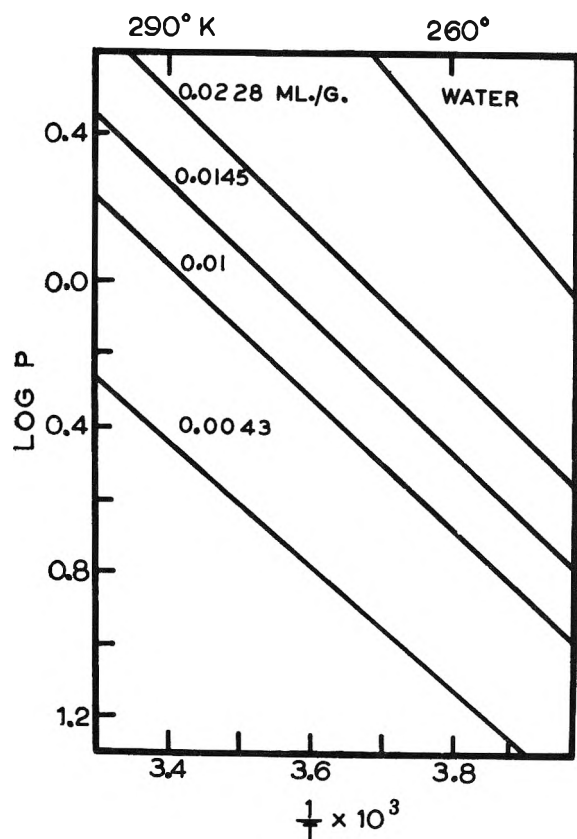
Figure 2. Isosteres for water vapor on AgI. Straight lines indicate no phase change over the conditions studied.

Figure 3. Isosteric heats of adsorption of water vapor on AgI. Two lower and two higher temperatures are averages of $1/T$: for A, -8.2; for B, $+9.6°$.

An odor of ammonia was detected from the sample prepared from ammonium iodide, particularly when heated. The powder tested basic to moist litmus. It is pertinent that the literature[11] refers to a number of silver ammonium salts. Adsorption isotherms similar to those reported by Birstein[6] and by Coulter and Candela[5] were obtained with this sample except that plateaus were found at low pressures not in accord with Type III plots. Apparent condensation pressures shifted to higher relative pressures as the ammonia contaminant was gradually removed by pumping and heating. The large adsorption (or absorption) appeared to be a direct consequence of the presence of ammonia. Thus, the peculiar results reported for such samples previously are simply due to the water-soluble contaminant. It is interesting to note, however, that our ammonium iodide preparation was the most efficient cloud seeder ever tested by Professor Sänger's Laboratory in Zurich.[12]

Adsorption measurements were also made on one sample with benzene to attempt to explain the result of Moskvitin, et al.[7] Using 50 Å.[2] for the close-packed area of benzene, as they did, good agreement with the argon area was obtained. Thus, our results and

those of Hall and Tompkins[4] are not in accord with theirs. Other differences in the water isotherms will also be revealed.

Water Adsorption Isotherms. The water isotherms obtained at -15.8, 0, 10, and 20° are given in Fig. 1. Note that more water was adsorbed the higher the temperature. The B.E.T. plots yielded two linear branches as reported previously.[4] For this reason, B-points were chosen for the monolayer values. These values generally agreed with those obtained from the lower branches of the B.E.T. plots, but were more consistent.

Desorption points fell on the adsorption curve. The absence of hysteresis suggests that no pores were present and that no further chemisorption occurred on the adsorbent surface during the adsorption runs.

Adsorption isosteres are plotted as log p vs. $1/T$ in Fig. 2. For the various amounts adsorbed, the experimental points all fell on the straight lines indicated. Therefore, no phase change is evident. In contrast, Moskvitin, et al.,[7] reported a phase transition near $0°$, but the break was based on a line drawn through only two points. Birstein also concluded there is ice

(11) "Gmelin's Handbuch der Anorganischen Chemie," E. H. E. Pietsch, Ed., No. 61, Verlag Chemie, Weinheim/Bergstrasse, 1962.

(12) A. C. Zettlemoyer, N. Tcheurekdjian, and C. L. Hosler, Z. angew. Math. Phys., 14, 496 (1963).

formation at $-20°$, but the ammonia contamination beclouds the issue.

Heats of Adsorption. The isosteric heats of adsorption were calculated from the two lower temperature and from the two higher temperature isotherms. Smoothed curves are plotted in Fig. 3. The shape of these curves does not differ appreciably from that presented by Hall and Tompkins.[4] Both sets of results yield heats of adsorption below the heat of liquefaction until the apparent monolayer coverage is approached in agreement with increasing adsorption with increasing temperature.
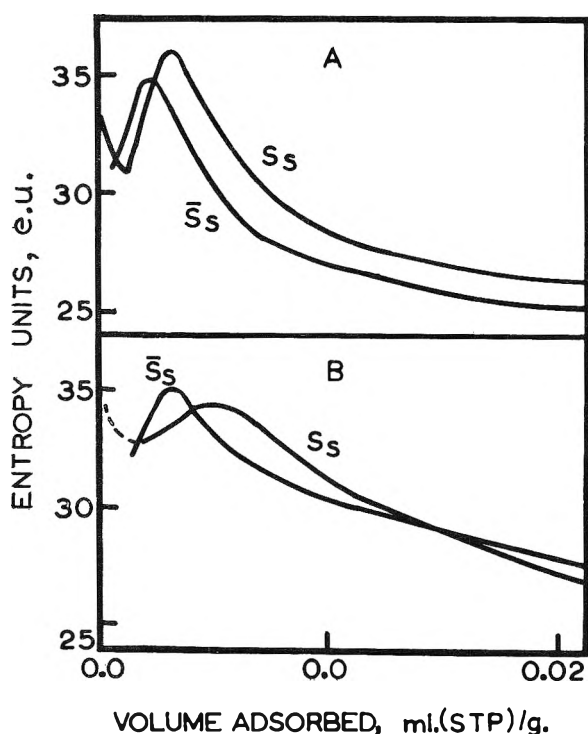
Figure 4. Integral and differential entropies:
at A, -8.2; at B, $+9.6°$.

The shape of these differential heat curves resembles those we reported earlier for Graphon.[13] In this case, the values could be determined more precisely because the high surface area enabled calculations to be made from heats of immersion and one isotherm. Similar heat curves have also been reported for water on Spheron-2800-6,[14] on molybdenum sulfide,[15] and on Teflon.[16]

Entropies of Adsorption. From the equilibrium heats of adsorption, calculated from $d \ln p/dT$ at constant spreading pressure, the integral entropies of the adsorbed water were obtained. These entropies were calculated with the assumption that the perturbation of the solid is negligible for the rather weak ad-

sorption. They are plotted in Fig. 4 along with the differential entropies obtained from the isosteric heats for the two average temperatures of -7.9 and $+9.6°$. The values lie between 25 and 35 e.u. in the region studied. In comparison, the molar entropy of water at $0°$ is 14.3 e.u., and that for ice is calculated to be 9.1 e.u.[17] Large entropies at very low coverages are expected due to the configurational entropy.

The nominal monolayer capacity from the B-points lies slightly above 0.01 ml. adsorbed. Hence, the minimum in the integral entropy curves falls far below $\theta = 1$. Obviously, what is called the Hill criterion for the monolayer[18] does not agree with the B-points, as Halsey[19] has recently pointed out for other systems. This situation seems to arise when interaction energies are low and lateral interaction is absent, although there was good concordance for the Graphon-water system. For argon on P33(2700) graphitized carbon black, Sams, Constabaris, and Halsey[19] did not get a minimum in the integral entropy curve.

Nature of Adsorbed Water on Silver Iodide. It seems to be firmly established that silver iodide (not made from the ammonium salt) possesses hydrophilic sites on a largely hydrophobic surface. On the average for the various samples tested, one in four sites which adsorbed argon also adsorbed water. Questions arise as to what the nature of the hydrophilic sites might be and as to the behavior of the adsorbed water on these sites.

Hall and Tompkins[4] propose that the halide surface is uniform and adsorbs first in an idealized manner across the lattice from iodide to iodide ion. Then, the increase in heat of adsorption with coverage is attributed to lateral interaction as doublets, triplets, and clusters form. No argument is presented for the lack of complete coverage and isolated cluster formation. It seems difficult to adhere to their idealized surface approach on the basis of the evidence at hand.

The variability in fraction of hydrophilic sites from sample to sample in itself suggests that variations in surface concentrations of polar impurities may be the cause. The fact that the number of sites which adsorbed water did not change with the large area decrease due to sintering also supports the impurity

(13) G. J. Young, J. J. Chessick, F. H. Healey, and A. C. Zettlemoyer, *J. Phys. Chem.*, **58**, 313 (1954).

(14) E. V. Baloo and S. Ross, *ibid.*, **57**, 653 (1953).

(15) D. Graham, *ibid.*, **66**, 1815 (1962).

(16) J. J. Chessick, F. H. Healey, and A. C. Zettlemoyer, *ibid.*, **60**, 1345 (1956).

(17) W. E. Giauque and J. W. Stout, *J. Am. Chem. Soc.*, **58**, 1144 (1936).

(18) T. L. Hill, *J. Chem. Phys.*, **17**, 520 (1949).

(19) J. R. Sams, Jr., G. Constabaris, and G. D. Halsey, Jr., *J. Phys. Chem.*, **66**, 2154 (1962).

concept. It is well known that impurities often congregate on the surfaces of solids.

The colored motion pictures taken by Professor B. J. Mason, Imperial College, of the nucleation and growth of ice crystals on single silver iodide crystals show that they form on isolated sites. These localities appear to be mostly at steps in the crystal face. Harris, Sparks, and Layton,[20] studying nucleation by lead iodide single crystals, also showed that steps and edges were the active sites. In the latter case, it was found that there was a strong tendency for growth to repeat at these specific sites. Exposure to liquid water, however, changed the locales. These findings in ice nucleation studies support the contention that impurities are the likely origin of the hydrophilic sites. These studies, however, did not reveal any distinctive characteristic at these places. The steps themselves and dislocations may also provide active sites along with contaminants and hydrolysis products such as hydroxyl groups located there and occasionally elsewhere.

Lead iodide is accepted to be a poorer nucleating agent for ice crystals than silver iodide. Fletcher[21] has shown that for idealized surfaces, an entropy effect in the ordering of water molecules on the substrate leads to the conclusion that it is the prism rather than the basal faces which are active as nuclei. The misfit for ice on the prism face is greater for lead iodide than for silver iodide; the basal misfit, on the contrary, is less for silver iodide. Thus, he explains the hitherto puzzling relative inefficiency of lead iodide. It is interesting to note that Hall and Tompkins[4] reported a much lower fraction of hydrophilic sites (0.054) on lead iodide. Therefore, it may be that the efficiency depends on an optimum concentration of such sites. If this is the case, then Fletcher's analysis based on idealized surfaces may be of secondary importance.

Graham[22] took a statistical mechanical approach to the behavior of adsorbed water in the monolayer on Graphon using our results. A similar approach may be fruitful here in assaying the area of freedom of an adsorbate molecule necessary to prevent interaction between adsorbed molecules. The monolayer entropy is about the same as in the case of water on Graphon, 29.3 e.u. Subtracting from this value similar contributions for configurational entropy, rotational entropy, and vibrational entropy with the surface, the residual entropy of two-dimensional translatory motion is 17.3 e.u. Putting this quantity into the equation for S_T

$$S_T = R \left[1 + \ln \frac{2\pi mkT}{h^2} a \right] \qquad (1)$$

(where R is the gas constant, m is the mass of each adsorbate molecule, k is the Boltzmann constant, T is the absolute temperature, a is the area covered by the wandering of each adsorbate molecule, and h is Planck's constant) gives a value of 120 Å.^{2} for the average area over which each water molecule wanders. The adsorption measurement suggests that each water molecule has only about 100 Å.^{2} at monolayer coverage not considering earlier clustering before the nominal monolayer coverage is reached. These values are in agreement considering the uncertainties in the analysis. Therefore, it appears that silver iodide surfaces, whatever the source of the hydrophilic sites may be, possess the maximum hydrophilic area possible without appreciable lateral interaction between the first molecules adsorbed.

Such hydrophilic sites on an essentially hydrophobic surface seem to be conducive to ice nucleation. Adsorption energy is low and clustering about the first down molecules readily occurs. If the surface would adsorb the water molecules in an ordered array over the entire surface, then the sticking coefficient for subsequent adsorption would no doubt be low, as suggested by the work of Eyring and Wanlass.[23] Then, growth of clusters would be slow.

This work has led to an understanding of the hydrophobic–hydrophilic balance on silver iodide surface. The evidence seems to favor impurity sites largely located in geometrical heterogeneous locations such as steps. The adsorption energy for water on these sites is low and the entropy of the adsorbed molecules is high. Adsorption of water molecules with increasing pressure leads to cluster formation. These clusters are no doubt formed in the nucleation process which is responsible for cloud seeding; subsequent to the cluster formation, ice crystals develop. From these concepts based on the nature of water adsorption on silver iodide, new and cheaper nucleation agents have been developed.[12] They possess the common attribute of having hydrophilic adsorption sites each located in a matrix of hydrophobic sites.

(20) F. S. Harris, Jr., D. C. Sparks, and R. G. Layton, *J. Atmospheric Sci.*, **20**, 149 (1963).

(21) N. H. Fletcher, *J. Chem. Phys.*, **30**, 1476 (1959).

(22) D. Graham, *J. Phys. Chem.*, **60**, 1022 (1956).

(23) H. Eyring and F. M. Wanlass, Advances in Chemistry Series, No. 33, American Chemical Society, Washington, D. C., 1962.

Rheological Properties of Polyethylene Melts: Effects

of Temperature and Blending[1]

by Masao Horio, Tsuguo Fujii, and Shigeharu Onogi

Department of Polymer Chemistry, Kyoto University, Kyoto, Japan   (*Received September 26, 1963*)

Dynamic viscosity η', dynamic rigidity G', and apparent viscosity η_a of polyethylene blends in the molten state have been measured by means of a concentric cylinder-type rheometer which enables us to measure not only dynamic but also steady flow properties. The frequency ranges from about 5×10^{-4} to 1 c.p.s., and the rate of shear from about 0.004 to 4 sec.$^{-1}$. η' and G' as functions of frequency as well as η_a as a function of rate of shear for each blend of two components at different temperatures (140–200°) can be superposed according to the usual time–temperature superposition principle, and shift factors a_T from η' and G' are practically the same. Master curves superposed with respect to temperature can also be superposed very well with respect to the blending ratio or to the weight-average molecular weight. For blends of two components whose molecular weights are not so different, the logarithm of the shift factor c_M bears a linear relationship to the blending ratio. On the other hand, for blends of two components differing very much in their molecular weights, the linearity holds only approximately. The theory proposed by Ninomiya for polymer blends can also be applied to G' of our systems, and the equilibrium compliance J_e and viscosity have been evaluated. The evaluated values coincide fairly well with the observed values, but J_e plotted against blending ratio shows no peak. This result differs from those reported by the previous authors for blends of amorphous polymers having different molecular weights.

Introduction

The flow properties of polymer melts are significant in connection with their internal structure and with their processing, and therefore have been studied by many authors.[2] However, the viscoelastic properties of polymer melts in a wide range of frequency have been studied only by Cox, *et al.*,[3] for polystyrene and polyethylene and by Ballman and Simon[4] for polystyrene, so far as the authors know. In the previous paper,[5] a concentric cylinder-type rheometer has been described, which was designed to measure not only the dynamic but also steady flow properties of polymer melts and solutions over the wide ranges of frequency and rate of shear. Measurements with this rheometer of rheological properties such as the dynamic viscosity η', the dynamic rigidity G', and the apparent viscosity η_a of polyethylene blends in a molten state have been reported in this paper. Our main

purpose is to investigate the effects of temperature and blending on the flow properties of the blends.

Experimental

Materials. Three types of commercial polyethylene were used as original samples. Two of them were Dow polyethylene 544 and 910M having melt indices

(1) Presented at the 145th National Meeting of the American Chemical Society, New York, N. Y., Sept., 1963, and supported by a grant from the scientific research funds (Kagaku Kenkyu-hi) of the Ministry of Education, Japan.

(2) See, for example, T. G Fox, S. Gratch, and S. Loshaek, "Rheology Theory and Applications," Vol. I, F. R. Eirich, Ed., Academic Press, New York, N. Y., 1956, Chapter 12.

(3) W. P. Cox, L. E. Nielsen, and R. Keeney, *J. Polymer Sci.*, 26, 365 (1957); W. P. Cox and E. H. Merz, Special Technical Publication of ASTM, No. 247, 1958, p. 178.

(4) R. L. Ballman and R. H. Simon, paper presented at the 145th National Meeting of the American Chemical Society, New York, N. Y., Sept., 1963.

(5) M. Horio, S. Onogi, and S. Ogihara, *J. Japan. Soc. Testing Mater.*, 10, 350 (1961).

2.2 and 20, respectively. The other was Epolene C of Eastman Chemical Products having a very low molecular weight. They will be designated hereafter as polymers A, B, and E.

Polymers A and B were blended in four different ratios by passing them through a nonvent-type extruder equipped with du Pont-type screw, whose diameter $D = 1.5$ in. and the ratio of length L to D was equal to 20. Stainless steel screens of 60, 100, and 60 mesh were mounted in front of a breaker plate of the extruder in order to remove impurities and enhance the blending effect. The blended polymer was obtained in a form of bristle having a diameter of 0.125 in. Polymers A and E, on the other hand, were blended between two rollers having 4 in. diameter and 15 in. length for 20 min. at 140°, because the difference in viscosities of these two polymers was too large to blend uniformly with the above extruder. The blends were obtained in a sheet form.

Uniformity of the blending was considered to be satisfactory, because the intrinsic viscosity and the melt viscosity of the blended samples from different portions of the bristles and sheets gave practically the same values.

Measurements. As mentioned above, the dynamic viscosity η', the dynamic rigidity G', and the apparent viscosity η_a were measured by means of a concentric cylinder-type rheometer specially designed for our study. The details of this rheometer have been described in the previous paper.[5] A merit of this apparatus is that it can be used as a torsionally oscillating rheometer, a forced vibration torsion pendulum, or a Couette-type viscometer by a minor change in the driving system. Another merit is that the oscillation and rotation of the outer and/or inner cylinders during the measurements are changed into electrical potential by means of a differential transformer device, and after being amplified are recorded on a X–Y recorder. The thermostat has been designed to keep temperature constant from room temperature to 300°, and inert gas such as nitrogen flows under a slight positive pressure through a spiral pipe in the thermostat over the surface of the sample in order to minimize chemical degradation at higher temperatures. By using many torsion wires and bobs having different diameters, a very wide range of rheological properties can be measured. The frequency and number of revolutions of the cup range from 5×10^{-4} to 1 c.p.s. and from 0.122 to 240 r.p.m., respectively.

When we use the rheometer as a torsionally oscillating rheometer, the complex viscosity η^* can be evaluated from the following equation, which is a reduced form of a general equation given by Markovitz[6,7]

$$\eta^* = \frac{\left[(A_1 + B_1\rho)\omega - \dfrac{C_1}{\omega} \right] \left[\dfrac{\sin \phi}{m} - i \left(1 - \dfrac{\cos \varphi}{m} \right) \right]}{\left(\dfrac{\sin \phi}{m} \right)^2 + \left(1 - \dfrac{\cos \phi}{m} \right)^2}$$

where A_1, B_1, and C_1 are apparatus constants, ω is the angular frequency, m is the amplitude ratio, ϕ is the phase angle, ρ is the density of the sample, and $i = (-1)^{1/2}$

When the rheometer is used as a forced vibration torsion pendulum, η' and G' can be evaluated from the following equations[8]

$$\eta' = \frac{R}{4\pi l} \left(\frac{1}{r_1^2} - \frac{1}{r_2^2} \right), \quad G' = \frac{K}{4\pi l} \left(\frac{1}{r_1^2} - \frac{1}{r_2^2} \right)$$

where, r_1 and r_2 are the radii of the bob and cup, l is an immersion length of the bob, and

$$R = \frac{kT_f \sin \phi}{2\pi m}, \quad K = k\left(\frac{\cos \phi}{m} - 1 \right) + \frac{4\pi I}{T_f^2}$$

where k is a torsion constant of the wire, T_f is the period of vibration of the bob, ϕ is the phase angle, m is the amplitude ratio, and I is the moment of inertia. In general the results obtained by the above two methods are practically the same as have been reported in the previous paper,[5] and therefore the former method was chiefly employed in this study.

Finally, when we use the rheometer as a Couette-type viscometer, the flow curves of non-Newtonian liquids can be determined accurately by the single-bob method proposed by Krieger and Maron.[9] Then the apparent viscosity η_a can be evaluated as a ratio of shearing stress to rate of shear or velocity gradient D.

The most important thing in the dynamic measurements is to choose a suitable torsion wire to give sufficient value to m and ϕ. Otherwise, one will obtain the final result including a systematic error which can not easily be detected when one relies upon only one method. The choice of the wire depends not only upon the nature of the sample but also upon the measuring frequency. This forced us to interchange wires very often even in a series of frequency-varying experiments of the same sample.

Results and Discussion

Effect of Temperature. The frequency dependence curves of η' and G' as well as the rate of shear dependence curves of η_a for blends and their components at

(6) H. Markovitz, *J. Appl. Phys.*, **23**, 1070 (1952).

(7) H. Markovitz, P. M. Yavorsky, R. C. Harper, Jr., L. J. Zapas, and T. W. DeWitt, *Rev. Sci. Instr.*, **23**, 430 (1952).

(8) T. Nakagawa, "Jikken Kagaku Koza," Vol. 8, Maruzen, Tokyo, 1957, Chapter 6.

(9) I. M. Krieger and S. H. Maron, *J. Appl. Phys.*, **25**, 72 (1954).
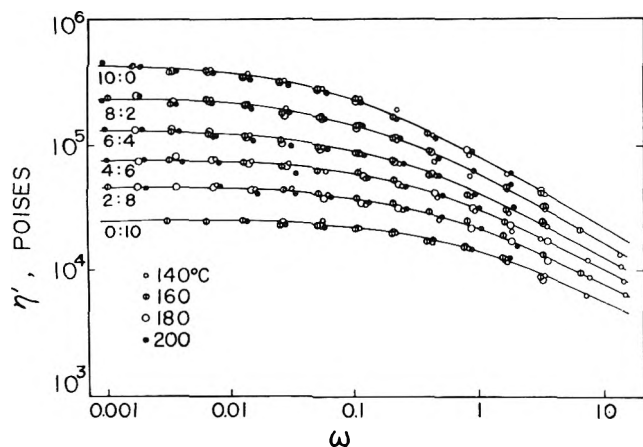
Figure 1. Master curves of η' for the system of polymers A and B. The reference temperature is 160°. ω denotes the angular frequency in sec.$^{-1}$.
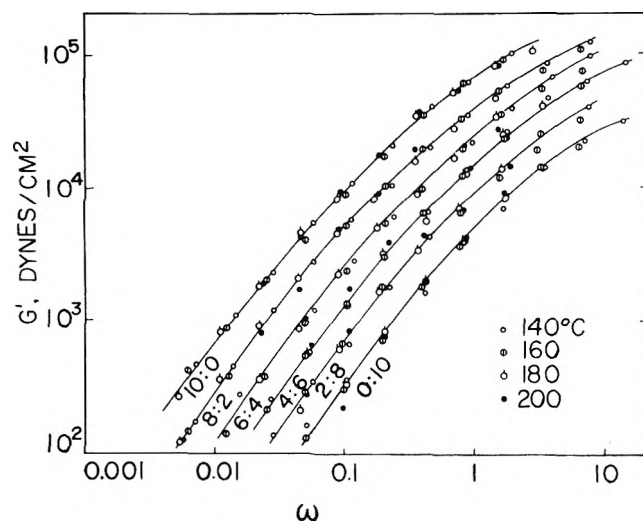
Figure 2. Master curves of G' for the system of polymers A and B. The reference temperature is 160°. ω denotes the angular frequency in sec.$^{-1}$.

various temperatures can be superposed very well to give master curves according to the usual method of time–temperature superposition without any correction for temperatures. Figures 1 and 2, for instance, give master curves of η' and G' measured for polymers A, B, and their blends at 140°, 160°, 180°, and 200°. Similarly, Fig. 3 and 4 give master curves of η' and G' for the blends from polymers A and E at the same temperatures, respectively. The ratio on the curves denotes the blending ratio in weight, A:B in Fig. 1 and 2 and A:E in Fig. 3 and 4. The values of the shift factor a_T determined from the data of η', G', and η_* are almost the same, and moreover independent of the composition or the blending ratio of the

blends, as illustrated in Fig. 5 for the blends from polymers A and B. Log a_T plotted against the temperature is almost linear and the activation energy for relaxation processes therefore varies with the temperature. For example, its value for polymer A at 160° is about 13.7 kcal./mole.

Effect of Blending. As is seen from Fig. 1 to 4, the rheological properties of the blends change systematically with their composition, indicating that there is great possibility of superposition in respect to the blending ratio or to the weight average molecular weight similar to the time–temperature superposition just men-
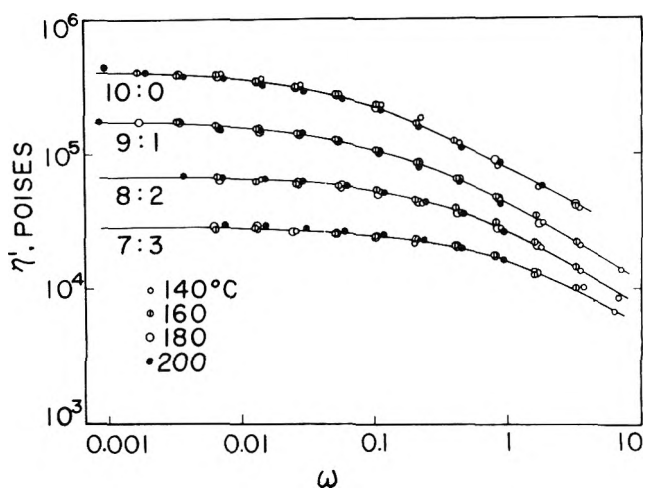
Figure 3. Master curves of η' for the system of polymers A and E. The reference temperature is 160°. ω denotes the angular frequency in sec.$^{-1}$.
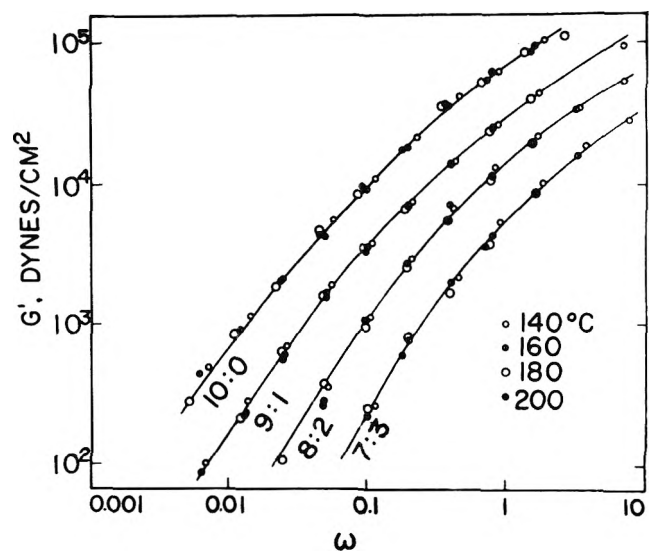
Figure 4. Master curves of G' for the system of polymers A and E. The reference temperature is 160°. ω denotes the angular frequency in sec.$^{-1}$.
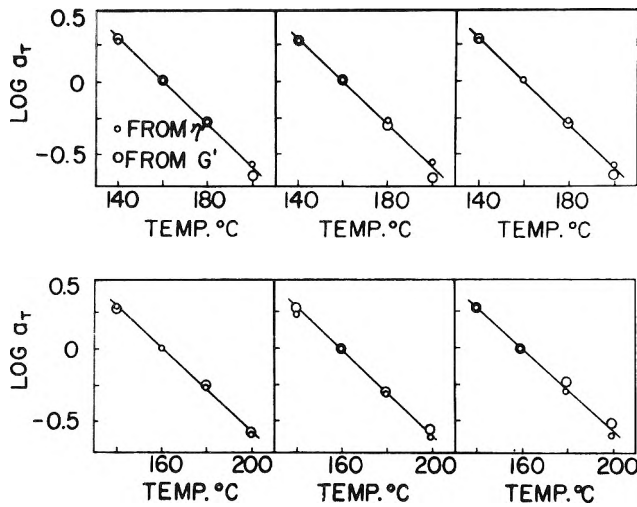
Figure 5. Log a_T vs. temperature for the system of polymers A and B.

Figure 7. Composite curves of η' and G' for the system of polymers A and E. The reference temperature is 160° and the reference composition is 8:2. ω denotes the angular frequency in sec.$^{-1}$.
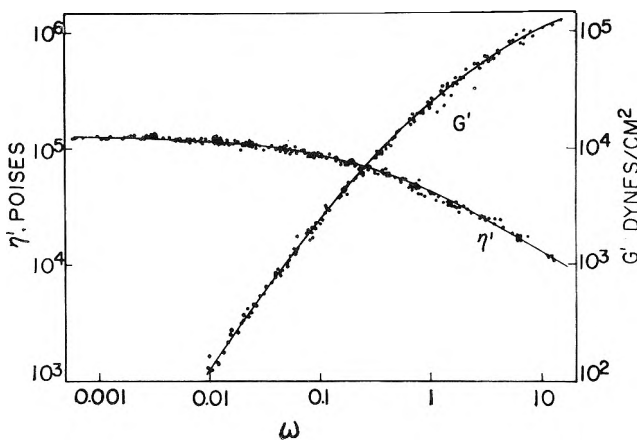
Figure 6. Composite curves of η' and G' for the system of polymers A and B. The reference temperature is 160° and the reference composition is 6:4. ω denotes the angular frequency in sec.$^{-1}$.
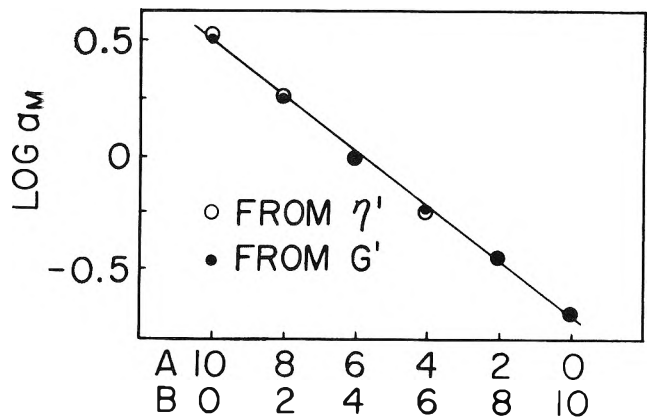
Figure 8. Log a_M vs. blending ratio for the system of polymers A and B.

tioned above. In fact, this superposition was applied satisfactorily to the master curves shown in Fig 1–4.

By shifting the viscosity curves along straight line having slope −1 and the rigidity curves along the abscissa, we could obtain new composite curves, which are shown in Fig. 6 for the blends from polymers A and B, and in Fig. 7 for the blends from polymers A and E. These composite curves include all the data for the blends having different blending ratios and the component polymers at different temperatures. The reference temperature and reference composition are, respectively, 160° and 6:4 for the system of polymers A and B, and 160° and 8:2 for the system of polymers A and E. In making this superposition, we can determine a new shift factor a_M similar to a_T in the case

Figure 9. Log a_M vs. blending ratio for the system of polymers A and E.
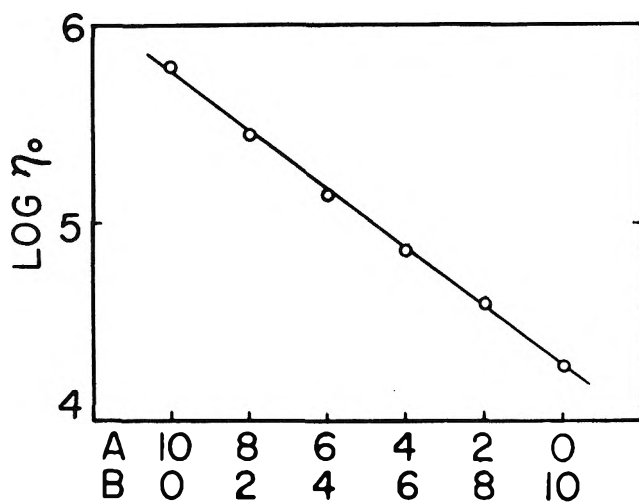
Figure 10. Log η_0 vs. blending ratio for the system of polymers A and B.
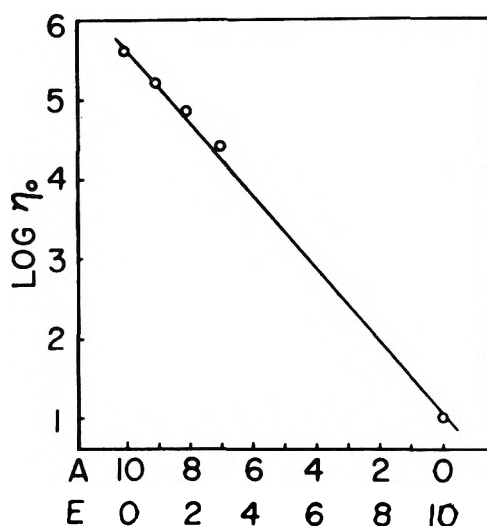
Figure 11. Log η_0 vs. blending ratio for the system of polymers A and E.

of the time-temperature superposition. Log a_M corresponds to the distance by which the viscosity or rigidity curve for any blend or component was shifted in the horizontal direction along the abscissa. Log a_M thus determined was plotted against the blending ratio in Fig. 8 for the first system and Fig. 9 for the second. The plots are substantially linear, and the shift factor from the viscosity data gives almost the same values as those from the rigidity data.

Since a_M is equal to the ratio of the steady flow viscosity of any blend or component to that in the reference state, the zero shear or zero frequency viscosity plotted logarithmically against the blending ratio should also give a straight line. These plots are shown

in Fig. 10 and 11 for the two systems. In the first system, in which the two components A and B do not differ greatly in their molecular weights, all the points for the blends are located on a straight line connecting the two points for the component polymers. This indicates that the zero shear viscosity η_{0b} and shift factor a_{Mb} of the blends can be represented by the following equations, respectively

$$\log \eta_{0b} = w_1 \log \eta_{01} + w_2 \log \eta_{02},$$

$$\log a_{Mb} = w_1 \log a_{M1} + w_2 \log a_{M2}$$

where w denotes the weight fraction of each component, and the subscripts 1 and 2 refer to the components of higher and lower molecular weight. On the other hand, in the case of the second system, in which the two components do have greatly differing molecular weights, the plots for the intermediate blends have a tendency to deviate somewhat from the straight line.

To the dynamic viscosity and rigidity data given above, the theory presented by Ninomiya[10] for polymer blends composed of two components differing only in molecular weights from each other was applied, and the interaction parameters λ_1 and λ_2 were determined from the rigidity data. These values for the system of polymers A and B are tabulated in Table I as an example. As is seen from this table, λ_1 increases and λ_2 decreases

Table I: Interaction Parameters λ_1 and λ_2 for the System from Polymers A and B at 160°

Blending ratio	λ_1	λ_2
8:2	1.33	0.678
6:4	1.45	0.443
4:6	1.55	0.320
2:8	1.56	0.295

monotonously with the blending ratio. With these interaction parameters and weight fractions of two components, w_1 and w_2, the steady flow viscosity η_0 and steady state compliance J_e of the blend are given, respectively, by the equations[10,11]

$$\eta_{0b} = w_1 \lambda_1 \eta_{01} + w_2 \lambda_2 \eta_{02}$$

$$J_{eb} = (w_1 \lambda_1^2 \eta_1^2 J_{e1} + w_2 \lambda_2^2 \eta_2^2 J_{e2})/\eta_{0b}^2$$

In Table II, the observed values of η_0 and J_e for the above system are compared with those calculated from these equations. The latter coincides fairly well with

(10) K. Ninomiya, J. Colloid Sci., 14, 49 (1959).

(11) K. Ninomiya, ibid., 17, 759 (1962).

Table II: A Comparison of the Observed Values of η_0 and J_e with the Calculated Values for the Same System

Blending ratio	η_0, 10^5 poises ($160°$) Obsd.	Calcd.	J_e, 10^{-4} cm.^{2}/dyne ($140°$) Obsd.	Calcd.
10:0	4.30		1.19	
8:2	2.32	2.39	1.64	1.51
6:4	1.30	1.29	2.02	1.73
4:6	0.740	0.782	2.68	2.73
2:8	0.480	0.564	4.32	5.19
0:10	0.250		6.68	

the former. However, J_e decreases monotonously with the blending ratio and does not show any peak at the intermediate composition. This result differs from those reported previously on other polymers such as polyisobutylene[12] and polyvinyl acetate.[10] The difference might be due to the polyethylene samples used in this study, which were different in their nature, especially in molecular weight distribution, from the other polymers cited above. A further study with fractionated species will be required.

Now, it is interesting to make clear the relation between our viscosity equation and Ninomiya's. When we put

$$\lambda_1 = (\eta_{02}/\eta_{01})^{w_2}$$

and

$$\lambda_2 = (\eta_{01}/\eta_{02})^{w_1}$$

into Ninomiya's formulation, then obtain

$$\eta_{0b} = (w_1 + w_2)\eta_{01}{}^{w_1} \times \eta_{02}{}^{w_2}$$

$$= \eta_{01}{}^{w_1} \times \eta_{02}{}^{w_2}$$

This is the same as our equation given above. As seen from this derivation, our case corresponds to a simple one of Ninomiya's general treatment in which the interaction parameters are functions of only weight fractions of the components.

The ratio λ_1/λ_2 is very simple and equal to the ratio η_{02}/η_{01}. Consequently, we can obtain

$$\eta_{0b} = \eta_{01}\lambda_1 = \eta_{02}\lambda_2$$

and the shift factor a_M is given as

$$a_M = \frac{\eta_{0b}}{\eta_{0b0}} = \frac{\eta_{01}\lambda_1}{\eta_{0b0}} = \frac{\eta_{02}\lambda_2}{\eta_{0b0}}$$

or

$$\lambda_1 = a_M \frac{\eta_{0b0}}{\eta_{01}}, \quad \lambda_2 = a_M \frac{\eta_{0b0}}{\eta_{02}}$$

where, η_{0b0} is the steady flow viscosity of the blend having the reference composition. These equations give connection between the shift factor a_M and the interaction parameters λ_1 and λ_2 given by Ninomiya, respectively.

(12) H. Leaderman, R. G. Smith, and R. W. Jones, *J. Polymer Sci.*, **14**, 47 (1954).

Urethane Elastomers Containing Disulfide and Tetrasulfide Linkages

by G. D. T. Owen, W. J. MacKnight, and A. V. Tobolsky

Department of Chemistry, Princeton University, Princeton, New Jersey   (*Received September 30, 1963*)

The chemorheology of two cross-linked polyurethane elastomers containing (1) disulfide groups and (2) tetrasulfide groups was investigated by stress relaxation experiments. It was found that the tetrasulfide-containing elastomer underwent stress decay at a rate 10 times faster than the disulfide-containing elastomer, showing that the tetrasulfide linkage undergoes bond interchange much more rapidly than the disulfide linkage. Spectroscopic evidence is cited tending to confirm the greater stability of the disulfide linkage. The behavior of a cross-linked polyurethane elastomer without polysulfide linkages is presented for comparison.

Introduction

The chemorheological behavior of thiokol-type polymers has been thoroughly investigated by a number of workers.[1] In the case of cross-linked polymers of this type it has been established by Tobolsky and co-workers that stress relaxation takes place by a mechanism of interchange between polysulfide linkages. This mechanism involves scission of the linkage and recombination to give an unstressed chain. The kinetics of the process have been completely worked out on the basis of this mechanism.[1] On the basis of a proposal of Gee[2] and of spectroscopic data on low molecular weight polysulfides[3,4] it would seem that the disulfide linkage should be more stable than the higher polysulfides. In order to test this hypothesis, two "model" compounds were prepared. Both are cross-linked polyurethane elastomers differing only in that one contains disulfide linkages while the other contains tetrasulfide linkages. Such polyurethane elastomers are conveniently prepared in the following manner.

A low molecular weight polyether or polyester, terminated with hydroxyl groups, is treated with excess diisocyanate (usually 2,4-toluene diisocyanate), to form polyurethane chains terminated by isocyanate groups. This material, the prepolymer, can be cured by reaction with hydroxyl-containing substances, and cross links can be introduced by curing with triols. The properties of these polymers have been described elsewhere.[5-7] Schonfeld[8] introduced monosulfide bonds into such a polymer by utilizing the hydroxy-terminated polythioacetal, namely, $HOCH_2CH_2(-SCH_2CHOCHO-$

$CH_2CH_2)_n-SCH_2CH_2OH$. However, the physical properties of the polymer were not described.

In the present work, the disulfide linkage was introduced into the polymer by partially replacing the curing agent (1,2,6-hexanetriol) with dithiodiglycol, namely, $HOCH_2CH_2-S-S-CH_2CH_2OH$. The tetrasulfide linkage was added in an identical manner except tetrathiodiglycol was used, namely, $HOCH_2-CH_2-S-S-S-S-CH_2CH_2OH$. The polyurethane elastomer prepared from 1,2,6-hexanetriol was studied as a basis for comparison.

Experimental

Urethane prepolymer, Cyanoprene 4590, was kindly donated by the Cyanamid Corporation. Cyanoprene 4590 is a polyester terminated by isocyanate linkages. The free NCO concentration of cyanoprene 4590 is about 2.75%.

Tetrathiodiglycol was prepared by treating 2 moles

(1) A. V. Tobolsky, "Properties and Structure of Polymers," John Wiley and Sons, Inc., New York, N. Y., 1960, Section IV, pp. 12, 13, and Section V, p. 8.

(2) F. Fairbrother, G. Gee. and G. T. Merrall, *J. Polymer Sci.*, **16**, 459 (1955).

(3) J. E. Baer and M. Carmack, *J. Am. Chem. Soc.*, **71**, 1215 (1949).

(4) J. A. Barltrop, P. M. Hayes, and M. Calvin, *ibid.*, **76**, 4348 (1954).

(5) J. A. Offenbach and A. V. Tobolsky, *J. Colloid Sci.*, **11**, 39 (1956).

(6) P. C. Colodny and A. V. Tobolsky, *J. Am. Chem. Soc.*, **79**, 4320 (1957).

(7) R. J. Athey, *Rubber Age* (N. Y.), **85**, 77 (1959).

(8) E. Schonfeld, *J. Polymer Sci.*, **49**, 277 (1961).

of 2-chloroethanol with 1 mole of sodium tetrasulfide in an aqueous medium according to the reaction

$$2HOCH_2CH_2Cl + Na_2S_4 \longrightarrow$$
$$HOCH_2CH_2S_4CH_2CH_2OH + 2NaCl$$
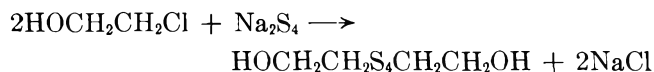
After adding the 2-chloroethanol over a period of 0.5 hr. (using 0.5 M quantities) the temperature had risen from 40 to 75°. The reactants were held at 70–80° for a period of 2 hr. On cooling to room temperature the product was isolated by ether extraction, filtered, and dried by heating for 2 days in a vacuum oven at 50°. The product was a yellow oil and the analysis corresponded very closely to the composition $C_4H_{10}O_2S_4$.

Dithiodiglycol was obtained commercially from the Wateree Chemical Co.

The cure recipes studied are shown in Table I. The required weight of prepolymer was weighed out and heated to 100° *in vacuo* and the required quantities of curing agents were added. The mixture was stirred well and poured into a mold preheated to 130–135°. The cure mixture became extremely viscous and almost solidified within a few minutes. The sample was

Table I

	Sample number		
	1	2	3
Urethane prepolymer	20 g.	20 g.	20 g.
1,2,3-Hexanetriol[a]	0.29 g.	0.29 g.	0.509 g.
Dithiodiglycol	0.411 g.	...	...
Tetrathiodiglycol	...	0.56 ml.	...

[a] Acetone solution containing 0.29 g. of 1,2,6-hexanetriol per ml.

then molded at 130° for 30 min. under a pressure of 10,000 p.s.i. Curing was completed by heating in a forced-draught oven at 100° for 24 hr. A Gehman torsion tester[9] was used to determine the 10-sec. modulus $(3G(10))$ as a function of temperature and the stress relaxation studies were made with a relaxation balance.[10]

Results and Discussion

Figure 1 shows the 10-sec. modulus temperature curves for samples 1, 2, and 3 prepared according to the recipes in Table I. Each network chain in sample 1 contains one disulfide linkage and has the structure

—OR'OCNHRNHCO(CH₂)₂S₂(CH₂)₂OCNHRCOR'O

$$\begin{array}{cccc} | \quad \| & \| & \| & \| \quad | \\ O \quad O & O & O & O \quad O \\ | & & & | \end{array}$$
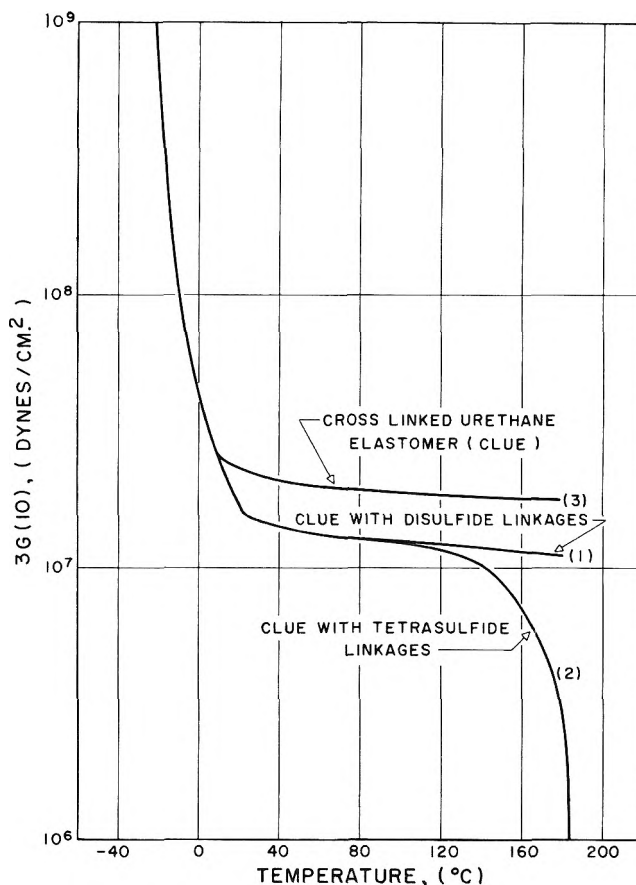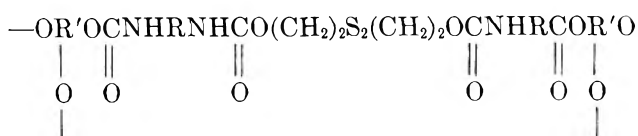
Figure 1. Ten-sec. modulus $(3G(10))$ plotted as a function of temperature for samples 1, 2, and 3.

where R is the urethane prepolymer backbone and R' is $CH_2C(C_2H_5)CH_2$. Sample 2 has a structure identical with the above except that S_2 is replaced by S_4.

Inspection of Fig. 1 shows that, up to 180°, samples 1 and 3 exhibit the characteristic viscoelastic behavior of a cross-linked polymer with the rubbery flow region entirely suppressed. Sample 2 on the other hand has an apparent rubbery flow region starting at just above 100°. Since polymers 1 and 2 are identical in structure with the exception of the polysulfide linkage, it is concluded that the apparent rubbery flow region in sample 2 is due to bond interchange between tetrasulfide groups. The various linkages of sample 3 and these plus the disulfide linkages of sample 1 are "stable" within the 10-sec. measurement interval up to 180°.

Figure 2 shows the relative stress decay of sample 3 at 120°.[6] This is compared with sample 1 at 120° and sample 2 at 100° and it can be seen that stress decay in sample 2 is faster than in the other polymers

(9) ASTM Book of Standards D1043-51, 1958.

(10) Ref. 1, Section IV, p. 1, and Plate IV, p. 1.
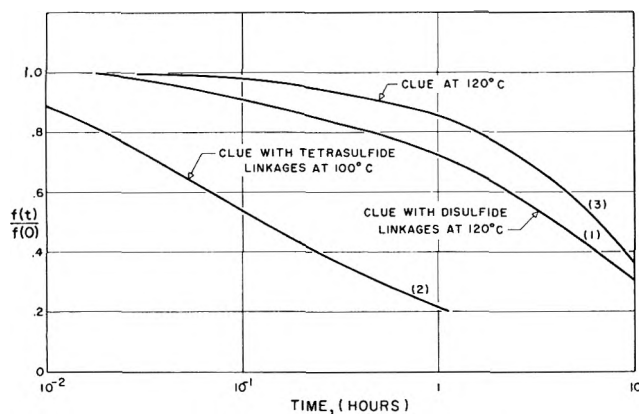
Figure 2. Relative stress at constant extension
vs. log time for sample 1 at 120°, for sample 2 at
100°, and for sample 3 at 120°.

though 20° lower in temperature. The chemical relaxation time, τ_{ch}, defined as the time when the ratio of the stress at time t to the initial stress ($f(t)/f(0)$) is equal to $1/e$, is presented in Table II for the three polymers at 120°. This further serves to point out the striking differences among the three samples.

Table II

Sample	Reference	τ_{ch}, sec.
1	This work	26.3×10^3
2	This work	3.5×10^2
3	Sample IV of ref. 6	34.9×10^3

Figure 3 gives a plot of the relative stress decay vs. logarithmic time of sample 2 at several temperatures
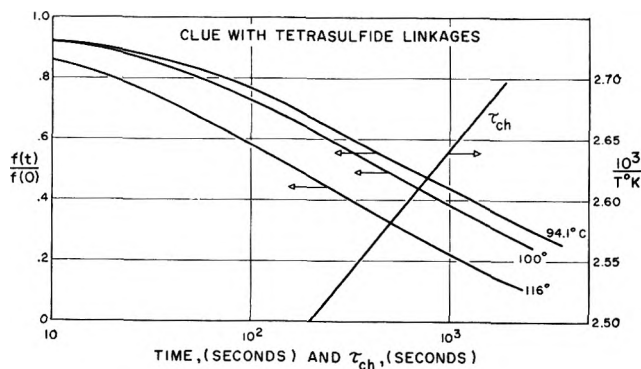
Figure 3. Relative stress at constant extension
vs. log time for sample 2 at various temperatures,
and also log τ_{ch} vs. $1/T$ for sample 2.

and also includes a plot of log τ_{ch} as a function of $1/T$. The slope of this line gives the activation energy for chemical flow[1] and this has a value of 24.4 kcal. mole^{-1}. The agreement between this value and the value of 25.9 kcal. mole^{-1} obtained for the activation energy for stress decay by bond interchange in cross-linked polyethylene tetrasulfide[11] is reasonably good.

The specific rate constant for the interchange reaction in sample 2 is 1.00×10^{-3} sec.$^{-1}$ at 100° For cross-linked polyethylene tetrasulfide,[11] the specific rate constant is 1.79×10^{-3} sec.$^{-1}$ at this temperature. The similarity between the two values tends to show that the mechanism of stress decay in sample 2 is the same as in cross-linked polyethylene tetrasulfide, that is, interchange between tetrasulfide linkages.

The results presented above indicate that the disulfide linkage is much more stable than the tetrasulfide linkage. That this is so can be explained by Gee's analogy[2] between the bonding in O_2 and that in S_2. He attributes the binding in S_2 to a normal single bond plus two three-electron bonds. Thus in the scission of a tetrasulfide (or higher polysulfide) linkage, the odd electron on each free-radical end will be able to form a three-electron bond with the adjacent sulfur atom as shown.

$$\text{\~\~\~}S_4\text{\~\~\~} \longrightarrow \text{\~\~\~}S\text{\_\_\_}S + S\text{\_\_\_}S\text{\~\~\~}$$

In the scission of a disulfide linkage, three-electron bond formation is not possible and thus the linkage is more stable than higher polysulfide linkages.

Calvin[4] and co-workers studied the ultraviolet absorption spectra of cyclic disulfides and attributed the absorption peak found at 2500 Å. to the transition

$$S\text{-}S \longrightarrow S\cdot + \cdot S$$
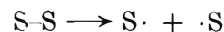
Baer and Carmack[5] observed the ultraviolet spectra of low molecular weight aliphatic disulfides and tetrasulfides and found the absorption peak for the disulfides to be at 2520 Å. corresponding to an energy of 115 kcal. mole^{-1} and the absorption peak for the tetrasulfides to be at 3000 Å. corresponding to an energy of 95.2 kcal. mole^{-1}.

If the ultraviolet absorption of polysulfides is due to the transition suggested by Calvin, the observations of Baer and Carmack tend to lend further support to the greater stability of the disulfide linkage relative to the tetrasulfide linkage. The disulfide linkage may however show rapid interchange in the presence of ionic catalysts such as mercaptides.

(11) A. V. Tobolsky, R. B. Beevers, and G. D. T. Owen, J. Colloid Sci., 18, 359 (1963).

Relaxation of Disulfide and Tetrasulfide Polymers

by A. V. Tobolsky, W. J. MacKnight, and M. Takahashi

Department of Chemistry, Princeton University, Princeton, New Jersey (Received September 30, 1963)

The chemorheology of cross-linked polyethylene disulfide, polyethylene tetrasulfide, and mixtures of these polymers with elemental sulfur is investigated. It is shown that stress decay in the disulfide polymer occurs by scission of the small quantities of higher polysulfide linkages present in the network. It is also shown that elemental sulfur decreases the chemical relaxation time in cross-linked polyethylene disulfide in a predictable manner.

Introduction

In the previous publication from this laboratory[1] it was shown that the disulfide linkage in the absence of catalysts possesses a stability equal to the weakest linkage of the polyurethane network. It was also shown that the tetrasulfide linkage is quite labile relative to the disulfide linkage. This was explained as a consequence of the formation of three-electron bonds[2] by the disulfide radical, a scission product of the tetrasulfide linkage. In previous papers it had been shown that ionic materials such as mercaptides catalyze disulfide interchange.[3-7]

In the light of these results and of a study of the chemorheology of cross-linked polyethylene tetrasulfide rubbers[8] it was decided to conduct an investigation of the viscoelastic properties of cross-linked polyethylene disulfide rubbers (known commercially as "thiokol" type rubbers) with a view to elucidating the mechanism of stress decay in these substances. The effect of elemental sulfur on the chemical relaxation time of these polymers was also studied.

Elemental sulfur (S_8) is a good plasticizer for polymeric sulfur,[9] "thiokol" type rubbers, and other polymers.[10] In particular, large amounts of S_8 can exist dissolved in a liquid condition in polysulfide polymers. In many cases S_8 shows no tendency to crystallize and the mechanical properties of such mixtures are just what would be expected for plasticized cross-linked amorphous polymers.[10]

In this paper the chemical relaxation time (τ_{ch}) of cross-linked polyethylene disulfide is studied as a function of temperature and of sulfur concentration. These data are compared with those obtained for cross-linked polyethylene tetrasulfide.

Experimental

The polysulfide polymers were prepared by the interfacial polycondensation of mixtures of ethylene dichloride, 1,2,3-trichloropropane, and sodium polysulfide of the appropriate sulfur rank. The method is described in the literature.[11,12] The cross-linked polyethylene disulfide was obtained by using sodium disulfide as the reactant. The cross-linked polyethylene tetrasulfide was obtained by using sodium tetrasulfide as the reactant. However, when using sodium disulfide as the reactant, there is still a likelihood that some trisulfide, tetrasulfide, etc., linkages are formed in the polymer.[12] This is probably due to an equilibration among the ionic species in the sodium disulfide solution.

(1) G. D. T. Owen, W. J. MacKnight, and A. V. Tobolsky, J. Phys. Chem., 68, 784 (1964).

(2) F. Fairbrother, G. Gee, and G. T. Merrill, J. Polymer Sci., 16, 459 (1955).

(3) P. C. Colodny and A. V. Tobolsky, J. Appl. Polymer Sci., 2, 39 (1959).

(4) G. Goren, A. V. Tobolsky, and G. Dougherty, J. Am. Chem. Soc., 71, 3551 (1949).

(5) D. T. McAllan, J. V. Cullum, R. A. Dean, and F. A. Fidler, ibid., 73, 3627 (1951).

(6) A. Fava, A. Fliceto, and E. Camera, ibid., 79, 833 (1957).

(7) A. V. Tobolsky, F. Leonard, and G. P. Roeser, J. Polymer Sci., 3, 604 (1948).

(8) A. V. Tobolsky, R. B. Beevers, and G. D. T. Owen, J. Colloid Sci., 18, 359 (1963).

(9) A. V. Tobolsky, W. J. MacKnight, R. B. Beevers and V. D. Gupta, Polymer, 4, 423 (1963).

(10) A. V. Tobolsky and M. Takahashi, J. Appl. Polymer Sci., in press.

(11) A. V. Tobolsky, R. B. Beevers, and G. D. T. Owen, J. Colloid Sci., 18, 353 (1963).

(12) "High Polymers. Volume XIII, Polyethers. Part III, Polyalkylene Sulfides and Other Polythioethers," N. G. Gaylord, Ed., Interscience Publishers. Inc., New York, N. Y., 1962.

Similarly the polymer formed with sodium tetrasulfide must contain other linkages as well. For convenience however we refer to these polymers as polyethylene disulfide and polyethylene tetrasulfide.

Sulfur was added by heating the polymers with sulfur at 155° until the mixtures were homogeneous according to the method of Tobolsky and Takahashi.[10] β-Naphthol was mixed with the polymers in the same way. Sulfur was extracted from the mixtures with benzene in a Soxhlet extractor.

Stress relaxation studies were carried out with a relaxation balance.[13]

Results and Discussion

Figure 1 illustrates the relative stress decay as a function of log time for cross-linked polyethylene disulfide while Fig. 2 is a similar plot for cross-linked polyethylene tetrasulfide. Both elastomers undergo stress decay by the same mechanism, namely, the reversible interchange of polysulfide linkages.[14]
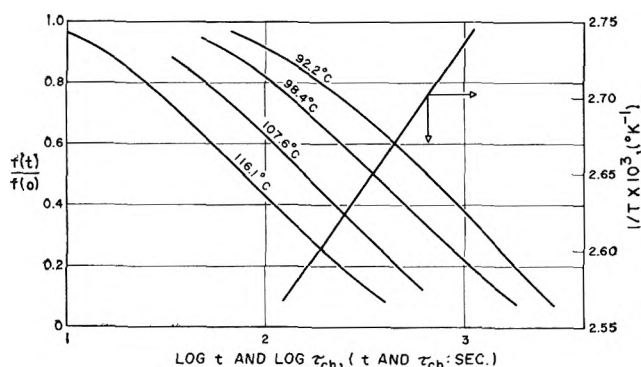
Figure 1. Relative stress decay vs. log time for polyethylene disulfide (sulfur rank 2.2) cross linked with 10 mole % of trichloropropane, and also log τ_{ch} vs. $1/T$ for the same polymer.
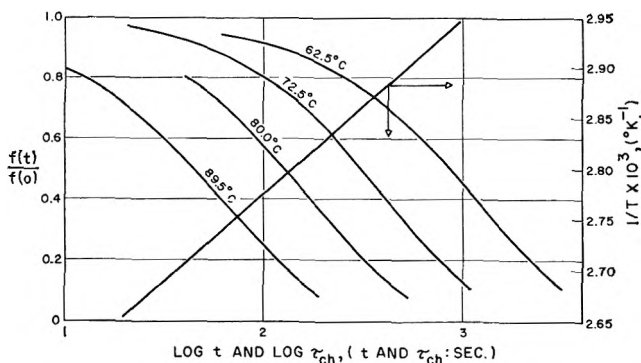
Figure 2. Relative stress decay vs. log time for polyethylene tetrasulfide cross linked with 10 mole % of trichloropropane, and also log τ_{ch} vs. $1/T$ for the same polymer.

The rate law for the disappearance of network chains supporting stress at time t in such a system is[15]

$$-\frac{dN(t)}{dt} = kmN(t) \tag{1}$$

where $N(t)$ is the moles of network chains per cc. supporting stress at time t, k is a specific rate constant for the interchange reaction, and m is the number of bonds per network chain capable of undergoing interchange.

Integration of eq. 1 gives

$$N(t) = N(0) \exp(-t/\tau_{ch}) \tag{2}$$

$$\frac{1}{\tau_{ch}} = km \tag{3}$$

From the equation of state for rubber elasticity, it can be shown[15] that for a cross-linked rubber maintained at constant extension

$$\frac{f(t)}{f(0)} = \frac{N(t)}{N(0)} = \exp(-t/\tau_{ch}) \tag{4}$$

where $f(t)$ is the stress on the rubber at time t, $f(0)$ is the initial stress, and $N(0)$ is the moles of network chains per cc. supporting the stress initially.

According to eq. 2 and 4, a plot of $f(t)/f(0)$ vs. log t should be Maxwellian with τ_{ch} occurring at the time when $f(t)/f(0) = 1/e$. The curves in Fig. 1 and 2 closely approximate the behavior of a single Maxwell element.

Figures 1 and 2 also show a plot of log τ_{ch} vs. the reciprocal of the absolute temperature. Since τ_{ch} is related to the specific rate constant by eq. 3, the slopes of such plots give the activation energy for the bond interchange process. This was found to be 24 ± 1 kcal. mole⁻¹ for both the disulfide and the tetrasulfide polymers.

Feher[16] found that the activation energy for the decomposition of the higher sulfanes (RS_mR where m may have any value up to about 350) is of the order of 25 kcal. mole⁻¹. This agrees well with the data obtained from stress relaxation.

In view of the relative stability of the disulfide linkage[1] and the similarity between the activation energies found for interchange in disulfide and tetrasulfide polymers, it seems reasonable to conclude that chemical

(13) A. V. Tobolsky, "Properties and Structure of Polymers," John Wiley and Sons, Inc., New York, N. Y., 1960, Section IV, p. 1, and Plate IV.

(14) M. Mochulsky and A. V. Tobolsky, Ind. Eng. Chem., 40, 2155 (1948).

(15) Ref. 13, Section IV. pp. 12, 13, and Section V, p. 8.

(16) F. Feher, Special Publication No. 12, The Chemical Society, London, 1958, p. 305.

stress relaxation of cross-linked polyethylene disulfide occurs by scission of occasional higher polysulfide linkages present along the network chains and not by scission of disulfide linkages. Further, it seems probable that the stability of all polysulfide linkages of rank higher than two is approximately the same since all are capable of three-electron bond formation[2] upon scission. We should point out however that a trisulfide linkage has two equivalent S–S bonds that can be cleaved, a tetrasulfide linkage has three nearly equivalent S–S bonds that can be cleaved, etc.

For cross-linked ethylene tetrasulfide polymers we have previously used eq. 1–4 to compute the absolute rate constant k for the interchange reaction of the tetrasulfide linkage.[8] We have calculated m in eq. 3 from the relative amount of ethylene dichloride and 1,2,3-trichloropropane used in the polymerization.[8] We made the tacit assumption that all the polysulfide linkages along the chain were tetrasulfide linkages, which is not exactly true but represents a good approximation.

On the other hand, for the cross-linked polyethylene disulfide polymer, the occasional tri-, tetra-, penta-, etc., sulfide linkages are the only ones that contribute to stress decay since the disulfide linkages are stable.

Table I gives the τ_{ch} for 10 mole % cross-linked polyethylene disulfide and for 10 mole % cross-linked polyethylene tetrasulfide at several temperatures. It is seen that τ_{ch} for the disulfide polymer is much greater than for the tetrasulfide polymer. Ideally, the tetrasulfide polymer has an average of seven tetrasulfide linkages per network chain, and the disulfide polymer has an average of seven disulfide linkages per network chain. From the values of τ_{ch} in Table I we infer that the disulfide polymer behaves as though 6% of its polysulfide linkages were tri-, tetra-, and/or pentasulfide linkages rather than disulfide linkages. Quantitatively speaking, the disulfide polymer behaves as though it contained 0.42 tetrasulfide equivalent linkages per network chain, i.e., the value of m in eq. 3 is 7 for the tetrasulfide polymer but only 0.42 for the disulfide polymer.

The Effect of Dissolved Sulfur. Table II shows the effect of admixed sulfur on τ_{ch} for polyethylene disulfide cross linked with 10 mole % of trichloropropane. It is seen that sulfur causes a marked decrease in τ_{ch} and the effect is strongly concentration dependent. The sulfur can be almost completely extracted from the mixtures whereupon τ_{ch} returns to approximately its value for pure polyethylene disulfide. On the other hand the effect of sulfur on the τ_{ch} of polyethylene tetrasulfide is very slight. For example τ_{ch} for a sample of polyethylene tetrasulfide cross linked with trichloropropane was measured at 62.5° and found to be 1280 sec. τ_{ch} for the same sample mixed with 20% sulfur by weight was 1220 sec. at 62.5°.

Table II: Chemical Stress Relaxation of 10% Cross-Linked Polyethylene Disulfide-Sulfur Systems at 100°

% Sulfur by wt.	τ_{ch} (exptl.), sec.	τ_{ch} (theoret.), sec.
0	470	470
5	180	260
10	132	179
20	96	101
30	64	65
40	52	44
60	23	23
30% β-naphthol	345	

There is a profound difference between the cross-linked polyethylene disulfide plasticized by elemental sulfur and the cross-linked polyethylene tetrasulfide polymer. In the former case the elemental sulfur can be extracted by carbon disulfide. Nothing can be extracted in the latter case.

Although the sulfur has a profound effect on τ_{ch} of cross-linked polyethylene disulfide, stress decay must still occur by polysulfide bond interchange since the plots of relative stress decay *vs.* log time are Maxwellian for the mixtures.

If the sulfur were to act merely as a diluent it would have no effect on τ_{ch} since it would reduce both $N(t)$ and $N(0)$ by the same amount leaving the ratio unchanged. Then, from eq. 4, $f(t)/f(0)$ would also remain unchanged and consequently τ_{ch} would remain constant. This point was checked experimentally by mixing the disulfide polymer with 30 weight % β-naphthol and measuring τ_{ch}. The result is shown in Table II. The probable reason for the slight reduction of τ_{ch} is a minor catalytic effect on disulfide interchange due to the β-naphthol. However, the effect on the reduction of τ_{ch} is very small compared to that produced by a comparable amount of dissolved elemental sulfur.

Table I

Temp., °C.	τ_{ch} disulfide, sec.	τ_{ch} tetrasulfide, sec.
92.2	1050	73
94.8	890	48
98.4	560	32
104.6	320	19

The effect of elemental sulfur on the chemorheology of cross-linked polyethylene disulfide may be explained by assuming that the elemental sulfur interchanges with the disulfide linkages. The process must be a dynamic one, because at any given moment, the elemental sulfur is completely extractable. However the dynamic interchange must allow the network chains to relax.

The fact that elemental sulfur can attack disulfide linkages in a reversible interchange reaction is reconcilable with our theoretical postulates. The S_8 rings must be able to cleave into diradicals, with a specific rate constant essentially the same as that established for the tetrasulfide linkage. These radicals can then cleave the disulfide bond in an interchange reaction.

$$S_8 \text{ (ring)} \rightleftharpoons \cdot S_8 \cdot \text{ (diradical chain)}$$

$$\cdot S_8 \cdot + R\text{-}S_2\text{-}R \rightleftharpoons RS_9 \cdot + \cdot SR$$
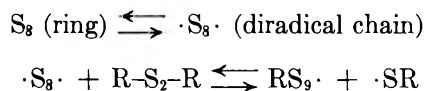
The attack of radicals on the disulfide linkage is well known from chain-transfer reactions in vinyl polymerization.[17]

We shall postulate that the rate-controlling reaction is the cleavage reaction rather than the radical transfer reaction.

We now write the following theoretical equation for τ_{ch} for the disulfide polymer plasticized by elemental sulfur. This equation follows immediately from our postulates.

$$\frac{1}{\tau_{ch}} = k\left(m + \frac{8}{3}\frac{S_8}{N(0)}\right) \tag{5}$$

In eq. 5 k is the specific rate constant for the cleavage of the tetrasulfide linkage, S_8 is the concentration of dissolved sulfur in moles per cc., and $N(0)$ is the moles of network chains per cc. The quantity m has been discussed in the previous section and was found to be 0.42. The factor 8/3 appears because there are eight equivalent sites for cleavage of S_8 and only three for the tetrasulfide linkage. All of the quantities in eq. 5 are predetermined from other experiments. We can thus compute τ_{ch} (theoretical) for the sulfur plasticized samples of cross-linked polyethylene disulfide on a completely a priori basis.

In Table II we show a comparison of τ_{ch} (theoretical) from eq. 5 with the experimentally determined values of τ_{ch}. In all cases the agreement is within a factor of two. Our mechanism is supported by these calculations.

(17) A. V. Tobolsky and B. Baysal, J. Am. Chem. Soc., 75, 1757 (1953).

The Thermodynamic and Physical Properties of Beryllium Compounds.

V. Heat of Formation and Entropy of Beryllium(I) Chloride(g)[1]

by Michael A. Greenbaum, M. Louis Arin, Madeline Wong, and Milton Farber

Rocket Power, Inc., Research Laboratories, Pasadena, California (*Received October 2, 1963*)

The equilibrium $BeCl_2(g)$ + Be(l) = 2BeCl(g) was studied over the temperature range 1573–1723°K. by the molecular flow effusion technique in order to obtain the heat of formation and entropy for BeCl(g). Over this temperature range ΔH_r was found to be 89.1 ± 7.6 kcal./mole and ΔS_r was 39.4 ± 4.6 cal./deg./mole. From recent experimental data and available thermal functions, the second law $\Delta H_{f,298}$ for BeCl(g) was +3.7 ± 3.8 kcal./mole, which compared favorably with the corresponding third law value of +2.0 ± 0.8 kcal./mole. The experimental value for $S°_{298}$ for BeCl(g) was found to be 53.0 ± 2.3 cal./deg./mole.

Introduction

The heat of formation of BeCl(g) has not been determined experimentally. As was the case with BeF(g),[2] estimates of the heat of formation have been based on the dissociation energy of the BeCl molecule, for which several values have been reported. The first spectroscopically determined dissociation energy value ($D_0°$) for the BeCl(g) species was reported by Fredrickson and Hogan[3] in 1934. By employing new physical constants and conversion factors, Herzberg,[4] in 1950, recalculated a new $D_0°$ value from the original data of Fredrickson and Hogan[3] and obtained a value of 4.2 e.v. Gaydon[5] applied further corrections dependent upon the ionic character of BeCl and obtained a value of 3.0 e.v. for $D_0°$. In 1960, Novikov and Tunitskii[6] obtained a new set of spectral data for BeCl(g) which yielded a value of 5.9 ± 0.5 e.v. for the dissociation energy of BeCl.

This wide variation in the dissociation energy of BeCl results in a correspondingly large variation in the heat of formation of this molecule. Using the heat of sublimation of beryllium of 78 kcal./mole[7] and the dissociation energy of chlorine of 57.8 kcal./mole,[8] the values obtained for the heat of formation of BeCl(g) are: +9.5 kcal./mole (Herzberg), +37.1 kcal./mole (Gaydon), and −29.7 kcal./mole (Novikov and Tunitskii).

Since all previously available values for the heat of formation of BeCl(g) were based on widely varying spectroscopic data, an experimental thermodynamic study of the reaction was carried out. This reaction

$$BeCl_2(g) + Be(l) \longrightarrow 2BeCl(g) \qquad (1)$$
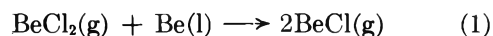
was studied over the temperature range 1573–1723°K. using the molecular flow effusion technique.[9]

Experimental

Introduction. The apparatus and general experimental procedures for the determination of thermodynamic properties of BeF as reported previously[2] have been employed in the present investigation. The

(1) This research was supported by the Air Research and Development Command of the United States Air Force.

(2) M. A. Greenbaum, R. E. Yates, M. L. Arin, M. Arshadi, J. Weiher, and M. Farber, *J. Phys. Chem.*, **67**, 703 (1963).

(3) W. R. Fredrickson and M. E. Hogan, *Phys. Rev.*, **46**, 454 (1934).

(4) G. Herzberg, "Molecular Spectra and Molecular Structure. I. Spectra of Diatomic Molecules," 2nd Ed., D. Van Nostrand Co., New York, N. Y., 1950.

(5) A. G. Gaydon, "Dissociation Energies and Spectra of Diatomic Molecules," Chapman and Hall, Ltd., London, 1953.

(6) M. M. Novikov and L. N. Tunitskii, *Opt. i Spektroskopiya*, **8**, 396 (1960).

(7) G. T. Armstrong, H. W. Wooley, W. H. Evans, and L. A. Krieger, National Bureau of Standards (U. S.), Report No. 6928, U. S. Govt. Printing Office, Washington, D. C., July 1, 1960.

(8) D. R. Stull and G. C. Sinke, "Thermodynamic Properties of the Elements," American Chemical Society, Washington, D. C., 1956.

(9) M. Farber, *J. Chem. Phys.*, **36**, 1101 (1962).

following sections discuss in some detail the modifications in this apparatus and procedure necessary for the study of the reaction of $BeCl_2$ and beryllium.

Apparatus. The molecular flow effusion method developed by Farber[9] was employed to determine the requisite experimental data for the reaction of gaseous beryllium chloride with liquid beryllium at temperatures between 1573 and 1723°K. This procedure consists of vaporizing solid $BeCl_2$ and allowing it to pass over the sample of Be which is heated to the desired temperature, and allowing the resulting vapor species to escape through an effusion orifice into a high vacuum.

The container for the $BeCl_2$ consisted of an aluminum oxide tube, 50 mm. in length and 20 mm. in diameter, closed at one end with a high purity, high density graphite plug. The other end was fitted with a graphite adapter. The alumina tube was wrapped with heating wire contained in an asbestos matrix. The sample of $BeCl_2$ was contained in a nickel boat placed inside the alumina cell. The graphite adapter had an opening 6 mm. in diameter. Connecting the $BeCl_2$ cell to the Be cell was a high purity BeO tube 150 mm. long with an inside diameter of 6 mm. This BeO tube was connected to the Be cell by another graphite adapter. The BeO cell was made of two tight-fitting BeO tubes. The back part had a 1-mm. orifice to allow entry of the gaseous $BeCl_2$, while the front section had a 0.7-mm. effusion orifice. No reaction was found to occur between the Al_2O_3 and the $BeCl_2$. This was established by passing $BeCl_2$ vapor through an empty Al_2O_3 tube over the temperature range of interest and weighing the tube after this treatment. No change in weight of the Al_2O_3 tube was found to occur under these conditions. The remaining parts of the cell were constructed of BeO.

To permit uniform distribution of heat over the BeO cell, as well as to prevent contamination of materials on the outside of the cell (and thus result in an apparent weight gain), the BeO cell was encased in a graphite shield. The opening in the shield above the cell orifice permitted unhindered effusion. Weighing of the BeO cell before and after reaction was done with the graphite shield removed.

Measurement of the Be temperature was accomplished by means of a Leeds and Northrup optical pyrometer which was calibrated before and after the experimental determinations. Correlation of the temperature inside the BeO cell with that read by the pyrometer on the outside of the cell was accomplished by using a calibrated platinum–rhodium thermocouple placed inside of the cell and taking readings with thermocouple and pyrometer simultaneously. This was done in the empty cell before and after experimental

determinations were made as well as during some experimental runs. No significant difference in temperatures was observed in any case.

Experimental Procedure. The extreme hygroscopicity of $BeCl_2(s)$ necessitated very special handling precautions. Even when these precautions were taken early samples of $BeCl_2$ were found to be totally unsatisfactory. The first samples of $BeCl_2$ obtained were reported to be in excess of 99% purity. However, they were provided in the form of a very fine, fluffy material. After many unsuccessful attempts to obtain reproducible data with this material some of it was resublimed *in vacuo.* Under these conditions large amounts of material were left behind. In addition, the sublimed materials had only a slightly larger crystalline size and thus did not significantly reduce the surface area of the material. Suitable material of 99.5+% purity in the form of large crystals was finally obtained from Beryllium Corporation of America. This material yielded reasonably reproducible results when handled in a drybox or drybag under dry nitrogen. All of the $BeCl_2$ cells were filled under these conditions and on completion of a reaction the entire three-part cell assembly was immediately placed in a drybag under nitrogen. For weighing purposes, the $BeCl_2$ remaining in the cell was transferred to a weighing bottle (nickel boat and all) and then weighed on a semimicro balance. Initial weighings were made in the same manner. The bottles of $BeCl_2$ were kept under dry nitrogen in a drybox at all times. The beryllium employed has been described previously.[2]

The Be sample was heated to the desired temperature in the 1573–1723° K. range. After reaching temperatures in the Be cell the temperature of the $BeCl_2$ cell was generally around 470–500°K. The temperature of the cell was then so raised that a reasonable pressure of $BeCl_2$ could be obtained. Based on a recent vapor pressure study of $BeCl_2(s)$[10] this was generally around 525–555°K. The length of the runs was between 1 and 3 hr. and corrections were made for the weight loss of $BeCl_2$ during the heat-up and cool-down cycle at each temperature studied. Temperatures of both $BeCl_2$ and Be containers were constantly monitored and controlled, the former manually and the latter automatically. The variation in temperature was usually less than ±7°K. while the temperature of the Be varied less than ±2°. Temperatures of both cells were recorded at 10–15-min. intervals during each run. The average temperature over the 1–2 hr. of the run was used in making the calculations.

(10) M. A. Greenbaum, R. E. Yates, and M. Farber, *J. Phys. Chem.,* **67,** 1802 (1963).

Table I: Summary of Data for the Be–BeCl₂ Reaction

T, °K.	Time, hr.	G_0, BeCl₂ wt. loss, mg.	G_{BeCl_2}', cor. BeCl₂ wt. loss, mg.	G, Be wt. loss, mg.	G_{Be}', cor. Be wt. loss, mg.	Log K	ΔF_r, kcal./mole	$\Delta H_{f,BeCl}$, kcal./mole
1724	1	243.9	81.8	14.1	6.6	−2.9287	23.105	−1.488
1722	1	216.3	62.4	13.1	5.6	−2.6428	20.825	−2.653
1696	1	132.5	34.8	11.5	5.3	−2.7580	21.405	−2.793
1695	1	114.3	30.1	11.1	4.9	−2.7433	21.278	−2.865
1664	1	214.3	123.6	11.6	6.9	−3.0594	23.296	−2.352
1636	1	246.1	206.1	9.7	6.4	−3.3469	25.056	−1.952
1603	2	287.0	224.8	9.6	7.0	−3.6078	26.464	−1.753
1573	2	138.8	103.6	6.0	4.0	−3.7575	27.081	−1.479
1574	3	269.1	205.7	10.2	7.2	−3.7208	26.794	−1.613
1575	2	349.2	291.5	8.5	6.5	−3.7844	27.275	−1.378

Weight loss corrections for vaporization of Be were found to be in excellent agreement with those previously reported.[2,11,12]

Treatment of Experimental Data. In the study of the reaction

$$BeCl_2(g) + Be(l) \longrightarrow 2BeCl(g) \qquad (1)$$
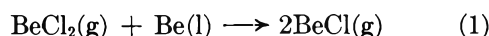
over the temperature range 1573–1723 °K. the experimentally determined weight loss data of Be and BeCl₂(s) were converted into partial pressures of BeCl(g) and BeCl₂(g) at equilibrium by using the basic Knudsen effusion equation

$$P(\text{mm.}) = 17.4 \frac{G'}{W_0 A t} \frac{\sqrt{T}}{M} \qquad (2)$$

where $P(\text{mm.})$ is the pressure (mm.) of the effusing compound, G' is the corrected weight loss (g.) of the compound due to effusion through an orifice of area A (cm.²) during time t (sec.), W_0 is the Clausing factor, T is the temperature (°K.), and M is the average molecular weight of the effusing material.

The weight loss of Be was corrected by subtracting the amount of Be vaporized G_v from the total weight loss measured G. The amount lost due to the vaporization of beryllium was determined experimentally for each temperature studied and these values were found to agree with the previously reported values[2] obtained in this same manner.

At equilibrium, according to eq. 1, 2 moles of BeCl are formed from the reaction of 1 mole of Be; thus, if G_r represents the weight loss of Be due to reaction, $89.0/9G_r$ or $9.89G_r$ will be the weight of BeCl effusing from the cell at equilibrium. Also, for each mole of Be reacting 1 mole of BeCl₂ reacts; if G_0 stands for the total weight loss of BeCl₂ during an experiment, $G_0 − 8.89G_r$ should be the weight of BeCl₂ effusing from the

cell at equilibrium. G_r is, however, equal to $G − G_v$ by definition. The weight loss of BeCl₂ due to the heat-up and cool-down cycle of the furnace, G_f, must also be subtracted from the total weight loss of BeCl₂. This value was determined experimentally for every temperature at which measurements were made. The final corrected value for the weight loss of BeCl₂ is $G_0 − 8.89(G − G_v) − G_f$.

In the present investigation A was found to be 5.514×10^{-3} cm.² and W_0 was determined to be 0.4006 by direct measurement. Substituting these values and the weight losses into eq. 2 and converting the equation to pressures in atm. and weight losses to mg., the equilibrium partial pressures of BeCl and BeCl₂ are given by

$$P_{BeCl} = 1.513 \times 10^{-2} \sqrt{\frac{T}{t}} (G − G_v) \qquad (3)$$

$$P_{BeCl_2} = 1.42 \times 10^{-3} \sqrt{\frac{T}{t}} (G_0 − 8.89[G − G_v] − G_f) \qquad (4)$$

The equation for the equilibrium constant for the reaction given in eq. 1 is

$$K = \frac{P_{BeCl}^2}{P_{BeCl_2}} \qquad (5)$$

Substituting into the above equation the expressions for P_{BeCl} and P_{BeCl_2} the following equation is obtained

$$K = 5.556 \times 10^{-5} \sqrt{\frac{T}{t}} \left(\frac{[G − G_v]^2}{G_0 − 8.89[G − G_v] − G_f} \right) \qquad (6)$$

(11) E. H. Gulbransen and K. J. Andrew, *J. Electrochem. Soc.*, **97**, 383 (1950).

(12) R. B. Holden, R. Spieser, and H. L. Johnston, *J. Am. Chem. Soc.*, **70**, 3897 (1948).

The reported vapor pressure values were calculated from eq. 3 and 4 and are reported in Table I along with the values for the equilibrium constant K, as calculated from eq. 6.

Validity of the Reaction. The reaction taking place between the gaseous beryllium chloride and liquid beryllium in the effusion cell at the temperatures studied was assumed to be that represented by eq. 1. The corresponding reaction between beryllium fluoride and beryllium was previously demonstrated to occur in this manner.[2] Dimerization of $BeCl_2$ in the vapor phase at these temperatures and pressures has also been shown not to occur.[10]

Although it was not possible to carry out a detailed analysis of the effect of the partial pressure of $BeCl_2$ on the equilibrium constant as was done in the case of BeF,[2] due to the much steeper vapor pressure curve of $BeCl_2$ coupled with the larger scatter in the data, some evidence of the nature of the reaction is available from the data. A plot of log P_{BeCl} *vs.* log P_{BeCl_2} based on the limited data available yields a slope around 2 in agreement with the slope predicted from reaction 1. In addition, the agreement of the vapor pressure data for $BeCl_2$ found in this study with that obtained in a detailed effusion study reported earlier[10]

demonstrates that neither $(BeCl_2)_2$ nor any dissociation products (Be, Cl, Cl_2, etc.) are the species reacting with Be(l). Further, the good agreement found between second and third law values for $\Delta H_{f,298}$, coupled with agreement between experimental and theoretical values for $S°_{298}$ of BeCl(g) (*vide infra*), lends further support to the fact that the indicated reaction is the only one occurring to a significant extent.

As demonstrated previously,[2] no reaction was found to occur between the BeO and graphite components of the cell. In addition neither BeO nor graphite loses any weight by volatilization at the temperatures employed in this study. No reaction was found to occur between $BeCl_2$ and any of materials used in this study (Ni, BeO, C, Al_2O_3). The passage of considerable quantities of $BeCl_2$ through an empty BeO tube at 1723°K., the highest temperature investigated, following the procedure previously described for $BeF_2(g)$,[2] resulted in no change in weight of the BeO tube.

Because of the previously demonstrated reaction between beryllium and graphite, the cell used in this study was so designed (*vide infra*) that no contact occurred between these materials. In no instance was any trace of beryllium carbide found in the graphite adapter. This was also considered good evidence for
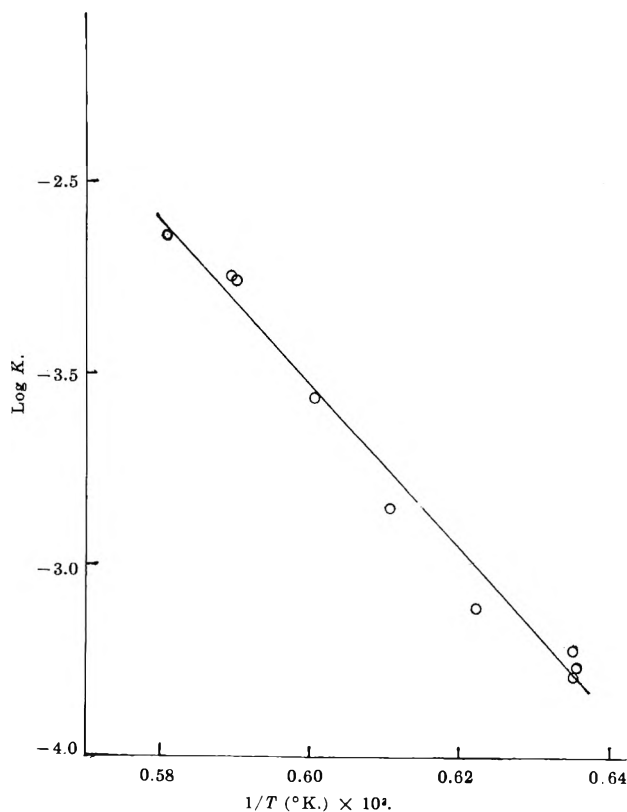
Figure 1. The equilibrium constant for the reaction $BeCl_2(g) + Be(l) = 2BeCl(g)$ as a function of temperature.
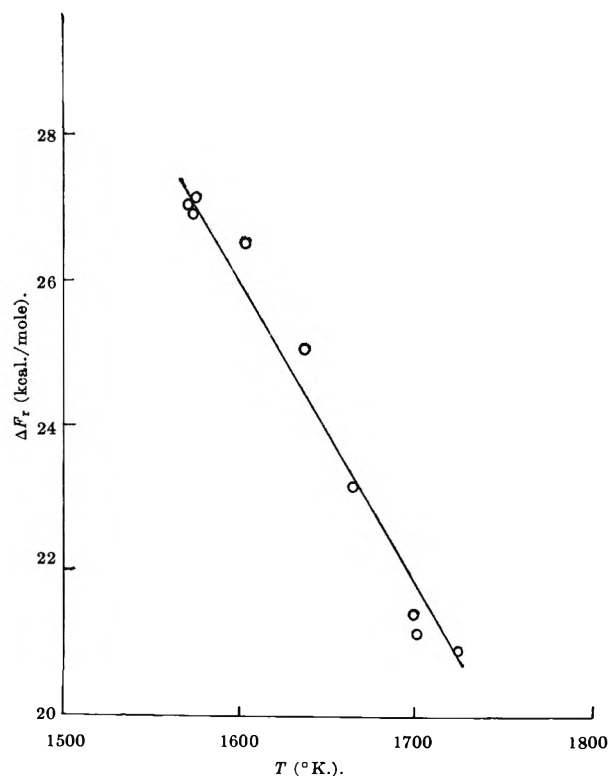
Figure 2. The ΔF_r for the reaction $BeCl_2(g) + Be(l) = 2BeCl(g)$ as a function of temperature.

the lack of back diffusion of Be(g) during the course of the experiments. However, further confirmation for the absence of back diffusion was obtained by varying the inlet diameter for the $BeCl_2$ as previously described for the study of BeF(g).[2]

Based on all the above observations it is considered that the postulated reaction of $BeCl_2(g)$ with Be(l), eq. 1, is the only reaction occurring within the experimental error of the resulting data.

Results and Discussion

The experimental data obtained from the study of reaction 1 over the temperature range 1573-1723°K. have been summarized in Table I. A plot of log K vs. $1/T$, as represented in Fig. 1, leads to a value for the second law heat of reaction. Similarly, a plot of ΔF vs. T in Fig. 2 yields a value for the entropy of reaction. Least-squares analyses of the experimental data leads to a value for the heat of reaction over the experimental temperature range of 89.1 ± 7.6 kcal./mole and an entropy of reaction of 39.4 ± 4.6 cal./deg./mole. The fairly high least-squares standard deviations are due largely to the extreme hygroscopicity of the $BeCl_2$ employed. This resulted in considerably more scatter in the points (due to liberation of HCl on heating the $BeCl_2$) than has previously been encountered. However, by taking the special precautions previously described (vide supra) this problem was reduced to a minimum.

Employing the experimental value for the heat of reaction, a value of −86.3 kcal./mole for $\Delta H_{f,298}$ for $BeCl_2(g)$[13] and estimated theoretical heat capacity data for the species involved, $BeCl_2(g)$, Be(l), and BeCl(g),[13] a value of 3.7 ± 3.8 kcal./mole is obtained for $\Delta H_{f,298}$ of BeCl(g). The experimental entropy of

reaction combined with a value of 57.9 cal./deg./mole for $S°_{298}$ for $BeCl_2(g)$[13] and 3.95 cal./deg./mole for $S°_{298}$ of Be(l),[13] together with the theoretical entropy data,[13] result in a value of 53.0 ± 2.3 cal./deg./mole for $S°_{298}$ of BeCl(g). This compares with a theoretical value for $S°_{298}$ of BeCl(g) of 52.0 cal./deg./mole.[13] The third law value for $\Delta H_{f,298}$ of BeCl(g) is 2.0 ± 0.8 kcal./mole, which is in excellent agreement with that obtained from the van't Hoff equation.

At the lowest temperature employed in this study, 1573°K., the contents of the BeO cell were examined after the runs to make sure that the beryllium metal, which was heated to only about 15° above its melting point, had actually melted; in all cases, the beryllium was found to be completely fused.

All previous values for the heat of formation of BeCl(g) have been based on spectroscopically determined dissociation energies. These dissociation energies are inherently of a low order of accuracy as a result of the very long extrapolations of vibrational quanta required for these calculations. The magnitude of these uncertainties are well illustrated both by the admitted deviations of 0.5-1.0 e.v. and by the large divergence of values which have been reported. It is not surprising, therefore, that the more precise, thermodynamically determined value of $\Delta H_{f,298}$ of BeCl, +3.7 kcal./mole, agrees reasonably well only with one of the three previously reported values. As was found to be the case in a comparable study of the BeF(g) molecule,[2] the experimental value obtained in this experimental study lies midway between the extremes of the spectroscopic values.

(13) JANAF Thermochemical Tables, USAF Contract No. AF 33(616)-6149, Advanced Research Projects Agency, Washington 25, D. C.

Solutions of Fluorochemicals and Hydrocarbons

by M. S. B. Munson

Humble Oil and Refining Company, Research and Development, Baytown, Texas
(Received October 7, 1963)

Critical solution temperatures for several paraffins and mixtures of paraffins in fluoro-chemicals can be correlated well with ΔE_v even though the Hildebrand–Scatchard solution theory is inadequate. A single curve of mole fraction composition *vs.* T/T_c will reproduce the solubility data for an isomeric series of compounds with $(C_4F_9)_3N$, and a solubility curve of volume fraction *vs.* reduced temperature, T/T_c, will adequately represent the solubility data for pentanes, hexanes, and heptanes in $(C_4F_9)_3N$. From the correlations of critical solution temperatures of a series of hydrocarbons with different fluorochemicals one would expect similar behavior for other noncomplexing fluorochemical–hydrocarbon systems. Chemical shifts for paraffins in $(C_4F_9)_3N$ showed no correlation with ΔE_v and gave no indication of any solution anomalies.

Introduction

Solutions of fluorochemicals and hydrocarbons furnish examples of highly nonideal mixtures (without the complication of complex formation) whose components may be varied through a wide range of chemically similar materials. It has been observed, however, that solutions of fluorochemicals and hydrocarbons do not behave as one would expect from Hildebrand–Scatchard solution theory. Although extensive comment has been forthcoming, no satisfactory reconciliation of theory with experiment has been achieved.[1]

The critical solution temperature is a reasonable, though indirect, measure of solution nonideality and one which is relatively easily obtained. Critical solution temperatures for various compounds with fluorochemicals have been measured and it has been found for many fluorochemical–hydrocarbon systems that predictions based upon the Hildebrand–Scatchard equations (including a correction for inequalities in molar volumes)[2]

$$RT_c \cong (\delta_1 - \delta_2)^2 (2V_1V_2)/(V_1^{1/2} + V_2^{1/2})^2$$

do not agree with the experimental values. V is the molar volume; δ is the solubility parameter, $(\Delta E_v/V)^{1/2}$, in which ΔE_v is the molar energy of vaporization; R is the gas constant; and T_c is the critical temperature in °K. Disagreement between theory and experiment should not be surprising since T_c is related to the second derivative of the excess free energy of mixing[3] and drastic approximations are made in the development of an equation for the excess free energy of mixing in solubility parameter theory. The parameters of the solution theory, δ or ΔE and V, have proved useful in describing "weakly interacting" systems and should be helpful with the noncomplexing fluorochemical–hydrocarbon systems.

Results and Discussion

Solubilities of several hydrocarbons were determined with portions of fluorochemical taken from one carefully purified sample. The purity of this sample of fluorochemical $(C_4F_9)_3N$, perfluorotributylamine from the Minnesota Mining and Mfg. Co., was estimated at $>95\%$ by gas chromatographic analysis. The impurities were close-boiling fully fluorinated compounds. The purification procedure involved passing through silica or alumina, refluxing with $KMnO_4$ + H_2SO_4, refluxing over KOH, and distilling. Of these procedures, only extremely careful fractionation had any effect on the distribution of fully fluorinated materials. The hydrocarbons were Phillips Research grade. A comparison of the critical solution tempera-

(1) R. L. Scott, *J. Phys. Chem.*, **62**, 136 (1958).

(2) J. H. Hildebrand, B. B. Fisher, and H. A. Benesi, *J. Am. Chem. Soc.*, **72**, 4348 (1950).

(3) J. S. Rowlinson, "Liquids and Liquid Mixtures," Butterworths Publications, Ltd., London, 1959, Chapter 5.

Table I :   Mixtures of Paraffins with $(C_4F_9)_3N$

	δ_{298}, (cal./cc.)$^{1/2}$	V_{298}, cc.	$\Delta E_{v, 298}$, kcal.	t_c, °C.	$(X_{HC})_c$
2,2-Dimethylbutane	6.71	133.7	6.024	26.29	0.780
2,3-Dimethylbutane	6.97	131.2	6.367	37.42	0.783
2-Methylpentane	7.02	132.9	6.545	45.04	0.781
3-Methylpentane	7.13	130.6	6.642	48.28	0.795
n-Hexane	7.27	131.6	6.947	59.90	0.786
		132.0 ± 1.0			0.785 ± 0.005
n-Pentane	7.02	116.1	5.723	36.94	0.807
2-Methylbutane	6.75	117.4	5.344	22.83	0.798
		116.8 ± 0.7			0.802 ± 0.005
n-Heptane	7.43	147.5	8.142	81.02	0.764
2,4-Dimethylpentane	6.96	149.9	7.267	50.63	0.763
		148.7 ± 1.2			0.764 ± 0.001
$(C_4F_9)_3N$	5.9[a]	358.0	13.2[a]		

[a] G. J. Rotariu, R. J. Hanrahan, and R. E. Fruin, *J. Am. Chem. Soc.*, **76**, 3752 (1954).

tures reported here and others in the literature affords fair agreement, which is all that one may reasonably expect.

The solubility curves were determined in the accustomed manner by changing the temperature of a mixture of known composition (with agitation of the sample vessels) until two phases appeared (or disappeared). The thermometers were calibrated and the accuracy of the temperature measurements is ±0.02°. Critical solution temperatures and compositions were obtained by plotting the average hydrocarbon concentration, $^{1}/_{2}(X_{HC}(\text{hydrocarbon phase}) + X_{HC}(\text{fluorochemical phase}))$, against temperature and noting the intersection with the solubility curve. The lines

exhibited only a slight curvature and were easily extrapolated.

The values of the critical solution temperatures and compositions, together with pure component properties, are given in Table I. For hydrocarbons of the same molar volumes, the critical concentrations are constant and decrease as the molar volume of the hydrocarbon increases toward that of the fluorochemical. From a plot of $T_c^{1/2}$ vs. δ_{HC} (which for the hexanes is not a good fit to the data) one obtains average values for the solubility parameter of the fluorochemical $(C_4F_9)_3N$: 4.87 from the pentanes, 4.46 from the hexanes, and 3.24 from the heptanes. This agreement is not good and the values thus obtained do not agree
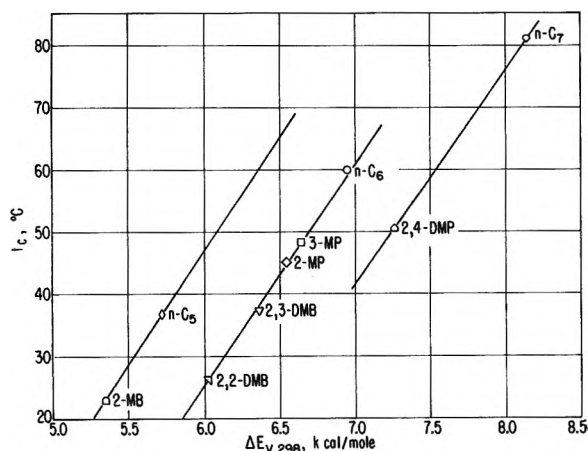
Figure 1.   Critical solution temperature vs. energy of vaporization.
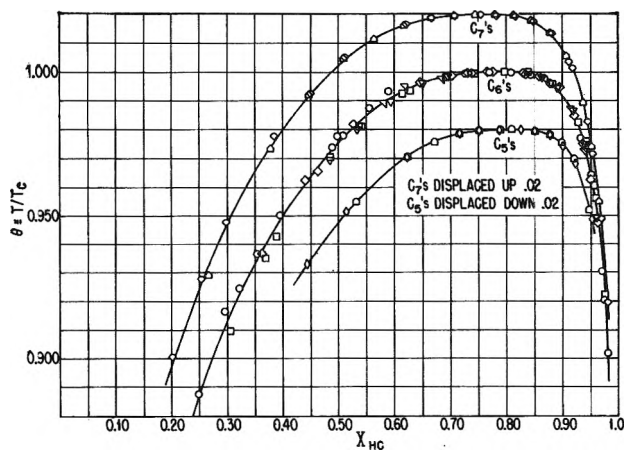
Figure 2.   Mole fraction solubility vs. reduced temperature.
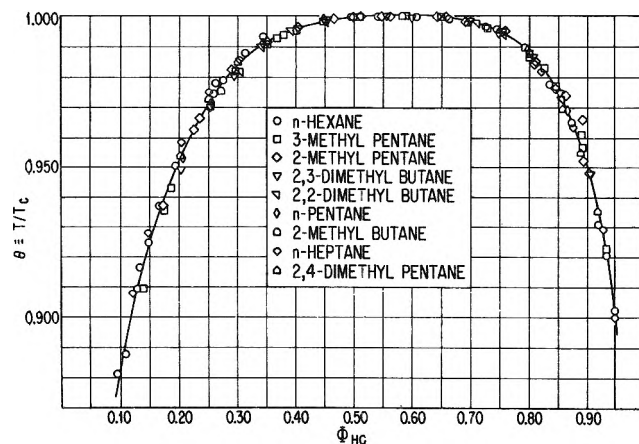
Figure 3. Volume fraction solubility vs. reduced temperature.

with that calculated from the properties of $(C_4F_9)_3N$. If one disregards the specific equations of the Hildebrand–Scatchard theory but still considers the energy of vaporization and molar volume to be measures of the interaction energy and size of the molecules, one may hope to find an empirical equation relating the critical solution temperature and these parameters. Figure 1 shows a plot of t_c vs. $\Delta E_v(298°K.)$ which gives a good fit to a straight line for the hexanes. The slopes of the lines are substantially the same for the homologs and the intercepts decrease with increasing hydrocarbon volume. A plot of t_c vs. δ_{HC} shows appreciably more scatter for the hexanes than does the plot of t_c vs. ΔE_v and does not allow the data for pentanes, hexanes, and heptanes to be plotted on one curve. A plot of t_c vs. δ^2 shows slightly more scatter of the data than indicated in Fig. 1 and does not allow the points to be considered as one curve. Although the quantitative description of the theory is poor, the qualitative agreement is good in that the critical concentrations of the isomeric species are the same and an increase in δ_{HC} (or ΔE_v) is paralleled by an increase in t_c. Similar behavior was noted for the hexanes with "perfluoroheptane"[4] and "perfluoropentane."[5]

By an obvious (although shaky) analogy to the corresponding states treatment of gases, one would expect a one-parameter equation to correlate the solubilities of isomers in a given solvent, since the molar volumes (which are perhaps the same as the sizes) are the same. Figure 2 shows the solubilities for the heptanes, hexanes, and pentanes plotted as functions of the reduced temperature, $\theta = T/T_c$. In this figure, the curve for the heptanes has been displaced upward by 0.02 and the curve for the pentanes downward by 0.02 to improve legibility. The data fit remarkably well to these curves. The solubility curves for the homologs are

not superimposable. The marked assymetry of the curves is that usually observed in systems with a large disparity of molecular sizes. These data also seem to indicate that there is no pronounced effect of molecular shape within this range.

Since a one-parameter equation was so successful for molecules of the same size, one is led to attempt to reduce all of these solubility data to a single curve. It has been observed repeatedly that the pronounced assymetry in solubility curves for mixtures of molecules of different size is reduced by using volume fractions instead of mole fractions. Figure 3 shows a plot of volume fraction solubility of hydrocarbon against reduced temperature. The volume fractions are calculated at 25° assuming no volume change on mixing— the volume change on mixing is small, though not zero.[6] The curve is much more nearly symmetric than those in the previous figure, but the critical solution composition is at $\phi_{HC} = 0.572 \pm 0.002$ (for pentanes, hexanes, and heptanes) and not $\phi_{HC} = 0.500$. As indicated by the legend in Fig. 3, the solubilities of nine paraffins (two pentanes, five hexanes, and two heptanes) are reproduced by one curve. The observed correlations may perhaps be fortuitous or perhaps the range of hydrocarbon volumes is not great enough to test it accurately, but the representation of the present data is good.

A hasty search of the literature indicates no other available tabulation of data on solubility of paraffin isomers in fluorochemicals. Some studies have been made but they are not extensive enough to be of utility in verifying a reduced equation of solubilities. Taking all of the available data on solubilities of various compounds with different fluorochemicals and plotting as volume fraction solubility against reduced temperature, one can obtain a "semiquantitative" fit to a single curve, with an appreciable scatter of the data points. Considering the general discordance of solubility data, one should not expect much more.

There are several other ways of plotting solubility data which may yield information of interest. These data are not accurate enough to add anything of value to the discussions of whether or not the solubility curve has an absolutely flat top,[7] since either a discontinuous or smooth curve can be drawn through the points in the critical region with equal confidence.

(4) J. B. Hickman, J. Am. Chem. Soc., 77, 6154 (1955).

(5) R. Dunlap, R. Digman, and J. Vreeland, Abstracts, 124th National Meeting of the American Chemical Society, Chicago, Ill., September, 1953.

(6) See, for example, R. G. Bedford and R. D. Dunlap, J. Am. Chem. Soc., 80, 282 (1958).

(7) See, for example, O. K. Rice, J. Chem. Phys., 23, 164 (1955).
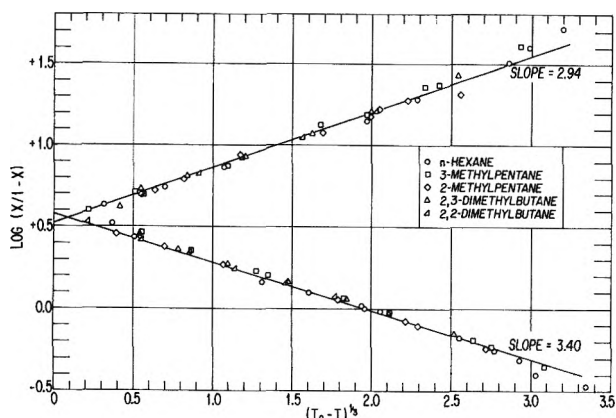
Figure 4. Log $(X_{HC}/1 - X_{HC})$ vs. $(T_c - T)^{1/3}$ for the hexanes with $(C_4F_9)_3N$.

Cox and Herrington[8] have reported that solubility data may be represented by the equations

$$(T_c - T) = [A' \log (x'/1 - x') + B']^3$$

and

$$(T_c - T) = [A'' \log (x''/1 - x'') + B'']^3$$

in which ' and '' refer to the two coexisting phases. They found for several mixtures that $A' \cong A''$. Rudd and Widom[9] in another examination of one of the systems for which Cox and Herrington found $A' \neq A''$ observed that within the experimental precision for pure ethylene glycol monoisobutyl ether with water $A' = A''$, but with impure materials $A' \neq A''$. Figure 4 shows a plot of log $(X/1 - X)$ vs. $(T_c - T)^{1/3}$ for the hexanes with $(C_4F_9)_3N$. The points for $(T_c - T)^{1/3}$ less than about 0.7 are not reliable because any reasonable value for the uncertainty in the critical temperature produces an appreciable uncertainty in these values. All of the points, however, fall close to the curves indicating that this method would probably be an excellent one for determining the critical temperature. The plots are good straight lines over a fairly wide temperature range, up to about $(T_c - T) = 25°$, where the precision of the data becomes bad, and intersect at $(T_c - T)$ almost zero. The intersection at $(T_c - T)^{1/3} < 0.1$ corresponds to only a trivial discrepancy in the critical temperature. As in the previous reduced equation (Fig. 2) all of the hexanes fit on the same curve. The slopes of the two curves are not the same and cannot be considered the same within experimental error. Whether this disagreement of slopes is to be considered as characteristic of fluorochemical–hydrocarbon mixtures or the results of known impurities in the fluorochemical is unknown. The slopes of the curves are different for the pentanes and heptanes as well: 2.97 and 3.41 for the pentanes
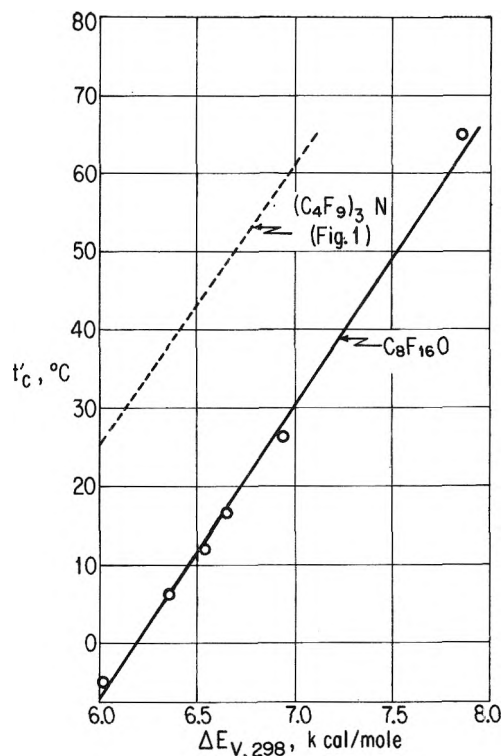
Figure 5. Critical solution temperature vs. energy of vaporization.

and 2.90 and 3.38 for the heptanes. The intercepts are slightly different, so that the curves are essentially parallel. A plot using volume fractions would make the curves for pentanes, hexanes, and heptanes superimposable but the slopes for the two phases would still be different.

From Fig. 2 or 3 one can see that the ratios of the temperatures of miscibility for two paraffins in $(C_4F_9)_3N$ are independent of concentration and that the temperature of miscibility of an equal volume mixture of fluorochemical and hydrocarbon is very close to the critical solution temperature. Consequently, since it was easier to measure the miscibility temperature of equal volume mixtures, t_c', than to determine the critical solution temperatures, these quantities, t_c', were determined for mixtures of hydrocarbons with another fluorochemical for comparison: $C_8F_{16}O$ from the Minnesota Mining and Mfg. Co., purified in the same manner as $(C_4F_9)_3N$. These data are listed in Table II.

Figure 5 shows a plot of t_c' vs. ΔE_v for hexanes with $C_8F_{16}O$. A good linear relationship is observed (the dotted line is drawn from Fig. 1 for comparison). The points on this curve represent the hexanes and

(8) J. D. Cox and E. F. G. Herrington, Trans. Faraday Soc., 52, 926 (1956).

(9) DeF. P. Rudd and B. Widom, J. Chem. Phys., 33, 1816 (1960).

Table II: Miscibility Temperatures of Equal Volumes of Fluorochemical and Hydrocarbon

	t_0', °C.	
	$(C_4F_9)_3N$	$C_8F_{16}O$
2,2-Dimethylbutane		−5.0
2,3-Dimethylbutane		6.0
2-Methylpentane		11.8
3-Methylpentane		16.0
n-Hexane		26.3
2,2,4-Trimethylpentane	53.3	18.2
n-Heptane		45.6
Methylcyclohexane		65.0

methylcyclohexane, which has essentially the same molar volume as the hexanes. Mixtures of hexanes and methylcyclohexane, even 2,2-dimethylbutane and methylcyclohexane whose miscibility temperatures differ by about 70°, fall close to this curve if plotted against average ΔE_v. Other data on solubilities of mixtures of paraffins show that that data can be well represented by a solubility curve as a function of reduced temperature as indicated in Fig. 2 and 3.

To illustrate the similarity in solution behavior for other noncomplexing fluorochemical–hydrocarbon systems, Fig. 6 shows a plot of t_c or t_c' for one set of hydrocarbons with a fluorochemical against t_0' for the same set of hydrocarbons with $(C_4F_9)_3N$. The data
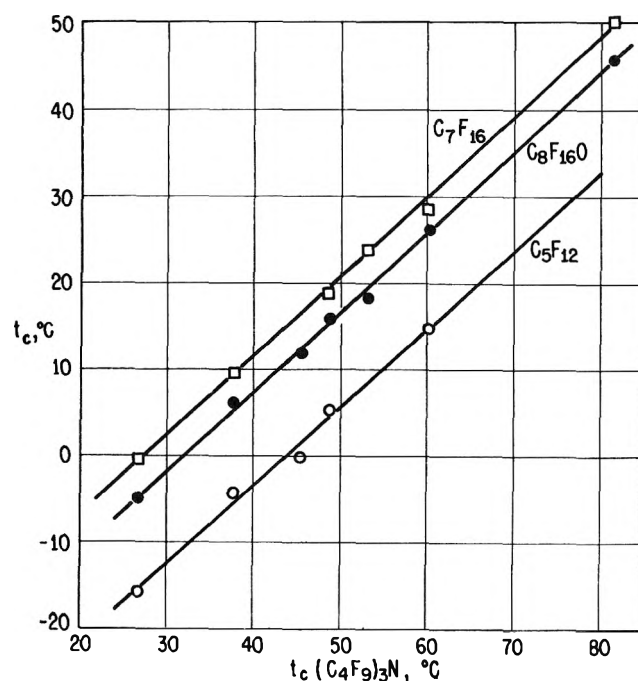
Figure 6. Correlation of critical solution temperature of a series of hydrocarbons with different fluorochemicals.

for C_5F_{12} are the critical solution temperatures from ref. 5 and the data for C_7F_{16} are from ref. 2 and 4. The similarities in behavior are striking and one can expect similar behavior for solutions of other noncomplexing fluorochemical–hydrocarbon systems.

Simple nuclear magnetic resonance studies were undertaken on solutions of fluorochemicals and hydrocarbons to see if any information could be obtained with regard to any anomalous solution behavior. A solvent shift in excess of that due to the differences in magnetic susceptibility has been observed for several systems for gas going into solution and has been considered as due to dispersion forces.[10,11]

The nuclear magnetic resonance data were obtained using a 60 Mc. Varian spectrometer with proton-controlled magnetic field. Benzene sealed into a melting point capillary was used as an external standard. The benzene standard and all samples were degassed by several freezing, evacuating, and melting cycles. The concentration of all samples was ~2%. Line separations were determined using a modification of the side-band superposition method.[12] Instead of superimposing a modulation side band from the standard directly on the peak to be measured, the modulation frequency was adjusted to place the benzene side band adjacent to the unknown peak. This region of the spectrum was then scanned repetitively in both increasing and decreasing field directions. The separation between the side band and the unknown peak was determined from the horizontal scale which had been calibrated previously using the side-band technique. This separation was added to the audio oscillator frequency to give the chemical shift data reported here. The frequency of the oscillator was monitored with a Hewlett-Packard Model 522B frequency counter. The solvent shift measurements were made at room temperature $29 \pm 3°$.[13] For 2,2,4-trimethylpentane and 2,2-dimethylbutane, the peak observed was the unresolved $-CH_3$ peak; for the other compounds the composite $-CH_2-$ peak was observed.

Table III shows the measured solvent shifts; the column headed Δ represents the experimental difference, in parts per million, of the chemical shift for the hydrocarbon in a 2% solution in the fluorocarbon $(C_4F_9)_3N$ minus the value for the pure hydrocarbon with reference to benzene as an external standard. The column

(10) A. A. Bothner-By, *J. Mol. Spectry.*, **5**, 52 (1960).

(11) A. D. Buckingham, T. Schaefer, and W. F. Schneider, *J. Chem. Phys.*, **32**, 1227 (1960).

(12) J. T. Arnold and M. G. Packard, *ibid.*, **19**, 1608 (1951).

(13) The author is grateful to Mr. R. K. Saunders and Dr. F. C. Stehling for performing the nuclear magnetic resonance experiments and for discussions concerning the interpretations thereof.

Table III: N.m.r. Solvent Shifts for Several Hydrocarbons

	δ_{298}	V_{298}	ΔH_{298}	$-K_1{}^a$	Δ	Δ'
Cyclopentane	8.10	95	8.54	0.629	-0.047 ± 0.022	$+0.171$
n-Decane	7.72	195	12.28	0.612	-0.056 ± 0.027	$+0.195$
2,2,4-Trimethylpentane	6.85	166	8.40	0.596	-0.172 ± 0.033	$+0.170$
n-Octane	7.57	163	9.92	0.595	-0.086 ± 0.011	$+0.203$
Methylcyclohexane	7.82	128	8.45	0.618	-0.025	$+0.215$
n-Hexane	7.27	132	7.54	0.567	-0.180	$+0.168$
2,2-Dimethylbutane	6.71	132	6.62	0.577	-0.144	$+0.182$
$(C_4F_9)_3N$	5.9	358	13.2	0.733^b		

[a] S. Broersma, *J. Chem. Phys.*, **17**, 873 (1949); volume susceptibility, all values $\times 10^{-6}$. [b] Determined by Dr. J. T. Richardson, Humble Oil and Refining Co., Baytown, Texas.

headed Δ' represents the solvent shift corrected for differences in magnetic susceptibility. A reasonable estimate of the precision of the data, as shown, indicates that the excess solvent shifts are equal within experimental error. The positive shift is to be expected in going from hydrocarbons to fluorochemicals ($\delta_{HC} > \delta_{FC}$; hydrocarbon intermolecular forces greater than fluorochemical intermolecular forces) as would be predicted from other data[10] and is of a reasonable value. The expected trend with δ was not observed. The solvent shifts (Table III, column Δ) show a variation with the difference in volume susceptibility of the fluorocarbon and hydrocarbon, but are not proportional to it. Further, the ratio of $\Delta/(K_2 - K_1)$, the ratio of solvent shift to magnetic susceptibility difference shows no constancy for hydrocarbons of the same volume and no trend with the volume of the hydrocarbon.[14] A further comparison was made of the nuclear magnetic resonance spectrum of 2,3-dimethylbutane as pure liquid and in solution in $(C_4F_9)_3N$ at various temperatures (25-90°). The spectra were essentially identical under all conditions. There is no evidence for any solution anomalies from the nuclear magnetic resonance measurements.

(14) R. E. Glick, D. F. Kates, and S. J. Ehrenson, *J. Chem. Phys.*, **31**, 567 (1959).

The Heat of Formation of Germanium Dioxide[1]

by James L. Bills[2] and F. Albert Cotton[3]

Department of Chemistry, Massachusetts Institute of Technology, Cambridge 39, Massachusetts
(Received October 10, 1963)

A new procedure has been used to measure the standard enthalpy of formation of hexagonal germanium(IV) oxide, $GeO_2(c, I)$, affording the value -132.2 ± 1.2 kcal./mole. This agrees very well with the result obtained by Yokokawa, *et al.* (-132.3 ± 1.0), and one which can be calculated from data of Jolly and Latimer (-132.6 ± 2.0), but differs by 3.9 kcal./mole from the value, based on combustion data, listed in the National Bureau of Standards Tables (-128.3 kcal./mole).

Introduction

In the course of some thermochemical studies of organogermanium compounds, reported elsewhere,[4] we became aware of some discrepancies and consequent uncertainty about the heat of formation of germanium-(IV) oxide. Since this quantity plays a role in the interpretation of our data, and will do so in other thermochemical studies of germanium compounds, a reinvestigation of the heat of formation of GeO_2 was carried out and is reported here.

The value of -128.3 kcal./mole listed in the National Bureau of Standards tables[5] for ΔH_f° (GeO_2, amorphous) is based upon two determinations of the heat of combustion of elemental germanium.[6,7] In both determinations, errors may possibly have been introduced by incomplete combustion and by the reaction of the GeO_2 with water, which was either introduced deliberately or formed by combustion of paraffin oil used as a combustion aid. Other difficulties are also encountered in this direct combustion method.[6,8]

Later, Jolly and Latimer[9] measured the heats of solution of Ge(c) and of $GeO_2(c, I)$ in basic hypochlorite solution, obtaining for ΔH_f° of $GeO_2(c, I)$ the value -129.2 ± 2.0 kcal./mole, which was considered to confirm the value derived from the combustion data. However, they used -24.5 kcal./mole for ΔH_f° of aqueous hypochlorite ion, whereas a more recent determination[10] yields -26.2 kcal./mole, thus leading to a ΔH_f° for $GeO_2(c, I)$ of -132.6 ± 2.0 kcal./mole, which does not agree satisfactorily with the combustion result.

Still more recently, a group of Japanese investigators[11] carefully measured the equilibrium

$$Ge(c) + 2H_2O(g) = GeO_2(c, I) + 2H_2(g)$$
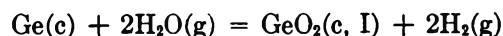
between 500 and 650°, from which data they calculated -132.3 ± 1.0 kcal./mole for ΔH_f° of $GeO_2(c, I)$ at 25°. They give reasons for believing that their result is more reliable than that (-141.8 kcal./mole) obtained in an earlier study[12] of the same equilibrium by a different method. While their result agrees

(1) This work was supported in part by the National Science Foundation and by the donors of the Petroleum Research Fund, administered by the American Chemical Society, to whom grateful acknowledgment is made.

(2) Standard Oil of Ohio Fellow, 1960–1961; National Science Foundation Cooperative Fellow, 1961–1962.

(3) Alfred P. Sloan Foundation Fellow.

(4) J. L. Bills and F. A. Cotton, *J. Phys. Chem.*, **68**, 806 (1964).

(5) F. D. Rossini, *et al.*, "Selected Values of Chemical Thermodynamic Properties," National Bureau of Standards Circular 500, U. S. Govt. Printing Office, Washington, D. C., 1952.

(6) G. Becker and W. A. Roth, *Z. physik. Chem.*, A161, 69 (1932).

(7) H. Hahn and R. Juza, *Z. anorg. Chem.*, **244**, 120 (1940).

(8) Although it is stated[6] that about two thirds of the GeO_2 was the hexagonal modification, the N.B.S. tables assign the ΔH_f° value to amorphous (or glassy) GeO_2. In this paper we shall follow the established nomenclature in which the hexagonal and tetragonal forms of GeO_2 are denoted $GeO_2(c, I)$ and $GeO_2(c, II)$, respectively.

(9) W. L. Jolly and W. M. Latimer, *J. Am. Chem. Soc.*, **74**, 5757 (1952).

(10) J. E. McDonald, J. P. King, and J. W. Cobble, *J. Phys. Chem.*, **64**, 1345 (1960).

(11) T. Yokokawa, M. Koizumi, M. Shimoji, and K. Niwa, *J. Am. Chem. Soc.*, **79**, 3365 (1957).

(12) K. Ono, Y. Inada, and I. Konno, *Bull. Res. Inst. Mineral Dressing Met.*, **11**, 159 (1955).

Table I: Data Pertaining to Calibration of Calorimeter

Run no.	Final temp., °C.	$-\Delta H_n$, cal./mole	Moles of acid neutralized	Calories evolved	Measured Δt, deg.	$\mathcal{E}$, cal./deg.	$\mathcal{E}_{std}$, cal./deg.
1	24.84	14,394	0.25028	3,602	1.0441	3,450	3,320
2	24.82	14,394	0.24967	3,594	1.0420	3,449	3,319
3	25.01	14,290	0.25022	3,576	1.0323	3,464	3,322
4	25.08	14,130	0.25000	3,532	1.0118	3,491	3,324

Mean value of $\mathcal{E}_{std}$: 3,321
Std. dev. of the mean: 1.1

well with that recalculated from Jolly and Latimer's measurements, the difficulties of the high temperature measurements raise some concern as to the certainty of that result, although, as will be seen, the result is indeed quite accurate.

In the course of our studies with germanium compounds, it was observed that both germanium and GeO_2 can be dissolved fairly rapidly in a solution of hydrogen peroxide and hydrofluoric acid. These reactions were used for a new and independent determination of $\Delta H_f°$ for GeO_2(c, I).

Experimental[13]

Apparatus. The rotating-bomb calorimeter described elsewhere[4] was used. In order to use it as a heat of solution calorimeter with hydrogen peroxide–hydrofluoric acid as solvent, the usual combustion bomb was replaced by a 16-oz. wide-mouth polyethylene bottle fitted with a leak-proof cap and a weighted brass sleeve, to which the gear girdle of the bomb was fitted. The tumbling motion usually imparted to the bomb immediately following combustion was then used to effect mixing and agitation of the solute and solvent. In all experiments, about 100 ml. of one solution was contained in the 16-oz. bottle, while 50 ml. of a second solution was contained in a 2-oz. wide-mouth polyethylene bottle, which was covered loosely and initially stood upright in the other solution.

Calibration. The energy equivalent of the calorimeter was determined using the heat of neutralization of hydrochloric acid by sodium hydroxide. The value of $-14,555$ cal./mole, given by Bender and Biermann[14] for the heat of neutralization of $4\ m$ HCl with $4\ m$ NaOH was used as the standard. Various corrections for heats of dilution were made by graphical interpolation of data in the N.B.S. tables[5] and checked against data in the literature[15,16] recalculated after Bender and Biermann.[14] A standard deviation of 40 cal./mole was assigned to each ΔH_n measurement, which includes the 0.1% uncertainty assigned by Bender and Biermann

to their own results. Correction of the ΔH_n values from 25° to the actual final temperatures were made using appropriate heat capacity data from the literature.[17-19] Table I summarizes the calibration data. $\mathcal{E}$ is the energy equivalent of the initial system including the heat capacities of the HCl and NaOH solutions and any excess water over the standard amount in the calorimeter can. $\mathcal{E}_{std}$ is the energy equivalent of the initial system after subtraction of these three contributions.

Materials. The elemental germanium was the "intrinsic metal" obtained from Eagle-Picher Co. It was crushed in a stainless steel press and ground in an agate mortar under absolute ethanol until it passed through a 200-mesh sieve, and then dried *in vacuo* at 100°. The oxygen content was estimated by the vacuum fusion method[20] as 0.003%.

Germanium(IV) oxide from three different sources was tested for use. Samples from Eagle-Picher Co. and from Fisher Scientific Co. were found to be incompletely soluble in hydrofluoric acid, presumably because they contain some of the tetragonal modification.[21] A third sample, which originated with the Raytheon Co., kindly provided by Professor J. W. Irvine, Jr., was found to be completely soluble. It was used for runs 1, 2, and 5 (Table III). The Fisher

(13) A more detailed description may be found in the Ph.D. thesis of J. L. Bills, Massachusetts Institute of Technology, 1963.

(14) P. Bender and W. J. Biermann, *J. Am. Chem. Soc.*, **74**, 322 (1952).

(15) G. Akerlof and J. W. Teare, *ibid.*, **59**, 1855 (1937).

(16) J. W. Bertetti and W. L. McCabe, *Ind. Eng. Chem.*, **28**, 247 (1936).

(17) F. T. Gucker, Jr., and K. H. Schminke, *J. Am. Chem. Soc.*, **54**, 1358 (1932).

(18) J. W. Bertetti and W. L. McCabe, *Ind. Eng. Chem.*, **28**, 375 (1936).

(19) L. J. Gillespie, R. H. Lambert, and J. A. Gibson, Jr., *J. Am. Chem. Soc.*, **52**, 3806 (1930).

(20) A. L. Beach and W. G. Guldner, *Am. Soc. Testing Mater., Spec. Tech. Publ.*, **222**, 15 (1958).

(21) A. W. Laubengayer and D. S. Morton, *J. Am. Chem. Soc.*, **54**, 2303 (1932).

Table II : Data Pertaining to the Heat of Solution of Elemental Germanium

	Run number 1	2	3	4
Wt. of Ge, g.	1.4518	1.4528	1.4535	1.4510
Wt. of 15% HF, g.	104.20	104.02	104.50	104.77
Wt. of 5% H_2O_2, g.	50.93	50.77	51.08	51.16
$\mathcal{E}$, cal./deg. (see text)	3466.6	3465.2	3465.8	3466.3
Δt, deg.	1.2012	1.2037	1.2021	1.1993
Q, cal.	4164.1	4171.1	4166.2	4157.1
Initial moles of $HF \cdot 6.294H_2O$	0.7811	0.7798	0.7819	0.7854
Final mole ratio $(H_2O + H_2O_2)/HF$	9.827	9.823	9.835	9.825
Q_{diln}, cal.	35.9	35.8	36.0	36.0
$Q_{cor} = Q - Q_{diln}$, cal.	4128.2	4135.3	4130.2	4121.1
Q_{cor}/mole, kcal./mole	206.41	206.62	206.27	206.17

Mean Q_{cor}/mole, kcal./mole: 206.37
Std. dev. of the mean: 0.10

Table III : Data Pertaining to the Heat of Solution of Germanium(IV) Oxide(c, I)

	Run number 1	2	3[a]	4[a]	5
Wt. of GeO_2, g.	2.0994	2.0912	2.0310	2.0651	2.0917
Wt. of 15% HF, g.	105.33	104.75	103.34	104.04	105.26
Wt. of 2.36% H_2O_2, g.	50.81	50.23	50.30	49.91	50.28
$\mathcal{E}$, cal./deg. (see text)	3467.5	3466.4	3465.5	3465.4	3468.2
Δt, deg.	0.1780	0.1770	0.1731	0.1754	0.1770
Q, cal.	617.2	613.6	599.9	607.8	613.9
Initial moles of $HF \cdot 6.294H_2O$	0.7896	0.7852	0.7747	0.7799	0.7891
Final mole ratio $(H_2O + H_2O_2)/HF$	9.826	9.805	9.858	9.806	9.792
$-Q_{diln}$, cal.	-36.2	-35.9	-35.7	-35.6	-36.0
$-Q_{vap}$, cal.	0.4	0.4	0.4	0.4	0.4
Q_{cor}, cal.	581.4	578.1	564.6	572.6	578.3
Q_{cor}/mole, kcal./mole	28.96	28.91	29.07	29.00	28.92

Mean Q_{cor}/mole,[a] kcal./mole: 28.93
Std. dev. of the mean: 0.015

[a] Results of runs 3 and 4 excluded; see text.

GeO_2 was used for runs 3 and 4 and a correction was made for the isolated residue.

The hydrofluoric acid (15%) and hydrogen peroxide (5.00 and 2.36%) solutions were prepared from Baker Analyzed reagents. The hydrogen peroxide was diluted with demineralized water to which 2 p.p.m. of sodium stannate was added as stabilizer. The stability of hydrogen peroxide in presence of fluorogermanate ion was established by analyzing the product solutions from runs 2 and 4 on GeO_2. These analyses were carried out by adding 15 g. of boric acid and then titrating with standard potassium permanganate solution.[22] The millimoles of H_2O_2 initially added and the total millimoles found in the titrations were, in that order: 34.85 and 34.88 in run 2 and 34.66 and

34.68 in run 4. The possibility of catalyzed peroxide decomposition during solution of the germanium metal was similarly tested. For the four runs, the millimoles found by titration compared to millimoles calculated to remain after stoichiometric reaction to oxidize the germanium were as follows: 34.7/34.9, 34.9/34.5, 35.4/35.0, and 35.3/35.3.

Procedure. Polypropylene graduated cylinders were used to measure 100 ml. of the HF solution and 50 ml. of the H_2O_2 solution into the polyethylene bottles. The actual amounts were measured by weight. The germanium or germanium(IV) oxide was weighed into

(22) I. M. Kolthoff and E. B. Sardell, "Textbook of Quantitative Inorganic Analysis," Third Ed., Macmillan Co., New York, N. Y., 1952, pp. 711, 712.

a polyethylene crucible which was loosely closed with a polyethylene stopper and placed on top of the loose cover over the small polyethylene bottle containing the H_2O_2 solution.

Tables II and III record the essential data for the heat of solution measurements. The energy equivalents, $\mathcal{E}$, of the initial systems were obtained by adding to the $\mathcal{E}_{std}$ value (Table I) the heat capacity contributions of the Ge or GeO_2, of the HF and H_2O_2 solutions, and of the polyethylene and any water in excess of the standard amount placed in the calorimeter can. The data used for calculation of these increments to $\mathcal{E}_{std}$ are listed in Table IV.

Table IV: Heat Capacities, cal./g. deg., Used in Calculating Energy Equivalents, $\mathcal{E}$, in Tables II and III

Material	C_p, cal./g. deg.	Ref.
Ge	0.074	a
$GeO_2(c, I)$	0.119	b
15% HF	0.892	c
5.00% H_2O_2	0.969	d
2.36% H_2O_2	0.985	d
Polyethylene	0.55	a

[a] C. D. Hodgman, Ed., "Handbook of Chemistry and Physics," 44th Ed., Chemical Rubber Publishing Co., Cleveland, Ohio, 1961, pp. 1554, 2353. [b] K. K. Kelley and A. U. Christensen, U. S. Bur. Mines, Rept. Invest., No. 5710, U. S. Govt. Printing Office, Washington, D. C., 1961. [c] T. Thorvaldsen and E. C. Bailey, *Can. J. Res.*, 24B, 51 (1946). [d] See ref. 24.

For the GeO_2 runs a correction of 0.4 cal. was made for the energy of vaporization of water.[23] The final temperatures for all measurements on GeO_2 were within 0.03° of 25°, while for the Ge runs, they were 25.28, 25.19, 25.02, and 25.01°. No corrections for these differences were made.

In computing the mean value of Q_{cor}/mole for GeO_2 (Table III), the results of runs 3 and 4 were omitted since the corrections for the insoluble residues make these results inherently less accurate. The mean value, when included, is 0.04 kcal./mole higher, so that for most purposes it may be said that they provide a check on the results obtained with the completely soluble GeO_2.

It should also be noted that the approximation has been made that the heat of dilution of the HF solution by $xH_2O \cdot yH_2O$ ($x \ll y$) solution is the same as would be found for dilution by $(x + y)H_2O$. In view of the similarities of liquid H_2O_2 and H_2O and the near cancellation of whatever error there may be this seems

a tolerable approximation. The required heat of dilution data were taken (by graphical interpolation) from the N.B.S. tables.[5]

Results

The following set of reactions is considered

$$2H_2O_2(aq) = 2H_2O(l) + O_2(g) \qquad \Delta H_1$$

$$GeO_2(c, I) + nHF \cdot xH_2O = \text{solution} \qquad -Q^{GeO_2}_{cor}$$

$$Ge(c) + nHF \cdot (x - y)H_2O + 2H_2O_2 \cdot (y - 2)H_2O =$$
$$\text{solution} \qquad -Q^{Ge}_{cor} - Q_{diln}$$

$$nHF \cdot (x - y)H_2O + yH_2O = nHF \cdot xH_2O \qquad -Q_{diln}$$

$$Ge(c) + O_2(g) = GeO_2(c, I) \qquad \Delta H_f°[GeO_2(c, I)]$$
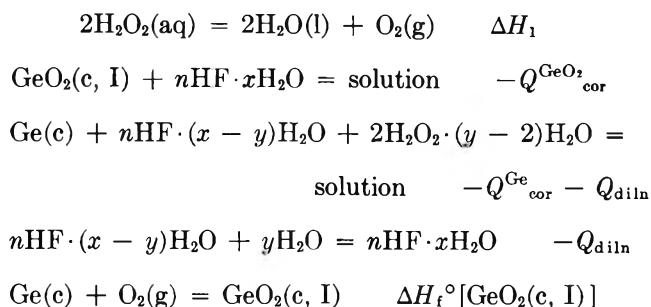
As explained above, dilution corrections have been made so as to make the two "solutions" formally identical; therefore

$$\Delta H_f°[GeO_2(c, I)] = -Q^{Ge}_{cor} + Q^{GeO_2}_{cor} - \Delta H_1 =$$
$$-206.37 + 28.93 + 45.24 =$$
$$-132.20 \text{ kcal./mole}$$

The value of ΔH_1 was taken from ref. 24. The standard deviation to be assigned to $\Delta H_f°$ was computed[25] to be 0.60 kcal./mole and taking the uncertainty interval to be twice this, the final result is that $\Delta H_f°$ for $GeO_2(c, I)$ is -132.2 ± 1.2 kcal./mole at 25°. This and all other quantities of heat are in terms of the defined calorie (4.1840 abs. joules) and are referred to atomic weights as given in the 1961 IUPAC table.[26]

Discussion

Bues and Wartenberg[27] found $Q = 29.9 \pm 0.2$ kcal./mole for the heat of solution of $GeO_2(c, I)$ in 20% HF; the difference between their results and ours should be equal to the difference between the heat of dilution of 20% HF to 10% HF and that of diluting a solution

(23) W. D. Good and D. W. Scott, "Experimental Thermochemistry," Vol. II, H. A. Skinner, Ed., Interscience Publishers, Inc., New York, N. Y., 1962, Chapter 2, p. 31.

(24) P. A. Giguere, B. G. Morissette, A. W. Olmos, and O. Knop, *Can. J. Chem.*, 33, 804 (1955).

(25) F. D. Rossini, "Experimental Thermochemistry," F. D. Rossini, Ed., Interscience Publishers, Inc., New York, N. Y., 1956, Chapter 14, pp. 309, 318.

(26) A. E. Cameron and E. Wichers, *J. Am. Chem. Soc.*, 84, 4175 (1962).

(27) W. Bues and H. von Wartenberg, *Z. anorg. Chem.*, 266, 281 (1951).

of Ge in 20% HF to give a solution of Ge in 10% HF, but the relevant data for a check are apparently unavailable.

Our final result, -132.2 ± 1.2 kcal./mole, for the ΔH_f° of $GeO_2(c, I)$ is in excellent agreement with that of Yokokawa, et al.[11] (-132.3 ± 1.0) and with the value recalculated from the data of Jolly and Latimer[9] (-132.6 ± 2.0). It therefore appears that the value in the N.B.S. tables[5] based on combustion measurements (-128.3) is in error by about 4.0 kcal./mole.

The Enthalpy of Formation of Tetraethylgermane and the

Germanium–Carbon Bond Energy[1]

by James L. Bills[2] and F. Albert Cotton[3]

Department of Chemistry, Massachusetts Institute of Technology, Cambridge 39, Massachusetts
(Received October 10, 1963)

The heat of formation of tetraethylgermane has been determined by combustion calorimetry. A rotating-bomb calorimeter of the type devised by Hubbard, Katz, and Waddington was used with 10% aqueous HF as the bomb liquid. The method of comparative measurements was employed to minimize errors. The chief results are: $\Delta H_f^\circ{}_{298\cdot16} = -50.0 \pm 1.9$ kcal./mole for $Ge(C_2H_5)_4(l)$; mean thermochemical bond energy of Ge–C bond $= 58 \pm 2$ kcal./mole.

Introduction

At the time this work was begun there was no reliable value for the germanium–carbon bond energy. In the interim, two different values have been reported. The entire literature on the thermochemistry of organogermanium compounds is very small and will be briefly reviewed here.

The first compound studied was tetra(β-styryl)germane,[4] for which the standard energy of combustion, ΔE_c°, was reported to be -4293.1 ± 2.9 kcal./mole. No effort was made to derive a Ge–C bond energy. Later, one of these authors burned tetraphenylgermane,[5] obtaining $\Delta E_c^\circ = -3277.4$ kcal./mole, from which a Ge–C bond energy of 32.2 kcal./mole was derived. However, because of various errors in the calculations,[6,7] this result should be 36 kcal./mole.

Very recently, some Russian workers[8] have measured the heats of combustion of tetraethylgermane (TEG) and hexaethyldigermane, obtaining for the former -1515.6 ± 1.5 kcal./mole. A comparison of this result with ours will be given in the Discussion section.

(1) Acknowledgment is made to the donors of the Petroleum Research Fund, administered by the American Chemical Society, and to the National Science Foundation for support of this work.

(2) National Science Foundation Cooperative Predoctoral Fellow.

(3) Alfred P. Sloan Foundation Fellow.

(4) K. H. Birr and D. Kraeft, *Z. anorg. allgem. Chem.*, **311**, 235 (1961).

(5) K. H. Birr, *ibid.*, **315**, 175 (1962).

(6) In evaluating ΔH_f° from ΔE_c°, auxiliary ΔH_f° values have been added directly to ΔE_c°. Using $\Delta(PV) = \Delta nRT$, ΔH_c° should be -3281.0 kcal./mole and this, together with the correct ΔH_f° for $GeO_2(c, I)$[7] gives ΔH_f° for $Ge(C_6H_5)_4(c)$ as 208.3 kcal./mole. Taking the heat of sublimation[5] of $Ge(C_6H_5)_4$ as 20.9 kcal./mole, ΔH_f° of $Ge(g)$ as 89 kcal./mole, and the heat of formation of the phenyl radical as 71 kcal./mole, the Ge–C bond energy comes out as 36 kcal./mole. It may also be noted that Birr's own data give 66.5 kcal./mole (not 51.3) for the Si–C bond energy, and that the numbers in column 4 of Table IV are actually $-\Delta H_f^\circ$.

(7) J. L. Bills and F. A. Cotton, *J. Phys. Chem.*, **68**, 802 (1964).

(8) I. B. Rabinovich, V. I. Tel'noi, N. V. Kariakin, and G. A. Razuvaev, *Dokl. Akad. Nauk SSSR*, **149**, 324 (1963).

Experimental[9]

Apparatus. Except for a few small changes, the calorimeter and platinum-lined bomb are identical with those of the U. S. Bureau of Mines, Bartlesville, Oklahoma, and designated by them as BMR2 and Pt-5.[10] Jacket temperature was regulated by a Model S Sargent Thermonitor, powered by a Sola constant voltage transformer, which provided regulation to within about 0.001°. An Automatic Timing and Controls electronic dial timer was used to limit the ignition current, drawn from a 6.3-v. transformer, to a fixed period of time. Quartz crucibles were used, rather than platinum ones, which were found to alloy with the germanium. Crucibles of 7-ml. capacity (Thermal American Fused Quartz Co.) were treated with HF to reduce their mass to 3–4 g.

Recording Thermometry. The practices of the Bureau of Mines workers were modified to provide thermistor temperature sensing and millivoltmeter recording. A 2000-ohm disk thermistor (Veco 32 D 12) was pre-aged at 110° for a few weeks to improve its stability and then coated with epoxy resin to maintain it in a constant immediate environment.[11] The use of this large thermistor required some modification of the lead arrangements, since it is too large to be inserted through the thermometer hole of the calorimeter can. The use of smaller thermistors was undesirable because they respond too quickly to a small volume of the water, thus giving a wavy recording trace.

The thermistor formed one arm of a Wheatstone bridge. The adjacent arm of the other branch was a 1–10,000-ohm decade box of 0.05% accuracy. The other two arms were 2000-ohm wound Manganin wire resistors. The bridge was powered by a Sorensen Model QM 3.0–0.66 transistorized d.c. power supply of nominal voltage 3.0 with 0.05% regulation, line and load. The bridge output was fed to a Leeds and Northrup Speedomax G millivolt recorder equipped with a special range switch providing for ranges of 0 to 1, 2, 5, 10, 20, 50, and 100 mv. The fore- and after-periods of each run were recorded on the 0–1-mv. range but the main reaction periods covered several spans of the 0–10-mv. range. The algebraic details of converting the mv. *vs* time traces to temperature rises will not be given here.[9]

Calibration and Test of Calorimeter. The energy equivalent of the bomb and calorimeter was determined using benzoic acid supplied by the National Bureau of Standards (sample 39h). Measurements were made over temperature intervals corresponding to those in the combustion and comparison experiments. The average values in cal./deg. and their standard deviations were 3519.2 ± 0.9 for $\Delta t \approx 1.3°$ and 3518.3

± 1.0 for $\Delta t \approx 2.2°$ (four measurements each). The heat of combustion of succinic acid was measured (four runs) against that of benzoic acid in a separate set of experiments, giving a value (with standard deviation) of 3020.1 ± 0.5 cal./g. which may be compared with the value of 3019.8 ± 0.4 cal./g. from the Bureau of Mines.[12]

Sample Enclosure. Several attempts to burn TEG sealed in thin-walled Pyrex bulbs were unsuccessful due to incomplete combustion and the impossibility of separating the residues from fused glass. We therefore had recourse to polyester film, which burns completely and thus also serves to promote combustion. Mylar Type A, 100 gage, was used and the procedure[9] for making bags, filling and sealing them, and correcting for the heat of combustion of the film was similar to that recommended in the literature.[13] Unmercerized cotton thread (heat of combustion taken[12] as 4050 cal./g.) was used as fuse material.

Materials. Tetraethylgermane was purchased from Peninsular ChemResearch Inc. It was redistilled under a reduced pressure of nitrogen through a 4-ft. Todd fractionating column at a high reflux ratio. A middle fraction was used for the combustions.

The germanium(IV) oxide was from the same batch as the completely soluble hexagonal material used earlier.[7]

Oxygen gas was purified by passage over hot copper oxide and then through Ascarite and Drierite.

The 10% hydrofluoric acid solution used in the bomb was prepared by dilution of Baker Analyzed reagent HF. A 25-ml. volume was weighed in a stoppered polypropylene vessel.

Procedure. The method of comparative measurements[14] was used. The comparison experiments were designed to produce the same amount of carbon dioxide as the corresponding combustion experiments. Thus corrections for dissolved carbon dioxide are nearly identical and residual errors about cancel. Equivalent amounts of benzoic acid (N.B.S. sample 39h) and $GeO_2(c, I)$ were substituted for tetraethylgermane. The temperature rises were about 1.3° in the comparison experiments as compared to 2.2° in

(9) A much more detailed account will be found in the Ph.D. thesis of C. L. Bills, Massachusetts Institute of Technology, 1963.

(10) W. D. Good, D. W. Scott, and G. Waddington, *J. Phys. Chem.,* **60,** 1080 (1956).

(11) S. A. Friedberg in "Temperature, Its Measurement and Control in Science and Industry," Vol. II, H. C. Wolfe, Ed., Reinhold Publishing Corp., New York, N. Y., 1955, pp. 364, 365.

(12) W. D. Good, *et al., J. Phys. Chem.,* **63,** 1133 (1959).

(13) H. A. Skinner, "Experimental Thermochemistry," Vol. II, Interscience Publishers, Inc., New York, N. Y., 1956, p. 19.

(14) See ref. 13, Chapter 4.

the combustion experiments; as noted earlier, calibrations were made for each of these approximate temperature rises.

In the comparison experiments, the GeO_2 was weighed into a quartz crucible. A platinum insert-type crucible cover served to cover the GeO_2 and to hold the polyester film and benzoic acid. With the appropriate materials in place, the bomb was flushed with about 3 l. of purified oxygen and filled to a pressure of 30 atm. Rotation of the bomb was begun when the temperature had risen about 60% of the expected amount and continued to the end of the experiment. (Subsequent calculations revealed the mid-time to lie closer to 58% for these experiments.)

Complete combustion of tetraethylgermane was not achieved; the residues of carbon, ranging from 0.2 to 0.5 mg. were assumed to have the same heat of combustion, -7.8 cal./mg., as pure carbon, and corrections made were taken to have an uncertainty of ± 0.10 mg. of carbon. A corresponding contribution was included in the standard deviation assigned to the combustion reaction.

Entirely negligible amounts (<0.012 mmole) of nitric acid were produced in the calibration reactions. Hence it was considered unnecessary to attempt analysis of the HF solutions for nitric acid.

Reduction to Standard States. This was accomplished with the computation form for fluorine compounds given in Chapter 2 of ref. 13. A few simple and obvious modifications were required to have it apply to germanium compounds. Since the effect of fluorogermanic acid on the properties of the final solution was unknown, the germanium was, for this purpose, treated as if it remained as $GeO_2(c, I)$. The heat of solution of GeO_2 was taken from ref. 7, although the concentrations of the final solutions are somewhat different. It is the purpose of the comparison experiments to assure cancellation of the errors resulting from such assumptions.

The quartz crucibles were found to dissolve in the HF to the extent of about 0.04 g. in both sets of runs. Assuming the rate of solution to be constant, there is no need to consider an energy correction. This is because rotation was begun very near the "mid-time," to which the initial and final slopes are extrapolated. The heat of any constant process which begins at that point simply adds to the final slope and is taken care of in the extrapolation.

The physical constants used for tetraethylgermane are density, 0.988 g./ml.; specific heat, 0.392 cal./g.-deg.; and $(\partial E/\partial P)_T$, -0.0065 cal./atm.-g. The last two values were unknown and assumed to be the same on a mole basis as for tetraethyllead.[15] The corresponding constants for the benzoic acid and polyester film were taken from the literature.[12,15]

Results

The Heat of Combustion of Tetraethylgermane. The results are expressed in terms of the defined calorie equal to 4.1840 absolute joules and the 1961 Table of International Atomic Weights. The weights of materials used in the five satisfactory combustion runs and four comparison runs are given in Table I.

Table I: Reactant Weights

Combustion experiments

Run no.	TEG, g.	Polyester, mg. (at 37% rel. hum.)	Thread, mg.	10% HF, g.
1	0.92864	43.37	3.78	26.31
2	0.88073	43.65	3.35	26.34
3	0.95295	43.19	3.67	26.23
4	0.91969	43.23	4.10	26.38
5	0.94659	42.74	4.36	26.29

Comparison experiments

Run no.	Benzoic acid, g.	Polyester, mg. (at % rel. hum.)	Thread, mg.	10% HF, g.[a]	GeO₂, g.
1	0.68226	43.38 (41)	3.36	26.30	0.51000
2	0.68718	42.63 (44)	3.41	26.45	0.51187
3	0.65118	43.43 (41)	3.35	26.17	0.48984
4	0.70270	43.13 (44)	3.05	26.26	0.52662

[a] Contained additional 0.60 g. of H_2O.

The manner in which the comparison runs were treated is indicated in Table II. Essentially, it amounted to a comparison of the quantity of heat measured with that expected on the basis of the various heats of combustion, solution, and vaporization. A discrepancy existed because of errors in evaluating the extent of one or more processes, and/or in assigning each process the energy associated with it. It is reasonable to expect this "error in reduction" to increase with sample size. Since the number of moles of Ge is a convenient measure of the sample size for combustions and comparisons, the reduction error is expressed in kcal./mole of Ge. (The results were also calculated assuming the average error per experiment, 4.3 cal., to apply regardless of sample size. The same final ΔE_c° resulted, with the same standard deviation.) The average error of the four comparison

(15) D. W. Scott, W. D. Good, and G. Waddington, *J. Phys. Chem.*, **60**, 1090 (1956).

Table II: A Typical Pair of Combustion and Comparison Experiments with Tetraethylgermane (TEG)[a]

	Combustion	Comparison
m(TEG), g.	0.91969	...
m(benzoic acid), g.	...	0.68226
m(polyester), g. (at % rel. hum.)	0.04323 (37)	0.04338 (41)
m(GeO$_2$), g.	...	0.51000
n^i(H$_2$O), mole	1.318	1.347
n^i(HF), mole	0.1319	0.1315
Δt_c, deg.	2.19119	1.32741
$\mathcal{E}$ (calor.)($-\Delta t_c$), cal.	-7709.3	-4671.4
$\mathcal{E}$ (cont.)($-\Delta t_c$), cal.	-61.5	-37.9
ΔE_{ign}, cal.	0.6	0.6
ΔE, cor. to std. states, cal.	9.5	11.9
$\Delta E^f{}_{comb}$(carbon), cal.	-2.7	...
$\Delta E^f{}_{soln}$(GeO$_2$), cal.	140.9	141.1
$-m\Delta E_c{}^\circ/M$(benzoic acid), cal.	...	4307.1
$-m\Delta E_c{}^\circ/M$(polyester), cal.	236.3	237.1
$-m\Delta E_c{}^\circ/M$(fuse), cal.	16.6	13.6
$m\Delta E_c{}^\circ/M$(TEG), cal.	-7369.6	...
ΔE_c(TEG), kcal./mole	-1513.2	...
Error in reduction, cal.	...	2.1
Error in reduction, kcal./mole of Ge	...	0.43
(Average error, kcal./mole)	...	(0.9)
Reduction correction, kcal./mole	-0.9	...
$\Delta E_c{}^\circ/$(TEG), kcal./mole	-1514.1	...
$\Delta E_c{}^\circ/M$(TEG), cal./g.	-8017.9	...

[a] Symbols follow the usage in ref. 10 and 15.

experiments was 0.88 ± 0.26 kcal./mole Ge, or 4.3 cal. per experiment. This is slightly less than 0.1% of the total heat evolved. On page 24 of ref. 13, it is reported that reduction errors this large have been encountered in the combustion of fluorine compounds.

Table III: Summary of Comparison-Measurement Results[a]

	$\mathcal{E}$(tot.)(Δt_o), cal.	ΔE_{cor},[b] cal.	$\Delta E^f{}_{soln}$ (GeO$_2$), cal.	$\Sigma(-m\Delta E_o{}^\circ/M)$, cal.	Reduction error, kcal./mole of Ge
1.	4709.3	12.5	141.1	4557.8	0.43
2.	4731.3	12.7	141.6	4584.9	1.61
3.	4506.9	12.2	135.5	4361.8	0.56
4.	4838.5	13.0	145.7	4684.2	0.88
				Mean reduction error:	0.88
				Standard deviation of mean:	0.26

[a] Symbols follow usage of ref. 10 and 15. [b] Includes ignition energy.

A summary of the reduction errors appears in Table III.

The results with tetraethylgermane have been summarized in Table VI. A reduction correction of

Table IV: Summary of Results with Tetraethylgermane[a]

	$\mathcal{E}$(tot.)(Δt_o), cal.	ΔE_{cor},[b] cal.	$-\Delta E_c{}^f$ (carbon), cal.	$\Delta E^f{}_{soln}$ (GeO$_2$), cal.	$\Sigma(-m\Delta E_o{}^\circ/M)$, cal.	$-\Delta E_c{}^\circ$ (TEG), kcal./mole
1.	7846.3	10.1	2.7	142.4	252.4	1513.0
2.	7457.4	9.7	1.6	134.9	252.2	1515.1
3.	8042.8	10.4	3.9	146.0	251.0	1514.7
4.	7770.8	10.1	2.7	140.9	252.9	1514.1
5.	7990.2	10.3	2.7	145.0	251.3	1514.3

$\Delta E^\circ{}_{298.16}$ (eq. 1), mean: -1514.2
$\Delta H^\circ{}_{298.16}$ (eq. 1), mean: -1517.8
Standard deviation of mean: 0.36
Total[c] deviation of mean: 0.75
Uncertainty interval ($2s'_{tot}$): 1.5

[a] Symbols follow the usage in ref. 10 and 15. [b] Includes ignition energy. [c] The total standard deviation includes terms from the combustion and comparison runs, both sets of calibrations, the carbon residue corrections, and the benzoic acid certification.

-0.9 kcal./mole was included in the values of $\Delta E_c{}^\circ$ (TEG) in the last column. These results apply to the equation

$$(C_2H_5)_4Ge(l) + 14O_2(g) =$$
$$8CO_2(g) + 10H_2O(l) + GeO_2(c, I) \quad (1)$$
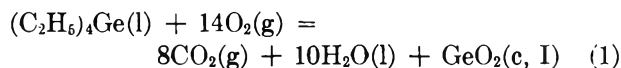
$$\Delta H^\circ{}_{298.16} = -1517.8 \pm 1.5 \text{ kcal./mole}$$

Derived Results. The values in the N.B.S. table[16] for the standard heats of formation of $CO_2(g)$ and $H_2O(l)$ were combined with $\Delta H_f{}^\circ$ of $GeO_2(c, I)$, -132.2 ± 1.2 kcal./mole,[7] and $\Delta H^\circ{}_{298.16}$ (eq. 1) to calculate the heat of formation of liquid tetraethylgermane. The result is

$$\Delta H_f{}^\circ{}_{298.16}(Et_4Ge, l) = -50.0 \pm 1.9 \text{ kcal./mole}$$

where the uncertainty includes that for GeO_2. Using 10.1 ± 0.3 kcal./mole for the heat of vaporization o tetraethylgermane,[8] this becomes

$$\Delta H_f{}^\circ{}_{298.16}(Et_4Ge, g) = -39.9 \pm 2.0 \text{ kcal./mole}$$

Discussion

Comparison with Other Results. The value of $\Delta H^\circ{}_{298.16}$ (eq. 1) found in this study, $-1517.8 = 1.5$ kcal./mole, does not differ significantly from the value

(16) F. D. Rossini, D. D. Wagman, W. H. Evans, S. Levine, and I Jaffe, "Selected Values of Chemical Thermodynamic Properties," National Bureau of Standards Circular 500, U. S. Govt. Printing Office, Washington, D. C., 1952.

of −1515.6 ± 1.5 kcal./mole reported by Rabinovich, et al.[8] However, little importance is to be attached to this close agreement, since the a priori accuracy of the Russian work is very uncertain and certainly much poorer than that implied by the assigned uncertainty of ±1.5 kcal./mole.[17]

The Ge–C Thermochemical Bond Energy. Using the following heats of formation in kcal./mole at 25° for the gaseous atoms, 170.9 for C, 52.09 for H, and 89 ± 4 for Ge, and the following bond energies, 82.6 kcal./mole for C–C and 98.7 kcal./mole for C–H, all taken from Cottrell,[18] the mean thermochemical Ge–C bond energy is calculated to be 58.4 ± 2 kcal./mole. The average Ge–C bond energy may also be estimated by using 25 ± 2 kcal./mole for the heat of formation of the ethyl radical[19]; the result is 57.2 ± 2 kcal./mole, in good agreement with the former estimate. For most

purposes, the result $E_{Ge-C} = 58 \pm 2$ kcal./mole should be appropriate. The result (∼36 kcal./mole) obtained by Birr for $Ge(C_6H_5)_4$ seems unlikely to be correct, even allowing for possible differences between Ge–C_2H_5 and Ge–C_6H_5 bonds.

(17) The Russian paper gives practically no experimental details, such as method of enclosing samples, sizes of samples, number of runs or data for individual runs, energy equivalent of calorimeter, or the temperature rises. There is no indication that they used the method of comparative measurements and some of their discussion suggests positively that they depended on direct comparison of combustions of TEG with calibrations using simply benzoic acid. Such a procedure is full of dangers. Finally, they give no details concerning reduction of data to standard states, and no mention is made of incompleteness of combustion and yet from our experience and that of Birr,[4,5] it is difficult to believe that combustion could have been complete.

(18) T. L. Cottrell, "The Strengths of Chemical Bonds," 2nd Ed., Academic Press, Inc., New York, N. Y., 1958.

(19) C. T. Mortimer, "Reaction Heats and Bond Strengths," Pergamon Press, New York, N. Y., 1962, p. 127.

Nuclear Magnetic Resonance Study of Molecular Complexes of

7,7,8,8-Tetracyanoquinodimethane and Aromatic Donors[1,2]

by Melvin W. Hanna and Alan L. Ashbaugh

Department of Chemistry, University of Colorado, Boulder, Colorado (*Received October 14, 1963*)

An n.m.r. method has been developed which gives the equilibrium quotients and shifts of pure complex for the association of 1:1 π-molecular complexes. A series of complexes between 7,7,8,8-tetracyanoquinodimethane and various methyl-substituted benzenes has been studied. The equilibrium quotients determined by the n.m.r. method agreed we ll with previous data determined spectroscopically by the Benesi–Hildebrand method. A curious concentration scale dependence was noted, and this indicated the care which mu st be exercised when any Benesi–Hildebrand-type method is used to evaluate equilibriu m quotients. Various contributions to the shift of pure complex are discussed in relation to the experimental shifts and the structure of the complex.

Introduction

The structure and chemistry of π-molecular complexes have been the subjects of extensive investigation in the last two decades. A recent book[3] and several reviews[4-6] summarize the work in this field through 1961. Information about the equilibria between components and π-complex and about the structure of π-complexes has come from many different experimental methods.[3-5] The most useful of these has been the use of visible, ultraviolet,[3,5] and infrared spectroscopic techniques.[7]

It is a natural next step to apply nuclear magnetic resonance (n.m.r.) to a study of these complexes. N.m.r. has been successfully used to evaluate equilibrium constants in hydrogen-bonding systems,[8] and should be similarly useful in π-complex equilibria since the two types of equilibria are formally the same. Further, n.m.r. is extremely sensitive to small changes in the electronic environment of a magnetic nucleus, and a study of the appropriate n.m.r. parameters may be another means of obtaining structural information about π-complexes. It is the object of this paper to report an investigation of these possibilities for π-complexes formed from 7,7,8,8-tetracyanoquinodimethane (TCNQ, I) and various aromatic donors.

The applicability of n.m.r. to a study of π-complex formation has been shown in several recent investiga-

I
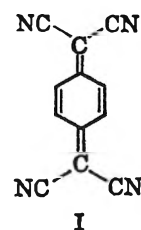
tions. Hatton and Richards[9] have discussed solvent effects on the chemical shifts of amides and other solutes in terms of complex formation. Hatton and Schneider[10]

(1) Supported in part by Grant GM 09187-0152 from the National Institutes of Health, Public Health Service, and by the Directorate of Chemical Sciences, Air Force Office of Scientific Research, under Grant AF-AFOSR-216-63.

(2) This paper is based on portions of a thesis submitted by A. L. Ashbaugh to the Graduate School of the University of Colorado in partial fulfillment of the requirements for the degree Master of Science.

(3) G. Briegleb, "Electronen-Donator–Acceptor Komplexe," Springer-Verlag, Berlin, 1961.

(4) L. J. Andrews, *Chem. Rev.*, **54**, 713 (1954).

(5) S. P. McGlynn, *ibid.*, **58**, 1113 (1958).

(6) R. S. Mulliken and W. B. Person, *Ann. Rev. Phys. Chem.*, **13**, 107 (1962).

(7) E. E. Ferguson, *J. chim. Phys.*, in press.

(8) See, for example, P. J. Berkeley, Jr., and M. W. Hanna, *J. Phys. Chem.*, **67**, 846 (1963).

(9) J. V. Hatton and R. E. Richards, *Mol. Phys.*, **5**, 139, 153 (1962).

(10) J. V. Hatton and W. G. Schneider, *Can. J. Chem.*, **40**, 1285 (1962).

have used a similar explanation in describing the shifts of toluene protons upon addition of acceptors such as acetonitrile, p-benzoquinone, and N,N-dimethylformamide. The results of these experiments and others are discussed in an excellent article by Schneider.[11] No attempt was made in these studies to evaluate equilibrium constants or the shift of pure complex. Such an attempt was made by Schug and Martin in their study of silver ion complexes of benzene and olefins.[12] The equilibrium constants obtained from n.m.r. did not agree with those determined earlier in solubility studies,[13] however.

Determination of Equilibrium Constants by N.m.r.

Consider the equilibrium

$$A + D = AD \qquad (1)$$

where A and D represent acceptor and donor molecules, respectively, and AD represents the π-molecular complex. Equilibrium constants or, more accurately, equilibrium quotients[14] for π-complex formation have usually been determined by the Benesi–Hildebrand method[15] or a modification therof.[16] This method takes advantage of the fact that most π-complexes have a new absorption band in the visible or ultraviolet region of the spectrum which is characteristic of the complex. From an appropriate plot of observed optical density vs. donor concentration, the equilibrium quotient and molar absorbancy index of the complex can be calculated.

It is possible to derive an expression analogous to the Benesi–Hildebrand equation for use with n.m.r. data. Consider the chemical shift of protons on A molecules which are undergoing rapid exchange[17] between the complexed and the uncomplexed state. Following treatments used in n.m.r. studies of hydrogen-bonding equilibrium[8,18,19] it can be shown that

$$\delta_{obsd}{}^A - \delta_0{}^A = \frac{\xi_D Q}{1 + \xi_D Q} (\delta_{AD}{}^A - \delta_0{}^A) \qquad (2)$$

where $\delta_0{}^A$ is the shift of acceptor protons in uncomplexed form, $\delta_{obsd}{}^A$ is the observed shift of acceptor protons in complexing media, $\delta_{AD}{}^A$ is the shift of acceptor protons in the pure complex, and ξ_D is the concentration of donor on some scale to be defined later.

Equation 2 requires that $\xi_D \gg \xi_A$. It further assumes that the solutions are ideal, in which case $Q = K$, or that the quotient $\gamma_{AD}/\gamma_A\gamma_D$ remains constant over the range of solutions studied.

Defining $\Delta_{obsd}{}^A = \delta_{obsd}{}^A - \delta_0{}^A$ and $\Delta_{AD}{}^A = \delta_{AD}{}^A - \delta_0{}^A$, eq. 2 becomes

$$\Delta_{obsd}{}^A = \frac{\xi_D Q}{1 + \xi_D Q} \Delta_{AD}{}^A \qquad (3)$$

Writing eq. 3 in reciprocal form gives[20]

$$\frac{1}{\Delta_{obsd}{}^A} = \frac{1}{Q\Delta_{AD}{}^A} \frac{1}{\xi_D} + \frac{1}{\Delta_{AD}{}^A} \qquad (4)$$

Equation 4 is analogous to the Benesi–Hildebrand equation except that the concentration of acceptor does not appear, and the shift of acceptor protons in pure complex replaces the molar absorbancy index of complex. The first difference means that the chemical shift of acceptor protons does not depend on acceptor concentration as long as $\xi_D \gg \xi_A$. This has been confirmed in experiments on several different types of complexes.[21] The shift of acceptor protons in pure complex is the quantity which holds the promise of providing structural information about these complexes.

The ideal system for n.m.r. study of molecular complexes would have the following properties.

1. Both donor and acceptor molecules should contain protons (or other magnetic nuclei), preferably giving a single sharp line.

2. Both donor and acceptor concentrations should be able to be made large with respect to the other component.

3. The n.m.r. absorptions of donor or solvent should not overlap the absorption of acceptor (vice versa if donor shifts are being studied).

If these three conditions hold, it would be possible to determine $\Delta_{AD}{}^A$, $\Delta_{AD}{}^D$, and two values of Q which should check each other. Unfortunately, it is very difficult to

(11) W. G. Schneider, J. Phys. Chem., 66, 2653 (1962).

(12) J. C. Schug and R. J. Martin, ibid., 66, 1554 (1962).

(13) L. J. Andrews and R. M. Keefer, J. Am. Chem. Soc., 71, 3644 (1949).

(14) The term equilibrium quotient Q represents just the quotient of concentrations of products and reactants. The equilibrium constant K is equal to the product of Q and the appropriate quotient of activity coefficients $\gamma_{AD}/\gamma_A\gamma_D$. Equilibrium quotient is the more accurate term if activity coefficients are not evaluated or known, and will be used in the rest of this paper.

(15) H. A. Benesi and J. H. Hildebrand, J. Am. Chem. Soc., 70, 2832 (1948); 71, 2703 (1949).

(16) R. L. Scott, Rec. trav. chim., 75, 787 (1956).

(17) H. M. McConnell, J. Chem. Phys., 28, 430 (1958).

(18) C. M. Huggins, G. C. Pimentel, and J. N. Shoolery, ibid., 23, 1244 (1955).

(19) E. D. Becker, U. Liddel, and J. N. Shoolery, J. Mol. Spectry., 2, 1 (1958).

(20) An identical equation can be written for the shift of donor protons.

(21) M. W. Hanna, W. Trigg, and A. L. Ashbaugh, to be published.

find an experimental system for which these conditions all hold. As a compromise, the complexes formed between TCNQ[22] and a series of aromatic donors were chosen. One advantage of these systems is that TCNQ forms reasonably strong π-complexes with a large number of aromatic donors.[23] Further, it has a single sharp n.m.r. absorption at 2.45 τ. The main disadvantage is that TCNQ is not very soluble in most organic solvents and, consequently, only the acceptor shifts could be studied. A further disadvantage is that, for complexes with polynuclear aromatic hydrocarbons, the n.m.r. absorptions of the donor overlap the absorption of TCNQ and prevent their study.

Experimental

Materials. An initial sample of TCNQ was supplied by Dr. T. L. Cairns of E. I. du Pont de Nemours and Company, and was used without further purification. Additional TCNQ was synthesized by the method of Acker and Hertler.[22] Reagent grade p-dioxane was distilled from over stannous chloride and then redistilled. All other liquids were reagent grade and were distilled before use. Pentamethylbenzene and hexamethylbenzene were recrystallized from methanol and ethanol, respectively, until a constant melting point was obtained.

Procedure. A standard solution of TCNQ in dioxane was prepared with the concentration of TCNQ just sufficient to observe an n.m.r. line (0.008 M). An appropriate amount of donor was weighed out in 10-ml. ground glass stoppered flasks. A 5.0-ml. aliquot of the standard solution was then added, and the flask reweighed. Concentrations of donor in dioxane could then be calculated in both molal and mole fraction units.

N.m.r. spectra were taken on a Varian Associates A-60 spectrometer. The dioxane line was used as an internal reference. Chemical shifts were measured by displaying the signal of interest and a modulation side band of the dioxane reference peak on the 50 c.p.s. sweep of the A-60. This sweep was carefully calibrated to 50.0 ± 0.2 c.p.s. full scale. A Hewlett Packard Model 202-A low frequency function generator and a Model 521-C electronic counter were used for the modulation source and frequency counter. Chemical shifts were reproducible to better than 0.3 c.p.s. All measurements were made at 37.0 ± 0.5°, the temperature of the probe.

Results and Discussion

Equilibrium Quotient. Typical plots of $1/\Delta_{obsd}{}^{A}$ vs. $1/m_D$ are shown in Fig. 1 and 2. It can be seen that good straight lines are obtained in all cases. The

Figure 1. Plots of $1/\Delta_{obsd}$ vs. $1/m_D{}^0$ for the n.m.r. shifts of TCNQ protons using as donors: benzene, O; toluene, □; and o-xylene, △.

increased deviation at high values of $1/m_D$ is to be expected since this corresponds to low molalities of donor and to the breakdown of the approximation that $m_D \gg m_A$. The range of donor concentration, the observed shifts, and the calculated values of equilibrium quotients and shifts of acceptor protons in pure complex for both the molal and mole fraction concentration scales are given in Table I.

The first question that arises is whether the equilibrium quotients derived from n.m.r. data are meaningful, or if some kind of general solvent effect on the spectra is being measured. This question is especially appropriate in view of the relatively small absolute value of the measured shifts.

There are three facts which argue that it is indeed the effect of molecular complexing that is giving rise to the observed shifts. The first is that the equilibrium constants go in the right order. That is, as the ionization potential of the donor becomes lower, the equilibrium constant increases. The second is that, when comparison with equilibrium quotients

(22) D. S. Acker and W. R. Hertler, *J. Am. Chem. Soc.*, **84**, 3370 (1962).

(23) L. R. Melby, R. J. Harder, W. R. Hertler, W. Mahler, R. E. Benson, and W. E. Machel, *ibid.*, **84**, 3374 (1962).

Table I: Measured and Calculated Properties of π-Molecular Complexes of TCNQ and a Series of Aromatic Donors in Dioxane

Donor	Range of donor concentration, m	Max. Δ_{obsd}^A, c.p.s.	Q_m, kg. of solvent/ mole	$(\Delta_{AD}^A)_m$, p.p.m.	Q_x, m.f.$^{-1}$	$(\Delta_{AD}^A)_x$, p.p.m.	Q_{lit}
Benzene	0.468–2.15	8.6	0.061	1.28	c	c	
Toluene	0.401–2.88	12.4	0.085	1.06	c	c	
o-Xylene[a]	0.353–2.54	13.7	0.12	0.91	0.47	2.86	
Mesitylene	0.298–2.18	12.7	0.16	0.80	1.10	1.43	
Durene	0.207–0.967	9.3	0.33	0.67	2.7	1.10	0.47[b]
Pentamethylbenzene	0.056–0.457	8.0	0.55	0.59	6.2	0.67	
Hexamethylbenzene	0.100–0.295	7.1	1.15	0.56	9.7	0.57	1.23[b]

[a] The results for the m- and p-xylenes were identical with those of o-xylene. [b] These are calculated values from the data of ref. 21. These authors determined K_x values at "room temperature." The values were 5.6 and 14.5 for the durene and hexamethylbenzene complexes, respectively. [c] Values undetermined, see text.

calculated from spectroscopic data is possible (the complexes with durene and hexamethylbenzene), the agreement is good. The third is that, when the TCNQ is replaced by an aromatic molecule which is not expected to complex with the donor, toluene for example, no shift (<0.5 c.p.s.) of the protons on this molecule is observed under the conditions that the TCNQ experiments were carried out. All of these facts argue strongly *against* the observed shifts of the
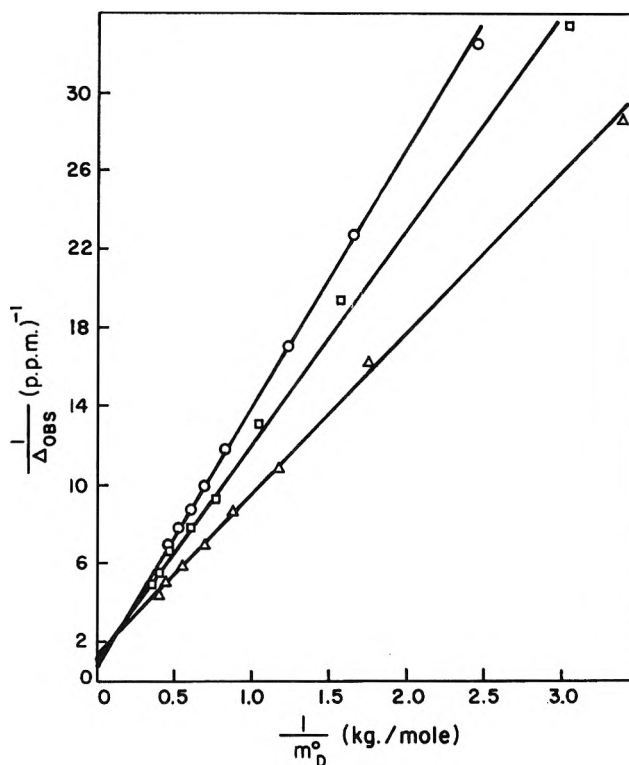

Figure 2. Plots of $1/\Delta_{obsd}$ vs. $1/m_D^0$ for the n.m.r. shifts of TCNQ protons using as donors: mesitylene, O; durene, □; pentamethylbenzene, ●; and hexamethylbenzene, △.

TCNQ protons being due to some kind of a general solvent effect, and *for* their being due to molecular complexing.

There are other problems apparent from the data of Table I that must be resolved before these n.m.r. results can be accepted with confidence. The first of these problems is that the calculated equilibrium quotients and shifts of acceptor protons in pure complex are dependent on the concentration scale used. Since the quantity Δ_{AD}^A is a function only of the structure of the complex, it should be independent of the concentration scale.[24] In fact, the values of Δ_{AD}^A determined on the molal scale are different from the corresponding quantities determined using the mole fraction scale. The values of $(\Delta_{AD}^A)_x$ could not even be determined for benzene and toluene because the intercept of a plot of $1/\Delta_{obsd}^A$ vs. $1/X_D$ was negative and equal to zero, respectively. It is important to note, however, that as the complexes become stronger, the values of Δ_{AD}^A determined from the two scales approach one another.

These facts are indicative of a situation discussed by King, Espensen, and Visco in their study of halide complexes of hexaamminecobalt(III),[25] and illustrate the care which must be taken in evaluating equilibrium quotients using a Benesi–Hildebrand procedure. A consideration of eq. 3 shows that, if the denominator is a constant, a plot of Δ_{obsd}^A vs. ξ_D will be a straight line whose slope is $Q\Delta_{AD}^A$. Under these conditions, it

(24) Strictly speaking, there may be differences in Δ_{AD}^A determined using the molal and mole fraction scales since the former refers to the shift of acceptor protons in a "1 m solution of pure complex in dioxane," while the latter refers to the shift of acceptor protons in "pure liquid complex." These shifts may differ by the order of solvent effects on spectra, 0.1 p.p.m.

(25) E. L. King, J. H. Espensen, and R. E. Visco, *J. Phys. Chem.*, **63**, 755 (1959).

is not possible to extract values of both Q and $\Delta_{AD}{}^A$ from the data, but only the value of their product. There are two sets of conditions which would make the denominator of eq. 3 a constant. The first condition is if $\xi_D Q \ll 1$. The second is if $\xi_D Q$ remains essentially constant over the range of concentrations studied. The basic point is that, before values of Q and $\Delta_{AD}{}^A$ can be trusted, a plot of $\Delta_{obsd}{}^A$ vs. ξ_D must give a *curved* line.

Plots of $\Delta_{obsd}{}^A$ vs. both mole fraction and molality of donor for the TCNQ-benzene system are shown in Fig. 3. It can be seen that a plot against mole fraction is a straight line, while that against molality is curved. Thus, values of Q_x and $\Delta_{AD}{}^A$ derived from a mole fraction plot will not be meaningful. This is in agreement with the observations listed in Table I.

The differences in behavior of the plots using molal and mole fraction units is difficult to explain in a completely satisfying manner. It is true that in the concentration range studied, concentrations on the molal scale are increasing faster than concentrations on the mole fraction scale, thus making the product $m_D Q_m$ increase faster than the product $X_D Q_x$. This may be the explanation of the observed difference between the two plots. A second factor which must be considered is the assumption of solution ideality. Since in this concentration range the two concentration scales are not proportional, it is impossible for the solutions to be ideal on both scales. A possible factor involved in the better behavior of the molal scale may be that the "hypothetical 1 m" standard state is more appropriate to these experiments than the "pure liquid complex" standard state.

The conclusion that can be drawn from this work is that the equilibrium quotients derived from n.m.r. measurements are valid as long as a plot of $\Delta_{obsd}{}^A$ vs. the appropriate concentration gives a curved line. The values of Q_m for benzene and toluene in this work are so small that the effects of molecular complexing are of the same order as solution nonideality effects. Their significance is uncertain. The remaining Q_m are significant, however.

The major advantage of the n.m.r. method is that complexes can be studied that have no separate charge-transfer band in the visible or ultraviolet spectrum, or where the charge-transfer band is buried beneath the spectrum of one of the components. This is the case with the first four donors listed in Table I.

A second advantage is that it is experimentally easier to measure a line position than an intensity.[26] The major disadvantages of the n.m.r. method is that it is difficult to find experimental systems which satisfy all of the requirements discussed above. It is obvious
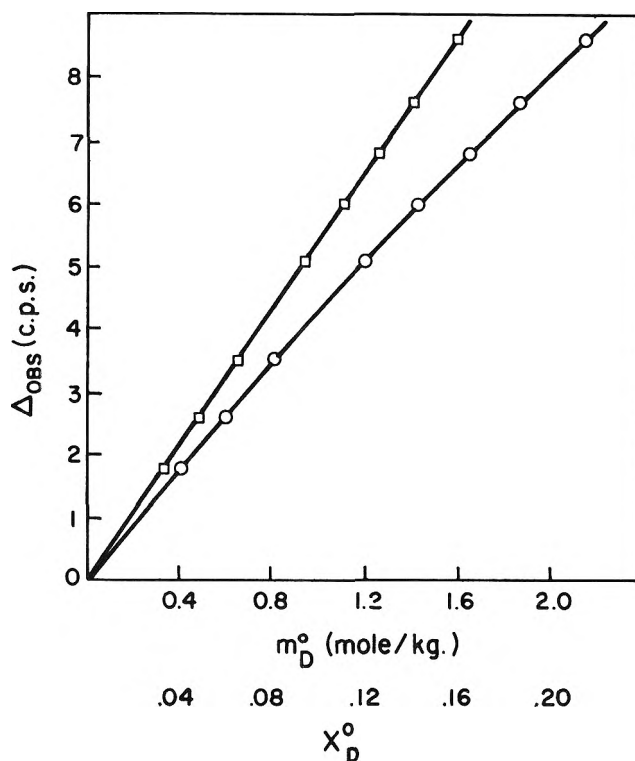
Figure 3. Comparison of plots of Δ_{obsd} of TCNQ protons vs. concentrations expressed on the molal scale, O, and the mole fraction scale, □. The molal plot is curved while the mole fraction plot is a straight line.

that in many cases the n.m.r. and optical spectroscopic methods can supplement each other.

The Shift of Pure Complex. One of the initial objectives of this work was to gain insight into the structure of molecular complexes from the value of the shift of pure complex. Ideally, both $\Delta_{AD}{}^A$ and $\Delta_{AD}{}^D$ should be found, but, since it was not possible to make the TCNQ concentration large compared with the donor concentration, it was not possible to calculate $\Delta_{AD}{}^A$.

A consideration of the shifts of pure complex in Table I shows first, that all complex shifts are to high field, and second, that as the complex becomes stronger, the upfield shifts become less. These results can be rationalized by a consideration of the possible effects on the acceptor proton resonance position that the donor might have. These effects are: 1. transfer of charge from donor to acceptor, 2. effect on acceptor protons of ring currents in the donor, 3. electric field effects of donor on acceptor protons, 4. modification of ring currents in acceptor, if present, by interaction with donor, 5. alteration of the paramagnetic contribution to the acceptor proton shifts.

(26) This point was discussed some time ago by G. C. Hood, O. Redlich, and C. A. Reilly, *J. Chem. Phys.*, **22**, 2067 (1954).

Effect 1 would result in an upfield shift if the electron density in the acceptor molecule were increased by transfer of charge from the donor. All theories of π-molecular complexes agree, however, that the amount of such charge transfer is very small. Using the results of Fraenkel, et al.,[27] which indicate that the shielding of a σ-proton is increased by approximately 10 p.p.m. for a one π-electron increase on the adjacent carbon, one calculates that there would have to be a "transfer" of from 0.5 to 0.9 electron from donor to acceptor to explain the shifts. This is clearly too large. Further, if effect 1 were the cause of the upfield shift, this shift should go to even higher fields as the complexes become stronger. Such is not the case, and therefore effect 1 is ruled out.

Effect 2 would also give an upfield shift. This can be seen by carrying out a classical ring current calculation[28] or making use of the more elaborate calculations of Johnson and Bovey.[29] The maximum shift predicted in these calculations is only about 0.3 p.p.m., and remains essentially the same even though the spacing between donor and acceptor is varied between 3.1 and 3.5 Å. Work by McWeeny has suggested that all classical ring current calculations may *underestimate* the ring current effect, however.[30] This effect is certainly of importance and may be the principal cause of the upfield shift of all complexes. The upfield shifts are the same order as those discussed by Schneider.[11]

Effect 3 would be very small since the donor molecules have very small dipole moments.

Effect 4 can be ruled out because, regardless of the way in which the acceptor ring currents were modified by interactions with the donor, the effect would be expected to increase as the complex became stronger. This effect, like effect 1, is unlikely to be important because complex formation is only a small perturbation on the ground state of the acceptor.

Effect 5 would predict a downfield shift of the acceptor protons. A combination of this effect with

effect 2 may be the explanation of the order and direction of the $\Delta_{AD}{}^A$ values. Thus, all complexes are shifted upfield by a constant amount due to effect 2. The excited state of the π-complex as a whole adds a new term in the sum of terms comprising the paramagnetic shift. The contribution of this new term to the sum would be inversely proportional to the frequency of the charge-transfer band since $\nu_{CT} = (E_{D^+A^-} - E_{DA})/h$. Thus, the downfield shift superimposed on effect 2 should increase as the complex gets stronger and the charge-transfer band shifts to longer wave lengths. This hypothesis can be tested if a series of complexes can be found in which the $\Delta_{AD}{}^A$ begins an upfield shift, goes through zero, and ends as a downfield shift as the complex becomes stronger.

In summary, this work has shown that n.m.r. can be used to evaluate equilibrium quotients for π-molecular complexes, but that special care must be taken in choosing the appropriate concentration scale. In this respect, it can serve as a valuable supplement to the Benesi–Hildebrand method. The shifts of acceptor protons in pure complex, which are also obtained in these experiments, can be rationalized in terms of the effect of ring currents of the donor on the acceptor molecule and a new contribution to the paramagnetic part of the chemical shift.

(27) G. Fraenkel, R. E. Carter, A. McLachlan, and J. H. Richards; *J. Am. Chem. Soc.*, 82, 5846 (1960).

(28) J. A. Pople, W. G. Schneider, and H. J. Bernstein, "High Resolution Nuclear Magnetic Resonance," McGraw-Hill Book Co., Inc., New York, N. Y., 1959, p. 180 ff.

(29) C. E. Johnson, Jr., and F. A. Bovey, *J. Chem. Phys.*, 29, 1012 (1958).

(30) R. McWeeny, *Mol. Phys.*, 58, 311 (1958).

Reactions between the Triplet State of

Fluorescein and Oxygen[1]

by Volker Kasche and Lars Lindqvist

Institute of Physical Chemistry, University of Uppsala, Uppsala, Sweden   *(Received October 14, 1963)*

The primary reactions between the triplet state of fluorescein and molecular oxygen have been studied in aqueous solutions by the flash photolysis method. Rate constants for physical and chemical quenching of the triplet state by oxygen were determined over a wide range of pH. The semioxidized dye is formed in the quenching reaction, and the possible role of this species in dye photosensitized reduction–oxidation reactions is discussed.

Introduction

In autoxidation reactions in solution, photosensitized by fluorescein dyes, the interaction between the photoexcited dye and the reactants generally seems to be of a chemical nature. Although the dye may react in the excited singlet state, there is strong evidence that the triplet state is in practice responsible for the photoactivity of the dye[2-4] due to the long lifetime of this state. Schenck[5] presented evidence for an association reaction between the photoexcited dye and oxygen to give a short-lived, reactive compound, which in turn oxidizes the oxidizable reactant and regenerates the dye in the ground state. This reaction mechanism has been supported in other studies.[6] A second sensitization mechanism that has been proposed in a number of cases[7-9] involves the reduction of the photoexcited dye by the oxidizable reactant to give a semireduced dye radical, which is re-oxidized to the ground state by the oxygen present in the solution. This mechanism is supported by the observed existence of a semireduced form of the dye.[3,9] A third sensitization mechanism can be imagined in which the photoexcited dye is oxidized by oxygen to a semioxidized dye radical, which is then re-reduced to the ground state by the oxidizable reactant.[7,10] This mechanism has been discussed very little, probably because evidence for the existence of a semioxidized form of the dye was lacking. However, the possibility of its formation has recently been established,[3] and its properties have been studied.[11] The results indicate that the semioxidized

radical may be important as an intermediate in photosensitized reactions. The present study was undertaken to investigate this possibility further. A kinetic analysis of the primary reactions between oxygen and the triplet state of fluorescein in aqueous solutions was made by means of the flash photolysis method, with particular regard to the formation of the semioxidized dye. A technique for preparing solutions with accurately known oxygen content, in the μM concentration range, is also described.

Experimental

The flash photolysis apparatus has been described previously.[12] An energy of 6 kj. (100 μf., 11 kv.) was dissipated in a pair of 60-cm. long quartz discharge tubes, the flash duration time being 60 μsec. (1/e-

(1) Research sponsored by the U. S. Department of the Army, through its European Office, under Contract No. DA-91-591-EUC-2162 OI-26528-B, with Prof. S. Claesson as supervisor.

(2) G. Oster and A. H. Adelman, *J. Am. Chem. Soc.*, **78**, 913 (1956).

(3) L. Lindqvist, *Arkiv Kemi*, **16**, 79 (1960).

(4) L. Lindqvist, *J. Phys. Chem.*, **67**, 1701 (1963).

(5) G. O. Schenck, *Naturwiss.*, **35**, 28 (1948); G. O. Schenck and E. Koch, *Z. Elektrochem.*, **64**, 170 (1960).

(6) G. Oster, J. S. Bellin, R. W. Kimball, and M. E. Schrader, *J. Am. Chem. Soc.*, **81**, 5095 (1959).

(7) J. Weiss, *Naturwiss.*, **23**, 610 (1935).

(8) R. Livingston and F. Hurd, *J. Phys. Chem.*, **45**, 547 (1941).

(9) M. Imamura, *Bull. Chem. Soc. Japan*, **31**, 962 (1958).

(10) R. Livingston, *J. Phys. Chem.*, **46**, 233 (1942).

(11) L. Lindqvist, to be published.

(12) S. Claesson and L. Lindqvist, *Arkiv Kemi*, **11**, 535 (1957).
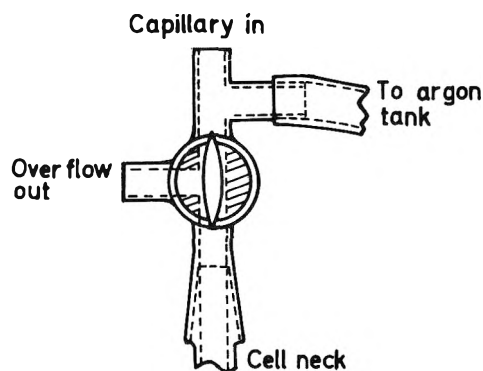
Figure 1. Device for preparation of solutions of known oxygen concentration in the micromolar concentration range.

time). The solution to be exposed was contained in a cylindrical silica cell with end windows (length 60 cm. or alternatively 20 cm. and inner diameter 2.3 and 2.7 cm., respectively). The photolysis light was filtered through a 0.5-cm. layer of filter solution transmitting from 390 to 630 mμ (10 g. of ferric alum, 200 g. of crystallized copper sulfate, 5 ml. of concentrated sulfuric acid, and water to make 1 l.). The filter solution was circulated through a jacket surrounding the reaction cell and through a thermostat maintained at 25°.

The transient changes in optical density (ΔE) of the flash-exposed solutions were measured as a function of time using a time-resolved single-beam spectrophotometer with oscilloscopic recording.[3,4] The band width was 1 mμ or less and the time resolution ca. 2 μsec. No appreciable excitation occurred 60 μsec. after the initiation of the flash, and this time point was chosen as the zero time for the "dark" reactions following excitation. A recording spectrophotometer (Bausch and Lomb Spectronic 505) was used for complementary measurements of the spectra of the solutions before and after flashing.

The solutions were prepared from chromatographically pure fluorescein[3] and triple-distilled water. The pH of the solutions was maintained using sulfuric acid at pH 2 and below, citrate buffer at pH 2.6 and 4.5, phosphate buffer at pH 8.4, and sodium hydroxide at pH 12. The ionic strength of the citrate and phosphate buffers was kept at 0.01. Sulfuric acid, reagent grade, was fractionally vacuum-distilled; other chemicals were reagent grade.

Fluorescein solutions of known oxygen content were prepared by mixing deaerated fluorescein solutions with air-saturated water. The aliquot required for filling the reaction cell was deaerated in a flask which was connected by means of greased glass joints both to the cell and to a mercury diffusion pump through a liquid

nitrogen trap. The ice-cooled solution was shaken 1 min. during evacuation and then exposed to oxygen-free argon (welding quality) for 1 min. under continued agitation at a pressure slightly below atmospheric pressure. This procedure was repeated eight times. After one further evacuation the solution was allowed to attain room temperature, poured into the reaction cell, and argon at atmospheric pressure was applied above the solution. The cell was removed from the degassing apparatus and was closed off by means of a stopper provided with a three-way stopcock (Fig. 1). To avoid the introduction of air, a stream of argon was blown around the cell neck during removal. A known amount of air-saturated water contained in a pipet was introduced into the cell through the opened stopcock via a stainless steel capillary which was extended to the bottom of the cell. An argon stream through the stopcock kept air from diffusing into the solution. Conditions were arranged such that a small amount (less than 0.5 ml.) of the degassed solution was pressed out through the stopcock during the mixing procedure. After removal of the capillary the stopcock was closed, thus leaving no empty space above the solution for the dissolved oxygen to escape. Under these conditions the oxygen concentration could be calculated directly from the volumes of the degassed and air-saturated solutions. In order to avoid the formation of bubbles by contraction of the solution, the cell was filled at a temperature slightly lower than that of the flash experiments. A thick layer of vacuum grease was applied between stopper and cell neck to allow for expansion of the solution and to prevent air diffusion into the cell. The solution was mixed by means of a number of glass balls within the cell. The oxygen concentration in the air-saturated water was determined by iodometry to be 2.83×10^{-4} M (at 22°). Blank tests showed that the accidentally introduced air produced an oxygen concentration in the solution of less than 0.03 μmole/l. This value was calculated from studies of the decay of the triplet state of fluorescein using the rate constant reported below. Blank runs also showed that neither the stainless steel capillary nor the grease in contact with the solution introduced any impurities that affected the triplet decay.

Results

Proposed Reaction Scheme. Fluorescein in aqueous solution, although stable to visible light in the absence of oxygen, is photobleached rapidly in the presence of oxygen. The fluorescence of the dye is not noticeably quenched by the oxygen present in air-saturated water, thus indicating that the fluorescent state is not involved in the oxidation process. A calculation of the

quenching effect, using known values of the lifetime of the fluorescent state,[13] and assuming that the quenching reaction is diffusionally controlled, gives a value of the order of only 0.1%. This effect is neglected in the following treatment of data. Instead, it is assumed that the oxygen attacks the dye in the lowest triplet state,[14] which is populated by intersystem crossing from the fluorescent state. The efficiency of this reaction is expected to depend upon the protolytic state of the triplet dye; the following forms have been reported[3,4]: the cation ($pK_a = -2.1$), the neutral molecule ($pK_a = 4$–5), the monovalent anion ($pK_a = 7.0$), and the divalent anion.

In a previous study,[3] the triplet state has been shown to undergo the following reactions in the absence of oxygen.

$$T \longrightarrow S \qquad \text{(rate constant } k_1) \qquad (1)$$

$$T + T \longrightarrow S + T \qquad (k_2) \qquad (2)$$

$$T + S \longrightarrow S + S \qquad (k_3) \qquad (3)$$

$$T + T \longrightarrow X + R \qquad (k_4) \qquad (4)$$

$$T + S \longrightarrow X + R \qquad (k_5) \qquad (5)$$
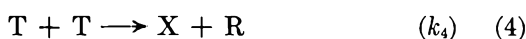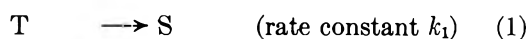
T, S, R, and X represent the triplet, ground state, semireduced, and semioxidized dye, respectively. In the same study the reactions between the triplet dye and molecular oxygen were investigated qualitatively and the results gave some evidence for the occurrence of a "physical-quenching" reaction

$$T + O_2 \longrightarrow S + O_2 \qquad (k_6) \qquad (6)$$
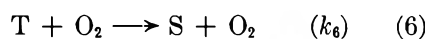
as well as a chemical quenching reaction

$$T + O_2 \longrightarrow X + HO_2 \text{ (or } O_2^-) \qquad (k_7) \qquad (7)$$
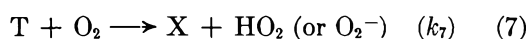
(the term "physical quenching" denotes here quenching processes where no chemical reaction was observed experimentally).

The kinetic analysis of the results is based on the assumption that the above reactions represent the only interactions between the triplet dye and oxygen.

Rate Constants of Triplet Quenching by Oxygen. Oxygen-containing aqueous solutions of fluorescein were flash-exposed, and transient changes in optical density were measured at wave lengths where the triplet state of the dye is the only absorbing species. The rate of disappearance of the triplet absorption was measured as a function of the oxygen concentration. The fluorescein concentration was kept low (0.2 μM, and alternatively, 0.5 μM) in order to suppress the concentration-quenching reactions 2–5. The oxygen concentration was 0–7 μM, the upper limit being set by the time resolution of the flash photolysis apparatus.
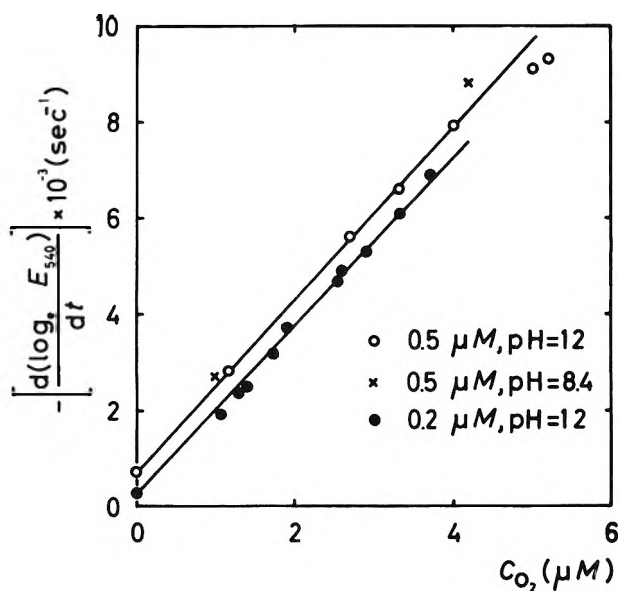
Figure 2. The initial logarithmic decay rate (see eq. 8) of the flash-induced light absorption at 540 mμ in solutions of 0.2 and 0.5 μM fluorescein at pH 8.4 and 12, as a function of the oxygen concentration. The dianionic form of the dye triplet is responsible for the light absorption at this wave length.

The amount of transient change in optical density produced by the flash and, hence, the transient concentration of triplet dye, were found to be independent of the oxygen concentration. Quantitative conversion of the dye to the triplet state was observed[3] in the absence of oxygen under the present conditions and is consequently realized also in the oxygen-containing solutions. The initial (indicated by a subscript zero) rate of triplet decay after flash exposure can in this case be expressed by the equation

$$-\left[\frac{d \ln c_T}{dt}\right]_0 = k_1 + (k_2 + 2k_4)C +$$

$$(k_6 + k_7)C_{O_2} \qquad (8)$$

where C and C_{O_2} are the concentrations of fluorescein and oxygen, respectively, before the flash.

The decay of the dianionic triplet was studied at 540 mμ at pH 8.4 and 12. The initial logarithmic rates of decay (left-hand side expression of eq. 8) are plotted in Fig. 2 as a function of the oxygen concentration. The linear relationship required by the above equation is verified experimentally. The results obtained at pH 8.4 and 12 agree with each other, as is expected from the fact that the same protolytic form of the triplet is formed in both cases. The slope of the line in Fig. 2

(13) E. A. Bailey, Jr., and G. K. Rollefson, *J. Chem. Phys.*, 21, 1315 (1953).

(14) G. N. Lewis and M. Calvin, *J. Am. Chem. Soc.*, 67, 1232 (1945).

Table I: Rate Constants of Quenching of the Fluorescein Triplet by Oxygen (k_q), and of the Chemical Reaction (7) between the Triplet and Oxygen (k_7)

Triplet species	pH	$k_q \times 10^{-9}$, M^{-1} sec.$^{-1}$	k_7, M^{-1} sec.$^{-1}$
Cation	-4^a	0.2	$<10^6$
Neutral molecule	2.0	1.2	$(1.0 \pm 0.5) \times 10^7$
	2.6	1.2	
Monoanion	4.5	1.2	
Dianion	8.4	1.7	
	12.0	1.7	$(1.4 \pm 0.1) \times 10^8$

^{a} The Hammett acidity function of 8 M sulfuric acid.

gives the rate constant of triplet quenching by oxygen ($k_q = k_6 + k_7$), presented in Table I.

Corresponding triplet decay measurements were done at 510 mμ in solutions of pH 2.0 and 2.6, where the neutral triplet predominates, and at pH 4.5, where the monoanionic triplet is expected to appear. A plot of the initial logarithmic rate of decay as a function of the oxygen concentration at these acidities is shown in Fig. 3. The points describe a line from which the quenching constant, given in Table I, was calculated.

Figure 3 and Table I also show the results pertaining to a study of the cationic triplet in 8 M sulfuric acid (Hammett acidity function $H_0 = -4$). In this case the linear relationship is also satisfied.

Chemical Quenching. The relative importance of chemical and physical quenching of the triplet dye by
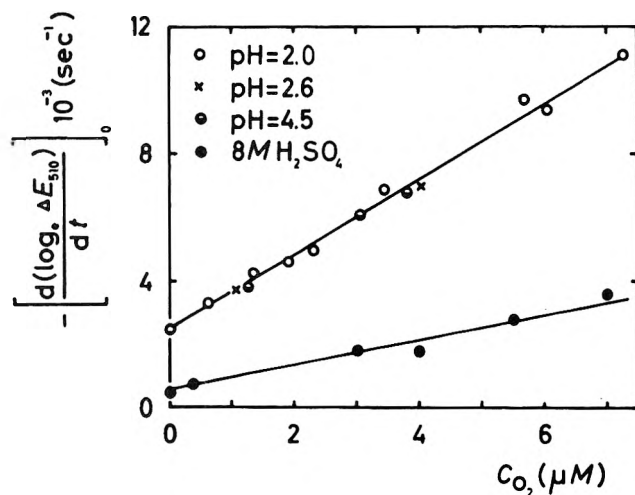
Figure 3. The initial logarithmic decay rate of the flash-induced light absorption at 510 mμ in 0.5 μM fluorescein solutions of different acidities, as a function of the oxygen concentration. The monoanionic form of the dye triplet is responsible for the light absorption at pH 4.5, the neutral form at pH 2.0 and 2.6, and the cationic form in 8 M sulfuric acid.

Figure 4. The flash-induced change in optical density at 428 mμ in 0.2 μM fluorescein solutions of pH 12, as a function of time, at different oxygen concentrations. The numbers given in the figure indicate the oxygen concentration in μmoles/l.; cell length, 60 cm.

oxygen was determined by measuring flash-induced changes in optical density of oxygen-containing solutions of fluorescein at wave lengths where the semioxidized dye has a high light absorption. Previous studies[3,11] have shown that in strongly acidic solutions this species has an intense absorption peak at 442 mμ (molar ext. coeff. 6×10^4), which is probably due to the cationic radical ($pK_a = -1.5$). The peak is shifted to 428 mμ (ext. coeff. 5×10^4) in moderately acidic and alkaline solutions, probably due to the formation of the neutral and anionic radical (the ionization of the carboxyl group does not affect the peak position).

The semioxidized dye is expected to be formed by the triplet–triplet and triplet–singlet dismutation reactions 4 and 5 in the absence of oxygen, and by the triplet–oxygen reaction 7 in the presence of oxygen. The total concentration, $(c_X)_{total}$, of semioxidized dye formed can be expressed as

$$(c_X)_{total} = Ck_7/k_q \qquad (9)$$

at oxygen to dye concentration ratios such that reactions 4 and 5 are unimportant compared to reaction 7, with the additional requirement that no appreciable deactivation of the triplets occurs during the flash. Since k_q is known (Table I), the value of k_7 can be determined by measuring the amount of semioxidized dye formed after the flash.

The curves in Fig. 4, obtained from measurements at 428 mμ, demonstrate the effect of oxygen on the amount of semioxidized dye formed after flash exposure of 0.2 μM fluorescein solutions at pH 12. At this wave length the semioxidized dye is the only strongly absorbing species present in the solution, and the changes in opti-
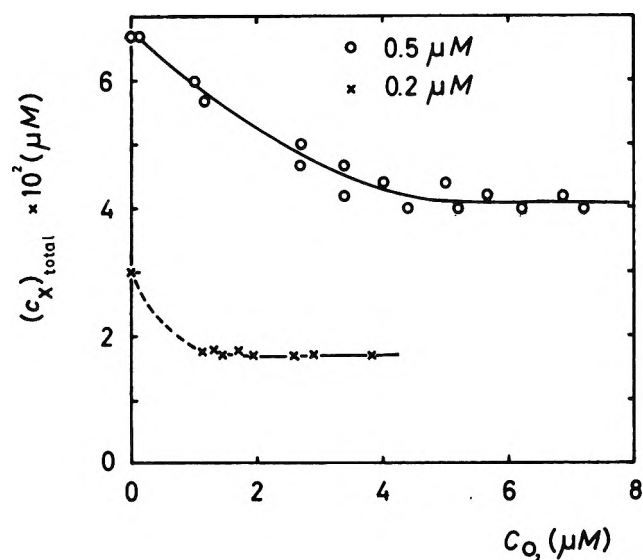
Figure 5. Maximum concentration, $(c_X)_{total}$, of semioxidized fluorescein appearing after flash-excitation of 0.2 and 0.5 μM fluorescein solutions at pH 12, as a function of the oxygen concentration.

cal density are therefore proportional to the amount of semioxidized dye formed. From the difference between the extinction coefficient of the semioxidized dye and of the ground state (4.5×10^4), the changes in optical density were converted to changes in concentration of the semioxidized dye. The steeply rising parts of the curves in Fig. 4 demonstrate the appearance of the semioxidized dye by reactions 4, 5, and 7, and the slightly descending parts indicate the slow disappearance by subsequent reactions. A value of $(c_X)_{total}$ was taken at each oxygen concentration from the point of the corresponding curve in the figure (and from other measurements) where the optical density change has a maximum. The small amount of triplet which had not reacted at this time and the small amount of semioxidized dye which had already disappeared by subsequent reactions were neglected. These values are plotted against the oxygen concentration in Fig. 5. At high oxygen concentrations, the yield of semioxidized dye reaches a limiting value, from which k_7 (Table I) was calculated.

A corresponding determination of k_7 was made at pH 2.0 where the neutral triplet appears. Reaction 7 was in this case found to be very inefficient compared to reactions 4 and 5, and it was necessary to use a high oxygen concentration in order to suppress the latter reactions. Measurements were done in air-saturated solutions at a fluorescein concentration of 0.5 μM using a 60-cm. cell. The optical density increased during the flash by 0.012 at 428 mμ, and then decreased compara-

tively slowly to a value 0.017 below the original value. Since it is not known if the permanent bleaching occurs during or after the flash, the mean value of 0.012 + 0.029 was used to calculate the concentration of semi-oxidized dye formed. (The difference between the extinction coefficients of the semioxidized dye and the dye in the ground state is 2.0×10^4 at this wave length.) In air-saturated solutions deactivation of the triplet state by reaction 6 may occur during the flash and several-fold conversion of the same molecule to the triplet state is possible. The number of times that each dye molecule can be reactivated to the triplet state during one flash was determined in a separate study. The amount of dye converted per flash to the triplet state in deaerated 0.5 μM fluorescein solution of pH 2.0 was measured as a function of the amount of light incident in the cell. The light input was varied by means of calibrated screens. At low light levels the triplet concentration was directly proportional to the light input, and an extrapolation to the light level of unscreened flash gave a triplet concentration of 1.5 μM. This means that each dye molecule in a 0.5 μM solution should be converted to the triplet state on an average of three times, provided that the triplet deactivation is instantaneous. The value of the concentration of semioxidized dye calculated above was, after reduction by this factor of three, inserted in eq. 9 (which applies to a onefold conversion to the triplet state), and a value of k_7 (Table I) was obtained.

The value of k_7 for the cationic triplet state was determined from measurements of the dye in 8 M sulfuric acid. The accuracy of the determination of the concentration of semioxidized dye was lower in this case, because the absorption peak of the cationic semioxidized dye which appears at this acidity is close to that of the cationic dye in the ground state. The difference in extinction coefficients amounts to 1.3×10^4 at 442 mμ, the most suitable measuring wave length. No absorption change was observed in air-saturated solution. From the limit of detectability of the measurements, an upper limiting value of k_7 was calculated (Table 1).

Reaction between Semireduced Fluorescein and Oxygen. Reactions 4 and 5, producing semioxidized and semireduced dye, compete with reactions 6 and 7 at low oxygen concentrations. The semireduced dye is known[3] to have a pronounced absorption peak at 355 mμ at pH below 9.5. At this wave length the extinction coefficients of the other species present in the reaction mixture are an order of magnitude smaller. The flash-induced formation and disappearance of the semireduced fluorescein was measured at 355 mμ at different oxygen concentrations, at pH 2 and 8.4. The results, presented in Fig. 6, show that when the oxygen concen-
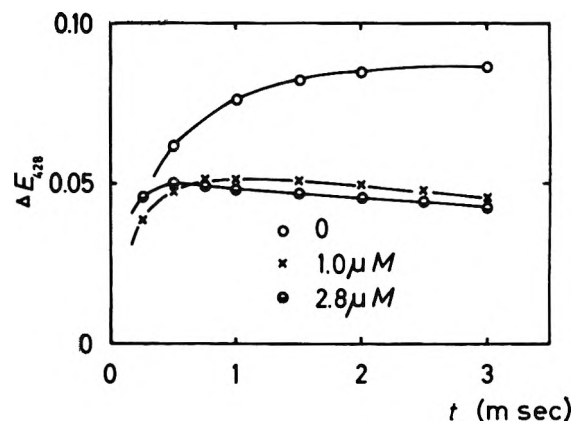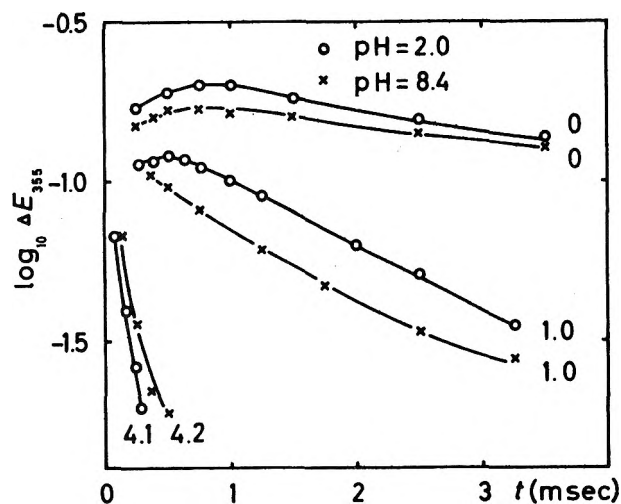
Figure 6. The logarithm of the flash-induced change in optical density at 355 mμ in 0.5 μM fluorescein solutions of pH 2.0 and 8.4, as a function of time, at different oxygen concentrations. The numbers given in the figure indicate the oxygen concentration in μmoles/l.; cell length, 60 cm.

tration is increased, the yield of semireduced dye is decreased, due to the increasing importance of the quenching reactions 6 and 7. At the same time, the rate of disappearance of the semireduced dye increases, probably due to the occurrence of the reaction

$$R + O_2 \longrightarrow S + HO_2 \text{ (or } O_2^-) \quad (k_{10}) \quad (10)$$
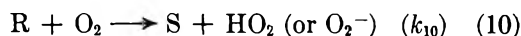
The simultaneous presence of semioxidized dye in the reaction mixture made a determination of k_{10} difficult, but a rough calculation gave a value in the range 10^8 to 10^9 M^{-1} sec.$^{-1}$.

Reactions of the Semioxidized Dye. The reactions of the semioxidized dye to form stable photooxidation products are not of direct importance in connection with the use of the dye as a photosensitizer, and were not studied in detail. It was observed, however, that in alkaline medium the permanent decrease in dye concentration after flash exposure was smaller than the concentrations of the transiently appearing semioxidized dye. Since the absorption spectrum of the photoproduct is known,[3] the permanent decrease in dye concentration could be obtained by measuring the decrease in optical density of the dye solution at the wave length of the absorption maximum of the dye in the visible region. It was found for air-saturated solutions that at pH 12, *ca.* 4% of the dye was oxidized by one flash, whereas the amount of semioxidized radical formed was 8% of the total dye concentration. At pH 2 the corresponding figures were 2 and 4%. Since at both pH values one-half of the semioxidized dye is reduced to give the

original dye, a reasonable mechanism for the recovery would be that two semioxidized dye radicals disproportionate when encountering. However, studies of the photooxidation of fluorescein by ferric salts[11] do not support this reaction and it seems more probable that the reaction

$$X + HO_2 \text{ (or } O_2^-) \longrightarrow S + O_2 \quad (11)$$
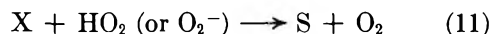
is occurring and that this reaction competes favorably with the reactions which give stable photoproducts.

Discussion

The results show that "physical" quenching of the triplet state of fluorescein by oxygen (reaction 6) is a very efficient process. It seems very probable that this quenching reaction involves the actual formation of a reactive compound between the excited dye and oxygen as proposed by Schenck,[5] but that the lifetime of this compound is shorter than the time resolution of the flash photolysis apparatus. Due to the high efficiency of this reaction it would appear to be important in autoxidation reactions photosensitized by fluorescein. On the other hand, the one-electron oxidation of the triplet dye (reaction 7), although less efficient, also may be important under certain conditions, considering the comparatively long lifetime of the semioxidized dye. At high oxygen-to-dye ratios the yield of this species per triplet molecule formed is equal to k_7/k_q, 0.0084 at pH 2, and 0.082 at pH 12. The fluorescence yield[15] is 0.31 at pH 2 and 0.93 at pH 12, giving a maximum yield of conversion from the excited singlet state to the triplet state of 0.69 and 0.07, respectively. The maximum quantum yield of formation of the semioxidized dye is 0.006 in both cases. However, this value is obtained by making the improbable assumption that no radiationless transition from the excited singlet to the ground state is occurring. It should be possible, in principle, to calculate the extent of the radiationless transition from the observed permanent photobleaching per flash, using known values of the quantum yield of photooxidation of the dye.[9] However, this could not be done in the present case because at the high light intensities used, photobleaching was observed even in the absence of oxygen, and the origin of this bleaching is not known.

The oxidized dye is produced not only by reaction of the triplet dye with oxygen but at ordinary light intensities also by the electron dismutation reaction with the dye in the ground state (reaction 5). The semireduced dye which is formed in this process

(15) G. Weber and F. W. J. Teale, *Trans. Faraday Soc.*, 54, 640 (1958).

reacts readily with oxygen (reaction 10) to regenerate the dye in the ground state, and to give the reduced species of oxygen. The net result of these reactions is the same as that of the direct reaction between oxygen and the triplet dye. Reaction 5 has a high rate constant in moderately acidic solutions where it may enhance the quantum yield of formation of the semioxidized dye. (For example, in an air-saturated 10 μM fluorescein solution of pH 2, the dismutation reaction is twice as efficient as the direct photooxidation reaction in producing semioxidized dye.) The above treatment of data shows that the production of semioxidized fluorescein in the photolysis of air-containing dye solutions is appreciable (except at acidities realized in concentrated sulfuric acid solutions) and this radical, therefore, should be taken into account in the discussion of photosensitized autoxidation reactions.

The values of the triplet quenching constants presented in Table I are of the order of magnitude calculated for diffusionally controlled reactions. The low value observed for the cationic triplet is accounted for by the high viscosity of the solvent used (8 M sulfuric acid), which has a viscosity four times greater than that of water. The results agree with previous observations that oxygen is an efficient quencher of the triplet state, as has been shown in the case of chlorophyll[16] and of anthracene.[17] In contrast to this, a rate constant for quenching of triplet eosin by oxygen *ca.* 1000 times smaller has recently been reported,[18] a difference compared to the present results on fluorescein that is surprising in view of the similarity of these dyes.

The HO_2 and O_2^- radicals formed in the chemical quenching reaction were not observed directly, and probably have too weak an absorption spectrum in the visible or near ultraviolet region of the spectrum to be detectable under the present conditions. Indirectly, the results show that the chemical reaction between two HO_2 radicals must be at least an order of magnitude less efficient than the observed reaction between semioxidized dye and the products of the one-electron reduction of oxygen (reaction 11). Baxendale[19] has estimated the rate constant of the reaction between two HO_2 radicals to be on the order of $10^6 M^{-1}$ sec.$^{-1}$. This is a sufficiently small value to agree with the results of this study. No effects were found of the protolysis of the HO_2 radical.

(16) E. Fujimori and R. Livingston, *Nature*, 180, 1036 (1957).

(17) G. Porter and M. W. Windsor, *Proc. Roy. Soc.* (London), A245, 238 (1958).

(18) E. F. Zwicker and L. I. Grossweiner, *J. Phys. Chem.*, 67, 549 (1963).

(19) J. H. Baxendale, *Radiation Res.*, 17, 312 (1962).

The Protonation and Deprotonation of Sulfamide

and Sulfamate in Aqueous Solutions

by Michael Garrett,[1] Terence Tao,[1] and William L. Jolly

Department of Chemistry, University of California, Berkeley 4, California   (Received October 17, 1963)

The width of the n.m.r. signal of water in aqueous solutions of sulfamide varies with the pH; maxima are observed at pH values 4.1 and 5.7. The data have been interpreted in terms of reactions of sulfamide with hydrogen ion and hydroxide ion. Similar data for aqueous solutions of sodium sulfamate have been analogously interpreted.

Introduction

Sulfamide acts as a very weak acid in aqueous solutions. Thus, although various salts of sulfamide have been isolated from alkaline aqueous solutions, solutions of pure sulfamide are practically nonconducting.[2,3] On the other hand, apparently no basic character has ever been detected in sulfamide in its aqueous solutions. In the present study, we have measured the broadening of the proton magnetic resonance signal of water in sulfamide solutions as a function of pH, and have interpreted the data in terms of an acid-catalyzed exchange reaction and a base-catalyzed exchange reaction. Each of these reactions has been studied in pH regions of moderately slow exchange (separate signals for sulfamide and water) and of fast exchange (one merged signal).

The sulfamate ion, $NH_2SO_3^-$, is known to be weakly basic[4] and to be very weakly acidic.[5] Although we never observed a separate n.m.r. signal due to the sulfamate ion, we found that the n.m.r. line broadening data of sulfamate solutions, like those for sulfamide solutions, could be interpreted in terms of acid- and base-catalyzed exchange reactions.

Experimental

Sulfamide from the General Chemical Division of Allied Chemical Corporation was purified by repeated recrystallization from 95% ethanol, followed by recrystallization from an acetone–ethyl acetate mixture. The purified product had a melting point of 90–93° (lit.[2] m.p. 93°) In each experiment, purified sulfamide was dissolved in the appropriate amount of buffer solution to make a solution 1.5 M in sulfamide. The

pH of the solution was determined with a pH meter, and the solution was transferred to an n.m.r. tube. In the pH range 3.2–5.2, 0.1 M acetic acid–acetate buffers were used; in the pH range 5.2–7.3, 0.1 M dihydrogen phosphate–monohydrogen phosphate buffers were used.

Sulfamic acid from the G. F. Smith Chemical Company was dissolved in the appropriate amount of sodium hydroxide solution to make solutions 2 M in sodium sulfamate. The pH was adjusted with potassium dihydrogen phosphate and borax at concentrations near 0.03 M.

A Varian Model A-60 n.m.r. spectrometer was used.

Results

Sulfamide. The measured line widths at half height of the water signal $\Delta\nu_{1/2}$ are plotted vs. pH in Fig. 1. The curve shows two maxima (at pH values $\sim$4.1 and $\sim$5.7) and a minimum (at pH 5.1). In the pH range between the two maxima, a broad signal due to sulfamide was observed approximately 104 c.p.s. to low field of the water signal. At pH values outside of this range, only one signal (essentially that of the water) was observed. We shall interpret the data in terms of the following two reactions, each of which

(1) Work performed by M. Garrett and T. Tao in partial fulfillment of the requirements for the B.S. degree.

(2) L. F. Audrieth, M. Sveda, H. H. Sisler, and M. J. Butler, *Chem. Rev.*, **26**, 49 (1940).

(3) E. C. Franklin, "The Nitrogen System of Compounds," Reinhold Publishing Corp., New York, N. Y., 1935, pp. 169–170.

(4) E. G. Taylor, R. P. Desch, and A. J. Catotti, *J. Am. Chem. Soc.*, **73**, 74 (1951); E. J. King and G. W. King, *ibid.*, **74**, 1212 (1952).

(5) Ref. 3, pp. 167–168.
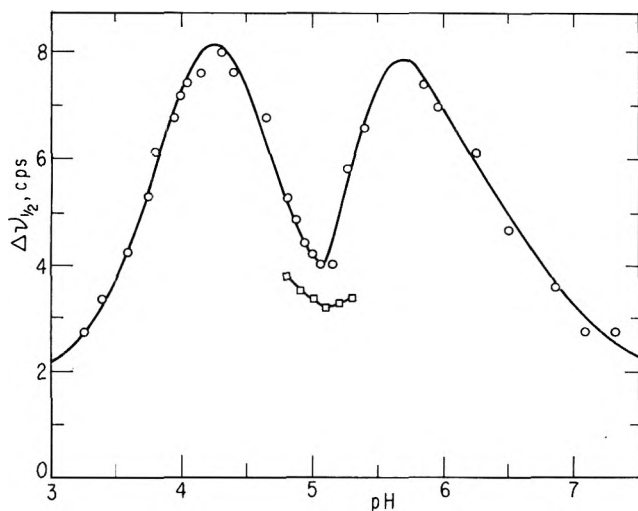
Figure 1. N.m.r. line width as a function of pH for 1.5 M sulfamide. The circles and squares represent separately determined data. It is believed that the squares represent more accurate data than the circles. $\Delta\nu_{1/2}^{0}$, the value of $\Delta\nu_{1/2}$ for the buffer solutions in the absence of sulfamide, has the values 1.27 and 1.0 c.p.s. for the circles and squares, respectively.

leads to an exchange of a proton between sulfamide and water.

$$NH_2SO_2NH_2 + H^+ \longrightarrow NH_2SO_2NH_3^+ \quad (1)$$

$$NH_2SO_2NH_2 + OH^- \longrightarrow NH_2SO_2NH^- + H_2O \quad (2)$$
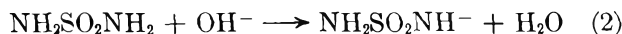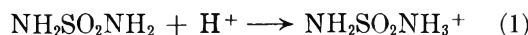
The sum of the rates of these reactions is represented by the equation

$$R = k_1(H^+)(NH_2SO_2NH_2) + k_2(OH^-)(NH_2SO_2NH_2)$$

At the minimum in the $\Delta\nu_{1/2}$ vs. pH curve, we use the relation

$$1/\tau = 1/T_2' - 1/T_2 \quad (3)$$

where τ is the mean lifetime of a proton on a particular site, and T_2' and T_2 are the transverse relaxation times in the presence of exchange and in the absence of exchange, respectively.[6] By using eq. 3 and the data $\Delta\nu_{1/2} = 3.2$ c.p.s. and $\Delta\nu_{1/2}^{0} = 1.0$ c.p.s., we obtain an approximate value for τ_w (τ for protons on water). From the relation

$$\tau_s/\tau_w = p_s/p_w \quad (4)$$

(where τ_s is τ for the protons on sulfamide, and p_s and p_w are the fractions of the protons on sulfamide and water, respectively) we calculate $\tau_s = 7.95 \times 10^{-3}$ sec. Equation 3 is valid only when $2\pi\tau(\nu_w^0 - \nu_s^0) \gg 1$, where $\nu_w^0 - \nu_s^0$ is the chemical shift (c.p.s.) between water and sulfamide in the absence of exchange.[6] From our data we calculate that, at the minimum, $2\pi\tau_s(\nu_w^0 - \nu_s^0) \approx 5$; thus, for

our purposes, eq. 3 is a fairly good approximation. Because $R = 4(NH_2SO_2NH_2)/\tau_s$, and because, at the minimum, the acid- and base-catalyzed reaction rates are equal, we may write

$$2/\tau_s = k_1(H^+) = k_2(OH^-)$$

Using the H^+ and OH^- concentrations corresponding to pH 5.1, we calculate $k_1 = 3.2 \times 10^7 M^{-1}$ sec.$^{-1}$ and $k_2 = 2.0 \times 10^{11} M^{-1}$ sec.$^{-1}$.

At pH 4.1 the two signals coalesce to one broad signal, and we may write

$$2\pi\tau(\nu_w^0 - \nu_s^0) \approx 1 \quad (5)$$

where τ is a "reduced" lifetime for the system.[7,8] We take τ_s as a good approximation for τ. The term k_2 (OH^-) is negligible compared to $k_1(H^+)$; thus $4/\tau_s \approx k_1(H^+)$. The data yield $k_1 \approx 3.1 \times 10^7 M^{-1}$ sec.$^{-1}$. At pH 5.7, the two signals coalesce to one broad signal, and again we use eq. 5. At this pH, we may neglect the term $k_1(H^+)$; thus $4/\tau_s \approx k_2(OH^-)$. The data yield $k_2 \approx 5 \times 10^{11} M^{-1}$ sec.$^{-1}$.

When $2\pi\tau(\nu_w^0 - \nu_s^0) \ll 1$, the "fast exchange" approximation is valid[8,9]

$$1/T_2' = p_w/T_{2w} + p_s/T_{2s} +$$
$$4\pi^2 p_A^2 p_B^2 (\nu_w^0 - \nu_s^0)^2 (\tau_w + \tau_s)$$

Such conditions prevail in solutions of very low pH and in solutions of very high pH. However, there are practical limits to the useful pH values because, if the exchange becomes too rapid, the difference between $1/T_2'$ and $(p_w/T_{2w} + p_s/T_{2s})$ becomes very small and subject to considerable uncertainty. We have chosen to use the data at pH 3.38 and 6.85, at which points $2\pi\tau_s(\nu_w^0 - \nu_s^0) \approx 0.2$. Although it was not possible to measure $1/T_{2s}$ directly, we obtained an approximate value of 19.5 sec.$^{-1}$ for this quantity from measurements of $1/T_{2w}'$ and $1/T_{2s}'$ in the region of moderately slow exchange and by application of eq. 3 and 4. This large value for T_{2s} is probably due to N^{14} quadrupole broadening of the resonance. From the $1/T_2'$ value at pH 3.38, we calculate $\tau_s = 2.9 \times 10^{-4}$ sec. and $k_1 = 3.3 \times 10^7 M^{-1}$ sec.$^{-1}$. From the $1/T_2'$ value at pH 6.85, we calculate $\tau_s = 3.25 \times 10^{-4}$ sec. and $k_2 = 1.7 \times 10^{11} M^{-1}$ sec.$^{-1}$.

Sulfamate. A plot of the measured line widths at

(6) J. A. Pople, W. G. Schneider, and H. J. Bernstein, "High-Resolution Nuclear Magnetic Resonance," McGraw-Hill Book Co., Inc., New York, N. Y., 1959, p. 221.

(7) H. S. Gutowsky and C. H. Holm, *J. Chem. Phys.*, 25, 1228 (1956); see ref. 6, pp. 222–223.

(8) A. Loewenstein and T. M. Connor, *Ber. Bunsenges. physik. Chem.* 67, 280 (1963).

(9) Ref. 6, pp. 221–222.

half height vs. pH for sulfamate solutions is similar to the corresponding plot for sulfamide solutions, except that the minimum is not as pronounced as in the case of the sulfamide solutions, and the maxima occur at pH values 7.2 and 8.8. Even in approximately 7 M sulfamate solutions, it was not possible to observe a separate signal for sulfamate; however, a shoulder on the water peak was observed at this high concentration in the region of pH 8.

Let us assume that proton exchange occurs by the reactions

$$NH_2SO_3^- + H^+ \longrightarrow (NH_2SO_3)H \qquad (6)$$

$$NH_2SO_3^- + OH^- \longrightarrow NHSO_3^{2-} + H_2O \qquad (7)$$
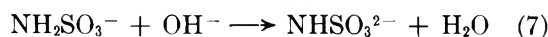
The sum of the rates of these reactions is then given by

$$R = k_6(H^+)(NH_2SO_3^-) + k_7(OH^-)(NH_2SO_3^-)$$

If we further assume that the chemical shift for sulfamate is similar to that for sulfamide and that the maxima at pH 7.2 and 8.8 correspond to "coalescence points," then we calculate, using eq. 5 as above, $k_6 \approx 10^{10}$ and $k_7 \approx 10^8$.

Discussion

The three different determinations of k_1 and k_2 are in accidentally good agreement. We shall take $k_1 = 3 \times 10^7 \ M^{-1}$ sec.$^{-1}$ and $k_2 = 2 \times 10^{11} \ M^{-1}$ sec.$^{-1}$.

The magnitude of k_1 (for the protonation of sulfamide) is similar to that of rate constants for the protonation of other weak bases such as H_2O_2 (2 $\times$ 10^7 M^{-1} sec.$^{-1}$) and methanol (10^8 M^{-1} sec.$^{-1}$).[8] The protonation rate constant for N-methylacetamide, which might be expected to be comparable to that for sulfamide, is very low (400 M^{-1} sec.$^{-1}$).[8] This low value is probably attributable to partial double bonding of the type
$$\overset{+}{^-O-C(CH_3)=NH(CH_3)},$$
and the data suggest that double bonding to the nitrogen atom is more important in the latter molecule than in sulfamide. The rate constant k_2 (for the reaction of sulfamide with OH$^-$) falls in line with the rate constants for the reactions of OH$^-$ with acids stronger than water ($k \sim 10^{10}$ to $10^{11} M^{-1}$ sec.$^{-1}$).[10]

The protonation rate constant for sulfamate ($k_6 \approx 10^{10} \ M^{-1}$ sec.$^{-1}$) is similar in magnitude to the corresponding rate constants for bases stronger than water ($k \sim 10^{10}$ to $10^{11} \ M^{-1}$ sec.$^{-1}$).[10] The rate constant for the reaction of OH$^-$ with sulfamate ($k \approx 10^8 \ M^{-1}$ sec.$^{-1}$) is reasonable when compared with the corresponding rate constants for water and methanol ($k = 5 \times 10^9$ and 3 $\times$ 10$^6 M^{-1}$ sec.$^{-1}$, respectively).[8]

(10) M. Eigen, *Pure Appl. Chem*, **6**, 97 (1963).

P–T–x Diagrams in the Critical Region.   Acetone-*n*-Alkane Systems

by Webster B. Kay

Ohio State University, Columbus, Ohio   *(Received October 18, 1963)*

The P–T–x phase diagrams of nine binary systems composed of the *n*-alkanes from ethane through *n*-octane plus *n*-decane and tridecane, with acetone as a common component, were determined in the critical region.   Critical positive azeotropes were found to exist in the *n*-pentane–acetone and *n*-hexane–acetone systems and possibly in the *n*-heptane–acetone system.   In general, systems which form positive critical azeotropes possess a minimum temperature point in the critical locus curve.   Exceptions to this rule are discussed.   The results suggest a general pattern of phase behavior of binary systems composed of the members of a homologous series of compounds and a common azeotrope-forming compound that may be used for a qualitative prediction of their critical locus.

The P–T–x relations of mixtures at elevated pressure, in addition to their practical value in engineering operations, are of interest to the physical chemist because they yield fundamental information on the molecular behavior of fluids.   Of particular interest are those systems whose solutions deviate from ideality to such an extent that azeotropes are formed.   Many years ago, Kuenen showed[1] that the principal difference in the phase diagrams of systems that form critical azeotropes and those that do not is the existence of a minimum or a maximum temperature point in the critical locus curve of the former, but not in the latter.   Kuenen did not explore the subject further.

In 1951, this laboratory began a study of azeotrope-forming systems[2–5] which indicated that their P–T–*x* diagrams may exhibit a great variety of forms dependent on the difference in the critical temperatures of the components.   This was demonstrated convincingly in a recent paper on the critical properties of perfluoro-*n*-heptane–*n*-alkane systems.[6]   Further evidence of this diversification is presented here as a result of a study of the binary systems of the *n*-alkanes from ethane through *n*-octane plus *n*-decane and *n*-tridecane, with acetone as the common component.   The present study deals with systems in which the common component, acetone, has a critical pressure greater than that of any hydrocarbon with which it is paired.   This is in contrast with the previous series where the common component, perfluoro-*n*-heptane, had a critical pressure less than that of the hydrocarbons.

Experimental

P–T–x relations at the liquid–vapor phase boundaries of the nine binary systems were obtained by the determination of the pressure–temperature border curves of a series of mixtures of known composition.   From plots of these curves the P–T–x diagrams were derived.   The apparatus and experimental procedures were, in general, the same as those employed in earlier studies.[3,7]   Briefly, an air-free sample of a mixture of known composition was confined over mercury in a glass capillary tube which was surrounded by a constant temperature bath.   The tube was fastened in a mercury-filled compressor with means provided for controlling and measuring the pressure on the sample.   Equilibrium between the liquid and vapor was established by a magnetic stirrer.   Bubble and dew point pressures were determined for a series of temperatures from which data the P–T border curves were derived.   Critical points were obtained by observing the temperature and pressure at which the meniscus visually disappeared.

(1) J. P. Kuenen, "Theorie der Verdampfung und Verflüssigung von Gemischen," Johann A. Barth, Publisher, Leipzig, 1906, pp. 78–94.

(2) W. B. Kay and D. B. Brice, *Ind. Eng. Chem.*, **45**, 615 (1953).

(3) W. B. Kay and G. M. Rambosek, *ibid.*, **45**, 221 (1953).

(4) W. B. Kay and F. M. Warzel, *A. I. Ch. E. J.*, **4**, 296 (1958).

(5) W. B. Kay and H. A. Fisch, *ibid.*, **4**, 293 (1958).

(6) L. W. Jordan and W. B. Kay, *Chem. Eng. Progr. Symp. Ser.*, **59**, No. 44, 46 (1963).

(7) W. B. Kay and W. E. Donham, *Chem. Eng. Sci.*, **4**, 1 (1955).
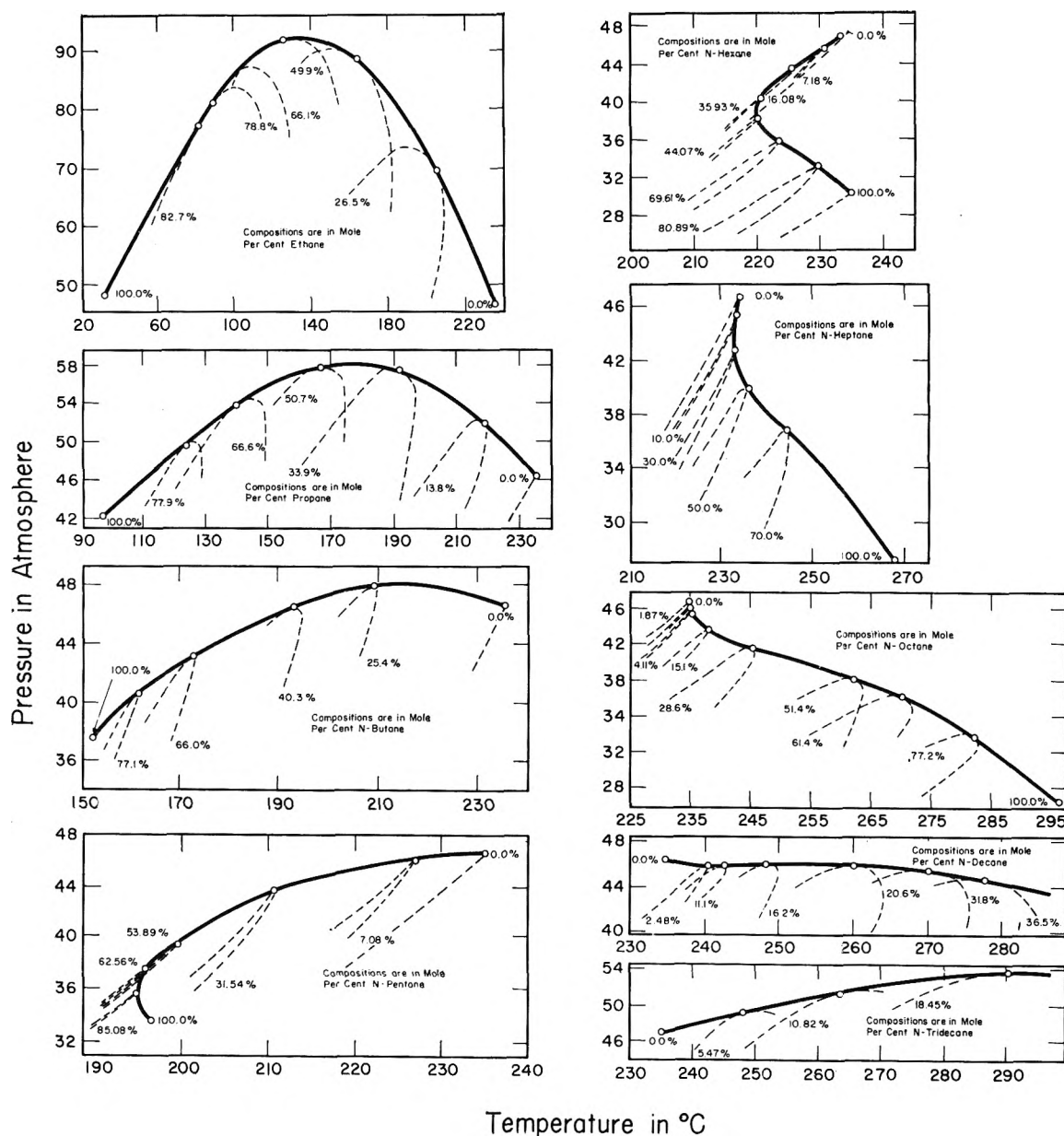
Figure 1. P–T–x diagrams in the critical region.

The temperature of the sample was measured to within 0.2° by means of a copper–constantan thermocouple and a sensitive potentiometer. For the pressure, a 16-in. dial precision spring gage graduated in 2-lb. (0.13 atm.) divisions was used.

Preparation of Materials. Reagent grade acetone was dried with dehydrated calcium sulfate and the decanted acetone distilled in a 1.5-m. silvered and vacuum-jacketed fractionating column using a reflux of 20:1. Samples of the paraffin hydrocarbons, ethane through n-octane of a purity of the order of 99.9 mole % and n-decane and n-tridecane of a purity

of about 99 mole %, were available and were used without further purification.

Mixtures of acetone with ethane, propane, and n-butane were prepared by loading the capillary tube with a sample of pure acetone, calculating its weight from the measured volume and density, and then adding a measured volume of gas at a known temperature and pressure to make a mixture of known composition. Mixtures of acetone with n-pentane and higher homologs were prepared by transferring small measured quantities of the pure components by molecular distillation to the experimental tube attached

to a high vacuum line. The estimated error in the composition of the mixtures that were studied was about 1–2%.

Table I: Critical Temperatures and Pressures of Binary Mixtures

Ethane–acetone system[a]			Propane–acetone system[a]		
Mole % ethane	T_c, °C.	P_c, atm.	Mole % propane	T_c, °C.	P_c, atm.
0	234.5	46.4			
26.5	204.8	68.9	13.8	218.3	51.9
49.9	163.3	87.8	33.9	191.2	57.3
66.1	122.9	90.9	50.7	164.9	57.5
78.8	88.1	80.0	66.6	139.8	53.6
82.7	75.0	79.8	77.9	122.9	49.2
100.0	32.3	48.7	100.0	96.8	42.0

n-Butane–acetone system[b]			n-Pentane–acetone system[b]		
Mole % butane	T_c, °C.	P_c, atm.	Mole % pentane	T_c, °C.	P_c, atm.
25.4	208.8	47.6	7.1	226.8	45.6
40.3	192.7	46.2	31.5	210.5	42.7
62.6	173.0	43.0	53.9	199.1	39.1
77.1	161.3	40.4	62.6	195.5	37.2
100.0	152.2	37.5	79.9	194.5	35.3

n-Hexane–acetone system[c]			n-Heptane–acetone system[d]		
Mole % hexane	T_c, °C.	P_c, atm.	Mole % heptane	T_c, °C.	P_c, atm.
7.2	230.6	45.0	6.06	233.4	45.3
16.1	225.5	43.0	20.0	232.6	42.4
35.9	220.4	39.8	36.7	235.5	39.9
44.1	219.9	37.6	57.5	244.1	36.9
69.6	223.2	35.3	100.0	267.4	27.3
88.9	229.4	32.7			
100.0	234.7	29.9			

n-Octane–acetone system[e]			n-Decane–acetone system[e]		
Mole % octane	T_c, °C.	P_c, atm.	Mole % decane	T_c, °C.	P_c, atm.
1.87	234.7	46.0	2.5	240.1	45.7
4.1	234.9	45.4	5.7	241.9	45.7
15.1	237.8	43.4	11.1	242.3	45.8
28.6	244.9	41.4	16.2	248.1	45.9
51.4	261.9	37.9	20.6	259.9	45.7
61.4	270.0	35.9	31.8	269.7	45.3
77.2	281.7	31.8	36.5	277.5	44.4

n-Tridecane–acetone system[c]		
Mole % tridecane	T_c, °C.	P_c, atm.
5.5	247.5	49.1
10.8	263.3	51.1
18.5	290.7	53.5

[a] L. Jones, M.S. Thesis, Ohio State University, 1958. [b] C. Brown, M.S. Thesis, Ohio State University, 1959. [c] S. Chun, M.S. Thesis, Ohio State University, 1959. [d] R. Congelliere, M.S. Thesis, Ohio State University, 1951. [e] E. McAdams, M.S. Thesis, Ohio State University, 1958.

Results and Discussion

The *P–T–x* diagrams of the nine binary systems are shown in Fig. 1. The critical data are given in tabular form in Table I. For each system the vapor pressure curves of the pure components and the *P–T* border curves of the various mixtures are indicated by broken lines. Tangent to each of the border curves in the critical point and terminating in the critical points of the pure components is the critical locus curve which forms the upper boundary of the liquid–vapor region.

The *P–T–x* phase diagram of the ethane–acetone system is typical of those systems whose components differ greatly in physical and chemical properties but which do not form azeotropes. Such systems invariably possess a point of maximum pressure in the critical locus curve. The diagrams of the propane– and n-butane–acetone systems are similar but due to the decrease in the volatility of the hydrocarbon component, there is a notable decrease in the value of the maximum critical pressure.

When n-pentane is substituted for n-butane, a folding of the *P–T–x* space occurs and a minimum temperature point appears in the critical locus curve in the pentane-rich region. As a consequence, the condition for the existence of a positive critical azeotrope is fulfilled. From an inspection of the diagram one can see that the critical azeotrope must occur in a mixture containing between 54 and 63 mole % n-pentane, whereas the minimum temperature point on the critical locus curve occurs in a mixture of about 85 mole % n-pentane. It is evident, therefore, that the critical azeotropic point and the minimum temperature point are separate and individual points, though it is possible that in some systems they may coincide.

As the critical temperatures of the components approach each other in the n-hexane–acetone system, the folding of the *P–T–x* space is more severe and the critical locus curve is nearly symmetrical around a constant pressure line drawn through the minimum temperature point. The composition of the minimum point is between 40 and 45 mole % hexane. In the n-heptane–acetone system, the critical locus curve terminates in a nearly vertical section in the acetone-rich region, making it difficult to decide whether or not a critical azeotrope is formed.

When n-octane replaces n-heptane, there is no minimum temperature point in the critical locus curve, though in the vicinity of pure acetone the slope of the curve approaches infinite slope. This becomes less pronounced in the n-decane–acetone and completely disappears in the n-tridecane system. To be noted also in the latter system is the return of the maximum pressure point in the critical locus curve.

Critical Pressure–Composition Relations. The variation of the critical pressure with composition, shown in Fig. 2, is noteworthy. The maximum critical pressure in the ethane–acetone system is 91 atm. in a mixture of 63 mole % ethane. This decreases to 58 atm. in a mixture of 45 mole % propane in the propane–acetone system and continues to decrease, becoming 47.5 atm. in a mixture of 20 mole % of n-butane in acetone. In all systems from n-pentane through n-octane, the critical pressure lies between the critical

The latter was not determined because of the thermal decomposition of the mixtures.

Critical Temperature–Composition Relationships. The critical temperature–composition relations for each of the systems are shown in Fig. 3. The broken line curve is the locus of the minimum temperature points. It is notable that only those systems whose critical temperatures lie within a given range of each other possess a point of minimum temperature. Since the latter are identifiable with systems that form azeotropes,

Figure 2. Critical pressure vs. composition relations.
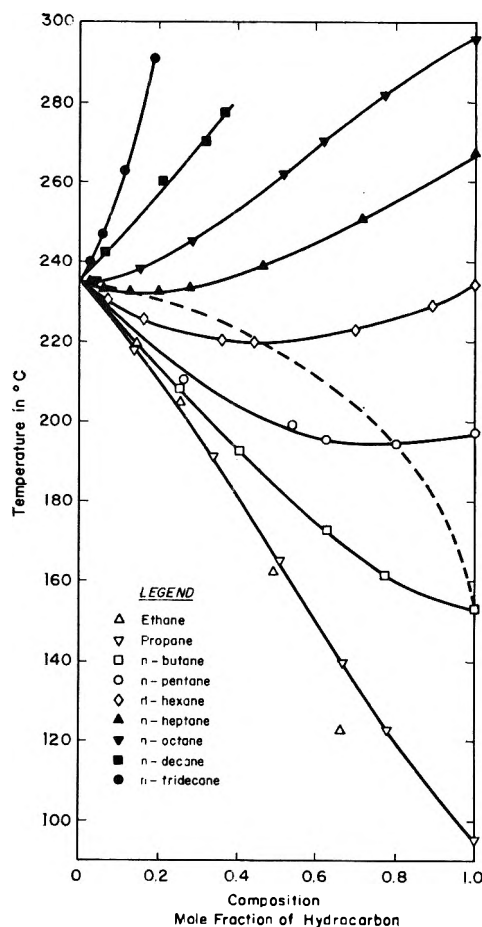
Figure 3. Critical temperature vs. composition relations.

pressures of the pure components with no maximum or minimum. In the n-decane–acetone system, the critical pressure decreases from the critical pressure of pure acetone, passes through a minimum pressure point of 45.6 atm. and a maximum pressure point of 45.9 atm. in mixtures containing 10 and 16% decane, respectively, and then decreases to the critical pressure of pure decane. Finally, in the n-tridecane system, the critical pressure shows a gradual increase and must eventually pass through a maximum pressure point.

this critical temperature range has been termed the critical "azeotropic range."[8] The azeotropic range of the systems under study is approximately 160 to 270°. Only the critical temperatures of n-pentane, n-hexane, and possibly n-heptane fall within this range. Kreglewski,[9] found similar relationships for the acetic acid–n-alkane and pyridine–n-alkane systems.

(8) A. Kreglewski, *Bull. Acad. Polon. Sci. Cl. III*, **5**, 323 (1957).

(9) (a) A. Kreglewski, *ibid.*, **5**, 329 (1957); (b) *Roczniki Chem.*, **31**, 1001 (1957).
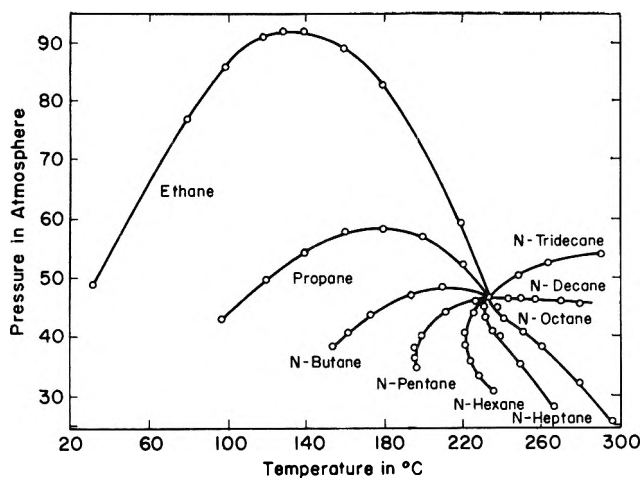
Figure 4. P-T critical locus curves.

These relations are quite similar to those existing between the standard boiling point and the azeotropic composition at atmospheric pressure, first noted by Swietoslawski in systems similar to those studied here.[10]

General Pattern of Phase Relations. When a composite plot is made of all of the critical locus curves, as in Fig. 4, there is revealed a pattern of phase relations which, in general, will be the same for many binary systems composed of a homologous series of compounds and a common positive azeotrope-forming compound. If the critical temperatures of the components differ greatly from each other, no azeotrope is formed and the critical locus curve will possess a point of maximum pressure. As the critical temperatures approach each other, the maximum critical pressure decreases until the critical temperature of the

homolog falls within the azeotropic range of the systems. When this occurs, the P-T-x space begins to fold, with the result that an azeotrope forms. Within the azeotropic range, the critical locus curve will possess a point of minimum temperature whose composition will vary from a mixture rich in the common component when the critical temperature of the homolog becomes greater than the critical temperature of the common component. Beyond the azeotropic range, the critical locus curve reverts to one with a maximum pressure.

The greatest deviation from this pattern of phase relations for systems whose components are completely miscible in the critical region may be expected when the critical pressures of the components differ greatly. For example, if the homolog has a critical pressure much lower than that of the common component and a critical temperature less than the common component but within the azeotropic range, a critical azeotrope may form without a minimum temperature point in the critical locus curve. Such conditions exist in the ethane–hydrogen sulfide system.[2] Other possible forms that the critical locus curve may take have been discussed in some detail in an earlier paper.[4]

(10) W. Swietoslawski, "Ebulliometric Measurements," Reinhold Publishing Corp., New York, N. Y., 1945, p. 114.

Carbon-13 Nuclear Magnetic Resonance Spectra of

Some Aromatic Amines and Imines

by Charles P. Nash and Gary E. Maciel

Department of Chemistry, University of California, Davis, California   *(Received October 19, 1963)*

The C^{13} nuclear magnetic resonance spectra of N,N-dimethylaniline, N,N-diethylaniline, and three N-phenyl-substituted cyclic imines have been examined. It is shown that the *para* chemical shift correlates well with other measures of phenyl-ring nitrogen resonance, such as ultraviolet spectroscopic data and molar refraction exaltation, for all the compounds studied. The *para* chemical shift correlates moderately well with the base strengths (in 50% ethanol) of all the compounds except N,N-diethylaniline. It is proposed that N,N-diethylaniline exhibits an anomalously high base strength in hydroxylic solvents arising from steric inhibition to hydrogen bonding in the free base.

Introduction

In a recent paper,[1] the ultraviolet spectra of N,N-dimethylaniline and a series of phenyl-substituted cyclic imines whose ring sizes varied from three to six members were reported. It was shown that the oscillator strengths of the two readily accessible absorption bands in the ultraviolet decreased in the same order as both the exaltation in molar refraction and the pK_A values of the compounds in 50% aqueous ethanol. By inference, the molecular property of major interest which changed from compound to compound was the degree of resonance interaction between the lone-pair electrons on nitrogen and the π-electrons of the benzene ring. Several experimental studies of C^{13} magnetic shieldings in aromatic rings[2-10] have shown that these parameters correlate with local π-electron densities. Karplus and Pople[11] recently investigated theoretically the various contributions to the C^{13} chemical shift in conjugated systems and showed that a significant charge-dependent term of this type is to be expected. We have chosen here to examine the C^{13} n.m.r. spectra of several phenyl-substituted cyclic imines, N,N-dimethylaniline, and N,N-diethylaniline to determine the extent to which the supposed resonance interaction is reflected in the magnetic shieldings of the various carbon atoms.

Experimental

Materials. The aromatic amines N,N-dimethyl-

aniline and N,N-diethylaniline were both Eastman White Label products, and were used without further purification.

The cyclic imines 1-phenylaziridine (three-membered ring), 1-phenylpyrrolidine (five-membered ring), and 1-phenylpiperidine (six-membered ring) were supplied by A. T. Bottini. Their preparation has been described earlier.[1] Spectro grade acetonitrile, benzene, and methanol were used in solvent studies to be discussed below. Ultraviolet spectra were taken with a Cary Model 14 recording spectrophotometer using matched 1.0-cm. glass-stoppered silica absorption cells.

N.m.r. Spectra. The carbon-13 magnetic resonance spectra were obtained at a fixed frequency of 15.1 Mc./sec. by measuring natural abundance C^{13} resonances, using dispersion mode and rapid passage condi-

(1) A. T. Bottini and C. P. Nash, *J. Am. Chem. Soc.*, **84**, 734 (1962).

(2) P. C. Lauterbur, *Ann. N. Y. Acad. Sci.*, **70**, (4), 841 (1958).

(3) P. C. Lauterbur, *J. Am. Chem. Soc.*, **83**, 1838 (1961).

(4) P. C. Lauterbur, *ibid.*, **83**, 1846 (1961).

(5) P. C. Lauterbur, *Tetrahedron Letters*, 274 (1961).

(6) P. C. Lauterbur, *J. Chem. Phys.*, **38**, 1406 (1963).

(7) P. C. Lauterbur, *ibid.*, **38**, 1415 (1963).

(8) P. C. Lauterbur, *ibid.*, **38**, 1432 (1963).

(9) H. Spiesecke and W. G. Schneider, *Tetrahedron Letters*, 468 (1961).

(10) H. Spiesecke and W. G. Schneider, *J. Chem. Phys.*, **35**, 731 (1961).

(11) M. Karplus and J. A. Pople, *ibid.*, **38**, 2803 (1963).

Table I: C^{13} Chemical Shifts and Other Properties of Aromatic Amines and Imines

Compound	Chemical shift (p.p.m. w.r.t. benzene)							f-sum	ΔR_D	pK_A
	C_1	C_{ortho}	C_{meta}	C_{para}	N–CH$_2$	C–C^{11}H$_2$	CH$_3$			
1-Phenylpyrrolidine	−20.3	15.5	−1.6	12.3	79.2[a]	100.4[a]	...	0.37	1.64	3.45
Diethylaniline	−19.9	15.3	−1.4	12.2	83.1	...	114.2	0.34	1.58	5.85
Dimethylaniline	−22.6	15.6	−1.0	11.5	...	...	89.0	0.33	1.49	4.39
Dimethylaniline (1:2 in acetonitrile)	−22.6	15.5	−0.9	11.8	...	...	88.4			
1-Phenylpiperidine	−24.7	10.9	−1.6	8.7	76.3[a]	101.0[a]	...	0.26	0.96	>5.2
1-Phenylaziridine	−27.4	7.3	−0.1	7.3	103.0	...	...	0.20	0.43	5.22
1-Phenylaziridine (1:2 in methanol)	−26.7	6.2	−1.5	6.2	99.1	...	...			

[a] The assignment of these peaks was based on a comparison with the chemical shift of cyclohexane carbons given by P. C. Lauterbur, *J. Chem. Phys.*, **26**, 217 (1957).

tions as described by Lauterbur.[3] The sample container was similar to that described by Spiesecke and Schneider[12] except for the absence of provisions for spinning the sample, and consisted of two concentric, thin-walled spherical bulbs about 0.2 and 1.4 cc. in volume, a geometry which eliminates the need for bulk susceptibility corrections in these results. The small inner bulb contained the reference, a saturated aqueous solution of sodium acetate enriched to 55% C^{13} at the carbonyl carbon. For calibration purposes, 300-c.p.s. side bands on the reference line were employed, and at least five forward and reverse sweeps were taken to minimize errors in line position caused by variations in sweep rate and saturation effects. The reproducibility of this technique was about ±5 c.p.s. or ±0.3 p.p.m. Since the shifts were determined with respect to a sodium acetate reference whereas it seemed desirable to report them with respect to benzene, a calibration of the acetate reference relative to benzene was obtained. The center of the benzene doublet was found to lie 804 ± 2 c.p.s. to higher field than the acetate reference. Thus a 53.6 ± 0.1 p.p.m. correction was applied to the raw data to convert them to shifts with respect to benzene, and the reproducibility of these derived shifts may also be considered to be about ±0.3 p.p.m.

Results and Discussion

Table I contains the C^{13} chemical shifts, referred to benzene, of all the interpretable peaks in the C^{13} n.m.r. spectra of the compounds we have examined. In addition we have included in the table the sum of the oscillator strengths (f-sums) of the ultraviolet absorption bands, the exaltation in molar refraction, ΔR_D, and the pK_A values of the bases in 50% aqueous ethanol. Most of the auxiliary data in Table I have been abstracted from ref. 1. The value of pK_A for

N,N-diethylaniline in 50% aqueous ethanol was determined by the method previously described.[1] The f-sum for N,N-diethylaniline has been estimated from the data of Wepster, *et al.*[13] The C^{13} n.m.r. spectrum of N,N-dimethylaniline has been reported previously by Spiesecke and Schneider[10] and by Lauterbur.[7] Our results for the chemical shifts of the benzene-ring carbons agree with those of Spiesecke and Schneider to within 0.3 p.p.m., all our values being smaller than theirs. The discrepancy is probably due to errors in the calibration of one or both of the external references with respect to benzene. Our values agree with Lauterbur's results for the ring carbons to within 0.7 p.p.m., no trend being present. Our value for the chemical shift of the N-methyl carbons exceeds Lauterbur's by 1.4 p.p.m. The agreement may be considered satisfactory, since Lauterbur's measurements were obtained at a lower radiofrequency (8.5 Mc./sec.), and he employed nonspherical sample containers.

One striking feature of Table I is the close similarity between the chemical shifts of N,N-diethylaniline and the five-membered ring compound. Evidently the electron distributions in the benzene rings of these two compounds are nearly the same, although the former is the strongest base in our series while the latter is the weakest. On the basis of their ultraviolet spectra, Wepster[13] has concluded that appreciable resonance interaction exists in all the higher N,N-dialkylated anilines, and the present n.m.r. data are in accord with this deduction. We shall shortly demonstrate that the exaltation in molar refraction, which is a commonly accepted measure of resonance interaction, correlates well with the *para*-carbon chemical shift of

(12) H. Spiesecke and W. G. Schneider, *J. Chem. Phys.*, **35**, 722 (1961).
(13) J. A. C. Browers, S. C. Bijlsma, P. E. Verkade, and B. M. Wepster, *Rec. trav. chim.*, **77**, 1080 (1958).

all the compounds here studied. The exaltation in the molar refraction of N,N-diethylaniline further indicates that there must be a substantial resonance interaction in this compound. It is therefore apparent that the relatively high basicity of this compound is anomalous, when viewed from the standpoint of its resonance stabilization.

It is well known that the pK_A values of the series of symmetrically substituted N,N-dialkyl anilines in alcohol or water solution display a maximum about 1 pK unit high at diethylaniline.[13,14] The basicities of the higher homologs are essentially constant. On the basis of inductive effects, as measured by the relative base strengths within numerous series of alkylamines having the same degree of substitution of the nitrogen atom,[15] one might reasonably expect the basicity of N,N-diethylaniline to exceed that of N,N-dimethylaniline by perhaps 0.6 pK unit, but no fall in pK_A at N,N-dipropylaniline is to be anticipated.

Taylor,[16] in a previous discussion of this problem, has attributed the observed drop in pK_A to a steric strain in the anilinium ion arising from interaction between the alkyl side chains and the *ortho* positions of the benzene ring when the alkyl groups contain three or more carbon atoms. We are in agreement with this view. His argument that basicity of free diethylaniline is enhanced by steric inhibition of resonance is, however, untenable in the light of the present results.

Recent work by Forman and Hume[17] has shown that a good correlation exists between the heat of neutralization of aromatic amines by hydrogen bromide in acetonitrile solution and the basicity of the amines in water, as measured by pK. The one conspicuous deviation from this correlation occurred with N,N-diethylaniline. These workers assume N,N-diethylaniline is a weaker base than it should be in acetonitrile. If we adopt a counter proposal, namely that N,N-diethylaniline is a stronger base than it should be in water, the curious behavior of the dialkyl anilines can be understood.

We suggest that the alkyl groups in free N,N-diethylaniline produce a sufficiently cluttered situation in the vicinity of the nitrogen atom that hydrogen bonding between hydroxylic solvent molecules and the nitrogen atom is inhibited. The resulting loss of solvation energy will increase the free energy of the free base, reduce the energy gap between N,N-diethylaniline and its anilinium ion, and correspondingly increase the base strength of the former, relative to dimethylaniline, by an additional amount over and above the "normal" increase which arises from inductive effects.

Indirect evidence for this proposal may be inferred

from miscibility studies of dialkylated anilines with hydroxylic solvents. In mixtures containing either ethylene glycol or glycerol, the critical solution temperature of N,N-diethylaniline exceeds that of N,N-dimethylaniline in each case,[18] and hence the excess free energy of mixing of the former compound must be the larger. Similarly, diacetone alcohol is completely miscible with N,N-dimethylaniline but immiscible with N,N-dipropylaniline,[19] a fact which also indicates a more positive free energy of mixing for the higher homolog.

Much more direct evidence for our hypothesis may be obtained from an examination of the ultraviolet absorption spectrum of N,N-diethylaniline dissolved in both methanol and acetonitrile. The principal absorption maxima in these two solvents differ in intensity by only 3%, and have essentially the same extinction coefficient as was observed by Wepster, *et al.*,[13] in isooctane solution. Moreover, the absorption maximum is at 261.9 mμ in acetonitrile, at 260.8 mμ in methanol, and at 259 mμ in isooctane. Our previous studies[1] indicate that if N,N-diethylaniline were as strong an electron donor as its pK leads one to believe, the absorption maxima in the two polar solvents would be separated by at least 5 mμ, the maximum in methanol would be displaced to shorter wave lengths relative to isooctane, and the extinction coefficient would be smaller in methanol than in either acetonitrile or isooctane by some 20%. As regards solvent effects on ultraviolet spectra, N,N-diethylaniline is again remarkably similar to 1-phenylpyrrolidine.

In summary, we propose that the order of base strengths of the N,N-dialkylanilines can be explained by assuming that the dimethyl and diethylanilinium ions have virtually equal free energies in solution but the free N,N-diethylaniline is less solvated than the free N,N-dimethylaniline, and hence appears to be too basic by several tenths of a pK unit. The free energies of the neutral N,N-diethyl- and N,N-dipropylanilines are nearly equal, but to form the dipropylanilinium ion requires a free energy expenditure attributable to steric strain, and hence the base strength of the N,N-dipropylaniline is correspondingly reduced.

The remainder of the data on the pure liquids in

(14) N. F. Hall and M. R. Sprinkle, *J. Am. Chem. Soc.*, **54**, 3469 (1932).

(15) H. K. Hall, *ibid.*, **79**, 5441 (1957).

(16) H. T. Taylor, *Nature*, **181**, 265 (1957).

(17) E. J. Forman and D. N. Hume, *J. Phys. Chem.*, **63**, 1949 (1959).

(18) A. W. Francis, "Critical Solution Temperatures," Advances in Chemistry Series, No. 31, American Chemical Society, Washington, D. C., 1961, pp. 70, 73.

(19) J. S. Drury, *Ind. Eng. Chem.*, **44**, 2744 (1952).

Table I require little discussion. The chemical shifts of the *meta* carbons are rather insensitive to structural variations, as is generally the case,[2-4,6-8] whereas the *para*-carbon shieldings reflect rather well the changes in the phenyl-ring nitrogen resonance interaction which are to be expected on the basis of the oscillator strengths, molar refraction exaltations, and even pK_A values.[7] For example, in 1-phenylaziridine, which gives the least other evidence of resonance interaction, the *para*-carbon shifts relative to benzene are the smallest tabulated.

It might be assumed that the small variations in the *meta*-carbon shieldings arise from effects which do not depend on the resonance interaction: e.g., changes in ring currents and local electron densities produced by inductive effects. Such effects might be expected to influence *meta* and *para* positions more or less equally. If we "correct" the observed *para* chemical shifts by the amount of the corresponding *meta* shifts, we may attempt to correlate the "corrected" shifts, as measures of the resonances contributions to the local π-electron densities, with other physical properties.

Some justification for considering our "corrected" *para* chemical shifts as being determined by resonance interactions can be found in the well-known correlations of the F[19] magnetic resonance shielding constants of *meta*- and *para*-substituted fluorobenzenes with
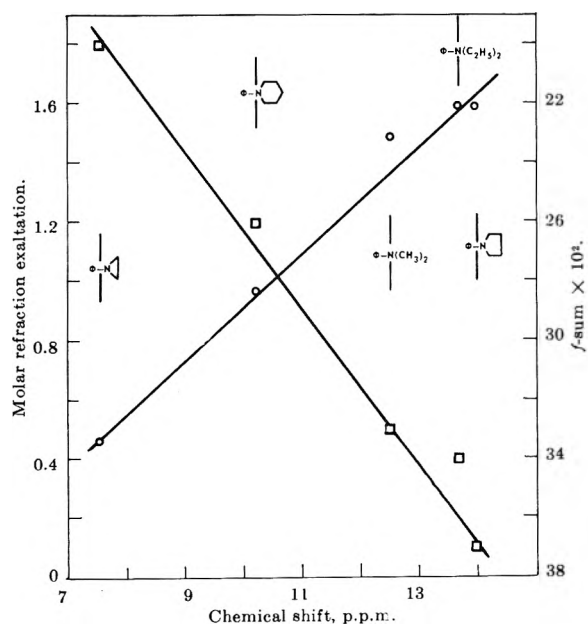
Taft's inductive and resonance parameters.[20-23] Taft has demonstrated that the *difference* between the F[19] chemical shifts of *para*- and *meta*-substituted fluorobenzenes is directly proportional to the resonance parameters σ_R[20] and σ_R^0[21] of the substituent. Whereas the F[19] shifts of *para*-substituted fluorobenzenes depend linearly on both the inductive parameter σ_I and on σ_R or σ_R^0, the F[19] shifts of *meta*-substituted fluorobenzenes are proportional to σ_I, but are independent of the resonance parameters.[20,21] These relationships bear an apparent resemblance to the present treatment if we assume that our uncorrected C[13] shifts are influenced by both inductive and resonance effects while the "corrected" shifts depend mainly on resonance interactions.

It is found empirically that a correction of the kind indicated yields definite improvement in the correlations to be discussed below. In Fig. 1 we have plotted the "corrected" *para* shift against both the *f*-sum and the ΔR_D values. Sensibly linear plots obtain in both cases, but whereas N,N-diethylaniline is well removed from the line for the *f*-sum, it is definitely in line with regard to the exaltation in refraction. On this fragmentary evidence we might conclude that the exaltation in refraction is probably the best simple measure of resonance interaction in the N-alkylated anilines.

To the extent that variations in magnetic anisotropy may be neglected within this class of closely similar compounds, we may conclude that the changes in the π-electron densities of the C-1 and the *ortho* carbon atoms parallel those on the *para* carbon, and are somewhat larger in magnitude.

Lauterbur[7] found that within a series of ring-methylated N,N-dimethylanilines the N-methyl shieldings decreased linearly as pK_A increased. Our data on 1-phenylpyrrolidine and 1-phenylpiperidine show a similar decrease in the shielding of the N-methylene carbons. In this respect N,N-diethylaniline again appears to be anomalous.

Our previous studies[1] indicated the possibility of appreciable amine–solvent interaction in polar and hydroxylic solvents. We assumed that a bathochromic shift in acetonitrile *vs.* isooctane could be interpreted as solvent-stabilization of the highly polar excited state, while the fact that the spectra in methanol show a hypsochromic shift relative to the acetonitrile medium was supposed to reflect a hydrogen-bonding stabiliza-

Figure 1. Correlation between "corrected" *para* chemical shift and molar refraction exaltation or oscillator strengths for three N-phenyl-substituted cyclic imines and two N,N-dialkylanilines.

(20) R. W. Taft, Jr., *J. Am. Chem. Soc.*, **79**, 1045 (1957).

(21) R. W. Taft, Jr., S. Ehrenson, I. C. Lewis, and R. E. Glick, *ibid.*, **81**, 5352 (1959).

(22) R. W. Taft, Jr., E. Price, I. R. Fox, I. C. Lewis, K. K. Andersen, and G. T. Davis, *ibid.*, **85**, 709 (1963).

(23) R. W. Taft, Jr., *J. Phys. Chem.*, **64**, 1805 (1960).

tion of the free base. If these explanations are correct, the C^{13} n.m.r. spectra in acetonitrile solution should be virtually unaffected while the ring carbons would be expected to experience changes in shielding in methanol solution due to hydrogen bonding. As the greatest bathochromic shift was observed with N,N-dimethylaniline and the greatest hypsochromic shift with N-phenylaziridine, these two systems were selected for the present experiments. In addition, 50 mole % solutions of N,N-dimethylaniline in benzene and N-ethylethylenimine were examined to assess the effects, if any, of dilution with structurally similar molecules. As the results in Table I show, the n.m.r. spectrum of N,N-dimethylaniline in acetonitrile is identical with that of the pure liquid within experimental error. Similar results were also obtained when benzene and N-ethylethylenimine were employed as diluents. The environments of the phenyl-ring carbons of 1-phenyl-aziridine, on the other hand, are definitely altered by

the presence of methanol. The resonance lines of the *ortho*, *meta*, and *para* carbons were all displaced downfield by about 1.1 p.p.m., while the C_1 resonance moved upfield by 0.7 p.p.m. Since the difference between the *para* and *meta* carbon shifts is essentially unchanged by the presence of methanol, one might conclude that the resonance interaction between the nitrogen atom and the benzene ring is largely unaffected by a hydrogen bond, while some change in the ring-carbon electron densities does occur as a result of a modified inductive effect. Similarly, the N-methylene carbons are very much less shielded in the presence of methanol. Evidently, an electron acceptor polarizes the charge distribution about nitrogen in such a way that electrons flow toward the nitrogen lone pair from both the phenyl ring and the imine ring. It is interesting that the C-1 position seems to behave like a bottleneck, in that its charge density appears to be enhanced by the flow from more remote locations within the molecule.

The Effects of Solvents and of Solid Substrates on the Visible

Molecular Absorption Spectrum of Cyanine Dyes

by W. West and A. L. Geddes

Kodak Research Laboratories, Eastman Kodak Company, Rochester, New York   *(Received October 26, 1963)*

The solvent displacement of the molecular absorption maximum of representative cyanine dyes was found to be linear in the refractive index of the solvent or in various refractive index functions. The dielectric constant, hydrogen-bonding capacity, or surface tension of the solvent had little influence on the displacement, which is determined essentially by dispersion interactions and can be interpreted as the "universal red shift" of Bayliss. In binary solvent mixtures of varying composition, deviations from linearity of the frequency of the absorption maximum with the refractive index, when the components differ considerably in polarity, point to selective solvation of the dye cations in the mixed solvents. At low coverages of an adsorbed cyanine dye on solid substrates, the structure of the absorption spectrum reduplicated that of the molecular spectrum in solution, and the position of the maximum was mainly governed by the refractive index of the substrate. The displacement coefficient, the frequency shift per unit change in refractive index or in refractive index function, for adsorbed dye was little more than half that for the dye in solution, probably because of the one-sided interaction of the medium in adsorption. The spectrum of the adsorbed molecular dye on silver chloride and silver bromide fell, for the most part, in line with those on other substrates, but silver iodide induced a uniquely great tendency to dye–dye aggregation, even at very low coverages. Anomalously small displacements of the molecular spectrum of the dye on some hydrated surfaces can be attributed to interaction between adsorbed dye and adsorbed water molecules. On unfired samples of zinc sulfide prepared under acid conditions by precipitation of zinc ion by hydrogen sulfide, proton transfer from active acidic sites in the surface of the substrate caused the dye to be adsorbed in a colorless form from solvents of acidic nature.

Part I. Spectra in Solution

Cyanine dyes exhibit only small bathochromic solvent displacements of their visible absorption spectra[1,2] in contrast to the relatively large displacements observed among merocyanine dyes, some of which exhibit hypsochromic displacements when dissolved in polar solvents.[3-6] The chromophore in both of these types of dye molecule consists of N or O atoms, of variable valence, linked by a conjugated chain of carbon atoms. The cyanine chromophore is the singly charged cation

$$>\overset{+}{N}=C-(C=C-)_nN<,\ n = 1,2\ldots,$$ which resonates with an equivalent terminal structure in which the positive charge is carried by the other N atom, with a concomitant rearrangement of single and double bonds.

A typical merocyanine chromophore is the resonance hybrid between the structure $>N(-C=C)_n-C=O$, $n = 1,2\ldots$, and the usually energetically nonequivalent, over-all uncharged but highly polar structure

(1) S. E. Sheppard, P. T. Newsome, and H. R. Brigham, *J. Am. Chem. Soc.*, **64**, 2923 (1942).

(2) S. E. Sheppard, *Rev. Mod. Phys.*, **14**, 303 (1942).

(3) L. G. S. Brooker, G. H. Keyes, R. H. Sprague, R. H. Van Dyke, E. Van Lare, G. Van Zandt, F. L. White, H. W. J. Cressman, and S. J Dent, Jr., *J. Am. Chem. Soc.*, **73**, 5332 (1951).

(4) L. G. S. Brooker, G. H. Keyes, and D. W. Heseltine, *ibid.*, **73**, 5350 (1951).

(5) L. G. S. Brooker, Experimenta Supplementum II, XIV Internat. Conf. Pure and Applied Chemistry, 1955, p. 229.

(6) A. I. Kiprianov, *Russ. Chem. Rev.*, **29**, 618 (1960).

$>N(=C-C)_n=C-O.$ [3] Brooker[3-5] interpreted the peculiarities of the solvent displacements of the spectra of merocyanine dyes as originating in the differential stabilization of the unpolarized and polarized structures by electrostatic interactions with the molecules of polar solvents, and essentially equivalent interpretations, in terms of differential stabilization of the dipoles of the ground and excited states of these dyes and of other molecules containing intramolecular ionoidic chromophores, have been proposed.[7-12]

Any solvent effect on the position of the absorption spectrum of a solute must originate in the differential interaction of solvent molecules on the ground and excited states of the solute (greater stabilization of the excited than of the ground state causing a shift to longer wave lengths, and preferential stabilization of the ground state causing a shift to shorter wave lengths), but the cyanines, because of their lack of strong permanent dipoles in the chromophore, cannot be subject to the types of solvent interaction responsible for the large spectral effects of solvents on the merocyanines. No systematic study of solvent effects on the absorption of cyanine dyes seems to have been published, and the following observations were therefore made to determine what properties of the solvent did govern the position of the absorption spectrum of those dyes.[13]

The refractive index turns out to be the macroscopic property of the solvent that essentially determines the absorption of dissolved cyanines; the dye–solvent interaction originates mostly in dispersion forces. In the adsorbed state of the dye at low concentrations on solid adsorbents, also, the refractive index of the adsorbent appears to be the most important factor in determining the position of the absorption band (part II).

This study is restricted to the spectrum of the dye as isolated molecules, contrasted with the dimers and multimolecular aggregates that appear with increasing concentration of the dyes in aqueous solution and in the adsorbed state. Dimers and higher aggregates rarely appear in organic solvents at room temperature. In the formation of adsorbed layers, conditions were chosen so that the absorption band of isolated adsorbed molecules alone was present or predominated in the spectrum.

Experimental

Dyes I, II, and III of the 2,2'-cyanine series were examined, along with the thiacyanine dyes, IV and V (Table I).

Molecules III, IV, and V are probably nearly co-

Table I
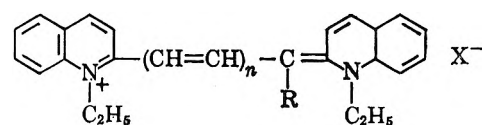
I.   1,1'-Diethyl-2,2'-cyanine chloride, $n = 0$, $R = H$, $X^- = Cl^-$

II.   1,1',9-Triethyl-2,2'-cyanine perchlorate, $n = 0$, $R = C_2H_5$, $X^- = ClO_4^-$

III.   1,1'-Diethyl-2,2'-carbocyanine chloride, $n = 1$, $R = H$, $X^- = Cl^-$
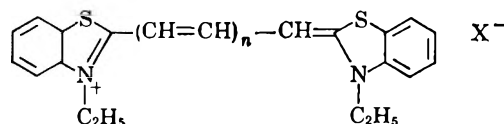
IV.   3,3'-Diethylthiacyanine iodide, $n = 0$, $X^- = I^-$

V.   3,3'-Diethylthiacarbocyanine chloride, $n = 1$, $X^- = Cl^-$

planar with respect to the atoms in the heterocyclic nuclei and the chromophore; in I, the two quinoline nuclei are probably slightly twisted from coplanarity about the methine bridge because of some steric impingement of the hydrogen atoms in the 3- and 3'-positions, and in II, the heterocyclic nuclei are strongly forced from coplanarity because of the severe crowding introduced by the ethyl group in the bridge.[14] Consequently, the intensity of absorption of II is considerably lower than that of I.[14]

The solvents used were Eastman Grade organic chemicals, selected to show wide variations in dielectric constant, D, refractive index, n, and in hydrogen-bonding capacity. They are listed in Table II, together with values of the dielectric constant and the refractive index and of the function $(n^2 - 1)/(2n^2 + 1)$, introduced into the analysis of spectral solvent displacements by Bayliss.[10,15]

The spectra were examined in dilute solution, about 10^{-5} M, by a Cary spectrophotometer, Model 14. The dye dissolved with difficulty in some of the sol-

(7)   T. Förster, Z. Elektrochem., 45, 548 (1939).

(8)   W. T. Simpson, J. Am. Chem. Soc., 73, 5359 (1951).

(9)   E. Lippert and F. Moll, Z. Elektrochem., 58, 718 (1954).

(10)   Y. Ooshika, J. Phys. Soc. Japan, 9, 594 (1954).

(11)   J. R. Platt, J. Chem. Phys., 25, 80 (1956).

(12)   E. G. McRae, Spectrochim. Acta, 12, 192 (1958).

(13)   Bathochromic shifts of the spectra of cyanine dyes dissolved in cellulose acetate films with increasing pressure have been reported recently by G. A. Samara, B. M. Riggleman, and H. G. Drickamer, J. Chem. Phys., 37, 1482 (1962).

(14)   L. G. S. Brooker, F. L. White, R. H. Sprague, S. G. Dent, Jr., and G. Van Zandt, Chem. Rev., 41, 325 (1941).

(15)   N. S. Bayliss, J. Chem. Phys., 18, 292 (1950).

Table II: Solvents Used

	Solvent	D_{25}	$n^{25}D$	$\dfrac{n^2 - 1}{2n^2 + 1}$
1	Methanol	32.6	1.329	0.169
2	Water	78.5	1.333	.171
3	Acetonitrile	37.0	1.345	.175
4	Methyl acetate	6.6	1.359	.181
5	Acetone	20.7	1.359	.181
6	Propionitrile	27.0	1.368	.183
7	n-Propyl alcohol	20.1	1.378	.187
8	2-Butanone	18.5	1.379	.187
9	n-Heptane	1.9	1.388	.192
10	Pentyl alcohol	13.9	1.397	.194
11	n-Butyl alcohol	17.1	1.399	.195
12	4-Methylvaleronitrile	15.0	1.404	.196
12a	Tetrahydrofuran	...	1.404	.196
13	Dichloromethane	9.1	1.424	.204
14	Octyl alcohol	10.1	1.430	.205
15	Dimethylnitrosoamine	52.0	1.437	.207
16	1,2-Dichloropropane	8.9	1.439	.208
17	Dodecyl alcohol	6.5	1.440	.208
18	1,2-Dichloroethane	10.4	1.445	.210
19	Formamide	107.0	1.447	.210
20	Cyclohexanone	18.2	1.451	.212
21	1,2,3-Trichloropropane	7.3	1.484	.222
22	Chloroform	4.7	1.490	.224
23	Benzene	2.3	1.501	.227
24	Pentachloroethane	3.7	1.504	.228
25	Pyridine	12.3	1.509	.230
26	Iodoethane	7.8	1.513	.231
27	Chlorobenzene	5.6	1.525	.234
28	Iodomethane	6.7	1.531	.236
29	1,2-Dibromoethane	4.8	1.538	.238
30	Dibromomethane	7.1	1.541	.240
31	Bromobenzene	5.4	1.560	.244
32	Ethyl cinnamate	6.1	1.560	.244
33	Bromoform	4.4	1.596	.254
34	Iodobenzene	4.6	1.620	.260
35	1,1,2,2-Tetrabromoethane	6.8	1.638	.264
36	1-Bromonaphthalene	4.8	1.658	269
37	Diiodomethane	5.3	1.740	.287

Figure 1. Absorption spectra of 1,1'-diethyl-2,2'-cyanine chloride in various solvents: (1) methanol; (2) pyridine; (3) methylene iodide.

vents, and in such cases, 0.5 to 1% methanol added to the solvent facilitated solution of dyes I, III, IV, and V, and 1% 1,2,3-trichloropropane aided that of dye II. In solvents in which the dye dissolved without difficulty, the addition of 2% methanol shifted the absorption maximum by no more than 0.5 mμ, and it appears reasonable to assume that the spectra in solvents containing no more than 1% of auxiliary solvent are, within the precision of measurement, insignificantly different from those in the pure solvents.

Results

As is shown in Fig. 1, the shape of the absorption bands is essentially the same in the different solvents, with only minor differences in the separation and in the intensity ratios of the submaxima with respect to the main maximum. The invariance of the band structure over such a range of solvents, differing greatly in polarity and tendency to form hydrogen bonds, suggests that the sequence of maxima and shoulders represent poorly resolved vibrational structure in a single electronic transition. There appears to be a vibrational interval of about 1300 cm.$^{-1}$, about that to be expected from a conjugated C=C linkage in the excited electronic state. The data reported refer to the position of the main maximum, which probably is approximately the frequency of the $0 \leftarrow 0$ transition of the spectrum.

The only property of the solvent which can be correlated with the observed positions of the maximum of the absorption band of these dyes is the refractive index; the absorption maximum is displaced regularly to longer wave lengths with increasing refractive index. In Fig. 2 and 3 the wave number of the absorption maximum is shown to be in essence linear in the function $(n^2 - 1)/(2n^2 + 1)$, suggested by Bayliss[15] to be the relevant solvent parameter that controls the "general red shift" caused by interaction between the solvent and the transition dipole moment of the solute
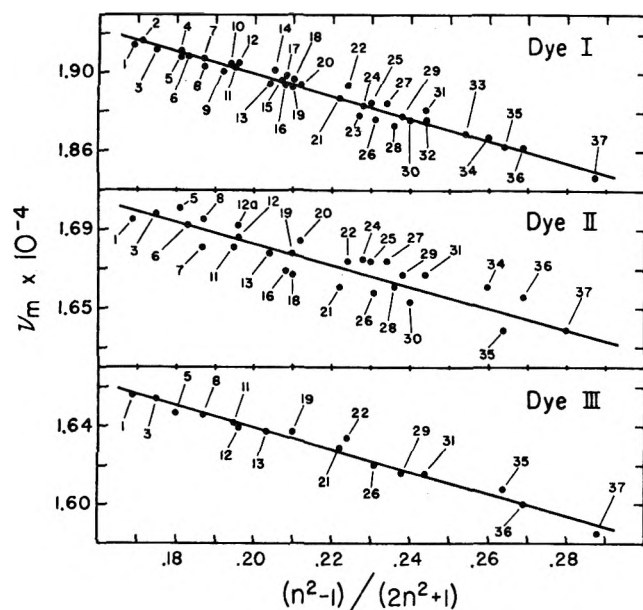
Figure 2.   Molecular absorption band maxima of 2,2'-cyanine dyes in relation to the Bayliss refractive index function.
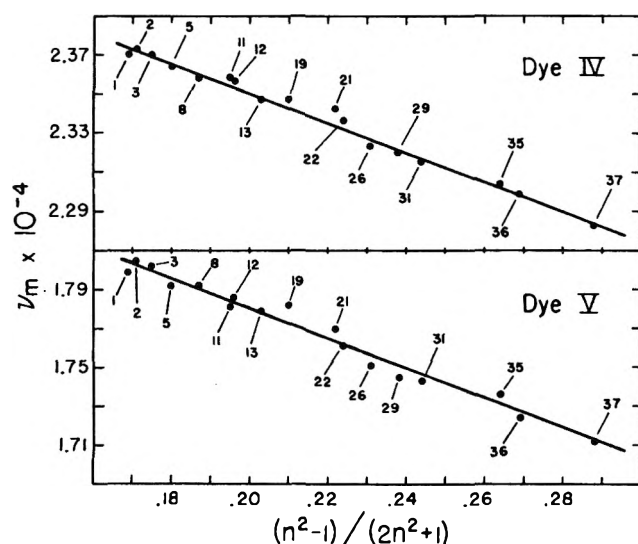
Figure 3.   Molecular absorption band maxima of thiacyanine dyes in relation to the Bayliss refractive index function.

chromophore.[15-17] A somewhat similar deduction of the spectral shift of nonpolar solutes in nonpolar solvents predicts a bathochromic shift proportional to the polarizability of the solvent,[18] or to $(n^2 - 1)/(n^2 + 2)$.[19a]

There is no correlation between the spectral shift of the cyanines and the dielectric constant of the solvent, or additive functions of the dielectric constant and the refractive index, or with Kosower's Z-value.[19b] Nor are the shifts well correlated with the surface

tension of the solvent, as might be expected if the effect of the restrictive solvent cage on the energies of the ground and excited states of the solute, as considered by Bayliss and Rees,[20,21] were an important factor. The solvents included in Fig. 2 and 3 differ greatly in hydrogen-bonding power, and the fact that the spectral displacements are so nearly linear in refractive index indicates that hydrogen bonding is not involved in the environmental interaction responsible for the shifts.

With regard to the refractive index factor, linearity of the spectral shift in the function $(n^2 - 1)/(2n^2 + 1)$ is not unique; the refractive index itself, plotted against the frequency of maximum absorption, yields as satisfactory a straight line, as does the electronic polarizability function $(n^2 - 1)/(n^2 + 2)$. What seems certain is that the refractive index is the essential macroscopic property of the solvent that determines the position of the molecular spectra of these dyes in solution. The observed scatter is partly attributable to experimental error, the precision of the maxima being about ± 0.5 mμ in wave length, equivalent to about ± 18 cm.$^{-1}$ in the wave number. The observed maxima may also differ from the position of the $0 \leftarrow 0$ transition by slightly different amounts in different solvents, and probably other factors than the refractive index, such as molecular size and shape, as well as permanent dipolar properties influence the absorption maximum to minor extents.

Discussion

The approximate equations of McRae[17] for the total solvent-induced displacement of the absorption spectrum associated with a strong optical transition in a dissolved chromophore may serve as the basis of discussion of the experimental observations on the cyanines. In McRae's treatment, the spectral shift is the result of additive contributions arising from the interaction of all the dipoles present in the system in the radiation field, including the transition dipole induced by the light in the solute molecule, any permanent dipoles in the solute and solvent molecules, and the induced dipoles associated with the polarizability of solute and solvent molecules. The interaction between the rapidly fluctuating transition moment and the solvent involves only the electronic polarizability

(16) N. S. Bayliss and E. G. McRae, J. Phys. Chem., 58, 1002 (1954).

(17) E. G. McRae, ibid., 61, 562 (1957).

(18) H. C. Longuet-Higgins and J. A. Pople, J. Chem. Phys., 27, 192 (1957).

(19) (a) F. A. Bovey and S. S. Yanari, Nature, 186, 1012 (1960); (b) E. M. Kosower, J. Am. Chem. Scc., 80, 3253 (1958).

(20) N. S. Bayliss and A. L. G. Rees, J. Chem. Phys., 8, 377 (1940).

(21) A. L. G. Rees, ibid., 8, 429 (1940).

of the solvent molecules, and can be described as a dispersive interaction. For strong transitions such as those associated with the visible absorption of cyanine dyes, the dispersive contribution to the shift is approximately[17]

$$\Delta\nu\text{(dispersive)} = -2.14 \times 10^{-14} \frac{Lf}{a^3} \frac{n^2 - 1}{2n^2 + 1} \quad (1)$$

The shift is measured from the position of the absorption in the vapor, f is the oscillator strength of the transition of the solute, and a is the Onsager cavity radius[22] of the solute molecule. L is a property of the solvent, the "weighted mean wave length," the value of which for solvents absorbing at wave lengths distant from the absorption band of the solute corresponds to a wave length in the far-ultraviolet region and can be regarded as approximately constant for different solvents, at about 1250 Å., and n is the refractive index of the solvent. The dispersive interaction produces a bathochromic displacement referred to as the "general red shift."

If the solute molecule contains permanent dipoles, a contribution to the spectral shift depending on the refractive index of the solvent arises from the reaction back on the solute of the dipoles induced by the solute in the solvent molecules. This contribution is approximately

$$\Delta\nu\text{(dipole-induced dipole)} = \frac{M_g^2 - M_e^2}{hca^3} \frac{n^2 - 1}{2n^2 + 1} \quad (2)$$

where M_g and M_e are the dipole moments of the solute in the ground and excited states, and h and c have their usual significance. Permanent solute dipoles also come under the influence of the fields of oriented permanent solvent dipoles, yielding a contribution to the shift, $\Delta\nu$(orientation), approximately expressed by a form similar to (2), but including terms in the dielectric constant and polarizability of the solute in the ground and excited states in addition to the refractive index. The spectral shifts of merocyanines and of other internal ionoidic compounds in different solvents are dominated by the orientation contribution,[11] or by an additive superposition of the dispersive and of the orientation contributions.[23]

The insignificance of any dielectric constant term in the solvent effect on the absorption of cyanine dyes shows that there is very little difference in the permanent dipole moments of their ground and excited states. It is not immediately obvious that cyanine cations are "nonpolar solutes." As ions they must exert an electrostatic attraction on polar solvent molecules, and the fact that their crystals from polar solvents tend to

be solvated[24] suggests appreciable interaction between dye cations and dipolar solute molecules. In nonaqueous solvents, the dye is probably present, even in dilute solution, largely as ion pairs, i.e., as polar aggregates of the cation and anion, and the positive charge of the dipole is in the chromophoric part of the dye.

Such dipole moments, however, are largely outside the chromophore, and must be small in comparison with the static moments present in the chromophore of strongly polar merocyanines. The concentration of absorption in the 0 ← 0 vibrational transition in the spectra of the cyanines indicates that bond lengths are not very different in the ground and excited states, and the fact that for fluorescent cyanines, the Stokes shift is not very large shows that the Franck–Condon configuration of the excited state is not highly strained. The shape of the molecule is not greatly changed on excitation and the static moments and polarizabilities are therefore not greatly different in the ground and excited states. These general considerations indicate why orientation polarization makes only minor contributions to the spectral shifts of cyanine cations, and the dispersive term must then predominate.

According to the Bayliss–McRae formulation, the magnitude of the dispersive contribution to the spectral shift is proportional to the quotient of the oscillator strength of the solute and the cube of the Onsager radius. In the third and fourth columns of Table III the displacement coefficient, the change in frequency of the absorption maximum per unit change of the function $f(n) = (n^2 - 1)/(2n^2 + 1)$, is compared with the value of the oscillator strength, f, of the dyes investigated.

Table III: Solvent Displacements and Oscillator Strengths of Cyanine Dyes

Dye	$E \times 10^{-5}$	$\int E d\nu \times 10^{-8}$	f	$\Delta\nu/\Delta[f(n)] \times 10^{-3}$	a(Å), calcd.
I	0.74	1.74	0.75	−5.7	8.3
II	0.20	0.72	0.31	−5.5	2.5
III	1.89	2.88	1.24	−5.6	5.9
IV	0.90	2.12	0.91	−7.5	8.2
V	1.54	2.36	1.02	−7.6	8.3

In the table, E is the molar extinction coefficient of the dye at the absorption maximum, and f is computed from the relation $f = 4.313 \times 10^{-9} \int E d\nu$. Dye III

(22) L. Onsager, J. Am. Chem. Soc., 58, 1486 (1936).

(23) O. Popovych and L. B. Rogers, ibid., 81, 4469 (1959).

(24) P. J. Wheatley, J. Chem. Soc., 3245 (1959).

is the higher vinylogous homolog of I, and shows the normal increase in E and f resulting from the addition of a double bond in the methine bridge of the chromophoric chain. Dyes IV and V are similarly related. The oscillator strength of the crowded dye II is less than half its value in dye I, but the displacement coefficient is about the same as that for dye I, as is also that for III, which has a higher oscillator strength than I and II. On the other hand, the displacement coefficient for the dyes IV and V containing benzothiazole nuclei is distinctly greater than for the dyes derived from quinoline, although the oscillator strengths are comparable. Using McRae's approximate value of 1250 Å. for the parameter L in eq. 1, one can evaluate a, the cavity radius of the solute molecule, from the experimental value of the displacement coefficient. The values thus calculated, listed in the fifth column of Table III, are considerably smaller than the values corresponding to the dimensions of the dye molecules.

If, for the moment, the small calculated value of the cavity radius is neglected, the conclusion to be drawn from the application of the Bayliss–McRae treatment is that in interaction with solvents the low value of the oscillator strength of dye II is compensated for by a smaller distance of approach of the perturbing solvent molecules to the chromophore of this dye. It is not clear from the structures of dyes I and II how this can be; the presence of the 9-ethyl substituent would appear to inhibit access of solvent molecules to this dye more than to dye I. In general, the theory is not in very satisfactory agreement with observation regarding the dependence of the spectral solvent shift on the intensity of the absorption band of the solute. The low values of the cavity radius a usually calculated from the shifts may possibly be explained, as suggested by Bayliss and Hulme,[25] if the transition moment is buried within the solute molecule, the outer parts of which may function as part of the solvent in its dispersion interaction with the chromophore, but the observed shifts of feeble bands, according to current data, seem to be much larger in comparison with those of strong bands than the Bayliss–McRae treatment predicts. For example, the observed shifts of the strong benzene transition at 2000 Å. and of the weak transition at 2600 Å. are only in the ratio of from 2:1 to 4:1, although the oscillator strengths are in the ratio of about 45:1.[25]

Spectra of Cyanines in Solvent Mixtures. The effect on the absorption spectrum of changing the refractive index of the solvent by using as solvent binary mixtures of different compositions is shown in Fig. 4 and 5. The mixtures used were acetonitrile–methylene iodide, acetone–methylene iodide, and methylene chloride–
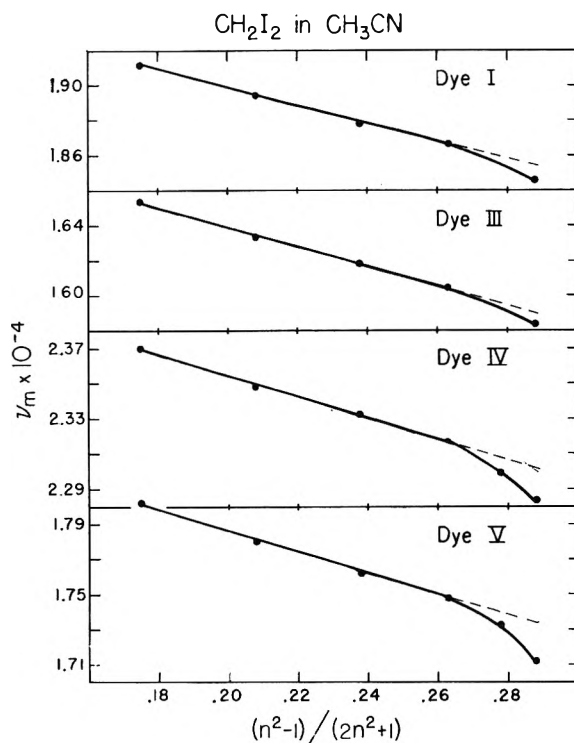
Figure 4. Molecular absorption band maxima of cyanine dyes in mixtures of CH_2I_2 and CH_3CN in relation to the Bayliss refractive index function.

methylene iodide. The two extreme points in each curve refer to the pure liquids as solvents. In acetonitrile–methylene iodide (Fig. 4), the displacements of the two thiacyanines examined, dyes IV and V, are practically linear in the Bayliss function (or in the refractive index itself) in solutions containing from 0 to about 90% by weight of methylene iodide; at higher concentrations of methylene iodide, the curve plunges downwards, indicating disproportionally large bathochromic displacements for the last additions of methylene iodide, or disproportionally large hypsochromic displacements caused by the first additions of acetonitrile to methylene iodide. The corresponding deviation from linearity is smaller in the case of the 2,2'-cyanines, dyes I and III, although it seems to exist. Mixtures of methylene iodide and acetone behaved similarly to the methylene iodide–acetonitrile mixtures, with somewhat smaller downward curvature at the high concentrations of methylene iodide, whereas in methylene chloride–methylene iodide mixtures, Fig. 5, deviations from linearity were small.

The dielectric constants of acetonitrile, acetone, methylene chloride, and methylene iodide at 25° are 37, 20.7, 9.1, and 5.3, respectively. For the mixed

(25) N. S. Bayliss and L. Hulme, *Australian J. Chem.*, 257 (1953).

CH₂I₂ in CH₂Cl₂
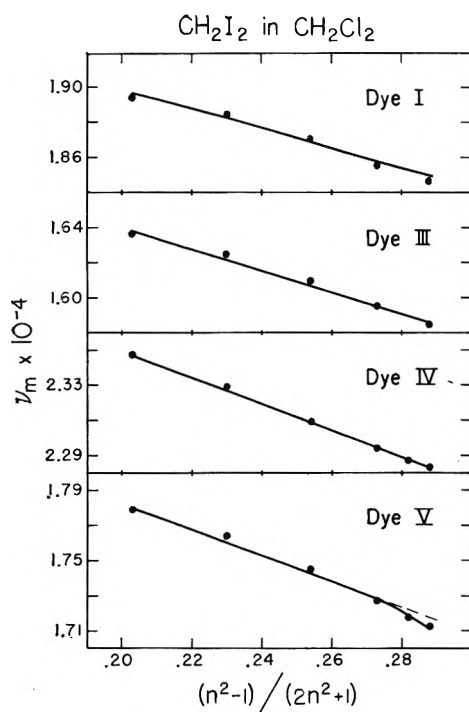
Figure 5. Molecular absorption band maxima of cyanine dyes in mixtures of CH₂I₂ and CH₂Cl₂ in relation to the Bayliss refractive index function.

solvents, the deviations from a linear dependence of the spectral displacement on the refractive index or the Bayliss function are greatest when the components differ most in polarity and size and are nearly absent for the mixture of the two methylene halides. The deviations indicate that small additions of the more polar and smaller molecule, which also possesses the lower refractive index, cause a disproportionally large hypsochromic shift, as if the microscopic refractive index in the neighborhood of the solute molecules were less than the average refractive index throughout the bulk of the solution. Preferential solvation of the dye cations, especially of the thiacyanine cations, by aceto-nitrile or acetone, respectively, in binary mixtures with methylene iodide would account for the observations. The more open structure of dyes containing benzothia-zole nuclei, compared with those containing quinoline nuclei, might accentuate the selective approach of the negative end of the dipoles in acetonitrile and acetone to the chromophore, in competition with methylene iodide. Effects on the conductivity and other properties associated with the dissociation equilibrium of quaternary ammonium salts in mixed solvents arising from selective solvation have been described in the literature.[26]

Part II. Spectrum of Diethyl-2,2'-cyanine Adsorbed to Solid Substrates

The optically sensitized photographic process, in which silver halide photographic layers are rendered sensitive to light of longer wave lengths than those absorbed by the silver salt, is brought about by adding an adsorbed layer of sensitizing dye to the surface of the silver halide crystallites in the sensitive layer and exposing the layer to light absorbed by the dye. Many studies have therefore been made of the absorption spectra of adsorbed sensitizing dyes in photographic gelatin emulsions and in model single-crystal or poly-crystalline silver halide systems, and of the relation between the spectral absorption and the spectral sensi-tization.

An important feature of the adsorption of dyes to silver halides is the marked tendency of the dye to enter into cooperative aggregated states having characteristic absorption spectra different from that of the adsorbed dye at very low surface coverage, when the dye appears to be adsorbed as isolated molecules. In normal photographic emulsions, sensitizing dyes are usually aggregated in some form. Dyes, however, can act as photographic sensitizers both in unaggre-gated and in aggregated states.[27] The present study was undertaken partly to find out how the spectral effects of adsorption of sensitizing dyes on silver bro-mide were related to the scheme of spectral effects of adsorption on substrates in general. For simplicity of interpretation, the present observations refer only to the molecular spectrum of a cyanine dye adsorbed to a number of finely divided solid substrates dyed under conditions of little or no aggregation.

Experimental

Three milliliters of a solution of dye I[28] in water or in an organic solvent was shaken with 1 g. of the powdered material, the suspension was centrifuged, freed from the supernatant liquid, washed once with the solvent, recentrifuged, and the powder was spread on a glass plate and rapidly dried in a current of air. A glass cover was applied, the "sandwich" was sealed with tape around the edges, and the diffuse reflectance spectrum of the dyed powder was measured by a

(26) H. Sadek and R. M. Fuoss, J. Am. Chem. Soc., 72, 301 (1950); Y. H. Inami, H. K. Bodenseh, and L. B. Ramsey, ibid., 83, 4745 (1961); J. Buffalini and K. H. Stern, ibid., 83, 4362 (1961); J. B. Hyne, ibid., 85, 304 (1963).

(27) C. E. K. Mees, "The Theory of the Photographic Process," Revised Ed., The Macmillan Co., New York, N. Y., 1954, Chapters 11 and 12.

(28) In the case of adsorption to solid halides as substrate, as AgCl, Hg₂Br₂, the anion of the dye used was the same as that of the sub-strate. The iodide was used for the other substrates.

General Electric recording spectrophotometer. The particle size of the substrates was small enough for Fresnel reflectance to make only a minor contribution.[29]

The substrates LiF, CaF_2, $SiO_2 \cdot xH_2O$, Al_2O_3, Bi_2O_3, Hg_2Br_2, ZnO, and $PbBr_2$ were analytical grade commercial preparations; silver halides and thallous halides were precipitated from the corresponding nitrates by the appropriate potassium halide in aqueous solutions, washed well with water, and dyed moist with water or organic solvent according to the solvent used for the dye.

Dye I, in concentrated aqueous solution or adsorbed to silver halides, readily aggregates in a form characterized by a sharp absorption band at about 573 $m\mu$, referred to as a J-band.[27] Of the substrates used in this study, the silver halides and lead bromide strongly induced J-aggregation of the dye adsorbed from aqueous solution, and the adsorbed layer on most of the other substrates contained a small proportion of J-aggregated dye, indicated by a small shoulder at about 575 $m\mu$. Except for the dye adsorbed to the silver halides and to lead bromide, the J-band associated with adsorption from aqueous solution did not interfere with the measurement of the absorption of the molecular band of the adsorbed dye. Aggregation on silver or lead halides was found to be eliminated or greatly reduced when small quantities of the dye, of the order of 10^{-5} mole per formula weight of substrate, dissolved in nitromethane or chloroform, were adsorbed on these substrates. To prepare dyed silver halides, the adsorbant, precipitated from aqueous solution, was freed from water by repeated washing with methanol and centrifuging; the methanol was then replaced by repeated

washing and centrifuging with the solvent from which the dye was to be added; the necessary amount of dye solution was then added to the precipitate suspended in the solvent, the suspension was centrifuged, and the dyed powder was rapidly air-dried on a glass plate and prepared for spectral examination as already described. Methanol can be used as a solvent, but if the substrate strongly favors J-aggregation, much dye aggregate may form on air-drying. Air-drying of dyed powders which have been dyed from solvents such as nitromethane, of lower water affinity than methanol, can be readily carried out without special precautions, without introducing disturbing amounts of aggregated dye.

No comparison of adsorbability of the dye on the various substrates is made in this paper. The specific surfaces of the substrates were not measured, and probably varied considerably. In all cases, the concentration of adsorbed dye was kept low, with the object of avoiding aggregation, and the fraction of the surface covered is probably low.

Results

The nature of the reflectance spectra of the dye adsorbed on these substrates is illustrated in Fig. 6, in which increasing percentage reflection is plotted downward as the ordinate against the wave length.

It is well known that the reflectance minima of the dyes in photographic emulsions coincide, within the accuracy of measurement, with absorption maxima, and the shapes of the reflectance spectra in Fig. 6, viewed as if the ordinates increased upward in the usual way, represent the shapes of the absorption curves, the peaks representing absorption maxima (and reflection minima) and the valleys absorption minima. In the subsequent discussion of the spectra of the adsorbed dye, the wave length of minimum reflectance will be referred to as "the wave length of the absorption maximum."

With the exception of the shoulders representing feeble J-bands that appear in some of the reflection curves, the shape of the inverted reflectance curves of the adsorbed dye in Fig. 6 is very similar to that of the absorption curves in organic solvents illustrated in Fig. 1. The structure in the absorption curve is reproduced in corresponding peaks and shoulders in the inverted reflection curve, and there can be little doubt that the absorbing species in the adsorbed layers under the condition of these experiments and in the solutions are the same; that is, they are essentially unaggregated
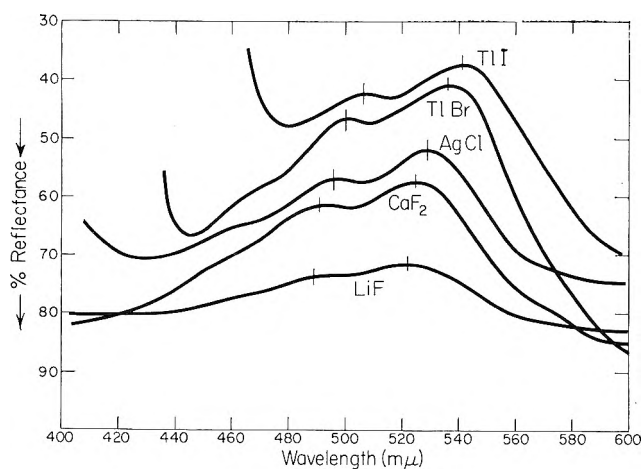
Figure 6. Reflectance spectra of 1,1'-diethyl-2,2'-cyanine cation at low concentration on various substrates. The decreasing reflectance at short wave lengths arises from the substrate.

(29) G. Kortüm, *Trans. Faraday Soc.*, **58**, 1624 (1962).

dye molecules interacting with the solvent or substrate, but only to a minor degree among themselves.

As in the solution spectra, the approximate invariance and the general appearance of the pattern in the reflection spectra of adsorbed dye I strongly suggest that the structure, probably incompletely resolved at room temperature, is determined by vibronic progressions, with about the same main interval of about 1300 cm.$^{-1}$, corresponding to that to be expected for a conjugated C=C linkage in the excited electronic state.

On many of the substrates examined, the wave length of the absorption maximum of the adsorbed dye did not depend on the solvent, nor on the coverage of the surface by dye, provided the coverage was low. When, however, the adsorbability of the dye on a substrate was sufficiently high, the absorption spectrum shifted with higher coverage to longer wave lengths by as much as 10 mμ, without change in shape, i.e., without introduction of new bands. For example, the absorption spectrum of dye I adsorbed from nitromethane on silver chloride in amounts varying from 0.5 × 10^{-5} to 2 × 10^{-5} mole per mole of substrate showed its main maximum at wave length 531 mμ, with a subsidiary maximum at 497 mμ and a shoulder at about 462 mμ, but at 5 × 10^{-5} and at 5 × 10^{-4} mole of dye per mole of adsorbent, the corresponding maxima were at 540 mμ, 504 mμ, and about 467 mμ. The displaced spectrum is still the molecular spectrum, and no new state of aggregation characterized by its own spectrum appears (except that with increasing concentration of the adsorbed dye, increasing small amounts of the J-aggregate band may appear, at wave lengths sufficiently removed from the molecular spectrum not to interfere with the spectral distribution of the molecular absorption). Nevertheless, some interaction between adsorbed dye molecules, less intense than those responsible for dimerization and for the polymerization, appears to set in as the concentration is increased, leading to a bathochromic displacement of the molecular absorption band. Displacements of the molecular band of dye I with increasing concentration of the adsorbed dye, similar to those observed on AgCl, have been found on AgBr, TlI, and Bi$_2$O$_3$.

The molecular absorption spectrum of adsorbed cyanine dyes seems therefore, in general, to be influenced (a) by the substrate, and (b) at sufficiently high concentration, by neighboring dye molecules. To isolate the effect of the substrate on the absorption spectrum, one considers the spectrum of the adsorbed dye at low concentrations, at which the maximum is independent of concentration. Figure 7 contains a plot of the wave number of maximum absorption at low concentration of adsorbed dye against the refractive

index function $(n^2 - 1)/(2n^2 + 1)$. The values of the refractive index, n, are from standard tables or from the original literature, and for anisotropic crystals, the mean of the values along the principal axes has been used. Most of the points fall fairly well on a straight line, but, as for the cyanines in liquid solvents, an equally valid linear relation holds between the wave number and the refractive index itself. Deviations from the line are greater than for the corresponding relation in solution, but the main factor governing the spectral shift of adsorbed mutually noninteracting cyanine molecules, as of those molecules in solution, appears to be the refractive index of the environment. The environmental interactions are therefore principally governed by dispersion forces. The line showing the displacement of the molecular band of dye I in solution is also drawn in Fig. 7. It can be seen that the "general red shift" in the molecular spectrum of the dye is less in adsorbed layers than in solution; for a given refractive index, the maximum absorption is at a higher frequency in the adsorbed state than in solution. The displacement coefficient, measured by the slope of the line, for the adsorbed dye is −3.1 × 10^{-3} cm.$^{-1}$ per unit increase in the Bayliss function, little more than half that for the dye in solution, −5.7 × 10^{-3}. The dispersion interaction of a solid substrate with the dye is only about half that of a liquid solvent of the same refractive index, probably because in adsorption the interaction occurs from one side only. It seems likely that the bathochromic shift of the molecular band of
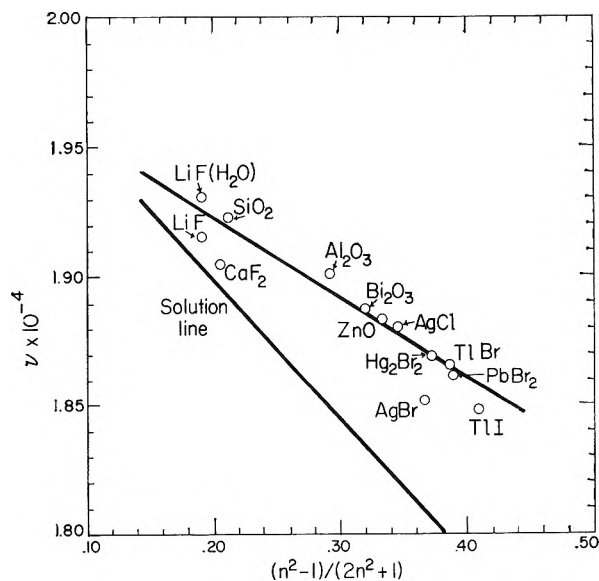
Figure 7. Molecular absorption band maxima of 1,1'-diethyl-2,2'-cyanine cation adsorbed to solid adsorbents in relation to the Bayliss refractive index function.

the adsorbed dye with increasing concentration likewise originates in dispersive interactions between the adsorbed dye molecules themselves.

The absorption spectrum of the molecular form of dye I on silver halides falls essentially in line with that on other substrates, although the deviation of the observed absorption maximum on silver bromide from the line in Fig. 7 is greater than for most other substrates. On silver iodide, the dye aggregated to a considerable degree even at very low concentrations, and a satisfactory molecular spectrum was not observed on this substrate. Of the solids examined, silver iodide was unique in this respect.

Adsorbed on powdered zinc oxide from water on methanol, dye I exhibited the maximum of its molecular absorption at about 520 mμ, a value consistent with a refractive index about 1.3 instead of the observed value of 2.0 for zinc oxide. Adsorbed from bromoform or nitromethane on zinc oxide which had been well shaken previously with these solvents and examined in a layer protected from the action of atmospheric water vapor, the dye showed its absorption maximum at 532 mμ, or 1.88×10^4 cm.$^{-1}$, close to the value, as shown in Fig. 7, to be expected for adsorbed dye on zinc oxide, for which the value of the Bayliss function is 0.333. On exposure of this layer to atmospheric water vapor, the absorption maximum shifted to 521 mμ. The appearance of molecular absorption spectra of adsorbed cyanines at wave lengths much shorter than is consistent with the refractive index of the substrate seems therefore very probably to be the effect of accompanying adsorbed layers of water.

Adsorption of Dye I in a Colorless Form on Zinc Sulfide. Zinc sulfide prepared by precipitation of zinc ion by hydrogen sulfide under alkaline conditions adsorbed the dye in the normal pink form from water or from nitromethane, showing maximum absorption near a wave length consistent with the refractive index of zinc sulfide. On material precipitated by hydrogen sulfide under acid conditions, the nature of the adsorbed dye depended on the solvent. From group 1 of solvents, including water, methanol, chloroform, pyridine, or pyrrol, the dye was adsorbed in the normal colored form, but from group 2, comprising solvents of acidic nature, like nitromethane, nitrobenzene, glacial acetic acid, dilute acetic acid in chloroform, o-chlorophenol, or bromoform, the dye was adsorbed in a colorless form. Solutions of the dye in solvents of both groups are strongly colored. The absence of color in the zinc sulfide treated with solutions of the dye in solvents of group 2 was not the result of poor adsorption or of permanent destruction of the dye, for addition of water to the white powder left after cen-

trifuging from the solvents of acidic nature immediately caused the appearance of strong color, which was found by centrifuging to reside in the zinc sulfide. Similarly, addition of a drop of water to a dry layer of white zinc sulfide which had been treated with a solution of the dye in nitromethane caused the development of an intense pink spot, and, on exposure to moist room air, the dry white layer of treated zinc sulfide slowly became uniformly pink. The interconversion between the colorless and colored forms of the dye on zinc sulfide was reversible from both sides. Addition of nitromethane to a sample of zinc sulfide deeply dyed from aqueous solution rendered the solid white, but the color was regained on addition of water to the surface.

The colorless form of the dye adsorbed from solvents of acidic nature was observed on commercial samples of precipitated zinc sulfide as well as on samples prepared by precipitation with hydrogen sulfide by Mr. D. Pearlman of these laboratories. All of these samples were prepared under acid conditions. The potentiometric pH values of aqueous suspensions of these various samples were about 3.25, while an aqueous suspension of zinc sulfide prepared under alkaline conditions, which adsorbed the dye in the colored form from all solvents, showed a pH value of 5.00. Acid-precipitated zinc sulfide which had been heated to a temperature of 600–700° in helium or air adsorbed dye in the colored form from all solvents, and the pH values of aqueous suspensions of the fired samples increased to between 6 and 7.

It is well known that cyanine dyes in acid solution can be reversibly protonated to yield colorless substances. The value of pK_a for the equilibrium between the colored and the protonated forms of dye I is about 4.0.[30] The decolorization of the dye in these adsorption experiments cannot, however, be attributed to protonation in the solution in equilibrium with the zinc sulfide. For example, when the dye is adsorbed from water, the pH of the solution in equilibrium with the zinc sulfide is such as to cause considerable, but incomplete protonation, but the adsorbed dye is unprotonated. If zinc sulfide is first vigorously shaken with nitromethane and then centrifugally settled, the addition of a solution of the dye in a little nitromethane to the supernatant liquid gives a colored liquid layer over the powder. Only after shaking with the zinc sulfide does decolorization occur. If a limited amount of dye is added, both the powder and the supernatant liquid are colorless after shaking; addition of dye can

(30) Dr. A. Herz, of these laboratories, private communication; cf. G. Scheibe and D. Brücke, Z. Elektrochem., 54, 403 (1950).

be made until the supernatant liquid remains colored after shaking with the zinc sulfide, but the powder remains white.

Decolorization of the dye added from acidic solvents to unfired, acid-precipitated zinc sulfide must therefore be attributed to protonation at active acidic sites in the zinc sulfide surface in equilibrium with the solvent. The situation appears similar to that discussed by Walling,[31] who utilized the ability of surfaces of powdered calcium fluoride, calcium sulfate, etc., to convert adsorbed indicating dye bases to their differently colored conjugated acids to measure the acid strengths of solid surfaces. In Walling's experiments, as in those reported here on zinc sulfide, the surface acid strength depended on the medium from which the indicator was adsorbed, weakly basic solvents such as

water and the other members of group 1 depressing the acid strength of the surface and promoting adsorption in the unprotonated form. These examples of proton transfer between surface sites and adsorbed molecules appear to be analogous to recently studied examples of electron transfer between surface sites and adsorbed molecules.[24,32]

(31) C. Walling, *J. Am. Chem. Soc.*, **72**, 1164 (1950).
(32) J. J. Rooney and R. C. Pink, *Trans. Faraday Soc.*, **58**, 1632 (1962).

Gold–Chlorine and Gold–Bromine Equilibria in Fused Salts

by Denis D. Durnan, Alan D. Mighell, Edward J. Zapolski, and Reuben E. Wood

Department of Chemistry, The George Washington University, Washington, D. C.
(Received October 26, 1963)

The reaction between gold and chlorine in fused zinc chloride and in fused NaCl–KCl and the reaction between gold and bromine in fused NaBr–KBr have been studied. Equilibrium concentrations have been determined and, from these, thermodynamic data have been calculated.

Introduction

Most of the existing thermodynamic data concerning fused salt solutions have been obtained by cell potential measurements. The relative scarcity of directly obtained data on chemical equilibria can be attributed to analytical difficulties inherent in the study of equilibria involving extremely small concentrations of some reactant and to the difficulty or practical impossibility of varying equilibrium concentrations sufficiently to permit reliable extrapolations to infinite dilution or to unit mole fraction, for example. The gold–halogen equilibrium studies reported here were

not hampered by the first difficulty. Because of the second difficulty, however, data for making the mentioned extrapolations were not obtained.

This paper reports the results of studies on these three reactions

$$2Au + Cl_2 \longrightarrow 2AuCl \qquad (1)$$

in fused zinc chloride at 736°K.

$$2Au + Cl_2 \longrightarrow 2AuCl \qquad (2)$$

in fused equimolar NaCl–KCl in the temperature range 1025 to 1100°K., and

$$2Au + Br_2 \longrightarrow 2AuBr \qquad (3)$$

in fused equimolar NaBr–KBr in the temperature range 1035 to 1200°K.

Experimental

There was much similarity in the procedures used in studying the three reactions. The reaction mixtures were heated in an electric furnace supplied through a constant-voltage transformer. The gold used was specified to be of 99.95% purity. The chlorine was specified by the manufacturer (Matheson) to be of at least 99.3% purity. It was used without further purification except for drying in the cases of the NaCl–KCl experiments. Other chemicals including the bromine were all of reagent grade. The reaction vessel in the zinc chloride experiments was Pyrex glass. In the NaCl–KCl and NaBr–KBr experiments, the vessel was an alundum tube. Temperatures were measured with a platinum–platinum rhodium thermocouple.

In each case the halogen was bubbled under prevailing atmospheric pressure through the fused salt in which the gold was immersed. One atmosphere was used in calculations as the halogen pressure. Actual departures from this value would lead to insignificant changes in the results of such calculations. In the case of the chlorine experiments, the exit gas was trapped or exhausted through the fume hood system. In the case of the bromine experiment, the gas was obtained by boiling liquid bromine in an apparatus in which the exhaust bromine was condensed and recycled. This system contained anhydrous $Mg(ClO_4)_2$ as a desiccant. In all cases the fused salt was dried by the passage of the halogen through it. In each case, the reaction vessels were arranged to permit the insertion of a sampling pipet.

The analytical procedure was gravimetric. The sample of fused salt, withdrawn into a pipet, was cooled and weighed. It then was mixed with water in which most of it dissolved, leaving a residue of precipitated gold. The dissolved gold was precipitated by sulfur dioxide. In all cases the total precipitated gold was weighed. In the NaCl–KCl experiments and in some of the NaBr–KBr experiments the gold precipitated before and after treatment with sulfur dioxide was weighed separately.

Results

Gold–Chlorine Reaction in Fused $ZnCl_2$. This was the first of the three reactions studied. The reaction was found to be very slow. The run reported here covered a period of 53 days during which 27 samples were taken and analyzed. The temperature of this run was 736 ± 5°K. The temperature fluctuations

observed were less than ±5°. Control and maintenance of the chlorine flow was not entirely satisfactory; the flow was interrupted several times. Samples taken during or shortly after the interruption of chlorine flow showed lessened gold content, a fact presumably resulting from escape of chlorine to the air and consequent reduction of chlorine concentration in the solution. This interpretation is supported by the facts that after chlorine flow interruption, very fine platelets of gold precipitated and this precipitate redissolved rapidly when chlorine flow was resumed.

The data are shown in Fig. 1. The dotted portions of the curve indicate periods where the chlorine flow was, or recently had been, cut off.

Gold–Chlorine Reaction in Fused NaCl–KCl. Equimolal NaCl–KCl was used as the solvent. The reaction was found to be much faster than in zinc chloride but the temperature was also much higher. The data from this experiment are shown in Table I. These represent two different runs. In the table, the first column is the time from the beginning of the run. The second is the observed temperature at the time of sampling. One entry is missing from this column because the thermocouple had been removed at the time of this sampling. The third and fourth columns express the concentrations in milligrams of gold per gram of sample and mole fraction of aurous chloride, respectively.

The last column gives the ratio of gold precipitated by treatment of the sample with water only to this gold plus the gold which was reduced by the sulfur dioxide. The significance of this column is that it confirms what would be predicted by extrapolation of lower temperature data,[1-3] namely, that most of the gold
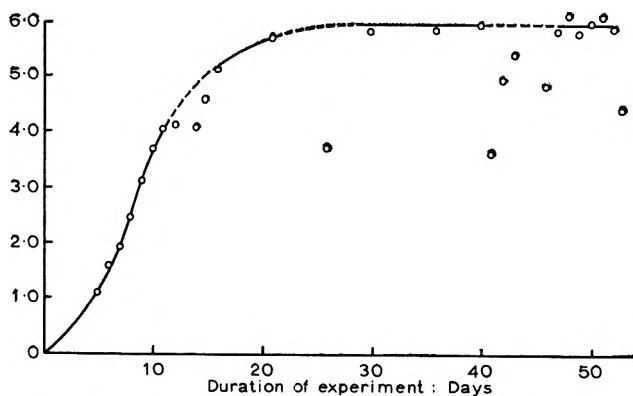
Figure 1. Approach to equilibrium in reaction between gold and chlorine in fused zinc chloride at 736 ± 5°K. Dotted lines indicate intervals during which chlorine flow was or recently had been interrupted.

Table I: Data of the Gold–Chlorine
Experiments in NaCl–KCl

Run	Time, hr.	Temp., °K.	Concn. of Au, mg./g.	Concn. of AuCl, mole fraction	Ratio
I	2.25	1025	296	0.133	0.645
	8.0	1033	529	0.322	0.600
	11.5	1020	528	0.322	0.619
	21.5	. . .	535	0.329	0.665
	25.5	1019	542	0.337	0.638
II	1.25	1096	457	0.251	0.657
	3.0	1089	464	0.257	0.655
	5.25	1097	468	0.262	0.654
	7.25	1094	468	0.262	0.655
	9.25	1089	481	0.272	0.630

is gold(I) at the temperatures of these experiments. The proportionation reaction

$$3AuCl \longrightarrow 2Au + AuCl_3$$
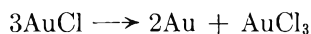
which presumably occurs when the fused salt sample cools indicates 0.667 as the number to be expected in the ratio column if in the melt all the gold were gold-(I). The fact that the experimental ratios are somewhat less than this and that they fluctuate more than the values for total gold concentration could be abcounted for in part, at least, by assuming that dissolved chlorine reacted with some of the AuCl during the cooling process. The fact that the lower temperature run gave a bit lower average ratio is of dubious significance although reliable data are not yet available to rule out the possibility that the observed difference could result in appreciable part from the greater concentration of gold(III) at the lower temperature.

Gold–Bromine Reaction in Fused NaBr–KBr. Two experimental runs are reported. In the first experiment the temperature was first held at 1059 ± 2.9°K. After equilibrium had been attained, as determined by sample analysis, the temperature was raised to 1178 ± 2.4°K. In the second experiment, the temperature was initially maintained at 1038 ± 4.3°K.; it was then raised to, and maintained at, 1202 ± 3.1°K.; then it was again lowered and the final data were obtained at 1037 ± 5.9°K. These temperatures are the means observed at 0.5-hr. intervals during equilibrium periods. The data from these experiments are presented in Table II. The first column is the time elapsed from the start of the experimental run at the particular rheostat setting which controlled the temperature of the reaction cell. The second column is the observed temperature of the melt just before sampling. The

third and fourth columns express the observed concentrations in milligrams of gold per gram of sample and mole fraction of aurous bromide, respectively. The last column again presents, for the cases in which the requisite data were obtained, the ratio described in connection with Table I.

Table II: Data of the Gold–Bromine
Experiments in NaBr–KBr

Run	Time, hr.	Temp., °K.	Concn. of Au, mg./g.	Concn. of AuBr, mole fraction	Ratio
I	14.5	1057	171	0.112	
	19.5	1057	173	0.114	0.614
	21.5	1057	168	0.110	
	22.5	1062	173	0.114	0.663
	24.0	1058	174	0.115	0.662
	3.0	1174	136	0.0865	
	6.0	1175	129	0.0815	0.670
	8.5	1186	142	0.0909	
II	9.0	1032	186	0.124	
	10.0	1031	192	0.129	
	13.0	1038	186	0.124	
	16.5	1047	191	0.126	
	17.5	1044	194	0.131	
	9.5	1201	138	0.0881	
	11.5	1202	138	0.0881	
	12.5	1206	143	0.0916	
	18.0	1032	192	0.129	
	19.5	1033	191	0.126	
	23.0	1034	178	0.118	

Treatment of Results

Several standard thermodynamic properties may be estimated from the data presented in Fig. 1 and in Tables I and II. The standard state to which these properties will be referred will be the hypothetical unit mole fraction solution having properties extrapolated from those of the solutions actually studied.

The work with the ZnCl$_2$ solvent, although an experiment of long duration (53 days), involved essentially a single temperature and therefore only a value for

(1) L. Brewer, L. A. Bromley, P. W. Gilles, and N. L. Lofgren, "Chemistry and Metallurgy of Miscellaneous Materials: Thermodynamics," L. L. Quill, Ed., McGraw-Hill Book Co., Inc., New York, N. Y., 1950.

(2) W. J. Hamer, M. S. Malmberg, and B. Rubin, *J. Electrochem. Soc.,* **103,** 8 (1956).

(3) A. Glassner, "The Thermodynamic Properties of the Oxides, Fluorides and Chlorides to 2500°K.," U. S. Atomic Energy Commission Report ANL-5750 (1957).

ΔG° of formation of AuCl can be calculated. This value, like the values for ΔG° calculated hereafter from the data in Tables I and II, is based on the familiar relation $\Delta G^\circ = -RT \ln K$, K in these cases being taken simply as the mole fraction of the aurous halide corresponding to the equilibrium solution. For AuCl in $ZnCl_2$ at 736°K., then, $\Delta G^\circ = 4.6$ kcal. mole^{-1}.

Since the reaction between Au and Cl_2 and Br_2 in the corresponding alkali halide eutectics involved a range of temperatures, more calculations could be made in these cases and certain extrapolations and interpolations were possible. First, by least-squares treatment of the primary data, empirical equations were developed for the equilibrium constants (equilibrium mole fraction of AuCl or AuBr) of the reactions

$$Au + 0.5Cl_2 \longrightarrow AuCl \text{ (in fused NaCl–KCl)}$$

$$Au + 0.5Br_2 \longrightarrow AuBr \text{ (in fused NaBr–KBr)}$$

as a function of temperature. From these empirical equations and applicable thermodynamic relations, values at 1000°K. for the ΔG°, ΔH°, and ΔS° of formation of the gold halide in the specified solvent were calculated. For these calculations the approximation was made that ΔH° (and then likewise ΔS°) was constant in the temperature range to which the calculations were applied. The results of these calculations are shown in Table III.

Table III: Values Computed from Data in Tables I and II

	AuCl	AuBr
log K	$(1.55 \times 10^3)/T - 2.00$	$(1.20 \times 10^3)/T - 2.07$
log K_{1000}	-0.45	-0.87
ΔG°_{1000}	2.1 kcal. mole^{-1}	4.0 kcal. mole^{-1}
ΔH°_{1000}	-7.1 kcal. mole^{-1}	-5.5 kcal. mole^{-1}
ΔS°_{1000}	-9.2 cal. mole^{-1} deg.$^{-1}$	-9.5 cal. mole^{-1} deg.$^{-1}$

For oxidation–reduction reactions, much of the experimental work and the published data are in terms of cell potentials. We therefore give in Table IV some cell potential figures to which our experimental data correspond.

Discussion

The only previously published experimental results we have found which can be compared directly with our data involve measurements by Gitman and Delimarskii[4] of the potential of the cell: Au/AuCl + KCl–

NaCl/KCl–NaCl + $PbCl_2$/Pb. They reported a cell potential of 1.00 ± 0.02 v. in the temperature range 700–738°. Flengas and Ingraham[5] report values

Table IV: Calculated Cell Potentials

Cell	Temp., °K.	E°, volt
Au–Cl_2 in $ZnCl_2$	736	-0.100
Au–Cl_2 in NaCl–KCl	1000	-0.042
Au–Br_2 in NaBr–KBr	1000	-0.087
Au–Cl_2 in NaCl–KCl	736	$+0.02$
(extrapolated to 736°K. for comparison)		

for the Pb, Pb^{+2} and Cl$^-$, Cl_2 electrodes in fused NaCl–KCl, the difference between which, interpolated to 727° (1000°K.), is 1.225 v. This, combined with our value of E° for the Au–Cl_2 reaction in the same solvent (Table IV) would lead to a prediction of 1.26 v. for the Gitman–Delimarskii cell.

If thermodynamic data for the pure gold halides were known with sufficient accuracy at the temperatures of our experiments, activity coefficients could be calculated. However, consideration of ref. 1 and 3 and of the dissociation pressures of the gold halides reported by Meyer[6] lead us to conclude only that our values of ΔG° for the gold halides in solution are the same as those for the pure compounds within the range of uncertainty of the pure-compound ΔG° values and that because of this considerable uncertainty, activity coefficients could be unity or either significantly greater or less than unity with the pure compound as reference state.

The results with zinc chloride compared to those with the alkali chloride melt are just the opposite of what one might predict on the basis of a simple common-ion effect and the assumption that zinc chloride contains relatively few chloride ions. The fact probably is that complex ion formation is importantly involved in these systems and that the zinc competes with gold more effectively than the alkali metals for the complexing chloride ions.

(4) E. B. Gitman and Y. K. Delimarskii, *Ukr. Khim. Zh.*, **22**, 731 (1956).

(5) S. N. Flengas and T. R. Ingraham, *J. Electrochem. Soc.*, **106**, 714 (1959).

(6) Meyer, International Critical Tables, Vol. 7, 1933, p. 273.

Magnetic Susceptibilities of Molten Bismuth–Bismuth Tribromide Solutions[1]

by L. E. Topol and F. Y. Lieu

Atomics International, A Division of North American Aviation, Inc., Canoga Park, California
(Received October 28, 1963)

Magnetic susceptibility measurements were made with a Gouy balance on the molten Bi–BiBr₃ system from 250 to 620°. The susceptibilities were diamagnetic throughout and in the composition range 0 through 20 mole % Bi were temperature independent as in the Bi–BiCl₃ system, whereas in the 30 to 100% metal region the susceptibilities became less diamagnetic with increasing temperature as in Bi–BiI₃ solutions. The molar susceptibility as a function of composition resembled that of the Bi–BiI₃ system and is described in terms of chemical entities, *e.g.*, BiBr, or completely localized electrons in the salt-rich melts, and in terms of the free electron model in the metal-rich compositions.

Introduction

In previous magnetic susceptibility studies on molten bismuth–bismuth halide solutions, the Bi–BiCl₃ system over the composition range 0 to 28.5 mole % Bi[2] and the Bi–BiI₃ system with 0 to 100% Bi[3] concentrations were measured. In Bi–BiCl₃ the susceptibilities were found to be linear with composition and temperature independent in the range 280 to 430°. In Bi–BiI₃ melts at 450 to 600°, on the other hand, the susceptibilities varied with composition and temperature throughout. Since it is known that at low concentrations Bi dissolves in BiCl₃ to form subhalides[4] of the type (BiCl)ₓ, where x equals one and higher integers such as four, the susceptibility data of the salt-rich iodide system were also related to the formation of a monovalent subhalide

$$2Bi + BiI_3 = 3BiI \qquad (1)$$

The susceptibility behavior in Bi–BiCl₃ and Bi–BiI₃ with low metal concentrations then indicates that the equilibrium constant for reaction 1 is smaller than that for the corresponding chloride. (It is assumed that no distinction can be made here between the specific susceptibility of BiX and (BiX)ₓ.) For metal-rich Bi–BiI₃ solutions the susceptibility data were consistent with the model of a free electron gas diluted by the salt anions. The phase diagram of the Bi–BiBr₃ system[5] appears to be very similar to that of Bi–BiCl₃,[6] and low metal concentration bromide melts also contain the subhalide (BiBr)ₓ.[7] Thus a magnetic suscepti-

bility investigation of Bi–BiBr₃ solutions should afford an interesting comparison between the different bismuth systems at low metal compositions. In addition, since the consolute temperature of the bromide system, 538°,[5] is much lower than that of the chloride, 780°,[6] the entire composition range can be covered at temperatures where vapor pressures are not too large for Vycor containers; this will enable a comparison to be made with the iodide system at higher metal concentrations.

Experimental

Materials. The purification of bismuth[3] and the preparation and treatment of BiBr₃[5] have been described previously.

Apparatus and Procedure. The susceptibility measurements were made with a Gouy balance and the apparatus and procedure were similar to those used in the iodide study.[3] Samples with metal compositions of 5 to 30 mole % were equilibrated at 450° in a rocking furnace for several hours to ensure complete solution.

(1) This work was supported by the Research Division of the U. S. Atomic Energy Commission.

(2) N. H. Nachtrieb, *J. Phys. Chem.*, **66**, 1163 (1962).

(3) L. E. Topol and L. D. Ransom, *J. Chem. Phys.*, **38**, 1663 (1963).

(4) L. E. Topol, S. J. Yosim, and R. A. Osteryoung, *J. Phys. Chem.*, **65**, 1511 (1961); also C. R. Boston, G. P. Smith, and L. C. Howick, *ibid.* **67**, 1849 (1963).

(5) S. J. Yosim, L. D. Ransom, R. A. Sallach, and L. E. Topol, *ibid.* **66**, 28 (1962).

(6) S. J. Yosim, A. J. Darnell, W. G. Gehman, and S. W. Mayer, *ibid.* **63**, 230 (1959).

(7) L. E. Topol and R. A. Osteryoung, *ibid.*, **66**, 1587 (1962).

Samples with metal concentrations of 40 mole % or higher were equilibrated at 600° for longer periods of time. The absence of ferromagnetic impurities was checked by testing the constancy of sample susceptibility with varying field strength.

The density of a 70.0 mole % Bi solution was measured as described elsewhere.[3] Since the vapor pressures above 540° are high, frequently resulting in rupture of the Pyrex pycnometer, a measurement at only one temperature could be obtained. This density, 6.69 g./ml. at 543°, was extrapolated to other temperatures by assuming a temperature dependence similar to the average of the 40 mole % and pure Bi melts.

Results and Discussion

The specific susceptibility χ' is calculated from the relation

$$\chi' = 2g\Delta w/H^2 ad \qquad (2)$$

where g is the gravitational constant, Δw the apparent change in weight of the sample on application of the magnetic field of strength H, a the cross-sectional area of the sample, and d the density of the solution. The density results of Keneshea and Cubicciotti for 0 to 40.0 mole % Bi–BiBr$_3$ solutions[8a] and for pure Bi,[8b] as well as the density of a 70.0 mole % Bi melt measured in this laboratory, were used. The densities of all the intermediate compositions involved in this study were obtained from the interpolated values of the measured molar volumes of the 0 to 40.0, 70.0, and 100% Bi solutions. The molar susceptibility χ is given by $\chi'\bar{M} = \chi'(N_1 M_1 + N_2 M_2)$ where N_1, N_2, M_1, and M_2 are the mole fraction and molecular weight of the two components, respectively.

The specific susceptibilities as a function of temperature for 0 to 100 mole % Bi are plotted in Fig. 1. The results for a 5% Bi solution have been omitted from the figure for the sake of clarity. For the composition range, 0 to 30% metal, the 250 to 450° temperature scale at the top of the graph should be used; for the 60 to 100% Bi solutions the 450 to 650° temperature scale at the bottom of the plot pertains. Susceptibilities for 40 and 50% samples were measured from 285 to 625° and are thus represented on both temperature ordinates. Duplicate samples were measured for the pure components as well as the 40 and 80% compositions; the agreement between the duplicates was good for all but the 40% solution. The susceptibility of pure fused BiBr$_3$ is $-0.265 \pm 0.005 \times 10^{-6}$ per g. and is essentially independent of temperature in the range 250 to 460°. This behavior is similar to that of BiCl$_3$[2] but is unlike the iodide,[3] the susceptibility of which exhibits a small temperature dependence. It is
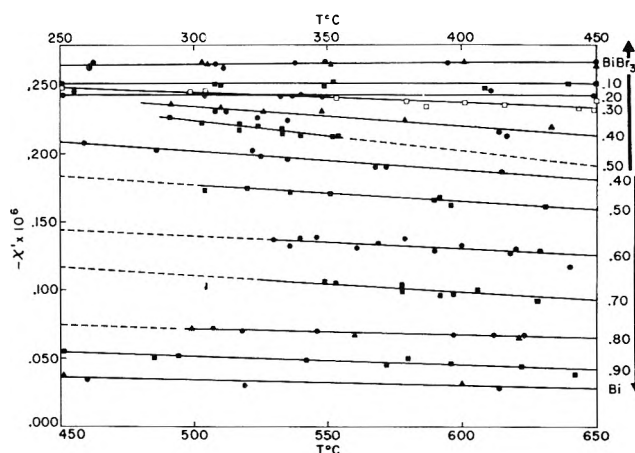
Figure 1. The specific susceptibilities of Bi–BiBr$_3$ solutions vs. temperature. Concentrations are in mole % Bi; the arrows designate the temperature range for that composition. The results of duplicate samples are distinguished by different points.

also interesting that the decrease in the diamagnetic susceptibility between solid and liquid BiCl$_3$, -0.322[9] and -0.280×10^{-6}, respectively, and solid and liquid BiBr$_3$, -0.303[9] and -0.265×10^{-6}, respectively, is about the same, 13%. The specific susceptibility of bismuth was found to vary with temperature from $-0.036 \pm 0.002 \times 10^{-6}$ at 450° to $-0.030 \pm 0.002 \times 10^{-6}$ at 600° in excellent agreement with the earlier results,[3] -0.038 and -0.032×10^{-6} at 450 and 600°, respectively.

As illustrated in Fig. 1 all the solutions are diamagnetic and a decrease in diamagnetism with increasing temperature is noted for compositions of 30% Bi or greater. The largest variation in susceptibility with temperature appears to occur in the 40 to 70% melts. Thus, it seems that for compositions of 20% Bi or less and for temperatures below 500° the bromide system resembles the chloride magnetically, whereas for the higher metal compositions above 450° a similarity with the iodide is evident. (It should be noted that no susceptibility measurements have been accomplished in metal-rich Bi–BiCl$_3$ melts due to the limited solubilities at these temperatures. Such measurements would be expected to show a similar behavior as the bromide and iodide, i.e., a temperature dependence.) The dotted lines in the 50 to 80% plots represent extrapolations of the data into the two phase liquid region. For the 50 mole % composition where measurements were taken

(8) (a) F. J. Keneshea, Jr., and D. Cubicciotti, J. Phys. Chem., 63, 1112 (1959); (b) ibid., 62, 843 (1958).

(9) M. Prasad, C. R. Kanekar, and L. N. Mulay, J. Chem. Phys., 19, 1440 (1951).

Table I: Molar Susceptibilities and the Effect of Bi in Bi–BiBr₃ Melts

N_{Bi}	$\bar{M}^a$	350° $-\chi \times 10^6$	350° $\Delta\chi^b \times 10^6$	350° $\dfrac{\Delta\chi \times 10^6}{N_{Bi}}$	450° $-\chi \times 10^6$	450° $\Delta\chi^b \times 10^6$	450° $\dfrac{\Delta\chi \times 10^6}{N_{Bi}}$	550° $-\chi \times 10^6$	550° $\Delta\chi^b \times 10^6$	550° $\dfrac{\Delta\chi \times 10^5}{N_{Bi}}$	650° $-\chi \times 10^6$	650° $\Delta\chi^b \times 10^6$	650° $\dfrac{\Delta\chi \times 10^5}{N_{Bi}}$
0	448.7	118.9	0	...	118.9	0	...	118.9^c	0	...	118.9^c	0	...
0.05	436.8	113.1	0.3	6.0	113.1	0.3	6.0	113.1^c	0.2	4.0	113.1^c	0.2	4.0
0.10	424.8	107.9	−0.1	−1.0	107.9	−0.2	−2.0	107.9^c	−0.2	−2.0	107.9^c	−0.3	−3.0
0.20	400.8	98.2	−1.4	−7.0	98.2	−1.6	−8.0	98.2^c	−1.8	−9.0	98.2^c	−1.9	−9.5
0.30	376.8	90.8	−5.1	−17.0	88.2	−2.8	−9.3	85.5^c	−0.3	−1.0	82.9^c	2.1	7.0
0.40	352.8	80.1	−5.4	−14.0	74.8	−0.5	−1.2	68.8	5.2	13.0	64.2	9.5	24.0
0.50	328.9	69.1	−5.4	−11.0	61.8^c	1.4	2.8	56.2	6.6	13.0	52.3	10.2	20.0
0.60	304.9	46.6^c	6.0	10.0	43.9^c	8.2	14.0	41.2	10.4	17.0	38.4	12.7	21.0
0.70	280.9	36.2^c	5.4	8.0	32.9^c	8.0	12.0	29.5	10.9	16.0	25.8	15.0	21.0
0.80	256.9	20.0^c	10.5	13.0	19.0^c	10.8	13.0	18.0	11.2	14.0	16.7	11.8	15.0
0.90	233.0	14.0^c	5.5	6.1	12.6	6.0	6.7	11.2	6.7	7.4	9.8	7.4	8.2
1.00	209.0	8.4	0	0	7.5	0	0	6.7	0	0	5.9	0	0

^{a} $\bar{M} = N_1 M_1 + N_2 M_2$. ^{b} $\Delta\chi = \chi - (N_1\chi_1 + N_2\chi_2)$, where $-\Delta\chi$ and $+\Delta\chi$ indicate deviations in diamagnetic and paramagnetic directions, respectively. ^{c} Extrapolated value.

both below and above this immiscibility region, it is difficult to ascertain if the data are continuous; *i.e.*, the slopes of the two sets of data appear to be somewhat different and susceptibility values of −0.291 and −0.284 × 10⁻⁶, respectively, are found at 450° by extrapolation of the measurements from below and above the two-phase region.

Since the slopes of the 30 to 70% compositions in Fig. 1 are greater than those of the pure components, it appears, as in the Bi–BiI₃ system, that one or more new species are formed. Furthermore, in order to be consistent with these data, these new species must be paramagnetic or less diamagnetic than the pure components and their concentrations must increase with temperature in the 30–70% Bi melts.

Typical molar susceptibilities as a function of composition are given at 350°, 450°, 550°, and 650° in Table I. For the 0 to 30 mole % Bi solutions at 550 and 650° as well as for those compositions that are in the two-phase liquid region (60–90% Bi at 350° and 50–80% at 450°) hypothetical susceptibilities were taken from extrapolated data in Fig. 1. The $\Delta\chi$ data, where $\Delta\chi = \chi_{soln} - (N_1\chi_1 + N_2\chi_2)$, indicate negligible deviations from simple additivity at all temperatures for melt compositions of 5 to 20 mole % Bi. At the higher metal compositions deviations occur at first in a more diamagnetic direction from additivity and then in a more paramagnetic direction. The diamagnetic deviations decrease in magnitude as the temperature is increased and at temperatures of 550° and above are virtually nonexistent. On the other hand, the paramagnetic deviations increase with increase in temperature. These effects are accentuated by comparing the deviations from additivity per addition of metal, $\Delta\chi/N_{Bi}$

(Table I), and here again, as in the Bi–BiI₃ system, a maximum paramagnetic effect is found at all temperatures around a composition corresponding to a Bi–anion ratio of unity.

As discussed previously,[3] the negligible deviations from additivity in melts of low metal concentration should not be taken to indicate that little or no interaction occurs between the components. Since bulk metals consist of cations and free electrons, the additive susceptibility behavior (see eq. 9 and 10) would be expected to follow that represented by curve 5 in Fig. 2. Furthermore, since strong interactions resulting in the new species, (BiBr)ₓ, are known to occur in this system,[7] an interpretation of these results must be
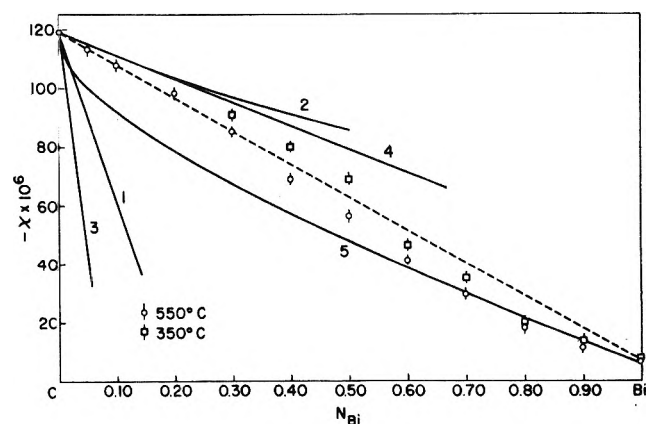

Figure 2. Molar susceptibilities in Bi–BiBr₃ at 350 and 550° as a function of mole fraction of Bi: 1, Bi atoms ($\chi = 456 \times 10^{-6}$ at 550°); 2, Bi₂ ($\chi = -80 \times 10^{-6}$); 3, BiBr₂ ($\chi = 390 \times 10^{-6}$ at 550°); 4, BiBr ($\chi = -67 \times 10^{-6}$); 5, Bi⁺³ Br⁻, and e⁻ (at 550°). The dashed line represents linear additivity between the two components.

made in this light. However, the possible occurrence of other chemical entities as well as the free electron gas model will also be considered.

I. Solution by Reaction. If solution of the metal in its molten salt occurs by a chemical reaction, the following possibilities must be considered

$$nBi = Bi_n \qquad (3)$$

$$2Bi + BiBr_3 = 3BiBr \qquad (4)$$

$$Bi + 2BiBr_3 = 3BiBr_2 \qquad (5)$$
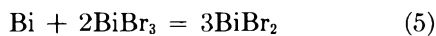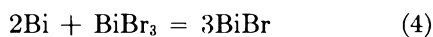
where Bi_n are metal polymers of the order n. The entities $BiBr_3$, $BiBr$, and Bi_n (n even) are diamagnetic and Bi_n (n odd) and $BiBr_2$ would be paramagnetic. Of these, reaction 4 is known to occur in solutions of low metal composition[7] and reaction 3 with an $n = 2$ has been observed in the gas phase.[10] As for reaction 5, no evidence for the existence of Bi^{+2} is known and its occurrence in this system is not readily apparent.

A comparison between the experimental results and the above mechanisms of solution will be made with the aid of the additivity relation

$$\chi = \sum_i N_i \chi_i \qquad (6)$$

Although this relation is an empirical one, it has been found to apply quite generally to mixtures of nonreacting diamagnetic liquids.[11] Since the susceptibilities of some of the equilibrium species, Bi(atoms), Bi_n, $BiBr$, and $BiBr_2$, are not available, estimates of these values will be made as described previously.[3] If the susceptibility of Bi^{+3} in molten $BiBr_3$ is taken equal to that in fused $BiCl_3$,[2] -20×10^{-6}, then the bromide ion susceptibility becomes -33×10^{-6}. With this value and the susceptibilities of Bi^+, -34×10^{-6} (derived[3] from $\chi_{BiCl} - \chi_{Cl} = -(57 - 23) \times 10^{-6}$) and Bi^{+2}, 456×10^{-6} at $550°$, susceptibility values of -67×10^{-6} and 390×10^{-6}, are arrived at for $BiBr$ and $BiBr_2$, respectively. The susceptibilities of the paramagnetic species, Bi^{+2} and Bi, 456×10^{-6} at $550°$, were calculated[3] from the Van Vleck equation[12]

$$\chi = [A\beta^2 4S(S + 1)/3kT] \qquad (7)$$

where A is Avogadro's number, β the Bohr magneton, and k the Boltzmann constant; it was assumed that both species contain only one unpaired electron, *i.e.*, the resultant spin moment $S = {}^1/_2$, and that there is complete quenching of the orbital angular momentum contribution of the electrons to the magnetic moment $(L = 0)$. Finally, for Bi_2 a minimum susceptibility value[3] of -80×10^{-6} is taken.

In Fig. 2 are plotted the experimental data at 350 and $550°$ and the calculated curves that would result at

$550°$ using relation 6 for the cases where the metal goes into solution completely as: a, discrete atoms (curve 1); b, metal dimers (curve 2); c, $BiBr_2$ (curve 3); and d, $BiBr$ (curve 4). The linear additivity dependence between the components has also been included (dashed line). Although the experimental results at low metal compositions resemble those for Bi–$BiCl_3$ in that they are linear and temperature independent, they fall somewhat below the calculated line for $BiBr$. (It should be recalled that the susceptibility values for $BiBr$ were based on the Bi–$BiCl_3$ results.) However, as in the Bi–BiI_3 system, curves 4 and 2 are the only ones that approach the experimental data at low metal concentrations. Although reaction 4 appears to be favored, the susceptibility results certainly do not preclude the occurrence of reaction 3 or a combination of reactions. If one reaction is predominant, *e.g.*, reaction 4, the data appear to indicate that this reaction goes furthest to completion in the chloride system and least in the iodide. The effect of an increase in temperature on the susceptibilities of the solutions is to increase the concentration of paramagnetic entities, *i.e.*, the mass action constant of reaction 4 (or 3) decreases with increase in temperature.

II. Solution of Bi as Ions and Electrons. Since many properties of liquid metals are described quite adequately by the free electron theory, the addition of bismuth to its fused salt may be considered analogous to adding cations and free electrons to the melt. Conversely, the addition of salt to the metal can be considered as a dilution of the free electron gas of the metal. To calculate the susceptibilities with this model, *i.e.*

$$Bi = Bi^{+z} + ze^- \qquad (8)$$

we shall utilize the additivity relation

$$\chi = N_1\chi_1 + N_2\chi_2 + \chi_e \qquad (9)$$

where the subscripts 1 and 2 denote iodide ion and bismuth(III) cation, respectively, and χ_e is the contribution to the molar susceptibility of the solutions made by free electrons

$$\chi_e = (8m\beta^2/3h^2)(9\pi^2 A N_{Bi})^{1/3}(\bar{M}/d)^{2/3} \qquad (10)$$

where, in turn, m is the mass of the electron and h is Planck's constant. It has been assumed in relation 10 that bismuth metal has three free electrons per atom, *i.e.*, $z = 3$. Although there is some evidence that there

(10) M. Yoshiyama, *J. Chem. Soc. Japan*, **62**, 204 (1940); E. Brackett and L. Brewer, UCRL-3712 (1957).

(11) P. W. Selwood, "Magnetochemistry," 2nd Ed., Interscience Publishers, Inc., New York, N. Y., 1956, p. 108.

(12) J. H. Van Vleck, "The Theory of Electric and Magnetic Susceptibilities," Oxford University Press, London, 1932, Chapter IX.

may actually be five electrons[13] per atom, the susceptibility results for three or five electrons per Bi in the metal-rich compositions are virtually identical.[3] (The weak dependence of χ_e on the number of electrons per atom of Bi in eq. 10 arises from the one-third power of the electron concentration, zAN_{Bi}.) With this result at high metal compositions and the fact that in the salt-rich solutions no oxidation state for bismuth higher than +3 is known, only the three electron case will be considered. Equation 9 can therefore be rewritten as

$$\chi = (1 - N_{Bi})\chi_{BiBr_3} + N_{Bi}\chi_{Bi^{+3}} + \chi_e \quad (11)$$

where $\chi_{BiBr_3} = -119 \times 10^{-6}$ and $\chi_{Bi^{+3}}$ is taken as -20×10^{-6}, and the results at 550° are presented in Fig. 2 as curve 5. The fit between curve 5 and the experimental points at 550° in the metal-rich composition range is fair, whereas in the salt-rich solutions there is no correspondence. Thus, as in the Bi–BiI$_3$ system, it appears that the metal-rich melts are, to a first approximation, metallic in their magnetic behavior, but no metallic behavior is evident in the low-metal composition range. If reaction 4 is assumed to be important in the salt-rich portion of this system and if

the free electron model persists at higher metal compositions, the system (except for the pure components) can be simply described by the equilibrium

$$Bi^{+3} + 2e^- = Bi(e)_2^+ \quad (12)$$
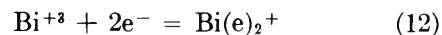
i.e., there is an equilibrium between free electrons and electron pairs localized around bismuth ion cores to form the entity Bi$^+$. The mass action "constant" for reaction 12 should decrease monotonically with increasing metal concentration and with increasing temperature.

Thus from the free electron viewpoint it appears that the Bi–BiBr$_3$ system is similar to the Bi–BiI$_3$. In the low metal compositions virtually all of the electrons are localized around bismuth ion cores and are in diamagnetic states. With continued addition of metal, overlap of electron orbitals occurs and in the metal-rich region of the system (70 to 100% Bi) free electron or metallic behavior is predominant. In the intermediate compositions both localized and delocalized electrons probably exist.

(13) S. Takeuchi and H. Endo, *Trans. Japan Inst. Metals*, **2**, 188, 243 (1961).

Kinetics of Ethylene Hydrogenation over a Platinum–Silica Catalyst

by J. H. Sinfelt

Esso Research and Engineering Co., Linden, New Jersey   (*Received October 30, 1963*)

The kinetics of ethylene hydrogenation have been investigated over a silica-supported platinum catalyst in the temperature range 45–93° using a flow reactor system. The reaction rate was found to be proportional to the square root of the hydrogen partial pressure. With respect to ethylene partial pressure, the rate was observed to decrease with increasing pressure at the lower ethylene pressures studied (0.007 to 0.10 atm.), but to approach a zero-order dependence at sufficiently high pressures. The apparent activation energy was 16 kcal./mole. The rate data support a mechanism involving adsorption of both hydrogen and ethylene on the active catalyst sites, the rate being determined by the rate of reaction between hydrogen atoms and ethylene molecules adsorbed on the surface.

The kinetics of ethylene hydrogenation over nickel catalysts have been studied extensively, but much less has been reported on the kinetics over other metals, such as platinum.[1] Furthermore, kinetic studies over supported metals have received much less attention than studies over metal films, wires, or powders. In the case of supported platinum catalysts, the reported data on the kinetics of ethylene hydrogenation appear to be limited to those of Bond,[2] along with some very briefly reported results of Schuit and van Reijen.[3] The latter results were obtained at low temperature (−40°), while the former were obtained in the temperature range 0–50°. The supported platinum catalysts employed by these investigators differed markedly in platinum content, the catalyst studied by Schuit and van Reijen containing about 50% Pt on SiO₂ as compared to 1–5% Pt on several different supports in the studies of Bond. Furthermore, these investigators observed marked differences in the way in which the reaction rates varied with the partial pressures of ethylene and hydrogen. This is not unreasonable, considering the differences in conditions and the nature of the catalysts employed. However, differences such as these observed over wide ranges of conditions can be illuminating with regard to the over-all mechanistic picture of the system and how it can vary with conditions.

In the present paper, the kinetics of ethylene hydrogenation over supported platinum have been extended to higher temperatures using a Pt–SiO₂ catalyst of much lower platinum content (0.05%). Reaction rates have been measured over a wide range of hydrogen and ethylene partial pressures (40–60-fold variation), and some significant differences from what has been reported at lower temperatures have been observed.

Experimental

Apparatus and Procedure. A flow reactor system at atmospheric pressure was used in this work. The reactor consisted of a stainless steel tube approximately 1.0 cm. in diameter and 8.0 cm. in length. In place, the reactor was held in a vertical position and was surrounded by an electrical heater. A small electrically heated coil was placed in the inlet line to the reactor to serve as a preheater. The catalyst was located midway along the length of the tube and occupied a space amounting to about 20% of the volume of the tube. The catalyst was supported on a fritted stainless steel disk and was held in place by packing quartz wool on top. The reaction temperature was measured with an iron–constantan thermocouple housed in a 3-mm. axial thermowell extending upward through

(1) G. C. Bond. "Catalysis by Metals," Academic Press Inc., New York, N. Y., 1962, p. 240.

(2) G. C. Bond. *Trans. Faraday Soc.*, **52**, 1235 (1956).

(3) G. C. A. Schuit and L. L. van Reijen. *Advan. Catalysis*, **10** 242 (1958).

the fritted steel disk to the center of the catalyst charge. The reactant gases, ethylene and hydrogen, were passed downflow through the reactor in the presence of helium as a diluent. The flow rates of the individual gases were measured with orifice-type flow meters. The total gas flow rate was maintained at 1 l./min. throughout, and the partial pressures of the hydrogen and ethylene could be varied individually by appropriate adjustment of the helium flow rate.

The reaction products were analyzed by a chromatographic unit coupled directly to the outlet of the reactor. The chromatographic column, 0.6 cm. in diameter and 1 m. in length, was packed with 100-mesh silica gel and operated at 40°. Excellent resolution of the ethylene and ethane was obtained. A thermal conductivity detector was used with the column, and helium was employed as the carrier gas.

The run procedure involved passing the reactant gases over the catalyst for a period of 3 min. prior to sampling the products for chromatographic analysis. The ethylene was then cut out and the hydrogen flow continued for 10 min. prior to another reaction period. Most of the reaction periods were bracketed by periods at a standard set of conditions, as an insurance against possible complications due to changing catalyst activity.

Materials. Research grade ethylene was obtained from the Matheson Co. A chromatographic analysis of the ethylene showed no detectable hydrocarbon impurities such as ethane or methane, although it is estimated that levels of the order of 100 p.p.m. would have been detected. High purity hydrogen obtained from the Linde Co. was further purified by passing it through a Deoxo unit containing palladium catalyst to remove trace amounts of oxygen as water and then drying with a molecular sieve.

The Pt–SiO$_2$ catalyst used in this work contained 0.050 wt. % Pt and was prepared by impregnating calcined silica gel with aqueous chloroplatinic acid, and then calcining the finished catalyst at 538° in air for 1 hr. The silica gel, obtained from Davison Chemical Co., was calcined for 4 hr. at 538° prior to impregnation with platinum. The B.E.T. surface area of the calcined silica gel was 388 m.^{2}/g. The particle size of the Pt–SiO$_2$ catalyst as used in the rate studies was approximately 0.3 mm. The catalyst was reduced in place in the reactor at 500° for 3 hr. in flowing hydrogen (200 cc./min.) prior to making any reaction rate studies.

Results

The hydrogenation of ethylene to ethane over the Pt–SiO$_2$ catalyst used in this work was studied over the

temperature range 45 to 93°. The reaction occurred very selectively, no side products being detected.

The approach in studying the kinetics was to measure initial reaction rates, and 90% of the data was obtained at conversion levels less than 5%. The rates were calculated using the relation

$$r = \frac{F}{W} x \qquad (1)$$

where F represents the ethylene feed rate in gram-moles per hour, W represents the weight in grams of platinum on the catalyst charged to the reactor, and x represents the fraction of the ethylene converted to ethane. The reaction rate r is then expressed as gram-moles of ethylene hydrogenated per hour per gram of platinum.

The effect of temperature on reaction rate is shown in Fig. 1. The data in the plot were obtained in successive reaction periods in a falling temperature sequence. During the measurements at the different temperatures, the hydrogen partial pressure p_H and the ethylene partial pressure p_E were maintained constant at 0.20 and 0.030 atm., respectively. From the slope of the Arrhenius plot of the data, the apparent activation energy is 16 kcal./mole. While the data in Fig. 1 show satisfactorily the effect of temperature on reaction rate, the absolute values of the rates are less meaningful. It has been observed that the activity of the catalyst can vary markedly over an extended series of measurements and is also sensitive to the length of time that the catalyst is reduced.
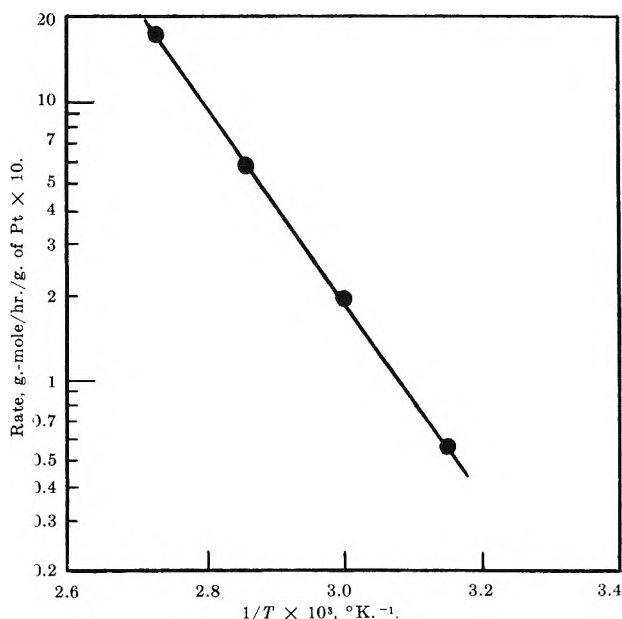
Figure 1. Effect of temperature on the rate of C$_2$H$_4$ hydrogenation; p_H = 0.20 atm., p_E = 0.030 atm.

In determining the effects of hydrogen and ethylene partial pressures on the rate of hydrogenation, it was decided to bracket all the reaction periods with periods at a standard set of conditions. This made it possible to detect variations in catalyst activity during the course of the measurements. The effect of hydrogen or ethylene partial pressure, varied one at a time away from the standard conditions, was then determined by simply comparing the rate, r, at the particular set of conditions with the average, r_0, of the rates at the standard conditions immediately before and after the period in question. This procedure serves to minimize the complications due to varying catalyst activity. The results on the effects of hydrogen and ethylene partial pressures on the relative rates, r/r_0, are presented in this form in Fig. 2 and 3.

In the logarithmic plot of r/r_0 vs. p_H at constant p_E in Fig. 2, a single line with a slope of approximately 0.5 fits the data for both temperatures. This indicates that the reaction rate is proportional to the square root of the hydrogen pressure over the range of pressures investigated. In Fig. 3, a similar logarithmic plot of r/r_0 vs. p_E at constant p_H shows that the effect of ethylene partial pressure varies somewhat with temperature. However, at both temperatures the rate falls with increasing ethylene partial pressure at the lower ethylene pressures, but tends to become independent of ethylene partial pressure at the higher pressures. Thus, at sufficiently high ethylene partial pressures, the reaction approaches zero order with respect to ethylene.

Figure 3. Effect of p_E on the rate of C_2H_4 hydrogenation at p_H = 0.20 atm.: O, 77°; △, 45°.

Discussion

The kinetic data on ethylene hydrogenation over the Pt–SiO₂ catalyst used in this work appear to be best explained by a mechanism involving adsorption of both reactants on the active catalyst sites. On the assumption that the hydrogen is chemisorbed dissociatively to atoms on the platinum surface, the surface reaction can be written

$$C_2H_4 \text{ (a)} \xrightarrow{H(a)} C_2H_5 \text{ (a)} \xrightarrow{H(a)} C_2H_6$$
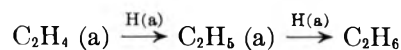
where the symbol (a) denotes an adsorbed species. The reaction rate is given by

$$r = k\theta_H\theta_E \qquad (2)$$

where θ_H and θ_E represent the fractions of the active surface covered by hydrogen and ethylene, respectively. Assuming that θ_H can be expressed in terms of a Langmuir isotherm, and that hydrogen is chemisorbed in competition with ethylene, we can write

$$\theta_H = \frac{b_H^{1/2}p_H^{1/2}}{1 + b_H^{1/2}p_H^{1/2}} (1 - \theta_E) \qquad (3)$$

If the term $b_H^{1/2}p_H^{1/2}$ is small compared to unity, corresponding to weak adsorption of hydrogen, the denominator of eq. 3 can be ignored, and eq. 2 for the rate expression becomes

$$r = kb_H^{1/2}p_H^{1/2}(1 - \theta_E)\theta_E \qquad (4)$$

This equation accounts for the observed dependence of the rate on the square root of the hydrogen partial

Figure 2. Effect of p_H on rate of C_2H_4 hydrogenation at p_E = 0.030 atm.: O, 77°; △, 45°.

pressure. The equation also predicts that at constant hydrogen pressure the rate will go through a maximum at $\theta_E = 0.5$ and then decrease with further increase of θ_E. Since θ_E is determined by the ethylene pressure p_E, the rate should then decrease with increasing p_E for values of p_E above that corresponding to $\theta_E = 0.5$. The results of the present study show that the rate decreases with increasing p_E even at the lowest ethylene pressures investigated, and to make the results consistent with eq. 4 it must be postulated that an ethylene coverage of 0.5 is attained at ethylene pressures lower than any covered in this work. This could well be the case. However, eq. 4 cannot readily account for the observation that the rate becomes essentially zero order with respect to ethylene at the higher ethylene pressures investigated, unless one assumes that θ_E approaches a maximum value less than unity as p_E is increased without limit. It is conceivable that the packing of ethylene molecules on the surface of the platinum crystallites is such that the ethylene cannot completely cover the platinum sites; i.e., a certain fraction of the sites is not accessible to ethylene, but is accessible to hydrogen. Making an assumption of this nature, we can write a modified Langmuir adsorption expression for θ_E

$$\theta_E = c \frac{b_E p_E}{1 + b_E p_E} \qquad (5)$$

where c represents the maximum degree of coverage by ethylene as p_E is increased without limit. On substitution of expression 5 for θ_E in eq. 4, the rate expression becomes

$$r = k b_H^{1/2} p_H^{1/2} \left\{ \frac{1 + (1 - c)b_E p_E}{1 + b_E p_E} \right\} \frac{cb_E p_E}{1 + b_E p_E} \qquad (6)$$

Equation 6 indicates that, at very low ethylene partial pressures, the rate will increase with increasing ethylene pressure up to a maximum value, beyond which the rate declines with further increase in ethylene pressure. As the ethylene pressure is increased without limit, however, the rate approaches a constant limiting value.

Applying eq. 6, we can write an expression for r/r_0, the rate at a particular set of conditions relative to the rate at standard conditions. Arbitrarily taking $c = 0.90$, and noting that $p_E = 0.030$ atm. at the standard conditions employed in this study, we obtain for r/r_0

$$\frac{r}{r_0} = 33.3 p_E \left\{ \frac{1 + 0.10 b_E p_E}{1 + 0.0030 b_E} \right\} \left\{ \frac{1 + 0.030 b_E}{1 + b_E p_E} \right\}^2 \qquad (7)$$

Taking a value of b_E equal to 500 atm.$^{-1}$, we obtain satisfactory agreement between eq. 7 and the data at 77° for the range of ethylene pressures investigated,
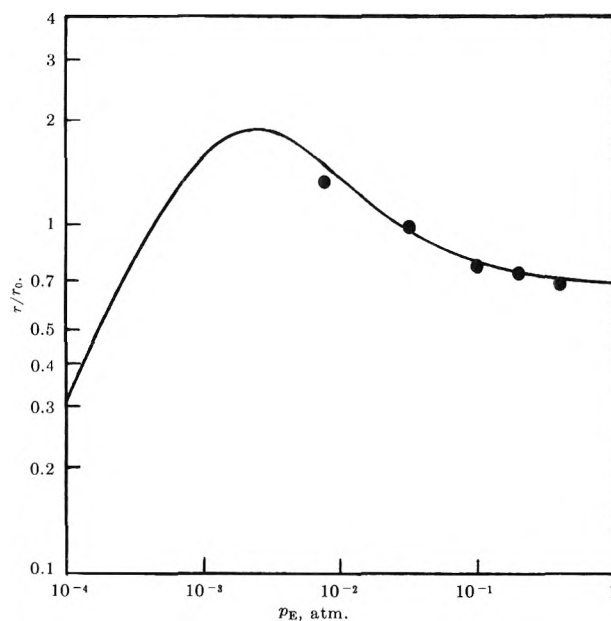
Figure 4. Comparison of eq. 7 with observed rate data; curve calculated from eq. 7; points represent data at 77°.

as illustrated in Fig. 4. We note that all the data were obtained in the region to the right of the maximum in the curve in Fig. 4. It was not possible to obtain data at low enough ethylene pressures to observe the maximum. In Fig. 3, the data indicated that the curve of r/r_0 vs. p_E was flatter at the lower temperature. This would be predicted by eq. 7 provided that a higher value of b_E was assumed at the lower temperature. Such an assumption is reasonable since adsorption constants should increase with decreasing temperature. The position of the maximum in the curve of r/r_0 vs. p_E would be expected to shift to a lower value of p_E at the lower temperature.

The apparent activation energy of 16 kcal./mole observed in this work is somewhat higher than has generally been observed for ethylene hydrogenation (about 11 kcal./mole). However, the catalyst employed in the present study represents a marked departure from the usual catalyst employed, e.g., metal films, or in the case of supported metals, much higher metal contents than the 0.05% used in this work.

The kinetic analysis presented in this paper is undoubtedly oversimplified, but it does appear to account reasonably well for the negative order with respect to ethylene at low ethylene pressures and for the shift toward zero order at the higher pressures. This type of analysis could tend to reconcile some of the apparent discrepancies in the literature regarding the effect of ethylene pressure, since part of this might arise simply from the fact that rate measurements were obtained in different ranges of conditions. However, it is likely

that the kinetic treatment presented here would not be satisfactory for situations where a large excess of ethylene relative to hydrogen is employed, since in such cases side reactions involving excess decomposition and possibly polymerization of unsaturated fragments could lead to irreversible poisoning of the surface.

The activity of the 0.05% Pt on SiO_2 catalyst used in this study, expressed as rate per unit weight of platinum, appears to be much lower than has been observed by Bond[2] for platinum catalysts containing 1 to 5% platinum. While this might merely reflect differences in catalyst preparation techniques, it might also indicate

heterogeneity of platinum centers, such that successive increments of platinum have different intrinsic catalytic activities. In support of this hypothesis, it has been observed that for a series of platinum-on-charcoal catalysts prepared in the same way, the rate of benzene hydrogenation per unit weight of platinum shows a sharp decrease below 0.1% platinum.[4] It is conceivable that this effect may be associated with an interaction between the platinum and support.

(4) A. M. Rubinshtein, K. M. Minachev, and N. I. Shuikin, *Dokl. Akad. Nauk SSSR*, **67**, 287 (1949).

The Free Energies of Formation of the Vanadium,

Niobium, and Tantalum Carbides[1]

by Wayne L. Worrell[2] and John Chipman

Department of Metallurgy. Massachusetts Institute of Technology, Cambridge, Massachusetts
(Received October 30, 1963)

By measuring the pressure of carbon monoxide in equilibrium with graphite–carbide–oxide mixtures at temperatures of 1180 to 1370°K , the free energies of formation of the carbon-rich carbides $V\overline{C}$, $Nb\overline{C}$, and $Ta\overline{C}$ have been determined. The notations $M\overline{C}$ and $\overline{M}C$ are introduced to denote carbide compositions, respectively, at the carbon-rich and at the metal-rich boundaries of the homogeneous field. The thermodynamic properties of other group VA carbides ($\overline{M}C$ and M_2C) are estimated from the $M\overline{C}$ data and the phase diagrams.

Introduction

With the increasing interest in refractory metal carbides, any determination of their thermodynamic properties at elevated temperatures should be very useful. In this investigation, the thermodynamic properties of vanadium carbide, niobium carbide, and tantalum carbide were determined by bringing a graphite–carbide–oxide pellet into equilibrium with a carbon monoxide atmosphere. Since the metal carbide is in equilibrium with carbon, the experimental results are valid for only the most carbon-rich composition of the carbide ($M\overline{C}$).

Because the group Va carbides exhibit a homogeneity range,[3] the simple formula MC is insufficient to designate a particular carbide composition. In this study, the formula for the carbide is modified to indicate precisely the carbide under discussion even when its exact

(1) This paper is based on a thesis submitted by Wayne L. Worrell in partial fulfillment of the requirements for the degree of Doctor of Philosophy at the Massachusetts Institute of Technology, May, 1963.

(2) Inorganic Materials Research Division, Lawrence Radiation Laboratory, University of California, Berkeley, Calif

(3) E. K. Storms, Los Alamos Scientific Lab Report LAMS-2674, 1962.

composition may be unknown. The use of $\overline{MC}$ indicates that carbide composition at the metal-rich phase boundary, while $\overline{MC}$ refers to that carbide composition at the carbon-rich boundary. Since the carbide phase boundaries vary with temperature, the compositions of the carbides $\overline{MC}$ and $\overline{MC}$ change with temperature. However, recent phase diagram investigations of the group Va carbides[3-5] show that the composition of $\overline{MC}$ varies only slightly with temperature.

Method

The experimental apparatus was very similar to that of Gleiser and Chipman.[6] The porcelain reaction tube was glass-sealed to a Pyrex tube which connected the reaction chamber to a vacuum pump, to gas cylinders, and to a mercury manometer used to measure pressures. After the reaction boat containing a sample pellet was placed in the reaction tube, a ground-glass stopper sealed the system.

A thin silica tube was used to withdraw gas samples from the reaction zone to a glass sampling bulb. The gas was analyzed for carbon dioxide and carbon monoxide in an Orsat apparatus.[7]

Elevated temperatures were obtained using a platinum-wound resistance tube furnace fitted with radiation shields and having a uniform temperature zone 5 cm. long. Temperatures were measured and controlled with a Pt-Pt + 10% Rh thermocouple which was accurate to $\pm 1°$ at the gold point.

Shieldalloy Corporation, Newfield, New Jersey, was the source of VC (vacuum grade, 81% V, 18.4% total C, 0.3% free C) and of TaC (Grade I with 1% Nb). The NbC (11.07% combined C, 0.66% free C) was purchased from the Vascoloy-Ramet Company.

Ta$_2$O$_5$ of reagent grade was used in the TaC investigation. V$_2$O$_3$ and NbO$_2$, which were used in the other studies, were prepared by the standard method[8,9] of hydrogen reduction of the pure pentoxide.

The finely powdered oxide and graphite in stoichiometric ratio were mixed with an equivalent quantity of carbide and cold-pressed into pellets weighing approximately 10 g. Usually two of these sample pellets were placed in an alumina reaction boat lined with small carbon rods. After the reaction boat was positioned in the reaction tube, the system was evacuated.

If no variation of the pressure in the reaction chamber was detected in 20 hr., an experimental run was started. After reaching the desired temperature, the system was evacuated again to remove gaseous impurities from the chamber. To avoid reducing the oxide in the sample pellet, the system was never evacuated for an extended period at elevated temperatures. The pressure in the system was measured with the mercury

manometer. By slightly evacuating the system one could reduce the pressure below the equilibrium value; the pressure could be increased above this value by introducing CO from the gas cylinder. Thus the equilibrium value was approached from both high and low pressures. After a constant pressure was observed (usually in 6 to 18 hr., depending on the reaction temperature), a gas sample was taken and the furnace evacuated. CO was then reintroduced, and the temperature setting was either decreased or increased so a new equilibrium pressure could be determined.

The gas samples contained no CO$_2$, and CO accounted for 94 to 99% of the total volume. The 1 to 6% residue was either H$_2$ or N$_2$, which most likely evolved from the graphite. In similar equilibrium studies with chromium carbide, Kelley, et al.,[10] found that 95 to 98% of the gas was CO in the experimental runs which used high-purity carbon. Only when carbon had been previously purified with chlorine gas to remove hydrogen did the gas from the reaction chamber analyze 99 to 100% CO.

An experimental run was terminated by completely evacuating the system and quenching with high-purity argon. The silica gas sampling tube and the radiation shields were removed, and the reaction boat was pulled to the cold zone of the reaction tube.

After each experiment, an X-ray diffraction pattern indicated that only the initial carbide, the initial oxide, and graphite were present in the sample pellet.

The experimental results are shown in Tables I, II, and III.

Discussion

In each carbide study, the investigated reaction is of the general form

$$M_xO_y(s) + (x + y)C(gr) \rightleftharpoons x\overline{MC}(s) + yCO(g) \quad (1)$$
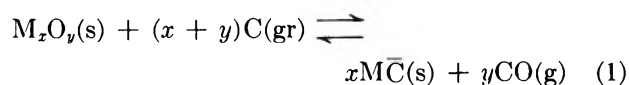
where M refers to either V, Nb, or Ta. With a determination of the temperature (T) and the equilibrium CO pressure (P_{CO}), the standard free energy change of

(4) E. K. Storms and R. J. McNeal, J. Phys. Chem., 66, 1401 (1962).

(5) E. K. Storms and N. H. Krikorian, ibid., 64, 1471 (1960).

(6) M. Gleiser and J. Chipman, ibid., 66, 1539 (1962).

(7) "Manual for Gas Analysis," Catalog No. 80, Burrell Technical Supply Co., Pittsburgh, Pa.

(8) A. D. Mah and K. K. Kelley, U. S. Department of the Interior, Bureau of Mines, Report of Investigation, No. 5858, Mines Bureau, Pittsburgh, Pa., 1961.

(9) E. G. King, J. Am. Chem. Soc., 80, 1799 (1958).

(10) K. K. Kelley, F. S. Boericke, G. E. Moore, E. H. Huffman, and W. M. Bangert, U. S. Department of the Interior, Bureau of Mines, Technical Paper No. 662, Mines Bureau, Pittsburgh, Pa, 1944.

Table I: Experimental Data from the Vanadium Carbide Study

T, °K.	P_{CO}, mm.	$\Delta F°$, cal.
1276	343	6130
1322	646	1269
1232	147	12175
1323	662	1090
1255	235	8785
1304	488	3401
1241	170	11071

Table II: Experimental Data from the Niobium Carbide Study

T, °K.	P_{CO}, mm.	$\Delta F°$, cal.
1249	743	114
1180	205	6154
1210	377	3322
1261	844	−577
1183	211	6008
1241	667	625
1201	344	3846
1175	185	6612
1211	408	2992

Table III: Experimental Data from the Tantalum Carbide Study

T, °K.	P_{CO}, mm.	$\Delta F°$, cal.
1311	314	11546
1265	145	20835
1355	590	3255
1366	654	2031
1289	217	16070
1332	411	8074

this reaction $(\Delta F_R°)$ can be calculated using the expression

$$\Delta F_R° = -yRT \ln P_{CO} \qquad (2)$$

Since the calculation is based on y moles of CO, the experimental interpretation depends heavily on the stoichiometry of the oxide phase. Only if the oxide is exactly M_xO_y will x be the correct number of moles of carbide. If the oxide possesses an extended homogeneity range, it would be very difficult to specify the correct value of x for reaction 1. However, there is evidence that V_2O_3[11] and NbO_2[12,13] are essentially stoichiometric compounds. Since a detailed phase investigation of Ta_2O_5 is unavailable, its stoichiometry is assumed.

Although the final X-ray diffraction patterns indicated the presence of both the M_xO_y and MC phases, oxide saturation of the MC phase could influence the results. Investigations of the carbon reduction of V_2O_3[14,15] above 1700° indicate that it is very difficult to eliminate oxygen completely from the VC phase. From his extensive investigations of the carbon reduction of niobium oxides, Shveikin[16] concludes that NbO_2 and NbC do not interact below 1200° but do form a solid solution above 1450°.

In the $N\overline{bC}$ investigation the effect of oxygen solubility on the activity of $N\overline{bC}$ can be estimated from the following reaction

$$NbO_2(s) + C(gr) \rightleftharpoons \langle NbO \rangle + CO(g) \qquad (3)$$
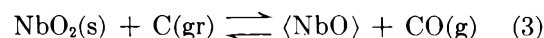
where $\langle NbO \rangle$ is considered to be dissolved in $N\overline{bC}$. Using the available free energy of formation data for NbO,[17] CO,[18] and NbO_2,[19] the standard free energy change of reaction 3 is calculated to be +12.6 kcal. at 1200°K. Since the measured CO pressure is approximately 0.5 atm. at this temperature (see Table II), one can calculate the equilibrium activity of NbO in the carbide to be 0.01. Assuming that the activity of $N\overline{bC}$ is thus reduced to 0.99 by the presence of this NbO, the calculated free energy of formation would be modified by only 25 cal. at 1200°K., which is considerably less than the experimental uncertainty from other causes. Similarly, the effect of oxygen contamination on the calculated thermodynamic properties of $Ta\overline{C}$ is probably negligible. However, the oxygen solubility in $V\overline{C}$ can be significant,[20] and its effect is considered in the subsequent analysis of the $V\overline{C}$ data.

The experimental temperature range was too small to permit evaluation of the entropy change $(\Delta S_R°)$ of reaction 1 from the linear variation of $\Delta F_R°$ with temperature. Instead a value for $\Delta S_R°$ calculated from available thermochemical data was used for the

(11) G. Anderson, *Acta Chem. Scand.*, **8**, 1599 (1954).

(12) G. Bauer, *Z. anorg. allgem. Chem.*, **248**, 1 (1941).

(13) L. Brewer, *Chem. Rev.*, **52**, 1 (1953).

(14) G. A. Meerson and O. E. Krein, *Zh. Neorgan. Khim.*, **5**, 1924 (1960).

(15) V. I. Zhelankin, V. S. Kutsev, and B. F. Ormont, *ibid.*, **3**, 1237 (1958).

(16) G. P. Shveikin, *Tr. Inst. Khim. Akad. Nauk SSSR, Uralsk. Filial*, **2**, 45 [translation AEC-TR-4303], 51 [translation AEC-TR-4304], 57 [translation AEC-TR-4305] (1958).

(17) V. I. Lavrent'ev, Ya. I. Gerasimov, and T. N. Rezakhima, *Dokl. Akad. Nauk SSSR*, **136**, 1372 (1961).

(18) J. F. Elliott and M. Gleiser, "Thermochemistry for Steelmaking," Vol. I, Addison-Wesley Publishing Co., Inc., Reading, Mass., 1960.

(19) W. L. Worrell, *J. Phys. Chem.*, **68**, 952 (1964).

(20) H. Krainer and K. Konopicky, *Berg- Huettenmaenn. Monatsh. Montan. Hochschule Leoben*, **92**, 166 (1947).

Figure 1. Standard free energy changes of the
$V\bar{C}$, $Nb\bar{C}$, and $Ta\bar{C}$ reactions.

the uncertainties in the free energy and enthalpy of formation of the carbide were evaluated.

Vanadium Carbide. The experimental data from the vanadium carbide study are shown in Table I.

The entropy of formation of VC at 298°K. is −1.5 e.u. using the value of Bieganski and Stalinski[22] for $S°_{298}$ of vanadium, since their metal was of higher purity than that on which Kelley and King's tabulation[23] is based. Values of Kelley and King were used for $S°_{298}$ of C and VC. The entropy of formation of VC at 1300°K. is also −1.5 e.u., because the high-temperature heat capacity of VC obeys Kopp's rule.[24] With this value and the thermal data for CO[18] and V_2O_3[8] at 1300°K., the entropy change of the $V\bar{C}$ reaction is +115.6 e.u. This fixes the slope of the dotted line drawn through the experimental data in Fig. 1 and gives

$$V_2O_3(c) + 5C(gr) \rightleftharpoons 2V\bar{C}(c) + 3CO(g)$$
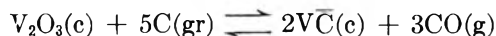
$$\Delta F°(\pm 850) = 154{,}150(\pm 1000) - 115.6T \text{ cal.} \quad (4)$$

However, VC and VO can form a continuous series of solid solutions,[20] and a significant amount of VO may be dissolved in the $V\bar{C}$. With the thermodynamic data for the vanadium oxides[8] and CO,[18] the activity of VO dissolved in the $V\bar{C}$ is calculated to be 0.42 ± 0.02 over the experimental temperature region using eq. 5 and the experimental data tabulated in Table I.

$$V_2O_3 + C \rightleftharpoons \langle 2VO \rangle + CO(g)$$
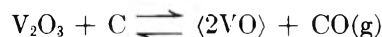
$$\Delta F° = 57{,}600 - 40.9T \text{ cal.} \quad (1200{-}1350°K.) \quad (5)$$

By assuming the solid solution to be ideal, the maximum correction to eq. 4 is obtained. With this assumption, the standard free energy change for reaction 4 would be 2800 cal. more positive, and this determines the lower boundary of the shaded area shown in Fig. 1.

Because VO and VC should separate into two immiscible phases at some critical temperature, one would expect positive deviations from ideality and a smaller correction to eq. 4. If the critical temperature for phase separation were known, the extent of the positive deviations from ideality could be calculated using regular solution theory.[25] The lowest temperature

slope of the lines shown in Fig. 1. Using the least-squares method,[21] this calculated slope was combined with the measured free energy changes to yield the enthalpy change of reaction 1. By combining these with the free energies and enthalpies of formation of the oxide and carbon monoxide, the free energy and enthalpy of formation of the carbide ($M\bar{C}$) were obtained.

The uncertainties in the reaction free energy changes were calculated from the estimated uncertainties in the temperature ($\pm 2°K.$) and pressure measurements ($\pm 5\%$) according to standard procedures.[21] The uncertainties in the enthalpy changes of reaction 1 were determined from the uncertainties in the measured free energy changes and in the values adopted for the entropy changes. By combining the uncertainties in the tabulated thermochemical data[18] for the oxides and for carbon monoxide with those of reaction 1,

(21) Y. Beers, "Introduction to the Theory of Error," Addison-Wesley Publishing Co., Inc., Reading, Mass., 1958.

(22) Z. Bieganski and B. Stalinski, *Bull. Acad. Polon. Sci.*, *Ser. Sci. Chim.*, 9, 367 (1961).

(23) K. K. Kelley and E. G. King, U. S. Department of the Interior, Bureau of Mines, Bulletin No. 592, U. S. Govt. Printing Office, Washington, D. C., 1961.

(24) K. K. Kelley, U. S. Department of Interior, Bureau of Mines, Bulletin No. 584, U. S. Govt. Printing Office, Washington, D. C., 1960.

at which complete solid solubility has been experimentally observed is 900°K.[20]; thus the maximum possible value for the critical temperature is 900°K. Using this value, one calculates that the minimum correction to eq. 4 is +700 cal., which determines the upper boundary of the shaded area in Fig. 1.

The correct equation for the standard free energy change of reaction 4 would be represented by a line parallel to the dotted line and lying within this shaded area. Lacking more precise information, eq. 4 is revised to eq. 6 which represents a line passing through the center of the shaded area; the distance between this line and the area boundaries is incorporated into the uncertainty term.

$$\Delta F^\circ(\pm 1100) = 155{,}900(\pm 1300) - 115.6T \text{ cal.} \quad (6)$$

Combining the free energy of formation equations for V_2O_3[8] and CO[18] at 1300°K. with eq. 6, the following expression for the free energy of formation of $V\bar{C}$ between 1200 and 1350°K. is obtained

$$\Delta F_f^\circ(\pm 600) = -24{,}100(\pm 700) +$$

$$1.5T \text{ cal./g.-atom of V} \quad (7)$$

Fujishiro[26] has measured the equilibrium pressure of vanadium over $V\bar{C}$ and graphite in a graphite Knudsen effusion cell between 2350 and 2550°K. and obtained a free energy of formation equation of $-23.300 + 2.0T$ cal. for $V\bar{C}$. The effusion of vanadium through the pores in the graphite cell and the vaporization of graphite itself accounted for 50 to 75% of the total weight loss; thus the experimental uncertainty may be as large as ±5 kcal./mole. Using the same data Fujishiro and Gokcen[27] calculated a value of -22.7 ± 5 kcal./mole for ΔH_f° of $V\bar{C}$ at 298°K.

Mah[28] has obtained -24.35 (± 0.4) kcal./g.-atom of V for the ΔH_f° of $V\bar{C}$ at 298°K. from recent heat of combustion experiments. Mah's value can be compared directly with our value of -24.1 (± 0.7) kcal./mole in eq. 7 since the high-temperature heat contents[24] of VC obey Kopp's rule.

Niobium Carbide. NbO_2 is the stable oxide under the experimental conditions of temperature and CO pressure, and no other oxide phase was detected in the final sample. The experimental data from the niobium carbide study are shown in Table II.

The entropy of formation of $Nb\bar{C}$ at 298°K. is -1.6 e.u. using the known entropies of Nb,[29] C,[23] and $Nb\bar{C}$.[30] Using Kelley's data[30] which are in excellent agreement with Gel'd and Kusenko's[31] high-temperature heat capacity data, -0.4 e.u. is obtained for the entropy of formation of NbC at 1200°K. With this

value and the available data for CO[18] and NbO_2[19] at 1200°K., the entropy change in the reaction is 80.3 e.u. This determines the slope of the line drawn in Fig. 1 and thus the free energy change in the reaction

$$NbO_2(c) + 3C(gr) \rightleftharpoons Nb\bar{C}(c) + 2CO(g)$$

$$\Delta F^\circ(\pm 400) = 100{,}400(\pm 800) - 80.3T \text{ cal.} \quad (8)$$

Combining the free energy of formation equations for NbO_2[19] and CO[18] at 1200°K. with eq. 8, the following expression for the free energy of formation of $Nb\bar{C}$ between 1170 and 1260°K. is obtained

$$\Delta F_f^\circ(\pm 600) = -31{,}100(\pm 900) +$$

$$0.4T \text{ cal./g.-atom of Nb} \quad (9)$$

Using the high-temperature heat content data for Nb,[29] C,[24] and NbC,[30,31] the heat of formation of NbC at 298°K. is calculated to be -31.8 (± 0.9) kcal./g.-atom of Nb. The heat of formation of NbC at 298°K. has been determined in the combustion calorimetric investigations of Mah and Boyle[32] as -33.6 ± 0.8 kcal., and of Huber, Head, Holley, Storms, and Krikorian[33] as -33.6 ± 0.6 kcal. Our value is less negative than the calorimetric values, but this may be the result of the compositional differences in the investigated carbide. Calorimetric values were obtained by extrapolation to a hypothetical $NbC_{1.0}$ composition, while our value is applicable to the graphite-saturated carbide which is $Nb\bar{C}_{0.99}$.[5]

Tantalum Carbide. Ta_2O_t was the oxide used in the $Ta\bar{C}$ study. Although other tantalum oxide phases have been reported,[34] tantalum pentoxide was the only oxide phase detected in the X-ray diffraction pattern of the sample pellet. The experimental data from the tantalum carbide study are shown in Table III.

(25) See, for example, G. N. Lewis, M. Randall, K. S. Pitzer, and L. Brewer, "Thermodynamics," 2nd Ed., McGraw-Hill Book Co., New York, N. Y., 1961, pp. 284–287.

(26) S. Fujishiro, *Trans. Japan Inst. Metals*, 1, 125 (1960).

(27) S. Fujishiro and N. A. Gokcen, *J. Electrochem. Soc.*, 109, 835 (1962).

(28) A. D. Mah, U. S. Department of the Interior, Bureau of Mines, Report of Investigation, No. 6177, Mines Bureau, Pittsburgh, Pa., 1963.

(29) R. Hultgren, R. L. Orr, P. D. Anderson, and K. K. Kelley, "Selected Values of Thermodynamic Properties of Metals and Alloys," John Wiley and Sons, New York, N. Y., 1963.

(30) K. K. Kelley, private communication, 1963.

(31) P. V. Gel'd and F. G. Kusenko, *Izv. Akad. Nauk SSSR, Otd. Tekhn. Nauk Met. i Toplivo*, 79 (1960).

(32) A. D. Mah and B. J. Boyle, *J. Am. Chem. Soc.*, 77, 6512 (1955).

(33) E. J. Huber, Jr., E. L. Head, C. E. Holley, Jr., E. K. Storms, and N. H. Krikorian, *J. Phys. Chem.*, 65, 1846 (1961).

(34) M. Hansen, "Constitution of Binary Alloys," McGraw-Hill Book Co., Inc., New York, N. Y., 1958.

Considering the similarity between NbC and TaC, the entropy of formation of TaC at 298°K. was estimated to be -1.6 (± 0.3) e.u. Using the tabulated entropies of Ta[29] and C,[23] this value would require that $S°_{298}$ of TaC equals 9.65, which is felt to be more reasonable than the 10.11 e.u. determined by Kelley.[23,35] Because the values of $S°_{298}$ for VC and NbC are both lower than $S°_{298}$ for pure V and Nb, respectively, it seems plausible that $S°_{298}$ for TaC should be less than the $S°_{298}$ of Ta which is 9.92 e.u. Since Kelley's study[35] was conducted in 1940, his TaC sample may have been inaccurately analyzed; even today it is extremely difficult to know precisely the composition of carbide samples.[1] There is also evidence[36] that Humphrey's[37] TaC, which was a similar commercial sample, was inaccurately analyzed. Thus a redetermination of the low-temperature heat capacity of TaC would be worthwhile.

To raise our estimated value of $\Delta S_f°$ at 298°K. for TaC to 1300°K., the high-temperature increments of TaC were assumed equal to those of NbC[30,31]; the high-temperature heat and entropy contents of TaN are virtually identical with those of NbN.[24] The resulting value of -0.5 e.u. for the entropy of formation of TaC and the thermochemical data for CO[18] and Ta$_2$O$_5$[18] at 1300°K. were combined with the data in Table III to yield the following equation for the line shown in Fig. 1.

$$Ta_2O_5(c) + 7C(gr) \rightleftharpoons 2Ta\bar{C}(c) + 5CO(g)$$

$$\Delta F°(\pm 800) = 274,900(\pm 1200) - 200.5T \text{ cal.} \quad (10)$$
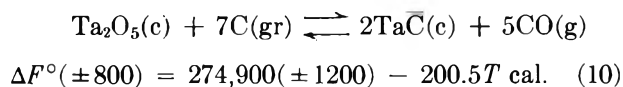
Combining the free energy of formation equations for Ta$_2$O$_5$[18] and CO[18] at 1300°K. with eq. 10, the following expression for the free energy of formation of TaC between 1250 and 1400°K. is obtained.

$$\Delta F_f°(\pm 600) = -34,900(\pm 700) +$$
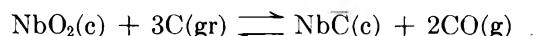$$0.5T \text{ cal./g.-atom of Ta} \quad (11)$$

Using the high-temperature heat content data for NbC,[30,31] the heat of formation of Ta$\bar{C}$ at 298°K. is calculated to be -35.6 (± 0.7) kcal./g.-atom of Ta.

The heat of formation of TaC at 298°K. has been measured by Huber, et al.[36] (-34.6 ± 0.9), by Humphrey[37] (-38.5), by McKenna[38] (-38.5 ± 5.0), and by Smironova and Ormont[39] (-35.7).

Our value agrees with the most recent investigation by Huber, et al., within the experimental uncertainties. Because they used TaC samples which probably contained free carbon, Humphrey's and McKenna's results have been questioned by Huber, et al. The close agreement between our value and that of Smironova and Ormont is probably fortuitous because their

heat of formation–composition data deviate widely from those of Huber, et al., who suggest that the samples of Smironova and Ormont were probably inhomogeneous.

In comparing our values for heat of formation with the calorimetric data, we do not imply equality of accuracy in $\Delta H°_{298}$. Our values are subject not only to the normal uncertainties in heat capacity but also to unknown contributions of the small shifts in equilibrium compositions of the M$\bar{C}$ phases, including solution of the oxide. Conversely, when it is the free energy of the equilibrium phase at elevated temperatures that is of primary interest, our values are to be preferred over those deduced from thermochemical measurements.

Estimates for the M$_2$C Carbides

In addition to the MC carbide phase, the group VA metal–carbide systems[3-5] also exhibit the M$_2$C carbide which has a narrow homogeneity range. Using the thermodynamic data obtained for the M$\bar{C}$ compositions, it is possible to assign limits for values of the $\bar{M}C$ carbides. Within somewhat wider limits, values for the M$_2$C carbides also can be estimated.

If the compositions of the carbide phase boundaries are known, the free energy of formation of the carbide at one phase boundary can be estimated from that of the carbide at the other phase boundary. For example, at 1000° the VC phase extents $\bar{V}C_{0.73}$ to $V\bar{C}_{0.88}$.[4] Since $V\bar{C}_{0.88}$ is that carbide in equilibrium with carbon and $\bar{V}C_{0.73}$ is that carbide at the metal-rich boundary, the following two reactions must occur spontaneously

$$V\bar{C}_{0.88} + V \longrightarrow 1.205\bar{V}C_{0.73} \quad (a)$$

$$\bar{V}C_{0.73} + C \longrightarrow V\bar{C}_{0.88} \quad (b)$$
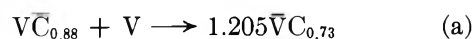
Thus, one can write

$$-\Delta F°V\bar{C}_{0.88} > -\Delta F°\bar{V}C_{0.73} > \frac{-1}{1.205}\Delta F°V\bar{C}_{0.88} \quad (c)$$

Using eq. 7 at 1273°K., $\Delta F°V\bar{C}_{0.88}$ is -22.2 kcal./g.-atom of V. From eq. c, therefore, $\Delta F°\bar{V}C_{0.73}$ must have a value between -22.2 and -18.4 kcal./g.-atom of V, and one can estimate that $\Delta F°\bar{V}C_{0.73} = -20.3 \pm 2.0$ kcal./g.-atom of V at 1273°K. Assuming the entropy of formation of $\bar{V}C_{0.73}$ has the same value as that of

(35) K. K. Kelley, J. Am. Chem. Soc., 62, 818 (1940).

(36) E. J. Huber, Jr., E. L. Head, C. E. Holley, Jr., and A. L. Bowman, J. Phys. Chem., 67, 793 (1963).

(37) G. L. Humphrey, J. Am. Chem. Soc., 76, 987 (1954).

(38) P. M. McKenna, Ind. Eng. Chem., 28, 767 (1936).

(39) V. I. Smironova and B. F. Ormont, Dokl. Akad. Nauk SSSR, 100, 127 (1955).

Table IV: Observed and Estimated Thermodynamic Properties of the Vanadium, Niobium, and Tantalum Carbides

Carbide	Calorimetric ΔH°_{298}, kcal.	This study ΔH°_{298}, kcal.	ΔS°_{298}, e.u.
		Obsd.	
$V\bar{C}_{0.88}$	-24.35 ± 0.4^a	-24.1 ± 0.7	-1.5
$Nb\bar{C}_{0.99}$	-33.6 ± 0.8^b	-31.8 ± 0.9	-1.6
$Ta\bar{C}_{0.99}$	-34.6 ± 0.9^c	-35.6 ± 0.7	-1.6
		Estd.	
$\bar{V}C_{0.73}$		-22.2 ± 2.0	-1.5
$\bar{Nb}C_{0.71}$	-28.2 ± 0.6^b	-28.0 ± 4.0	-1.6
$\bar{Ta}C_{0.71}$	-28.1 ± 1.5^c	-31.0 ± 4.0	-1.6
V_2C		-35.2 ± 5	-1.0^d
Nb_2C	-46.4 ± 1.2^b		-1.0^d
Ta_2C	-47.2 ± 3.4^c		-0.5^d

^{a} See ref. 28. ^{b} See ref. 33. ^{c} See ref. 36. ^{d} See ref. 41.

$V\bar{C}_{0.88}$, the following free energy of formation equation is obtained for $\dot{V}C$

$$\Delta F_f^\circ(\pm 2000) = -22,200 + 1.5T \text{ cal./g.-atom of V} \tag{12}$$

The thermodynamic properties of the other $\bar{M}C$ carbides were estimated using a similar procedure.

Properties of the M_2C phases can be estimated only very roughly, and the calorimetric data lie well within the limits of these estimates. The entropies of formation of the M_2C carbides have been estimated by Krikorian[40] and by Worrell.[41] The heat of formation of V_2C is estimated from the ratio of the calorimetric values for M_2C to MC, which for the other elements of the series is 1.375 ± 0.01. To apply this ratio to VC requires first extrapolation of the $V\bar{C}$ and $\bar{V}C$ data to $VC_{1.0}$ which gives about -25.6 kcal. at the stoichiometric ratio. Then for V_2C the estimate becomes -35.2 kcal. The uncertainty is large.

The estimates, along with the observed values for the heat and entropy of formation, are summarized in Table IV.

(40) O. H. Krikorian, Lawrence Radiation Lab Report UCRL-2888' 1955.

(41) W. L. Worrell, *J. Phys. Chem.*, **68**, 954 (1964).

Dynamic Mechanical Properties of Dilute Polyisobutylene Solutions

and Their Interpretation by an Extension of the Zimm Theory[1a]

by N. W. Tschoegl[1b] and John D. Ferry

Department of Chemistry, University of Wisconsin, Madison, Wisconsin (*Received October 31, 1963*)

Storage (G') and loss (G'') shear moduli have been measured for solutions of a sharply fractionated polyisobutylene ($M_v = 840,000$) in a naphthenic oil, at concentrations of 1% and 2%, temperatures of 0° and 25°, and frequencies between 0.016 and 160 c./sec., using the apparatus of Birnboim and Ferry. The results, expressed either as the polymer contributions to the complex modulus, G' and $G'' - \omega v_1 \eta_s$, or as the relative contributions to the complex viscosity, $(\eta' - v_1\eta_s)/(\eta - v_1\eta_s)$ and $\eta''/(\eta - v_1\eta_s)$, exhibited a frequency dependence intermediate between the predictions of the Rouse and Zimm theories. (Here ω is the circular frequency, v_1 the volume fraction of polymer, and η_s the solvent viscosity.) The frequency dependence was described by a recent extension of the Zimm theory with ϵ, a parameter describing deviation from gaussian chain statistics, set at 0.080, and h, an adjustable parameter describing the strength of hydrodynamic interaction, set at 7.5 for the 1% and 2 for the 2% solution. Earlier data on two polyisobutylenes of lower molecular weight (63,000 and 129,000) are closely fitted by the extended theory with $\epsilon = 0.03$ to 0.04 and $h = \infty$, representing a scarcely perceptible departure from the original Zimm theory. The molecular weights calculated by matching theory to experiment are too high, however, by a factor of 1.5 to 2.3.

Introduction

Measurements of the dynamic viscoelastic properties of dilute solutions of two fractionated polyisobutylenes of moderately low molecular weight (63,000 and 129,000) have been reported in an earlier paper.[2] The frequency dependence of the contributions of the polymer to the storage and loss shear moduli, G' and $G'' - \omega\eta_s$, conformed closely to the theory of Zimm.[3] (Here ω is the circular frequency and η_s the solvent viscosity, so $\omega\eta_s$ is the solvent contribution to the loss modulus.) Another polyisobutylene with much higher molecular weight ($M_v = 1,100,000$) and a broad molecular weight distribution showed a frequency dependence of G' and $G'' - \omega\eta_s$ which resembled more closely the theory of Rouse.[4]

In the present paper, measurements on a sharply fractionated high molecular weight polyisobutylene, undertaken to clarify this difference, are presented. The concentration dependence of the viscoelastic properties is examined; the frequency dependence of the components of the complex modulus, as well as of the complex viscosity, is compared with a recent extension of the Zimm theory[5,6] in which varying hydrodynamic interaction together with deviations from gaussian chain statistics are taken into account.

Materials and Method

A sample of polyisobutylene fractionated by a continuous chromatographic method[7] was generously provided by Dr. R. S. Porter and Dr. J. F. Johnson of the California Research Corporation. Its viscosity-

(1) (a) Part XLV of a series on mechanical properties of substances of high molecular weight; (b) Stanford Research Institute, Menlo Park, Calif.

(2) N. W. Tschoegl and J. D. Ferry, *Kolloid-Z.*, **189**, 37 (1963).

(3) B. H. Zimm, *J. Chem. Phys.*, **24**, 269 (1956).

(4) P. E. Rouse, Jr., *ibid.*, **21**, 1272 (1953).

(5) N. W. Tschoegl, *ibid.*, **39**, 149 (1963).

(6) N. W. Tschoegl, *ibid.*, **40**, 473 (1964).

(7) M. J. R. Cantow, R. S. Porter, and J. F. Johnson, *J. Polymer Sci.*, **C1**, 187 (1963).

average molecular weight was 840,000, and it is believed[8] to have a sharp molecular weight distribution, though probably broader than in the two samples studied previously.

Solutions containing 1% and 2% polymer by weight were prepared in Primol D, a naphthenic oil of suitable viscosity for the viscoelastic measurements.[2] Several more dilute solutions were prepared for measurements of steady-flow viscosity in a capillary viscosimeter,[9] from which the intrinsic viscosity in Primol D was calculated to be 1.94 dl./g.

The storage and loss moduli, G' and G'', of the 1% and 2% solutions were measured over a frequency range from 0.016 to 160 c./sec. by the apparatus of Birnboim and Ferry,[10] with modifications which have been described in subsequent publications.[2,11]

Results

Measurements were made at 0° and 25°. The former were reduced to 25° as previously described.[2,11] In Fig. 1 and 2, the reduced values of the contributions of the polymer to the components of the complex shear modulus, namely, G' and $G'' - \omega v_1 \eta_s$, are plotted logarithmically against reduced frequency for the 1% and 2% solutions. Here v_1 is the volume fraction of solvent, calculated on the assumption that the volumes of solvent and polymer are additive. In earlier papers,[2,11] this factor was omitted, and the polymer contribution to the loss modulus was written as $G'' - $

Figure 2. Logarithmic plots of G' and $G'' = \omega v_1 \eta_s$ for 2% polyisobutylene, $M = 840,000$. Key to temperature same as in Fig. 1. Curves represent extended Zimm theory with $\epsilon = 0.080$, $h = 2$, origin of dimensionless plot at cross.

$\omega \eta_s$. The difference is small except for quite high concentrations, but it is more appropriate[12] to include the factor v_1.

The superposition of data from the two temperatures is very good in both cases, showing that all relaxation times depend identically on temperature. The frequency dependence shows a distinct departure from the theory of Zimm; at the high frequency end, the ratio $(G'' - \omega v_1 \eta_s)/G'$ is about 1.3 instead of 1.73, and the slopes of the logarithmic plots in this region are about 0.55 to 0.60 instead of 0.667 as specified by the Zimm theory. Both these deviations are in the direction of the theory of Rouse, so it may be concluded that the Rouse-like behavior observed earlier for an unfractionated polyisobutylene of high molecular weight[2] was associated primarily with the magnitude of the molecular weight rather than with its broad distribution.

Discussion

Reduction of Components of Complex Viscosity. An alternative reduction which in principle provides for dependence on both temperature and concentration

Figure 1. Logarithmic plots of G' and $G'' - \omega v_1 \eta_s$ for 1% polyisobutylene, $M = 840,000$, in Primol D, referred to 25.0°: pip down, measured at 0.0°; pip left, at 25.0°. Curves represent extended Zimm theory with $\epsilon = 0.080$, $h = 7.5$, origin of dimensionless plot at cross.

(8) R. S. Porter and J. F. Johnson, personal communication.

(9) We are indebted to Mr. J. E. Frederick for these measurements.

(10) M. H. Birnboim and J. D. Ferry, *J. Appl. Phys.*, **32**, 2305 (1961).

(11) R. B. DeMallie, M. H. Birnboim, J. E. Frederick, N. W. Tschoegl, and J. D. Ferry, *J. Phys. Chem.*, **66**, 536 (1962).

(12) K. Ninomiya, *J. Colloid Sci.*, **17**, 759 (1962), and private communication.
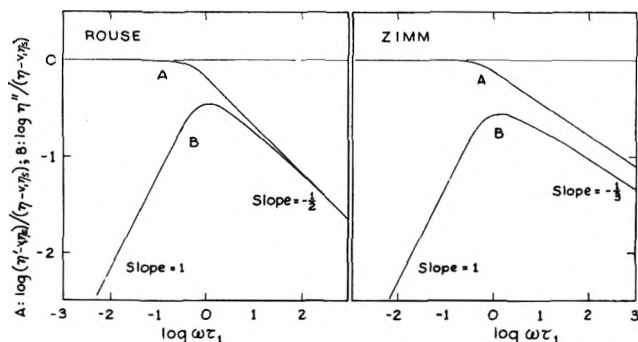
Figure 3. Logarithmic plots for the contributions of a polymer solute to the components of the complex viscosity, expressed in dimensionless form, as predicted by the theories of Rouse and Zimm.

may be employed with the following dimensionless variables

$$\eta_R' = (\eta' - v_1\eta_s)/(\eta - v_1\eta_s) \tag{1}$$

$$\eta_R'' = \eta''/(\eta - v_1\eta_s) \tag{2}$$

Theoretical logarithmic plots of η_R' and η_R'' against $\omega\tau_1$, where τ_1 is the terminal or longest relaxation time, are shown in Fig. 3 for the Rouse and Zimm theories. In terms of the components of the dimensionless complex modulus G_R' and G_R'' previously defined,[2,11] $\eta_R' = G_R''/\omega\tau_1 S$ and $\eta_R'' = G_R'/\omega\tau_1 S$. Here $S = \Sigma\tau_k/\tau_1$, where τ_k is the k'th relaxation time specified by the theory; $S = 2.369$ for Zimm and 1.645 for Rouse.

The appropriate frequency reduction for experimental plots can be inferred from the relation between the terminal relaxation time and the steady flow viscosity for either Zimm or Rouse theory

$$\tau_1 = [(\eta - v_1\eta_s)/cRT]M/S \tag{3}$$

where c is the concentration in g. of polymer per ml. and M is the molecular weight. A plot of η_R' and η_R'' against $\omega(\eta - v_1\eta_s)/cRT$ should give coincidence of data at different concentrations provided all relaxation times have the same concentration dependence.

The data of Fig. 1 and 2 are plotted logarithmically in this manner in Fig. 4. The two concentrations are nearly coincident, though the maximum in η'' is slightly lower at the higher concentration. Similar plots are given in Fig. 5 and 6 for the earlier data[2] on sharply fractionated polyisobutylenes of lower molecular weight. Here the coincidence of data at different concentrations is also rather close.

Plots of η_R' and η_R'' have an advantage in matching against theoretical curves to determine the apparent molecular weight; the ordinate position is fixed, unlike
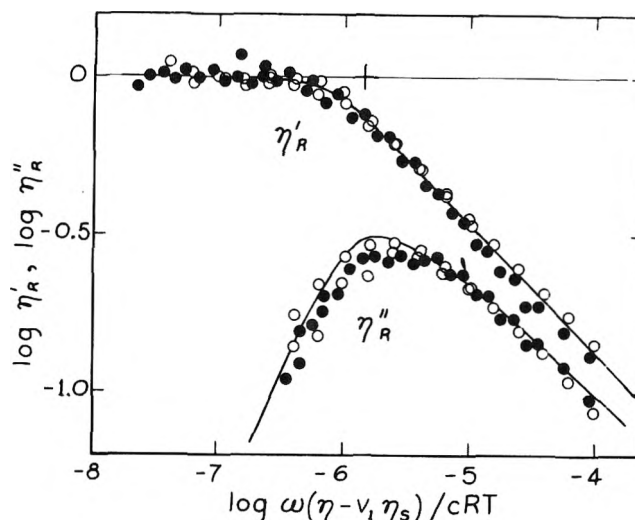
Figure 4. Logarithmic plots of η_R' and η_R'' against $\omega(\eta - v_1\eta_s)/cRT$ for data of Fig. 2 and 3: open circles, 1% (Fig. 2); black circles, 2% (Fig. 3). Curves represent extended Zimm theory with $\epsilon = 0.080$, $h = 5$.
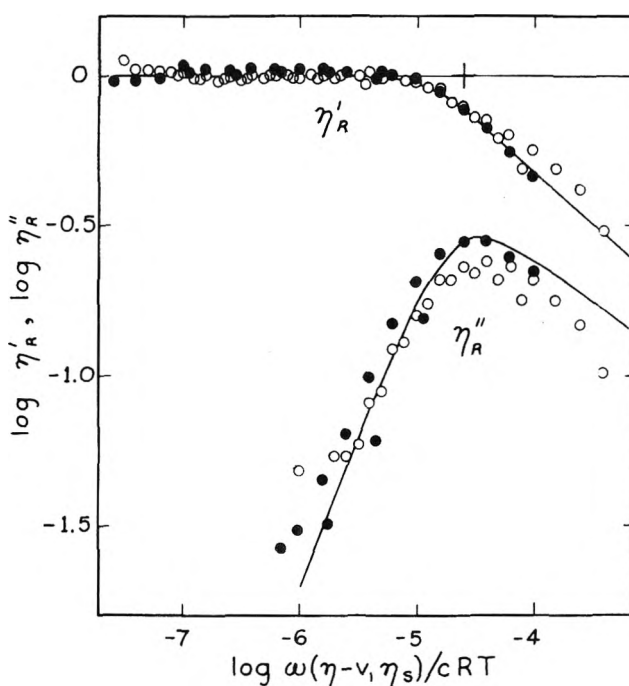
Figure 5. Logarithmic plots of η_R' and η_R'' against $\omega(\eta - v_1\eta_s)/cRT$ for polyisobutylene, $M = 63,000$, from data of ref. 2: open circles, concentration 2%; black circles 4%. Curves represent extended Zimm theory with $\epsilon = 0.031$, $h = \infty$.

the case for matching G_R' and G_R'' against theory as previously described.[11] Thus, a single shift of the abscissa scale for coincidence of theoretical and experimental curves identifies $\omega\tau_1 = 1$ at $\omega(\eta - v_1\eta_s)/$
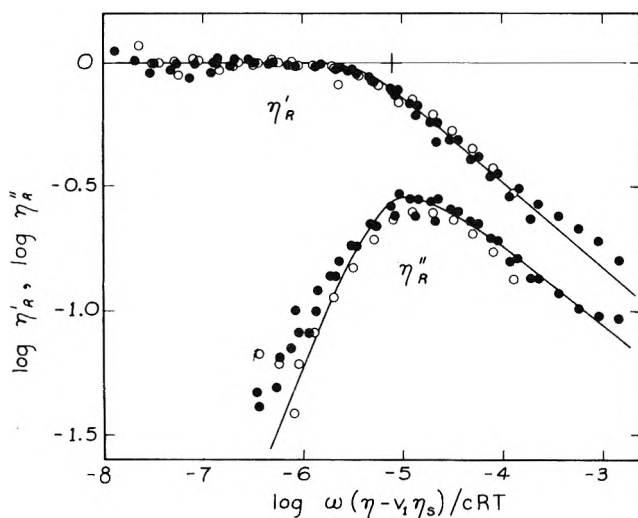
Figure 6. Logarithmic plots of η_R' and η_R'' against $\omega(\eta - v_1\eta_s)/cRT$ for polyisobutylene, $M = 129{,}000$, from data of ref. 2: open circles, concentration 2%; black circles, 4%. Curves represent extended Zimm theory with $\epsilon = 0.042$, $h = \infty$.

$cRT = S/M$. Then the position of the theoretical cross of origin on the experimental abscissa scale is simply $\log S/M$.

The data of Fig. 1–2 and 4–6 do not exactly fit either the Rouse or the Zimm theoretical plots, however, and we therefore apply a recent extension of the Zimm theory[5,6] in which behavior intermediate between the Rouse and Zimm types is predicted on the basis of varying hydrodynamic interaction and departures from gaussian chain statistics.

Theoretical Curves for Complex Viscosity from Extended Zimm Theory. In the extended theory, the frequency dependence of the complex modulus and complex viscosity is specified by two dimensionless parameters, h and ϵ. The first is Zimm's strength of the hydrodynamic interaction; $h = \infty$ corresponds to the Zimm case of dominant interaction, and $h = 0$ to the Rouse theory. The parameter ϵ is that used by Ptitsyn and Eizner[13] to describe expansion of a random coil in good solvents. The mean square separation of chain ends, for example, is proportional to $M^{1+\epsilon}$ instead of to M as would be specified by gaussian statistics in a Θ-solvent. For $h = \infty$, increasing values of ϵ toward the theoretical maximum of $^1/_3$ cause a shift in the character of the frequency dependence of dynamic mechanical behavior from the Zimm type partially toward the Rouse type.[6]

An estimate of ϵ can be obtained from the molecular weight dependence of the intrinsic viscosity $[\eta]$ in a given solvent, leaving h as an adjustable parameter. Following Stockmayer and Fixman,[14] a plot of $[\eta]/M^{1/2}$

against $M^{1/2}$ should be linear and the intercept a and slope b can be used to calculate the molecular weight dependence of the expansion factor α. From the relation $\epsilon = \partial\ln\alpha^2/\partial\ln M$, it follows[6] that

$$\epsilon = (M^{1/2}b/a)/[(3M^{1/2}b/a + 0.497) + 2.308(3M^{1/2}b/a + 0.497)^{1/2}] \quad (4)$$

The intrinsic viscosity values given in Table I have been treated in this manner to give a value of ϵ for each of the molecular weights, and these are also listed in the Table. Equation 4 was chosen in preference to the simpler eq. 39 of ref. 5 since it predicts lower ϵ-values and is therefore more in accordance with the experimental results for the lower molecular weight polymers whose solutions have been shown previously[2] to fit the Zimm theory for $\epsilon = 0$ quite closely. In the latter solutions it could be anticipated from this close approach to the Zimm theory that $h = \infty$. To determine h for the solutions with $M = 840{,}000$, the frequency dependence of η_R' and η_R'' was calculated for various values of h and $\epsilon = 0.080$, using a Control Data Corporation 1604 computer, from the relations given by the extended theory[5]; the curves whose shapes most closely matched the experimental data were selected. For the 1% concentration, $h = 7.5$ and for 2%, $h = 2$.

Comparison of Theory with Experiment and Calculation of Molecular Weight. Theoretical curves for G' and $G'' - \omega v_1\eta_s$ are drawn in Fig. 1 and 2 for $h = 7.5$ and $h = 2$, respectively, with $\epsilon = 0.080$, and the agreement with experimental points is excellent in both cases. No basic theoretical significance can be attributed to the change in h with concentration, however, since the theory is really limited to infinite dilution. It can only be said that there is a slight apparent shift toward Rouse-like behavior with increasing concentration. A similar effect has been noted in polystyrene solutions.[11,15]

In Fig. 4, a compromise pair of theoretical curves for η_R' and η_R'' has been drawn for $\epsilon = 0.080$ and $h = 5$, and these fall quite near the data at both concentrations. In Fig. 5 and 6, theoretical curves for the appropriate values of h and ϵ agree with the experimental points quite well. These curves differ very little from those for the original Zimm theory, since $h = \infty$ and ϵ is only slightly greater than zero.

The values of S calculated theoretically[6] for the appropriate values of h and ϵ are intermediate between

(13) O. B. Ptitsyn and Yu. E. Eizner, *Zh. Fiz. Khim.*, 32, 2464 (1958).

(14) W. H. Stockmayer and M. Fixman, *J. Polymer Sci.*, C1, 137 (1963).

(15) J. E. Frederick, N. W. Tschoegl, and J. D. Ferry, *J. Phys. Chem.*, submitted.

Table I: Parameters Obtained from Extended Zimm Theory Reduced to 25°

Polymer	F-17[a]		F-22[a]		H.M.[b]	
log M	4.80		5.11		5.924	
$[\eta]$ in Primol D, dl./g.	0.437		0.641		1.94	
ϵ	0.031		0.042		0.080	
Concn., wt. %	2	4	2	4	1	2
Concn., g./ml.	0.0176	0.0352	0.0176	0.0352	0.0088	0.0176
h	∞	∞	∞	∞	7.5	2
S		2.323		2.309	2.124	1.977
Abscissa cross, η_R' and η_R''	-4.63		-5.11		-5.85	-5.85
log M from eq. 3	4.99		5.47		6.17	6.15

[a] See ref. 2. [b] H.M. = high molecular weight.

the extreme values for the Rouse and Zimm theories; they are also given in Table I. From these together with the positions of the cross of origin on the experimental abscissa scale, values of molecular weight have been obtained as described above. The values (last row of Table I) for the lower molecular weights are practically the same as those derived previously[2] from the original Zimm theory. The apparent molecular weight from viscoelastic measurements is too large by a factor which lies between 1.5 and 2.3; it does not depend much on concentration in the range covered and its dependence on molecular weight appears to be erratic with the limited data thus far available. It may be remarked that the procedure for deriving the molecular weight by matching scales of experimental and theoretical curves will give a complicated molecular weight average if there is any molecular weight distribution. If the selection is made primarily on the basis of the left limb of η_R'' and the Zimm theory is followed, this average can be shown to be $M_z M_w M_n^2/ (\overline{M^{1/2}})^2$, where $\overline{M^{1/2}}$ is $\int M^{1/2}\varphi(M)\mathrm{d}M$, $\varphi(M)$ being the number-distribution of molecular weights.[16] The high molecular weights are weighted somewhat more than in M_w, but not enough to account for the observed discrepancy unless the molecular weight distribution were quite broad. Further work will be necessary, therefore, to clarify this discrepancy. However, the agreement of theory and experiment in all other respects is gratifying.

Applications of the extended Zimm theory to dilute polystyrene solutions will be presented subsequently.[15]

(16) S. E. Lovell and J. D. Ferry, *J. Phys. Chem.*, **65**, 2274 (1961).

On the Origin of Unpaired Electrons in Metal-Free Phthalocyanine

by J. M. Assour and S. E. Harrison

RCA Laboratories, Princeton, New Jersey   (Received November 4, 1963)

Metal-free phthalocyanine single crystals were found to contain 10^{17} unpaired electrons/cm.[3]. By heat treatments under vacuum and in oxygen and hydrogen ambients, the centers responsible for the "free radical" resonance were found to be oxygen impurities absorbed by the compounds. Experimental evidence indicates that the unpaired electrons may be either in the bulk or on the surface of the phthalocyanine. The absorbed oxygen may be associated with the electronically active centers in phthalocyanine semiconduction.

I. Introduction

Free radicals in residues of diamagnetic phthalocyanine metal derivatives were first detected through e.s.r. experiments by Ingram and Bennett.[1] Winslow, et al.,[2] observed similar free radicals in metal-free phthalocyanine (H$_2$Pc) and suggested that the origin of the unpaired electron occurs as a result of a broken π-bond in the phthalocyanine matrix. FuYen, Erdman, and Saraceno[3] believed that diradical structures of phthalocyanines might be responsible for the free radical concentration obtained in petroleum asphaltene. We have observed the "free radical" resonance both in metal-free phthalocyanine (H$_2$Pc) powder purchased from du Pont and that synthesized in our laboratory. The strong e.s.r. signal of the radical indicated that its concentration is large. Quantitative estimates of unpaired spins were made by comparison with the absorption of 1,1-diphenyl-2-picrylhydrazyl (DPPH) which contains 10^{21} unpaired electrons/g.

Our initial experimental studies began with H$_2$Pc crystals grown by sublimation from du Pont crude powder. A semiquantitative chemical emission spectrograph analysis for the compound revealed Cu as the major metallic impurity (200–2000 p.p.m.). The e.s.r. spectra of the single crystals consisted of Cu^{+2} hyperfine and nitrogen superhyperfine structures.[4] No evidence of the free radical resonance was observed. However, when the crystals were lightly crushed into powder, the free radical resonance was observed in addition to the Cu^{+2} and nitrogen lines. Subsequently, crystals were sublimed from "pure" H$_2$Pc and no metallic resonances were found; only the free radical resonance was observed. Evaporated thin films using single crystals as a starting material also revealed the free radical resonance.

Since the phthalocyanine compound are being studied in our laboratory as organic semiconductors,[5] the existence of free radicals in the system may prove to be significant in the semiconduction of the compound. Large concentrations of free radicals were shown to increase the electrical conductivity of some organic compounds.[2] The possibility of the radical contributing to the free carrier concentration[6] as a donor or acceptor of free carriers will determine the polarity of the involved carriers. Furthermore, if the radical is situated on the surface, it may have an influence on the relative importance of surface and bulk conductivities.

In the present paper, attempts to study the nature of the free radical, its location, as well as its chemical bonding and stability are reported. The investigations were carried out primarily by e.s.r. measurements with samples that were heat-treated under vacuum and in oxygen and hydrogen ambients. In attempting to

(1) D. J. E. Ingram and J. E. Bennett, Phil. Mag., 45, 545 (1954).

(2) F. H. Winslow, W. O. Baker, and W. A. Yager, J. Am. Chem. Soc., 77, 4751 (1955).

(3) T. FuYen, J. G. Erdman, and A. J. Saraceno, Anal. Chem., 34, 694 (1962).

(4) S. E. Harrison and J. M. Assour, Proceedings of the First International Conference on Paramagnetic Resonance, Academic Press, New York, N. Y., 1963.

(5) For a discussion of organic semiconductors, see C. B. G. Garett in "Semiconductors," N. B. Hannay, Ed., Reinhold Publ. Corp., New York, N. Y., 1959.

(6) L. S. Singer and J. Kommandeur, J. Chem. Phys., 34, 133 (1961).

create radicals by irradiation, samples treated with γ- and neutron rays were also examined.

II. Experimental Methods

The microwave resonance equipment used was a Varian spectrometer. The magnetic field modulation was 100 kc. while the microwave frequency was 9.5 kMc. The magnetic field was determined by a Harvey Wells n.m.r. gauss meter in conjunction with a Hewlett Packard 524D counter. The samples were placed in quartz tubes purchased from Varian with 2.9-mm. i.d. A calibrated quartz rod was used for accurate positioning of the samples in the microwave cavity. The radiofrequency power was properly adjusted to prevent saturated e.s.r. signals while the amplitude modulation was set to be less than one-tenth of the free radical line width. In all measurements reported here, the derivative of the absorption is recorded at ∼25° and the line width ΔH is taken between two points of maximum slope.

The actual spin concentration, spins/cm.^{3}, in the powdered samples was not established because only the relative change in the spin concentration was of interest. Therefore, the variation in the unpaired electron concentration in each sample as a function of heat-treatment temperature is expressed in arbitrary units.

III. Experimental Results

Pure H_2Pc was synthesized according to the method of Linstead.[7] Crystals grown from this powder contained the following metallic impurities by emission spectroscopy (in p.p.m.): Cu, 0.3–3; Li, 3–30; Al, 1–10; Si, 0.3–3; Mg, 3–30. Electron spin resonance of single crystals of 15-mm. length and 0.1-mm. width was examined at 25° in air. The resonance spectra were recorded for the ac plane of the H_2Pc crystal to determine their angular dependence. The spectra consisted of one narrow line shown in Fig. 1. The line width ΔH = 4.3 ± 0.5 gauss and the g-value was 2.0026 ± 0.0003. Both ΔH and g were isotropic and no metallic resonances were found in these crystals. To our knowledge this is the first time that H_2Pc single crystals exhibited the free radical resonance. The concentration of the free radicals in the single crystals was determined by a comparison method using the DPPH as a standard sample. The unpaired electron concentration in the H_2Pc crystals was found to be approximately 10^{17}/cm.^{3}.

Single crystals were lightly crushed into powder between two sheets of glassine paper and packed into a quartz tube which was then evacuated to 10^{-4} torr and sealed. The tube was placed in a furnace for
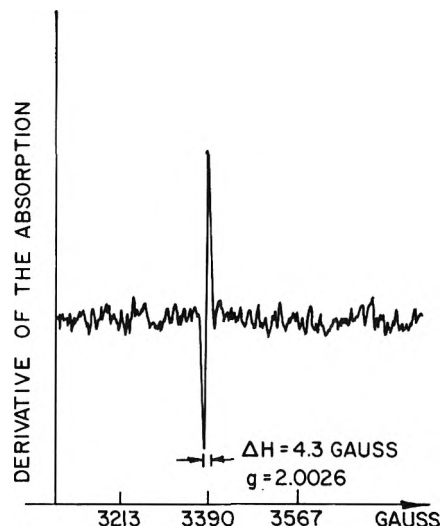
Figure 1. Electron spin resonance of free radical in metal-free phthalocyanine crystal.

AH = 4.3 GAUSS
g = 2.0026
3213   3390   3567   GAUSS

heat treatment at temperatures ranging from 25 to 500°. After each heat-treatment period which lasted for 2 hr., the spectrum of each sample was recorded. The spin concentration increased slightly up to 300° and then decreased at 400°. The decrease in spin concentration was found to be caused by sublimation of H_2Pc. At this temperature the powder began to sublime and small crystallites grew in the cooler zone of the quartz tube. At 600° the powder sublimed completely. Under vacuum, the total increase in spin concentration was negligible. The line width ΔH = 5.3 ± 0.5 gauss and g = 2.0026 ± 0.0003. These values remained essentially constant during the entire heat-treatment process.

A second powdered sample was first evacuated and then filled with oxygen and sealed. The sample was heat-treated as above. Figure 2 represents the plot of the variation of the unpaired electron concentration as a function of heat-treatment temperature. The concentration remains almost constant to 200° and then increases linearly with temperature. In this case a significant increase in spin concentration is obtained. The line width ΔH = 5.4 ± 0.5 gauss varied slightly with heat treatment while g = 2.0024 ± 0.0003 remained constant.

In a third quartz tube containing H_2Pc powder, hydrogen was allowed to flow continuously while the sample was heat-treated at 300°. The spectrum of this sample was recorded every hour. The spin concentration is seen to decrease in a hydrogen ambient as shown in Fig. 3. The decrease is seen to reach a

(7) R. P. Linstead, et al., J. Chem. Soc., 1719 (1936).
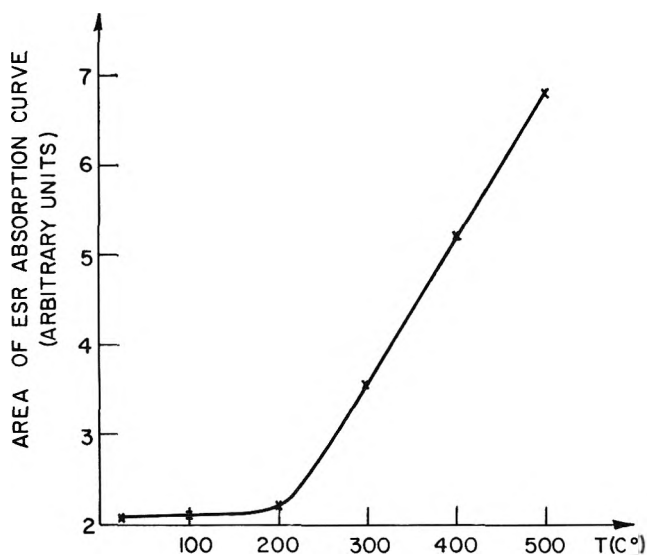
Figure 2.   Electron spin resonance of free radical in sublimed H₂Pc powder heat-treated in oxygen ambient.
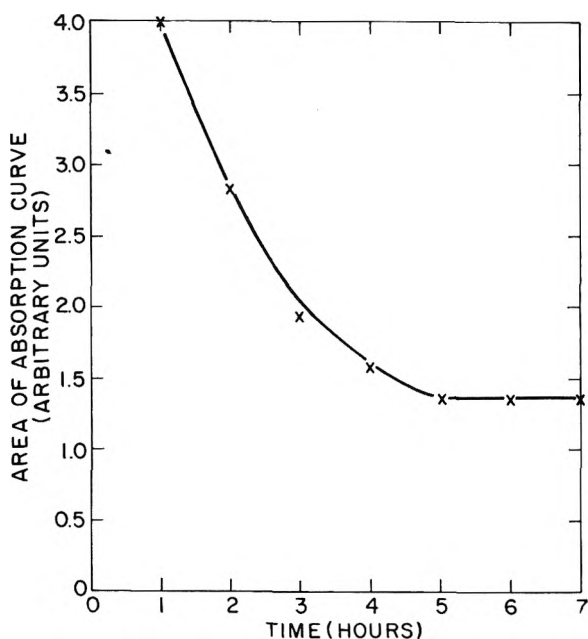
Figure 3.   Electron spin resonance of free radical in H₂Pc heat-treated at 300° in hydrogen ambient.

constant level after 6 hr. of heat treatment. To investigate the reversibility of the experimental results, the flow of hydrogen was stopped after 7 hr. of heat treatment and oxygen was allowed to flow through the same sample. Indeed, the spin concentration was found to increase at a rapid rate. During the heat-treatment process, the line width and the g-value did not vary at all. In this case, the heat-treatment temperature, 300°, was below the sublimation temper-

ature and after 9 hr. of heat treatment no evidence of sublimation was observed. The entire procedure was repeated for two different samples and in each case the same results were obtained.

IV.   Discussion

The spin concentration of the order of 10^{17} unpaired electrons/cm.[3] found experimentally in the H₂Pc compound is surprisingly high considering the fact that the molecule is diamagnetic and highly stable.[8] The spectra recorded for the ac plane show that the line width ΔH and the g-factor are independent of the angular variation with respect to the applied magnetic field. The line width in the single crystal is approximately equal to that obtained in the crystalline powder and seems to be invariant to the changing ambients and to the changing spin concentration. The single crystals utilized in these experiments have a large surface-to-volume ratio. In comparing the radical concentration/cm.[3] to the surface area of the crystals, it is found that a surface concentration of the order of 10^{14} unpaired electrons/cm.[2] would manifest the same e.s.r. characteristic. Assuming that the crystal contains 10^{21} sites/cm.[3], the density of surface sites is $\sim 10^{14}$ sites/cm.[2]. Therefore, it appears possible that these unpaired electrons are located in surface sites rather than in the bulk of the material.

The experimental results obtained from the heat-treatment method show that the number of free radicals remained essentially constant under vacuum, increased with oxygen treatment, and decreased with exposure to a hydrogen ambient. During the entire heat treatment in different ambients, the only parameter which varied significantly was the unpaired electron concentration. These results are quite different from those obtained with similar experiments on carbon blacks[9] and charred hydrocarbons.[10] In these compounds, it was found that the presence of molecular oxygen severely broadens[9] the unpaired electron resonance line and decreases[10] the unpaired spin concentration in the samples. The origin of the unpaired electron in the above compounds has been identified as a broken π-bond in the molecular matrix. Our experimental results clearly show that a reversible effect which gives an increase in spin concentration was obtained when a powdered sample was heat-treated in air. This result is in accord with that obtained by Winslow, et al.[2]

The mechanism for the reduction of spin concentra-

(8) J. M. Robertson, "Organic Crystals and Molecules," Cornell University Press, Ithaca, N. Y., 1953.

(9) R. I. Collins, M. D. Bell, and G. Kraus, J. Appl. Phys., 30, 56 (1959).

(10) J. Uebersfeld, Ann. Phys., 1, 393 (1956).

tion in the presence of a hydrogen ambient can be explained in terms of the experimental results obtained by Calvin, Cockbain, and Polanyi.[11] Their studies indicate that H_2Pc and its metal derivatives act as catalysts in the formation of water from its elements. Their experiments were carried out by heating a mixture of hydrogen and oxygen between 250 and 370° in the presence of H_2Pc crystals and observing the catalytic reaction. It seems reasonable to expect that in our experiments hydrogen may remove oxygen in much the same catalytic process. Therefore, our experimental results suggest that the unpaired spins may have their origin in reversibly absorbed oxygen. Oxygen is known to assume the role of a free radical. It may, in fact, exist as a diradical, though such a role is not implied by our spectra with a single sharp resonance. Our results indicate that oxygen may attach itself to the surface or diffuse into the bulk of the material.

In the case of carbon blacks and similar compounds, in which free radical resonances have been found and to which the phthalocyanine resonance has been compared,[1-3] the unpaired spins react differently. When oxygen diffuses in these compounds, which are assumed to contain free radicals, it attaches itself to the free radicals and may annihilate them.[10] Consequently, a decrease in spin concentration is observed. Singer, Spry, and Smith[12] have noted that in sucrose charred at 670°, only the line width decreases and the total absorption remains constant as the oxygen pressure increases. However, in sucrose charred at 450°, the resonance line width increases and the spin concentration decreases as a function of oxygen pressure. Now the effects of oxygen on charred carbons may be due to either the compensation of the broken π-bond or a broadening of the line due to the paramagnetism of the oxygen. In our case, the presence of oxygen manifests itself in an increase of spin concentration which indicates the absence of free radicals due to broken π-bonds in the phthalocyanine matrix. Our results are then in disaccord with prevailing assumption[1-3] that the unpaired electron responsible for the free radical is a delocalized electron from a broken π-bond in the phthalocyanine molecule.

Additional evidence for the absorption of oxygen by phthalocyanines has been obtained from conductivity measurements in various ambients. In H_2Pc, conductivity measurements on single crystals without guard rings indicate a reversible 1000-fold increase in conductivity on exposure to an oxygen atmosphere at room temperature along with a 15% decrease in activation energy.[13] With guard rings the same crystals show no change of conductivity. This indicates that the oxygen centers are effective on the

surface in increasing the conductivity but not in the bulk. This result, however, does not rule out the diffusion of oxygen into the bulk of the compound, for it has been found, on the other hand, that oxygen will affect the bulk conductivity of $CuPc$ and this oxygen can be identified with a deep-lying electron donor.[14] Though the interaction of $CuPc$ and H_2Pc with oxygen may not be identical, the diffusion processes should be similar because of the congruence of the molecular and crystal structures of these two derivatives.[8] In H_2Pc single crystals measurements of space-charge-limited currents reveal the existence of effective traps in the bulk of the crystal of the order of $10^{14}/cm.^3$ at a trap depth of 0.8 e.v. below the bottom of the conduction band.[15] Whether the oxygen active in the conduction processes gives rise to these traps and is the same as the oxygen that is responsible for the e.s.r. signal cannot be unequivocally established at the present time.

It is difficult at the present state of our knowledge to determine with certainty the site of the trapped oxygen. The absence of hyperfine structure suggests that the unpaired electron spin density on the surrounding nuclei is very small. Also, the narrowness of the resonance line shows that the free radical is an unpaired electron localized or possibly "trapped" in limited orbits which do not overlap with the phthalocyanine molecular orbitals. We have excluded exchange narrowing as the source for the narrow line width for two reasons. The first is that the spin density is so low compared to that of DPPH (i.e., 10^{21} spins/cm.^{3}). Secondly and more importantly, even if there were exchange narrowing with densities for less than 10^{21} spins/cm.^{3}, we would have expected the line width to vary as the spin concentration was altered. Further evidence that the resonance signal is not altered by exchange is given by the fact that Li_2Pc dissolved in 1-chloronaphthalene also manifests a resonance signal that is very similar in both ΔH and g-value[4] to the H_2Pc signal.

It may be that in phthalocyanine the free radical center is a complex of oxygen and some other unknown item in the phthalocyanine crystal. This unknown moiety of the free radical may be intrinsic to the

(11) M. Calvin, E. G. Cockbain, and M. Polanyi, *Trans. Faraday Soc.*, **32**, 1436 (1936).

(12) L. S. Singer, W. J. Spry, and W. H. Smith, Proceedings of the Third Conference on Carbon, Pergamon Press, New York, N. Y., 1959, p. 121.

(13) J. M. Assour and S. E. Harrison, unpublished.

(14) G. H. Heilmeier and S. E. Harrison, *Phys. Rev.*, **132**, 2010 (1963).

(15) G. H. Heilmeier and G. Warfield, *J. Chem. Phys.*, **38**, 163 (1962).

phthalocyanine crystals or a chemical or physical (*e.g.*, lattice imperfection) impurity.

The generation of free radical resonances on exposure to oxygen has been noted in experiments on biological materials by Miyagawa, Gordy, Watabe, and Wilbur.[16] In that work the oxygen was also reversibly absorbed. Even though the free radical resonances described in ref. 16 are somewhat asymmetrical whereas the resonances generated by oxygen in Pc are symmetrical and approximately half the width of the biological resonances, it may be that the centers that cause the oxygen to be absorbed in that material are electronically similar to the absorbing centers in Pc.

Samples of fine H_2Pc powder were irradiated with γ- and neutron rays. Preliminary studies of the ir-

radiated samples point out that the resulting e.s.r. spectra indicate that the free radical, as well as the phthalocyanine molecule, is stable under irradiation. The stability of phthalocyanines with regard to ionizing radiation may, as in the case of porphyrins,[17] be due to the very high resonance energy of the compound.

Acknowledgments. The authors wish to acknowledge helpful discussions with Dr. N. E. Wolff and the assistance of L. Korsakoff in supplying pure metal-free phthalocyanine powder.

(16) I. Miyagawa, W. Gordy, N. Watabe, and K. M. Wilbur, *Natl. Acad. Sci.*, **44**, 613 (1958).

(17) B. Pullman and A. Pullman, *Nature*, **196**, 1137 (1962).

Conductance of Potassium Chloride in Highly Purified

N-Methylpropionamide from 20 to 40°[1]

by Thomas B. Hoover

National Bureau of Standards, Washington, D. C.   (*Received November 7, 1963*)

The conductance of potassium chloride in N-methylpropionamide was measured at 5° intervals from 20 to 40° and in the concentration range of 5×10^{-5} to $3 \times 10^{-2}\,N$. The Fuoss–Onsager conductance equation represents the data with only a small contribution from the term linear in concentration. The ion size parameter $å_J$ increases from 0.6 to 1.5 with increasing temperature, while the mean hydrodynamic (Stokes) radius is 3.1 Å.

N-Methylpropionamide (NMP) is of interest as a solvent for electrolytes because of its unusually high dielectric constant (176 at 25°). Dawson, Graves, and Sears[2] have shown that a Kohlrausch plot represents the conductance data for potassium chloride fairly satisfactorily to much higher concentrations in NMP than in water. They found, however, that the slope of the plot differed by a few per cent from the theoretical limiting value of the Onsager equation. The present study was undertaken in order to obtain data

of sufficient precision to permit application of the extended conductance equation of Fuoss and Onsager.[3]

(1) Presented before the Division of Physical Chemistry at the 145th National Meeting of the American Chemical Society, New York, N. Y., September 9–13, 1963.

(2) L. R. Dawson, R. H. Graves, and P. G. Sears, *J. Am. Chem. Soc.*, **79**, 298 (1957).

(3) R. M. Fuoss and F. Accascina, "Electrolytic Conductance," Interscience Publishers, Inc. New York, N. Y., 1959, p. 195.

Experimental

The Jones–Dike conductance bridge[4] used in this work was found, by comparison with precision a.c. coils, to introduce a frequency-dependent error. In order to keep the error from this source negligible, frequencies were restricted to 2 kc.p.s. when the cell resistance was greater than 2000 ohms, and to 4 kc.p.s. at lower resistances.

Conductance cell I, with constant of 0.010747, had concentric cylinders of bright platinum as electrodes. The outer electrode was the longer and was constricted at the ends to provide partial shielding of the inner cylinder, which was always connected to the high potential corner of the bridge. Cell II, with a constant of 0.10684, was of the Jones and Bollinger[5] design and was calibrated against potassium chloride.[6] Concentrations of 0.01, 0.005, and 0.001 N revealed no Parker effect greater than 0.05%. Cell I was calibrated by intercomparison with II by means of 10^{-3} and 10^{-4} M solutions of sodium bicarbonate[7] and 0.1 M boric acid. Lead resistances were determined by measuring the conductance of constant-boiling hydrochloric acid in each cell in series with a precision 1000-ohm resistor.

The automatically regulated oil bath was stable to $\pm 0.002°$ for several hours. Temperatures were measured with a calibrated platinum resistance thermometer.

Solutions were prepared by weight in 125-ml. flasks and were transferred to the conductance cells under dry nitrogen. Magnetic stirrers were used to dissolve the salt; the stirring bars were enclosed in glass or polytetrafluoroethylene. Within the range of molalities (m) and temperatures covered by this investigation, the densities of the solutions could be represented by the equation

$$\rho = \rho_0(1 + km) \tag{1}$$

where k has the value 0.042 ± 0.002. Molarities (c) were calculated from molalities by the equation

$$c/m = \rho_0(1 + km)/(1 + 0.07456m) \tag{2}$$

Measured viscosities were fitted by least squares to an equation of the form

$$\eta/\eta_0 - S_\eta c^{1/2} = 1 + Bc \tag{3}$$

where S_η, the Falkenhagen coefficient, was estimated from Λ_0 on the assumption of equal ionic mobilities.[8] Values of B are given in Table I.

The conductance measurements, summarized in Table II, covered the concentration range of 5×10^{-5} to 3.3×10^{-2} M. Each solution was prepared independently and each was measured at three or more temperatures. Because plots of R vs. f^{-1}, where R

Table I: Viscosity Coefficients for Potassium Chloride Solutions in N-Methylpropionamide

t	20	25	30	35	40
B	1.39	1.37	1.35	1.33	1.31

is resistance and f is frequency, usually showed a slight curvature, resistances were extrapolated to infinite frequency by the equation

$$R_t = R_\infty + af_t^{-b} \tag{4}$$

which can be fitted exactly to three points for which the frequencies lie in geometric progression. Thus

$$R_\infty = (R_1R_3 - R_2^2)/(R_1 + R_3 - 2R_2)$$
$$(\text{for } f_2^2 = f_1f_3) \tag{5}$$

At least five such frequencies in the range 0.5 to 4 kc.p.s. were used and the equation was fitted to the widest range consistent with the graph of all the points. The exponent b in eq. 4 varied from 0.76 to 1.10, being higher in the more concentrated solutions. The maximum difference between the extrapolated resistance and that measured at 2 kc.p.s. was 0.4%. The conductance of the solvent was subtracted from that of the solution.

Dielectric Constant. The substitution method[9] was used to obtain the dielectric constant of NMP at audio frequencies with the same bridge and cell as were used for the conductance measurements. Calibration of cell I with chlorobenzene, 1,2-dichloroethane, and water yielded an extrapolated vacuum capacitance of 8.64 pf. (the conductance cell constant corresponds to 7.41 pf.). The results for NMP, given in Table III, have an estimated error of $\pm 0.5\%$. Literature values[10] are about 2% lower. The effect of moisture was investigated and the discrepancy, which is slightly greater than the combined estimates of error, could be accounted for by less than 0.2% water in the sample used by Leader and Gormley.

N-Methylpropionamide. The solvent was prepared by the procedure of Leader and Gormley[10] and was purified by repeated fractional distillation at 5 mm. in a 1000 × 4 cm. column packed with 3-mm. glass helices.

(4) P. H. Dike, *Rev. Sci. Instr.*, **2**, 379 (1931).

(5) G. Jones and G. M. Bollinger, *J. Am. Chem. Soc.*, **53**, 411 (1931).

(6) J. E. Lind, Jr., J. J. Zwolenik, and R. M. Fuoss, *ibid.*, **81**, 1557 (1959).

(7) J. E. Lind, Jr., and R. M. Fuoss, *J. Phys. Chem.*, **65**, 999 (1961).

(8) See ref. 3, p. 234.

(9) C. P. Smyth, "Dielectric Behavior and Structure," McGraw-Hill Book Co., Inc., New York, N. Y., 1955, p. 212.

(10) G. R. Leader and J. F. Gormley, *J. Am. Chem. Soc.*, **73**, 5731 (1951).

Table II: Conductance of Potassium Chloride in N-Methylpropionamide

———20°———		———30°———		———35°———		———40°———	
10^4c	Λ	10^4c	Λ	10^4c	Λ	10^4c	Λ
6.76	8.906	0.53	11.621	3.91	13.326	3.89	15.042
14.66	8.891	3.92	11.723	4.05	13.270	4.04	14.979
47.48	8.882	4.07	11.681	8.58	13.278	6.65	15.062
81.67	8.894	6.71	11.702	19.80	13.289	8.54	14.996
155.63	8.907	8.62	11.693	35.46	13.307	19.71	15.022
204.25	8.915	14.54	11.711	41.00	13.274	35.31	15.031
204.25	8.913	14.54	11.720	66.21	13.301	40.79	15.006
312.88	8.927	19.88	11.697	80.62	13.317	46.67	15.018
———25°———		35.61	11.711	110.62	13.326	65.92	15.026
		41.14	11.685	186.25	13.360	110.14	15.052
14.60	10.240	66.49	11.699	237.80	13.382	185.45	15.105
47.28	10.227	111.10	11.717	308.87	13.406	200.77	15.108
81.32	10.244	154.30	11.744			236.77	15.126
154.97	10.257	187.06	11.754			307.54	15.155
203.38	10.269	238.83	11.764				
311.55	10.290	310.21	11.783				

Table III: Properties of N-Methylpropionamide

t	ρ	D	100η	$10^7\kappa_0$
20	0.9347	185	6.06	1.94
25	.9308	176	5.25	2.23
30	.9268	167	4.58	2.53
35	.9228	159	4.03	2.85
40	.9188	151	3.56	3.15

A conductivity cell in the line to the receiver was used to monitor the purity of the product. The NMP was stored and transferred under dry nitrogen. Gas chromatography of a sample 8 months after its preparation showed 0.1% water and an unidentified peak corresponding to a substance present in the amount of about 0.02%. This substance was eluted just before the water. The specific conductance of different batches of solvent fell within 2% of the values given in Table III, which are an order of magnitude lower than those of the previous study.[2] The freezing point, $-30.9°$, was 12° higher than the literature value[11]; other physical properties are given in Table III.

Potassium Chloride. Reagent grade potassium chloride was further purified by ion-exchange treatment with the use of Dowex 50 resin. A 0.1 N aqueous solution of the salt was passed through the column and eluted with the same concentration of hydrochloric acid prepared from bromide-free potassium chloride.[12] The middle half of the eluate was put on a second column and eluted with 30% hydrochloric acid, discarding the first and last quarters of the eluate. The salt obtained by evaporation of the eluate was re-crystallized once from conductivity water to free it from soluble resin. After drying at room temperature, the salt was fused under nitrogen. Spectrographic analysis showed less than 10 p.p.m. each of Al and Si, less than 1 p.p.m. of Ca and Mg, and no other detectable impurities. The pH of a 3.5 N solution in carbon dioxide-free water (pH 7.1) was 6.4.

Results and Discussion

The function Λ_η', defined by

$$\Lambda_\eta' = (\eta/\eta_0)\Lambda + Sc^{1/2} - Ec \log c = \Lambda_0 + Jc \quad (6)$$

was accurately linear in concentration. The viscosity correction to the observed equivalent conductance, Λ, consisted of the right side of eq. 3 $(1 + Bc)$ without inclusion of the Falkenhagen term[8]; S and E are theoretical terms whose values are given in Table IV. A least-squares fitting of eq. 3 gave Λ_0 and J, which are given in Table IV along with the estimates of their standard deviations. In order to reduce the effect of experimental scatter at the lower concentrations, the points were weighed by c. Consequently, the derived parameters depend chiefly on the four or five measurements obtained at concentrations greater than 0.01 N.

Values for Λ_0 at 30 and 40° may be compared with 11.6 and 14.9, respectively, reported by Dawson, Graves, and Sears.[2] These authors also called attention to the fact that the Walden product (last column of Table IV) varies somewhat with changes of temperature.

(11) G. F. D'Alelio and E. E. Reid. *J. Am. Chem. Soc.*, **59**, 109 (1937).
(12) G. D. Pinching and R. G. Bates, *J. Res. Natl. Bur. Std.*, **37**, 311 (1946).

Table IV: Conductance Parameters and Constants for Eq. 6

t	S	$-E$	Λ_0	Std. dev.	J	Std. dev.	$\Lambda_0\eta_0$	$\dot{a}_J$
20	6.4340	0.1828	8.884	0.003	1.4	0.1	0.5377	0.65
25	7.5584	.2109	10.225	.003	2.1	.1	.5368	0.92
30	8.8420	.2408	11.691	.004	3.0	.2	.5354	1.18
35	10.2685	.2669	13.280	.005	4.2	.2	.5347	1.43
40	11.8374	.2926	15.002	.005	5.1	.3	.5341	1.52

The J coefficients provide a measure of the ion size parameter, $\dot{a}_J$, if short-range interionic attractions are neglected and if the proper allowance has been made for the viscosity of the medium. The resulting values for $\dot{a}_J$, shown in Table IV, are impossibly small. Some other estimates of the ion sizes may be made if it is assumed that both ions have the same radius and mobility. The Walden product, at 30°, corresponds to a hydrodynamic (Stokes) radius of 3.06 Å. Inclusion of the Sutherland correction[7] gives 4.59 Å. If the large values of the viscosity coefficient B in Table I are interpreted as a purely hydrodynamic phenomenon due to the Einstein volume effect[13] they correspond to a mean ionic radius of 4.74 Å. However, the electrostatic interaction of the ions with solvent dipoles constitutes a far more plausible explanation of the viscosity effect. Zwanzig[14] has recently derived an equation for the contribution of this effect to conductance, but the dielectric relaxation time of NMP, which would permit a test of this theory, is not known.

The apparent molar volume of potassium chloride at 30° is 36 cc., corresponding to an ionic diameter of 3.85 Å. The small values calculated for $\dot{a}_J$ indicate that this parameter has been forced to include other short range effects. The most likely of these is ionic association, although it is also possible that an under-correction was made for viscosity. If a plausible value for $\dot{a}_J$ is used in the calculation of J, e.g., 3.33 Å. (the

value found for potassium chloride in water[7]) then an ion pair association constant of 0.5 is required, to account for the slope of the Λ_η' vs. c curve at 30°.

It is clear that the sphere-in-continuum model is unsatisfactory for potassium chloride in N-methylpropionamide. Indeed, this model could scarcely be expected to apply strictly as it is well-established[15] that the structure of N-substituted amides is that of long, polymeric chains held together by hydrogen bonds. There is evidence, however, of ion–solvent interactions. These effectively increase the viscosity and decrease the dielectric constant near an ion, as indicated by the large apparent hydrodynamic radii and by the existence of ion pairs despite the very high bulk dielectric constant.

(13) See ref. 3. p. 63.

(14) R. W. Zwanzig, *J. Chem. Phys.*, **38**, 1603 (1963).

(15) R. Lin and W. Dannhauser, *J. Phys. Chem.*, **67**, 1805 (1963).

Electrode Kinetics with Adsorbed Foreign Neutral Substance

by Akiko Aramata and Paul Delahay

Coates Chemical Laboratory, Louisiana State University, Baton Rouge, Louisiana
(Received November 9, 1963)

The kinetics of discharge of Zn(II) on a hanging Zn(Hg) drop was studied by the galvanostatic method in perchlorate medium without and with n-amyl alcohol. The Frumkin correction for the double layer structure was verified in the absence of n-amyl alcohol for $Mg(ClO_4)_2$ and $Ba(ClO_4)_2$, but departure was considerable for $NaClO_4$ and $Al(ClO_4)_3$. This discrepancy is tentatively explained. The variations of apparent exchange current density in the presence of n-amyl alcohol and $Mg(ClO_4)_2$ were essentially accounted for up to coverages of 0.5 by the change of current density with coverage and by the change of potential across the diffuse double layer. At higher coverage, exchange current densities appear to be somewhat smaller than the values computed on the basis of the above two corrections. An explanation is offered, and the significance of coverage, as computed from thermodynamic surface excesses, is discussed. The transfer coefficient was not affected by the presence of n-amyl alcohol.

Electrode processes in the presence of an adsorbed neutral substance, which is not directly involved in the charge-transfer reaction, have been considered from two points of view,[1-4] namely the effects of adsorption (a) on processes controlled by mass transfer and (b) on kinetics of charge transfer. Adsorption kinetics is also relevant, particularly with the dropping mercury electrode.[4,5] This paper deals with the second problem in a somewhat novel way.

Conditions were selected to simplify as much as possible the interpretation of experimental results and to eliminate effects which are only incidental to the problem. The discharge of Zn(II) on zinc amalgam was selected because its kinetics can be investigated by a relaxation method (e.g., the galvanostatic method) over a narrow interval of potentials in which coverage by the adsorbed additive hardly varies. Furthermore, this process occurs at sufficiently negative potentials to preclude anion specific adsorption. Complexation was avoided by the use of a perchlorate medium,[6] and the charge of the discharged species was unambiguously known. Complications due to adsorption kinetics, as would have been encountered with a dropping amalgam electrode, were eliminated by the use of a hanging zinc–amalgam electrode.

Experimental

Solutions. Solutions of $Ba(ClO_4)_2$, $Mg(ClO_4)_2$, and $Zn(ClO_4)_2$ were prepared by dissolution of the corresponding oxides. $Al(ClO_4)_3$ was prepared by dissolution of aluminum foil in $HClO_4$ (in the presence of Hg to speed up metal attack), and the solution was analyzed by an ion-exchange technique. Analytical grade $NaClO_4$ was utilized without further purification. Solutions were prepared with double-distilled water (once over $KMnO_4$) and were treated with purified activated charcoal to remove adsorbable impurities.[7]

(1) For a review see A. N. Frumkin, paper presented at the C.I.T.-C.E. Moscow meeting, Aug., 1963; abstract in *Electrochim. Acta*, 8, iii (1963).

(2) R. Parsons, "Advances in Electrochemistry and Electrochemical Engineering," Vol. I, P. Delahay, Ed., Interscience Publishers, New York, N. Y., 1961, pp. 54–58.

(3) In polarography: (a) J. Weber, J. Koutecky, and J. Koryta, *Z. Elektrochem.*, 63, 583 (1959); J. Koutecky and J. Weber, *Collection Czech. Chem. Commun.*, 25, 1423 (1960); (c) J. Kuta, J. Weber, and J. Koutecky, *ibid.*, 25, 2376 (1960); (d) J. Weber and J. Koutecky, *ibid.*, 25, 2993 (1960).

(4) For a review in polarography see C. N. Reilley and W. Stumm, "Progress in Polarography," Vol. I, P. Zuman, Ed., Interscience Publisher, New York, N. Y., 1962, pp. 81–121.

(5) See ref. 2, pp. 20–26.

(6) J. Bjerrum, G. Schwarzenbach, and L. G. Sillén, "Stability Constants," The Chemical Society, London, 1958, p. 111.

Zinc amalgam was prepared by electrolysis of zinc perchlorate in acidic solution and was stored, with cathodic protection, under a layer of 0.01 M $HClO_4$. The zinc concentration was determined by treatment of the amalgam with perchloric acid and subsequent polarographic analysis. n-Amyl alcohol was redistilled at 135–136°.

Cell for Galvanostatic Measurements. An all-glass H-cell was used with a fritted glass disk between the arms of the cell. Both compartments were filled with the solution being studied. One compartment contained a zinc–amalgam pool, a dropping amalgam electrode, and a hanging amalgam drop, which was prepared according to DeMars and Shain.[8] The zinc–amalgam pool served as auxiliary electrode in galvanostatic measurements. The other compartment was connected by a 1 M NaCl bridge to a calomel electrode prepared with 1 M NaCl. The latter electrode was part of the potential stabilization circuit, described below, and the liquid junction potential was of no consequence. The solution in the compartment with the zinc–amalgam electrodes was freed of oxygen by nitrogen bubbling. Nitrogen was purified over activated charcoal at Dry Ice temperature and by a vanadous sulfate solution according to standard polarographic practice.

Galvanostatic Measurements. The conventional bridge[9] was fed by a Tektronix pulse generator, Type 161. The potential of the zinc–amalgam drop was somewhat unstable with n-amyl alcohol in solution, possibly because of slow hydrogen gas evolution, and the resulting error in galvanostatic measurements was minimized by polarization of the electrode at the equilibrium potential with the 1 M NaCl–calomel electrode as counter electrode. The polarization circuit was opened with a Clare mercury relay, Type 1010, just before the galvanostatic determination of the overvoltage–time curve. Overvoltages at $t = 0$ were determined by extrapolation against $t^{1/2}$ in the interval $t = 2$ to 50 msec.

Surface Tension. Measurements were made with a Gouy electrometer after substitution of Zn(II) by Mg(II) in equivalent amount, regardless of the supporting electrolyte. Conditions corresponding to an ideal polarized electrode were thus practically achieved. The resulting error was negligible since, at any rate, the Zn(II) concentration was small in comparison with that of the supporting electrolyte. Charge densities and surfaces excesses were computed from electrocapillary curves.[10] Double layer capacity data, which lead to more precise values of the charge density in the absence of adsorbed organic substance, were not determined here because their interpretation is complicated by a frequency-dependent mass-transfer component[5] when n-amyl alcohol is present.

Discussion and Results

Zn(II) Discharge without n-Amyl Alcohol. The transfer coefficient α for Zn(II) discharge was determined by application of[11]

$$I_a^0 = nFk^0 C_{Zn(II)}^{1-\alpha} C_{Zn}^\alpha \exp\left[\frac{-(1-\alpha)nF}{RT}\Delta\varphi\right]$$

$$(1)$$

where I_a^0 is the apparent exchange current density; $n = +2$; k^0 is the standard rate constant for the reaction Zn(II) + 2e = Zn(Hg) in the medium being studied; the C values are the concentrations; $\Delta\varphi$ is the difference of potential from the plane of closest approach to the bulk of the solution at the equilibrium potential; and F, R, and T are as usual. One had $I_a^0 = 1.75, 2.66, 4.52,$ and 7.47 ma. cm.$^{-2}$, respectively, for 1, 2, 4, and 8 mmoles l.$^{-1}$ of Zn(II); other conditions were $C_{Zn(II)} = 0.048$ mole l.$^{-1}$ for Zn(Hg), $C = 0.25$ M $Mg(ClO_4)_2$ for supporting electrolyte. A plot[12] of log I_a^0 against log $C_{Zn(II)}$ yielded $\alpha = 0.30$. The same value of α was also computed from measurements with 0.05 M $Mg(ClO_4)_2$.

Validity of the Frumkin correction was ascertained from the linearity of a plot of log I_a^0 against $\Delta\varphi$ for a varying concentration of supporting electrolyte and for fixed concentrations of Zn(II) and Zn(Hg). Results for $Mg(ClO_4)_2$ and $Ba(ClO_4)_2$ (Table I) yielded $\alpha = 0.30$, in good agreement with the above determination of α. Results for $NaClO_4$ gave the absurd value of $\alpha = -0.38$; likewise, $\alpha = 0.53$ for $Al(ClO_4)_3$ was abnormal. This indicated a definite departure from the Frumkin correction for the $\Delta\varphi$ values calculated from the plane of closest approach to the bulk of the solution. The disagreement may be ascribed to the differences in ionic charges[13] or, more likely, to differences in ionic radii of Zn(II) and Na(I) or Al(III). One has the following radii in solution according to Monk[14]: 1.83 [Na(I)], 2.88 [Ba(II)], 3.45 [Mg(II)],

(7) G. C. Barker, "Transactions of the Symposium on Electrode Processes," E. Yeager, Ed., John Wiley and Sons, Inc., New York, N. Y., 1961, pp. 325–365.

(8) R. D. DeMars and I. Shain, *Anal. Chem.*, **29**, 1825 (1957).

(9) See ref. 2, pp. 305–306.

(10) D. C. Grahame, *Chem. Rev.*, **41**, 441 (1947).

(11) For a review see ref. 2, pp. 237–247.

(12) The more rigorous plot of log I_a^0 vs. log $C_{Zn(II)} - (0.434nF/RT)\Delta\varphi$ yielded $\alpha = 0.28$, but variations of α resulting from the change of equilibrium potential, as C of Zn(II) varied, were so small (0.4 mv.) to hardly affect the determination of α.

(13) K. Asada, P. Delahay, and A. K. Sundaram, *J. Am. Chem. Soc.*, **83**, 3396 (1961).

Supporting electrolyte, mole l.$^{-1}$	$\Delta\varphi$, mv.	I_a^0, ma. cm.$^{-1}$	I^0, ma. cm.$^{-2}$
0.025 M Mg(ClO$_4$)$_2$	-63.0	12.0	0.40
0.05	-56.8	9.0	0.43
0.125	-46.3	4.7	0.37
0.25	-41.1	2.7	0.38
0.025 M Ba(ClO$_4$)$_2$	-60.8	9.1	0.33
0.05	-52.7	5.7	0.39
0.125	-42.8	3.2	0.31
0.250	-36.0	2.1	0.39

[a] For $C_{Zn(II)} = 2$ mmoles l.$^{-1}$, $C_{Zn(Hg)} = 0.048$ mole l.$^{-1}$. The exchange current density I^0, defined as $I^0 = I_a^0$ for $\Delta\varphi = 0$, was computed for $\alpha = 0.30$.

and 3.47 Å. [Zn(II)]. The difference in ionic radii in mixed electrolytes, as pointed out by Joshi and Parsons,[15] is a cause of departure from the Gouy–Chapman theory. Specific cation effects might possibly play a role.[16] At any rate, all work with adsorbed n-amyl alcohol was done with Mg(ClO$_4$)$_2$ since the Frumkin correction did hold in that case.

Zn(II) Discharge with Constant n-Amyl Alcohol Concentration and Varying Supporting Electrolyte Concentration. Before applying eq. 1 to Zn(II) discharge in the presence of adsorbed n-amyl alcohol, one must consider the main assumptions made in the derivation of this equation. These assumptions are: (a) The discharge process is of the first order with respect to all reactants, and its rate-determining step involves the same number of electrons as the over-all reaction. (b) The double layer correction is made by using $\Delta\varphi$, as calculated from the plane of closest approach and the bulk of the solution; and the concentration of Zn(II) in the plane of closest approach is correlated to that in the bulk of the solution on the assumption of purely electrostatic interactions. We shall *assume* that these assumptions can also be made when n-amyl alcohol is adsorbed on the electrode. The difference of potential $\Delta\varphi$ is now calculated by combination of the theoretical dependence of the charge density q on the electrode as a function of $\Delta\varphi$ with the experimental dependence of q on the electrode potential. The former relationship is given by the Gouy–Chapman theory, and the function $q = f(E)$ is obtained from electrocapillary curves. The procedure is the same as for solutions free of adsorbed neutral organic species, and its extension to electrodes with adsorption was made by Parsons.[2]

The rate constant k^0 in eq. 1 is some unknown func-

tion of the n-amyl alcohol coverage θ, but one deduces from this equation that a plot of log I_a^0 against $E - \Delta\varphi$ is linear and has the slope $0.434(1 - \alpha)(nF/RT)$ provided θ and the Zn(Hg) concentration are kept constant. This relationship provides one means of ascertaining the validity of the above method of calculation of $\Delta\varphi$, especially if α is constant whether or not n-amyl alcohol is present. At constant n-amyl alcohol concentration, $\Delta\varphi$ can be changed by variation of the supporting electrolyte concentration. The n-amyl alcohol coverage then varies slightly but could be kept constant, in principle, by adjustment of the potential E at which I_a^0 is measured. The Zn(II) concentration therefore should be adjusted to maintain θ constant, as the supporting electrolyte concentration varies. In practice, however, variations of θ due to the change of the supporting electrolyte concentration are smaller than the experimental error on θ. Measurements thus were made at constant E, *i.e.*, with constant concentration of Zn(II) and Zn(Hg), and data were plotted as log I_a^0 against $\Delta\varphi$. Results in the presence of 0.1 M n-amyl alcohol (Table II) gave a linear plot with a slope corresponding to $\alpha = 0.32$. This value of α for a high electrode coverage ($\theta = 0.78$) is the same within experimental error as that determined without n-amyl alcohol ($\alpha = 0.30$). It appears that α, *in this case*, is not affected by the presence of n-amyl[17] alcohol and that the Frumkin correction holds for the value of $\Delta\varphi$ calculated by the above method.

Zn(II) Discharge with Constant Supporting Electrolyte Concentration and Varying n-Amyl Alcohol Concentration. Values of I_a^0 were determined for different n-amyl alcohol concentrations in order to determine the influence of coverage. Since it was shown above that the correction for $\Delta\varphi$ can be made in presence of n-amyl alcohol, one can calculate the value of $(I_a^0)_{\theta=0}$ that would be measured if only $\Delta\varphi$ varied by addition of n-amyl alcohol and θ remained equal to zero (Table III). A plot of the ratio $I_a^0(\text{measured})/(_aI^0)_{\theta=0}$ then gives the influence of coverage (Fig. 1). The

(14) C. B. Monk, "Electrolytic Dissociation," Academic Press, Inc., New York, N. Y., 1961, p. 271.

(15) K. M. Joshi and R. Parsons, *Electrochim. Acta*, **4**, 129 (1961).

(16) (a) A. Aramata and P. Delahay, *J. Phys. Chem.*, **66**, 2710 (1962); (b) F. Lamy, J. J. Tondeur, and L. Gierst, paper presented at the C.I.T.C.E. Moscow meeting, August, 1963; abstract in *Electrochim. Acta*, **8**, xii (1963).

(17) The method for the determination of α in the absence of n-amyl alcohol cannot be applied here because θ varies too rapidly with the equilibrium potential as a result of the change in the Zn(II) concentration. An attempt to apply this method for 0.1 n-amyl alcohol gave the abnormal value $\alpha = 0.63$. Thus, when $C_{Zn(II)}$ increases, $C_{Zn(Hg)}$ being constant, E becomes more positive and θ increases; hence, I_a^0 is lower than the value expected for the same $C_{Zn(II)}$ and a constant θ. The plot of log I_a^0 against log $C_{Zn(II)}$ yields too low a value of $1 - \alpha$. This is indeed observed.

Table II: Variations of I_a^0 with Supporting Electrolyte Concentration in the Presence of 0.10 M n-Amyl Alcohol[a] at 26 ± 1°

$C_{Mg(ClO_4)_2}$, mole l.$^{-1}$	$\Delta\varphi$, mv.	I_a^0, ma. cm.$^{-1}$	I^0, ma. cm.$^{-1}$
C.05	−40.0	0.32	0.037
C.125	−30.5	0.20	0.037
C.25	−23.5	0.14	0.039

[a] For $C_{Zn(II)}$ = 2 mmole l.$^{-1}$, $C_{Zn(Hg)}$ = 0.048 mole l.$^{-1}$. I^0 computed for α = 0.30.

Table III: Variation of I_a^0 with n-Amyl Alcohol Concentration in 0.05 M Mg(ClO$_4$)$_2$[a] at 26 ± 1°

$C_{alcohol}$, mole l.$^{-1}$	$\Delta\varphi$, mv.	I_a^0 (measured), ma. cm.$^{-2}$	$(I_a^0)_{\theta=0}$, ma. cm.$^{-2}$
0	−55.8	9.0	9.0
0.02	−53.5	7.7	8.1
0.04	−49.2	4.2	6.4
0.08	−43.6	0.65	4.5
0.12	−37.5	0.23	3.4

[a] For $C_{Zn(II)}$ = 2 mmoles l.$^{-1}$, $C_{Zn(Hg)}$ = 0.048 mole l.$^{-1}$. I_a^0 (for θ = 0) computed from eq. 1 for α = 0.30.

significance of the coverage plotted in Fig. 1, however, must be scrutinized. Thus, θ was *defined* as Γ/Γ_m were Γ is the surface excess of n-amyl alcohol and Γ_m is the maximum value of Γ. One had Γ = 1.26 × 10^{-9} mole cm.$^{-2}$ at E = −0.55 v. *vs.* n.c.e. for 0.12 M n-amyl alcohol. This value of Γ was adopted[18] as being Γ_m in the preparation of Fig. 1. There results some uncertainty on Γ_m, as determined in this way, and, furthermore, experimental errors on Γ can be as large as 10% under the best experimental conditions.[21] One should also expect the covered area per
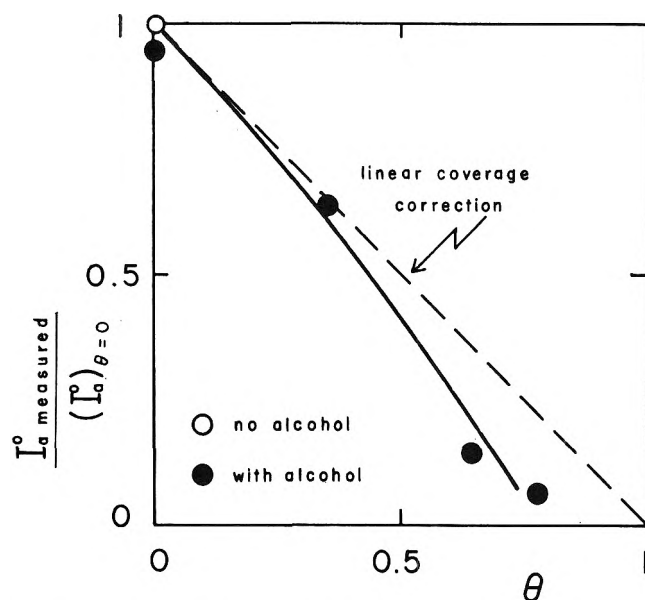
Figure 1. Influence of coverage after correction for $\Delta\varphi$.

molecule to vary with θ, as pointed out by Frumkin.[1] *Keeping in mind these reservations*, one concludes from Fig. 1 that, *in the present case*, the influence of adsorbed n-amyl alcohol is essentially accounted for up to θ = 0.5 by consideration of two effects: variation of I_a^0 with $\Delta\varphi$ and the concomitant variation of current density with coverage. At high coverages (θ > 0.5), exchange current densities are somewhat smaller than the values expected after correction for the above effects. Reservations made about the definition of θ, made above, may be invoked to explain results for θ > 0.5.

Further work is now in progress to examine the validity of this interpretation for other systems. The validity of the $\Delta\varphi$-calculation for a variable ϑ is also being re-examined.

(18) It is somewhat larger than Γ_m = 1.03 × 10^{-9} mole cm.$^{-2}$ computed by Parsons[19] for 0.1 M n-amyl alcohol in 1 M NaClO$_4$ from data from this laboratory.[20] Differences in conditions and experimental errors may account for the difference.

(19) R. Parsons, *J. Electroanal. Chem.*, **5**, 397 (1963).

(20) M. Breiter and P. Delahay, *J. Am. Chem. Soc.*, **81**, 2939 (1959).

(21) E. Blomgren, J. O'M. Bockris, and C. Jesch, *J. Phys. Chem.*, **65**, 2000 (1961).

Surface Area Measurement of Graphite[1] Using the γ-Radiation of Kr[85]

by John T. Clarke

Brookhaven National Laboratory, Upton, New York   (*Received November 14, 1963*)

A method has been developed to measure the surface area of small samples of low surface area materials using the γ-radiation of Kr^{85}-traced Kr to determine the amount of Kr adsorbed. Since the count rate observed is directly proportional to the Kr adsorbed, the method is much more rapid and the calculations much less time-consuming than other methods of surface area measurement. The method is applicable over a wide range of surface areas (0.001 to 10 m.²/g.) and to sample sizes of 0.5 g. or less. The long half-life of Kr^{85} (10.4 years) minimizes the corrections necessary for radioactive decay. The usual advantages of Kr over nitrogen (inertness, low vapor phase corrections, and spherical shape) are utilized in this method. Using this new method, it was found that the surface area of TSX nuclear graphite increased by a factor of four as the particle size was reduced from 3-mm. cubes to 80-mesh. This is interpreted as indicating that the increased surface area results primarily from the opening of closed pores; this allows one to estimate the surface area of graphite samples having different sizes and shapes.

Introduction

The properties of graphite can be markedly changed by varying the coke, binder, and graphitization temperature and atmosphere. They can also be modified by impregnation and degassing at high temperature. As a consequence, nuclear grade graphites are generally characterized[2a] in terms of the starting materials and the conditions of their manufacture rather than by their observable properties. Surface area is an important property in investigating chemical reaction rates between a solid and a gas; therefore, a simple, rapid method of measuring it is of considerable importance. The specific surface of a graphite and its variation with degassing temperatures and with particle size, can be used to help characterize it in terms of its present properties rather than by specifying its method of manufacture.

In studying the reaction of graphite with a gas, the results are found to vary depending on the size and shape of the graphite sample. Thus the change of surface area with particle size is particularly important as it allows one to estimate the shape factor.

Before developing the present method, the surface area of graphite samples was determined using a standard nitrogen adsorption apparatus. It was necessary to use large samples and minimize the gaseous volume in the sample cell in order to obtain the desired 5% accuracy.

Various additional modifications of the standard B.E.T. apparatus were considered. The substitution of Kr for N_2 would minimize the gaseous volume correction since the vapor pressure of Kr is only 2.3 mm. at liquid N_2 temperature. This method however, requires an entirely different apparatus. The use of nonradioactive Kr for surface area measurements is reported in detail by Rosenberg[2b] and Tomlinson.[3] This method does allow accurate measurement of small surface areas with gram-size samples, but it is as slow and tedious as the nitrogen method. In either method, the amount of gas adsorbed on the surface at liquid nitrogen temperature is determined by accurately measuring the amount of gas in an exterior system before and after the adsorption, and involves many measurements and arithmetical calculations.

Aylmor and Jepson[4] have simplified the Kr method

(1) This work was performed under the auspices of the U. S. Atomic Energy Commission.

(2) (a) R. E. Nightingale, Ed., "Nuclear Graphite," Academic Press, New York, N. Y., 1962, pp. 182–185;   (b) A. J. Rosenberg, *J. Am. Chem. Soc.*, 78, 2929 (1956).

(3) L. Tomlinson, United Kingdom Atomic Energy Authority, Industrial Group Report 1032, 1959, Her Majesty's Stationery Office, London, England.

by counting the β-radiation of Kr[85]-traced Kr in a thermostated constant-volume cell to determine the pressure; the pressure is directly proportional to the count rate. They used a constant amount of Kr (adsorbed and unadsorbed) for one isotherm, and varied the external volume to vary the equilibrium pressure. The method works satisfactorily, but the amount of Kr adsorbed is still obtained by subtracting the amount of gas in the external system from that originally present. It is also necessary to control carefully the amount of Kr added to the volumetric system so that a monolayer covers the sample surface; this may vary widely with different samples.

Experimental

In the present method, the amount of Kr adsorbed by the sample is measured directly by counting the γ-radiation from the Kr[85]-traced Kr. This simplifies the calculations and allows one to work with small samples having widely different surface areas. We have measured 0.5–1.0-g. samples with surface areas varying from 0.001 to 10.00 m.^{2}/g., but these are not its limits. The time involved in a surface area measurement is about one-third of that using the earlier B.E.T. apparatus. Samples having only 0.01 of the surface area/g. can be determined. Kr[85] has a half-life of 10.4 years so radioactive decay is a small correction.

A schematic drawing of the apparatus is given in Fig. 1. The essentials of the apparatus consist of a tube containing the sample which is connected to a reservoir of Kr[85]-traced Kr. The sample tube is held at liquid N$_2$ temperature while the Kr storage tube is held at a series of constant temperatures below liquid nitrogen temperature to keep the vapor pressure of the solid Kr at a desired value. The sample adsorbs Kr at constant pressure until it equilibrates with Kr in the storage tube. The amount adsorbed is a function of the surface area and is measured by counting the 0.53 Mev. γ-radiation of Kr[85]-traced Kr. This measures directly the amount of Kr adsorbed, and only a small correction is needed for the Kr in the gas phase detected by the counter. The equilibrium Kr pressure (100 to 500 μ) is determined by a thermistor gage[2a] to an accuracy of 1 μ. The Kr storage tube is shut off from the cell for this pressure measurement. The amount of Kr adsorbed as a function of the Kr pressure above the sample allows one to calculate its surface area. The rate of Kr adsorption can also be measured directly with this apparatus. The apparatus for maintaining the solid Kr storage tube at different temperatures below 77°K., greatly simplifies the surface area measurement, since it supplies the amount of Kr
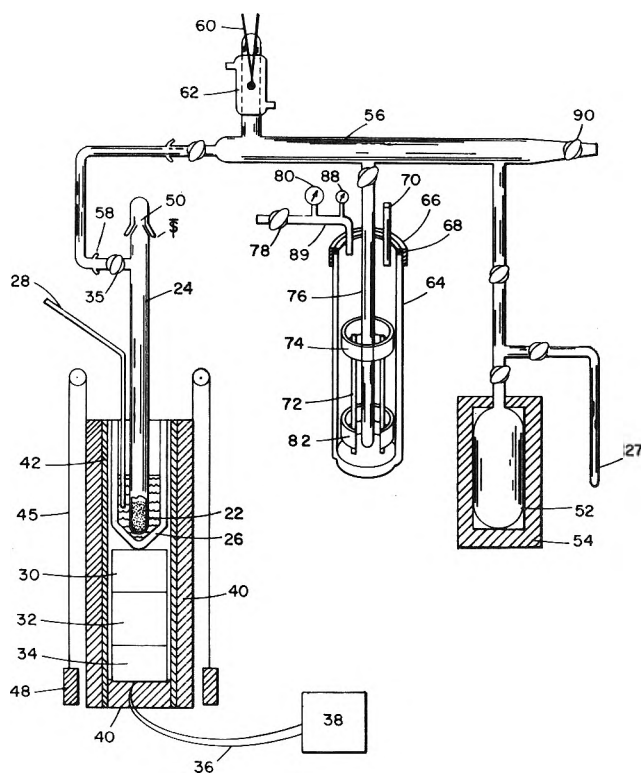
Figure 1.

needed at a suitable pressure whether the sample has a small or large surface area.

A measure height of the sample (22), whose surface area is to be measured, is placed in a sample tube (24) which has been removed from the apparatus for loading and weighing. The counterweighted assembly containing the dewar and scintillation crystal is then raised so that the sample tube (24) is centrally located and rests on the bottom of the thin-walled dewar (26). A nitrogen thermometer (28) is used to determine the temperature of the liquid nitrogen. A 1.0 × 1.5-in. Al-covered scintillation crystal (30) is mounted directly below the dewar (26) and above the photomultiplier tube (32); the preamplifier (34) is connected to a discriminator and scaler (38) by coaxial leads (36). The sample tube and detection apparatus are enclosed in a brass tube which is shielded by 8 mm. of lead and counterweighted by weights (48) so that the assumbly may be raised or lowered.

Kr[85]-traced Kr is stored in a Pyrex bulb (52) surrounded by 0.5 in. of lead (54) and is connected to the pumping manifold (56). The assembly (64–88) is used to control the temperature in the Kr storage tube (76) and thus the Kr pressure. A metal dewar (64)

(4) D. W. Aylmor and W. P. Jepson, J. Sci. Instr., 38, 156 (1961).

with a stainless steel cover (66) and vacuum sealed with an "O"-ring is connected to a vacuum pump by a valve (78). A bundle of 0.375-in. copper tubes is held in a vertical position by brass rings (74 and 82) to maintain a uniform temperature inside the dewar (66). This dewar is half-filled with liquid N₂ through the port (70) and closed by a rubber stopper which also serves as a safety valve. The pressure is measured with a vacuum gage (80) and gaseous nitrogen can be added through the valve (88). The Kr storage tube is vacuum sealed to the cover (66) by means of a short piece of rubber tubing. A thermocouple has also been introduced at this point. By pumping on the nitrogen in the dewar; the temperature can be controlled between 55 and 77°K. This storage tube also serves as a convenient means of keeping the Kr pure; cooling the Kr to below the solid point reduces its pressure to <5 μ and allows one to pump off O_2 or N_2 without appreciable loss of Kr.

Counting Equipment. Kr^{85} decays by β- and γ-emission. Rider and Peterson[6] have experimentally found that the 0.513 Mev. $\gamma:\beta$ ratio is 0.0036 ± 0.0008. Thus Kr^{85} gives off 280 β for 1 γ. The β-rays do not penetrate far into the graphite or Pyrex wall, but in the process of being stopped, give rise to "bremsstrahlung" which are only partially absorbed by the Pyrex and activate the counter. The "bremsstrahlung" reaching the counter may not be proportional to the Kr adsorbed. In addition, our proximity to the Brookhaven Research Reactor with its Ar^{41} effluent gives a background which varies with wind conditions.

To correct for these two sources of error, two scalers with separate discriminators were used.[6] One discriminator was set to screen the "bremsstrahlung" which were experimentally found to be below 0.46 Mev. The other discriminator was set at 0.60 Mev. and the ratio of the two discriminated count rates determined as a function of the background activity when no Kr^{85} was in the sample cell. In measuring Kr, the two discriminators were run simultaneously so the count rate could be corrected for the observed background. In most locations the 0.60 Mev. discriminator would be an unnecessary addition.

Geometry and Activity. The apparatus was designed to count as much of the γ-radiation from the Kr^{85} adsorbed as was practical. The diameter of the sample tube and the height of the sample can be arbitrarily fixed. Once fixed and calibrated, however, either the same or a similar sample tube must be used. Two different size cells were used in this work, but all the reported results were made by using precision glass 7-mm. i.d. tubes and a sample height of 1.0 in. The over-all geometry, including the integrated solid angle,

the absorption by glass, and absorption by the sample, gave about 13% efficiency for the count of the total γ-emmission from the Kr adsorbed on the graphite.

This may be broken down as:
1. Average solid angle of NaI crystal with respect to the total sample equals 0.9π or 22.5% is absorbed.
2. 96% of the γ-rays from Kr^{85} on the sample is transmitted through the graphite.
3. The walls of the sample tube and dewar absorb 5%; 95% is transmitted.
4. For a 1 × 1.5-in. NaI crystal, 64% of the γ-rays are absorbed and activate the counter.

Thus, $0.22 \times 0.96 \times 0.95 \times 0.64 = 12.8\%$ of the γ-rays emitted by Kr^{85} adsorbed on the graphite surface activate the photodetector and are counted. The efficiency is not used in any absolute sense, but rather for sizing the equipment and estimating the Kr^{85} activity needed.

For calibration, a measured volume (STP) of Kr^{85}-traced Kr is condensed on a 1-in. graphite sample in a standard cell at liquid nitrogen temperature. The cell is then closed and kept as a standard sample. The graphite used has sufficient surface area so that less than one-half of a monolayer of Kr is adsorbed at liquid N₂ temperature; this insures uniform coverage and low Kr pressure in the tube. The observed count was 16,700 counts/min./ml. of Kr (STP) on January 1, 1963. This corresponds to 1.0 mc./ml. for total $\beta + \gamma$ activity and 3.6 mc./l. of γ-activity. In subsequent work the activity was increased to over 10^6 counts/min./ml. of Kr (STP).

To obtain Kr of the proper activity, Kr^{85}-traced Kr, as received, was diluted with pure Kr. It was purified additionally by cooling to approximately 55°K. and pumping off any O_2 or N_2. This purification was done routinely in the course of the runs to remove any air impurities that might inadvertently have been introduced.

Procedure. In carrying out a surface area measurement, the sample tube was filled to a height of 1 in. and weighed. The sample tube was mounted on the apparatus surrounded by a small furnace maintained at 200° and evacuated for 15 min. The movable dewar and crystal assembly was raised and the sample tube centered accurately at the bottom of the dewar cone. Liquid nitrogen was added to a height of 2 in. and maintained within 0.125 in. of this during the course of the run.

(5) B. F. Rider and J. P. Peterson, General Electric GEAP-3496 (1960).
(6) This method was suggested by R. L. Chase of the Instrument Division of Brookhaven National Laboratory.

Before opening the Kr storage tube to the graphite sample, it was cooled by pumping on the storage tube dewar so that the vapor pressure of the Kr was 500 μ. The Kr storage tube was then opened to the sample tube. The adsorption was followed by the rate meter, but it was found that a leveling off of the pressure as measured by the thermistor gage was more satisfactory.

The storage tube was then closed and equilibrium adsorption indicated by a constant pressure on the thermistor gage and a constant count rate on the scaler. The equilibrium pressure of Kr over the sample was measured by means of a Rosenberg[2b] thermistor gage (60) and was sensitive in the pressure range 10–1500 μ. The sample was then counted for three 5-min. periods and the results recorded. Each count rate was corrected for the background and gas pressure. The counts/min. were converted to ml. of Kr adsorbed by using the counts/min./ml. of Kr obtained in calibrated Kr^{85} standard sample. Since Kr^{85} has a 10.4-year half-life, the standard changes vary slowly.

The temperature of the Kr in the storage tube was then lowered to another fixed value by pumping on the solid nitrogen trap. The storage tank was connected to the sample tube and the excess Kr condensed in the storage tube. The adsorption at four or five points was measured. The sample tube was then allowed to warm and the Kr transferred to the storage tube. The amount of Kr adsorbed at each pressure was used to calculate the surface area of the sample.

Calculations

Various methods of calculating the data are available and have been reviewed by Emmett.[7] A plot is made of ml. of Kr (STP) adsorbed vs. P/P_0, where P = observed pressure, and P_0 = extrapolated vapor pressure of liquid Kr at the observed liquid N_2 temperature.

The intersection of the lower pressure slope with that between $P/P_0 = 0.05$ to 0.15 gives a close approximation to the volume of gas contained in the monolayer.

The B.E.T. approach uses the equation

$$\frac{P/P_0}{V(1 - P/P_0)} = \frac{1}{V_m C} + \frac{(C - 1)}{V_m C} (P/P_0) \quad (1)$$

where V = ml. of Kr at STP adsorbed at a pressure P, V_m = ml. of Kr at STP adsorbed for a monolayer, and C = constant. Thus by plotting $(P/P_0)/V(1 - P/P_0)$ vs. P/P_0 one obtains $1/V_m C$ for the intercept and $(C - 1)/V_m C$ for the slope. The B.E.T. method was used as it reduces the data to a straight line in the region of

interest. The experimental results gave straight lines for eq. 1 between $P/P_0 = 0.05$ to 0.15.

Corrections

(a) *Amount of Kr in the Vapor Phase.* The bulk density of most of the pulverized graphite samples is about 1.0 while the helium density is 2.25. The vapor volume is thus $V(1 - (1/2.25))$ or 55.5% of the cell volume.

Since the volume of the cell is 0.58 ml., the gas volume is 0.32 ml. At the pressure of Kr necessary to form a monolayer (200 μ for graphite), this corresponds to 2.5 counts/min. or 0.15% for a sample of 0.5 m.^{2}/g. This has been experimentally verified but is normally an insignificant correction.

(b) *Surface Area of Cell.* The cell with a diameter of 0.63 cm. is immersed in liquid nitrogen to a depth of 2.0 in. This has a surface area of 10 cm.^{2} or 0.001 m.^{2}. For a 0.5-g. sample of 0.5 m.^{2}/g., this amounts to a 0.4% correction. Experimentally, this correction appears larger than calculated, i.e., about 0.005 m.^{2}/g. Whether this results from tube roughness or trace amounts of carbon from glass blowing is not known.

(c) *Effect of Sample Height.* Since the sample is mounted perpendicular to the scintillation crystal, different sections of the sample are at different distances from the crystal and are recorded at different efficiencies. Table I shows the results obtained for 80-mesh TSX graphite with the tube filled to different heights. The top 0.25 in. of the sample contributes less than half as much as bottom 0.25 in. Thus the variation in the height of 5% would introduce an error of only 2% in the surface area measurement.

Table I: Effect of Sample Height on Count Rate

Sample height, in.	Total relative count	Contribution from last 0.25 in.	% of total for each 0.25-in. section
0.25	0.86	0.86	38.0
0.50	1.42	0.56	24.8
0.75	1.92	0.50	22.1
1.00	2.26	0.34	15.1

(d) *Thermal Transpiration.* Since the Kr is absorbed at liquid nitrogen temperature and the pressure is read at 46°, the pressure over the sample is less than that read at the thermistor. For a 1.0-mm. capillary, an observed pressure of 200 μ has only a pressure of 182 μ at liquid N_2 temperature. For this reason, a 6-

(7) P. H. Emmett, *Catalysis*, 1, 31 (1954).

mm. i.d. sample tube was used. It was found better not to decrease the vapor phase correction by putting a glass tube inside the sample tube, for this greatly increased the thermal transpiration. With a 6-mm. tube, the true pressure is 198 μ for an observed pressure of 200 μ. Calculations were made by using the equation of Liang[8] as reported by Rosenberg.[2b]

Results

In the initial runs with the Kr^{85} apparatus using 20 to 40-mesh samples of TSX graphite, the surface area was found to be 1.0 m.²/g. compared to 0.40 m.²/g. for 15-g. cylinders obtained using a standard nitrogen B.E.T. apparatus modified to measure these low surface areas. Further runs with the Kr^{85} apparatus on more finely ground TSX showed that the surface area increased much more rapidly than one would anticipate from the increase in external surface. In making these comparisons the surface area of a monolayer of N_2 was taken to be 4.37 m.²/ml. of N_2 at STP while that of Kr was taken to be 5.21 m.²/ml. of Kr at STP. These are the values reported by Tomlinson[3] in his comparison of surface area measurements obtained using N_2 and Kr and appear to be the best values available.

Since this sample size effect was so large, it was necessary to compare the N_2 absorption apparatus and the Kr^{85} apparatus on the same size samples. This was done on a variety of samples and the results are summarized in Table II.

Table II: Comparison of Surface Area Measurements Use Kr^{89} Method vs. Standard B.E.T. Nitrogen Method

Graphite (TSX)	Surface area, m.²/g. 16,700 c./min. per ml. of Kr	Radio-active decay factor	Surface area, m.²/g. (corrected)	Surface area, m.²/g. of N_2 (B.E.T.)	% varia-tion Kr-N_2
0.125-in. cubes	0.435	0.987	0.429	0.421	+1.9
20-mesh	1.018	1.000	1.018	1.00	1.8
40-mesh	1.59	1.000	1.59	1.47	8.1
80-mesh	3.43	0.989	3.46	3.27	3.4
80-mesh	3.45	0.998	3.46	3.27	3.4

The two methods agree within 4% over an eightfold change in surface area. The nitrogen apparatus was designed to give an accuracy of 4% on 10-g. samples, and repeat runs agreed better than this. For the Kr^{58} apparatus using 0.5-g. samples having 1.0 m.²/g., approximately 0.1 ml. of Kr is adsorbed. For a 5-min.

count, this corresponds to 8 × 10³ counts or a precision of 2% for background counts less than 10³ counts/min. For counting rates less than 10⁴ counts/min., the results of three 5-min. count periods were averaged. The surface area as measured by Kr appears somewhat larger than by N_2 adsorption, but is within the accuracy of the calibration constants. Pore volume measurements on graphite indicate that it has many pores less than 20 Å. so packing on the surface could be different for N_2 and Kr. The two methods do agree within the planned reproducibility of 5%.

The observed increase in surface area with decreased particle size is of particular interest since it is approximately 100 times the increased external or geometric surface area. A plot of total surface area vs. geometrical surface area gives a straight line whose intercept at zero geometrical surface area equals the surface area obtained for large single piece samples. Thus determining the surface area for two or three samples of known external area allows one to obtain the surface area of any size sample. This effect can be accounted for by assuming that large samples have internal pores that may be opened by subdividing the graphite. These internal pores must be very small since the helium density shows that with 80-mesh material the internal volume is <1%. Work is continuing on this and other types of nuclear graphite, and results will be reported and discussed in a subsequent paper.

Conclusions

1. A new method, involving the counting of the γ-radiation of adsorbed Kr^{85}-traced Kr, has been developed to measure the surface area of porous materials.

2. The method is rapid and the calculations simpler than other methods since the amount of Kr adsorbed is directly proportional to the count rate observed.

3. The method gives the same results as standard N_2-adsorption methods, but is about three times as rapid and can be used on samples of one-tenth the weight and having much lower specific surfaces.

4. The surface area of TSX-grade nuclear graphite varies as a function of particle size; it has a lower limiting value for large pieces and increases linearly with external surface area as the particle size is reduced. This allows one to calculate the surface area for any regularly shaped graphite specimen.

(8) S. C. Liang. *J. Appl. Phys.*, **22**, 148 (1951).

Hydrogen Chloride in Anhydrous Benzonitrile: Electrical

Conductance, Time Effect, and Ion—Solvent Interactions

by George J. Janz, Iqbal Ahmad,[1a] and H. V. Venkatasetty[1b]

Department of Chemistry, Rensselaer Polytechnic Institute, Troy, New York   (Received November 14, 1963)

The conductance of hydrogen chloride in benzonitrile for the concentration range 0.823×10^{-3} to 0.13 mole/l. at 25° has been investigated. The conductance–time effect is found to be less marked than in the acetonitrile solutions. The conductance data for the aged solutions were examined by the various extrapolation techniques for weak electrolytes. The values for Λ_0, K, and a thus obtained are, respectively, 1.5 ± 0.2 ohm^{-1} cm.$^{-1}$, $2.5 \pm 0.5 \times 10^{-4}$, and 1.6 Å. The sharp decrease in Λ with concentration in the dilute solution range can be attributed to ion pair formation. Two solid substrates of composition corresponding to $C_6H_5CN \cdot HCl$ and $C_6H_5CN \cdot 2HCl$ can be isolated from the saturated solutions. The structural data and physical properties of these substrates are considered in the light of possible chemical interactions in the system.

Introduction

Benzonitrile is the simplest aryl derivative of hydrogen cyanide. The relatively high dielectric constant (25.2 at 25°) is understood in large part as due to the polar nature of the nitrile group which gives the force field a highly directional character (dipole moment 4.05). Like acetonitrile ($D = 35.99$ at 25°) the values of its viscosity and Trouton constant indicate that association in the liquid state is much less than in other organic solvents, making it a less complex solvent for the study of ion–solvent interactions. The properties of HCl as an electrolyte in acetonitrile have recently have been reported from this laboratory.[2] The present communication reports an investigation of the electrical conductance of this solute in anhydrous benzonitrile, particularly with reference to the values for aged solutions. Attention was also directed to the problem of the time effect and the solid substrates, first noted for CH₃CN–HCl systems.

Experimental

Benzonitrile. Benzonitrile (Eastman Organic Chemicals) was magnetically stirred with CaH₂ (20 g./l.)[3] for 24 hr., decanted, and then refluxed for 18 hr. with freshly added CaH₂ (20 g.). It was next fractionally distilled using a vacuum-jacketed strip-silvered distillation column (100 × 25 cm.) packed with 0.125-in Hastelloy stainless steel helices (Podbielniak Inc.) and a solenoid-controlled partial take-off condenser. Separate fractions were collected using a magnetically controlled policeman distributor.[4] Unless otherwise indicated, at all times the exits to the atmospheric pressure on the flasks and conductance cells were through Mg(ClO₄)₂ guard tubes. The middle cut of this distillate (b.p. 191.0°) was again refluxed (18 hr.) with fresh CaH₂ (20 g.) and refractionated. The specific conductivity of the solvent thus purified was 5–9×10^{-8} ohm^{-1} cm.$^{-1}$ (25°). The water content (Karl Fischer titration) was found to be less than 0.009 wt. %.

Hydrogen Chloride. The hydrogen chloride gas, available commercially (Matheson Co.), was passed successively through a sulfuric acid bubbler and columns of SiO₂ gel and Mg(ClO₄)₂ prior to use.

Preparation of Solutions. For the conductance–time effect study, the solutions were made directly in the conductivity cell (cylindrical electrode type).[2c]

(1) (a) Postdoctorate Fellow, 1962–1963; (b) Postdoctorate Fellow, 1961–1962.

(2) (a) G. J. Janz and S. S. Danyluk, *J. Am. Chem. Soc.*, **81**, 3846 (1959); (b) *ibid.*, **81**, 3850 (1959); (c) *ibid.*, **81**, 3854 (1959).

(3) J. F. Coetzee, *et al.*, *Anal. Chem.*, **34**, 1139 (1962).

(4) G. J. Janz and E. J. Rock, *ibid.*, **22**, 626 (1950).

Excess hydrogen chloride gas from the solution and the cell flask was removed by a dry nitrogen sweep. For regular concentration–conductance runs, a concentrated stock solution was made in a similar fashion and the dilutions in an experiment were by weight–pipet technique. All concentrations were checked after each conductance measurement by a volumetric analysis of a small amount of the solution. The accuracy of this, down to 0.005 M HCl, was ±1%; at lower concentrations because of the poor end point, it was not better than ±3%.

Conductance. Measurements were made with the cells in a thermostated bath at 25° (±0.002°) using a Jones–Dike conductance bridge and accessories. The cell constants for the conductance cells determined in the conventional manner were 1.258, 0.05403, 1.3363. Bright platinum electrodes were used; corrections for polarization were made by taking measurements at frequencies of 1000, 2000, and 10,000 c.p.s. as required for extrapolation to the infinite frequency. This correction was less than 0.05% (on resistance) at all times.

Conductance–Time Effects. To study this effect, the measurements of the resistance were initiated immediately after the preparation of this solution and its temperature equilibration in the bath. The measurements were made first at 5 min., followed by 30-min. intervals for the first 6 hr., after which readings were spread in accord with the total time of the experiments.

The concentration, aging time, specific conductance at $t = 0$ by extrapolation and $t = t$ (final) and the per cent increase of conductance are given in Table I. Figure 1 illustrates the change of conductance with time for a 0.13 M HCl solution over some 360 hr.

Figure 1. Conductance–time effects for 0.13 M HCl solution.
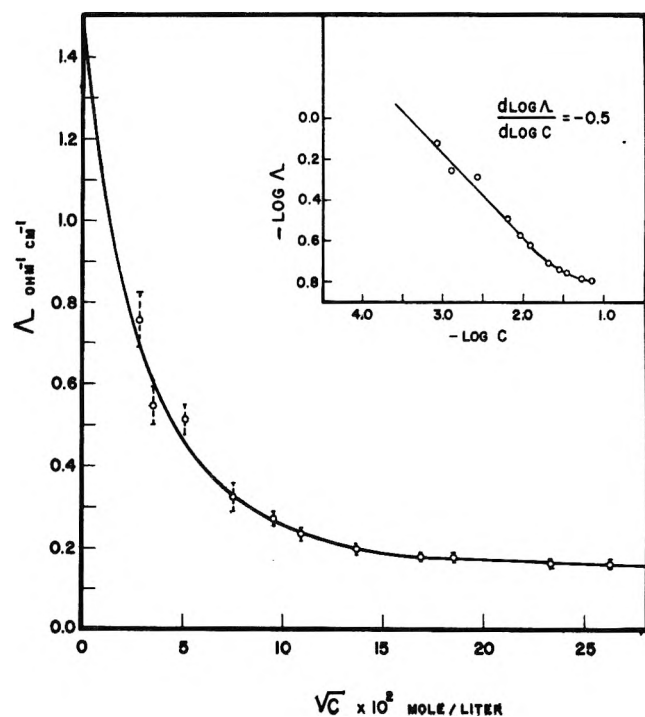
Figure 2. Phoreogram of the "aged" HCl–benzonitrile solutions.

Table I: Conductance–Time Effect in HCl–Benzonitrile Solution (25°)

Concn., mole/l.	Aging period, hr.	Sp. conductance, ohm^{-1} cm.$^{-1}$ × 10^5 Initial	Final	Sp. conductance increase, %
0.0575	75	1.70	2.87	69
0.0693	49	2.40	3.73	55
0.0810	49	5.20	6.06	16
0.2660	50	14.20	25.11	77
0.130	40	17.00	18.90	11
0.130	400	17.00	21.66	27.5

Equivalent Conductance. In Table II, the specific conductivity and equivalent conductance data for various aged solutions are summarized. At lower concentrations, the conductivity of the solvent was significant, and therefore due account of this was taken in calculating the Λ-values for these concentrations. Figure 2 gives the phoreogram of this system. The limits of accuracy shown in this table have been calculated by taking into account the errors involved in the chemical analysis (±1–3%), resistance measurement, and temperature variation of the bath (±0.1% on resistance), as well as errors due to the conductance–time effect.

Solid Substrates. When a saturated solution of HCl in benzonitrile was chilled to −8° and allowed to

Table II: Equivalent Conductance of the "Aged" HCl Solutions in Benzonitrile (25°)[a]

Concn., mole/l.	$\sqrt{C}$	Sp. conductivity, ohm⁻¹ cm.⁻¹ × 10⁶	Sp. conductivity corrected for solvent × 10⁶	Equivalent conductance, ohm⁻¹ cm.⁻¹
0.0686	0.2620	11.080	10.996	0.160 ± 3%
0.0545	0.2335	8.854	8.760	0.161 ± 3%
0.0342	0.1849	6.044	5.950	0.174 ± 3%
0.0285	0.1688	5.064	4.970	0.175 ± 3%
0.0188	0.1371	3.805	3.711	0.197 = 3%
0.0119	0.1091	2.870	2.776	0.233 = 3%
0.0091	0.0954	2.550	2.456	0.270 = 3%
0.0057	0.0755	1.932	1.838	0.323 = 4%
0.0026	0.0510	1.406	1.312	0.510 = 6%
0.00124	0.0352	0.774	0.680	0.547 ± 10%
0.000823	0.0286	0.156	0.062	0.753 ± 10%

[a] Specific conductivity of benzonitrile = 0.094 × 10⁻⁶ ohm⁻¹ cm.⁻¹.

stand for a long time, a white crystalline substrate was obtained. This was insoluble in benzene, carbon tetrachloride, and diethyl ether, but soluble in methyl alcohol and acetone. The substrate was fairly stable at room temperature; in a sealed capillary, it sintered at 57° and melted at 62–65°. Analytical results confirmed it to correspond stoichiometrically to a 1:1 addition compound $C_6H_5CN \cdot HCl$ (%HCl: theoretical, 26.13; experimental, 25.3, 25.16, 24.26).

The infrared spectrum of the crystalline product was obtained with a Perkin-Elmer Model 21 spectrometer having NaCl optics and the KBr disk technique. It showed a complete absence of C≡N stretching frequency (2240 cm.⁻¹). A strong absorption band at 1640–1660 cm.⁻¹ was also apparent; the latter corresponds to the characteristic C=N stretching mode of Imino-type compounds.[5]

When HCl gas was bubbled for prolonged periods into benzonitrile cooled in a freezing mixture (−10°) another crystalline compound was obtained. This was highly unstable and readily decomposed into 1:1 substrate and HCl. On analysis it was found to correspond stoichiometrically to a 1:2 addition compound $C_6H_5CN \cdot 2HCl$: (% HCl: theoretical, 41.45; experimental, 38.00, 39.70, 39.32). Because of its high instability, attempts to gain the infrared spectrum were not successful.

Discussion

The only other work on the conductance of HCl in benzonitrile reported in the literature is by Zil'berman, et al.[6] Unfortunately, the results are reported as a

small scale phoreogram which precludes precise values. It can be estimated that the value of Λ is less than 0.1 ohm⁻¹ cm.⁻¹ (0.04–0.12 M HCl). The solutions were apparently aged for 24 hr.; this may account for the over-all lower values as compared with those obtained in this study (Table II, Fig. 2). The phoreogram in Fig. 2, for solutions which were aged for 21 days, conclusively shows that HCl behaves as a weak electrolyte in benzonitrile.

By a free-hand extrapolation of a large-scale phoreogram, the value of 1.5 ohm⁻¹ cm.⁻¹ is obtained for Λ_0'. Attempts to use this value for subsequent Shedlovsky[7]-type extrapolation were not fruitful, since the function S

$$S_{(z)} = 1 + Z + \frac{Z^2}{2} + \frac{Z^3}{8} \cdots$$

does not coverge. With somewhat higher values, i.e., 16, this function is convergent, and the extrapolation gives 1.44 ohm⁻¹ cm.⁻¹ and 2.33 × 10⁻⁴ for Λ_0 and K, respectively (Fig. 3(i)).

Less accurate relationships for the weak electrolytes were also examined and are listed here.

(i) From the equation given by Robinson and Stokes[8]

$$\Lambda = \Lambda_0'' - \frac{(\Lambda_0'\alpha + \beta)\sqrt{C}}{1 + \kappa a}$$

where $(\alpha\Lambda_0' + \beta)$ = Onsager function (Λ_0' taken as 1.5), $\kappa = (2.9127 \times 10^8 \sqrt{C}/D^{1/2}_{25°}$ and a = distance of closest approach (taken as 4 Å. in this case), the Λ_0'' values were gained and plotted against C. The extrapolated Λ_0'' at $C = 0$ is Λ_0 (Fig. 3(ii)).

(ii) The Ostwald dilution[9] law: Λ_0 and K are obtained, respectively, from the intercept and slope of the graph of $1/\Lambda$ vs. $C\Lambda$ (Fig. 3(iii)).

(iii) Davies' method[10]: the dissociation constant K is obtained from the graph of $\sqrt{C_i}$ (where C_i is the ionic fraction of the solute) vs. $\log C_i^2/C_u$ (where C_u is the fraction of the undissociated molecules) (Fig. 3(iv)).

(iv) K can be obtained[11] from a graph of C_u vs. ($\log K - \log f_\pm^2$), where the activity coefficients are

(5) L. J. Bellamy, "Infrared Spectra of Complex Molecules," J. Wiley and Sons, Inc., New York, N. Y., 1956.

(6) E. N. Zil'berman, et al., J. Gen. Chem. USSR, 31, 1905 (1961).

(7) T. Shedlovsky, J. Franklin Inst., 225, 739 (1938).

(8) R. H. Stokes and R. A. Robinson, "Electrolyte Solutions," Academic Press, Inc., New York, N. Y., 1955, p. 144.

(9) C. A. Kraus and W. C. Bray, J. Am. Chem. Soc., 35, 1315 (1913).

(10) C. W. Davies, "The Conductivity of Solutions," John Wiley and Sons, Inc., New York, N. Y., 1933.

(11) H. S. Harned and B. B. Owen, "Physical Chemistry of Electrolyte Solutions," Reinhold Publishing Corp., New York, N. Y., 1958, pp. 171, 312.
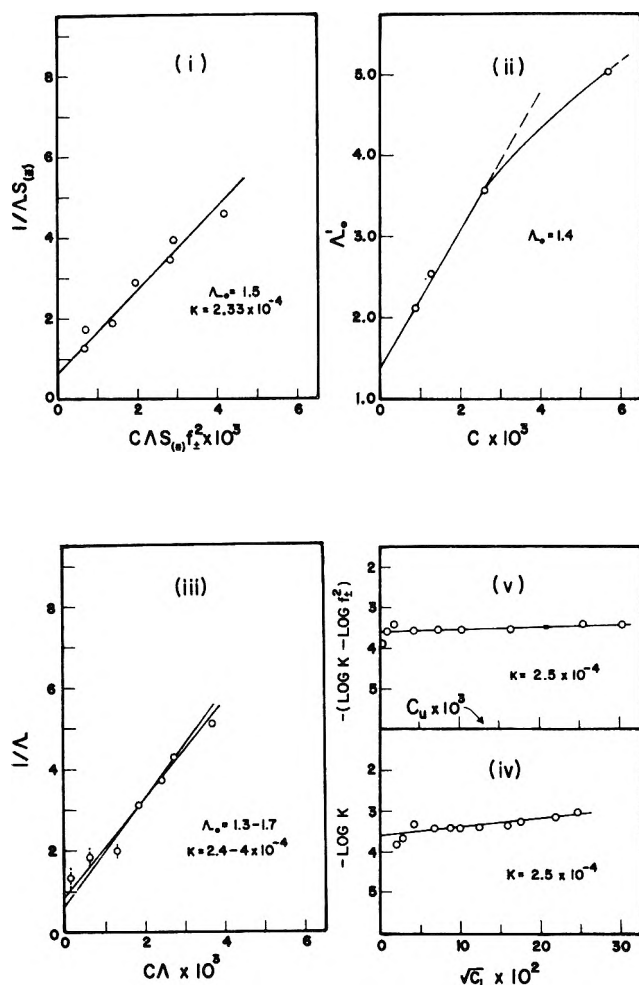
Figure 3. Extrapolation curves according to various relationships: (i) Shedlovsky; (ii) Robinson and Stokes; (iii) Ostwald's dilution law; (iv) Davies; (v) taking into account the activity coefficient in Davies.

estimated by the Debye-Hückel limiting law (Fig. 3(v)).

The values of Λ_0 and K thus obtained are summarized in Table III. Taking into consideration the lack of refinement in the latter analyses, the values of 1.5 ± 0.2 ohm^{-1} cm.$^{-1}$ and 2.5 ± 0.5 × 10^{-4} for Λ_0 and K, respectively, are recommended.

The initial rapid decrease in Λ with concentration suggests strong association. The slope of log Λ vs. log C (inset Fig. 2) is -0.5 in this concentration range (characteristic of ion pair formation[12]). The critical distance calculated from Bjerrum's[13] theory is 11.2 Å., i.e., ionic association is not improbable for simple solutes in benzonitrile. The distance of the closest approach can be calculated if the value of K is known from the relationship[14]

Table III: Summary of Λ_0 and K Calculated by Various Extrapolation Methods

Method	Λ_0	K
Free-hand extrap.	1.5	...
Robinson and Stokes	1.4	...
Ostwald	1.3–1.7	3.1 × 10^{-4}
Davies	...	2.5 × 10^{-4}
Taking into account activity coeff. in Davies	...	2.5 × 10^{-4}
Shedlovsky	1.44	2.33 × 10^{-4}

$$-\log K = 6.12 - 3 \log D + \log Q(b)$$

where D is the dielectric constant and $Q(b)$ is a numerical function of b, values of which are available.[11] From $Q(b)$ thus gained, a can be readily calculated. Taking $K = 2.5 × 10^{-4}$, the a is found to be 1.6 Å. in this manner. Recognizing that the internuclear distance in the HCl molecule is 1.28 Å., the distance of the closest approach thus found seems quite reasonable. From the infrared spectral evidence it follows that the 1-1 benzonitrile-HCl substrate may be formulated as an imino chloride, $C_6H_5(Cl)C=NH$. Further interaction with HCl can be foreseen, e.g.

$$C_6H_5(Cl)C=NH + HCl \rightleftarrows [C_6H_5(Cl)C=NH_2]^+Cl^-$$

$$(1)$$
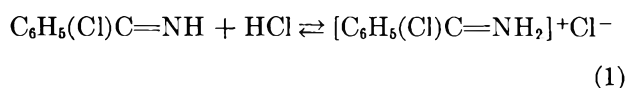
Thus an imino dihydrochloride is seen the likely structure of the 1:2 compound. Such compounds are notably unstable and evolve HCl readily.

The time effect for conductance also warrants comments. This effect is not as marked as in the HCl-acetonitrile solutions. After 50 hr., the specific conductance increased at the most by 77% as compared with as much as 400% in acetonitrile. This is one of the major reasons of the larger scatter in the results of the equivalent conductance vs. concentration in acetonitrile as compared with benzonitrile. Some insight in the nature of the time effect can be gained from a consideration of the various possible solute-solvent interactions in these solutions.

The ionization process of hydrogen chloride in C_6H_5-CN, by analogy with the scheme advanced for acetonitrile,[2a] may be expressed as

$$C_6H_5CN + HCl \rightleftarrows C_6H_5CN \cdot HCl \qquad (2)$$

$$C_6H_5CN \cdot HCl \rightleftarrows C_6H_5CNH^+Cl^- \qquad (3)$$
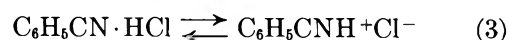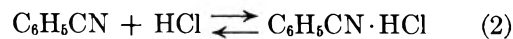
(12) C. A. Kraus, *Trans. Electrochem. Soc.*, **66**, 182 (1934).

(13) N. Bjerrum, *Kgl. Danske Videnskab. Selskab*, **7**, No. 9 (1926).

(14) R. M. Fuoss and C. A. Kraus, *J. Am. Chem. Soc.*, **55**, 1019 (1933).

$$C_6H_5CNH^+Cl^- \rightleftharpoons C_6H_5CNH^+ + Cl^-_{(solv)}$$

$$(4)$$
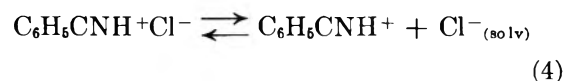
In (2), the nitrile acts as an onium donor and HCl as $h\sigma_D$ acceptor, according to the donor–acceptor classification of Mulliken.[15,16] The rearrangement from the "outer" to the "inner" complex (3) is normally considered as the slow step, and may contribute to the time effect. In addition, in this system, chemical interactions such as iminochloride formation (slow) with subsequent acid–base interactions (1) may further contribute to this effect through the formation of additional ionic species. It may be possible to assess the relative contributions of the two types of processes to the time effect by temperature-dependence studies, since charge-transfer processes are generally temperature insensitive.

(15) R. S. Mulliken, *J. Phys. Chem.*, **56**, 801 (1952).
(16) R. S. Mulliken, *J. Am. Chem. Soc.*, **74**, 811 (1952).

Charge-Transfer-to-Solvent Spectra of Polyvalent Anions.

I. General Theory

by Avner Treinin

Department of Physical Chemistry, Hebrew University, Jerusalem, Israel   (*Received November 16, 1963*)

The charge-transfer-to-solvent (c.t.t.s.) spectra of polyvalent anions are considered. The treatment is based on the continuum model and extends the previous treatment of monovalent anions. An expression for the transition energies is derived and this is used to explain the environmental effects on these spectra. The theory is compared with available data.

Polyvalent anions do not exist in the gas phase. The small electron affinity for the formation of univalent anions makes it improbable that even a second electron could be attached with decrease of energy, *i.e.*, the electron affinity of a univalent anion is always negative.[1,2] Polyvalent anions in crystals and solutions owe their existence to the interactions with their surroundings. Consider the process

$$X_g^z \longrightarrow X_g^{z-1} + e \qquad (1)$$
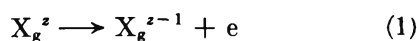
where z denotes the number of negative charges. The endothermicity of this reaction is by definition the electron affinity of X^{z-1} or the ionization potential (detachment energy) of X^z. If the process is carried out in water to give an electron which is completely unbound[3]

$$X^z(aq) \longrightarrow X^{z-1}(aq) + e \qquad (2)$$
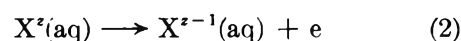
the endothermicity of (2) will be greater than that of (1) by an amount representing the difference between the heats of solvation of X^z and X^{z-1}. For the bivalent anion with a radius of 2 Å., the difference amounts to about 250 kcal.[4]

(1) H. S. W. Massey, "Negative Ions," Cambridge University Press, Cambridge, England, 1950.
(2) H. O. Pritchard, *Chem. Rev.*, **52**, 529 (1953).
(3) The inner potential of the solvent is ignored since in all the processes considered here the electron does not leave the solvent.

Absorption of light may lead to detachment of electrons from negative ions. In the case of univalent anions, this is known to occur in the gas phase. Recently, appreciable concentrations of nearly free halide ions were produced and their light absorption was measured.[5] The corresponding excitation process is adequately described by eq. 1, and the onset of absorption gives the electron affinity of the halogen atom. More generally, the spectroscopic method will lead to the vertical ionization potential, since the positions of the nuclei remain unchanged in the electron-detachment process (Franck–Condon principle). Electron detachment from anions in solution is very well known. The so-called charge-transfer-to-solvent (c.t.t.s.) spectra of univalent anions have been discussed in detail.[6,7] The c.t.t.s. process differs essentially from process 2 by: (a) the nonequilibrium state of solvent and X^{z-1} resulting from the electron transfer, according to the Franck–Condon principle; (b) the binding of the detached electron to the medium. These two important points were considered in detail for univalent anions. Using the oversimplified continuum model,[8] the energies,[7,8] intensities,[9] and environmental effects[7,10] were calculated.

Evidently, a process like (1) cannot be carried out with polyvalent anions. On the other hand, some of these ions show intense bands in the ultraviolet which behave like c.t.t.s. bands toward environmental effects. Such bands are the 215-mμ band of $S_2O_3^{-2}$,[11,12] the 360-mμ band of S^{-2},[13] and that of $Fe(CN)_6^{-4}$ below 300 mμ.[14,15] The origin of other bands assigned to c.t.t.s. (e.g., that of SO_3^{-2}) is still not clear and should be investigated, but first the theory of such bands must be developed and compared with the available experimental results. By means of such a theory we expect to derive information about some important properties of polyvalent anions as their ionization potentials, radii, solvation energies, etc. This is the purpose of the following discussion, which is essentially an extension of a previous treatment.[7,10]

The Binding of the Electron in the C.t.t.s. State. For X^-, the continuum model considers the binding energy as due partly to the persistent polarization of the medium and partly to the electronic polarization induced by the electron in its excited state (the c.t.t.s. state). In this state the electron is on the average fairly removed from the neutral radical X, so that the effect of the latter on the binding energy could be neglected. Now consider the general excitation process

$$X^z(aq) \xrightarrow{h\nu} \{X^{z-1}(aq)\} + e_{bound} \qquad (3)$$
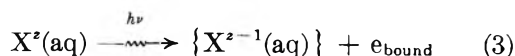
$\{\}$ represents the nonequilibrium conditions where

all the nuclei keep their positions as in the ground state. The electrostatic repulsion exerted by X^{z-1} should now be taken into account. The repulsion potential at a distance r is $(z-1)e/rD_{op}$, where D_{op} is the optical dielectric constant. The use of D_{op} is due to the atomic nuclei being unable to follow the electronic motion. The attraction potential exerted by the persistent polarization of the medium, polarized around the ion X^z, is $(ze/r)(1/D_{op} - 1/D_s)$, where D_s is the static dielectric constant. Therefore the net potential by which the electron is bound to the medium is $V(r) = (e/r)(1/D_{op} - z/D_s)$. For polar solvents (i.e., large D_s) this gives a potential which differs only little from that corresponding to a univalent anion.[8] Thus within the approximation of the continuous medium we expect for all anions nearly the same binding energy of the electron in the c.t.t.s. state and the same average distance from the center of the radical. The values of the binding energy B in various solvents show little variation with the nature of the solvent, being about 35–32 kcal. for H_2O, acetonitrile, and alcohol.[10]

The Transition Energy. Consider the cycle

$$X_g^z + \{aq\} \xrightarrow{I_x} \{X_g^{z-1}\} + \{aq\} + e_g$$

$$\uparrow E_1 \qquad\qquad\qquad \downarrow -E_2 - B$$

$$X^z(aq) \xrightarrow{h\nu_{max}} \{X^{z-1}(aq)\} + e_{bound}$$
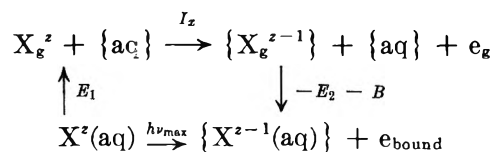
This is a generalization of a previous cycle.[7] I_x is the vertical ionization potential of the ion in the gas phase. In order to calculate E_1 and E_2 it is first assumed that the ion occupies a cavity of radius r_x in a continuous medium with dielectric constants D_s and D_{op}. Then a correction term will be added to take account of dielectric saturation.

$$E_1 = \frac{z^2e^2}{r_x}(1/D_{op} - 1/D_s) + \frac{z^2e^2}{2r_x}(1 - 1/D_{op})$$

(4) Calculated by means of the Born equation.

(5) R. S. Berry, C. W. Riemann, and G. N. Spokes, *J. Chem. Phys.*, 37, 2278 (1962).

(6) M. Smith and M. C. R. Symons, *Trans. Faraday Soc.*, 54, 338 (1958).

(7) G. Stein and A. Treinin, *ibid.*, 55, 1086, 1091 (1959).

(8) R. L. Platzman and J. Franck, "Farkas Memorial Volume," Weizmann Press, Jerusalem, 1952, p. 21; *Z. Physik.* 138, 411 (1954).

(9) J. Jortner and A. Treinin, *Trans. Faraday Soc.*, 58, 1503 (1962).

(10) I. Burak and A. Treinin, *ibid.*, 59, 1490 (1963).

(11) M. Smith, Thesis, University of Southampton, Southampton, England. 1958; M. Smith and M. C. R. Symons, *J. Chem. Phys.* 25, 1074 (1956).

(12) R. Sperling and A. Treinin, to be published.

(13) M. J. Blandamer, J. M. Gross, and M. C. R. Symons, *Proc. Chem. Soc.*, 147 (1963).

(14) W. S. Fyfe, *J. Chem. Phys.*, 37, 1894 (1962).

(15) M. Shirom and G. Stein, to be published.

where the first term represents the binding of a charge ze by the persistent polarization of the medium, and the second term represents the electronic polarization induced by this charge.

$$E_2 = \frac{(z-1)ze^2}{r_x} (1/D_{op} - 1/D_s) +$$

$$\frac{(z-1)^2 e^2}{2r_x} (1 - 1/D_{op})$$

where the two terms represent the corresponding interactions for an ion of charge $(z-1)$ in a medium which keeps all the positions of the nuclei fixed as in the ground state. Altogether the following expression is derived from the cycle

$$h\nu_x = I_x + e^2 \left(\frac{z}{r_x}\right)(1 - 1/2z + 1/2zD_{op} - 1/D_s) - B \quad (4)$$

The cavity radius r_x is related to the crystallographic radius R_x: $r_x = \alpha R_x$, where α is a factor larger than one, accounting for the loose packing of solvent molecules around the ion. For many ions in water, α was shown to be nearly constant irrespective of their charge,[16] $\alpha \sim 1.25$ at room temperature.

The foregoing calculation ignored the dielectric saturation effect near the ion. This becomes of increasing importance with increasing charge of the ion. The effect will be treated here using a simple method introduced by Jortner[17] and based on Buckingham's treatment of ion–solvent interaction.[18] The dependence of the dielectric constant on the field intensity E is given by the expression

$$D_s' = D_s + bE^2 + \cdots \quad (5)$$

The field at a distance r from X^z is thus

$$E = \frac{ze}{D_s' r^2} \sim \frac{ze}{D_s r^2} - \frac{z^3 e^3 b}{D_s^4 r^6} \quad (6)$$

From the relation between the displacement vector ze/r^2 and the field intensity, the total polarization of the medium P is calculated

$$P = \frac{ze}{4\pi r^2} (1 - 1/D_s) + \frac{z^3 e^3 b}{4\pi D_s^4 r^6} \quad (7)$$

By subtracting the electronic polarization $P_E = (ze/4\pi r^2)(1 - 1/D_{op})$, the persistent polarization P_D is obtained

$$P_D = \frac{ze}{4\pi r^2} (1/D_{op} - 1/D_s) + \frac{z^3 e^3 b}{4\pi D_s^4 r^6} \quad (8)$$

The potential due to this polarization at the ionic cavity of radius r_x is

$$V(r_x) = \int_{r_x}^{\infty} \left(\frac{P_D}{r^2}\right) 4\pi r^2 dr =$$

$$\frac{ze}{r_x} (1/D_{op} - 1/D_s) + \frac{z^3 e^3 b}{5 D_s^4 r_x^5} \quad (9)$$

Using this expression of $V(r_x)$ in our previous calculation we obtain

$$h\nu_x = I_x + e^2(z/r_x)(1 - 1/2z +$$

$$1/2z D_{op} - 1/D_s) + \frac{z^3 e^4 b}{5 D_s^4 r_x^5} - B \quad (10)$$

For water, $b = -3 \times 10^{-7}$ e.s.u.[18]; hence, the correction term accounting for dielectric saturation is $-11z^3/r_x^5$ kcal. (r_x is given in Å). For the halide ions with $z = 1$ and $r_x \sim 2.5$ Å., the correction term is negligible, but this term may be quite important for polyvalent anions.

For divalent anions in water ($D_{op} = 1.77$, $D_s = 80$, $\alpha = 1.25$), eq. 10 reduces to

$$h\nu_x = I_x + 465/R_x - 29/R_x^5 - 35$$

$$(R_x \text{ in Å., } h\nu \text{ in kcal.}) \quad (11)$$

Table I contains the available data concerning some divalent anions. (HS^- was also included for comparison with S^{-2}, its $h\nu_{max}$ calculated in a similar way.) In the few cases where $h\nu_{max}$ is known, the agreement is satisfactory, taking into account all the approximations involved. Apart from the oversimplification involved in the continuum model, the present theory ignores all but simple electrostatic interactions. In some cases the contribution of the X^{z-1} orbitals to the binding should not be overlooked.

Environmental Effects. According to the theory derived for X^-, the environmental effects on c.t.t.s. spectra are mainly due to variations in r_x, *i.e.*, in α.[7,10] The study of solvent effects has shown that $h\nu_{max}$ of X^- in various solvents varies nearly linearly with their c.t.t.s. values.[10] (The c.t.t.s. value, C, of a solvent is defined as $h\nu_{max}$ of I^- in that solvent.) The slope of the line β measures the solvent sensitivity of the c.t.t.s. band. This relation was given a simple theoretical interpretation,[10] which will now be extended to polyvalent anions. It is based on the assumption that in analogy with H_2O, α is the same for all anions in the same solvent.

From the definition of the c.t.t.s. value, C, and by using eq. 4 (*i.e.*, the dielectric saturation effect is neglected), the following relation is obtained

(16) J. Jortner, unpublished work.

(17) J. Jortner, Thesis, Hebrew University, Jerusalem, 1959.

(18) A. D. Buckingham, *Discussions Faraday Soc.*, **24**, 151 (1957).

$$h\nu_x = \beta_x C + I_x - \beta_x I_I + B(\beta_x - 1) \quad (12)$$

where $\beta = z(R_I/R_x)(1 - 1/2z + 1/2zD_{op} - 1/D_s) \cdot (1/2 + 1/2D_{op} - 1/D_s)^{-1}$. For monovalent anions $\beta = R_I/R_x$ and so we obtain the simple expression already derived.[10] In general, for solvents with $D_{op} \sim 2$, $\beta \sim z(R_I/R_x)(4/3 - 1/3z)$. This means that the solvent sensitivity of the c.t.t.s. band of an ion should be nearly proportional to its electrical potential, z/R. Indeed, this relation was shown to apply to monovalent anions[10,19] and also to $S_2O_3^{-2}$.[12] Its origin is very simple: the electron transfer results in the ion losing one electron at a potential which is proportional to z/R.

The situation is quite different with respect to tem-

perature and pressure effects. To show this, eq. 4 is differentiated with respect to λ, where λ denotes T or P. Ignoring the small dependence of the dielectric properties on λ we obtain

$$d(h\nu_x)/d\lambda \sim -e^2(1 - 1/4z)(z/\alpha r_x)(d\alpha/d\lambda) \quad (13)$$

$d\alpha/d\lambda$ represents the effect of changing λ on the average distance between the ion and the solvation layer. This effect should be inversely proportional to the electrostatic potential of the ion, since the larger the potential the more tightly the solvation layer is held. Therefore, altogether it follows from eq. 13 that $d(h\nu)/d\lambda$ should be nearly independent of the ionic potential. And indeed nearly the same temperature sensitivity is displayed by the peaks of the c.t.t.s. bands of I^-,[7] $S_2O_3^{-2}$,[12] and S^{-2}.[13] As for the pressure effect, this was measured at the onset of the c.t.t.s. band of $S_2O_3^{-2}$ (260 mμ) and was found to be twice that on the peak of I^-,[14] but since the temperature effect on the onset is also twice that on the peak,[7] we should expect the same pressure effect on the peaks of $S_2O_3^{-2}$ and I^-.

Thus, to inflict a certain change upon the solvation layer of an ion becomes more difficult as its potential increases, but once the change is accomplished, its effects increase with potential. The study of c.t.t.s. bands in mixtures of solvents differing largely in solvation power is also in accord with this conclusion.[12]

Table I: Experimental and Calculated Data Concerning C.t.t.s. Bands of Divalent Anions

Ion	R_x, Å.	I_x, kcal.	$h\nu_{max}$ (exptl.), kcal.	$h\nu_{max}$ (calcd.), kcal.
S^{-2}	1.84[a]	-128[c,d]	79.5[e]	87.5
HS^-	1.95[b]	53[c]	124[e]	123
O^{-2}	1.40[a]	-210[d]		81.5
Se^{-2}	1.98[a]	$-(\geqslant 137)$[d]	70[f]	$\leqslant 62$

[a] Pauling crystallographic radius. [b] K. B. Yatsimirskii, *Bull. Acad. Sci., URSS*, 753 (1947). [c] D. A. Ansdell and F. M. Page, *Trans. Faraday Soc.*, **58**, 1084 (1962). The vertical ionization potential of HS^- is probably a little larger. [d] See ref. 2. The value for Se^{-2} is questionable. [e] See ref. 13. [f] D. J. G. Ives and R. W. Pittman, *J. Chem. Soc.*, 766 (1948); a peak of unknown origin in the spectrum of H_2Se in water.

(19) The smaller solvent sensitivity of the onset relative to the peak[10] agrees with this conclusion, since the radius of the cavity corresponding to the onset is larger.

Charge-Transfer-to-Solvent Spectra of Polyvalent Anions. II.

The Electronic Spectrum of $S_2O_3^{-2}$

by Ruth Sperling and Avner Treinin

Department of Physical Chemistry, Hebrew University, Jerusalem, Israel (*Received November 16, 1963*)

The electronic absorption spectrum of $S_2O_3^{-2}$ in solution was investigated. For this purpose environmental effects on the spectrum were studied. In the 190–300-mμ region the spectrum consists of at least three bands, labeled A, B, and C. Band A, which is of moderate intensity ($\epsilon \sim 200$ l. mole^{-1} cm.$^{-1}$) has a peak at about 240 mμ and is assigned to $\pi^* \leftarrow$ n transition involving the no-bonding electrons on the sulfur atom. Band B (λ_{max} at about 215 mμ) originates from a charge transfer to the solvent (c.t.t.s.). Band C, the peak of which is at the vacuum ultraviolet, is assigned to the allowed $\pi^* \leftarrow$ n transition involving the no-bonding electrons on the oxygen atoms. The environmental effects on the c.t.t.s. band are related to the theory derived in part I of this series. The photochemistry of $S_2O_3^{-2}$ at 229 mμ was studied by using suitable electron scavengers. The photochemical behavior is in general similar to that displayed by the halide ions, but the limiting and residual quantum yields are appreciably smaller. $S_2O_3^{-2}$ itself is shown to act as an efficient electron scavenger.

The ultraviolet absorption spectrum of $S_2O_3^{-2}$ in solution appears as a single intense band with a peak at about 215 mμ.[1,2] It has been assigned to a charge-transfer-to-solvent (c.t.t.s.) type of excitation.[2–4] The evidence for this assignment is limited and is entirely based on the study of some environmental effects including temperature[2] and pressure[4] effects. No attempt has been made to detect other electronic transitions which may be concealed under the main band.

The photochemistry of $S_2O_3^{-2}$ has hardly been investigated. The recent photochemical studies of I^- in the presence of specific electron scavengers (H^+, N_2O, O_2)[5] have established a method to detect electron release to the solvent. Such release results from the spectroscopic excited state (c.t.t.s. state) with an efficiency Φ, which depends on the competition between the deactivation of the c.t.t.s. state and its decomposition to a radical and solvated electron in the photochemical cage.[5b,c] Provided that the efficiency is not too small, the electron scavenging method thus adds photochemical evidence for c.t.t.s. transitions. However, by itself it is not conclusive, since it does not deal directly with the spectroscopic excited state. Thus electron release to the solvent may result from the

thermal dissociation of an intramolecular excited state, as in the case of the phenolate ion.[5d]

The photochemical method together with an extensive study of environmental effects were used in the present work to identify the electronic transitions responsible for the ultraviolet absorption spectrum of $S_2O_3^{-2}$ in solution. The environmental effects are related to the theory derived in part I of this series.[6]

Experimental

Absorption Spectra and Materials. The spectrophotometer, its calibration, and the solvents used were described elsewhere.[7] Unless otherwise stated, the temperature was kept constant at 25 ± 0.5°.

(1) H. Ley and E. König, *Z. Physik. Chem.*, **B41**, 365 (1937); A. Kiss, *Z. anorg. Chem.*, **246**, 28 (1941); A. D. Autrey and R. E. Connick, *J. Am. Chem. Soc.*, **73**, 1842 (1951).

(2) M. Smith, Ph.D. Thesis, University of Southampton, 1958; M. Smith and M. C. R. Symons, *J. Chem. Phys.*, **25**, 1074 (1956).

(3) D. P. Ames and J. Willard, *J. Am. Chem. Soc.*, **75**, 3267 (1953).

(4) W. S. Fyfe, *J. Chem. Phys.*, **37**, 1894 (1962).

(5) (a) M. Ottolenghi, Ph.D. Thesis, Hebrew University, Jerusalem, 1962; (b) J. Jortner, M. Ottolenghi, and G. Stein, *J. Phys. Chem.*, **66**, 2029 (1962); (c) *ibid.*, **66**, 2037 (1962); (d) *J. Am. Chem. Soc.*, **85**, 2712 (1963); (e) *J. Chem. Phys.*, **37**, 2488 (1962).

(6) A. Treinin, *J. Phys. Chem.*, **68**, 893 (1963).

$Na_2S_2O_3$ (Analar) was used without further purification. Tetraethylammonium thiosulfate was prepared by adding an excess of freshly prepared BaS_2O_3 to a solution of tetraethylammonium sulfate in methanol, shaking for 24 hr., filtering, and evaporating the filtrate to dryness under vacuum (at room temperature to avoid decomposition). The thiosulfate was then recrystallized from dimethylformamide and dried over alumina. Its purity was checked by measuring its spectrum in aqueous solution, which was found to be nearly identical with that of $Na_2S_2O_3$. All other materials used were Analar.

In all measurements the sample differed from the reference solution only by containing the thiosulfate. The concentration of the latter was kept as low as possible (10^{-3} to 10^{-4} M) in order to diminish the effect of ionic association. Small deviations from Beer's law (up to 3%) were still observed at this concentration range, and hence for recording the whole spectrum (from ϵ 1) the concentration was kept constant ($\sim 10^{-3}$ M) and the cell thickness was varied (from 40 to 1 mm.).

Photochemical Experiments. Light Sources. Most photochemical experiments were carried out at 2288 Å. using an Osram Cd/1 cadmium lamp operated at 12 v. and 1.5 amp. In all solutions used, the optical path was 3 cm. and conditions of total absorption were attained. The light output at 2288 Å. was determined by a differential actinometric method using the uranyl oxalate actinometer.[5d] The total output was first measured by irradiating the actinometer in the reaction vessel without filter. The output at $\lambda > 2400$ Å. was then measured by performing the same experiment with a filter of 3-cm. path length 4 N acetic acid. From the difference between the two values, the light intensity at 2288 Å. was determined as $J = 8.4 \times 10^{-7}$ einstein l.$^{-1}$ sec.$^{-1}$.

Some experiments were conducted at 2537 Å. using a Thermal Syndicate low pressure mercury lamp. A I_2/I^- filter[5a] was employed to cut off other lines. The light intensity at this wave length was $J = 2.2 \times 10^{-6}$ einstein l.$^{-1}$ sec.$^{-1}$.

Procedure. $Na_2S_2O_3$ solutions containing 5×10^{-3} KH_2PO_4–Na_2HPO_4 buffer (pH 7.5) and 1 M methanol were evacuated until their gas pressure was 1–2×10^{-5} mm. This was best achieved by a brief evacuation followed by leaving the solution stirred overnight and then another brief evacuation. The methanol served to scavenge O^- (or OH) resulting from the irradiation.

The preparation of N_2O containing solutions and the pressure measurement after irradiation were performed as described elsewhere.[5c] At low temperatures,
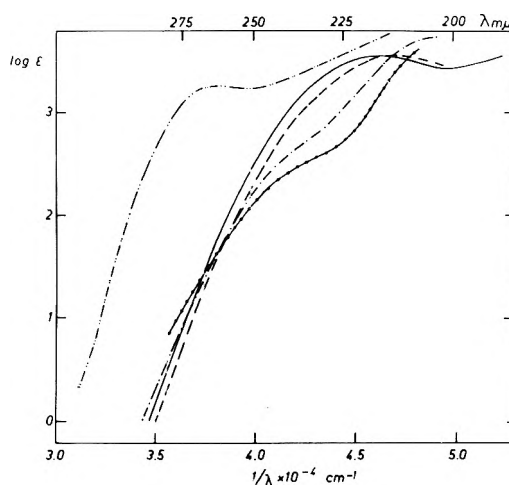
Figure 1. The absorption spectrum of $(Et_4N)_2 S_2O_3$ in MeCN (—··—) and of $Na_2S_2O_3$ in H_2O (———), 1 M sucrose (— —), CH_3OH (—·—), and ethylene glycol (—·—·—).

N_2 seems to be occluded in ice (probably by forming a clathrate) and hence special care was taken to condense all the water vapor in a CO_2–acetone trap and then to disconnect the trap from the system. In some experiments hydrogen was evolved. Its identity and pressure were determined by collecting the gas over a trap of silica gel at liquid air temperature.[8]

Results

Spectra. Figure 1 shows the spectrum of $S_2O_3^{-2}$ in various solvents. In water, a peak appears at about 215 mμ and there is also an indication of another transition at shorter wave lengths (labeled band C). In alcohols, two opposite effects are observed: at wave lengths shorter than about 250 mμ there is a remarkable blue shift, while at longer wave lengths there is a small shift to the red. Some intensification of the peak also occurs, probably due to increasing overlap by band C, which is red-shifted by alcohols. The spectrum in alcohols thus reveals a new transition (labeled band A) which in water merges into another band (labeled band B) to yield (with considerable overlap of C) the apparently single band of $S_2O_3^{-2}$ at 215 mμ. The alcohols, by having opposite effects on A and B, succeed in separating them a little, causing band A to appear as a shoulder on the long wave length branch of B.

In ethylene glycol, where the separation is the largest, the properties of band A were determined by means of a rough graphical analysis: $\lambda_{max} \sim 245$ mμ, $\epsilon_{max} \sim 200$. In MeCN all three bands are shifted to

(7) I. Burak and A. Treinin, *J. Chem. Phys.*, **39**, 189 (1963).

(8) G. Kuhn, *Z. angew. Chem.*, **44**, 757 (1931).

the red, but band B suffers the largest shift and appears as a well-defined peak at $\lambda \sim 260$ mμ with $\epsilon_{max} \sim 2000$.[9] Bands A and C, which shift to a smaller extent, lag behind with A probably lying at the onset of the much more intense band C. The decrease in overlap with bands C and B leads to the lowering of the peak and to increase in the steepness of the onset.

The high solvent sensitivity and its nature suggest that band B is a c.t.t.s. band, which in water contributes the major part of the absorption in the 215–240-mμ region (the c.t.t.s. region). On the other hand, bands A and C behave like $\pi^* \leftarrow n$ transitions, exhibiting the regular blue shifts when passing from a less polar to a more polar solvent. This interpretation is consistent with the following observations.

(a) The transition energy in various solvents (at ϵ 1000)[10] is plotted against $h\nu_{max}$ of I^- in those solvents (Fig. 2). Apart from the MeCN + H$_2$O mixtures, the various media fit a linear relation, the slope of the line obtained is ~ 1.8.

(b) Figure 3 shows that, in general, the c.t.t.s. region behaves like the c.t.t.s. band of I^- toward ionic

Figure 3. The spectrum of 10^{-4} M Na$_2$S$_2$O$_3$ alone (curve 1) and in presence of: 1 M NaCl (curve 2), 1 M NaClO$_4$ (curve 3), and 2, 4, 6, 8 M KF (curves 4, 5, 6, 7).

effects,[11a] but there are still some differences, especially in the cationic effect, which displays a more pronounced specifity, being largely dependent on the charge of the cation (Fig. 4).

(c) The effect of sugar, which is of particular importance for the identification of c.t.t.s. transitions,[7] is most pronounced in the c.t.t.s. region (Fig. 1).

(d) The temperature effect shows clearly that at least two transitions contribute to the long wave length branch of the spectrum. In Fig. 5, the temperature coefficient d$(h\nu)$/dt is given at four different extinction coefficients. Moving from the peak to longer wave lengths, d$(h\nu)$/dt first increases and then decreases, so that its value at the onset is nearly the same as that at the peak. This is completely different from the behavior of the c.t.t.s. band of I^-, which displays a regular increase of d$(h\nu)$/dt with λ, being at the onset nearly twice as large as at the peak.[11b]

(e) Photochemical experiments with solutions of Na$_2$S$_2$O$_3$ containing N$_2$O indicate that the quantum yield of N$_2$ is much larger at 228 mμ than at 254 mμ.

Photochemistry. The ultraviolet irradiation of aqueous thiosulfate solutions results in formation of sulfur,

Figure 2. $h\nu(S_2O_3^{-2})$ at ϵ 1000 against $h\nu_{max}$ of I^- at the same solvent (*i.e.*, its c.t.t.s. value): (1) MeCN; (2) 97.5% MeCN; (3) 95% MeCN; (4) 90% MeCN; (5) 25% NH$_3$; (6) 76% MeCN; (7) H$_2$O; (8) 1 M sucrose; (9) 4 M KF; (10) CH$_3$OH; (11) 8 M KF; (12) ethylene glycol.

(9) S$_2$O$_3^{-2}$ is unstable in MeCN; the spectrum changes slowly with time. After rapidly recording the spectrum of a fresh solution, an equal volume of water was added, and the spectrum of the solution obtained was nearly identical with that of the aqueous solution. This was considered as a proof that a chemical reaction has not yet occurred, since in the solutions which had reacted, the spectrum of S$_2$O$_3^{-2}$ could not thus be regained.

(10) ϵ 1000 was chosen because band B seems to have the largest contribution there.

(11) (a) G. Stein and A. Treinin, *Trans. Faraday Soc.*, 56, 1393 (1960); D. Meyerstein and A. Treinin, *J. Phys. Chem.*, 66, 446 (1962); (b) G. Stein and A. Treinin, *Trans. Faraday Soc.*, 55, 1091 (1959).
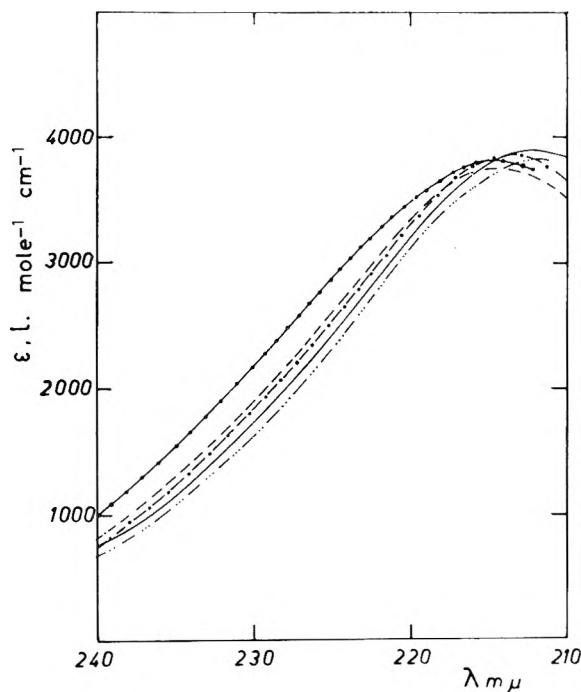
Figure 4. The spectrum of 10^{-4} M $Na_2S_2O_3$ alone (———·———·———) and in presence of 1 M of the following salts: $N(CH_3)_4Cl$ and NH_4Cl (— — —), NaCl and KCl (—·—·—), $MgCl_2$ (————), $CaCl_2$ (—··—··—). NH_4Cl and KCl bring about slightly larger shifts than $N(CH_3)_4Cl$ and NaCl, respectively.
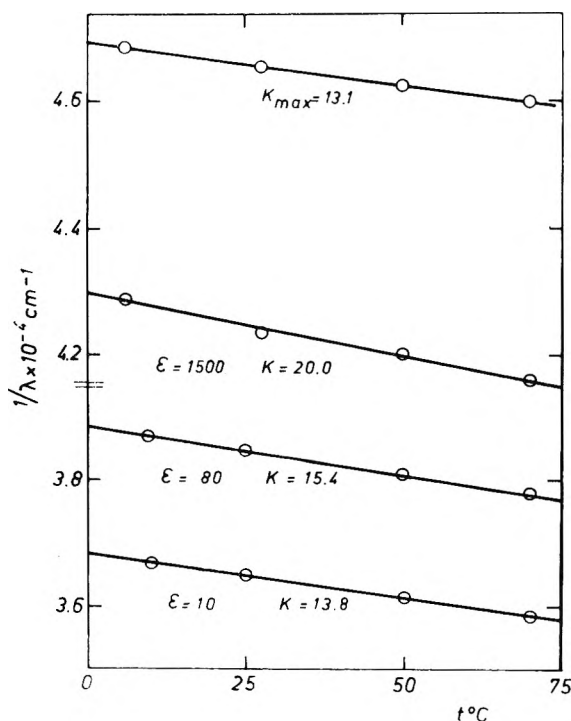
Figure 5. The temperature effect on the spectrum of $S_2O_3^{-2}$ at various extinction coefficients. (The thermal expansion of water was taken into account.)

sulfite, H_2S, and probably other products which have not yet been identified. The gases which result from the irradiation (H_2S is readily detected) can be condensed in a CO_2–acetone trap.

Irradiation at 228.8 mμ of N_2O-containing solutions led to the formation of N_2. The initial quantum yield of N_2 (φ_{N_2}) could be determined easily since in all our experiments (up to 25 min. of irradiation) the yields were linearly dependent on time of irradiation. At constant concentration of N_2O, φ_{N_2} was found to depend strongly on the concentration of $S_2O_3^{-2}$. Thus at $C_{N_2O} \leqslant 2 \times 10^{-2}$ M and $C_{S_2O_3^{-2}} \geqslant 0.1$ M, φ_{N_2} is negligible. At constant C_{N_2O} the yield increases with decrease of $C_{S_2O_3^{-2}}$ until it reaches a limiting constant value. This suggests a competition between N_2O and $S_2O_3^{-2}$ for the solvated electrons, a subject which will be discussed later. In order to study the dependence of φ_{N_2} on C_{N_2O}, we irradiated 10^{-3} M $Na_2S_2O_3$ solutions at $C_{N_2O} \geqslant 7 \times 10^{-4}$ M. The lower limit for C_{N_2O} was chosen so that further decrease of the thiosulfate concentration (at total absorption conditions) had no detectable effect on φ_{N_2}. Figure 6 shows the dependence of φ_{N_2} on C_{N_2O}. At high concentrations, an upper limiting yield is approached. Its exact value could not be determined by extrapolation, being about 0.08. The fall of φ below this value is ascribed to the competition between the scavenging action of N_2O and the secondary recombination of $S_2O_3^-$ and the electron in the solvent cage. Figure 7 shows that the experimental results are consistent with the general equation for diffusion-controlled scavenging.[5b]

$$\ln (1 - \varphi/\Phi) = A - B\sqrt{C_{N_2O}}$$

(The value $\Phi = 0.080$ seems to give better agreement.) From the slope and intercept of the line we obtain[5b] $\varphi_r \sim 0$, $2a(\pi k)^{1/2} \sim 17$ $M^{-1/2}$, where φ_r is the residual yield, k is the rate constant for scavenging of the electron by N_2O, and a is a parameter characteristic of the cage. The plot of φ against $\sqrt{C}$ (Fig. 7) also indicates that $\varphi_r \sim 0$.

Few photochemical experiments were conducted with $H_2PO_4^-$ as an electron scavenger.[5e] An excess of methanol was added to convert H atoms to H_2. For a mixture containing 10^{-3} M $Na_2S_2O_3$, 1.54 $\times$ 10^{-1} M KH_2PO_4, 2 $\times$ 10^{-2} M Na_2HPO_4, and 1 M methanol, the quantum yield of H_2 was 0.055.

Discussion

The electron structure of $S_2O_3^{-2}$ has hardly been discussed. The ion is structurally analogous to SO_4^{-2} with one sulfur atom replacing an oxygen atom. Raman spectra of $S_2O_3^{-2}$ in aqueous solution[12] prove
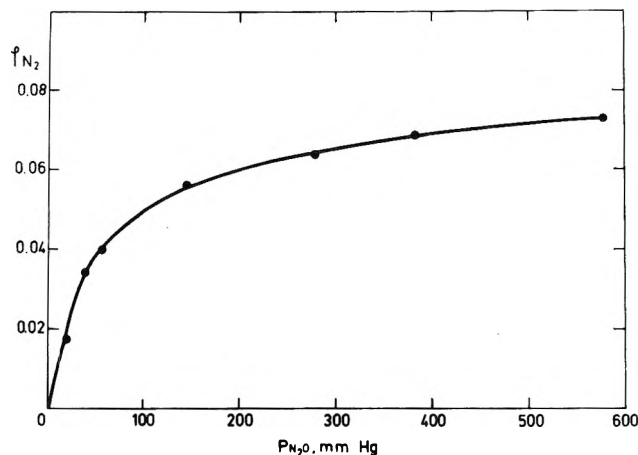
Figure 6. Dependence of φ_{N_2} on N_2O concentration.
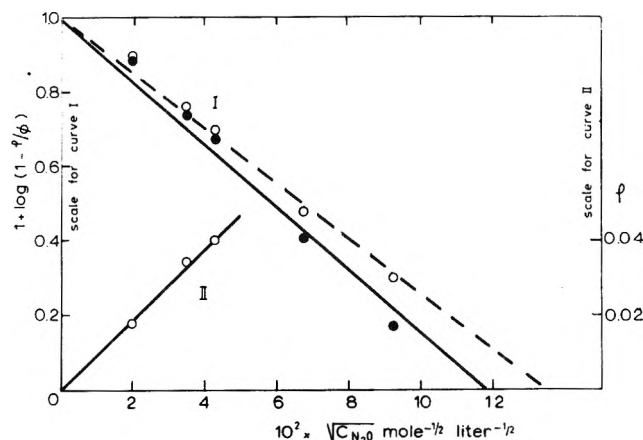
Figure 7. Scavenging plots for N_2O: continuous line, $\Phi = 0.075$; dashed line, $\Phi = 0.080$.

that it possesses the C_{3v} symmetry, with bond angles differing only slightly from those in the tetrahedral SO_4^{-2} ion. The S–O bond length in $S_2O_3^{-2}$ is nearly the same as in SO_4^{-2},[13] showing that in both ions the S–O bond has the same π-bond order, 50%.[14] The length of the S–S bond 1.97 Å. is 0.11 Å. shorter than a single bond[15] and 0.08 Å. larger than the double bond in S_2. Assuming a linear relation between π-bond order and shortening, the value obtained for S–S in $S_2O_3^{-2}$ is 58%. Hence in $S_2O_3^{-2}$ the double system of π-orbitals is nearly equally shared by the four bonds. The same conclusion was also reached from force constants consideration.[12b]

The electronic structure of SO_4^{-2} has been discussed in some detail[14-17]; the molecular orbital treatment has been used for its description.[14,17] The highest filled energy level is a triply degenerate MO (t_1) involving the no-bonding electrons on the oxygen atoms. The

first empty orbital is probably the doubly degenerate π-antibonding orbital (e), which is mainly concentrated on the central S atom. Thus the lowest energy electronic transition in SO_4^{-2}, (the peak of which appears in the vacuum ultraviolet) is the allowed $\pi^* \leftarrow n$ transition[18] e $\leftarrow t_1$. On going from SO_4^{-2} to $S_2O_3^{-2}$, two main differences should be considered: (a) the symmetry is lowered from T_d to C_{3v}; (b) the binding of the no-bonding p-electron on sulfur is appreciably weaker. The lowering of symmetry leads to the splitting of t_1 into a doublet and a singlet.[19] Thus on going from SO_4^{-2} to $S_2O_3^{-2}$ the $\pi^* \leftarrow n$ transition is expected to split into two components: the low energy one essentially involving the no-bonding electrons on the sulfur atom, while the other, not much removed from the band of SO_4^{-2}, involves the no-bonding electrons on the oxygen atoms. This prediction seems to be confirmed by our results. The low energy $\pi^* \leftarrow n$ transition of $S_2O_3^{-2}$ (band A) appears at about 245 mμ in ethylene glycol with moderate intensity and it displays the regular blue shift when changing to a more polar solvent. Band C is accordingly interpreted as being due to the second component of the $\pi^* \leftarrow n$ transition, since SO_4^{-2} starts to absorb in this region.[20] The solvent sensitivity of band C seems to be larger than that of A, which we ascribe to the larger negativity of oxygen compared with sulfur: oxygen is more liable to H-bond formation than sulfur.

The C.t.t.s. Band of $S_2O_3^{-2}$. Between the two $\pi^* \leftarrow n$ components $S_2O_3^{-2}$ displays a c.t.t.s. band probably originating from a transfer of one no-bonding electron on the sulfur atom to a discrete level largely defined by the polarized medium. The nature and theory of such bands were discussed in detail.[6] An expression was derived for relating $h\nu_{max}$ of a polyvalent anion to its crystallographic radius R and vertical ionization potential I

$$h\nu_{max} = I + 465/R - 29/R^5 - 35$$

(R in Å., $h\nu$ in kcal.)

(12) (a) H. Gerding and K. Eriks, *Rec. trav. chim.*, **69**, 659 (1950); (b) E. Siebert, *Z. anorg. allgem Chem.*, **275**, 225 (1954).

(13) "Interatomic Distances," Special Publication No. 11, The Chemical Society, London, 1958.

(14) D. W. J. Cruickshank, *J. Chem. Soc.*, 5486 (1961).

(15) L. Pauling, "The Nature of the Chemical Bond," Cornell University Press, Ithaca, N. Y., 1960. In $S_2O_6^{-2}$ where S has no available free p-orbitals for double bond, the S–S distance is 2.08 Å.

(16) G. W. Chantry and R. A. Plane, *J. Chem. Phys.*, **32**, 319 (1960).

(17) D. S. Urch, *J. Inorg. Nucl. Chem.*, **25**, 771 (1963).

(18) S. P. McGlynn and M. Kasha, *J. Chem. Phys.*, **24**, 481 (1956).

(19) L. Helmholtz and H. Brennan, *ibid.*, **23**, 853 (1955); U. Kläning and M. C. R. Symons, *J. Chem. Soc.*, 3204 (1961).

(20) J. L. Weeks, G. M. A. C. Meaburn, and S. Gordon, *Radiation Res.*, **19**, 559 (1963).

Taking $R_{S_2O_3^{-2}} = 2.4$ Å.[21] and $h\nu_{max} = 133$ kcal., we obtain $I_{S_2O_3^{-2}} = -26$ kcal. The normal ionization potential is probably more negative, since the vertical ionization process leads to a strained radical.

The environmental effects in general are in accord with the theory.[6] Thus the solvent sensitivity β is nearly twice that of I^-, while the temperature sensitivity is nearly the same.[22] The deviations of the H_2O + MeCN mixtures from the line (Fig. 2) are of particular interest. They indicate that the water molecules in the solvation layer of $S_2O_3^{-2}$ are replaced by molecules of MeCN with more difficulty than in the case of I^-. This is due to the higher electrical potential of $S_2O_3^{-2}$, but once the solvation layer is totally replaced, the spectroscopic shift is nearly doubled.

Spectroscopic Shifts and Ionic Association. In several works[3,24] ionic effects were studied at the long wave length branch of the absorption spectrum of $S_2O_3^{-2}$, and the spectral shifts were attributed to ionic association. Accordingly, the effect of alcohol was ascribed to increasing ionic association as the polarity of the solvent decreases.[24b] From the spectral shifts, association constants were determined[24] for $Na^+S_2O_3^{-2}$, $K^+S_2O_3^{-2}$, etc. It was assumed that the molar absorption coefficient of $S_2O_3^{-2}$ is not affected by the change of environment and that the ion pairs have a discrete spectrum. That this assumption is wrong was already pointed out by Smith and Symons,[2] who studied some ionic effects on the peak. Our results completely support their conclusions, as can be readily seen from the nearly parallel shifts of the whole spectrum up to very high concentrations of added salts (Fig. 3). Furthermore, there is a pronounced anionic effect which is very similar to that displayed by I^-. Thus at the same concentration the difference between the effects of NaCl and $NaClO_4$ is larger than that between NaCl and KCl (Fig. 3 and 4). Such specific anionic effects were observed by us at the concentration range investigated by Gimblett and Monk,[24] who completely ignored them in their calculations. As in the case of I^-,[11a] our results led us to attribute the major part of the ionic effect to the changes induced in the solvation layer of the light absorbing ion. These changes probably go in parallel with ion-pair formation, if only the nature of the cation is varied. The term "ion-pair" was recently discussed in detail,[25] and was shown to apply to several types of ionic association differing in closeness of contact between anion and cation. Only very intimate contacts are expected to bring about an abrupt change in the spectrum of the light absorbing ion.[26] Thiosulfates belong to the group of ion pairs where solvation is a predominant factor; the association constants increase with

decreasing size of *solvated* cation.[25] This is also the order of increasing spectroscopic effects (Fig. 4), but none of the cations studied changes the nature of the excitation. This becomes even clearer when we vary the nature of the solvent. The association constant does increase with decrease of polarity, but this is not the origin of the large solvent shifts observed at low concentrations of $S_2O_3^{-2}$. (The small deviations from Beer's law should be ascribed to this effect.) Actually, in the c.t.t.s. region there is no relation between solvent polarity and the spectroscopic shift,[23] as can be easily checked by comparing the effects of MeCN and MeOH.

The Photochemistry of $S_2O_3^{-2}$ at 229 mμ. In aqueous solution, the absorption at 229 mμ is probably due to both internal ($\pi^* \leftarrow n$) and c.t.t.s. transitions, the latter contributing the major part. Our work has a bearing only on the c.t.t.s. contribution, leading to $S_2O_3^-$ radical and solvated electron according to the scheme

$$S_2O_3^{-2} \underset{\longleftarrow}{\overset{h\nu}{\rightleftarrows}} S_2O_3^{-2*} \longrightarrow (S_2O_3^- + e)$$
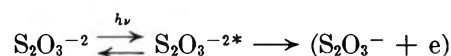
$S_2O_3^{-2*}$ represents the c.t.t.s. state and ( ) represents the solvent cage where the particles may undergo secondary recombination.[5] The quantum yield Φ for the formation of the cage can be determined by the photochemical yield under total scavenging conditions. This is attained at N_2O concentrations larger than 2×10^{-2} M. The value 0.08 obtained for Φ is relatively small (for I^-, $\Phi = 0.29^{5b}$). This is only partly due to the "internal filter effect" of the $\pi^* \leftarrow n$ transition, which absorbs less than half of the light. It seems to result mainly from a large probability of decay of the c.t.t.s. state back to the ground state. Assuming the validity of the continuum model,[6] the average radius of the excited orbital in $S_2O_3^{-2*}$ is at most 6 Å. (it is probably less[11a]), i.e., the excited electron resides at most 4 Å. from the center of the sulfur atom, from where it was detached. This may be the reason for the high deactivation yield. It seems that even

(21) The thermochemical radius of SO_4^{-2} is 2.3 Å. (A. F. Kapustinskii, *Quart. Rev.* (London), **10**, 283 (1956)); 0.1 Å. is added to account for the difference between the radii of S and O averaged over the four ligands.

(22) Moving from the onset of a c.t.t.s. band toward its peak, the solvent sensitivity β increases while the temperature sensitivity $d(h\nu)/dT$ decreases.[23,11b] Hence at the peak $\beta_{S_2O_3^{-2}}$ should be larger than 1.8 while $d(h\nu_{max})/dT$ is probably not far from that observed at 215 mμ.

(23) I. Burak and A. Treinin, *Trans. Faraday Soc.*, **59**, 1490 (1963).

(24) (a) F. G. R. Gimblett and C. B. Monk, *ibid.*, **51**, 793 (1955); (b) C. B. Monk and G. D. Thomas, *ibid.*, **52**, 685 (1956).

(25) C. W. Davies, "Ion Association," Butterworths, London, 1962.

(26) T. R. Griffiths and M. C. R. Symons, *Mol. Phys.*, **3**, 90 (1960).

in the cage, the recombination probability is very high: the residual yield φ_r is very low and a high concentration of scavenger is required to overcome secondary recombination completely (Fig. 6).

Moreover, our results show that $S_2O_3^{-2}$ itself acts as an efficient electron scavenger, being able to compete with N_2O for the solvated electrons. The rate constants ratio for scavenging by $S_2O_3^{-2}$ and N_2O could be determined in the following way: $5 \times 10^{-2}\ M$ $Na_2S_2O_3$ was irradiated in presence of $C_{N_2O} > 10^{-2}\ M$ and the quantum yield of N_2 was measured. (At such N_2O concentrations there is nearly total electron scavenging even at $10^{-3}\ M$ $Na_2S_2O_3$.) The electrons are now scavenged by N_2O and $S_2O_3^{-2}$ which act in parallel; the fraction δ scavenged by N_2O is given by the expression

$$\delta = \frac{\varphi_{N_2}}{\Phi} = \frac{k_{(N_2O\ +\ e)}C_{N_2O}}{k_{(N_2O\ +\ e)}C_{N_2O}\ +\ k_{(S_2O_3^{-2}\ +\ e)}C_{S_2O_3^{-2}}}$$

φ_{N_2} observed at $1.82 \times 10^{-2}\ M$ and $1.23 \times 10^{-2}\ M$ N_2O were 0.046 and 0.040, respectively. This gives $[k_{(S_2O_3^{-2}\ +\ e)}]/[k_{(N_2O\ +\ e)}] = 0.2$, which shows that $S_2O_3^{-2}$ is actually a very efficient electron scavenger.

The possible occurrence of self-electron scavenging in the photochemistry of polyatomic anions should always be considered. It probably plays an important role in the photolysis of $S_2O_3^{-2}$, N_3^{-},[27] and CNS^{-}.[28] The chemical effect of this self-scavenging should be considered in such cases.

(27) M. Smith and P. Kelly, *J. Chem. Soc.*, 1479, 1487 (1961).

(28) M. S. Matheson, W. A. Mulac, and J. Rabani, to be published

Calibration of High-Resistance Conductance Cells[1]

by James J. Zwolenik[2] and Raymond M. Fuoss

Contribution No. 1746 from the Sterling Chemistry Laboratory of Yale University, New Haven, Connecticut (Received November 13, 1963)

Constants Λ_0, J, and K_A in the conductance equation $\Lambda = \Lambda_0 - Sc^{1/2}\gamma^{1/2} + Ec\gamma \log c\gamma + Jc\gamma - K_Ac\gamma f^2\Lambda$ were determined for tetrabutylammonium tetraphenylboride in ethylene chloride at 25°. A convergent series of successive approximations then permits Λ to be calculated, given the concentration. It is shown that this system may be used as a secondary standard for determining constants for conductance cells in the range of 0.01 cm.$^{-1}$, with an accuracy of 0.1%. Data are also given for the same salt in o-dichlorobenzene in the range $0.24 \leq 10^{-4}c \leq 36$; these specific conductances, in the range $3\text{-}25 \times 10^{-6}$, are reproducible and stable, and may also be used for calibration.

For precision conductance work on dilute solutions in solvents of dielectric constant lower than about 15, cells with constants of the order of 0.01 or less must be used. These constants are too low to be determined by the use of aqueous potassium chloride solutions[3] and the cells must be calibrated by intercomparison. The purpose of this paper is to present data for a secondary standard, tetrabutylammonium tetraphenyl-boride in ethylene dichloride, which will permit direct calibration of such cells with an accuracy of about 0.1%.

The following method was used. A Jones–Bollinger[4] cell was calibrated using potassium chloride in water, then an Erlenmeyer cell[5] was calibrated against the Jones–Bollinger cell by comparison, and finally a Nichol–Fuoss[6] cell was calibrated by comparison against the Erlenmeyer cell. Then the conductance of tetrabutylammonium tetraphenylboride in ethylene chloride over the range $1–7 \times 10^{-4} N$ was determined in the Erlenmeyer cell. The data were analyzed to obtain the constants Λ_0, K_A, and J of the conductance equation[7]

$$\Lambda = \Lambda_0 - Sc^{1/2}\gamma^{1/2} + Ec\gamma \log c\gamma +$$
$$Jc\gamma - K_A c\gamma f^2 \Lambda \quad (1)$$

where the viscosity coefficient F has been absorbed in J and the $c^{3/2}$ term has been dropped. Activities are calculated[5] by the limiting law

$$-\ln f = \frac{\epsilon^2 \kappa}{2DkT} \quad (2)$$

Next a program (the Gamma program) was developed which solves eq. 1 for Λ, given c, Λ_0, J, and K_A; we are grateful to Dr. John E. Lind, Jr., and to Mr. James F. Skinner for their aid in the computer work. Finally, a series of the same solutions was measured in the N–F cell. From the known concentrations in this cell and the Gamma program, Λ was calculated; then the cell constant k_{N-F} was obtained from the definition

$$k_{N-F} = \frac{c\Lambda R_\infty}{1000} \quad (3)$$

where R_∞ is the cell resistance extrapolated to infinite frequency. By the comparison method, $k_{N-F} = 0.013382 \pm 6 \times 10^{-6}$; by the Gamma method, k_{N-F} was found to be $0.013400 \pm 7 \times 10^{-6}$. The constants of the equation are given by the coefficients in eq. 4

$$\Lambda = \gamma(49.77 - 428c^{1/2}\gamma^{1/2} +$$
$$4400c\gamma \ln c\gamma + 29{,}100c\gamma) \quad (4)$$

with $K_A = 950$.

Experimental

The conductance cells have already been described[4–6]; electrical equipment and general technique were as given by Lind and Fuoss.[5] Tetrabutylammonium tetraphenylboride[8] was recrystallized from 3:1 acetone–water (1 g. of salt/50 ml. of mixed solvent); m.p. 235°. Ethylene dichloride (Matheson Coleman and Bell 5636, b.p. 83–85°) was fractionated in the Todd still. The material collected after a 10% discarded forerun boiled sharply at 83.7° at a reflux ratio

of 5:1. Properties at 25° of the solvent are: density, 1.2460 g./ml.; dielectric constant, 10.35 at 300 kc.; and viscosity, 0.007834. A 0.02 N solution of tetrabutylammonium tetraphenylboride in ethylene chloride had a density of 1.2472; our solutions were so dilute that solvent density could be used to calculate volume concentrations from the experimental weight concentrations. The solvent conductance was less than 10^{-9} and completely negligible.

Some measurements were also made in o-dichlorobenzene. Solvent from Matheson Coleman and Bell (b.p. 179.5–180.5°) was redistilled at 11 mm. in the Todd still to b.p. 60.4°. Solvent properties are: density, 1.3010; dielectric constant, 10.07; viscosity,[9] 0.01324.

Results

Calibration[3] of the Jones–Bollinger cell was done using aqueous potassium chloride solutions in the range 0.00172219 to 0.00258738; the corresponding cell resistances (corrected for water conductance and extrapolated to infinite frequency on an $R - f^{-1/2}$ scale) were 976.31 to 654.93 ohms. Eleven determinations were made which gave $k_{J-B} = 0.24733 \pm 0.00005$ cm.$^{-1}$. Deviations $(\times 10^5)$ of the individual determinations from the average were $+10$, -6, $+2$, -6, $+2$, -6, $+2$, -1, -2, -2, and $+5$.

Tributylammonium picrate in isopropyl alcohol was used as the electrolyte for the calibrations by comparison. It was found that the resistance of these solutions drifted with time for several days after their preparation, but after a week or so, the resistance thenceforth remained constant (except for small systematic changes obviously due to evaporation of solvent). All comparisons were therefore made with aged solutions. For the comparison of the Jones–Bollinger cell and the Erlenmeyer cell, solutions of tributylammonium picrate in isopropyl alcohol ranging from 0.017 to 0.0043 N were used. The resistances in the J–B cell ranged from 4106.9 to 9678.4 ohms and in the Erlenmeyer cell from 643.52 to 1516.58 ohms. Twelve comparisons were made; the ratio R_E/R_{J-B} was found to be 0.15670 ± 0.00002. Deviations $(\times 10^5)$ of individual ratios were -0.8, $+0.1$, -3.0, -2.8,

(3) J. E. Lind, Jr., J. J. Zwolenik, and R. M. Fuoss, *J. Am. Chem. Soc.*, **81**, 1557 (1959).

(4) G. Jones and G. M. Bollinger, *ibid.*, **53**, 411 (1931).

(5) J. E. Lind, Jr., and R. M. Fuoss, *J. Phys. Chem.*, **65**, 999 (1961).

(6) J. C. Nichol and R. M. Fuoss, *ibid.*, **58**, 696 (1954).

(7) R. M. Fuoss, *J. Am. Chem. Soc.*, **81**, 2659 (1959).

(8) F. Accascina, S. Petrucci, and R. M. Fuoss, *ibid.*, **81**, 1301 (1959).

(9) V. Griffing, M. A. Cargle, L. Carvese, and D. Eby, *J. Phys. Chem.*, **58**, 1054 (1954).

$-0.1, +1.9, +1.9, +1.5, -2.9, +0.3, -1.4,$ and -0.3. The result is $k_E = 0.038757 \pm 5 \times 10^{-6}$. In a similar fashion, the ratio R_{N-F}/R_E was found to be 0.34527 ± 0.00003, (average over six determinations) whence $k_{N-F} = 0.013382 \pm 1 \times 10^{-6}$. Adding the uncertainty in each of the three operations which lead to the value of k_{N-F}, we estimate that the cell constant of the latter is determined to $\pm 0.05\%$ and therefore expect the accuracy to be no worse than 0.1%.

Table I gives the conductance data for tetrabutylammonium tetraphenylboride in ethylene dichloride at $25°$. It will be noted that no data for concentrations greater than 7×10^{-4} are included; here $\kappa a = 0.16$ for $a = 7 \times 10^{-8}$. At a dielectric constant this low, deviations from the functional form of eq. 1 appear rather sharply; values of Λ_0 which are obviously incorrect appear, along with negative values of K_A, when data points at too high concentration are included in the imput to the computer, or else the program refuses to converge.

Table I: Conductance of Tetrabutylammonium Tetraphenylboride in Ethylene Chloride (Superscripts Designate Series of Determinations)

10^4c	Λ	10^4c	Λ	10^4c	Λ
6.6871[a]	32.028	6.3100[d]	32.303	5.5112[h]	33.023
3.7982	35.374	4.5001	34.308	4.3004	34.493
2.8040	37.109	3.1206	36.441	3.0746	36.427
2.4102	37.936	1.5653	40.140	2.0774	38.576
2.0253	38.915	5.3960[e]	33.192	1.1629	41.467
6.9390[b]	31.658	4.4740	34.293	6.2937[i]	32.243
3.6711	35.439	3.2332	36.182	4.6250	34.058
2.5361	37.543	2.1926	38.336	3.1054	36.377
2.0815	38.597	1.2211	41.280	1.7916	39.368
1.7193	39.596	4.9014[f]	33.742	6.2371[j]	32.303
4.3380[c]	34.510	3.2412	36.151	4.5884	34.112
3.1097	36.434	1.5870	39.994	3.2562	36.100
2.2567	38.215	5.5593[g]	32.986	2.3601	37.906
1.4468	40.502	3.8818	35.094	1.1578	41.488
		2.9101	36.739		
		1.6093	39.904		

The data of Table I were analyzed by the IBM 709 computer in order to obtain the constants Λ_0, K_A, and J. The average values, with standard deviations, are: $\Lambda_0 = 49.77 \pm 0.10$, $J = 29{,}100 \pm 230$, and $K_A = 950 \pm 40$.

Given the values of the constants, we may now use eq. 1 and observed resistances at known concentrations in a given cell in order to obtain its constant. The problem: "given c, to find Λ" must be solved by successive approximations, because γ and f are related by the transcendental equation

$$-\ln f = \frac{\beta\kappa\gamma^{1/2}}{2} \tag{5}$$

while c, f, and γ are related by the mass action equation. The latter can be solved for γ in terms of the variable

$$m = 4K_A cf^2 \tag{6}$$

to give

$$\gamma = \frac{2[(1 + m)^{1/2} - 1]}{m} \tag{7}$$

so a value of f is needed to compute γ and vice versa. In order to break this cycle of interdependence, we set $f = 1$ as zeroth approximation in eq. 6, which then by eq. 7 gives an initial value γ_0. This is used in eq. 5 to get the first approximation to f, which is next fed back into eq. 6. The cycle is continued until $|\gamma_n - \gamma_{n-1}| < 5 \times 10^{-5}$. Then Λ is computed, using eq. 1 in the form

$$\Lambda = \gamma(\Lambda_0 - Sc^{1/2}\gamma^{1/2} + Ec\gamma \log c\gamma + Jc\gamma) \tag{8}$$

Table II shows the results of the determination of the cell constant of the N-F cell by this method. Six series (Table II) of determinations were made. Deviations from the average value of the data within a given series show no systematic pattern common to all series. The first column gives the known concentra-

Table II: Cell Constant (Superscripts Designate Series of Determinations)

10^4c	R	$100k_{N-F}$
2.8487[a]	1273.94	1.3408
2.1040	1650.32	1.3406
1.5397	2164.67	1.3398
3.5880[b]	1047.73	1.3391
2.4089	1468.46	1.3399
1.5408	2162.14	1.3391
5.9525[c]	688.81	1.3392
4.5505	859.58	1.3389
3.7638	1007.80	1.3406
2.6911	1335.98	1.3398
1.6730	2013.52	1.3403
5.9676[d]	688.34	1.3411
4.1132	935.69	1.3402
3.0423	1204.63	1.3403
1.9663	1749.41	1.3403
1.2257	2647.06	1.3389
4.1996[e]	919.50	1.3399
2.7103	1328.47	1.3403
1.9970	1726.69	1.3408
1.3006	2511.62	1.3392
6.0671[f]	678.90	1.3408
4.3702	889.28	1.3395
3.3649	1106.20	1.3397
2.1184	1640.58	1.3406

tion of salt, and the second the corrected cell resistance. The last column gives the individual values of the cell constants, which average to $0.013400 \pm 7 \times 10^{-6}$. The maximum deviation is 11×10^{-6}.

In our case, solvent conductance was negligibly small. The method may still be used if a correction, which is not negligible, must be considered. In this case, the observed cell resistance R_∞ measures the specific conductance σ_s of the salt plus the specific conductance σ_0 of the solvent; then

$$k/R_\infty = \sigma_s + \sigma_0 \tag{9}$$

From R_∞ and c, the computer calculates an apparent cell constant k'

$$k' = \sigma_s R_\infty \tag{10}$$

It is obvious that

$$k' = k - \sigma_0 R_\infty \tag{11}$$

A plot of the values of k' against cell resistance, extrapolated to zero resistance, then gives the true constant k.

In principle, the method can be extended to cells with constants still lower than 0.01, because the reliability of extrapolation by eq. 1 to lower concentrations (and hence higher cell resistances) has been established. Adsorption on the electrodes, however, begins to be noticeable below about 10^{-4} N, and precautions[10] to eliminate its effects must be taken. Briefly described, one prepares a small amount of solution of about the desired concentration in a Pyrex flask, uses it to rinse the walls of the flask, and discards it. This operation saturates the adsorption capacity of the glass walls. Then a large batch of solution is made in this flask; successive portions are added to the conductance cell, measured, and discarded, until the resistance for two successive fillings agrees to the desired precision, say 0.02%.

Table III: Conductance of Tetrabutylammonium Tetraphenylboride in o-Dichlorobenzene

$10^4 c$	Λ	$10^4 c$	Λ
0.24258	24.943	1.0447	19.141
0.41300	23.092	1.4977	17.532
0.69637	20.963	2.6767	14.983
2.2036	15.700	4.0439	13.252
3.3275	14.020	11.570	9.498
4.7726	12.604	16.596	8.459
7.089	11.152	23.530	7.561
11.330	9.607	36.411	6.593

The conductance of tetrabutylammonium tetraphenylboride in o-dichlorobenzene was measured in the N–F cell whose calibration has just been described. The data are summarized in Table III. Approximate values of the constants are $\Lambda_0 = 29.6$ and $K_A = 8300$; more data in the range below 10^{-4} N would be needed to permit a reliable extrapolation. This system is quite stable, and could also serve as a calibrating system, because in the range $0.0003 \leq c \leq 0.003$ it provides a reproducible set of specific conductances in the approximate range $4 \times 10^{-6} \leq \sigma \leq 20 \times 10^{-6}$. Since the equivalent conductance changes only slowly with concentration in this range, empirical interpolation from the values given in Table III is relatively easy and precise. The association constant K_A for tetrabutylammonium tetraphenylboride in o-dichlorobenzene is about one order of magnitude greater than in the isodielectric solvent ethylene dichloride. A similar difference was found[11] for tetrabutylammonium perchlorate in these two solvents; $K_A = 641$ in the latter and 9340 in the former.

(10) N. L. Cox, C. A. Kraus, and R. M. Fuoss, *Trans. Faraday Soc.*, **168**, 749 (1935).

(11) Y. H. Inami, H. K. Bodenseh, and J. B. Ramsey, *J. Am. Chem. Soc.*, **83**, 4745 (1961).

Electrolyte–Solvent Interaction.   XIV.   Triisopropanolamine

Borate with Triisoamylbutylammonium Salts[1]

by Thomas L. Fabry[2] and Raymond M. Fuoss

*Contribution No. 1749 from the Sterling Chemistry Laboratory of
Yale University, New Haven, Connecticut   (Received December 7, 1963)*

The conductance of solutions of triisoamylbutylammonium tetraphenylboride, picrate, and iodide was determined in mixtures of acetonitrile and triisopropanolamine borate in the dielectric range $36 < D < 61$. Initial addition of the highly polar borate (moment, 8.0 D. in dioxane) decreases conductance due to short-range ion–dipole interaction. The Walden product then goes through a minimum, conductance finally increasing with increasing D as the long-range relaxation effect predominates.

Electrostatic forces between the ions and the solvent dipoles of an electrolytic solution have two different effects on the conductance. First, the polarization and relaxation in the volume of the solvent as ions move through it decreases conductance by adding to the work required to move the ions. This effect[3-5] decreases with increasing dielectric constant; hence in mixtures of a polar and a nonpolar solvent, the limiting conductance increases with increasing content of polar component. This is a volume effect, in that it is produced by long-range interaction between a given ion and its entire dielectric environment. A second effect, which acts in the opposite direction, has also been observed.[6] Addition of p-nitroaniline to solutions of electrolytes in acetonitrile decreases conductance. Such a decrease would be expected if ion–dipole forces were so strong that ion–dipole pairs behaved like kinetic units in their motion in an electric field. This effect was observed when the p-nitroaniline concentration was in large excess over that of the electrolyte, but not high enough to increase the dielectric constant significantly. Solubility limited the concentration range which could be studied in the case of p-nitroaniline. Triisopropanolamine borate is highly polar and quite soluble in acetonitrile. We therefore investigated the conductance of several electrolytes in mixtures of the borate and acetonitrile in the range of high dielectric constants ($36 < D < 61$). The Walden product goes through a minimum, demonstrating the competition between the short-range and long-range effects of ion–dipole forces.

Experimental

Materials. Triisoamylbutylammonium iodide, picrate, and tetraphenylboride were prepared by Dr. M. A. Coplan.[7] Dioxane was purified according to Lind's procedure[8] (b.p. 101.3°, density 1.0280). Acetonitrile (Matheson) was refluxed over Drierite and then fractionated; solvent conductance, $\sigma_0 \approx 3 \times 10^{-8}$. The conductance increased on standing, so acetonitrile was always distilled just before use.

Triisopropanolamine borate (TPAB) as obtained from the U.S. Borax Research Corp. melted at 148–151°; literature values[9] are 153–156°. (The material is a mixture of optical isomers; the molecule contains three asymmetric carbon atoms.) The borate was recrystallized from benzene (150 g./400 ml. of hot benzene) in a drybox. On pumping, the large transparent crystals lost benzene of crystallization and became chalky white, m.p. 154–156°. TPAB can also be recrystallized from dioxane, but the product

(1) This paper is based on part of a thesis submitted by T. L. Fabry to the Graduate School of Yale University in September, 1963, in partial fulfillment of the requirements for the degree of Doctor of Philosophy.

(2) Du Pont Teaching Fellow, 1962–1963.

(3) R. M. Fuoss, *Proc. Natl. Acad. Sci. U. S.*, **45**, 807 (1959).

(4) R. H. Boyd, *J. Chem. Phys.*, **35**, 1281 (1961).

(5) R. Zwanzig, *ibid.*, **38**, 1603 (1963).

(6) A. D'Aprano and R. M. Fuoss, *J. Phys. Chem.*, **67**, 1722 (1963).

(7) M. A. Coplan, Thesis, Yale University, 1963.

(8) J. E. Lind, Jr., and R. M. Fuoss, *J. Phys. Chem.*, **65**, 999 (1961).

(9) H. Steinberg and D. L. Hunter, *Ind. Eng. Chem.*, **49**, 174 (1957); *J. Am. Chem. Soc.*, **82**, 853 (1960).

gradually turns yellow, possibly due to interaction with the peroxide which rapidly forms in dioxane exposed to air.[10]

In the borate $N(CH_2 \cdot CHCH_3 \cdot O)_3B$, which has a "tryptych boraxazolidine"[9] structure, there is a highly polar transannular $N:B$ bond. Pugh and Stokes[11] found for the moment, measured in benzene, $\mu = 6.69 \pm 0.04$ D. Triethanolamine borate, measured[12] in dioxane, gave $\mu = 8.8$ D. We measured dielectric constants, densities, and indices of refraction of solutions of TPAB in dioxane; the data are shown in Table I. Dielectric constants were measured at $25.00°$ and 1 Mc., using Lind's cell.[8] Refractive indices were measured at $25.0°$, using light from a sodium lamp and a Spencer refractometer. In Table I, f_2 is mole fraction of borate in the dioxane solution. The densities can be reproduced by the equation[13]

$$\rho/\rho_0 = 1 + (Mc/1000)(v_0 - v_s) \qquad (1)$$

where $v_s = 0.890$ for dioxane solutions and $v_s = 0.877$ for acetonitrile solutions of TPAB. We obtain $\mu = 8.00 \pm 0.04$ D., using Guggenheim's method[14] of treating the data. Interaction between dioxane and TPAB enhances the moment of the latter; other instances of higher moments being found in dioxane than in benzene have been reported.[15,16]

Table I: Properties of Tripropanolamine Borate in Dioxane

$10^3 f_2$	D	ρ	$n^{25}D$
0.00	2.207	1.02800	1.4203
7.01	2.72	1.02930	1.4208
8.61	2.86	1.02962	1.4210
11.32	3.11	1.03026	1.4216
13.97	3.35	1.03069	1.4218
15.20	3.49	. . .	. . .
17.87	3.78	. . .	. . .
20.30	4.05	1.03188	1.4219
23.76	4.48	. . .	. . .

Conductances of three electrolytes were measured in various mixtures of acetonitrile and TPAB: the properties of the mixtures are given in Table II where w is weight % TPAB in the mixture. Methods and equipment have been described[8] earlier. All solutions were made up on a weight basis, using the equation

$$c/m = \rho_0 + Am \qquad (2)$$

where

$$A = (\rho - \rho_0)/m - M\rho_0/1000 \qquad (3)$$

to relate molarity c and molality m, for a solution of

density ρ of a solute of molecular weight M in a solvent of density ρ_0. Table III summarizes the density data and the A-values for the systems studied. Composition of solvents is given by the code numbers of the first column of Table II. Precautions to exclude moisture were taken since TPAB is hygroscopic. All measurements were made at $25.00°$. The conductance data are summarized in Table IV.

Table II: Properties of Solvents

No.	w	ρ	100η	D
1	0.0	0.77681	0.335	36.01
2	10.71	.80460	.400	40.60
3	11.01	.80549	.403	40.67
4	20.63	.83166	.477	46.32
5	27.14	.85027	.548	51.30
6	33.58	.86954	.641	56.81
7	37.40	.88180	.719	61.24 .
8	45.77	. . .	. . .	72.95

Table III: Densities of Salt Solutions in Mixtures

No.	$10^3 m$	ρ	$-A$
		i-Am$_3$BuNI	
3	18.23	0.80731	0.232
5	19.42	.85235	.242
7	24.16	.88407	.228
		i-Am$_3$BuNPi	
2	9.57	0.80582	0.285
4	16.05	.83351	.311
6	20.96	.87161	.347
		i-Am$_3$BuNBPh$_4$	
3	13.12	0.80549	0.389
5	16.98	.85158	.436
7	20.80	.88321	.465

Discussion

Analysis of the data gave the constants Λ_0 and J of the equation

(10) R. MacFarland and R. M. Fuoss, J. Am. Chem. Soc., **77**, 2194 (1955).

(11) J. M. Pugh and R. H. Stokes, Australian J. Chem., **16**, 204 (1963).

(12) H-C. Fu, T. Psarras, H. Weidmann, and H. K. Zimmermann, Ann., **641**, 116 (1961).

(13) D. F-T. Tuan and R. M. Fuoss, J. Phys. Chem., **67**, 1343 (1963).

(14) E. A. Guggenheim, Trans. Faraday Soc., **47**, 573 (1951).

(15) C. Curran and G. K. Estok, J. Am. Chem. Soc., **72**, 4575 (1950).

(16) A. V. Few and J. W. Smith, J. Chem. Soc., **753**, 2663 (1949).

$$\Lambda = \Lambda_0 - Sc^{1/2} + E'c \ln c + Jc \qquad (4)$$

which describes conductance in solvents of high dielectric constant. Here the e^b term in the relaxation field,[17] which gives a cf^2 term in conductance, has been combined with the linear term by approximating the activity coefficient $f = e^{-r}$ by unity. The results are summarized in Table V. Values for acetonitrile (zero % TPAB) are included; these were determined by Coplan.[7]

Table IV: Conductance in Mixtures

i-Am₃BuNI		i-Am₃BuNPi		i-Am₃BuNBPh₄	
10^4c	Λ	10^4c	Λ	10^4c	Λ
$D = 40.67$		$D = 40.60$		$D = 40.67$	
9.462	126.67	5.972	108.73	10.633	89.44
17.811	123.80	10.590	106.83	19.833	87.07
25.818	121.67	16.377	104.97	28.946	85.25
35.040	119.63	24.411	103.07	40.292	83.51
45.423	117.71	29.393	101.89	51.415	82.09
$D = 51.30$		$D = 46.32$		$D = 51.30$	
17.722	91.88	15.768	88.54	22.826	63.13
34.343	89.35	30.147	86.03	35.196	61.73
50.472	87.49	51.651	83.35	52.504	60.21
66.25	85.94	64.922	82.11	66.945	59.16
85.26	84.38	79.174	80.83	84.944	58.05
$D = 61.24$		$D = 56.81$		$D = 61.24$	
21.348	71.15	33.30	65.31	24.70	48.31
41.948	69.23	66.09	62.70	45.82	46.82
62.524	67.80	98.65	60.86	68.99	45.57
83.39	66.58	125.03	59.59	93.01	44.53
103.15	65.53	147.49	58.60	116.19	43.68

Table V: Constants of Conductance Equation

D	Λ_0	J
	i-Am₃BuNI	
36.01	160.68 ± 0.00	1440 ± 2
40.67	135.04 ± 0.05	987 ± 15
51.30	98.81 ± 0.03	319 ± 6
61.24	76.18 ± 0.03	131 ± 4
	i-Am₃BuNPi	
36.01	135.70 ± 0.01	1550 ± 7
40.60	115.00 ± 0.07	1009 ± 35
46.32	96.06 ± 0.06	572 ± 11
56.81	72.33 ± 0.04	193 ± 4
	i-Am₃BuNBPh₄	
36.01	116.26 ± 0.02	1678 ± 12
40.67	97.10 ± 0.05	970 ± 14
51.30	69.90 ± 0.03	370 ± 6
61.24	53.08 ± 0.03	168 ± 4
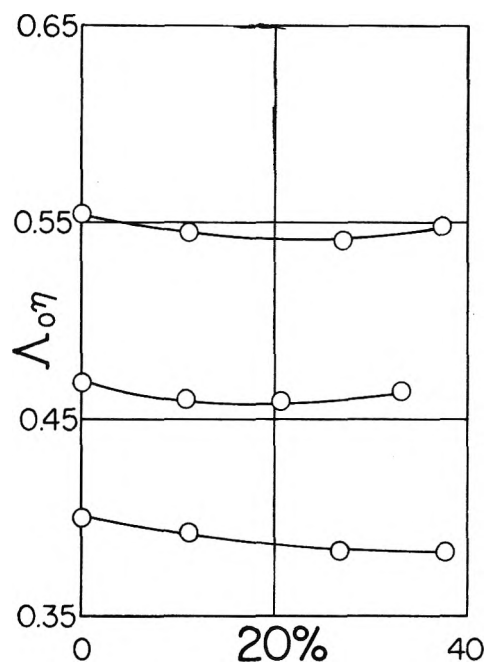
Figure 1. Dependence of Walden products $\Lambda_0\eta$ on solvent composition.

The effect of adding the highly polar amine borate is shown in Fig. 1, where the Walden products are plotted against composition of solvent. The product decreases initially for all three salts, showing that addition of TPAB decreases the mobility of the ions, just as was observed on the addition of p-nitroaniline.[6] As the content of borate is increased, however, the $\Lambda_0\eta$–w curve goes through a minimum and the Walden products increase in the range of higher dielectric constants. Two effects are clearly involved. As the dielectric constant increases, short-range ion–dipole interaction is decreased, and hence the initial decrease in mobility which was ascribed to dipole solvation disappears. Then the long-range relaxation effect[3] produced by the motion of ions in a polarizable dielectric takes control, and the Walden product increases with increasing dielectric constant as expected from the relation

$$\Lambda_0\eta = (\mathfrak{F}\epsilon/1800\pi)\Sigma_{i=1,2}R_i^{-1}(1 + A_i/DR_i^2)^{-1} \qquad (5)$$

where R_1 is the hydrodynamic radius of the cation and R_2 that of the anion. As D increases, the denominators in (5) decrease, and hence the sum of the two terms increases.

The shift of the minima in Fig. 1 toward higher dielectric of the anion is as expected. The small ions have large slopes on an R–D^{-1} plot[3] in aprotonic sol-

---

(17) R. M. Fuoss and L. Onsager, *J. Phys. Chem.*, **67**, 621 (1963).
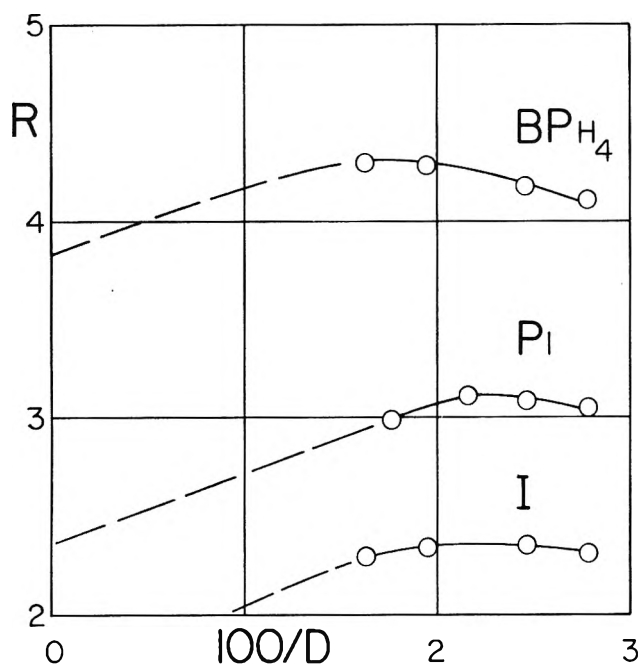
Figure 2. Dependence of Stokes radii on dielectric constant.

vents and therefore the long-range relaxation effect will dominate the short-range solvation at a lower value of dielectric constant. As seen in Fig. 1, the minimum comes at about 20% borate for the iodide (top curve), and appears around 40% for the tetraphenylboride, with the picrate intermediate.

It has been shown[7] that the single ion conductances of the two ions i-Am$_3$BuN$^+$ and BPh$_4'$ are equal within 1% in methanol. If we assume them equal in the present mixtures, then halving the limiting conductance of i-Am$_3$BuNBPh$_4$ gives $\lambda_0(BPh_4')$ = $\lambda_0(Bu_4N^+)$ = $\Lambda_0/2$ as a function of composition, and then the single ion conductances of the iodide and picrate in the mixtures become known. From these, the Stokes radii of the anions can be calculated from the equation

$$R_s{}^{\pm} = 0.8194 \times 10^{-8}/\lambda_0{}^{\pm}\eta \qquad (6)$$

Their dependence on dielectric constant is shown in Fig. 2; in our range of dielectric constants (36 < D < 61), R goes through a maximum. The dashed extrapolations to $D = \infty$ are drawn to terminate at the values of R_∞ found for the anions in nitrobenzene–carbon tetrachloride mixtures.[18,19] It is evident that the sphere-in-continuum model fails completely to describe these systems hydrodynamically; on the other hand, the variation of the Stokes radius with composition of the solvent can be rationalized if both short- and long-range effects of ion–dipole forces are considered.

(18) R. M. Fuoss and E. Hirsch. *J. Am. Chem. Soc.*, **82**, 1013 (1960).
(19) E. Hirsch and R. M. Fuoss, *ibid.*, **82**, 1018 (1960).

Osmotic and Activity Coefficients for the Symmetrical Tetraalkyl

Ammonium Halides in Aqueous Solution at 25°[1]

by S. Lindenbaum and G. E. Boyd

Chemistry Division, Oak Ridge National Laboratory, Oak Ridge, Tennessee   (*Received November 26, 1963*)

The symmetrical tetraalkyl ammonium halides have been employed in a study of the effect of cation size on electrolyte behavior in aqueous solution. Osmotic and activity coefficients were measured by the gravimetric isopiestic vapor pressure technique for tetramethyl-, tetraethyl-, tetrapropyl-, and tetrabutylammonium chlorides, bromides, and iodides. For concentrations below 1 m, the osmotic coefficients for the chlorides increased with the size of the cation: $Bu_4N^+ > Pr_4N^+ > Et_4N^+ > Me_4N^+$. The bromides and iodides, however, showed the reverse order. At higher concentrations, the osmotic coefficients of the larger cation salts decreased sharply and some of the sequences were reversed. The dependence of the osmotic and activity coefficients on cation size and concentration is explained as the result of three effects. The order for the chlorides in dilute solution is due to the ability of large organic cations to enforce the water structure, and the more carbon atoms on an ion, the larger this effect will be. However, with the bromides and iodides, "water structure-enforced ion pairing" overshadows the "structure making" ability of the cations, causing an opposite order in the osmotic coefficients. At higher concentrations the tetrabutyl salts form micelles, and hence a sharp lowering of the osmotic coefficient is observed.

Introduction

The symmetrical tetraalkyl ammonium halides form a useful homologous series for the study of the effect of cation size on the equilibrium and transport properties of aqueous electrolyte solutions. Measurements of the osmotic coefficients of dilute solutions on some of these salts at the freezing point were first reported by Ebert and Lange[2] in 1928 and by Lange[3] in 1934. The osmotic coefficients of the chloride salts showed a behavior characteristic of strong 1–1 electrolytes. The values for the iodides, however, fell below the limiting law prediction, suggesting that strong ion association occurred even in dilute solution.

Interest has been stimulated recently by the paper of Devanathan and Fernando[4] which reports activity coefficient values for tetraalkyl ammonium iodides derived from measurements of cells with liquid junctions. Extremely high coefficients (*e.g.*, $f_{R_4NI} = 13.5$ for 1 N Et_4NI) were found. Stokes[5] has suggested that these results are unreasonable and in disagreement with those of Lange. Soon afterward, however,

a paper by Frank[6] appeared in which the cell measurements are reported to have been confirmed, but they are interpreted to yield the ratio of iodide single ion activity coefficients between R_4NI and KI in aqueous solutions.

Very recently, Bower and Robinson[7] have published activity coefficients for tetraethylammonium iodide solutions at 25° which were derived from measurements employing the isopiestic vapor pressure comparison technique. Values for the osmotic and activity coefficients in good agreement with the freezing point data

(1) Presented before the Division of Colloid Chemistry, 145th National Meeting, American Chemical Society, New York, N. Y., September 8–13, 1963; see Abstract 17, p. 71.

(2) L. Ebert and J. Lange. *Z. physik. Chem.*, **139A**, 584 (1928).

(3) J. Lange, *ibid.*, **168A**, 147 (1934).

(4) M. A. V. Devanathan and M. J. Fernando, *Trans. Faraday Soc.*, **58**, 784 (1962).

(5) R. H. Stokes, *ibid.*, **59**, 761 (1963).

(6) H. S. Frank, *J. Phys. Chem.*, **67**, 1554 (1963).

(7) V. E. Bower and R. A. Robinson, *Trans. Faraday Soc.*, **59**, 1717 (1963).

Table I: Molalities of Isopiestic Solutions

Salt[a]	$(CH_3)_4NCl$	$(C_2H_5)_4NCl$	$(C_3H_7)_4NCl$	$(C_4H_9)_4NCl$	$(CH_3)_4NBr$	$(C_2H_5)_4NBr$	$(C_3H_7)_4NBr$	$(C_4H_9)_4NBr$
0.2350	0.2446				0.2498			
0.2470	0.2556				0.2645			
0.4523		0.4780	0.4715	0.4625		0.5270	0.5404	0.5504
0.4709		0.4983	0.4911	0.4810		0.5516	0.5646	0.5759
0.5042	0.5377				0.5683			
0.5059	0.5379				0.5684			
0.7183		0.7674	0.7421					
0.7197		0.7668	0.7421	0.7251		0.8775	0.8869	0.9245
1.018	1.107				1.219			
1.039	1.125				1.243			
1.050		1.116	1.005	1.040		1.320	1.298	1.446
1.092		1.162	1.091	1.077		1.376	1.344	1.517
1.105		1.167						
1.274	1.390				1.541			
1.343		1.424	1.317	1.319		1.720	1.646	2.008
1.348	1.455				1.630			
1.516		1.597	1.459	1.487		1.945	1.836	2.381
1.668	1.800				2.049			
2.201		2.269	2.010	2.238		2.818	2.585	4.306
2.255		2.311	2.045	2.296		2.875	2.633	4.397
2.358	2.544				2.972			
2.530	2.724				3.201			
2.641	2.842				3.353			
2.867		2.864	2.491	3.074		3.588	3.265	6.258
2.924		2.924	2.533	3.154		3.654	3.324	6.454
3.128	3.363				4.014			
4.174		4.001	3.483	5.143		5.062	4.753	9.417
4.227		4.042	3.529	5.238		5.111	4.834	9.893
6.135		5.605	5.119	8.355		7.140	7.464	14.36
6.138		5.613	5.121	8.341		7.148	7.454	14.37
A					2.694			
B					3.498			
C	4.562				5.585			
D	5.392							
E	6.788	5.601	5.136	8.386		7.172	7.465	14.25
F		5.681	5.226	8.519		7.272	7.597	14.53
G		6.335	6.008	9.77		8.145	8.964	16.29
H	9.955	7.911	8.138	12.70		10.31		21.02
I		9.471	10.55	15.61		12.65		26.39
J	14.594	13.29						
K	14.853	13.57						
L	19.060	18.66						

[a] Pertinent data are given for salts (A–L) other than NaCl. A: satd. KNO_3, a_w = 0.9248; B: satd. $BaCl_2 \cdot 2H_2O$, a_w = 0.9019; C: satd. KCl, a_w = 0.8426; D: satd. KBr, a_w = 0.8071; E: satd. NaCl, a_w = 0.7528; F: 4.4182 m H_2SO_4, a_w = 0.7484; G: satd. $SrCl_2 \cdot 6H_2O$, a_w = 0.7083; H: satd. NH_4NO_3, a_w = 0.618; I: satd. $Mg(NO_3)_2 \cdot 6H_2O$, a_w = 0.5286; J: 8.526 m H_2SO_4, a_w = 0.4472; K: 8.647 m H_2SO_4, a_w = 0.4397; L: satd. $MgCl_2 \cdot 6H_2O$, a_w = 0.3300.

of Lange[3] were found, considering the temperature difference between the two sets of measurements. Bower and Robinson also were able to reproduce the very high potentials for the cells used by Devanathan and Fernando,[4] but they suggest that the interpretation of the cell reaction by the latter was incorrect.

Experimental

Materials. The tetraalkyl ammonium halides employed in this research were obtained from Matheson Coleman and Bell, East Rutherford, N. J.; Eastman Organic Chemicals, Rochester, N. Y.; and K & K Laboratories, Jamaica, N. Y. In those cases for which only the iodide salt was available, the chloride and bromide salts were prepared as follows. A solution of the iodide salt in methanol was treated with excess silver hydroxide and filtered. The filtrate was neutralized with HCl or HBr, the solvent was boiled off, and the salt dried *in vacuo*. All salts were recrystallized

from suitable solvents following the work of Kraus and others[8-16]; their purity, which was confirmed by halide analyses, showed that all salts were at least 99.4% pure.

Isopiestic Vapor Pressure Comparisons. Osmotic coefficients were determined by the gravimetric isopiestic vapor pressure method of Robinson and Sinclair.[17-19] A special apparatus was constructed from a "low" form Pyrex vacuum desiccator which was equipped with a mechanism for the remote closure of the sample dishes. The dishes were made of silver and were gold-plated. They rested in depressions in a gold-plated copper block. The gold plating was essential because some of the solutions measured were severely corrosive to silver.

Duplicate samples of the dry salts were weighed into the tared dishes and dissolved in a minimum of added water. Two dishes contained sodium chloride reference solutions; at the lower water activities where these were saturated, sulfuric acid was used. In a depression in the center of the copper block was a large gold-plated silver dish which contained either a saturated solution of known vapor pressure[18] or, at the higher water activities, a solution of sodium chloride.

The entire unit was immersed in a 625-l. constant-temperature water bath held at 25.000 ± 0.005° and evacuated with an aspirator. The unit was rocked gently while being evacuated and during the entire vapor equilibration period. The dishes were always covered before admitting air into the unit and removing it from the bath. Changes in the composition of the solutions thereby were avoided during the time required for removing the unit from the bath and weighing the sample dishes. The dishes were weighed at intervals varying from 3 days to 2 weeks (depending on the time found necessary to reach equilibrium). Equilibrium was assumed to have been attained if the solutions in duplicate dishes arrived at the same molality (within 0.5%) and if the molalities of the two reference solutions agreed with the water activity of the saturated solution in the large center dish. Equilibrium was approached alternately from higher and lower water activities. The equilibrium isopiestic molalities obtained are given in Tables I and II. Measurements were carried out to the solubility limit of each salt; the highest values of the molalities listed in each case are therefore approximate measures of the solubilities.

Results and Discussion

Osmotic coefficients were evaluated from the equation

$$\nu m \phi = \nu_r m_r \phi_r \qquad (1)$$

where ν is the number of ions ($= 2$), m is the molality of

quaternary ammonium salt, ϕ is the osmotic coefficient (molal scale) of the quaternary ammonium salt, m_r is the molality of the reference electrolyte (NaCl), and ϕ_r is the osmotic coefficient of the reference electrolyte.

The required ϕ_r-values were interpolated from the tables of Robinson and Stokes.[19] For water activities lower than that of saturated NaCl, eq. 2 was used

$$\nu m \phi = -55.51 \ln a_w \qquad (2)$$

Table II: Molalities of Isopiestic Solutions

NaCl	$(CH_3)_4NI$	$(C_2H_5)_4NI$	$(C_3H_7)_4NI$
0.0688	0.0722	0.0742	. . .
.0748		.0807	0.0830
.1093		.1204	.1235
.1187	.1262	.1308	
.1393	.1498	.1565	
.1549		.1766	.1884
.1603		.1832	.1941
.1701	.1854	.1946	.2090
.1978	.2168	.2301	.2495
.2092	.2314	.2467	.2706
.2605		.3166	.3577
.2621		.3214	.3653
.2913		.3638	.4183
.3307		.4222	.5075
.4230		.5735	
.5297		.7695	
.8433		1.440	
1.041		1.910	
1.048		1.927	

Tables of a_w (water activity at 25°) for various saturated aqueous solutions are available in the literature.[18,19] Mean molal activity coefficients, γ, were calculated from the osmotic coefficients with the Gibbs–Duhem equation (eq. 3).

(8) L. M. Tucker and C. A. Kraus. *J. Am. Chem. Soc.*, 69, 454 (1947).

(9) W. E. Thompson and C. A. Kraus, *ibid.*, 69, 1016 (1947).

(10) E. G. Taylor and C. A. Kraus, *ibid.*, 69, 1731 (1947).

(11) C. R. Witschonke and C. A. Kraus, *ibid.*, 69, 2472 (1947).

(12) W. F. Luder and C. A. Kraus, *ibid.*, 69, 2481 (1947).

(13) M. B. Reynolds and C. A. Kraus. *ibid.*, 70, 1709 (1948).

(14) A. K. R. Unni, L. Elias, and H. I. Schiff, *J. Phys. Chem.*, 67, 1216 (1963).

(15) S. C. Blum and H. I. Schiff, *ibid.*, 67, 1220 (1963).

(16) R. L. Kay, S. C. Blum, and H. I. Schiff, *ibid.*, 67, 1223 (1963).

(17) R. A. Robinson and D. A. Sinclair. *J. Am. Chem. Soc.*, 56, 1830 (1934).

(18) R. H. Stokes and R. A. Robinson. *Ind. Eng. Chem.*, 41, 2013 (1949).

(19) R. A. Robinson and R. H. Stokes, "Electrolyte Solutions," 2nd Ed., Academic Press, New York, N. Y., 1959.

Table III: Osmotic and Activity Coefficients of Tetraalkyl Ammonium Chlorides

m	(CH₃)₄NCl φ	(CH₃)₄NCl γ	(C₂H₅)₄NCl φ	(C₂H₅)₄NCl γ	(C₃H₇)₄NCl φ	(C₃H₇)₄NCl γ	(C₄H₉)₄NCl φ	(C₄H₉)₄NCl γ
0.1	0.914	0.746	0.913	0.750	0.917	0.753	0.918	0.752
0.2	.892	.683	.901	.688	.896	.694	.904	.701
0.3	.880	.644	.880	.647	.886	.655	.898	.670
0.4	.872	.617	.874	.620	.882	.633	.899	.650
0.5	.867	.597	.870	.600	.883	.615	.902	.637
0.6	.863	.580	.868	.586	.887	.604	.907	.629
0.7	.861	.566	.868	.574	.894	.598	.914	.626
0.8	.860	.556	.870	.565	.902	.595	.922	.625
0.9	.860	.546	.872	.557	.913	.596	.932	.625
1.0	.862	.539	.875	.554	.926	.598	.943	.627
1.2	.865	.527	.891	.549	.954	.610	.963	.629
1.4	.871	.520	.907	.548	.986	.627	.975	.638
1.6	.879	.516	.922	.549	1.023	.648	.978	.639
1.8	.888	.514	.937	.551	1.059	.673	.980	.640
2.0	.898	.514	.951	.554	1.095	.702	.982	.640
2.5	.926	.516	.993	.568	1.181	.797	.980	.636
3.0	.957	.525	1.047	.600	1.264	.918	.972	.627
3.5	.989	.542	1.108	.650	1.346	1.043	.957	.614
4.0	1.023	.564	1.172	.710	1.426	1.171	.936	.597
4.5	1.054	.588	1.239	.777	1.489	1.303	.920	.583
5.0	1.084	.610	1.308	.865	1.533	1.435	.913	.574
5.5	1.112	.632	1.379	.966	1.567	1.569	.910	.568
6.0	1.138	.654	1.453	1.073	1.593	1.703	.911	.564
7.0	1.190	.705	1.596	1.410	1.631	1.950	.920	.562
8.0	1.238	.762	1.722	1.742	1.653	2.170	.932	.564
9.0	1.280	.822	1.818	1.985	1.666	2.373	.958	.574
10.0	1.321	.885			1.673	2.564	.985	.587
11.0	1.361	.952			1.676	2.747	1.013	.603
12.0	1.400	1.022			1.679	2.923	1.042	.621
13.0	1.435	1.094			1.680	3.100	1.068	.644
14.0	1.469	1.170			1.678	3.253	1.096	.667
15.0	1.501	1.250			1.674	3.391	1.123	.688
16.0	1.532	1.332			1.668	3.518		
17.0	1.562	1.418			1.661	3.633		
18.0	1.591	1.506			1.654	3.745		
19.0	1.617	1.596						

$$-\ln \gamma = 1 - \phi + 2 \int_0^{\sqrt{m}} [(1 - \phi)/\sqrt{m}] \, d\sqrt{m}$$

$$(3)$$

The integral in the right-hand member of eq. 3 was evaluated graphically. Graphs of the osmotic and activity coefficients were drawn from the experimental data in Tables I and II, and these were employed to prepare Tables III, IV, and V.

Computer methods[20] were not used to calculate the osmotic and activity coefficients from the isopiestic molalities, because no single expression would adequately fit the widely divergent behavior exhibited by the series of salts studied.

The calculation of the activity coefficients with eq. 3 involves an extrapolation to infinite dilution. Since the nature of this extrapolation is not known exactly,

the γ-values reported may be subject to a small constant correction (applied to log γ) when data on more dilute solutions become available. The error introduced by this uncertainty, however, is not expected to be greater than 0.010 in the activity coefficient. The activity coefficients for tetraethylammonium iodide (Table V) are in good agreement with those reported by Bower and Robinson. The concentration dependence of the activity coefficients is shown in Fig. 1 for the chloride and bromide salts. The osmotic coefficients of the iodide salts are compared with those of Ebert and Lange and Bower and Robinson in Fig. 2.

In the dilute solutions the coefficients for the chlorides increase with cation size, while for the bromides

(20) M. H. Lietzke and R. W. Stoughton. *J. Phys. Chem.*, **66**, 508 (1962).

Table IV: Osmotic and Activity Coefficients of Tetraalkyl Ammonium Bromides

m	(CH₃)₄NBr φ	(CH₃)₄NBr γ	(C₂H₅)₄NBr φ	(C₂H₅)₄NBr γ	(C₃H₇)₄NBr φ	(C₃H₇)₄NBr γ	(C₄H₉)₄NBr φ	(C₄H₉)₄NBr γ
0.1	0.910	0.746	0.892	0.716	0.886	0.708	0.889	0.714
0.2	.879	.672	.855	.631	.842	.620	.843	.620
0.3	.857	.624	.828	.575	.813	.560	.808	.558
0.4	.840	.587	.807	.536	.791	.517	.782	.513
0.5	.826	.558	.793	.505	.776	.486	.763	.478
0.6	.815	.533	.781	.479	.765	.461	.751	.452
0.7	.806	.513	.772	.458	.757	.441	.743	.431
0.8	.799	.497	.764	.441	.752	.424	.734	.413
0.9	.794	.483	.758	.427	.749	.411	.726	.397
1.0	.790	.471	.753	.414	.749	.400	.718	.384
1.2	.786	.450	.748	.393	.754	.383	.702	.357
1.4	.784	.435	.746	.377	.763	.373	.686	.335
1.6	.785	.423	.746	.364	.775	.366	.671	.316
1.8	.787	.413	.748	.354	.789	.362	.655	.299
2.0	.789	.406	.751	.346	.805	.360	.640	.284
2.5	.796	.391	.764	.335	.843	.360	.602	.251
3.0	.803	.381	.786	.331	.881	.366	.570	.226
3.5	.811	.372	.818	.330	.917	.373	.541	.205
4.0	.820	.365	.856	.332	.952	.382	.520	.188
4.5	.831	.360	.898	.338	.984	.393	.504	.177
5.0	.840	.354	.938	.348	1.010	.403	.492	.166
5.5	.842	.349	.976	.362	1.026	.410	.482	.156
6.0			1.014	.377	1.038	.416	.476	.148
7.0			1.087	.411	1.052	.425	.473	.134
8.0			1.159	.449	1.062	.432	.476	.125
9.0			1.225	.490	1.069	.439	.484	.120
10.0			1.284	.534			.499	.116
11.0			1.334	.576			.514	.112
12.0			1.375	.619			.528	.109
13.0							.541	.106
14.0							.552	.104
15.0							.563	.102
17.0							.584	.098
19.0							.608	.096
21.0							.630	.095
23.0							.650	.094
25.0							.665	.093
27.0							.672	.091

a decrease with increasing size occurs. At higher concentrations the order for the chlorides remains the same except for tetrabutylammonium chloride, for which the activity coefficient curve rises to a maximum and crosses all the others. No discernible pattern appears to exist for the bromide curve crossovers. The iodide osmotic coefficients, Fig. 2, are in the same sequence as the bromides in dilute solution, and this order is maintained throughout the concentration range

The behavior of the chlorides in dilute solution is readily understood in terms of theories of the effect of large unhydrated ions on water structure. The decrease in entropy on dissolving a hydrocarbon in water has been interpreted by Frank and Evans[21] as indicating a tightening of the water structure around the

molecule. By analogy it is to be expected that the large, nonpolar quaternary ammonium ions will enforce the structure of water around themselves. The more carbon atoms surrounding the nitrogen, the more hydrophobic these ions will be, the more the water structure will be enforced, and the greater the free energy of the ion. Therefore, the larger the cation the larger the activity coefficient, and this is observed with the chlorides in dilute solution.[22] The order of the iodide salts is the opposite and, therefore, some other

(21) H. S. Frank and M. W. Evans, J. Chem. Phys., 13, 507 (1945).

(22) An analogous regularity may be observed in the osmotic and activity coefficients for the sodium salts of the fatty acids; see E. R. B. Smith and R. A. Robinson, Trans. Faraday Soc., 38, 70 (1942).
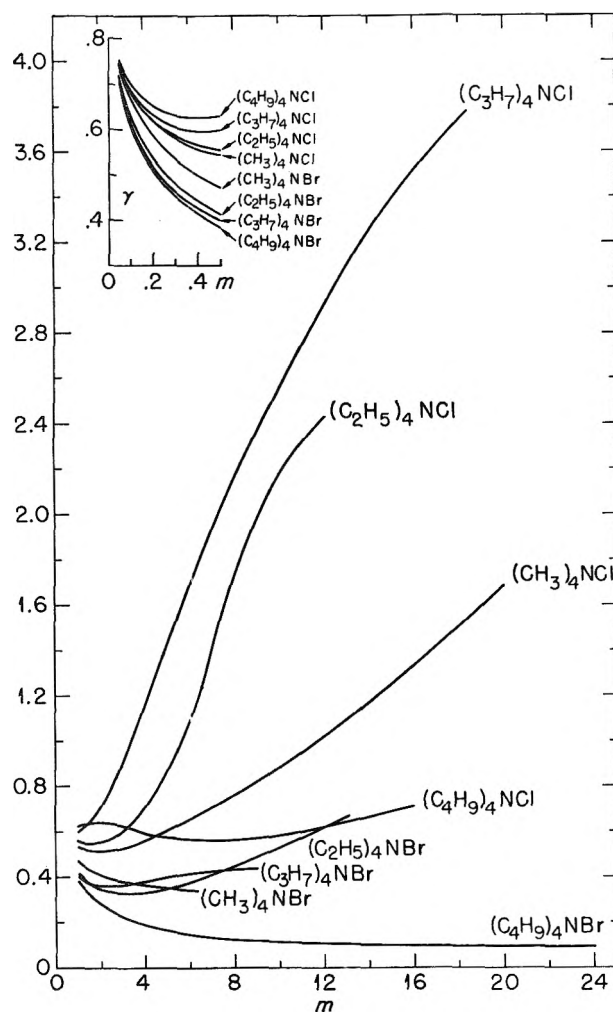
Figure 1. Activity coefficients of tetraalkyl
ammonium chlorides and bromides.

Table V: Osmotic and Activity Coefficients
of Tetraalkyl Ammonium Iodides

m	$(CH_3)_4NI$ ϕ	$(CH_3)_4NI$ γ	$(C_2H_5)_4NI$ ϕ	$(C_2H_5)_4NI$ γ	$(C_3H_7)_4NI$ ϕ	$(C_3H_7)_4NI$ γ
0.10	0.885	0.708	0.855	0.683	0.830	0.634
.15	.866	.668	.831	.616	.794	.572
.20	.846	.630	.806	.568	.759	.519
.25	.828	.590	.783	.528	.727	.476
.30			.762	.496	.696	.438
.35			.743	.468	.669	.406
.40			.726	.445	.644	.378
.45			.710	.424	.622	.354
.50			.696	.406	.603	.332
.6			.670	.374		
.7			.648	.346		
.8			.630	.324		
.9			.615	.306		
1.0			.601	.290		
1.2			.574	.263		
1.4			.549	.239		
1.6			.528	.221		
1.8			.514	.206		
1.9			.510	.199		
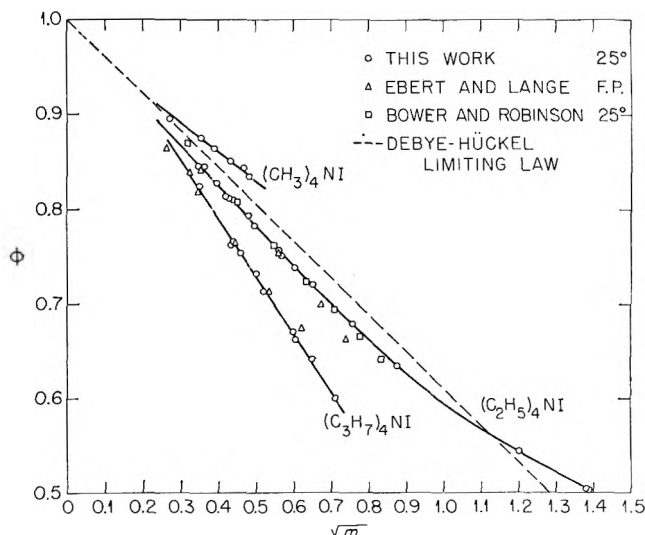
Figure 2. Osmotic coefficients of tetraalkyl
ammonium iodides.

effect must predominate. Diamond[23] recently has
suggested an explanation very similar to the phenomenon
of *hydrophobic bonding* which has been treated by
Némethy and Scheraga.[24] This type of bond may be
defined as one which forms ". . .when two or more non-
polar groups come into contact, thereby decreasing the
extent of the interaction with the surrounding water."
Thus, it has been proposed that large, hydrophobic
cations and anions will tend to combine with each other
to minimize their interaction with the surrounding
water as well as to decrease the electrostatic free
energy of the system. This process has been described
as "water structure-enforced ion pairing," and it will
occur to a greater extent the larger the cation. Also,
the iodide salts would be expected to associate in this
manner more readily than the chlorides and bromides.
The formation of such ion pairs will, of course, lead to a

drastic lowering of the activity coefficients, and this is
observed with the iodide salts. The bromides at low
concentrations show the same behavior as the iodides,
suggesting that ion pairing occurs. At higher concen-
trations the bromide curves cross each other, suggesting
a behavior intermediate between that of chloride and

(23) R. M. Diamond, *J. Phys. Chem.*, **67**, 2513 (1963).

(24) G. Némethy and H. A. Scheraga, *J. Chem. Phys.*, **36**, 3382,
3041 (1962); *J. Phys. Chem.*, **66**, 1773 (1962).

iodide. The formation of "water structure-enforced ion pairs" is probably prevented in the case of the chlorides by the hydration of the chloride ion.

Structure-enforced ion pairing is only possible in a strongly structured solvent such as water. Kraus and co-workers have shown by conductivity measurements that in solvents such as ethylene chloride,[8,9] nitrobenzene,[10,11] pyridine,[12] and acetone,[13] the association constants for the tetraalkyl ammonium halides decrease with increasing cation size and the chloride salts are more associated than the bromides and iodides. Similar results have been reported recently by Schiff and co-workers[14-16] for conductivity and transference measurements in nitromethane. This is the expected order for electrostatic ion pairing, and the opposite of the order observed by us in aqueous solution.

Activity coefficients of the tetraalkyl ammonium methane- and ethanesulfonates in aqueous solution have been published recently.[25] In these measurements it was also found that the curve for the tetrabutyl salt passed through a maximum and crossed all other curves. The authors have suggested that the explanation for this phenomenon is that the tetrabutylammonium ions aggregate to form micelles.

The critical micelle concentration (c.m.c.) of tetrabutylammonium methanesulfonate was estimated with the dye solubilization technique and a value of 0.03 M was obtained. We have made c.m.c. measurements on solutions of tetrabutylammonium bromide using the spectral change method[26] with the dye 2,6-dichloroindophenol, and a value of 0.039 M was obtained. Smith and Robinson[22] have suggested that micelle formation was responsible for the crossovers they found in the osmotic coefficients of the sodium salts of the n-fatty acids. Light scattering measurements were later reported by Debye[27] on the potassium salts, and the presence of micelles was verified. An important factor in the association of the tetraalkyl ammonium cations doubtless is the lowering of energy accompanying the reduction of the hydrocarbon–water interface on micelle formation. The nature of these micelles and a direct proof of the existence of structure-enforced ion pairs in solution remain as problems for the future.

(25) H. C. Gregor, M. Rothenberg, and N. Fine. J. Phys. Chem. 67, 1110 (1963).

(26) M. L. Corrin and W. D. Harkins, J. Am. Chem. Soc., 69, 679 (1947).

(27) P. Debye, J. Phys. Colloid Chem., 53, 1 (1949).

Self-Exchange Measurements in a Chelating Ion-Exchange Resin[1]

by A. Schwarz,[2] J. A. Marinsky, and K. S. Spiegler

Department of Chemistry, State University of New York at Buffalo, Buffalo 14, New York
(Received August 2, 1963)

Self-exchange measurements using Na^{22}, Co^{60}, and Zn^{65} were made with Dowex A-1 chelating resin, a polystyrene–divinylbenzene copolymer containing the iminodiacetic acid functional group attached to the hydrocarbon matrix. The experimental results indicate that a particle diffusion mechanism is the rate-controlling step in the self-exchange process.

Introduction

The preparation of an ion-exchange resin with iminodiacetic acid functional groups to provide chelating properties was reported by Morris, *et al.*[3] Their objective was to produce a resin with sufficient cation specificity to improve chromatographic separations. Such specificity was indeed exhibited by their product.[4,5] Its rate of exchange, however, was shown to be somewhat slow, leading to diffuse elution bands[5,6] and the exchange involving one or two strongly chelated cations was reported to be controlled by a second-order chemical reaction.[6] This result was unexpected since it was the first observation of a chemically controlled process in an ion-exchange reaction.[7] Self-exchange experiments similar to those performed by Boyd and Soldano[8] with Dowex 50 were initiated[9] to reduce the complexity of the system. In that study it was shown that if the isotopic exchange is controlled by chemical reaction, a three-parameter equation is needed to describe the rate curves.

In this investigation, we have made additional self-exchange studies of Na^+ and the strongly chelated ions Zn^{2+} and Co^{2+} in unbuffered systems and have found that the rate of the self-exchange is diffusion- rather than chemically controlled.

Experimental

Materials. Dowex Chelating Resin A-1, a product of the Dow Chemical Co., Midland, Mich., was employed in the experimental program. Two different resin preparations were used. The isotopic exchange experiments with sodium were performed at the Technion-Israel Institute of Technology, with one resin sample source, while the experiments with cobalt and

zinc were performed at the State University of New York at Buffalo with the second resin sample source.

The nuclides, 5.27-year Co^{60} and 250-day Zn^{65}, were received from the Radioisotopes Division of the Oak Ridge National Laboratory. Carrier-free 2.6-year Na^{22} was obtained from The Radiochemical Centre, Amersham, England. Reagent grade chemicals were used throughout the program.

Resin Preparation. The resin was cycled repeatedly with 2 *M* HCl and 2 *M* NaOH. After the sixth conversion to the hydrogen form, the resin was washed with distilled water until the effluent gave a negative test for chloride ion. The resin was then dried at room temperature over P_2O_5. The dry resin, after separation into four size fractions, 40/60, 60/80, 80/100, and 100/120 mesh (U. S.), was stored over P_2O_5 at the ambient temperature.

Preparation for a self-exchange experiment consisted of converting 1.0 g. of the dry resin (2.70 mmoles of iminodiacetic acid) to the sodium form with con-

(1) Dowex Chelating Resin A-1, a product of the Dow Chemical Co., Midland, Mich.

(2) Postdoctoral Research Fellow, 1962-1963; address correspondence to Oak Ridge National Laboratory, Oak Ridge, Tenn.

(3) L. R. Morris, R. A. Mock, C. A. Marshall, and J. H. Howe, *J. Am. Chem. Soc.*, **81**, 377 (1959).

(4) R. Turse and W. Rieman, III, *Anal. Chim. Acta*, **24**, 202 (1961).

(5) R. Christell, S. Forberg, and T. Westermark, *J. Inorg. Nucl. Chem.*, **19**, 187 (1961).

(6) R. Turse and W. Rieman, III, *J. Phys. Chem.*, **65**, 1821 (1961).

(7) F. Helfferich, "Ion-Exchange," McGraw-Hill Book Co., Inc., New York, N. Y., 1962, pp. 250-322.

(8) G. E. Boyd and B. A. Soldano, *J. Am. Chem. Soc.*, **75**, 6091 (1953).

(9) A. Schwarz, Ph.D. Thesis, Technion-Israel Institute of Technology, Haifa, Israel, 1962.

centrated $NaNO_3$ solution which was then diluted with a small excess of sodium hydroxide solution. The resin in the sodium form was then washed free of excess $NaNO_3$–$NaOH$ solution and an excess of the metal nitrate solution of the desired concentration was added. This conversion path was selected since the exchange reaction is more rapid and proceeds further toward completion when the resin is originally in the sodium rather than the hydrogen form.

Equilibrium of the resin with the metal nitrate solution was assured by replacing the external solution three or four times, after a contact time for at least 24 hr. After the first solution change, no observable loss of metal from the external solution was detectable and the pH of the solution usually remained constant.

The chelated metal in the resin was then tagged with its radioactive isotope by equilibration for at least 1 week with a metal nitrate solution containing the radioactive nuclide. This method ensured attainment of equilibrium between resin and solution.

Particle Size Measurement. The diameter of the wet resin beads of a given mesh size in equilibrium with the desired solution was measured by microscopic examination with a calibrated eye piece ocular which had been previously standardized against a stage micrometer. Measurement of 300 to 400 beads was employed to obtain a representative average particle size.

Experimental Arrangement. A schematic representation of the apparatus for monitoring the isotopic exchange is shown in Fig. 1. A four-necked 250-ml. flask was used to contain the resin and solution in a thermostated bath. A stirrer extended into the mixture through the center neck of the flask. A filter stick of coarse sintered glass confined the resin in the flask during continuous circulation of the solution (by means of a peristaltic pump) through a Plexiglass flow cell situated in the crystal well of a shielded scintillation counter attached to a recording count-rate

meter. The flow all was held firmly in the well by tape, thus assuring constant geometry.

Experimental Procedure. In a typical experiment, tracer-free metal ion solution of the same concentration as that used for the resin equilibration was pumped in and through the system until thermal equilibrium was attained. The pumping rate was sufficiently high to assure circulation of the entire solution at least once every minute.

Self-exchange was initiated by introducing the wet radioactive resin through the fourth flask neck (Fig. 1) into the circulating solution, followed by rinsing with a small quantity of the metal salt solution. Uniform mixing of the solution and resin particles was achieved by vigorous stirring. The volume of the final solution was adjusted to make the ratio between total exchanging ion in the resin and that in solution (w) equal to 0.1. With this ratio $^{10}/_{11}$ of the radioactive isotope will eventually enter the solution. Progress of the self-exchange process, as indicated by the increasing activity in the solution, was followed by the recording rate meter.

A self-exchange reaction was considered to be complete when no change in solution activity was noticeable in a 24-hr. period. A radioactive material balance was periodically carried out to check on the attainment of equilibrium. The background was measured at the completion of each run by removing the flow cell from the scintillation counter and by recording the rate meter reading while the resin and solution were still in place. The time constant of the rate meter was increased in the final solution activity measurement to give 1% standard deviation. Because of the importance of this final activity value for the accurate estimate of the fractional exchange, a separate check on instrument stability was made by recording the activity of a Co^{60} reference source before and after representative runs. (No correction for instability was ever needed, however.)

Results

The results of the self-exchange experiments with Na^{22}, Co^{60}, and Zn^{65} are summarized in Tables I–IV. If the self-exchange is controlled by ion diffusion in the resin, the equations shown in Table IV apply. The conventional test for this condition is a plot of Bt, as determined from the experimental values of fractional attainment of equilibrium by this formula, against time. If this yields a straight line through the origin, it is proven that B remained indeed constant during the experiment, as demanded by the theory. An additional criterion is the variation of the slope of the line inversely with the square root of the radius, r_0,
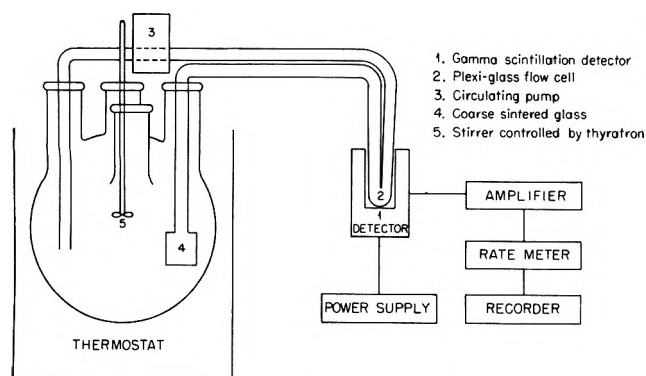

1. Gamma scintillation detector
2. Plexi-glass flow cell
3. Circulating pump
4. Coarse sintered glass
5. Stirrer controlled by thyratron

Figure 1. Schematic representation of experimental arrangement for study of isotopic exchange.

Table I: Self-Exchange of Sodium in Dowex A-1[a] at 29.0 ± 0.1°

Solution	pH in soln.	Particle radius, cm. × 10²	Half-exchange, sec.	Rate meter time const., sec.	w	Water content[b]	D × 10⁷, cm.² sec.⁻¹
NaNO₃[c] 0.08 M	3.2	1.17	34	3	0.01	0.52	1.2
NaAc 0.1 M	7.6	1.43	5	1	0.1	1.37	11
NaOH 0.1 M	12.6[d]	1.44	9	1	0.2	1.72	6.7

[a] Self-exchange studies with Na²² were made with a different batch from those reported for Zn and Co. [b] Grams of water per gram of dry resin in the H form. [c] Solution also contained 0.05 M acetic acid. [d] pH uncorrected for sodium error.

Table II: Self-Exchange of Zinc and Cobaltous Ions in Dowex A-1[a] in 0.1 M Metal Nitrate Solutions at 29°

Expt. no.	Wet radius, cm. × 10²	Half-exchange, min.	Apparent diffusion coefficient[b], D_{app} × 10⁹, cm.² sec.⁻¹	Remarks
	Zn⁶⁵		pH 5.3 ± 0.3	
1	0.874 ± 0.05	6.2	6.4	0.1 M Zn(NO₃)₂
2	1.05 ± 0.09	8.4	6.3	0.1 M Zn(NO₃)₂
3	1.32 ± 0.09	17.0	5.1	0.1 M Zn(NO₃)₂
4	1.76 ± 0.14	28.4	5.4	0.1 M Zn(NO₃)₂
5	1.32	9.5	9.1	0.1 M ZnSO₄
6	1.32	11.9	7.4	0.2 M Zn(NO₃)₂ w = 0.05
	Co⁶⁰		pH 4.6 ± 0.1	
7	1.05	9.0	6.1	
8	1.29	11.6	7.4	
9	1.69	19.1	7.5	

[a] Resin water content = (38.5 ± 1.4)% water by weight in the zinc form and 42.5% water by weight in the cobalt form.
[b] See Appendix for explanation and definition of this term.

Table III: Reproducibility of Self-Exchange of Zn in Dowex A-1 in 0.1 M Metal Nitrate Solution at 29°

Expt. no.[a]	Wet radius, cm. × 10²	Half-exchange, min.	Apparent diffusion coefficient, D_{app} × 10⁹, cm.² sec.⁻¹
3	1.32	17.0	5.1
10	1.32	14.5	5.9
11	1.32	18.5	5.0
6b	1.32	19.2	4.6
6f		33.0	
6g[b]		8.9	
1	0.874	6.2	6.4
1c	0.874	9.0	4.2

[a] An experiment number without a letter (column 1) corresponds to a fresh sample. Experiments designated by a number followed by a letter were carried out by recharging a used sample. Consecutive letters refer to consecutive experiments. [b] In this experiment the sample was treated with acid and base prior to use.

of the resin spheres used.[10,11] The results in Fig. 2 demonstrate that both criteria were met in the self-exchange of zinc, at least throughout the major part of the reaction. A similar test applied to the self-exchange of sodium[9] and cobalt also leads to the conclusion that the self-exchange of these ions is particle-diffusion controlled.

In these calculations, the values of Bt as functions of F were read from Reichenberg's table,[10] which applies when the ratio, w, of total metal ion in the resin to that in solution is close to zero; in this case the rate of the reverse reaction (re-absorption of radioactive ion into the resin) may be neglected. This table was used in all experiments in which w was 0.1 or smaller. For the evaluation of all those experiments in which w was larger than 0.1, however, we used a table due to Boyd (ref. 7, p. 585), based on a more complicated rate

formula, which takes due account of the reverse exchange reaction.

The diffusion coefficient values that are presented in Table I were calculated from one point between 50 and 60% exchange. Since the self-exchange of Na⁺ is relatively fast, the rate meter was operated at a low time constant setting and the statistical deviation was 5% at the half exchange; the over-all accuracy for the diffusion coefficient is believed to be ±10%. The results indicate that this exchange is particle-diffusion controlled. Rieman and Turse also found the same mechanism in exchange reactions in which one of the ions was sodium. The increase of the diffusion coefficient with increasing water content of the resin in the first two experiments in Table I can be correlated with enhanced rate of diffusion in the less tortuous path

(10) D. Reichenberg, J. Am. Chem. Soc., 75, 589 (1953).
(11) G. E. Boyd, A. W. Adamson, and L. S. Myers, Jr., ibid., 69, 2836 (1947).
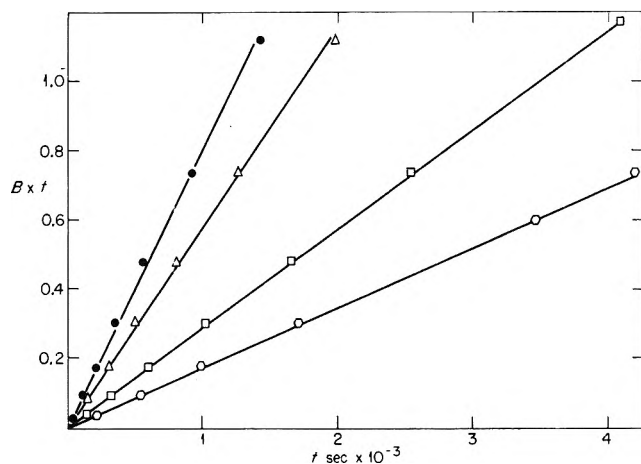
Figure 2. Infinite bath diffusion plot for self-exchange of zinc between Dowex A-1 resin of different particle radius, r_0, and 0.1 M $Zn(NO_3)_2$ solutions: ●, $r_0 = 0.874 \times 10^{-2}$ cm., expt. no. 1; △, $r_0 = 1.05 \times 10^{-2}$ cm., expt. no. 2; □, $r_0 = 1.32 \times 10^{-2}$ cm., expt. no. 3; ○, $r_0 = 1.76 \times 10^{-2}$ cm., expt. no. 4.

Table IV: Numerical Evaluation of the Self-Diffusion Coefficient for a Representative Experiment[a]

t, sec.	F	Bt	B, sec.$^{-1} \times 10^4$
43.2	0.2	0.0386	8.94
115.2	0.3	0.0928	8.06
211.5	0.4	0.177	8.37
369	0.5	0.301	8.16
560	0.6	0.479	8.55
927	0.7	0.734	7.92
1440	0.8	1.120	7.78
			8.25 ± 0.7 (av.)

$$D_{app} = \frac{Br_0^2}{\pi^2} = 6.38 \times 10^{-9} \text{ cm.}^2 \text{ sec.}^{-1}$$

[a] Solution, 0.103 M $Zn(NO_3)_2$; resin, Dowex A-1 in the zinc form; average particle radius, $r_0 = 8.74 \times 10^{-3}$ cm.; $w = 0.1$. Infinite bath equation used to calculate the apparent diffusion coefficient from the fractional attainment of equilibrium, F, at time t

$$F = 1 - \frac{6}{\pi^2} \sum_{n=1}^{\infty} \frac{1}{n^2} \exp(-n^2 Bt)$$

$$B = D_{app}\pi^2/r_0^2$$

Numerical values of Bt as a function of F are from Reichenberg.[10]

available in the more swollen resin. These two sodium exchange reactions involve the first ionized carboxylate group of the imino diacetic acid and the comparison is straightforward. In the third experiment, however, the geometry of the system is probably changed by the presence of the second ionized carboxylate group.

The resin becomes a less open structure as shown by the lower water content per sodium atom at higher pH. Although the total water content of the resin is higher, the structure is more restrictive to movement of the sodium ion.

The diffusion coefficient values reported in Table II for Zn^{2+} and Co^{2+} are each an average of seven points. An example of a detailed numerical evaluation of the self-diffusion coefficient is given in Table IV.

From experiments 1, 2, 3, and 4 with zinc, and experiments 7, 8, and 9 with cobalt, the strong dependence of the exchange rate on particle size is clearly evident. The half-exchange time changes from 6 min. for the smallest particle examined to 28 min. for the largest particle in the case of Zn and from 9 min. to 19 min. for Co. On the other hand, a single diffusion coefficient with average values of $(5.7 \pm 0.7) \times 10^{-9}$ cm.^{2} sec.$^{-1}$ and $(7.0 \pm 0.9) \times 10^{-9}$ cm.^{2} sec.$^{-1}$ for zinc and cobalt, respectively, describes the complete exchange reaction.

By comparing experiments 3, 10, and 11 (Table III), we can judge the reproducibility of the experiments. These experiments were performed with new samples from a prepared resin source. Apparent diffusion coefficient values of $(5.7 \pm 0.7) \times 10^{-9}$ cm.^{2} sec.$^{-1}$ were always obtained.

However, when an experiment was repeated with the same sample by recharging the resin with fresh radioactive tracer, the rate of the self-exchange always decreased. This phenomenon is illustrated by the results obtained from experiments 1 and 1c and from experiments 6 to 6f. When trying to repeat experiment 1, after carrying out an experiment at a lower temperature, the rate was observed to decrease (experiment 1c).

In experiments 6b to 6f, a single sample of resin was exchanged in five runs including a run at 50°, and the decrease of exchange rate was quite large. It is believed that poor chemical and physical stability of Dowex A-1 is responsible for this difficulty.

The Dowex A-1 batch used to carry out the self-exchange study was only 1% DVB cross linked.[12] Also, it has been shown[13] that a polymeric mixture is leached from the low cross-linked resin into the equilibrating solution. This leach material may block diffusion through the pores and thus decrease the exchange rate.

In an attempt to support this hypothesis, the resin sample after experiment 6f was regenerated and cycled twice between 2 M HCl and 2 M NaOH solutions. After

(12) R. M. Wheaton, The Dow Chemical Co., private communication, 1961.

(13) C. Eger and J. A. Marinsky, private communication, 1963.

this treatment an additional run was made. The half-exchange time dropped to 8.9 min. A microscopic examination of the beads at this stage revealed that a high percentage was broken, as compared to 95% sphericity of the fresh resin sample. The water content of the sample after this experiment was also higher (43%) than the average value reported in Table II.

It is of interest to note that a sodium hydroxide treatment is also recommended[14] by the Dow Company when the resin loses its exchange ability due to long storage in the hydrogen form. A possible explanation for this recommended procedure is the opening of the structure and removal of trapped soluble material when the resin is converted to the sodium form.

No further attempt was made to investigate this breakdown of the resin. Despite this difficulty, freshly prepared samples gave repeatable diffusion coefficients. The resin decomposition is apparently much slower than the self-exchange process so that by taking a fresh sample for each experiment, meaningful diffusion coefficient values are obtained.

By changing the salt solution, the effect of concentration (Table II, expt. 6) and nature of the co-ion (Table II, expt. 5) was studied. When the external solution concentration is doubled, the rate increases by about 20%. It is believed that the increase in counter-ion diffusion coefficient with the increase in external solution concentration is due to electrolyte invasion as observed with other resins.[15] In Dowex A-1 this effect will be magnified when the resin is loaded with a chelate-forming metal ion because of the decrease of Donnan exclusion due to the metal–ligand bond.

A pronounced co-ion effect is found; self-exchange is much faster with an external solution of 0.1 M ZnSO$_4$ than with 0.1 M Zn(NO$_3$)$_2$. The sulfate ions are known to form ion pairs with zinc and about 55% of the Zn is estimated to be bound to SO$_4$$^{-2}$ [16] at the concentration of the experiment. Thus much of the diffusible zinc in the resin pores is in the form of the noncharged ZnSO$_4$ molecule, and one species instead of two or three species as in the case of Zn(NO$_3$)$_2$ prevails in the resin phase. Both effects increase the rate of exchange.

Discussion

The theory of ion-exchange kinetics is well-established. Evidence in the extensive literature[7] indicates that the rate-determining step is interdiffusion of the exchanging counter-ions either in the particle (particle-diffusion mechanism) or in a film of solution surrounding the resin sphere (film-diffusion mechanism). Furthermore, diffusion exchange was also found to be a

rate-controlling step in a different chelating resin studied by Hojo.[17] The rate equations for homogeneous reaction were inapplicable to the absorption of Ag, Hg, and Cu by (3-hydroxyphenyl)thiourea–phenol resin. The diffusion of ions in the resin phase seemed to be the rate-determining step in this case. We conclude from our results that the self-exchange of Zn and Co in Dowex A-1 is also diffusion-controlled in contradiction to the results of earlier work[6] with this resin.

We believe that the lack of dependence of exchange rate on particle size observed by Turse and Rieman[6] in their earlier work was due to a composite of complicating effects resulting largely from the difference between exchange of different ions and of isotopic ions. The analogy between heat transfer and ion exchange which leads to the basic equations for particle-diffusion controlled exchange is justified only for exchange of ions of equal mobility and charge, as in isotopic exchange experiments, and not for other cases (ref. 7, p. 269). Moreover, swelling and deswelling during the exchange reactions of Turse and Rieman may have further complicated their exchange kinetics and obscured the effect of particle size variation on the rate.

Additional experimental evidence on which Turse and Rieman base their earlier conclusion is the dependence on the external solution concentration. This observation, however, does not exclude a diffusion process,[15] especially in a system where electrolyte invasion can become significant. Finally, recent work by Rieman and Varon[18] also supports particle-diffusion control as the rate-limiting factor.

Most complexes of Zn^{2+} and Co^{2+} are known to be labile, i.e., exchange rapidly with isotopic free ions, and there is no apparent reason for them to become inert when chelated in a resin when only three bonds need to be broken simultaneously. The iminodiacetic acid group in Dowex A-1 is connected to the polymer chain through a methylene bridge and is therefore relatively free to oscillate.

It might be expected that a truly chemically controlled self-exchange reaction will be encountered in the case where the metal ion is inert (e.g., Ni^{2+} and Cr^{3+}). Work on Cr^{51} $^{3+}$ self-exchange has been initiated and preliminary results indicate that the exchange may be chemically controlled.

(14) "Dowex Chelating Resin A-1," The Dow Chemical Co., Midland, Mich., 1959.

(15) R. Schlögl, Z. Elektrochem., 57, 195 (1953).

(16) R. A. Robinson and R. H. Stokes, "Electrolyte Solutions," Academic Press, Inc., New York, N. Y., 1955, p. 402.

(17) N. Hojo, J. Chem. Soc. Japan, Ind. Chem. Sect., 62, 1145 (1959); Chem. Abstr., 57, 10756 (1962).

(18) W. Rieman, III, private communication, 1963.

Appendix

Self-Diffusion in a Traced Chelating Resin. Consider the internal dissociation

$$M^+R^- \rightleftharpoons M^+ + R^- \tag{1}$$

where M^+ is the metal ion and R^- the resin anion. The effect of electrolyte invasion is neglected. This equilibrium is assumed to be instantaneous.

Theorem. The self-diffusion flux of the metal ions can be treated as if there were no chelating or other binding between M^+ and R^-; however, the *apparent* self-diffusion coefficient, D_{app}, calculated from this procedure is smaller than the *true* self-diffusion coefficient of M^+, D_M. In fact, $D_{app} = \alpha D_M$, α being the ratio of free M^+ to total M $(M^+R^- + M^+)$ in the resin.

Proof. The basic flux equation for *free* ions M^+ in the resin is

$$\phi^*_{M^+} = -\frac{D_M}{RT} \bar{C}^*_{M^+} \frac{d\mu^*_{M^+}}{dx} = -\frac{D_M}{RT} \alpha \bar{C}^*_{st} \frac{d\mu^*_{M^+}}{dx} \tag{2}$$

The asterisk refers to the radioactive species. $\bar{C}^*_{st}$ is the total (stoichiometric) concentration of the radioactive ion, bound and free, in the resin (mole cm.$^{-3}$), $\bar{C}^*_{M^+}$ the concentration of the *free* radioactive ions only.

Because of the equilibrium (1), the chemical potential of the radioactive compound M^+R^- is equal to the sum of the chemical potentials of the respective ions

$$\mu^*_{MR} = \mu^*_{M^+} + \mu_{R^-} \tag{3}$$

and since μ_{R^-} is independent of position within the resin particle, because there is no concentration gradient of R^- within the particle

$$\frac{d\mu^*_{M^+}}{dx} = \frac{d\mu^*_{MR}}{dx} \tag{4}$$

By definition

$$\mu^*_{MR} = (\mu^*_{MR})_0 + RT \ln \bar{a}^*_{MR} = (\mu^*_{MR})_0 + RT \ln f\bar{C}^*_{MR} \tag{5}$$

Note that the concentration, $\bar{C}^*_{MR}$, in the resin is almost identical with the total stoichiometric concentration of M^*, $\bar{C}^*_{st}$, in the resin. Remembering that the activity coefficient, f, is not a function of x

$$\frac{d\mu^*_{MR}}{dx} = \frac{RT}{\bar{C}^*_{st}} \frac{d\bar{C}^*_{st}}{dx} \tag{6}$$

According to eq. 4 this expression equals $d\mu^*_{M^+}/dx$. Substituting it in eq. 2, we obtain

$$\phi^*_{M^+} = -\alpha D_M \frac{d\bar{C}^*_{st}}{dx} \tag{7}$$

or, if we define

$$D_{app} \equiv \alpha D_M \tag{8}$$

we obtain

$$\phi^*_{M^+} = -D_{app} \frac{d\bar{C}^*_{st}}{dx} \tag{9}$$

The meaning of eq. 9 is that for the self-diffusion flux of free ions, M^+, in the resin, one does not have to use the Fick law for free ions (whose concentration, after all, one does not know, because the degree of dissociation and the extent of invasion are unknown). Instead one can use, in Fick's law, the total stoichiometric concentration of radioactive ions. The apparent diffusion coefficient obtained when this is done is simply the true ionic diffusion coefficient multiplied by the fraction of the free ions in the resin. The same treatment applies when electrolyte invasion is not entirely negligible, provided the ratio of invading M^+ to the total (stoichiometric) amount of M in the resin is small, which was no doubt the case in our experiments, because dilute electrolyte solutions were used.

Symbols

All symbols refer to the resin phase.

$\bar{a}^*_{MR}$ activity of radioactive M^+R^-, mole cm.$^{-3}$

B constant defined in Table IV, sec.$^{-1}$

$\bar{C}^*_{M^+}$ concentration of free radioactive M^+ ions, mole cm.$^{-3}$

$\bar{C}^*_{MR}$ concentration of radioactive M^+R^-

$\bar{C}^*_{st}$ concentration of radioactive M^+R^- plus free radioactive M^+

D_{app} self-diffusion coefficient obtained from Fick's law when concentration gradient of radioactive M^+R^- is used in that law, cm.^{2} sec.$^{-1}$

D_M true ionic self-diffusion coefficient of M^+ obtained from Fick's law when gradient of radioactive M^+ is used in that law

f activity factor of M^+R^-

F fractional attainment of equilibrium

r_0 resin radius, cm.

R gas constant, joule mole^{-1} deg.$^{-1}$

t time, sec.

T absolute temperature, °K.

w the ratio of total metal in the resin to that in solution at the end of a self-exchange experiment. Its numerical value is determined by the equilibrium distribution of the tracer between resin and solution

x length coordinate, cm.

α ratio of free ions M^+ to total M in the resin

ϕ^*_M = flux of radioactive M^+, mole cm.$^{-2}$ sec.$^{-1}$

μ^*_M = chemical potential of radioactive ions M^+, joule mole^{-1}

μ^*_{MR}, $(\mu^*_{MR})_0$ chemical potential and standard chemical potential of radioactive M^+R^-, respectively

μ_{R^-} chemical potential of R^-

Experimental Investigations on the Light Scattering of Colloidal

Spheres. VI. Determination of Size Distribution Curves by

Means of Turbidity Spectra[1]

by Morton L. Wallach and Wilfried Heller

Department of Chemistry, Wayne State University, Detroit, Michigan   *(Received August 13, 1963)*

Spectra of turbidity exhibited by polystyrene latices were investigated and the results were used to derive the size distributions in these systems. The turbidity spectra method was found to be equivalent in performance to that based upon the study of spectra of the scattering ratio (depolarization) provided the spectral turbidity maximum is within or near the spectral range investigated. Turbidity spectra were determined for systems showing a negatively skewed, a positively skewed, and a gaussian-type distribution. The distribution curves derived from the spectra were compared with electron microscopic distribution curves obtained on the same systems. Simplifications of the method proposed here are outlined which may be sufficient if the objective is merely a determination of the modal and/or mean particle diameter or if the concentration of the scattering material is not exactly known.

Introduction

The preceding paper in this series[2] dealt with a method for determining size distribution curves in heterodisperse systems of colloidal spheres by means of the spectra of the scattering ratio. An alternate method may be based upon the use of turbidity spectra. The theory of this alternate method was given some time ago.[3] The present paper is concerned with the experimental test of this alternate method, using again heterodisperse polystyrene latices as model systems. The distribution curve is again assumed to be of the type

$$f(r) = (r - r_0)e^{-[(r-r_0)/s]^2} \qquad (1)$$

$$= 0, \; r < r_0$$

Here, $Cf(r)\,dr$ is the number of particles per unit volume of a system containing particles with radii between r and $r + dr$, s is a parameter proportional to the width

(1) This work was supported by the Office of Naval Research. The results given in the present paper were presented at the 134th National Meeting of the American Chemical Society, Chicago, Ill., Sept., 1958.

(2) W. Heller and M. L. Wallach, *J. Phys. Chem.*, **67**, 2577 (1963).

(3) M. L. Wallach, W. Heller, and A. F. Stevenson, *J. Chem. Phys.*, **34**, 1796 (1961).

of the distribution, and r_0 is the radius of the smallest particles present in consequential numbers. Particles with a radius smaller than r_0 are quantitatively defined here as those having a radius smaller than 99% of all the particles present in the system. This definition, for the present systems, is based upon electron microscopic histograms.

Experimental

The systems investigated were the same latices as used previously.[2] They represent a positively skewed distribution (H.D. 1) in line with eq. 1, a negatively skewed distribution (H.D. 2), and a gaussian distribution (H.D. 3). The apparatus used and preparation and treatment of the latex samples were the same as in the preceding investigation.[2] Details of the optical setup were on the whole the same as before when turbidity measurements were carried out on monodisperse systems.[4] Modifications already described[2] were taken advantage of. In addition, the following changes were introduced: (1) Since it was desirable to have radiation of the highest possible spectral purity, the radiation emerging from the incandescent light source was passed through interference filters supplemented by colored glass filters prior to entry of the light beam into the monochromator proper. (2) The solid angle was decreased to 1.1×10^{-4} steradian in order to eliminate, as much as possible, the contribution of forward scattering.[5]

Turbidity measurements were carried out at each wave length at systematically varied concentrations, the lowest concentration within a series being given by $\phi = 0.24 \times 10^{-5}$ (ϕ, volume fraction of the polymer). The specific turbidity, $\lambda\tau/\phi$ (λ, the wave length in the medium; τ, the turbidity), was then plotted against concentration and extrapolated to infinite dilution. The turbidity spectra to be given apply therefore to infinitely dilute systems. The respective $\lambda\tau/\phi$ values are differentiated from those actually measured by a subscript, viz. $(\lambda\tau/\phi)_0$.

Results

Figure 1 summarizes the specific turbidity spectra derived from experiment for the three systems. The width of the rectangles represents the maximum uncertainty in λ_0; their height is the maximum uncertainty in $(\lambda\tau/\phi)_0$. The data indicated by the black dots are the most probable values. In the case of H.D. 3, the combined use of a Hg-vapor lamp (instead of the Pointolite lamp used in the other two cases), a monochromator, and interference filters reduced the former uncertainty to a negligible value at two of the three wave lengths used.

Figure 1. Actual $(\tau/\phi)_0$ spectra of the heterodisperse systems H.D. 1 and 3 investigated. Numerical data identifying the three characteristic parameters of the distribution curves are due to electron microscopy (subscript e): dots, most probable values; height of rectangles, total width of spectral band entering apparatus. (In two instances, use of Hg-vapor lamp, instead of incandescent source—in combination with monochromator, interference filters, and color filters—reduced width of rectangle to practically zero.)

The shapes of the curves differ characteristically. The turbidity maximum is seen to move toward shorter wave lengths in the direction H.D. 2 → H.D. 1 → H.D. 3. This indicates, as will be seen, a decrease, in this direction, of the modal diameter, D_m. The direction in the shift is therefore qualitatively the same as that expected in monodisperse systems.

In order to derive distribution curves, the experimental spectra are compared with a series of theoretical spectra until that theoretical spectrum is found which fits the experimental spectrum in a satisfactory approximation. These theoretical spectra are constructed by varying systematically the p_R and q_R values defined as

$$p_R = p\lambda/\lambda_R \qquad (2)$$

$$q_R = q\lambda/\lambda_R \qquad (3)$$

where

$$p = 2\pi r_0/\lambda \qquad (4)$$

$$q = 2\pi s/\lambda \qquad (5)$$

$$s = (r_m - r_0)\sqrt{3} \qquad (6)$$

The quantity p depends on the radius of the smallest

(4) R. M. Tabibian, W. Heller, and J. N. Epel, J. Colloid Sci., 11, 195 (1956).

(5) For a discussion of this effect, see R. M. Tabibian and W. Heller, ibid., 12, 25 (1957).

particles present in consequential numbers, r_0; and the quantity q is a measure of the spread of the distribution curve, r_m being the modal radius. These quantities are related to the $(\lambda\tau/\phi)_0$ value by the equation

$$(\lambda\tau/\phi)_0 = \frac{3\pi \int_p^\infty \Sigma(\alpha)(\alpha - p)\exp\{-[(\alpha - p)/q]^3\}d\alpha}{\int_p^\infty \alpha^3(\alpha - p)\exp\{-[\alpha - p]/q]^3\}d\alpha} \quad (7)$$

In these equations, r is the particle radius, $dr = (\lambda/2\pi)d\alpha$, and $\alpha = 2r\pi/\lambda$. The electronically computed theoretical values of $(\lambda\tau/\phi)_0$ have been given[3] for a wide range of p and q values for $m = 1.05(0.05)$ 1.30, where $m = (\mu_2/\mu_1)$, μ_2 being the refractive index of the particles and μ_1 that of the medium. In contradistinction to p and q, p_R and q_R are normalized with respect to the reference wave length λ_R which, in the present work (the medium being water at $25°$), is 4093.57 Å. (the corresponding vacuum wave length is the green Hg line, 5460.73 Å.). The procedure followed in finding the best theoretical spectrum is as follows: The values of q_R, p_R pairs are varied first within large intervals. Having come reasonably close to the normalized experimental spectra, the intervals in the numerical values of q_R and p_R are reduced to 0.4 or 0.2. (After some experience, the first step of wide variations in q_R and p_R can be eliminated). Four (Fig. 2) or three (Fig. 3) theoretical spectra are reproduced for each of the three systems investigated. They cover the entire range of acceptable q_R, p_R combinations. The best q_R, p_R pair is obtained subsequently. This final selection may be made by simply picking

Figure 3. Normalized experimental and theoretical $(\lambda\tau/\phi)_0$ spectra of H.D. 2. A third theoretical curve (i_3) is omitted (see text for details).

that theoretical spectrum which comes closest to the experimental one. Instead, one may, for a still better approximation, obtain the best q_R, p_R pair by interpolation between the two or three closest fitting theoretical spectra. The spectra used for such interpolations are identified in Fig. 2 and 3 by the symbols i_1 and i_2, respectively. In order not to crowd Fig. 2 and 3, only three or four instead of the larger number of actually considered theoretical spectra are shown. The i_2 curve in Fig. 2, pertinent to H.D. 3, is omitted ($q_R = 1.8$, $p_R = 5.6$). Similarly, an i_3 curve in Fig. 3 (1.8, 7.2) is omitted.

The experimental spectra are also normalized by plotting $(\lambda\tau/\phi)_{0,\lambda}/(\lambda\tau/\phi)_{0,\lambda_R}$. This eliminates uncertainties connected with concentration determinations and corrections in the numerical values associated with the use of a finite solid angle.[6] It also allows one to accommodate several spectra in a single graph.

The normalized experimental $(\lambda\tau/\phi)_0$ spectra are represented by the heavily drawn curves in Fig. 2 and 3. The open circles correspond to the most probable experimental values given in Fig. 1. The black circles are obtained by interpolation by means of the curves in Fig. 1.

Figures 4, 5, and 6 give the optical distribution curves and electron microscopic histograms obtained for H.D.
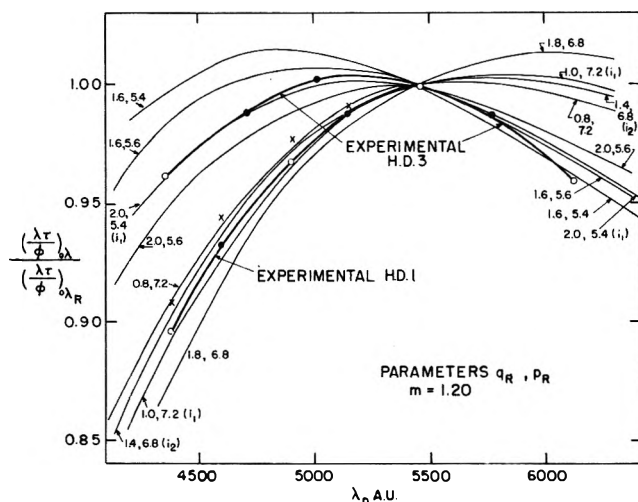

Figure 2. Normalized experimental and theoretical $(\lambda\tau/\phi)_0$ spectra of H.D. 1 and H.D. 3: heavily drawn curves, spectra derived from experiment; other curves, theoretical spectra.
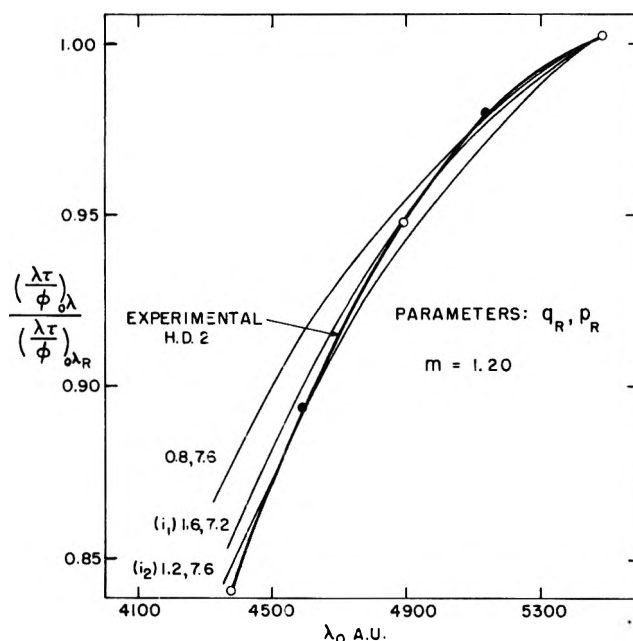
---

(6) Electronic computation would, of course, carry out automatically the equivalent of such interpolations.
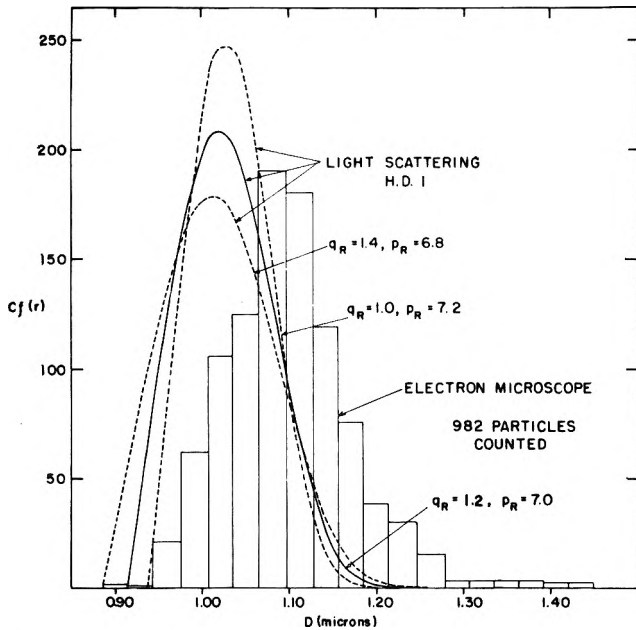
Figure 4. Size distribution curves derived from turbidity
spectra and comparison with electron microscopic histogram.
System (H.D. 1) with positively skewed distribution
conforming to eq. 1: fully drawn curve, using interpolated
q_R, p_R values; dotted curves, using the two q_R, p_R pairs
which come closest to achieving spectral fit on using Δq_R
and Δp_R intervals of 0.4.
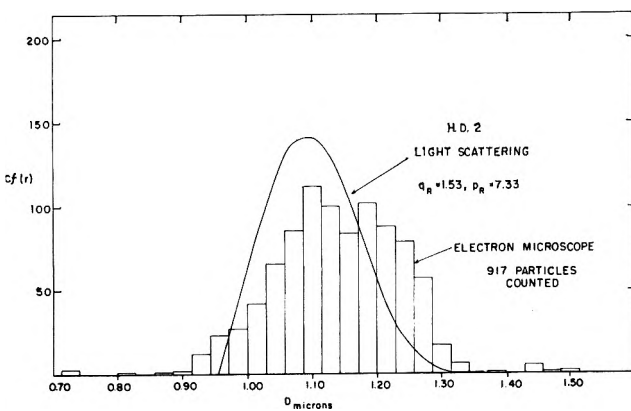
Figure 5. Size distribution curve derived from turbidity
spectra and comparison with electron microscopic histogram.
System (H.D. 2) with negatively skewed distribution curve
(interpolated q_R, p_R values used).

1, H.D. 2, and H.D. 3, respectively. (The procedure
used for the electron microscopic determinations of
the size distribution has been described previously.[2])
The fully drawn curve in Fig. 4 (H.D. 1) results from
the interpolated q_R and p_R values intermediate between
those of the i_1 and i_2 spectra in Fig. 2.[6] The dotted
curves pertain to the i_1 and i_2 spectra themselves.
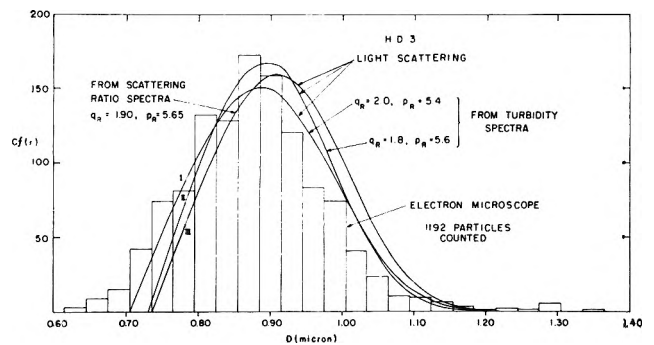
Figure 6. Size distribution curves derived from turbidity
spectra and comparison with curves obtained from spectra
of scattering ratio and with electron microscopic histogram.
System (H.D. 3) approximating gaussian distribution:
I and II, using turbidity spectra and the two q_R, p_R pairs
which came closest to achieving spectral fit on using Δq_R
and Δp_R intervals of 0.2. (Interpolation of q_R and p_R values
would yield curve within area bounded by curves I and II);
III, using σ-spectra and interpolated q_R and p_R values.

The modal diameter is hardly affected by the interpola-
tion. On the other hand, the peak height of the curve
is improved by it. Figure 5 (H.D. 2) contains only
the curve obtained by interpolation among the i_1,
i_2, and i_3 curves (see Fig. 3). Figure 6 gives two
distribution curves (I, II) derived for H.D. 3 from the
i_1 and i_2 pairs of q_R, p_R values (see Fig. 2). The dis-
tribution curve which would result from an interpola-
tion between the i_1 and i_2 pairs is omitted. It would
be intermediate between the curves I and II.

Instead of extrapolating the experimental spectra to
zero concentration it may be sufficient to operate at
a single reasonably small concentration if optimum
accuracy is not required for the distribution data.
Although the individual $(\lambda \tau / \phi)$ values are then slightly
different from the extrapolated $(\lambda \tau / \phi)_0$ values, the shape
of the normalized $(\lambda \tau / \phi)$ vs. λ_0 curve is not materially
affected. This is tested for H.D. 1. Normalized
data of $(\lambda \tau / \phi)$ obtained at the very small concentra-
tion of 0.827×10^{-3} g. of solids/100 g. of latex are
identified by crosses in Fig. 2. They agree throughout
to within 1% with those obtained by extrapolation to
zero concentration (circles). The q_R, p_R pair satisfying
these alternate data (1.0, 7.0) would give a distribu-
tion curve very similar to that of the pair 1.0, 7.2
except for a slightly lower modal diameter. On using
this approximation method, it is really not necessary
to know the absolute concentration provided that one
has proof that one operates within a "safe" range of
low concentrations. The safe range is defined by the
fact that τ varies, within it, linearly with the degree
of dilution at all wave lengths used (negligible multiple
scattering).

Table I gives a comprehensive survey of the numerical results obtained for the number average diameter, $\bar{D}_n$; modal diameter, D_m; diameter of the smallest particles present in consequential numbers, D_0; and half-width, W. (The half-width W considered here is twice the half-width, w, defined previously.[2] The

Table I: Summary of Numerical Results[a]

System	$\bar{D}_n$	D_m	D_0	W
H.D. 1	$1.02_8(6.5)$	$1.02_0(5.6)$	$0.91_2(3.3)$	$0.14_1(\sim1)$
H.D. 2	$1.10_2(3.3)$	$1.093(0.6)$	$0.955(4.5)$	$0.18_0(26)$
H.D. 3	$0.90_0(2.5)$	$0.888(2.1)$	$0.717(6.5)$	$0.22_3(27)$

[a] All data are in μ except bracketed data which represent % deviations relative to electron microscopic data.

latter would apply if the independent variable were the particle radius, r, rather than the diameter used here.) In each instance, the % deviation with respect to the electron microscopic data is given in parentheses. The quantities enumerated being those of principal importance, it can be stated from the results obtained here that the present method for determining size distribution curves is very satisfactory in those cases where the actual distribution curve does not differ much in type from that assumed (eq. 1). If the distribution curve is not of this type then the results for $\bar{D}_n$, D_m, and D_0 are still satisfactory, but the half-width W is obviously very much in error. If better results are to be obtained for the half-width in such a case, it is necessary to use the two term equation or other procedures discussed previously.[2] It is, fortunately, easy to ascertain when this contingency arises. A major departure of the distribution curve from that assumed by eq. 1 is indicated by the fact that it is impossible to obtain good agreement with experiment for any q_R, p_R pair. In Fig. 2 the experimental curve for H.D. 1 which satisfies eq. 1 is nearly parallel to any of the best fitting theoretical curves. On the other hand in Fig. 3, no theoretical curve can be found which fits more than $^1/_3$ or $^1/_2$ of the spectral range considered. This indicates at once that the system investigated does not possess the distribution assumed. For the gaussian distribution in Fig. 2 (H.D. 3) the situation is intermediate. Here, it is seen from the degree of agreement between experimental and theoretical spectra that the distribution curve differs, but not as much as in the preceding case from that assumed. The rather poor partial fit in Fig. 3 leads to the distribution curve in Fig. 5 which has the wrong skew, but does not— except for this feature—differ radically from the actual

distribution curve. It therefore depends on the objective as to whether or not in such cases use of the more time consuming two term equation or of other procedures is warranted.

Approximation Methods for Attaining Limited Objectives

Less exacting procedures are warranted if the objective is merely the determination of $\bar{D}_n$, D_m, and D_0. The reason is that the numerical value of these quantities changes relatively little on varying q_R and p_R within modest limits. Thus, the agreement between the electron microscopic D_m value and that derived from *any* of the theoretical spectra in Fig. 2 and 3 is within at least 7, 3, and 2% for H.D. 1, H.D. 3, and H.D. 2, respectively. Similarly, the agreement between the electron microscopic D_0 values and those derived from any of the theoretical spectra in Fig. 2 and 3 is within at least 5%, 12%, and 9%, respectively. An approximate fit of theoretical and experimental spectra is therefore sufficient if one is satisfied with a determination of these three quantities.

If the objective is even more limited, *i.e.*, if one is merely interested in determining an *approximate* value of D_m or $\bar{D}_n$, one may dispense with spectra entirely and operate at a single wave length. The diameter thus obtained is an *apparent* quantity since the system is treated as if it were monodisperse. It is of interest to evaluate the error committed by using such a very simple technique on heterodisperse systems. Choosing, for this purpose, the data obtained at the green mercury line, the theoretical specific turbidities would yield a particle diameter of 1.196, 1.214, and 0.736 μ for H.D. 1, H.D. 2, and H.D. 3, respectively. The differences between these diameters and the modal diameters obtained from the optical distribution curves are 15, 10, and 21%, respectively. The numerical error would be larger in systems more heterodisperse than those used here and smaller in the reverse case. Similarly, in a given system, the error would obviously vary with the wave length. Therefore, the ratio of the apparent diameters obtained at two wave lengths—treating the system as if it were monodisperse $(q = 0)$—can provide a rough measure of the relative degree of heterodispersion. It is clear that the apparent diameter should increase with decreasing wave length if the spectral range considered comprises wave lengths larger than that at which the turbidity maximum occurs. It should decrease with decreasing wave length in the inverse case.

Probable Range of Usefulness of Turbidity Spectra

The usefulness of turbidity spectra (within the visible spectral range) for determining size distribution curves

and the sensitivity of the spectra to changes in the degree of heterodispersion have been investigated in the present work for size distributions extending from particle diameters of about 0.7–1.4 μ and for half-widths from 0.14–0.24 μ. It can be anticipated (see Fig. 1 in ref. 3) that the sensitivity to heterodispersion for systems with particles smaller than 0.7 μ and with larger half-width is similar to that found here. While experiments in this lower range of particle diameters and with wider distributions are desirable, the situation which one is bound to find if D_0 is as small as 0.26 μ ($p_R = 2.0$) can be derived from an inspection of Fig. 3 of ref. 3. An increase of q_R from 1.0 to 4.0 changes the normalized $(\lambda\tau/\phi)_0$ spectrum just as profoundly no matter whether p_R has the value 6.0 ($D_0 \sim 0.8$ μ) or the value 2.0. Finally, it should be noted that the method described here, like any other light scattering method, will, of course, be wholly insensitive to particle size distributions if all the particles are so small compared to the wave length that Rayleigh scattering applies.

Turbidity spectra will become quite insensitive to particle size distributions if the particles are large relative to the wave length. Inspection of Fig. 1 and 2 in ref. 3 shows that the range of sensitivity terminates for slightly heterodisperse systems at $p \sim 16$ and for moderately heterodisperse systems ($q = 4.0$) at $p \sim 12$. Thus a system with a distribution half-width W of 0.5 μ will not respond well to the analysis if D_0 is about 2 μ. Work done by Wu in continuation of the present work shows that the sensitivity within the visible range of the spectrum begins in fact to fall off seriously if the distribution extends appreciably into the microscopic range.

On being faced with systems in which the particles are too small (Rayleigh range) or too large (upper microscopic range) to apply turbidity spectra usefully within the visible spectral range, one may, of course, in favorable instances (no true absorption), resolve the problem by making use of turbidity spectra in the ultraviolet or intermediate infrared, respectively.

Comparison of the Present Method With That Based on the Spectra of the Scattering Ratio

On comparing the results presented here with those given previously,[2] it is clear that the method of determining size distribution curves from turbidity spectra is, for the systems investigated, comparable in performance to that based upon spectra of the scattering ratio. A specific example is given in Fig. 6. The size distribution curve obtained for H.D. 3 from σ-spectra (curve III) is compared to that obtained by the method described in this paper. The curves are in satisfactory

agreement. For a closer check, the results given in Table I may be compared with the results obtained for the same systems by the alternate method (see Table I, ref. 2). An advantage of the present method is its relative experimental simplicity inasmuch as any properly modified spectrophotometer may be used. A further advantage is the fact that the sensitivity of turbidity spectra to heterodispersion is preserved even at very high degrees of heterodispersion (a half-width of 0.5 μ) provided $D_0 < 1$ μ. In addition, owing to their monotonic character, theoretical $(\lambda\tau/\phi)_0$ $vs.$ λ curves can be derived and constructed faster. Also, a high brightness of the light source is not as imperative here as in the case of scattering ratio spectra.

On the other hand, an advantage of the method based upon the scattering ratio is that the spectra of the latter are more profoundly affected by changes in p_R (by the smallest particle size at which the distribution curves effectively begin). The larger the quantity p_R is, the larger is the number of maxima and minima exhibited by the spectra. Thus, giving a q_R value of 1.4, one has one maximum if $D_0 \sim {}^1\!/_3$ μ, one maximum and one minimum if $D_0 \sim {}^2\!/_3$ μ, and two maxima and one minimum if $D_0 \sim 1$ μ on investigating a spectrum extending from the vacuum wave length of 4500 Å. to 6000 Å.[7] There is, therefore, no upper limiting p_R value beyond which the method is not applicable except that the occurrence of many maxima and minima in the upper microscopic range may make the resolution of the spectra a difficult task. This may well be the most important advantage of scattering ratio spectra over turbidity spectra, the latter of which should, as stated, become rather insensitive to size distributions if D_0 is in the microscopic range. As regards the sensitivity of the spectra of the scattering ratio, σ, to heterodispersion, it will most likely exceed that of the turbidity spectra as long as the degree of heterodispersion is small or moderate. This is due to the strong effect of q_R upon the amplitude of the σ $vs.$ λ oscillations.[7]

Some of these differences between the two types of spectra also lead to differences in the ease with which one may find, for a given system, the best q_R, p_R combination. The number of maxima and minima observed in a σ-spectrum, within a given spectral range, suggests at once the range of p_R values to be examined. The amplitude of the spectral oscillations suggests the range of q_R values to be examined (see, $e.g.$, Fig. 4, 5, and 6 in ref. 7). In the case of the turbidity spectra, on the other hand, the number of possible maxima is reduced to one. A quick analysis is therefore possible

(7) A. F. Stevenson, W. Heller, and M. L. Wallach, $J.$ $Chem.$ $Phys.$, **34**, 1789 (1961).

only if the $(\lambda\tau/\phi)_0$ maximum occurs within the visible range. The presence of such a maximum immediately limits the number of p_R values that may be considered. The degree of shallowness of the maximum is a reliable indicator of the approximate q_R range to be considered. The absence of a maximum within or very close to the experimental spectrum of $(\lambda\tau/\phi)_0$ increases the labor of finding the best q_R, p_R pair; it does, however, not interfere with the applicability of the $(\lambda\tau/\phi)_0$ method. Only one of the three systems investigated here exhibited a $(\lambda\tau/\phi)_0$ maximum.

The availability of both the $\sigma(\lambda)$ and $(\lambda\tau/\phi)_0$ vs. λ methods provides a welcome opportunity to check the results obtained with one against those obtained with the other. It allows one to make a quicker decision as to the proper q_R and p_R combination than with one spectrum alone. Furthermore, a combination of the two methods and, if necessary, consideration of a third

(variation of lateral scattering with the angle of observation) may allow one to derive distribution curves without having to make any assumption about its basic type. This possibility which appears very promising—provided the degree of heterodispersion is not so large as to wipe out spectral and angular maxima and minima completely—is being explored at the present time.

In conclusion, it may be noted that with systems which show a strong dispersion (of the refractive index), the dispersion should be taken into account in the calculation of the theoretical spectra on applying the method described here. With the systems investigated here, these corrections proved to be negligible.

Experimental Investigations on the Light Scattering of

Colloidal Spheres. VII. Resolving Power of the σ-Spectra

Method for Determining Size Distribution Curves[1]

by Wilfried Heller and Morton L. Wallach

Chemistry Department, Wayne State University, Detroit 2, Michigan   (*Received August 15, 1963*)

The resolving power of a previously described method for determining size distribution curves in colloidal dispersions of spheres was examined. The method is based upon use of the spectra of the scattering ratio or of the depolarization of scattered light. The systems used were two of those Dow latices of polystyrene which have a distribution curve so narrow that they are often referred to as monodisperse. The spectra of the scattering ratio showed that these systems are not strictly monodisperse and, in addition, allowed one to derive this distribution curve. The half-width of the distribution curve thus determined differed by 2.6 and 0%, respectively, from that obtained by electron microscopy. Similar good agreement with electron microscopic data was found for the mean and modal diameters and other quantities of statistical interest. Since the half-width was, in the systems investigated, one order of magnitude smaller than the modal diameter, the resolving power of the method can be stated to be most satisfactory.

Introduction

In two preceding papers the theory[2] and experimental test[3] of a method were given which allows one to determine the size distributions of spherical colloidal particles from spectra of the scattering ratio. It was found that the modal diameter D_m can be obtained with a high degree of accuracy, the % deviation with respect to electron microscopic results being at the most 5% no matter whether or not the particular type of distribution curve agreed or disagreed with that assumed. This is just within the range of uncertainty of electron microscopic data. If the distribution was of the type assumed,[2] the diameter of the smallest particles present in consequential numbers, D_0, and the "half-spread" $(D_m - D_0)$, of the distribution curve were obtained with an error not in excess of 6% and 2%, respectively. For other types of distribution, the error in D_0 and $(D_m - D_0)$ was somewhat but not appreciably larger. The same applied to the number average diameter, $\bar{D}_n$. Only the result for the half-width of the distribution curve proved to be quite sensitive to the type of distribution actually present.

A question not explored previously was the sensitivity of the method to deviations of a system from strict monodispersity. This problem of the resolving power of the method, based upon σ-spectra, is the subject of the present paper.

It may be recalled[3] that $\sigma = I_{||}/I_{\perp}$ where $I_{||}$ is the intensity of light scattered from an incident polarized beam of unit intensity whose electric vector vibrates parallel to the plane of observation. Similarly, $I_{\perp}$ refers to the light scattered from an incident polarized beam vibrating perpendicular to the plane of observation. The angle of observation with respect to the incident beam is again 90°.

Experimental

Electron microscopy gave the following information on the number average diameter, $\bar{D}_n$, and the standard deviation, S, of the two "monodisperse"

(1) This work was supported by the Office of Naval Research.

(2) A. F. Stevenson, W. Heller, and M. L. Wallach, *J. Chem. Phys.*, **34**, 1789 (1961).

(3) M. L. Wallach, and W. Heller *J. Phys. Chem.*, **68**, 924 (1964).
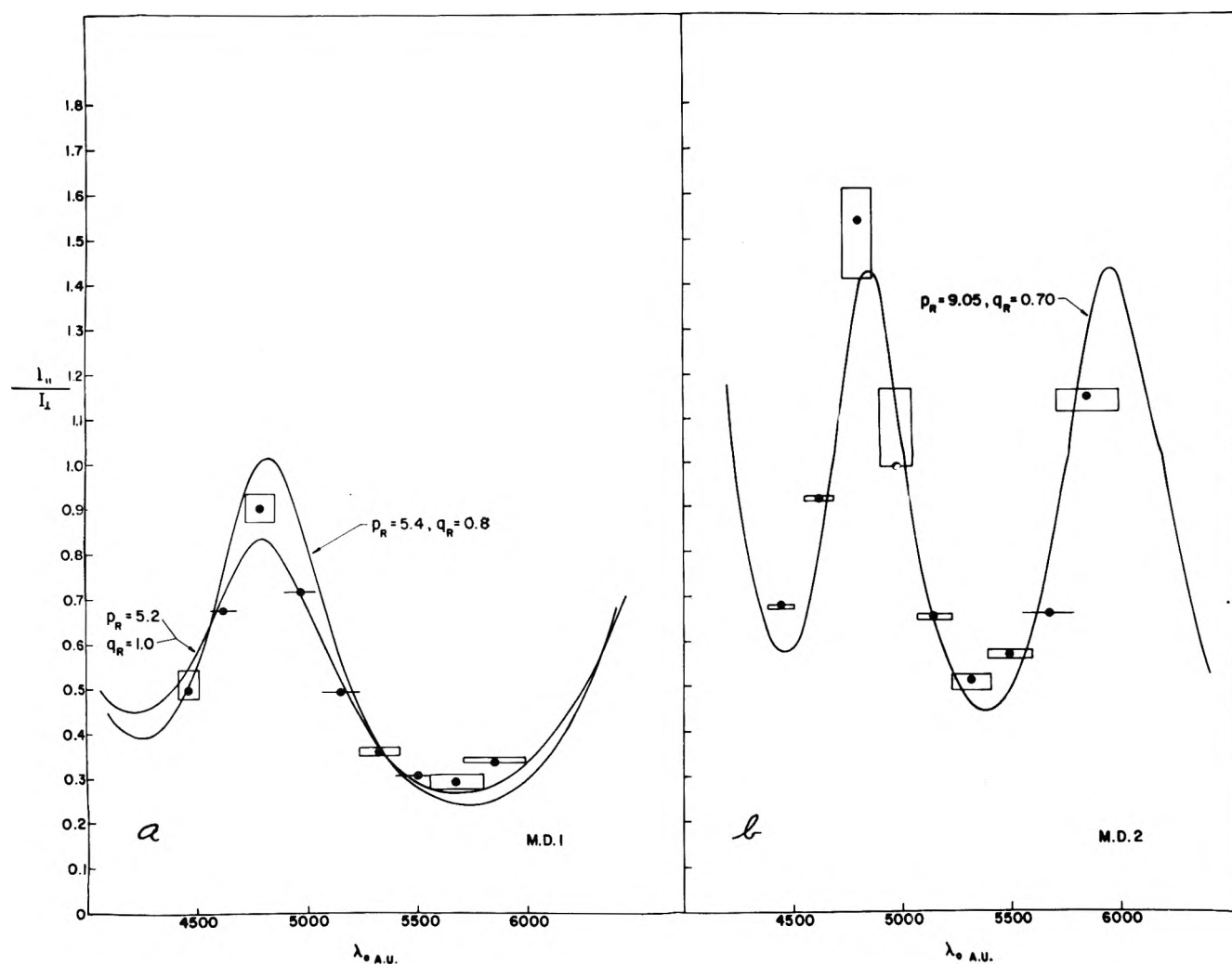
Figure 1. σ-Spectra of "monodisperse" latex M.D. 1 (part a) and M.D. 2 (part b).   Part a: black circles, most probable experimental value; rectangle, range of experimental uncertainty; two curves, theoretical curves which satisfy experimental data best on varying p_R and q_R in intervals of 0.2.   Part b: curve represents result of interpolation between four p_R and q_R values.

Dow latices investigated, both $\bar{D}_n$ and S being expressed in μ: M.D. 1, $\bar{D}_n = 0.761$; $S = 0.039$; M.D. 2, $\bar{D}_n = 1.230$; $S = 0.042$. The use of quotation marks for "monodisperse" means here, as is customary, that the size distribution curve in these latices, though remarkably narrow, is finite; i.e., the systems are not ideally monodisperse.

The apparatus used for the optical studies, the treatment of the systems prior to the light scattering measurements, and all of the experimental details including electron microscopy were throughout the same as in the preceding investigation.[3]

Results

The spectra of the scattering ratio are given in Fig. 1. Two theoretical curves which come closest
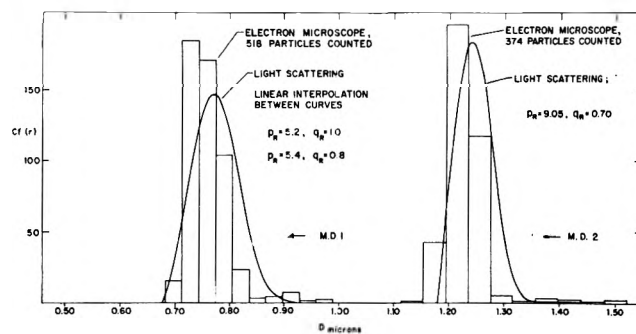
Figure 2.   Size distribution curves of M.D. 1 and M.D. 2. M.D. 1: Curve obtained by linear interpolation between two distribution curves derived from the two spectra in Fig. 1, part a. M.D. 2: Curve derived from interpolated spectrum in Fig. 1, part b.

to satisfying the experimental data of M.D. 1 are traced in Fig. 1, part a; only one is given in Fig. 1, part b, for M.D. 2.

In the case of M.D. 1, separate distribution curves were derived from the two theoretical spectra. The distribution curve actually given in Fig. 2 is the result of interpolation between these two primary distribution curves. This technique approximates the performance of the two-term distribution function.[3] It will be noted that by virtue of this interpolation procedure the rigidity in form of the basic distribution assumed is removed as documented particularly by the appearance of a curvature near the lower end of the distribution curve.[4]

The single $\sigma(\lambda)$ spectrum of M.D. 2 in Fig. 1, part b, was obtained by using the previously described procedure of interpolating between the p_R and q_R values pertinent to the four best fitting theoretical spectra (p_R, q_R pairs: 9.0, 0.6; 9.0, 0.8; 9.2, 0.6; 9.2, 0.8).[5] From the resulting single theoretical $\sigma(\lambda)$ spectrum of M.D. 2, the distribution curve in Fig. 2 was derived.

It may be recalled that

$$p_R = p\lambda/\lambda_R \tag{1}$$

$$q_R = q\lambda/\lambda_R \tag{2}$$

where

$$p = 2\pi r_0/\lambda \tag{3}$$

$$q = 2\pi s/\lambda \tag{4}$$

λ_R is the reference wave length, in the medium used for normalization (it corresponds to the vacuum wave length 5460.73 Å.); λ is the wave length, in the medium, used in a given experiment; r_0 is the radius of the smallest particle present in consequential numbers (still smaller particles accounting for not more than 1% of the total number); s is a quantitative measure of the spread of the distribution, i.e., it is a measure of the degree of departure from monodispersity. The defining relation is

$$s = (r_m - r_0)/\sqrt{3} \tag{5}$$

where r_m is the modal radius.

The electron microscopic histograms, also given in Fig. 2, agree very well with the distribution curves derived from the σ-spectra.

Table I gives the numerical values for the modal diameter, $\bar{D}_m$; number average diameter, $\bar{D}_n$; and diameter of the smallest particles present in consequential number, D_0. In addition, the half-width W is given.[6] The values in parentheses represent the % deviation of these data relative to those obtained from the electron microscopic histograms.[7] The agree-

ment of the numerical data obtained by electron microscopy, on the one hand, and from the σ-spectra, on the other, is excellent. The deviations are throughout within the limits of the combined uncertainty of the two methods.

Table I: The Diameters, D_0, D_m, $\bar{D}_n$,[a] and the Half-Width, W,[b] as Derived from the σ-Spectra of "Monodisperse" Latices M.D. 1 and M.D. 2, and Comparison with the Apparent Diameter, D_a, Obtained at 5460.73 Å. on Assuming Strict Monodispersity[c]

	M.D. 1			M.D. 2	
D_0	678	(0.9)	D_0	1179	(3.0)
D_m	773	(5.9)	D_m	1242	(1.0)
$\bar{D}_n$	776	(2.0)	$\bar{D}_n$	1246	(3.0)
W	106	(2.6)	W	82	(0.0)
D_a	800	[3.4]	D_a	1213	[-2.4]

[a] D_0, D_m, and $\bar{D}_n$ are in mμ. [b] See ref. 6. [c] Data in parentheses, % deviation from electron microscopic data; data in brackets, % deviation from D_m value.

It is of interest to note the large difference in the frequencies and amplitudes of the oscillations in the $\sigma(\lambda)$ curves of Fig. 1a and 1b. This illustrates well the fact that it is rather easy to pick out those p_R and q_R values which should be considered in a given instance.[8]

Discussion

The principal conclusion to be drawn from the results is that the method proposed is sensitive to relatively minor degrees of heterodispersity, i.e., it has a very high resolving power. One clearly can determine the essential features of size distribution curves in practically monodisperse systems.

It may be recalled that nearly monodisperse Dow latices of the type investigated here were used in this laboratory for the purpose of experimentally verifying light scattering functions predicted by the Mie theory.[9]

(4) Interpolation between the p_R and q_R values of the two curves given in Fig. 1, part a, one of the procedures used previously,[3] would lead to a distribution curve almost identical with that given here except that it would reproduce rigidly the type of distribution assumed by eq. 1.[3]

(5) The four curves were obtained by varying p_R and q_R in intervals of 0.2 and picking those four spectra which came closest to a fit with the experimental data.

(6) The half-width W is the numerical difference between the two particle dimensions—expressed in terms of diameters—for which the particle number is ¹/₂ of the number at the peak of the curve. Thus $W = 2w$, the latter quantity having been used in some of the preceding publications.

(7) The electron microscopic value of D_0 is obtained by disregarding those cells at the lower end of the polygonal frequency distribution in which the number of particles is less than 1% of the total number of particles present in all cells.

(8) See also, for example, Fig. 5 and 6 in ref. 2.

One is now in a position to compare the modal particle diameter obtained by the method described in this paper to the particle diameter to be expected from those earlier experiments which were carried out in monochromatic light by using the Mie data and on assuming ideal monodispersity. To that effect Table I gives the particle diameter D_a, derived from the scattering ratio obtained at the green Hg line assuming ideal monodispersity ($q_R = 0$). Comparison with the modal diameter obtained from the size distribution analysis shows that the % deviations are within the range of uncertainty of the electron microscopic diameters used as a reference in the experiments carried out by

Tabibian.[9] It follows from the near coincidence of the D_m and $\bar{D}_n$ values in Table I that the same statements apply also to the number average diameter, $\bar{D}_n$, as compared to the apparent diameter, D_a, obtained in nearly, but not strictly, monodisperse systems from monochromatic scattering experiments.

(9) W. Heller and R. Tabibian, *J. Phys. Chem.*, 66, 2059 (1962), and earlier papers.

Combustion Calorimetry of Organic Chlorine Compounds. The Heat

of Combustion of 2,3,5,6-Tetrachloro-*p*-xylene[1]

by N. K. Smith,

Department of Chemistry, Oklahoma State University, Stillwater, Oklahoma

D. W. Scott, and J. P. McCullough

Contribution No. 130 from the Thermodynamics Laboratory, Bartlesville Petroleum Research Center, Bureau of Mines, U. S. Department of the Interior, Bartlesville. Oklahoma (Received November 1, 1963)

A rotating-bomb method was developed for precision combustion calorimetry of organic chlorine compounds. The heat of combustion of 2,3,5,6-tetrachloro-*p*-xylene was determined. Two reducing agents, hydrazine dihydrochloride and arsenious oxide, were used to reduce the free chlorine produced in the combustion reaction to chloride ion. Arsenious oxide proved to be the superior reducing agent. The heat of formation of tetrachloro-*p*-xylene from graphite and gaseous hydrogen and chlorine was found to be -42.0_6 kcal. mole^{-1}.

Introduction

Most combustion calorimetry of organic chlorine compounds has been done by static-bomb methods. The status of such methods for chlorine compounds was reviewed by Smith and Hubbard in 1956.[2] The chief problem, aside from the corrosive nature of the combustion products, is the appearance of chlorine as both

HCl and Cl_2 in these products. To obtain a chemically well-defined final state, a reducing agent is placed in

the bomb initially to convert Cl_2 to HCl. Arsenious oxide and hydrazine dihydrochloride both have been used as reducing agents. Because the reaction with the reducing agent is slow, the surface area of the solution has been increased by supporting the solution on quartz fibers or glass cloth. However, even with that expedient, complete homogeneity of the final bomb solution and equilibrium with the gas phase are not attained.

Moving-bomb methods have been very effective in ensuring homogeneity and equilibrium in the final state for combustion calorimetry of sulfur compounds, fluorine compounds, bromine compounds, and a variety of organometallic compounds. Such methods have not been developed extensively for chlorine compounds heretofore, although pioneering work was done by Popoff and Schirokich[3] and by Smith and co-workers.[4]

The purpose of the present investigation was to develop moving-bomb methods for chlorine compounds and to investigate the relative merits of arsenious oxide and hydrazine dihydrochloride as reducing agents. To that end, a compound was chosen with a high enough chlorine content to provide a rigorous test of the special techniques, namely, 2,3,5,6-tetrachloro-p-xylene (58% Cl). Series of calorimetric experiments were done with each reducing agent using identical samples of the chlorine compound. It was hoped that the compound also would prove suitable as a reference substance for combustion calorimetry of chlorine compounds; it will be seen that this hope was not realized, although the primary aims of the investigation were attained.

Experimental

Apparatus. The rotating-bomb calorimeter BMR-2 has been described.[5,6] For reasons given below, it was necessary to minimize the amount of platinum inside the combustion bomb. To do this, a tantalum-lined bomb (Ta-1) was equipped with tantalum internal fittings (flushing tube, crucible support, and valve inlet fittings), and specially prepared, thin-walled Vycor crucibles were used. The crucibles, complete with supporting side arms, weighed from 300 to 550 mg. The bomb was sealed with a gold gasket. The only platinum present in bomb Ta-1 was 80 mm. of 0.05-mm. diameter ignition wire. The volume of the bomb was 0.341 l. A schematic sectional view of the bomb is shown in Fig. 1.

Materials. A commercial sample of tetrachloro-p-xylene was purified by recrystallization from benzene and then by zone melting.[5] An indicator–impurity dye was removed from four-fifths of the column after six passes of the molten zone, and a sample then
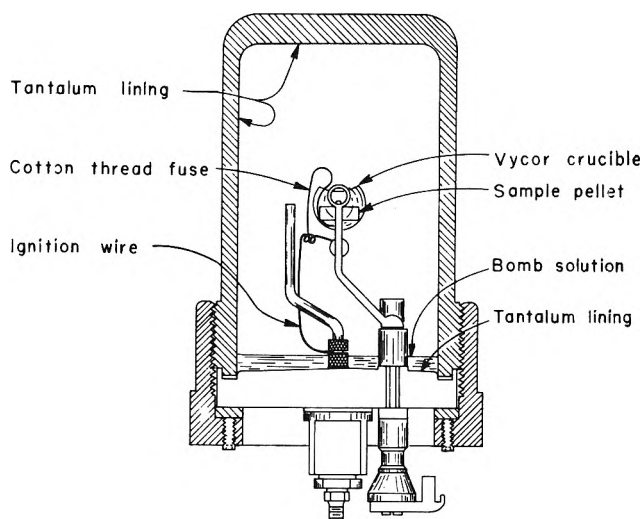
Figure 1. Schematic sectional view of combustion bomb Ta-1.

was melted from the tube. This sample exhibited a pale yellow color; the substance apparently is unstable at its melting point (248°), but the decomposition products were removed by the zone-melting process as fast as they formed. To avoid decomposition of the purified product, another sample was removed from the tube, without melting, by inverting and shaking the tube. For analysis, a sample was burned in an oxygen bomb in the presence of arsenious oxide, and the resulting chloride ion was precipitated and weighed as silver chloride. The yield of silver chloride was 100.0% of theoretical.

A commercial sample of hydrazine dihydrochloride was purified by dissolving it in water and then precipitating a portion by slowly adding hydrogen chloride gas; this sample then was recrystallized from water. Titration with standard iodine solution[7] indicated a purity of 99.8%.

Reagent grade arsenious oxide and arsenic oxide were used without further purification.

Iodine solutions, prepared from reagent grade iodine and potassium iodide, were standardized against National Bureau of Standards sample 83a arsenious oxide.

(3) M. M. Popoff and P. K. Schirokich, *Z. physik. Chem.*, **A167**, 183 (1933).

(4) L. Smith, L. Bjellerup, S. Krook, and H. Westermark, *Acta Chem. Scand.*, **7**, 65 (1953).

(5) W. D. Good, D. W. Scott, and G. Waddington, *J. Phys. Chem.*, **60**, 1080 (1956).

(6) W. D. Good, D. R. Douslin, D. W. Scott, A. George, J. L. Lacina, J. P. Dawson, and G. Waddington, *ibid.*, **63**, 1133 (1959).

(7) R. A. Penneman and L. F. Audrieth, *Anal. Chem.*, **20**, 1058 (1948).

The samples of auxiliary oil and cotton thread fuse material have been described.[5,6] The value of $\Delta Ec^\circ/M$ for the auxiliary oil obtained in experiments chronologically near the experiments with tetrachloro-p-xylene was $-10{,}983.8 \pm 0.2$ cal. g.$^{-1}$.

The benzoic acid was National Bureau of Standards sample 39h, with a certified heat of combustion of $26{,}434 \pm 3$ abs. joules g.$^{-1}$. Conversion from certificate conditions to standard conditions[8] gives -6312.97 ± 0.72 cal. g.$^{-1}$ for $\Delta Ec^\circ/M$, the energy of the idealized combustion reaction.

Combustion Experiments. Samples of tetrachloro-p-xylene were compressed into pellets; the amount of sample was adjusted to give a temperature increment of 1° for experiments with arsenious oxide and 2° for experiments with hydrazine dihydrochloride. An aliquot of reducing agent solution was added to the bomb, 10 ml. in the experiments with hydrazine dihydrochloride and 25 ml. in the experiments with arsenious oxide. The bomb was flushed and charged with oxygen to 30 atm. in all combustion experiments. The combustions were initiated at temperatures such that the final temperatures were in each case very nearly 25°. The calorimetric observations were made in the usual way.[5,9]

Comparison Experiments. The apparent energy equivalent of the calorimetric system was determined by a series of comparison experiments.[5] The samples in these experiments consisted of benzoic acid and paraffin oil; the amounts were adjusted to give an evolution of energy and a quantity of carbon dioxide both nearly the same as in the combustion of the chlorine compound. The bomb initially contained an aqueous solution of hydrazine dihydrochloride and hydrochloric acid (or arsenious oxide, arsenic oxide, and hydrochloric acid) which, upon dilution with the water produced by combustion of the sample, produced a solution of nearly the same amount and concentration as obtained from combustion of the chlorine compound. The paraffin oil was contained in small Pyrex containers placed on top of the benzoic acid pellets in the Vycor crucibles. Comparison experiments were used because of a lack of experimental data necessary for corrections to standard states.[8] In particular, the solubility and heat of solution of carbon dioxide in solutions of arsenious oxide–arsenic oxide–hydrochloric acid and in solutions of hydrazine dihydrochloride–hydrochloric acid as a function of concentration have not been measured.

Analytical Procedures. At the conclusion of the calorimetric part of the experiment, the bomb was discharged and the contents were rinsed with hot water into a beaker. The entire solution then was titrated with standard iodine solution. The solution was transferred to a 500-ml. volumetric flask and made up to volume; aliquots were taken for further analysis. In experiments with hydrazine dihydrochloride as the reducing agent, ammonium ion was determined by Kjeldahl distillation. Immediately afterward, and in the same apparatus, nitrate ion was determined by Devarda's method. In experiments with arsenious oxide as the reducing agent, only nitrate ion was determined, again by Devarda's method.

The platinum ignition wire remained intact in about half of the experiments, so it was possible to show that no corrosion of the platinum occurred, by weighing the wire before and after the experiments. A qualitative test for gold in the solutions from trial combustions gave negative results.

Results

Units of Measurement and Auxiliary Quantities. All data reported are based on the 1961 atomic weights,[10] the 1951 fundamental constants,[11] and the definitions: $0^\circ C. = 273.15^\circ K.$; 1 cal. $= 4.184$ joules (exactly). The laboratory standard weights had been calibrated at the National Bureau of Standards. For use in reducing weights in air to *in vacuo*, and in correcting to standard states, the following values were used for physical properties of tetrachloro-p-xylene: density, $\rho = 1.688$ g. ml.$^{-1}$; specific heat, $c_p = 0.289$ cal. deg.$^{-1}$ g.$^{-1}$; and $(\partial E/\partial P)_T = -0.0028$ cal. atm.$^{-1}$ g.$^{-1}$. The density value is from measurements of a pellet; others are estimates. The value used for the heat of reaction 6 (see Discussion) was that of Bjellerup, Sunner, and Wadsö,[12] -77.4 ± 0.1 kcal. mole^{-1}. Values used for heats of reactions 7 and 8 were -132.68 kcal. mole^{-1} and $+4.25$ kcal. mole^{-1}, respectively, as given by Smith and Hubbard.[2] To compute the value of the standard heat of formation of tetrachloro-p-xylene, the following values were used for the standard heats of formation of carbon dioxide, water, and hydrochloric acid, in kcal. mole^{-1}: $CO_2(g)$, -94.0517; $H_2O(l)$, -68.3149; $HCl(in\ 14\text{-}H_2O)$, -38.975; and $HCl(in\ 85H_2O)$, -39.687. These values are from N.B.S. Circular 500^{13} with

(8) W. N. Hubbard, D. W. Scott, and G. Waddington, "Experimental Thermochemistry," Vol. I, F. D. Rossini, Ed., Interscience Publishers, Inc., New York, N. Y., 1956, Chapter 5, pp. 75-128.

(9) W. N. Hubbard, C. Katz, and G. Waddington, *J. Phys. Chem.*, **58**, 142 (1954).

(10) A. E. Cameron and E. Wichers, *J. Am. Chem. Soc.*, **84**, 4175 (1962).

(11) F. D. Rossini, F. T. Gucker, Jr., H. L. Johnston, L. Pauling, and G. W. Vinal, *ibid.*, **74**, 2699 (1952).

(12) L. Bjellerup, S. Sunner, and I. Wadsö, *Acta Chem. Scand.*, **11**, 1761 (1957).

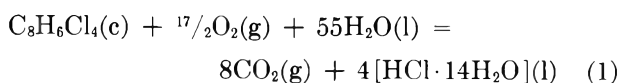**Table I:** Summary of Typical Calorimetric Experiments[a]

	Reducing agent	
	$N_2H_4 \cdot 2HCl$	As_2O_3
	Comparison experiments	
m'(benzoic acid), g.	0.73407	0.41740
m''(oil), g.	0.30490	0.12145
m''''(fuse), g.	0.00116	0.00121
$n^i(H_2O)$, mole	0.5135	1.3626
$n^i(HCl)$, mole	0.03961	0.01630
$n^i(N_2H_4 \cdot 2HCl)$, mole	0.0004676	
$n^i(As_2O_3)$, mole		0.0004637
$n^i(As_2O_5)$, mole		0.0017902
m(Vycor), g.	0.38078	0.38665
m(Pyrex), g.	0.05728	0.05395
Δt_c, deg.	1.99551	0.98969
$n^f(NH_4Cl)$, mole	0	
$n^f(N_2H_4 \cdot 2HCl)$, mole	0.004552	
$n^f(As_2O_3)$, mole		0.0004461
$m'\Delta Ec°/M$(benzoic acid), cal.	−4634.16	−2635.03
$m''\Delta Ec°/M$(oil), cal.	−3348.97	−1333.99
$m''''\Delta Ec°/M$(fuse), cal.	−4.70	−4.90
$-\Delta E^f_{dec}(HNO_3)$, cal.	−0.18	−0.33
$-\Delta E$, cor. to std. states, cal.	−9.93[b]	−8.28[c]
$-\Delta E_{ign}$, cal.	−0.74	−0.48
$-\Delta E^f_{oxid}(NH_4Cl)$, cal.	0.00	
$-\Delta E^f_{red}(N_2{}^*)$, cal.	−1.64	
$-\Delta E^f_{decomp}(As_2O_5)$, cal.		−1.37
ε(cont.)(Δt_c),[d] cal.	21.92	26.03
ε_{app}(calor.)($-\Delta t_c$), cal.	−7879.40	−3958.35
ε_{app}(calor.), cal. deg.$^{-1}$	3998.18	3999.59
	Combustion experiments[e]	
$m'(C_8H_6Cl_4)$, g.	1.95145	0.99604
m''''(fuse), g.	0.00110	0.00121
m(Vycor), g.	0.54878	0.47834
Δt_c, deg.	1.99234	0.98835
$n^f(NH_4Cl)$, mole	0.0001478	
$n^f(N_2H_4 \cdot 2HCl)$, mole	0.0004411	
$n^f(As_2O_3)$, mole		0.0004631
ε_{app}(calor.)($-\Delta t_c$), cal.	−7966.63[f]	−3952.25[g]
ε(cont.)($-\Delta t_c$), cal.	−25.12	−27.09
ΔE_{ign}, cal.	0.67	0.85
ΔE, cor. to std. states, cal.	8.89[b]	8.22[c]
$\Delta E^f_{dec}(HNO_3)$, cal.	1.18	0.23
$\Delta E^f_{oxid}(NH_4Cl)$, cal.	−0.63	
$\Delta E^f_{red}(N_2{}^*)$, cal.	508.47	
$\Delta E^f_{decomp}(As_2O_5)$, cal.		138.39
$-m''''\Delta Ec°/M$(fuse), cal.	4.46	4.90
$m'\Delta Ec°/M(C_8H_6Cl_4)$, cal.	−7468.71	−3826.75
$\Delta Ec°/M(C_8H_6Cl_4)$, cal. g.$^{-1}$	−3827.26	−3841.96

[a] The symbols and abbreviations in this table are those of ref. 8 except as noted. [b] Items 81–85, 87–91, 91c, 93, and 94 of the computation form of ref. 8. [c] Items 81–85, 87–91, 91b, 93, and 94 of the computation form of ref. 8. [d] ε^i(cont.)(t_i − 25°) + ε^f(cont.)(25° − t_f + t_{cor}). [e] 9.97₆ ml. of 0.4357₇ M N_2H_4·2HCl solution added to bomb for experiments with this reducing agent; 24.99₆ ml. of 0.0900₆ M As_2O_3 solution added to bomb for experiments with As_2O_3. [f] Calculated from average value of ε_{app}(calor.), 3998.63 cal. deg.$^{-1}$, from eight comparison experiments. [g] Calculated from average value of ε_{app}(calor.), 3998.84 cal. deg.$^{-1}$, from eight comparison experiments.

corrections for changes in molecular weights of CO_2 and H_2O.

Reduction to Standard States. The computation forms of Hubbard, Scott, and Waddington[8] were used to reduce experimental results to standard states. In several instances, it was necessary to estimate numerical data used in the computation forms.

Calorimetric Results. Detailed results of calorimetric experiments selected as typical with each reducing agent are given in Table I. The results of eight experiments with each reducing agent are shown in Table II. The value of $\Delta Ec°/M$ obtained from experiments with hydrazine dihydrochloride as the reducing agent refers to the reaction

$$C_8H_6Cl_4(c) + {}^{17}/_2O_2(g) + 55H_2O(l) =$$
$$8CO_2(g) + 4[HCl \cdot 14H_2O](l) \quad (1)$$

The value of $\Delta Ec°/M$ obtained from experiments with arsenious oxide as the reducing agent refers to the reaction

$$C_8H_6Cl_4(c) + {}^{17}/_2O_2(g) + 339H_2O(l) =$$
$$8CO_2(g) + 4[HCl \cdot 85H_2O](l) \quad (2)$$
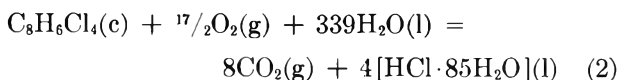
Table II: Summary of Experimental Results

	Reducing agent	
	$N_2H_4 \cdot 2HCl$	As_2O_3
$\Delta Ec°/M(C_8H_6Cl_4)$,	−3827.26	−3841.96
cal. g.$^{-1}$	−3828.11	−3841.14
	−3827.95	−3841.70
	−3828.82	−3841.41
	−3827.52	−3841.19
	−3828.00	−3840.71
	−3825.15	−3841.66
	−3827.24	−3841.50
Mean value	−3827.51[a]	−3841.41[b]
Std. dev. of the mean	±0.38	±0.14

[a] For reaction 1. [b] For reaction 2.

Derived Results. The molal values of $\Delta Ec°$, the standard change in internal energy, and $\Delta Hc°$, the standard heat of combustion, are given in Table III. The uncertainties given are the "uncertainty intervals" equal to twice the final over-all standard deviation of the mean.[14]

(13) F. D. Rossini, D. D. Wagman, W. H. Evans, S. Levine, and I. Jaffe, "Selected Values of Chemical Thermodynamic Properties," National Bureau of Standards Circular 500, U. S. Govt. Printing Office, Washington, D. C., 1952.

(14) F. D. Rossini, "Experimental Thermochemistry," Vol. I, F. D. Rossini, Ed., Interscience Publishers, Inc., New York, N. Y., 1956, Chapter 14, pp. 297–320.

Table III: Comparison of Results

| | Reducing agent | |
	$N_2H_4 \cdot 2HCl$	As_2O_3
$\Delta Ec°$ (eq. 1)	-933.72 ± 0.21 kcal. mole^{-1}	
(eq. 2)		-937.11 ± 0.14 kcal. mole^{-1}
$\Delta Hc°$ (eq. 1)	-934.02 ± 0.21	
$\Delta H°_{diln}{}^a$	-2.85	
$\Delta Hc°$ (eq. 2)	-936.87 ± 0.21	-937.41 ± 0.14
$\Delta Hf°(c)^b$		-42.06

^{a} According to the reaction $4[HCl \cdot 14H_2O](l) + 234H_2O(l) = 4[HCl \cdot 85H_2O](l)$; data from N.B.S. Circular 500.[13] ^{b} Based on experiments with As_2O_3.

Discussion

Chemistry of the Bomb Process. When a compound containing carbon, hydrogen, and chlorine is burned in an oxygen bomb, the following reactions occur

$$C_aH_bCl_d(c \text{ or } l) + [a + (b - d)/4]O_2(g) +$$
$$[dn - (b - d)/2]H_2O(l) =$$
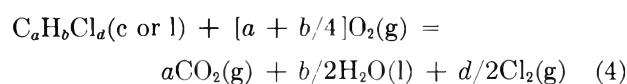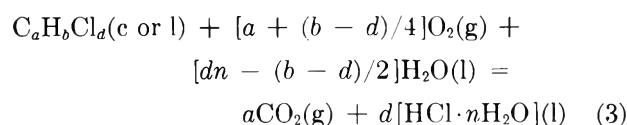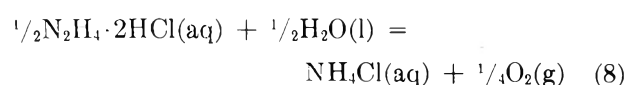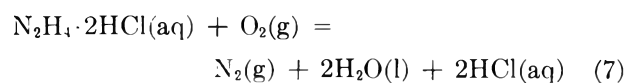$$aCO_2(g) + d[HCl \cdot nH_2O](l) \quad (3)$$

$$C_aH_bCl_d(c \text{ or } l) + [a + b/4]O_2(g) =$$
$$aCO_2(g) + b/2H_2O(l) + d/2Cl_2(g) \quad (4)$$

If arsenious oxide is present in the bomb, the following reaction also occurs

$$d/2Cl_2(g) + d/4As_2O_3(aq) + d/2H_2O(l) =$$
$$d/4As_2O_5(aq) + dHCl(aq) \quad (5)$$
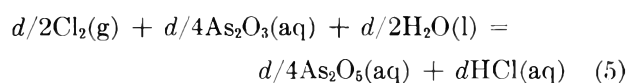
From an examination of these stoichiometric relations, it may be seen that a quantitative description of the reactions occurring is given by considering that all of the organic chlorine compound reacts according to eq. 3, and that all of the arsenious oxide reacts according to the equation

$$d/4As_2O_3(aq) + d/4O_2(g) = d/4As_2O_5(aq) \quad (6)$$
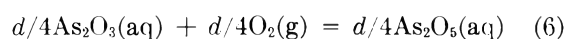
Similarly, if hydrazine dihydrochloride is present in the bomb, a quantitative description of the bomb process is given by considering that all of the organic chlorine compound reacts according to eq. 3, and that the hydrazine dihydrochloride reacts according to the equations

$$N_2H_4 \cdot 2HCl(aq) + O_2(g) =$$
$$N_2(g) + 2H_2O(l) + 2HCl(aq) \quad (7)$$

$$^1/_2N_2H_4 \cdot 2HCl(aq) + ^1/_2H_2O(l) =$$
$$NH_4Cl(aq) + ^1/_4O_2(g) \quad (8)$$

Thus, with the proper thermochemical corrections for reactions 6, 7, and 8, one may relate the observed energy evolution to eq. 3, the idealized combustion reaction.

Evaluation of Reducing Agents. Preliminary tests of the stabilities of hydrazine dihydrochloride and arsenious oxide under bomb conditions were performed in each of two bombs, Ta-1 described above and a platinum-lined bomb of similar construction. Aliquots of standard solutions of the reducing agents were placed in the bombs and the bombs were closed and charged with oxygen to 30 atm.. After various periods of time, the bombs were discharged, opened, and rinsed. The resulting solutions then were titrated with standard iodine solution. Quantitative recovery of arsenious oxide was obtained from both bombs. Quantitative recovery of hydrazine dihydrochloride was obtained only from the tantalum-lined bomb. It was concluded that platinum catalyzes a decomposition reaction of hydrazine dihydrochloride; and that this combination of reducing agent and bomb lining material must be avoided in precision combustion calorimetry of organic chlorine compounds. This situation places a severe restriction on the use of hydrazine dihydrochloride for this purpose.

A potential advantage associated with the use of hydrazine dihydrochloride is its high solubility in water. A relatively small aliquot of hydrazine dihydrochloride solution placed in the bomb will suffice to reduce the free chlorine, and with a small volume of solution the problem of homogeneity with respect to gas solubilities is reduced. However, for several reasons, arsenious oxide has proved to be the preferred reducing agent. Homogeneity is assured through the use of a rotating-bomb calorimeter, despite a large volume of bomb solution. The thermal effect associated with the reduction of chlorine by arsenious oxide is only about one-half that involved in the use of hydrazine dihydrochloride, on a molar basis. Finally, both the chemistry and thermochemistry of arsenious oxide are better defined. In related work, the authors have noted that the amount of ammonium chloride found in the bomb at the conclusion of experiments with hydrazine dihydrochloride varies widely for as yet unknown reasons.

As seen in Table III, the results obtained with the two reducing agents differ by 0.54 kcal. mole^{-1}, and the sum of the uncertainties is only 0.35 kcal. mole^{-1}. The N.B.S. Circular 500[13] value for the heat of formation of $N_2H_4 \cdot 2HCl(aq)$, -84.0 kcal. mole^{-1}, is apparently the average of three values cited by Roth[15]:

(15) W. A. Roth, *Z. Elektrochem.*, **50**, 111 (1944).

−83.2, −82.7, and −86.2 kcal. mole⁻¹. Thus the uncertainty in the heat of formation of $N_2H_4 \cdot 2HCl$-(aq) might explain the difference obtained with the two reducing agents. The results of this work favor a more negative value for the heat of formation of $N_2H_4 \cdot 2HCl(aq)$.

Tetrachloro-p-xylene as a Reference Substance. As discussed by Beckers,[16] a reference substance must satisfy certain minimum requirements: (1) it should be obtainable in a pure state; (2) it should be stable; (3) it should not be hygroscopic; (4) it should not be too volatile; (5) it should be easily compressed into pellets; and (6) it should ignite readily and burn completely in the bomb. Tetrachloro-p-xylene is unstable at its melting point, making purification by zone melting questionable, and its crystal habit does not favor purification by recrystallization. The last four requirements listed above are fulfilled by tetrachloro-p-xylene; however, in the absence of a suitable method of purification, this compound is not proposed as a reference substance. Several organic chlorine compounds have been studied in this laboratory for possible use as reference substances in combustion calorimetry; no entirely satisfactory compound has yet been found.

(16) M. Beckers, *Bull. soc. chim. Belges,* **40**, 871 (1931).

The Heats of Combustion, Sublimation, and Formation

of Four Dihalobiphenyls[1]

by N. K. Smith, G. Gorin,

Department of Chemistry, Oklahoma State University, Stillwater, Oklahoma

W. D. Good, and J. P. McCullough

Contribution No. 131 from the Thermodynamics Laboratory of the Bartlesville Petroleum Research Center, Bureau of Mines, U. S. Department of the Interior, Bartlesville, Oklahoma   (*Received November 1, 1963*)

The structure and energetics of dihalobiphenyls were investigated by thermochemical methods. Heats of combustion of four dihalobiphenyls were determined by rotating-bomb combustion calorimetry, and the vapor pressure of each was measured by the Knudsen effusion technique. The following values, in kcal. mole^{-1}, are reported for the heat of formation in the vapor state, $\Delta Hf°_{298.15}$, from graphite and gaseous hydrogen, fluorine, and chlorine: 2,2'-difluorobiphenyl, -45.4; 4,4'-difluorobiphenyl, -46.5; 2,2'-dichlorobiphenyl, $+30.4$; and 4,4'-dichlorobiphenyl, $+28.8$. The results are shown to be consistent with known values of interplanar angles of the molecules and earlier calculations of delocalization energy.

Introduction

Electron diffraction, dipole moment, and other kinds of studies have shown that biphenyl and its derivatives exist in the gas state with the phenyl rings in a non-ooplanar configuration.[2] The angle between the rings, measured with respect to rotation about the central C–C' bond, increases with increasing size of substituent groups in the 2,2'-positions. Resonance conjugation between the rings would be greatest when the rings are coplanar and also should vary with the size of substituents in the 2,2'-positions. The development of precision methods for combustion calorimetry of organic halogen compounds[3,4] has made possible an experimental study of the effects of 2,2'-substituents on the extra delocalization energy resulting from conjugation between the rings of biphenyl.

In this research, the heats of combustion and formation of 2,2'- and 4,4'-difluorobiphenyl and of the corresponding dichlorobiphenyls were determined by rotating-bomb calorimetry and vapor pressure measurements. The angle between the rings in each 4,4'-derivative is approximately the same as in biphenyl; thus, the observed differences in energy between the isomers should be greater for the chloro compounds because the greater size of the substituents forces a greater deviation from coplanarity. The experimental results confirm this supposition and provide an experimental verification of some theoretical calculations of delocalization energy in biphenyls.

Experimental

Calorimetric Apparatus and Procedures. The rotating-bomb calorimeter BMR-2 has been described.[5] Platinum-lined bomb Pt-3b,[6] internal volume 0.353 l., was used for the experiments with the difluorobiphenyls. Tantalum-lined bomb Ta-1,[4] internal vol-

(1) Abstracted from the Ph.D. thesis submitted by N. K. Smith to the Graduate School of Oklahoma State University.

(2) G. H. Beaven and D. M. Hall, *J. Chem. Soc.*, 4637 (1956).

(3) W. D. Good and D. W. Scott, "Experimental Thermochemistry," Vol. II, H. A. Skinner, Ed., Interscience Publishers, Inc., New York, N. Y., 1962, Chapter 2, pp. 15–39.

(4) N. K. Smith, D. W. Scott, and J. P. McCullough, *J. Phys. Chem.*, **68**, 934 (1964).

(5) W. D. Good, D. W. Scott, and G. Waddington, *ibid.*, **60**, 1080 (1956).

(6) W. D. Good, D. R. Douslin, D. W. Scott, A. George, J. L. Lacina, J. P. Dawson, and G. Waddington, *ibid.*, **63**, 1133 (1959).

ume 0.341 l., was used for the experiments with the dichlorobiphenyls.

The basic procedures used in this investigation for the combustion calorimetry of organic fluorine compounds have been described.[3] The volatility of the difluorobiphenyls was judged to be of borderline significance; therefore, pellets of these compounds were sealed in polyester bags to prevent loss of sample.[7] In all experiments with the difluorobiphenyls, the bomb initially contained 10 ml. of water. For the comparison experiments,[3] a solution of HF was put into the bomb initially in such amount and concentration that the solution obtained after combustion was nearly the same as that produced in the combustion of the difluorobiphenyls.

The procedures used for the combustion calorimetry of the dichlorobiphenyls are described in the preceding paper.[4] Sample confinement was not necessary. In all experiments with the dichlorobiphenyls, the bomb initially contained 9.97$_6$ ml. of 0.1156$_3$ M hydrazine dihydrochloride solution. For the comparison experiments, the bomb initially contained a solution of hydrazine dihydrochloride and hydrochloric acid, which upon dilution with the water produced by combustion of the sample, produced a solution of nearly the same amount and concentration as that obtained from combustion of the dichlorobiphenyls.

Combustion calorimetry of the dichlorobiphenyls was done before the work reported in the preceding paper[4] showed that arsenious oxide is superior to hydrazine dihydrochloride as a reducing agent. The uncertainty about the thermochemistry of hydrazine dihydrochloride discussed in that paper affects the accuracy of the present results; however, they are reported in enough detail that they can be revised, if necessary, whenever better thermochemical data for hydrazine dihydrochloride become available. The results for the 2,2'- and 4,4'-compound are affected nearly the same, so the *difference* between the heats of formation reported here would be unchanged by such a revision.

Vapor Pressure Apparatus and Procedures. The vapor pressures of the four dihalobiphenyls were measured by the Knudsen effusion method.[8,9] The effusion cells, made of aluminum with brass lids and polytetrafluoroethylene gaskets, weighed about 8 g. The areas of the two orifices used were computed from measurements of their diameters and the assumption that the orifices were circular. The diameters were measured with a microscope-stage micrometer, with a traveling microscope, and with an optical comparator; an average of the values so obtained was used in the calculations. The rate of effusion was

determined by weighing the cells before and after evacuation for a known period of time. Timing of the experiments (using an electric timer) was started when a Pirani gage indicated a pressure of 10^{-3} mm. and stopped when air was admitted into the system through the same three-way stopcock through which the system was evacuated. The cells were contained in a metal vacuum chamber that was immersed in a bath thermostatically controlled to ±0.001°. Temperatures were measured with a platinum resistance thermometer and a Mueller bridge.

Before measurements were made on a sample, it was subjected to a preliminary process of evacuation for 1 hr.

Materials. The 2,2'- and 4,4'-difluorobiphenyl were synthesized by Drs. H. B. Gottlieb and J. D. Park of the University of Colorado Chemistry Department. Elemental analyses of the two compounds were: Calcd. for $C_{12}H_8F_2$: C, 75.78; H, 4.24; F, 19.98. Found for 2,2'-difluorobiphenyl: C, 75.90; F, 19.65. Found for 4,4'-difluorobiphenyl: C, 75.55; H, 4.49; F, 19.89. Both compounds were further purified by J. L. Lacina of this Center using a zone-melting procedure.[5] An indicator–impurity dye, initially present at a concentration of 0.01 wt. %, was completely removed from the 2,2'-difluorobiphenyl sample used for combustion experiments; some of the dye remained in the final sample of 4,4'-difluorobiphenyl.

Commercial samples of 2,2'- and 4,4'-dichlorobiphenyl were purified by recrystallization from methanol and toluene, respectively, and further purification was attempted by zone melting. The indicator–impurity dye was removed from three-quarters of the 4,4'-dichlorobiphenyl after eight passes of the molten zone. The 2,2'-dichlorobiphenyl was not purified by zone melting. The materials were analyzed by combustion in an oxygen bomb in the presence of arsenious oxide and determination of the chlorine as silver chloride. *Anal.* Calcd. for $C_{12}H_8Cl_2$: Cl, 31.78. Found for 2,2'-dichlorobiphenyl: Cl, 31.75. Found for 4,4'-dichlorobiphenyl: Cl, 31.84.

Gas–liquid chromatographic analysis of the biphenyls[10] showed no impurity peaks for the difluorobi-

(7) J. L. Lacina, W. D. Good, and J. P. McCullough. *J. Phys. Chem.*, **65**, 1026 (1961).

(8) G. W. Thompson, "Physical Methods of Organic Chemistry," Third Ed., A. Weissberger, Ed., Interscience Publishers, Inc., New York, N. Y., 1959, Chapter IX, Part 1.

(9) J. L. Margrave, "Physico-Chemical Measurements at High Temperatures," J. O'M. Bockris, J. L. White, and J. D. Mackenzie, Ed., Academic Press, Inc., New York, N. Y., 1959, Chapter 10.

(10) H. Weingarten, W. D. Ross, J. M. Schlater, and G. Wheeler, Jr., *Anal. Chim. Acta*, **26**, 391 (1962).

Table I: Summary of Typical Combustion Experiments[a]

	2,2'-Difluoro-biphenyl	4,4'-Difluoro-biphenyl	2,2'-Dichloro-biphenyl	4,4'-Dichloro-biphenyl
Comparison experiments[b]				
m'(benzoic acid), g.	0.99111	0.99425	0.91669	
m''(oil), g.	0.15906	0.15737	0.19973	
m''''(fuse), g.	0.00113	0.00111	0.00127	
$n^i(H_2O)$, mole	0.5353	0.5358	0.5301	
$n^i(HF)$, mole	0.01079	0.01079		
$n^i(HCl)$, mole			0.01250	
$n^i(N_2H_4 \cdot 2HCl)$, mole			0.0004211	
m(Vycor), g.			0.46698	
m(Pyrex), g.			0.03186	
Δt_c, deg.	1.99652	1.99686	1.99416	
$n^f(NH_4Cl)$, mole			0.0582	
$n^f(N_2H_4 \cdot 2HCl)$, mole			0.0004110	
$m'\Delta Ec°/M$(benzoic acid), cal.	−6256.85	−6276.67	−5787.04	
$m''\Delta Ec°/M$(oil), cal.	−1747.15	−1728.58	−2193.80	
$m''''\Delta Ec°/M$(fuse), cal.	−4.58	−4.50	−5.14	
$−\Delta E^f_{dec}(HNO_3)$, cal.	−3.82	−3.85	−0.25	
$−\Delta E$, cor. to std. states, cal.	−9.99[c]	−10.04[c]	−9.56[d]	
$−\Delta E_{ign}$, cal.	−0.41	−0.38	−0.71	
$−\Delta E^f_{oxid}(NH_4Cl)$, cal.			0.03	
$−\Delta E^f_{red}(N_2{}^*)$, cal.			−0.80	
ε(cont.)(Δt_c),[e] cal.	26.37	26.21	23.97	
ε_{app}(calor.)($−\Delta t_c$), cal.	−7996.43	−7997.81	−7973.30	
ε_{app}(calor.), cal. deg.$^{-1}$	4005.18	4005.19	3998.32	
Combustion experiments				
m'(compound), g.	1.02633	1.02616	1.24371	1.24367
m'''(polyester), g. (at % rel. hum.)	0.06679 (54)	0.06739 (58)		
m''''(fuse), g.	0.00106	0.00112	0.00109	0.00119
$n^i(H_2O)$, mole	0.5530	0.5530		
m(Vycor), g.			0.51370	0.34636
Δt_c, deg.	1.99660	1.99727	2.00207	1.99504
$n^f(NH_4Cl)$, mole			0.0000365	0.0000442
$n^f(N_2H_4 \cdot 2HCl)$, mole			0.0004161	0.0004194
ε_{app}(calor.)($−\Delta t_c$), cal.	−7996.20[f]	−7999.05[g]	−8004.52[h]	−7976.41[h]
ε(cont.)($−\Delta t_c$),[e] cal.	−26.78	−26.78	−25.51	−25.35
ΔE_{ign}, cal.	0.41	0.60	0.76	0.47
ΔE, cor. to std. states, cal.	10.25[c]	10.25[c]	9.58[d]	9.59[d]
$\Delta E^f_{dec}(HNO_3)$, cal.	3.40	3.76	0.33	0.30
$\Delta E^f_{oxid}(NH_4Cl)$, cal.			−0.16	−0.19
$\Delta E^f_{red}(N_2{}^*)$, cal.			95.42	94.47
$−m'''\Delta Ec°/M$(polyester), cal.	364.84	368.05		
$−m''''\Delta Ec°/M$(fuse), cal.	4.29	4.54	4.41	4.82
$m'\Delta Ec°/M$(compound), cal.	−7639.79	−7638.63	−7919.69	−7892.30
$\Delta Ec°/M$(compound), cal. g.$^{-1}$	−7443.79	−7443.90	−6367.79	−6345.98

[a] The symbols and abbreviations of this table are those of ref. 11, except as noted. [b] One series of comparison experiments was used for both series of combustion experiments with the dichlorobiphenyls. [c] Items 81–85 incl., 87–91 incl., 93, and 94 of the computation form of ref. 3. [d] Items 81–85 incl., 87–91 incl., 91c, 93, and 94 of the computation form of ref. 11. [e] ε^i(cont.)($t_i - 25°$) + ε^f(cont.)(25° − t_f + Δt_{corr}). [f] Calculated from average value of ε_{app}(calor.), 4004.91 cal. deg.$^{-1}$, from eight comparison experiments. [g] Calculated from average value of ε_{app}(calor.), 4004.99 cal. deg.$^{-1}$, from six comparison experiments. [h] Calculated from average value of ε_{app}(calor.), 3998.12 cal. deg.$^{-1}$, from eight comparison experiments.

phenyls or for 4,4'-dichlorobiphenyl. An impurity with a relative retention time corresponding to that of 2-chlorobiphenyl was found in the 2,2'-dichlorobiphenyl. Comparison of peak areas indicated the im-

purity to be present to the extent of 0.50 ± 0.05%. These analyses were performed by H. J. Coleman of this Center.

The benzoic acid used was National Bureau of

Standards sample 39h, with a certified heat of combustion of 26,434 ± 3 abs. joules g.$^{-1}$. Conversion from certificate conditions to standard conditions[11] gives -6312.97 ± 0.72 cal. g.$^{-1}$ for $\Delta Ec^\circ/M$, the energy of the idealized combustion reaction.

The samples of auxiliary oil, polyester film, and cotton thread fuse material have been described.[5,6] Values of $\Delta Ec^\circ/M$ for the auxiliary oil obtained chronologically near the experiments with the difluorobiphenyls and the dichlorobiphenyls were $-10,984.2 \pm 0.5$ and $-10,983.8 \pm 0.2$ cal. g.$^{-1}$, respectively.
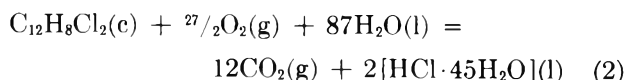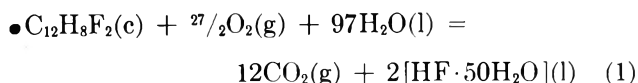
The samples of hydrazine dihydrochloride and iodine are described in the preceding paper.[4]

Results

Units of Measurement and Auxiliary Quantities. All data reported are based on the 1961 atomic weights,[12] the 1951 fundamental constants,[13] and the definitions: $0^\circ C. = 273.15^\circ K.$; 1 cal. = 4.184 joules (exactly). The laboratory standard weights had been calibrated at the National Bureau of Standards. For use in reducing weights in air to *in vacuo*, the following values were used for the densities of the materials: 2,2'-$C_{12}H_8F_2$, 1.331; 4,4'-$C_{12}H_8F_2$, 1.336[14]; 2,2'-$C_{12}H_8Cl_2$, 1.349; and 4,4'-$C_{12}H_8Cl_2$, 1.439 g. ml.$^{-1}$.[14] The values for the 2,2'-compounds were determined from measurements on pellets. In correcting the energy of the actual bomb process to the isothermal bomb process and in correcting to standard states, estimates of 0.385 cal. deg.$^{-1}$ g.$^{-1}$ and -0.0028 cal. atm.$^{-1}$ g.$^{-1}$ were used for specific heat and $(\partial E/\partial P)_T$, respectively, for each compound. The thermochemical corrections applied for the reaction of hydrazine dihydrochloride were the same as in the preceding paper.[4]

Reduction to Standard States. The computation form of Good and Scott[3] was followed for reduction to standard states of the data obtained for the fluorine compounds. Reduction to standard states for the chlorine compounds was done as prescribed by Hubbard, Scott, and Waddington,[11] who discuss the modifications necessary to make their detailed correction scheme devised for sulfur compounds applicable to chlorine compounds. Reliable experimental values for some of the numerical quantities that enter into the corrections are lacking; estimates were made in these instances.

Calorimetric Results. Table I lists the detailed results of representative calorimetric experiments for each dihalobiphenyl. The results refer to the reactions

$$\bullet C_{12}H_8F_2(c) + {}^{27}/_2 O_2(g) + 97H_2O(l) =$$
$$12CO_2(g) + 2[HF \cdot 50H_2O](l) \quad (1)$$

$$C_{12}H_8Cl_2(c) + {}^{27}/_2 O_2(g) + 87H_2O(l) =$$
$$12CO_2(g) + 2[HCl \cdot 45H_2O](l) \quad (2)$$

HF recovery from the combustion experiments with the difluorobiphenyls averaged 100.1% of theoretical. The results of all experiments are summarized in Table II.

Vapor Pressure Results. Measurements of the effusion cell orifices yielded the following values, in cm.: orifice A, diameter 0.0666 ± 0.0003, length (thickness of lid) 0.0160 ± 0.0005; orifice B, diameter 0.0537 ± 0.0002, length 0.0130 ± 0.0005. Values of the Clausing factor, interpolated from the table of Dushman,[15] were 0.8075 and 0.8068 for orifices A and B, respectively.

The experimental data and calculated vapor pressures are shown in Table III. The vapor pressures were calculated from the equation

$$p = \frac{W}{aKt} \sqrt{\frac{2\pi RT}{M}}$$

where p is the vapor pressure, W the weight loss over a corresponding time t, a the area of the orifice, R the gas constant, T the absolute temperature, M the molecular weight of the effusing species, and K the Clausing factor. The effect of the impurity in the sample of 2,2'-dichlorobiphenyl was neglected in the vapor pressure calculations.

To calculate heats of sublimation, equations of the form $\log p = a + b/T$ (p in mm. and T in $^\circ K.$) were fitted to the vapor pressure data by the method of least squares. The equations are as follows: 2,2'-$C_{12}H_8F_2$, $\log p = 13.880 - 4967/T$; 4,4'-$C_{12}H_8F_2$, $\log p = 13.584 - 4771/T$; 2,2'-$C_{12}H_8Cl_2$, $\log p = 13.837 - 5019/T$; 4,4'-$C_{12}H_8Cl_2$, $\log p = 13.460 - 5416/T$. The heats of sublimation were calculated from the vapor pressure equations by application of the Clausius–Clapeyron equation.

Derived Results. To correct for the presence of 2-chlorobiphenyl in the sample of 2,2'-dichlorobiphenyl, a value for the heat of combustion of the former was estimated as follows: Brüll[16] gives the value -7697.9

(11) W. N. Hubbard, D. W. Scott, and G. Waddington, "Experimental Thermochemistry," Vol. I, F. D. Rossini, Ed., Interscience Publishers, Inc., New York, N. Y., 1956, Chapter 5, pp. 75–128.

(12) A. E. Cameron and E. Wichers, *J. Am. Chem. Soc.*, **84**, 4175 (1962).

(13) F. D. Rossini, F. T. Gucker, Jr., H. L. Johnston, L. Pauling, and G. W. Vinal, *ibid.*, **74**, 2699 (1952).

(14) N. A. Lange, "Handbook of Chemistry," Handbook Publishers, Inc., Sandusky, Ohio, 1956.

(15) S. Dushman, "Scientific Foundations of Vacuum Technique," John Wiley and Sons, New York, N. Y., 1949, p. 99.

(16) L. Brüll, *Gazz. chim. ital.*, **65**, 17 (1935).

Table II: Summary of Combustion Experiments

	Compound			
	2,2'-Difluoro-biphenyl	4,4'-Difluoro-biphenyl	2,2'-Dichloro-biphenyl	4,4'-Dichloro-biphenyl
$\Delta E_c^\circ / M$(compound), cal. g.$^{-1}$	−7444.48	−7443.90	−6366.34	−6345.98
	−7443.79	−7442.18	−6367.79	−6345.75
	−7444.18	−7444.20	−6367.50	−6345.59
	−7444.69	−7444.48	−6367.99	−6345.90
	−7444.44	−7443.52	−6367.78	−6345.54
	−7444.74	−7443.23	−6368.10	−6345.91
	−7444.87		−6367.95	−6345.10
	−7444.71		−6368.32	−6344.88
Mean value	−7444.49	−7443.58	−6367.72[a]	−6345.58
Std. dev. of the mean	±0.13	±0.34	±0.22	±0.14

[a] Uncorrected for 2-chlorobiphenyl impurity. See text.

Table III: Vapor Pressure Data for Dihalobiphenyls

T, °K.	Time, 10^3 sec.	Orifice A Weight loss, mg.	Orifice A Pressure, μ	Orifice B Weight loss, mg.	Orifice B Pressure, μ
2,2'-Difluorobiphenyl					
301.68	12.42	2.74	2.61	4.17	2.58
303.11	16.02	4.32	3.20	6.49	3.12
306.04	11.22	4.24	4.50	6.45	4.45
308.64	29.58	14.99	6.06	22.82	5.99
313.20	11.64	10.36	10.7	15.77	10.6
318.26	10.32	16.03	18.9	24.34	18.6
4,4'-Difluorobiphenyl					
294.92	11.34			3.73	2.50
298.99	26.70	9.69	4.27	14.98	4.29
303.24	10.14			9.13	6.93
303.24	7.20	4.43	7.30		
309.93	8.64	11.06	15.3	17.46	15.7
312.72	6.60	11.55	21.1	18.72	22.2
313.23	7.20			19.83	21.6
313.26	7.68	14.22	22.3		
318.60	3.60	12.11	40.9		
2,2'-Dichlorobiphenyl					
310.27	21.96	9.24	4.66	14.13	4.62
314.57	12.84	8.80	7.64	13.47	7.59
319.04	7.20	8.09	12.6	12.38	12.5
323.59	8.46	15.94	21.3	23.97	20.8
328.07	3.60	11.15	35.2	17.01	34.9
4,4'-Dichlorobiphenyl					
303.03	16.98	1.67	1.12	2.62	1.14
339.73	13.50	3.78	3.24	5.81	3.24
349.93	18.78	15.13	9.47	23.44	9.53
360.15	24.18	53.83	26.6	83.76	26.8

cal. g.$^{-1}$; correction for combustion to $HCl \cdot 90H_2O$ gives −7725 cal. g.$^{-1}$. The value obtained by adding the difference between the heats of combustion of ethylbenzene[17] and o-chloroethylbenzene[18] to that for

biphenyl[19] was −7695 cal. g.$^{-1}$. The average of the experimental and calculated values, −7710 cal. g.$^{-1}$, was used for the heat of combustion of 2-chlorobiphenyl. The following equation was then written, in which x is the heat of combustion of 2,2'-dichlorobiphenyl: $0.995x + 0.005(-7710) = -6367.72$. The solution is $x = -6360.97$ cal. g.$^{-1}$.

Table IV lists the derived results. The uncertainties shown for ΔE_c° and ΔH_c° are the uncertainty intervals equal to twice the final "over-all" standard deviation[20] except for 2,2'-dichlorobiphenyl, which has a larger uncertainty because of the impurity in the sample.

To compute the values of the standard heats of formation, the following values were used for the standard heats of formation of hydrochloric and hydrofluoric acids: HCl(in 45H$_2$O), −39.550 kcal. mole^{-1}; and HF(in 50H$_2$O), −75.660 kcal. mole^{-1}.[21] Values used for carbon dioxide and water are given in the preceding paper.[4]

Discussion

Comparison with Previous Work. The heats of combustion of 2,2'- and 4,4'-dichlorobiphenyl were found by Brüll[16] to be −6251.2 and −6231.5 cal. g.$^{-1}$,

(17) "Selected Values of Physical and Thermodynamic Properties of Hydrocarbons and Related Compounds," American Petroleum Institute Research Project 44, Carnegie Press, Pittsburgh, Pa., 1953, Table 5n.

(18) W. N. Hubbard, J. W. Knowlton, and H. M. Huffman, *J. Phys. Chem.*, **58**, 396 (1954).

(19) G. S. Parks and L. M. Vaughan, *J. Am. Chem. Soc.*, **73**, 2380 (1951).

(20) F. D. Rossini, "Experimental Thermochemistry," Vol. I, F. D. Rossini, Ed., Interscience Publishers, Inc., New York, N. Y., 1956, Chapter 14, pp. 297–320.

(21) F. D. Rossini, D. D. Wagman, W. H. Evans, S. Levine, and I. Jaffe, "Selected Values of Chemical Thermodynamic Properties," National Bureau of Standards Circular 500, U. S. Govt. Printing Office, Washington, D. C., 1952.

Table IV: Derived Thermochemical Data at 298.15°K., kcal. mole^{-1}

	State	2,2'-Difluoro-biphenyl	4,4'-Difluoro-biphenyl	2,2'-Dichloro-biphenyl	4,4'-Dichloro-biphenyl
$\Delta Ec°$	Crystal	-1415.90 ± 0.15^a	-1415.72 ± 0.22^a	-1419.16 ± 0.41^b	-1415.72 ± 0.15^b
$\Delta Hc°$	Crystal	-1416.79 ± 0.15^a	-1416.61 ± 0.22^a	-1420.05 ± 0.41^b	-1416.61 ± 0.15^b
$\Delta Hf°$	Crystal	-68.09	-68.27	$+7.39$	$+3.95$
ΔHs		$+22.7 \pm 1$	$+21.8 \pm 1$	$+23.0 \pm 1$	$+24.8 \pm 1$
$\Delta Hf°$	Gas	-45.4	-46.5	$+30.4$	$+28.8$

^{a} For eq. 1. ^{b} For eq. 2.

respectively. A static-bomb calorimeter was used and no details were given regarding the bomb solutions or the determination of final states within the bomb, but it is stated that the results were calculated for the formation of Cl_2 gas. With data from Circular 500,[21] the results reported here can be converted to the equation

$$C_{12}H_8Cl_2(c) + 14O_2(g) =$$
$$12CO_2(g) + 4H_2O(l) + Cl_2(g) \quad (3)$$
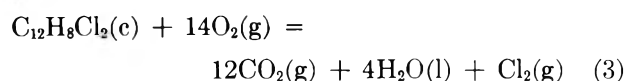
The results are -6313.8 cal. g.$^{-1}$ for 2,2'-dichlorobiphenyl and -6298.4 for the 4,4'-isomer. The results of this research are about 15 kcal. mole^{-1} more negative than Brüll's and they differ from one another by 1.0 kcal. mole^{-1} less.

Vapor Pressure Results. The agreement of the results from the two effusion cells is an indication that equilibrium vapor pressures were measured; the ratio of effective orifice areas of the two cells was 1.54. As may be seen from Table III, the smaller orifice gave slightly higher results for two of the four compounds, and slightly lower results for the other two.

The ratio of mean free path (λ) to orifice diameter (d) was calculated for these experiments, and the data given in Table III cover a range of λ/d ratios from 0.5 to 15. Data from experiments in which the λ/d ratio was below 0.5 were rejected because there was indication that the flow conditions through the orifice changed from molecular to viscous. The mean free paths were calculated from the relation

$$\lambda = \frac{kT}{\pi\sqrt{2}\sigma^2 p}$$

Values for σ, the collision diameter of the molecule, were obtained by taking the average of the three dimensions of the molecule calculated from the molecular parameters tabulated by Beaven and Hall.[2]

Energy Differences between Biphenyl Isomers. The characteristics of biphenyl and its derivatives pose an interesting question. Do the two benzene rings interact

in such a way as to reduce the energy of the molecule relative to benzene?

Theoretical calculations have been made of the hypothetical case in which the rings would be coplanar; these calculations have led to a delocalization energy of 6.1 kcal. mole^{-1}.[22] However, steric interference between the hydrogen atoms in the *ortho* positions forces the two rings out of the same plane; electron diffraction studies indicate an interplanar angle $\theta = 41.6°$.[23] Dewar[24,25] has suggested that the delocalization energy is proportional to $\cos^2 \theta$; the calculated delocalization energy of the actual biphenyl molecule then becomes 3.4 kcal. mole^{-1}. This value may be compared with the value 1.5 kcal. mole^{-1} obtained from Wheland's table,[26] with revisions utilizing more recent data for the heat of combustion[19] and heat of sublimation[27] of biphenyl.

The interplanar angles for 4,4'-difluoro-, 2,2'-difluoro-, and 2,2'-dichlorobiphenyl also have been measured.[28,29] For the first compound, the value is 44°, which is very similar to the angle in biphenyl, as should be expected; for the second and third compounds, the angles are, respectively, 60 and 74°, in accordance with the greater van der Waals radii of fluorine and chlorine. These data and the thermochemical energy differences found in this research can be used to calculate the delocalization energy, ΔE_p, for the hypothetical coplanar form, by the equation

$$\Delta E_p = \Delta E/(\cos^2 \theta - \cos^2 44°)$$

(22) A. Streitwieser, Jr., "Molecular Orbital Theory for Organic Chemists," John Wiley and Sons, New York, N. Y., 1955, p. 243.

(23) A. Almenningen and O. Bastiansen, *Kgl. Norske Videnskab. Selskabs. Skrifter*, 1 (1958); *Chem. Abstr.*, 53, 11917c (1959).

(24) M. J. S. Dewar. *J. Am. Chem. Soc.*, 74, 3345 (1952).

(25) L. L. Ingraham, "Steric Effects in Organic Chemistry," M. S. Newman, Ed., John Wiley and Sons, New York, N. Y., 1956, Chapter 11.

(26) G. Wheland, "Resonance in Organic Chemistry," John Wiley and Sons, New York, N. Y., 1955, p. 98.

(27) A. H. Jones. *J. Chem. Eng. Data*. 5, 196 (1960).

(28) O. Bastiansen. *Acta Chem. Scand.*, 4, 926 (1950).

(29) O. Bastiansen and L. Smedvik, *ibid.*, 8, 1593 (1954).

where ΔE is the observed energy difference. From Table IV, it may be seen that the 4,4'-dihalobiphenyls are more stable than the 2,2'-isomers, by 1.1 kcal. mole^{-1} for the difluoro compounds, and 1.6 kcal. mole^{-1} for the dichloro compounds. The results calculated from the above equation are 4.1 kcal. mole^{-1} for ΔE_p for the difluorobiphenyls and 3.6 kcal. mole^{-1} for the dichlorobiphenyls. A similar calculation for biphenyl, based on the experimental stabilization energy of 1.5 kcal. mole^{-1}, leads to the result 2.8 kcal. mole^{-1} for ΔE_p. Because the results of the present work were obtained from paired experiments, performed under nearly identical conditions, the uncertainty associated with the energy difference under discussion is much smaller than the uncertainties in the heats of formation.

In the calculations described above, the assumption is made that the entire difference in energy between the 2,2'- and 4,4'-isomer is caused by the distortion from coplanarity. A better approximation would correct for the stabilization attributable to the attraction between the 2,2'-substituent atoms. That such an attraction exists is shown by the fact that the halogen atoms are found in the *cis* rather than the *trans* position. A quantitative estimate of the energy involved is difficult to make, but it is expected to be smaller than the respective heats of vaporization of hydrogen,

carbon tetrafluoride, and carbon tetrachloride, and to parallel their increase in that order. This correction would bring the values of ΔE_p calculated from the data for the difluoro and the dichloro isomers closer together, but would increase the discrepancy between them and biphenyl.

Independent estimates of the stabilization energy of the planar form of biphenyl have been made in conjunction with calculations of rates of racemization of optically active biphenyls; Westheimer[30] has estimated a value of 3 kcal. mole^{-1}, and Howlett[31] reported 7 kcal. mole^{-1}. The accumulated evidence, considered together and with no attempt at a critical evaluation of the assumptions underlying each estimate, suggests the stabilization energy of a planar biphenyl structure relative to benzene is about 4 to 5 kcal. mole^{-1}

(30) F. H. Westheimer, "Steric Effects in Organic Chemistry," M. S. Newman, Ed., John Wiley and Sons, New York, N. Y., 1956, Chapter 12.
(31) K. E. Howlett, *J. Chem. Soc.*, 1055 (1960).

NOTES

The Heats of Formation of Trisilane and Trigermane[1]

by Stuart R. Gunn and LeRoy G. Green

Lawrence Radiation Laboratory, University of California; Livermore, California (Received September 13, 1963)

Simple bond energy additivity rules do not hold for light alkanes. Thus the standard heat of formation of CH_4[2] is -17.89 kcal. mole^{-1} and that of C_2H_6 is -20.24, an increment of -2.35 for the CH_2 group; C_3H_8 is -24.82, an increment of -4.59. The increment for straight-chain hydrocarbons becomes constant at -4.93 per CH_2 group only beyond *n*-pentane. Using 52.09 and 170.9 for the heats of atomization of hydrogen and carbon,[3] the C–H bond energy in methane

is 99.29 and the C–C bond energies in ethane and propane are 78.85 and 79.97, respectively. In the present investigation, the heats of formation of Si_3H_8 and Ge_3H_8 have been measured for comparison with previous determinations[4] for SiH_4, Si_2H_6, GeH_4, and Ge_2H_6 to ascertain corresponding trends in these similar series.

Experimental

Trisilane was prepared by reaction of magnesium silicide with hydrochloric acid and purified by bulb-

(1) This work was performed under the auspices of the U. S. Atomic Energy Commission.
(2) E. J. Prosen and F. D. Rossini, *J. Res. Natl. Bur. Std.*, 34, 263 (1945).
(3) T. L. Cottrell, "The Strengths of Chemical Bonds," 2nd Ed., Butterworth Scientific Publications, London, 1958.

to-bulb distillation. Although the vapor pressure approached the literature value, analysis of the melting curve[5] indicated several per cent impurity. The material was then purified by gas-liquid partition chromatography using a column of Octoil-S on firebrick. Melting point analysis then indicated a purity of 99.5 mole % and an extrapolated melting point of −114.8° (lit.[6] −117.4°).

Trigermane was prepared by J. E. Drake of the University of California, Berkeley, by reaction of germanium dioxide and potassium hydroborate in sulfuric acid.[7,8] Melting point analysis indicated a purity of 99.9 mole % and an extrapolated melting point of −101.8° (lit.[9] −105.6°).

Measurements were performed by explosion in mixtures with stibine in glass cells as previously described.[4,10] A new copper-block calorimeter, laboratory designation XXIX,[11] with copper surface thermometer was used. This system is more precise than that previously used. Three runs with stibine only at 25° gave 34.99, 34.99, and 34.95 kcal. mole^{-1} for $-\Delta E$; the previously used average[4] was 34.98 ± 0.10. Duplicate calibrations were performed for all runs and agreed on the average within 0.04%.

Results

Results of the trisilane-stibine runs are given in Table I. The percentage of Si_3H_8 decomposed is

Table I: Heat of Decomposition of Si_3H_8 at 25°

Run	Si_3H_8, mmoles	SbH_3, mmoles	Si_3H_8 decomposed, %	Condensable gas, %	(qSi_3H_8), cal.	$-\Delta E$, kcal. mole^{-1}
1	0.554	2.412	99.3	0.6	15.25	27.73
2	0.766	2.713	97.4	1.7	20.67	27.71
3	0.859	2.266	97.9	2.9	23.23	27.62
4	0.898	1.579	92.9	11.1	23.18	27.79

calculated from the total hydrogen found after the run minus that expected from stibine. The condensable gas found is expressed as percentage of the trisilane; it tends to be somewhat larger than the hydrogen deficiency, probably indicating some decomposition into di- and monosilane, but since the heat shows no trend with completeness of decomposition, the thermal effect of this is evidently negligible. In all cases, flaming the tube to the softening point liberated hydrogen corresponding to about 0.1% of the Si_3H_8. The heat is corrected for the fuse energy and the stibine contribution and ΔE is calculated from the amount of trisilane decomposed. Taking the average, 27.71,

for $-\Delta E$ and converting to constant pressure, $\Delta H_f°$ (Si_3H_8) is +25.9.

Results for the Ge_3H_8 runs are given in Table II.

Table II: Heat of Decomposition of Ge_3H_8 at 75°

Run	Ge_3H_8, mmoles	SbH_3, mmoles	Ge_3H_8 decomposed, %	Condensable gas, %	$q(Ge_3H_8)$, cal.	$-\Delta E$, kcal. mole^{-1}
1	0.791	1.573	99.8	...	41.30	52.35
2	0.894	1.369	99.7	<0.1	47.27	52.99
3	0.736	0.791	99.0	0.5	39.48	54.16
4	0.841	0.450	98.9	0.7	45.72	54.95
5	0.762	0	89.6	5.8	37.97	55.59

Flaming tubes from runs 2, 3, and 4 gave hydrogen corresponding to about 0.1% of the Ge_3H_8; run 5 gave 0.6%. Probably some polymeric germanium hydrides were formed, but the value is consistent with the other runs; as before, ΔE is calculated from the amount of Ge_3H_8 decomposed. A value of −34.71 is used for $\Delta E_{348}(SbH_3)$, calculated from the enthalpy data of Sunderam[12] for SbH_3 and Stull and Sinke[13] for Sb and H_2.

Least-squares fitting of a straight line to the plot of $\frac{1}{3}\Delta E$ vs. Sb–Ge gives an intercept of −18.59 and a slope of 1.70 ± 0.08 (probable error). Similar fitting of the earlier data for GeH_4 and Ge_3H_8 gives for ΔE (GeH_4), −22.22 with a slope of 1.48 ± 0.15 and for $\frac{1}{2}\Delta E(Ge_2H_6)$, −19.94 with a slope of 1.48 ± 0.07. Since the heat of formation of the Ge–Sb alloy presumably produced should vary very little with temperature, we take a weighted average, 1.57, for the slope and fit this by least squares again to obtain −22.29, −19.98, and −18.54 for $\Delta E(GeH_4)$, $\frac{1}{2}\Delta E(Ge_2H_6)$, and $\frac{1}{3}\Delta E_{348}(Ge_3H_8)$, respectively. Then converting to constant pressure, we obtain the slightly revised values of +21.7 and +38.8 for $\Delta H_f°(GeH_4)$ and $\Delta H_f°$ (Ge_2H_6), and +53.6 for $\Delta H°_{348}(Ge_3H_8)$.

(4) S. R. Gunn and L. G. Green, J. Phys. Chem., 65, 779 (1961).

(5) S. R. Gunn, Anal. Chem., 34, 1292 (1962).

(6) A. Stock, "Hydrides of Boron and Silicon," Cornell University Press, Ithaca, N. Y., 1933.

(7) W. L. Jolly, J. Am. Chem. Soc., 83, 335 (1961).

(8) J. E. Drake and W. L. Jolly, J. Chem. Soc., 2807 (1962).

(9) L. T. Dennis, R. B. Corey, and R. W. Moore, J. Am. Chem. Soc., 46, 657 (1924).

(10) S. R. Gunn, W. L. Jolly, and L. G. Green, J. Phys. Chem., 64, 1334 (1960).

(11) S. R. Gunn, Rev. Sci. Instr., in press.

(12) S. Sunderam, Can. J. Phys., 39, 370 (1961).

(13) D. R. Stull and G. C. Sinke, "Thermodynamic Properties of the Elements," Advances in Chemistry Series, No. 18, American Chemical Society, Washington, D. C., 1956.

In order to correct this to 25°, we must estimate the heat capacity of Ge_3H_8. Using the spectroscopic data of Gutowsky and Styskal[14] for Si_2H_6 and Dows and Hexter[15] for Ge_2H_6, we calculate the heat capacities at 325° by standard statistical-mechanical procedures to be approximately 19.6 and 21.4, respectively. Using heat capacities for CH_4, C_2H_6, C_3H_8, SiH_4, and GeH_4 at 325° from Rossini, et al.,[16] and Kelley,[17] we then estimate values for Si_3H_8 and Ge_3H_8 by correlations indicated in the diagram.
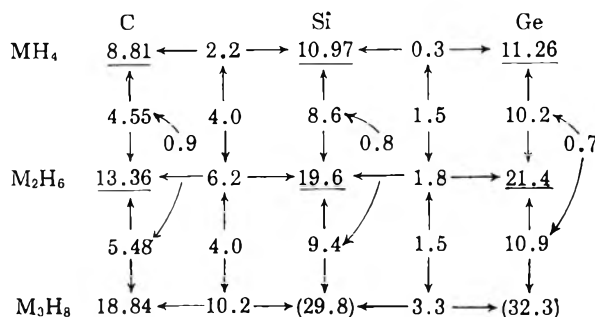
Taking data from Stull and Sinke[13] for Ge and H_2, we obtain $+54.2$ for $\Delta H_f°(Ge_3H_8)$.

X-Ray diffraction analyses of the products were not performed, but they presumably would be similar to those found earlier with monosilane and monogermane.[4] The uncertainty in the nature of the Si might contribute an error of 1 kcal./g.-atom or more to the heats of formation of the silanes; the uncertainty for the germanes should be less. These uncertainties cancel out in derivation of differences between the mono-, di-, and tri- species.

Discussion

The change of heat of formation upon adding a SiH_2 group to SiH_4 is $+9.8$ kcal. and upon adding SiH_2 to Si_2H_6, $+8.8$; adding GeH_2 to GeH_4, $+17.1$ and GeH_2 to Ge_3H_8, $+15.4$. The thermochemical bond energy $E(Si-Si)$ is 0.5 kcal. greater in Si_3H_8 than in Si_2H_6, and $E(Ge-Ge)$ is 0.8 kcal. greater in Ge_3H_8 than is Ge_2H_6, while $E(C-C)$ in C_3H_8 is 1.1 kcal. greater than in C_2H_6. These differences appear to be somewhat outside our experimental uncertainty, and do not represent a monotonic trend with increasing atomic number in the group.
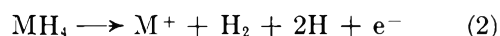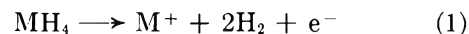
The thermochemical bond energies for silanes and germanes are given in Table III. Values not in parentheses are based on heats of sublimation selected by Cottrell[3]; those in parentheses, on values selected by Rossini, et al.[18] The current JANAF tables[19] select 106 ± 4 for $\Delta H_f°(Si,g)$. A value of 52.09 kcal. mole^{-1} is used for $\Delta H_f°(H,g)$.

Saalfeld and Svec have reported mass spectrometric

Table III: Thermochemical Bond Energies

	Si	Ge
$\Delta H_f°(M,g)$	105 (88)	89 (78)
$E(M-H)$ in MH_4	76.5 (72.3)	68.9 (66.2)
$E(M-M)$ in M_2H_6	46.4 (37.9)	38.2 (32.7)
$E(M-M)$ in M_3H_8	46.9 (38.4)	39.1 (33.6)

appearance potentials of Si^+ and Ge^+ from SiH_4 and GeH_4.[20] The potentials in electron volts attributed to the three processes

$$MH_4 \longrightarrow M^+ + 2H_2 + e^- \qquad (1)$$

$$MH_4 \longrightarrow M^+ + H_2 + 2H + e^- \qquad (2)$$

$$MH_4 \longrightarrow M^+ + 4H + e^- \qquad (3)$$

are 11.7 ± 0.2, 16.4 ± 0.2, and 20.8 ± 0.2 for Si and 10.7 ± 0.2, 14.1 ± 0.5, and 18.3 ± 0.3 for Ge. The differences between successive values in these series should be the dissociation energy of hydrogen, 104.18 kcal. or 4.52 e.v. The Si values are consistent on this basis but the Ge values are not.

Heats of formation and bond energies can be obtained from the appearance potentials if the fragments are assumed to have no excess potential energy. From reaction 1

$$\Delta H_f°(MH_4) = \Delta H_f°(M^-) - \Delta H_1 =$$
$$\Delta H_f°(M,g) + I(M) - \Delta H_1 \qquad (4)$$

where I is the ionization potential. Since

$$E(M-H) = \frac{1}{4}[\Delta H_f°(M,g) +$$
$$4\Delta H_f°(H,g) - \Delta H_f°(MH_4)] \qquad (5)$$

substituting eq. 4 into 5 gives

$$E(M-H) = \Delta H_f°(H) + \frac{1}{4}[\Delta H_1 - I_M] \qquad (6)$$

Comparing eq. 4 and 6, it is seen that determination of $\Delta H_f°(MH_4)$ from the appearance potential requires both the ionization potential and the heat of subli-

(14) H. S. Gutowsky and E. D. Styskal, *J. Chem. Phys.*, **22**, 939 (1954).

(15) D. A. Dows and R. M. Hexter, *ibid.*, **24**, 1029 (1956).

(16) F. D. Rossini, et al., "Selected Values of Physical and Thermodynamic Properties of Hydrocarbons and Related Compounds," American Petroleum Institute, 1953.

(17) K. K. Kelley, U. S. Bureau of Mines Bulletin 584, U. S. Govt. Printing Office, Washington, D. C., 1960.

(18) F. D. Rossini, et al., "Selected Values of Chemical Thermodynamic Properties," National Bureau of Standards Circular 500, U. S. Govt. Printing Office, Washington, D. C., 1952.

(19) JANAF Interim Thermochemical Tables, The Dow Chemical Co., Midland, Mich., 1962.

(20) F. E. Saalfeld and H. J. Svec, *Inorg. Chem.*, **2**, 46 (1963).

mation whereas determination of $E(M-H)$ requires only the ionization potential and the well established $\Delta H_f{}^\circ(H)$. From calorimetry, on the other hand, the heat of formation is obtained directly, but calculation of $E(M-H)$ requires use of the heat of sublimation.

For SiH_4, using $\Delta H_1 = 11.7$ e.v. or 270 kcal. and $I = 189.4$,[18,21] $E(Si-H)$ is 72 kcal. For GeH_4, using $H_1 = 10.7$ e.v. or 247 kcal. and $I = 183.2$[18] (converted from $0^\circ K$. to $25^\circ C$.), $E(Ge-H)$ is 68 kcal.

Saalfeld and Svec[22] also measured appearance potentials of Si^+ and Ge^+ from Si_2H_6, Ge_2H_6, and Ge_3H_8, assuming the processes

$$M_2H_6(g) \longrightarrow M^+(g) + M^\circ(g) + 3H_2 \quad (7)$$

$$M_3H_8(g) \longrightarrow M^+(g) + 2M^\circ(g) + 4H_2 \quad (8)$$
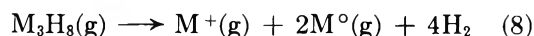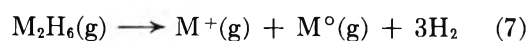
From eq. 7

$$\Delta H_f{}^\circ(M_2H_6) = 2\Delta H_f{}^\circ(M,g) + I(M) = \Delta H_7 \quad (9)$$

Since

$$E(M-M) = 2\Delta H_f{}^\circ(M,g) + 6\Delta H_f{}^\circ(H) -$$
$$\Delta H_f{}^\circ(M_2H_6) - 6E(M-H) \quad (10)$$

substituting 6 and 9 into 10 gives

$$E(M-M) = \Delta H_7 - {}^{1/2}\Delta H_1 + {}^{1}/{}_2 I(M) \quad (11)$$

For Si_2H_6, using $\Delta H_7 = 15.2$ e.v. or 350 kcal., $E(Si-Si)$ is 40. For Ge_2H_6, using $\Delta H_7 = 13.3$ e.v. or 307 kcal., $E(Ge-Ge) = 28$.

For Ge_3H_8, by similar reasoning

$$\Delta H_f{}^\circ(M_3H_8) = 3\Delta H_f{}^\circ(M,g) + I(M) - \Delta H_8 \quad (12)$$

$$E(M-M) = {}^{1}/{}_2 \Delta H_8 - \Delta H_1 + {}^{1}/{}_2 I(M) \quad (13)$$

Using $\Delta H_8 = 16.3$ e.v. or 376 kcal., $E(Ge-Ge) = 33$.

The bond energies from the appearance potential work are more consistent with the calorimetric work if the lower values of the heats of sublimation of Si and Ge are used. However, recent work rather strongly supports the higher value in both cases.

Stone and co-workers[23,24] have reported appearance potential work indicating that the bond dissociation energies $D(H-SiH_3)$ and $D(H_3Si-SiH_3)$ are much higher than the thermochemical bond energies $E(Si-H)$ and $E(Si-Si)$ from our work. This seems surprising, since for the carbon analogs the values are quite similar. In general, the thermochemical measurements leading to E are much less ambiguous than appearance potential measurements leading to D; a reinvestigation of D might well be in order.

Fehér, Jansen, and Rohmer[25] have recently reported values of -11.3, -36.2, and -54.4 kcal. mole^{-1} for the heats of formation of $SiH_4(g)$, $Si_2H_6(g)$, and $Si_3H_8(l)$ at 20° from combustion calorimetry. The calculations are apparently based on -205.4 for the heat of formation of quartz,[18] and the derived heats of formation would be even more negative if the better value of -217.5 for quartz were used.[26,27] These large discrepancies apparently illustrate the difficulty of obtaining correct results for silicon compounds by ordinary combustion calorimetry.

Acknowledgments. We wish to thank Professor William Jolly for providing the trigermane, and Mr. Virgil DuVal for performing the gas chromatographic purification of trisilane.

(21) C. E. Moore, "Atomic Energy Levels," Vol. III, National Bureau of Standards Circular 467, U. S. Govt. Printing Office, Washington, D. C., 1958.

(22) F. E. Saalfeld and H. J. Svec, *Inorg. Chem.*, 2, 50 (1963).

(23) W. C. Steele and F. G. A. Stone, *J. Am. Chem. Soc.*, 84, 3600 (1962).

(24) W. C. Steele, L. D. Nichols, and F. G. A. Stone, *ibid.*, 84, 444 (1962).

(25) F. Fehér, G. Jansen, and H. Rohmer, *Angew. Chem.*, 75, 859 (1963).

(26) C. N. Cochran and L. M. Foster, *J. Phys. Chem.*, 66, 380 (1962).

(27) W. D. Good, *ibid.*, 66, 380 (1962).

The Heats of Formation of H_2Se and H_2Te. Correlations of Simple Covalent Hydrides[1]

by Stuart R. Gunn

Lawrence Radiation Laboratory, University of California, Livermore, California (Received September 13, 1963)

Measurements of the heats of formation of several hydrides of groups IV and V[2-4] and of boron[5,6] by the method of explosion in mixtures with stibine have been previously reported. This method appeared rather unattractive for H_2Te and H_2Se because of compounds in the product Sb-Te and Sb-Se systems[7] with unknown heats of formation. However, SnH_4 had been found to explode by itself,[3] more violently than SbH_3, and it appeared possible that H_2Te, lying

(1) This work was performed under the auspices of the U. S. Atomic Energy Commission.

(2) S. R. Gunn, W. L. Jolly, and L. G. Green, *J. Phys. Chem.*, 64, 1334 (1960).

(3) S. R. Gunn and L. G. Green, *ibid.*, 65, 779 (1961).

(4) S. R. Gunn and L. G. Green, to be published.

(5) S. R. Gunn and L. G. Green, *J. Phys. Chem.*, 65, 2173 (1961).

(6) S. R. Gunn and L. G. Green, *J. Chem. Phys.*, 36, 1118 (1962).

(7) M. Hansen, "Constitution of Binary Alloys," McGraw-Hill Book Co., Inc., New York, N. Y., 1958.

in the same row of the periodic table, might also explode by ignition with a fuse, although extrapolation would suggest it to be less explosive than SbH₃. Preliminary experiments showed this indeed to be the case; it does not explode as completely at low pressures or propagate as readily into narrow tube sections as does SbH₃, although its spontaneous slow decomposition is considerably more rapid.

Experimental

Materials. H_2Te and H_2Se were prepared by the hydrolysis of Al_2Te_3 and Al_2Se_3, essentially according to the procedure of Watkins and Shutt.[8] The yield of H_2Te was much poorer, perhaps 10% that of H_2Se. Purifications were performed by bulb-to-bulb distillations, after a preliminary passage through $CaCl_2$ and P_2O_5 in the case of H_2Te. The principal criterion of purity was equality of vapor pressure of initial and final small fractions distilled from the total purified batch. Measurements of H_2Te were especially poor because of deposition of Te metal in the manometers; the value was approximately 95 mm. in a chlorobenzene slush bath (−45.2°); the vapor pressure equation of Kelley[9] gives 105 mm. The vapor pressure of H_2Se was about 230 mm. in a chloroform slush bath (−63.5°); Kelley's equation[9] gives 247 mm. Chemical analysis of the Te metal produced in the calorimeter runs showed less than 0.1% Se.

Calorimetry. The reaction tubes were as previously described[2] except for being 10 cm. long instead of 20 cm. and having a volume of about 45 ml.; this was done because of the difficulty of preparation of H_2Te and the apparently improved decomposition yield at higher pressures. The bulbs were equipped with ungreased Teflon-tipped high vacuum needle valves.[10] The gases were measured by weighing in the reaction tubes, H_2Se being loaded first when used. There appeared to be some evidence that H_2Te was decomposed by the room fluorescent lighting, so it was handled largely in the dark. Some decomposition of H_2Te still occurred during the weighing, so after completion of the weighing the gases were frozen out with liquid nitrogen and the hydrogen was pumped off and measured; this usually amounted to about 0.2 or 0.3%. The tube was then sealed off and placed in the calorimeter; further decomposition occurring during the somewhat shorter interval before firing is neglected in the calculations below.

Copper block calorimeter XXIX, described elsewhere,[11] was used. It was calibrated six times using a dummy glass cell, similar to the reaction cells, with a heater wound on its outer surface. Temperature intervals used were 0.25 to 0.5° (70 to 150 cal.); the

total spread of the calibrations was 0.15%. After reaction runs, the cells were weighed and a small correction was applied to the calibrated heat capacity to allow for the weight difference of the experimental cells and the calibration heater cell. Runs were performed at $25.0 \pm 0.2°$.

After the runs, the hydrogen was transferred with a Toepler pump through traps at −196° and measured; in the case of H_2Te–H_2Se runs, the traps were then warmed and the condensable gas also was measured.

Results

Four runs were performed with H_2Te only. The amounts in millimoles, corrected for decomposition during weighing, were 1.809, 2.041, 2.607, and 3.348. Observed heats, q, corrected for fuse energies, were 43.18, 48.32, 61.82, and 79.30 cal. The hydrogen found was 1.807, 2.024, 2.597, and 3.336 mmoles, or 99.9, 99.2, 99.6, and 99.6% of theoretical, respectively. The molar heats of reaction, ΔH, calculated with respect to the hydrogen found, are then −23.90, −23.87, −23.81, and −23.77 kcal mole⁻¹, respectively. X-Ray diffraction observations of the powder produced gave strong, clear patterns for the known structure of Te.

Five runs were performed with H_2Te–H_2Se mixtures. The data are summarized in Table I.

The amounts of H_2Se and H_2Te are calculated from the sample weights, the H_2Te being corrected for decomposition during weighing. "H_2Se decomposed" is taken as H_2 found minus 99.5% of the H_2Te. The value q_{tot} is the observed heat corrected for fuse energy; q_{H_2Se} is q_{tot} minus 0.995 times 23.83 kcal. mole⁻¹ times the amount of H_2Te (0.990 was used instead of 0.995 for run no. 3, where firing was considerably delayed). ΔH_{H_2Se} is then q_{H_2Se} divided by H_2Se decomposed.

The sum of H_2 and condensable gas found agrees quite well with the sum of H_2Se and H_2Te taken. Chemical analysis of Se and Te in the powder produced gave results which, while not very precise, were consistent with the gas measurements except for run no. 5, where the chemical ratio of Se to Te was significantly higher than calculated from the gas measurements. The condensable gas from all runs was condensed in tubes which were then sealed off and stored in light at room temperature. Run no. 5 developed

(8) G. R. Watkins and R. Shutt, "Inorganic Synthesis," Vol. II W. C. Fernelius, Ed., McGraw-Hill Book Co., Inc., New York. N. Y., 1946, pp. 183–186.

(9) K. K. Kelley, Bureau of Mines Bulletin 383, U. S. Govt. Printing Office, Washington, D. C., 1935.

(10) Fischer and Porter Co., Warminster, Pa.

(11) S. R. Gunn, *Rev. Sci. Instr.*, in press.

Table I: Heats of Explosion of H_2Te–H_2Se Mixtures

Run	H_2Te, mmoles	H_2Se, mmoles	H_2 found, mmoles	Condensables, mmoles	H_2Se decomposed mmoles	q_{tot}, cal.	q_{H_2Se}, cal.	$-\Delta H_{H_2Se}$, kcal. mole⁻¹
1	2.991	0.661	3.289	0.360	0.313	72.92	2.00	6.39
2	2.264	0.919	2.694	. . .	0.441	56.11	2.43	5.50
3	2.506	1.329	3.114	0.713	0.621	62.08	2.94	4.73
4	2.264	1.562	2.958	0.861	0.705	56.47	2.80	3.97
5	1.655	2.068	2.160	1.542	0.513	41.08	1.84	3.59

Table II: Heats of Formation of Simple Hydrides

CH_4, −17.89 (+25.2)	(+6.8)	NH_3, −11.04 (+12.3)	(−46.8)	H_2O, −57.80 (+53.0)	(−6.4)	HF, −64.2 (+42.1)
SiH_4, +7.3 (+14.3)	(−6.0)	PH_3, +1.3 (+14.6)	(−6.1)	H_2S, −4.82 (+13)	(−17.2)	HCl, −22.06 (+13.4)
GeH_4, +21.6 (+17.3)	(−5.7)	AsH_3, +15.9 (+18.9)	(−8)	H_2Se, +8 ? (+16)	(−17)	HBr, −8.66 (+14.8)
SnH_4, +38.9 (−4.2)		SbH_3, +34.7 (−10.9)		H_2Te, +23.8 (−17.6)		HI, +6.20

a much stronger mirror than the others; it is evident that in this run considerably more H_2Te was undecomposed. It may be noted that the per cent of H_2Se decomposed, calculated from the gas measurements, ranges from 48 to 45% in the first four runs, tending to decrease with increasing $H_2Se:H_2Te$ ratio, but is 25% for run no. 5. X-Ray diffraction analysis of the products showed them to be crystalline solid solutions.[12]

Discussion

The results for H_2Te seem to be straightforward and adequately precise; the explosions give well defined crystalline tellurium. The standard heat of formation, $\Delta H_f°$, is +23.83 kcal. mole⁻¹, with ±0.20 as an estimated over-all limit of error. Bichowsky and Rossini[13] give +34.2 (at 18°) based on work of Berthelot and Fabre[14]; Rossini, et al.,[15] give +36.9, referring to the same work. Awad[16] has proposed 23.1 for $\Delta F_f(H_2Te)$ at 30°; neglecting heat capacities and using tabulated entropies,[16] this corresponds to +26.9 for $\Delta H_f°$ at 25°.

Our values for H_2Se show a regular trend, slightly curved, when plotted against the $H_2Se:H_2Te$ ratio, which extrapolates to about +8 kcal. mole⁻¹ for $\Delta H_f°$ at a ratio of zero. This could be rationalized if an increasing fraction of H_2Te were undecomposed as the $H_2Se:H_2Te$ ratio in the runs was increased. However, there is no direct evidence for this except in the case of run no. 5. Tellurium and selenium are

isomorphous and completely miscible as solids[7]; the heat of solution would not be expected to be large.

Bichowsky and Rossini[13] give +18.5 (at 18°) for $\Delta H_f°$ (H_2Se) based on several investigations. Fabre[17] measured the heat of oxidation of H_2Se by $FeCl_3$; this gives 18.5 for $\Delta H_f°$. This is the same method that gave a high value for H_2Te. Fabre[17] also measured the heat of reaction of H_2Se with aqueous SeO_2; this gives 19.8 for $\Delta H_f°$. Equilibrium data of Rolla[18] for the reaction of H_2Se with I_2 and of Pelabon[19] for the dissociation of H_2Se to the elements give 16.9 and 19.0 for $\Delta H_f°$, respectively. Rossini, et al.,[15] give 20.5 for $\Delta H_f°$, referring only to Fabre.[17] More recently, Kapustinskii and Kankovskii[20] have reported a value of +18.16 from measurements of the heat of combustion of H_2Se.

Table II gives standard heats of formation (as gases)

(12) E. Grison, *J. Chem. Phys.*, **19**, 1109 (1951).

(13) F. R. Bichowsky and F. D. Rossini, "The Thermochemistry of the Chemical Substances," Reinhold Publishing Co., New York, N. Y., 1936.

(14) M. Berthelot and M. C. Fabre, *Ann. Chim. Phys.*, (6) **14**, 92 (1888).

(15) F. D. Rossini, *et al.*, National Bureau of Standards Circular 500, U. S. Govt. Printing Office, Washington, D. C., 1952.

(16) S. A. Awad, *J. Phys. Chem.*, **66**, 890 (1962).

(17) C. Fabre, *Ann. Chim. Phys.*, (6) **10**, 472 (1887).

(18) L. Rolla, *Atti. Accad. Nazl. Lincei, Mem. Classe Sci. Fis., Mat. Nat. Sez.*, **21 II**, 278 (1912).

(19) H. Pelabon, *Ann. Chim. Phys.*, (7) **25**, 365 (1902).

(20) A. F. Kapustinskii and R. T. Kankovskii, *Zh. Fiz. Khim.*, **33**, 722 (1959).

from Rossini, *et al.*,[15] and our earlier[2,3] and present work.

The values in parentheses are the differences between successive compounds. For periods 3, 4, and 5 these differences are remarkably regular, both horizontally and vertically, and a value near +20 for H_2Se would be entirely out of line. All in all, a value of around +8 kcal. mole^{-1} for ΔH_f° (H_2Se) appears most probable, with an unknown but large uncertainty. Using Cottrell's[21] values for the heats of formation of the gaseous atoms: H, 52.1; Se, 49; Te, 48, the thermochemical bond energies E(Se–H) and E(Te–H) are 73 and 64, respectively, forming a regular trend with the values of 110.6 for E(O–H) and 83 for E(S–H).

The 4 × 4 matrix of heats of formation of simple gaseous binary hydrides given in Table III should provide a valuable test of theory when and if theoretical chemistry becomes capable of giving reasonably rigorous *a priori* calculations of molecular bonding energies. An attempt has been made to correlate the thermochemical bond energies derived from these heats of formation with electronegativity schemes[22–24]

$$\Delta = E(M\text{–}H) - \tfrac{1}{2}[E(M\text{–}M) - E(H\text{–}H)]$$

$$X_M - X_H = 0.208\sqrt{\Delta}$$

Results are unsatisfactory, except for the halogens. For Si, Ge, and Sn, Δ is negative, and for groups V and VI the E(M–M) values to be used are poorly defined.

The regular trends shown in Table I suggest that fairly good estimates may be made for period 6. Assuming that the differences between periods 6 and 5 will be somewhat greater than those between 5 and 4, as those between 5 and 4 are greater than between 4 and 3, reasonable values would be PbH_4, 60; BiH_3, 55; H_2Po, 45; HAt, 25. However, the intervening lanthanide contraction might perturb this extrapolation somewhat. Saalfeld and Svec[25] have given values of 60 and 66 for ΔH_f° for SnH_4 and BiH_3, respectively, from mass spectrometric appearance potentials; this method in general is subject to fairly large experimental uncertainties, although their values for several other hydrides are in rather good agreement with ours.

(21) T. L. Cottrell, "The Strengths of Chemical Bonds," 2nd Ed., Butterworth, London, 1958.

(22) L. Pauling, "The Nature of the Chemical Bond," 3rd Ed., Cornell University Press, Ithaca, N. Y., 1960.

(23) A. L. Allred, *J. Inorg. Nucl. Chem.*, **17**, 215 (1961).

(24) H. O. Pritchard and H. A. Skinner, *Chem. Rev.*, **55**, 745 (1955).

(25) F. E. Saalfeld and H. T. Svec, *Inorg. Chem.*, **2**, 46 (1963).

The Free Energy of Formation of Niobium Dioxide between 1100 and 1700°K.[1]

by Wayne L. Worrell

*Inorganic Materials Research Division,
Lawrence Radiation Laboratory,
University of California, Berkeley, California*
(*Received October 7, 1963*)

The free energy of formation of NbO_2 has been determined by measuring the carbon monoxide equilibrium pressure of reaction 1 between 1050 and 1200°K.

$$Nb_2O_5(s) + C(gr) \rightleftharpoons 2NbO_2(s) + CO(g) \quad (1)$$
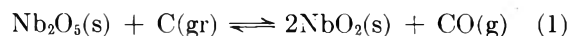
Combining these results with recent thermal data[2] and with another equilibrium study[3] yields free energy of formation values for NbO_2 which are more precise than those tabulated by Elliott and Gleiser[4] and by Coughlin.[5]

To obtain an expression for the free energy of formation of NbO_2 between 1100 and 1700°K., the standard free energy change of the reaction

$$Nb_2O_5(s) \rightleftharpoons 2NbO_2(s) + 0.5O_2(g) \quad (2)$$
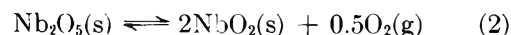
was calculated from the results of the three investigations.

In this study a solid pellet of NbO_2–Nb_2O_5–C was equilibrated with a carbon monoxide atmosphere at elevated temperatures. The experimental apparatus and procedures are described elsewhere.[6,7] The amount of CO (usually >94%) was determined by Orsat analysis,[8] and an X-ray diffraction pattern of the remaining pellet indicated that only the initially charged phases were present. The results are summarized in Table I, in which $\Delta F^\circ_{(1)}$ and $\Delta F^\circ_{(2)}$ are the standard free energy changes of reactions 1 and 2,

(1) This note is based on a thesis submitted in partial fulfillment of the requirements for the degree of Doctor of Philosophy at the Massachusetts Institute of Technology, May, 1963. The work was supported principally by the National Science Foundation and the U. S. Atomic Energy Commission.

(2) E. G. King and A. O. Christensen, U. S. Bur. Mines Rept. Invest. 5789, U. S. Govt. Printing Office, Washington, D. C., 1961.

(3) V. I. Lavrent'ev, Y. I. Gerasimov, and T. N. Rezakhina, *Dokl. Akad. Nauk SSSR*, **136**, 1372 (1961).

(4) J. F. Elliott and M. Gleiser, "Thermochemistry of Steelmaking," Vol. I, Addison-Wesley Publishing Co., Inc., Reading, Mass., 1960.

(5) J. P. Coughlin, U. S. Bur. Mines Bull. 542, U. S. Govt. Printing Office, Washington, D. C., 1954.

(6) W. L. Worrell and J. Chipman, *J. Phys. Chem.*, **68**, 860 (1964).

(7) M. Gleiser and J. Chipman, *ibid.*, **66**, 1539 (1962).

(8) "Manual for Gas Analysis," Catalog No. 80, Burrell Technical Supply Co., Pittsburgh, Pa.

respectively; values for $\Delta F^{\circ}{}_{(2)}$ are obtained by subtracting the free energy of formation of $CO(g)$[4,5] from $\Delta F^{\circ}{}_{(1)}$ and are shown in Fig. 1.

Table I: Standard Free Energy Changes of Reactions 1 and 2

T, °K.	P_{CO}, mm.	$\Delta F^{\circ}{}_{(1)}$, cal.	$\Delta F^{c}{}_{(2)}$, cal.
1175	662	323	51,948
1143	452	1182	52,132
1074	135	3682	53,182
1090	205	2341	52,681
1172	754	25	51,585
1127	302	2062	52,682

Lavrent'ev, Gerasimov, and Rezakhina[3] have measured the steam-to-hydrogen equilibrium pressure ratios between 1473 and 1673°K. for reaction 3.

$$Nb_2O_5(s) + H_2(g) \rightleftharpoons 2NbO_2(s) + H_2O(g) \quad (3)$$
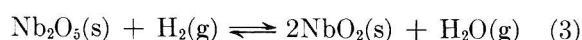
Their data for reaction 2 are shown in Fig. 1.
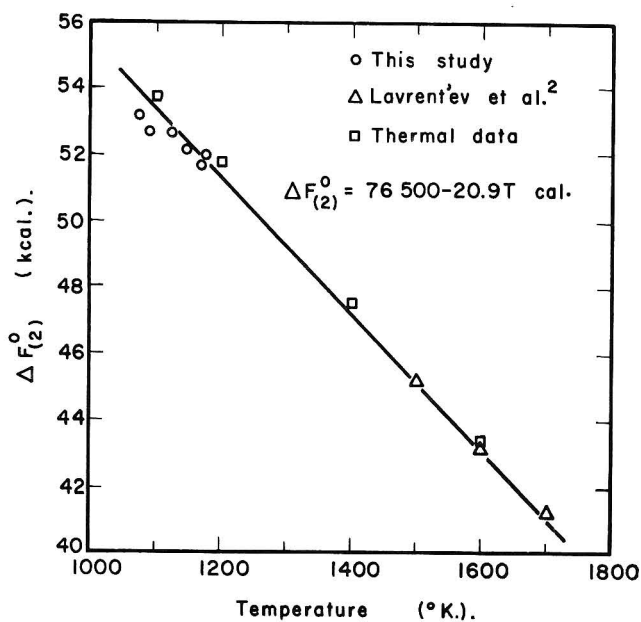
Figure 1. Standard free energy change of the reaction $Nb_2O_5(s) \rightleftharpoons 2NbO_2(s) + 0.5O_2(g)$.

The standard free energy change of reaction 2 at 298°K. can be calculated from Mah's measured heat of reaction[9] and the available entropy data.[10] Com-

bining this value with high-temperature thermal data for Nb_2O_5,[11] $O_2(g)$,[11] and NbO_2,[2] one obtains the thermal values for the standard free energy change of reaction 2 shown in Fig. 1.

The results presented in Fig. 1 agree within the experimental uncertainties. However, the two low temperature values from this study appear not to have been at equilibrium, possibly due to the inertness of graphite below 1100°K.[12] Hence, these two values were disregarded in the subsequent calculations.

Using available thermal data,[2,10,11] one obtains 20.9 cal./deg. for the temperature variation of $\Delta F^{\circ}{}_{(2)}$ between 1100 and 1700°K. Combining this value with the results shown in Fig. 1 yields the following equation for $\Delta F^{\circ}{}_{(2)}$ between 1100 and 1700°K.

$$\Delta F^{\circ}{}_{(2)} (\pm 600) = 76,500 - 20.9T \text{ cal.} \quad (4)$$

With this equation and the free energy of formation values for Nb_2O_5,[4,5] one obtains the following equation for the free energy of formation of NbO_2 between 1100 and 1700°K.

$$\Delta F^{\circ}{}_{NbO_2} (\pm 500) =$$
$$-185,600 + 38.9T \text{ cal./mole} \quad (5)$$

The uncertainty in $\Delta F^{\circ}{}_{(2)}$ was calculated by the usual method[13] of assessing the deviation of the individual points from the straight line variation shown in Fig. 1. The uncertainty in $\Delta F^{\circ}{}_{NbO_2}$ of ± 500 cal. was obtained by applying the usual technique[13] for combining the independent uncertainties in $\Delta F^{\circ}{}_{(2)}$ and $\Delta F^{\circ}{}_{Nb_2O_5}$.[14]

Using eq. 5 and recent thermal data,[2] one obtains an average value of -190.7 kcal./mole for the standard heat of formation at 298°K. of NbO_2, which is in good agreement with Mah's value[9] of -190.9 (± 0.4) kcal./mole determined from combustion calorimetry.

(9) A. D. Mah, *J. Am. Chem. Soc.*, **80**, 3872 (1958).

(10) K. K. Kelley and E. G. King, U. S. Bur. Mines Bull. 592, U. S. Govt. Printing Office, Washington, D. C., 1961.

(11) K. K. Kelley, *ibid.*, Bull. 584, 1960.

(12) J. Chipman, *J. Phys. Chem.*, **60**, 1467 (1956).

(13) Y. Beers, "Introduction to the Theory of Error," Addison-Wesley Publishing Co., Inc., Reading, Mass., 1958.

(14) G. L. Humphrey, *J. Am. Chem. Soc.*, **76**, 978 (1954).

Estimation of the Entropy of Formation
at 298°K. for Some Refractory Metal Carbides[1]

by Wayne L. Worrell

Inorganic Materials Research Division,
Lawrence Radiation Laboratory,
University of California, Berkeley, California
(Received October 7, 1963)

Although their heats of formation are fairly well known, few entropies of formation at 298°K. (ΔS°_{298}) of refractory metal carbides have been determined. Until such data become available, any estimation of ΔS°_{298} should be very useful. By combining the estimated ΔS°_{298} with the measured ΔH°_{298}, one can obtain a free energy of formation equation for the carbide at 298°K. Because Kopp's rule ($\Delta Cp \approx 0$) is usually a good approximation for carbides,[2] this equation is also applicable at elevated temperatures.

Krikorian[3] has estimated values for ΔS°_{298} for some refractory metal carbides by correlating the entropy of formation of the carbides from the gaseous elements. In his calculations, the electronic contributions to the entropies of the gaseous atoms were neglected and only their translational entropies were considered. By comparing the results of similar calculations for the oxides and for some nitrides with the tabulated entropies of Kelley,[4] Krikorian[3] demonstrated that quite reasonable entropy values were obtained for the refractory metal carbides, nitrides, and oxides.

In 1949, Richardson[5] attempted to correlate the sign of ΔS°_{298} with the structure and melting point of the carbide. He noted that a face-centered-cubic carbide had a melting temperature significantly higher than that of its parent metal and a negative ΔS°_{298}, but that a hexagonal-close-packed carbide usually melted at a comparable or lower temperature than its parent metal and had a positive ΔS°_{298}.

However, further research[6] has indicated that the vanadium group metals form a hexagonal-close-packed carbide (M_2C) which melts at a higher temperature than its parent metal and probably has a negative ΔS°_{298}. Although this indicates that the sign of ΔS°_{298} of a carbide probably is not linked to its crystal structure, a correlation should be possible between its melting temperature and its value for ΔS°_{298}.

Recent melting point data for the titanium group, the vanadium group, and the chromium group metal-carbide systems[6] have been used to calculate t_M/t_C values where t_M and t_C are the melting points of the metal and the carbide, respectively. The melting points, the calculated t_M/t_C values, and the available entropy

data[7] for these metal-carbide systems are tabulated in Table I. If the melting temperature varies with the composition of the carbide, its maximum value, which is not necessarily that at the stoichiometric composition, is tabulated. The peritectic temperature is used to calculate t_M/t_C for those carbides which peritectically decompose.
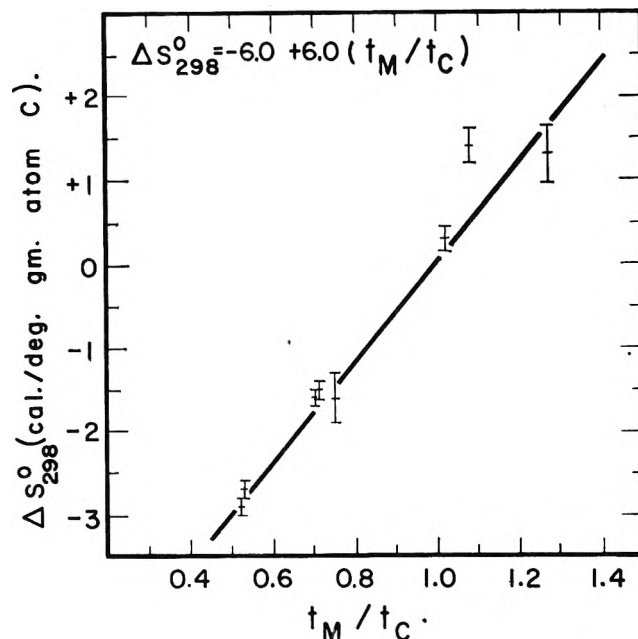
Figure 1. Variation of ΔS°_{298} with t_M/t_C for some refractory metal carbides.

A qualitative correlation between the melting point quotient (t_M/t_C) and ΔS°_{298} can be expected.[8] The main contribution to the entropy of formation

(1) This note is based on a thesis submitted in partial fulfillment of the requirements for the degree of Doctor of Philosophy at the Massachusetts Institute of Technology, May, 1963. The work was supported principally by the National Science Foundation and the U. S. Atomic Energy Commission.

(2) O. Kubaschewski and E. L. Evans, "Metallurgical Thermochemistry," Pergamon Press, New York, N. Y., 1958.

(3) O. H. Krikorian, Lawrence Radiation Lab Report UCRL-2888, 1955.

(4) K. K. Kelley, U. S. Bur. Mines Bull. 477, U. S. Govt. Printing Office, Washington, D. C., 1950.

(5) F. D. Richardson, *J. Iron Steel Inst.* (London), 163, 382 (1949).

(6) E. K. Storms, Los Alamos Scientific Lab Report LAMS-2674, 1962.

(7) K. K. Kelley and E. G. King, U. S. Bur. Mines Bull. 592, U. S. Govt. Printing Office, Washington, D. C., 1961.

(8) See L. Brewer, L. A. Bromley, P. W. Gilles, and N. L. Lofgren, Paper 6, "Chemistry and Metallurgy of Miscellaneous Materials: Thermodynamics," Vol. 19 B, National Nuclear Energy Series, ed. by L. L. Quill, 1950. They have estimated entropy values for some halides by considering S°_{298} to be a linear function of the melting temperature.

Substance	Melting point, °C.	t_M/t_C	$\Delta S°_{298}$, cal./deg. g.-atom C
Ti	1660		
TiC (fcc)	3180	0.52	-2.9 ± 0.07
Zr	1855		
ZrC (fcc)	3480	0.53	-2.69 ± 0.1^a
Hf	2222		
HfC (fcc)	3890	0.57	. . .
V	1888		
V$_2$C (hcp)	2165	0.87	. . .
VC (fcc)	2650	0.71	-1.5 ± 0.1^b
Nb	2467		
Nb$_2$C (hcp)	3090	0.80	. . .
NbC (fcc)	3500	0.71	-1.6 ± 0.1^b
Ta	3000		
Ta$_2$C (hcp)	3500	0.86	. . .
TaC (fcc)	4000	0.75	-1.6 ± 0.3^b
Cr	1915		
Cr$_{23}$C$_6$ (fcc)	1520	1.27	1.32 ± 0.35
Cr$_7$C$_3$ (hcp)	1780	1.08	1.39 ± 0.19
Cr$_3$C$_2$ (orth)	1895	1.01	0.30 ± 0.12
Mo	2620		
Mo$_2$C (hcp)	2410	1.09	. . .
MoC (hcp)	2575	1.02	. . .
W	3407		
W$_2$C (hcp)	2800	1.22	. . .
WC (hcp)	2720	1.25	. . .

[a] Obtained from the low temperature heat capacity data of E. F. Westrum, Jr., and G. Feick reported in Tech. Doc. Rept. No. ASD-TDR-62-204, part II, May, 1963. [b] Obtained from W. L. Worrell and J. Chipman, *J. Phys. Chem.*, **68**, 860 (1964).

of the refractory metal carbides would be from vibrational effects because changes in the electronic and configurational entropies are very small. A carbon atom is more loosely bonded in the carbide than in pure graphite; hence the lattice vibrations and the vibrational entropy of a carbon atom should be greater in the carbide. However, $\Delta S°_{298}$ of a carbide is probably influenced more by the entropy changes of the metal atom because the vibrational entropy of a pure metal at 298°K. is five to seven times that of carbon.

A metal should be more rigidly bonded in a carbide whose melting point quotient (t_M/t_C) is less than one. The lattice vibrations and the vibrational entropy of the metal in this carbide would be less than that in the pure metal, and $\Delta S°_{298}$ is probably negative. A similar argument would predict a positive $\Delta S°_{298}$ for a carbide which has a lower melting point than that of its parent metal $(t_M/t_C > 1)$.

The linear variation of $\Delta S°_{298}$ with the melting point quotient (t_M/t_C) is shown in Fig. 1 and can be represented by the equation

$$\Delta S°_{298} = -6.0 + 6.0(t_M/t_C) \text{ cal./deg. g.-atom of C} \tag{1}$$

This expression has been used to calculate values of $\Delta S°_{298}$ tabulated in Table II. Krikorian's estimates[3] and recommended values are also presented in Table II.

Table II: Estimated Values of $\Delta S°_{298}$ for Some Refractory Metal Carbides

Carbide	t_M/t_C	$\Delta S°_{298}$, cal./deg. g.-atom C		
		This study	Krikorian[3]	Recommended
HfC	0.57	-2.6	-4.0 ± 1.0	-3.0 ± 1.5
Nb$_2$C	0.80	-1.2	-1.0 ± 1.5	-1.0 ± 1.0
V$_2$C	0.87	-0.8	-2.0 ± 1.0	-1.0 ± 1.0
Ta$_2$C	0.86	-0.8	-0.4 ± 1.0	-0.5 ± 1.0
MoC	1.02	0.1	0.0 ± 1.0	0.0 ± 1.0
Mo$_2$C	1.09	0.6	2.1 ± 1.0	1.5 ± 1.0
W$_2$C	1.22	1.3	2.5 ± 1.5	2.0 ± 1.5
WC	1.25	1.5	0.6 ± 1.0	1.0 ± 1.0

A precision of $\pm 100°$ in the melting points of the carbides would result in a variation of approximately $\pm 10\%$ in the calculated values of $\Delta S°_{298}$. However, because of the empirical nature of eq. 1, no quantitative estimate of the uncertainties associated with the values of $\Delta S°_{298}$ calculated in this study has been made. The uncertainties quoted for the recommended values in the last column of Table II are based arbitrarily on those of Krikorian[3] and on the agreement between his estimates and those of this study.

The Nuclear Magnetic Resonance

Spectra of Bromodiborane[1]

by Donald F. Gaines and Riley Schaeffer

Contribution No. 1172 from the Department of Chemistry, Indiana University, Bloomington, Indiana
(Received October 2, 1963)

From studies of the aminodiboranes, Burg and Randolph[2] postulated that the halogen atom occupied a bridge position in the halodiboranes. However, the

preliminary microwave study of Cornwell[3] could be interpreted only in terms of a terminal bromine in bromodiborane. This paper presents the [11]B and [1]H n.m.r. spectra of bromodiborane and interprets them in terms of a terminal substituted model.

Experimental

Bromodiborane was prepared and purified by the method of Schlesinger and Burg.[4] The purified product had a vapor pressure of 40 mm. at $-45°$, in good agreement with the literature.[4,5] Samples of the liquid for the n.m.r. spectra were contained in 5-mm. o.d. Pyrex tubing. The [11]B and ^{1}H spectra were obtained using a Varian Model 4300B high resolution spectrometer operating at 19.3 and 60 Mc./sec., respectively. To minimize decomposition, the temperature of the sample was maintained at about $-40°$ using the standard Varian variable temperature accessories.

Results

The [11]B n.m.r. spectrum (Fig. 1) of bromodiborane can be interpreted only in terms of a terminal bromine. The boron to which the bromine is bonded is coupled to a single terminal hydrogen, giving rise to the large doublet at lower field. Each member of the doublet is further split into a triplet, with relative intensities of 1:2:1, by the two less strongly coupled bridge hydrogens. The other boron is coupled to two terminal hydrogens giving rise to a large triplet each member of which is also split into smaller triplets by the bridge hydrogens, as in diborane.[6] The resonances of the two borons are partially overlapped, so that the central portion of the spectrum is a composite of the different resonances.

The [1]H n.m.r. spectrum of bromodiborane also indicates two types of terminal hydrogens in a ratio of 2:1 (Fig. 2). The peaks arising from one terminal hydrogen coupled to [11]B ($I = {}^3/_2$), marked a, occur at lower field while those arising from two terminal hydrogens coupled to [11]B, marked b, occur at higher field.[7] Coupling of the bridge hydrogen with two different borons, using coupling constants obtained from the [11]B spectrum, results in a sixteen-lined group, marked c. Only the highest field members of the group are clearly visible, and they are partially overlapping.

The contribution of [10]B coupling with the hydrogen has not been included in the derived spectrum. The chemical shifts for hydrogens coupled to [10]B would be expected to be the same as for hydrogens coupled to [11]B,[8] but the coupling constant is smaller by a factor of about three, and there are seven lines (the spin of [10]B is 3) instead of four. Thus the presence of 20% [10]B produces only a background, which is of little signifi-
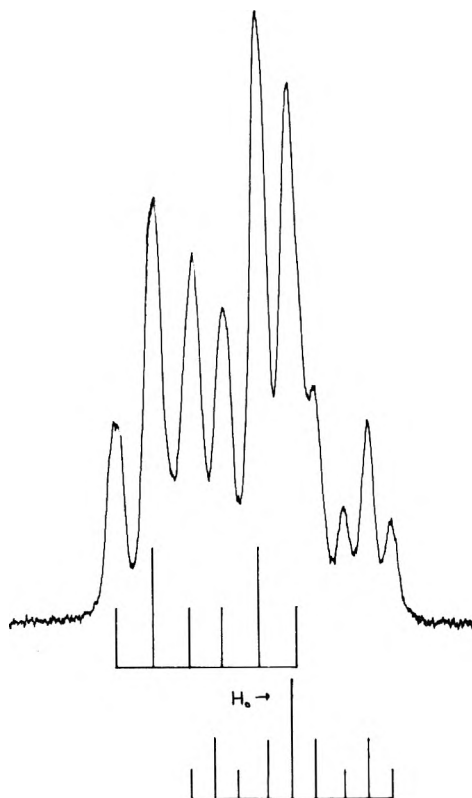
Figure 1. The [11]B n.m.r. spectrum of bromodiborane.
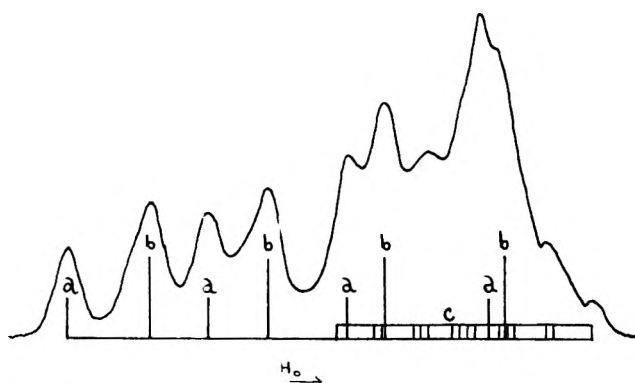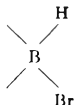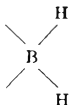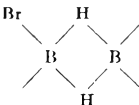
Figure 2. The [1]H n.m.r. spectrum of bromodiborane.

(1) Studies of Boranes X. For paper IX, see I. A. Ellis, D. F. Gaines, and R. Schaeffer, *J. Am. Chem. Soc.*, **85**, 3885 (1963).

(2) A. B. Burg and C. L. Randolph, *ibid.*, **71**, 3451 (1949).

(3) C. D. Cornwell, *J. Chem. Phys.*, **18**, 1118 (1950).

(4) H. I. Schlesinger and A. B. Burg, *J. Am. Chem. Soc.*, **53**, 4321 (1931).

(5) A. Stock, E. Kuss, and O. Priess, *Ber.*, **47**, 3115 (1914).

(6) R. A. Ogg, Jr., *J. Chem. Phys.*, **22**, 1933 (1954); J. N. Shooler, *Discussions Faraday Soc.*, **19**, 215 (1955); W. D. Phillips, H. C. Miller, and E. L. Muetterties, *J. Am. Chem. Soc.*, **81**, 4496 (1959); D. F. Gaines, *Inorg. Chem.*, **2**, 523 (1963).

(7) It has been found that general chemical shift trends observed in [11]B n.m.r. spectra of boron hydrides are also observed in [1]H n.m.r. spectra, though there is at present no theoretical justification for this correlation.

cance in terms of the over-all spectrum observed.

Though the ^{11}B and ^{1}H n.m.r. spectra of bromodiborane contain regions where the overlap is sufficient to render interpretation difficult, other regions are sufficiently free of overlap so that there is no doubt as to the assignments shown. Thus the structure of bromodiborane has been confirmed by an entirely independent method.

Table I: Chemical Shifts and Coupling Constants for the ^{11}B and ^{1}H n.m.r. Spectra of Bromodiborane

		H	H	Br H
^{11}B	δ^a (± 0.5), p.p.m.	-18.9	-12.2	
	J (± 3), c.p.s.	163	141	56.4,^{c} 44.2^d
^{1}H	δ^b (± 0.1), p.p.m.	-4.98	-4.02	-1.2 (est.)
	J (± 3), c.p.s.	167	140	

^{a} With reference to BF$_3$·O(C$_2$H$_5$)$_2$. ^{b} With reference to (CH$_3$)$_4$Si. ^{c} Bridge hydrogen coupling to the boron attached to bromine. ^{d} Bridge hydrogen coupling to the boron attached to two terminal hydrogens.

(8) D. F. Gaines, R. Schaeffer, and F. Tebbe, *J. Phys. Chem.*, **67**, 1937 (1963).

Association of Silver(I) and Chloride in Molten Cesium Nitrate and in Molten Mixtures of Potassium Nitrate with Cesium Nitrate or Lithium Nitrate[1]

by C. Thomas and J. Braunstein

Department of Chemistry, University of Maine; Orono, Maine (*Received October 28, 1963*)

The solvent effect on the association constants of silver(I) with chloride, bromide, or iodide in the molten solvents NaNO$_3$ and KNO$_3$ has been correlated with the relative sizes of the cations and the relative sizes of the anions in terms of a "reciprocal coulomb effect."[2,3] The solvent effect of Na$^+$ or K$^+$ on the association constants of lead(II) or cadmium(II) with bromide in mixtures of NaNO$_3$ and KNO$_3$[4] also is in the direction
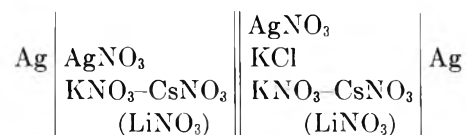
predicted by the reciprocal coulomb effect.[4] In mixtures of LiNO$_3$ and KNO$_3$, however, association constants of cadmium(II) with bromide *increase* with increasing proportions of lithium ion in the solvent,[5] in apparent disagreement with the reciprocal coulomb effect.

This note describes measurements of association constants of silver(I) with chloride in molten CsNO$_3$, in molten 67–33 mole % KNO$_3$–CsNO$_3$, and in molten 67–33 mole % KNO$_3$–LiNO$_3$. We show that the results in CsNO$_3$ are consistent with the reciprocal coulomb effect while the solvent effect of lithium ion is anomalous if a single "effective radius" of nitrate ion is used for all the alkali nitrate solvents.

Experimental

Cesium nitrate was prepared by treating cesium carbonate (purified) from Fisher Scientific Co. with a slight excess of nitric acid, recrystallizing twice from water, and drying at 140°. All other chemicals were reagent grade from Mallinckrodt or J. T. Baker and were used without further purification other than drying.

Electromotive force measurements were made, by methods described previously,[6] of the cell

$$\text{Ag} \left| \begin{array}{c} \text{AgNO}_3 \\ \text{KNO}_3\text{–CsNO}_3 \\ (\text{LiNO}_3) \end{array} \right\| \begin{array}{c} \text{AgNO}_3 \\ \text{KCl} \\ \text{KNO}_3\text{–CsNO}_3 \\ (\text{LiNO}_3) \end{array} \right| \text{Ag}$$

both in the presence and in the absence of KCl.

Results

In the absence of chloride, the e.m.f. of the cell followed the Nernst equation in the concentration of AgNO$_3$. The change of e.m.f. on addition of KCl is given in Table I as a function of the mole ratios, R, (moles of solute/mole of solvent) of AgNO$_3$ and of KCl (CsCl).

Association constants for the formation of AgCl in the three solvents were evaluated graphically by methods described previously.[7] The constants are

(1) Supported by the U. S. Atomic Energy Commission under Contract No. AT(30-1)-2873.

(2) D. L. Manning, R. C. Bansal, J. Braunstein, and M. Blander, *J. Am. Chem. Soc.*, **84**, 2028 (1962).

(3) R. E. Hagman and J. Braunstein, *J. Phys. Chem.*, **67**, 2881 (1963).

(4) D. L. Manning, M. Blander, and J. Braunstein, *Inorg. Chem.*, **2**, 345 (1963).

(5) J. Braunstein and A. S. Minano, *ibid.*, **3**, 218 (1964).

(6) (a) M. Blander, F. F. Blankenship, and R. F. Newton, *J. Phys. Chem.*, **63**, 1259 (1959); (b) J. Braunstein and M. Blander, *ibid.*, **64**, 10 (1960).

(7) J. Braunstein, M. Blander, and R. M. Lindgren, *J. Am. Chem. Soc.*, **84**, 1529 (1962).

listed in Table II along with values of the specific Helmholtz free energy of association, ΔA, which were calculated from the equation of the quasi-lattice model[8]

$$K_1 = Z(\exp(-\Delta A/RT) - 1)$$

for values of Z, the quasi-lattice coordination number, 4, 5, and 6. Also listed in Table II, for comparison, are previously reported values of ΔA in KNO_3[9] and in $NaNO_3$,[10] and an estimate of ΔA in $LiNO_3$ based on a linear extrapolation of the values of ΔA in pure KNO_3 and in the mixed solvent, 0.67 KNO_3–0.33 $LiNO_3$.

Discussion

The results in Table II indicate that AgCl is more stable in $CsNO_3$ than in KNO_3 by 0.65 kcal./mole. This is in the direction predicted by the reciprocal coulomb effect, but the observed stabilization is smaller than the value of 2.0 kcal./mole calculated for the exchange of nearest neighbor ions[2,3,6] using the Pauling radii[11] for Cs^+, K^+, and Cl^- and 2.19 Å. for the radius of nitrate ion.[12] The observed solvent effect is 0.32 of the calculated effect, which is high because of the neglect in the calculation of the effect of next nearest neighbor and more distant ions.[2]

Table I: Change of E.m.f. (in millivolts) on Addition of KCl

(a) $CsNO_3$, $T = 441°$

$R_{AgNO_3} = 0.102 \times 10^{-1}$		$R_{AgNO_3} = 0.218 \times 10^{-1}$		$R_{AgNO_3} = 0.305 \times 10^{-1}$		$R_{AgNO_3} = 0.522 \times 10^{-1}$	
$R_{CsCl} \times 10^3$	$-\Delta e.m.f.$	$R_{CsCl} \times 10^3$	$-\Delta e.m.f.$	$R_{CsCl} \times 10^3$	$-\Delta e.m.f.$	$R_{CsCl} \times 10^3$	$-\Delta e.m.f.$
0.162	4.49	0.219	6.17	0.192	4.87	0.216	4.61
0.335	9.06	0.522	14.69	0.506	12.97	0.516	10.13
0.864	24.18	1.441	39.44	1.105	27.61	0.807	17.45
1.538	40.06	2.327	57.74	2.352	55.45	1.515	33.79
2.644	63.21	3.397	77.56	3.144	70.77	2.308	50.05
3.522	79.81	4.510	92 ± 3	4.315	91.56	3.497	71.24
4.486	95.81					4.783	91.14

$R_{AgNO_3} = 0.944 \times 10^{-1}$		$R_{AgNO_3} = 1.133 \times 10^{-1}$	
$R_{CsCl} \times 10^3$	$-\Delta e.m.f.$	$R_{CsCl} \times 10^3$	$-\Delta e.m.f.$
0.144	3.20	0.146	3.34
0.421	9.81	0.404	8.69
0.791	18.85	0.787	16.37
1.522	33.39	1.466	27.69
2.071	44.99	2.267	44.46
2.941	60.90	3.669	69.12
4.413	85.01	5.010	91.49

(b) 0.33 $CsNO_3$–0.67 KNO_3, $T = 385°$

$R_{AgNO_3} = 0.1018 \times 10^{-1}$		$R_{AgNO_3} = 0.3161 \times 10^{-1}$		$R_{AgNO_3} = 0.511 \times 10^{-1}$		$R_{AgNO_3} = 0.863 \times 10^{-1}$	
$R_{KCl} \times 10^3$	$-\Delta e.m.f.$	$R_{KCl} \times 10^3$	$-\Delta e.m.f.$	$R_{KCl} \times 10^3$	$-\Delta e.m.f.$	$R_{KCl} \times 10^3$	$-\Delta e.m.f.$
0.1095	3.34	0.0814	2.17	0.505	13.27	0.915	22.76
0.1971	4.67	0.230	7.50	1.139	27.49	1.222	29.86
0.329	8.59	0.349	10.31	1.980	45.07	1.812	41.98
0.656	17.47	0.851	22.28	3.132	67.31	2.543	55.97
0.873	22.40	1.285	32.96	4.005	82.46	3.279	68.97
1.392	35.63	1.756	43.92	4.962	96.33	4.232	88.26
2.008	49 ± 1	2.408	58.56				
2.558	58.25	3.219	74.35				

$R_{AgNO_3} = 1.282 \times 10^{-1}$		$R_{AgNO_3} = 1.568 \times 10^{-1}$		$R_{AgNO_3} = 2.729 \times 10^{-1}$		$R_{AgNO_3} = 4.112 \times 10^{-1}$	
$R_{KCl} \times 10^3$	$-\Delta e.m.f.$	$R_{KCl} \times 10^3$	$-\Delta e.m.f.$	$R_{KCl} \times 10^3$	$-\Delta e.m.f.$	$R_{KCl} \times 10^3$	$-\Delta e.m.f.$
0.170	3.99	0.452	9.17	0.190	6.58	0.338	6.21
0.595	14.17	0.985	19.54	0.7778	16.13	0.973	15.04
1.0755	23.46	1.707	32.76	1.356	24.12	1.885	25.57
2.122	44.08	2.327	44.95	2.033	36.37		
2.747	55.08	3.699	66.85				
3.404	67.62						
4.520	85.72						

Table I (*Continued*)

(c)   0.33 LiNO₃–0.67 KNO₃, $T = 391°$

$R_{AgNO_3} = 0.1095 \times 10^{-3}$		$R_{AgNO_3} = 0.412 \times 10^{-3}$		$R_{AgNO_3} = 0.653 \times 10^{-3}$		$R_{AgNO_3} = 0.866 \times 10^{-3}$	
$R_{KCl} \times 10^3$	$-\Delta e.m.f.$	$R_{KCl} \times 10^3$	$-\Delta e.m.f.$	$R_{KCl} \times 10^3$	$-\Delta e.m.f.$	$R_{KCl} \times 10^3$	$-\Delta e.m.f.$
0.0975	1.77	0.544	9.90	0.348	5.98	0.460	7.90
0.245	5.52	1.316	23.74	0.965	16.78	1.277	20.35
0.565	13.27	2.056	34.60	1.622	26.30	1.526	24.29
1.154	24.20	2.649	41.90	2.098	33.05	1.906	30.15
1.758	37.27	3.309	50.56	2.737	41.56	2.252	36.11
2.475	50.00	3.902	57.88	3.614	52.70		
3.459	65.00	4.427	64.55	4.054	57.71		

$R_{AgNO_3} = 0.964 \times 10^{-3}$		$R_{AgNO_3} = 1.747 \times 10^{-3}$		$R_{AgNO_3} = 2.615 \times 10^{-3}$	
$R_{KCl} \times 10^3$	$-\Delta e.m.f.$	$R_{KCl} \times 10^3$	$-\Delta e.m.f.$	$R_{KCl} \times 10^3$	$-\Delta e.m.f.$
0.321	5.36	0.181	3.30	0.283	5.51
0.817	13.20	0.781	9.95	0.713	8.50
1.219	19.44	1.092	14.20	1.801	18.62
1.505	24.87	1.574	21.30		
1.910	31.06	2.187	31.95		
2.318	36.41				

Table II : Association Constants, K_1 (moles/mole of solvent)$^{-1}$, and Specific Helmholtz Free Energies of Association, $-\Delta A$ (kcal./mole), for $Z = 4$, 5, or 6

Solvent, mole %			T, °K.	K_1	$-\Delta A$		
CsNO₃	KNO₃	LiNO₃			$Z = 4$	$Z = 5$	$Z = 6$
100	0	0	713	506 ± 20	6.85	6.55	6.29
33	67	0	658	530 ± 10	6.38	6.10	5.86
0	67	33	664	380 ± 25	6.0	5.7	5.5
0	100[a]	0	623–709				5.64
0	NaNO₃[b]	0	604–773				4.59
0	0	100[c]	713				5.2[c]

[a] See ref. 9.   [b] See ref. 10.   [c] Extrapolated value.

The value of ΔA for the mixed solvent 0.67 KNO₃–0.33 CsNO₃ is given, within the experimental error, by the linear expression $N_{KNO_3}\Delta A_{KNO_3} + N_{CsNO_3}\cdot\Delta A_{CsNO_3}$ where the N are mole fractions of the solvents KNO₃ and CsNO₃ in the mixed solvent. Such linearity has been observed also for the AgCl association in the mixed solvent NaNO₃–KNO₃[13] and for the formation of CdBr⁺ in mixtures of LiNO₃ and KNO₃.[5] Since cells with high proportions of LiNO₃ in the solvent did not give stable e.m.f. values at temperatures high enough to keep AgCl in solution, ΔA in LiNO₃ was estimated from the measured value of ΔA in the solvent 0.67 KNO₃–0.33 LiNO₃ and the known value of ΔA in pure KNO₃ by assuming a linear relation in the mole fractions of KNO₃ and LiNO₃. This led to a value of ΔA *more negative* in LiNO₃ than in NaNO₃ by nearly 0.6 kcal./mole in spite of the small radius

of Li⁺. (It is unlikely that the error in the estimate of ΔA in LiNO₃ can be high enough to account for this.) Thus, although the direction and approximate magnitude of the solvent effect in NaNO₃, KNO₃, and CsNO₃ can be correlated with the ionic radii, the results with LiNO₃ indicate the possibility of a smaller "effective radius" of nitrate ion in LiNO₃ than in the other alkali nitrates.[5]

(8)   M. Blander, *J. Chem. Phys.*, **34**, 432 (1961).

(9)   D. L. Manning, J. Braunstein, and M. Blander, *J. Phys. Chem.*, **66**, 2069 (1962).

(10)   D. G. Hill, J. Braunstein, and M. Blander, *ibid.*, **64**, 1038 (1960).

(11)   "Handbook of Chemistry and Physics," 9th Ed., Handbook Publishers, Inc., Sandusky, Ohio, 1956, p. 108.

(12)   O. J. Kleppa and L. S. Hersh, *J. Chem. Phys.*, **36**, 544 (1962).

(13)   D. G. Hill and M. Blander, *J. Phys. Chem.*, **65**, 1866 (1961).

The Vapor Pressures of Silicon Tetrachloride and Germanium Tetrachloride below Their Melting Points

by P. Balk and D. Dong

International Business Machines Corporation, Thomas J. Watson Research Center, Yorktown Heights, New York
(Received October 17, 1963)

In the course of an investigation of the interaction of chlorine with silicon and germanium,[1] the need arose for accurate data on the temperature dependence of the saturation vapor pressures of $SiCl_4$ and $GeCl_4$ in the range from 0.01 to 0.5 mm. Since no published data below 1 mm. were available, it was decided to measure these quantities. For both substances the pressures at the melting points are about 0.6 mm.; thus in the pressure range of interest both substances are solids. Considerable undercooling (by more than 20°) was observed when trying to freeze the liquids in both cases. This provided a convenient opportunity to extend the range of liquid vapor pressure data, particularly since the published values show considerable scatter between 1 and 10 mm. for $SiCl_4$[2] as well as for $GeCl_4$.[3] The present note describes the measurements and discusses their results.

Experimental

A 100-g. sample of semiconductor grade $SiCl_4$ (or $GeCl_4$) was transferred in a dry nitrogen atmosphere to a glass apparatus consisting of a purification section, a pressure-measuring section, and a vacuum station, separated from each other by a set of metal valves (Hooke A 434 K). After sealing off the apparatus, the sample was subjected to several cycles of freezing, evacuating, and melting to remove traces of dissolved permanent gases. Next, the sample was distilled over mercury to remove chlorine. Finally, the liquid was fractionated, retaining a middle fraction of about 20 g. After flushing several times with vapor, about 0.5 g. of sample was introduced into the evacuated pressure measuring section. Here, the compound was frozen out in a side arm and subsequently sublimed into a cryostated container kept at a temperature where the saturation vapor pressure is approximately 0.01 mm. The residual vapor was pumped off.

Mercury was used in the cryostat as a heat transfer medium. The desired temperatures, measured with a calibrated copper–constantan thermocouple, were obtained by adjusting the input to a built-in heater, while cooling continuously with liquid nitrogen. The pressure was monitored continuously with a thermistor gage.[4] After the temperature and the vapor pressure

had reached constant values, the pressure was measured with a McLeod gage. Then the heater current was increased slightly and the next point was taken. When repeating a run, the sample was removed from the pressure measuring section by pumping and a new charge was introduced. From this point, the same procedure was applied as described above. The melting points or, more accurately, the triple points, were taken from the onset of a plateau in the plot of the thermistor bridge off-balance voltage *vs.* temperature, for a continuous slow temperature rise.

During the measurements, the McLeod gage was separated from the cryostat by a U-tube immersed in an ice–salt mixture. The readings were corrected for the mercury vapor pressure. Thermomolecular pressure effects at the cryostat were estimated following Liang,[5] using collision diameters calculated according to Jona and Mandel.[6] The corrections were always less than 0.2% and were therefore omitted. The uncertainty of the McLeod gage readings (the gage had a 3-mm. precision bore capillary) ranged from 2% at the lowest pressures to 0.2% at the melting points. The accuracy of the temperature readings was better than 0.1°. It is thought that the scatter in the experimental data is mainly caused by material condensed in the temperature transition zone at the top of the cryostat and by sticking of the mercury in the gage.

The vapor pressures for the undercooled liquids were obtained using the thermistor gage, after sealing off the McLeod gage from the system. The thermistor gage was first calibrated, using the vapor pressure data for the corresponding solids, at increasing temperatures. After passing through the melting point, the direction of temperature change was reversed and the liquid vapor pressure data were taken. The error in the pressures obtained with the thermistor gage is about 0.3% over the entire range, discounting systematic errors in the calibration.

Results and Discussion

The data points for independent runs on each solid are indistinguishable and yield straight lines when plotted as log pressure *vs.* $1/T$, as shown in Fig. 1. They can thus be represented by an equation of the form

$$\log p \text{ (mm.)} = -a/T + b \qquad (1)$$

(1) P. Balk, to be published.
(2) A. Stock, C. Somieski, and R. Wintgen, *Ber.*, **50**, 1754 (1917).
(3) A. W. Laubengayer and D. L. Tabern, *J. Phys. Chem.*, **30**, 1047 (1926).
(4) A. J. Rosenberg, *J. Am. Chem. Soc.*, **78**, 2929 (1956).
(5) S. C. Liang, *J. Phys. Chem.*, **57**, 910 (1953).
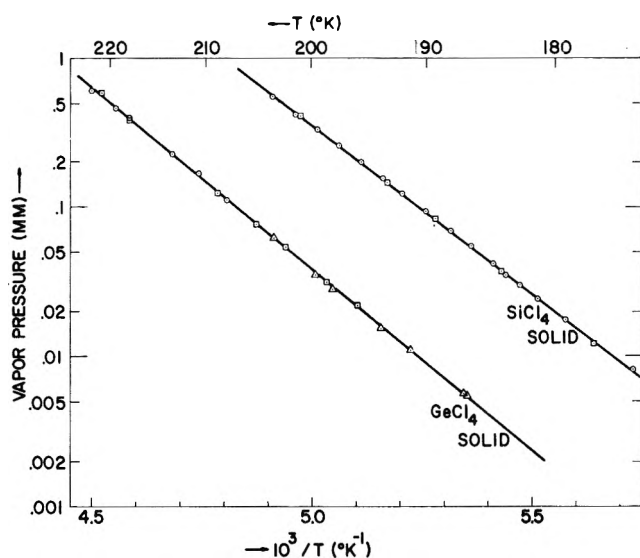(6) F. Jona and G. Mandel, *J. Chem. Phys.*, **38**, 346 (1963).

Figure 1. Vapor pressures of solid $SiCl_4$ and $GeCl_4$.
Different symbols indicate different independent
runs. Solid lines are least-square representations
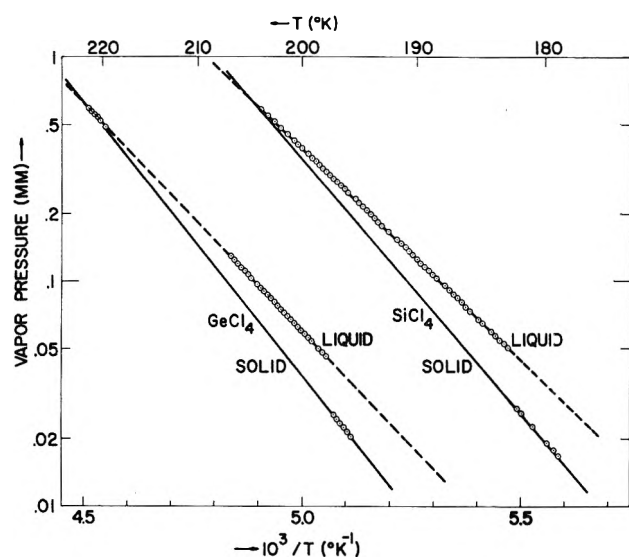(eq. 1, Table I) of experimental points.

Figure 2. Vapor pressures of undercooled liquid $SiCl_4$ and
$GeCl_4$. Dashed and solid lines are least-square representations
(eq. 1, Table I) of experimental points for liquids and solids,
respectively.

Values of the constants a and b, obtained by a least-square treatment, are listed in Table I, along with the probable errors (Δ) in the pressures. Experimental points for the undercooled liquids (Fig. 2) can also be represented by an expression of the form of eq. 1 (see Table I). There seems to be a very slight curvature in the plot of the $SiCl_4$ data points, and the values for a and b computed for the first half set of points from the melting point down are slightly different from those

obtained for the entire set. It should be noted that the straightness of the plot of the data for the under-cooled liquid is conditioned by the straightness of that for the solid, since the latter data were used in the form of eq. 1, to calibrate the thermistor gage for the measurements on the undercooled liquid. Upon solidification

Table I: Values for a, b, and Δ

	Range, °K.	a	b	Δ, %
$SiCl_4$				
(Solid)	174.5–m.p.	2262 ± 5	10.86 ± 0.03	1.3
(Undercooled liq.)	182.7–m.p.	1879 ± 2	8.99 ± 0.01	0.5
(Undercooled liq.)	193.0–m.p.	1871 ± 4	8.95 ± 0.02	0.3
$GeCl_4$				
(Solid)	186.8–m.p.	2437 ± 8	10.77 ± 0.12	2.0
(Undercooled liq.)	197.8–m.p.	2036 ± 1	8.959 ± 0.004	0.3

of the liquid the data points fall on the vapor pressure line of the solid (Fig. 2), which is indicative of the absence of volatile impurities in the tetrachlorides. The melting points (triple points) were found to be 204.3 ± 0.1°K. for $SiCl_4$ (lit.[7] 204.4°K.) and 221.6 ± 0.1°K. for $GeCl_4$. The melting point for $GeCl_4$ seems to indicate that the solid was identical with the metastable β-phase, for which melting point values of 221.4°K.[8] and 221.2°K.[9] have been reported, as compared to 223.7°K.[10] for the stable α-phase. It is believed that the lack of success in obtaining the stable phase may be due to the large degree of undercooling which was invariably exhibited by the very pure liquid in several trials and which could not be reduced by vibrating the apparatus during cooling.

By application of Clapeyron's equation to the vapor equilibria[11] one calculates for the heats of vaporization (liquid data from 193.0°K. to the melting point), sublimation, and fusion of $SiCl_4$ 8.56 ± 0.03, 10.35 ± 0.02, and 1.79 ± 0.03 kcal. mole^{-1}, respectively. The value for the heat of fusion is compatible with Latimer's calorimetric value of 1.845, ±2%.[12] The heats of vaporization, sublimation, and fusion of $GeCl_4$

(7) Landolt-Börnstein, "Zahlenwerte und Funktionen aus Physik, Chemie, Astronomie, Geophysik, Technik," II. 2a, Springer, Berlin, 1960, p. 39.

(8) P. A. Bond and E. B. Crone, J. Am. Chem. Soc., 56, 2028 (1934).

(9) H. H. Sisler, W. J. Wilson, B. J. Gibbins, H. H. Batey, B. Pfahler, and R. Mattair, ibid., 70, 3818 (1948).

(10) See ref. 7, p. 52.

(11) E. A. Guggenheim, "Thermodynamics," 4th Ed., North-Holland Publishing Co., Amsterdam, 1959, pp. 148, 149.

are 9.31 ± 0.01, 11.14 ± 0.04, and 1.83 ± 0.02 kcal. mole^{-1}, respectively. The data permit calculation of the entropies of the solids. Starting from Kelley and King's value for the standard entropy of SiCl$_4$ vapor (79.1 ± 1.0 e.u.),[13] one obtains the entropy at the melting point and 760 mm. by subtracting 7.75 e.u. (from Kelley's specific heat equation),[14] and the entropy of the vapor at the saturated vapor pressure at the melting point by subsequently adding a pressure correction term (to 0.617 mm.) of 14.14 e.u. By subtraction of the entropy of sublimation: 10350/204.3 = 50.65 e.u. (present data), a value of 34.8 ± 1.3 e.u. is found for the entropy of solid SiCl$_4$ at the melting point. This value is close to that obtained in ref. 13 from a recalculation of Latimer's data[12] (35.05 e.u.), and it is still compatible with Latimer's original value (33.85 e.u.).[12] The entropy of GeCl$_4$ vapor at the melting point and saturated vapor pressure (0.590 mm.) is obtained similarly by subtracting 6.53 e.u.[15] from the standard entropy of the vapor (83.0 ± 0.8 e.u.)[16] and next adding a pressure term of 14.22 e.u. A value of 40.4 ± 1.2 e.u. for solid GeCl$_4$ follows after subtraction of 11,140/221.6 = 50.30 e.u. for the entropy of sublimation (present data). No value for solid GeCl$_4$ has been listed in the literature.

Vapor pressure equations for the liquid tetrachlorides also follow from Kelley's free energy equations.[17] They are of the form

$$\log p = -A/T + B + C \log T \qquad (2)$$

where C is the difference between the specific heats of vapor and liquid, divided by the gas constant R, and the constants A and B were apparently chosen to fit the experimental data above 10 mm. The present data for undercooled SiCl$_4$ are about 5% higher than the values obtained from Kelley's expression. Inspection shows that a satisfactory fit to the present data and the higher pressure data can be obtained by a slight adjustment in the values of A and B. For undercooled GeCl$_4$, the data reported in this note are 20% higher. It is not unlikely that this discrepancy is caused by the larger scatter in the experimental points from which the constants of eq. 2 were derived, and by the rather high estimate of the value for the difference in the specific heats.

(12) W. M. Latimer, *J. Am. Chem. Soc.*, **44**, 90 (1922).

(13) K. K. Kelley and E. G. King, Bureau of Mines Bulletin 592, U. S. Govt. Printing Office, Washington, D. C., 1961, p. 83.

(14) K. K. Kelley, Bureau of Mines Bulletin 584, U. S. Govt. Printing Office, Washington, D. C., 1960, p. 163.

(15) See ref. 14, p. 72.

(16) See ref. 13, p. 42.

(17) K. K. Kelley, Bureau of Mines Bulletin 383, U. S. Govt. Printing Office, Washington, D. C., 1935, pp. 47, 91.

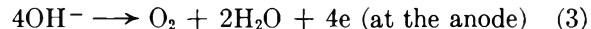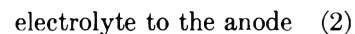# Electrolytic Separation and Purification of Oxygen from a Gas Mixture

by Stanley H. Langer* and Robert G. Haldeman

Central Research Division, American Cyanamid Company, Stamford, Connecticut (*Received September 9, 1963*)

Oxygen is usually prepared by fractional distillation of air or electrolysis of water. The latter has the disadvantages of overvoltage, resulting in greater than theoretical power requirements, and the need to separate and dispose of simultaneously evolved hydrogen. An alternate convenient electrolytic technique would be separation of oxygen from air or other gaseous mixtures using porous catalytic oxygen electrodes working in opposite directions with an electrolyte transport and barrier phase between them. Oxygen is selectively removed, transported, and regenerated according to the following equations in basic aqueous solution.

$$O_2 + 2H_2O + 4e \longrightarrow 4OH^- \text{ (at the cathode)} \qquad (1)$$

$4OH^-$ transported through the

$$\text{electrolyte to the anode} \qquad (2)$$

$$4OH^- \longrightarrow O_2 + 2H_2O + 4e \text{ (at the anode)} \qquad (3)$$

Thus, oxygen is separated from other less electroactive materials which are relatively insoluble in the electrolyte barrier phase. The applied external voltage must be sufficient to overcome the characteristic overvoltage loss for reactions 1 and 3 as well as concentration and ohmic polarization. This may still be considerably less than the 1.5 v. or more generally necessary for the electrolysis of water; furthermore, no hydrogen is evolved.

In acid solution, reaction may be represented as

$$O_2 + 4H^+ + 4e \longrightarrow 2H_2O \text{ (cathode)} \qquad (4)$$

$$2H_2O \longrightarrow O_2 + 4H^+ + 4e \text{ (anode)} \qquad (5)$$
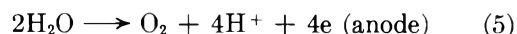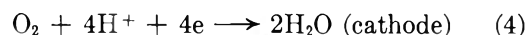
Using the schemes above and molded catalyst–polyethylene or catalyst–polytetrafluoroethylene[1,2] gas permeable electrodes, we have obtained substantially pure oxygen from air (purity > 97%, mass spectrometrically) with acid, base, and ion-exchange membrane

* Chemical Engineering Dept., University of Wisconsin, Madison 6, Wisc.

(1) (a) G. V. Elmore and H. A. Tanner, *J. Electrochem. Soc.*, **108**, 669 (1961); (b) W. T. Grubb, "Proceedings of the 16th Annual Power Sources Conference," PSC Publications Committee, Red Bank, N. J., pp. 31–34.

(2) S. H. Langer and R. G. Haldeman, *Science*, **142**, 225 (1963).

Table I: O_2 Purification Cell Performance Data (Cell Initially at 25°)

Electrodes	Electrolyte	Initial cell resistance, ohms	Voltage drop at given current		Inlet gas
			Volts	Amp.	
Pt (11.2 mg./cm.²) on stainless steel screen	5 disks of filter paper saturated with 23% KOH	0.44	0.62	0.05	O_2
			0.95	0.2	O_2
			1.00	0.2	Air
Pt (9 mg./cm.²) on tantalum screen	5 disks of filter paper saturated with 6 N H_2SO_4	0.23	0.78	0.1	O_2
			1.05	0.5	O_2
			1.08	0.3	Air
Ni (1.6 mg./cm.²) deposited on graphite (14.4 mg./cm.²)	3 disks of filter paper saturated with 23% KOH	0.43	1.19	0.3	O_2
			1.24	0.15	Air

electrolyte phases. The purified oxygen is saturated with water vapor as is the inlet air (except when water is added directly to the electrolyte phase). Platinum, silver–carbon, and nickel–carbon have all been found to be effective catalysts for oxygen purification.

· For the work described here, we have used a purification cell (electrode area 4.9 cm.²) and ancillary apparatus similar to that which we have described previously for hydrogen purification.[2,3] The arrangement differs in that the impure gas stream impinges on the cathode while purified oxygen emerges from the anode compartment. Voltage and current, coulombicly related to the amount of oxygen purified, are monitored in the same fashion as previously.[2] Some operating data are given in Table I. Performance can be improved by varying catalyst, electrolyte, and pore distribution, to minimize gas diffusion polarization.[4]

A polarization curve for a high performance cell with platinum black catalyst (9 mg./cm.²) is shown in
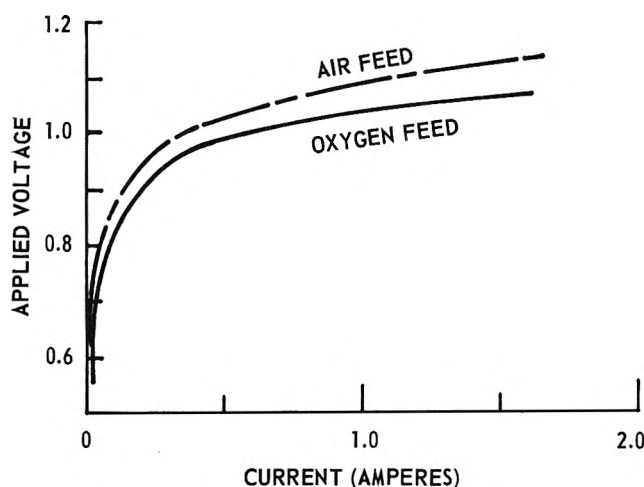

Figure 1. Performance of O_2 purification cell: Pt black–polytetrafluoroethylene electrodes; electrolyte, glass fiber disk saturated with 2 N $HClO_4$; internal resistance, 0.07 ohm.

Fig. 1. We have compared the rate of evolved oxygen with current supplied to the cell with both acid and base electrolyte and found the over-all four-electron mechanism to be operative. On this basis, 1 amp.-min. is equivalent to about 4 ml. of O_2 at our operating conditions. Where power requirements are a consideration, it would be desirable to have the oxygen react through a two-electron mechanism[5] if it were possible.

The cell described is useful for pumping and metering oxygen in addition to providing a convenient source of the pure gas. It also provides a tool for studying catalytic materials and mechanisms at the oxygen electrode and makes possible simultaneous studies of polarization at both the oxygen-reducing and oxygen-evolving electrode.

(3) See also J. E. McEvoy, R. A. Hess, G. A. Mills, and H. A. Shalit, Petroleum Preprints, Symposium on Production of Hydrogen, 145th National Meeting of the American Chemical Society, New York, N. Y., September, 1963, p. B61.

(4) H. B. Urbach, "Fuel Cells," Vol. II, E. G. Young, Ed., Reinhold Publishing Corp., New York, N. Y., 1963, Chapter 7; L. G. Austin, ibid., Chapter 8.

(5) W. G. Berl, Trans. Electrochem. Soc., **83**, 253 (1943); M. O. Davies, M. Clark, E. Yeager, and F. Hovarka, J. Electrochem. Soc., **106**, 56 (1959), and references therein.

An Effusion Study of the Decomposition of Iron(III) Bromide

by R. R. Hammer and N. W. Gregory

Department of Chemistry, University of Washington, Seattle, Washington

The kinetic behavior of vaporization–decomposition processes appears quite varied and unpredictable. We have been studying a number of reactions of the type

$$A(s) = B(s) + C(g)$$
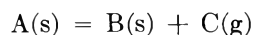
by effusion methods.[1-3] An analysis of steady-state pressures of $Fe_2Cl_6(g)$ and of chlorine in effusion cells containing solid iron(III) chloride shows that, with proper allowance for dependence of steady-state pressures on cell geometry, equilibrium vaporization characteristics of Fe_2Cl_6 can be obtained; however, the effusion pressures of chlorine, which effuses simultaneously with Fe_2Cl_6, do not provide a reliable source of equilibrium data for the decomposition reaction $2FeCl_3(s) = 2FeCl_2(s) + Cl_2(g)$.[2] On the other hand, satisfactory equilibrium data for the similar reaction $2CuBr_2(s) = 2CuBr(s) + Br_2(g)$ were obtained by the effusion method.[3]
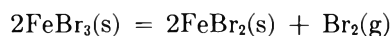
We now wish to report results of an effusion study of the decomposition

$$2FeBr_3(s) = 2FeBr_2(s) + Br_2(g)$$

The iron(III) bromide solid and vapor phases are very similar in structure and molecular composition, respectively, to those of the chloride system. The principal difference is that the bromide is less stable; bromine decomposition pressures are expected to be in the effusion range below room temperature (based on diaphragm gage study of the system at higher temperature).[4] The vapor pressures of the iron bromides are negligible at temperatures of interest for an effusion study of the decomposition reaction, in contrast to the vapor pressure of Fe_2Cl_6 in the chloride system.

Experimental

The torsion effusion apparatus used has been described previously.[3,5] It consists of a double orifice Pyrex (or quartz) effusion cell, ca. 4 cm. long and 2 cm. in diameter, suspended by a tungsten fiber. The cell was surrounded by a copper cylinder heated inside the vacuum system by radiation from photoflood lamps. Temperatures of the cell were assumed to be the same as those measured by a thermocouple inserted into a well on an adjacent dummy cell. The apparatus was calibrated by comparison of measured vapor pressures of zinc and mercury with well-established values from the literature.[6] The effusion measurements on FeBr₃ were made between 40 and 70°.

Samples of anhydrous FeBr₃ were prepared by reaction of Merck's reagent grade bromine, previously dried over P_2O_5, and reagent grade iron wire. The iron was placed in one leg of a V-shaped Pyrex tube and held at 175–200° while the liquid bromine in the other leg was held at ca. 120°. After standing for several weeks, virtually a 100% yield of FeBr₃ was obtained. Samples were transferred in a drybox to effusion cells and the orifices temporarily sealed while cells were

mounted in the torsion tower. The weight loss of the cell after a series of measurements was compared with the amount of bromine calculated to have effused through the orifices during the measurements to determine the degree of decomposition at various points. After brief degassing periods, the entire pressure indicated by the twist of the torsion fiber was attributed to bromine.

Results and Discussion

Bromine steady-state pressures in effusion cells showed considerable scatter. Pressures were dependent on sample size unless more than ca. 0.5 g. of undecomposed FeBr₃ was present. With from 0.5 to 3-g. samples, reasonably consistent pressures were obtained. Results shown in Fig. 1 correspond to the
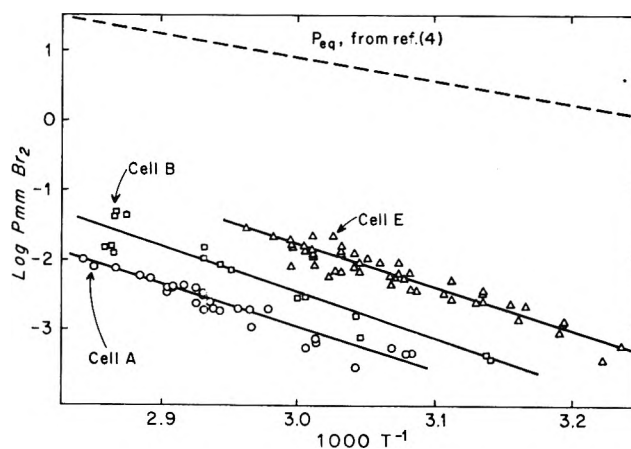
Figure 1. Effusion bromide steady-state pressure above iron(III) bromide. Cell: A_0, total area (cm.²) of the two nearly identical orifices; A_s, cell cross-sectional area (cm.²); A, 0.0375, 4.8; B, 0.00715, 7.3; E, 0.00219, 6.3.

observed behavior when the solid composition was between 12 and 80% FeBr₂. On either side of these approximate limits, pressures were appreciably lower, falling toward zero as the reaction neared completion and rising slowly in the initial stages of the decomposition. In the intermediate steady-state pressure plateau region, the temperature could be varied ran-

(1) E. Kay and N. W. Gregory, J. Phys. Chem., 62, 1079 (1958).

(2) R. R. Hammer and N. W. Gregory, ibid., 66, 1705 (1962).

(3) R. R. Hammer and N. W. Gregory, ibid., 68, 314 (1964).

(4) N. W. Gregory and B. A. Thackrey, J. Am. Chem. Soc., 72, 3176 (1950).

(5) R. J. Sime and N. W. Gregory, J. Phys. Chem., 64, 86 (1960).

(6) For zinc: R. F. Barrow, et al., Trans. Faraday Soc., 51, 1354 (1955); K. K. Kelley, U. S. Bureau of Mines Bulletin 385, U. S. Govt. Printing Office, Washington, D. C., 1935; for mercury: R. H. Busey and W. F. Giauque, J. Am. Chem. Soc., 75, 806 (1953).

domly with reproducible pressures (within the large scatter shown) obtained at any given temperature.

It will be observed that effusion pressures are from $1/10,000$ to $1/500$ as large as expected equilibrium values, extrapolated from the higher temperature diaphragm gage study.[4] Whereas the pressures increase as the orifice diameters decrease, no simple systematic relationship could be found to correlate the pressures with effusion cell geometries or to predict from the various steady-state pressures the value of the equilibrium limit. It appears that the condensation coefficient is very small, of the order of 10^{-7}, similar in magnitude to the apparent value for the iron(III) chloride decomposition reaction.[2] The appearance of the sample after removal of considerable amounts of bromine suggests that decomposition occurs largely at the edges of the plate-like crystals. No appreciable yellow coloration ($FeBr_2$) could be seen on the large faces of $FeBr_3$ crystals. The effective surface area for the decomposition may be limited to the edges of these crystals, similar to the behavior (loss of water) in the $Mg(OH)_2$ system.[1] The condensation coefficient on these edges alone may be considerably larger; the average value of α could appear very small because the reacting edges constitute only a small fraction of the total area of the sample. The large scatter of data may well be caused by variations in the effective reacting surface area as well as possible variations in the condensation and vaporization coefficients as the decomposition progresses.

The slopes of the least-squares lines in Fig. 1, drawn through effusion data from the various cells, are different from that of the equilibrium line. From the variation in condensation coefficient with temperature suggested by these slopes, an apparent heat of activation for condensation of 12 kcal. mole^{-1} of bromine, and for vaporization of 28 kcal. mole^{-1}, is obtained.[7] In view of the large difference between steady-state and equilibrium pressures, these apparent values may have little significance. It is of interest, however, that the apparent heat of activation for vaporization of bromine is virtually the same as that indicated for release of chlorine from $FeCl_3$ (26).[2] However, the value for condensation of chlorine appeared to be near zero. Simultaneous vaporization of Fe_2Cl_6 in the chloride case provides a mechanism for renewing the $FeCl_3$ solid surface which was not present in the bromide system.

These results emphasize that caution must be exercised in the application of the effusion method to the study of decomposition reactions. The method is not useful as a means for determination of relative

thermodynamic properties of iron(III) and iron(II) bromides and chlorides, respectively.

(7) N. W. Gregory, *J. Phys. Chem.*, **67**, 618 (1963).

The Vapor Pressure and Heat and Entropy of Sublimation of Solid Magnesium Fluoride

by Michael A. Greenbaum, Hon Chung Ko, Madeline Wong, and Milton Farber

Rocket Power, Inc., Research Laboratories, Pasadena, California (*Received October 3, 1963*)

The first vapor pressure measurements of MgF_2 were reported by Ruff and LeBoucher[1] in 1934. These investigators used a manometric method to obtain a vapor pressure curve for liquid MgF_2 between 1934 and 2129°K. In 1945, Naylor[2] reported values for the melting point and heat of fusion of MgF_2. Using these values, a heat of sublimation at 298°K. was calculated for MgF_2.[3] The value obtained in this manner was 85.6 ± 1.0 kcal./mole. In 1962, Berkowitz and Marquart[4] reported the first experimental determination of the vapor pressure of solid MgF_2 together with the heat of sublimation. The solid was studied at 1220–1450°K. by means of a mass spectrometer. However, only nine points were measured in this range. From a plot of log P vs. $1/T$ the authors obtained a second-law value of 86 kcal./mole for the heat of sublimation of MgF_2 at 1330°K. Their third-law value for ΔH_{sub} was found to be only 81 kcal./mole, however.

Because of the limited amount of experimental data available on the vapor pressure of solid MgF_2 coupled with the lack of a definitive value for the heat of sublimation, it was decided to undertake a detailed measurement of the vapor pressure of $MgF_2(c)$ by means of the torsion effusion procedure.

Experimental

The measurement of the vapor pressure of $MgF_2(c)$ was carried out over the temperature range 1273–

(1) O. Ruff and L. LeBoucher, *Z. anorg. allgem. Chem.*, **219**, 376 (1934).

(2) B. F. Naylor, *J. Am. Chem. Soc.*, **67**, 150 (1945).

(3) JANAF Thermochemical Tables, USAF Contract No. AF33(616)-6149, Advanced Research Projects Agency, Washington 25, D C., December, 1960.

(4) J. Berkowitz and J. R. Marquart, *J. Chem. Phys.*, **37**, 1853 (1962).

1513°K. by means of the torsion effusion procedure. This procedure is sufficiently well established and widely used to eliminate the necessity of any detailed discussion of the theory of experimental procedure involved. Such discussions and descriptions of the specific apparatus and experimental procedures used can be found in several previous papers from these laboratories[5-7] as well as in a recent article by Schulz and Searcy.[8]

The MgF_2 employed in this investigation was 99.8+ % material obtained from City Chemical Corp. Since MgF_2 is nonhygroscopic, no special handling precautions were necessary in this study. The material was placed in graphite effusion cells which were in turn placed in the torsion apparatus. The cells used in this work have previously been described in detail.[5-7] Two different cells which had orifice areas differing by a factor of four were used in this work. The temperature of the furnace, which was identical with one previously described,[7] was recorded and automatically controlled to $\pm 1°$. The suspension wire employed in these studies was a 1.5-m. length of 2-mil molybdenum.

Measurements were made at 10° intervals within the temperature range studied after baking of the MgF_2 sample for 18 hr. at 1125°K. Runs were repeated in the same cell on three consecutive days to ensure that no minor amounts of impurities were present in the MgF_2 sample. After completion of this procedure, the sample was cooled, the apparatus opened, and a fresh sample of MgF_2 contained in the second cell was placed in the apparatus and the above procedure repeated. In no case was there any evidence of a measurable amount of impurity in the MgF_2 sample.

Data Treatment

The effusion of vapor through an orifice imparts a torque to the wire supporting the effusion cell. The angle through which the cell (and wire) rotates is calculated from the displacement of a beam of light by a galvanometer mirror attached to the torsion wire. The displacement distance is measured experimentally by using a cathetometer to observe the readings on a meter stick. The experimental values obtained are the rest point of the cell when no material is effusing and the distance the light beam moves on the meter stick at temperatures where vapors are effusing from the cell. These distances (in cm. or mm.) are combined with the measured perpendicular distance of the mirror from the meter stick to yield, via the tangent relationship, the angle of rotation.

The vapor pressure is calculated from the angle of rotation by eq. 1 where P is the vapor pressure; D is the torsion constant of the suspension wire in dyne-cm./ radian; θ is the angle of rotation in radians; a_i is the cross-sectional area of orifice i in .cm.^{2}; f_i is the Searcy correction factor for nonideality of orifice i; and q_i is the horizontal distance of orifice i from the suspension wire in cm. (moment arm).

Results and Discussion

The vapor pressure of $MgF_2(c)$ was measured at 40 different points in the temperature range 1273–1513°K. using the torsion effusion apparatus. The results of these measurements are presented in Table I. The geometrical factors of the effusion cells employed in this work are presented in Table II.

Since the torsion effusion procedure yields vapor pressure values which are independent of the molecular weight of the effusing species, the validity of the vapor pressure data reported here is dependent on a knowledge of the nature of the effusing species. The identity of the species effusing from the orifice of the graphite cells can be obtained in three ways. First, a mass spectrometric study of the effusing species will yield the most accurate analysis of the effusing gases. Second, simultaneous torsion and gravimetric effusion studies will permit the calculation of the average molecular weight of the effusing gas. The third method of identifying the effusing species is an indirect one and depends upon agreement between the second- and third-law values for the heat of sublimation as calculated from the experimental vapor pressure data. As the slope of the vapor pressure curve is independent of the nature of the vapor species while the third-law value does depend on this factor, it is obvious that good agreement between these two values is evidence for the existence of the assumed species.

The study of the vapor species of MgF_2 in the temperature range of interest in the present investigation has been carried out by several groups. Berkowitz and Marquart[4] carried out a detailed spectroscopic examination of MgF_2 vapor to 1450°K. At these temperatures it was determined that no more than 1% of $(MgF_2)_2$ was present. No evidence for the existence of any MgF was obtained. Thermodynamic calculations also indicate that the existence of $MgF(g)$ at these temperatures and pressures is highly improbable. Hammer[9,10] has studied the vapor species of

$$P_{mm} = \frac{\theta D}{\sum a_i f_i q_i} \times 7.5 \times 10^{-4} \qquad (1)$$

(5) M. A. Greenbaum, J. N. Foster, M. L. Arin, and M. Farber, *J. Phys. Chem.*, **67**, 36 (1963).

(6) M. A. Greenbaum, R. E. Yates, and M. Farber, *ibid.*, **67**, 1802 (1963).

(7) R. E. Yates, M. A. Greenbaum, and M. Farber, *ibid.*, in press.

(8) D. A. Schulz and A. W. Searcy, *ibid.*, **67**, 103 (1963).

Table I : Summary of Data from Vapor Pressure Studies on $MgF_2(c)$ by Torsion Effusion

T, °K.	Cell	θ, radian	P, atm. $\times$ 10^6	ΔF_{sub}, kcal./ mole	ΔH_{sub}, kcal./ mole
1273	1	0.045	2.218	32.936	78.955
1273	1	0.053	2.613	32.522	78.541
1283	1	0.052	2.563	32.826	79.142
1292	1	0.060	2.958	32.689	79.349
1293	1	0.075	3.697	32.140	78.766
1304	1	0.076	3.747	32.379	79.362
1314	1	0.104	5.128	31.808	79.086
1323	1	0.112	5.522	31.832	79.381
1323	2	0.031	7.872	30.899	78.448
1333	1	0.155	7.642	31.212	79.067
1343	1	0.177	9.726	31.092	79.252
1343	1	0.170	8.382	31.199	79.359
1352	1	0.227	11.192	30.631	79.073
1363	1	0.274	13.513	30.370	79.138
1373	1	0.339	16.711	30.013	79.084
1373	2	0.070	17.776	29.845	78.916
1373	2	0.081	20.564	29.447	78.518
1383	1	0.408	20.118	29.722	79.095
1383	2	0.086	21.841	29.496	78.869
1393	1	0.425	20.947	29.826	79.500
1393	2	0.114	28.945	28.927	78.601
1394	2	0.109	27.683	29.073	78.769
1403	1	0.491	24.211	29.635	79.610
1403	2	0.127	32.235	28.837	78.812
1404	1	0.624	30.765	28.988	78.984
1413	2	0.158	40.118	28.429	78.704
1414	1	0.644	31.750	29.106	79.416
1415	2	0.184	46.726	28.040	78.372
1423	1	0.712	35.105	29.007	79.580
1423	2	0.177	44.934	28.309	78.882
1433	1	0.838	41.316	28.747	79.604
1433	2	0.231	58.654	27.745	78.602
1444	2	0.268	68.051	27.535	78.725
1454	2	0.307	77.961	27.333	78.819
1465	2	0.384	97.511	26.888	78.705
1473	2	0.426	108.171	26.739	78.780
1484	2	0.520	132.105	26.341	78.711
1494	2	0.582	147.763	26.187	78.853
1504	2	0.716	181.842	25.742	78.698
1513	2	0.866	219.868	25.325	78.552

Table II : Geometrical Constants of Torsion Cells

Cell	D, dyne-cm./ radian	a_i, cm.^{2}	f_i	q_i, cm.
Cell 1, four 1.0-mm. holes	0.6337	7.856×10^{-3}	0.734	0.55
Cell 2, four 0.5-mm. holes	0.6337	1.964×10^{-3}	0.570	0.55
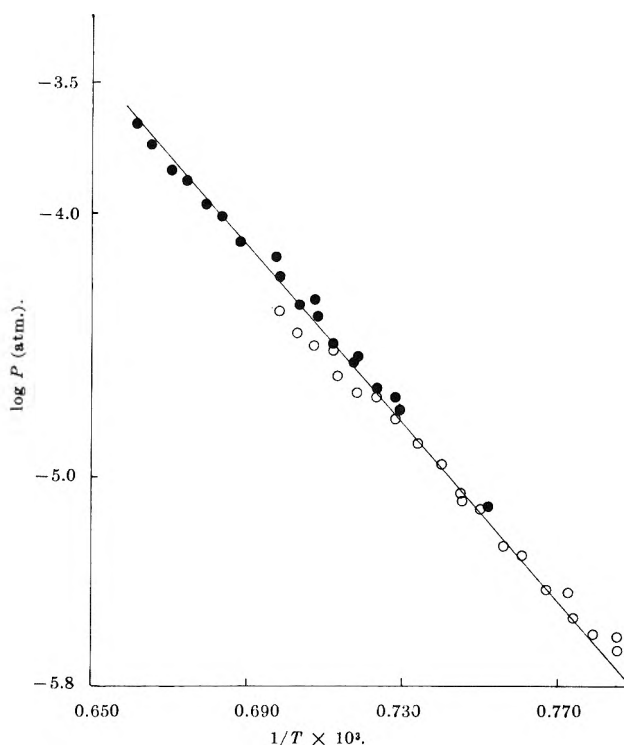
Figure 1. Vapor pressure of MgF_2 as a function of temperature: O, cell I; ●, cell II.

MgF_2 by effusion procedures and calculated the average molecular weight of gas. Within experimental error this was found to be that of MgF_2 monomer. This result was subsequently confirmed by Hildenbrand.[11] Similar results have been obtained in the study of the vapor pressure of CaF_2.[9,12]

Based on these experimental data, the vapor pressures in this study were considered to be those of $MgF_2(g)$ only. A plot of the data in Table I in the form of log P vs. $1/T$ was made (Fig. 1). A least-squares analysis of the data yields a value for the slope of -17.10 ± 0.23, which corresponds to a ΔH^{1400}_{sub} of 78.23 ± 1.03 kcal./mole. A plot of ΔF vs. T yields a value of 35.16 ± 0.75 cal./deg./mole for the ΔS^{1400}_{sub}. Using the available thermal functions for MgF_2 gas and solid,[3] conversion of these values to 298°K. yields ΔH^{298}_{sub} 83.21 ± 1.03 kcal./mole and ΔS^{298}_{sub} 41.78 ± 0.75 cal./deg./mole. The vapor pressure in the

(9) R. R. Hammer, "The Vapor Pressure of Magnesium Fluoride," Ph.D. Thesis, University of California, Berkeley, Calif., September, 1961.

(10) R. R. Hammer, D. R. Messier, and J. A. Park, University of California Ceramic Laboratories, Series 18, Issue 8, 1960.

(11) D. L. Hildenbrand and L. P. Theard, Aeronutronic Report U-1187, Newport Beach, Calif., March, 1961.

(12) G. D. Blue, J. W. Green, R. G. Bautista, and J. L. Margrave, J. Phys. Chem., **67**, 877 (1963).

temperature region studied (1273–1513°K.) is defined by

$$\log P_{atm} = \frac{-17,096}{T} + 7.6845 \qquad (2)$$

Using the available values for the entropies of solid and gaseous MgF_2[3] coupled with the experimentally determined vapor pressures, a third-law value for $\Delta H^{298}{}_{sub}$ of MgF_2 of 83.95 ± 0.64 kcal./mole is obtained. The excellent agreement between second- and third-law values obtained in this investigation for $\Delta H^{298}{}_{sub}$ of MgF_2 coupled with the fine agreement of the $\Delta S^{298}{}_{sub}$ with the theoretical value of 42.2 cal./deg./mole confirms the previous experimental observation that the vapor species above $MgF_2(c)$ consists of only $MgF_2(g)$ within experimental error (1–2%).

The value of $\Delta H^{298}{}_{sub}$ obtained in this work is in reasonably good agreement with the value previously calculated[3] by combining the vapor pressure data of the liquid[1] and the melting point and heat of fusion[2] (85.6 ± 1.0 kcal./mole), and the third-law value of Berkowitz[4] (~85 kcal./mole). It should also be mentioned that the vapor pressure of $MgF_2(c)$ at 1450°K. reported by Berkowitz[4] (2.8×10^{-5} atm.) is only about one-third of the measured value (7.3×10^{-5} atm.) reported here. Based on the excellent agreement between the second- and third-law values for $\Delta H^{298}{}_{sub}$ obtained in the present investigation, coupled with the very large number of points obtained in the 240° temperature range studied, it is considered that the present vapor pressure curve and the heat and entropy of vaporization reported here are more definitive than those previously reported.

It should be pointed out that in this investigation, in which two effusion cells were employed having orifice areas differing by a factor of four, no dependence of the vapor pressure on orifice area was observed. This is consistent with previous experimental observations made in this laboratory in studies of BeF_2[5] and $BeCl_2$,[6] where orifice areas of cells were varied by as much as a factor of sixteen.

Mass Spectra, Radiolysis, and Photolysis of Phenyl Alkyl Ketones

by Seymour Meyerson

Research and Development Department, American Oil Company, Whiting, Indiana   *(Received October 31, 1963)*

A recent paper[1] reported that radiolysis of n-butyrophenone is dominated by a reaction leading to ethylene

and acetophenone, and that no such specificity of product formation is displayed by isobutyrophenone or benzoylcyclopropane. The parallel with the Norrish Type II photolytic reaction of aliphatic ketones[2–4] suggested that similar mechanisms may be important in radiolysis and photolysis of phenyl alkyl ketones. At the same time, the paper reported failure to find any correlation between these results and mass spectra. The spectra were stated to be so similar as to be useless for predicting how radiolytic reactions of the three ketones might differ. The present writer furnished the spectra referred to, but does not concur in this judgment.

The statement cited is correct if only the grossest spectral features are taken into consideration. For example, the three most intense fragment-ion peaks in each of the three spectra are those due to $C_7H_5O^+$, $C_6H_5^+$, and $C_4H_3^+$, of masses 105, 77, and 51. Among peaks of lower intensity, however, the partial spectra shown in Table I reveal significant differences, some of which parallel closely differences found in radiolysis. In particular, the normal peak at 120 and the metastable peak at 97.3 arise from primary rearrangement–dissociation of n-butyrophenone to ethylene and acetophenone (enol) ion[5]; no indication of an analogous process is observed in the spectra of isobutyrophenone and benzoylcyclopropane. This reaction, characteristic of a wide variety of carbonyl compounds under electron impact provided they have the requisite structural features, has been shown[5] to parallel precisely the Norrish Type II photolysis of aliphatic ketones.

Admittedly, the reaction leading to acetophenone in radiolysis of n-butyrophenone looms far larger than the analogous reaction in the mass spectrum. Such a difference might have been anticipated even if reaction mechanisms in radiolysis were assumed identical with

(1) D. J. Coyle, *J. Phys. Chem.*, **67**, 1300 (1963).

(2) R. G. W. Norrish, *Trans. Faraday Soc.*, **33**, 1521 (1937); W. Davis and W. A. Noyes, *J. Am. Chem. Soc.*, **69**, 2153 (1947); J. R. McNesby and A. S. Gordon, *ibid.*, **80**, 261 (1958); N. C. Yang and D. H. Yang, *ibid.*, **80**, 2913 (1958); P. Ausloos and E. Murad, *ibid.*, **80**, 5929 (1958); R. Srinavasan, *ibid.* **81**, 5061 (1959); P. Ausloos, *J. Phys. Chem.*, **65**, 1616 (1961); R. P. Borkowski and P. Ausloos, *ibid.*, **65**, 2257 (1961).

(3) The well-known correspondence between primary rearrangement–dissociation reactions of aliphatic ketones in photolysis and under electron impact [A. J. C. Nicholson, *Trans. Faraday Soc.*, **50**, 1067 (1954); T. W. Martin and J. N. Pitts, *J. Am. Chem. Soc.*, **77**, 5465 (1955); P. P. Manning, *ibid.*, **79**, 5151 (1957); F. W. McLafferty, *Anal. Chem.*, **31**, 82 (1959)] was recently extended to include also radiolysis [J. N. Pitts and A. D. Osborne, *J. Am. Chem. Soc.*, **83**, 3011 (1961)].

(4) Reference 1 reports, on the basis of preliminary experiments, that "the photolysis with 2537-Å. radiation of the neat aralkyl ketones *in vacuo* yields products anticipated on the basis of the photochemistry of dialkyl ketones."

(5) S. Meyerson and J. D. McCollum. *Advan. Anal. Chem. Instr.*, **2**, 179 (1963), and references cited there.

Table I: Partial Mass Spectra of Phenyl Alkyl Ketones[a]

Mass	n-C₃H₇	i-C₃H₇	cyclo-C₃H₅
		Relative intensity	
39	2.33	2.38	4.89
41	1.60	2.18	3.63
42	0.40	0.34	0.28
43	1.26	1.40	0.12
51	7.21	7.28	7.41
77	16.0	15.5	13.6
105	37.9	47.6	27.5
120	2.75	0.01	0.01
Parent less 1	0.30	0.06	1.84
Parent	6.00	2.78	7.56

Metastable peaks corresponding to primary reaction steps[b]

	n-C₃H₇	i-C₃H₇	cyclo-C₃H₅
74.5	0.06	0.08	. . .
75.5	. . .	. . .	0.69
97.3	0.15	. . .	. . .
144.0	. . .	. . .	0.13
146.0	0.04	. . .	. . .

Transitions denoted by metastable peaks[b]

74.5	$(148^+) \rightarrow (105^+) + 43$
75.5	$(146^+) \rightarrow (105^+) + 41$
97.3	$(148^+) \rightarrow (120^+) + 28$
144.0	$(146^+) \rightarrow (145^+) + 1$
146.0	$(148^+) \rightarrow (147^+) + 1$

[a] Total ion intensity = 100.0. No corrections made for contributions of naturally occurring heavy isotopes. [b] For interpretation of metastable peaks, see ref. 5.

those in the mass spectrometer. Extrapolation of results from the gas phase at 10^{-5} torr to the liquid phase may be possible for primary reaction steps and especially for low-energy processes, but would seem progressively less likely for succeeding steps and for higher-energy processes. Moreover, involvement in radiolytic processes of reactive intermediates, such as those appearing in mass spectra, might well be obscured in the ultimate reaction products even if the latter were all isolated and identified.

Common intermediates and reaction paths in mass spectra—as in photolysis—and radiolysis of phenyl alkyl ketones are certainly not established by available evidence. However, the parallel is striking. Interpreted with care, mass spectra can furnish helpful guidance in exploring radiolytic systems.

Experimental

Mass spectra were measured with 70-v. electrons on a modified[6] Consolidated 21-103 instrument with the sample-introduction system at 250°.

(6) H. M. Grubb, C. H. Ehrhardt, R. W. Vander Haar, and W. H. Moeller, presented before ASTM Committee E-14 on Mass Spectrometry, Los Angeles, Calif., May, 1959.

Charge-Transfer Complexes of Oxygen and Inorganic Anions

by G. Navon

Department of Physical Chemistry, The Hebrew University, Jerusalem, Israel (Received October 31, 1963)

Oxygen was recently found to bring about an extra light absorption when dissolved in various solvents.[1-5] The linear dependence of the transition energy on the ionization potential of the solvent molecule has led to the conclusion that this absorption is of charge-transfer type.[1,4,5] For the same reason Meyerstein and Treinin,[6] following the suggestion of Mulliken,[7] concluded that the spectrum of the trihalide ions is also of charge-transfer character, where the halogen molecule acts as an acceptor and the halide ion as a donor. The purpose of this note is to present spectroscopic evidence for the existence of analogous complexes between oxygen and the iodide, bromide, chloride, and thiocyanate ions in solution.

Experimental

Materials. The oxygen used was the Extra Dry Grade of the Matheson Co., with minimum purity of 99.6%. The nitrogen was the Perpurified Grade of the Matheson Co., with minimum purity of 99.996%. Water was triply distilled. Ethylene glycol of Riedel-De Haën Ag. was distilled *in vacuo*. All other chemicals were of A.R. grade without further purification.

Spectrophotometric measurements were carried out at room temperature (24 ± 1°) using a Hilger Uvispek spectrophotometer. Quartz cells (4 cm.) with ground glass stoppers were used.

Procedure. All solutions were near neutral pH. No buffers were used. Oxygen was bubbled through the solutions for 5 min. and the absorption spectra were

(1) D. F. Evans, J. Chem. Soc., 345 (1953); J. Chem. Phys., 23, 1424 (1955).

(2) A. U. Munck and J. F. Scott, Nature, 177, 587 (1956).

(3) L. J. Heidt and L. E. Ekstrom, J. Am. Chem. Soc., 79, 1260 (1957).

(4) H. Tsubomura and R. S. Mulliken, ibid., 82, 5966 (1960).

(5) J. Jortner and U. Sokolov, J. Phys. Chem., 65, 1633 (1961).

(6) D. Meyerstein and A. Treinin, Trans. Faraday Soc., 59, 1114 (1963).

(7) R. S. Mulliken, J. Am. Chem. Soc., 72, 600 (1950).

Table I

Salt present	Solvent	$\Delta D_{max}/l(O_2)(X^-)$, mole^{-2} cm.$^{-1}$	$\lambda_{max}(O_2X^-)$, mμ	$\lambda_{max}(I_2X^-)$, mμ	$h\nu(O_2X^-) - h\nu(I_2X^-)$, kcal.
1. 0.2 M NaI	Ethanol	43	285[a]	360[b,c]	21
2. 0.5 M KI	Glycol	207	286	361[b]	21
3. 1 M KI	Water	>55	<278	352[c]	>22
4. 0.2 M KSCN	Ethanol	36	274.5	313[b]	13
5. 0.2 M KSCN	Glycol	158	277	315[b]	12.5
6. 1 M KSCN	Water	>70	<265	310[b,d]	>15
7. 1 M NaBr	Water	>47	<236	270[e]	>15
8. 1 M NaCl	Water	>31	<214	248[e]	>18

[a] An approximate value estimated from a shoulder. [b] Present work. [c] L. I. Katzin, *J. Chem. Phys.*, **23**, 2055 (1955). [d] C. Lewis and D. A. Skoog [*J. Am. Chem. Soc.*, **84**, 1101 (1962)] and ref. 2 gave a value of 303 mμ. This value is probably not due to the I_2SCN^- ion but to the $I(SCN)_2^-$ ion (see Experimental). [e] Ref. 2.

measured against the same solutions through which nitrogen was bubbled instead of oxygen. The results were reproducible and did not change during the time of the measurements. This is true also for the iodide solutions in which an absorption at 350–360 mμ (due to the autoxidation product, the I_3^- ion) appears only after a few hours. When nitrogen was bubbled through solutions previously saturated with oxygen, the absorption spectra became nearly identical with those of the reference solutions. All these facts confirm that the absorption bands found are not due to oxidation products. To avoid false maxima due to stray light the total optical density of the solutions was kept below $D = 1.3$.

Preliminary experiments with the I_2SCN^- complex have shown that the λ_{max} of the complex varies with the concentration of SCN^-. This seems to indicate the existence of the equilibrium

$$I_2SCN^- + SCN^- \rightleftharpoons I(SCN)_2^- + I^-$$
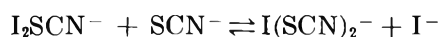
In order to supress the formation of $I(SCN)_2^-$ the spectrum of I_2SCN^- in the various solvents was measured in the presence of added iodide and the absorption of I_3^- was subtracted. The concentration of I_3^- was determined by the absorbance at 380–410 mμ where the absorption of the thiocyanate complexes is negligible. Because of the slow reduction of iodine by the thiocyanate ion all absorption measurements were repeated several times moving back and forth from the shorter to the longer wave length, and an average was taken.

The positions of band maxima recorded in this work are accurate within ± 1 mμ.

Results and Discussion

Figure 1 presents the difference in optical density between various salt solutions saturated with oxygen
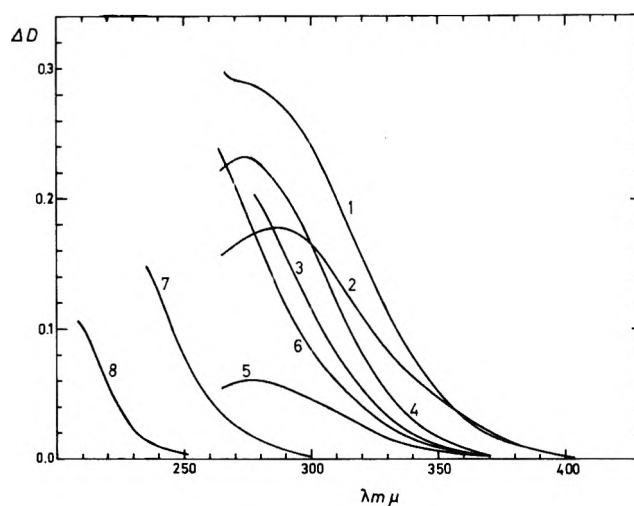

Figure 1. Absorption spectra of O_2X^- in solution at room temperature. The optical path length l is 4 cm. For the numbers see Table I.

and the same solutions saturated with nitrogen. The absorbance of oxygen itself in the corresponding solvents was subtracted when necessary.

The absorbance of the anions themselves made absorption measurements in the ultraviolet impossible. This is probably the reason why we could not find absorption maxima in the aqueous solutions. In ethanol and ethylene glycol the absorption bands of the halides (and other charge-transfer-to-solvent bands) are shifted to the blue[8,9] while internal charge-transfer bands of the type considered here are usually shifted to the red, compared to aqueous solutions.[6,8,10] These

(8) M. Smith and M. C. R. Symons, *Trans. Faraday Soc.*, **54**, 338 (1958).

(9) I. Burak and A. Treinin, *ibid.*, **59**, 1490 (1963).

(10) E. M. Kosower, *J. Am. Chem. Soc.*, **80**, 3253 (1958).

shifts of opposite directions allow the absorption maxima of the O_2I^- and O_2SCN^- ions to be observed. Unfortunately, the large correction for the oxygen absorbance in ethanol and ethylene glycol made the absorption spectra of O_2Br^- and O_2Cl^- in these solvents unreliable.

Experiments with air-saturated and pure oxygen-saturated solutions indicate that the absorbance due to the oxygen–iodide complex is proportional to the oxygen partial pressure. The dependence of this absorption on the concentration of the iodide was measured to 4 M in aqueous solutions and was found to be roughly proportional to the iodide concentration. The accuracy of the experiments was not sufficient for the determination of the stability constant by the Benesi and Hildebrand method.[11] However an upper limit of $K < 0.1$ M^{-1} can be estimated.

Using known and estimated oxygen solubilities[12] the quantities $K\epsilon_{ef} = \Delta D_{max}/1(O_2)(X^-)$ were calculated and recorded in Table I. The relatively small variation of $K\epsilon_{ef}$ in the various solvents suggests that a dominant part of the total absorption intensity is due to contact charge-transfer pairs.[13]

In Table I the absorption maxima of O_2X^- and I_2X^- are compared. This comparison provides an opportunity to check the assumption of Jortner and Sokolov[14] that for a series of oxygen and iodine charge-transfer complexes with various electron donors (D), the difference $h\nu(DO_2) - h\nu(DI_2)$ is constant and equal to the difference in the vertical electron affinities of oxygen and iodine molecules. The values of this difference recorded in the last column of Table I should be compared with the corresponding value of 19 ± 3 kcal. for complexes with organic solvents.[14] The general trend of the transition energies of the anion–oxygen pairs shows clearly that they are of charge-transfer character.

The existence of anion–oxygen complexes has a bearing on the mechanism of their thermal and photochemical autoxidation. It supports the suggestion of Abel[15] about the participation of iodide–oxygen complex in the thermal autoxidation of iodide ion. However some of the subsequent stages in Abel's mechanism are liable to criticism.

Acknowledgment. The author is indebted to Prof. G. Stein and Dr. A. Treinin for helpful discussions and comments.

(11) H. A. Benesi and J. H. Hildebrand, *J. Am. Chem. Soc.*, **71**, 2703 (1949).

(12) Gmelin, "Handbuch der anorganischen Chemie," 8 Auf., Verlag Chemie, G.M.B.H., Weinheim/Bergstrasse, 1958. For oxygen solubilities in the organic solutions a salting-out constant $k_s = 0.2$ was assumed. The results do not depend appreciably upon this choice.

(13) L. E. Orgel and R. S. Mulliken, *J. Am. Chem. Soc.*, **79**, 4839 (1957).

(14) J. Jortner and U. Sokolov, *Nature*, **190**, 1003 (1961).

(15) E. Abel, *Monatsh. Chem.*, **89**, 313 (1958).

Conductance of the Alkali Halides. VIII. Lithium-7 Chloride in Dioxane–Water Mixtures at 25°[1]

by Thomas L. Fabry[2] and Raymond M. Fuoss

Contribution No. 1747 from the Sterling Chemistry Laboratory of Yale University, New Haven, Connecticut
(*Received November 26, 1963*)

The conductance of lithium-7 chloride in dioxane–water mixtures covering the range $12.95 \leq D \leq 62.43$ in dielectric constant which is presented here completes our study of the chlorides of the alkali metals.[3] Symbols used in discussion have been defined in preceding papers of this series.

Experimental

Lithium-7 chloride was used as received from the Isotope Division of the Oak Ridge National Laboratory; it was certified to contain 99.9926 atomic % Li^7. Stock solutions (approximately 0.1 and 0.025 N) were made up in water. No precautions were taken to avoid water take-up by the salt during weighing; concentrations were determined by conductance. Portions of the stock solution were diluted by weight in a conductance cell to give solutions in the range $0.002 \leq c \leq 0.012$ N. Kunze's data[4] were analyzed to give the constants in the conductance equation as shown

$$\Lambda = 115.117 - 86.91c^{1/2} + 40.29c \log c + 170.2c \quad (1)$$

(1) This paper is based on part of a thesis presented by T. L. Fabry to the Graduate School of Yale University in partial fulfillment of the requirements for the Degree of Doctor of Philosophy, September, 1963.

(2) Du Pont Teaching Fellow, 1962–1963.

(3) (a) NaCl, R. W. Kunze and R. M. Fuoss, *J. Phys. Chem.*, **67**, 911 (1963); (b) KCl, J. E. Lind, Jr., and R. M. Fuoss, *ibid.*, **65**, 999 (1961); (c) RbCl, R. W. Kunze and R. M. Fuoss, *ibid.*, **67**, 914 (1963); (d) CsCl, J. C. Justice and R. M. Fuoss, *ibid.*, **67**, 1707 (1963).

(4) In eq. 1 of ref. 3c, the $J_2c^{3/2}$ term was unfortunately omitted; the constants of Tables III and IV of ref. 3c are for the equation with the $c^{3/2}$ term retained. Here, in order to simplify the interpolation, we omitted the $c^{3/2}$ term, and our Λ_0 and J-values therefore differ slightly from Kunze's.

From the observed cell resistance R and the cell constant k, one calculates

$$Z = 1000k(R^{-1} - R_0^{-1}) \qquad (2)$$

where R_0^{-1} is the resistance with water in the cell. Now

$$Z = c\Lambda \qquad (3)$$

The concentration of the lithium chloride solution is known approximately from the weight of lithium chloride and water used to make up the stock solution; call it c_1. Substituting c_1 in (1) gives Λ_1, whence

$$c_2 = Z \text{ (obsd.)}/\Lambda_1 \qquad (4)$$

Then c_2 is returned to (1), and the cycle continued until $|c_n - c_{n-1}| < 10^{-4}c$. From the volume concentrations, the weight concentrations are calculated and from these, the weight concentration of the corresponding stock solution is determined. Concentration of stock solution was checked at least once a week. For conductance measurements, appropriate amounts of dioxane, water, and stock solution were weighed to give the initial concentration for a run. Subsequent points were obtained by diluting this solution with a dioxane–water mixture adjusted to exactly the same solvent ratio as that at the initial point.

Electrical equipment and cells have already been described.[3b] One modification was made in cell design, thanks to a suggestion from Prof. R. H. Stokes. The platinum tube seals through Pyrex have been replaced by tungsten; the tungsten electrode supports are considerably more sturdy than the thin-walled platinum tubes. All measurements were made at $25 \pm 0.002°$.

Properties of the mixed solvents, where w is weight % of dioxane, are summarized in Table I. Conductances are given in Table II, where $\Delta\Lambda$ is the difference between observed conductance and that computed by the equation

$$\Lambda = \Lambda_0 - Sc^{1/2}\gamma^{1/2} + E'c\gamma \ln c\gamma +$$
$$Jc\gamma - K_A c\gamma f^2 \Lambda \qquad (5)$$

Activity coefficients were calculated by the limiting law, $f^2 = e^{-2\tau}$.

Discussion

The data were analyzed by the IBM 709 computer in order to obtain the constants of eq. 5. We are treating J, the coefficient of the linear term, as an empirical constant, pending the completion of a revision[5] of the interpretation of J and K_A, the coefficients of the $c\gamma$ and $c\gamma f^2$ terms. The values of the constants are summarized in Table III. For systems

Table I: Properties of Solvents

No.	w	ρ	D	100η	$10^6\sigma_0$
1	0.0	0.99707	78.54	0.8903	2.44
2	18.8	1.01308	62.43	1.268	2.20
3	45.9	1.03154	39.44	1.845	0.195
4	65.1	1.03670	23.14	1.976	0.123
5	69.8	1.03680	19.30	1.928	0.065
6	75.6	1.03619	14.98	1.827	0.055
7	78.4	1.03577	12.95	1.761	0.009

Table II: Conductance of Lithium-7 Chloride in Dioxane–Water Mixtures at 25°

10^4c	Λ	$100\Delta\Lambda$	10^4c	Λ	$100\Delta\Lambda$
$D = 62.43$			$D = 19.30$		
38.063	78.304	−1.6	5.811	35.001	0.4
66.470	77.155	3.0	10.972	33.125	−1.2
86.912	76.477	−0.2	15.515	31.948	0.5
103.933	76.016	−1.1	20.244	30.969	0.7
			25.275	30.116	−0.6
$D = 39.44$			$D = 14.98$		
8.724	51.336	−0.6	3.971	30.412	0.5
16.388	50.491	0.6	7.611	27.921	−1.6
26.371	49.673	0.6	11.356	26.235	0.7
35.733	49.058	−0.5	15.117	24.985	1.1
			18.961	23.989	−0.8
$D = 23.14$			$D = 12.95$		
6.815	38.213	−0.1	3.424	27.041	0.6
8.735	37.666	0.1	6.594	24.092	−1.9
12.655	36.745	0.1	9.832	22.241	1.1
17.086	35.905	0.0	13.192	20.887	1.2
20.490	35.362	0.0	16.619	19.857	−0.8

2 and 3, at high dielectric constants, $\mathring{a}$ was taken equal to 6.4 to compute $J(a)$, and K_A and Λ_0 were determined by the Λ_K method.[6]

A plot of log K_A against reciprocal dielectric constant is shown in Fig. 1 for the five alkali chlorides. For $D > 30$, association constants were determined by the Λ_K method; the others were computed from the data by means of eq. 5. Lithium chloride is seen to be the least associated of the group, and comes nearest to giving a linear plot. From the slope of the linear portion at low dielectric constants, we obtain $\mathring{a} = 6.4$; this value was used to determine the association constants for systems 2 and 3. This value of $\mathring{a}$ is con-

(5) R. M. Fuoss and L. Onsager, J. Phys. Chem., 66, 1722 (1962); 67, 621 (1963); 67, 628 (1963); 68, 1 (1964).

(6) R. M. Fuoss, J. Am. Chem. Soc., 81, 2659 (1959); eq. 39 and 40. Correction: in the same paragraph, delete "or as the slope . . . against x."
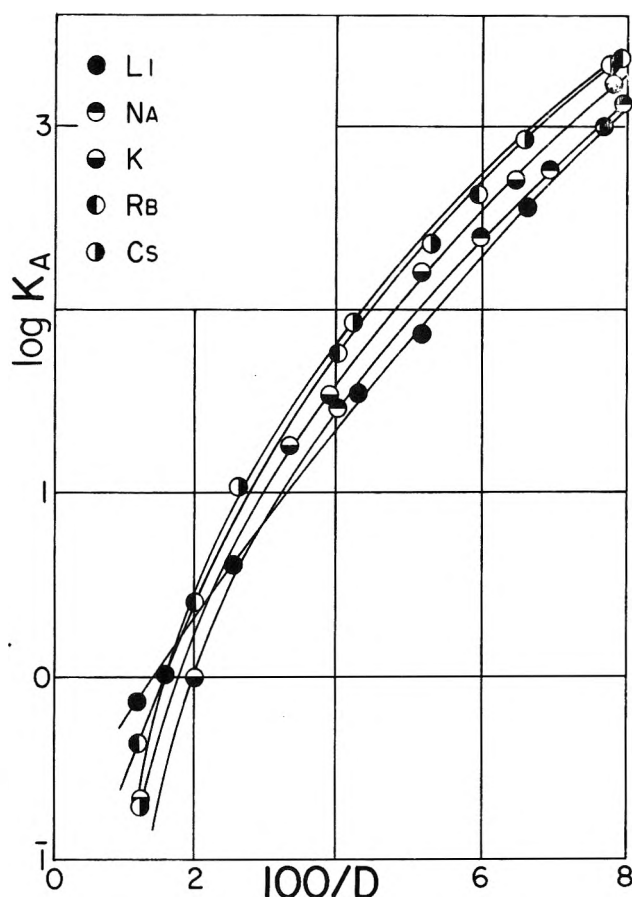
Figure 1. Dependence of association constants of the alkali chlorides on dielectric constants.

siderably higher than the sum of the lattice radii and suggests that the lithium ion remains hydrated, even in a contact pair with chloride ion.

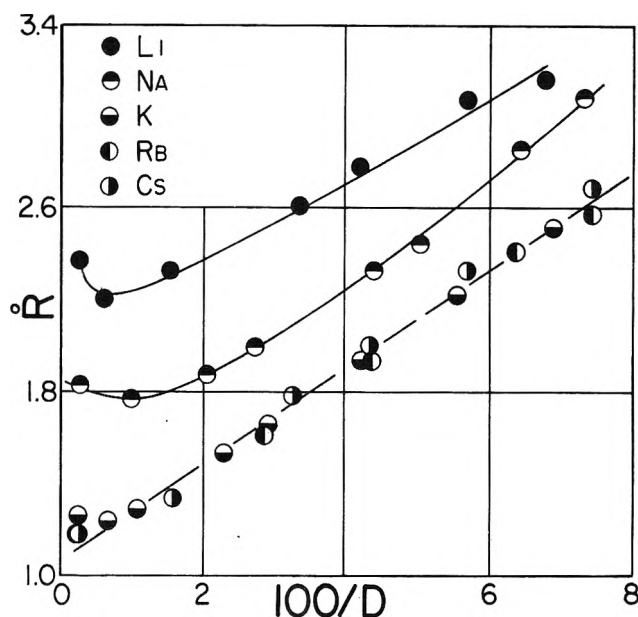A comparison of the Stokes radii for the alkali ions is shown in Fig. 2. Here

Table III: Derived Constants

No.	Λ_0	J	K_Λ
2	82.67 ± 0.04	217.5 = 5.0	2.1 ± 0.1
3	53.76 ± 0.01	420 ± 4	7.9 ± 0.3
4	42.12 ± 0.01	1770 ± 20	34.5 ± 1.1
5	39.77 ± 0.05	2780 ± 50	72.8 ± 5.6
6	36.91 ± 0.08	5900 ± 70	339 ± 14
7	35.74 ± 0.11	9250 ± 80	915 ± 28
	S	$E^.$	σ
2	74.32	9.86	0.016
3	75.75	16.98	0.008
4	110.6	46.06	0.001
5	131.1	67.85	0.012
6	169.0	118.9	0.016
7	197.6	165.0	0.019

Figure 2. Dependence of Stokes radii of the alkali cations on dielectric constant.

$$R_+ = 0.8194 \times 10^{-8}/\lambda_0^+ \eta \qquad (6)$$

Like the other alkali cations, the apparent radius is linear in reciprocal dielectric constant over the range of intermediate and low dielectric constants, showing a drag on the ion due to polarization and relaxation of solvent dielectric as ions move through it.[7-9] Extrapolation to $D = \infty$ gives $R_\infty = 1.06$, which, as expected, is the largest among the alkalis. This value is, however, certainly smaller than the actual radius of the kinetic cation in lithium solutions containing water. It will be noted that the greatest curvature among the alkalis of the $R-1/D$ plots in the water-rich region is shown by lithium. This must be a consequence of the strong interaction expected between the nearest neighbor water molecules and the small lithium ions. There is a close parallel between the structure of the $R-1/D$ plots of Fig. 2 and the viscosity B-coefficients,[10] which are Li$^+$, +0.147; Na$^+$, +0.086; K$^+$, −0.007; Rb$^+$, −0.029; and Cs$^+$, −0.045. As B increases with decreasing atomic number, the curvature in the $78 \geqslant D \geqslant 50$ range steadily increases. At $D = 50$, the mole ratio of the solvent is about 10 water : 1 dioxane; for mixtures containing more dioxane than this, the $R-1/D$ curves become linear. These results suggest

(7) R. M. Fuoss, *Proc. Natl. Acad. Sci. U. S.*, **45**, 807 (1959).

(8) R. H. Boyd, *J. Chem. Phys.*, **35**, 1281 (1961).

(9) R. Zwanzig, *ibid.*, **38**, 1603 (1963).

(10) R. W. Gurney, "Ionic Processes in Solution," Dover Publications, Inc., New York, N. Y., 1962, p. 168.

that the water structure persists in the mixtures up to about 30 wt. % dioxane and that beyond this, the mixed solvent behaves like an ordinary liquid. We plan to study the viscosities of the alkali chlorides in this region.

Relaxation data are available for dioxane–water mixtures containing less than 50% dioxane[11]; from these data, $\tau/\eta = 8.0 \times 10^{-14}$ sec./poise, where τ is dielectric relaxation time and η is viscosity. From Fig. 2, the slope s of the line

$$R^+ = R_\infty(1 + s/D) \tag{7}$$

is found to be 17 Å. Boyd's equation gives

$$s_B = 2e^2\tau/27\pi\eta R^3 \tag{8}$$

where e is the unit charge. With $R = 3$ Å., the calculated slope is 16. Zwanzig's equation is

$$s_Z = (e^2\tau/9\pi\eta R^3)(1 - \epsilon_\infty/\epsilon_0) \tag{9}$$

where ϵ_∞ and ϵ_0 are, respectively, the limiting dielectric constants at infinite and zero frequencies. For our mixtures $\epsilon_\infty/\epsilon_0 \ll 1$; eq. 9 gives $s_Z = 22$. Since the theoretical slope depends on the *cube* of the radius, the agreement between experiment and either theoretical value must be considered satisfactory.

(11) J. B. Hasted, G. H. Haggis, and P. Hutton, *Trans. Faraday Soc.*, **47**, 577 (1951).

Conductance of the Alkali Halides. IX.
Rubidium Iodide in Dioxane–Water
Mixtures at 25°[1]

by Thomas L. Fabry[2] and Raymond M. Fuoss

Contribution No. 1748 from the Sterling Chemistry Laboratory of Yale University, New Haven, Connecticut (*Received November 26, 1963*)

The conductances of rubidium bromide[3] and chloride[4] in dioxane–water mixtures have been reported previously. We present here the conductance of rubidium iodide in dioxane–water mixtures in order to complete the series of rubidium halides. The conductance in water of rubidium chloride, prepared from our iodide by ion exchange, was also determined in order to obtain another check on the limiting conductance of the rubidium ion.[5] Our final result is $\lambda_0(Rb^+, H_2O, 25°) = 77.18 \pm 0.10$.

Experimental

Rubidium iodide, as received from A. D. MacKay Co., gave a conductance in water about three units higher than expected. It was purified by first washing with ice-cold methanol until it became white and then recrystallizing from methanol. The washed residue from 10 g. of starting material was dissolved in 50 ml. of methanol; slow evaporation under a nitrogen stream gave two crops of crystals, which were heated *in vacuo* in an Abderhalden drier for a week at 131°. A second crystallization gave a product whose limiting conductance agreed with that of the first within 0.01%. Analysis in the flame photometer showed 0.033% LiI, 0.026% NaI, 0.046% KI, and 0.028% CsI. These impurities lead to a correction[6] $\Delta\Lambda_0 = -0.026$ in water.

Rubidium chloride was prepared from recrystallized iodide by ion exchange on a Dowex 1-X8 column. The resin was conditioned by five cycles of alternate charging with 1 N potassium iodide and 2 N hydrochloric acid; it was then boiled in distilled water for 1 hr. The column was made up again and regenerated with 2 N hydrochloric acid prepared from constant-boiling acid.[7,8] The column was then washed with deionized water until the effluent had a conductance of 0.10×10^{-6}. Finally, 1 N rubidium iodide solution was fed in at 1 drop/sec. and eluted at the same rate with deionized water. Analysis by flame photometry showed 0.020% LiCl, 0.005% NaCl, 0.035% KCl, and 0.041% CsCl, which led to a correction $\Delta\Lambda = -0.057$. The rubidium chloride eluate was then further diluted to about 0.1 N as stock solution for the conductance determinations. The solution was standardized by potentiometric titration against silver nitrate solution (silver indicating electrode, Beckman glass electrode as reference). The precision[9] was better than 0.01%.

The properties of the solvents are given in Table I and the conductance data in Tables II and III.

(1) This paper is based on part of a thesis presented by T. L. Fabry to the Graduate School of Yale University in partial fulfillment of the requirements for the Degree of Doctor of Philosophy, September, 1963.

(2) Du Pont Teaching Fellow, 1962–1963.

(3) J. E. Lind, Jr., and R. M. Fuoss, *J. Phys. Chem.*, **66**, 1727 (1962).

(4) R. W. Kunze and R. M. Fuoss. *ibid.*, **67**, 914 (1963).

(5) R. W. Kunze, R. M. Fuoss, and B. B. Owen, *ibid.*, **67**, 1719 (1963).

(6) See ref. 4, eq. 6–11.

(7) S. Williams and W. Weiss, *J. Assoc. Offic. Agr. Chemists*, **36**, 354 (1953); **37**, 462 (1954).

(8) I. M. Kolthoff and M. Stenger. "Volumetric Analysis," Vol. II, Interscience Publishers. Inc., New York. N. Y., 1947. p. 67.

(9) E. Bishop. *Anal. Chim. Acta*, **20**, 315 (1959).

Table I: Properties of Solvents

No.	w	ρ	D	100η	$10^6\sigma_0$
1	0.0	0.97707	78.54	0.8903	2.09
2	47.6	1.03226	37.96	1.869	0.36
3	63.7	1.03661	24.39	1.983	0.122
4	70.7	1.03677	18.68	1.918	0.125
5	76.1	1.03613	14.73	1.819	0.035
6	77.2	1.03592	13.53	1.782	0.028

Table II: Conductance of Rubidium Chloride in Water at 25°

10^4c	Λ	$100\Delta\Lambda$	10^4c	Λ	$100\Delta\Lambda$
19.598	149.64	3.4	23.725	149.21	−0.8
37.684	148.10	−4.5	45.696	147.64	−0.4
59.124	146.90	−0.4	67.147	146.53	0.2
82.338	145.86	0.8	90.167	145.62	3.8
93.720	145.43	0.6	114.709	144.72	−2.7

Table III: Conductance of Rubidium Iodide in Dioxane–Water Mixtures at 25° (Superscripts Designate Series of Determinations)

10^4c	Λ	$100\Delta\Lambda$	10^4c	Λ	$100\Delta\Lambda$
	$D = 78.54$			$D = 18.68$	
15.692[a]	150.30	0.0	4.699	43.14	0.4
30.996	148.87	−0.4	9.467	40.88	−1.2
46.718	147.80	0.8	14.253	39.33	0.8
61.385	146.97	0.0	18.537	38.25	0.4
77.489	146.20	−0.3	23.455	37.27	−0.4
14.975[b]	150.37	−0.5			
30.062	148.93	−0.4		$D = 14.73$	
44.921	147.90	1.5	3.292	38.07	0.7
60.300	147.02	0.4	6.347	35.27	−2.1
75.012	146.29	−0.9	9.570	33.30	0.5
	$D = 37.96$		12.333	32.03	2.1
11.135	61.12	0.0	15.353	30.90	−1.3
21.827	59.97	−0.7			
32.372	59.17	0.4		$D = 13.53$	
43.748	58.49	0.9	2.902	35.99	0.7
55.949	57.88	−0.7	5.755	32.75	−2.0
	$D = 24.39$		8.522	30.74	0.6
6.349	48.61	0.6	11.585	29.14	2.1
11.090	47.33	−1.3	14.393	28.00	−1.4
19.143	45.83	−1.0			
31.941	44.21	−0.2			

Discussion

Analysis of the data of Table III gives the values of the constants Λ_0, K_A, and J which are summarized in Table IV. The values of K_A for systems 1 and 2 were obtained by the Λ_K-program, using $\mathring{a}$ = 5.7 (from the slope of the log K_A–D^{-1} plot at low dielectric

constants). In the table are also given the theoretically calculated coefficients S and E', and σ, the standard deviation between calculated and observed conductances in a given run. Figure 1 shows the dependence
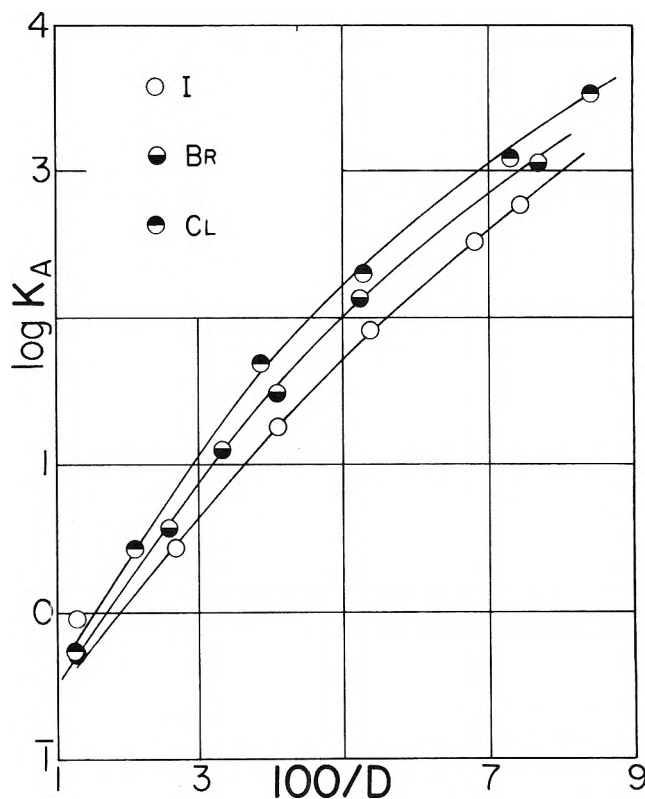

Figure 1. Dependence of association constant on dielectric constant for rubidium halides.

of association constant on dielectric constant for the three rubidium halides. At a given value of dielectric constant, association increases in the sequence $Cl' > Br' > I'$; that is, the smallest halide ion is most associated. This is just the reverse of the sequence found for the alkali cations where lithium is least associated (for a given halide); this difference supports the argument that cations are hydrated while halide ions are not.

A plot of Stokes radius against reciprocal dielectric constants for the iodide ion in rubidium iodide is linear (including the water point) with a slope s of 10 Å. Using the value $\tau/\eta = 8 \times 10^{-14}$ sec./poise,[10] Boyd's equation[11] gives $s = 16$ and Zwanzig's equa-

(10) J. B. Hasted, G. H. Haggis, and P. Hutton, Trans. Faraday Soc., **47**, 577 (1951).

(11) R. M. Boyd, J. Chem. Phys., **35**, 1281 (1961).

tion[12] gives $s = 22$. Agreement with either is satisfactory, since an arbitrary parameter (radius) enters as a cube.

Finally we consider the limiting conductance of the rubidium ion in water at $25°$. The limiting conductance of rubidium iodide (corrected for known impurities) is 154.01 ± 0.01 from the data of Table II. Extrapolation of the data of Owen and Zeldes[13] for potassium iodide gives $\Lambda_0 (KI) = 150.48 \pm 0.02$. Using Longsworth's[14] value $n^+ = 0.4906$ and Lind's[15] value $\Lambda_0(KCl) = 149.89$, $\lambda_0(K^+) = 73.54$, whence $\lambda_0(I') = 76.94$ and $\lambda_0(Rb^+) = 77.08$.

Table IV: Derived Constants

No.	κ_0	J	K_A
1	154.01 ± 0.01	204 ± 2	1.1 ± 0.1
2	64.14 ± 0.01	604 ± 2	5.8 ± 0.2
3	52.40 ± 0.06	1910 ± 80	16.8 ± 4.5
4	48.22 ± 0.04	3990 ± 50	77.8 ± 4.3
5	45.03 ± 0.11	7860 ± 140	331 ± 19
6	44.02 ± 0.11	10300 ± 130	587 ± 23

No.	S	E'	σ
1	95.82	26.42	0.01
2	85.19	112.1	0.01
3	118.1	359.6	0.02
4	152.8	748.3	0.01
5	195.4	1441	0.02
6	213.9	1824	0.01

The data of Table II for the chloride in water can be summarized by the equation

$$\Lambda = 153.72 - 95.75Sc^{1/2} + 26.34c \ln c + 228c$$

The corrected value of the limiting conductance for the chloride is $\Lambda_0(RbCl) = 153.66$; from Longsworth's transference number and Lind's limiting conductance for potassium chloride, we find $\lambda_0(Cl') = 76.36$, whence $\lambda_0(Rb^+) = 77.30$. (Differences of ±0.01 in this paragraph are trivial: the arithmetic was done carrying three digits after the decimal point, and the figures cited have been rounded off to two.) Taking the average of these values and earlier ones,[5] we find $\lambda_0(Rb^+, H_2O, 25°) = 77.18 \pm 0.10$.

(12) R. Zwanzig, *J. Chem. Phys.*, **38**, 1603 (1963).

(13) B. B. Owen and H. Zeldes, *ibid.*, **18**, 1083 (1950).

(14) L. Longsworth, *J. Am. Chem. Soc.*, **54**, 2741 (1932).

(15) J. E. Lind, Jr., and R. M. Fuoss, *J. Phys. Chem.*, **65**, 999 (1961).

Nuclear Magnetic Resonance Studies of BF₃ Addition Compounds. II. The Exchange of BF₃ between $C_6H_5OCH_3 \cdot BF_3$ and $(C_2H_5)_2O \cdot BF_3$

by A. C. Rutenberg, A. A. Palko, and J. S. Drury

Chemistry Division, Oak Ridge National Laboratory,[1] Oak Ridge, Tennessee (Received November 1, 1963)

Boron trifluoride forms stable 1:1 molecular addition compounds with many ethers. In many systems containing BF_3 and more than one ether, rapid exchange of BF_3 occurs between the ether·BF_3 species. This paper presents the results of n.m.r. kinetic studies of the system $(C_6H_5OCH_3)-(C_2H_5)_2O-BF_3$ using the ^{19}F resonance. The present system differs from the previously reported $(CH_3)_2O-(C_2H_5)_2O-BF_3$ system[2] primarily because anisole $(C_6H_5OCH_3)$ forms a much weaker BF_3 addition compound than $(CH_3)_2O$ and $(C_2H_5)_2O$. Thus, if sufficient BF_3 is added to a mixture of anisole and $(C_2H_5)_2O$ to form observable quantities of the anisole·BF_3 species, essentially all of the $(C_2H_5)_2O$ is complexed. From the standpoint of kinetics, such a system is more amenable to analysis than one also containing free $(C_2H_5)_2O$.

The present system is also better suited for accurate rate measurements since the equilibrium compositions of the three major constituents are more accurately known, and the rate measurements could be taken over a more advantageous temperature and composition range. Rate constants and activation energies were calculated for the reaction of $(C_2H_5)_2O \cdot BF_3$ with $C_6H_5OCH_3 \cdot BF_3$ and with $C_6H_5OCH_3$.

Experimental

Eight mixtures of $C_6H_5OCH_3-(C_2H_5)_2O$ and BF_3 were prepared from purified chemicals using high vacuum techniques. N.m.r. measurements of these solutions were made over a temperature range of about $70°$ using a Varian Associates high resolution spectrometer operating at 56.445 Mc. Modulation frequencies were determined with a Hewlett Packard 521C frequency counter. The experimental techniques were described in a previous paper.[2]

Calculations

The values of τ, the mean lifetime in seconds of an ether·BF_3 addition compound, were calculated[2,3]

(2) A. C. Rutenberg, A. A. Palko, and J. S. Drury, *J. Am. Chem. Soc.*, **85**, 2702 (1963).

Table I: Characteristics of the Eight $C_6H_5OCH_3$-$(C_2H_5)_2O$-BF_3 Mixtures

	A	B	C	D	E	F	G	H
Initial composition								
$(C_2H_5)_2O$, moles	1.00	1.00	1.00	1.00	1.00	1.00	1.00	1.00
$C_6H_5OCH_3$, moles	14.06	5.63	1.67	2.99	6.80	1.86	1.01	1.00
BF_3, moles	1.96	1.99	1.33	2.00	3.92	2.09	1.78	1.97
Equilibrium composition at 0°								
$(C_2H_5)_2O \cdot BF_3$, moles/l.	0.61	1.34	3.32	2.12	1.08	2.84	4.01	3.97
$C_6H_5OCH_3 \cdot BF_3$, moles/l.	0.59	1.33	1.11	2.12	3.13	3.09	3.13	3.87
$C_6H_5OCH_3$, moles/l.	8.03	6.22	4.43	4.23	4.19	2.20	0.93	0.095
BF_3 as $C_6H_5OCH_3 \cdot BF_3$, mole fraction	0.490	0.497	0.250	0.500	0.745	0.522	0.438	0.492
$\tau \times 10^5$ at 0°, sec.	39.4	59.4	31.1	91.9	124	155	279	401
$\tau \times 10^5$ at 25°, sec.	7.63	8.61	6.44	14.4	16.3	20.6	30.2	35.6
$\Delta E'$, kcal. mole^{-1}	10.6	12.5	10.2	12.0	13.2	13.1	14.4	15.7
95% confidence limits on $\Delta E'$	0.5	0.5	0.5	0.6	0.8	0.4	0.5	1.4
$R \times 10^{-3}$ at 0°, moles l.$^{-1}$ sec.$^{-1}$	0.76	1.12	2.67	1.15	0.65	0.96	0.63	0.49
$R \times 10^{-3}$ at 25°, moles l.$^{-1}$ sec.$^{-1}$	3.85	7.56	12.4	7.22	4.80	7.02	5.60	5.28

from experimental line width and peak separation data. A least-squares equation of the form

$$\log \tau = m/T + c$$

was obtained for each of the eight mixtures. τ-Values at 0 and 25° were calculated from the least-squares equations. An equation was then set up for each mixture in terms of the rate of exchange R, concentration of the species involved, and rate constants for each exchange path

$$R = \frac{[(C_2H_5)_2O \cdot BF_3]p_1}{\tau} = \frac{[C_6H_5OCH_3 \cdot BF_3]p_2}{\tau} \quad (1)$$

where R is the rate of exchange of an ether·BF_3 complex in moles l.$^{-1}$ sec.$^{-1}$; p_1 and p_2 are mole fractions of $C_6H_5OCH_3 \cdot BF_3$ and $(C_2H_5)_2O \cdot BF_3$, respectively; and the brackets denote molar concentrations. Thus

$$R = k_1[(C_2H_5)_2O \cdot BF_3][C_6H_5OCH_3 \cdot BF_3] +$$
$$k_2[(C_2H_5)_2O \cdot BF_3][C_6H_5OCH_3] \quad (2)$$

Values of k_1 and k_2 were obtained from a least-squares solution of eight rate equations of the above form.

Results and Discussion

Compositions, mean lifetimes, and rates of exchange for the eight mixtures studied are presented in Table I. The R values were calculated from the mean lifetimes using eq. 1.

Most of the experimental τ-values in this study were obtained from measurements on the single peak of the combined complexes. These calculations required values for the separation between the two ether·BF_3 peaks, in the absence of exchange, at the temperatures of interest. The separation changed with tempera-
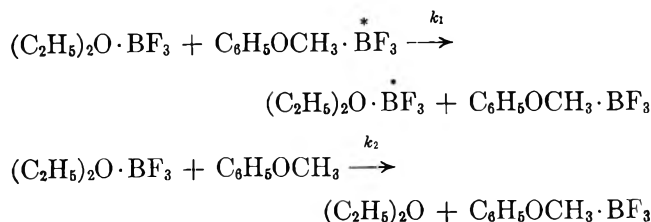
ture; the values used in the calculations were obtained from extrapolation of low temperature measurements of the separation between the individual peaks. This extrapolation was a source of error in the rate measurements and was least satisfactory in the case of mixture H, contributing to the poorer fit of the data for that mixture.

Figure 1 shows the experimental τ-values plotted as a function of reciprocal temperature. The curves shown are the least-squares straight lines. The $\Delta E'$ values in Table I were calculated from the slopes of these lines. $\Delta E'$ represents an average activation energy for the various paths contributing to the BF_3 exchange. A similar average activation energy may be calculated from the 0 and 25° rates of exchange. The temperature coefficients of the rates of exchange give values of $\Delta E'$ that are 1–2% lower than the slope values, since the concentration of $(C_2H_5)_2O \cdot BF_3$ is slightly lower at the higher temperature due to a change in solution density.

A previously studied mixture[2] of $(C_2H_5)_2O$, $(CH_3)_2O$, and BF_3 similar in composition to mixture D $(R = 1.15 \times 10^3$ moles l.$^{-1}$ sec.$^{-1}$) had an R value of $\sim 2 \times 10^4$ moles l.$^{-1}$ sec.$^{-1}$. Since the main reaction for the mixtures under consideration, in both cases, was the transfer of BF_3 from $(C_2H_5)_2O \cdot BF_3$ to a free ether, the reaction of $(C_2H_5)_2O \cdot BF_3 + (CH_3)_2O$ is more rapid than $(C_2H_5)_2O \cdot BF_3 + C_6H_5OCH_3$.

Table II gives the values of k_1 and k_2 at 0 and 25° calculated from the n.m.r. measured rates of exchange using eq. 2. The reactions associated with the rate constants are

(3) J. A. Pople, W. G. Schneider, and H. J. Bernstein, "High-Resolution Nuclear Magnetic Resonance," McGraw-Hill Book Co., Inc., New York, N. Y., 1959, Chapter 10.

$$(C_2H_5)_2O \cdot BF_3 + C_6H_5OCH_3 \cdot \overset{*}{BF_3} \xrightarrow{k_1}$$

$$(C_2H_5)_2O \cdot \overset{*}{BF_3} + C_6H_5OCH_3 \cdot BF_3$$

$$(C_2H_5)_2O \cdot BF_3 + C_6H_5OCH_3 \xrightarrow{k_2}$$

$$(C_2H_5)_2O + C_6H_5OCH_3 \cdot BF_3$$

Reaction 1, which should involve more rearrangement of the solution, has the larger activation energy and
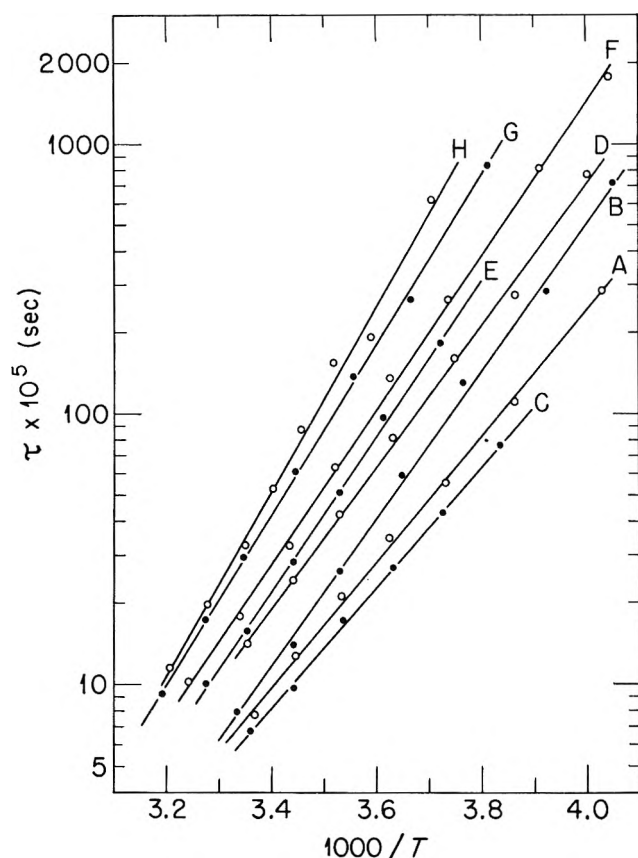
Figure 1. Temperature dependence of τ for eight mixtures of $(C_2H_5)_2O$, $C_6H_5OCH_3$, and BF_3.
Compositions of mixtures are given in Table I.

Table II: Rate Constants and Activation Energies for Reactions of $(C_2H_5)_2O \cdot BF_3$ with $C_6H_5OCH_3 \cdot \overset{*}{BF_3}$ and $C_6H_5OCH_3$[a]

	k_1, l. mole^{-1} sec.$^{-1}$	k_2, l. mole^{-1} sec.$^{-1}$
25°	353 ± 11	798 ± 42
0°	28.5 ± 2.2	155 ± 13
ΔE, kcal. mole^{-1}	16.3 ± 0.5	10.6 ± 0.6

[a] Confidence limits all at 95% level.

smaller rate constant. Reaction 2 appears to proceed by way of a displacement mechanism since its activation energy is somewhat less than the heats of formation of the ether·BF_3 complexes.[4,5]

An upper limit for the equilibrium constant for the reaction

$$(C_2H_5)_2O \cdot BF_3 + C_6H_5OCH_3 \rightleftharpoons$$

$$(C_2H_5)_2O + C_6H_5OCH_3 \cdot BF_3$$
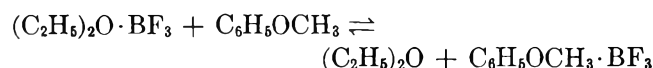
was estimated from low temperature observations of several reaction mixtures containing a large excess of anisole

$$K_{eq} = \frac{k_{forward}}{k_{reverse}} < 0.005$$

Since $k_{forward} = k_2 = 798$ l.·mole^{-1} sec.$^{-1}$ at 25°, we may set a lower limit on the rate constant for the reaction of $C_6H_5OCH_3 \cdot BF_3$ with $(C_2H_5)_2O$ ($k_{reverse}$) at 25°.

$$k_{reverse} > 10^5 \text{ l. mole}^{-1} \text{ sec.}^{-1}$$

The available kinetic data on these systems indicate the fastest BF_3 exchanges between different ethers involve the transfer of a BF_3 molecule from a weaker complex to a free ether to give a stronger complex.

(4) A. A. Palko, R. M. Healy, and L. Landau, J. Chem. Phys., 28, 214 (1958).

(5) D. E. McLaughlin and M. Tamres, J. Am. Chem. Soc., 82, 5618 (1960).

The Standard Molar Free Energy of Formation of Thorium Carbide by Electromotive Force Measurements[1]

by J. J. Egan

Brookhaven National Laboratory, Upton, New York
(Received November 8, 1963)

The thermodynamic properties of ThC_2 have been studied by Prescott and Hincke[2] at high temperatures by measuring the equilibrium of the reaction, $ThO_2 + 4C = ThC_2 + 2CO$. Several authors have used the resulting data to obtain the heat and free energy of formation of ThC_2, but the free energy values remain uncertain to ± 10 kcal.[3]

This work employs a solid-state galvanic cell[4] in the temperature range 700 to 970° in order to measure the free energy of formation directly. The cell may be represented as
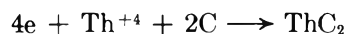
$$Mo|Th,ThF_4(s)|CaF_2(s)|ThF_4,ThC_2,C(s)|Mo$$
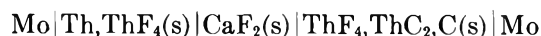
where the CaF_2 acts as an auxiliary electrolyte and the two adjoining tablets are powders of the constituents, intimately mixed. Molybdenum served as an inert electrode material.

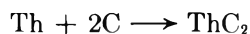At the left-hand electrode

$$Th = Th^{+4} + 4e$$

At the right-hand electrode

$$4e + Th^{+4} + 2C \longrightarrow ThC_2$$

and the over-all reaction on passing 4 f. is

$$Th + 2C \longrightarrow ThC_2$$

with CaF_2 conducting by means of F^- ions from right to left.

Thus the standard molar free energy of formation of ThC_2 is given by

$$\Delta F°_{ThC_2} = -4FE$$

Experimental

The cell arrangement was the same as that used previously to measure the free energy of formation of solid chlorides[5] with the exception that molybdenum was used as an electrode material in place of platinum.

The thorium carbide was prepared by mixing thorium powder with a stoichiometric excess of graphite powder, pressing the resulting mixture into a pellet, and then heating the pellet with an induction furnace for approximately 0.5 hr at 1650° in a graphite crucible under vacuum. The thorium carbide containing excess carbon was then rapidly crushed and mixed with ThF_4 and again pressed into a pellet suitable for the cell. The cells were operated for approximately 2 weeks.
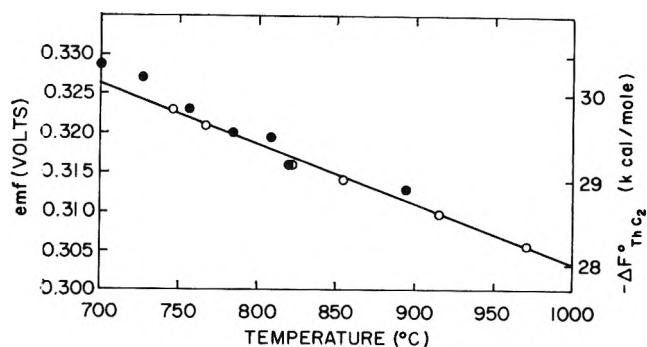

Figure 1. Results of two cells operated at various temperatures.

Only results of the last week of operation were used since it generally took 4 days to 1 week to attain complete equilibrium at 800°.

Results

The results of two separate cells at various temperatures are shown in Fig. 1. At 800° the standard molar free energy of formation of ThC_2 is -29.4 ± 0.3 kcal./mole. Since entropy measurements made from temperature coefficients of cells are in general not always accurate, one may only estimate the entropy and heat of formation of ThC_2 from the results. These calculations yield the values $\Delta S°_{ThC_2} = -7.2$ e.u. and $\Delta H°_{ThC_2} = -37.1$ kcal./mole in the temperature range of the experiments.

(3) O. Kubaschewski and E. Evans, "Metallurgical Thermochemistry," Pergamon Press Ltd., New York, N. Y., 1958.

(4) K. Kiukkola and C. Wagner, *J. Electrochem. Soc.*, **104**, 308 (1957).

(5) J. J. Egan, W. McCoy, and J. Bracker in "Thermodynamics of Nuclear Materials," International Atomic Energy Agency, Vienna, 1962, p. 163.

COMMUNICATIONS TO THE EDITOR

First Observation of a Solution of Li₃Bi, An Intermetallic in Molten Lithium Chloride and Lithium Chloride–Lithium Fluoride[1]

Sir: Evidence has been obtained for the first time of the existence of an intermetallic species in a molten salt. The first indication that such a solution might exist occurred during the study of the bimetallic concentration cell

$$Li(l) | LiCl-LiF(l) | Bi(l) \text{ saturated with } Li_3Bi(s)$$
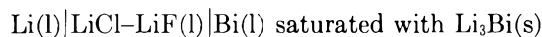
over the temperature range of 500 to 1000°. The fused salt electrolyte, which had been maintained under a helium atmosphere, became intensely red in color. Analysis of the electrolyte revealed that both bismuth and lithium were present. Solubility and spectrophotometric measurements were undertaken to gain a better understanding of the nature of the molten salt solution.

The solubilities of high-purity, activated bismuth in LiCl–LiF eutectic were measured at 600, 700, 800, and 900° and were found to be 0.9×10^{-3}, 1.6×10^{-3}, 2.0×10^{-3}, and 1.8×10^{-3} wt. %, respectively. The liquid bismuth metal equilibrated with the fused lithium salts gave colorless solutions.

High-purity lithium (99.99%, sodium and potassium content each less than 30 p.p.m.) was added to the bismuth to prepare an alloy containing 70 atom % lithium. The alloy was equilibrated with the fused salt at various temperatures between 600 and 1000°. The bismuth content of the solutions was determined by β-counting, the lithium content by titration of hydrolyzed samples of the fused salt solutions. The experiments were carried out in a glove box containing a very high-purity helium atmosphere.

The solubility data are given in Table I and are shown in Fig. 1 as mole % Li₃Bi *vs.* $1/T$, °K.

Equilibration of the Li–Bi alloy with the eutectic resulted in clear, deep red solutions. The solutions contained from about 350 to 2000 times the bismuth found in solutions equilibrated with pure bismuth in the temperature range of 600 to 900°. The clear deep red fused salt solutions quickly became black with a fine dispersion of insoluble bismuth precipitating when the solutions were allowed to come in contact with air. The lithium content appears to be of the same order of magnitude as found for the equilibration of pure lithium metal in lithium chloride, *ca.* 0.5 mole % lithium at 640° in lithium chloride[2] compared to 0.3 mole % in the 70 mole % lithium chloride–30 mole % lithium fluoride eutectic salt mixture. The latter value was

obtained by multiplying the Li₃Bi mole % at 640° in Fig. 1 by three. The lithium fluoride would have the effect of decreasing the solubility of pure lithium metal, but the exact value of the solubility of lithium metal in lithium chloride–lithium fluoride eutectic salt mixture is not known.
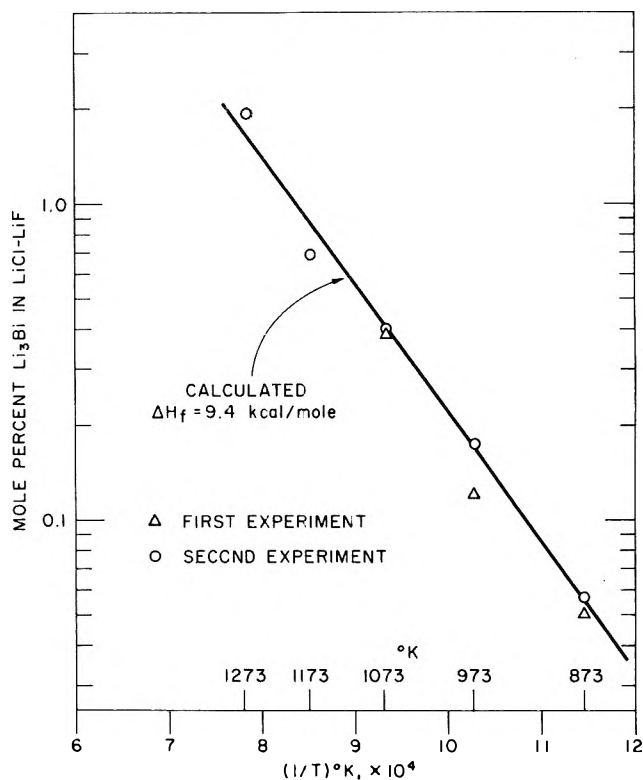

Figure 1. Solubility of Li₃Bi in LiCl–LiF eutectic salt mixture.

Approximately 0.5 g. of Li₃Bi was prepared *in situ* in a small tantalum crucible by fusing together the appropriate amounts of lithium and bismuth metals. About 25 g. of purified LiCl–LiF eutectic (70 mole % LiCl, m.p. 505°) was placed in the tantalum crucible, and a saturated solution of Li₃Bi in the molten eutectic was prepared by heating the crucible to 800°. The mixture was decanted from the tantalum crucible, crushed, and placed in the rectangular well of a 0.5 × 1.5-in. rectangular sapphire absorption cell. The sapphire cell was placed in a quartz outer envelope consisting of a rectangular bottom and a round upper portion provided with a vacuum stopcock. The fore-

(1) This work was performed under the auspices of the U. S. Atomic Energy Commission.

(2) A. S. Dworkin, H. R. Bronstein, and M. A. Bredig, *J. Phys. Chem.*, **66**, 572 (1962).

going steps were carried out in a high-purity helium atmosphere. The quartz and sapphire assembly was evacuated and placed in the heated sample chamber of a Cary 14H spectrophotometer.

The spectrum of the red solution was measured at 525° in the range 5000–30,000 cm.$^{-1}$. The spectrum is characterized by an intense absorption band whose long wave length edge is located at 2.0 e.v. (16,300 cm.$^{-1}$) at 525°. Preliminary studies of the temperature shift of the band have shown that the band edge shifts ~0.1 e.v. to lower energies for each 100° rise in temperature.

The absorption spectra of lithium metal in LiCl[3] and of bismuth metal in BiCl$_3$[4] have been reported in the literature. The absorption bands reported for both of these systems have their energy maximum at ~18,000 cm.$^{-1}$.

Since the Li–Bi ratio of the soluble species was very close to three, we wish to suggest that the absorption spectrum is due to an Li$_3$Bi entity. The data presented constitute the first evidence for the existence of intermetallic species in a molten salt.

It is of interest to note that a large number of intermetallic compounds form solutions in liquid ammonia. However, Zintl, Goubeau, and Dullenkopf[5] found Na$_3$-Bi$_3$ and Na$_3$Bi$_5$ soluble in liquid ammonia while Na$_3$Bi was not soluble (no study was reported for Li$_3$Bi).

Table I: Lithium and Bismuth Metal Solubilities Found in Fused LiCl–LiF Eutectic Salt Mixture Equilibrated with 0.70 Atom Fraction of Lithium in Bismuth

Temp., °C.	⌐—Wt. % Li[a]—⌐	⌐—Wt. % Bi[b]—⌐	Atom ratio Li:Bi
600	0.0322 ± 0.0005	0.314 ± 0.004	3.09 ± 0.06
		0.259 ± 0.05[c]	
700	0.098 ± 0.002	0.968 ± 0.012	3.03 ± 0.06
		0.64 ± 0.05[c]	
800	0.207 ± 0.003[c]	2.19 ± 0.03	2.84 ± 0.06
	0.223 ± 0.003[c]	2.16 ± 0.04[c]	
900	0.380 ± 0.006	3.74 ± 0.05	3.05 ± 0.07
1000	0.957 ± 0.014	10.01 ± 0.13	2.88 ± 0.06
		Average	3.0 ± 0.1

[a] Hydrolysis and titration with a standard hydrochloric acid solution. [b] Bismuth containing Bi-210 tracer at a known specific activity was used in making the alloy. [c] Results of first experiment.

(3) J. P. Young, *J. Phys. Chem.*, **67**, 2507 (1963).

(4) C. R. Boston and G. P. Smith, *ibid.*, **66**, 1178 (1962).

(5) E. Zintl, J. Goubeau, and W. Dullenkopf, *Z. physik. Chem.*, **15A**, 1 (1931).

ARGONNE NATIONAL LABORATORY   M. S. FOSTER
ARGONNE, ILLINOIS   C. E. CROUTHAMEL
                                     D. M. GRUEN
                                     R. L. McBETH

Study of Electrode Kinetics at Open Circuit with an Electrode of Varying Area

Sir: The algebraic sum of the faradaic and double layer charging currents is equal to zero at open circuit for an electrode of varying area. Current–potential characteristics thus can be determined[1] from calculated capacity currents and measured potentials (electrometer amplifier). Correction for mass transfer is made, if necessary. Study of electrode processes should be possible in electrolytes of very low conductivity because no external polarization device is needed and the electrometer input resistance is very high. This seems hardly possible with present methods. Details are given for application of the streaming mercury electrode to fast processes, and potentialities of some other electrodes (solid, mercury) are examined.

Streaming Mercury Electrode. The capacity current *at constant E* is (see discussion of sign and transient below)

$$|i_{d1}| = |c(E - E_z)(2m/r\delta)| \qquad (1)$$

where c is the double layer integral capacity per unit area; E, potential; E_z, zero charge point; m, mercury rate of flow; r, mercury column radius; and δ, mercury density. $(2m/r\delta)$ represents the renewal rate of the electrode surface, *i.e.*, the electrode area $2\pi rl$ divided by the time, $\pi r^2\delta l/m$, an element of surface travels the length l of the mercury column. It is assumed that r is constant along the column, and that the exposed area at the column end, if any, is negligible.

The faradaic current for $O + ne = R$ (O and R soluble) and an overvoltage η not exceeding a few millivolts is

$$i_f = -\cfrac{1}{\cfrac{1}{I_a^0} + \cfrac{1}{I_C^d} + \cfrac{1}{I_A^d}} \frac{nF}{RT} \eta(2\pi rl) \qquad (2)$$

where I_a^0 is the apparent exchange current density; I_C^d and I_A^d are diffusion current densities for the cathodic and anodic processes, respectively; F, R, and T are as usual. One has: $i_f \gtrless 0$ and $\eta \lessgtr 0$ for cathodic and anodic processes, respectively; $I_C^d > 0$ and $I_A^d > 0$. Equation 2 was derived by introducing the concentrations C_O and C_R at the electrode surface, calculated according to the diffusion layer model, in the linearized $I - \eta$ characteristic. The explicit form[2] of the I^d's

(1) Double layer capacities were measured by Watanabe with a vibrating mercury–electrolyte interface. Application to electrode kinetics is not mentioned. See A. Watanabe, *J. Electrochem. Soc.*, **110**, 72 (1963).

is now introduced in eq. 2, and the resulting equation is combined with eq. 1. Signs are such that $i_f \gtrless 0$ for $E \gtrless E_z$. Thus

$$-\frac{1}{\eta} = 2\frac{(nF)^2}{RT} \frac{1}{\frac{1}{C_O^0 D_O^{1/2}} + \frac{1}{C_R^0 D_R^{1/2}}} \times$$

$$\frac{r\delta^{1/2}}{c(E - E_z)} \left(\frac{l}{m}\right)^{1/2} \left[1 - \frac{1}{\lambda}\ln(1 + \lambda)\right] \quad (3)$$

$$\lambda = \frac{\pi r \delta^{1/2}}{nF}\left(\frac{1}{C_O^0 D_O^{1/2}} + \frac{1}{C_R^0 D_R^{1/2}}\right)\left(\frac{l}{m}\right)^{1/2} I_a^0 \quad (4)$$

(D's are diffusion coefficients; C^0's are bulk concentrations). The function $1 - (1/\lambda)\ln(1 + \lambda)$ varies from 0 for $\lambda = 0$ to 1 for $\lambda \to \infty$, and these two limits correspond to pure control by charge transfer and by diffusion, respectively. Hence, $-1/\eta$ is proportional to l/m for $\lambda \to 0$ and to $(l/m)^{1/2}$ for $\lambda \to \infty$. In the general case, I_a^0 can be computed either directly from eq. 3 or from a plot of $d[(l/m)^{1/2}]/d(-1/\eta)$ against $(m/l)^{1/2}$. Apparent standard rate constants up to at least 5×10^{-2} cm. sec.$^{-1}$ could be measured.

The above treatment was modified to include the transient resulting from the term $|c(dE/dt)A|$ (A is the electrode area) to be added in eq. 1 when E varies. It was concluded that the transient for fast processes dies out too rapidly to interfere.

Since $i_f \gtrless 0$ for $E \gtrless E_z$, anodic processes cannot be studied for $E > E_z$ (and cathodic processes for $E < E_z$) with the streaming mercury electrode. This is not a drawback with fast processes since they can be studied in either direction, but application to slow processes in the Tafel region is limited (see below).

Other Electrodes. Generalization to any electrode is based on the fundamental equation (c is constant)

$$cA(dE/dt) + c(E - E_z)(dA/dt) - I_fA = 0 \quad (5)$$

where A is the electrode area, and $I_f \gtrless 0$ for $\eta \lessgtr 0$. If $A = A_0 \exp(pt)$ ($p \gtrless 0$), E is constant, when A varies, after the transient has died out. A "*funnel mercury electrode*" of easily calculated profile can be used to measure E while mercury flows at a constant rate (for slow processes when the streaming electrode cannot be utilized). Or, a solid electrode with suitable profile may be used for slow processes. Fast processes could possibly be studied with a metallic membrane electrode whose area varies according to a known function of time, and the case corresponding to $A = A_0 + A_1 \sin \omega t$ was treated. The foregoing ideas were also applied to the dropping mercury electrode, and I_a^0 can be determined from potential–time curves during drop life. The capacity current density is very large in the initial moments of drop life, and large overvoltages then prevail. This difficulty is avoided with a drop (expelled from a microsyringe) with interruption of drop growth to allow equilibrium to be reached before drop growth is resumed.

In conclusion, the above ideas should allow the study of slow or fast processes in media of very poor conductivity (*e.g.*, nonaqueous solvents of low dielectric constant) when conventional methods fail. Experimental data and further results will be reported in a subsequent paper.

(2) Survey and validity conditions: I. M. Kolthoff and Y. Okinaka, "Progress in Polarography," P. Zuman, Ed., Interscience Division, John Wiley and Sons, Inc., New York, N. Y., Vol. 2, 1962, pp. 367–372. The equation for I_A^d for anodic oxidation of a metal (amalgam) used here is valid provided the diffusion layer thickness is very small in comparison with r. Migration can also be corrected for, if necessary.

COATES CHEMICAL LABORATORY   PAUL DELAHAY
LOUISIANA STATE UNIVERSITY
BATON ROUGE, LOUISIANA